Mobile Information Systems

Artificial Intelligence for Remote and Mobile Multimedia

Lead Guest Editor: Chi Lin
Guest Editors: Ning Wang and Chang Wu Yu

Artificial Intelligence for Remote and Mobile Multimedia

Mobile Information Systems

Artificial Intelligence for Remote and Mobile Multimedia

Lead Guest Editor: Chi Lin
Guest Editors: Ning Wang and Chang Wu Yu

Contents

Contents

Contents

Hindawi
Mobile Information Systems
Volume 2023, Article ID 9829310, 1 page
https://doi.org/10.1155/2023/9829310

Retraction

Retracted: Regular Flow Field Sparse Processing and Blue Finance of Ocean City Research Based on GIS System

Mobile Information Systems

Received 31 October 2023; Accepted 31 October 2023; Published 1 November 2023

This article has been retracted by Hindawi following an investigation undertaken by the publisher [1]. This investigation has uncovered evidence of one or more of the following indicators of systematic manipulation of the publication process:

(1) Discrepancies in scope
(2) Discrepancies in the description of the research reported
(3) Discrepancies between the availability of data and the research described
(4) Inappropriate citations
(5) Incoherent, meaningless and/or irrelevant content included in the article
(6) Peer-review manipulation

The presence of these indicators undermines our confidence in the integrity of the article's content and we cannot, therefore, vouch for its reliability. Please note that this notice is intended solely to alert readers that the content of this article is unreliable. We have not investigated whether authors were aware of or involved in the systematic manipulation of the publication process.

Wiley and Hindawi regrets that the usual quality checks did not identify these issues before publication and have since put additional measures in place to safeguard research integrity.

We wish to credit our own Research Integrity and Research Publishing teams and anonymous and named external researchers and research integrity experts for contributing to this investigation.

The corresponding author, as the representative of all authors, has been given the opportunity to register their agreement or disagreement to this retraction. We have kept a record of any response received.

References

[1] Y. Sun and K. Anurag, "Regular Flow Field Sparse Processing and Blue Finance of Ocean City Research Based on GIS System," *Mobile Information Systems*, vol. 2022, Article ID 7650704, 10 pages, 2022.

Hindawi
Mobile Information Systems
Volume 2023, Article ID 9897383, 1 page
https://doi.org/10.1155/2023/9897383

Retraction

Retracted: Analysis of Computer Visualized Sound Parameters of Vocal Music Singing Based on Deep Learning

Mobile Information Systems

Received 17 October 2023; Accepted 17 October 2023; Published 18 October 2023

This article has been retracted by Hindawi following an investigation undertaken by the publisher [1]. This investigation has uncovered evidence of one or more of the following indicators of systematic manipulation of the publication process:

(1) Discrepancies in scope
(2) Discrepancies in the description of the research reported
(3) Discrepancies between the availability of data and the research described
(4) Inappropriate citations
(5) Incoherent, meaningless and/or irrelevant content included in the article
(6) Peer-review manipulation

The presence of these indicators undermines our confidence in the integrity of the article's content and we cannot, therefore, vouch for its reliability. Please note that this notice is intended solely to alert readers that the content of this article is unreliable. We have not investigated whether authors were aware of or involved in the systematic manipulation of the publication process.

Wiley and Hindawi regrets that the usual quality checks did not identify these issues before publication and have since put additional measures in place to safeguard research integrity.

We wish to credit our own Research Integrity and Research Publishing teams and anonymous and named external researchers and research integrity experts for contributing to this investigation.

The corresponding author, as the representative of all authors, has been given the opportunity to register their agreement or disagreement to this retraction. We have kept a record of any response received.

References

[1] N. Mo, J. S. Ai, and S. Y. Ran, "Analysis of Computer Visualized Sound Parameters of Vocal Music Singing Based on Deep Learning," *Mobile Information Systems*, vol. 2022, Article ID 1121092, 9 pages, 2022.

Hindawi
Mobile Information Systems
Volume 2023, Article ID 9824052, 1 page
https://doi.org/10.1155/2023/9824052

Retraction

Retracted: Statistical Measurement and Influencing Factors of Green Total Factor Productivity of China's Tourism Industry Based on DEA-EBM Model

Mobile Information Systems

Received 8 August 2023; Accepted 8 August 2023; Published 9 August 2023

This article has been retracted by Hindawi following an investigation undertaken by the publisher [1]. This investigation has uncovered evidence of one or more of the following indicators of systematic manipulation of the publication process:

(1) Discrepancies in scope
(2) Discrepancies in the description of the research reported
(3) Discrepancies between the availability of data and the research described
(4) Inappropriate citations
(5) Incoherent, meaningless and/or irrelevant content included in the article
(6) Peer-review manipulation

The presence of these indicators undermines our confidence in the integrity of the article's content and we cannot, therefore, vouch for its reliability. Please note that this notice is intended solely to alert readers that the content of this article is unreliable. We have not investigated whether authors were aware of or involved in the systematic manipulation of the publication process.

Wiley and Hindawi regrets that the usual quality checks did not identify these issues before publication and have since put additional measures in place to safeguard research integrity.

We wish to credit our own Research Integrity and Research Publishing teams and anonymous and named external researchers and research integrity experts for contributing to this investigation.

The corresponding author, as the representative of all authors, has been given the opportunity to register their agreement or disagreement to this retraction. We have kept a record of any response received.

References

[1] Z. Xiang, S. Che, and S. Zhou, "Statistical Measurement and Influencing Factors of Green Total Factor Productivity of China's Tourism Industry Based on DEA-EBM Model," *Mobile Information Systems*, vol. 2022, Article ID 4069291, 13 pages, 2022.

Hindawi
Mobile Information Systems
Volume 2023, Article ID 9757060, 1 page
https://doi.org/10.1155/2023/9757060

Retraction

Retracted: Design of Accurate Association System of QR Code Information for Cigarette Sorting

Mobile Information Systems

Received 8 August 2023; Accepted 8 August 2023; Published 9 August 2023

This article has been retracted by Hindawi following an investigation undertaken by the publisher [1]. This investigation has uncovered evidence of one or more of the following indicators of systematic manipulation of the publication process:

(1) Discrepancies in scope
(2) Discrepancies in the description of the research reported
(3) Discrepancies between the availability of data and the research described
(4) Inappropriate citations
(5) Incoherent, meaningless and/or irrelevant content included in the article
(6) Peer-review manipulation

The presence of these indicators undermines our confidence in the integrity of the article's content and we cannot, therefore, vouch for its reliability. Please note that this notice is intended solely to alert readers that the content of this article is unreliable. We have not investigated whether authors were aware of or involved in the systematic manipulation of the publication process.

Wiley and Hindawi regrets that the usual quality checks did not identify these issues before publication and have since put additional measures in place to safeguard research integrity.

We wish to credit our own Research Integrity and Research Publishing teams and anonymous and named external researchers and research integrity experts for contributing to this investigation.

The corresponding author, as the representative of all authors, has been given the opportunity to register their agreement or disagreement to this retraction. We have kept a record of any response received.

References

[1] C. Hao, W. Taicheng, and Z. Haoran, "Design of Accurate Association System of QR Code Information for Cigarette Sorting," *Mobile Information Systems*, vol. 2022, Article ID 2466801, 12 pages, 2022.

Hindawi
Mobile Information Systems
Volume 2023, Article ID 9860170, 1 page
https://doi.org/10.1155/2023/9860170

Retraction

Retracted: Analysis of Ancient Literary Works Based on Intelligent Image Text Recognition

Mobile Information Systems

Received 1 August 2023; Accepted 1 August 2023; Published 2 August 2023

This article has been retracted by Hindawi following an investigation undertaken by the publisher [1]. This investigation has uncovered evidence of one or more of the following indicators of systematic manipulation of the publication process:

(1) Discrepancies in scope
(2) Discrepancies in the description of the research reported
(3) Discrepancies between the availability of data and the research described
(4) Inappropriate citations
(5) Incoherent, meaningless and/or irrelevant content included in the article
(6) Peer-review manipulation

The presence of these indicators undermines our confidence in the integrity of the article's content and we cannot, therefore, vouch for its reliability. Please note that this notice is intended solely to alert readers that the content of this article is unreliable. We have not investigated whether authors were aware of or involved in the systematic manipulation of the publication process.

Wiley and Hindawi regrets that the usual quality checks did not identify these issues before publication and have since put additional measures in place to safeguard research integrity.

We wish to credit our own Research Integrity and Research Publishing teams and anonymous and named external researchers and research integrity experts for contributing to this investigation.

The corresponding author, as the representative of all authors, has been given the opportunity to register their agreement or disagreement to this retraction. We have kept a record of any response received.

References

[1] J. Fan, "Analysis of Ancient Literary Works Based on Intelligent Image Text Recognition," *Mobile Information Systems*, vol. 2022, Article ID 1113856, 9 pages, 2022.

Hindawi
Mobile Information Systems
Volume 2023, Article ID 9817515, 1 page
https://doi.org/10.1155/2023/9817515

Retraction

Retracted: Application of Computer Network Technology in Network Music Education System

Mobile Information Systems

Received 1 August 2023; Accepted 1 August 2023; Published 2 August 2023

This article has been retracted by Hindawi following an investigation undertaken by the publisher [1]. This investigation has uncovered evidence of one or more of the following indicators of systematic manipulation of the publication process:

(1) Discrepancies in scope
(2) Discrepancies in the description of the research reported
(3) Discrepancies between the availability of data and the research described
(4) Inappropriate citations
(5) Incoherent, meaningless and/or irrelevant content included in the article
(6) Peer-review manipulation

The presence of these indicators undermines our confidence in the integrity of the article's content and we cannot, therefore, vouch for its reliability. Please note that this notice is intended solely to alert readers that the content of this article is unreliable. We have not investigated whether authors were aware of or involved in the systematic manipulation of the publication process.

Wiley and Hindawi regrets that the usual quality checks did not identify these issues before publication and have since put additional measures in place to safeguard research integrity.

We wish to credit our own Research Integrity and Research Publishing teams and anonymous and named external researchers and research integrity experts for contributing to this investigation.

The corresponding author, as the representative of all authors, has been given the opportunity to register their agreement or disagreement to this retraction. We have kept a record of any response received.

References

[1] X. Chao, "Application of Computer Network Technology in Network Music Education System," *Mobile Information Systems*, vol. 2022, Article ID 8754424, 11 pages, 2022.

Hindawi
Mobile Information Systems
Volume 2023, Article ID 9686763, 10 pages
https://doi.org/10.1155/2023/9686763

Research Article

Dynamic Student Data Management Using Resource Optimization Technology in Higher Education Platforms

Chenghao Lu[1,2] and Omer Saeed[3]

[1]*School of Public Policy&Management, China University of Mining and Technology, Xuzhou, China*
[2]*Office of Academic Affairs, Jinling Institute of Technology, Nanjing, China*
[3]*Institute of Management, Kyrgyz International Universal College, Bishkek, Kyrgyzstan*

Correspondence should be addressed to Omer Saeed; omersaeed@mail.cu.edu.kg

Received 3 September 2022; Revised 22 September 2022; Accepted 3 October 2022; Published 12 April 2023

Academic Editor: Chi Lin

This study combines intelligent resource optimization technology to build a dynamic student data management model and suggests a fuzzy hierarchical network representation model based on isomorphism and homogeneity in order to increase the effectiveness of dynamic student data management in colleges and universities. The important semantics of nodes in the network are also captured in this study using fuzzy k-kernel decomposition as a technique for multigranularity partitioning. Based on the SIR model, FHNE compares the production of the sequence to the process of information transmission in the random walk stage, which increases the node sequence's accuracy. According to the research, the dynamic student data management system that is used in the higher education platform that is suggested in this study can significantly increase the effectiveness of managing student data.

1. Introduction

The student model ITS (intelligent teaching system) changes dynamically according to the interaction between students and the system and the learning situation, which provides the basis for the determination of teaching strategies and teaching resources required by the system for further teaching. The student model is currently the most difficult part of ITS design and a hot issue in ITS research [1]. Guided by relevant teaching theories and learning theories, starting from the individual learning situation and learning needs of learners, based on research and analysis of factors affecting learning, a student model of an intelligent teaching system is designed [2]. There are many factors in the design of the student model. For instance, it must be able to accurately describe students' learning situations, work with the system's representation of course information, help the system design new teaching tactics, and help with implementation [3].

The coverage model expresses the domain knowledge that students want to learn and their constraints as a directed knowledge structure graph, the student's learning state is regarded as a subgraph of this graph, and the learning process is regarded as the approximation process of the subgraph to the original graph. The system based on this model can obtain the knowledge structure defects of students according to the comparison between the domain knowledge structure diagram and the students' knowledge state diagram, to recommend the content to be learned to the students [4].

Deviation model: This model records the deviation of the student's problem-solving path from the expert's path. These deviations describe a certain deficiency of the student at this knowledge point and can give specific remedial measures according to the type of deviation [5].

The cognitive model reflects the differences in cognitive ability and cognitive structure of each learner. We can comprehend pupils' initial learning capacity and knowledge structure by examining their cognitive peculiarities. The purpose of analyzing students' cognitive ability and cognitive structure is to formulate effective teaching strategies for

specific teaching tasks [6]. Mental model: It refers to a collection of interrelated speech or representation propositions, which is the deep knowledge base for people to make inferences and predictions. Mental models describe and record the psychological changes of students as they learn, as well as their effects on the learning process [7].

Different student models represent different theoretical foundations of learning. In the educational field, behaviorist learning theory has always occupied an important position. In the intelligent teaching system established on the basis of the teaching practice of this teaching theory, the corresponding student model is the covering student model. In this model, to understand the student's learning foundation or the student's learning mastery level, students can be tested, and the test results can be analyzed. Generally speaking, a course consists of multiple units, each unit has multiple subsections, and each subsection contains multiple knowledge points [8]. To test the students' mastery of a course, it can be obtained by weighting the mastery of each knowledge point. The feature of the coverage model is that it only considers the students' right and wrong answers. The correct rate of answering questions is lower than a certain percentage when learning a certain knowledge point. Because there is no analysis of the mistakes made by the students, it is impossible to give targeted learning guidance, and the consequences of students' simple repetition of learning are often repeated mistakes. The consequence of this continuous cycle is often that students lose interest in learning and lose confidence in themselves [9]. It can be seen that the coverage model is only suitable for describing the learning situation of declarative knowledge and simple procedural knowledge, and it is not convenient to describe the learning situation of complex procedural knowledge. An introduction to the bias model addresses the aforementioned issues. In order to identify various error kinds and associated faults, it analyzes, summarizes, and contrasts the errors made by students with the appropriate problem-solving techniques. In this way, students only need to relearn the corresponding weak links, and the learning will be more targeted, and the learning effect will naturally be better [10]. In order to establish a deviation model, it is necessary to diagnose the students' learning process, and domain experts set a number of possible errors for each knowledge point. Every time a student gets a question wrong, it must correspond to one or more of the wrong sets. The cognitive model is an indispensable part of the student model [11].

In order to determine a student's cognitive ability, the question of how cognitive ability is represented must first be addressed. In practical applications, a relatively simple and practical cognitive model for students is established. It is believed that educational goals should include the content of three domains, namely, cognitive ability domain, motor skill domain, and affective domain [12]. Cognitive ability determines the choice of learning content. Those with higher cognitive ability can arrange learning content with greater knowledge difficulty. Psychological factors have an important impact on learning. Personality has an effect on learning effect, according to research on the connection between learner personality and learning effect: (1) Students with tenacious-stable personalities lack empathy and place a greater emphasis on facts than on feelings during learning. The subjects frequently receive high marks. Conversely, learners with sensitive personalities tend to do well in arts subjects. (2) The introverted and extroverted personality characteristics of learners are also related to the learning effect: learners with extraverted personality characteristics tend to ignore academic research and prefer stimulating social activities, so they need stronger stimulation when learning. It is suitable for processing information provided quickly; while, learners with introverted characteristics are more suitable for learning with slower information processing and reflective learning [13]. Studies have shown that learners with a field-dependent learning style are suitable for structured learning methods based on facts, well-structured teaching materials, and clear teaching goals. If they are not, they should carry out an individualized learning method based on learner control and encourage them to maximize their learning such as inquiry, discovery, and discussion [14].

"Mastery degree" indicates the degree of mastery of the knowledge point. The system can set a threshold. If the test score is higher than the threshold, the system will no longer arrange learning; if the test score is higher than the threshold, the system will no longer arrange learning. It will be arranged to continue learning; if it is near the threshold, students will be prompted whether they need to continue to strengthen, and the students will choose [15]. The "error number" indicates the type of error that the student made in the knowledge point test. The system can obtain the corresponding error description information and learning prompt information from the error type table and provide it to the student for targeted learning. The learning strategy library records the learning strategies of each knowledge point in the next round of learning obtained after the decision. The following cycle of learning could involve reviewing some of the material from the most recent unit, or it could involve learning something entirely new. The techniques include selecting the subject matter to be taught, how to deliver information, how to teach, and how to create exam questions [16]. The error type table is a collection of all possible errors in the student's study of the subject. This collection is drawn up by experts in advance. New types can be added according to the actual learning process (this will increase the complexity of the system), or they can remain unchanged. Based on this table, the system calculates the student's learning deviation and gives relevant prompt information. The learning assessment table records the learning results of each knowledge point in the unit after each test, which is the basis for adjusting students' knowledge table and error type table, calculating cognitive ability, and then forming teaching strategies. The psychological status table describes the psychological factors of students during learning, and its initial value can be entered by students when they register to indicate their preferences. During the learning process, the system tracks students' learning behaviors and automatically draws judgments [17].

This study combines intelligent resource optimization technology to construct a dynamic student data management model to improve the management effectiveness of the student data management data model.

2. Fuzzy Hierarchical Network Representation Based on Isomorphism and Homogeneity

Fuzzy k-kernel decomposition is proposed to learn more robust node representations and encode more semantics. To overcome the limitations of the original k-kernel decomposition, FHNE proposes fuzzy decomposition to replace the original strict decomposition and establishes a fuzzy k-kernel decomposition model. In the fuzzy k-kernel decomposition method, the membership function of nodes assigns membership values according to the similarity between node degrees and k values. Therefore, nodes that are very close to the k-kernel will be activated during the fuzzy k-kernel decomposition. The core of this membership function is that the membership value should be positively correlated with the semantics of node importance.

Its model framework is shown in Figure 1.

Based on the k-core decomposition theory, the network can be divided into subnetworks with different degrees of aggregation according to the importance of nodes. The larger the value of k, the stronger the aggregation of nodes. Although k-core decomposition can distinguish the importance of nodes well, it still suffers from the drawback that its "recursive pruning" process is too strict. As shown in Figure 2, if we want to obtain the 2-core subnetwork $H = (C, EIC)$, the condition $\forall v \in C$: $degree_{H(v)} \geq 2$ must be satisfied. Figure 3(a) shows the first pruning from 1-core to 2-core, and Figure 3(b) shows the final 2-core subnet. In the small network shown in Figure 2, the degree of node v is 4, which is relatively important. However, node v will be removed in the process of generating the 2-core network because it does not meet the strict definition of a 2-core network. To better capture the importance of nodes, the strict conditions of the k-kernel decomposition need to be changed by adopting a fuzzy map.

Fuzzy sets are used as a reliable means to quantitatively express inherent ambiguity and uncertainty information and break the boundaries of sets described by characteristic functions. Any element can belong to multiple fuzzy subsets at the same time, and its degree can be represented by a membership value in the interval [0, 1], which is closer to human perception. To solve the problem caused by exact k-kernel decomposition, fuzzy k-core decomposition is proposed.

The key problem of fuzzy systems is the use of membership functions. Generally speaking, fuzzy membership functions are divided into linear and nonlinear. In the FHNE model, the feature of fuzzy k-core decomposition is only node degree. The model hopes that as the value of k increases, the membership degree calculated by the node degree can cover more semantics. It can be seen that the typical characteristics of nonlinear membership functions do not match this, which may lead to a sharp rise or fall in membership. Therefore, the trapezoidal membership

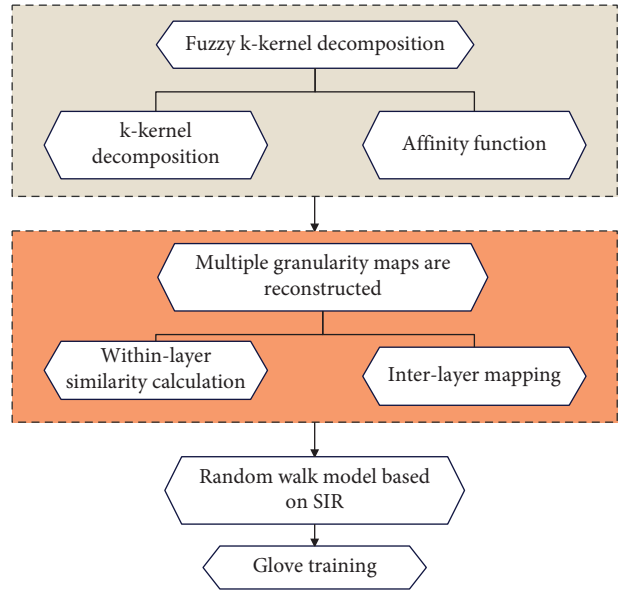

Figure 1: FHNE frame diagram.

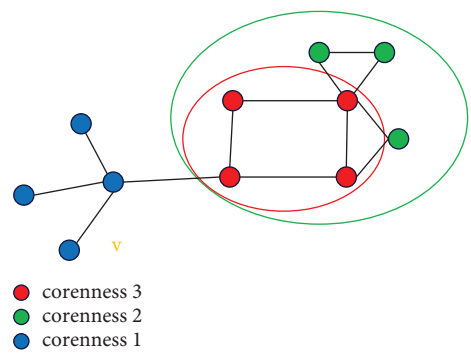

Figure 2: Example of k-core.

function as shown in Figure 4 is adopted, and its corresponding expression is shown in the following formula:

$$\forall v \in G, A(v)_k = \begin{cases} 0, & d(v) < k, d(v) < k, \\ \dfrac{d(v) - k}{b - k}, & k \leq d(v) \leq b, \\ 1, & b < d(v). \end{cases} \quad (1)$$

Among them, $d(v)$ represents the degree of node v, and $A(v)_k$ represents the membership degree of node v belonging to k-core. As shown in Figure 4, node v belongs to k-core if $A(v)_k > \lambda$, where λ is the cutoff set of membership functions.

Definition 1. (Fuzzy k-core decomposition): In the k-core decomposition process, if the membership degree of a node is greater than or equal to the cut set a, the node belongs to k-core, otherwise, it does not belong. If and only if $\forall v \in C$: $A(v)_k > \lambda$ and FH is the largest subgraph with this property, $FH_k = (C, E|C)$ denotes a fuzzy k-core network.

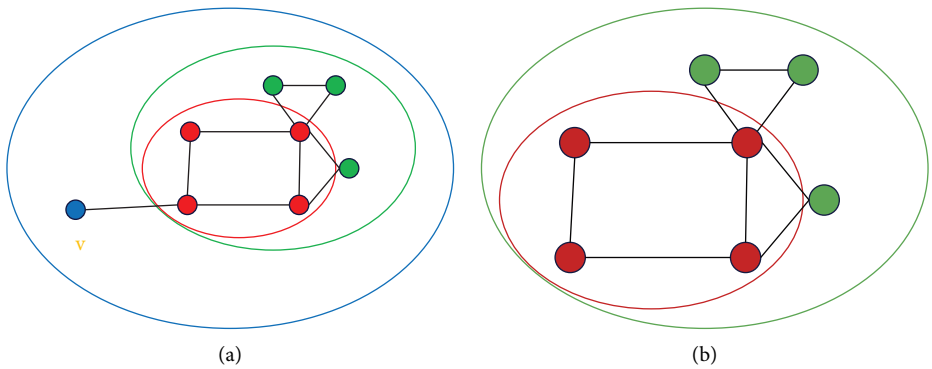

Figure 3: k-core decomposition process. (a) The first pruning. (b) 2 kernels network.

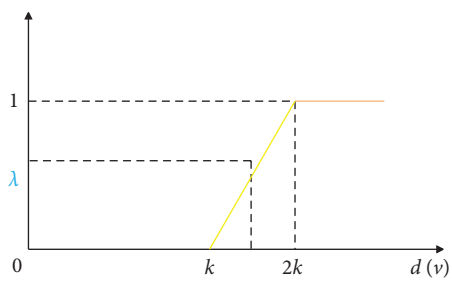

Figure 4: Trapezoidal membership function.

In this section, the original network is divided into multigranularity networks by fuzzy k-core decomposition, and the maximum k value of the network is denoted as max_k. If the step size of fuzzy k-core decomposition is set to 1, it will bring two problems. First, the constructed multigranularity subgraphs will be very large and computationally expensive. Second, the importance of nodes on different granulation layers is not very different, which will lead to an unsatisfactory granulation effect. Therefore, this study defines the step size to control the number of layers l through the fuzzy k-core decomposition algorithm, and the relationship is defined as follows:

$$\eta = \left\lfloor \frac{\max\_k}{l} \right\rfloor. \tag{2}$$

Among them, l represents the number of layers.

Granular computing is a way of thinking from different levels, different perspectives, and different granularities. The original network is divided into multiple subnetworks based on fuzzy k-core decomposition, and each subnetwork with different k-cores represents a granular layer. The larger the value of k, the smaller the subnet size and the stronger the aggregation of nodes in the subnet. To better capture the homogeneity and isomorphism of the network at the same time, this section reconstructs the subnetwork of each granular layer by introducing the structural similarity of nodes. First, the structural similarity between nodes u and j is defined:

$$Sim_k(i, j) = \frac{\min\left(degree(i), deg(j)\right)}{\max\left(degree(i), deg(j)\right)}, i, j \in FH_k. \tag{3}$$

Among them, k represents the kth granular layer, and Sim_k represents the structural similarity matrix of nodes. As shown in formula (3), if the degrees of nodes i and j are equal, then $Sim_k(i, j) = 1$. It is worth noting that in the process of building a multigranularity network, the neighborhood information of nodes also needs to be considered. Among them, the adjacency matrix is used to capture the relationship between nodes in each layer to fuse the link information of the network. Therefore, the adjacency matrix of the kth layer can be defined as follows:

$$Adj_k(i, j) = \begin{cases} 1, (i, j) \in E, \\ 0, (i, j) \notin E. \end{cases} \tag{4}$$

Combining the above two aspects, two nodes in the same layer are adjacent and have similar importance; then, they will be more likely to get closer representation. The final weight matrix is determined by the adjacency matrix Ad and the structural similarity matrix Sim, and the weight of the kth layer is defined as follows:

$$W_k(i, j) = \delta * Sim_k(i, j) + (1 - \delta) * Adj_k(i, j). \tag{5}$$

Among them, δ is the hyperparameter governing the matrices Sim and Adj, and the matrix W can capture the homogeneity and isomorphism of the original network. After reconstructing the multigranularity graph, there is currently no connection between the granular layers, and the core of the mutual mapping between the granular layers is to find similar nodes. Obviously, similar nodes exist not only in the same layer but also in other layers. The larger the value of k, the closer the nodes in the granular layer and the stronger the similarity of nodes. In this section, the weight matrix W is used to calculate the transition probability between granular layers, and it tends to make nodes jump to the granular layer with a larger k value. The interlayer mapping function is expressed as follows:

$$Map_i(k, k+1) = \sum_j \frac{W_k(i, j)}{\left(|V_k| - 1\right)}, \tag{6}$$

$$Map_i(k, k+1) = 1 - Map_i(k, k+1). \tag{7}$$

Map $(k, k+1)$ represents the mapping function from the kth layer to the $(k+1)$ th layer, and Map $(k, k-1)$ is the

mapping function from the kth layer to the $(k-1)$ layer, where $|V_k|$ represents the number of nodes in the kth layer. The model establishes a mapping relationship for most of the adjacent granular layers, but the first layer only has the mapping to the second layer, and the last layer only has the mapping to the previous layer. All in all, the interlayer mapping function addresses the connectivity problem of multigranularity graphs.

The first infected user of the SIR infectious disease model corresponds to the seed node of the random walk, and the infection process corresponds to the random walk process. When a node transitions to the removed state, it means that the random walk terminates. Different from the traditional SIR model, the infection probability in this model is no longer a fixed 0, but the similarity between nodes. Similarly, the immune probability is no longer a fixed β, and the immune conditions of nodes are shown in the following formula:

$$W(i,j) < \sum_{v \in V_k} \frac{W_k(i,v)}{\left(|V_k| - 1\right)}. \tag{8}$$

In general, the selection of subsequent nodes is only related to the current node. However, the actual situation is that other tail nodes that are already in the walk sequence will also affect the subsequent walk. The model introduces a multinode influence mechanism to allow nodes to consider more information in the process of walking, which is defined as follows:

$$SIMI(i,j) < \prod_{n \in ns[-ls:]} W(i,n). \tag{9}$$

Among them, ns represents the existing node sequence, and ls represents the last few nodes in the sequence ns. Taking into account the time complexity of random walk and the obtained sequence effect, the value of ls is set to half of the glove training window.

This study models the training process of the node sequence. First, some symbols are explained. The matrix of node co-occurrence counts is denoted by X, and X_i represents the number of occurrences of node j in the context sequence of node i, $X_i = \sum_k X_{ik}$ represents the number of occurrences of any node in the context of node i, and $P_{ij} = (Pj/i) = X_{ij}/X_i$ represents the probability of node j appearing in the context of node i.

The same is true for the training of nodes in the network, and nodes can be compared to words. For nodes i and j, this section examines the relationship between nodes by introducing probe node k. The general model can be represented as follows:

$$F(\Phi(i), \Phi(j), \Phi(k)) = \frac{P_{ik}}{P_{jk}}. \tag{10}$$

Among them, $\Phi \in R^d$ is the vector of the node itself, and $\overline{\Phi} \in R^d$ is the vector that is the context of other nodes. The possibilities of the function F are various, but by performing some operations, it can be induced to convert it into an understandable formula. First, F encodes information at a ratio P_{ik}/P_{jk} in the node vector space. Since vector spaces are inherently linear in structure, the most natural approach is to use vector difference. With this goal in the hand, the model can construct F as a function that embodies the node differences, so that formula (10) can be modified as follows:

$$F(\Phi(i) - \Phi(j), \overline{\Phi}(k)) = \frac{P_{ik}}{P_{jk}}. \tag{11}$$

In formula (11), the parameter of F on the left is a vector and the parameter on the right is a scalar. While F can be thought of as a complex function parameterization, such as a neural network, doing so confuses the linear structure one is trying to model. To avoid this problem, the left side of the formula can be dot-product first:

$$F\left((\Phi(i) - \Phi(j))^T \overline{\Phi}(k)\right) = \frac{P_{ik}}{P_{jk}}. \tag{12}$$

This is to prevent F from changing the vector dimension in an incorrect way. It is worth noting that for the node co-occurrence matrix, the roles between the node itself and the context node are interchangeable. To do this, the function needs to satisfy the symmetry, and formula (12) does not satisfy the symmetry, but it can be satisfied by the multistep transformation, and the specific operation is as follows:

$$F\left((\Phi(i) - \Phi(j))^T \overline{\Phi}(k)\right) = \frac{P_{ik}}{P_{jk}} = \frac{F\left(\Phi(i)^T \widetilde{\Phi}(k)\right)}{F\left(\Phi(i)^T \widetilde{\Phi}(k)\right)}, \tag{13}$$

$$F\left(\Phi(i)^T \widetilde{\Phi}(k)\right) = P_{ik} = \frac{X_{ik}}{X_i}. \tag{14}$$

The left side of the formula represents subtraction and the right side represents division. We can execute exponential operations on the left and right sides to transform them into equivalent expressions, that is, $F = \exp$.

$$\Phi(i)^T \widetilde{\Phi}(k) = \log\left(P_{ik}\right) = \log\left(X_{ik}\right) - \log\left(X_i\right). \tag{15}$$

Without the term b on the right-hand side, (15) satisfies exchange symmetry. Although this term is independent of k, it can be absorbed into the bias term b_i of $\Phi(i)$. Then, $\widetilde{\Phi}(k)$ adds an extra bias term $\overline{b}_k$, and the formula restores symmetry.

$$\Phi(i)^T \widetilde{\Phi}(k) + b_i + \overline{b}_k = \log\left(X_{ik}\right). \tag{16}$$

Formula (16) is a simple visualization of formula (10). Since the logarithmic function is meaningless when its argument is zero, one way to solve this problem is to add a term to the logarithm, such as $\log(X_{ik}) \longrightarrow \log(X_{ik} + 1)$, which guarantees the sparsity of X and avoids the divergence problem of the logarithm. Next, formula (16) is converted into a least squares problem, and the model can learn the node sequence. At the same time, the weight function $f(X_{ij})$ is introduced into the loss function, and the model is defined as follows:

$$\Phi(i)^T \widetilde{\Phi}(k) + b_i + \overline{b}_k = \log\left(X_{ik}\right). \tag{17}$$

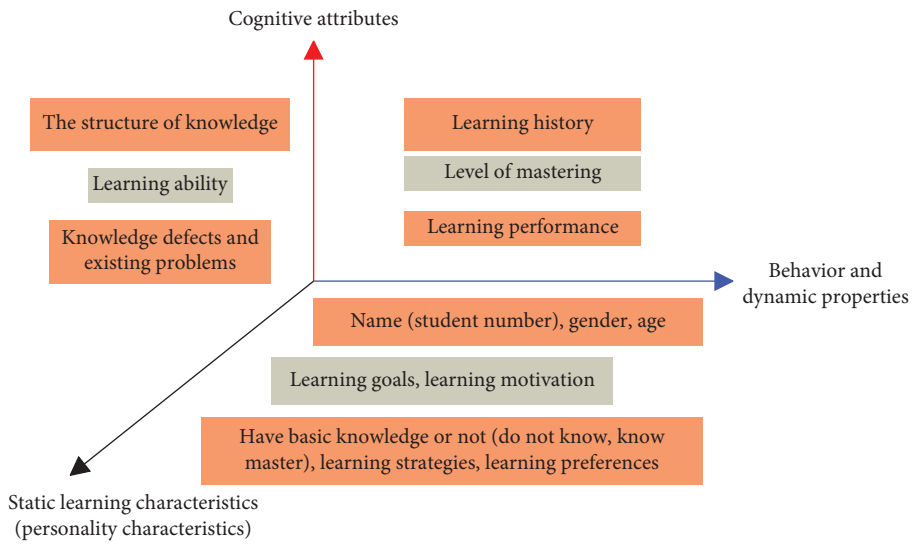

Figure 5: 3D model of learner feature attributes.

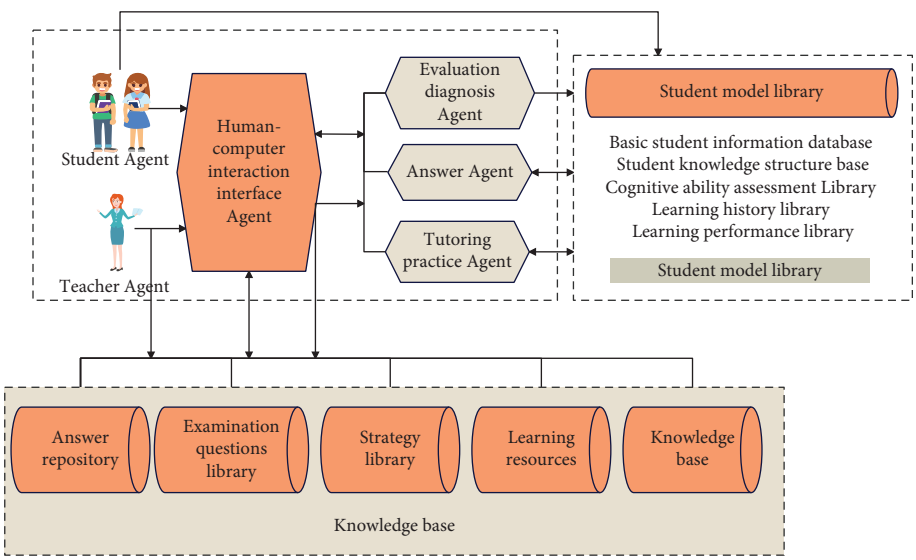

Figure 6: Student model library.

Among them, IV is the set of network nodes. If the same weight is used for each co-occurring node, the important difference between nodes cannot be reflected. Therefore, this section introduces the weight function $f(X_{ij})$, which needs to meet the following properties:

(1) $f(0) = 0$. When the number of co-occurrences of words is 0, the corresponding weight should be 0.

(2) F must be a nondecreasing function, so as to ensure that the weight will not decrease as the number of node co-occurrences increases

(3) For large values of x, the upward trend of f(x) should be relatively small, so that the weight of frequently occurring co-occurring nodes is not too large

Combining the above three points, the definition of the weight function f(x) is as follows:

$$f(x) = \begin{cases} \left(\dfrac{x}{x_{\max}}\right)^{\alpha}, & if\, x < x_{\max}, \\ 1, & otherwise. \end{cases} \tag{18}$$

The performance of the model depends to a small extent on the cutoff value. This model fixes it as $x_{\max} = 100$ for all experiments. According to expert experience and many experiments, the model effect is improved to a certain extent when $\alpha = 3/4$.

3. Dynamic Student Data Management

The model is constructed according to the basic information of the learner, and it is simplified into a three-dimensional student model as shown in Figure 5.

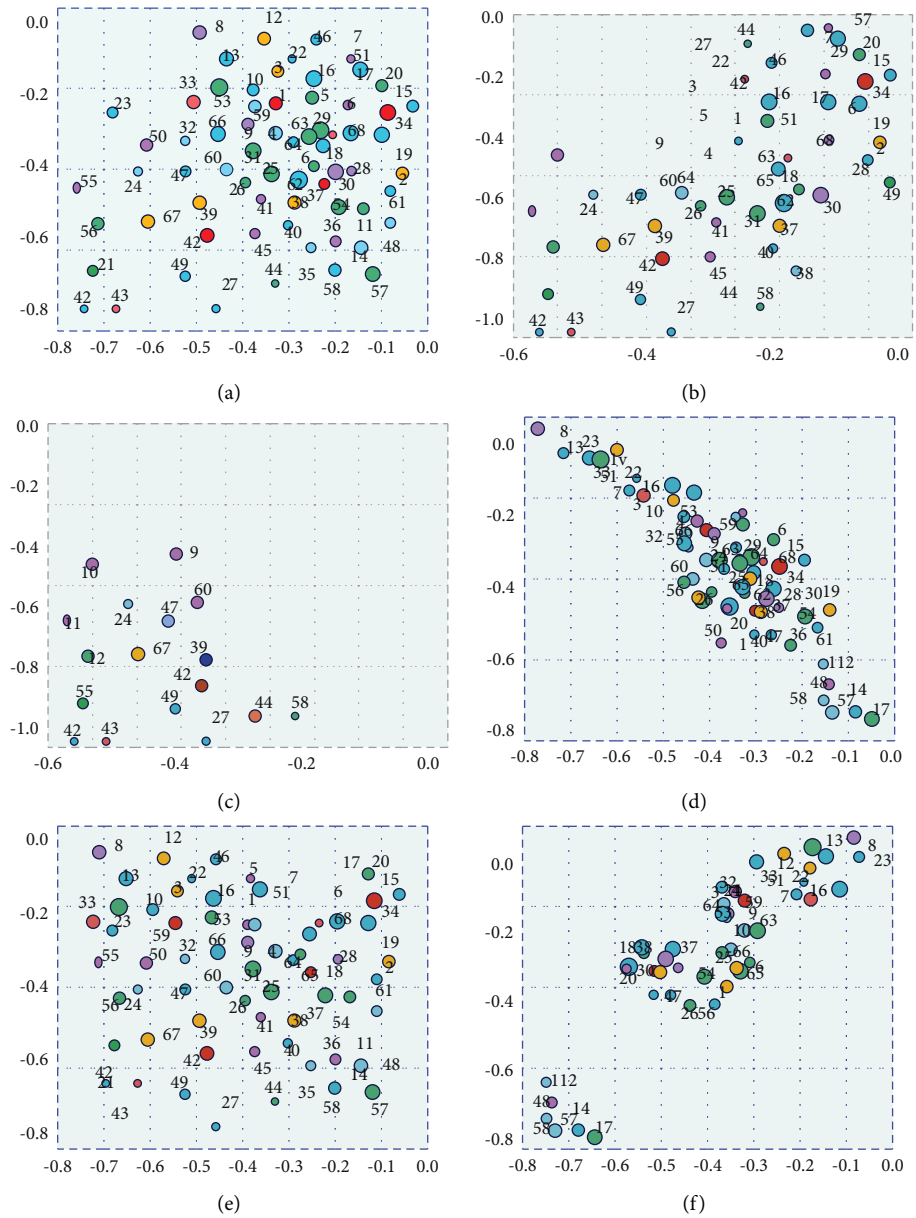

Figure 7: The spatial visualization of the network vector of the students' teaching process. (a) Deep walk. (b) Node2vec. (c) SDNE. (d) Struc2vec. (e) HARP(LINE). (f) FHNE.

The process and working principle of the system are shown in Figure 6.

Multilabel classification refers to assigning one or more labels to each sample in a dataset. This section will validate the ability of the FHNE model on the multilabel classification task on the BlogCatalog and PPI datasets. In the previous chapter, we have defined four prediction cases (TP, FP, FN, TN) for binary classification. According to these four cases, this section can calculate the classification precision and recall, where the calculation formula of the accuracy is as follows:

$$Precision = \frac{TP}{TP + FP}. \tag{19}$$

The formula for calculating recall is as follows:

$$Recall = \frac{TP}{TP + FN}. \tag{20}$$

When using precision or recall to evaluate the classification results, if the value of precision or recall is high, it is the most ideal situation. Many times, the values of precision and recall are often not positively correlated. As an extreme example, it is assumed that the number of positive and negative samples in a dataset is 50, the prediction result shows that there is only one positive sample, and the prediction is correct. In this case, the precision result is 100%, but the recall rate is very low, only 1/50. The $F1$ value combines the above two indicators and is a fairer evaluation indicator. The calculation method is as follows:

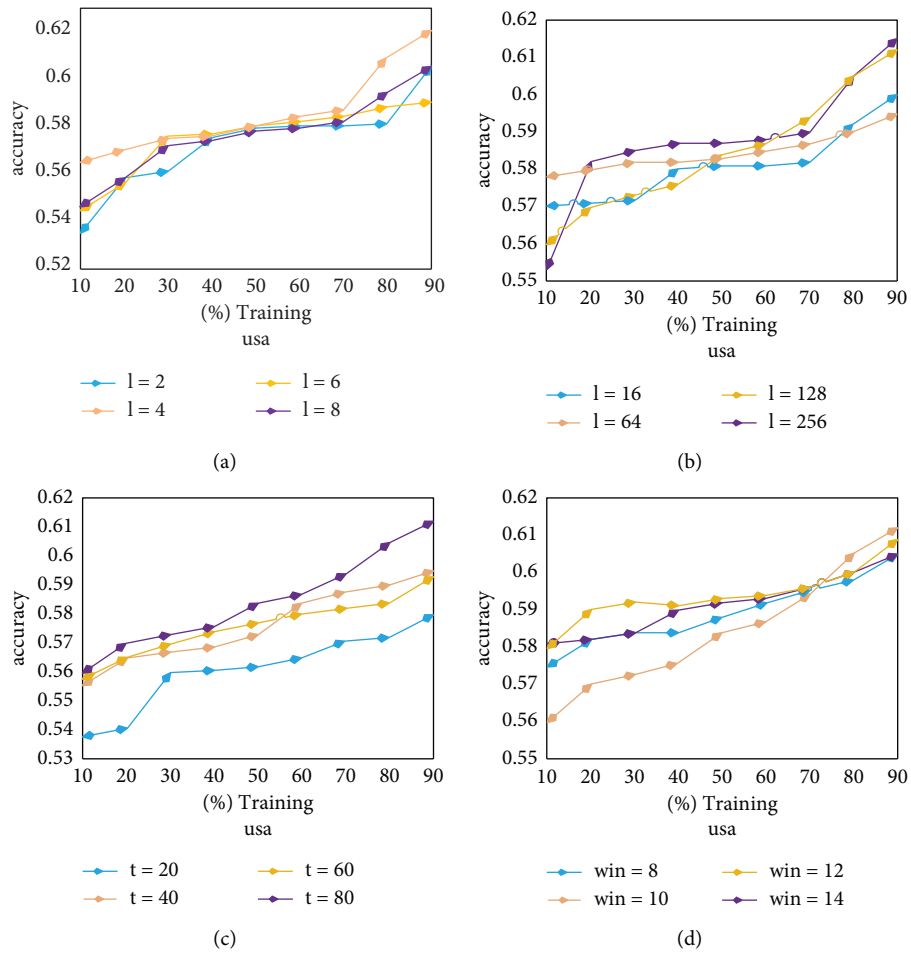

Figure 8: Parameter sensitivity analysis.

$$F1 = \frac{2 * precision * recall}{precision + recall}. \tag{21}$$

This section takes the teaching process of students as an example to verify the ability of the FHNE model in teaching visualization. Since this dataset is relatively small, we directly use the baseline method and FHNE to learn the 2D vector representation of nodes. The visualization results are shown in Figure 7.

As shown in Figures 7(a), 7(b), and 7(e), DeepWalk, node2vec, and HARP(LINE) fail to capture the homogeneity of the network. As shown in Figure 7(c), SDNE can capture the structure of nodes to a certain extent. Most of the light blue nodes are almost coincident (lower left corner), but other types of nodes are scattered. Struc2vec and FHNE capture structural equivalence very well. For the struc2vec algorithm, in Figure 7(d), nodes of the same type have a certain degree of aggregation, but the degree of discrimination of nodes of different types is not large. Overall, FHNE performs better than struc2vec. From Figure 7(f), it can be seen that most of the nodes of the same type are clearly clustered into one class, and the underlying representations between different types of nodes have obvious differences.

The parameter sensitivity analysis of the FHNE model is performed in this work. The FHNE method includes various parameters, and this part confirms, as depicted in Figure 8, how different settings affect the classification performance of student dynamic data. Except for the parameter to be tested, all other parameters have default values.

The classification works best when $l = 4$, because the nodes in the dataset are labeled with four types of labels (corresponding to the number of layers $l = 4$) according to the activity level.

On the basis of the above research, the effect of dynamic student data management is verified, and the effect of resource optimization and student data management is studied, as shown in Tables 1 and 2, respectively.

Table 1: Resource optimization effect.

Number	Resource management	Number	Resource management
1	83.850	13	79.425
2	80.354	14	79.579
3	85.072	15	80.570
4	81.162	16	82.230
5	84.654	17	84.032
6	81.645	18	81.272
7	83.604	19	83.049
8	79.438	20	80.567
9	79.128	21	80.278
10	79.799	22	83.917
11	84.077	23	83.357
12	79.381	24	84.758

Table 2: The effect of student data management.

Number	Student management	Number	Student management
1	86.016	13	92.513
2	92.368	14	84.467
3	89.911	15	87.851
4	87.289	16	92.173
5	89.708	17	91.524
6	84.609	18	90.388
7	91.801	19	89.754
8	85.291	20	92.117
9	85.857	21	84.061
10	89.846	22	88.389
11	91.591	23	84.809
12	89.468	24	87.343

From the above research, we can see that the dynamic student data management using resource optimization technology in the higher education platform proposed in this study can effectively improve the efficiency of college student data management.

4. Conclusion

The student model is one of the core components to realize intelligence, and ITS can implement personalized teaching for learners according to the student model. The student model is a data structure representing the cognitive characteristics of the learner. On the one hand, it captures fundamental data like the student's name, gender, and student ID. On the other hand, it correctly reflects the learner's degree of knowledge, capacity for learning, state of mind, and other factors. The student knowledge base describes and records the student's learning progress and level, as well as the student's error type at each knowledge point. This study combines the intelligent resource optimization technology to construct a dynamic student data management model to improve the management effectiveness of the student data management data model. The research shows that dynamic student data management using resource optimization technology in the higher education platform proposed in this study can effectively improve the efficiency of college student data management.

Data Availability

The experimental data used to support the findings of this study are available from the corresponding author upon request.

Conflicts of Interest

The authors declare that there are no conflicts of interest.

References

[1] J. Holloway, "Teacher evaluation as an onto-epistemic framework," *British Journal of Sociology of Education*, vol. 40, no. 2, pp. 174–189, 2019.

[2] M. Han, N. Zhou, and Z. Qiao, "Analysis of Extension strategies for improving Adaptive teaching ability of college Teachers," *International Journal of Emerging Technologies in Learning (iJET)*, vol. 15, no. 15, pp. 147–161, 2020.

[3] M. D. C. Salazar, "Interrogating teacher evaluation: Unveiling whiteness as the normative center and moving the margins," *Journal of Teacher Education*, vol. 69, no. 5, pp. 463–476, 2018.

[4] M. L. Derrington and J. W. Campbell, "High-stakes teacher evaluation policy: US principals' perspectives and variations in practice," *Teachers and Teaching*, vol. 24, no. 3, pp. 246–262, 2018.

[5] S. J. Zepeda and A. M. Jimenez, "Teacher Observation and Reliability: Additional Insights Gathered from inter-rater Reliability Analyses," *Journal of Educational Supervision*, vol. 2, no. 2, pp. 11–26, 2019.

[6] E. Brunner, J. M. Cowen, K. O. Strunk, and S. Drake, "Teacher labor market responses to statewide reform: evidence from Michigan," *Educational Evaluation and Policy Analysis*, vol. 41, no. 4, pp. 403–425, 2019.

[7] M. L. Donaldson and S. Woulfin, "From tinkering to going "rogue": how principals use agency when enacting new teacher evaluation systems," *Educational Evaluation and Policy Analysis*, vol. 40, no. 4, pp. 531–556, 2018.

[8] R. Vagi, M. Pivovarova, and W. Miedel Barnard, "Keeping our best? A survival analysis examining a measure of preservice teacher quality and teacher attrition," *Journal of Teacher Education*, vol. 70, no. 2, pp. 115–127, 2019.

[9] K. C. Bastian, D. Lys, and Y. Pan, "A framework for improvement: analyzing performance-assessment scores for evidence-based teacher preparation program reforms," *Journal of Teacher Education*, vol. 69, no. 5, pp. 448–462, 2018.

[10] G. Skedsmo and S. G. Huber, "Top-down and bottom-up approaches to improve educational quality: their intended and unintended consequences," *Educational Assessment, Evaluation and Accountability*, vol. 31, no. 1, pp. 1–4, 2019.

[11] J. A. Grissom, R. S. L. Blissett, and H. Mitani, "Evaluating school principals: Supervisor ratings of principal practice and principal job performance," *Educational Evaluation and Policy Analysis*, vol. 40, no. 3, pp. 446–472, 2018.

[12] K. Kim and Y. Park, "A development and application of the teaching and learning model of artificial intelligence education for elementary students," *Journal of The Korean Association of Information Education*, vol. 21, no. 1, pp. 137–147, 2017.

[13] O. Zawacki-Richter, V. I. Marín, M. Bond, and F. Gouverneur, "Systematic review of research on artificial intelligence applications in higher education–where are the educators?" *International Journal of Educational Technology in Higher Education*, vol. 16, no. 1, pp. 39–27, 2019.

[14] S. C. H. Yang, W. K. Vong, R. B. Sojitra, T. Folke, and P. Shafto, "Mitigating belief projection in explainable artificial intelligence via Bayesian teaching," *Scientific Reports*, vol. 11, no. 1, pp. 9863–9917, 2021.

[15] Y. Lee, "An analysis of the influence of block-type programming language-based artificial intelligence education on the learner's attitude in artificial intelligence," *Journal of The Korean Association of Information Education*, vol. 23, no. 2, pp. 189–196, 2019.

[16] J. M. Alonso, "Teaching explainable artificial intelligence to high school students," *International Journal of Computational Intelligence Systems*, vol. 13, no. 1, pp. 974–987, 2020.

[17] R. Yang, "Artificial intelligence-based strategies for improving the teaching effect of art Major courses in colleges," *International Journal of Emerging Technologies in Learning (iJET)*, vol. 15, no. 22, pp. 146–160, 2020.

Hindawi
Mobile Information Systems
Volume 2023, Article ID 8215434, 10 pages
https://doi.org/10.1155/2023/8215434

Research Article

Higher Education Multimedia Teaching System Based on the Artificial Intelligence Model and Its Improvement

Xiaoyu Yang [1,2]

[1]*School of Culture and Media, Zhanjiang University of Science and Technology, Zhanjiang, Guangdong 524000, China*
[2]*Graduate School, Srinakharinwirot University, Bangkok 10110, Thailand*

Correspondence should be addressed to Xiaoyu Yang; yangxy202107@163.com

Received 18 August 2022; Revised 22 September 2022; Accepted 8 October 2022; Published 10 April 2023

Academic Editor: Chi Lin

In order to improve the quality of multimedia teaching in higher education, this article analyzes the problems existing in multimedia education in higher education, improves the multimedia teaching system, and proposes a three-dimensional multimedia image surface extraction method based on crease. Moreover, this article uses the level set method to segment the Gaussian smoothed multimedia data to obtain the preliminarily divided target fault area and then extracts the fault surface as the feature of the target area. The analysis demonstrates that the multimedia teaching system of higher education based on the artificial intelligence model can effectively enhance the multimedia teaching mode and promote its further development.

1. Introduction

Online learning has the characteristics of open field, high complexity, and redundant information. The unreasonable use of media and resources may cause confusion and cognitive overload of learners and affect their academic performance. Cognitive load is the cognitive resources consumed by learners in the process of information processing and processing [1]. In addition, as the most important cognitive element in multimedia learning, cognitive load has a significant effect on the effectiveness of multimedia learning. How to accurately measure cognitive load is a pressing research issue that must be resolved as soon as possible.

Humans inevitably consume cognitive resources in the process of learning and problem solving, and the information elements that individuals can process in unit time are limited. Cognitive overload occurs when the number of cognitive resources required to process information exceeds the capacity of personal working memory resources [2]. Learning in a multimedia environment involves the use of different types of technical media. At the same time, different teaching media, resource presentation methods, and application of various clues make it difficult to effectively control the cognitive load of learners. Therefore, the problem of cognitive load in the multimedia learning environment is more worthy of study [3]. Mayer explored the cognitive process of learners in the field of multimedia learning and summed up the famous multimedia learning theory to balance the cognitive load level of learners. In addition to this, the basis of multimedia learning theory is the dual-coding theoretical assumption and the dual-channel theoretical assumption. Combining these two assumptions with generative learning methods, generative theories of multimedia learning assert that learners actively select relevant visual and linguistic information from learning materials. In addition, it stores visual and linguistic working memory separately by establishing a link between them. Furthermore, by allocating cognitive resources and working memory capacity to establish reference links and integrating mental representations and prior knowledge, the cognitive load effect will occur when the amount of information received by the learner exceeds the working memory capacity [4]. At present, the cognitive load measurement methods used in the field of multimedia learning include subjective measurement, behavior analysis, dual-task analysis, performance analysis, eye tracking, and physiological measurement. The application of various methods provides the possibility for

the objectivity and accuracy of cognitive load measurement. This article uses the method of literature analysis to sort out the cognitive load measurement methods and related indicators used in the field of multimedia learning and analyze the advantages and disadvantages of various methods to provide reference for subsequent research [5].

The media network has the following characteristics: resource distribution, whether it is a physical resource or a logical resource, its functions show strong distribution, and users can share resources; real-time transmission, the signal is generally continuous, which requires that the transmission must have strong real-time performance, and if there is a delay, the quality of playback will be reduced; interactivity, in the multimedia system, users can process and modify information. From the above characteristics, the multimedia system is more complex, and the requirements for service quality are also higher [6]. Therefore, better service-aware control capability can help the system to detect problems more timely and reduce transmission delay. Based on this, related scholars have made the following research. Kim and Park [7] propose a comprehensive service quality monitoring system based on user perception. We analyze the security privacy affecting multimedia information data, construct the interaction model between security factors and network services, explore the location of important nodes, build a service quality perception platform, and effectively control service perception. Zawacki-Richter et al. [8] proposed a network service-aware control method based on stochastic learning. The network topology change is sensed through the heartbeat packet observation mechanism. At the same time, in order to reduce the observation error, a combination of Markov partial sensing and random learning adaptive sensing is used to achieve the purpose of sensing adjustment. However, the above two traditional methods cannot guarantee the service perception range, and due to the complexity and variability of multimedia networks, they cannot adapt to network changes, and the adaptive control performance is poor. In order to solve these problems, Yang et al. [9] proposed their study based on the QoS adaptive multimedia service awareness control method. QoS stands for quality of service, and this adaptive control technology can control various services under the condition that the network infrastructure remains unchanged. By understanding the requirements of multimedia services for QoS, combined with adaptive control theory [10], a QoS service-aware control model is constructed to improve service quality and make multimedia technology better serve users.

Multimedia technology is used in many different ways. Using multimedia in the classroom will have a positive teaching impact for university instructors. The university's new curriculum reform includes the addition of the general technology course as a new course. The purpose is to improve students' ability to creatively solve practical problems, stimulate students' interest in learning, and strengthen students' technical literacy through the application of technical ideas and methods [11]. The rapid development of society has made more and more teaching use multimedia technology, and the rational use of general technology at the university stage is also of great help to students, so as to expand students' knowledge in classroom teaching and learn from them. This increases the channels for students to acquire knowledge so that students can effectively understand the development of students while learning communication technology [12]. The university stage is a critical period for students to learn, and it is also an effective stage for students to cultivate in many aspects. Cultivating students' technical literacy is more conducive to students' understanding of multimedia, and in the process, they can also better understand the content of communication technology [13]. Therefore, in the process of teaching, teachers need to infiltrate communication technology into the classroom according to the specific content of classroom teaching, thereby effectively stimulating students' interest in learning. The development of communication technology is multifaceted. The most prominent one is that it is closely related to science and technology so that students and teachers can explore the mysteries of communication technology together. The application of multimedia technology in the classroom is also more conducive to students' memory of knowledge, so as to effectively improve the learning efficiency of students [14]. Communication technology is also a kind of technical learning, and it needs the correct guidance of teachers to cultivate students' technical literacy, thereby contributing to the all-round development of students. In order to improve students' technical literacy and general quality in the face of university communication technology, professors should actively encourage students to learn more about communication technology through multimedia. Students are essentially able to comprehend the educational importance of communication technology thanks to the professors' and students' cooperative cooperation [15]. Teachers skillfully use multimedia technology in the process of teaching to improve students' technical literacy, thereby effectively improving the effect of classroom teaching. The addition of multimedia technology at the university stage is more conducive to improving students' interest in learning. Compared with the traditional teaching mode, the rapid development of information technology is more conducive to students to improve their learning efficiency, and learning new content will become easier to understand, and teachers will become more effective in classroom teaching. Giving full play to the role of multimedia technology can effectively improve the quality of classroom teaching [16].

In order to comprehensively improve teachers' multimedia teaching technology and increase the design and integration of multimedia courseware, it should be divided and studied from two perspectives. Among them, it is necessary to strengthen the training of school teachers, increase the opportunities for teachers to learn and exchange experience, and strengthen teachers' ability to learn and master multimedia teaching technology through training, so as to effectively increase the design and integration of multimedia courseware and improve courseware. We design content and mode and use the learning and training of multimedia courseware teaching technology knowledge to improve their professional skills and promote the improvement of teachers' multimedia courseware design ability [17]. In order to enhance their ability to design

multimedia courses, teachers must not only develop their own multimedia knowledge and abilities but also increase professional training opportunities in the field, create supportive work environments for them, and support the seamless integration of multimedia course materials into college history teaching [18].

For the application of multimedia courseware in college history teaching, the evaluation mechanism of multimedia teaching should be comprehensively improved. For the application of multimedia courseware in history teaching under the current rapid development of network environment, the extension and development of teachers' multimedia teaching ability needs to be established. On the basis of improving the multimedia teaching evaluation mechanism, on the one hand, increasing the implementation of multimedia informatization has a very important role and significance for all fields and aspects of teachers' teaching [19]. On the other hand, in the application of multimedia courseware, it is necessary to use multimedia information technology to design and prepare history courseware according to the fundamental needs of history courses and to use multimedia technology in course narration [20].

This article analyzes the problems existing in multimedia education in higher education, improves the multimedia teaching system, and improves the effect of multimedia teaching in modern colleges and universities.

2. Intelligent Multimedia Image Processing Technology

2.1. The Process of Extracting Teaching Information of 3D Level Set Based on Crease. In this research, a crease-based information extraction method for three-dimensional level set instruction is proposed. Figure 1 depicts the primary process. Before the process is implemented, Gaussian smoothing is performed on the ant volume data. Firstly, the three-dimensional data volume is segmented by the level set method, and the target area and background area of multimedia teaching information in the data volume are preliminarily divided. Since the target area of the multimedia teaching information segmented by the level set is a volume structure with thickness, further processing is required to obtain a three-dimensional surface reflecting the spatial topology of the target area. The skeleton structure of the target body can completely retain the topological shape information of the target body under the condition of reducing the redundant components of the original target body as much as possible. Therefore, this article regards the teaching information as the skeleton feature of the segmented data body to extract.

2.2. Level Set Partitioning of 3D Data Volume. For images with uneven gray distribution, the model establishes an image model to describe the real distribution of the image and combines the clustering properties of local gray values to construct an energy term to measure the correctness of region division.

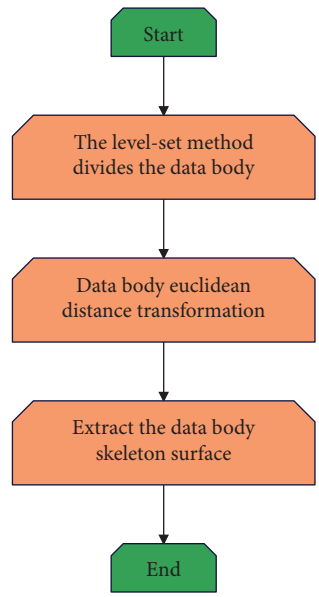

Figure 1: Schematic diagram of the process of extracting teaching information of 3D level set based on crease.

The established image model is shown in formula (1). Among them, I is the data obtained by measurement and J represents the real data value, which measures the physical properties of the target itself. It is, therefore, assumed that h can be estimated with a piecewise constant, that is, J can be divided into N disjoint regions $\Omega_1, \Omega_2, \ldots, \Omega_N$, and this division must satisfy $\Omega = \cup_{i=1}^{N} \Omega_i, \Omega_i \cap \Omega_j = \varnothing$. When $\neq j$, for each disjoint area, there is a corresponding constant $c_1, c_2, \ldots, c_N$ as the mean value of the multimedia teaching information attribute value of each area. b is the deviation field used to measure the unevenness of the gray level. Since b itself is assumed to vary slowly, it can be considered as a constant in the local field. n is additional noise.

Next, this article discusses the clustering properties of local gray values. For each point y of the entire data domain Ω, with the point as the center and a given ρ as the radius, a circular domain $o_y \triangleq \{x\colon |x - y| \leq \rho\}$ can be obtained. Based on the assumption that the deviation field d changes slowly, there is an equivalence relationship shown in formula (2) for points within o_y. Based on the assumption that J can be estimated with a piecewise constant, since for a point in each region Ω_i, its real data value $J(x)$ can be approximately replaced by a constant C_i, the image model of formula (1) can be approximated to the approximate model shown in formula (3). Moreover, it is approximately considered that the noise satisfies the zero mean, and the distribution obeys the normal distribution:

$$I = bj + n, \tag{1}$$

$$b(x) = b(y), x \in o_y, \tag{2}$$

$$I(x) \approx b(y)c_i + n(x), x \in o_y \cap \Omega_i. \tag{3}$$

The range of o_y is divided into N clusters by intersection with each Ω_i, the cluster centers of which are denoted as

$m(y) \approx b(y)c_i, i = 1, \ldots, N$. The gray value of the region o_y is divided by the K-means clustering algorithm, and the clustering criterion equation of each point y can be obtained as shown in (4). Among them, $K(y-x)$ is a nonnegative window function, also called a kernel function, which satisfies $K(y-x) = 0, x \notin o_y$:

$$\xi_y = \sum_{i=1}^{N} \int_{\Omega_i} K(y-x)\left|I(x) - b(y)c_i\right|^2 \mathrm{d}x. \tag{4}$$

The local clustering criterion function ξ_y is used as the evaluation index o_y to divide $\{o_y \cap \Omega_i\}_{i=1}^{N}$. The smaller the value of function ξ_y is, the better the effect of this division is. Therefore, when the optimal partition $\{\Omega_i\}_{i=1}^{N}$ is determined for the entire Ω, the value ξ_y of the local clustering criterion equation of all points y must also be the smallest. By integrating ξ_y over all points in the entire Ω domain, the energy term shown in (5) will be obtained. Both the final segmentation result of the image and the estimation of the deviation field can be obtained by minimizing the energy term shown in (5). In practical application, the kernel function K can be freely selected, and the truncated Gaussian function shown in formula (6) is used in this article. The radius ρ is the same as the domain radius of o_y, and its selection should be determined according to the actual degree of inhomogeneity of the 3D data volume:

$$\xi \triangleq \int \left(\sum_{i=1}^{N} \int_{\Omega_i} K(y-x)\left|I(x) - b(y)c_i\right|^2 dx \right) \mathrm{d}y \tag{5}$$

$$K(u) = \begin{cases} \dfrac{1}{a} e^{-|u|^2/2a^2}, |u| \le \rho, \\ 0, |u| > \rho. \end{cases} \tag{6}$$

The value of the level set function takes a positive or negative sign, which can divide the data domain 2 into two disjoint regions Ω_1 and Ω_2. The function ϕ: $\Omega \longrightarrow R$ is defined as the level set function, and the entire data body can be divided as in formula (7) by judging the sign of the function value. For the case of $N > 2$, it is necessary to specify multiple level set functions to divide the subregion $\{\Omega_i\}_{i=1}^{N}$:

$$\Omega_1 = \{x\colon \phi(x) > 0\}, \Omega_2 = \{x\colon \phi(x) < 0\}. \tag{7}$$

The membership functions of regions Ω_1 and Ω_2 are defined as $M_1(\phi) = H(\phi)$ and $M_2(\phi) = 1 - H(\phi)$, where H is the Heaviside function, and the energy function of (5) can be expressed in the form of (8) by exchanging the integration order. For convenience, $C_1, \ldots, C_N$ is expressed in the form of a vector $c = (c_1, \ldots, c_N)$, and the level set function ϕ, the vector c, and the deviation field b are used as variables for the energy ξ. Among them, in order to simplify the expression of ξ, the part shown in (9) is represented by e_i:

$$\xi(\phi, c, b) = \int \sum_{i=1}^{N} e_i(x) M_i(\phi(x)) \mathrm{d}x, \tag{8}$$

$$e_i(x) = \int K(y-x)\left|I(x) - b(y)c_i\right|^2 \mathrm{d}x, \tag{9}$$

The energy $\xi(\phi, c, b)$ defined above can be used as the data item of the energy function of the model, and the energy function of the model is shown in (10). Among them, $L(\phi) = \int |\nabla H(\phi)| \mathrm{d}x$ represents the area value of the zero-level contour of ϕ, so it can be used to constrain the smoothness of the contour. $R_p(\phi) = \int p(|\nabla\phi|)\mathrm{d}x$ is the signed distance function, where ρ represents an energy density function, which is defined as shown in (11):

$$F(\phi, c, b) = \xi(\phi, c, b) + \nu L(\phi) + \mu R_p(\phi). \tag{10}$$

$$p(s) = \frac{1}{2}(-1)^2. \tag{11}$$

This article uses the level set method for nonuniformly distributed images to process the ant volume data after Gaussian smoothing. The main steps of the method are as follows:

(1) The initial contour can be chosen at random because the model utilized in this article is not sensitive to that decision. Additionally, variables are set for the time iteration step size, the scale parameter used in the convolution operation, and the local clustering's neighborhood radius. At the same time, for the convenience of numerical calculation, the equations involved in the model are approximated.

(2) Next, this article performs iterative operations on the variables, c and b. The whole algorithm aims to minimize the energy function and guides and controls to update the values of c and b sequentially in each iteration process. This article uses formula (12) and combines the standard gradient descent method to iteratively update φ. Meanwhile, in each iteration, the formulas shown in (13) and (14) are used to update c and b, respectively:

$$\begin{aligned} \frac{\partial\phi}{\partial t} &= -\delta(\phi)(e_1 - e_2) + \nu\delta(\phi)\mathrm{div}\left(\frac{\nabla\phi}{|\nabla\phi|}\right) \\ &\quad + \mu\mathrm{div}\left(d_p(|\nabla\phi|)\nabla\phi\right), \end{aligned} \tag{12}$$

$$\widehat{c} = \frac{\int (b * K) I u_i \mathrm{d}y}{\left(b^2 * K\right) I u_i \mathrm{d}y}, i = 1, \ldots, N \text{且} u_i = M(\phi(y)), \tag{13}$$

$$\widehat{b} = \frac{\left(IJ^{(1)}\right) * K}{J^{(2)} * \mathrm{K}}, J^{(1)} = \sum_{i=1}^{N} c_i, u_i. J^{(2)} = \sum_{i=1}^{N} c_i^2 u_i. \tag{14}$$

(3) In the process of each iteration calculation, the algorithm calculates $L(\phi) = \int |\nabla H(\phi)| dx$, that is, the area value of the evolution surface, and then calculates the difference between it and the area value of

the evolution surface after the previous iteration. Moreover, this article judges by the preset threshold T. If it is less than T, it means that the surface is in a state of convergence; that is, the contour surface approaches the boundary of the target body, and the algorithm ends. At this time, the area contained by the zero level set surface is determined as the target area of multimedia teaching information.

2.3. Extracting Multimedia Teaching Information with Skeleton Features. It can be seen from the foregoing that the skeleton structure is one of the main ways to describe the topological structure of objects in image processing. The skeleton is located in the center of the target body, and on the premise of completely retaining the shape information of the original target body, the redundant components of the original object are reduced as much as possible. The data volume for segmenting the target area of multimedia teaching information has been obtained in the foregoing, but the current multimedia teaching information structure is a volume structure with thickness. Therefore, this article regards the teaching information as the skeleton feature of the target area to extract and finally obtains a three-dimensional surface reflecting the spatial topology of the multimedia teaching information structure.

Distance transform has been widely used since it was first proposed and has important applications in digital image processing, motion trajectory planning, and navigation. Among them, the Euclidean distance transformation is more widely used because of its high precision and consistent with the actual distance. Usually, in a two-dimensional space, a binary image can be considered to contain only two kinds of points, where the value of the target point is 1, and the value of the background point is 0. After Euclidean distance transformation, the image is transformed from a binary image to a gray value image that looks very similar to the original image. The value of the target volume will rise layer by layer from the boundary to the interior as each pixel in the inner region of the target volume takes on the Euclidean distance between it and the closest background point.

The data to be processed in this article is three-dimensional, and the amount of data is relatively large. Therefore, the multidimensional Euclidean distance transform algorithm is used to process the data volume divided by the level set method. This method can effectively process multidimensional data and has high efficiency.

For binary data in three-dimensional space, the data points can be divided into target points and background points. O is used to represent the point set of the target body, and the complement of O, that is, the set of background points, is represented by $B = \overline{O}$. Any point in the 3D data volume I is denoted by $X = (x_1, x_2, x_3) \in Z^n$, and $m = |0|$ is the number of points inside the target volume. The value of X for each point is defined by

$$f(X) = \begin{cases} 1, X \in O, \\ 0, X \in B. \end{cases} \tag{15}$$

The neighborhood of point X is $N(X)$. When g is a point in three-dimensional space, its neighborhood range is defined as the 26-neighboring points of point X (except X is the boundary of the three-dimensional data volume), which can be represented by

$$N(X) = \left\{Y | Y = (y_1, y_2, y_3) \in I, \left|y_i - x_i\right| \le 1, 1 \le i \le 3, Y \ne X\right\}. \tag{16}$$

At the same time, the definition of the boundary point set of the target body is given. They belong to the background points and the adjacent points of the target point. The boundary point set can be represented by

$$S = \{Y | Y \in B, \exists X \in O\colon Y \in N(X)\}. \tag{17}$$

For any point X, its Euclidean distance transformation is to find the point with the smallest Euclidean distance between the background points and the point X. At the same time, it is equivalent to finding the point in the boundary point set S that can make the minimum distance between X and the background. g represents the Euclidean distance transformation from the original three-dimensional data volume I to the distance field data volume I', and d represents the Euclidean distance. The expression of function g is shown in

$$\begin{aligned} g(X) &= d(X, B) = d(X, S), \\ &= \min\{d(X, Y), Y \in S\}. \end{aligned} \tag{18}$$

For any point v in the target point set, the closest point to the background is defined as $NP(X)$, as shown in formula (19). Often, there may be multiple points with the smallest Euclidean distance, in which case one of them is generally chosen at random. When $X \in S$, $NP(X)$ also has a corresponding definition as shown in formula (20), and for the points in the boundary point set, the Euclidean distance is 0:

$$NP(X) = \operatorname{argmin}\{d(X, Y), Y \in S\}, \tag{19}$$

$$NP(X) = X, X \in S. \tag{20}$$

The whole algorithm starts from the boundary point, then advances the search target point inward layer by layer, saves the points of each layer through the container queue Q Z $d\min(Z) = d(Z, NP(Y))$ $NP(X)$, and then iterates continuously until the entire queue is empty. For any point X in the target point set, information such as its nearest boundary point $NP(X)$ and the minimum Euclidean distance $d_{\min}(X)$ between them is recorded. The main operations for queues are insertion points from the tail of the queue and removal points from the head of the queue.

Step 1: The algorithm traverses the three-dimensional data volume processed by the level set method and determines the value of each data point. If the value is negative, we mark the point as the target point and add it to the target point set O. If the value is nonnegative, we mark the point as a background point and add it to the background point set B, where the value is 0, and we

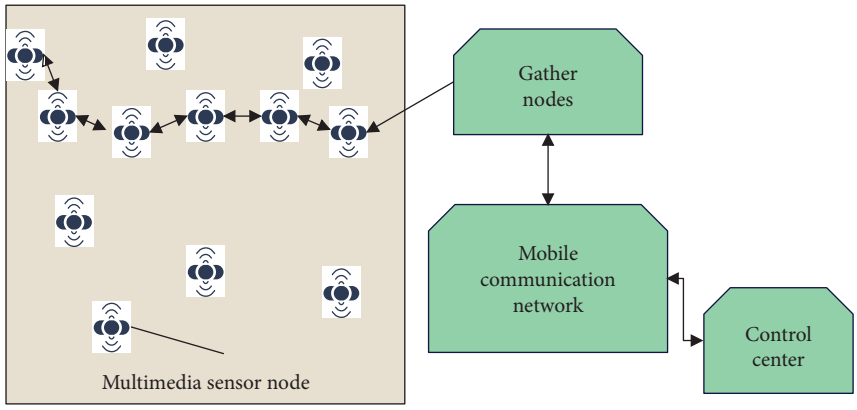

Figure 2: Structure diagram of multimedia network system.

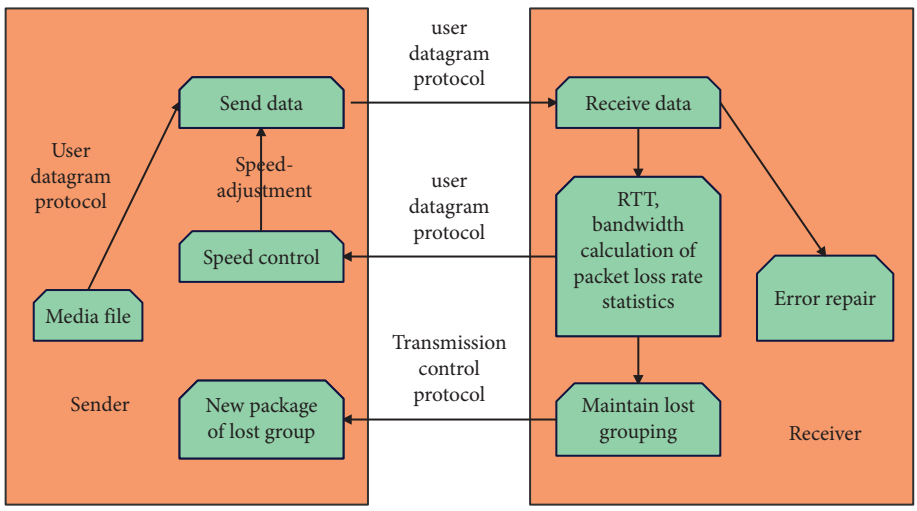

Figure 3: Quick transmission process of command information.

mark it as a boundary point and add it to the boundary point set S.

Step 2: The algorithm initializes all the point information in the target point set O, and the minimum distance point $NP(Y)$ between it and the background is initially empty, and the minimum Euclidean distance $NP(Y)$ between it and $d_{\min}(X)$ is initially positive infinity, and the queue Q is initialized to the boundary point f.

Step 3: If the queue is not empty, iterative processing is being done because the target point has not yet been processed. For each point Y in the queue, the algorithm advances towards the interior of the target body through its set of adjacent points $N(Y)$. If the neighboring point Z of the target point has not been processed and the minimum Euclidean distance $d_{\min}(X)$ recorded by Z is larger than the minimum Euclidean distance between Z and $NP(Y)$, the algorithm inherits the minimum distance point $NP(Y)$ from Y to the background point, that is, $NP(Z) = NP(Y)$ and $d\min(Z) = d(Z, NP(Y))$. Then, the algorithm adds Z to the queue, and removes Yr from the queue Q if all the neighbors of Y are processed.

Step 4: When the third step is over, the last recorded $NP(X)$ and minimum Euclidean distance $d_{\min}(X)$ of all target points will be optimal. Therefore, the algorithm replaces the value of the target point itself with the recorded $d_{\min}(X)$ and updates all point values of the background point set to 0.

Step 5: The Euclidean distance transformation is completed, and the operation is ended.

3. Higher Education Multimedia Teaching System Based on the Artificial Intelligence Model and Its Improvement

The classic multimedia network system mainly includes multiple sensor nodes, a convergence node, and a control center. The architecture is shown in Figure 2.

In the embedded multimedia terminal control system, any function needs to complete the task instruction through information transmission. However, with the rapid increase of media files, the system control rate will slow down and the

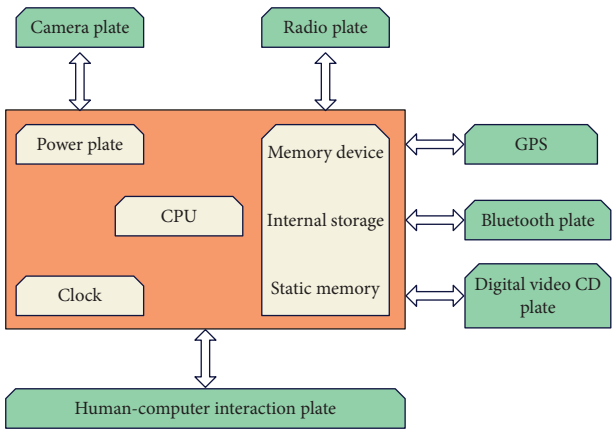

Figure 4: The overall hardware architecture of the multimedia terminal control system.

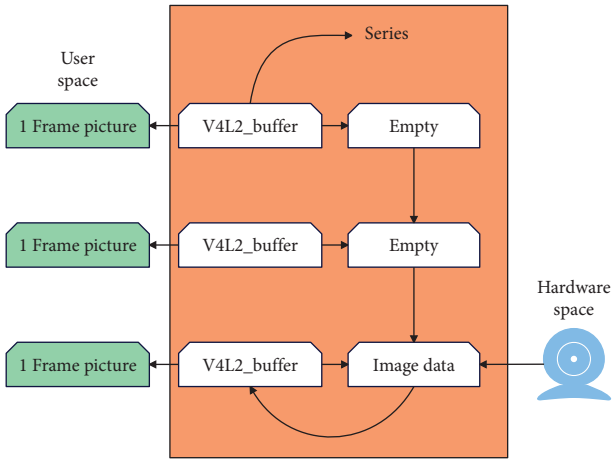

Figure 5: Operation instruction code.

resource consumption will also increase. In order to improve the real-time data transmission rate, the EMFTP proposed in this article can make the system have better timeliness, reduce resource consumption, and improve the overall performance of the system. EMFTP mainly adopts transmission control protocol (TCP) and user datagram protocol (UDP) and uses application layer control to complete the fast transmission of instruction information. Its architecture is shown in Figure 3.

The core of the embedded vehicle multimedia terminal control system hardware is the Freescale *i*. MX31 processor. It consists of power supply board, storage device, video monitoring board, radio board, GPS navigation board, Bluetooth board, human-computer interaction board, DVD board, etc., as shown in Figure 4.

Since the Windows CE 5.0 system has a camera driver, the application program only needs to use the system call function to open the camera equipment and clarify the image information contained in the camera. This article uses the Linux video device driver V4L2 to manage the camera image information, and its working principle is shown in Figure 5.

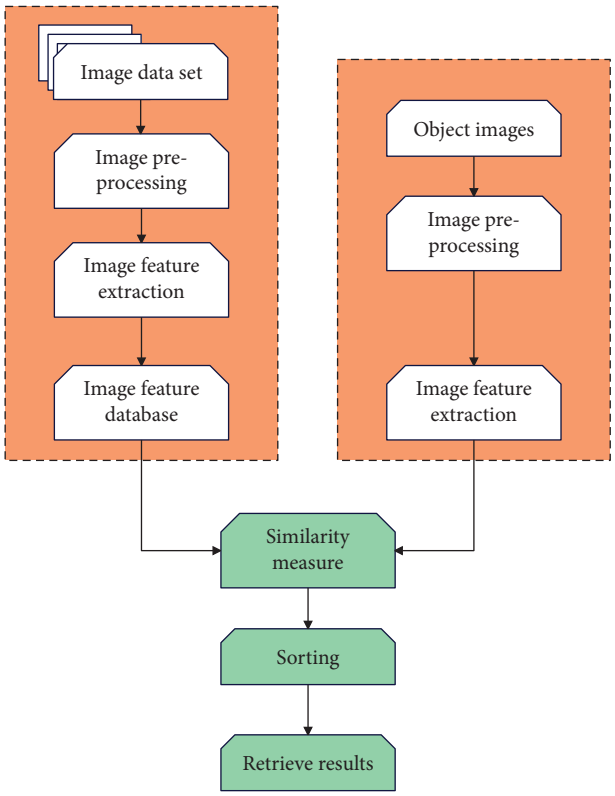

Figure 6: Principle framework of image retrieval method.

This work extracts picture features, fuses the extracted features, and enhances the accuracy of image retrieval by combining a variety of features after a thorough analysis of the original deep learning. The framework of the fast retrieval method for multimedia image information based on improved deep learning is shown in Figure 6.

This system is based on C/S architecture, uses MySQL database to store data, and uses C++ development environment to generate audio and video codec library to send and receive streaming media data, as shown in Figure 7.

The structure of the GUI is not fixed, which facilitates flexible changes in the future. For example, instead of putting several functions in one window, the windows are divided by function so that the function of each window is concise and simple. In this layer of program development, visual programming tools are mainly used, such as 4GL's visualBasic and PowerBuildep DelDhi. It is mainly used to check the legitimacy and validity of data input and to control the amount of data input. Through simple control, the amount of data exchange between this layer and the functional layer can be reduced, which is especially important in network transmission. Figure 8 shows the system architecture.

Figure 9 shows a case diagram of image recognition of multimedia teaching courseware by the higher education multimedia teaching system based on the artificial intelligence model.

On the basis of Figure 9, this article conducts multimedia teaching evaluation for the higher education multimedia

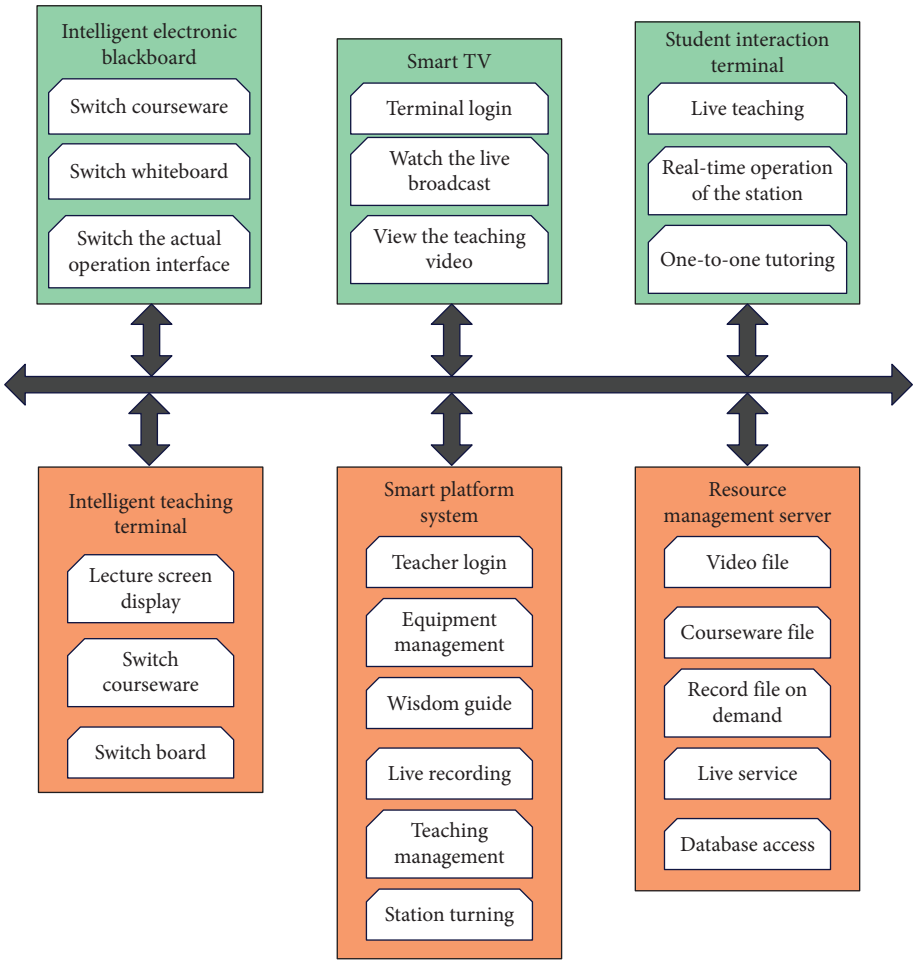

Figure 7: Architecture diagram of the multimedia teaching system.

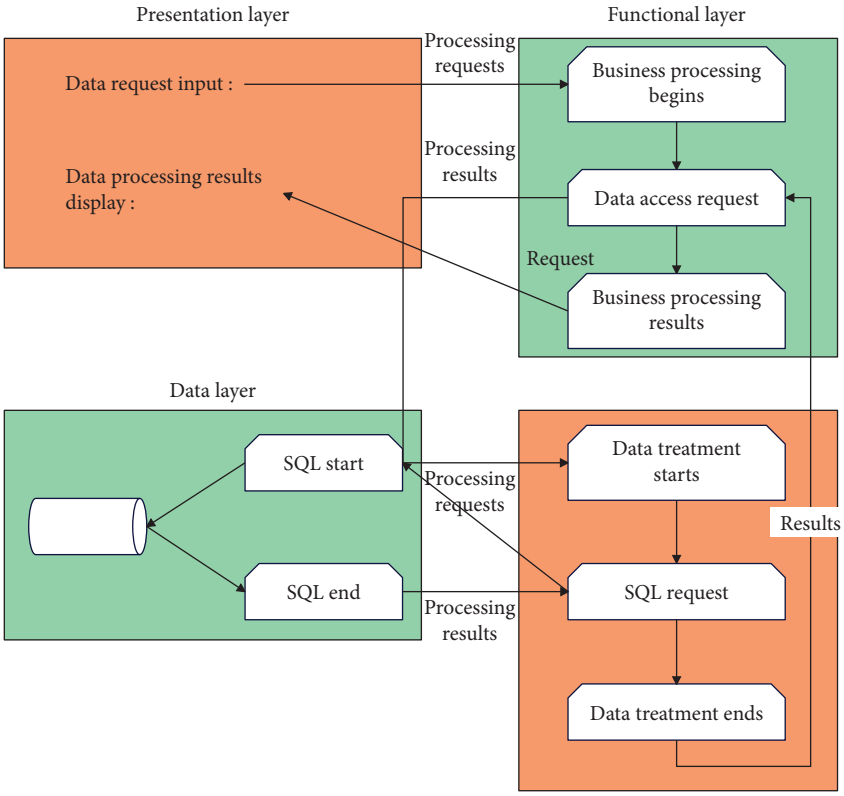

Figure 8: System frame structure.

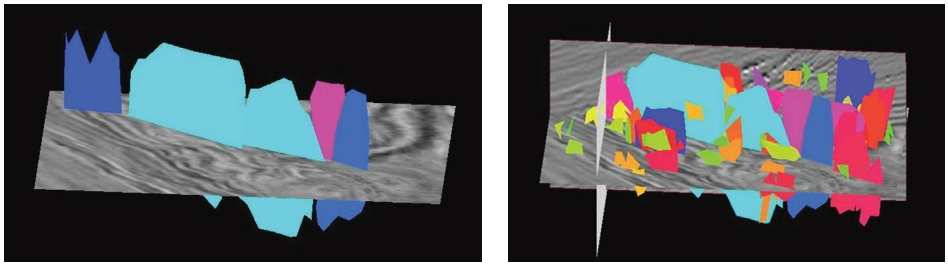

(a) (b)

Figure 9: Case diagram of image recognition of multimedia teaching courseware by higher education multimedia teaching system based on the artificial intelligence model: (a) case 1 of multimedia stereo image recognition courseware and (b) case 2 of multimedia stereo image recognition courseware.

Table 1: Teaching rating of higher education multimedia teaching system based on the artificial intelligence model.

Num	Teaching improvement	Num	Teaching improvement
1	88.28	15	84.65
2	85.35	16	87.29
3	84.60	17	83.51
4	84.29	18	88.15
5	87.33	19	88.58
6	83.19	20	87.80
7	88.82	21	83.44
8	83.26	22	86.78
9	86.50	23	86.04
10	88.39	24	86.54
11	87.42	25	84.75
12	87.41	26	84.52
13	86.36	27	84.92
14	83.32	28	85.56

teaching system based on the artificial intelligence model proposed in this article and obtains the results shown in Table 1 through the final results of multiple evaluation statistics.

It can be seen from the above analysis that the higher education multimedia teaching system based on the artificial intelligence model can effectively improve the multimedia teaching mode and promote the further improvement of multimedia teaching.

4. Conclusion

University is a very critical period in a student's academic life, and there is a lot to be learned. Since general technology is only a unified examination subject, students' attention is not high. The students' initiative, freedom, and originality in the learning process will be severely hampered if the standard teaching method is employed to impart knowledge. Additionally, as they learn, pupils will eventually tire out and lose interest in what they are learning. Therefore, appropriate use of multimedia display can effectively stimulate students' various senses and thereby improve learning efficiency so that students' learning life becomes no longer boring and effectively improve teaching quality and teaching efficiency. This article analyzes the problems existing in multimedia education in higher education to improve the multimedia teaching system and improve the effect of multimedia teaching in modern colleges and universities. The analysis shows that the multimedia teaching system of higher education based on the artificial intelligence model can effectively improve the multimedia teaching mode and promote the further improvement of multimedia teaching.

Data Availability

The experimental data used to support the findings of this study are available from the author upon request.

Conflicts of Interest

The author declared that there are no conflicts of interest regarding this work.

References

[1] J. R. Mianroodi, N. H Siboni, and D. Raabe, "Teaching solid mechanics to artificial intelligence—a fast solver for heterogeneous materials," *Npj Computational Materials*, vol. 7, no. 1, pp. 99–10, 2021.

[2] X. Li, "The construction of intelligent English teaching model based on artificial intelligence," *International Journal of Emerging Technologies in Learning (iJET)*, vol. 12, no. 12, pp. 35–44, 2017.

[3] S. Zou, "Designing and practice of a college English teaching platform based on artificial intelligence," *Journal of Computational and Theoretical Nanoscience*, vol. 14, no. 1, pp. 104–108, 2017.

[4] F. Kong, "Application of artificial intelligence in modern art teaching," *International Journal of Emerging Technologies in Learning (iJET)*, vol. 15, no. 13, pp. 238–251, 2020.

[5] M. Pantic, R. Zwitserloot, and R. J. Grootjans, "Teaching introductory artificial intelligence using a simple agent framework," *IEEE Transactions on Education*, vol. 48, no. 3, pp. 382–390, 2005.

[6] C. Yang, S. Huan, and Y. Yang, "A practical teaching mode for colleges supported by artificial intelligence," *International Journal of Emerging Technologies in Learning (IJET)*, vol. 15, no. 17, pp. 195–206, 2020.

[7] K. Kim and Y. Park, "A development and application of the teaching and learning model of artificial intelligence education for elementary students," *Journal of The Korean Association of Information Education*, vol. 21, no. 1, pp. 137–147, 2017.

[8] O. Zawacki-Richter, V. I. Marín, M. Bond, and F. Gouverneur, "Systematic review of research on artificial intelligence applications in higher education–where are the educators?" *International Journal of Educational Technology in Higher Education*, vol. 16, no. 1, pp. 39–27, 2019.

[9] S. C. H. Yang, W. K. Vong, R. B. Sojitra, T. Folke, and P. Shafto, "Mitigating belief projection in explainable artificial intelligence via Bayesian teaching," *Scientific Reports*, vol. 11, no. 1, pp. 9863–9917, 2021.

[10] Y. Lee, "An analysis of the influence of block-type programming language-based artificial intelligence education on the learner's attitude in artificial intelligence," *Journal of The Korean Association of Information Education*, vol. 23, no. 2, pp. 189–196, 2019.

[11] J. M. Alonso, "Teaching explainable artificial intelligence to high school students," *International Journal of Computational Intelligence Systems*, vol. 13, no. 1, pp. 974–987, 2020.

[12] S. F. M. Alfalah, "Perceptions toward adopting virtual reality as a teaching aid in information technology," *Education and Information Technologies*, vol. 23, no. 6, pp. 2633–2653, 2018.

[13] G. Cooper, H. Park, Z. Nasr, L. P. Thong, and R. Johnson, "Using virtual reality in the classroom: preservice teachers' perceptions of its use as a teaching and learning tool," *Educational Media International*, vol. 56, no. 1, pp. 1–13, 2019.

[14] J. Zhao, X. Xu, H. Jiang, and Y. Ding, "The effectiveness of virtual reality-based technology on anatomy teaching: a meta-analysis of randomized controlled studies," *BMC Medical Education*, vol. 20, no. 1, pp. 127–210, 2020.

[15] S. J. Bennie, K. E. Ranaghan, H. Deeks et al., "Teaching enzyme catalysis using interactive molecular dynamics in virtual reality," *Journal of Chemical Education*, vol. 96, no. 11, pp. 2488–2496, 2019.

[16] S. F. M. Alfalah, J. F. M. Falah, T. Alfalah, M. Elfalah, N. Muhaidat, and O. Falah, "A comparative study between a virtual reality heart anatomy system and traditional medical teaching modalities," *Virtual Reality*, vol. 23, no. 3, pp. 229–234, 2019.

[17] M. Reymus, A. Liebermann, and C. Diegritz, "Virtual reality: an effective tool for teaching root canal anatomy to undergraduate dental students–a preliminary study," *International Endodontic Journal*, vol. 53, no. 11, pp. 1581–1587, 2020.

[18] V. L. Dayarathna, S. Karam, R. Jaradat et al., "Assessment of the efficacy and effectiveness of virtual reality teaching module: a gender-based comparison," *International Journal of Engineering Education*, vol. 36, no. 6, pp. 1938–1955, 2020.

[19] O. Hernandez-Pozas and H. Carreon-Flores, "Teaching international business using virtual reality," *Journal of Teaching in International Business*, vol. 30, no. 2, pp. 196–212, 2019.

[20] V. Andrunyk, T. Shestakevych, and V. Pasichnyk, "The technology of augmented and virtual reality in teaching children with ASD," *Econtechmod: Scientific Journal*, vol. 7, no. 4, pp. 59–64, 2018.

Hindawi
Mobile Information Systems
Volume 2023, Article ID 8453791, 13 pages
https://doi.org/10.1155/2023/8453791

Research Article

Construction of Digital Art Education Platform under the "Internet+" Environment

Chen Zhang and Xiaoxia Li

School of Fine Arts and Design, Hainan University, Haikou 570228, Hainan, China

Correspondence should be addressed to Chen Zhang; 993794@hainanu.edu.cn

Received 25 July 2022; Revised 13 September 2022; Accepted 23 September 2022; Published 10 February 2023

Academic Editor: Chi Lin

With the development of society and the rapid development of the Internet, there are currently about 100 million web pages and 100 million hyperlinks, and in the future, the number of web pages and hyperlinks will also intensify. How to make this huge Internet better used by people has become a common concern of the international community. In recent years, with the acceleration of the reform of China's basic education curriculum, people have become more and more aware of the special status and superiority of art education in overall education, and the general consensus that "lack of art education is an incomplete education." Therefore, this paper proposes the construction of a platform for digital art education under the "Internet+" environment. This paper first introduces how to perform data mining in the Internet era, and proposes an interactive data fusion algorithm and model for Internet and crowdsourcing. Then, a statistical analysis was made on the preschool art education syllabus of 20 colleges and universities in different provinces and cities. The experimental results have shown that there are eight undergraduate colleges and universities that have not written syllabuses for College Aesthetic Education majors in art courses, and they still account for 40% of the total sample size. This shows that some Chinese colleges and universities have not paid enough attention to the art courses of College Aesthetic Education majors, have loopholes in curriculum management, and neglected teaching staff.

1. Introduction

The 21st century is an information age, with massive amounts of information and data coming in like a tide. In today's scientific and technological progress, the wave of informatization has promoted the modernization of society and the modernization of education. In 2015, the Premier of the State Council proposed "Internet+" for the first time at the 12th National People's Congress. Since then, the rapid development of "Internet+" has driven the reform and development of various industries. The deep integration of "Internet+" and education is an important topic in the field of Chinese pedagogy. As the center of teaching reform, the classroom has become an important research topic. As learners grow about what attracts to people and have a direct say in how their work will turn out, art education aids in decision making, increases self-confidence, and enables individuals become more self-assured. They can develop into lifelong learners that push themselves regularly and sharpen their focus on reaching their objectives. Collaboration and group study are also promoted through art education. It frequently brings individuals and kids together, allowing them to benefit from and support one another as they continue in producing anything. It enhances emotional stability and fosters teamwork in children. Kids take ownership of their errors and assume accountability for them while functioning collaboratively, which increases responsibility.

As the main way of aesthetic education for students, art course teaching is not only a simple skill and skill training, but also a cultural study. In today's environment of advocating quality education, it plays a very important role in popularizing art education for primary and secondary school students. Through the research on the meaning and function of art education, this paper draws the importance of art education. It is mainly reflected in five aspects: students'

aesthetic evaluation ability, physical and mental literacy and cognitive ability, hand-brain coordination, and students' creativity. Therefore, increasing the art and aesthetic education for primary and secondary school students can bring a good promotion effect to the cultivation of high-quality talents in China. Internet data fusion combines information from different sources to just provide knowledge which is more reliable, precise, and practical than that offered by any one source of data alone. Only Internet data fusion can be used by both users and programmers to access management services provided in the live project. Digital and context-aware gadgets are used by the modern instructional paradigms, such as smart educational experiences, to speed up the learning process. Therefore, in order to merge different sources of multimedia learning data in arts integration, it is required to employ information fusion methods and approaches appropriately. Aesthetic education is a way of teaching and learning that involves students exploring, questioning, discussing, and creating art as they study about pieces of art. People who are educated in aesthetics are better able to judge beauty. It teaches how to properly feel, enjoy oneself, and manage emotions. People are encouraged to be imaginative via creating a learning environment. Meeting the requirements of perceptual, intellectual, and social learning is the goal of aesthetic education.

This paper mainly talks about the use of data mining for data statistics in the context of Internet big data. Then, the interactive data fusion algorithm and its model of Internet and crowdsourcing are proposed. This paper then makes a statistical analysis of the undergraduate course syllabus of 20 colleges and universities in different provinces. Cities and regions collect data from 12 colleges and universities and designs experiments. The innovation of this paper is to use big data algorithm to analyze and discriminate, and analyze various data of colleges and universities, so the final experimental results are also very authoritative.

2. Related Work

College Aesthetic Education is the core content of the education and teaching system, and art is an indispensable professional course. College art teachers should not only pay attention to students' learning ability, but also pay attention to their professional ability, and also pay attention to the improvement of students' aesthetic awareness and personal accomplishment from the perspective of modern innovation and entrepreneurship education. Art is an important course to improve students' aesthetic awareness and personal accomplishment. At present, many undergraduate college aesthetic education institutions have listed professional art courses as one of the compulsory courses, but there are still many problems in college aesthetic education. Yan put forward some measures to promote the innovation and entrepreneurship development of college students [1]. With the popularization of computer-aided technology, universities, as important institutions of knowledge dissemination, are actively exploring the combination mode of modern information technology and curriculum. Hanfei analyzed the innovative teaching modes and methods of art design courses in the context of information technology. In the process of art design and expression, students majoring in art design need to understand the detailed steps of painting and show their teaching results [2]. In this visual essay, cosmopolitanization is used as a method to evoke an attunement to being, being, and belonging through common experiences and emotions. Blaikie told multimodal stories composed of theory and practice that provide rethinking of fine arts, pedagogy, and scholarship as practice [3]. In this visual essay, we describe multimodal scenarios that are structured by research and models that provide reassessments of the arts, education, and research as practice, drawing on discussing the matter as method to induce sensitivity to being, emerging, and connecting through daily experiences and emotions. Discussions with Danny are presented alongside her art works and writing as piece of the overall representations of a developing self-spanning location, place, and time, contextualized by young ethnic communities, permeable visual appearances, materiality, physique control, clothes, pop culture, and social networks. Nacak aimed to identify current trends in published articles on arts education and society for a systematic review of the field. Literature analysis as a qualitative research method was used in research to achieve this goal. The data of this study comes from Google Scholar database, obtained by searching keywords such as "art education," "communication," and "society" [4]. They all explained the importance of art education very well, but they did not study in detail, and did not go to college classrooms to really analyze experimental data, which is relatively one-sided.

The Internet is supported by emerging sensing, communication, cloud computing, and big data analytics technologies, and has received extensive attention in the industrial field for its potential to be smarter and more efficient in industrial production. With the fusion of smart devices, smart systems, smart decisions, and the latest information technology, the Internet will increase productivity and reduce costs and waste across the entire industrial economy. Using data from a longitudinal survey of undergraduates at Midwestern universities, Nelson found that digital civic engagement fills the void left by the decline of more traditional forms of political engagement. It was also found that educators play an important role in developing and sustaining young people's civic engagement both online and offline. Conclusions have shown that academics and undergraduate educators need to develop curricula based on the way students currently engage in democracy [5]. In this paper, Papagiannidis et al. proposed the use of a new big data mining method and the Internet as a new source of useful metadata for industry classification. The method he proposes can be used as a decision support system for the near real-time identification of industrial clusters in a specific geographic area, which contributes to strategic cooperation and policy formulation of operations and supply chain management across organizational boundaries through big data analytics [6]. The article provides an overview of the industrial Internet, focusing on the architecture, enabling technologies, applications, and existing challenges, beginning with a survey of a brief history of the industrial Internet.

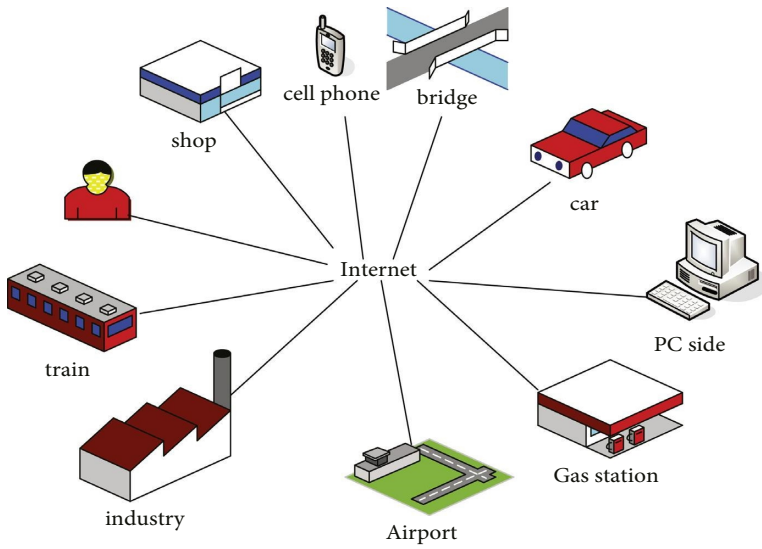

Figure 1: Internet+ model diagram.

Then, Li et al. introduced the 5C architecture that is widely used to characterize industrial Internet systems. In addition, he has carried out research on enabling technology from various aspects such as industrial network, industrial intelligent sensing, cloud computing, big data, intelligent control, and security management [7]. They have all done research on Internet technology to inform everyone about the importance of the Internet, but they have not done research in combination with digital technology.

3. Digital Data Fusion Algorithm in the "Internet+" Environment

3.1. The Era of "Internet+". "Internet+" connects everything. The networked connectivity of individuals, processes, data, and objects is defined by the phrase "Internet+ connects anything." The benefit this greater connectivity produces when "everything" comes back online and the factors which influence of making connections, processes, information, and objects are what make IoE beneficial. It connects together individuals, processes, information, and objects to make networked relationships more useful and meaningful than ever before. By transforming knowledge into actions, it gives organizations, individuals, and nations unheard-of economic opportunities. As shown in Figure 1, it always presents an open and fair attitude. The simple relationship of instilling and receiving, giving and being given in the past will no longer be used here.

The number of Internet users in China reached 710 million in June 2016, mainly mobile phones, desktop computers, and laptops. The number of mobile phone users has reached 656 million, accounting for 92.5%, far exceeding other Internet devices, which can be seen in Figure 2 [8] and Table 1.

3.2. Internet Data Fusion. With the development of society and the rapid development of the Internet, how to make this huge Internet better for people has become a common concern of the international community. On the one hand, people hope to obtain information quickly, accurately, and comprehensively, on the other hand, it is difficult to make a choice due to the variety of information on the Internet. In the past, most of them were still in the very primary stage of data collection, with manual classification of web pages, machine retrieval, etc., which lacks of knowledge processing and understanding, as well as the mining and utilization of the Internet, which made its intelligence level not high.

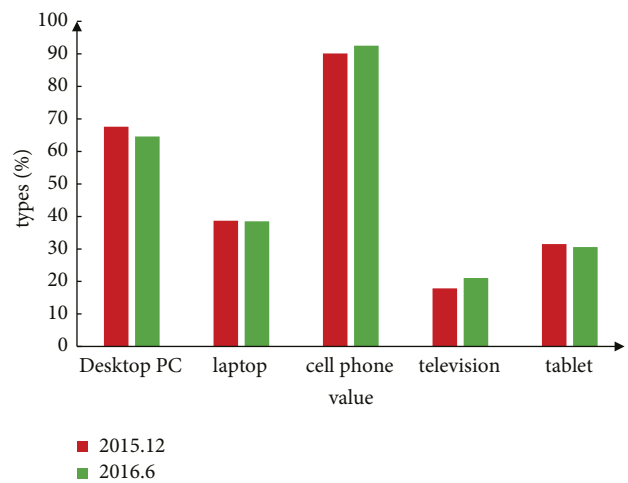

Figure 2: December 2015–June 2016 intervention and use of Internet equipment in China.

To this end, this paper proposes an interactive data fusion technology based on the Internet and crowdsourcing. It can perform different pattern matching and physical matching in different situations to achieve better fusion effect. In this way, more information can be obtained and the potential can be better tapped. In addition, this paper presents a new model that combines the advantages of the above two methods and addresses their limitations [9].

Table 1: Usage of Internet equipment in China.

Types	Usage of Internet in December 2015 (%)	Usage of Internet in June 2016 (%)
Desktop PC	66	64
Laptop	38	37
Cell phone	90	96
Television	19	21
Tablet	30	28

3.2.1. Record Matching Likelihood Estimation. First, the logical sigmoid function is used to reduce the above complex function to a linear function, rather than completely computing the dependencies between attributes. A sigmoid function is a limited, differentiable, performs the functions that has precisely one turning point, a non-negative derivative at every juncture, and is specified for all actual input values. Only one parameter was then used to control the effect of dependencies between attributes on the likelihood of record matching. That is, the effect of attributes on the matching likelihood of records is smoothed in an interpretable way by the sigmoid function. Furthermore, in order to overcome the error accumulation problem, it is need to define a contribution function and use the logarithmic function to map the values in $[0, 1]$.

To achieve this, first all attribute pairs are assumed to be opposite to each other, so that a linear function can be used to calculate the matching probability (similar to the Noisy-All model). The only systems in this category that can forecast a specific occurrence known as static probabilities similarity are linear models. Additionally, it is demonstrated that models belonging to this class that have the additional characteristic known as marginal consistency forecast approximation probabilistic match. A damping factor is then introduced to compensate for the assumption that the properties are independent of this setting. Then, the calculation method of the matching probability of d and w can be expressed by the following formula:

$$\phi_{KN}(d, w) = 1 + h^{-\alpha \cdot W\left(X^1 \leftrightarrow Y, d, w\right)}. \tag{1}$$

An object's damping coefficient reveals whether a substance will rebound or supply energy to a system. The following are some reasons why the damping ratio matters. It is employed to assess the system's dampening degree. Among them, ϕ is the damping coefficient used to compensate for the interdependence between attributes (this coefficient can be reconciled on the data validation set) and $W(X \leftrightarrow Y, d, w)$ is the total contribution score of the matching attributes to set $\{X \leftrightarrow Y\}$, which is calculated as follows:

$$W(X \leftrightarrow Y, d, w) = \sum_{(X \leftrightarrow Y) \in \{X \leftrightarrow Y\}} \beta(X, Y) \cdot \mathrm{ctr}(d[X], w[Y]). \tag{2}$$

$\beta(X, Y) \in$ uses the logarithmic function to map values between 0 and 1 to the entire real axis as follows:

$$\beta(X, Y) = -\ln\left(1 - \phi_{WN}(X, Y) \cdot IdC(X \leftrightarrow Y)\right). \tag{3}$$

Among them, $\phi_{WN}(X, Y)$ is the matching likelihood of X and Y. The last $\mathrm{ctr}(d[X], w[Y])$ are the $d[X]$ and $w[Y]$ similarity contribution functions, which are calculated as follows:

$$\mathrm{ctr}(d[X], w[Y]) = \begin{cases} 0, \text{if } d[X] = \text{null or } w[Y] = \text{null}, \\ \mathrm{sim}(d[X], w[Y])_{1-\varepsilon}, \text{if } \mathrm{sim}(d[X], w[Y]) \geq 0, \\ \mathrm{sim}(d[X], w[Y])_{\varepsilon}, \text{if } \mathrm{sim}(d[X], w[Y]) > 0. \end{cases} \tag{4}$$

Among them, $\mathrm{sim}(d[X], w[y])$ is the similarity calculated by the string similarity function, such as the Levingston similarity function, $(d[X], w[y])$, ε is the turning point defined by experts to judge whether an attribute value provides a positive or negative contribution. The distance value specifies the smallest number of incisions, deletion, or replacements needed to convert the source string into the destination string. The contribution function defined in equation (4) addresses the error accumulation problem instead of directly using $\mathrm{sim}(d[X], w[y])$ as the contribution. In that case, the scores of the larger $W(X \leftrightarrow Y, d, w)$ may accumulate through the smaller similarity $\mathrm{sim}(d[X], w[y])$ among the multiple attributes $\{X \leftrightarrow Y\}$ and cause false matches [10, 11].

To sum up, the proposed model has the following two advantages: it can solve the problem of record matching probability calculation in the case of nonindependence between attributes at a small cost; it solves the problem of error accumulation. It can be found in Figure 3 that the Noisy-All model is relatively stiff and changes very quickly when x is small. The ϕ_{WN} curve is smoother and corresponds to a large area on the x-axis. In addition to this, when applying equation (4), the model does not introduce negative values like the Noise-All model, because that would be meaningless.

3.2.2. Attribute Matching Likelihood Estimation. Now, how to estimate the probability of 1 and 2 matching is discussed. When the currently matched record pair is $\{D_d \leftrightarrow D_w\} = \{(d_1 \leftrightarrow w_1), (d_2 \leftrightarrow w_2), (d_3 \leftrightarrow w_3) \cdots (d_m \leftrightarrow w_m)\}$, the same model used in record matching is used to calculate the probability of two attributes matching. But here a damping coefficient is not needed to control the correlation dependencies between the records, because they are usually independent of each other. Unfortunately, unlike a system's mass or rigidity, the damping coefficient of a system cannot be determined intrinsically. It has an impact on the oscillator's inherent speed in addition to the progressive fading of output waveform. The formal expression for the property matching likelihood is given below:

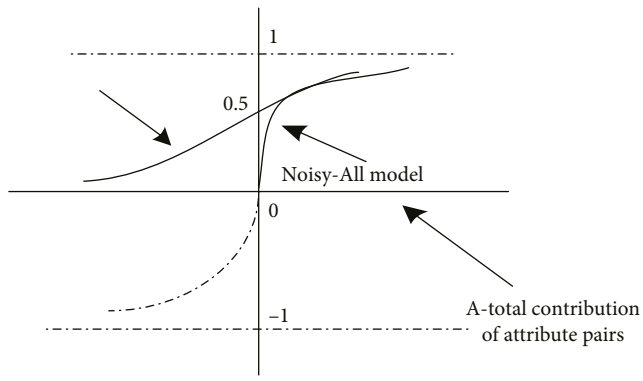

Figure 3: Schematic diagram of model comparison.

$$\phi_{WN}(X,Y) = 1 + h^{-W\left(D_d \leftrightarrow D_w, X, Y\right)}. \tag{5}$$

Among them, $W(D_d \leftrightarrow D_w, X, Y)$ is the total contribution score of matching records to set $D_d \leftrightarrow D_w$, which is calculated as follows:

$$W(D_d \leftrightarrow D_w, X, Y) = \chi \cdot \sum_{(d \leftrightarrow w) \in \{D_d \leftrightarrow D_w\}} \beta(d,w) \cdot \mathrm{ctr}(d[X], w[Y]). \tag{6}$$

As the iterative process proceeds, more and more attribute pairs and record pairs are matched together. After each iteration, the currently calculated matching probability needs to be updated, and the connected attribute pairs and record pairs also need to be readjusted.

There is a mutually reinforcing relationship between attribute pairs and record pairs. As shown in Figure 4, a bipartite graph can be used to show the relationship between attribute pairs and record pairs. The weight on the edge represents the contribution score of an attribute pair or a record pair. Specifically, if an edge is from a record pair (d,w) to an attribute pair (X,Y), the weight of their edge is $\beta(d,w) \cdot \mathrm{ctr}(d[X], w[Y])$. If an edge is from a record pair (X,Y) to an attribute pair (d,w), the weight of their edge is $\chi(X,Y) \cdot \mathrm{ctr}(d[X], w[Y])$. Then function $p(x) = 1 + h^{-\eta x}$ can be applied to the full-time sum of all edges pointing to the record pair itself. This method can also be used to calculate the matching probability of attribute pairs, and the matching possibilities of record pairs and attribute pairs are recorded as vectors $\vec{k}$ and $\vec{x}$, respectively. The above interactive algorithm is denoted as IntSRM, and the formal conclusion is given:

The IntSRM interaction algorithm is convergent, and the matching record pairs and matching attribute pairs will be uniquely determined in the end [12]. All of these hypotheses would have been in line with the idea that an arts education might increase students' motivation. One simply needs to make the case that arts education is inspiring as a result of the intricate web of variables connected to such instruction. The best way to show that there is a high likelihood that the arts increase academic performance is to randomize students to one school with an arts programmed and the other with no such programmed, then monitor their development over time.

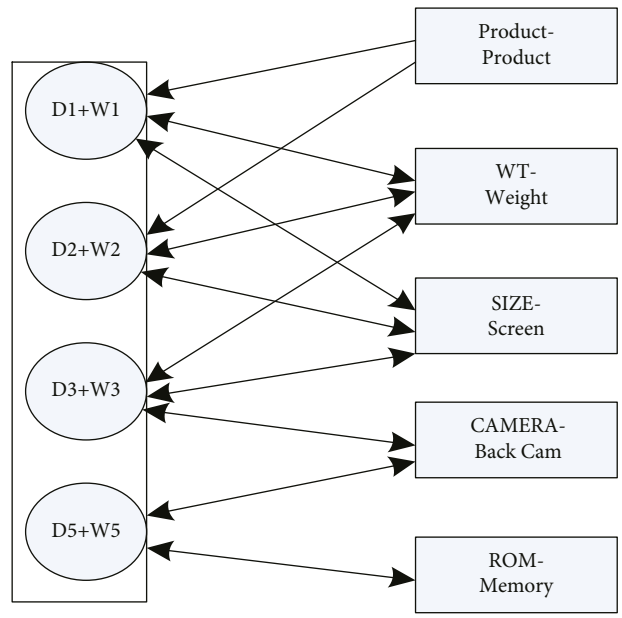

Figure 4: Two-part demonstration of the iterative process.

Proof: The bipartite graph of the algorithm is denoted as $F = F_1 \cup F_2$, where $F_1 = \{U_2, H_2\}$, $F_2 = \{U_2, H_2\}$. U_1 is the node set of all record pairs, and U_2 is the combination of all attribute pairs of nodes; H_1 is a combination of edges in F_1, and H_2 is a set of edges in F_2. Let denote X and Y denote an adjacency matrix of (U_1, H_1), (U_2, H_2), respectively. For the convenience of expression, the values in X and Y need to be redefined. If there is an edge from a node in U_1 to a node in U_2, then the corresponding value in the adjacency matrix X is defined as the contribution value in equation (4). If there is an edge from the node in U_2 to the node in U_1, then the corresponding value in the adjacency matrix Y is also defined as the contribution value. In j-step iterations, the matching possibilities of attribute pairs and record pairs are vectors $\vec{k}_j$ and $\vec{x}_j$, respectively. Now the following four functions on matrices are defined.

(1) $F_1(N)$ is the operation of applying function $p_1(x) = 1 + h^{-\eta x}$ to each x value in matrix M;

(2) $F_2(N)$ is the operation of applying function $p_2(x) = 1 + h^{-x}$ to each x value in matrix M;

(3) $E_1(N)$ is to apply function $q_1(x) = -\ln(1 - c - x)$ to each x value in matrix M where c is a constant

(4) $E_2(N)$ is to apply function $q_2(x) = -\ln(1 - x)$ to each x value in matrix M. In addition, denote $X^{(r)}(N)$ as applying the rth function X to the matrix N, where $X = \{F_1, F_2, E_1, E_2\}$ is used, and the following two formulas can be obtained:

$$\vec{x}_j = F_1\left(X^D \cdot E_1\left(\vec{k}_j^D\right)\right), \tag{7}$$

$$\vec{k}_j = F_2\left(Y^D \cdot E_2\left(\vec{x}_{j-1}^D\right)\right). \tag{8}$$

After substituting equation (7) into equation (8), and then substituting equation (8) into equation (7), it can be gotten:

$$\begin{aligned}\vec{x}_j^D &= F_1\left(X^D \cdot E_1\left(F_2\left(Y^D \cdot E_2\left(\vec{k}_{j-1}^D\right)\right)\right)\right),\\ \vec{k}_j^D &= F_2\left(X^D \cdot E_2\left(F_1\left(X^D \cdot E_1\left(\vec{k}_{j-1}^D\right)\right)\right)\right).\end{aligned} \tag{9}$$

To get a more explicit expression, some conversions need to be done. Similar to the method of series convergence proof, the following formula can be obtained:

$$\begin{aligned}\lim_{r\longrightarrow+\infty}\left(E_1F_2\right)^{(r)}(N) - N &= \Delta_1,\\ \lim_{r\longrightarrow+\infty}\left(E_2F_1\right)^{(r)}(N) - N &= \Delta_2.\end{aligned} \tag{10}$$

Therefore, the following expressions for 1 and 2 can be obtained:

$$\begin{aligned}\lim_{r\longrightarrow+\infty}\vec{x}_j^D &= \Delta_1' + F_1\left(X^DY^D\right)^{r-1}\cdot\vec{x}_1^D),\\ \lim_{r\longrightarrow+\infty}\vec{k}_j^D &= \Delta_2' + F_2\left(Y^DX^D\right)^{r-1}\cdot\vec{k}_1^D\Big).\end{aligned} \tag{11}$$

Δ_1', Δ_2' is a constant vector.

3.3. Interactive Data Fusion of Internet and Crowdsourcing. Due to the high number of missings in both datasets, interactive algorithms often fail to complete. However, specific pattern matching or entity matching can be performed through the network and crowdsourcing to fill in a small amount of missing data, or directly determine the matching of attributes and records [13, 14]. Then it may make the interaction process better, so as to achieve a better data fusion effect. To characterize the art education data and each sublayer, pattern matching utilized data fusion analysis and pattern recognition methods. This allows for the merging of multisource information, and running operational data on the sublayer scale. The outcomes demonstrate that the multisource sublayer information fusion method using pattern recognition can acquire the multidimensional characteristics of each sublayer, saving a significant amount of manually analysis time, lowering the subjective nature and one-sidedness of analysis, and offering expert and data assistance for the accurate determination of corresponding variables [15].

First, the missing values of attributes under a certain number of record pairs are filled with the help of the Internet, and then the matching model proposed above is used to recalculate the possibility of matching attribute pairs or record pairs. If the matching possibility of the recalculated attribute pair or record pair still does not reach the specified threshold, there are only two possibilities. The first is that missing values crawled on the Internet are unreliable, and the second is that the two attributes do not actually match. The second reason is that due to the limitation of the data itself, it cannot be changed. For the first reason, it can be tried to solve it with crowdsourcing. Thus, the strategy is to use the Internet-based method in preference, and if it does not work, use the crowdsourcing-based method. If the crowdsourcing-based method has no more attribute pairs to match in the current pattern matching, the interaction process is considered to be over. The difficulty of collecting and understanding task outcomes is embedded inside the framework when developing crowd-based processes, which include learners engaging with simple actions that pertain to homogenous entities.

3.3.1. Filling Framework Based on Internet and Crowdsourcing. This section introduces the matching framework on how to use the Internet and crowdsourcing. As shown in Figure 5, the basic flow of the framework can be illustrated by the following steps: First, the grouper groups the missing values of the currently matched records, so that the same data can be used to fill the model in the same group. Then, the data that needs to be populated is selected and an Internet-based population model is used to help populate the data. If the use of these padding values is not sufficient to continue the interaction process, a crowdsourcing-based approach is used to directly perform attribute or record matching. The Packetizer and Internet-based data filling model in this framework are described in detail next.

The data are once again analyzed to be a part of better matching patterns and extracted using packetized from various data restriction process. Once the data are extracted, the values are inquired with the analysis of pattern with the usage of Internet. Further, validation process is carried out in the crowd-sourcing platform and finds the pattern matching with trained data of maximum probability.

Grouper: The grouper will pad some records with missing values into different groups. It is mainly based on the following two points: the distribution of missing values in each tuple; data constraints such as FDs, CFDs, and some user-defined rules. Through this grouping, it is hoped that records with missing values in the same group can use the same query method to obtain data from the Internet. Each of these query modes uses a collection of attribute values and an associated schema to form a query. Thus, records within the same group can use the same Internet-based population model.

Internet-based data population model: This model fetches data from the Internet by entering the population query generated in the previous steps. The model not only fetches relevant data from the Internet, but also selects more accurate data from multiple return values to help us complete high-quality pattern and entity matching. As shown in Figure 6, two sets of parameters need to be considered in this model: the accuracy of the relevant website and the accuracy of the crawler (corresponding to each query style) [16].

3.3.2. Internet-Based Quality Control of Missing Values. In order to ensure high-quality data fetched from the Internet for better interactive fusion, a probability model is used to estimate the correct rate of attribute values fetched from the Internet. To make it easier for people to understand, first a website s and a crawler h are considered as a whole, which is denoted as (s, h). Then, using (s, h) to provide a fill-in value for a missing value, the probability that (s, h) provides a value d to y can be obtained as follows:

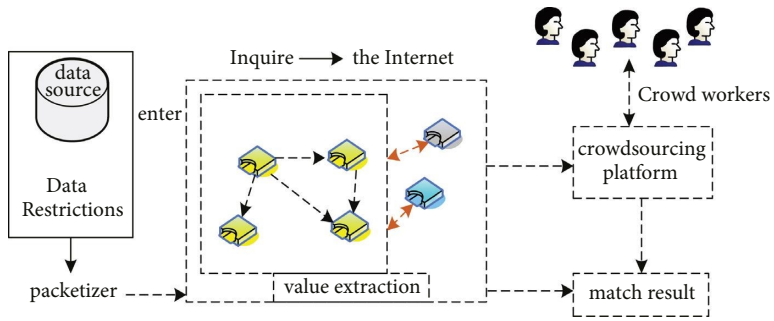

Figure 5: Internet- and crowdsourcing-based matching framework.

$$qk(s,h) \longrightarrow d\Big|(y) = \begin{cases} q(s,h), & \text{if } d_c^y = d, \\ \eta(s,h,y,d)\cdot(1-q(s,h) & \text{otherwise} \end{cases}. \tag{12}$$

$q(s,h)$ is the accuracy of (s,h), d_c^y is the correct value to fill in b, and $\eta(s,h,y,d)$ is the probability that (s,h) provides a wrong value for y and the wrong value is d. However, it is not known which value is correct, so equation (12) cannot be calculated for the time being. Here, an iterative EM method is used to estimate the accuracy of each combination of (s,h), that is, estimate $q(s,h)$. A strategy for carrying out maximum likelihood estimation in the context of latent constructs is the expectation-maximization method. To achieve this, the models are first optimized, then the latent constructs values are estimated, and so on until convergence. The Gaussian Mixture Model and other clustering methods frequently use this efficient and all-encompassing method for densities estimate using incomplete information.

$\overrightarrow{D}^y = [d_{1,1},\cdots d_{j,i}\cdots d_{n,m}]$ is represented as a padding y vector of all filled values (including duplicates) scraped from the website, where $(s_j,h_i)(1\le j\le n, 1\le i\le m)$ is the value returned by site-crawler combination 3, then the joint distribution for all filled values for y is:

$$qk\left(\overrightarrow{D}^y|d_c^y = d,(y) = \prod_{(s_j,h_i)\in WH} qk\left((s_j,h_i)\right) \longrightarrow d_{j,i}\,|\,d_c^y = d, y\right). \tag{13}$$

The goal of the EM method is to find a v that maximizes $qk(\overrightarrow{D}^y|d_c^y = d, y)$. Specifically, the derivation steps are as follows:

E-step: At the E-step, given the set of filled values $\overrightarrow{d}^y$ for each missing value y, the probability of $d_c^y = d$ can be calculated by the following Bayes rule:

$$qk\left(d_c^y = d|\overrightarrow{D}^y, y\right) = qk\left(\overrightarrow{D}^y|d_c^y = d, y\right)\bullet qk(d_c^y = d, y) \sum_{D'\in\left|\overrightarrow{D}^y\right|} qk\left(\overrightarrow{D}^y|d_c^y = d, y\right). \tag{14}$$

$\left\{\overrightarrow{D}^y\right\}$ is the set of all distinct values in D^y. In the first E-step, all $qk(d_c^y = d, y)$ are given a uniform prior probability so that we do not need to consider prior knowledge of the correct value.

M-step: During the M-step, the value of y is updated to replace the value of d_c^y, and then $qk(\overrightarrow{D}^y|d_c^y = d, y)$ is maximized among all alternative values, which is:

$$\hat{d}_c^y = \operatorname{argmax} qk\left(d_c^y = d|\overrightarrow{D}^y, y\right). \tag{15}$$

Then, the following formula is used to update all $q(s,h)$.

$$q(s,h) = \frac{\sum_{((s,h)\longrightarrow d_c^y|y\in Y} qk\left(d_c^y = d|\overrightarrow{D}^y, y\right)}{\sum_{((s,h)\longrightarrow d_c^y|y\in Y^1}}. \tag{16}$$

This formula represents the average probability that treating (s,h) as (s,h) provides the correct value for Y. E-steps and M-steps are performed alternately until all $q(s,h)$ have reached a stable value.

$$qk((s,h)\longrightarrow d|y) = \begin{cases} q(w)\cdot K(h), & \text{if Trube} = d \\ \eta(s,h,y,d)q(s)(1-q(h)), & \\ +\eta(s,h,y,d)k(1-q(s), & \text{otherwise} \end{cases}. \tag{17}$$

Among them, $q(s)$ is the accuracy rate of website s, $q(h)$ is the accuracy rate of crawler h, and $K(h)$ is the recall rate of crawler h.

4. Sampling Experiment of Digital Art Education in the Environment of "Internet+"

4.1. Data Sampling of College Art Course Syllabus

4.1.1. Data Collection and Teaching Staff. This study adopts the method of purpose sampling, and collects the syllabus of College Aesthetic Education major art courses in major colleges and universities through Internet search, direct access to teachers and families, and indirect access to friends. According to China's regulations on curriculum setting, all courses in the teaching plan should have corresponding syllabus. However, in fact, in the process of collecting the syllabus of art courses for College Aesthetic Education majors in major colleges and universities, this article found that some formal undergraduate colleges did not write curriculum teaching in the compulsory art courses specified in the College Aesthetic Education curriculum teaching plan, that is, there is no course syllabus written in text form [17, 18].

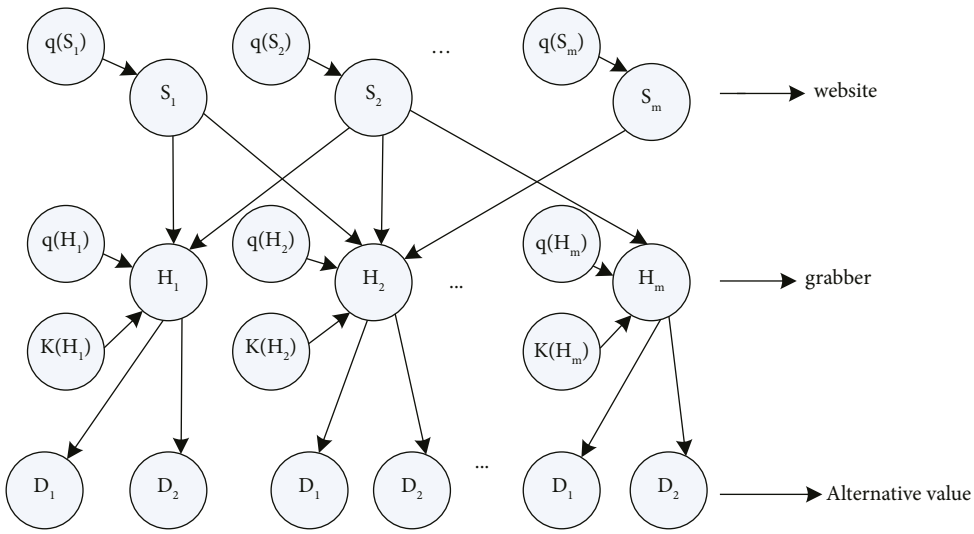

Figure 6: Internet-based data quality control model.

This paper selects colleges and universities in different provinces and cities as samples for collection. During the collection process, about 20 undergraduate colleges and universities with College Aesthetic Education majors were learned. However, among these 20 undergraduate colleges and universities, this paper only collects 12 undergraduate colleges and universities that have written syllabus texts for art courses in College Aesthetic Education, accounting for 60% of the total sample size. Relevant personnel from eight undergraduate colleges said that the school did not write a textual syllabus for College Aesthetic Education majors in art courses, accounting for 40% of the total sample size.

This paper finds that among the eight undergraduate colleges that have not compiled the syllabus of art courses for College Aesthetic Education (Note: School names are coded with numbers), there are 1985 colleges, 1211 colleges, 4 first-level key colleges, and 2 ordinary second-level colleges. As shown in Table 2, the locations of these eight undergraduate universities are: East China, North China, Northeast China, Central China, and Southwest China. It can be seen that there is a phenomenon that undergraduate colleges and universities at different levels in different regions of our country do not pay attention to the text compilation of art courses in colleges and universities, as shown in Table 2.

4.1.2. Types and Distribution of Schools. According to the type and distribution of these 12 undergraduate colleges and universities, this study will conduct statistics on the types and regions of the 12 colleges and universities obtained by sampling, as shown in Figure 7. The sampling subjects of this study are 12 undergraduate colleges and universities, and the selected sample is the syllabus of art courses for College Aesthetic Education majors in 12 colleges and universities.

From the perspective of regional distribution, among the 12 colleges and universities, 2 normal universities are located in North China, 2 normal universities, and 1 comprehensive university are located in East China. There are 2 normal universities, 1 normal college, and 1 comprehensive university in central China. There are 2 normal universities in Southwest China and 1 normal university in South China. From the perspective of distribution area, the 12 institutions of higher learning are mainly in Central China and East China. This is not intentional, but is completely selected according to the convenience of collecting samples, the pertinence of sampling and the mature years of colleges and universities to cultivate College Aesthetic Education majors. It is not collected according to the status quo of economic development in various regions of China and the overall distribution of colleges and universities enrolling College Aesthetic Education majors [19].

In terms of school types, among the 12 institutions of higher learning, there are 9 normal universities, 1 normal college, and 2 comprehensive universities. The sample conforms to the training units in China that recruit undergraduates majoring in College Aesthetic Education, with normal colleges and universities as the main body. The syllabus of art courses for College Aesthetic Education undergraduates in 12 colleges and universities can basically represent the current situation of the syllabus of College Aesthetic Education undergraduate art courses in Chinese colleges and universities. Therefore, the sampling of this study is representative and typical, which also lays the foundation for further in-depth analysis of this study [20].

4.1.3. The Length and Form of the Syllabus. From the perspective of detail, the art courses of each school are different, so the number and size of the collected syllabus documents are also uneven. In this paper, 12 colleges and universities are coded in the form of A–L letters, and they are sorted and analyzed, as shown in Figure 8. It can be seen that the total number of words in the syllabus of the College Aesthetic Education major art courses in these 12 undergraduate colleges and universities is quite different. For example, the number of words in school J is the largest, reaching 10,953 words, while the total number of words in the syllabus of art courses in school E is only 560

Table 2: Eight undergraduate colleges and universities without preschool art course syllabus.

School name	1	2	3	4	5	6	7	8
School grade	985	Second	First	Second	First	First	First	211
Whether the school	No	Yes	Yes	Yes	Yes	No	Yes	No
Your area	Huadong region	North China	North China	North China	North-east area	Central China	South China	Southwest region

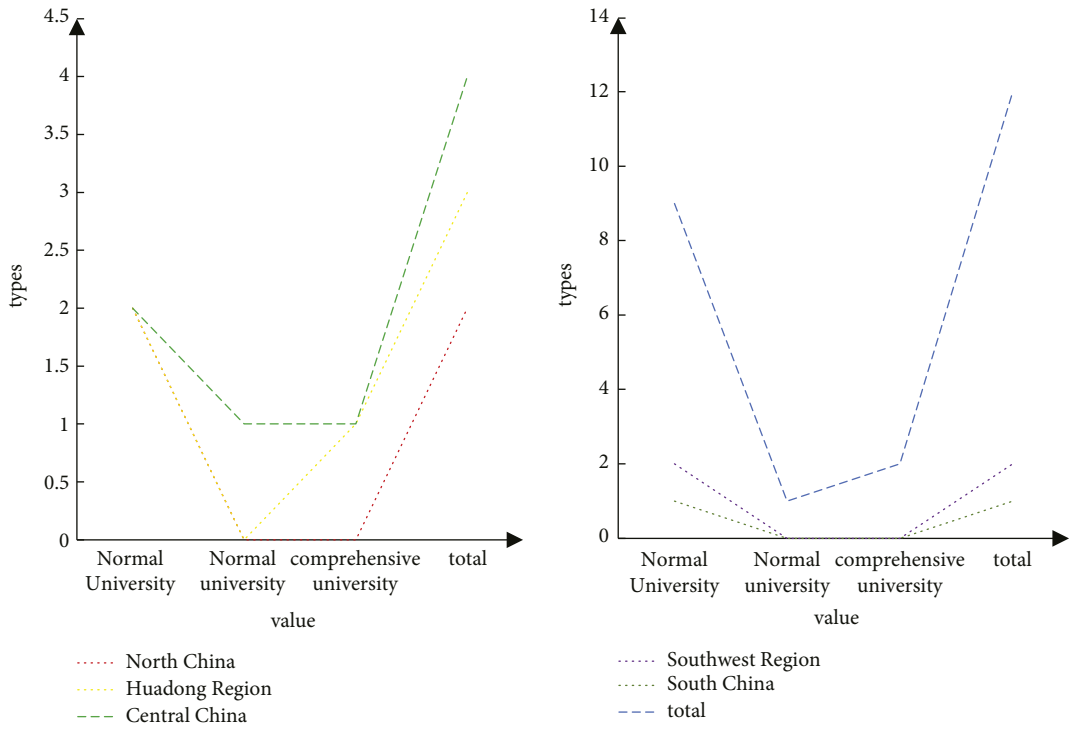

Figure 7: Statistical chart of types and distribution of 12 institutions of higher learning.

words, the J school is about 19 times that of the E school. Due to the difference in the opening time of each school's curriculum, the number of syllabus documents in each school is also different, such as A, I, H, D, B, C, the number of documents is consistent with the number of semesters in which the course is offered. Of course, there are exceptions, for example, the preschool art courses for K, B, and G are all two semesters long, but they are all written as one document.

In addition, it can also be seen from Figure 9 that the 12 undergraduate colleges and universities have different durations for preschool professional art courses [21]. For example, A only offers one-semester art courses, while H, E, D, B, L, and C all offer two-semester art courses, while I, G, F, J, and K offer three-semester fine arts program. This also shows that each school pays different attention to the art courses of College Aesthetic Education majors.

Based on the above, it can be seen that there are still huge differences in the art courses of preschool majors in Chinese undergraduate colleges. From the difference in the structure and length of the syllabus, it can be seen that some colleges and universities have written relatively detailed and explained the requirements and standards for the course content as clearly as possible. However, some colleges and universities are relatively perfunctory, and there is insufficient attention to the course. It can also be seen from the way of writing that Chinese preschool art courses are generally divided into a combination of theoretical knowledge and practical skills, and the opening hours and semesters are different, which also reflects the reform of preschool teachers in colleges and universities. The learning of art courses is a process of time accumulation and skill training. It not only allows students to understand systematic art knowledge, but also requires students to strengthen the learning and training of skills on the basis of understanding knowledge. Art courses for College Aesthetic Education majors are to train preschool teachers who will be engaged in College Aesthetic Education in the future. They should also learn basic art system knowledge and basic art skills, which also require a certain amount of training to master.

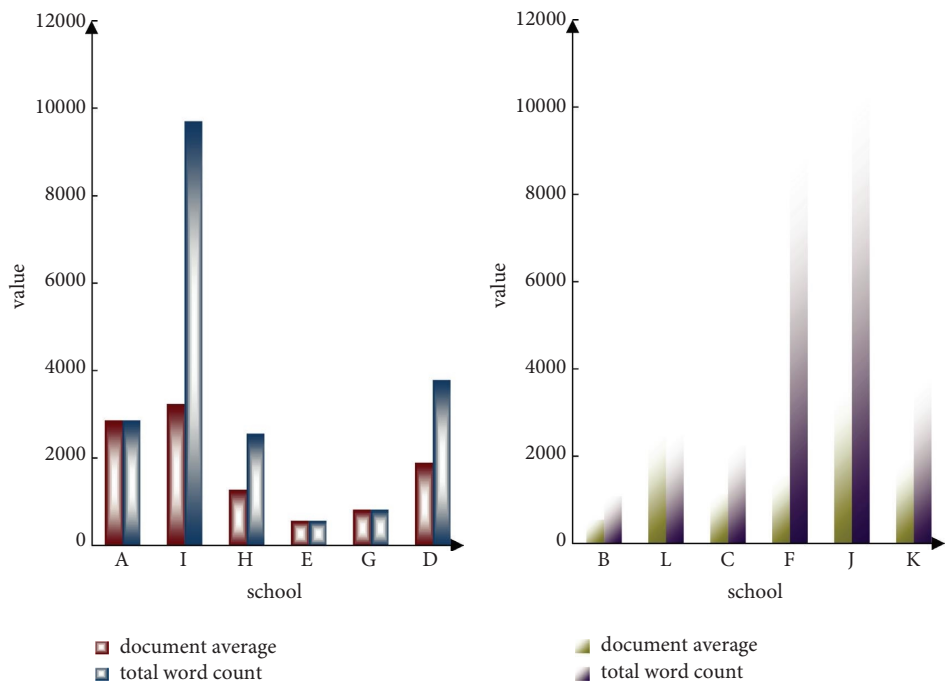

Figure 8: Word count chart of 12 pre-undergraduate professional art course syllabus documents.

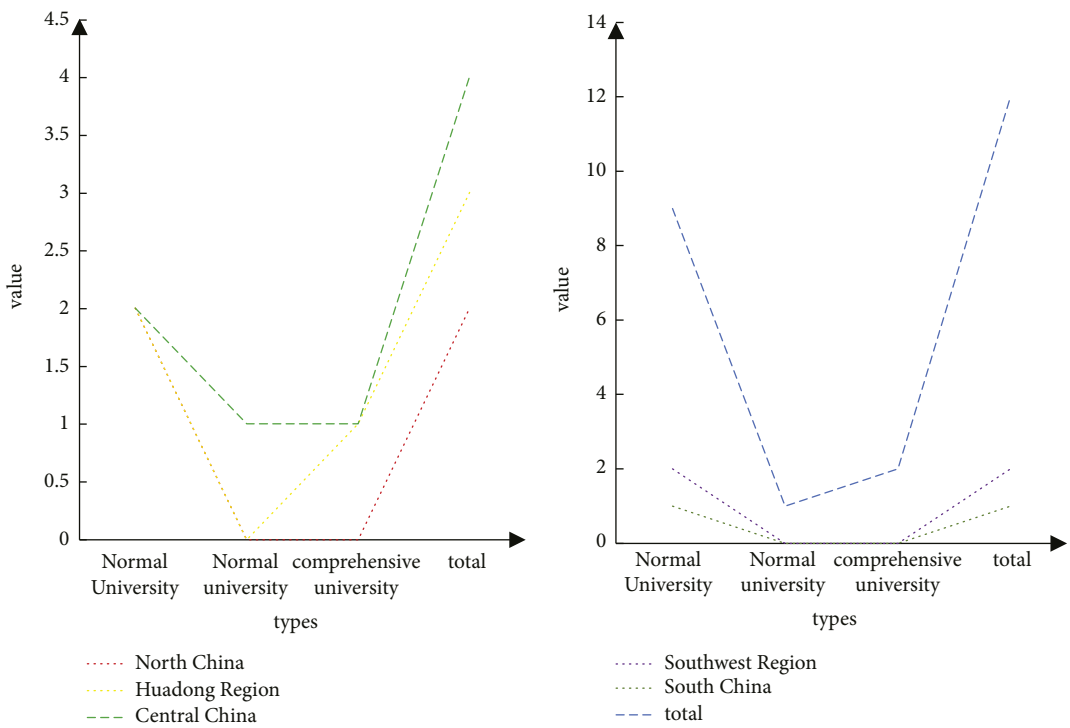

Figure 9: A line chart of the semester opening of 12 pre-undergraduate professional art courses.

4.1.4. Structural Elements of the Syllabus. Due to the different training conditions and goals of various colleges and universities, the elements of each part of the syllabus of art courses for College Aesthetic Education majors are also different. Statistics were made according to the first-level titles and their word frequencies in the 12 syllabuses of art courses for College Aesthetic Education majors in undergraduate colleges and universities. For "Course Introduction," "Course Basic Information," "Course Nature and Tasks," "Teaching Purpose, Course Objectives, Teaching Purpose and Tasks," the statistical results are shown in Table 3. The statistical results of "teaching content and requirements, and arrangement of teaching chapters" are shown in Table 4 [22].

Table 3: Main content words and frequency statistics of the syllabus of art courses for college aesthetic education majors in 12 colleges and universities.

First-level title	Syllabus and alias	Frequency of use	Total
Course nature	Basic course information	6	8
	Course nature and tasks	2	
Teaching objectives	Teaching goals and tasks	5	11
	Teaching purpose and requirements	3	
	Teaching purpose, course goal	3	

Table 4: Main content words and frequency statistics of the syllabus of art courses for college aesthetic education majors in 12 colleges and universities (b).

First-level title	Syllabus and alias	Frequency of use	Total
Teaching content	Teaching chapter content	2	9
	Teaching content and arrangement	4	
	Teaching content and requirements	3	
Teaching method	Teaching requirements and methods	2	8
	Suggestions on teaching methods and methods	2	
	Teaching methods and means	2	
	Teaching organization and arrangement	2	

Table 5: Main content words and frequency statistics of the syllabus of art courses for college aesthetic education majors in 12 colleges and universities.

First-level title	Syllabus and alias	Frequency of use	Total
Class hour allocation	School hours	7	8
Assessment method	Course assessment and evaluation	4	11
	Teaching assessment methods and grades	6	
	Learning process record	1	
Other	Link to related courses	2	2

Among the 12 syllabuses of art courses for College Aesthetic Education majors in colleges and universities, only 8 syllabuses explained the "basic information and course nature" of their courses; 8 syllabuses mentioned "teaching methods and means"; the 11 syllabuses all involve the positioning of "teaching objectives," and only 7 syllabuses clearly stipulate the specific "hour allocation" of art courses; 11 syllabuses stipulate their "reference lists," and 7 syllabuses clarify the connection with related courses, the relationship with other courses, teaching equipment and facilities, teaching week assignments, syllabus instructions and other details. All the syllabuses clearly pointed out the description of "the method of performance evaluation and assessment," and the statistical results are shown in Table 5.

The above data show that the syllabus is formulated by the colleges and universities themselves, and each college has its own opinion on the content that should be involved in the syllabus of art courses for College Aesthetic Education majors and has its own emphasis on the elements, which makes the elements of the current syllabus of art courses for undergraduates majoring in College Aesthetic Education not completely unified, even incomplete and systematic. However, most syllabuses can still cover some core elements of the syllabus, such as course nature, teaching objectives, teaching content and time allocation, teaching methods and means, and assessment methods. Although it can reflect the training characteristics of undergraduates majoring in College Aesthetic Education, it still needs to be further standardized and improved.

4.2. Contents of the Syllabus of Art Courses for College Aesthetic Education Majors in 12 Undergraduate Colleges and Universities. As can be seen from Figure 10, in the College Aesthetic Education major art courses offered by 12 undergraduate colleges and universities, the knowledge and skill objectives appear most frequently, that is, to master art skills and techniques (11 times). Followed by the process and method goals, namely practical ability (6 times), creative ability (6 times), and appreciation ability (5 times). The goals of emotion, attitude, and values were the least frequently used among all goal statements, almost only passing by. For example, "to form a correct aesthetic view, develop a healthy personality, show a positive interest in painting, like to use art to express children's life, and cultivate the morality of truth, goodness and beauty through art courses." These goals appear only once in the syllabus of individual colleges and universities. It is not difficult to find that the teaching objectives of art courses in College Aesthetic Education are still to focus on knowledge and skills and ignore emotions,

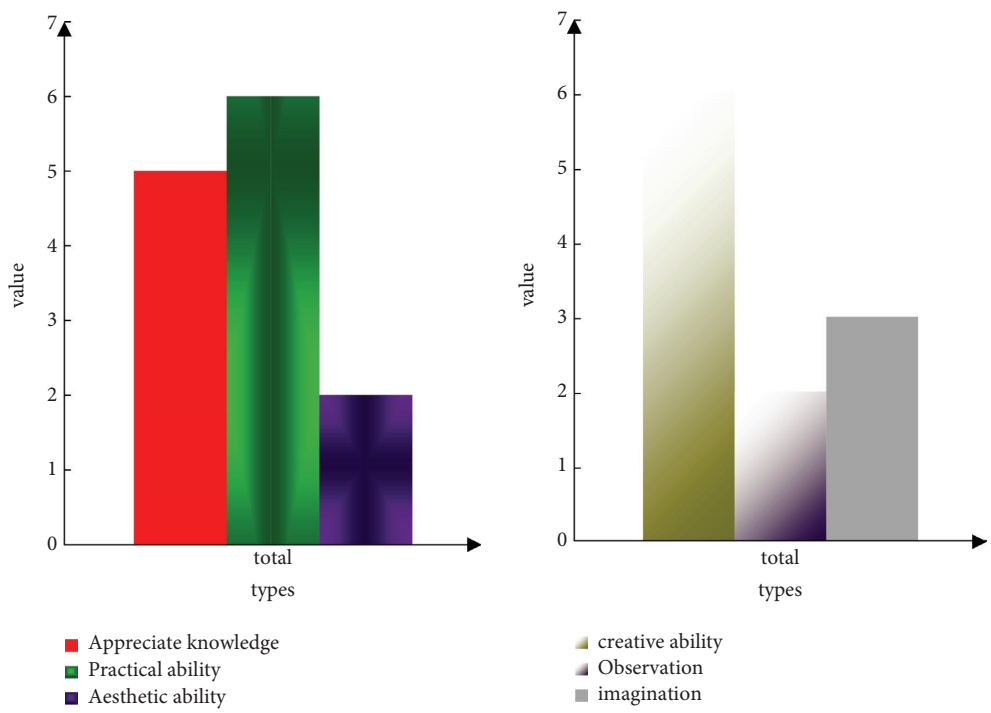

Figure 10: Coding summary of teaching objectives of art courses for college aesthetic education majors in 12 colleges and universities.

attitudes, and values. As stated in the nature of the course, the fine arts course is a practical course for the training of skills and skills for the College Aesthetic Education major.

5. Conclusions

Collecting the syllabus of art courses in 12 colleges and universities for investigation and analysis, from the perspective of static text, it reflects the current value orientation and problems of art courses for College Aesthetic Education undergraduates in China's higher normal colleges and universities. The study found that due to the influence of many factors, the syllabus of art courses for College Aesthetic Education majors in colleges and universities has some practical problems such as deficiencies and functional deficiencies in terms of course objectives, course content, course implementation, and evaluation. However, with China's concern for education, scholars' appeals, and the updating and improvement of the educational concepts of higher education institutions, these problems will be solved, and China's College Aesthetic Education will continue to develop and grow.

Data Availability

The data used to support the findings of this study can be obtained from the corresponding author upon reasonable request.

Conflicts of Interest

The authors declared no potential conflicts of interest with respect to the research, authorship, and/or publication of this article.

Acknowledgments

This work was supported by the education and teaching reform project no. hnjg2020-22 of the Colleges and Universities in Hainan Province and the education and teaching reform research project no. hdjy2032 of Hainan University.

References

[1] Y. Yang, "Teaching research on higher vocational pre-school education of professional art course based on innovation and entrepreneurship education," *Creative Education*, vol. 9, no. 5, pp. 713–718, 2018.

[2] L. Hanfei, "Innovative research on the teaching mode and method of art design course under the environment of advanced information technology," *Boletin Tecnico/Technical Bulletin*, vol. 55, no. 19, pp. 83–90, 2017.

[3] F. Blaikie, "Worlding Danny: being, becoming, and belonging," *Studies in Art Education*, vol. 61, no. 4, pp. 330–348, 2020.

[4] A. Nacak and Y. Yucesoy, "Art education for communication in the society: a content analysis," *Revista Tempos e Espaços em Educação*, vol. 13, no. 32, pp. 1–15, 2020.

[5] J. L. Nelson, D. A. Lewis, and R. Lei, "Digital democracy in America: a look at civic engagement in an internet age," *Journalism & Mass Communication Quarterly*, vol. 94, no. 1, pp. 318–334, 2017.

[6] S. Papagiannidis, E. W. K. See-To, D. G. Assimakopoulos, and Y. Yang, "Identifying industrial clusters with a novel big-data methodology: are SIC codes (not) fit for purpose in the Internet age?" *Computers & Operations Research*, vol. 98, pp. 355–366, 2018.

[7] J. Q. Li, F. R. Yu, G. Deng, C. Luo, Z. Ming, and Q Yan, "Industrial internet: a survey on the enabling technologies,

applications, and challenges," *IEEE Communications Surveys & Tutorials*, vol. 19, no. 3, pp. 1504–1526, 2017.

[8] V. Zagkotas and I. Fykaris, "Approaching the "Death of Socrates" through art education A teaching proposal and the introduction of a new typology for teaching with similar artworks," *Journal of Classics Teaching*, vol. 23, no. 45, pp. 60–72, 2022.

[9] M. Morari, "Number 13/Part I. Music. 1. The laws of musical art as a resource for the early education methodology," *Review of Artistic Education*, vol. 13, no. 1, pp. 7–16, 2017.

[10] M. A. Kang, "Theoretical study on the field of dance education in the education of art," *The Journal of Korean Dance*, vol. 36, no. 2, pp. 239–266, 2018.

[11] A. Özdemir, "Where are we in the art education required? Looking at life through the eyes of art," *Art and Design Review*, vol. 09, no. 02, pp. 123–130, 2021.

[12] A. Corell-Almuzara and J. Lopez-Belmonte, "Covid 19 in the fie1d of education state of the art," *Sustainability*, vol. 13, no. 10, pp. 1–17, 2021.

[13] S. K. Hong, "Teachers' roles in the practice of art education for life: art classes that reflect students' lives," *Journal of Research in Art Education*, vol. 22, no. 1, pp. 83–115, 2021.

[14] O. Malytska, "Developmental potential of artistic synthesis in the art education of a future teacher," *Educational Discourse: Collection of Scientific Papers*, vol. 28, no. 11, pp. 61–69, 2020.

[15] X. Li, M. Kagita, and R. L Kumar, "Machine learning techniques for multi-media communications in business marketing [J]," *Journal of Multiple-Valued Logic and Soft Computing*, vol. 36, no. 1-3, pp. 135–150, 2021.

[16] J. Y. . A. Lee, "A study on the connection between humanities and art: inquiry into the humanistic value of art education," *Journal of Research in Art Education*, vol. 21, no. 2, pp. 1–25, 2020.

[17] S. Aliyeva, "Use of examples of folk art in the artistic and aesthetic education of preschool children," *Azerbaijan Journal of Educational Studies*, vol. 1, no. 1, pp. 11–20, 2020.

[18] E. Bs, "The revision of the course of training and syllabus for the certificate of proficiency in the nursing of mental defectives," *Art and Design*, vol. 8, no. 6, pp. 689–700, 2018.

[19] A. Kolacinska, "How can we improve education of breast surgeons across europe?" *Chirurgia*, vol. 112, no. 4, pp. 365-366, 2017.

[20] S. Juneja, R. L. Kumar, Y. Yan, and Y. Zhang, "Improving college ideological and political education based on deep learning," *International Journal of Information and Communication Technology*, vol. 1, no. 1, p. 1, 2022.

[21] A A Berikbaev, "Development of competence skills of art education students," *International Journal of Psychosocial Rehabilitation*, vol. 24, no. 4, pp. 6984–6988, 2020.

[22] C. Lawrence and H. King, "Hippocrates: The "Father of Medicine" in the Internet Age (Bloomsbury Studies in Classical Reception)," *International Journal of the Classical Tradition*, Bloomsbury Academic, vol. 28, no. 2, pp. 246–248, London, 2019.

Hindawi
Mobile Information Systems
Volume 2023, Article ID 9897383, 1 page
https://doi.org/10.1155/2023/9897383

Retraction

Retracted: Analysis of Computer Visualized Sound Parameters of Vocal Music Singing Based on Deep Learning

Mobile Information Systems

Received 17 October 2023; Accepted 17 October 2023; Published 18 October 2023

This article has been retracted by Hindawi following an investigation undertaken by the publisher [1]. This investigation has uncovered evidence of one or more of the following indicators of systematic manipulation of the publication process:

(1) Discrepancies in scope
(2) Discrepancies in the description of the research reported
(3) Discrepancies between the availability of data and the research described
(4) Inappropriate citations
(5) Incoherent, meaningless and/or irrelevant content included in the article
(6) Peer-review manipulation

The presence of these indicators undermines our confidence in the integrity of the article's content and we cannot, therefore, vouch for its reliability. Please note that this notice is intended solely to alert readers that the content of this article is unreliable. We have not investigated whether authors were aware of or involved in the systematic manipulation of the publication process.

Wiley and Hindawi regrets that the usual quality checks did not identify these issues before publication and have since put additional measures in place to safeguard research integrity.

We wish to credit our own Research Integrity and Research Publishing teams and anonymous and named external researchers and research integrity experts for contributing to this investigation.

The corresponding author, as the representative of all authors, has been given the opportunity to register their agreement or disagreement to this retraction. We have kept a record of any response received.

References

[1] N. Mo, J. S. Ai, and S. Y. Ran, "Analysis of Computer Visualized Sound Parameters of Vocal Music Singing Based on Deep Learning," *Mobile Information Systems*, vol. 2022, Article ID 1121092, 9 pages, 2022.

Hindawi
Mobile Information Systems
Volume 2022, Article ID 1121092, 9 pages
https://doi.org/10.1155/2022/1121092

Research Article

Analysis of Computer Visualized Sound Parameters of Vocal Music Singing Based on Deep Learning

Na Mo,[1,2] Jin Shun Ai,[1] and Shi Yi Ran[3]

[1]*Northeast Normal University, Jilin 130000, China*
[2]*Jilin University of the Arts, Jilin 130000, China*
[3]*Jilin University, Jilin 130000, China*

Correspondence should be addressed to Jin Shun Ai; jinsa@nenu.edu.cn

Received 5 July 2022; Revised 10 August 2022; Accepted 13 August 2022; Published 12 October 2022

Academic Editor: Chi Lin

The first impression of the early historical recordings on the contemporary audience is often not ideal; the overall speed is relatively fast, the rhythm is relatively loose and free, and the strings are slippery. In recent years, a large number of research achievements have emerged at home and abroad that apply computer visualization analysis methods to music performance practice. It is feasible and necessary to gradually apply the visual audio parameter analysis method to music research and performance practice teaching. In this study, a prosody hierarchy prediction model based on the CNN (convective neural network) is proposed, and word vectors are added as semantic features. The DL (deep learning) method is applied to vocal music recognition, and a recognition method based on the DL framework is proposed by combining traditional audio signal processing methods. After introducing word vectors as features in the CNN model, the F-score value increased from 77% to 80%. The feasibility of the proposed vocal music recognition algorithm based on DL is verified by experiments.

1. Introduction

The history of vocal music art can be traced back to a long time. In Egypt, Asia Minor, and some eastern countries, especially ancient Greece, artistic singing had already existed as early as a century ago. As singing sound is a kind of compound sound, we can use acoustic instruments to analyze the sound spectrum, calculate the frequency and amplitude (sound intensity) of each component in singing sound, and display it in the form of sound spectrum. For many years, most teachers have been accustomed to correcting 'students' intonation, rhythm, and other basic problems by traditional means such as piano and metronome and involve further expressive problems through the oral description, personal demonstration, or listening to other masters' recordings [1]. Prosodic structure analysis is an important part of the speech synthesis system. Accurately predicting the prosodic boundary position and its grade of text is an important link in speech synthesis, and it is an important prerequisite and guarantee for synthesizing natural and smooth output speech. Most of the teachers and students' time and energy are often spent on such universal and basic issues as intonation, rhythm, speed, intensity, and timbre.

In music performance, the speed and rhythm parameters directly related to time have the most basic structural skeleton, which determines the basic characteristics of a particular performance and has universal validity and comparability across musical instrument types and performance forms. The computer visual analysis of music parameters is not new, such as the visual presentation of waveform diagram for the layout of playing intensity and the objective description of playing timbre and overtone distribution by spectrum diagram. Marinkovic et al. studied monosyllabic samples of French speakers under different emotions, removed the influence of prosodic features on emotions, and mainly studied the differences of sound quality parameters in different emotions [2]. Aubin and Bremond put forward a method of similarity measurement based on Aubin pitch and rhythm information and

Euclidean distance and developed a new vocal music recognition system by using this technology [3]. Senevirathna and Jayaratne divided the process of vocal music recognition into three stages, namely, pitch extraction, melody matching, and note matching and put forward three algorithms for each stage, which combined the results of the three stages to recognize vocal music [4]. Zhang et al. pointed out that, in music performance, the speed of the traditional symphony can be changed between the soil topic, subtopics, paragraphs, and even within the phrase. The importance of the relative speed relationship exceeds the importance of the composer's prescribed speed. The layout is the key to grasp the performance speed of the symphony [5]. Different prosody prediction studies are different in language, language materials, and definition of prosody level, and the evaluation methods adopted for the results are different, so we cannot directly compare the advantages and disadvantages of each model method.

Combining music teaching research with modern information technology, especially computer multimedia technology, is a general trend in the international academic frontier. In the analysis of acoustic features of emotional speech, previous studies mainly focused on the features such as fundamental frequency, sound intensity, and sound length [6] because these feature values are easy to extract by computer software, and they also play a certain role in distinguishing some emotions, but they are not enough to be the basis for accurately predicting the speaker's emotions. The denser the spectral lines on the sound spectrum, the lower the sound. The thinner the spectral line, the higher the sound. Not every harmonic has to appear in the sound spectrum. If the harmonic amplitude is zero or close to zero, a spectral line will be vacant in the sound spectrum. Based on DL (deep learning) technology, this study analyzes the sound parameters of vocal music singing with the aid of computer visualization, and the conclusions obtained through data analysis of visualization software are combined with vocal music teaching, so as to continuously deepen the artistic practice.

2. Related Work

2.1. Research on the Computer Visual Audio Parameter Analysis Method. It is the most varied parameter in vocal music singing, and it is also the most difficult factor to explain clearly through subjective description. Compared with instrumental music, vocal music teaching usually takes more time and energy to correct and adjust timbre. For beginners, the piano can certainly be a less effective and imperfect auxiliary tool. For high-level singers, if the keyboard pitch of the twelve-average law is used as an absolute reference standard for a long time, it is likely to destroy the sense of intonation which should be an expressive factor.

Vall et al. introduced a method to discuss the two most important dimensions of music performance, namely, speed and intensity in the same visual model, which has been widely used in the research of music expression and performance style pattern recognition [7]. McFee et al. proposed a bidirectional echo hiding algorithm [8] by using the front masking phenomenon of human hearing. The audio generated by this method has good auditory transparency, but the accuracy of extracting secret information will decrease with the decrease of echo amplitude. The minimum distortion embedding framework proposed by Bisharad and Laskar lays the foundation for the research of mainstream adaptive steganography algorithms in recent years [9]. Hu et al. gave the carrier elements with large differences between the original audio and the compressed and decompressed reconstructed audio a higher embedded distortion cost [10].

Music alignment technology is particularly important in automatic accompaniment, which can synchronize accompaniment and singing. Automatic accompaniment is to use computer algorithms and knowledge of music arrangement to generate music through some logic. Zhang proposed the modeling problem of inferring note events by identifying the duration of music [11]. Zhang proposed to add asynchronous compensation in audio note alignment to solve the problem of the local alignment error caused by the unsynchronized playing of music melody [12]. Murthy and Koolagudi proposed an alignment framework between audio and MIDI (musical structure digital interface) notes based on spectrum decomposition and dynamic time warping [13]. Lerch et al. put forward linear scaling matching at the level of vocal singing sentences and obtained the optimal path through the dynamic programming algorithm, which overcame the disadvantage that dynamic programming might lose the global optimal path in long path search [14].

2.2. DL-Related Technology. DL (deep learning) is an important branch of machine learning. It is called the prototype of the artificial neural network model, which opens a precedent for scholars to study the artificial neural network model. However, due to the limitation of computer hardware, the later DL research developed slowly, and as a marginal discipline, it did not attract the attention of scholars. However, some theories put forward during this period still guide the development of today's discipline.

Tsagkaraki et al. put forward the perceptron model, which is the first model that can learn feature weights according to sample data [15]. Pouyanfar et al. proposed a backpropagation algorithm, which greatly reduced the time required for training neural networks. While the neural network training algorithm is improved, the rapid development of computer technology also makes the computing power increase by leaps and bounds [16]. Pouyanfar et al. improved the Gaussian mixture model by using the five-layer DBN (deep belief network) structure and achieved remarkable improvement in speech recognition accuracy. The feedforward sequential memory network is used to model sentence speech signals through multilayer convolution layers, and the long-term related information of speech is summarized and expressed, which improves the recognition rate by more than 15% on the basis of the best two-way recurrent neural network speech recognition system in academia and industry [16].

Kim et al. proposed an algorithm to recognize transcribed songs by using the CNN (convective neural network) and trained the CNN model by using cross-similarity matrix generated from a pair of songs as input [17]. Meng et al. put forward a note following system based on chromaticity features and the DTW (dynamic time warping) algorithm, which is used to assist the computer to turn pages automatically [18]. Carter and Briens used the method of layer-by-layer training based on the greedy algorithm to effectively reduce the training difficulty of the multilayer neural network [19]. With the improvement of computing power and training methods, people can further exert the learning ability of multilayer neural networks to solve complex tasks. Güder and Içekli proposed to use the one-dimensional CNN for end-to-end audio steganalysis [20]. Compared with the audio steganalysis algorithm based on feature design, the detection effect is obviously improved.

3. The Research Method

3.1. DL and Audio Analysis. It is the most varied parameter in vocal music singing and the most difficult variable to explain clearly through subjective description. For different singing methods, different singers, and different styles of music works, there is no correct timbre; timbre is always in constant dynamic change. For example, on the commanding point of melody (vowel I), the four versions all have different degrees of timbre brightening and nonmusical components (mainly consonants, lips and teeth rubbing, breath sounds, etc.) tend to increase, etc. Due to the modulation of vocal tract resonance, its overtone amplitude gradually decreases with the increase of its frequency, which will be changed by the selectivity of vocal tract. In the process of training and recognition, it is necessary to detect the starting point of the note, intercept the dataset from the starting point of the note, eliminate the interference of silent noise, and improve the validity of the data.

Compared with traditional machine learning, the biggest advantage of DL is that it can extract nonlinear information from complex data, and it does not need tedious feature engineering. Therefore, for the music recommendation studied in this study, we will explore whether DL has more advantages in learning music-related features than traditional machine learning. Audio files store the waveform information of music signals, while MIDI files store music in the format of binary sequences. Instead of outputting any music signals, they send control information instructions to sound sources for playing music, so playing MIDI with different sound sources will generate music with different timbres.

Constructing a good steganalysis feature greatly depends on the experience and knowledge of steganalysis researchers and the degree of mastering the side information such as carrier model and the steganalysis algorithm. Generally speaking, the lower two peaks, namely, the first formant and the second formant, basically define the vowel tone of sound, while the higher third formant, fourth formant, and fifth formant affect the personal characteristics and musical tone of sound.

The CNN is a kind of deep neural network, which was first used in the image field. Among them, the convolution layer can be regarded as a feature extractor based on sliding window, and each neuron in the convolution layer receives the local feature information from the previous level. The CNN convolution layer, the pool layer, and its activation function transform the input data into abstract feature vectors, and the full connection layer is the marker vector that transforms the feature vectors into the expected values of the data. Figure 1 shows the structure of the CNN, including the input layer, the convolution layer, the pool layer, the full connection layer, and the output layer.

In the latest progress, DL-based recommendation has overcome the obstacles of the traditional linear model, thus significantly improving the quality of recommendation. DL can effectively capture the nonlinear relationship between users and goods and obtain the vector representation of users or goods through vectorization or coding.

The combination of multiple perceptrons is a perceptron, while the neural network is actually a perceptron model with one or more hidden layers. The supervision information in the training stage of classifier can guide the learning of steganalysis features. The overall framework of the vocal music recognition framework based on DL is shown in Figure 2.

The training dataset is input into the vocal music recognition neural network, and the training is carried out in batches. After each iteration, the loss function value is calculated by using the verification set, and the training is stopped after reaching a certain accuracy requirement. The performance of the neural network is tested and evaluated by appropriate evaluation indexes, which can be used as the basis for repeatedly adjusting the training process and parameter selection of the neural network. One can also use a set of model parameters trained by the neural network training module to test the network performance and the end-to-end test of the prototype system on different data sets.

Pre-emphasis digital filter: this kind of filter has the ability to improve the high-frequency characteristics, and it often uses a first-order digital filter. After pre-emphasis, the audio signal can be expressed as follows:

$$H(Z) = 1 - \mu Z^{-1}, \tag{1}$$

where Z is the input vocal singing signal and μ is called the pre-emphasis coefficient, and its value is usually a fraction slightly less than 1. The value used in this experiment is 0.94.

If the signal-to-noise ratio of vocal music singing signal is high, the starting point of vocal music singing can be determined by using short-term energy characteristics. Considering that the signal-to-noise ratio is difficult to reach a high level in practical application, the short-term average zero-crossing rate is further used to assist judgment.

In this study, the double threshold method is used to detect the starting point. The double-threshold method first examines the short-term energy of vocal music singing signal, and the short-term average energy E_n of the voice signal at n time is as follows:

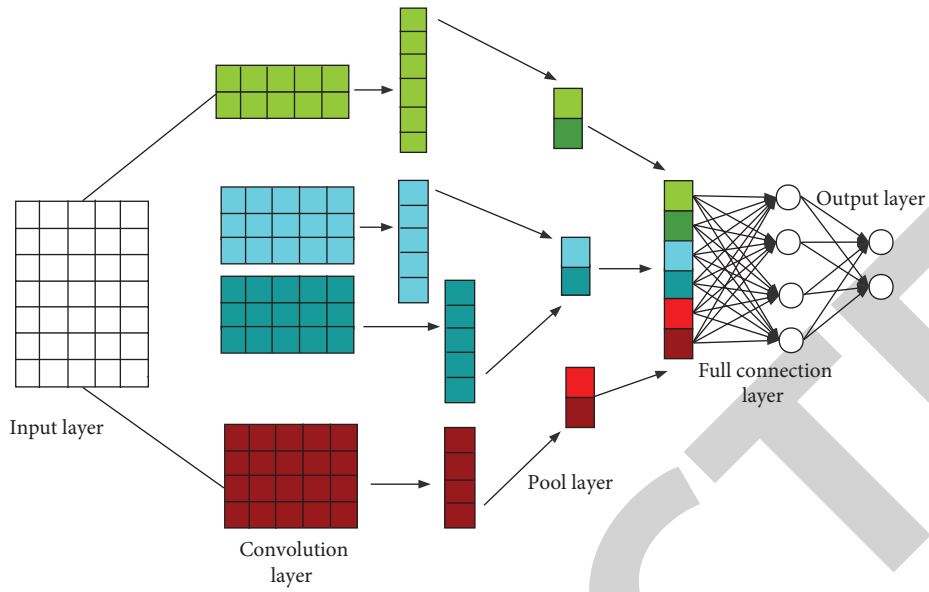

Figure 1: CNN structure diagram.

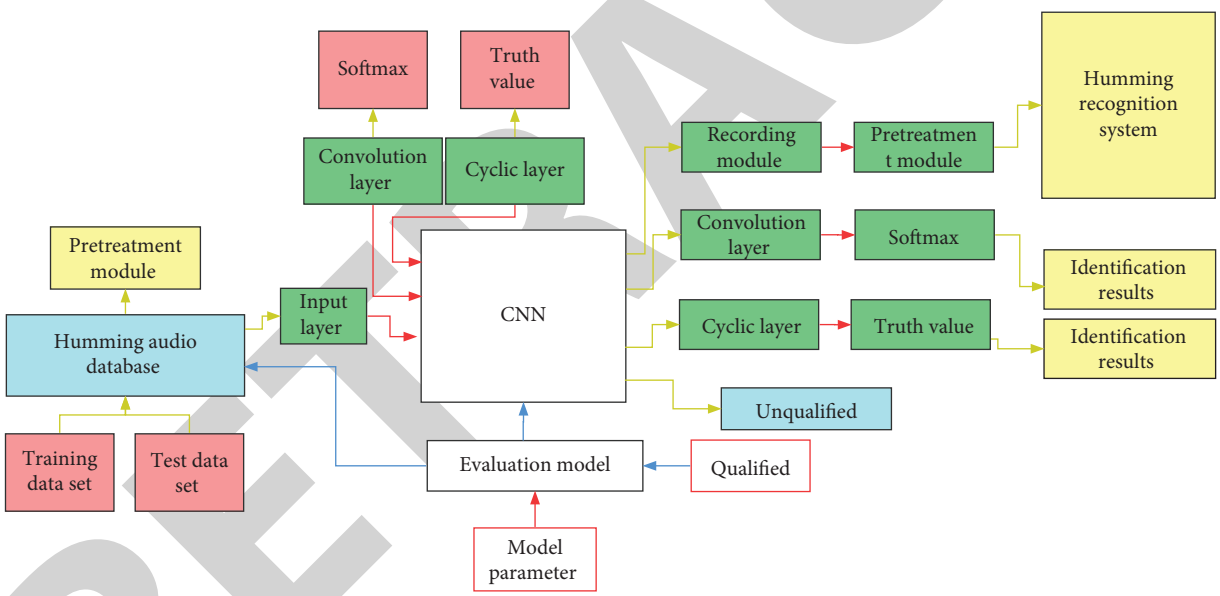

Figure 2: The DL framework of vocal music recognition.

$$E_n = \sum_{m=-\infty}^{\infty} x(m)^2 * h(n-m), \tag{2}$$

where x is the input signal and h is the weight.

HNR (harmonics-to-noise ratios) describes the ratio of the periodic part to the noise part of a speech signal, which mainly reflects the hoarseness of the voice. The autocorrelation function $r(x)$ of the speech delay signal q is defined as follows:

$$r(x) = \int s(t)s(t+x)dt, \tag{3}$$

where $s(t)$ is a stable time signal, and the function takes the global maximum when $x = 0$ is taken.

The glottic waveform diagram shows the difference between the maximum and minimum amplitude in a period. The larger its value, the greater the amplitude of glottic vibration. First, we use linear predictive coding inverse filtering to get the glottic wave and then extract this parameter from the glottic wave. The most common expression of linear predictive model is as follows:

$$\hat{x}(n) = -\sum_{i=1}^{p} a_i x(n-i)\hat{x}(n) = -\sum_{i=1}^{p} a_i x(n-i), \tag{4}$$

where $\hat{x}(n)$ is the predicted signal value, $x(n-i)$ is the previously observed value, and a_i is the prediction coefficient.

Because different users listen to songs for different times, and in order to eliminate the influence of data among users, we normalize the rating data with the maximum value and the minimum value. That is, for the j th element R_{ij} of the i th row in the scoring matrix R, as shown in the following formula:

$$\widehat{R}_{ij} = \frac{R_{ij}}{\mathrm{Max}\left(R_{ij}\right)}, \tag{5}$$

where $\mathrm{Max}(R_{ij})$ represents the maximum value in the i th row of elements and $\widehat{R}_{ij}$ represents the normalized score matrix.

3.2. Note Endpoint Extraction of Audio Signal. Time-related dimensions, such as rhythm, beat, and speed, are the most universal fundamental elements in all forms of music performance, and vocal singing is no exception. They are often used as an important means to outline the structure of music, express mood and expression, and convey the rhythm of a particular style. We can visually present and compare the abovementioned special laws quantitatively and intuitively. It will probably become one of the most important methods of this kind of learning to analyze the sound parameters qualitatively and quantitatively by the visual method. Obviously, if traditional methods such as constant metronome are still used as auxiliary teaching methods in daily teaching, it is unlikely that these deep-seated factors closely related to the second creation of music performance will be directly touched.

Generally speaking, the more compatible the stage environment is with the work, the more realistic the performance of the whole opera is, and it gives people the feeling of being there. In Turandot, in order to achieve this effect, Puccini also made great efforts to create a Chinese stage and bring the audience back to the time when the story happened. At that time, Puccini had only a synopsis of the story, and in order to meet the needs of opera performance, he recreated monologues and lyrics in other ways, making the Chinese style of his works more prominent. In the whole opera, Puccini made six variations on jasmine flower according to the needs of the plot of Turandot. Some of these passages are long, some are very short, and even there is only one line. Some only use solo and chords to express deep silence, while others use orchestra ensemble and chorus to highlight the grandeur. Macroscopically and microscopically, it is a rough and delicate Chinese life.

Excellent music performance itself should not only take "accuracy" as the first pursuit just to respect the spirit of the music score and the original work but also to have some reasonable and meaningful "deviations" from the music score. The elastic expansion and contraction of speed and rhythm is inevitable in any case, and there is only a difference in degree, but there is no difference between there and there. On such a small microscale, the fluctuation of speed has actually changed into the rhythm relationship between sound and sound. Instead of examining the tightness of speed pulsation, it is better to study which sound is longer and which sound is shorter, which can more intuitively and effectively reflect the expansion and contraction of microrhythm.

Without considering the features, the linear model is first used to train the coefficients of linear model fusion. We select the following exponential loss function during training:

$$L(y, f) = e^{-yf(x)}. \tag{6}$$

where $y \in \{-1, 1\}$ and f is the output value of the classifier.

The steganalysis noise caused by steganography is usually much weaker than the content information of the carrier itself. Therefore, using ReLU activation in the shallow layer of the neural network constructed for steganalysis task may lose the negative area information and introduce a large amount of carrier content information in the positive area. It is close to saturation, and the gradient value of the activation unit is close to 0, which is prone to gradient disappearance. Therefore, we introduce the linear truncation activation unit TLU in the first convolution layer of the network as follows:

$$TLU(x) = \begin{cases} -T, & x < -T, \\ x, & -T \le x \le T, \\ T, & x > T. \end{cases} \tag{7}$$

The characteristics of audio signals are nonstationary, and successive notes are superimposed and not hidden from each other, so the end points of notes cannot be directly detected from the time-frequency domain characteristics of audio signals.

The common practice is to convert audio frames into feature sequences that can highlight the starting point of notes after preprocessing. There are two main algorithms, namely, algorithms based on the probability model and algorithms based on signal features. Figure 3 shows a two-way LSTM (Long short-term memory) model with the attention mechanism.

The short-term features are learned by bidirectional LSTM, and then, the attention of the feature vectors output by the cyclic neural network is calculated by the attention mechanism. The calculation formula is as follows:

$$u_i = \tanh\left(W_i \cdot h_i + b_i\right). \tag{8}$$

where h_i is the output of bidirectional LSTM, W_i is the weight matrix, b_i is the offset value, and h_i is calculated by the simple neural network to get its hidden state u_i.

In the scenario of multiclassification steganalysis, the secret carrier generated by the unknown type of steganography algorithm can be regarded as an abnormal sample [18]. The purpose of anomaly detection is to detect the sample points in the dataset that do not meet expectations. CNN networks that solve classification problems often set the Softmax activation layer at the end, and its output can be regarded as the prediction probability $p(m^k)$ of each classification category. From this, we calculate the entropy value $H(m)$ of the output prediction probability of the multi-classification network:

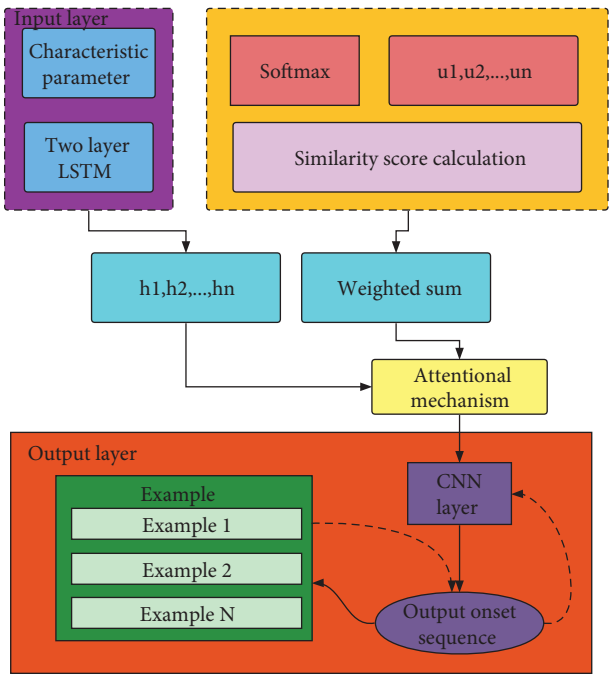

Figure 3: The network model based on attention mechanism.

$$H(m) = -\sum_{k=0}^{M-1} p(m^k)\log p(m^k). \tag{9}$$

According to the knowledge of information theory, the entropy value $H(m)$ gets the maximum value $\log M$ when the output probability is evenly distributed. We use formula (10) to set the normalized confidence C:

$$C = \frac{H(m)}{H(m)_{\max}} = \frac{H(m)}{\log M}. \tag{10}$$

It is easy to push $C \in [0, 1]$. Thereby setting the empirical confidence threshold CT. When the confidence is $C \geq CT$, it is considered that the prediction probability distribution of the network output is uniform, and at this time, the network is not sure about the prediction probability of each type of the algorithm.

4. Result Analysis

Western musicians usually think that using the pentatonic scale in their works can reflect the oriental charm. Mahler's Song of the Earth and Stravinsky's Song of the Nightingale all use pentatonic scales with Chinese characteristics. Puccini also created some melodies written in pentatonic scale in Turandot, in order to better create a Chinese atmosphere.

In addition, Turandot contains many pentatonic motives, which either exist or are created by composers. We found that Puccini especially likes to use G flat major and E flat minor in the creation of exotic music. This is obviously because the piano's black keys present pentatonic notes and are easy to play. This section will comprehensively analyze Turandot in the dimensions of speed, rhythm, and beat by using several most important visual analysis methods.

Table 1: Single sample k-s test results.

Emotion	Jitter	Shimmer
Sad	0.436	0.814
Joy	0.028	0.236
Fear	0.302	0.015
Anger	0.556	0.529
Neutral	0.149	0.566
Disgust	0.759	0.584
Surprise	0.501	0.238

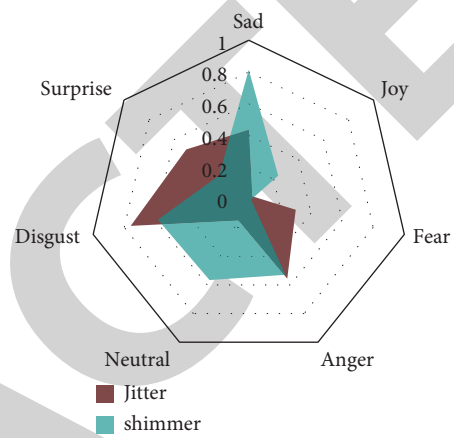

Figure 4: Radar chart of detection result.

In order to study the significant differences in parameters under different emotions, it is necessary to perform one-way ANOVA for each parameter. To ensure the availability of data, we first perform the one-sample k-s test on the data samples before performing one-way ANOVA. The test results of Jitter and shimmer are shown in Table 1 and Figure 4.

It can be seen that the significance of the jitter parameter in happy emotion and the shimmer parameter in scared emotion is less than 0.05, and the sample does not conform to the standard normal distribution. The two-tailed significance of the samples of other parameters is greater than 0.05, so there is no reason to reject the original hypothesis.

In order to better fit the residual error, this study also uses the GBRT (gradient boosting regulation tree) method. The more important super parameters are the maximum number of leaf nodes, the learning rate, the number of forests, and the ratio of positive and negative samples. The idea of combination feature selection in this study is to adopt the principle similar to the greedy method, that is, to add possible binary combination features. If the f-score effect is improved on the basis of cross-validation, this feature is considered to be better, see Table 2.

In this study, the information of word vector word2vec is especially considered as the feature. Generally, it is considered a DL model, and word2vec can express each word as a feature of an N-dimensional vector through training. So, the distance between two words can be expressed by the similarity of word vector space (see Figure 5).

Experiments show that, after introducing word vectors as features in the CNN model, the F-score value increases

Table 2: *F*-score results of the LSTM model.

Overfitting parameter	Number of features	Corpus prosodic phrases (%)
1	120	61.24
0.7	120	75.28
0.4	120	66.93
0.1	120	76.18

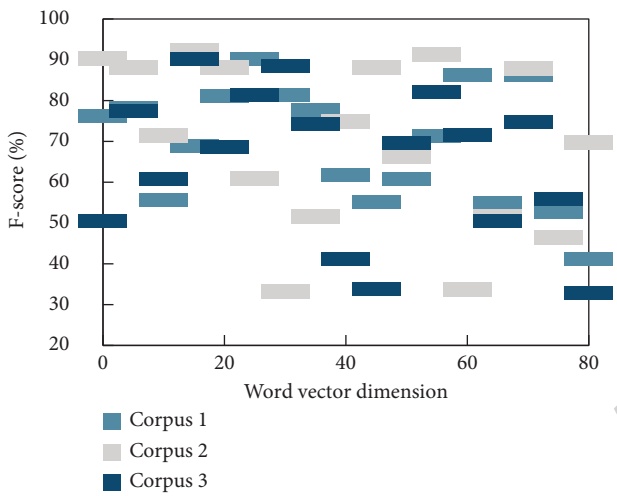

Figure 5: *F*-score results of the CNN model.

from 77% to 80%. The vector feature of this explanatory word can better adapt to the CNN model. However, adding word vectors to the LSTM model will greatly reduce the accuracy of the decision tree model.

As the expressive factors of music performance inevitably require that the performance deviates from the music score, this trend of precision and regularization actually gradually limits the basic space of artistic creation from a scientific point of view. Performance conventions such as over-symbol points, under-symbol points, uneven notes, and arpeggio treatment of chords have a long history and are often part of the complete artistic conception in the creative stage. Therefore, contemporary performance, while sticking to the accuracy of the spectrum, is probably far away from the authenticity of the work and the original intention of the composer.

Sometimes, the research will involve qualitative or quantitative analysis of the rhythm of the whole music, which requires statistical analysis of the microrhythm. In order to avoid the influence of accidental factors, Figure 6 sums up the rhythms of 70 bars of the whole song with 7 beats per bar to get the average value and takes the length of the first tone as a reference to get the relative lengths of other tones. It can be seen that the six beats are not evenly distributed.

The ratio of strong beat to strong beat is very similar, and the extension of the last beat is obvious, while performer 2 emphasizes the overall sense of 5/7 beat rhythm, and each bar is divided into two levels of elastic ups and downs on a microscopic level, thus causing some kind of periodic

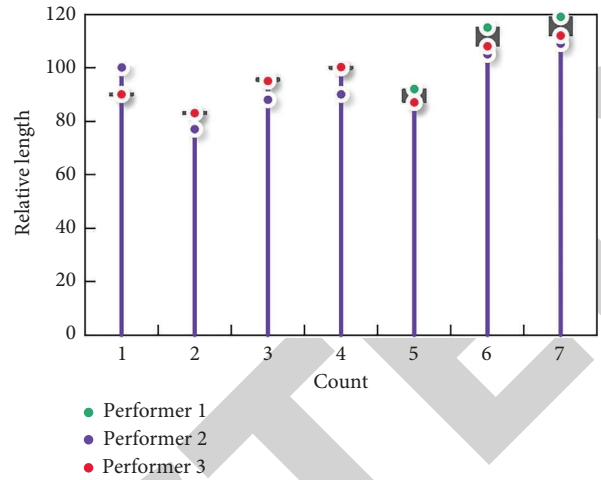

Figure 6: Analysis of rhythm proportion of each bar beat.

fluctuations with a sense of expectation. The tightness difference of this microrhythm is usually closely related to the performer's artistic conception. The unique five-tone style of Chinese music, *G* major, four or four beats, and adagio is adopted, and the melody is very stretched and full of singing. Especially, the repeated use of four-tone groups shows the unique warmth and femininity of oriental women to the fullest.

Puccini endows these characters with character, temperament, and soul with musical melody, treats these ordinary women in life with infinite love, shows them the most essential mentality and angle of human beings, and makes us feel their greatness. Turandot, based on fairy tales, has a strong appeal. However, Puccini, as a school of realism, was not finished when the opera was written for four years. I think it is mainly because the characters are difficult to grasp. Puccini died after writing Liu Er's aria in Turandot. Liu Er's death coupled with Puccini's death virtually added some content to this sad singing.

Figure 7 shows the test set accuracy of the above steganalysis method under different embedding rates of various steganalysis algorithms, in which less than 51% of the results can be considered as steganalysis failure. It can be seen that the CNN proposed in this study has achieved the highest detection accuracy for matching steganography algorithms with different embedding rates.

Similar to the high-order difference filter kernel, the secret information is adaptively embedded in the region with large audio amplitude and drastic changes, so the steganalysis model proposed in this section does not work for it. It shows that the CNN model proposed in this section is more reliable.

As the tested sample contains seven different emotions, it is impossible to judge which parameters have significant differences in which emotional combinations and which emotional combinations have no significant differences only based on the results of the previous section. In order to explore the differences of parameters in specific emotion groups and the difficulty of distinguishing emotion combinations by parameters, this study tests the rank sum of

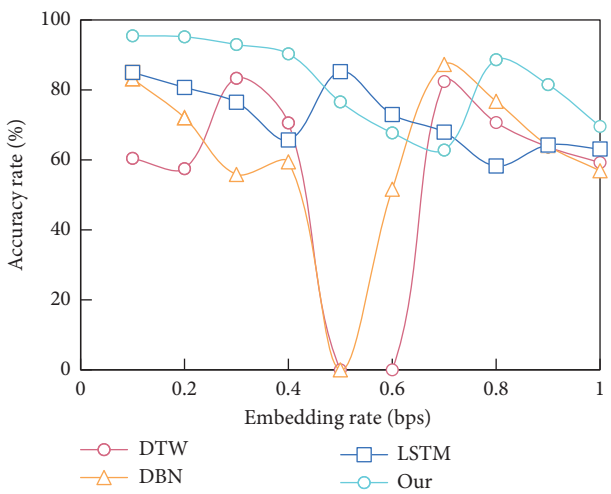

Figure 7: Accuracy of the matching algorithm.

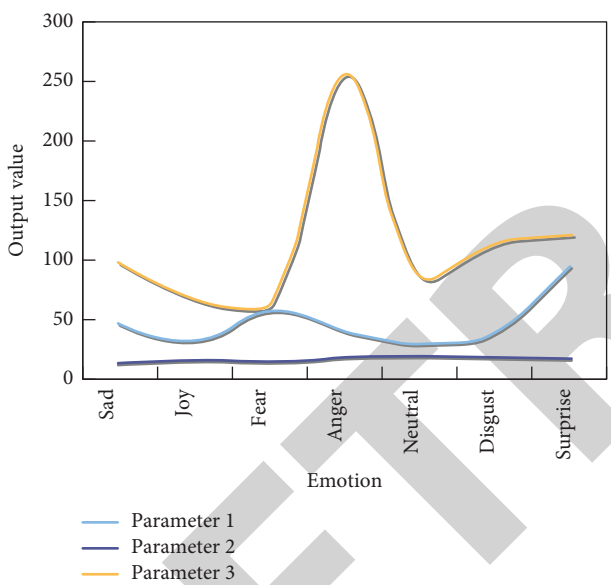

Figure 8: Typical values of vowels correspond to emotions.

emotion pairwise combinations of a vowel. The specific results are shown in Figure 8.

Different voices have different formant modes, and formant is the basic factor that determines the different auditory perception of this voice. Formant speech synthesis mainly depends on formant filters, which are combined in certain rules (usually including series and parallel connection). In the process of simulating vocal tract resonance, many harmonics are usually generated, that is, there are many resonance frequencies. Studies have shown that, at least five resonance frequencies should be selected to make the synthesized speech have high intelligibility and naturalness [17].

Puccini has broken the tradition that creators do not participate in dance design and put forward specific ideas and suggestions on the collection and display of props and the costumes of characters. At the premiere, behind the stage was a huge palace, in front of which was a street lined with shops. The Little Square was on the left and the execution ground was on the right, which was properly arranged. Puccini, according to his own understanding, made great efforts to render the "Chinese style" from the aspects of rhythm, harmony, and band orchestration. This external secondary factor has become an indispensable factor in the overall style of opera, and judging from the actual effect of music performance, Puccini's success is beyond doubt.

5. Conclusion

Vocal music teaching is a complex systematic project, and the sound spectrum analysis technology can provide powerful help for vocal music teaching. Through the analysis method of computer visual sound parameters, we can intuitively "see" the dynamic change process of the various parameters they care about, such as pitch, timbre, intensity, and speed. In this study, through the case analysis of Turandot's classic vocal music works, the basic idea of computer visual method for auxiliary analysis of common elements in vocal performance and teaching, such as timbre, intonation, vibrato, intensity, rhythm, beat, and speed, is fully demonstrated. The CNN DL method is used to predict the prosodic boundary. Through training and testing on the test data set and repeatedly adjusting the model, better model parameters are obtained. The experiment shows that the F-score value of the CNN model increased from 77% to 80% after introducing word vectors as features. The vector feature of this explanatory word can better adapt to the CNN model.

Data Availability

The data used to support the findings of this study are included within the article.

Conflicts of Interest

The authors declare that they have no conflicts of interest.

References

[1] H. Yue, B. Zhang, Y. Wu et al., "Simultaneous and signal-to-noise ratio enhancement extraction of vibration location and frequency information in phase-sensitive optical time domain reflectometry distributed sensing system," *Optical Engineering*, vol. 54, no. 4, Article ID 047101, 2015.

[2] Z. Marinkovic, N. Ivkovic, O. Pronic-Rancic, V. Markovic, and A. Caddemi, "Analysis and validation of neural network approach for extraction of small-signal model parameters of microwave transistors," *Microelectronics Reliability*, vol. 53, no. 3, pp. 414–419, 2013.

[3] T. Aubin and J. C. Bremond, "The Process of Species-specific Song Recognition in the Skylark Alauda arvensis. An Experimental Study by Means of Synthesis:pecific song recognition in the skylark alauda arvensis. an experimental study by means of synthesis," *Zeitschrift für Tierpsychologie*, vol. 61, no. 2, pp. 141–152, 2010.

[4] E. N. W. Senevirathna and L. Jayaratne, "Audio music monitoring: analyzing current techniques for song

Hindawi
Mobile Information Systems
Volume 2023, Article ID 9824052, 1 page
https://doi.org/10.1155/2023/9824052

Retraction

Retracted: Statistical Measurement and Influencing Factors of Green Total Factor Productivity of China's Tourism Industry Based on DEA-EBM Model

Mobile Information Systems

Received 8 August 2023; Accepted 8 August 2023; Published 9 August 2023

This article has been retracted by Hindawi following an investigation undertaken by the publisher [1]. This investigation has uncovered evidence of one or more of the following indicators of systematic manipulation of the publication process:

(1) Discrepancies in scope
(2) Discrepancies in the description of the research reported
(3) Discrepancies between the availability of data and the research described
(4) Inappropriate citations
(5) Incoherent, meaningless and/or irrelevant content included in the article
(6) Peer-review manipulation

The presence of these indicators undermines our confidence in the integrity of the article's content and we cannot, therefore, vouch for its reliability. Please note that this notice is intended solely to alert readers that the content of this article is unreliable. We have not investigated whether authors were aware of or involved in the systematic manipulation of the publication process.

Wiley and Hindawi regrets that the usual quality checks did not identify these issues before publication and have since put additional measures in place to safeguard research integrity.

We wish to credit our own Research Integrity and Research Publishing teams and anonymous and named external researchers and research integrity experts for contributing to this investigation.

The corresponding author, as the representative of all authors, has been given the opportunity to register their agreement or disagreement to this retraction. We have kept a record of any response received.

References

[1] Z. Xiang, S. Che, and S. Zhou, "Statistical Measurement and Influencing Factors of Green Total Factor Productivity of China's Tourism Industry Based on DEA-EBM Model," *Mobile Information Systems*, vol. 2022, Article ID 4069291, 13 pages, 2022.

Hindawi
Mobile Information Systems
Volume 2022, Article ID 4069291, 13 pages
https://doi.org/10.1155/2022/4069291

Research Article

Statistical Measurement and Influencing Factors of Green Total Factor Productivity of China's Tourism Industry Based on DEA-EBM Model

Zikun Xiang,[1] Shirui Che,[2] and Sijia Zhou[3]

[1]*School of Economics, Wuhan University of Technology, Wuhan, Hubei 430070, China*
[2]*School of Economics, Zhongnan University of Economics and Law, Wuhan, Hubei 430073, China*
[3]*School of Economics, Wuhan Donghu University, Wuhan, Hubei 430212, China*

Correspondence should be addressed to Sijia Zhou; 2020020019@stu.cdut.edu.cn

Received 20 July 2022; Revised 26 August 2022; Accepted 29 August 2022; Published 12 October 2022

Academic Editor: Chi Lin

In order to explore the statistical measurement and influencing factors of green total factor productivity in tourism, this paper proposes the use of gray absolute correlation to measure the similarity between input variable sequences. Moreover, this paper obtains the key parameters of the combination of radial and nonradial in the model based on the proximity index of gray correlation and calculates the economic efficiency of the decision-making unit according to the steps. In addition, this paper combines the DEA-EBM model to carry out the statistical measurement of China's tourism industry green total factor productivity and the analysis of influencing factors and verify it through data. Through research, it can be seen that the DEA-EBM model proposed in this paper can play an important role in the statistical measurement and analysis of influencing factors of green total factor production in the tourism industry.

1. Introduction

Tourism is a comprehensive and linked industry. In a society with diverse cultures and ethnic diversity, tourism builds bridges for human communication and promotes mutual understanding between different races and different cultures. At the same time, there are a series of social and economic activities in the process of tourism consumption, which promote the allocation and circulation of people, materials, and funds [1]. According to relevant data from the United Nations World Tourism Organization (UNWTO), currently, tourism accounts for 10% of global GDP, 7% of world exports, and 30% of labor exports. Moreover, modern tourism is a new economy, a comprehensive industry that integrates the primary, secondary, and tertiary industries, which not only promotes the appreciation of agricultural products but also drives the development of industrial products that meet consumer needs [2]. UNWTO's research shows that the contribution of the entire tourism sector to global warming caused by human factors has reached about 5%–14% [3]. This shows that tourism is closely related to global climate change.

From the macrolevel of the entire economic field, efficiency refers to the rational allocation of resources invested so as to maximize the total surplus value that all members of society can obtain. It is a specific indicator that reflects the research object's ability to use resources and the results obtained. For any economic entity, a high level of efficiency is an important prerequisite for its sustainable development. The issue of efficiency has become the core issue in the current economic development, and it is also a hot spot of domestic research.

This paper combines the EA-EBM model to carry out the statistical measurement and analysis of the influencing factors of the green total factor productivity of China's tourism industry, which provides a theoretical reference for the subsequent development of green tourism.

2. Related Work

Literature [4] studied the main source markets and compared single and multivariable models. From the model research results, it can be seen that the prediction models showed different research results in the main source markets. Literature [5] pointed out that there are many factors that influence tourism demand, and they are a series of factors and not a single factor. Literature [6] pointed out that different countries and regions have differences in prices or income, and their impact on international tourism demand is also different. Literature [7] believes that the economic development of a region or a city is too dependent on the international economic market, which may have a reactionary force on the economic development of the city and affect the development of urban tourism. Literature [8] studied the main reasons that affect rural tourism demand and found that the economic impact was limited and most rural consumers spent their expenditures on food and outdoor activities. Literature [9] conducted an in-depth investigation and exploration of the structural factors of tourism demand after readjusting the gravity model. Literature [10] used hotel overnight tourists as the research object, combined with the tourism demand model and artificial neural network model, carried out a specific analysis of the case, and proposed a prediction model to guide interested tourism suppliers to provide better product supply to meet the needs of tourists. Literature [11] uses a novel evolutionary negative correlation combined with the LSPME model to study tourism demand estimation, compares the LSPME model with other integrated models, and believes that the estimation accuracy of the LSPME model is significantly better than other integrated models. Literature [12] proposes to select a tourism demand model for measurement based on actual conditions. If the independent variable is known, it is best to use a neural network prediction model. When the independent variable is only a fuzzy value, the regression model analysis is more accurate. If the independent variable value is not known, the time series prediction model should be used. Literature [13] believes that there are many influencing factors in the generation of tourism demand, among which the most important factors are the price of tourism products, transportation, and personal disposable income. It also believes that economic growth can stimulate more tourism demand. Literature [14] proposed the concept of tourism compound cost, which included time, income, and other aspects into the model for consideration, and took the travel rate and tourism compound cost as the main measurement indicators so as to establish the tourism demand function for tourism demand and conduct calculation research. At present, domestic scholars have also begun to try to use single or combined forecasting methods to achieve forecasting goals. Literature [15] used the average absolute error and average absolute percentage error to construct multiple mathematical calculation models.

Literature [16] studied the supply of tourism through qualitative and quantitative methods and concluded that the management of water resources should be strengthened in tourist destinations where water is scarce. From the perspective of supply, literature [17] believes that the tourism supply chain includes not only direct suppliers but also indirect suppliers that provide tourism products and services to meet the needs of tourists; literature [18] puts forward an in-depth analysis of the process of tourism activities. Tourism supply chain is a tourism business network formed by multiple stakeholders, which involves various private enterprises, public departments, large enterprises, and so on. Literature [19] believes that the government should undertake the construction of basic public facilities in tourist destinations. However, the construction of tourism public service system has the characteristics of public welfare, so the profit is too small and may cause some enterprises to provide poor or even unqualified tourism products.

3. DEA-EBM Cross-Efficiency Model for Green Tourism considering Singularity and Competition and Cooperation

In DEA-EBM, due to the quantitative relationship between the input and output of the decision-making unit and the internal correlation in the evaluation to a certain extent, the rationality of the specific efficiency evaluation method has attracted more attention.

We assume that there are n DMUs, and each DMU has m inputs and s outputs. $x_{ij}\,(i = 1, 2, \ldots, m)$ represents the i-th input of unit $DMU_j\,(j = 1, 2, \ldots, s)$, $y_{rj}\,(r = 1, 2, \ldots, s)$ represents the r-th output. For the j-th decision-making unit, its efficiency can be defined as [20]

$$\theta_j = \frac{\sum_{r=1}^{s} u_r y_{rj}}{\sum_{i=1}^{m} v_r x_{ij}}\,(j = 1, 2, \ldots, n). \tag{1}$$

Among them, $v_i\,(i = 1, \ldots, m)$ and $u_r\,(r = 1, \ldots, s)$ represent the weight of input and output.

Considering that the decision-making unit is $DMU_d, d \in \{1, 2, \ldots, n\}$, the efficiency of this unit relative to other DMUs is called the CCR model, as shown in

$$\max E_{dd} = \frac{\sum_{r=1}^{s} u_{rd} y_{rd}}{\sum_{i=1}^{m} v_{id} x_{id}},$$

$$s.t.\begin{cases} E_{dd} = \dfrac{\sum_{r=1}^{s} u_{rd} y_{rd}}{\sum_{i=1}^{m} v_{id} x_{id}} \le 1 \;\; j = 1, 2, \ldots, n, \\ u_{rd} \ge 0 \quad r = 1, 2, \ldots, s, \\ v_{rd} \ge 0 \quad i = 1, 2, \ldots, m. \end{cases} \tag{2}$$

The goal of the plan is to find a set of input and output weights that are most beneficial to DMU_d.

By using the Charnes-Cooper transformation, model (2) can be converted into an equivalent linear program to solve, as shown in [21]

Table 1: Cross-efficiency matrix for n units.

Target DMU	DMU						Cross-eff
	1 (a_1)	2 (a_2)		1 (a_1)	2 (a_2)		1 (a_1)
1	E_{11}	E_{12}	1	E_{11}	E_{12}	1	E_{11}
2	E_{21}	E_{22}	2	E_{21}	E_{22}	2	E_{21}
...	...	...	...	...	...	...	...
P	E_{1p}	E_{2p}	P	E_{1p}	E_{2p}	P	E_{1p}
...	...	...	...	...	...	...	...
n	E_{n1}	E_{n2}	n	E_{n1}	E_{n2}	n	E_{n1}

$$\max \quad \sum_{r=1}^{s} u_r y_{rd} = E_{dd},$$
$$s.t. \begin{cases} \sum_{i=1}^{m} \omega_i x_{ij} - \sum_{r=1}^{s} u_r y_{rj} \geq 0 \; j = 1, 2, \ldots, n, \\ \sum_{i=1}^{m} \omega_i x_{ij} = 1, \\ \omega_i \geq 0 \quad i = 1, 2, \ldots, \mathrm{m}, \\ u_r \geq 0 \quad r = 1, 2, \ldots, s. \end{cases} \tag{3}$$

Among them, E_{dd} is the CCR efficiency of the decision-making unit U_d; that is, the optimal efficiency that the unit can achieve, reflecting the self-evaluation of the unit. The optimal weight coefficient of each decision unit DMU_d, $(d = 1, 2, \ldots, n)$ is $\omega_d^* = (\omega_{1d}^*, \ldots, \omega_{md}^*, \mu_{1d}^*, \ldots, \mu_{sd}^*)$. Since each unit can get its own set of ω_d^*, the efficiency of other units can be calculated according to co, which is called cross efficiency. Sexton et al. defined the crossover efficiency obtained by DMU_p using U_d's weight as

$$E_{dp} = \frac{\sum_{r=1}^{s} u_{rd}^* y_{rp}}{\sum_{r=1}^{s} \omega_{rd}^* x_{ip}} \leq 1, d, p = 1, 2, \ldots, n, d \neq p. \tag{4}$$

This model reflects the evaluation results of DMU_d on DMU_p. Model (3) needs to be run n times to solve the efficiency of each DMU. Therefore, for n DMUs, n sets of input-output weights will be obtained, forming n-1 sets of cross efficiency and a CCR efficiency, thereby forming a cross-efficiency matrix (CEM), as shown in Table 1 [22].

Model (3) may have multiple sets of optimal solutions; that is, the nonuniqueness of input and output weights will destroy the use of cross-efficiency evaluation. In order to solve this problem, Sexton proposed a set of quadratic goals to optimize the input and output weights while ensuring the efficiency of model (3). It uses an aggressive strategy to calculate the cross efficiency. The aggressive cross efficiency of the decision-making unit p based on d is shown in model (5), and the efficiency value is $\underline{E}_{dp}$. The benevolent cross efficiency of decision-making unit p based on d is shown in model (6), and the efficiency value is $\underline{E}_{dp}$.

$$Minimize \quad \sum_{r=1}^{s} u_{rd} \left(\sum_{p=1, j \neq d}^{n} y_{rp} \right),$$
$$s.t. \begin{cases} \sum_{i=1}^{m} v_{id} \left(\sum_{p=1, p \neq d}^{n} x_{rp} \right) = 1, \\ \sum_{r=1}^{s} u_{rd} y_{rp} - E_{dd} \sum_{i=1}^{m} v_{id} x_{rp} = 0, \\ \sum_{r=1}^{s} u_{rd} y_{rp} - \sum_{i=1}^{m} v_{id} x_{rp} \leq 0 \quad p = 1, 2, \ldots, n, \\ v_{id} \geq 0 \quad i = 1, 2, \ldots, \mathrm{m}, \\ u_{rd} \geq 0 \quad r = 1, 2, \ldots, s. \end{cases}$$
$$Maximize \quad \sum_{r=1}^{s} u_{rd} \left(\sum_{p=1, \mathrm{p} \neq d}^{n} y_{rp} \right),$$
$$s.t. \begin{cases} \sum_{i=1}^{m} v_{id} \left(\sum_{p=1, p \neq d}^{n} x_{rp} \right) = 1, \\ \sum_{r=1}^{s} u_{rd} y_{rp} - E_{dd} \sum_{i=1}^{m} v_{id} x_{rp} = 0, \\ \sum_{r=1}^{s} u_{rd} y_{rp} - \sum_{i=1}^{m} v_{id} x_{rp} \leq 0 \quad p = 1, 2, \ldots, n, \\ v_{id} \geq 0 \quad i = 1, 2, \ldots, \mathrm{m}, \\ u_{rd} \geq 0 \quad r = 1, 2, \ldots, s. \end{cases} \tag{5}$$

The above two models ensure the worst and the best overall efficiency of other units while maintaining the DMU_d efficiency score.

In addition, DEA-EBM also includes some other common secondary target models:

(a) $Minimize \quad \sum_{r=1}^{s} u_{rd} (\sum_{j=1, j \neq d}^{n} y_{rk}) - \sum_{i=1}^{m} v_{id} (\sum_{j=1, \mathrm{j} \neq d}^{n} x_{ij})$.

(b) It replaces $Minimize 1/n \sum |\alpha_j' - \overline{\alpha}'|$ with $\sum_{r=1}^{s} u_{rd} y_{rj} - \alpha_d \sum_{i=1}^{m} v_{id} x_{rj} \geq 0$ in model (5). Among them, $\alpha_d \in (\min_{1 \leq j \leq n} E_{jj}, 1)$ is a parameter that controls the range of DMU_d efficiency scores.

(c) $MinMaximize \quad \alpha'_j$ or $Minimize 1/n \sum_{j=1}^{n} |\alpha'_j - \overline{\alpha}'|$

$$s.t. \begin{cases} \sum_{i=1}^{m} v_{id} x_{id} = 1, \\ E_{dd} = \sum_{r=1}^{s} u_{rd} y_{rd}, \\ \sum_{r=1}^{s} u_{rd} y_{rd} - \sum_{i=1}^{m} v_{id} x_{id} + \alpha_j^r = 0 \quad j = 1, 2, \ldots, n. \end{cases} \tag{6}$$

Among them, $\overline{\alpha}' = 1/n \sum_{j=1}^{n} \alpha'_j$.

Models (4) to (6) give the general DEA cross-efficiency calculation method, and model (5) treats all decision-making units as hostile situations. However, model (6) regards all decision-making units as Allies. They simply regard all decision-making units as alliance or hostile relations.

The mutual information of discrete and continuous variables can be expressed as follows:

Continuous type: $I(X,Y) = \iint p(x,y) \log_2 p(x,y) / p(x)p(y) dx dy$.

Discrete type: $I(X,Y) = \sum \sum p(x,y) \log_2 p(x,y) / p(x)p(y)$.

Among them, $p(x, y)$ represents the joint probability distribution of random variable X and random variable Y. It can be seen from the above two forms that when the random variable X and the random variable Y are independent of each other, the mutual information $I(X,Y) = 0$.

We set a sample set $U = \{x_1, x_2, \ldots, x_n\}, x_i \in R^N$. Δ is the distance function defined on U, satisfying $\Delta(x_i, x_j) \geq 0$. In applications, 2-norm distance (also known as Euclidean distance) is often used: $(\sum_{k=1}^{N} |x_{ik} - x_{jk}|^2)^{1/2}$. We assume that $\delta \geq 0$, and the neighborhood of labeled sample x_i is $\delta(x) = \{x_i | \Delta(x_i, x_j) \leq \delta\}$. At the same time, we are given two feature spaces R and S, and $\delta_R(x)$ and $\delta_S(x)$ are, respectively, the neighborhood of X calculated based on the distance in these feature spaces. The neighborhood has the following attributes: $\delta_{R \cap S}(x) = \delta_R(x) \cap \delta_S(x)$. In addition to the distance function given above, there are many ways to measure the distance between heterogeneous features and missing data. Definition 1 and Definition 2 refer to Huetal's description.

Definition 1. We are given a sample set $U = \{x_1, x_2, \ldots, x_n\}$, which is described by a numerical or discrete $R, S \subseteq F$ attribute subset. The neighborhood of sample x_i on attribute S can be denoted as $\delta_S(x_i)$. The neighborhood uncertainty of the sample can be defined as

$$NH_\delta^{x_i}(S) = -\log \frac{\|\delta_S(x_i)\|}{n}. \tag{7}$$

Moreover, the average uncertainty of the sample set can be defined as

$$NH_\delta(S) = -\frac{1}{n} \sum_{i=1}^{n} \log \frac{\|\delta_S(x_i)\|}{n}. \tag{8}$$

Definition 2. $R, S \subseteq F$ is two attribute subsets, and the neighborhood mutual information defined based on R and S is

$$NMI_\delta(R;S) = -\frac{1}{n} \sum_{i=1}^{n} \log \frac{\|\delta_R(x_i)\| \cdot \|\delta_S(x_i)\|}{n \|\delta_{S \cup R}(x_i)\|}. \tag{9}$$

If we give two attribute subsets R and S and $NMI_\delta(R;S)$ is the mutual information between these two attribute subsets, then the following equation holds:

(1) $NMI_\delta(R;S) = NMI_\delta(S;R)$

(2) $NMI_\delta(R;S) = NH_\delta(R) + NH_\delta(S) - NH_\delta(R,S)$

(3) $NMI_\delta(R;S) = NH_\delta(R) + NH_\delta(S) - NH_\delta(R,S)$

We assume that there are n decision-making units to be evaluated, and each decision-making unit has m inputs and s outputs. Moreover, we use x_{ij} and y_{rj} to represent the i ($i = 1,2, \ldots$, m) input and r ($r = 1,2, \ldots$, s) output of the j-th decision-making unit, respectively.

e_J represents the average other-evaluation efficiency score of decision-making unit j, and h_{jj} represents the self-evaluation optimal efficiency score of the model. h_{kj} represents the evaluation value of the decision unit j when the decision unit k is optimized; that is, the decision unit j is evaluated with the optimal weight of the decision unit k. M_J represents the singularity index. Then, the formula for calculating the singular index is

$$M_j = \frac{h_{jj} - e_j}{e_j}, e_j = \frac{\sum_{k \neq j} h_{kj}}{n-1}. \tag{10}$$

What M_J expresses is the difference and changes in the efficiency of the decision-making unit between other- and self-evaluation. The larger h_{jj}, the smaller e_J. The larger M_J is, the easier the decision-making unit j is to be regarded as a singular person; that is, the decision-making unit j is pseudoeffective. The smaller M_J is, the closer the self-evaluation value is to his evaluation value, and the easier the final evaluation value of decision-making unit j is to be accepted.

Under the optimistic (optimal) frontier, the DEA-EBM model pursues the maximization of efficiency to determine the input and output weights. The optimistic efficiency of the k-th decision unit can be obtained by solving

$$\theta_{kk} = \max \sum_{r=1}^{s} u_{rk} y_{rk},$$

$$s.t. \begin{cases} \sum_{i=1}^{m} v_{ik} x_{ik} = 1, \\ E_{dd} = \sum_{r=1}^{s} u_{rd} y_{rd}, \\ \sum_{r=1}^{s} u_{rd} y_{rd} - \sum_{i=1}^{m} v_{id} x_{id} + \alpha_j^r = 0 \quad j = 1, 2, \ldots, n. \end{cases} \tag{11}$$

Among them, v_{ik} and u_{rk} represent the weights of the i-th input and r-th output of the k-th ($k = 1,2, \ldots$, n) decision-making unit, and the optimistic efficiency value of the k-th

decision-making unit is within $\theta \in [0, 1]$. If $\theta_{kk} = 1$, the k-th decision-making unit is called optimistic and effective; otherwise, the decision-making unit is called optimistic and noneffective.

Under the pessimistic (worst) frontier, the DEA-EBM model pursues the minimization of efficiency to determine the input-output weight. The pessimistic efficiency of the k-th decision unit can be obtained by solving

$$\phi_{kk} = \min \sum_{r=1}^{s} u_{rk} y_{rk},$$
$$s.t. \begin{cases} \sum_{i=1}^{m} v_{ik} x_{ik} = 1, \\ \sum_{r=1}^{s} u_{rk} y_{rj} - \sum_{i=1}^{m} v_{ik} x_{ij} \geq 0, j = 1, 2, \ldots, n, \\ u_{rk} \geq 0, v_{ik} \geq 0, r = 1, 2, \ldots, s, i = 1, 2, \ldots, \mathrm{m}. \end{cases} \tag{12}$$

In the above formula, the pessimistic efficiency of the k-th decision-making unit is $\phi_{kk} \geq 1$. If the force >1, the decision-making unit k is called pessimistic and invalid; otherwise, the decision-making unit is called pessimistic noninvalid.

Decision-making units are each other's Allies, and each unit between classes is each other's opponents. Then, we assume that the k-th decision-making unit is in the Tt category, that is, $k \in Tt$, and use the decision-making unit k ($k = 1, 2, \ldots, \mathrm{n}$) to evaluate other decision-making units separately, so that we try to make the efficiency of the units belonging to the Tt category as high as possible, and vice versa, as low as possible. Finally, we use the arithmetic average method to fuse self-evaluation and other-evaluation efficiency to obtain the overall crossover efficiency of competition and cooperation. The model is shown in

$$\min \sum_{j \neq k, j \in T_t} s_{kj}^{CP} - \sum_{jj \in T_t} s_{kj}^{CP},$$
$$s.t. \begin{cases} \sum_{r=1}^{s} u_{rk} y_{rj} - \sum_{i=1}^{m} v_{ik} x_{ij} + s_{kj}^{CP} = 0, j = 1, 2, \ldots, n, j \neq k, \\ \sum_{r=1}^{s} u_{rk} y_{rk} - \theta_{kk}^{*} \sum_{i=1}^{m} v_{ik} x_{ik} = 0, \\ s_{kj}^{CP} \geq 0, j = 1, 2, \ldots, m, j \neq k, \\ u_{rk} \geq 0, v_{ik} \geq 0, r = 1, 2, \ldots, s, i = 1, 2, \ldots, m. \end{cases} \tag{13}$$

Model (13) embodies the competitive and cooperative relationship between decision-making units, enabling the decision-making unit to establish a competitive or cooperative relationship with other units based on personal preference.

This paper first uses the bounded DEA-EBM model to provide an efficiency interval for each decision-making unit. The model is shown in

$$\psi_{kk} = \frac{\max}{\min} \sum_{r=1}^{s} u_{rk} y_{rk},$$
$$s.t. \begin{cases} \sum_{i=1}^{m} v_{ik} x_{ik} = 1, \\ \sum_{r=1}^{s} u_{rk} y_{rj} - \sum_{i=1}^{m} v_{ik} x_{ij} \leq 0, j = 1, 2, \ldots, n, \\ \sum_{r=1}^{s} u_{rk} y_{rj} - \alpha \sum_{i=1}^{m} v_{ik} x_{ij} \geq 0, j = 1, 2, \ldots, n, \\ u_{rk} \geq 0, v_{ik} \geq 0, r = 1, 2, \ldots, s, i = 1, 2, \ldots, m. \end{cases} \tag{14}$$

Among them, $\alpha = \max \theta^* / \min \varphi^*$ $(0 < \alpha \leq 1)$ represents the adjustment coefficient of pessimistic efficiency, and θ^* and φ^* are obtained by models (11) and (12), respectively. Due to the inconsistency of the two efficiency scores, the values of optimistic efficiency and pessimistic efficiency can be adjusted to be within the interval $[\alpha, 1]$. We use model (14) to evaluate the k-th decision-making unit, and the maximum value of the objective function is $\psi_{kk}^{U^*}$, which shows the best relative efficiency of the decision-making unit. The minimum value of the objective function is $\psi_{kk}^{L^*}$, which represents the worst relative efficiency of the decision-making unit. The two together constitute the efficiency interval $[\psi_{kk}^{L^*}, \psi_{kk}^{U^*}]$ of the k-th decision-making unit.

Based on model (13), we construct a new cross-efficiency model (15). By ensuring that the evaluation efficiency of the evaluated decision-making unit is not lower than its worst relative efficiency $\psi_{kk}^{L^*}$, we enable the decision-making unit to adopt different evaluation strategies for other units according to the degree of association.

$$\min \left[z_1 \left(\theta_{dd} - \sum_{r=1}^{s} u_{rk} y_{rd} \right) - z_2 \left(\theta_{dd} - \sum_{r=1}^{s} u_{rk} y_{rd} \right) \right],$$
$$s.t. \begin{cases} \sum_{i=1}^{m} v_{ik} x_{id} = 1, \\ \sum_{r=1}^{s} u_{rk} y_{rk} - \psi_{kk}^{U^*} \sum_{i=1}^{m} v_{ik} x_{ik} = 0, \\ \psi_{kk}^{L^*} \sum_{i=1}^{m} v_{ik} x_{id} - \sum_{r=1}^{s} u_{rk} y_{rd} \leq 0, \\ \sum_{r=1}^{s} u_{rk} y_{rj} - \sum_{i=1}^{m} v_{ik} x_{ij} \leq 0, j = 1, 2, \ldots, n, \\ u_{rk} \geq 0, v_{ik} \geq 0, r = 1, 2, \ldots, s, i = 1, 2, \ldots, m, \\ z_1 = 1, z_2 = 0, \{k, d\} \subset H; z_1 = 0, z_2 = 1, \{k, d\} \not\subset H. \end{cases} \tag{15}$$

We first use model (14) to calculate the optimal relative efficiency of each decision unit $\psi_{kk}^{U^*}$ and the worst relative efficiency of $\psi_{kk}^{L^*}$ and then evaluate decision unit d under the condition that the optimal relative efficiency of decision unit k keeps $\psi_{kk}^{U^*}$ unchanged. At the same time, we ensure that the

other-evaluation efficiency of unit d is not less than its worst relative efficiency $\psi_{kk}^{L^*}$. As a singular index, $\theta_{dd} - \sum_{r=1}^{s} u_{rk} - y_{rd}$ indicates the difference between self-evaluation and other evaluations. If the decision-making units k and d are in the same set, then $z_1 = 1, z_2 = 0$, which means that the decision-making unit d's other-evaluation efficiency is as large as possible. On the contrary, it is necessary to make the decision-making unit d's other-evaluation efficiency as small as possible. In addition, model (15) ensures that the other-evaluation efficiency of the decision-making unit d is not lower than its worst relative efficiency and can improve the acceptability of the evaluation results.

The same DEA-EBM model has many expressions. For example, model (3) is called a multiplier model of CCR. By solving this model n times, the efficiency score of each unit from DMU to DMU can be obtained. Although model (3) is linear, the calculation of efficiency scores often needs to be transformed into a dual form, as shown in

$$\max \quad \theta,$$
$$s.t. \begin{cases} \sum_{i=1}^{m} \lambda_j x_{ij} \le \theta x_{ro}, j = 1, 2, \ldots, n, \\ \sum_{r=1}^{s} \lambda_j y_{rj} \ge y x_{ro}, \\ \lambda_j \ge 0, j = 1, 2, \ldots, n. \end{cases} \tag{16}$$

Model (16) is the envelope form of the input-oriented CCR model (Farrell model). It means that the input to the DMU shrinks as much as possible without reducing the current output level. Both inputs and outputs are highly disposable:

$$T = \left\{ (x, y): \sum_{j=1}^{n} z_j x_{ij} \le x_i \sum_{j=1}^{n} z_j y_{rj} \ge y_r, r = 1, 2, \ldots, s z_j \ge 0 \quad j = 1, 2, \ldots, n \right\}. \tag{17}$$

Among them, $x = (x_1, x_2, \ldots, x_n)$ and $y = (y_1, y_2, \ldots, y_n)$ are input and output vectors, respectively. T is the reference technology set containing all possible input-output combinations.

In the traditional DEA-EBM model as shown in Figure 1, if $(x, y) \in T$ and $x' \ge x$ (or $y' \le y$), then $(x', y) \in T$ or $(x, y') \in T$.

Under the DEA-EBM framework, the weakly disposable reference technology is also called the environmental DEA-EBM technology, which can be expressed as model (18):

$$T_e = \left\{ (x, y, u): \sum_{j=1}^{n} z_j x_{ij} \le x_i, i = 1, 2, \ldots, m \sum_{j=1}^{n} z_j y_{rj} \ge y_r, r = 1, 2, \ldots, s \sum_{j=1}^{n} z_j u_{kj} = u_k k = 1, 2, \ldots, \mathrm{t} z_j \ge 0 \quad j = 1, 2, \ldots, n \right\}. \tag{18}$$

Among them, $u = (u_1, u_2, \ldots, u_t)$ represents the undesired output vector, and the difference between T and Te is that, in Te, it is not feasible to reduce only the undesired output, but it is feasible to reduce the expected output and the undesired output proportionally.

We assume that there are n homogeneous units as $DMU_j\,(j - 1, 2, \ldots, n)$, and the input vector, expected output vector, and undesired output vector of each decision-making unit are expressed as $x = (x_1, x_2, \ldots, x_m)$, $y = (y_1, y_2, \ldots, y_s)$, and $z = (z_1, z_2, \ldots, z_t)$, respectively, which consumes m types of inputs and produces s types of expected output and t kinds of undesired output.

In order to properly describe the production process with expected output and undesired output, the following two assumptions need to be added to the production technology set T proposed by Fare:

(1) Weak disposability of output. That is, if $(x, y, b) \in T \quad and \quad 0 \le \theta \le 1$, then $(x, \theta y, \theta b) \in T$.

(2) Zero combination of undesired output and expected output. That is, if $(x, y, b) \in T \quad and \quad b = 0$, then $y = 0$. These two assumptions show that it is not feasible to reduce only undesired output, and the reduction of undesired output must be accompanied by the reduction of expected output.

There are many models that DEA-EBM technology uses to measure environmental performance in an environment with constant returns to scale. Among these models, the model only allows adjustments to undesired output.

$$PEI_1 = \min \lambda$$
$$s.t. \left\{ \sum_{k=1}^{K} z_k x_{nk} \le x_{n0} \quad n = 1, \ldots, \mathrm{N} \sum_{k=1}^{K} z_k y_{mk} \ge y_{m0} \quad m = 1, \ldots, \mathrm{M}. \sum_{k=1}^{K} z_k u_{jk} = \lambda u_{j0} \quad j = 1, \ldots, J z_k \ge 0 \quad k = 1, 2, \ldots, \mathrm{K}. \right. \tag{19}$$

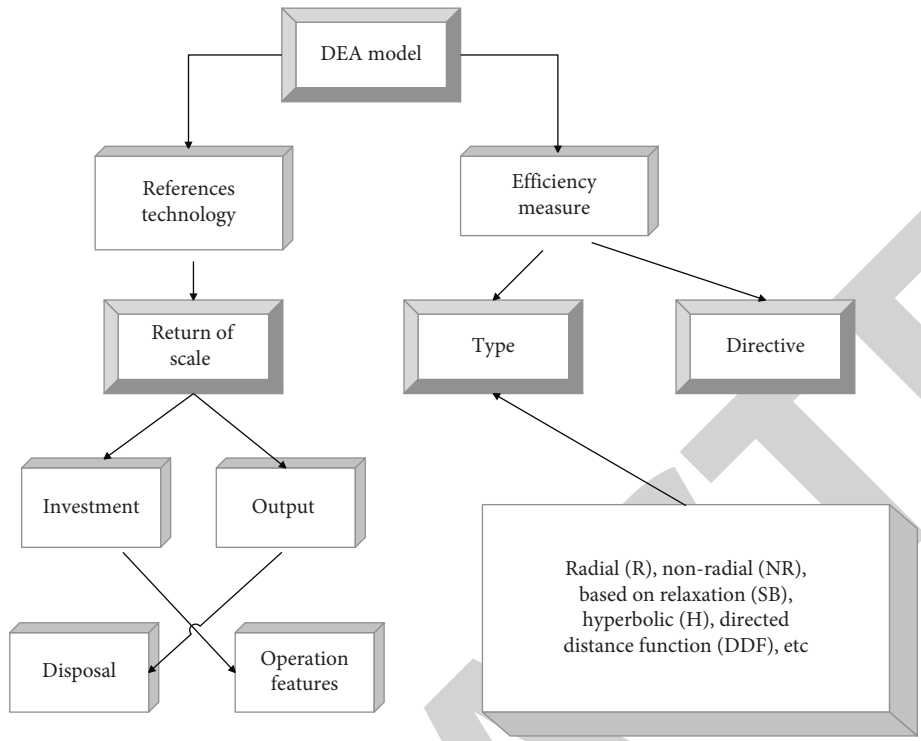

Figure 1: The general structure of the DEA-EBM model.

This paper proposes the following input-oriented EBM-GR-U model framework. The economic and ecological efficiency of n units can be obtained by solving the model n times. This paper assumes weak disposability of pollutants that play an important role in environmental impact, such as

$$\gamma^* = \min \beta - \varepsilon \sum_{i=1}^{m} \frac{w_i^- s_{i0}^-}{x_{i0}},$$

$$s.t. \begin{cases} \beta x_{i0} - \sum_{j=1}^{n} x_{ij}\lambda_j - s_{i0}^- \quad i = 1, \ldots, m, \\ \sum_{j=1}^{n} y_{rj}\lambda_j \geq y_{r0} \quad r = 1, \ldots, s, \\ \sum_{j=1}^{n} b_{pj}\lambda_j = pb_{po} \quad p = 1, \ldots, t, \\ \lambda_j \geq 0, s_{ij}^- \geq 0 \quad i = 1, \ldots, m \quad j = 1, \ldots, n. \end{cases} \tag{20}$$

θ in the above formula is the fraction of radial efficiency, which represents the degree of radial efficiency. $\sum_{i=1}^{m} w_i^- s_{i0}^- / x_{i0}$ represents the nonradial relaxation term. ε is a key parameter that combines the radial efficiency score and nonradial relaxation. w_i^- represents the weight of the i-th input and satisfies $\sum_{i=1}^{m} w_i^- = 1\,(\forall i, w_i^- \geq 0)$. In this formula, the values of ε and $w_i^-\,(i = 1, \ldots, m)$ need to be obtained in advance. ρ represents the environmental efficiency level of $\mathrm{DMU_o}$. Therefore, the eco-economic efficiency of $\mathrm{DMU_o}$ can be integrated through economic efficiency and environmental efficiency; that is, economic eco-efficiency $eco - efficiency = \gamma^* \cdot \rho$.

Definition 3 (EBM-GR-U input-oriented efficiency).
$\mathrm{DMU_o}$ is called EBM-GR-U input valid $\Leftrightarrow \gamma^* = 1$.

Definition 4. The optimal solution of model (19) is expressed as $(\theta^*, \lambda^*, s^{-*})$.

The projection of $DMU_o\,(x_o, y_o)$ can be defined as follows:

$$\begin{aligned} x_o^* &= X\lambda^* = \theta^* x_o - s^{-*}, \\ y_o^* &= Y\lambda^*, \\ z_o^* &= Z\lambda^*, \end{aligned} \tag{21}$$

As shown in model (19), the values of two types of important parameters ε and $w = (w_i, i = 1, \ldots, m)$ need to be obtained in advance, as shown in Table 2.

In addition, since the information expressed by the two types of input data overlaps to a certain extent, the eigenvalues and eigenvectors of the proximity matrix can be solved based on the idea of principal component analysis. When the closeness between the input indicators is higher, the characteristic roots compressed by principal components will be larger. According to the functional relationship between ε and the characteristic root, ε is reduced at this time, and the nonradial features of the model are reduced; that is, the radial compression is more suitable for input at this time. Conversely, when the input index is closer, the data is more scattered, the characteristic root will be smaller, and ε will increase. At this time, it is more suitable for projection based on nonradial relaxation.

Table 2: Input sequence used in correlation construction.

	$x_1(X_1)$	...	$x_i(X_i)$		$x_j(X_j)$		$x_m(X_m)$
DMU_1	x_{11}	...	x_{i1}	...	x_{j1}	...	x_{m1}
...		...		...		...	
DMU_k	x_{1k}	...	x_{ik}	...	x_{jk}	...	x_{mk}
...		...		...		...	
DMU_n	x_{1n}	...	x_{in}	...	x_{jn}	...	x_{mn}

Proposition 1. *We set the behavior column of the system $X_i = (x_i(1), x_i(2), ..., x_i(n))$ and mark the broken line $x_i(1) - x_t(1), x_i(2) - x_t(1), ..., x_i(n) - x_t(1)$ as $X_i(1) - x_t(1)$ and $s_i = \int_1^n (X_i - x_t(1))ds$.*

Then,

(1) When X_i is an increasing sequence, $s_i \geq 0$

(2) When X_i is the attenuation sequence, $s_i \leq 0$

(3) When X_i is an oscillating sequence, the symbol of s_i is uncertain

Proposition 2. *We set the behavior sequence of the system as $X_i = (x_i(1), x_i(2), ..., x_i(n))$ and $X_j = (x_j(1), x_j(2), ..., x_j(n))$. The two sequences have the same length. By operating $x_i^0 = x_i(k) - x_i(1), k = 1, 2, ..., n$ on the elements in the sequence, the zeroized images of the starting point of the two sequences can be obtained as*

$$X_i^0 = \left(x_i^0(1), x_i^0(2), ..., x_i^0(n)\right), X_j^0 = \left(x_j^0(1), x_j^0(2), ..., x_j^0(n)\right). \tag{22}$$

Moreover, we set $s_i - s_j = \int_1^n (X_i^0 - X_j^0)ds$.
Then,

(1) When X_i^0 is above X_j^0, $s_i - s_j \geq 0$.

(2) When X_i^0 is below X_j^0, $s_i - s_j \geq 0$.

(3) When X_i^0 intersects at X_j^0, the sign of $s_i - s_j$ is uncertain.

Definition 5. We assume that the sequences X_i and X_j have the same length and the definitions of s_i and s_j are as shown in Proposition 1, and then we call

$$s_{ij} = \varepsilon_{ij} = \frac{1 + |s_i| + |s_j|}{1 + |s_i| + |s_j| + |s_j - s_i|}. \tag{23}$$

It is the gray absolute correlation degree of X_i and X_j, the similarity index s_{ij} of these two sequences can be defined as $s_{ij} = \varepsilon_{ij}$.

Definition 6. We assume that the two sequences X_i and X_j have the same length, and the definitions of s_i and s_j are shown in Proposition 1. Then, the similarity index $s(i, j)$ of these two sequences can be defined as follows:

Table 3: Proximity matrix based on proximity index.

	...	X_i	...	X_j
X_1	...	ε_{1i}	...	$\varepsilon_{1j}(S_{ij})$
...	...	...	...	...
X_j	...	ε_{ji}	...	ε_{jj}

$$s_{ij} = \varepsilon_{ij} = \frac{\sqrt{|s_j s_i|} + |s_i| + |s_j|}{\sqrt{|s_j s_i|} + |s_i| + |s_j| + |s_j - s_i|},$$
$$s_{ij} = \varepsilon_{ij} = \frac{1 + \sqrt{|s_j s_i|} + |s_i| + |s_j|}{1 + \sqrt{|s_j s_i|} + |s_i| + |s_j| + |s_j - |s_i||}. \tag{24}$$

Formulas (22) and (23) have the following four properties:

(1) Reflexivity, $\forall i, s(i, j) = 1$

(2) Symmetry, $\forall i, j, s(i, j) = s(j, i)$

(3) Normative, $\forall i, j, 0 \leq s(i, j) \leq 1$

(4) Proximity.

Proof 1

(1) Reflexivity: $|s_j - s_i| = 0, \forall i, s(i, j) = 1$.

(2) Symmetry: $|s_i - s_j| = |s_j - s_i|$ and $\min 1 - 1/m\sum s_1^-/x/1/m\sum s_1^-/x$

$$s.t. \begin{cases} \beta x_{i0} - \sum_{j=1}^{n} x_{ij}\lambda_j - s_{i0}^- \quad i = 1, ..., m \\ \sum_{j=1}^{n} y_{rj}\lambda_j \geq y_{r0} \quad r = 1, ..., s \\ \sum_{j=1}^{n} b_{pj}\lambda_j = pb_{po} \quad p = 1, ..., t \\ \lambda_j \geq 0, s_{ij}^- \geq 0 \quad i = 1, ..., m \quad j = 1, ..., n \end{cases}.$$

(3) Normative: Obviously, $s_{ij} = \varepsilon_{ij} > 0$, and $|s_j - s_i| \geq 0$, so $s_{ij} = \varepsilon_{ij} \leq 1$.

(4) Proximity: Obviously, it is established. □

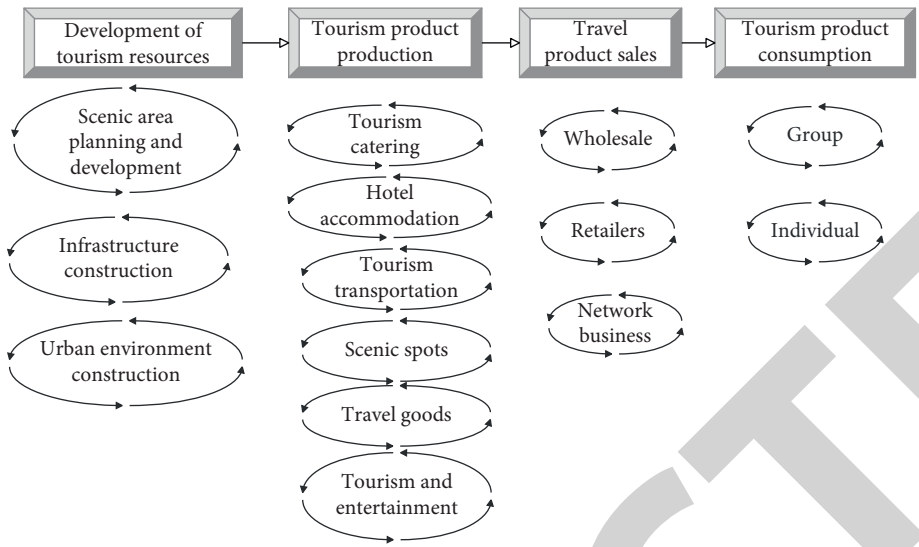

Figure 2: The core tourism industry chain.

Step 1. The algorithm projects all DMUs onto the front surface of the VRS.

$$\min \quad \frac{1 - 1/m \sum_{i=1}^{m} s_1^- / x_{io}}{1 + 1/s \sum_{r=1}^{s} s_1^+ / y_{io}},$$

$$s.t. \begin{cases} x_{i0} = \sum_{j=1}^{n} x_{ij}\lambda_j + s_i^- \quad i = 1, \ldots, m, \\ y_{r0} = \sum_{j=1}^{n} y_{rj}\lambda_j - s_r^+ \quad r = 1, \ldots, s, \\ b_{p0} = \sum_{j=1}^{n} b_{pj}\lambda_j \quad p = 1, \ldots, t, \\ \sum_{j=1}^{n} \lambda_j = 1, \\ \lambda_j \geq 0, s_i^- \geq 0 \quad s_r^+ \geq 0, \forall i, j, r. \end{cases} \tag{25}$$

The algorithm can improve the accuracy of estimation by projecting all DMUs onto the frontier under the assumption of variable returns to scale. The projection model is shown in model (24).

The projection using slack input and output can be defined as $\begin{matrix} \tilde{x}_{io} = x_{io} - s_i^{-*} \ (i = 1, \ldots, m) \\ \tilde{y}_{ro} = y_{ro} - s_r^{-*} \ (r = 1, \ldots, s) \end{matrix}$.

DMUS for N effective VRS units can be expressed as $\overline{X} = \overline{x}_1, \ldots, \overline{x}_m \quad \overline{Y} = \overline{y}_1, \ldots, \overline{y}_s$, and all DMUs with valid CRS and VRS are also included in this set.

Step 2. Because Step 1 uses different projection models to get different projection results, you can also replace the projection based on the actual data observed.

That is, the algorithm uses $X = \begin{pmatrix} x_1 \\ \cdots \\ x_m \end{pmatrix} = \begin{pmatrix} x_{11} & \cdots & x_{1n} \\ \vdots & \ddots & \vdots \\ x_{m1} & \cdots & x_{mn} \end{pmatrix}$ and $Y = \begin{pmatrix} y_1 \\ \cdots \\ y_m \end{pmatrix} = \begin{pmatrix} y_{11} & \cdots & y_{1n} \\ \vdots & \ddots & \vdots \\ y_{s1} & \cdots & y_{sn} \end{pmatrix}$ instead of $\overline{X}$ and $\overline{Y}$. According to formula (19), we only consider the proximity of the input sequence, and the proximity matrix $S = [s_{ij}] \in R^{m \times m}$ is composed of elements $s_{ij} = s(\overline{x}_i, \overline{x}_j)$ or $s_{ij} = s(\overline{x}_i, \overline{x}_j)$. As shown in Table 2, x_i, x_j is the sequence of the i-th and j-th input actual data of all units, where $i,j = 1,2, \ldots, m$. $s_{ij} = \varepsilon_{ij} = s(x_i, x_j)$ is the closeness index between the two input sequences obtained according to the actual input data and the definition of formula (21) or (22), and the final closeness matrix is shown in Table 3. According to the relevant properties of the formula, all elements in the matrix are obtained: $0 \leq s_{ij} = \varepsilon_{ij} \leq 1$.

Step 3. The algorithm solves the maximum eigenvalue of the similarity matrix and its corresponding eigenvector.

The matrix S is a nonnegative symmetric matrix, and the diagonal elements are all 1. According to the Perron–Frobenius theorem, S has the largest characteristic root ρ_x and its corresponding nonnegative characteristic vector w_x. The nonnegative vector w_x corresponds to the weight of each input element. According to the P–F theorem, $m \geq \rho_x \geq 1$.

In Step 4, the algorithm uses the largest feature root and feature vector model in Step 3 to calculate the values of ε and w^-. If $m > 1$, then $\varepsilon = m - \rho_x / m - 1$; and if $m = 1$, then $\varepsilon = 0$, and $w^- = w_x / \sum_{i=1}^{m} w_x$.

Step 4. The algorithm uses the obtained values of ε and w^- to use model (19) to calculate EBM-GR-U.

In summary, model (19) reasonably combines radial and nonradial models under the weak disposability of

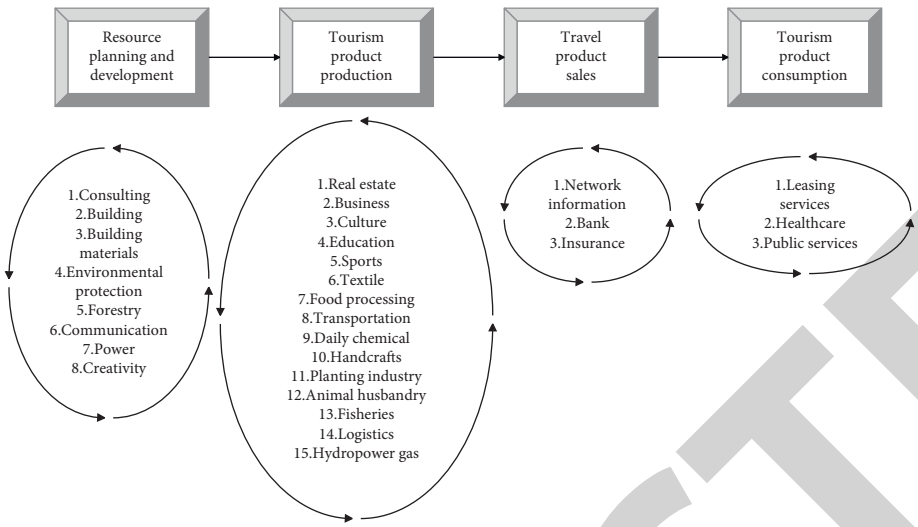

Figure 3: The tourism-related industry chain.

Table 4: Indicators in the study of tourism efficiency and tourism total factor productivity.

Investment indicators	Output indicators
Average price problem Service level Number of hotels Number of rooms	Customer satisfaction
Number of employees Number of rooms Hotel occupancy rate Operating expenses	Accommodation income Hotel income (dining and beverage) Other incomes
Number of employees The number of wages and wealth Operating cost Other costs	Operating income Customer volume Number of overnight stays
Number of employees Capital	Operating income Added value, profit
Number of employees in the tertiary industry Fixed asset investment Actual use of foreign capital	Star-rated hotel operating income
Number of employees in the tourism industry Tourism net fixed assets	Total tourism revenue
Tourism fixed assets Number of employees in the tourism industry Number of employees in the tertiary industry	Total operating income of tourism enterprises
Fixed capital stock Comment on the number of scenic spots Number of star hotels	Total tourism revenue Total number of tourists
Number of travel agencies Number of employees in the tertiary industry Fixed asset investment	Operating income Number of tourists served by travel agencies
Tourism net fixed assets Number of employees in the tourism industry	Total tourism revenue CO2 emissions from tourism

undesired output. Moreover, its proximity index based on gray correlation obtains the key parameters of the combination of radial and nonradial in the model and measures the economic efficiency of the decision-making unit according to the steps. Similarly, it can be calculated by building an output-oriented model.

Table 5: Total factor productivity evaluation indicator system.

Category	Indicator name	Specific indicators
Investment indicators	Labor force	Number of employees in the tertiary industry/10,000 people
	Capital	Urban investment in fixed assets/100 million yuan
Output indicators	Output value	Total tourism revenue/100 million yuan
	Scale	Total number of tourists/10,000 people

Table 6: Productivity and decomposition of tourism total factors.

Time	Effch	Techch	Pech	Sech	Tfpch
2012-2013	1.135	0.924	1.104	1.039	1.039
2013-2014	1.067	1.138	1.045	1.030	1.203
2014-2015	0.995	1.122	1.000	1.005	1.106
2015-2016	0.993	1.188	0.999	1.003	1.167
2016-2017	0.896	1.343	1.048	0.863	1.192
2017-2018	1.057	0.990	1.061	1.007	1.037
2018-2019	0.969	1.150	0.974	1.005	1.103
2019-2020	0.941	1.196	0.911	1.043	1.114
2020-2021	1.024	1.129	0.988	1.046	1.144
Average value	1.006	1.125	1.013	1.003	1.121

Table 7: Analysis table of the total factor productivity indicator of urban tourism.

Years	<1 city/count	City/*a* below average	Variance	Max	Minimum	Average value
2011-2012	64	76	0.031	1.722	0.364	1.039
2012-2013	14	87	0.022	1.736	0.717	1.203
2013-2014	27	97	0.014	1.468	0.830	1.106
2014-2015	12	96	0.014	1.717	0.932	1.167
2015-2016	7	80	0.019	1.206	0.554	1.192
2016-2017	58	71	0.022	1.919	0.514	1.037
2017-2018	22	77	0.012	1.436	0.540	1.103
2018-2019	19	68	0.017	1.627	0.581	1.114
2019-2020	19	96	0.028	1.892	0.464	1.144
2020-2021	8	80	0.004	1.314	0.906	1.121

Table 8: Analysis table of urban tourism technical efficiency indicator.

Years	<1 city/count	City/*a* below average	Variance	Max	Minimum	Average value
2012-2013	45	84	0.041	1.939	0.458	1.135
2013-2014	51	81	0.016	1.586	0.655	1.067
2014-2015	101	92	0.008	1.258	0.795	0.995
2015-2016	102	96	0.010	1.388	0.789	0.993
2016-2017	141	82	0.013	1.264	0.464	0.896
2017-2018	48	69	0.019	1.385	0.504	1.057
2018-2019	125	81	0.008	1.353	0.472	0.969
2019-2020	128	76	0.013	1.335	0.467	0.941
2020-2021	78	86	0.024	1.699	0.399	1.024
Average value	87	83	0.003	1.176	0.876	1.006

4. Statistical Measurement and Influencing Factors of Green Total Factor Productivity of China's Tourism Industry

The tourism industry chain is an input-output system of material, capital, technology, and information completed by different enterprises in the whole process from the development of tourism resources to the consumption of tourism products. We summarize the tourism industry chain into the core tourism industry chain (shown in Figure 2) and the tourism-related industry chain (shown in Figure 3).

When evaluating the total factor productivity of the tourism industry and its subsectors, due to the availability of data or different research purposes, a unified evaluation index system has not been formed. Researchers make diversified choices of indicators and variables according to different specific research goals. Moreover, even in the face

Table 9: Analysis table of urban tourism technology progress indicator.

Years	<1 city/count	City/*a* below average	Variance	Max	Minimum	Average value
2012-2013	123	100	0.016	1.178	0.708	0.924
2013-2014	9	158	0.008	1.469	0.895	1.138
2014-2015	7	111	0.008	1.287	0.946	1.122
2015-2016	0	74	0.001	1.252	1.094	1.188
2016-2017	0	81	0.016	1.599	1.079	1.343
2017-2018	142	139	0.002	1.134	0.815	0.990
2018-2019	3	65	0.002	1.221	0.962	1.150
2019-2020	0	83	0.003	1.312	1.052	1.196
2020-2021	0	87	0.003	1.202	1.050	1.129
Average value	1	78	0.001	1.198	0.983	1.125

of the same research object, scholars will construct different evaluation index systems (see Table 4).

The total number of tourists includes the number of domestic tourists and the number of international tourists. The total number of tourists reflects the city's tourism reception volume and directly reflects the tourism benefits of a city's tourism. Therefore, the total number of tourists in this paper reflects the tourism scale of the tourist city. Total tourism revenue includes domestic tourism revenue and international tourism revenue, which is the most direct economic benefit of a city's tourism development. Moreover, it is also the tourism output value of the region and an important indicator to measure the level and quality of urban tourism development. The total factor productivity evaluation index system is shown in Table 5.

The model proposed in this paper should be used to calculate the total factor productivity of tourism in tourist cities. From Table 6, it can be seen that the total factor productivity of tourism is showing a general upward trend.

Through data sorting (Table 7), it is found that the total factor productivity of the tourist city research sample during the study period fluctuates greatly.

The technical efficiency change index is the product of pure technical efficiency and scale efficiency. The specific performance is output maximization and input minimization; that is, the maximum output is achieved when the input elements are fixed or the input element items are minimized under the given conditions of output, as shown in Table 8.

In terms of technological progress in tourism, the overall variance of the various years fluctuates relatively small and relatively stable, indicating that the technological progress of each city is different but small, as shown in Table 9.

It can be seen from the above research that the DEA-EBM model proposed in this paper can play an important role in the statistical measurement and analysis of influencing factors of green total factor production in the tourism industry.

5. Conclusion

Tourism efficiency relates to the inclusive growth and sustainable development of the tourism industry. It is a comparison between input and output in the process of tourism development within a certain area. Moreover, it is an important indicator used to measure the ability of the entire tourism industry to achieve effective competition, the ability to use resources, the ability to achieve sustainable development, the ability of the tourism industry to compete in the market, the ability of input and output, and the ability of sustainable development. The level of tourism efficiency will directly determine the position of a region in the competitive environment. In addition, better industrial operation efficiency can effectively reduce production costs and increase economic returns, which plays an important role in the development of tourism. This paper combines the EA-EBM model to carry out the statistical measurement of China's tourism industry green total factor productivity and the analysis of influencing factors and verify it through data. Through research, it can be seen that the DEA-EBM model proposed in this paper can play an important role in the statistical speed measurement and influencing factor analysis of green total factor production in the tourism industry.

Data Availability

The data used to support the findings of this study are included within the article.

Conflicts of Interest

The authors declare that they have no conflicts of interest.

References

[1] T. A. Bhutto, R. Farooq, S. Talwar, U. Awan, and A. Dhir, "Green inclusive leadership and green creativity in the tourism and hospitality sector: serial mediation of green psychological climate and work engagement," *Journal of Sustainable Tourism*, vol. 29, no. 10, pp. 1716–1737, 2021.

[2] C. H. Chin, C. L. Chin, and W. P. M. Wong, "The implementation of green marketing tools in rural tourism: the readiness of tourists?" *Journal of Hospitality Marketing & Management*, vol. 27, no. 3, pp. 261–280, 2018.

[3] L. T. Tuan, "Environmentally-specific servant leadership and green creativity among tourism employees: dual mediation paths," *Journal of Sustainable Tourism*, vol. 28, no. 1, pp. 86–109, 2020.

[4] Y. Yusof, Z. Awang, K. Jusoff, and Y. Ibrahim, "The influence of green practices by non-green hotels on customer satisfaction and loyalty in hotel and tourism industry," *International Journal of Green Economics*, vol. 11, no. 1, pp. 1–14, 2017.

Hindawi
Mobile Information Systems
Volume 2023, Article ID 9817515, 1 page
https://doi.org/10.1155/2023/9817515

Retraction

Retracted: Application of Computer Network Technology in Network Music Education System

Mobile Information Systems

Received 1 August 2023; Accepted 1 August 2023; Published 2 August 2023

This article has been retracted by Hindawi following an investigation undertaken by the publisher [1]. This investigation has uncovered evidence of one or more of the following indicators of systematic manipulation of the publication process:

(1) Discrepancies in scope
(2) Discrepancies in the description of the research reported
(3) Discrepancies between the availability of data and the research described
(4) Inappropriate citations
(5) Incoherent, meaningless and/or irrelevant content included in the article
(6) Peer-review manipulation

The presence of these indicators undermines our confidence in the integrity of the article's content and we cannot, therefore, vouch for its reliability. Please note that this notice is intended solely to alert readers that the content of this article is unreliable. We have not investigated whether authors were aware of or involved in the systematic manipulation of the publication process.

Wiley and Hindawi regrets that the usual quality checks did not identify these issues before publication and have since put additional measures in place to safeguard research integrity.

We wish to credit our own Research Integrity and Research Publishing teams and anonymous and named external researchers and research integrity experts for contributing to this investigation.

The corresponding author, as the representative of all authors, has been given the opportunity to register their agreement or disagreement to this retraction. We have kept a record of any response received.

References

[1] X. Chao, "Application of Computer Network Technology in Network Music Education System," *Mobile Information Systems*, vol. 2022, Article ID 8754424, 11 pages, 2022.

Hindawi
Mobile Information Systems
Volume 2022, Article ID 8754424, 11 pages
https://doi.org/10.1155/2022/8754424

Research Article

Application of Computer Network Technology in Network Music Education System

Xiao Chao

Huanghe Jiaotong University, Jiaozuo, Henan, China

Correspondence should be addressed to Xiao Chao; 18291020420@stu.suse.edu.cn

Received 7 July 2022; Revised 26 August 2022; Accepted 29 August 2022; Published 11 October 2022

Academic Editor: Chi Lin

In order to explore the application of network music education system, this paper proposes an application of computer network technology in the network music education system. This method explores the application of network music education systems through the key technical problems and solutions of information recommendation based on computer network technology. The research shows that the efficiency of network music education system based on computer network technology is about 30% higher than that of traditional methods. This paper implements the system according to the layered mode and tests the operation of the software system. The test results show that, through the use case test of each functional module of the foreground and background, the system can execute the issued commands smoothly and normally. Finally, it is concluded that the average risk occurrence rate is 2.02 hours/hour, and the probability of high risk is 17.4%. *Conclusion*. After testing, the operation of the software system has achieved the expected goal.

1. Introduction

With the development of information science, advanced information technology represented by computer, multimedia, communication, and network has penetrated into all fields of science and social development and has had a far-reaching impact on society, changing people's work, life, learning, and lifestyle, thus putting forward higher requirements for the quality of workers. Education should face modernization, the world, and the future. It will lead to major changes in educational thought, teaching theory, teaching mode, teaching method, and teaching means [1, 2]. This change provides an excellent opportunity for China's basic education to achieve the goal of "Three Orientations." In traditional music teaching, due to the single content and lack of variability in form, the amount of information in the unit class is too narrow, and the information transmission link is not smooth, which greatly restricts students' understanding of more music works and cannot meet students' aesthetic needs for works of different music styles. Therefore, how to use modern teaching methods in music education, change the traditional teaching mode, build a learning environment conducive to students, give full play to students' main role, effectively improve teaching effectiveness, and promote the comprehensive development of students' quality have become a subject worthy of experiment in our music teaching.

Compared with traditional music education models and teaching methods, multimedia teaching music system has many advantages, such as rich music teaching content, reducing teachers' workload, and making the teaching process more vivid and interesting. The traditional music teaching mode is a teacher-centered way of "teachers teach, students learn," which mainly aims at teachers' imparting knowledge. In today's world, science and technology are booming, education is in the basic position in the formation of comprehensive national strength, and the status of students and teachers has changed greatly [3]. Today, with the rapid development of science and technology, the traditional music teaching mode can no longer adapt to the modern music teaching environment. Music education is also an aesthetic education. Its content is rich and colorful, and its feelings are rich and diverse. Multimedia has entered the classroom one after another, replacing the previous music

teaching, which has achieved twice the result with half the effort and solves the shortcomings of the traditional music teaching mode and teaching methods. And it is conducive to the application of constructivist teaching theory in music teaching.

2. Literature Review

Yajima et al. believe that the traditional music classroom teaching method has various disadvantages, such as the stylization of teaching form, the simplification of teaching content, the emphasis of teaching process on teaching rather than exploration, and the emphasis of teaching on results rather than process [4]. However, these drawbacks have been greatly improved after the use of "Internet +." Music teachers should view music education from a developmental perspective, maintain an open and inclusive teaching attitude, and update teaching thinking in the context of "Internet +." "Internet +" music classes will eventually spread across the country and open a new charter for music education. E. Nakamura believes that the use of "Internet +" in primary school music classes has made the originally boring classroom lively [5]. Music teachers should conform to the development of the times and actively explore how to use information technology to skillfully combine with music classroom. We should screen and integrate the teaching resources of the network in order to better stimulate students' interest in music learning and actively use the power of information network to cultivate students' creative ability to wear new clothes. Music teachers should actively explore how to use "Internet +" to better serve students and education with the help of network information technology platform. Isabirye believes that the era of "Internet +" has brought unprecedented opportunities and challenges to high school music education [6]. "Internet +" has a large amount of information, including positive and healthy information and negative and indecent information, so it is a double-edged sword. Music teachers should actively guide students to use "Internet +" to search and learn music works conducive to their healthy growth. In the context of the "Internet +" era, music teachers no longer only act as porters of knowledge but become guides in the process of students' learning, encourage and guide students to use network information technology for autonomous learning, and cultivate students' awareness and ability of autonomous learning. Bayley and Waldron believe that music education should pay attention to three points when taking the "Internet +" bus: (1) hardware is necessary, and technology is the key; (2) "Internet +" is not just about using the Internet; (3) it is not substitution but increase. We should carry out innovation on the basis of adhering to tradition and use "Internet +" to sow the seeds of music in the hearts of young musicians [7]. Fang, in his master's thesis, elaborated on the characteristics of music education under the background of "Internet +" from four aspects, "music education and Internet connection," "optimizing music teaching classroom by Internet means," "music education digitization," and "self-help learning" based on "cloud technology," and believed that it has three development trends, namely, main service trend, technology trend, and growth trend [8].

When analyzing the system while collecting data, if problems are found in the process of system analysis, we can further collect more relevant data and make further analysis to solve the problems encountered. Analysis is to prepare for the design, take the results of the analysis as the basis of system design, determine the function of the system according to the results of demand analysis, and design the model and data relationship of the system. After completing the analysis and design of the system, the system still stays in the model. The realization of the system is to change the model of the system to a computer-executable system through computer technology so as to realize the function of music distance education system design. Before the music distance education system is put into use, it is necessary to further test the music distance education system, correct the errors and existing problems in the system, and ensure the normal operation of the system.

3. Method

3.1. System Function Model. The system function model is designed by the system developer to reflect the system model according to the user's needs, the user's business needs, the user's requirements for the system, and the functional requirements. When designing the functional model, we communicate with users through questionnaires, talks, and other methods and convert the user's description of the system and functional requirements into formal documents. Figure 1 shows the overall functional modules of the students.

3.2. System Data Model. Through the analysis, we can get the entities of the system and the connections between entities, which are analyzed as follows.

Entity and entity attributes are as follows.

Student: user ID, user name, real name, password, gender, registration date, last login date, and status [9].

Learning record: learning record ID, user ID, course ID, course name, and last learning time.

Assessment record: test record ID, user ID, test paper ID, test paper name, test time, test score, and test answer.

Teacher: teacher ID, user name, real name, password, and level.

Course classification: course classification ID, course class name, and parent class ID.

Course: course ID, course name, classification ID, classification name, author, adding time, video address, introduction, course duration, recommendation level, and status.

News classification: news classification ID, news class name, and parent class ID.

News: News ID, title, classification ID, classification name, author, adding time, introduction, Title Image URL, content, recommendation level, and status.

Test paper: test paper ID, test paper name, parent ID, and status.

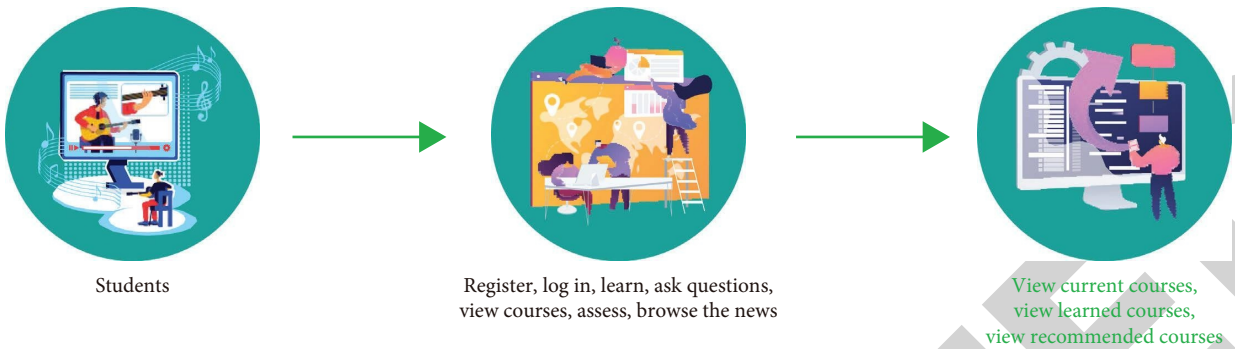

Figure 1: Overall function module diagram of trainees.

Test question: test question Id, classification ID, question, question type, question score, and question answer.

Question: question Id, parent ID, questioner ID, questioner user name, respondent ID, respondent user name, question or answer content, status, and type.

The links between entities are as follows:

Teachers and students: a teacher can manage multiple students, and a student can be managed by multiple teachers, so the relationship between teachers and students is many to many.

Teachers and problems: a teacher can manage multiple problems, and the same problem can be managed by multiple teachers, so the relationship between teachers and problems is many to many.

Teachers and news: a teacher can manage multiple news, and the same news can be managed by multiple teachers, so there is a many-to-many relationship between teachers and news.

Teachers and news categories: a teacher can manage multiple news categories, and a news category can be managed by multiple teachers, so there is a many-to-many relationship between teachers and news categories. News and news category: there can be multiple news under a news category, and a news can only belong to one news category, so there is a one-to-many relationship between them.

Teachers and courses: the same teacher can manage several courses, and the same course can be managed by several teachers, so there is a many-to-many relationship between the two.

Teachers and course categories: a teacher can manage multiple course categories, and a course category can be managed by multiple teachers, so there is a many-to-many relationship between them.

Course and course category: the same course can only belong to a certain course category, and a certain course category can correspond to several courses, so there is a one-to-many relationship between them.

Teachers and test papers: a teacher can manage multiple test papers, and the same test paper can be managed by multiple teachers, so there is a many-to-many relationship between them.

Teachers and assessment records: a teacher can view the assessment records of multiple students, and the assessment records of the same student can be viewed by multiple teachers, so they have a many-to-many relationship.

Test questions and papers: one test question can only belong to one test paper, and one test paper can have multiple test questions, so there is a one-to-many relationship between them.

Students and questions: a student can raise multiple questions, and a question can only be raised by one student, so there is a one-to-many relationship between them.

Students and news: a student can view multiple news, and a news can be viewed by multiple students, so there is a many-to-many relationship between them.

Students and test papers: a student can test multiple test papers, and the same test paper can be tested by multiple students, so there is a many-to-many relationship between them.

Student and assessment record: a student can generate multiple assessment records, and a record can only be generated by a student, so there is a one-to-many relationship between them.

Students and learning records: a student can generate multiple learning records, and a record can only be generated by a student, so there is a one-to-many relationship between them.

Students and courses: a student can learn multiple courses, and a course can be learned by multiple students, so there is a many-to-many relationship between them.

3.3. System Behavior Model. The behavior of the system is mainly generated by students and teachers (administrators). The behavior of both students and teachers basically follows these steps: login ⟶ issue commands ⟶ display operation results ⟶ exit the system/continue operation. Therefore, the behavior of students and teachers is simplified into two state diagrams, as shown in Figures 2 and 3, which are the state diagrams of teachers (administrators) and students' operation behavior, respectively.

The operations of the two state diagrams are the behaviors of students or teachers after logging in. They are a high summary of all the behaviors of the system. If they are subdivided, many specific operations can be divided. Because the operations are very similar, we will not describe

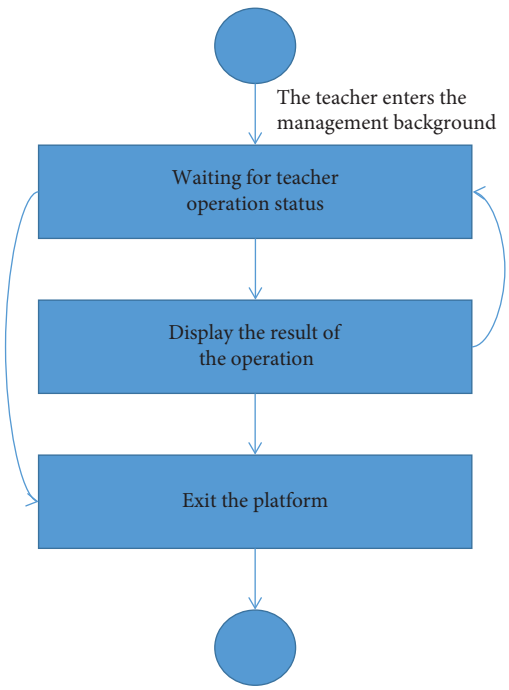

Figure 2: State diagram of teachers' operation behavior.

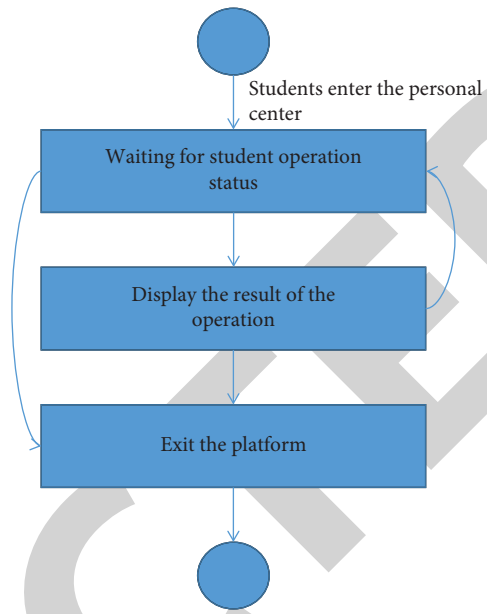

Figure 3: Student operation behavior state diagram.

them in detail. Now we will only make a specific state analysis of the login behaviors of students. Figure 4 shows the user login behavior state diagram.

When a user (student) logs in, the system will check the user's login information. If the user information is correct, the user will change from not logged in to logged in. If the user information is wrong, the system will give a second login opportunity. When the second login is successful, the user will change from not logged in to logged in. If it fails, the system will give a third login opportunity. If the third login is successful, the user will change from not logged in to logged in. If the login fails for three consecutive times, the user account will be locked and will no longer be allowed to try to log in [10, 11].

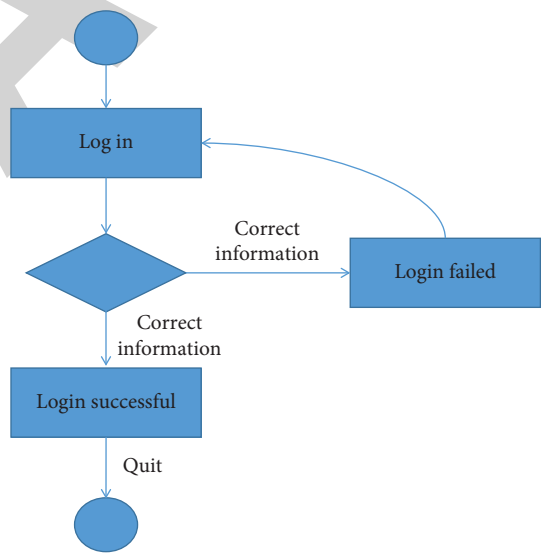

Figure 4: User login behavior state diagram.

3.4. System Architecture. This system is based on the network and belongs to the B/S architecture. B (browser) is a common application software running on the client, which can also be said to unify all clients and put the core functions of the system into the network server. Compared with the traditional c/s mode, it simplifies the development, maintenance, and use of the system. As long as the client installs a browser and enters the system website in the browser address bar, it is convenient to use the system. The architecture diagram of the system network operation is shown in Figure 5.

As can be seen from Figure 5, the system uses a web server and a database server because, considering the scalability of the system and the pressure on the server during multiuser access, they are allowed to undertake different tasks [12].

3.5. System Architecture Implementation Process. According to the system architecture diagram designed above, combined with the implementation, the architecture processing flow of the system can be obtained, as shown in Figure 6.

In Figure 6, the presentation layer (web page layer) is written in JSP to show the page to the user and realize the interaction with the user. When the user needs to request data, it is sent out by the JSP page, and then Struts sends the received request to the corresponding class for processing according to the configuration in struts.xml. In the business layer (service), Spring is responsible for providing business model components and DAO components needed in action

Figure 5: B/S architecture diagram.

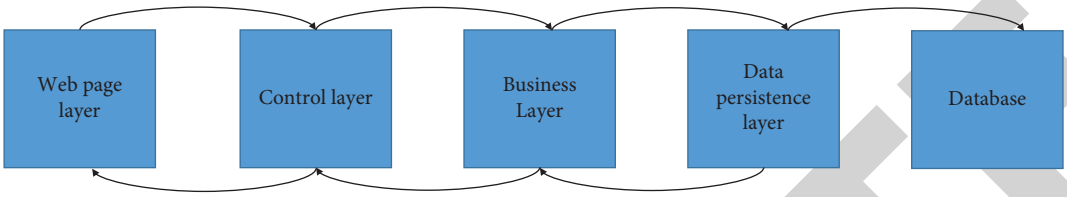

Figure 6: Framework business processing flowchart.

to action and providing unified transaction processing, which is equivalent to taking over the transactions of database operations. In the database persistence layer, Hibernate automatically maps the database and JavaBeans through hbm.xml files so that programmers can manipulate Java beans to operate the database and return the results of the operation to the business layer. After the business layer finishes processing, it returns the results to the control layer and finally receives the response through JSP [13, 14].

3.6. System Database Design. As the bottom layer of system application, the database provides data storage, modification, deletion, query, and other services for the upper layer, which plays a vital role in system design. A good design will improve the storage, query, and statistical efficiency of data, so the following principles must be considered in database design:

(1) *Database Security*. The normal operation of the system depends on the data database, and the system generally stores some sensitive information, such as user name and password. If the data is leaked due to the intrusion of illegal users, the system will not operate normally or be maliciously changed, resulting in a series of adverse consequences. Therefore, the authorization problem should be considered in the design of the database.

(2) *Database Integrity*. The corresponding constraint mechanism and audit mechanism should be designed in the database to prevent data synchronization between two or more tables with relationships and ensure the integrity of the data.

(3) *Database Scalability*. After the system is officially operated for a period of time, it may be further expanded or transplanted for some reason, so the database design should have good scalability.

(4) *Database Specification Design*. It is very important to understand 3NF and apply it to the database design of the software system. In addition, unified naming rules must be used for database naming, table naming, and domain name naming to facilitate maintenance and query.

(5) Ensure the consistency of data in the database. For a certain table, the possibility of concurrency control should be considered to ensure data consistency when updating data [15].

3.7. System Function Realization. Music distance education system is an application program running on the Internet, and the B/S (browser/server) mode is selected. Set up an application server on the server to provide services to customers. As long as a browser is installed on the client, it can be accessed and used. The music distance education system is developed based on the SSH framework of Java language. According to the functional modules of the system, the software system is divided into four levels, and each level of the software system corresponds to the corresponding functions of SSH. In terms of server building, the DBMS of MySQL building software is selected for data storage [16]. In terms of application server, Tomcat server is selected. The cooperation between Tomcat server and MySQL has good stability, high security performance, and high execution efficiency. The implementation of music distance education system adopts the popular layered idea in J2EE project at present. The system is divided into interface layer, service layer, and database persistence layer. On this basis, different modules are divided according to different functions. All modules are implemented by "interface-oriented" programming.

The system adopts a three-tier architecture with MVC code separation [17, 18]. After the introduction of the three SSH frameworks, compared with the three-tier architecture in MVC, their division of labor is basically decided: Hibernate acts as the model layer, responsible for generating objects corresponding to data tables and associating the generated objects with tables. Through the manipulation of JavaBeans to achieve the operation of data tables, Struts acts as the control layer, which is responsible for associating the data layer and the view layer (implemented through JSP), receiving the data submitted by users, then processing it (such as verification and encapsulation), and sending and controlling the direction of the operation process of the whole system. Spring is responsible for managing Hibernate and Struts, providing IOC containers, and generating the

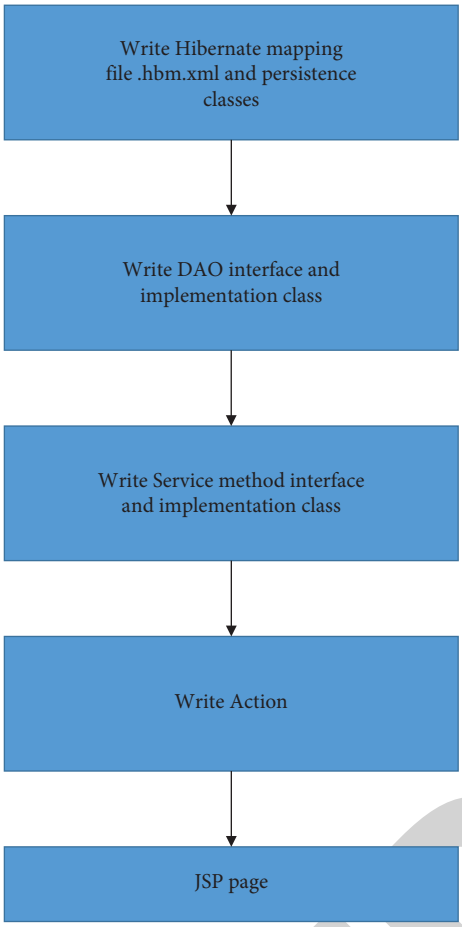

Figure 7: System function module compilation architecture diagram a.

Figure 8: System function module compilation architecture b.

required classes for Hibernate and Struts according to the actual situation of the system so that the code is loosely coupled. Based on the above analysis, the implementation of the system function modules is written according to the process in the following figure, as shown in Figures 7 and 8.

In order to overcome the impact of dynamic changes in the network on network transmission, network QoS monitoring technology is introduced, and real-time monitoring lays a good foundation for intelligent transmission control [19, 20]. Add a timestamp at the protocol layer to monitor the network delay, add two fields to each message, and record the last received timestamp (LRT) and the current sent timestamp (CST). After receiving the message, the receiving end calculates the local packet delay according to the LRT and SCT of the message. At the same time, the processing delay of the message in the network can be obtained by subtracting the processing delay of the opposite end according to the last timestamp (LST) saved by the receiving end and the time when the message is currently received.

When end B replies to A message,

$$\begin{aligned} LRT &= TB + \Delta t1, \\ CST &= TB + \Delta t1 + \Delta t2. \end{aligned} \tag{1}$$

When end A receives the message from end B, its local LRT is

$$LRT = TA + \Delta t1. \tag{2}$$

And its current time is

$$CT = TA + \Delta t1 + \Delta t2 + \Delta t3. \tag{3}$$

At this time, it can be calculated that the bidirectional delay of message sending is

$$CT - LST - (CST - LRT). \tag{4}$$

4. Results and Analysis

Software testing can also be carried out at different stages of the software implementation process. The software system is a whole, but software testing should not only regard the software system as a whole but also be carried out step by step. In the initial functional design of the software system, it is divided according to the functional modules of the system. When programmers divide the work, they also divide the work and code according to the functional modules. When

Table 1: User registration module test table.

Module name	User registration module				Tested by	Foreground user
Case number	1				Test time	2022.3.2
Test purpose	Test the effectiveness of user registration function					
Browser	General browsers such as IE11					
Correct data	User name: 4–10 digits; password: 5–15 digits; real name: required					
	Test input					
Operation steps	User name	Password	Duplicate password	Real name	Expected output	Actual output
1	Guest	12345	12345	Zhang San	Normal registration	Normal registration
2	Guest	12345	12345	Zhang San	Prompt user name length error	Prompt user name length error
3	Guest	12345	1234	Zhang San	Prompt that the two passwords are inconsistent	Prompt that the two passwords are inconsistent
4	Guest888888	12345	12345	Zhang San	Prompt user name length is too long	Prompt user name length is too long
5	Guest	1234567891011111	1234567891011111	Zhang San	Prompt password length is too long	Prompt password length is too long
6	Guest	12345	1234	Zhang San	Prompt that the two passwords are inconsistent	Prompt that the two passwords are inconsistent
7	Guest	12345	123456	Zhang San	Prompt that the two passwords are inconsistent	Prompt that the two passwords are inconsistent
8	Guest	1234	1234	Zhang San	Prompt password length is too short	Prompt password length is too short
9	Empty	12345	1234	Zhang San	Prompt user name cannot be empty	Prompt user name cannot be empty
10	Guest	Empty	1234	Zhang San	Prompt password cannot be empty	Prompt password cannot be empty
11	Guest	12345	Empty	Zhang San	Prompt duplicate password cannot be empty	Prompt duplicate password cannot be empty
12	Guest	12345	12345	Empty	Prompt that the real name cannot be empty	Prompt that the real name cannot be empty
13	Empty	Empty	Empty	Empty	Prompt user name cannot be empty	Prompt user name cannot be empty

the function of the module is completed, the function module needs to be integrated into the subsystem and finally integrated into a complete system. After the system is put into operation, it is necessary to continue to test the stability of the system. Testing is required in the process of software implementation, so software testing can be divided into the following tests.

4.1. Module Testing. Module test is a test conducted by programmers when completing module functions. Module testing requires not only testing whether the module completes the set function from the function but also completing the logic test from the internal code to test whether the process executed inside the module is correct [21, 22].

4.2. Subsystem Test. Subsystem test is a test conducted after the integration of functional modules, which needs to test whether the functions of each module are compatible and whether the data exchange between modules meets the design requirements [23, 24].

4.3. System Test. System testing is conducted after the completion of system integration. System testing is a systematic process, which includes function testing (using black box testing method) and program logic code testing [25].

4.4. Acceptance Test. After the acceptance test software is written, check whether the software meets the required test, create the normal operation environment of the software, and check whether the function of the software meets the design requirements. The acceptance test can verify whether the software system meets the design requirements.

4.5. Parallel Operation. Some software system errors will cause immeasurable losses, and these software systems need to be strictly tested before they can be put into operation. After putting into operation, the original system will not be removed immediately but run at the same time with the original system to check whether the new system has problems. When problems are found in the new system, they can be corrected after it is officially put into operation. The music system belongs to the B/S structure, and the roles of

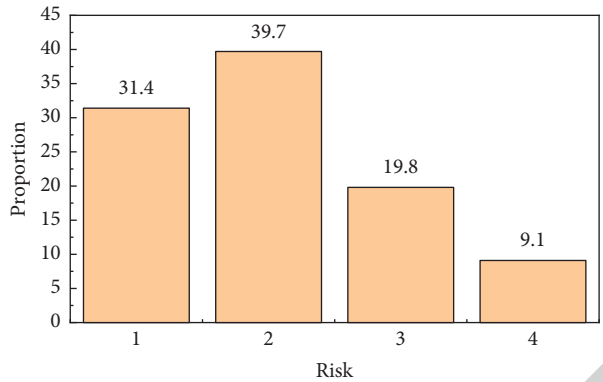

Figure 9: Risk classification.

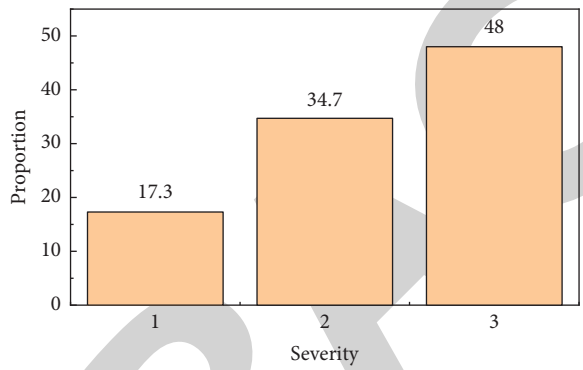

Figure 10: Severity.

Table 2: User login module test table.

Module name	User login module			Tested by	Foreground user
Case number	2			Test time	2022.3.2
Test purpose	Verify whether the legal and illegal login meet the requirements				
Browser	General browsers such as IE11				
Correct data	User name: chengbao; password: baolei				
	Test input				
Operation steps	User name	Password	Verification code	Expected output	Actual output
1	Chengbao	Empty	Empty	Prompt for password	Prompt for password
2	Empty	Baolei	Empty/error	Prompt for user name	Prompt for user name
3	Chengbao	Baolei	Empty/error	Prompt for verification code	Prompt for verification code
4	Chengbao	Guest	Fill in correctly	Prompt user name/password error	Prompt user name/password error
5	123456	Guest	Fill in correctly	Prompt user name/password error	Prompt user name/password error
6	Empty	Empty	Fill in correctly	Prompt for user name	Prompt for user name
7	Chengbao	Baolei	Fill in correctly	Normal login	Normal login
8	Empty	Empty	Empty	Prompt for user name	Prompt for user name
9	At will	At will	At will	Go back and clear the input box	Go back and clear the input box
10			Click on the verification code image	Replace verification code	Replace verification code

Table 3: Background administrator menu test table.

Module name	Background administrator menu	Tested by	Background user
Case number	3	Test time	2022.3.2
Test purpose browser	Check whether the menu switch is correct general browsers such as IE11		
Operation steps	Pedagogical operation	Expected output	Actual output
1	Click global settings	Display the menu of website settings and registration settings	Display the menu of website settings and registration settings
2	Click course management	Display the added course and category management menu	Display the menu of adding courses and category management
3	Click student management	Show add student, student list menu	Show add student, student list menu
4	Click assessment management	Display the test paper category management and test question management menu	Display the test paper category management and test question management menu
5	Click news management	Display the menu of adding news, news list, and news classification management	Display the menu of adding news, news list, and news classification management
6	Click problem management	Show question list menu	Show question list menu

Table 4: Test form of the backstage student management module.

Module name	Backstage student management module	Tested by	Background user
Case number	4	Test time	2022.3.2
Test purpose	Check the functions of the backstage student management module		
Browser	General browsers such as ie11 IE11		
Operation steps	Pedagogical operation	Expected output	Actual output
1	Click add student menu	Show the add student page	Show the add student page
2	Click the student list menu	Show student list	Show student list
3	Click the division menu in the list	Display the prompt whether to delete it really	Display the prompt whether to delete it really
4	Click the modify menu in the list	Display the modify student page	Display the modify student page
5	Fill in the information in the add student page	Check whether the data is correct	Correct data verification
6	Fill in and modify the information in the student page	Check whether the data is correct	Correct data verification
7	Click the "yes" button to delete the prompt	Delete data	Delete data
8	Click the "no" button to delete the prompt	There is no change in the data	There is no change in the data

Table 5: Statistical table of software test analysis.

Test software name	Music distance education platform		
Number of use cases	38	Number of risks	121
Test time	60	Average risk discovery rate (person/hour)	2.02

the foreground and background are completely independent, so the test plan will separate the foreground and background. The top and background will be tested, respectively, according to the program function, and the input value will be set with edge value and error value to ensure the normal operation of the program. Some test cases of music system functions are shown in Tables 1–4.

The user registration module test form, user login module test form, background administrator menu test form, and background student management module test form have been displayed in the test case. What is shown here is only one part of the test. There are other test parts in the music system.

In software testing, we found some problems, such as logic errors in programming, poor reliability caused by some illegal data not being detected, and the output data not reaching the standard. These problems were recorded in the test cases so as to check and correct the errors in the software.

Through the use case test of each functional module of the foreground and background, the system can smoothly and normally execute the commands issued. The final test

analysis statistics are shown in Table 5 and Figures 9 and 10. From Table 5 and Figures 9 and 10, the average risk occurrence rate is 2.02 hours/hour, and the probability of high risk is 17.4%, as shown in Table 5 and Figures 9 and 10.

5. Conclusion

From the software system design technology, this paper analyzes and studies the technology needed to design the music remote system, including unified modeling language UML, software system B/S architecture technology, database design technology, and entity relationship data model Finally, it analyzes the implementation technology of the software system and determines the design tool of the software system according to the needs of the music system. In the design process, considering that the music distance education system is an Internet-based system, we chose the Internet-based development Java language. In order to improve the efficiency of Java, MVC architecture and SSH framework technology are adopted in the software implementation. The application of SSH framework technology in the music remote system can well layer the system, which is conducive to the expansion and transplantation of programs, and enhance the flexibility of the system. The database adopts open source MySQL and uses toad for MySQL visual database operation software to accelerate the development of the database.

Through the test and trial operation of this system, the students' feedback on the system is good. The unified page design style, reasonable layout and structure, simple and clear operation, and smooth running speed give students a good experience. Online learning, online testing, viewing the learning situation of the course, and other functions are practical and easy to use, which makes it convenient for students to freely choose time and place for independent learning. Interactive online Q & A provides a new way for students to communicate with teachers. For teachers, the management of courses, test questions, news, students, and problems can be easily realized in the system, and the continuous increase of teaching resources, information, and students can be freely controlled. Therefore, the system has important practical significance for teaching and learning across time and space.

Data Availability

The data used to support the findings of this study are included within the article.

Conflicts of Interest

The author declares that there are no conflicts of interest.

References

[1] Y. H. Lin and H. H. Chen, "Tag propagation and cost-sensitive learning for music auto-tagging," *IEEE Transactions on Multimedia*, vol. 23, no. 99, p. 1, 2020.

[2] D. M. Gutierrez, G. H. Penaloza, A. B. Hernandez, and F. Alvarez, "A multimodal end-to-end deep learning architecture for music popularity prediction," *IEEE Access*, vol. 8, no. 99, p. 1, 2020.

[3] J. R. Castillo and M. J. Flores, "Machine learning for music genre: multifaceted review and experimentation with audioset," *Journal of Intelligent Information Systems*, vol. 55, no. 1, pp. 1–31, 2020.

[4] K. Yajima, H. Kanematsu, D. M. Barry et al., "Application of biological information from eye blinking to mutual communication for e-learning: results of pbl activities for students," *Procedia Computer Science*, vol. 176, pp. 3029–3036, 2020.

[5] E. Nakamura, Y. Saito, and K. Yoshii, "Statistical learning and estimation of piano fingering," *Information Sciences*, vol. 517, pp. 68–85, 2020.

[6] J. Isabirye, "Can indigenous music learning processes inform contemporary schooling?" *International Journal of Music Education*, vol. 39, no. 2, pp. 151–166, 2021.

[7] J. G. Bayley and J. Waldron, ""it's never too late": adult students and music learning in one online and offline convergent community music school," *International Journal of Music Education*, vol. 38, no. 1, pp. 36–51, 2020.

[8] K. Fang, "Equipment remote visual support maintenance system," *Procedia Computer Science*, vol. 166, pp. 335–338, 2020.

[9] A. A. Sagadevan and S. S. Chirayath, "Design and analysis of an internal remote monitoring system for spent nuclear fuel stored in a dry cask," *Nuclear Technology*, vol. 208, no. 3, pp. 428–436, 2021.

[10] H. Fukumoto, T. Yamaguchi, M. Ishibashi, and T. Furukawa, "Developing a remote laboratory system of stepper motor for learning support," *IEEE Transactions on Education*, vol. 64, no. 99, pp. 1–7, 2020.

[11] L. Liu, L. Li, Z. Zhao, and Y. Wang, "A remote laser focusing system with spatial light modulator," *Computer Communications*, vol. 154, pp. 92–98, 2020.

[12] X. Dong, J. Li, J. Wu, and J. Liu, "A window detection algorithm for remote laser gas leakage detection system," *Procedia Computer Science*, vol. 174, pp. 720–728, 2020.

[13] D. Arivudainambi, K. Varun, K. R. Vinoth, and P. Visu, "Ransomware traffic classification using deep learning models: ransomware traffic classification," *International Journal of Web Portals*, vol. 12, no. 1, pp. 1–11, 2020.

[14] S. Hakak, M. Alazab, S. Khan, T. R. Gadekallu, P. K. R. Maddikunta, and W. Z. Khan, "An ensemble machine learning approach through effective feature extraction to classify fake news," *Future Generation Computer Systems*, vol. 117, no. 6, pp. 47–58, 2021.

[15] M. Shi, Y. Tang, X. Zhu, and J. Liu, "Topic-aware web service representation learning," *ACM Transactions on the Web*, vol. 14, no. 2, pp. 1–23, 2020.

[16] P. Morais, M. J. Ferreira, and B. Veloso, "Improving student engagement with project-based learning: a case study in software engineering," *IEEE Revista Iberoamericana de Tecnologias del Aprendizaje*, vol. 16, no. 1, pp. 21–28, 2021.

[17] R. H. Hwang, M. C. Peng, C. W. Huang, P. C. Lin, and V. L. Nguyen, "An unsupervised deep learning model for early network traffic anomaly detection," *IEEE Access*, vol. 8, pp. 30387–30399, 2020.

[18] H. Wang, J. Li, Q. Yu, T. Hong, J. Yan, and W. Zhao, "Integrating recurrent neural networks and reinforcement learning for dynamic service composition," *Future Generation Computer Systems*, vol. 107, pp. 551–563, 2020.

[19] M. Abbasipour, S. Yazdi, J. Milimonfared, and K. Rouzbehi, "Technical constrained power flow studies for idc-pfc

Hindawi
Mobile Information Systems
Volume 2022, Article ID 3374674, 11 pages
https://doi.org/10.1155/2022/3374674

Research Article

Construction of Mobile Internet Financial Risk Cautioning Framework Based on BP Neural Network

Wu Zang

College of Accounting and Finance, Taizhou Vocational College of Science & Technology, Taizhou 318020, Zhejiang, China

Correspondence should be addressed to Wu Zang; 2012000436@tzvcst.edu.cn

Received 23 August 2022; Revised 13 September 2022; Accepted 22 September 2022; Published 11 October 2022

Academic Editor: Chi Lin

With the emergence of the 21st-century global economy, the international financial system faces economic risks. A competitive cautioning model for financial management is required to mitigate risks and losses in the financial sector. The financial losses of the banking industry have been categorized and analyzed using the Internet of Things (IoT) and big data technologies to minimize the economic risk of commercial banks in mobile internet finance (MIF). This article proposes a new financial risk cautioning framework (FRCF) based on the IoT, big data, and back propagation-neural network (BP-NN) to ensure steady growth of MIF in the long term. In this article, a big data technology-based approach for data recognition and mining has been suggested. A BP-NN-based method for risk identification and assessment in MIF is also presented. The BP-NN technique calculates each neural network (NN) layer's node count, transfer functions, learning rate, and other characteristics. The proposed FRCF has been developed through the proper construction, analysis, and testing of many information samples. A conceptual understanding of the use of IoT, big data, and artificial intelligence (AI) technologies through NN models in the financial industry has been described in the article. The proposed FRCF can predict the MIF risks associated with the MIF lending infrastructure with a 98.2% accuracy.

1. Introduction to Cautioning of MIF Risk in Financial Enterprises

The growth of Internet technology has aided socio-economic development, is now widely employed in many spheres of society, and has altered the financial sector's operations. The financial industry bases its action on Internet technology and leverages big data to move toward digitization. It achieves corporate change and undermines the conventional economic model [1]. A rational self is seen as a cohesive, noncontradictory whole in conventional economic theory. The financial survey of an organization has historically been a crucial resource for stakeholders. It is also an essential source for the general public, bankers, and trade partners to grasp the facts about the organization. When there are no longer any avenues for people to learn about an organization, they will seek for the organization's yearly report to study. They will base their investment choices on their own experiences [2]. Fitzpatrick matched samples of bankrupt and nonbankrupt firms in 1932, during the first economic recession, and thus began the tradition of the statistical study of early financial cautioning. Fitzpatrick's 19 pairs of samples were split into two groups (bankrupt and nonbankrupt) using the single factor financial ratio index. Finally, it has been discovered that the value of capital, shareholders' assets, and debts were the three indices with the best potential to forecast the financial crisis [3].

Internet finance is an economic practice where various owners fulfill their demands for money by using digital technology like mobile computing [4]. Due to information asymmetry and other issues, China's banking system is not yet flawless. Banks frequently fail to get comprehensive financial information from lenders while expanding credit operations, which puts banks at risk for Internet finance [5]. An innovative financial business model called "Internet finance" uses the Internet and information and communication technologies to undertake financing, payments, capital, and informational intermediary services between established financial institutions and online businesses. The risks taken on by banks have developed along with the

financial concerns that have evolved as the globalization process of economic liberalization gains momentum. Given this context, banks are currently required to update the management mechanism for MIF risk assessment [6] using advancements in science and technology. The systematic process of identifying, measuring, monitoring, and managing the many risks that an organization faces is known as risk management. Risk management systems and capacity-building activities have mostly concentrated on financial and operational concerns inside microfinance institutions (MFIs).

The big data produced by the growth of mobile, Internet, and information systems have sparked a revolution and significantly influenced the advancement of many industries. A collection of data that can be quickly gathered, archived, maintained, and evaluated by a computer is what big data is, in essence [7]. The efficiency of data transport, retention, computing, and dissemination has increased in the big data era. Enterprise business information, financial information, and associated data may all be accessible simultaneously using big data. It offers a sizable data source for early cautioning of the risks related to MIF [8]. Big data analytics makes use of these vast amounts of data on MIF risk possible, enhancing the precision and objectivity of earlier detection and cautioning. Traditional risk assessment techniques, such as the multiple discriminant approach and logistic regression decision trees, may correctly estimate MIF risk. The drawback of these conventional approaches is that they depend too much on previous data and need a lot of actual data as the foundation, which limits their capacity to provide proactive cautioning [9].

Data management and development have been delayed in China. Many clients' financial and business information is not wholly disclosed, which presents unique challenges in predicting and evaluating financial risks [10]. Complex nonlinear issues can be resolved using the NN model. Therefore, early MIF risk may be easily assessed by using a BP-NN finance cautioning model to merge big data with MIF risk cautioning, and the steps to lower the danger of MIF are appropriate [11].

An early cautioning FRCF model to predict MIF risk using BP-NN has been constructed, and the NN is enhanced to boost the accuracy of cautioning of MIF risks. The FRCF accurately evaluates MIF risks and raises the financial sector's level of advancement. To identify, remove, and reduce risks, businesses utilize the risk management framework as a framework and guidance. The National Institute for Standards and Technology created it first in order to safeguard the American government's information systems. In addition, it serves as a guide for developing a risk cautioning system for banks' MIF operations. Thus, the main contributions of this article are as follows:

(i) Big data and IoT technology are employed for MIF data recognition and mining to facilitate risk identification in the banking industry

(ii) To examine the predicted gap value of risk evaluation and objectively examine the different MIF risks faced by the banking sector, Risk Rate Model (RRM) and IoT have been used

(iii) Construct an FRCF framework using the BP-NN to achieve compelling financial risk assessment and ensure steady growth of MIF

(iv) The proposed FRCF has been developed through the proper construction, analysis, and testing of appropriate data samples from the rural financial institution in China

The remaining article has been ordered: Section 2 defines associated research on MIF risk and cautioning techniques. Section 3 gives a new financial risk cautioning framework (FRCF) based on the IoT, big data, and BP-NN. Experimental results and discussion have been given in Section 4. Finally, the conclusion, limitations, and scope for further research have been shown in Section 5.

2. Related Works on MIF Risk and Cautioning Techniques

Structured risk is an exogenous, non-diversifiable risk that threatens the macroeconomic environment instead of just a few banking firms. Non-diversifiable risk results from variables that have an impact on the entire market, such as overseas investment policy, financial policies, changing socio-economic parameters, changing taxation provisions, and threats to and actions taken in relation to global security. Systematic risk is a type of market risk that cannot be diversified. Economic, political, and social considerations, for example, are outside the control of the company or investor. Unsystematic risks, meantime, are microeconomic issues that have an impact on businesses. Nevertheless, the worldwide financial crisis of 2008 made regulatory agencies and academia realize that structured risk has several degrees of impact on the actual economy. As a result, a new notion for systemic risk has emerged, known as contagion risk, which states that one banking institution's failure will cause other banking firms' failure [12]. Systemic financial hazards have received much attention from governmental bodies and academics ever since the global financial crisis of 2008. Systemic risk "induces a significant amount of market players to experience substantial losses simultaneously and swiftly propagate the loss into the whole economic system" [13].

Authors in [14] examined the primary factors of loan loss provision (LLP), which are categorized as either voluntary (revenue flattening, investment management, and communication) or nonvoluntary using information from a group of more than 410 Italian banks for the years 2002 to 2016 (based on the business loop). An item on the income statement called a loan loss provision is set aside to cover unpaid loans and loan payments. To offer a realistic picture of their overall financial health, banks must take into consideration prospective loan defaults and expenditures. According to the findings, LLP in Italian banks appears to be contractionary, with nonvoluntary factors and socio-economic disruptions exerting a substantial influence. Additionally, because regional banks' liabilities are better secured

and their conduct is more heavily influenced by adequate supervision, LLP is less cyclical in this circumstance [14].

The "Fractional Predicted Loss Method," Conditional Risk-at-Value Method ($CoVaR$), and specific other novel risk evaluation techniques are proposed to characterize the general level of systemic risk further. These techniques also quantify the contribution of individual banking firms to more comprehensive economic risk when the financial sector is unstable. However, because $CoVaR\ and\ \Delta CoVaR$ only take into account correlation into account, two companies with the same connection to the market but different turbulence levels will be evaluated equally by $CoVaR$, even if one is almost secure and has turbulence of zero [15].

The median estimated shortcomings (MES) measuring approach does not consider the size of banking firms, liquidity ratio, or solvency ratio. Still, it does show the capital that businesses would need to augment in the case of a financial crisis [16]. As a result, the process of determining risk factors may be biased.

Due to their nonlinear correlations among variables that may significantly boost the effectiveness of MIF early cautioning, nonlinear models have increasingly supplanted the usage of linear models, such as time-series data, in financial forecasting, and cautioning systems. Zou et al. suggested a multiscale NN model predict the risk of selling crude oil [17]. These risk projections were combined as the ensemble members using the convolutional neural network (C-NN)-based nonlinear ensemble model, which results in the best ensemble predictions. The suggested model's effectiveness has been empirically evaluated using a large dataset built using daily price records from the leading crude oil markets.

Ensemble approaches have been effective in predicting financial distress. Gradient boosting was employed to forecast bankruptcy accurately among the other ensemble approaches. Shares of ordinary stock will stop yielding dividends and effectively lose all value. When a corporation files for bankruptcy, the stock may be delisted from the main stock exchanges and the symbol may be changed to Q. In [18], the authors developed CatBoost, a unique method for categorizing attribute values using gradient boosting decision trees. Initially, they started by looking into the significance of the characteristics found in the CatBoost model. CatBoost is a technique for decision trees that uses gradient boosting. It was created by Yandex engineers and researchers and used for weather prediction, personal assistance, self-driving automobiles, and search. Second, the suggested technique was compared to eight baseline machine learning models employed between one and three years before failure. Compared to other cutting-edge techniques, the model shows a significant enhancement in the ability of classification results.

Deep learning has advanced in recent years, and specifically, deep learning techniques, including the LSTM NN, have been increasingly integrated into MIF risk forecasting. Yang and Wang (2019) discovered that the accuracy rate was much better than the BP when using the LSTM NN to study the prediction of three different maturities of 30 international stock indices. Deep learning techniques have the edge over conventional machine learning since they can handle complex, high-dimensional, unpredictable data more efficiently. With limited cognitive resources in a small sample set, the attention-LSTM network further presents a learning algorithm based on the LSTM network that can swiftly filter out critical data from a massive amount of available data [19].

The effectiveness of data processing has significantly increased with the introduction of big data technologies and machine learning. Risk management has become increasingly digital and loaded with information due to the novel correlation analysis of several algorithms and big data technologies [20]. Zhang developed an intelligent fuzzy neural network-based financial investment risk model. This study provides reliable assessments of the cautioning signs of MIF risk for a sample of businesses from an economic standpoint, derives inferences from empirical comparison research, and recommends appropriate regulatory changes [21].

The NN can suit nonlinear problems without depending on the job configuration to provide an effective prediction result, allowing it to assess the FRCF's prediction impact more precisely. In essence, the article builds a BPNN-based FRCF using big data and IoT technology to identify and evaluate the financial hazards associated with the MIF. Then, the real MIF platforms are selected for investigation based on the early risk prediction research conducted on the recently established MIF application. This study aims to offer a crucial source of information for the steady growth of MIF.

3. Financial Risk Cautioning Framework (FRCF) for MIF in the Banking Sector

The banking industry collaborates with the Internet, mobile computing, IoT, and other technologies to develop MIF. MIF has seen a significant change in governance, procedures, and technology compared to conventional financial approaches. The MIF model that is expanding is Internet credit financing due to its easy implementation and high returns on investment.

3.1. MIF Credit Risk. MIF credit is obtaining and lending loans to individuals and between individuals and businesses on a digital site. This borrowing strategy departs from conventional banking in the implementation process. The borrowing strategy calculator uses different interest rates and repayment plans to demonstrate the fundamentals of banking borrowing and repayment. Your clients will gain from careful examination of their mortgage and payment alternatives in order to make choices that enable their funds to work harder for them. People have preferred it since it is based on digital technologies and relatively cheap but has a comparatively high return on investment.

Figure 1 depicts the two MIF credit operation modes in the banking sector. Figure 1(a) demonstrates how the online mode of MIF operation may accomplish all credit and financial operations using the Internet framework and IoT technologies. Still, it can also produce a very high default probability, necessitating the acceptance of the associated risk. As shown in Figure 1(b), the second mode blends

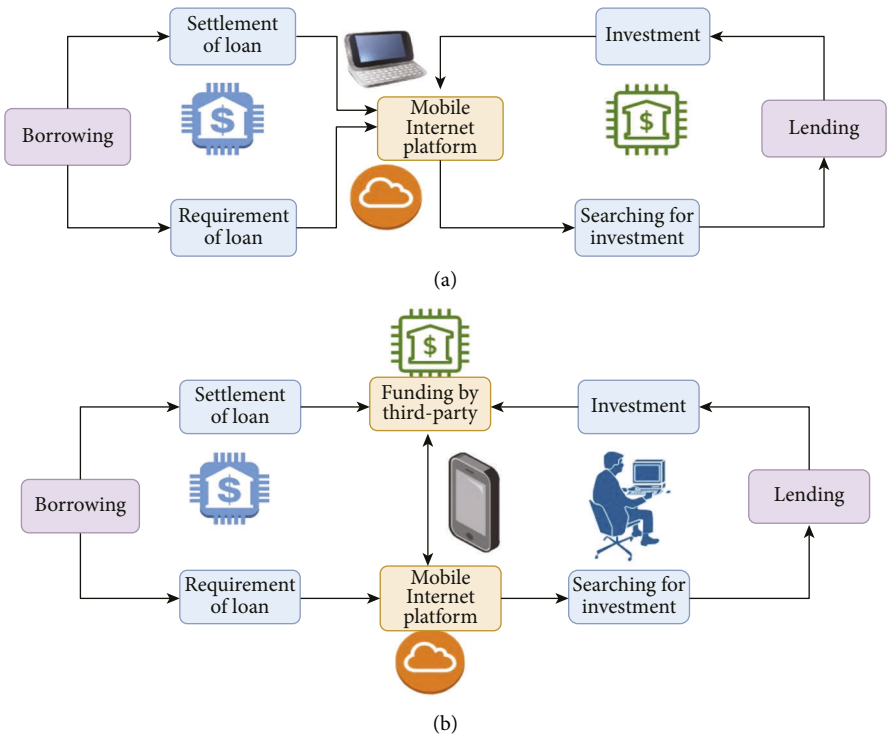

Figure 1: Modes of operation of MIF credit in the banking sector. (a) Online mode of operation of MIF. (b) Combined (online and offline) mode of operation of MIF.

online and offline transactions; while the loan may be raised online, "searching for investment," and evaluations must be completed offline. Information dependability may improve as a result, but running expenses will increase. Despite the differences in their features, these two operational modes will produce some credit risks for MIF.

3.2. Data Recognition and Mining of MIF Data Using Big Data and IoT Technology. The big data technique refers to the concept of data mining with the advent of specific unstructured multimedia data, such as images and audio files—the fast expansion of such unstructured information results from the development of storage technologies. In order to uncover hidden patterns and forecast upcoming trends and behaviors in the financial markets, data-gathering techniques have been applied. Mining such data, particularly high-frequency financial data, often requires advanced statistical, mathematical, and artificial intelligence approaches. The proliferation of distributed programming and cloud-based systems in the IoT age has led to a change in the research focus of big data technologies to fog computing and distributed processing architectures. Mobile data now has the features of dispersion and fragmentation due to the ongoing popularity of smartphones and the exponential increase of data in social media-based networks. These qualities make storing and analyzing the banking sector's mobile data related to IF a challenging process.

Figure 2 shows the data recognition and mining of mobile MIF data using big data. Big data technology is used to handle a significant volume of mobile data. As shown in Figure 2, certain vital technologies related to big data and the IoT extract combine and store various types of MIF data. The MIF data has been analyzed through analogous computation and deep learning algorithms. The analog deep learning method includes hurling incredibly fast protons through materials. The device's electrical conductivity is modulated by electrochemically inserting the proton, the smallest ion, into an insulating oxide. RapidMiner, a rather sophisticated data mining system, may offer some assistance with extensive data analytics via a graphical user interface to display the output MIF data [22]. Data transformation, modeling, analysis, assessment, and information processing are just a few of the many operations found in RapidMiner. Data loading and transformation (ETL), data preparation and visualization, data modeling and statistical modeling, assessment, and deployment are just a few of the data mining and machine learning processes that RapidMiner offers. RapidMiner is a potent data mining program that supports model deployment, model operations, and data mining. All the specific loading and machine learning skills required to make a significant effect throughout your business are provided by our end-to-end data science platform. It has been widely utilized because of its strong data mining skills, extensive algorithm functionality, and advanced analytics. The analyzed MIF data can be processed through deep learning algorithms to predict the risk involved through appropriate computation and human-machine interaction to get the desired output for MIF risk prediction. HMIs may be utilized for both straightforward and intricate tasks. An HMI's user interface can be customized by the user to meet their needs.

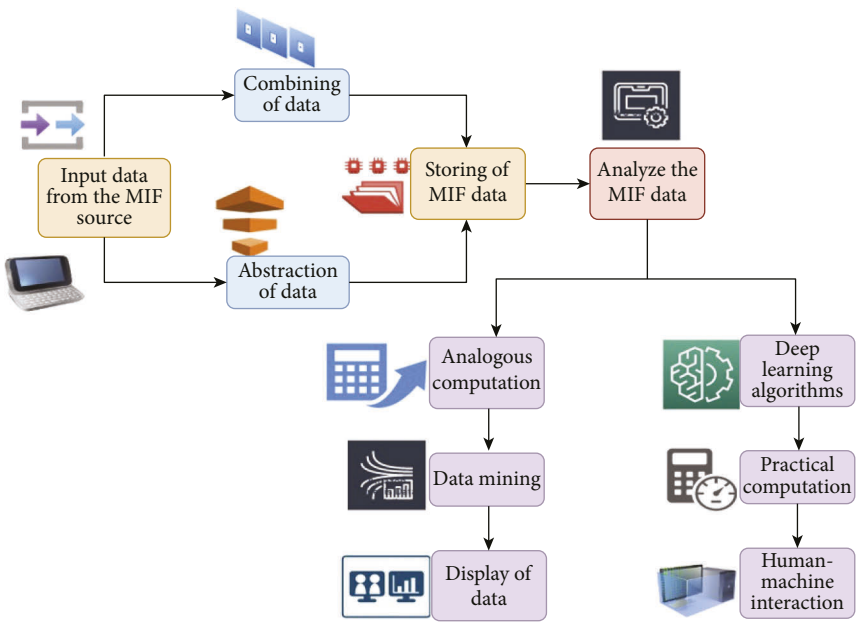

Figure 2: Data recognition and mining of mobile MIF data using big data.

3.3. Detection of MIF Risks Using Big Data Techniques. Big data expertise has been employed to determine the risks associated with MIF. When RapidMiner is used for risk modeling and examination of MIF, the web crawler technique is employed to gather information [23]. An Internet bot that routinely browses the Internet and is primarily run by browsers for the sake of Web indexing is known as a Web crawler, sometimes known as a spider or spiderbot and frequently abbreviated to crawler (web spidering). There is simply too much information at times. It is simple to deceive the crawler. Websites include secret information that may be used to trick users into thinking they are seeing something they are not. The required preprocessing is accomplished in RapidMiner to obtain the correct MIF information module and enable the use of big data technologies for information assessment.

Figure 3 depicts the detection of MIF risks using big data techniques. The following stages are often used to segment data mining and detect MIF risk: initially, the web crawler's data is selected to obtain the relevant statistical information and progressive information regarding MIF. Following the analysis and preprocessing to detect data anomalies and incompleteness, the data set's features have been determined, and data conversion and cleaning are carried out. The processed information is used as modeling data for the random forest (RF) algorithm and logistic regression model [24] for MIF data classification to detect and evaluate MIF risks and provide analysis findings. Random forest has a greater true and false positive predictive value as the number of explanatory factors in a dataset rise, but regression analysis performs better in general when the number of noisy variables is less or equal to the total of explanatory variables.

The RF algorithm must be implemented, which necessitates the creation of different data sets. Subsequently, the information has been trained, and the decision tree for classification may be retrieved. The data not retrieved throughout the collection process will make up the unbiased data set. During feature extraction, these decision trees must be categorized according to their classification capacities. Then a recursive function may be used to acquire the whole classification decision tree, and an optimization model has been used to detect the MIF risks. Without supervision, the decision tree may grow to the maximum, reducing error and enabling many decision trees to grow together to build an RF.

3.4. MIF Risk Analysis Using IoT Technology. IoT technology advancement offers financial firms substantial and practical technological assistance in managing risk management. IoT risk management is a collection of procedures and techniques used to find and assist in removing possible threats and detrimental effects of IoT vulnerabilities. IoT risk management employs risk management procedures and controls the associated business risk depending on all parts of that firm's usage of technology. Modern technical frameworks do, however, also carry with them several new operational dangers like MIF. Depending on the fundamental logical framework of IoT, the operational risks may be divided into the following three types. Threats from the data detection layer are within the first group. Bar codes, Quick Response (QR) codes, different sensors, and sensing technology like satellite location are the key components of the detection layer. Banking firms usually use these sensors to gather and analyze the MIF data. Various sensors often have varying degrees of precision, leading to inconsistent operational risk awareness.

Multiple levels of functioning risks in the perceptual layer will also originate from terminal failures, information source failures, or denial of QR codes. Risks from the

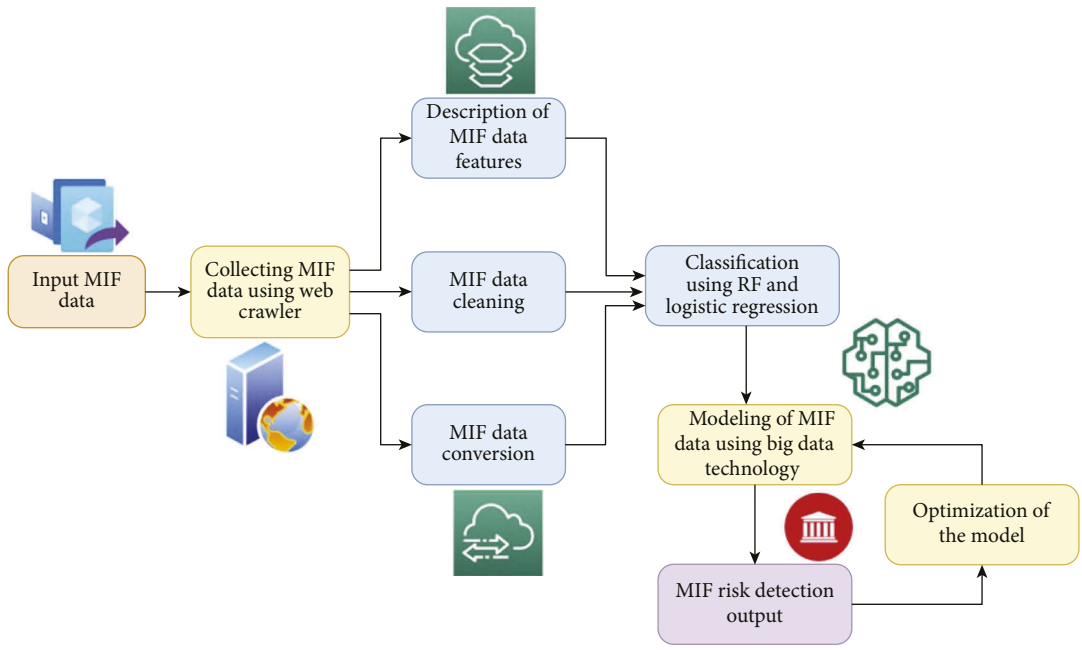

Figure 3: Detection of MIF risks using big data techniques.

network and transport layer are under the classification. MIF data is primarily sent and received by the network and transport layer across the broadband Internet. Once this layer delivers and analyses data collected at the perceptual layer, operational risks might arise due to imperfect technology and guidelines. The physical layer, or perception layer, contains sensors for perceiving and collecting environmental data. It detects certain physical factors or locates other intelligent devices in the surrounding area. MIF data exposure, breach, communication latency, data encryption, asymmetric information, and hostile intrusion are the primary hazards the network and transport layer must overcome.

The application layer presents risks in the third category. The application layer is primarily used to analyze the information and data transmitted by other levels of the IoT network, send them to financial institutions for processing, and offer workable mobile applications for banking activities, including economic decision-making and status monitoring. The risks in the application layer nest vulnerabilities in other levels that are further complicated, such as the risks of securing intellectual property and coordinating with stakeholders because the application layer comprises a diverse variety of businesses and individuals.

3.4.1. RRM and IoT to Examine MIF Risks. The RRM and IoT have been used to examine the predicted gap value of risk evaluation and objectively construct the different MIF risks faced by the banking sector. MIF's IoT-based mathematical risk formulation is built on the RRM as the basis for its operational risk assessment. (1) shows the mathematical model of MIF risk based on RRM. A vital tool for making loan choices and managing and building portfolios is a risk rating model. They provide lenders, analysts, and asset managers with a fairly objective method of classifying borrowers or particular assets according to their trustworthiness and default risk. Value at risk (VaR) is a metric that measures how much money might be lost by a company, investment, or position over a certain period of time. The Value at Risk (VaR) at a threshold value x for MIF in the banking sector is given as

$$VaR^x = \begin{cases} \dfrac{x}{(zy)}\left[\dfrac{q}{p}(1+\beta)\right]^{-y} - 1, & y < 0, \\ x + zln\left[\dfrac{q}{p}(1+\beta)\right], & y = 0, \\ \dfrac{x}{(zy)}\left[\dfrac{q}{p}(1+\beta)\right]^{-y} + 1, & y > 0, \end{cases} \tag{1}$$

where x is the threshold value for MIF in the banking sector, p is the MIF data samples higher than x. q is the MIF data samples lower than the threshold x. $y\,and\,z$ are MIF risk factors. β is the survival rate of the banking sector, despite MIF risks. The mathematical computation of high MIF risks using VaR^x has been carried out using the expected shortcomings (ES) value and is given as

$$ES_x = \left[\frac{VaR^x}{1+z}\right] - \left[\frac{(y-xz)}{(1+z)}\right], \tag{2}$$

where VaR^x is the value at risk at a threshold value x for MIF in the banking sector, $y\,and\,z$ are MIF risk factors. National financial institutions now lack a comprehensive database for operating MIF risks and losses. A MIF risk analysis model may be created based on the findings of the developed mathematical model, which can compute and identify various forms of financial business risk loss value.

3.4.2. FRCF Using BP-NN to Detect MIF Risks. Huge quantity, cross diversity, quick creation, and fragmented value are the four components of big data which broadens its valuation arena. The most effective technique for extensive data processing is the NN, a calculating method that mimics the comprehensive data analysis techniques of the nervous system. The BP-NN aims to simulate and represent the issue from the network's point of view. The interlinked transmission topology of every neuron in the network has been stored and identified. More variables can be controlled, and versatility can be improved. The recent data must be entered again into the NN for the calculation to provide updated values for risk prediction. The adaptive development and each neuron's link weight can be adjusted to influence this procedure.

Figure 4 depicts the structure of BP-NN used in FRCF to predict the MIF risks in the banking sector. The neuron is a part of the NN that has a typical configuration, as illustrated in Figure 4, with many input terminals and one output terminal. The input values given to NN are denoted as $\{A1, A2, \ldots . An\}$ for i^{th} neuron and the corresponding weights are given as $\{Wi1, Wi2, \ldots . Win\}$. The limiting value of the NN is provided by α. The most popular converter or transfer function is the sigmoid function, which has been used to alter the magnitude of the NN model output. One of the sigmoid units of a neural network. It is a given that the output of a unit will always fall between 0 and 1 when the activation function of a neuron is a sigmoid function. The purpose of the transfer function is to obtain the output Bi for neuron i to attain the limiting value of α based on the input values $\{A1, A2, \ldots . An\}$. As seen in Figure 4, the BP-NN has three layers: an input layer, an output layer, and a hidden layer, with $M, 1, and\ N$ nodes, correspondingly. Each input node's link weight value to each hidden state node is M_{ki}. Similarly, each output node's link weight value to each hidden state node is M_{kj}.

Figure 5 shows the flow diagram of the BP-NN process. The NN parameters have been set at the beginning, including defining the quantity of input and output nodes. The input vector and the expected outcome of the algorithmic process will be fed to the NN. The following are the design principles for neuron models: the BP-NN employs a multiple-layer feedforward NN with reinforced learning and a fault backpropagation algorithm to match the correlation between input and output and the widely applicable structure. For the chain rule method's neural network training, backpropagation is performed. To put it simply, this technique does the backward pass after each feedforward run through a network in order to modify the model's parameters depending on weights and biases. Backpropagation is sluggish and unstable since each authority is only used for a small number of input instances. Furthermore, the assortment of experts is unable to swiftly modify its parsing when new situations emerge. Existing blends of specialists cannot add a new type of specialty if a situation calls for it. For reinforcement methods of artificial networks employing gradient descent, backpropagation—short for "rewinding of errors"—is a method. The approach determines the grade of the error function in relation to the weights of the artificial

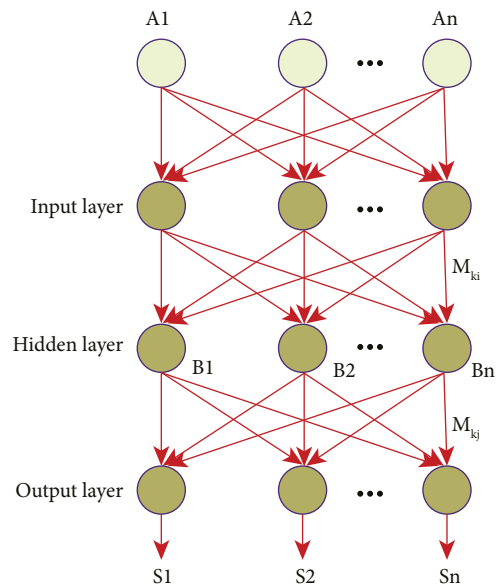

Figure 4: Structure of BP-NN used in FRCF to predict the MIF risks.

neural network given an error function and an artificial neural network. The weighting factor is adjusted following the feedback mechanism at the output based on the learning function of NN. The fault value in the learning outcome is given as $f = I - h$ if the intended output and the definite output value is given as h.

The learning procedure is split into two parts in the BP-NN algorithm's flowchart given above: the onward transmission of the operational data and the BP of the fault value. The resulting value of the ith neuron located in the hidden level corresponds to the feedforward transmission of the operational data and is given as

$$Bi = Fn\left[\sum_{i=1}^{I} M_{ki}Ai + \alpha \mathrm{i}\right], \tag{3}$$

where Bi is the value of the ith neuron located in the hidden level. The intended output is, and the value of the ith neuron located in the input level is given as Ai. The limiting value of the ith neuron is given by αi. Each input node's link weight value to each hidden state node is M_{ki}.

The resulting value of the jth neuron located in the output level corresponds to the BP of the fault value and is given as

$$Sj = Fn\left[\sum_{j=1}^{N} M_{kj}Bj + \alpha \mathrm{j}\right], \tag{4}$$

where Sj is the value of the jth neuron located in the output level that determines the FRCF value. The number of nodes in the hidden group is, and the value of the jth neuron located in the output level is given as Bj. The limiting value of the jth neuron is given by αj. Each output node's link weight value to each hidden state node is M_{kj}.

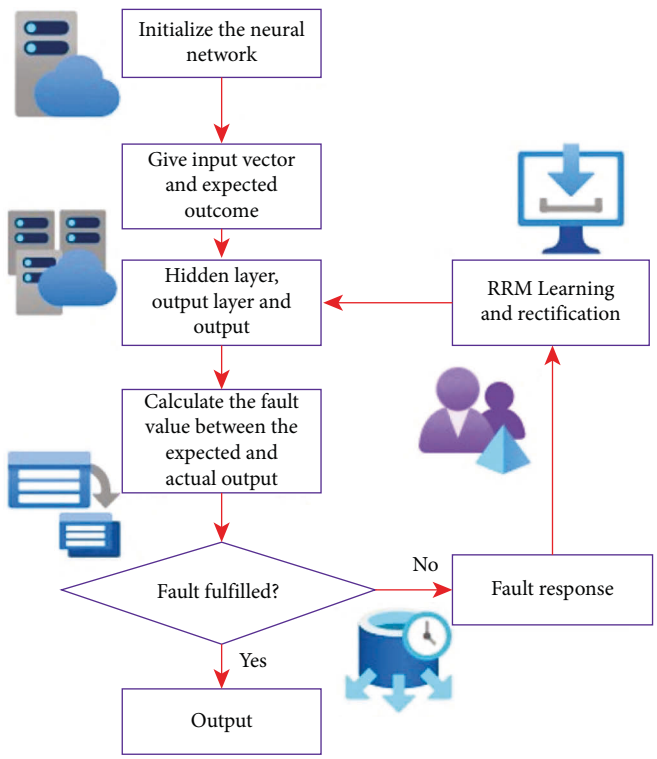

Figure 5: Flow diagram of the BP-NN process.

The fault value of BP-NN is given as

$$f(n) = 0.5\left[\sum_{j=1}^{N}(Ij - hj)^2\right], \tag{5}$$

where $f(n)$ is the fault value of a node j in NN. The quantity of nodes in the hidden level is N. The intended output of node j is, and the actual output value is given as hj. Finding optimal filter coefficients that produce the smallest average square of the process variable is how least mean square (LMS) algorithms, a kind of adaptive filter, imitate the desired filter. The corresponding weight values of BP-NN have been adjusted based on the least mean square (LMS) error algorithm for i^{th} and j^{th} neurons and are given as follows:

$$\begin{aligned} \delta M_{kj} &= \rho(Ij - hj)Bi, \\ \delta M_{ki} &= \rho\sum_{j=1}^{N}(Ij - hj)M_{kj}Ai, \end{aligned} \tag{6}$$

where δ is the weight adjusting factor. ρ is the effectiveness of the RRM learning process. The number of nodes in the hidden level is N. The intended output of node j is, and the actual output value is given as hj. Each input node's link weight value to each hidden state node is M_{ki}. Each output node's link weight value to each hidden state node is M_{kj}. Ai and Bi are the values of ith neuron in the input and hidden level.

Standardized metrics include the nonfinancial metric So, and the four comprehensive metrics (bank stability score, bank operational capacity score, capital adequacy score, and bank-scale possible score) have been chosen for FRCF using BP-NN. The data is then used as the input, with five input nodes ($N = 5$). The complete FRCF value falls inside the one output node, which is the MIF risk prediction based on, $Sj = Fn[\sum_{j=1}^{N} M_{kj}Bj + \alpha j]$.

The suggested FRCF performs well in forecasting and classification when employing BP-NN, big data, and IoT. The proposed FRCF is crucial to categorizing and managing banks in IF with similar risk profiles. Considering the link between the financial metrics, ecological indicators, and MIF risk level of relevant banks, BP-NN can determine the coherency and discrepancy between banks and relevant indicators. This coherency allows it to retrieve pertinent, helpful information relating to the chosen research banks based on the corresponding function correlation. The FRCF can be studied and assessed using the procedures mentioned above. The high learning effectiveness of BP-NN, particularly its incredible performance in fault BP and weight adjustment, can assist in controlling the fault for evaluating MIF and risk within the permissible range. This effectiveness of BP-NN can improve the accuracy of the FRCF evaluation result compared to other

mathematical methods. Thus, the BP-NN is chosen as the evaluation instrument to evaluate banks' MIF and FRCF based on the analysis mentioned above.

4. Results and Discussion

Rural Financial Institution (RFI) in China [25] has been chosen as the research entity. The organization statistics coherent with the trivial and medium-level businesses from multiple areas and having an account with RFI are selected. This analysis looks at the impact of the FRCF model based on BP-NN to predict MIF risk levels. Regarding the information sources, the loans that have been granted but still pose a risk of MIF risks have essentially been the primary focus. Under ordinary situations, the risk assessment of the MIF loan typically relates to the pertinent debtor data. It determines the likelihood of nonpayment based on the bank managers' consuming ideology and credibility. Big data technologies may be used to find relevant details, and the web-crawler technique has been used in this article to collect and archive the information [23]. Three years' worth of statistics are examined, assessed, and to create records, a sample of the data that appears in the event window is randomly picked. The sample data for testing is chosen from 25% of the total data samples, while the training dataset is selected from the remaining 75%. RapidMiner uses SplitData to determine the MIF risk levels and grading functions on the training and test samples [22].

The MIF risk levels have been classified based on the "3sigma" rule [26]. The statistical term used to determine the Degree of Deviation (DoD) in data samples is the "3sigma" criterion. This probability interval's definition is a foundation for the progressive grading of MIF risks. Implementing this rule enables the systematic grading of nonpayment rates to be quantified, allowing for a more logical examination and assessment of MIF risks.

Table 1 shows the MIF risk level identification using the "3sigma" criterion in FRCF. Standardized metrics in FRCF include the nonfinancial metric *So*, and the four comprehensive metrics (bank stability score, bank operational capacity score, capital adequacy score, and bank-scale potential score) have been chosen as input for BP-NN to find the risk level ($Sj = Fn[\sum_{j=1}^{N} M_{kj}Bj + \alpha j]$). After data preprocessing, the average value of Sj is found to be Avg = 0.512 an d DoD = 0.399. The output of FRCF using BP-NN is the five MIF levels classified as "Highly secure, Secure, Caution, Risky, and Highly risky" based on the "3sigma" criterion.

A total of 1000 samples have been considered for FRCF analysis, and 750 samples have been used in the training set. The remaining 250 samples from the data sample are included in the test set. The MIF risk levels and rate of nonpayment for training samples have been displayed in Figure 6. Calculations of the actual nonpayment percentage and predicted nonpayment percentage of different samples are used to assess whether IoT, mobile computing, and big data can effectively identify MIF risks. The fraction of debtors to the total quantity of samples in the dataset is the actual nonpayment rate. The mean number obtained after

Table 1: Identification of MIF risk levels using the "3sigma" criterion in FRCF.

"3sigma" period	Value	MIF risk levels
[(Avg-DoD), (Avg + DoD)]	[0.113, 0.911]	Highly secure
[(Avg + DoD),(Avg+3DoD)]	[0.911, 1.709]	Secure
[(Avg+3DoD), +∞]	[1.709, +∞]	Caution
[(Avg-3DoD), (Avg-DoD)]	[0.685, 0.113]	Risky
[-∞, (Avg-3DoD)]	[-∞, 0.685]	Highly risky

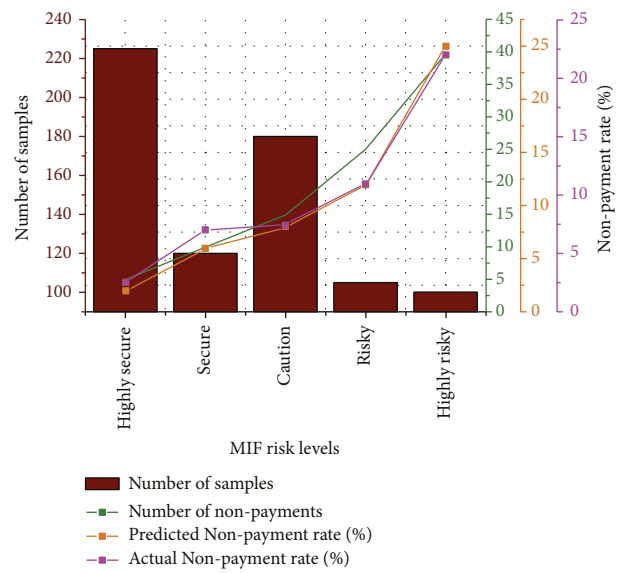

Figure 6: Comparison between MIF risk levels and nonpayment rate for various training samples in FRCF.

forecasting the nonpayment rate in the sample dataset is the predicted nonpayment rate. The training set contains 75% of the data sample chosen from the dataset [25]. The sample size and nonpayment rate of each MIF risk level may be obtained using the FRCF calculating technique based on IoT and big data technologies. It has been observed from Figure 6 that the actual and predicted nonpayment rate has increased with the decrease of MIF risk levels.

Figure 7 compares MIF risk levels and nonpayment rates for various test samples. The test set's sample data has an aggregate nonpayment rate of roughly 10.1%. The nonpayment rate for samples with MIF risk at the level "highly risky" is 32.9%, increasing as MIF risk levels decline. The actual nonpayment percentage and predicted nonpayment percentage of various data samples are determined to assess the viability of IoT, mobile computing, and big data technologies in recognizing MIF risks. According to Figure 7, there is a positive link between the actual and expected nonpayment rates, which means that both rise when MIF risk levels fall.

In this article, we aim to review five types of neural networks for binary classification problems. These are back propagation-neural network (BP-NN) [8], radial basis function-neural network (RBF-NN) [9], general regression-neural network (GR-NN) [10], probabilistic-neural network

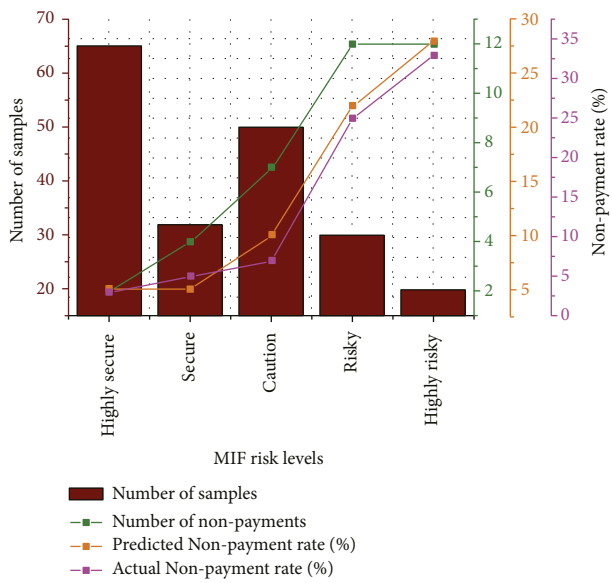

Figure 7: Comparison between MIF risk levels and nonpayment rate for various test samples in FRCF.

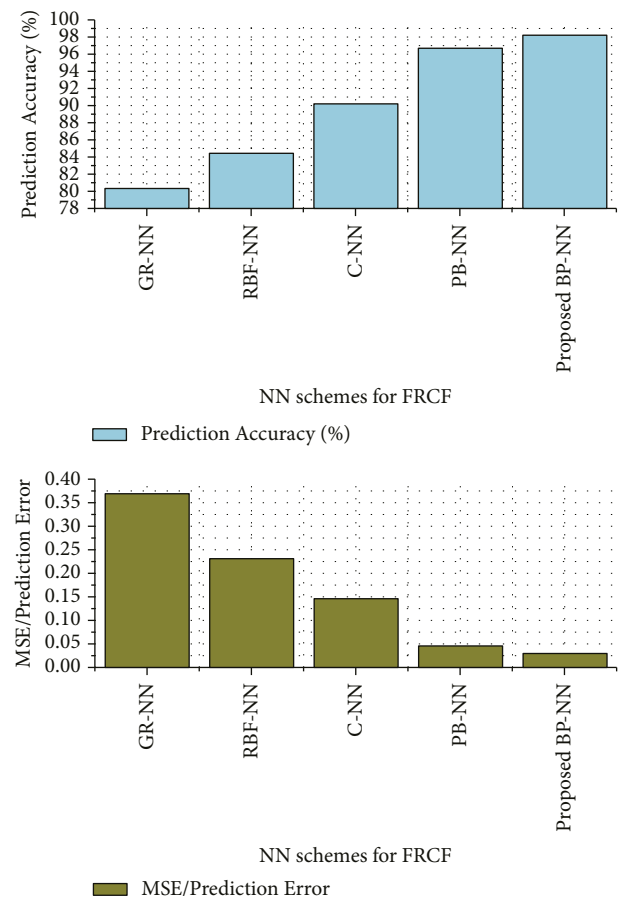

Figure 8: Prediction accuracy (%) and prediction error value for various NN schemes in FRCF.

(PNN) [11], and complementary-neural network (CMTNN) [12].

In this article, prediction accuracy and mean square error (MSE) of MIF risk levels for the proposed FRCF using BP-NN have been compared with other NNs [27]: radial basis function-neural network (RBF-NN), general regression-neural network (GR-NN), probabilistic-neural network (PB-NN), and complementary-neural network (C-NN).

Figure 8 depicts the prediction accuracy (%) and MSE value for various NN schemes in FRCF. The prediction accuracy of MIF risks for the proposed FRCF is given by

$$\text{prediction accuracy}\,(\%) = \left[\frac{\text{true positive}}{\text{true positive} + \text{false negative}}\right] * 100. \tag{7}$$

True positive is the figure of correctly identified MIF risks in FRCF. False negative is the figure of correctly identified MIF security. The MSE has been calculated as

$$\text{MSE or prediction error} = \frac{1}{DS}\sum_{j=1}^{DS}\left(\widehat{S}_j - S_j\right)^2, \tag{8}$$

where DS is the total amount of information samples, $\widehat{S}_j$ and S_j are the predicted and actual values of MIF risks in FRCF, respectively. The FRCF is accurate if it can predict the MIF risks with low prediction error values. Among the NN schemes for FRCF, the proposed BP-NN can predict the MIF risk levels with the highest accuracy of 98.2% and the least MSE of 0.028 due to its optimized fault response mechanism. GR-NN has the highest prediction error and the lowest accuracy among NN schemes.

This article examines the effectiveness of the BP-NN-based FRCF model in predicting MIF risk levels. The loans that have been approved but still have a risk of MIF hazards have essentially been the main emphasis in terms of the data sources. The MIF risk levels have been classified based on the "3sigma" rule using one nonfinancial and four comprehensive metrics.

5. Conclusion, Limitations, and Future Study

This study suggests a novel financial risk cautioning framework (FRCF) based on IoT, mobile computing, and big data technologies, and BP-NN to ensure a significant rise in MIF. This article proposes a big data technology-based data mining and recognition strategy. A BP-NN-based method for identifying and evaluating risks in MIF is also provided. The node count, transfer functions, learning rate, and other properties of each NN layer are calculated using the BP-NN approach. The proper training and testing of numerous information samples led to the development of the suggested FRCF. The output of FRCF using BP-NN is the five MIF levels classified as "Highly secure, Secure, Caution, Risky, and Highly risky" based on the "3sigma" criterion. Due to its optimized fault response mechanism, the suggested BP-NN among the NN schemes for FRCF can forecast the MIF risk levels with the most remarkable accuracy of 98.2% and the least MSE of 0.028.

Nevertheless, there are still certain restrictions on this research work. It primarily concentrates on risk assessment of the newly emergent credit structure, which is insufficient for MIF. Uniting a few other representative sectors is necessary to make future study findings more compelling. A specific volume of data samples must be needed to analyze the BP-NN model. The quantity and reliability of the data samples significantly impact how well NN models learn and function in the end. Consequently, to assure the correctness and applicability of the results obtained, the datasets' legitimacy, dependability, and diversity should be guaranteed as feasible in future research.

Data Availability

All data generated or analyzed during this study are included in the manuscript.

Conflicts of Interest

The author declares no conflicts of interest.

References

[1] G. Du, Z. Liu, and H. Lu, "Application of innovative risk early warning mode under big data technology in Internet credit financial risk assessment," *Journal of Computational and Applied Mathematics*, vol. 386, Article ID 113260, 2021.

[2] E. Peters, T. Kliestik, H. Musa, and P. Durana, "Product decision-making information systems, real-time big data analytics, and deep learning-enabled smart process planning in sustainable industry 4.0," *Journal of Self-Governance and Management Economics*, vol. 8, no. 3, 2020.

[3] Z. He, X. Tang, X. Yang et al., "Clinical trial generalizability assessment in the big data era: a review," *Clinical and translational science*, vol. 13, no. 4, pp. 675–684, 2020.

[4] J. Chen, "Big data boosts commercial bank credit business and risk management innovation," *Investment and Financing*, vol. 12, pp. 62–64, 2019.

[5] X. Zhu, "Research on credit risk management of China's commercial banks under the background of interest rate marketization," *Financial Community*, vol. 9, no. 9, 2018.

[6] Y. Dendramis, E. Tzavalis, and G. Adraktas, "Credit risk modelling under recessionary and financially distressed conditions," *Journal of Banking & Finance*, vol. 91, pp. 160–175, 2018.

[7] J. Gao, "Research on the corporate financial transformation with big data technologies," *International Journal of Progressive Sciences and Technologies*, vol. 32, no. 2, pp. 08–12, 2022.

[8] L. Gao and J. Xiao, "Big Data Credit Report in Credit Risk Management of Consumer Finance," *Wireless Communications and Mobile Computing*, vol. 2021, Article ID 4811086, 7 pages, 2021.

[9] S. Moradi and F. Mokhatab Rafiei, "A dynamic credit risk assessment model with data mining techniques: evidence from Iranian banks," *Financial Innovation*, vol. 5, no. 1, pp. 15–27, 2019.

[10] J. Doering, R. Kizys, A. A. Juan, A. Fito, and O. Polat, "Metaheuristics for rich portfolio optimisation and risk management: c," *Operations Research Perspectives*, vol. 6, Article ID 100121, 2019.

[11] X. Sun and Y. Lei, "Research on financial early warning of mining listed companies based on BP neural network model," *Resources Policy*, vol. 73, Article ID 102223, 2021.

[12] E. G Baranoff, P. Brockett, T. W Sager, and B. Shi, "Was the US life insurance industry in danger of systemic risk by using derivative hedging prior to the 2008 financial crisis?" *Quantitative Finance and Economics*, vol. 3, no. 1, pp. 145–164, 2019.

[13] Q. Xu, B. Jin, and C. Jiang, "Measuring systemic risk of the Chinese banking industry: a wavelet-based quantile regression approach," *The North American Journal of Economics and Finance*, vol. 55, Article ID 101354, 2021.

[14] G. M. Caporale, M. Alessi, S. Di Colli, and J. S. Lopez, "Loan loss provisions and macroeconomic shocks: some empirical evidence for Italian banks during the crisis," *Finance Research Letters*, vol. 25, pp. 239–243, 2018.

[15] Q. Xu, M. Li, C. Jiang, and Y. He, "Interconnectedness and systemic risk network of Chinese financial institutions: a LASSO-CoVaR approach," *Physica A: Statistical Mechanics and Its Applications*, vol. 534, Article ID 122173, 2019.

[16] H. Zhou, W. Liu, and L. Wang, "Systemic risk of China's financial system (2007–2018): a comparison between Δ CoVaR, MES and srisk across banks, insurance and securities firms," *The Chinese Economy*, vol. 53, no. 3, pp. 221–245, 2020.

[17] Y. Zou, L. Yu, G. K. Tso, and K. He, "Risk forecasting in the crude oil market: a multiscale Convolutional Neural Network approach," *Physica A: Statistical Mechanics and Its Applications*, vol. 541, Article ID 123360, 2020.

[18] S. B. Jabeur, C. Gharib, S. Mefteh-Wali, and W. B. Arfi, "CatBoost model and artificial intelligence techniques for corporate failure prediction," *Technological Forecasting and Social Change*, vol. 166, Article ID 120658, 2021.

[19] Q. Yang and C. Wang, "A study on forecast of global stock indices based on deep LSTM neural network," *Statistical Research*, vol. 36, no. 6, pp. 65–77, 2019.

[20] M. Pejić Bach, Ž. Krstić, S. Seljan, and L. Turulja, "Text mining for big data analysis in financial sector: a literature review," *Sustainability*, vol. 11, no. 5, p. 1277, 2019.

[21] J. Zhang, "Investment risk model based on intelligent fuzzy neural network and VaR," *Journal of Computational and Applied Mathematics*, vol. 371, Article ID 112707, 2020.

[22] https://rapidminer.com/glossary/data-mining-tools/.

[23] L. Yu, Y. Li, Q. Zeng, Y. Sun, Y. Bian, and W. He, "Summary of web crawler technology research journal of physics: conference series," *Journal of Physics: Conference Series*, vol. 1449, no. 1, Article ID 12036, 2020.

[24] K. Shah, H. Patel, D. Sanghvi, and M. Shah, "A comparative analysis of logistic regression, random forest and KNN models for the text classification," *Augmented Human Research*, vol. 5, no. 1, pp. 12–16, 2020.

[25] https://www.ceicdata.com/en/china/banking-balance-sheet-and-its-related/banking-total-asset-rural-commercial-bank.

[26] M. Lin, "Innovative risk early warning model under data mining approach in risk assessment of internet credit finance," *Computational Economics*, vol. 59, no. 4, pp. 1443–1464, 2022.

[27] A. N. Sharkawy, "Principle of neural network and its main types," *Journal of Advances in Applied & Computational Mathematics*, vol. 7, pp. 8–19, 2020.

Hindawi
Mobile Information Systems
Volume 2022, Article ID 2343021, 11 pages
https://doi.org/10.1155/2022/2343021

Research Article

Art Design Teaching Based on the Multidata Fusion Algorithm and Virtual Simulation Technology

Bin Liang

Taishan University, Taian 271000, Shandong, China

Correspondence should be addressed to Bin Liang; liangbin@tsu.edu.cn

Received 9 August 2022; Revised 12 September 2022; Accepted 16 September 2022; Published 11 October 2022

Academic Editor: Chi Lin

Virtual Reality (VR) technologies are widely applied to teaching art design. VR has been created with high-level techniques that create the artificial environment to support virtual aesthetics. Especially ceramics art design requires technical advancement to enhance business individuals. However, the user requires the virtual reality experience to improve the art design teaching performance. During the teaching process, reality learning patterns, experiences, and fusion ceramic product design are required to enhance art design teaching. So, in this research, modern art design has been optimized using virtual reality with a deep learning architecture for craftsmanship, style, ideals, creative aesthetics, cultural ramifications, and inherited designers to create an effective model. The deep learning-assisted gate array algorithm (GAA) is used to optimize the modern art structure in system design. Therefore, this approach reveals some experimental findings that produce better performance benefits than saving time and resources in traditional manual detection systems.

1. Introduction to Ceramic Art

Ceramic painting is a traditional folk art trait. It's a science with a long history. It's a combination of content and culture. It can promote the unity and consistency of ceramic and decorative templates. Contemporary brand management, to be exact, is a necessary work of modern basic graphic design [2]. If ceramic production increases, the new designer wants its beauty and its aesthetic appeal [3]. However, they have different cultures and have been skillfully mixed with escaping total porcelain features and purposes. Ceramic materials and brand management are intimately interlinked [4].

The regular use of ceramics in mosaics and investment reports is part of the application of boiling and ceramics [5]. It represents the cultural identity and even the global essence of contemporary brand management to give a better concept to be promoted entirely. The development of multimedia and virtual reality (VR) technologies greatly influences aesthetic learning. Aesthetic education is a method of educating as well as studying that involves learners in exploring, questioning, discussing, and creating art as they study from works of art. The VR utilises the different technologies that are incorporated with images, animations, audio, video, and other multimedia information. The capacity of the memory to integrate visual and verbal depictions of knowledge results in a better comprehension and helps the application of knowledge in various contexts, and it is one of the features of multimedia instruction. This information creates an impact on the art designing process. In addition, VR helps to provide a guideline for understanding the information to deliver details intuitively. Moreover, the VR process supports art and design; its characteristics express the particular art. The virtual reality process demonstrates the subject's appearance and object requirements and creates the aesthetic illustration that gives great attention to art and technology. To create art and design teaching, the VR process requires several modellings such as interaction analysis, animation making, collision analysis, texture map design, system controls, and texture making. These characteristics are investigated by observing the objects that require artificial intelligence to extract the features [6]. The thesis suggested discrimination between the prototype

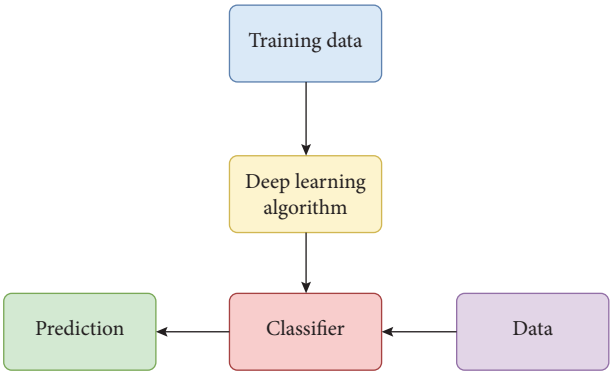

Figure 1: Machine learning algorithm.

object that uses the convolutional neural network (CNN) [7], as show in figure 1.

The estimation model subsection is a grouping of instructor training images based on training knowledge that could be required to define a predetermined class mark for the testing data item [8]. The economic analyzers are Bayesian predictors. The likelihood that a specific packet corresponds to a certain class is one example of a category participation likelihood that may be predicted using Bayesian learners. For starters, a Bayesian classification model can be used to filter a mail. If an incoming voicemail predicts that this can be categorized as spam or nonspam, the report checks it [9]. Naive Bayes' family identification is also centered on the probabilistic theory's success for the label, particularly in recognizing and diagnosing diseases in the document [10]. The purpose of probability theory is to allow us to discover more likely outcomes in a universe where every instant is affected by an endless set of complex variables. Knowing this helps us make judgments that are more accurate and efficient.

An easy and a well-managed system has been proposed. It has been compared to several traditional approaches resulting from multiple CNN templates. It improves the classification algorithm of the selected CNN model and the efficiency of the algorithm [11]. When learning neural networks, the two main types of gradient descent are cross entropy and mean absolute deviation. The learning picture of the system (convolution section) must learn from material classification functionality.

The software is completed and includes several logical foundations for programming. The network reference connection can control these by using the field-programmable gate array with a hardware description programming language [12]. The customizable logic block (CLB) grid at the centre of field programmable gate arrays (FPGAs), a technological gadget, is coupled via controllable connectors. After production, FPGAs can be reconfigured to meet specific industry or feature needs. The programming of a strong one is probable. Besides, the firm, FPGA, will decide its computation energy capacity. They are quickly tiny and economical, so the narrator must be involved in this paper's framework when he assumes the close to zero FPGA.

Initially, the ceramic material is melted to form annealing, and it is tested for processing whether it works or not. Finally, it is ready to package and ship. Further clarifications have been given below. Figure 2 defines ceramic processing products and their five forms (initial ceramic, flowers, colourants, fining, and cleaning products) (caret). An object (1600–1725°C) is perfect, but sulfate is too large to dissolve [13]. For example, various forms of electrical flow, such as Na_2O, may be used to minimize silica thermal conductivity.The raw metal is vaporized, forming an explosive reaction that escapes CO_2 and H_2O in the reactor [14].

Ceramic was obtained from the original ingredient to extract water vapour from melts, such as sulfide oxide, potassium, and sodium iodine [15]. The solubility of the melted at hot pressures to raise the air pockets to prevent low particles influences the heterogeneity of the bottle so that the molten ones from either the melt that is retained on the outer portion must be separated [16]. Commodities are prepared, furnace moulded, and finished, and in five processes, ceramics are made. Different methods for the shaping of the crystal differ based on application fields. The most commonly used glass shape may be categorized as plain, steel, or glass plate [17].

Researchers have built and deployed a computer porcelain space strategy focused on a ceramic remote server platform [18] to resolve any such question. This method reduces the waste of time and energy and enhances the engagement and happiness of consumers. In brief, the following could be seen in specific submissions to the article [19].

A simulated porcelain environment architecture and configuration based on the ceramic data centre is suggested. The layout of the pottery generation and the ceramic auditorium is seen. The ceramic data centre framework classifier is developed [20] for the online pottery region.

The education of art and design frequently makes use of virtual reality (VR) technology. High-level approaches have been used in the creation of VR to construct an artificial world that supports virtual aesthetics. In order to optimize the state-of-the-art system design structure, the gate array algorithm (GAA) with deep learning assistance is applied. This method displays certain experimental results that outperform more conventional manual detection techniques in terms of performance gains.

The text is organized as given below. Section 2 discusses the research background relevant to the proposed research. A general design and architectural capabilities are implemented in Section 3 for the ceramic commodity virtual reality cloud server based on the deep learning-assisted gate array algorithm (GAA). Section 4 illustrates the simulated ceramic room's configuration of the proposed deep knowledge-assisted gate array algorithm (GAA). The conclusion and scope of future research are explained in Section 6.

2. Background to Modern Ceramic Art

Most current research studies do not entirely explore how a simulated ceramic environment can be integrated with the

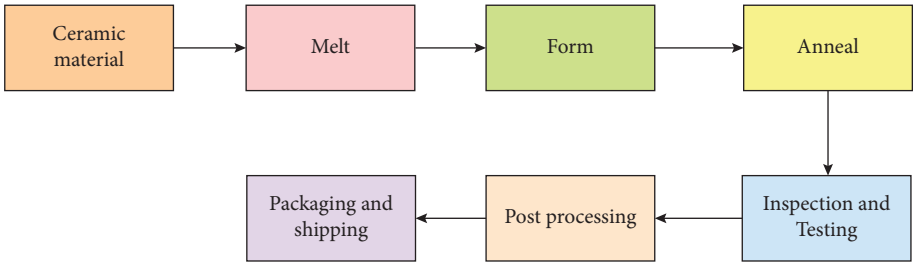

Figure 2: Ceramic art material workflow.

public cloud. Device QP will immediately create a digital ceramic system in which users must insert initial touchscreen conditions [21]. The author provides a pattern for making 3D pottery template forms with forearms, changing them, and navigating them. The researcher proposes a displacement framework based on the Unity3D program that uses a hand motion connection. The authors can use a practical guide to handle 3D models in a simulated environment [22]. A computer machine with a VR interface is an immersion machine. The authors recommended an app that simulates the interactive reality voice sculpture leveraging the action of gravitational technologies.

The potential to restore historical objects in an exact and fair period will be significant as archaeologists investigate modern and transitional living things. They have substantial knowledge of historical society. Investigators and many others used technological advances in this age of virtual and enlarged perception to make work quicker and more productive. This has made it simpler, more rewarding, and more efficient to work in a working world that is now referred to as an "intelligent environment." It is also helpful to apply computational methods to solve crucial problems in the world of archaeology [23].

Some experiments have also tried to address the healing issue. For example, the researchers found that a device that could destroy a warship used two secondary development techniques: a profile type system model of the complete warship and a user name fragmentation system. Its efficiency can be greatly improved depending on the satisfaction of some constraints, it needs more research to strengthen the accuracy [24].

Additionally, researchers compared description and reproduction procedures based on experience with colour and pattern photographs of demolished archaeological ceramic fragments [25]. They used the scale invariant function transform (SIFT) and the total variance geometry function identifier (TVG). In order to compare and recognise images, the scale invariant feature transform (SIFT) is used as a visual description. This description and associated imagery characteristics are employed in a wide range of tasks in machine learning, including view-based image classification and feature comparison among several perspectives of a 3D environment. Nevertheless, the reliability and precision of these identifiers were not sufficient. The researchers' analysis even suggested a method using SIFT [17]. The machine uses computer vision techniques to classify and analyze pictures of the building elements of bottles using "Raman spectroscopy." Raman scattering, also referred to as elastoplastic photonic dispersion, is the basis of Raman spectroscopy. Although X-rays can also be employed, homogeneous illumination is often produced by lasers in the visual, radiation in the infrared, or nearly UV spectrum. As a manager, measuring and evaluating the necessary characteristics for model training are essential. Raman has several advantages over IR, including significantly simpler and faster preconcentration. Performance is essential for the research since shorter execution times allow for the examination of further data.

This method also separates collected pictures and removes their attributes for the description of pottery. To do this, the authors have opted for an SIFT procedure, which extracts and matches the facial landmarks with corresponding couples. Because this method builds on the previous one, it is inadequate to provide a highly accurate optimized value that opens the door to study further [26].

Moreover, the author concentrated on technology to identify uncut gems correctly and automatically. The procedure was used in four stages: extraction of functions, fusion of characteristics, collection of operations, and identification [27]. With the "BoW" process, the features taken from images were used to generate "international iterator" vectors for pictures in this methodology to minimize the machine sophistication question. However, this approach has been very successful [28].

Eventually, the research recommends a sphere manifestation feature vector, which image processing technicians use in the potsherds' automated study [29]. This approach analyzes the exterior frontal view alone, uses only the range coordinates, manages three-dimensional images using colour, shape, or picture, and compresses data quickly from the range's coordinates [30]. It is said that complete-time reductions in potsherds' arrangement are an easy way to obtain the picture including all drawbacks, which illustrates that the benefits of image recognition strategies are now innate.

Computer vision and machine learning are evolving among numerous new digital techniques, which are increasingly important to archaeological study [31]. Seeing is the brain's capacity to experience and view the world of light mirrored in environmental objects. This approach is seen in the manual form of potsherd alignment implemented by archaeologists [32]. On the other hand, computer vision is a technology of designing structures, making valuable choices to gather information through optical pictures or complex

picture data—the computer's capability is what human logic can see and do. Computer vision (CV) could identify, locate, fuse, and pick the function and then draw conclusions interpreted from objects or imaging data to prove it. Other machine learning possibilities include restoring, recording, regeneration, restoration, and training [33]. Furthermore, a built computerized system improves efficiency.

It is also not hard for people to believe the infrastructure of virtuous ceramic processing and deflection offered by specific current structures [34]. Practical aspects that are not advantageous to exchanging ceramic items are overlooked. The proposed system provides a streamlined ceramic creation and communication module method, enabling members to download their templates in simulated ceramic spaces. It provides users with flexibility for ceramic development by integrating a preview pane into the digital ceramic environment of current technology.

The authors in [35] discussed artificial intelligence with the virtual reality-based digital media and art creation teaching process. The virtual reality process helps to understand the object vividness used to increase the teaching mode. Here, student and teacher teaching experiences are analyzed by applying artificial intelligence approaches. The intelligence techniques derive the digital media art patterns that increase the overall teaching process. In [36], the video was analyzed for developing virtual reality technologies. This work uses oil painting images to create the virtual reality-based learning process. The collected images are investigated by applying the deep learning approach that derives the features, and high-quality image-related features are fused. Then, the preprocessing technique is incorporated to remove the unwanted details. After that, extracted features are processed by an optimal matching process that creates the template for developing the learning pattern. This process is developed with the help of TensorFlow, and the images help to create an effective learning pattern.

3. Framework of Modern Art Design

3.1. Digital Pottery Network Centered on the Robust Architecture. The prototypes are stored in the cloud servers in the simulated ceramic process definition. The first is the ASCII-dependent FBX system, and the second is a template conducted to analyze the framework in a database table. One may explore the document for knowledge discovery using the FBX ASCII format, which provides a common communication rendition of the file type. For file types with OR SDK or Python, users can choose ASCII type. This device is furnished in file variants to save 3Dimages. Researchers enable users to access everyone's custom showroom, and information from galleries will also be protected in JSON database formats. Since it facilitates quick information exchange and software platform outcomes, JSON has grown in popularity in API code writing and Internet platforms. It is text-based, compact and features a simple data structure that does not need any further programming to understand. Besides, this initiative assists many users in almost the same exhibition space in creating ceramics concurrently.

The assembly process of the proposed gate Array (GAA) algorithm is shown in Figure 3. It is separated primarily into three layers: VR customer client customer, application layer and overall service system, and data tier that interacts with the application. According to the application layer, art and design have been created to improve the overall learning process.

3.1.1. Client Layer. The term client layer relates to third-party applications like Microsoft Office as well as native terminals utilised to create, generate, analyze, display, and disseminate a variety of material. The layer of the client is a customer-focused platform. Members can view ceramic showrooms and model and interact with custom ceramic clients throughout this surface. The report predominantly contains the customer's country coordination, ceramic capture, virtual reality room transport, hall production, ceramic model, and ceramic transfer. Ceramic catch knows concrete grabs, and ceramic scales monitor the scale of material since grabs are often used to coordinate several consumers' conditions in the same scenario. Space teleportation carries out a range of consumer portal services, which implies that customers can travel in a small capacity without limitation. In optical photonic laboratories all over the globe, teleportation has evolved into a regular procedure. The method is based on the peculiar tangling phenomena. This happens whenever two classical things, like particles, arise at the same time and location in spacetime and hence share a similar reality. The development of show halls allows custom construction of show grounds, and all consumers could submit information on the database storage from its exhibition spaces and then use it. The ceramic system requires VRTK software to customize clay. Virtual Reality Toolkit (VRTK) is a free software, cross-platform toolset that enables users to quickly create virtual reality (VR) encounters by offering simple fixes to everyday issues.

3.1.2. Server Layer. The server element's central aspect is the server module. Two servers make up the server aspect: a Java browser as well as a Web service. These servers support multiple threads. The server layer offers (client level) software development kit and context awareness in virtual environments, with system integration and policy synchronization. In that same layer, connection software is used for latency sensory scenarios. It uses the node configuration, transmits the directions to the database repair facility, and then collects the orders to the customer's nearest cloud infrastructure to measure and transfer the user sensor data via the device equilibrium. Application implementations under network protocols are used for convolution operators in certain delay-insensitive situations such as authentication, registry, and uploading a ceramic design. Designers often use digital distribution channels to preserve other dynamic tools, including image files. These layers primarily involve allocating services, synchronizing the nation, storing sequences, and transmitting and linking ceramic materials and customer data using an API system. Application

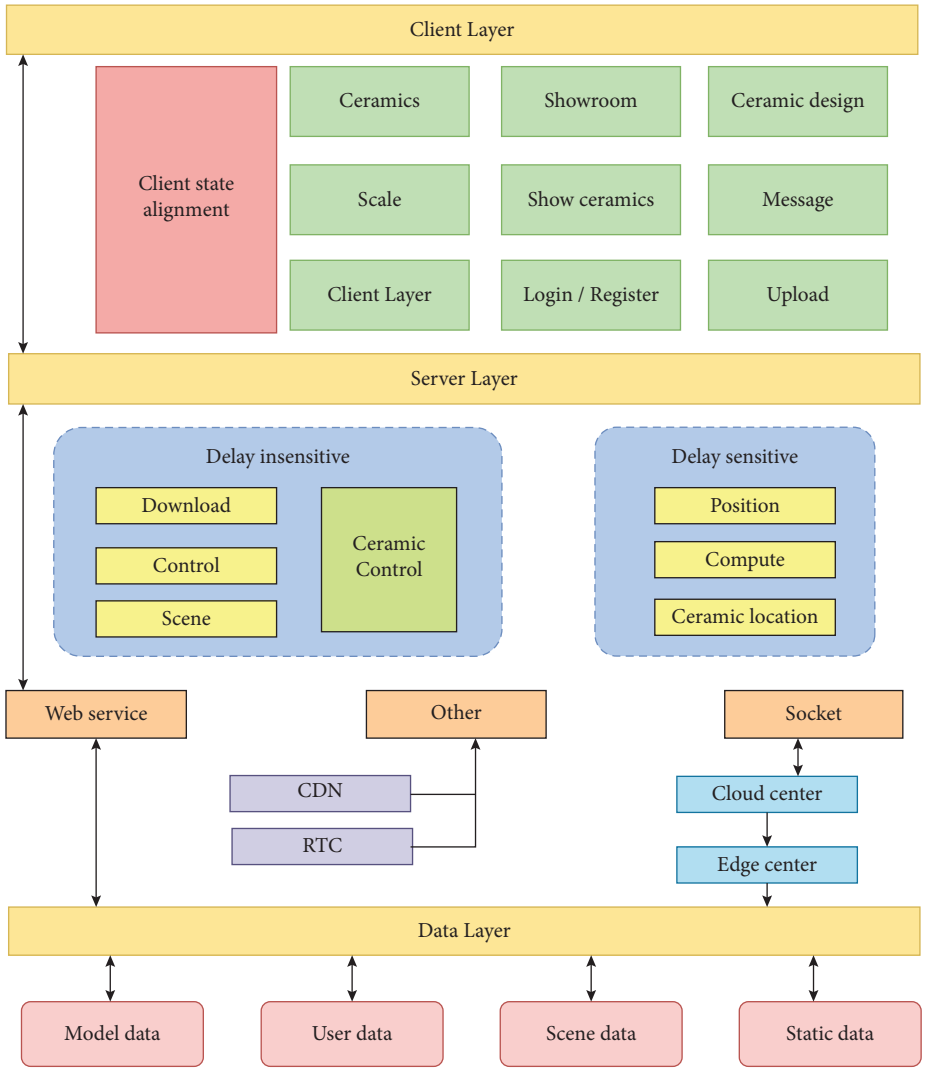

Figure 3: Gate array algorithm (GAA) architecture.

programming interface, or API, is a technology bridge that enables the communication between two programmes. We utilise an API every moment we need a smartphone application such as Facebook, composing an urgent message, or examining the weather. It is an essential tool for companies in all sectors of the economy. Technically speaking, APIs are crucial because they enable the utilisation of one computing system's features by the other. Interfaces are a channel for communication between two dissimilar programmes.

3.1.3. Data Layer. A JavaScript object called information level is employed to send knowledge from the web page to the Tag Manager containers. After that, one may utilise data to fill parameters and turn on the triggered in the tag setups. The repository data sublayer offers client information support, specifically for personalized ceramic design software, encoded scenario information, customer records, images, and voice storage. The ceramic is fused to have good performance.

3.2. Pottery Space Workflow on Ceramic Platforms. After the requirement is obtained, researchers use the separator building as their initial location. Between the exhibition space and the clay custom space is the shield building. Upon customer queries from the cloud network, the simulated display environment is set up and the consumer has to remain in the monitor space. The convention centre is designed simultaneously throughout these days for the consumer, so that the buyer's impression would not be impaired. Consumers will build the outline of the clay in the ceramic decoration space. The above relations were established in selective ceramic displacement management and shooting and can be downloaded to a database repository by shot cement consumers. Unless the consumer requires a specific tile, the device distributes the simulated ceramic template to manufacturers.

4. Design of the Gate Array Algorithm (GAA)

4.1. Ceramic Generator Design

4.1.1. Generation of Ceramic Models. Researchers like to use Unity3D's framework architecture to produce virtual reality

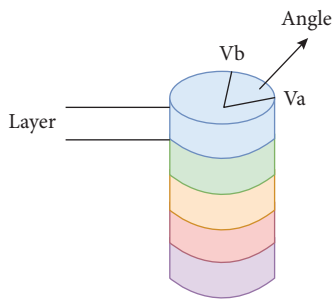

Figure 4: Ceramic model in the gate array algorithm (GAA).

clay, and once consumers can manipulate the ceramic, researchers must initiate a unique ceramic model. An effective cross-platform 3D technology and user-friendly software framework is Unity3D. Anyone looking to easily build 3D games and applications for smartphones, desktops, the Internet, and platforms will be interested in Unity, as it is suitable for both beginners and professionals. Cross-platform connectivity, component inventory control by Unity, amazing presentation excellence, a unified interface, clear architecture, and captivating gaming are some of its extra features. Community offers a coordinate structure that uses a vertical system and spheres interconnected by several edges to simulate the performance. Researchers placed the ceramic creation measurement on intelligent cities to minimize the total cost of consumers. The cloud platform has to be supplied with only the location where the ceramic is formed, and the information owner will display the measured simulated data. Figure 4 illustrates the specifications necessary to manufacture the ceramic prototype.

Figure 4 consists of several levels, but every level of the higher mantle is associated. The radial value of the contain attitude through the triangular and curve central is supposed to be the Angle, but that variable is determined by the design model's information. Unless the information is equivalent to 40, there have been 40 edges on the surface's diameter, which has the same observational size. Or how to display the thickness of a piece of paper, the researchers assume that A_{count} and V_0 is the 3d image professional and not the diameter. The coordination of each sheet below the first surface has shifted, and one element can be determined from all those three specifications. The corresponding equations (1), (2), (3), and (4) will help us articulate the issue.

$$\text{Angle} = \frac{2\pi}{A_{\text{count}}}, \tag{1}$$

$$V_{i\_x} = R * \text{Sin}(\text{Angle} * i), \tag{2}$$

$$V_{i\_y} = 0, \tag{3}$$

$$V_{i\_z} = R * \text{Cos}(\text{Angle} * i). \tag{4}$$

The coordinate V_{i_x}, V_{i_y}, and V_{i_y} of the i dimension in the initial surface is X, Y, and Z. The oscillation describes the first ever surface diameter. But only the measurement of Y coordinate amplitudes H_L has to be changed when measuring coordinates of the lowest $V_{i\_y\_\text{bottom}}$ ground after the initial layer (the higher portion of the final interface).

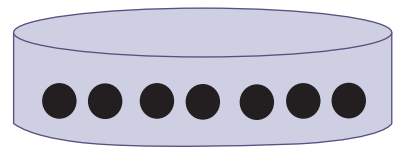

Figure 5: A layer of ceramic in the gate array algorithm (GAA).

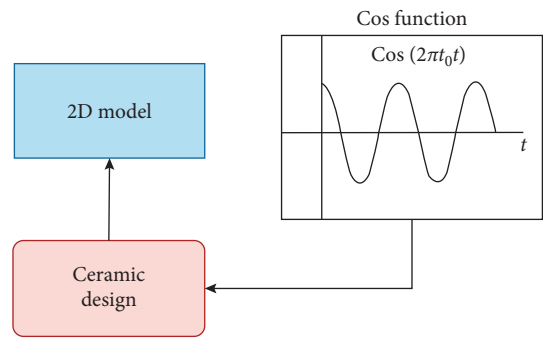

Figure 6: Cos function mapping with a ceramic model.

$$V_{i\_y\_\text{bottom}} = 0 - H_L. \tag{5}$$

Three vertexes will generate a triangle surface, and each element's position on the edges is displayed in Figure 5.

4.1.2. Ceramic Model Bottom Sealing. Artificial ceramic's primary focus could be produced, but the ceramic designer's floor has not been closed. For screening the floor, only the edges on the lowest portion of the higher layers are to be used to conclude the selection process by using the lowest edge of the foundation as the last edge of every other triangle.

4.1.3. Ceramic Model Deformation. The consumers must individualize the ceramic design when it is finished. The customization concept first involves ceramic displacement control. As seen in ceramics in regular activities, clay's deformation typically resembles the curved cos in the $-\pi, \pi$ mathematical equation, and the structure of the clay template is always formed due to the overlap of several types of trigonometry. If researchers expect this influence to be realized in virtual reality, researchers ought to monitor the vertical dimensions to replicate the equation process gradient. Weaknesses are manufacturing-related errors, obvious blemishes, or additions that must be mentioned in the specification. Destruction refers to flaws that occur during usage, treatment, washing, or preservation. Nicks, fractures, scrapes, colour fading, and cracks are examples of deterioration. The morphology, interior flaw size and form, sampling length and frame, speed of change, ambient conditions (degree, transparency, pH, etc.), tension level, and strain are the parameters that determine the durability of mechanical properties. Figure 6 shows the projection of the cos function to both simulated ceramic templates.

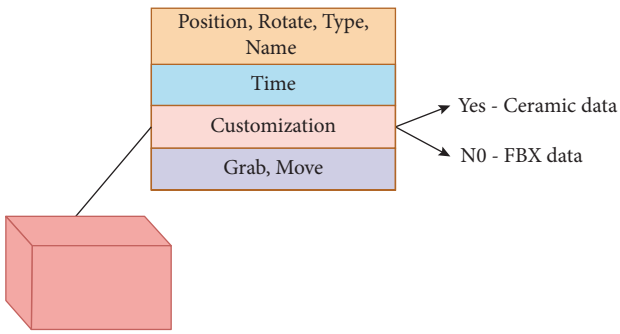

Figure 7: Parameters in the gate array algorithm (GAA).

The digital design, by manipulating the edge $-\pi, \pi$, would have had protrusions, identical to the cos function, in the distance [low, high] of the clay axis, to travel in specific directions. By the regulation of the projecting space [low, high], one can adjust the displacement duration. Researchers should use Unity's simulation curved system to directly visualize figures created on the artificial calculus design.

4.1.4. Edge Computation and Localized Generation. Whenever several virtual ceramic design levels exist, the system deformation process occurs. Deformation can make the device to the same degree as the consumer comfortable stay. Researchers can use artificial intelligence to quantify design deformation information.

4.2. Ceramic Exhibition Hall Design

4.2.1. Object Serializing Variables. Researchers must serialize everything to provide all people access to the open space. So one must understand how much the exhibits will be serialized in the exhibition hall before serialization. When evaluating virtual reality specifications, researchers defined objects' typical characteristics, including the entity description, entity nature, development effort, and other measurements. In Figure 7, the critical variables are shown.

(a) Simple variables: this segment of constraints is a general asset for all artefacts such as the location of the digital environment, rounding, and rotation. Researchers want to use the form function to discern the form and naming parameters in every digital environment.

(b) Customization: researchers can create a customized ceramic design during this research work, which could be saved in the server similar to other users using this ceramic design. That being said, some programmers may use many 3DMax or Mixer to build a three-dimensional ceramic model that users may value. Therefore, there are two methods of uploading templates. Custom models of virtual reality ceramics developed by the software will be uploaded, but ASCII based FBX templates are uploaded. When loading design details centrally, this should determine whether the template is a personalized version or not. Otherwise, they query to see if the FBX framework is loaded centrally.

(c) Grab, Move: researchers, therefore, need to define two characteristics to verify whether an entity is in confrontation with the consumer, to give consumers the selection or the displacement.

Table 1: Variables vs declarations.

Variables	Declaration
Scene	Room to exhibit objects
Cache	Showing available cache memory
List	Listing the available objects
Create	Creating a new object

4.2.2. Ceramic Exhibition Hall Serialization Parameters. There are some exhibits and several characteristics in the show space. The server contains a prototype chart by searching the JSON information on the demanded show hall from a database service. Entities and matrices are the sole two data formats that JSON provides. A collection is a number of values, but an item is a collection of name-value combinations. For serializing and transferring large datasets over a computer network, the JSON language is utilised. Data transmission among a Web server and web apps is its main purpose. JSON systems employ more memory speed and versatility, offer many search patterns, improve design versatility, and simply convert to SQL architecture. Since it lacks a structure, the extensively utilised JSON format enables semistructured information. This gives you more freedom to collect and search for information that does not necessarily conform to strict datasets and standards. The prototype information of web service entities is still required (such as FBX and virtual ceramic data). Researchers chose a distributed approach for constructing the exhibition hall to optimize the UI. The virtual reality ceramic exhibition hall-syndicated JSON specifications are shown in Table 1.

4.2.3. Virtual Reality Ceramic Display Hall Generation Procedure. The building phase of the exhibit centre and its process are as follows:

(i) The customer demands are reprinted from JSON sensor information from the virtual reality ceramic showroom

(ii) JSON is decoded to get all the product lists and asynchronously transfer statistical parameters from the CDN to the device

(iii) Consumers are permitted to access the convention centre after the launch of the showroom

To reduce the burden on the central server, static tools are downloaded such as FBX and pictures. Figure 8 shows the method of constructing a hall.

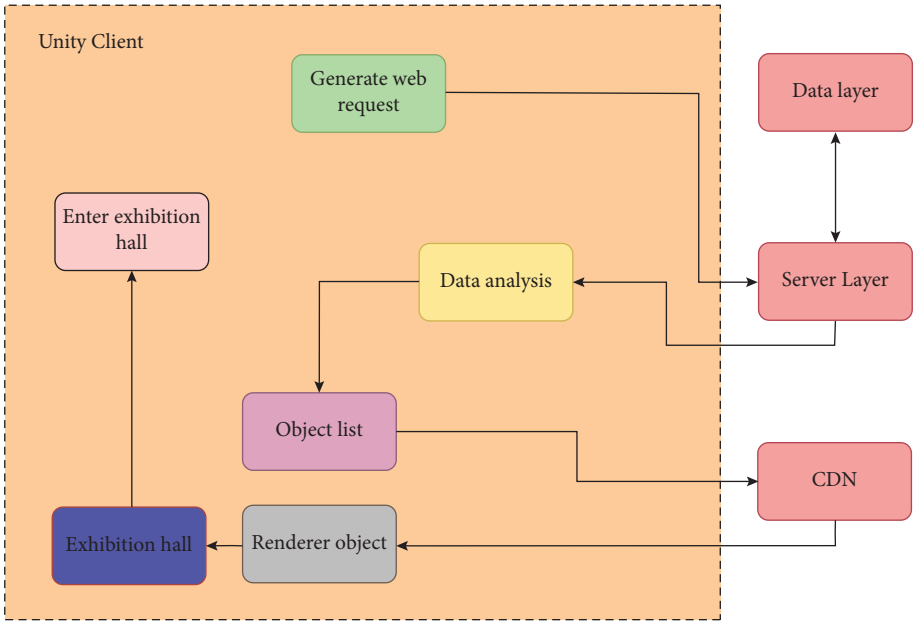

Figure 8: Exhibition model.

5. Development of Modern Art Design Based on Fused Ceramic Materials with Deep Learning

This section describes the modern art design teaching process initiated by fusing ceramic materials using deep learning approaches. The teaching process is started by creating the virtual reality-related fused ceramic modelling device applications and by creating the layouts, ceramic show hall application, and learning structure implementation. According to these steps, modern art design has been created for developing the teaching process.

5.1. Virtual Reality-Fused Ceramic Modelling Device Application. Users should click the button on virtual reality handling for teleportation before accessing the virtual room. A popular kind of virtual mobility that enables people to travel outside of the boundaries of the tracking area with little risk of experiencing virtual reality (VR) discomfort is translocation, and consumers can build a different substrate template that can be produced and distort the ceramic pattern in a fixed location. Consumers should push the discharged button to correct the ceramic form until they are pleased with the customized ceramic (Figure 9).

(1) Creating ceramic designs: researchers presented in Section 4 a method to produce and modify ceramic designs and use a mesh structure in Unity 3D to develop the ceramic strategy. In comparison to the opposing distributed systems, such as the star, bus and point-to-point architecture, it is more expensive. In the mesh, setup is really challenging. Given that each network will have to contribute to the load and be operational constantly, the energy requirement is larger.

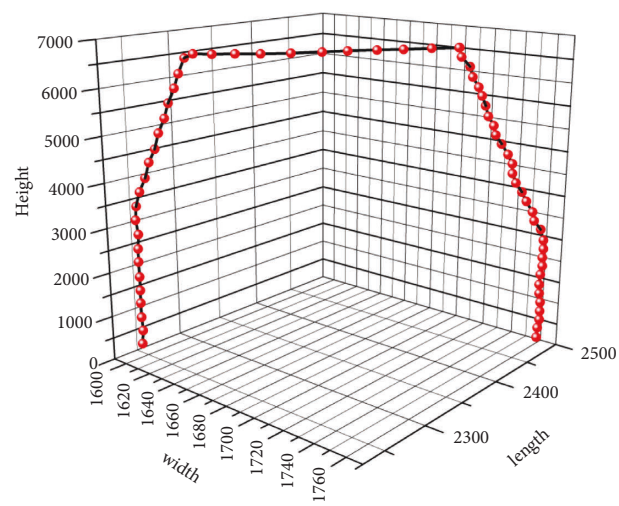

Figure 9: Edge plotting.

(2) Ceramic design deformation: designers can make multiple malformations on the produced ceramic template.

5.2. Virtual Reality Buffer Housing Layout. Researchers have created a boundary between the fused ceramic creation hall and the clay hall to enjoy an adequate space. Consumers should expect the cloud service provider to include the show centre data throughout the placeholder and ceramic decoration rooms.

5.3. Virtual Reality Ceramic Show Hall Application. In Section 4, the serialization of the exhibition space is implemented. The query data center displays hall information in order for its customers to create it. Researchers

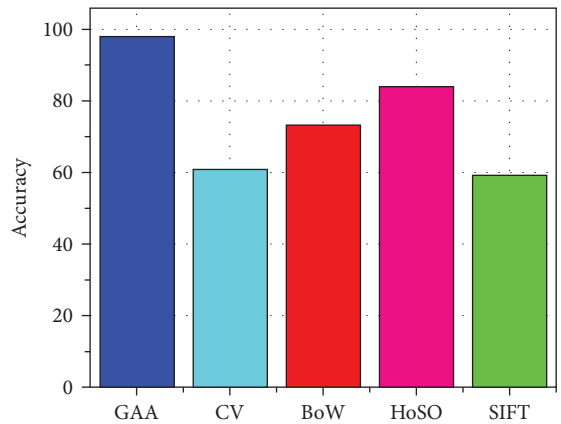

Figure 10: Accuracy comparison with the gate array algorithm (GAA).

Table 2: Accuracy comparison with different models.

Models	Accuracy
GAA	92.17
CV	56.20
BoW	68.65
HoSo	78.85
SIFT	55.43

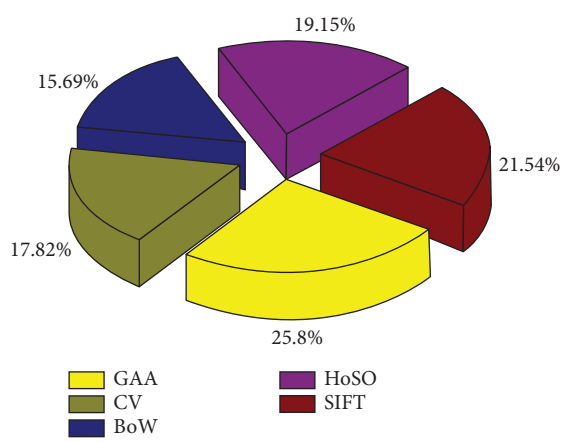

Figure 11: Efficiency comparison with the gate array algorithm (GAA).

used JSON as an asynchronous template to create a convention centre in order to get lost in a placeholder hall. The consumer will then enter the database showroom of other clients.

5.4. Digital Pottery Structure's Implementation Impact. This digital pottery room technology impact focused on the cloud-based ceramic framework demonstrates that the usage of ceramic development tools is minimized efficiently. Meanwhile, the digital exhibition space program could be used as a conceptual and applied framework.

Figure 10 and Table 2 represent the accuracy comparison of the proposed gate array algorithm (GAA) with existing

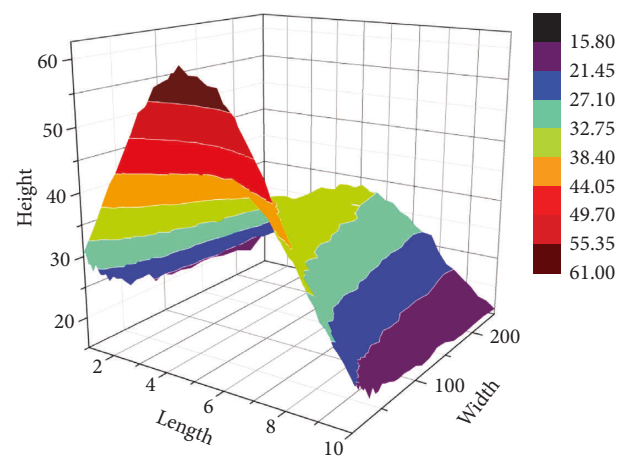

Figure 12: The surface plot in the gate array algorithm (GAA).

methods. The proposed GAA method has the highest accuracy, whereas the CV method has the lowest. The proposed gate array algorithm (GAA) performed well because of its deep learning network.

Figure 11 depicts the proposed gate array algorithm (GAA) efficiency in comparison with the existing methods. The proposed gate array algorithm (GAA) system has the highest efficiency because it requires meagre input from the user and designs the required fine art in the 3D model with limited time. But the existing methods fail to provide fast results because they lack a learning network.

Figure 12 shows the existing methods' surface plot of length, width, and height in the proposed gate array algorithm (GAA). The software designs the desired input in GAA. Then, the design is implemented by 3D software. The figure shows the surface where different colours represent different ceramic fusion components. The fused ceramic is used to maintain high durability and heat resistance.

Figure 13 and Table 3 show the magnitude plot in terms of time concerning the proposed gate array algorithm (GAA) system. The magnitude variations offer the fine art creation from almost nothing to a complete product. The final 3D fine art is created when the magnitude and surface

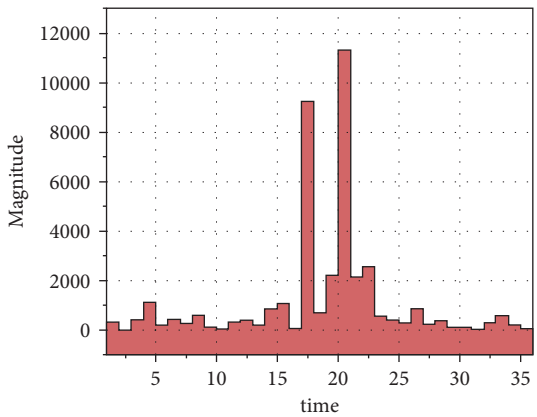

Figure 13: Magnitude plot vs time in the gate array algorithm (GAA).

Table 3: Magnitude plot vs time.

Time	Magnitude
5	1913.14
10	1128
15	8712
20	2862
25	10446.9
30	3171.43
35	1196

plot are combined. From the analysis, the proposed gate array algorithm (GAA) outperforms all other existing methods as well.

6. Conclusion

The room for digital cardboard-making functionality in this research work can create digital and archive ceramic designs, and scenarios are created using ceramic data centres for developing the teaching process. Consumers can use an online ceramic storage framework built on a ceramic data centre network to develop and distribute their virtual ceramic arts around the planet. For those other systems with related features, the proposed deep learning-assisted gate array algorithm (GAA) and conceptual design of this device may provide a philosophical and functional basis. As well as the integrated form of transport used with this framework would also allow consumers more control. Meanwhile, ceramic producers could also use this method to mitigate waste production and prophase expenditure. More than most current simulated ceramic structures, the framework is far more versatile.

The framework helps users to share their simulated ceramic workspace at lower costs and sell their brands. Researchers will look at how ceramic prototypes will be painted manually in the virtual reality setting or how sophisticated ceramic equations will be learned. Discrete Fourier transform estimates the process model's political extremes, provides smoother process curves, and uses the process graph to construct a symbol method. The information from edge points is not significant. Researchers can use political extremes to immediately create perfectly straight ceramics as a computer network's performance to build a deep convolutional neural network. In the future, the efficiency of the proposed methodology will be much improved with the help of new techniques.

Data Availability

No datasets were generated or analyzed during the current study.

Conflicts of Interest

The author declares that there are no conflicts of interest.

References

[1] Z. Gao, H. Wang, G. Feng, F. Guo, H. Lv, and B. Li, "RealPot: an immersive virtual pottery system with handheld haptic devices," *Multimedia Tools and Applications*, vol. 78, no. 18, pp. 26569–26596, 2019.

[2] M. Islam, A. N. Mahmood, P. Watters, and M. Alazab, "Forensic detection of child exploitation material using deep learning," in *Deep Learning Applications for Cyber Security*, pp. 211–219, Springer, Cham, Switzerland, 2019.

[3] R. Vinayakumar, K. P. Soman, P. Poornachandran, M. Alazab, and S. Thampi, "AmritaDGA: a comprehensive data set for domain generation algorithms (DGAs) based domain name detection systems and application of deep learning," in *Big Data Recommender Systems-Volume 2: Application Paradigms*, pp. 455–485, Institution of Engineering and Technology (IET), London, UK, 2019.

[4] B. Muthu, S. Cb, P. M. Kumar et al., "A framework for extractive text summarization based on deep learning modified neural network classifier," *ACM Transactions on Asian and Low-Resource Language Information Processing (TALLIP)*, vol. 20, no. 3, 2021.

[5] G. Zhang, C. H. R. Hsu, H. Lai, and X. Zheng, "Deep learning based feature representation for automated skin histopathological image annotation," *Multimedia Tools and Applications*, vol. 77, no. 8, pp. 9849–9869, 2018.

[6] S. Montgomery, "Dissertations in fine art. What is good academic writing?" *Insights into Discipline-Specific Student Writing*, vol. 135, 2020.

[7] C. L. Hsu, D. X. Hsu, T. J. Hsueh, S. P. Chang, and S. J. Chang, "Transparent gas senor and photodetector based on Al doped ZnO nanowires synthesized on glass substrate," *Ceramics International*, vol. 43, no. 7, pp. 5434–5440, 2017.

[8] Z. Wei, "The Teaching of Fine Art Design in Fine Arts Education in Higher Vocational Colleges," in *Proceedings of the 2019 4th International Social Sciences and Education Conference (ISSEC 2019)*, Xiamen, China, June 2019.

[9] F. Ullah, J. Wang, S. Jabbar, F. Al-Turjman, and M. Alazab, "Source code authorship attribution using hybrid approach of program dependence graph and deep learning model," *IEEE Access*, vol. 7, pp. 141987–141999, 2019.

[10] N. Lawrence and R. Huffman, *Melding the Mediums: Combining Fine Art, Graphic Design, and Product Photography to Create Commercial Images*, Pittsburg state university, Pittsburg, KS, USA, 2019.

[11] F. Ullah, S. Jabbar, and F. Al-Turjman, "Programmers' deanonymization using a hybrid approach of abstract syntax

tree and deep learning," *Technological Forecasting and Social Change*, vol. 159, Article ID 120186, 2020.

[12] K. B. Kadirova and C. B. Abdullaeva, "Lexico-Semantic aspects: national applied and fine art terms," *Journal of Critical Reviews*, vol. 7, no. 4, pp. 444–451, 2020.

[13] K. Dimililer, H. Dindar, and F. Al-Turjman, "Deep Learning, Machine Learning and Internet of Things in Geophysical Engineering Applications: An Overview," *Microprocessors and Microsystems*, vol. 80, p. 103613, 2020.

[14] N. Krishnaraj, M. Elhoseny, M. Thenmozhi, M. M. Selim, and K. Shankar, "Deep learning model for real-time image compression in Internet of Underwater Things (IoUT)," *Journal of Real-Time Image Processing*, vol. 17, no. 6, pp. 2097–2111, 2020.

[15] M. Elhoseny, M. M. Selim, and K. Shankar, "Optimal deep learning based convolution neural network for digital forensics face sketch synthesis in internet of things (IoT)," *International Journal of Machine Learning and Cybernetics*, vol. 12, no. 11, pp. 3249–3260, 2020.

[16] J. Shi, X. Yuan, M. Elhoseny, and X. Yuan, "Weakly supervised deep learning for objects detection from images," in *Urban Intelligence and Applications*, pp. 231–242, Springer, Berlin, Germany, 2020.

[17] X. Xu, Y. Chen, J. Zhang, Y. Chen, P. Anandhan, and A. Manickam, "A novel approach for scene classification from remote sensing images using deep learning methods," *European Journal of Remote Sensing*, vol. 54, no. sup2, pp. 383–395, 2020.

[18] A. Kumar, S. Mukherjee, and A. K. Luhach, "Deep learning with perspective modeling for early detection of malignancy in mammograms," *Journal of Discrete Mathematical Sciences and Cryptography*, vol. 22, no. 4, pp. 627–643, 2019.

[19] A. Khamparia, A. Singh, A. K. Luhach, B. Pandey, and D. K. Pandey, "Classification and identification of primitive Kharif crops using supervised deep convolutional networks," *Sustainable Computing: Informatics and Systems*, vol. 28, Article ID 100340, 2020.

[20] Z. J. Yalew, S. H. Ahmed, Y. J. Choi et al., "Machine Learning/AI for IoT, M2M, and Computer Communication," *Transactions on Emerging Telecommunications Technologies*, vol. 30, no. 9, 2019.

[21] S. R. Chaudhuri, E. Eban, H. Li, M. Moroz, and Y. Movshovitz-Attias, "Fine-grained stochastic architecture Search," 2020, https://arxiv.org/abs/2006.09581.

[22] R. Clarke, S. Heitlinger, A. Light, L. Forlano, M. Foth, and C. Salvo, "More-than-human participation: a design for sustainable smart city futures," *Interactions*, vol. 26, no. 3, pp. 60–63, 2019.

[23] H. Huo, Y. Chen, J. Luo, X. Yang, X. Guo, and X. Sun, "Rational design of hierarchical "Ceramic-in-Polymer" and :"Polymer-in-Ceramic" electrolytes for dendrite-free solid-state batteries," *Advanced Energy Materials*, vol. 9, no. 17, Article ID 1804004, 2019.

[24] A. Abdullayev, M. F. Bekheet, D. A. Hanaor, and A. Gurlo, "Materials and applications for low-cost ceramic membranes," *Membranes*, vol. 9, no. 9, p. 105, 2019.

[25] A. D. Badge, A. M. Kuthe, S. R. Nagdeve et al., "Geometric modeling and finite element simulation for architecture design of 3D printed bio-ceramic scaffold used in bone tissue engineering," *Journal of the Indian Institute of Science*, vol. 99, no. 3, pp. 1–14, 2019.

[26] K. Akella, "Multilayered ceramic-composites for armour applications," *Handbook of Advanced Ceramics and Composites: Defense, Security, Aerospace and Energy Applications*, pp. 403–433, Springer, Berlin, Germany, 2020.

[27] T. Mu, F. Wang, X. Wang, and H. Luo, "Research on ancient ceramic identification by artificial intelligence," *Ceramics International*, vol. 45, no. 14, pp. 18140–18146, 2019.

[28] C. Cintas, M. Lucena, J. M. Fuertes et al., "Automatic feature extraction and classification of Iberian ceramics based on deep convolutional networks," *Journal of Cultural Heritage*, vol. 41, pp. 106–112, 2020.

[29] G. A. O. Xiang, L. I. Guanghui, T. A. N. Rong, and Y. Leijiang, "Using deep neural networks to predict the tensile property of ceramic matrix composites based on incomplete small dataset IOP conference series: materials science and engineering," *IOP Conference Series: Materials Science and Engineering*, vol. 647, no. 1, Article ID 012004, 2019.

[30] C. Sandoval, E. Pirogova, and M. Lech, "Two-stage deep learning approach to the classification of fine-art paintings," *IEEE Access*, vol. 7, pp. 41770–41781, 2019.

[31] A. Lecoutre, B. Negrevergne, and F. Yger, "Recognizing art style automatically in painting with deep learning," in *Proceedings of the 9th Asian Conference on Machine Learning | ACML 2017*, pp. 327–342, Seoul, Korea, November 2017.

[32] D. Kim, J. Xu, A. Elgammal, and M. Mazzone, "Computational analysis of content in fine art paintings," in *Proceedings of the 2019 5th IEEE International Conference on Computer and Communications (ICCC)*, pp. 33–40, Chengdu, China, December 2019.

[33] S. Smirnov and A. Eguizabal, "Deep learning for object detection in fine-art paintings," in *Proceedings of the 4th International Conference on Metrology for Archaeology*, pp. 45–49, Cassino, Italy, October 2018.

[34] R. Bai, H. Ling, Z. Kai, D. Qi, and Q. Wang, "Author recognition of Fine-Art paintings," in *Proceedings of the 38th Chinese Control Conference (CCC2019)*, pp. 8513–8518, Guangzhou, China, July 2019.

[35] Y. Gong, "Application of virtual reality teaching method and artificial intelligence technology in digital media art creation," *Ecological Informatics*, vol. 63, Article ID 101304, 2021.

[36] W. Mao, "Video analysis of intelligent teaching based on machine learning and virtual reality technology," *Neural Computing & Applications*, vol. 34, no. 9, pp. 6603–6614, 2022.

Hindawi
Mobile Information Systems
Volume 2022, Article ID 9572413, 10 pages
https://doi.org/10.1155/2022/9572413

Research Article

Student-Centered Learning Environment Based on Multimedia Big Data Analysis

Erxi Zhao,[1] **Jian He**,[2] **Zhou Jin**,[1] **and Yue Wang**[3]

[1]*School of Nuclear Science and Engineering, North China Electric Power University, Beijing, China*
[2]*Graduate School, North China Electric Power University, Beijing, China*
[3]*School of Energy Power and Mechanical Engineering, North China Electric Power University, Beijing, China*

Correspondence should be addressed to Erxi Zhao; 51201648@ncepu.edu.cn

Received 23 August 2022; Revised 22 September 2022; Accepted 28 September 2022; Published 10 October 2022

Academic Editor: Chi Lin

The application of current information technology in education, especially multimedia network technology, has brought about major changes in the content and methods of instruction. It has replaced the conventional teacher-centered, textbook-centered, and classroom-centered teaching environment with a student-centered, information technology-based learning environment that includes a rich network of multimedia learning resources and virtual reality. Through the interaction between students and students and between students and the learning environment, students can acquire knowledge on the basis of observation, understanding, and cognition, so as to grasp the essence of things. It is an effective cognitive tool for students to explore freely and visualize various knowledge and skills. Therefore, the teacher is no longer the authority of knowledge imparting, but the learner's guide and helper or even the senior partner in the learner's learning activities. This shift will allow teaching staff to focus more on the design and development of learning environments and resources. This paper proposes a new clustering algorithm CURE, which overcomes the shortcomings of the detection rate and stability of the classical clustering algorithm and is suitable for solving the clustering problem in the learning environment of big data analysis. Experiments are carried out on some international standard network security dataset KDDCUP101, and the running time of the algorithm is 1230 s. The results show that the stability of the proposed algorithm is increased by 30.22% and the detection rate is increased by 10.98% compared with the common algorithm. Compared with the global K-means algorithm, the time complexity is also greatly enhanced.

1. Introduction

The continual development of information technology produces a learning environment suited to the specific needs of each student, provides a wealth of information resources and a variety of useful tools, and encourages the individualization of students' education. The construction of a learning environment is the basis for realizing the reform of learning and teaching methods, and providing learners with a more convenient, comfortable, and effective learning environment will be an important direction for the development of educational informatization in the future [1]. The traditional learning method is centered on teachers' teaching, and students are passive and receptive to learning. It is difficult to teach students in accordance with their aptitude and provide targeted guidance and education. The "student-centered" teaching method can be realized because of the development of big data technology [2]. Construct the feedback system of education and teaching evaluation and reconstruct the "student-centered" teaching feedback mode through the dynamic learning diagnosis and evaluation throughout the whole process of classroom teaching [3]. The "student-centered" teaching mode is mainly based on the humanistic theory, emphasizing that people are the first, and any activity should be centered on people's needs. It emphasizes "student-centered" and encourages students to stimulate high-level learning motivation, fully develop students' potential, and enable students to self-education [4]. Second, through experiential learning and meaningful learning, establish the teaching concept of "student-

centered," promote students to learn learning methods, and enhance adaptability. Third, the innovation of the teaching mode is also deeply influenced by mixed learning theory. With the development of network technology, network learning begins to rise. In the "student-centered" teaching mode, it emphasizes not only the master status of students and the leading role of teachers but also the essence of mixed learning as a way of information transmission [5].

Under the background of the education network era, the integration of "student-centered" must be based on "cloud, network, and end," with "Internet intelligent analysis and learning" as the new teaching method, and with the thinking mode of "big data +" to realize the accuracy and individuality of learning, realize the "activity-centered" of classroom teaching form and constantly improve the level and level of effective teaching by applying big data, so that the concept of effective teaching can be better developed [6]. Multimedia teaching resources can provide a variety of courseware. Through the application of dynamic presentation, linking, and other technologies, the learning resources are richer and the content organization is more flexible. Video or TV teaching materials can directly use the existing better audiovisual teaching materials in the classroom and provide convenience for the collection of real situational learning resources. We can also use network resources to increase the richness of learning content [7]. The "student-centered" teaching mode of education big data requires mobile terminals that can be used by students, whether it is intelligent analysis or intelligent push, whether it is data collection or data analysis, to realize real-time intelligent analysis and push, help students learn independently, and realize intelligent analysis and intelligent push. For students, they can understand the occurrence mechanism of the learning process from the perspective of learners' behavior and use it to optimize learning and carry out adaptive learning and self-directed learning [8].

In the network era, databases tend to be centralized and large, but applications are extending in the direction of decentralization and miniaturization. For current e-learning platforms, the required data sources come from many distributed databases [9]. The key technologies required in this environment are mainly aimed at the storage of massive data and the operation of massive data. Since most of the current e-learning platforms are developed based on relational databases, the relational database models are difficult to express complex nesting needs, and support data types are limited, so researchers generally start with data models and propose unstructured databases [10]. Using the process and outcome data obtained from big data analysis, we can intelligently diagnose the learning state of relevant classes and students and select the appropriate "teaching content and learning methods" in a targeted way. According to the big data platform, timely feedback whether the adjusted "teaching contents and learning methods" are suitable for most students' learning. For those students who fail to achieve the teaching effect, actively give guidance or adjust the "teaching contents and learning methods" again and finally realize the improvement of the "student-centered" teaching environment. The innovation of this paper lies in the following:

(1) The constructivist approach is used to organize resources based on the characteristics of learners in order to match resources with learners. The application of humanism to the education system makes personalized learning feasible, aids in the promotion and absorption of personalized learning, attempts to facilitate cross-cultural regional learning exchanges, and broadens the methods in which students can get assistance.

(2) The proposed intelligent learning system creates an independent learning environment for learners and provides a diagnosis of the learning situation, recommendations of learning resources, guidance on the learning path, evaluation of the learning effect, and documentation of the learners' personalized learning process. Analyze the content of student-centered learning performance in order to identify the indications of student-centered learning performance analysis and construct a student-centered learning performance analysis model with reference to the "response" level of the training evaluation theory.

This article is organized into seven sections.

The Section 1 is the introduction part. This part introduces the background of multimedia network technology, which is student-centered, relies on information technology, is rich in network multimedia learning materials, and has a virtual reality learning environment. The Section 2 mainly summarizes the relevant literature, summarizes the advantages and disadvantages, and proposes the research ideas of this paper. Section 3 deconstructs the intelligent learning environment design based on big data in detail. Section 4 describes and analyzes the clustering algorithm in this paper. The Section 5 conducts the experiment on the learning situation of the multimedia learning environment. Section 6 provides about research outlook and strategies. The Section 7 concludes, summarizing the findings of the full text.

2. Related Work

Although current researchers are aware of the importance of these data to the construction of a learning environment, how to classify massive big data and extract important relevant data for analysis is still a major technical problem. In most cases, students do not have the opportunity to communicate with teachers, and the opportunities for interaction and communication between students and teachers are not balanced.

Burns l took the lead in putting forward the concept of an intelligent learning environment, which is an intelligent and open digital virtual reality learning space composed of matching equipment, technology, and media with learners' learning as the center. It believes that it not only supports the independent construction of learners' learning but also provides timely learning guidance [11]. Main also explains the elements involved in the intelligent learning environment, pointing out that learning resources, intelligent tools, learning communities, learning methods, and teaching

methods are the main constituent elements of the intelligent learning environment, and proposes a new system model for this basis [12]. Kasim emphasizes that as a "student-centered" teaching mode supported by education big data, it needs to integrate multitype and diversified data based on students' learning behavior and result data and assisted by analysis of teaching behavior and result data [13]. Baeten et al. scholars pointed out that in the current network era, the rapid development of massive online learning content and the in-depth research of data mining technology and learning analytics technology have boosted the developmental achievements of teaching evaluation [14]. According to Yang and Xiao, intelligent learning is based on intelligent equipment and learning analysis technology, which predicts learners' learning results and then guides learners to conduct self-directed learning [15]. Ms et al. sorted out the development of personalized learning and thought that personalized learning went from advocating the intelligence of the teaching system to the application of the adaptive network teaching system and then to the development of the personalized learning situation and intelligent question-answering system based on mobile Internet at present [16]. Tong Y and others believe that digital learning refers to a brand-new learning mode that can fully reflect the role of learners through the establishment of an Internet platform in the field of education. It brings people not only the convenience of obtaining educational resources but also a brand-new concept different from traditional classroom learning [17]. Andone and Vasiu believe that a student-centered learning environment is a smart learning environment. In social learning, the intelligent learning environment can perceive the place where the learners are located, actively push the learning resources related to the environment where the learners are located according to the place and the learning style of the learners, and realize adaptive ubiquitous learning [18]. Ivanova and Nayakama' quantitative analysis of learning behavior data can provide timely insight into students' learning needs and predict education and teaching effects. Adjust teaching modules and teaching methods in a targeted manner, so as to achieve effective guidance, turn traditional teaching into a companion for students' learning and growth, and better integrate teaching and learning. The development of the new generation of information technology has made it possible to change the concept and practice of the learning environment [19]. Therefore, the scholar Sears indicated in his research that "the development of technology stimulates researchers and educators to expand the concept of learning and the design of learning environment" [20].

3. Design of an Intelligent Learning Environment Based on Big Data

The education business has unavoidably undergone revisions and advances as a result of the "Internet Plus" paradigm and big data technologies. One of the biggest changes is the learning environment. From traditional learning environments to online learning environments, mobile learning environments, and today's smart learning environments, modern education models and advanced computer technology play an important role. A smart learning environment is an intelligent, advanced, flexible, and humanized learning environment built on the basis of big data and cloud computing with the learner as the center. Its intelligence is mainly in two aspects. First, it has advanced facilities and technical means such as big data centers and cloud computing in the overall structure. Lay technical and architectural foundations for the entire learning environment. Second, artificial intelligence, face recognition, intelligent auxiliary tools, intelligent service software, and other software and hardware are used in smart classrooms, smart training rooms, smart labs, and other terminals to further enhance the intelligence of the terminals (Figure 1). In the past, school teaching management, evaluation, and classroom were separated, and the quality of classroom teaching could not be monitored in real-time. But now, schools can closely integrate teaching management and evaluation into classroom teaching activities through multimedia technology.

Technology-mediated learning environments should also embody a teacher-led, learner-centered tenet. Leverage the combined strengths of teachers, learners, and multimedia to create computer-assisted learning environments and improve learner performance. Here, we propose an interactive multimedia learning environment framework to analyze the relationship between learners, multimedia technology, and teachers (Figure 2). Due to the intervention of multimedia and modern communication technology, the creation of a learning environment is strongly stimulated. According to the instructional content, teachers should generate genuine tasks in real scenarios with the assistance of multimedia, inspire students' motivation to study, and allow them to feel the social worth of gaining information. The problem-based teaching supported by information technology creates a problem situation of real tasks, which has an obvious effect on the cultivation of students' cognitive ability.

Multimedia network, with its rich resources, interactivity, integration, nonlinearity, real-time, convenience of information use, and flexibility of learning methods, provides good external support conditions for students' autonomous learning. However, as students' knowledge increases, multimedia redundancy begins to emerge, that is, the benefits of combining visual and audio information eventually diminish. One form of information may become redundant information. At this time, they only learn pictures/charts or only accept text information, and the learning effect is the best. Therefore, we appropriately use the knowledge reversal effect to make learners control learning interests and motivation, make teaching meet different learning styles and realize adaptive teaching, and promote individuals to actively construct and actively process information. On the surface, all the above are the advantages of learners controlling the learning environment. However, in order to make these advantages work, we must consider the existing knowledge level of learners.

Autonomous learning requires changing the roles of teachers and students and changing the teaching philosophy,

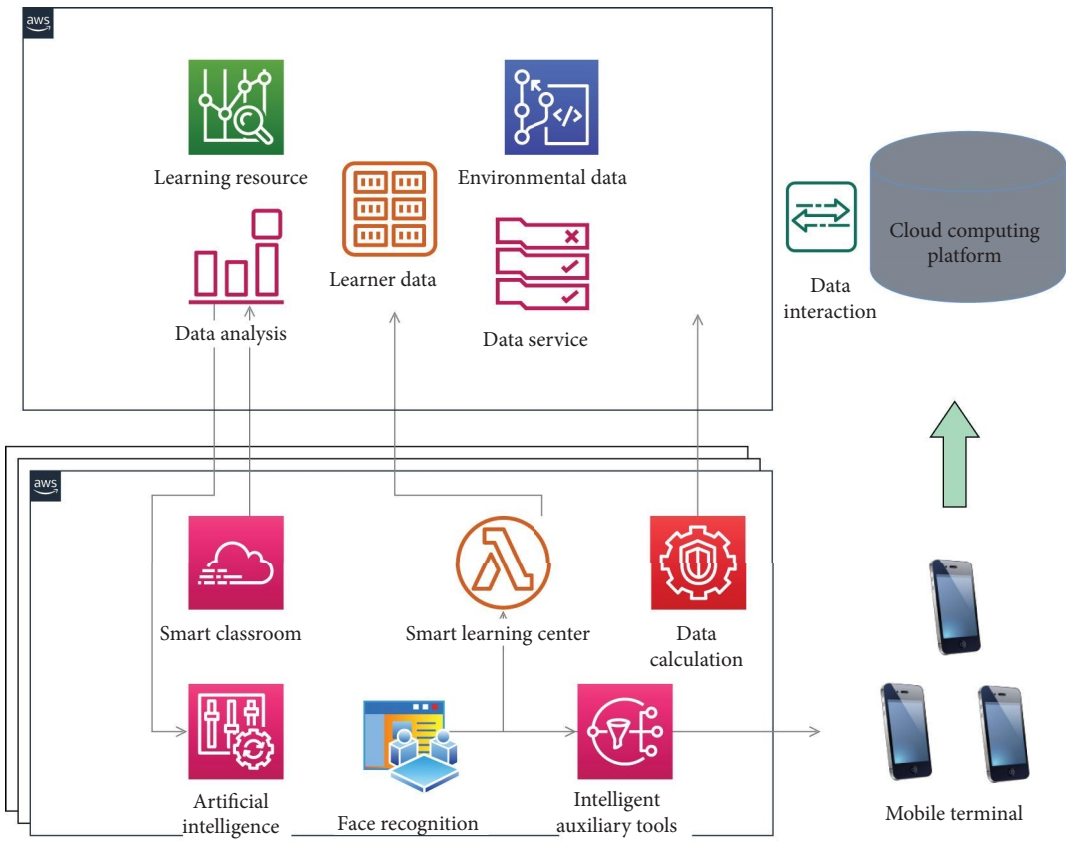

Figure 1: Framework of the intelligent learning environment.

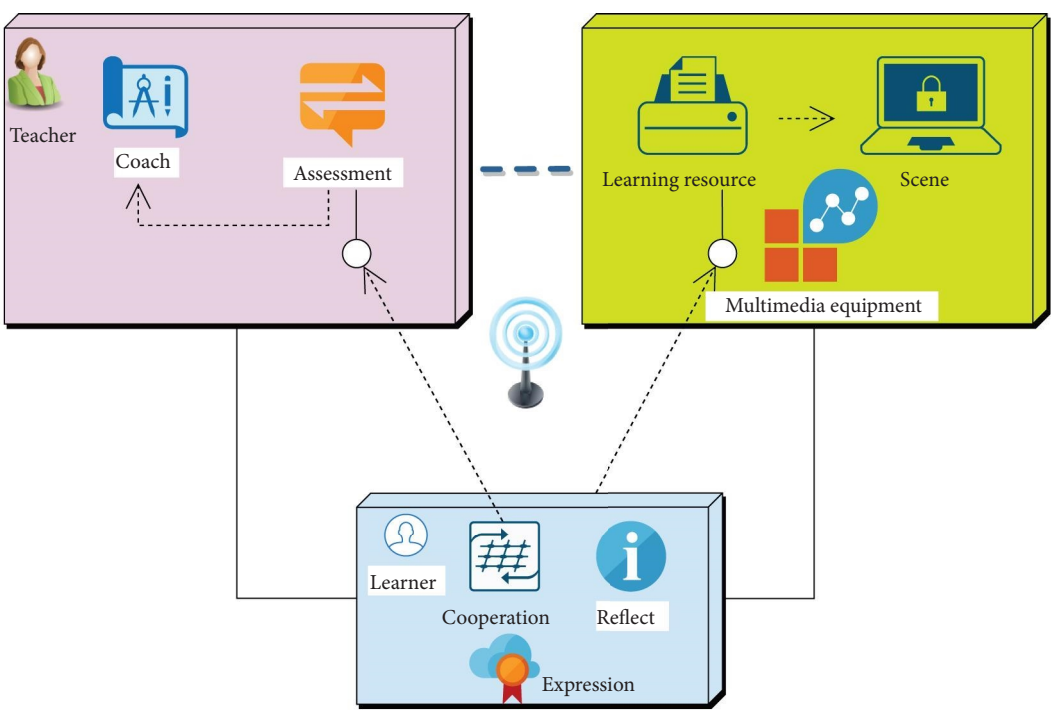

Figure 2: Components of the multimedia learning environment.

so that students can be in the dominant position and truly realize the learner-centered autonomous learning model. Self-regulated learning faces a process of knowledge digestion and absorption. In this process, students sometimes face many difficulties in understanding and application, and teachers are required to give timely guidance to

improve the effect of self-regulated learning. With the help of the characteristics of "Internet plus," students can give timely feedback when they encounter problems in the learning process, and the learning style is flexible and the learning time can be arranged by learners themselves, providing students with convenient and personalized learning style (Figure 3). When learners use computers to learn, they will continuously interact with teachers, classmates, and learning content. Therefore, the designers of the teaching environment believe that the design of the interactive interface for learning is the most important part of the design of the learning environment. The smart learning system supported by big data can be connected with other systems, such as examination and score analysis systems, student status management systems, and career planning systems. Extract useful data from it and improve the learner information database. At the same time, the smart learning system can carry out refined data collection on the learning process of learners and continuously update learner characteristic information through data mining and learning analysis.

4. Algorithm Description

The use of clustering in the field of data mining is very adaptable, and the clustering technique is situation-dependent; thus, it cannot be universal. The clustering algorithm abstracts the data objects, defines the metric function of clustering to describe the similarity between the data, and classifies the sample objects according to the similarity. The sample objects with high similarity are classified into one class, and the sample objects with low similarity are classified into other classes. Therefore, as a measure of the clustering metric function, the similarity distance function of the data objects is very important. There are three types of distance functions commonly used in clustering algorithms:

$$D(x, y) = \sqrt{\sum_{k=1}^{n} \left|x_k - y_k\right|^t}, \tag{1}$$

where t is a positive integer. When $t = 1$, it represents the Manhattan distance:

$$D(x, y) = \sum_{i=1}^{n} \left|x_k - y_k\right|. \tag{2}$$

When $t = 2$, it represents the Euclidean distance:

$$D(x, y) = \sqrt{\sum_{i=1}^{n} \left|x_k - y_k\right|^2}. \tag{3}$$

In practical problems, the corresponding weight w may be assigned according to the importance of each attribute.

$$D(x, y) = \sqrt{\sum_{i=1}^{n} w_k \left|x_k - y_k\right|^t}. \tag{4}$$

Let X be a data sample of an unknown class, and let C be a certain assumption: the data sample x belongs to a specific class $P(C \longrightarrow X)$. C is the probability that C holds given the observation data sample X. Then,

$$P(C \longrightarrow X) = \frac{P(X \longrightarrow C) \cdot P(C)}{P(X)}. \tag{5}$$

A weighted summation method is used to calculate the user's predictive rating for multimedia learning environment factors, thereby generating recommendations. The target user's predicted scoring formula for an item is

$$P_i = \frac{\sum_{i=1} \text{similar}\left(S_n * R_{u \cdot n}\right)}{\sum_{n=1} \text{similar}\left(\left|S_{u \cdot n}\right|\right)}. \tag{6}$$

In the formula, $S_{u \cdot n}$ represents the similarity between items u and n. $R_{u \cdot n}$ represents user u' rating on item n in the set of similar items.

The problem of data sparsity is caused by the insufficient scoring rate of users on resources. This will cause the user resource score matrix to be extremely sparse, which makes it difficult for the system to successfully generate the neighbor user set, and it is difficult to calculate the similarity between users. Finally, it will seriously affect the recommendation effect.

In the report on the learning situation of knowledge points, instructors can be urged to do remedial instruction for knowledge points with a relatively low degree of mastery, and they can also be prompted for knowledge points with a relatively high level of mastery. In combination with the daily learning behavior data of learners, the teachers can be prompted to judge according to the teaching experience, which can appropriately accelerate the teaching progress or improve the abstraction of the teaching content. The calculation formula is

$$A_i = \frac{f(x_i) - y_j + \omega}{\sum_{i=1}^{n}\left(f(x_i) - y_j\right) + \sigma}, \tag{7}$$

$$S_i M \times \frac{y_j - f(x_i) + \omega}{\sum_{i=1}^{n}\left(y_j - f(x_i)\right) + \sigma}. \tag{8}$$

When learners complete their learning, we need to evaluate the learning resources and tools recommended by the system to determine the pros and cons of their teaching effects, so as to screen out high-quality resources and guide the development of subsequent resources and tools. Use L_0 to represent the knowledge and ability level of the learner, L_{i0} to represent the knowledge and ability level of the learner at the beginning of the learning stage, L_{i1} to represent the knowledge and ability level after learning the learning object, and ΔL_0 to represent the improvement degree of the knowledge and ability level of the learner. Then, the calculation formula of ΔL is

$$\Delta L_0 = \frac{L_{i1} - L_{i0}}{\left|1 - L_{i0}\right|}. \tag{9}$$

$$CL_{tj} = 1 - \left|d_j - L_{t0}\right|. \tag{10}$$

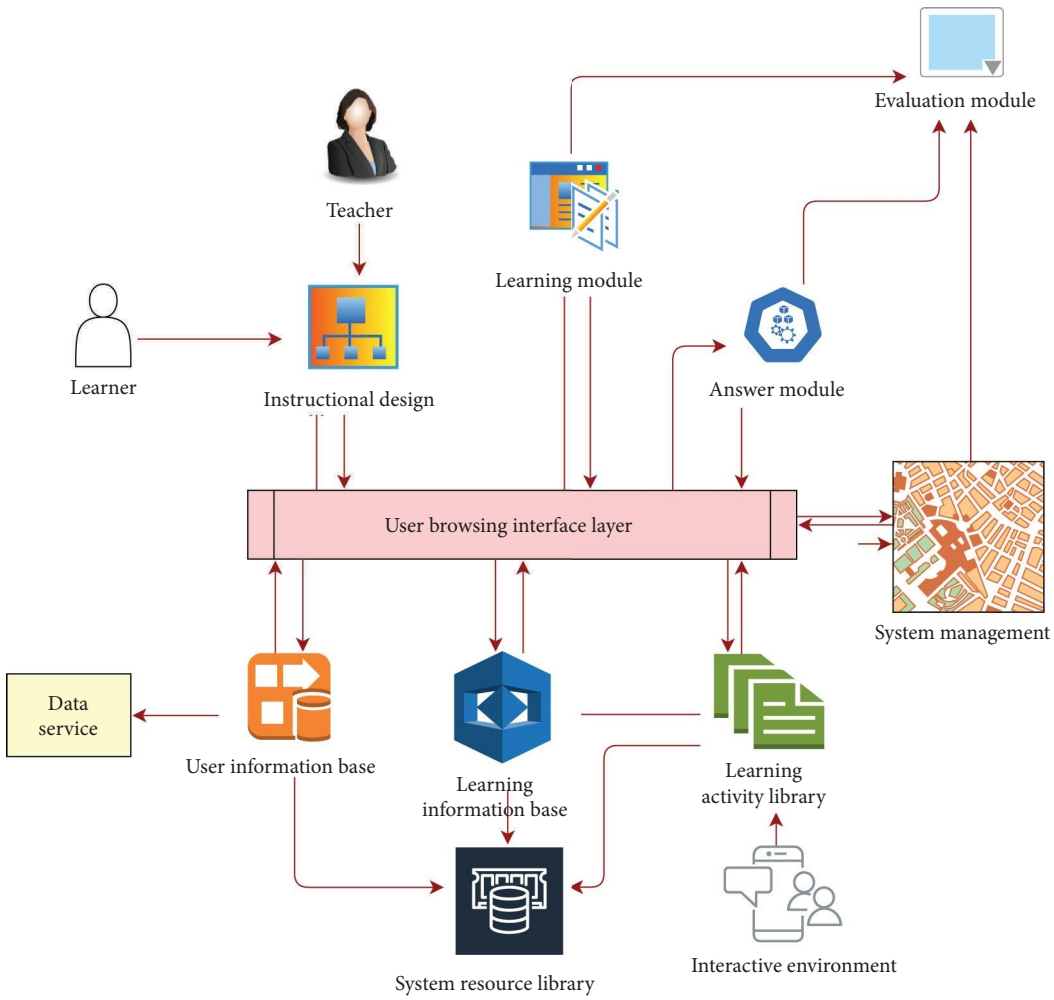

Figure 3: Big data analysis learning environment design.

In the formula, CL_{tj} represents the degree of matching between the learner's original knowledgeability level and the difficulty of the learning object.

Use V_j to represent the average effectiveness of learning object O_j, that is, the evaluation in all learning stages. The calculation formula is

$$V_j = \frac{\sum_{i=1}^{M} V_{ij}}{m}. \tag{11}$$

In the formula, V_{ij} represents the effectiveness of learning object O_j in learning stage P_i, and m is the number of all learning stages for all students.

5. Experiments

The experimental data in this paper is a small-scale test of 100 students from a university. These students are allowed to carry out various forms of intelligent autonomous environment learning in this system. The personal information of the learners and the learning activity records of the learners are taken as the attributes of the resource model, and the learning resources are taken as the target data source to recommend possible learning resources for the learners. The model emphasizes the ubiquity of learning, that is, learners can learn at any time, at any place, and with any device. Therefore, the recommendation system of ubiquitous learning resources should be suitable for the device needs of both mobile and mobile terminals. Tables 1–3 design both the ubiquitous learning resource model and the learner model. Resource managers can create new resources according to the learning resource model introduced in Section 3, including the basic information of resources, learning contents and corresponding exercises, and save them in the database and corresponding paths for learners to learn and use in the future.

The content-based recommendation is suitable for recommending resources of text type, but not for recommending resources of multimedia type because it needs to abstract several keywords representing text characteristics to form a feature vector based on the analysis of the structure of text resources to describe the content characteristics of resources.

In the multimedia learning environment, the teaching and related information provided to learners can be divided into two categories, one is direct teaching guidance

Table 1: Design of learner information table.

Attribute	Type	Describe
personID	Varchar (30)	Learner ID
personName	Varchar (20)	Learner name
Password	Varchar (50)	Learner registration
Sex	Varchar (2)	Gender
Age	Varchar (7)	Age
Edu-level	Varchar (5)	Educational level

Table 2: Learning behavior record design table.

Attribute	Type	Describe	Primary key
actld	Varchar (32)	Learning behavior ID	Yes
personID	Varchar (33)	Learner ID	No
resourceID	Varchar (34)	Learning resource ID	—
Click	Int	1 means clicked; 0 means not clicked	—
Collect	Int	1 means collected; 0 means not collected	—
Download	Int	1 means downloaded; 0 means not downloaded	—
Comment	Int	1 means commented; 0 means not commented	—
Score	Int	1–5 specific score; 0 means no score	—

Table 3: Learner resource evaluation matrix.

C/R	R1	R2	R3	...	Rn
C1	Q11	Q12	Q13	...	Q1n
C2	Q21	Q22	Q23	...	Q2n
C3	Q31	Q32	Q33	...	Q3n
	...	...	...	...	...
Cm	Qm1	Qm2	Qm3	...	Qmn

information and the other is auxiliary supporting information. With the improvement of learners' knowledge level, an inquiry-based or problem-based learning environment will further promote learners' development. At this time, it is necessary to provide them with auxiliary information resources, such as problem-solving strategies and tips and answers to frequently asked questions. In the design of a multimedia learning environment, we usually need to consider three factors: the support, interactivity, and diversity of teaching information. Figure 4 shows the reference strategies for designing these four aspects with the change in learners' knowledge level.

When learners learn independently after class, they mainly conduct systematic interactive learning in the form of self-directed learning. The types of visits are divided into collaboration, communication, and evaluation, and the number of visits proves the degree of learning interaction (Figure 5). The teacher selects resources from the resource pool or makes and uploads them by himself. The system pushes them to the students according to the push strategy or the students choose them independently. Here, the teacher should provide the students with task-driven resources, personalized listening resources, and various resources that can support personalized inquiry. Specific resources can be expressed in the form of video, audio, pictures, animation, and

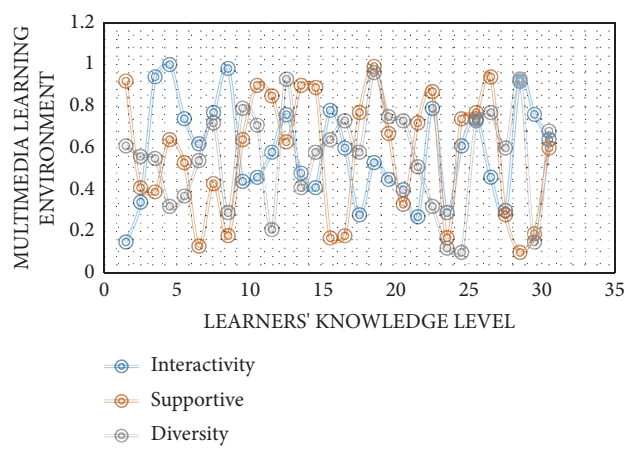

Figure 4: Analysis of design factors of the multimedia learning environment.

construction tools. To create learning guidance resources of various paths, the resources are arranged differently during pushing in accordance with the specific subject teaching content, subject characteristics, learning situation, and learning methods in order to adapt to the learning of students at different levels and realize personalized teaching and hierarchical teaching. In the

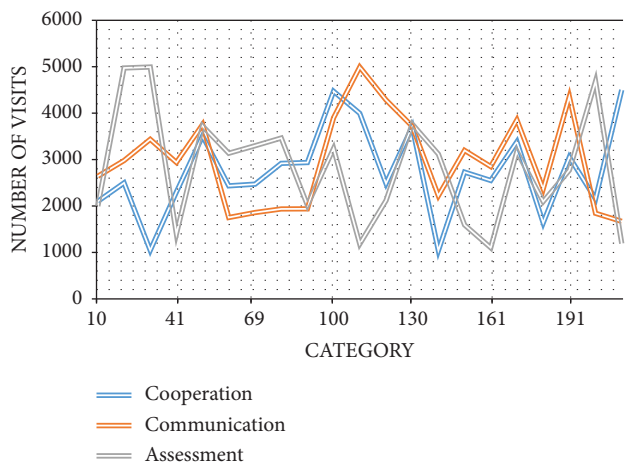

Figure 5: The number of visits to the multimedia self-learning platform.

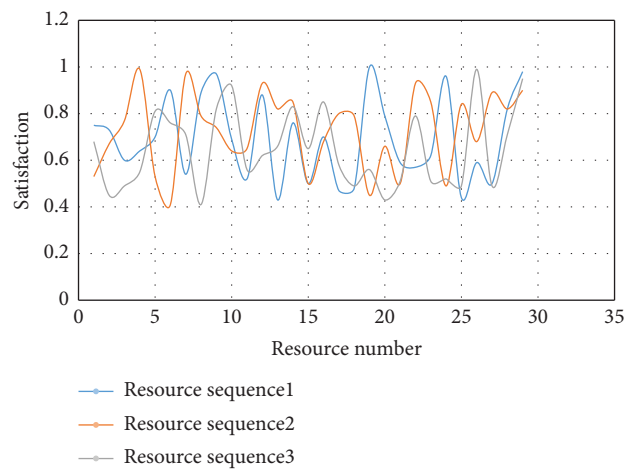

Figure 6: Satisfaction with teaching resources.

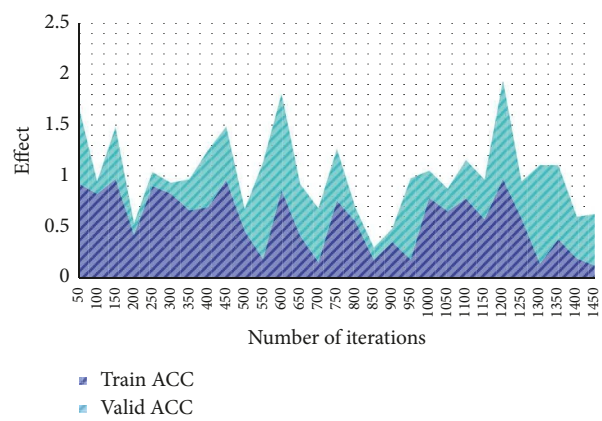

Figure 7: Resource model usage effect.

process of learning, students can choose their own path according to their learning situation.

Big data and learning analytics can predict learners' online learning behavior and learning effect and give them positive feedback. Learners can analyze and predict their own learning conditions, set their own learning goals, and formulate personalized learning plans that are most suitable for their own learning needs. Students' learning content is nonsystematic and presents the characteristics of fragmentation. Students who use the library of educational information resources may quickly find extensive materials both inside and outside of the classroom and become aware of how freely accessible information is. Teachers take on the role of mentors for their students' learning and can direct them toward resources based on big data research. The target dataset was divided into two groups, and 50 students in each group were assessed by means of a satisfaction questionnaire. Recommend different personalized learning resources according to the characteristics of different students and evaluate the feasible satisfaction of learning resources to learning (Figure 6).

The resource model should be in line with the learner's learning style in the use stage. The resource model should be defined accurately, and new technologies should not be blindly pursued. When designing a resource model, it is necessary to consider whether the model can generalize the real learners, and more importantly, the adaptability of the model to the learning platform. And the attribute value of the model needs to be obtained by tracking the use of resources by the learner, and the use of the resource model can be evaluated in time (Figure 7).

Finally, by calculating the similarity of resource objects, the cure algorithm is applied to group resource objects. The algorithm results are compared with the evaluation of the manual questionnaire, as shown in Figure 8. According to the link between resources and learners' characteristics, the learning materials suited for learners are recommended to learners. Through intelligent diagnosis of students' learning status, select appropriate teaching contents and learning methods. Build a teaching data platform to realize the learning exchange and interaction without time and space constraints and achieve the expected goal of the teaching mode.

Combined with previous research, it is found that the stability of the CURE algorithm proposed in this paper is 30.22% higher than that of common algorithms, and the detection rate is increased by 10.98%. The time complexity has also been significantly increased when compared to the global K-means algorithm. In view of this, combined with the CURE clustering algorithm and the learning characteristics of the learners, the resource objects are grouped reasonably, and the learning resources suitable for the characteristics of the learners are found. The traditional mode of learning resources for learners is transformed into a mode that allows resources to automatically find learners to match, which reduces the time and trouble of learners in finding suitable learning resources during the learning process, and improves learning efficiency.

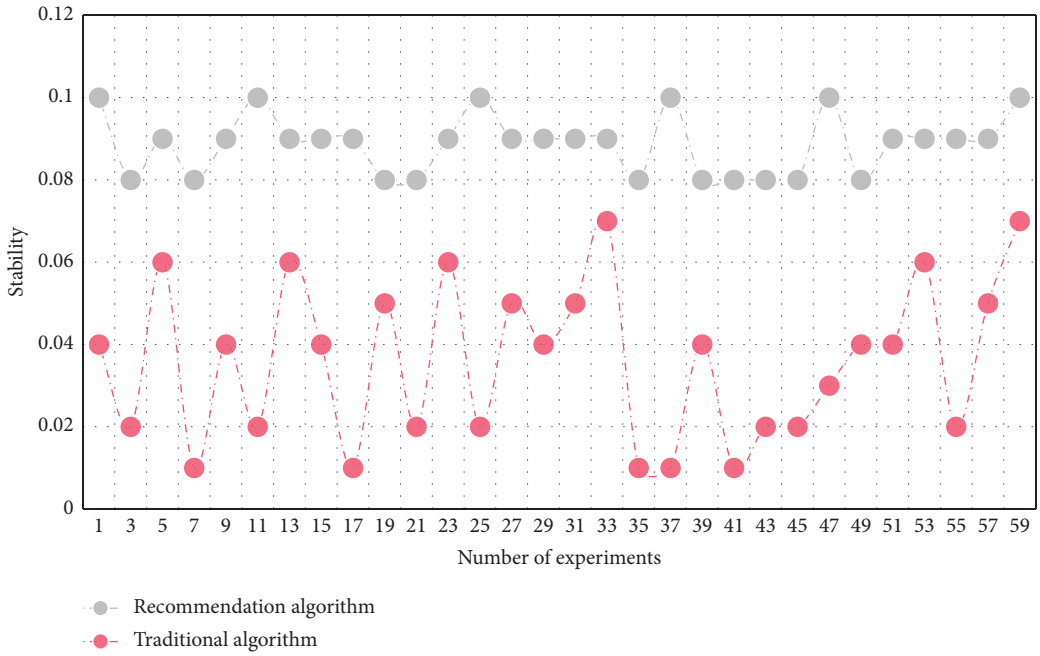

Figure 8: Algorithm application comparison.

6. Research Outlook and Strategies

In the multimedia network environment, to ensure learning efficiency, we should not only improve our own factors but also it is necessary to improve the external conditions for students to learn independently. That is, according to different teaching theories, teaching management models and management requirements, different learning objectives, and different personalities of learners, different technologies are used to build different intelligent learning environments. This environment is learner-centered, everything is beneficial to learners' learning as the starting point, and the end result is to promote learners' learning process. It is human-oriented, personalized according to the individual characteristics of learners, and intelligent based on high-tech. Therefore, the following aspects are prospected and analyzed.

(1) Reasonable teaching design: The big data analysis method is used in online learning. By collecting students' learning data, the student's learning situation is analyzed and evaluated. Discover problems in teaching in time, improve teaching, and improve students' learning efficiency.

(2) Cultivate students' metacognitive ability: Only students with strong metacognitive ability can develop more cognitive resources, more information, and more strategies. Only in this way can we better complete the cognitive task to become the leader of learning. Carry out autonomous learning.

(3) The change of teachers' roles and the improvement of their own level: Under the multimedia network environment, teachers help students develop good habits of autonomous learning, give them constructive suggestions in time, and become active promoters of autonomous learning. When students are engaged in autonomous learning, especially in the early stage of autonomous learning, teachers should be changed from traditional transmitters to guides and organizers.

7. Conclusions

Under the guidance of multimedia technology and big data analysis, the learning environment created by multimedia technology is widely used to carry out the interaction between students and the environment. Enhance students' sense of cooperation through interpersonal communication. Through the cooperation between humans and computer, the learning style of students is changed and the efficiency of solving problems is improved. Through communication between teachers and students, highlight the dominant position of students and teachers. This extensive interactive environment promotes the improvement of students' subject literacy and information literacy at the same time. According to the big data platform, timely feedback whether the adjusted "teaching contents and learning methods" are suitable for the learning of most students. For students who fail to achieve the teaching effect, actively guide them or readjust the "teaching contents and teaching methods" to finally achieve the teaching objectives, turn traditional teaching into a companion for students' learning and growth, and better integrate teaching and learning.

Data Availability

The data used to support the findings of this study are included within the article.

Conflicts of Interest

The authors declare that they have no conflicts of interest.

References

[1] S. Sasikala, S. Gomathi, and V. Geetha, "A proposed framework for cloud-aware multimodal multimedia big data analysis toward optimal resource allocation," *The Computer Journal*, vol. 28, no. 5, p. 389, 2020.

[2] T. Lauc, S. Kišiček, and P. Bago, "Students' usage and access to multimedia learning resources in an online course with respect to individual learning styles as identified by the VARK model," *Springer-Verlag*, vol. 48, no. 33, p. 2089, 2021.

[3] D. U. Bolliger, "Investigating student learning in a constructivist multimedia-rich learning environment," *Association for Educational Communications & Technology*, vol. 58, no. 4, p. 21, 2021.

[4] L. Min, J. Olmanson, and L. Horton, "Motivational multimedia: examining students' learning and motivation as they use a multimedia enriched learning environment," *American Educational Research Association Annual Meeting*, vol. 29, no. 6, pp. 300–321, 2017.

[5] S. Jones and J. Richardson, "Designing an IT-augmented student-centred learning environment," *Science and Mathematics Education*, vol. 589, no. 6, p. 390, 2018.

[6] A. H. Fatima and N. Ahmad, "Student-centred learning in a passive learning environment: students' perception and performance," *International Journal of Economics & Management*, vol. 7, no. 1, pp. 84–107, 2017.

[7] G. Fernandez, S. John, and G. Netherwood, "Teaching engineering with an on-line student-centred environment," *Faculty of Built Environment and Engineering, Queensland University of Technology*, vol. 209, no. 4, p. 9, 2018.

[8] J. Seppala and K. Yajima, "Development of student-centred language learning environment," *Information Technology and Electrical Engineering*, vol. 99, no. 1, p. 49, 2018.

[9] L. Wakeling, A. Green, and M. Naiker, "An active learning, student-centred approach in chemistry laboratories: the laboratory as a primary learning environment," *Science and Mathematics Education*, vol. 92, no. 02, p. 40, 2019.

[10] L. Klerkx, N. Totté, and M. Vriens, "Mobile learning in a student-centred learning environment: a surplus value?" *Multimedia Systems*, vol. 02, no. 5, p. 30, 2019.

[11] L. Burns, "Integrating digital literacy in a student-centred learning environment through online learning resources," *Australianliteracyeducatorsassociation*, vol. 39, no. 7, p. 408, 2019.

[12] K. Pramod, "Developing and incorporating an interactive IS project management coursework into a student-centred learning environment," *Computers in Human Behavior*, vol. 209, no. 7, p. 380, 2019.

[13] K. A. S. IM. Creating, "Lifelong learning environment through student-centred learning," *Teaching research*, vol. 49, no. 5, p. 487, 2018.

[14] M. Baeten, E. Kyndt, K. Struyven, and F. Dochy, "Using student-centred learning environments to stimulate deep approaches to learning: factors encouraging or discouraging their effectiveness," *Educational Research Review*, vol. 5, no. 3, pp. 243–260, 2010.

[15] W. Yang and Y. U. Xiao, "Research on the application mechanism of big data and learning analysis in a blended learning environment of universities," *Journal for Higher Education Management*, vol. 290, no. 6, p. 39, 2019.

[16] A. Ms, C. Mshb, and A. An, "Harnessing the power of big data analytics in the cloud to support learning analytics in mobile learning environment," *Computers in Human Behavior*, vol. 92, no. 6, pp. 578–588, 2019.

[17] H. E. Tong-Yu and J. X. University, "Big data era of network learning environment data integration," *Modern Educational Technology*, vol. 489, no. 6, p. 49, 2018.

[18] D. Andone and R. Vasiu, "Development of an ICT open learning environment for teaching multimedia," in *Proceedings of the New Educational Benefits of ICT in Higher Education, Erasmus Universiteit Rotterdam*, July 2004.

[19] M. Ivanova and M. Nakayama, "Analysis of a personal learning environment from multimedia perspective," *Multimedia Education Research*, vol. 190, no. 5, p. 40, 2019.

[20] R. B. Sears, "Evaluating the effectiveness of multimedia information graphics in the learning environment," *Texas A&M University - Commerce*, vol. 20, no. 8, p. 490, 2017.

Hindawi
Mobile Information Systems
Volume 2023, Article ID 9757060, 1 page
https://doi.org/10.1155/2023/9757060

Retraction

Retracted: Design of Accurate Association System of QR Code Information for Cigarette Sorting

Mobile Information Systems

Received 8 August 2023; Accepted 8 August 2023; Published 9 August 2023

This article has been retracted by Hindawi following an investigation undertaken by the publisher [1]. This investigation has uncovered evidence of one or more of the following indicators of systematic manipulation of the publication process:

(1) Discrepancies in scope
(2) Discrepancies in the description of the research reported
(3) Discrepancies between the availability of data and the research described
(4) Inappropriate citations
(5) Incoherent, meaningless and/or irrelevant content included in the article
(6) Peer-review manipulation

The presence of these indicators undermines our confidence in the integrity of the article's content and we cannot, therefore, vouch for its reliability. Please note that this notice is intended solely to alert readers that the content of this article is unreliable. We have not investigated whether authors were aware of or involved in the systematic manipulation of the publication process.

Wiley and Hindawi regrets that the usual quality checks did not identify these issues before publication and have since put additional measures in place to safeguard research integrity.

We wish to credit our own Research Integrity and Research Publishing teams and anonymous and named external researchers and research integrity experts for contributing to this investigation.

The corresponding author, as the representative of all authors, has been given the opportunity to register their agreement or disagreement to this retraction. We have kept a record of any response received.

References

[1] C. Hao, W. Taicheng, and Z. Haoran, "Design of Accurate Association System of QR Code Information for Cigarette Sorting," *Mobile Information Systems*, vol. 2022, Article ID 2466801, 12 pages, 2022.

Hindawi
Mobile Information Systems
Volume 2022, Article ID 2466801, 12 pages
https://doi.org/10.1155/2022/2466801

Research Article

Design of Accurate Association System of QR Code Information for Cigarette Sorting

Chen Hao, Wei Taicheng, and Zhu Haoran

China Tobacco Guangxi Industrial Co. Ltd, 530001, Nanning, China

Correspondence should be addressed to Zhu Haoran; 2019020428@stu.cdut.edu.cn

Received 23 June 2022; Revised 17 July 2022; Accepted 20 July 2022; Published 9 October 2022

Academic Editor: Chi Lin

This study employs the EIQ analysis approach to quantitatively examine the real order data of the cigarette distribution center in an effort to further increase the efficiency of cigarette sorting and distribution. To further increase the accuracy and efficiency of sorting labor, a sorting system based on QR code information and an accurate identification algorithm is proposed with the use of statistical data and the associated planning scheme. According to the system simulation findings, the sorting efficiency of the system's sorting line is 18570 pieces per hour. However, by adding packing equipment, the efficiency of the system can be raised by 61.55 percent and can reach 30000 pieces per hour. Additionally, it confirms the viability of the system design. The two-dimensional code' properties determine which global threshold method the binarization algorithm chooses. The two-dimensional code' coding principle is investigated, and a two-dimensional code decoding algorithm is developed. The results of the experiment indicate that the decoding algorithm can fulfill these requirements.

1. Introduction

In recent years, the competition in China's tobacco industry has become more and more fierce. Especially after joining Wyo, the competition in the tobacco industry is not only for the domestic market. Facing the strong challenges from international tobacco giants, the competition in the tobacco industry has undergone great changes. The main focus of tobacco titans is on how to succeed in the severe market rivalry through effective logistical services. How to complete the cigarette sorting task more quickly and affordably considering such internal and external circumstances is not only a requirement of the state tobacco monopoly administration but also a crucial factor that should be considered when optimizing the cigarette sorting system.

This study uses the EIQ analysis method to analyze the order data of a city based cigarette distribution center to provide a decision-making basis for the planning and design of a cigarette sorting system, and it selects the sorting mode and strategy of the sorting system based on the results of the order data analysis.

2. Literature Review

According to the idea of time delay and comprehensively considering the work efficiency of sorting operation and sorting packaging, a dynamic time window design and judgment method to eliminate the waiting time and block demand imbalance caused by the batch imbalance of time windows is proposed, which ensures the continuity and balance of the picking system [1]. In the research on order sorting strategy, it is proposed that the method for determining the sorting strategy should be divided into two steps. First, all orders are divided into five categories, and then, the sorting strategy suitable for each type of order is determined through computer simulation [2]. Hassoun and others used a genetic algorithm to study order batching to minimize the walking distance of sorting [3]. Semenov and others studied the batch strategy of orders with data mining technology [4].

Hewage and others discussed the order picking optimization problem of multiple rows of shelves and multiple lanes on the basis of giving the operation principles and warehouse structure parameters in advance. Using the highest picking efficiency as the aim function, multiple order

batch picking procedures were created. An order addition batch approach and a weighted postponed batch strategy are included. Using the idea of weighting, the priority assignment of orders with varying degrees of urgency according to postponed processing is explained. The simulation analysis utilizes a small sample of wood harboring fungi. The conclusion demonstrates that the batch processing technique requires fewer computational resources and can satisfy the needs of small batch order picking [5]; Kvon and others discussed the picking operation optimization of automatic three-dimensional warehouses in the form of multiple lanes, selected the case that a single stacker has a dwell point in multiple lanes for discussion, and established the corresponding model. Taking the shortest access time as the objective function, an improved ant colony algorithm is proposed, and the pheromone volatilization coefficient is adaptively adjusted to achieve a compromise between the global search ability of the algorithm and the convergence speed of the algorithm. To verify the effectiveness of the algorithm, a small sample containing 10 orders is used for simulation analysis. The conclusion shows that the convergence and global search ability of the algorithm are better than the unadjusted ant colony algorithm [6]; Ronzhina and others combined the heuristic algorithm with the genetic algorithm to consider the optimization problem of single machine access strategy in multiroadway [7]; Meng and others discussed the fixed shelf picking optimization problem of an automatic warehouse with multi roadway and single machine structure and combined niche theory with a genetic algorithm, the algorithm adopts natural number coding, uses sharing function to make the population show diversity, and adds local disturbance operation and improved crossover and mutation operation, trying to improve the global optimization ability of the algorithm [8]; Wu and others put forward an improved ant colony algorithm based on the rotating shelf automatic three-dimensional warehouse as the research object. They believe that the improved ant colony algorithm can quickly find the optimal goods by picking a path, and the solution quality is high and the calculation time is short [9].

This study examines the current state of express sorting based on the available research, develops a system for automatically extracting information from QR codes on express sheets, sorts the express in accordance with the information, and chooses and enhances each step in the QR code recognition algorithm process in light of the unique challenges that express sorting presents. The main work is as follows: the current situation of the existing express sorting system is studied. Aiming at the problems of low efficiency and a high error rate in manual sorting, a set of express sorting systems based on QR code recognition technology has been designed. The system has the characteristics of no manual assistance, independent acquisition of express QR code images, strong adaptability to the environment, and low cost. In this study, the algorithm flow of two-dimensional code recognition is designed, in which the weighted average method is selected according to the complex background in the express sorting system.

3. Sorting System Based on QR Code Information Recognition

3.1. System Design. The express sorting system connects five parts: control equipment, conveying equipment, information collection equipment, classification equipment, and sorting crossing through communication technology. Sometimes, it must cooperate with manual assistance to form a complete express sorting system [10, 11]. An automatic sorting system mainly has two characteristics: high sorting efficiency and low sorting error rate.

The express automatic sorting system based on QR code recognition technology is composed of a sorting area, control equipment, conveying equipment, image acquisition system, sorting equipment, and sorting crossing, as shown in Figure 1 [12]. The unloaded express is stacked in the unloading area and then enters the sorting area through the conveying equipment. The express is sorted into a queue and then enters the image acquisition system.

At this time, if you directly enter the image acquisition system, you cannot complete the collection of express images one by one. The schematic diagram is shown in Figure 2. The small blue block in the figure represents express delivery. After sorting in the sorting area, the express delivery placed disorderly in the unloading area can become a neat column and enter the image acquisition system [13, 14].

The overall flowchart of the express sorting system based on QR code recognition is shown in Figure 3, which can be divided into two parts: software and hardware [15]. In terms of hardware, first, unload the express to the unloading area, then select the express that cannot enter the sorting system according to the requirements of the sorting system, and then enter the sorting structure, sort the express into a queue, pass through the image acquisition system in turn, and then enter the sorting equipment.

3.2. Image Acquisition System

3.2.1. Design of the Image Acquisition System. Figure 4 is the flowchart of the image acquisition system. The image acquisition system collects the QR code image on one side of the express through image processing and manipulator control [16, 17].

3.2.2. Hardware Selection of the Image Acquisition System. Image acquisition equipment is the core part of an image acquisition system, which is composed of a light source, a camera, and an image acquisition card [18]. It is vital to consider if there are any express surface sheets with smooth surfaces that may reflect light when illuminated, resulting in the direct reflection of light to the camera, while choosing the configuration of LED lights in the express automatic sorting system. This will cause the reflected light to take the place of that portion of the information. Common light source types are shown in Figure 5.

The image acquisition system is an important part of the express automatic sorting system, and the industrial camera is a key part of the image acquisition system. Its specific function

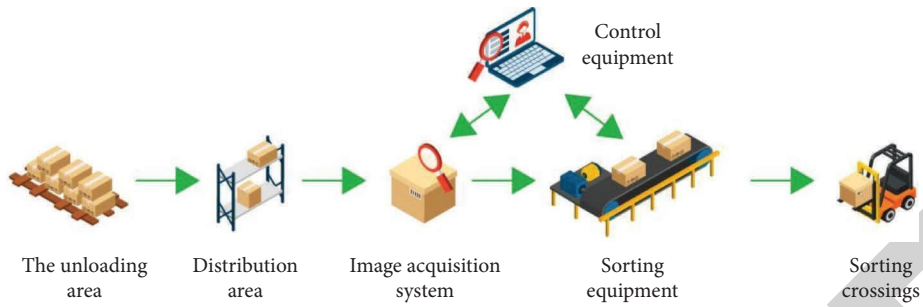

Figure 1: Block diagram of the automatic express sorting system.

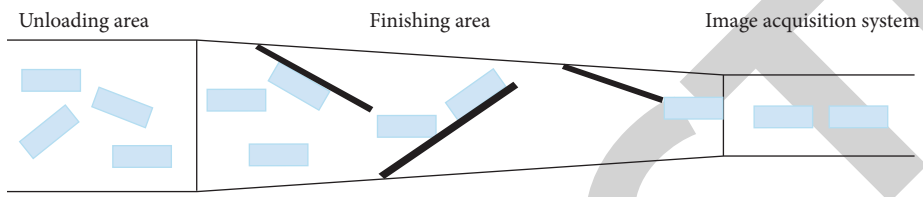

Figure 2: Schematic diagram of finishing area.

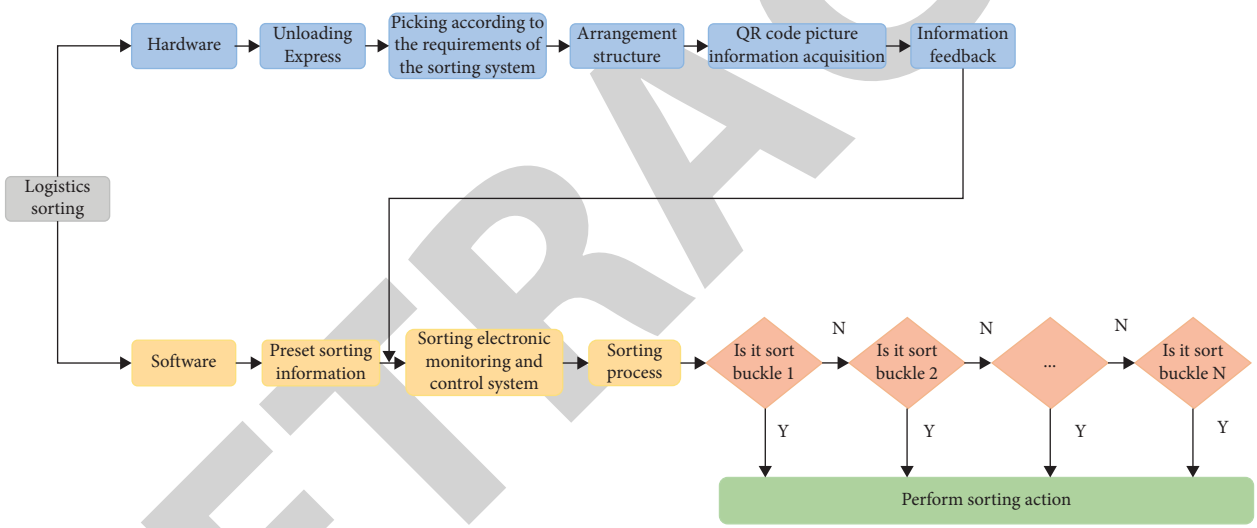

Figure 3: Flowchart of the automatic express sorting system.

is to collect and output an image of the target object [19, 20]. The structure of CCD is relatively complex. The biggest difference between CCD and CMOS is that CMOS is the charge signal in the unit of point, while CCD is the current signal in the unit of behavior. The comparison of performance parameters between CCD and CMOS is shown in Table 1.

The sorting equipment often used in the express automatic sorting system includes inclined guide wheel types, cross belt types, scraper types, and turnover plate types. As can be seen from Table 2, the cross-belt sorting equipment is very suitable for express sorting. However, because the structure of the cross-belt sorting equipment is too complex, each cross-belt car needs an independent motor and control system, and the overall cost is too high [21].

3.3. QR Code Processing Algorithm in the Sorting System

3.3.1. Two-Dimensional Code Identification Process in the Sorting System. The problems, such as a small amount of wear on QR codes, can be solved by the fault-tolerant mechanism of QR codes. The QR code recognition process in the express automatic sorting system is shown in Figure 6 [22].

3.3.2. QR Code Image Preprocessing. The conversion of a color image into a grayscale version is known as grayscale image processing. The grayscale approach can decrease the amount of image data, decrease the number of operations, and increase the effectiveness of operations. Generally, the following three methods can be used for graying [23].

First, the formula means method: take the arithmetic mean of R, G, and b values of all pixels in the original image as the gray value of the corresponding points, and the calculation formula is shown in the following formula.

$$\text{Gary} = \frac{(R + G + B)}{3}. \tag{1}$$

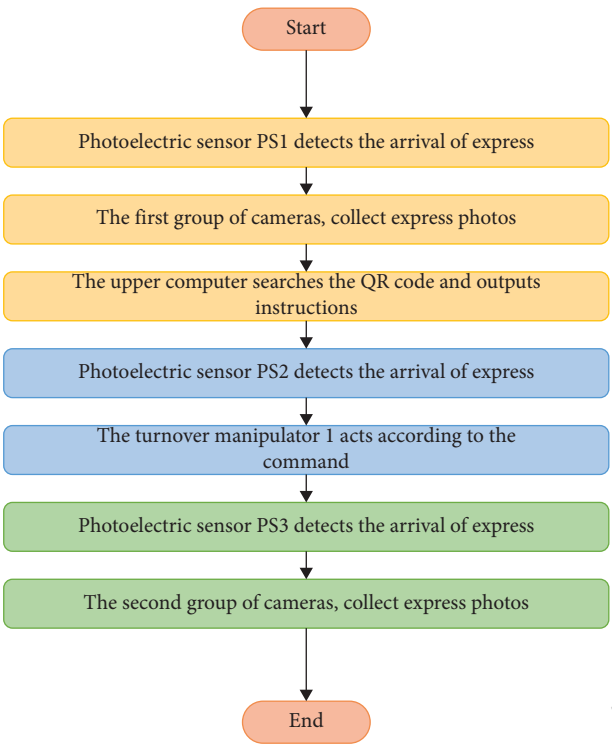

Figure 4: Flowchart of the image acquisition system.

The second is the maximum value method: it takes the maximum values of R, G, and B of all pixel points in the original image as the gray value of the corresponding points, and the calculation formula is shown in the following formula.

$$\text{Gary} = \text{Max}(R, G, B). \tag{2}$$

Furthermore, it is the weighted average method: when calculating the average value of R, G, and B, the weight of each value is also considered. The calculation formula is shown in formula (3). W_R, W_G, and W_B represent the weights of R, G, and B, respectively. This method aims to achieve the best graying effect. The weights of the three values were 0.299, 0.587, and 0.114, respectively.

$$\text{Gary} = \frac{W_R \cdot R + W_G \cdot G + W_B \cdot B}{W_R + W_G + W_B}. \tag{3}$$

The objective evaluation indexes of images mainly include peak signal-to-noise ratio PSNR and edge-preserving index EPI. PSNR is an index used to measure the degree of image distortion.

$$\text{PSNR} = 10 \times \log_{10}\left(\frac{(2^n - 1)^2}{\text{MSE}}\right). \tag{4}$$

EPI indicates the ability of the corresponding filtering method to maintain the edges in the horizontal and vertical directions of the image after the image is processed by different filtering methods. The larger EPI is, the better the edge retention ability of the filtering method is. EPI_H represents the edge retention ability of the filtering method for the image in the horizontal direction, and its calculation formula is shown in equation (5). EPI_V represents the edge retention ability of the filtering method for the image in the vertical direction, and its calculation formula is shown in equation 3.6. I_y represents the image after filtering, and I represents the standard image [24].

$$\begin{aligned} EPI_H &= \frac{\sum i \sum j \left| I_y(i, j+1) - I_y(i, j) \right|}{\sum i \sum j \left| I(i, j+1) - I(i, j) \right|}, \\ EPI_V &= \frac{\sum i \sum j \left| I_y(i+1, j) - I_y(i, j) \right|}{\sum i \sum j \left| I(i+1, j) - I(i, j) \right|}. \end{aligned} \tag{5}$$

By analyzing the data in Table 3, it can be seen that the peak signal-to-noise ratio of the median filter is greater than the mean filter, and the edge preservation index is also greater than the mean filter, that is, the median filter has a better edge preservation ability for the two-dimensional code image than the mean filter.

Finding the distortion control point precisely is essential to the distortion correction procedure, and doing so calls for accurate detection of the QR code's edge. The precise algorithm flow looks like this. First, the Otsu algorithm is used to obtain the optimal threshold, which is used as the high threshold T_0 of the Canny algorithm. The idea of the Otsu algorithm is to divide all pixel areas in the target image into two different areas, namely, foreground and background. Then, through the formula, the interclass variance of the background and foreground reaches the maximum threshold, that is, the best threshold for image edge detection [25]. Let their segmentation threshold be T, the total number of pixels in the image is N, the number of pixels in the foreground in the image is N_1, and the number of pixels in the background in the image is N_2. The proportion of foreground and background pixels to the total number of pixels is w_1 and w_2, respectively, the average gray value is u_1 and u_2, respectively, and the total average gray value of the image is u. The following formula holds.

$$\begin{aligned} w_1 &= \frac{N_1}{N}, \\ w_2 &= \frac{N_2}{N}, \\ w_1 + w_2 &= 1, \\ u &= w_1 \times u_1 + w_2 \times u_2, \\ g &= w_1 \times (u_1 - u)^2 + w_2 \times (u_2 - u)^2. \end{aligned} \tag{6}$$

The maximum interclass variance can be obtained from the above formula:

$$g = w_1 w_2 (u_1 - u_2)^2. \tag{7}$$

The final step in the distortion correction process is a spatial transformation. Assuming that the original image of the QR code is $f(x, y)$ and the distorted image is $g(x', y')$, the mapping relationship from $g(x', y')$ to $f(x, y)$ is determined according to the spatial transformation function

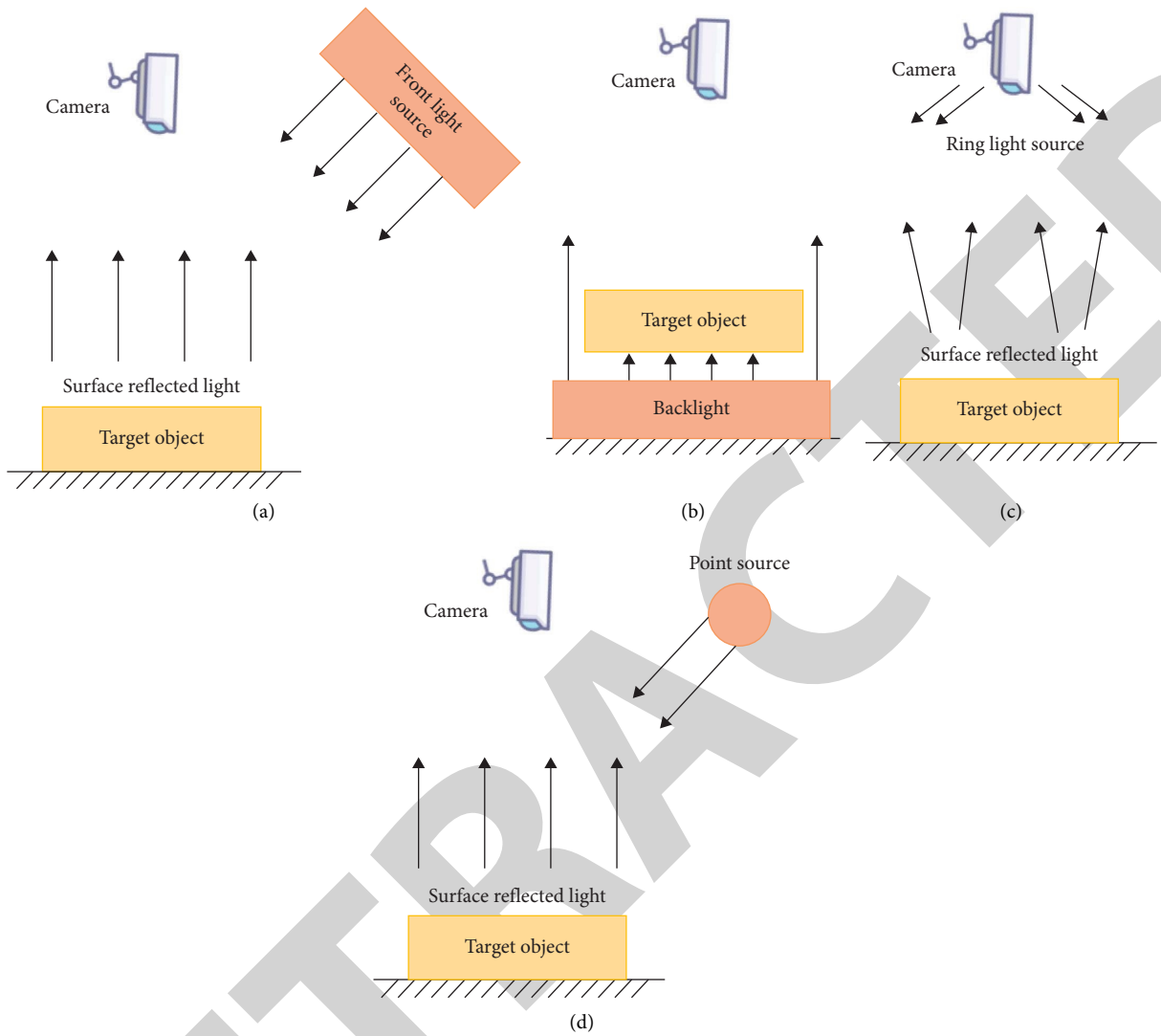

Figure 5: Schematic diagram of four common light source categories.

Table 1: Performance comparison between CCD and CMOS.

Category	CCD	CMOS
Dynamic range	3000:1	500:1
Uniformity	Good	Bad
Integration degree	Low	High
Signal-to-noise ratio	High	Low
ISO sensitivity	High	Low

shown in (8) and (9), and the correction operation of the distorted image of the QR code is completed.

$$x = s(x', y') = k_1 x' + k_2 y' + k_3, \tag{8}$$

$$y = t(x', y') = k_4 x' + k_5 y' + k_6. \tag{9}$$

Then find all the intersections of the straight line and get the four vertex coordinates of the upper left corner, upper right corner, lower left corner, and lower right corner of the original image, which are (x_1, y_1), (x_2, y_2), (x_3, y_3), (x_4, y_4), respectively. Then, determine the width and height after distortion correction through the vertex coordinates, as shown in the following equations.

$$A = \sqrt{(x_1 - x_2)^2 + (y_1 - y_2)^2}, \tag{10}$$

$$B = \sqrt{(x_1 - x_3)^2 + (y_1 - y_3)^2}, \tag{11}$$

where A and B, respectively, represent the width and height of the corrected figure. The four new vertices of the corrected QR code are derived from the original vertices, and equations (12)–(15) are the calculation formulas of the new vertex coordinates.

$$\begin{cases} x_1' = x_1, \\ y_1' = y_1, \end{cases} \tag{12}$$

$$\begin{cases} x_2' = x_1, \\ y_2' = y_1 + A. \end{cases} \tag{13}$$

Table 2: Principle and characteristics of sorting equipment.

Sorting mechanism type	System principle	Performance characteristics
Scraper type	Push the scraper to send the express out once the products have arrived at the selected location.	Low price and simple installation; wide range, mainly nonfragile products; with large space requirements, only one-way sorting is allowed
Cross belt type	The main conveying system moves each "trolley" to the specified position, and the "trolley" receiving the command rotates the belt in the cross direction to send the express.	Applicable to all kinds of small and unshaped express delivery; it can be sorted on the left and right sides, and there are many sorting outlets; horizontal or vertical circulation;
Inclined guide wheel type	Change the travel direction of the express by changing the direction of the guide wheel.	Small impact force, suitable for classification of fragile products. More exits to save space; small impact force, suitable for classification of fragile products; it is suitable for flat bottom goods such as cartons.
Flip type	The main conveying system moves each "trolley" to the specified position, and the "trolley" receiving the command tilts to the cross direction to make the express slide out.	Reliable and durable, easy to maintain; fragile goods cannot be sorted; it is applicable to the sorting of large quantities of products.

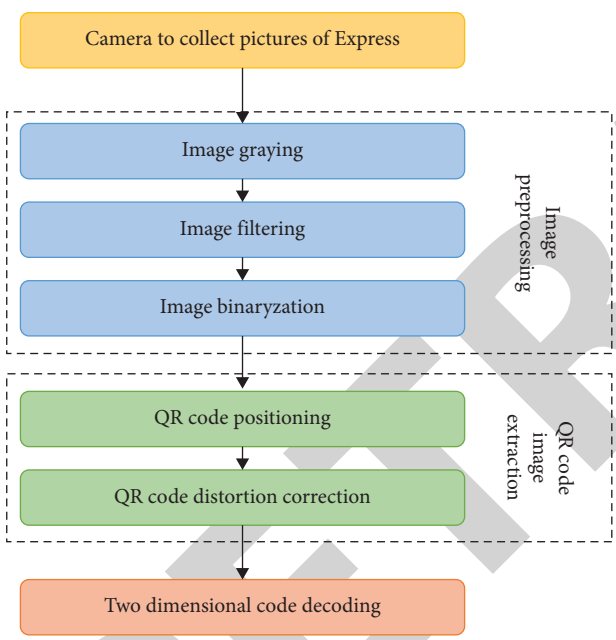

Figure 6: QR code image recognition process in the sorting system.

Table 3: Comparison of objective evaluation indexes of image filtering.

Image objective evaluation index	RSNR	EPI_H	EPI_V
Mean filtering	76.5084	0.5535	0.5377
Median filtering	82.0187	0.6325	0.6120

$$\begin{cases} x_3' = x_1 + B, \\ y_3' = y_1, \end{cases} \tag{14}$$

$$\begin{cases} x_4' = x_1 + B, \\ y_4' = y_1 + A. \end{cases} \tag{15}$$

By substituting the coordinates of the original vertex and the new vertex into (8) and (9), the six coefficients in the equation can be obtained, and then, the spatial transformation function can be obtained.

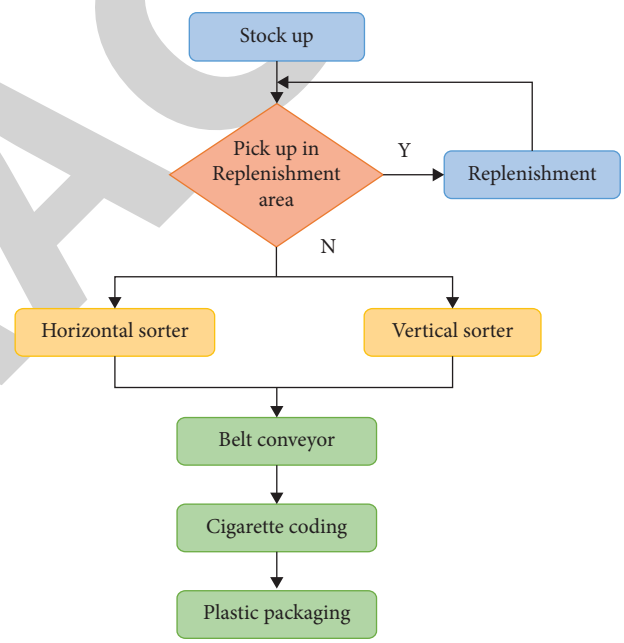

Figure 7: Sorting business flowchart of the automatic sorting system in cigarette distribution center.

4. Design Optimization of the Automatic Cigarette Sorting System

4.1. Operation Flow of Automatic Cigarette Sorting. The sorting business process of the automatic sorting system of the distribution center is shown in Figure 7.

The goal of the sorting equipment configuration optimization model is to reduce the total cost of sorting cigarettes; however, the values for each cigarette are independent of one another regardless of the sorter that is used. Consequently, the target function can be broken down into decreasing the sorting expense per cigarette. It can be shown from the analysis of sorting costs that the sorting costs of cigarettes in the automatic sorting system mostly consist of sorting equipment costs, site costs, and people costs for

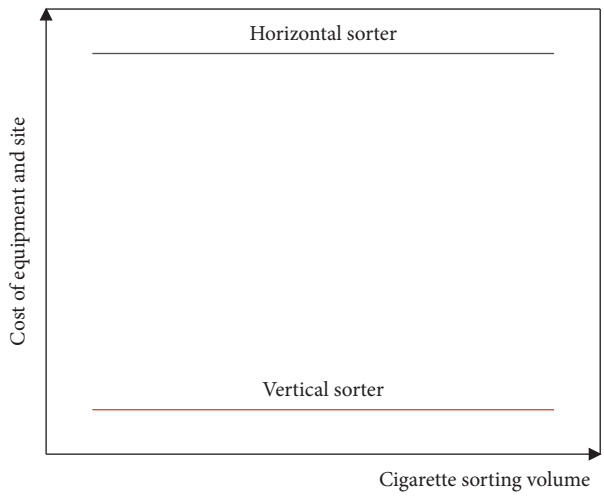

Figure 8: Change trend of equipment and site cost.

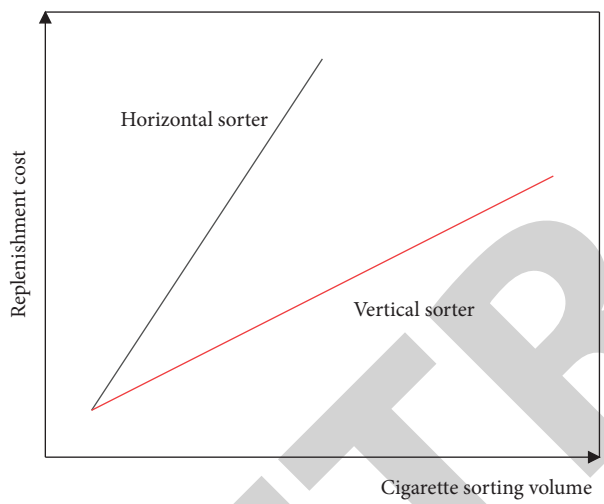

Figure 9: Change trend of replenishment cost.

replenishment. The equipment cost is fixed for every type of cigarette, regardless of whether a horizontal sorter or vertical sorter is chosen for sorting. The equipment is the equipment purchase cost and maintenance cost allocated to the daily depreciation cost, which will not change with the change in cigarette sorting volume. In this study, the purchase cost of the two sorting equipment is different. The purchase cost of the horizontal sorter is relatively high, so the equipment depreciation cost of the horizontal sorter is higher than that of the vertical sorter. In terms of site cost, because the floor area of a single horizontal sorter is larger than that of a vertical sorter, the site cost occupied by the horizontal sorter is high. The site cost is similar to the equipment cost and is fixed, so it can be combined with the equipment cost, as shown in Figure 8.

For a certain cigarette with a certain sorting volume, the sorting and replenishment times of the horizontal sorter are short, and the corresponding replenishment cost is low. The changing trend is shown in Figure 9. It can be seen from Figure 9 that the slope of the replenishment cost straight line of the vertical sorter is greater than that of the horizontal sorter, that is, the replenishment cost of the vertical sorter per unit cigarette is higher than that of the horizontal sorter.

Table 4: Equipment parameter values.

Parameter	Value	Company
c_1	3	10000 yuan/channel
l_1	0.5	m/channel
s_1	2	Square meter
b_1	170	Pieces/hour
r_1	300	Pieces/hour
c_2	0.8	10000 yuan/channel
l_2	0.14	M/channel
s_2	0.3	Square meter
b_2	25	Pieces/hour
r_2	130	Pieces/hour
c_3	0.8	10000 yuan/M
c_4	0.4	Yuan/m^2/day
c_5	15	Yuan/hour
μ	10%	
γ	10	Year (250 days/year)

4.2. Equipment Configuration Results

4.2.1. Data Analysis. According to the equipment quotation of an enterprise, determine the parameter values of the purchase and maintenance cost of sorting equipment that affect the cost of the sorting system, as shown in Table 4.

Summarize the sorting quantity of 100 orders in the cigarette distribution center on a certain day and calculate the average sorting quantity of an order, as shown in Figure 10. Among them, the maximum sorting volume of single variety cigarettes is 932, and the minimum is only 3. It can be seen that the shipment volume of different cigarettes varies greatly. Therefore, it is very necessary to consider the efficiency and cost of sorting when selecting sorting equipment.

In order to verify the rationality of equipment configuration based on the cost critical point method, this result is compared with the EIQ-ABC analysis results of cigarette orders, as shown in Table 5.

It can be concluded from the table that the sorting cost of the system is reduced from 9.85 million yuan to 8.72 million yuan by using the cost critical point method. It can not only realize the management of key cigarette brands and ensure their timely delivery but also ensure the smooth completion of the sorting operation of cigarettes with a small sorting volume and improve the utilization rate of the equipment. Additionally, a clearer configuration of the number of sorting machines may be made by contrasting the cost critical point approach with the EIQ-ABC analysis method. The sorting apparatus for each cigarette can be identified by comparing the sorting volumes of each one with those of the crucial point. Implementing this approach is fairly straightforward.

4.3. System Modeling and Simulation Test

4.3.1. FlexSim Modeling Process. The modeling process is shown in Figure 11.

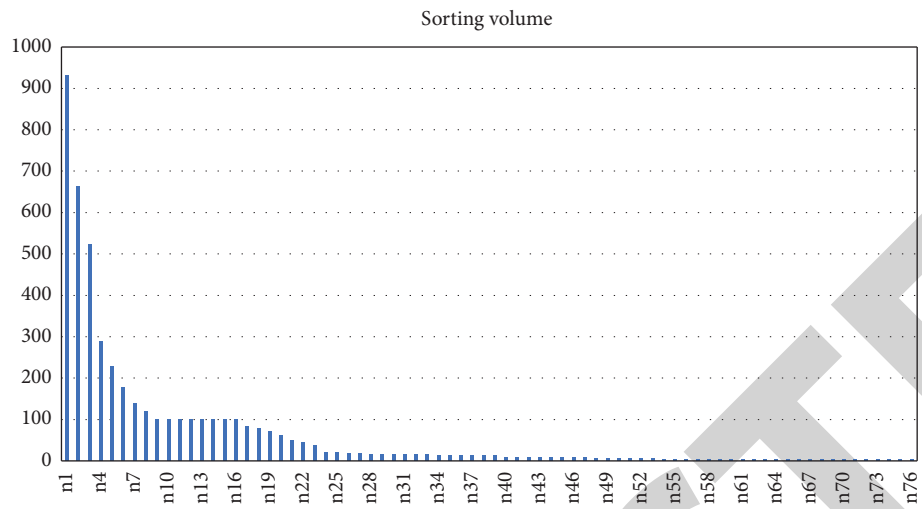

Figure 10: Cigarette order data.

Table 5: Comparison of equipment configuration results.

	EIQ-ABC method	Cost critical point method
Vertical sorter	50 channels	44 channels
Horizontal sorter	26 channels	32 channels
Sorting cost	9.85 million yuan	8.72 million yuan

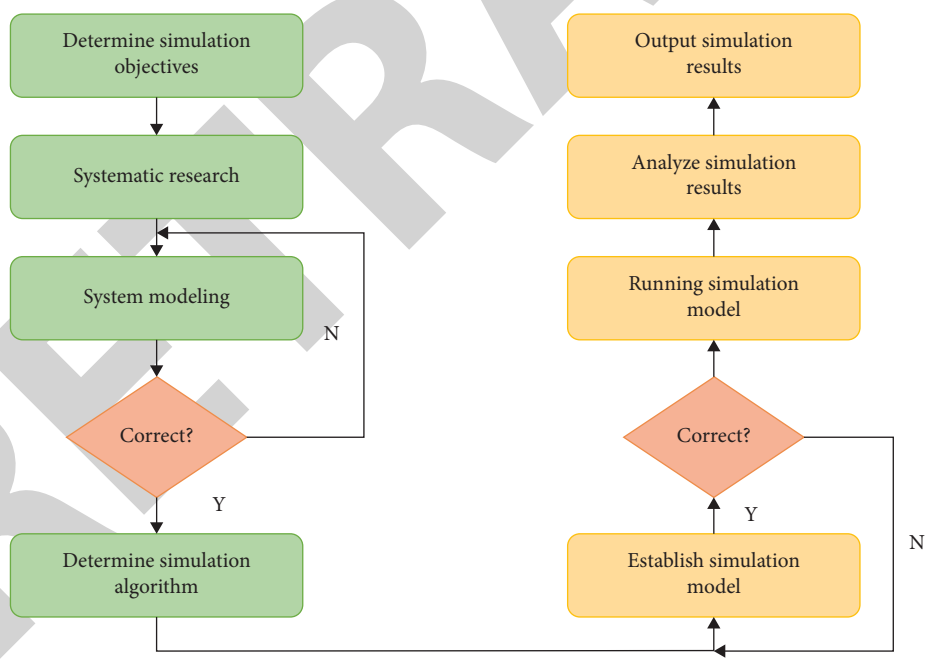

Figure 11: System simulation flowchart.

The specific steps of the system simulation can be summarized as follows:

Determining simulation objectives is the process of determining simulation objects and specific problems that will be solved by simulation. Conducting system research entails a thorough understanding of the system's operating process and collecting system simulation operation data. To create a system model, you must first determine the basic process and relevant parameters of the system operation. System models can take the form of text expressions, flowcharts, icons, mathematical expressions, and so on. Flowcharts are commonly used for the simulation of discrete event systems. To determine the simulation algorithm, you must first determine the method for controlling the simulation model's operation. The most common methods are event scheduling, activity scanning, and process interaction. Creating a simulation

Table 6: Equipment composition of the cigarette replenishment system and corresponding relationship with FlexSim entity.

Equipment name	Remarks	Corresponding entity in FlexSim	Auxiliary need entity
Unpacking station	3	Resolver ∗ 3 + operator ∗ 3	Simple cigarette replenishment system (conveyor belt ∗ 3 + sorting conveyor belt ∗ 3 + synthesizer ∗ 1 + generator ∗ 2)
Replenishment trolley	3 sets	Stacker ∗ 3	Trolley support (basic fixed entity) ∗ 3
Horizontal sorter	11 smoke bins/set ∗ 3 sets	Shelf (11 columns ∗ 5 layers) ∗ 3	Initial generator ∗ 1
Vertical sorter	44 smoke bin/set ∗ 1 set	Shelf (44 columns ∗ 1 floor) ∗ 1	Manual replenishment shelf + operator ∗ 1 + initial generator ∗ 1
Empty container recycling area	Conveyor belt/empty container recovery staging area	Conveyor belt ∗ 3 + temporary storage area ∗ 1	Empty container sorting worker (operator ∗ 1)

Table 7: Equipment composition of the cigarette sorting and packaging system and corresponding relationship with FlexSim entity.

Equipment name	Remarks	Corresponding entity in FlexSim	Auxiliary need entity
Third floor main line	Sorting transfer belt ∗ 3	Conveyor belt ∗ 3 + synthesizer ∗ 3	Suborder generator ∗ 3
Order closing station	1 (three orders in one)	Synthesizer ∗ 1	Single generator ∗ 3
Packer	1 set	Synthesizer ∗ 1	

Table 8: Equipment composition of the delivery temporary storage system and corresponding relationship with FlexSim entity.

Equipment name	Remarks	Corresponding entity in FlexSim	Auxiliary need entity
Labeling inspection machine	2 sets	Processor ∗ 2	Loading and unloading operator ∗ 2 + temporary storage area ∗ 2
Shipment staging area	6	Staging area ∗ 6	Task actuator ∗ 2

model is the process of creating a computer simulation model and writing a simulation program code. Establishing and validating the simulation model entails determining whether the model accurately reflects the reality of the system, including the operation simulation model, analyzing simulation results, and producing simulation results.

4.3.2. Visual Simulation of the Automatic Cigarette Sorting System. In the complete set of automatic logistics equipment systems, the occurrence of events depends on whether the conditions for triggering events are met to adapt the Petri net model. This study adopts a simulation strategy based on a combination of the event scheduling method and the activity scanning method: the entity in the system is tested by scanning, that is, the change. Once the preconditions are met, the activity process of the entity is activated, so that the relevant events can occur, change the state of the system, and arrange the occurrence time of relevant events. In the case of time change, start the corresponding timer to make the logistics system work on the computer as in the actual production environment through the process, without setting the system simulation clock. On the basis of the preceding study, a simulation model of the automatic cigarette splitting system can be developed to visually replicate the system's operation. Analyze and validate the model's and system's design scheme by using the simulation's user-friendly platform to observe the system's actual operation effect and to analyze and validate the model's and system's design logic. The statistics of each equipment's utilization rate, idle rate, blocking rate, and other data offer the foundation for decision-making and optimization.

According to the analysis of the design scheme of the sorting system, the sorting system includes four basic subsystems: cigarette replenishment, cigarette sorting, cigarette packaging, and delivery of temporary storage. The equipment of each subsystem and its corresponding relationships with the entities in the simulation system, as well as the auxiliary entities required to realize the simulation function, are shown in Tables 6 to 8.

Collection and analysis of the equipment parameters of a sorting system: The system data obtained according to the data are shown in Table 9.

The running time unit of the simulation setting is 1, and the length unit is 1. Therefore, to achieve the efficiency shown in table, it is necessary to set the data correspondence in the FlexSim simulation model, as shown in Table 10.

4.3.3. Analysis of Operation Results of Each Business Link. Calculated from the input of the horizontal sorter:

Replenishment efficiency of the trolley = $(9681 + 9651 + 9573)/1.5 = 19270$ pieces/hour.

Calculated from the input of the vertical sorter:

Table 9: Brief analysis of system data.

Station	Efficiency
Manual unpacking efficiency	100–150 pieces/person ∗ hour
Trolley replenishment efficiency	145 PCS/h
Replenishment efficiency of vertical tobacco silo	1500–2000 cartons/hour
Packaging efficiency of packaging machine	22000 cartons/hour
Belt running speed	1 m/s

Table 10: Simulation data analysis.

Station	Efficiency	FlexSim entity parameters to be adjusted	Reachable efficiency
Manual unpacking efficiency	100–150 pieces/person ∗ hour	Resolver processing time 0.5	120 pieces/hour
Trolley replenishment efficiency	145 pieces (7200 cartons)/hour	The stretching speed of stacker is 30, the acceleration/deceleration is 20, and the maximum speed is 2	7200 cartons/hour
Replenishment efficiency of vertical tobacco silo	1500–2000 pieces/hour	Maximum speed of replenishment operator 2. Acceleration/deceleration 1, capacity 4	1800 cartons/hour
Sorting efficiency	15000–22000 cartons/hour	Synthesizer processing time 5	17000 cartons/hour
Belt running speed	1 m/s	Belt running speed 1	1 m/S

Manual replenishment efficiency of the vertical machine = 3294/1.5 = 2196 pieces/hour.

The output of the horizontal sorter and vertical sorter is calculated as follows:

Sorting efficiency of the sorting line = (7401 + 7452 + 8238 + 3204)/1.5 = 18330 pieces/hour.

Through the calculation of the output of the single synthesizer:

Sorting efficiency of the sorting line = 29355/1.5 = 18750 pieces/hour.

The above data show that the system can achieve the expected overall efficiency.

From the data listed in the table, we can see the utilization rate of each equipment. Through the system data, it is found as follows:

The average utilization rate of the unpacking station of the resolver is 1.7%, but because the resolver acts as a cigarette buffer section, its utilization rate is 74.3%, and the overall utilization rate is more than 75%, which is an ideal application state.

The utilization rate of the replenishment trolleys is 78%. Workers only assist in unpacking the resolver, and the vacancy rate of unpacking workers is as high as 98%. The investment of workers is fully saved.

The idle rate of the four synthesizers of the three-tier sorting main line is 0%. It can be seen that the sorting equipment layer has been in a full load working state, and the sorting efficiency has reached the average value of the ideal state, i.e., 16500 pieces/hour.

During the operation of the system, the blocking rate of the three suborder execution synthesizers of the three-tier sorting main line exceeds, that is, if the downstream process is smooth, the separation efficiency can continue to improve. After adding a packer, the sorting efficiency of the system can reach 30000 pieces/hour.

Through the simulation of the sorting system of a tobacco distribution center in a city, it is found that the overall efficiency of the system is high, the equipment layout is reasonable, the integration is high, and the whole operation process is clearly visible. In sum up, the design scheme of the sorting system achieves the following results.

The system adopts humanized design, the labor intensity of workers is greatly reduced, the number is reduced, the operation is simple, and the sorting work can be completed efficiently.

The order processing was completed on the previous day, saving the processing time of the order upon arrival. The sorting line adopts the latest three-tier main line sorting and order combination technology, which greatly improves the sorting efficiency of the equipment, and the equipment efficiency operates stably at more than 15000 pieces/hour.

The horizontal machine has a large smoke bin capacity, flexible scheduling, and strong adaptability to different orders; the equipment is highly integrated, and the shape is unified and coordinated. Compared with the equipment with the same sorting efficiency, the floor area is small, and the empty box is set with a fixed recycling area. The operation process in the whole sorting system is clear.

5. Discussion

This work analyzes and studies the current situation of express sorting, designs an express sorting system based on QR code recognition without human participation, implements the automatic extraction of QR code information from the express sheet, sorts the express based on the information, and selects and improves each part of the QR code recognition algorithm process based on the particular problems encountered in express sorting. The primary work is the following: Examining the current state of the existing

express sorting system. The design of an express sorting system based on QR code recognition technology is motivated by the low efficiency and high error rate of human sorting. The technology features no manual assistance, independent collection of express QR code images, great environmental adaptability, and a reasonable price. The algorithm flow of two-dimensional code recognition is designed, with the weighted average method chosen due to the complexity of the background in the express sorting system; the median filter is chosen as the filtering algorithms to address the problem of noise interference in the process of express delivery; the binarization algorithm determines the global threshold method based on the properties of the two-dimensional code; and the coding principle and decoding algorithm of the two-dimensional code are investigated. The results of the experiments indicate that the decoding algorithm meets the requirements. However, this study briefly introduces the basic knowledge of Petri net and uses Petri net to establish the designed automatic sorting model of the cigarette distribution center. Based on this model, the design scheme of the automatic sorting system is simulated with the help of FlexSim software, and the results are run and output. Through the statistics of the utilization rate, idle rate, blocking rate, and other data of each equipment, the system simulation experimental results show that the sorting efficiency of the system sorting line is 18570 pieces/hour, and after adding packaging equipment, the sorting efficiency of the system can reach 30000 pieces/hour, and the efficiency can be improved by 61.55%. The rationality of the scheme was verified.

6. Conclusion

Automatic cigarette sorting systems are being employed more and more frequently in the distribution of cigarettes because the intensifying automation and informationalization of tobacco logistics. Based on an in-depth analysis of the characteristics of cigarette sorting, this study uses the EIQ analysis method to analyze the distribution center's order data to provide a decision-making framework for the planning and design of a cigarette sorting system. The sorting mode and strategy of the sorting system are chosen in accordance with the analysis results of the order data. Due to the prior qualitative analysis method's significant subjectivity and blindness, it is challenging to consider both the effectiveness and cost of the sorting system at the same time when choosing the equipment for the split building system. To optimize the configuration of the planned sorting system equipment, this study provides an equipment configuration approach based on the sorting cost critical point method. Finally, the cigarette sorting system is simulated and examined using the simulation program. The effectiveness and viability of the design scheme are examined through the operation process and result output.

Data Availability

The data used to support the findings of this study are included within the article.

Disclosure

The authors attest China Tobacco Guangxi Industrial Co., Ltd. has had no influence on design of this study or its outcomes.

Conflicts of Interest

Authors Chen Hao, Wei Taicheng, and Zhu Haoran are affiliated to and funded by China Tobacco Guangxi Industrial Co., Ltd.

Acknowledgments

This work was supported by the Science and Technology Planning Project of China Tobacco Guangxi Industrial Co., Ltd. "Research on Key Technology of Collecting Cigarette Two-Dimensional Code in Commercial Sorting Line" (GXZYCX2020E002).

References

[1] B. Li, Z. Li, Y. Xu, Y. Tao, and J. An, "Design of weak current control system for express sorting," *International Core Journal of Engineering*, vol. 6, no. 1, pp. 153–159, 2020.

[2] Q. Yang and Z. Shi, "Performance analysis of the phase swap sorting strategy for an isolated intersection," *Transportation Research Part C: Emerging Technologies*, vol. 77, pp. 366–388, 2017.

[3] A. Hassoun, K. A. Brady, R. Arefi, I. Trifonova, and K. Tsirilakis, "Vaping-associated lung injury during covid-19 multisystem inflammatory syndrome outbreak," *Journal of Emergency Medicine*, vol. 60, no. 4, pp. 524–530, 2021.

[4] N. D. Semenov, V. M. Muravev, I. V. Andreev, and I. V. Kukushkin, "Renormalization of the cyclotron frequency in a screened two-dimensional electron system with strong retardation," *JETP Letters*, vol. 114, no. 10, pp. 616–619, 2022.

[5] N. Hewage, U. Wijesekara, and R. Perera, "Association between insulin resistance and metabolic syndrome with thyroid status in normal and overweight/obese population: a review," *Journal of Biosciences and Medicines*, vol. 10, no. 4, p. 18, 2022.

[6] Z. D. Kvon, E. B. Olshanetsky, M. A. Drofa, and N. N. Mikhailov, "Anderson localization in a two-dimensional electron–hole system," *JETP Letters*, vol. 114, no. 6, pp. 341–346, 2021.

[7] M. I. Ronzhina, L. A. Manita, and L. V. Lokutsievskiy, "Solutions of a Hamiltonian system with two-dimensional control in a neighbourhood of a singular second-order extremal," *Russian Mathematical Surveys*, vol. 76, no. 5, pp. 936–938, 2021.

[8] Y. Meng, F. Li, C. Lan, X. Bu, and J. C. Ho, "Artificial visual systems enabled by quasi–two-dimensional electron gases in oxide superlattice nanowires," *Science Advances*, vol. 6, no. 46, 2020.

[9] M. Moralidou, A. Di Laura, J. Henckel, H. Hothi, and A. J. Hart, "Three-dimensional pre-operative planning of primary hip arthroplasty: a systematic literature review," *EFORT open reviews*, vol. 5, no. 12, pp. 845–855, 2020.

[10] M. Omar and H. O. Abdelal, "Current status of intestinal parasitosis among patients attending teaching hospitals in zagazig district, northeastern Egypt," *Parasitology Research*, vol. 121, no. 6, pp. 1651–1662, 2022.

Hindawi
Mobile Information Systems
Volume 2022, Article ID 7875137, 12 pages
https://doi.org/10.1155/2022/7875137

Research Article

Assessment of Fog Enabled Sensor Cloud Platform for Smart Logistics Park

Xuejiang Wei [1,2] **and Libing Wu** [1]

[1] *School of Computer Science, Wuhan University, Wuhan 430072, Hubei, China*
[2] *School of Logistics, Wuhan Technology and Business University, Wuhan 430065, Hubei, China*

Correspondence should be addressed to Libing Wu; wu@whu.edu.cn

Received 5 August 2022; Revised 7 September 2022; Accepted 17 September 2022; Published 7 October 2022

Academic Editor: Chi Lin

This paper is a comparative study on the performance of the fog-enabled sensor cloud (FSC) and traditional cloud computing and fog computing modes in a smart logistics park. Based on our previous work, we describe the physical sensor virtualization scheme and framework of the proposed FSC, construct the network model, and mathematically describe the parameters of the FSC. To assess the performance of the proposed platform, we take a large logistics enterprise in China as an example and illustrate the network setup of the proposed platform in a real logistics scenario. The experiment proves that the FSC for smart logistics parks has a practical advantage over the traditional cloud computing and fog computing modes in terms of bandwidth consumption and service latency.

1. Introduction

Sensor Cloud (SC) is the combination of the Internet of Things (IoT) and cloud computing [1, 2], which can be widely used in the smart logistics park to promote the sharing of physical (wireless) sensors (PS) and reduce the redundant deployment of PS too [3]. SC is built on top of PSs and composed of virtual sensors (VSs) which are virtualized from PSs [4]. A virtual sensor is, by definition, a class of computer programme that, given the information at hand, performs the functions that a physical sensor would ordinarily do. As it takes note of readings from several devices and learns to comprehend the correlations between the various factors. The map between PSs and VSs is one-to-one or many to one [5]. The VS is predefined as a piece of code-named VS template that is stored in the cloud, and the VS instance is created based on the VS template while there is a service request [6, 7]. One VS template can create multiple VS instances according to the number of requests (or end users), and multiple VS instances created from different VS templates can form a virtual sensor group (VSG) [8]. Virtual sensors are a type of software layer that uses a fusion function to combine data from physical (or other virtual) sensors to produce oblique measurements of a process variable or an abstract condition. Different end users can control the same PS (including setting sampling frequency, time window, collecting data, sending instructions, etc.) through their own VS instance without interference with each other based on the autonomous coordinate mechanism of SC, so the same PS resources can be shared among multiple users or applications [9].

Fog computing has attracted the attention of researchers since it was proposed by Cisco and has been used to support real-time applications in the context of IoT [10]. As a type of edge computing, fog computing moves the computing and storage resources closer to the application, such as the edge of the Internet, to reduce the transmission delays and realize real-time responses to time-sensitive applications [11]. Applications that need to be executed quickly in response to external events like frame capture or regularly may be required by time-sensitive applications. Fog devices are generally routers, gateways, access points, or some powerful sensor nodes, so fog computing has limited computing and storage capacity compared with cloud computing and can only support simple applications that require little computing and storage resources [12, 13]. Cloud offers a high

latency, whereas fog offers a low latency. A cloud system disintegrates in the absence of an Internet connection. As distinct protocols and standards are used in fog computing, the likelihood of failure is quite low. Fog's dispersed architecture makes it a more secure technology than the Cloud. Fog computing can also be widely used in smart logistics to support time-sensitive applications and distributed intelligence, such as intelligent scheduling of logistics devices, intelligent security of park boundaries, intelligent monitoring of storage environments, and so on [14, 15].

In our previous work, we proposed a fog-enabled sensor cloud platform for smart logistics and discussed the architecture, virtualization schemes, and service modes of the platform [16–21]. Clouds have high latency, while fog has low latency. In the absence of an Internet connection, a cloud system fails. Fog computing employs various protocols and standards, reducing the likelihood of failure. Fog has a distributed architecture, which makes it a safer system than the cloud. Software is used in virtualization to imitate hardware features and build a virtual computer system. This makes it possible for IT companies to operate many virtual systems, as well as various operating systems and applications, on a single server. Scale economies and increased effectiveness are two advantages that follow. The previous work is a preliminary consideration of the application of sensing cloud and fog computing in smart logistics parks, and the feasibility and effectiveness of the platform need to be further verified through experiments. So in this paper, we focus on the assessment of the proposed platform. We construct the network model, characterize the performance metrics mathematically, and perform a comparative study of a traditional cloud-based platform with our proposed platform by setting a study case. The novelty of the paper is to model the paradigm of fog-enabled sensor cloud platforms and perform a comparative study in terms of data fusion and latency with respect to cloud-based platforms. A new paradigm for cloud computing called sensor-cloud employs physical sensors to gather data and send it to a cloud computing infrastructure.

The rest of the paper is organized as follows. Section 2 briefly introduces the architecture of the platform, and we construct the network model for the platform in Section 3. In Section 4, we present performance metrics for the platform. Section 5 and Section 6 are the experimental setups for the case study and the performance evaluation of the platform compared with the cloud computing and fog computing-based platforms. Fog computing is a dispersed, decentralised infrastructure, whereas cloud computing is a centralised system. This is the major distinction between the two types of computing. Between computer hardware and a distant server, fog acts as an intermediate. It decides what data should be handled locally and what should be forwarded to the server. Finally, the work is concluded in Section 7.

2. Overview of the Proposed Platform

2.1. Sensor Virtualization. As shown in Figure 1, in the proposed platform, a multilayer physical sensor virtualization solution is applied to realize the reuse of PSs and data fusion of sensing data.

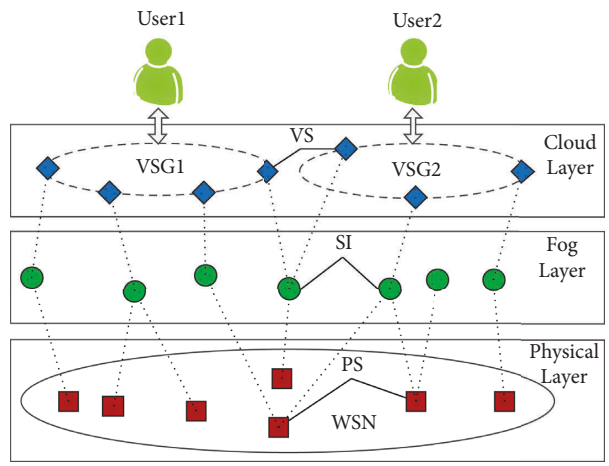

Figure 1: Multilayer physical sensors virtualization solution.

In the fog layer, PSs are virtualized as service instances (SIs). The SIs bridge the PSs deployed in the physical layer and the VSs located in the cloud layer. For batch and real-time processing, Cloud Data fusion provides prebuilt transforms. It allows users to build an external library of unique connections and changes that can be verified, distributed, and used again by different teams. The SIs receive the sensing data collected by PSs and preprocess the data according to preset data fusion policies that are listed in Table 1. The s and p represent the SI and PS, respectively. The b is a bundle of PSs, and an individual PS is considered a special bundle. The h is the aggregator function and the f is the qualifier fusion. An energy-efficient method in WSNs is data aggregation. Sensor networks with a high node density experience redundancy because the same data is perceived by several nodes. Details are shown in our previous work. After the sensing data is preprocessed, the result is either temporarily stored in the fog or forwarded to the cloud (VS) according to the application requirements. In some cases, the SIs can also provide services to local users to reduce the consumption of bandwidth and the response time of requests.

In the cloud layer, the PSs are virtualized as VSs, which receive data forwarded by SIs and provide services to end users. In order to reduce the consumption of the IT resources of the platform, the PSs are temporarily created to respond to the requests of the end-user and will be disposed of once the service is finished. One SI can map to multiple VSs, and multiple VSs can be grouped as one VSG based on specific application scenarios and service requests.

2.2. Framework of the Proposed Platform. As shown in Figure 2, the proposed platform is divided into three PS layer, fog layer, and cloud layer from bottom to top.

The PS layer is composed of PSs, which are deployed in smart logistics parks to collect context information about logistics operations, such as temperature and humidity sensors for warehouse environment monitoring, flame sensors for fire detection, infrared sensors for human

Table 1: Policies of data fusion from PSs to SIs.

Policy	Definition	Relation
Singular	$s_i \longrightarrow p_i$	One PS to one SI
Selector	$s_i \longrightarrow \{p_i \mid p_i \in b\}$	A bundle of homogenous PSs to one SI
Accumulator	$s_i \longrightarrow b$	A bundle of heterogeneous PSs to one SI
Aggregator	$s_i \longrightarrow h\ (b)$	A bundle of PSs to one SI
Qualifier	$s_i \longrightarrow \{p_i \mid \forall p_i \in b \longrightarrow f\ (p_i)\}$	A bundle of PSs to one SI
Context qualifier	$s_i \longrightarrow \{p_i \mid \forall p_i \in b \longrightarrow f\ (p_i,\ b)\}$	A bundle of PSs to one SI

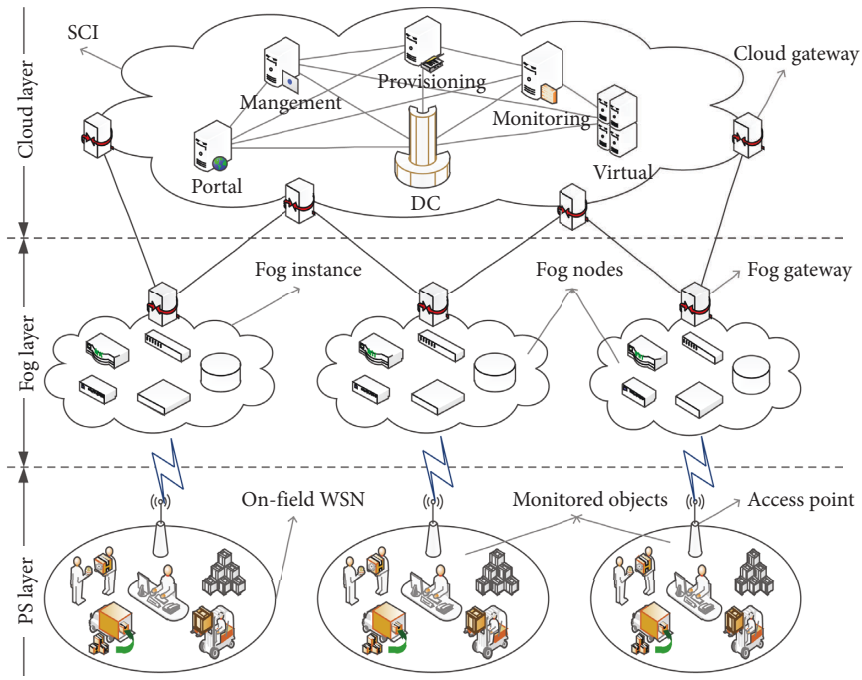

Figure 2: Fog enabled sensor cloud framework.

intrusion detection, and so on. A thermo-hygrometer is a tool that measures both humidity and temperature in one convenient tool. Your gas heating system's flame sensor is an essential safety feature. A shock or a surface temperature ignitor will really ignite the gas in your gas furnace during the ignition cycle. PSs are generally wireless sensors, and some PSs are mobile, such as sensors embedded in forklifts. An electronic device known as a forklift detection sensor is used to detect or sense the presence of people or objects in the path of a moving vehicle to boost forklift operating safety. PSs form on-field wireless sensor networks (WSNs) in the form of an AD-hoc network, and the number of WSNs in one logistics park is decided by the requirements of logistics management. Ad hoc networks are multi-hop networks made up of wireless independent hosts, where each host might function as a router to help with traffic from other nodes. Each WSN accesses the fog instance through an access point (AP). An AP is a LAN subdevice that gives devices other points of connection, allowing for the addition of more devices without affecting network performance. A large number of wireless sensors are placed in an ad hoc way to create a wireless sensor network (WSN), which lacks any physical infrastructure and is used to track system, physical, and environmental factors.

The fog layer is composed of fog instances, and each fog instance includes multiple fog nodes, which have limited capabilities for computing and data storage. Fog nodes are intelligent intermediate devices and can generally be gateways, routers, switches or special fog devices. In our proposed platform, fog nodes are used to preprocess sensing data to achieve data fusion, to reduce the consumption of network bandwidth, and to deploy some simple applications or some functions of these applications in the fog nodes to reduce the network transmission delay.

The cloud layer is the place where sensor cloud infrastructure (SCI) is located. A brand-new approach to cloud computing called Sensor Cloud transmits all sensor information into a cloud technology architecture using physical sensors to gather data. Numerous monitoring applications employ sensor data, which Sensor Cloud effectively manages. The primary components of SCI are data centers (DCs), portal servers, management servers, provisioning servers, monitoring servers, and virtual servers. To store, process, and distribute data and applications, an organization's common IT operations and hardware are centralised in a data centre. Data centers are essential to the continuity of everyday operations since they store the most important and proprietary assets of a business. DCs are used for the

permanent storage of preprocessed sensing data. Portal servers are the interfaces through which users log into the platform. Virtual servers provide companies with an innovative, cloud-oriented service for the future, while servers represent the tried and powerful data centre deployments of the past. The choice is not simple but, at the same time. The main functions of management servers are to manage VSs, fog nodes, and IT resources of SCI, while provisioning servers mainly provide VSs to end users. Virtual servers provide the base running environment for the VS and VSG, while monitoring servers monitor the status of VSs, VSGs, and virtual servers.

3. Network Model of the Proposed Platform

3.1. Definition of Components. As shown in Table 2, the set of PSs is denoted by $P = \{p_i | i \in N, |P| = N\}$, where p_i is the ith PS and N is the total number of PSs. PSs are divided into multiple bundles based on the requirements of application scenarios which are denoted by b_i, and the set of bundles is denoted by $B = \{b_i\}$, such that $\sum_{b_i \in B} |b_i| = N$. The set of SIs is denoted by $S = \{s_i | i \in |B|, s_i = F(b_i), |S| = |B|\}$ and s_i is the virtualization of b_i in the fog layer according to the policies listed in Table 1. The sets of VSs, APs, fog gateways, and cloud gateways are denoted by $v = \{vi\}$, $a = \{ai\}$, $g = \{gi\}$ and $c = \{ci\}$ correspondingly, where v_i, a_i, g_i and c_i denote the ith VS, AP, fog gateway, and cloud gateway, respectively.

3.2. Modeling the Network. This paper focuses on evaluating the performance of the proposed platform in terms of service latency and bandwidth consumption compared to traditional cloud computing and fog computing paradigm, and the key links are between APs and cloud gateways, so it is assumed that the data transmission bandwidth within the on-field WSN and SCI are unrestricted, while those of the key links are restricted. An excessive amount of bandwidth use can harm a network in many ways, including sluggish upload and downloading speeds and poor site performance.

The data collected by all PSs deployed in the on-field WSNs is transported to the fog layer through the (p, a, s) link, $\forall a \in A$ and $\forall s \in S$. $\forall p_i \in b$, the p_i has the common destination s_i and is one of the input values of the data fusion function F, so $\forall b_i \in B$, the b_i is treated as a whole and the transmission route is $b_i \longrightarrow a \longrightarrow s_i$, $\forall a \in A$ and $\forall s_i \in S$. For local real-time applications, the preprocessed result of the data is temporarily stored in fog nodes and directly provided to the application. Otherwise, the result is forwarded to the cloud layer through the (s, g, c, v) link, $\forall s \in S$, $\forall g \in G$, $\forall c \in C$, and $\forall v \in V$.

Table 2: Definition of components in the proposed platform.

Symbol	Definition	Description
P	$P = \{p_i \mid i \in N, \lvert P\rvert = N\}$	The set of PSs
b	$b = \{p_i \mid p_i \in P, \lvert b\rvert > 0\}$	A bundle of PSs
B	$B = \{b_i\}$	The set of bundles
S	$S = \{s_i \mid i \in \lvert B\rvert, s_i = F(b_i), \lvert S\rvert = \lvert B\rvert\}$	The set of SIs
V	$V = \{vi\}$	The set of VSs
A	$A = \{a_i\}$	The set of APs
G	$G = \{g_i\}$	The set of fog gateways
C	$C = \{c_i\}$	The set of cloud gateways

The data collected by b_i in time-slot t is defined as $D_o^{b_i}(t)$, in bytes, and $D_r^{b_i}(t)$ is the amount of the data from b_i that needs to be redirected to the cloud in time-slot t, in bytes too. We have:

$$D_r^{b_i}(t) = \begin{cases} 0, & \text{local real} - \text{time application}, \\ \delta D_o^{b_i}(t), & \text{otherwise}, \end{cases} \tag{1}$$

where δ is the data fusion coefficient determined by the fusion function F, and $\delta \in (0, 1]$. For the local real time application, the preprocessed result will not be forwarded to the cloud, so $D_r^{b_i}(t) = 0$. Otherwise, the result will be forwarded to the cloud, so $D_r^{b_i}(t) = \delta D_o^{b_i}(t)$. $\forall b_i \in B$, the data fusion function F is fixed on the basis of a predefined data fusion policy, so δ is fixed too for definite b_i. According to detailed data fusing policies, formula (1) can be refined as follows:

$$D_r^{b_i}(t) = \begin{cases} 0 & \text{local real} - \text{time application} \\ D_o^{b_i}(t) & \text{Singular} \\ D_o^{b_i}(t)/|b_i| & \text{Selector} \\ nD_o^{b_i}(t)/|b_i|\,(approximately) & \text{Accumulator} \\ D_o^{b_i}(t)/|b_i| & \text{Agrregator} \\ \theta D_o^{b_i}(t)/|b_i| & \text{Qualifier} \\ \theta D_o^{b_i}(t)/|b_i| & \text{Context Qualifier} \end{cases}, \tag{2}$$

Where n is an integer and is the number of arguments in the output value of F. θ is the probability of a particular event occurring while the qualifier function f returns true, and $\theta \in (0, 1)$.

The routing variables of the fog layer (FLRV) and cloud layer (CLRV) are defined as $X^{fog}_{b_i,a,s_i}(t)$, $X^{cld}_{s_i,gc,v}(t)$, respectively, $\forall b_i \in b$, $\forall a \in a$, $\forall s_i \in s$, $\forall g \in g$, $\forall c \in c$, $\forall v \in v$. The FLRV $X^{fog}_{b_i,a,s_i}(t)$ means the route through which the data collected by b_i in time-slot t reaches the SI s_i and the CLRV $X^{cld}_{s_i,g,c,v}(t)$ means the route through which the data from s_i to the destination v in time-slot t. Distributed fog computing units, known as fog nodes, which are made up of one or more physical objects with processor and sensing capabilities, enable the deployment of fog services. The Border Gateway Protocol is used by cloud routing to handle links between different virtual cloud networks or between cloud networks and an on-premises network dynamically (BGP). Routing in the cloud adjusts itself automatically to shifting network circumstances. For any given route, the corresponding FLRV and CLRV values are the proportion of the total data sent from the starting point in time-slot t which transmits through the route, so we can get:

$$X^{fog}_{b_i,a,s_i}(t) = \begin{cases} 0 & \text{invalid} \\ \varepsilon & \text{valid} \end{cases}, \quad X^{cld}_{s_i,g,c,v}(t) = \begin{cases} 0 & \text{invalid} \\ \varepsilon & \text{valid} \end{cases}, \tag{3}$$

where invalid means there is no data transmitted through the given route and $\varepsilon \in (0, 1]$. If the data is successfully transferred from the starting point to the destination without any loss, we can also get $\sum_{b_i \in B, a \in A, s_i \in S} X^{fog}_{b_i,a,s_i}(t) = 1$ and $\sum_{s_i \in S, g \in G, c \in C, v \in V} X^{cld}_{s_i,g,c,v}(t) = 1$. The set of all FLRVs in time-slot t is defined as formula (5) and that of all CLRVs is defined as formula (6).

$$\begin{aligned} X^{fog} &= \left\{ X^{fog}_{b_i,a,s_i}(t) \middle| X^{fog}_{b_i,a,s_i}(t) = [0, 1], \right. \\ &\left. \sum_{b_i \in B, a \in A, s_i \in S} X^{fog}_{b_i,a,s_i}(t) = 1, \forall b_i \in B, \forall a \in A, \forall s_i \in S \right\}, \\ X^{dd} &= \left\{ X^{dd}_{s_i,g,c,v}(t) \middle| X^{dd}_{s_i,g,c,v}(t) = [0, 1], \right. \\ &\left. \sum_{s_i \in S, g \in G, c \in C, v \in V} X^{dd}_{s_i,g,c,v}(t) = 1, \forall s_i \in S, \forall g \in G, \forall c \in C, \forall v \in V \right\}. \end{aligned} \tag{4}$$

4. Performance Metrics of the Network Model

4.1. Bandwidth Consumption. In the proposed platform, the data fusion is accomplished in the fog layer, so the data transmission is divided into two phases. In the first phase, which is from on-field WSN to the fog instance, the proposed platform has the same bandwidth consumption compared with traditional cloud computing and fog computing modes. The main difference lies in the second phase, that is, from the fog instance to the cloud platform, so in this section, we focus on the bandwidth consumption reduction of the proposed platform in the second phase, and mathematically describe the expression of the same.

The total amount of data traveling through the (b, a, s) link can be expressed as follows:

$$D^{total}_{o}(t) = \sum_{i=1}^{|B|} \left\{ D^{b_i}_{o}(t) \sum_{b_i \in B, a \in A, s_i \in S} X^{fog}_{b_i,a,s_i}(t) \right\}, \tag{5}$$

and the total amount of data traveling through the (s, g, c, v) link is:

$$D^{total}_{r}(t) = \sum_{i=1}^{|B|} \left\{ D^{b_i}_{r}(t) \sum_{s_i \in S, g \in G, c \in C, v \in V} X^{cld}_{s_i,g,c,v}(t) \right\}. \tag{6}$$

In the traditional cloud mode, all the data collected by $b_i \in B$ is directly sent to the cloud platform without data fusion, Cloud Data Fusion is a corporate data integration solution for developing and maintaining data pipelines rapidly that is completely managed and cloud-native, so the total amount of the data is expressed as follows:

$$D^{total}_{cld}(t) = D^{total}_{o}(t) = \sum_{i=1}^{|B|} \left\{ D^{b_i}_{o}(t) \sum_{b_i \in B, a \in A, s_i \in S} X^{fog}_{b_i,a,s_i}(t) \right\}, \tag{7}$$

where $D^{total}_{cld}(t)$ denotes the total amount of data sent to the cloud in the traditional cloud mode. Based on formulas (8) and (9), we can get the reduction $(\Delta D_{cld}(t))$ of the proposed platform compared with the cloud mode:

$$\Delta D_{cl\,d}(t) = D_{cl\,d}^{total}(t) - D_r^{total} = \sum_{i=1}^{|B|}\left\{D_o^{b_i}(t)\sum_{b_i\in B,a\in A,s_i\in S} X_{b_i,a,s_i}^{fog}(t) - D_r^{b_i}(t)\sum_{s_i\in S,g\in G,c\in C,v\in V} X_{s_i,g,c,v}^{cl\,d}(t)\right\}. \tag{8}$$

In the traditional fog mode, all the data collected by $b_i \in B$ is directly sent to the fog layer at first, and then will be redirected to the cloud except for the data requested by the local real time applications. Different to the proposed platform, there is no data fusion in the process of data transmission, so the total amount of data redirected to the cloud is:

$$D_{fog}^{total}(t) = \sum_{i=1}^{|B|}\left\{D_o^{b_i}(t)\sum_{b_i\in B,a\in A,s_i\in S} X_{b_i,a,s_i}^{fog}(t) \quad \left(F(D)_o^{b_i}\right)(t) = D_r^{b_i}(t) > 0\right), \tag{9}$$

where $D_{fog}^{total}(t)$ denotes the total amount of the data redirected to the cloud in the traditional fog mode. From formulas (8) and (11), we can get the reduction ($\Delta D_{fog}(t)$) of the proposed platform compared with the fog mode:

$$\begin{aligned}\Delta D_{fog}(t) = D_{fog}^{total}(t) - D_r^{total}(t) = \sum_{i=1}^{|B|}&\left\{D_o^{b_i}(t)\sum_{b_i\in B,a\in A,s_i\in S} X_{b_i,a,s_i}^{fog}(t)\right\}\\ &-\left\{D_r^{b_i}(t)\sum_{s_i\in S,g\in G,c\in C,v\in V} X_{s_i,g,c,v}^{cl\,d}(t)\right\}\left(F(D)_o^{b_i}\right)(t) = D_r^{b_i}(t) > 0).\end{aligned} \tag{10}$$

4.2. Service Latency. In this paper, the service latency is the response time of the request sent by the terminal node within or near the on-field WSN and is divided into the transmission latency and the processing latency. It takes time for a router to process a packet header. A packet's time in the routing queues is often known as the queuing delay. A packet's bits must be pushed onto the connection, which adds to the transmission latency. A signal's propagation delay is the amount of time it takes for it to go across a medium. As mentioned in Section 3, the bandwidth within the on-field WSN and the cloud is assumed to be unlimited, so we focus on the link between the on-field WSN and the cloud, that is, the link (b, a, s, g, c, v), $\forall b \in B$, $\forall a \in A$, $\forall s \in S$, $\forall g \in g$, $\forall c \in C$, $\forall v \in v$.

4.3. Transmission Latency. Similar to the previous part, the link (b, a, s, g, c, v) is divided into the link (b, a, s) and the link (s, g, c, v), and φ_{bs}, φ_{sv} are defined as the time delay constant for unit byte data respectively, so in time-slot t, the corresponding transmission latencies (φ_{tr}^{fog}, $\varphi_{tr}^{cl\,d}$) are expressed as:

$$\varphi_{tr}^{fog} = \varphi_{bs} \sum_{i=1}^{|B|} \left\{ D_o^{b_i}(t) \sum_{b_i \in B, a \in A, s_i \in S} X_{b_i, a, s_i}^{fog}(t) \right\},$$
$$\varphi_{tr}^{cl\,d} = \varphi_{sv} \sum_{i=1}^{|B|} \left\{ D_r^{b_i}(t) \sum_{s_i \in S, g \in G, c \in C, v \in V} X_{s_i, g, c, v}^{cl\,d}(t) \right\}. \quad (11)$$

The mean transmission latency in time-slot t ($\Delta_{tr}^{sc}(t)$) can be computed as:

$$\Delta_{tr}^{sc}(t) = \frac{\varphi_{bs} \sum_{i=1}^{|B|} \left\{ D_o^{b_i}(t) \sum_{b_i \in B, a \in A, s_i \in S} X_{b_i, a, s_i}^{fog}(t) \right\} + \varphi_{sv} \sum_{i=1}^{|B|} \left\{ D_r^{b_i}(t) \sum_{s_i \in S, g \in G, c \in C, v \in V} X_{s_i, g, c, v}^{cl\,d}(t) \right\}}{\sum_{i=1}^{|B|} \left\{ D_o^{b_i}(t) \sum_{b_i \in B, a \in A, s_i \in S} X_{b_i, a, s_i}^{fog}(t) \right\}}. \quad (12)$$

Similarly, in the traditional fog computing mode, the mean transmission latency in time-slot t ($\Delta_{tr}^{fog}(t)$) is expressed as:

$$\Delta_{tr}^{fog}(t) = \frac{\varphi_{bs} \sum_{i=1}^{|B|} \left\{ D_o^{b_i}(t) \sum_{b_i \in B, a \in A, s_i \in S} X_{b_i, a, s_i}^{fog}(t) \right\} + \varphi_{sv} D_{fog}^{total}(t)}{\sum_{i=1}^{|B|} \left\{ D_o^{b_i}(t) \sum_{b_i \in B, a \in A, s_i \in S} X_{b_i, a, s_i}^{fog}(t) \right\}}. \quad (13)$$

In the traditional cloud computing mode, the mean transmission latency in time-slot t ($\Delta_{tr}^{cl\,d}(t)$) is expressed as:

$$\Delta_{tr}^{cl\,d}(t) = \frac{\varphi_{bv} \sum_{i=1}^{|B|} \left\{ D_o^{b_i}(t) \sum_{b_i \in B, a \in A, s_i \in S} X_{b_i, a, s_i}^{fog}(t) \right\}}{\sum_{i=1}^{|B|} \left\{ D_o^{b_i}(t) \sum_{b_i \in B, a \in A, s_i \in S} X_{b_i, a, s_i}^{fog}(t) \right\}}, \quad (14)$$

where φ_{bv} is time delay constant for unit byte data transmission from an on-field WSN to the cloud platform, and $\varphi_{bv} \leq \varphi_{bs} + \varphi_{sv}$.

4.4. Processing Latency. Let δ^{fog} and $\delta^{cl\,d}$ are the processing delays per byte in the fog layer and cloud layer, respectively, and it is clear that $\delta^{fog} \geq \delta^{cl\,d}$ for the limited computing and storage power of the fog nodes. In the proposed platform, the total amount of time spent on data processing ($\varphi_{\mathrm{pr}}^{fog}$) in the fog layer can be computed as follows:

$$\varphi_{\mathrm{pr}}^{fog} = \delta^{fog} \sum_{i=1}^{|B|} \left\{ D_o^{b_i}(t) \sum_{b_i \in B, a \in A, s_i \in S} X_{b_i, a, s_i}^{fog}(t) \right\}, \quad (15)$$

and that of the cloud layer ($\varphi_{\mathrm{pr}}^{cl\,d}$) is:

$$\varphi_{\mathrm{pr}}^{cl\,d} = \delta^{cl\,d} \sum_{i=1}^{|B|} \left\{ D_r^{b_i}(t) \sum_{s_i \in S, g \in G, c \in C, v \in V} X_{s_i, g, c, v}^{cl\,d}(t), \right\}, \quad (16)$$

so the mean processing delay of the proposed platform is expressed as:

$$\Delta_{\mathrm{pr}}^{sc}(t) = \frac{\delta^{fog} \sum_{i=1}^{|B|} \left\{ D_o^{b_i}(t) \sum_{b_i \in B, a \in A, s_i \in S} X_{b_i, a, s_i}^{fog}(t) \right\} + \delta^{cl\,d} \sum_{i=1}^{|B|} \left\{ D_r^{b_i}(t) \sum_{s_i \in S, g \in G, c \in C, v \in V} X_{s_i, g, c, v}^{cl\,d}(t) \right\}}{\sum_{i=1}^{|B|} \left\{ D_o^{b_i}(t) \sum_{b_i \in B, a \in A, s_i \in S} X_{b_i, a, s_i}^{fog}(t) \right\}}. \quad (17)$$

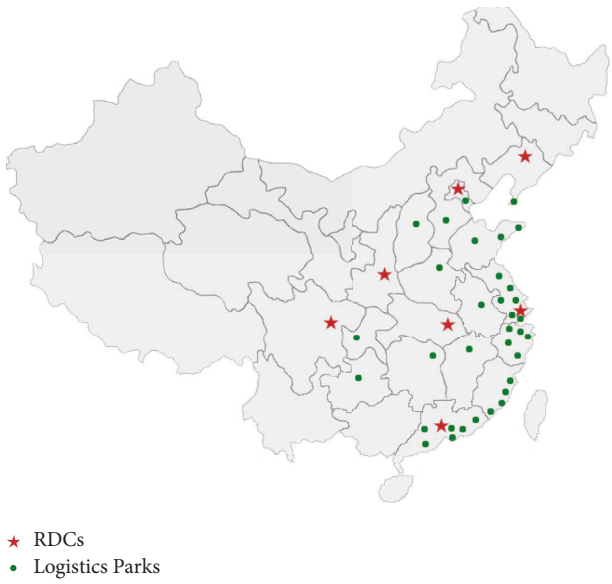

Figure 3: Distribution of logistics facilities.

Similarly, in the traditional fog computing mode, the mean processing latency ($\Delta_{tr}^{fog}(t)$) can be computed as:

$$\Delta_{\mathrm{pr}}^{fog}(t) = \frac{\delta^{fog}\sum_{i=1}^{|B|}\left\{D_o^{b_i}(t)\sum_{b_i\in B,a\in A,s_i\in S}X_{b_i,a,s_i}^{fog}(t)\right\} + \delta^{cl\,d}D_{fog}^{total}(t)}{\delta^{fog}\sum_{i=1}^{|B|}\left\{D_o^{b_i}(t)\sum_{b_i\in B,a\in A,s_i\in S}X_{b_i,a,s_i}^{fog}(t)\right\}}, \tag{18}$$

and that of the traditional cloud computing mode is:

$$\Delta_{\mathrm{pr}}^{cl\,d}(t) = \frac{\delta^{cl\,d}\sum_{i=1}^{|B|}\left\{D_o^{b_i}(t)\sum_{b_i\in B,a\in A,s_i\in S}X_{b_i,a,s_i}^{fog}(t)\right\}}{\sum_{i=1}^{|B|}\left\{D_o^{b_i}(t)\sum_{b_i\in B,a\in A,s_i\in S}X_{b_i,a,s_i}^{fog}(t)\right\}} = \delta^{cl\,d}. \tag{19}$$

5. Case Study: Simulation Setup

In this section, we take a large logistics enterprise in China as an example and illustrate the network setup for the proposed platform in the real logistics scenario.

5.1. Network Topology. As shown in Figure 3, the logistics enterprise has seven regional distribution centers (RDCs) and 34 logistics parks distributed mainly in southeast China. A regional distribution centre (RDC) is a facility that gathers and consolidates completed goods, parts, and accessories made by its own group of businesses for its own brand for distribution to dealers, importers, subsidiaries, or other unrelated businesses domestically or abroad. The RDC is also the data center (DC) of the region where the SCI is deployed and corresponds to the cloud layer of the proposed platform. The logistics park is where the fog instances are located, to realize data fusion and respond to local real-time applications.

There are 75 refrigerated warehouses for food, 4 refrigerated warehouses for medicine, and 91 e-commerce warehouses located in the 34 logistics parks. Each warehouse includes several on-field WSNs, and each on-field WSN is divided into multiple bundles of PSs according to the requirements of the logistics applications. The free software ensure that all of your warehouse and logistics requirements are met. This tool makes it simple to maintain tabs on deliveries, drivers, and customers. This is the instrument to link all your distribution network connections whenever you need help with your operations.

5.2. Network Traffic. The data traffic of the logistics park is proportional to the number of PSs deployed in the park. Data from the on-field WSNs is transmitted to the fog layer in packets. Considering the energy efficiency of WSNs, the sizes of the packets are set to be between 8 bytes and 200 bytes. Packet arrival is considered to follow a Poisson distribution, with the mean packet arrival rate being 1 packet per second. Discrete probability distributions include those in the Poisson distribution. It provides the likelihood that an event will occur k times within a predetermined period of time or space. As mentioned before, the bandwidth within on-field WSN and the cloud is assumed to be unlimited, but that between the on-field WSN and the cloud ((b, v) link, $\forall b \in B$, $\forall v \in V$) is limited. The communication between the WSN and the fog instance ((b, s) link, $\forall b \in B$, $\forall s \in S$) relies on the Intranet of the logistics park with a bandwidth of 1 Gbps, while the communication between the fog instance and the DC ((s, v) link, $\forall s \in S, \forall v \in V$) relies on the national backbone network of China with a bandwidth of 10 Gbps.

5.3. Physical Sensors. The total number of PSs deployed in the logistics parks is about 100,000. In the process of logistics operation, only active PSs collect the data of logistics, and the active PSs are proportional to real-time logistics traffic, and the number of active PSs changes over time, enabling the assessment of the proposed platform performance in varied network conditions. In this paper, the proportion of active PSs is set in the range [0.65, 0.95] based on the business statistics of the enterprise, as shown in Table 3. Additionally, the proportion of local real-time applications changes dynamically too, with a range of 0.05–0.35.

All the PSs are divided into about 40,000 bundles, the ratios of each type of bundle and the typical PS counts within each type of bundle are shown in Table 4. The number of bundles in each of the 34 logistics parks is proportional to the inventory capacity of the logistics park.

6. Case Study: Performance Evaluation

In details of the results obtained in terms of the performance metrics are presented and analyzed in this section. The simulation setup is mentioned in detail in Section 5. Additionally, we compare the performance of the proposed platform with that of the traditional fog computing and cloud computing architectures and present a thorough study against the same.

Table 3: Business statistics in 2022.

Indicators	Jan.	Feb.	Mar.	Apr.	May.	Jun.
Income (billion CNY)	15.59	10.56	13.79	13.21	13.53	15.12
Volume (billion bill)	0.90	0.67	0.88	0.83	0.87	0.95

Table 4: Proportions of each type bundle.

Types	Proportions	$\lceil b_i \rceil$
Singular	0.2	1
Selector	0.2	5
Accumulator	0.2	5
Aggregator	0.2	5
Qualifier	0.1	5
Context qualifier	0.1	5

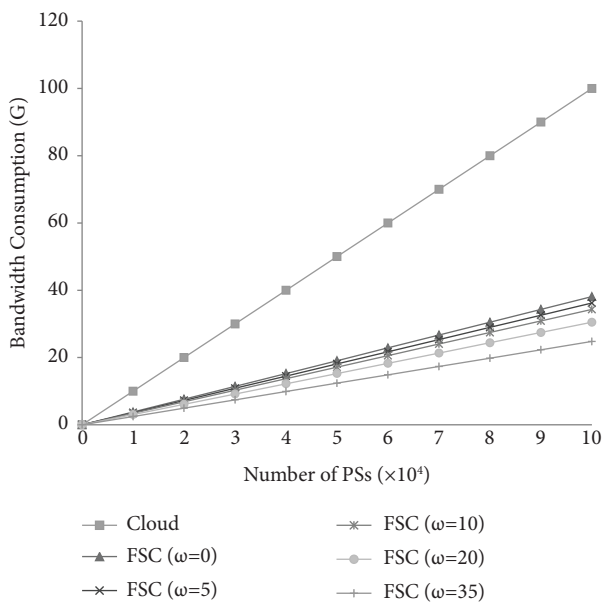

Figure 4: Cloud computing mode versus FSC in bandwidth consumption.

6.1. Bandwidth Consumption. Bandwidth consumption is affected by the number of PSs, sensor activation rate, and real-time application ratio, which is represented by ω, in the range of [5, 35]. As shown in Figures 4 and 5, bandwidth consumption is proportional to the number of active status sensors.

Figure 4 shows a comparison between the cloud computing mode and FSC bandwidth consumption. As shown in Figure 4, compared with the traditional cloud computing mode, the proposed FSC for a smart logistics park has good data fusion performance. Meanwhile, as the proportion of real-time applications increases, the bandwidth consumption of FSC gradually decreases.

6.2. Service Latency. Service latency consists of transmission latency and processing latency, so in this part, we compare the sensing delay and processing delay first, and

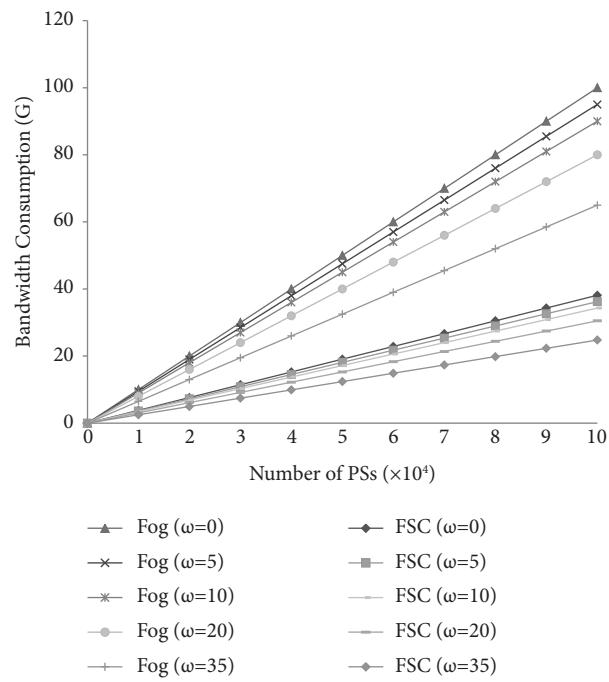

Figure 5: Fog computing mode versus FSC in bandwidth consumption.

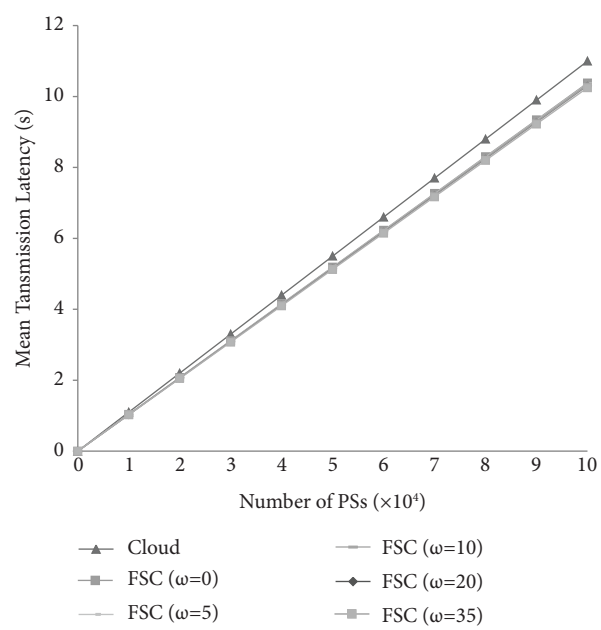

Figure 6: Cloud computing mode versus FSC in mean transmission latency.

then comprehensively compare the service delay. As in the previous part, this part takes ω to be 0, 5, 10, 20, and 35, respectively. A customer order and a cloud storage provider's answer are separated by a period of time called cloud service latency. Device use and enjoyment are significantly impacted by latency. For communications

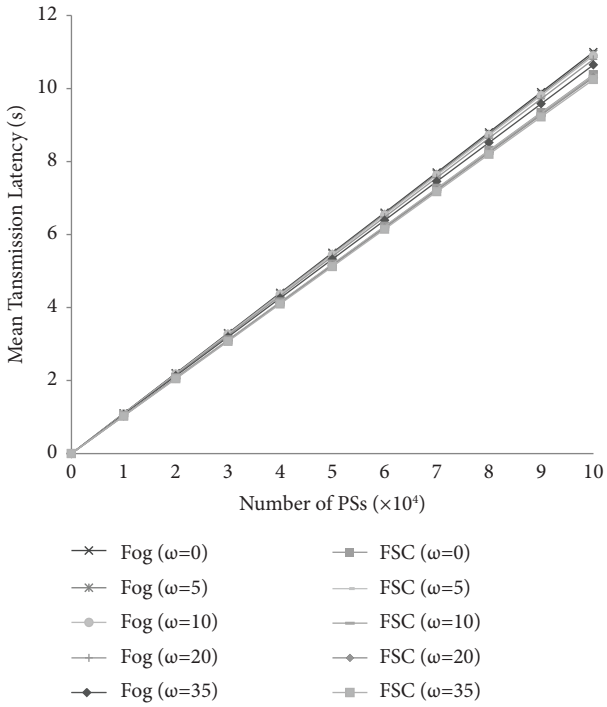

Figure 7: Fog computing mode versus FSC in mean transmission latency.

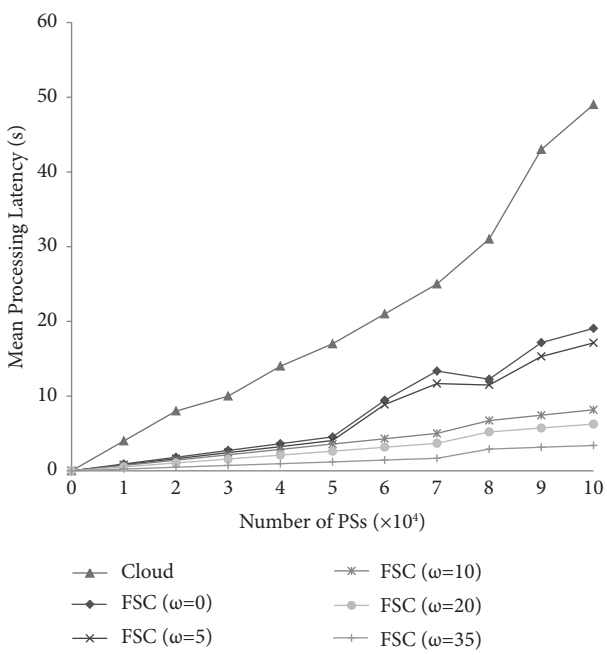

Figure 8: Cloud computing mode versus FSC in mean processing latency.

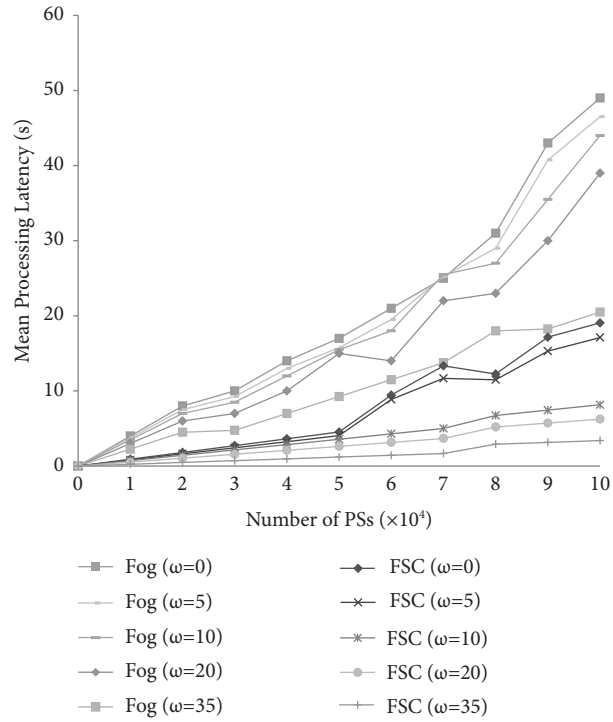

Figure 9: Fog computing mode versus FSC in mean processing latency.

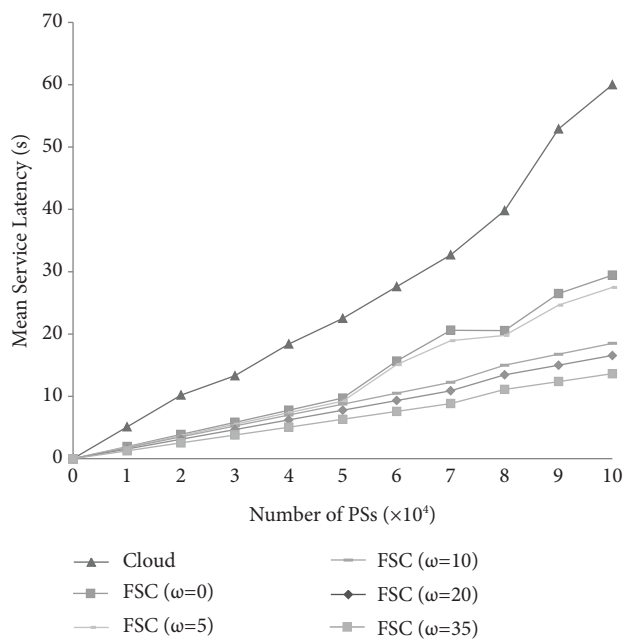

Figure 10: Cloud computing mode versus FSC in mean service latency.

using cloud services, which might be particularly susceptible to delays for various reasons, these issues may be exacerbated. The time elapsed between a client's needs and the cloud service provider's answer is known as cloud service latency. How useful and pleasurable gadgets and communications are is significantly impacted by latency. These issues may be made worse by cloud storage communications, which may be particularly susceptible to delays for various reasons.

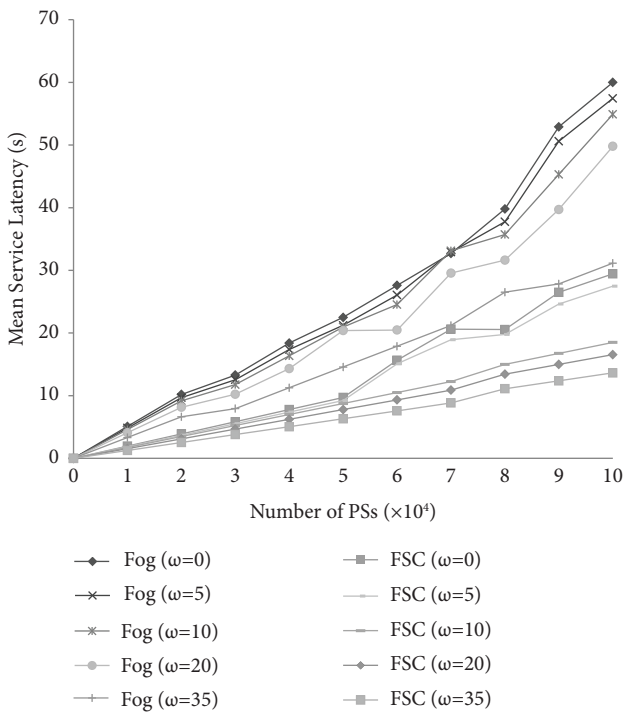

Figure 11: Fog computing mode versus FSC in mean service latency.

As shown in Figure 6, the FSC has some advantages over the traditional cloud computing model, but it is not obvious. When the proportion of local real-time applications increases, the average network transmission delay decreases slightly.

As shown in Figure 7, compared with the traditional fog computing mode, FSC has a certain advantage in the mean network transmission latency, but it is not very obvious. When the proportion of local applications increases, the mean transmission delay decreases slightly.

As shown in Figures 8 and 9, compared with the traditional cloud computing and fog computing modes, FSC reduces the mean processing latency. As the number of local real-time applications increases, the mean processing latency decreases. When the mean transmission latency and processing latency are combined, the mean service latency shows similar characteristics, as shown in Figures 10 and 11.

7. Summary and Conclusion

The assessment of the FSC proposed in our previous work is a key issue and stage in the research of the combination of sensor cloud and smart logistics park. In this paper, we construct a network model for the FSC for a smart logistics park and evaluate parts of its performance. The experiment proves that the FSC for smart logistics parks has a practical advantage over the traditional cloud computing and fog computing modes. The proposed FSC's physical sensor virtualization framework builds the network model and calculates the FSC's parameters. Using a big logistics company in China as an example, we demonstrate the network configuration for the suggested platform in a real-world logistics scenario to evaluate the performance of the platform.

In the future, we will expand the range of performance indicators, such as energy consumption, construction and operating costs, carbon emissions, etc. Meanwhile, based on the model proposed in this paper, sensor virtualization, data fusion, and intra-domain task scheduling in the FSC will be further studied.

Data Availability

The figures and tables used to support the findings of this study are included in the article.

Conflicts of Interest

The authors declare that they have no conflicts of interest.

Acknowledgments

This project is supported by the Natural Science Foundation of Hubei Province (project no. 2019CFC930) and China Society of Logistics (project no. 2020CSLKT3-213).

References

[1] C. Zhu, V. Leung, J. Rodrigues, S Lei, W Lei, and Z Huan, "Social sensor cloud: framework, greenness, issues, and outlook," *IEEE Network*, vol. 32, no. 5, pp. 100–105, 2018.

[2] A. Alamri, W. S. Ansari, M. Hassan, M. A. Hossain, and M. S. Hossain, "A survey on sensor-cloud: architecture, applications, and approaches," *International Journal of Distributed Sensor Networks*, vol. 2013, Article ID 917923, 18 pages, 2013.

[3] Y. Lv, S. Xiang, T. Zhu, and S. Zhang, "Data-driven design and optimization for smart logistics parks: towards the sustainable development of the steel industry," *Sustainability*, vol. 12, no. 17, p. 7034, 2020.

[4] S. Geetha and P. Deepalakshmi, "Rapid retrieval of secured data from the sensor cloud using a relative record index and energy management of sensors," *International Journal of Intelligent Enterprise*, vol. 6, no. 3, p. 1, 2019.

[5] S. Madria, V. Kumar, and R. Dalvi, "Sensor cloud: a cloud of virtual sensors," *IEEE Software*, vol. 31, no. 2, pp. 70–77, 2014.

[6] S. A. Chaudhry, K. Yahya, F. Al-Turjman, and M. H. Yang, "A secure and reliable device access control scheme for IoT based sensor cloud systems," *IEEE Access*, vol. 8, no. 99, pp. 139244–139254, 2020.

[7] M. Wieland, Y. Li, and S. Martinis, "Multi-sensor cloud and cloud shadow segmentation with a convolutional neural network," *Remote Sensing of Environment*, vol. 230, Article ID 111203, 2019.

[8] C. Zhu, L. Shu, V. C. M. Leung, S. Guo, Y. Zhang, and L. T. Yang, "Secure multimedia big data in trust-assisted sensor-cloud for smart city," *IEEE Communications Magazine*, vol. 55, no. 12, pp. 24–30, 2017.

[9] Y. Liao and S. Liu, "Research on key technologies of smart logistics dynamic positioning based on NB-iot," *Journal of Physics: Conference Series*, vol. 1634, no. 1, Article ID 012086, 2020.

[10] A. V. Dastjerdi and R. Buyya, "Fog computing: helping the internet of Things realize its potential," *Computer*, vol. 49, no. 8, pp. 112–116, 2016.

[11] M. Peng, S. Yan, K. Zhang, and C. Wang, "Fog computing based radio access networks: issues and challenges," *IEEE Network*, vol. 30, no. 4, pp. 46–53, 2016.

[12] S. V. Oprea and A. Bâra, "Edge and fog computing using IoT for direct load optimization and control with flexibility services for citizen energy communities," *Knowledge-Based Systems*, vol. 228, Article ID 107293, 2021.

[13] P. Pop, B. Zarrin, M. Barzegaran et al., "The FORA Fog Computing Platform for Industrial IoT," *Information Systems*, vol. 98, Article ID 101727, 2021.

[14] T. Wang, Y. Mei, and W. Jia, "Edge-based differenital privacy computing for sensor-cloud systems," *Journal of Parallel and Distributed Computing*, vol. 136, 2019.

[15] Y. B. Ooi, W Beh, L Wai-Kong, and S Shervin, "Using the Cloud to Improve Sensor Availability and Reliability in Remote Monitoring," *IEEE Transactions on Instrumentation and Measurement*, vol. 68, 2019.

[16] H. Cheng, D. Yang, C. Lu, Q. Qin, and D. Cadasse, "Intelligent oil production stratified water injection technology," *Wireless Communications and Mobile Computing*, vol. 2022Article ID 3954446, 7 pages, 2022.

[17] H. Cheng, P. Ma, G. Dong, S. Zhang, J. Wei, and Q. Qin, "Characteristics of Carboniferous Volcanic Reservoirs in Beisantai Oilfield, Junggar Basin," *Mathematical Problems in Engineering*, vol. 2022, Article ID 7800630, 2022.

[18] H. Cheng, J. Wei, and Z. Cheng, "Study on Sedimentary Facies and Reservoir Characteristics of Paleogene sandstone in Yingmaili Block, Tarim basin," *Geofluids*, vol. 2022, Article ID 1445395, 15 pages, 2022.

[19] W. Zhang, Z. Cheng, H. Cheng, Q. Qin, and M. Wang, "Research of tight gas reservoir simulation technology IOP conference series: earth and environmental science," *IOP Conference Series: Earth and Environmental Science*, vol. 804, no. 2, Article ID 022046, 2021.

[20] X. Wei and L. Wu, "A New Proposed Sensor Cloud Architecture Based on Fog Computing for Internet of Things," in *Proceedings of the 2019 International Conference on Internet of Things (iThings) and IEEE Green Computing and Communications (GreenCom) and IEEE Cyber, Physical and Social Computing (CPSCom) and IEEE Smart Data (SmartData)*, Atlanta, Georgia, USA, July 2019.

[21] K. Rajakumari, P. Punitha, R. Lakshmana Kumar, and C. Suresh, "Improvising packet delivery and reducing delay ratio in Mobile ad hoc network using neighbor coverage-based topology control algorithm," *International Journal of Communication Systems*, vol. 35, no. 2, 2022.

Hindawi
Mobile Information Systems
Volume 2022, Article ID 4616959, 9 pages
https://doi.org/10.1155/2022/4616959

Research Article

Analysis of the Influence of Back Home to Start Undertaking and Rural Revitalization Based on Artificial Intelligence

Shengyan Wu, Yue Chang, and Xingjiang Liao

School of Medicine and Health Management, Guizhou Medical University, Guiyang, Guizhou, China

Correspondence should be addressed to Shengyan Wu; 1717010305@xy.dlpu.edu.cn

Received 25 August 2022; Revised 22 September 2022; Accepted 28 September 2022; Published 7 October 2022

Academic Editor: Chi Lin

The strategy of rural revitalization is to take measures to deal with the big problem of rural decline, mainly from the aspects of developing rural economy, getting rid of poverty, and adjusting rural structure, and changing the traditional thinking of rural development when implementing policies. With the number and scale of rural laborer's back home to start undertaking expanding continuously, it is more important to improve the quality of rural laborer's back home to start undertaking. On the basis of analyzing the motivation and problems of rural laborer's back home to start undertaking, this paper puts forward a risk identification model based on artificial intelligence (AI) algorithm and explores the development path of rural laborer's back home to start undertaking under the background of rural revitalization. Through simulation experiments, the effectiveness and superiority of this algorithm are analyzed. The results show that the accuracy rate of venture risk assessment in this paper is 93.95%, and the error is 10.24% lower than that of the back propagation neural network (BPNN). It can be seen that this method has a significant effect in the analysis of the risk and influencing factors of rural laborer's back home to start undertaking. The overall requirements of rural revitalization strategy for industrial prosperity will inevitably encourage and attract more rural laborer's to back home to start undertaking, and "starting a business to help the poor" will become a new path for rural poverty alleviation and development in the future.

1. Introduction

Urban and rural development must be continually integrated and supportive of each other in the areas of resource development and people mobility in the new era. With the gradual deepening of the policy of "mass entrepreneurship and innovation," more and more rural laborer's choose back home to start undertaking, but the phenomenon of entrepreneurial failure affects their entrepreneurial motivation and willingness. With the steady advancement of the rural revitalization strategy, the countryside has shown a strong development momentum. Under the dual influence of the unsatisfactory work and life in the city and the good development prospects in the countryside, rural laborer's have the idea of back home to start undertaking [1, 2]. The strategy of rural revitalization is to take measures to deal with the big problem of rural decline, mainly from the aspects of developing rural economy, getting rid of poverty, adjusting rural structure, and so on, and changing the traditional thinking of rural development when implementing policies [3]. On the one hand, rural laborer's back home to start undertaking can bring investment, technology, and new market opportunities to their hometown, and drive the economic development of their hometown. On the other hand, the uncertainty of starting a business may also put it at risk or even fail to start a business and choose to go out to work again. With the number and scale of rural laborer's back home to start undertaking expanding continuously, it is more important to improve the quality of rural laborer's back home to start undertaking [4]. Enhancing the entrepreneurial risk awareness of rural laborer's back home, establishing a risk early warning system, monitoring and preventing entrepreneurial risks, and taking timely countermeasures are helpful to enhance the enterprise's ability to resist risks, prolong the operating cycle of enterprises, and promote economic development.

Under the background of rural revitalization strategy, rural laborer's back home to start undertaking injects new kinetic energy into rural economic development, which helps to improve rural industrial structure and promote urban-rural integration [5]. Many coastal enterprises in China began to develop inland, speeding up the pace of rural laborer's back home. Moreover, many rural laborers have chosen the road of self-employment when they return home. From the outbreak of the information revolution to the present, its influence has now penetrated into everyone's daily life. Nowadays, rural laborers have become an important factor for China to build a well-off society in an all-round way, and back home to start undertaking is a new way to help rural laborers get rid of poverty and get rich and solve the current predicament [6, 7]. With the continuous development of information technology, an AI-based risk assessment algorithm for homecoming entrepreneurship emerged, which fitted the results of homecoming entrepreneurship risk assessment with high precision and got a good result. On the basis of analyzing the motivation and problems of rural laborer's back home to start undertaking, this paper puts forward a risk identification model based on AI algorithm, and explores the development path of rural laborer's back home to start undertaking under the background of rural revitalization.

It closely resembles the modernization and urbanization conditions found in the majority of nations worldwide. As a result of ongoing development and economic growth, farmers' incomes in rural China have improved in recent years. In many rural areas, there has been a decline, whether it is the environment or irrigation and water conservancy [8]. The massive loss of labor force leads to problems such as urbanization and aging in rural areas, which is an important reason for the decline of rural areas in China. Because of their rich working experience, rural laborer's back home plays a positive role in promoting the goal of rural prosperity and development, and they are the main force of rural modernization [9]. Entrepreneurship of rural laborer's can promote the development of economy and technology, promote the employment of people, and solve the problems of empty nesters and left-behind children. Initially, the entrepreneurial risk was evaluated by manual method, the evaluation process of this method was very tedious, and the evaluation results deviated from the actual risk level, so the blindness of the evaluation results was serious. In this paper, the risk identification and analysis of rural laborer's back home to start undertaking based on the AI algorithm is proposed. The main innovations are as follows:

(1) This paper puts forward a risk assessment algorithm based on AI algorithm and analyzes the effectiveness and superiority of this algorithm through simulation and comparison experiments.

(2) From the perspective of individual entrepreneurs, and using grounded theory, we try to dig out the key factors that affect the success or failure of rural laborer's back home to start undertaking. To a certain extent, we can make up for the lack of attention paid to entrepreneurs' main body and entrepreneurial process in the existing research, and serve as a reference for the following research.

The rest of the article is arranged as follows: The second section is related work, which expounds the research of related scholars on rural development and entrepreneurship; the third section is the method part, which realizes the risk assessment of back home to start undertaking through the AI algorithm. The fourth section is the experimental analysis, which verifies the effectiveness of this method through simulation experiments and puts forward the development strategy of rural laborer's back home to start undertaking. The fifth section is the summary, which expounds the methods and contributions of this article, summarizes the realistic path of back home to start undertaking, and puts forward the future development direction.

2. Related Work

Under the urging of the city and hometown, rural laborers interact with each other to encourage rural laborer's back home to start undertaking. Serrano and others analyzed the motivation of rural laborer's back home to start undertaking from the difficulties of rural laborer's integration into cities and the abundant resources of back home to start undertaking [10]. Wang et al. pointed out that social integration difficulties, economic integration difficulties, and psychological integration difficulties are the main factors of financial difficulties, which have become the main thrust factors for rural laborer's to back home to start undertaking, while natural resources, human resources, and social resources provide powerful conditions for rural laborer's to back home to start undertaking and are the main pulling factors for rural laborer's to back home to start undertaking [11]. Martínez et al. analysts believe that the multiple causes leading to rural laborer's back home to start undertaking include the global economic downturn, industrial upgrading in large- and medium-sized cities, high housing prices and living costs in cities and towns, the extensive application of the AI technology, and the limitation of professional ceiling [12]. Zhou and Li, by studying the generation mechanism of rural laborer's back home to start undertaking to absorb surplus rural labor force, pointed out that rural laborer's back home to start undertaking has positive significance for driving poor farmers out of poverty and getting rich, helping poor farmers to increase their income, and embarking on a well-off road of prosperity [13]. Feinerman and Komen pointed out that after back home to start undertaking, rural laborer's will encounter livelihood risks from three levels, and the livelihood risks encountered at this time will be more risky. The sources of risks mainly include capital, technology, and management, and further pointed out that once rural laborer's fail to start a business, they will follow the rational logic of survival to minimize the risks and make another choice of livelihood [14]. The study by Cieslik and D'Aoust found that education level, work experience, personal ability, partners, local resources, and industry threshold have a very significant impact on rural laborer's choice of entrepreneurial mode [15]. Ngorora and Mago

found that the main factors affecting rural laborer's back home to start undertaking are related to their age, education, family factors, and government assistance [16]. Deng pointed out that learning culture, policy culture, and rural information culture have a significant impact on rural laborer's entrepreneurial behavior when they return home and put forward some targeted policy suggestions [17]. Naminse et al. pointed out through analysis and research that there are still some problems to be solved in the policy of supporting rural laborer's to back home to start undertaking and proposed that the government should take multidimensional measures to support rural laborer's to back home to start undertaking [18]. Güzel et al.'s point of view is that it is also very important to study farmers' entrepreneurial psychology. The most important thing for farmers to start entrepreneurial behavior is the social repercussions [19].

3. Methodology

3.1. Joint Mechanism of Rural Laborer's Back Home to Start Undertaking and Targeted Poverty Alleviation. With the continuous emergence of the strategic advantages of rural revitalization, the conditions required for returning rural laborers to start businesses tend to be better, which will attract a large quantity of knowledgeable, capable, and capital-reserved rural laborer's back home to start undertaking. Their return brings new ideas, which can not only change the concept of rural economic development but also greatly promote the promotion of regional economic competitiveness [20]. Accurate poverty alleviation focuses on the hematopoietic function of the poor, which depends on the endogenous power of rural economic growth. Rural laborer's back home to start undertaking is the endogenous power source of rural economic growth. They complement each other and promote each other, which can boost rural economic growth while improving poverty alleviation benefits. Rural laborer's back home to start undertaking will stimulate the local employment rate in rural areas, and to a certain extent, increase farmers' income. Successful rural laborer's enterprises can also set an example for other rural laborer's who back home to start undertaking and stimulate their enthusiasm for back home to start undertaking. Rural laborers need to rely on the advantages of local resources to help rural poverty alleviation. On the one hand, rural laborers choose to back home to start undertaking, because the labor-intensive industries in large- and medium-sized cities have shrunk in recent years, which leads to the rising pressure of continuous employment competition. On the other hand, it is influenced by the gradual improvement of preferential policies for rural entrepreneurship.

In order to realize the overall revitalization of rural areas and effectively increase farmers' income and rural employment rate, it is necessary to improve and perfect the rural industrial structure. In this process, rural laborer's back home to start undertaking has gradually become an indispensable force. Most of the rural laborers who back home to start undertaking are small- and medium-sized enterprises, which have affinity for farmers. Promoting and developing in their hometown have more advantages and can improve the efficiency of poverty alleviation in rural areas [21]. However, rural laborers are faced with problems such as land, capital, and entrepreneurship guidance in the process of returning to their hometowns, which requires that the precise poverty alleviation policy should be tilted towards rural laborer's enterprises in the implementation, and effective capital, land, and technical support should be provided for returning rural laborer's to start their own businesses by relying on the government platform and the advantages of rural resources. Endogenous motivation is the key to poverty alleviation in rural areas. Supporting rural laborer's to back home to start undertaking not only breaks the original pattern of one-way flow of urban and rural human resources but also provides talent support for rural development. The key to rural development lies in talents. Only when talents flourish can rural economic construction show a good development trend. It is necessary to improve the rural industrial structure, stimulate the vitality of rural economic development, encourage and support rural laborer's to back home to start undertaking, further increase the employment rate of rural residents, practically raise the income level of farmers, narrow the gap between urban and rural areas, and realize a new pattern of urban-rural integration.

3.2. Risk Assessment Algorithm for Back Home Entrepreneurship. We add new kinetic energy for accelerating the building of a well-off society in an all-round way and boosting the modernization of agriculture and rural areas. The linkage development of rural laborer's entrepreneurship and precision poverty alleviation is based on the commonality between them. Employment can achieve accurate assistance through back home to start undertaking to drive employment, so as to transfer agricultural surplus labor force, realize the two-way flow of human resource elements between urban and rural areas, create more room for farmers to increase their income, and create demographic dividend for rural development. From the perspective of rural laborer's back home to start undertaking and precision poverty alleviation, on the one hand, rural laborer's have poured into cities in one direction to realize the two-way flow between urban and rural areas, and a large quantity of rural laborer's back home to start undertaking have injected new blood into county economic development and poverty alleviation in the central and western regions.

The venture risk assessment of rural laborer's back home is a very complicated problem, which is caused by the high difficulty, strong professionalism, and many constraints and influences on the success of venture capital. At the same time, the main body of entrepreneurship is the special group of rural laborers who return home. They often have some defects and uncertainties in entrepreneurship, which leads to the greater risk of entrepreneurship than other groups. The risk assessment process of back home to start undertaking based on AI is shown in Figure 1.

Assuming that there are a total of m risk assessment indicators for back home to start undertaking, which are represented as $\{x_1, x_2, \ldots, x_m\}$, then the risk assessment

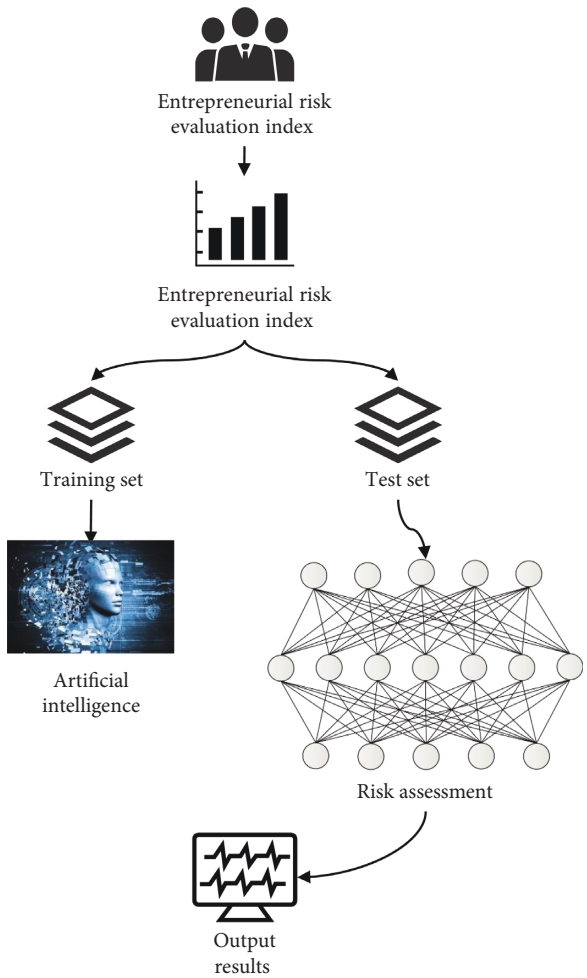

Figure 1: Risk assessment process for back home to start undertaking.

level for back home to start undertaking can be described as follows:

$$y = f(x_1, x_2, \ldots, x_m). \tag{1}$$

In the formula, $y = f(\cdot)$ is the risk assessment function of back home to start undertaking.

We collect the corresponding risk assessment indicators for back home to start undertaking and then calculate the eigenvector and maximum eigenvalue $\lambda_{\max}$ of the risk assessment index for back home to start undertaking, and then perform a consistency check as follows:

$$\mathrm{CI} = \frac{\lambda_{\max} - n}{n - 1}. \tag{2}$$

In the formula, n represents the order of the risk assessment matrix for back home to start undertaking. If the random one-time ratio CR satisfies (3), then it means that the user is satisfied with the risk assessment matrix for back home to start undertaking, which is acceptable, otherwise it is unacceptable:

$$\mathrm{CR} = \frac{\mathrm{CI}}{\mathrm{RI}} < 0.1, \tag{3}$$

where RI is the average random consistency index.

As the returning entrepreneurs have been working abroad for many years, they do not know much about their hometown's entrepreneurship support policies, how to handle relevant documents, and what information they need to provide. Therefore, grass-roots service entities such as county and township government departments should set up entrepreneurial service centers for rural laborer's back home to provide all-round services for rural laborer's back home to start undertaking, and timely track and grasp the entrepreneurial situation of rural laborer's back home. Rural laborer's entrepreneurship and precision poverty alleviation have a common effect link in the implementation. Rural laborers whose back home to start undertaking have more extensive contact with the outside world and have a deeper understanding of social development and progress. Rural laborer's entrepreneurship in their hometowns has a diffusion effect, which can stimulate more rural laborer's to back home to start undertaking and employment, and create a good atmosphere for employment and entrepreneurship in rural areas. While distributing economic benefits, however, villages confront several challenges due to the relative backwardness of rural economic growth.

3.3. Coupling Interaction and Risk Resolution between Back Home to Start Undertaking and Rural Revitalization. Venture identification refers to the signs that entrepreneurs show in the process of starting a business according to their entrepreneurial activities. It is a process of systematically and continuously discovering risks by using various methods to identify and distinguish risks before all kinds of risk events occur. In the process of starting a business, we should not only identify the risks of the external business environment and market but also the risks of technology, management, finance, and personnel within the enterprise. The fruitful results of rural revitalization strategy will also stimulate more rural laborer's back home to start undertaking. The virtuous circle that follows is that the implementation of rural revitalization strategy and rural laborer's back home to start undertaking complement each other and promote each other. The interaction between rural laborer's entrepreneurship and rural revitalization is shown in Figure 2.

From the point of view of maximizing the benefits of entrepreneurs, the best situation should be that the barriers to entry are high and the barriers to exit are low. In this case, new entrants will be resisted, while unsuccessful enterprises in this industry will easily leave this industry. On the contrary, low barriers to entry and high barriers to exit are regarded as the most unfavorable situation. Because under this situation, many businesses may readily enter this industry to share earnings when there is a positive outlook for the market; however, when there is a recession, many businesses face difficulty in closing their doors. Let the risk assessment data of back home to start undertaking be $x_i(k)$, and all data forms are a sequence as follows:

$$X_i = (x_i(1), x_i(2), \ldots, x_i(n)), i = 1, 2, \ldots, m. \tag{4}$$

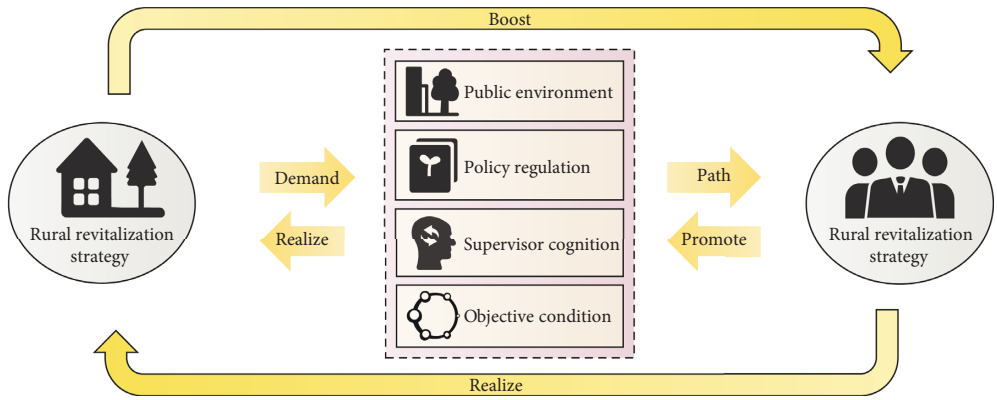

Figure 2: The interaction between rural laborer's back home to start undertaking and rural revitalization.

We perform a dimensionless operation on X_i to get X_i' and select a part to form a reference sequence for risk assessment of back home to start undertaking as follows:

$$X_i' = (x_i'(1), x_i'(2), \ldots, x_i'(n)), i = 1, 2, \ldots, m. \quad (5)$$

We calculate the difference between all return-home entrepreneurial risk assessment reference sequences as follows:

$$\Delta_i(k) = |x_i(k) - x_i'(k)|. \quad (6)$$

Then, we find the maximum and minimum differences of the sequence as follows:

$$\begin{aligned} M &= \max_i \max_k \Delta_i(k), \\ m &= \min_i \min_k \Delta_i(k). \end{aligned} \quad (7)$$

We calculate the grey correlation coefficient of the risk assessment index for back home to start undertaking as follows:

$$r_i(k) = \frac{m + \varsigma M}{\Delta_i(k) + \varsigma M}, \quad (8)$$

where ς is the resolution coefficient. We find the grey comprehensive correlation degree as follows:

$$r_i = \sum_{k=1}^{n} \omega_i r_i(k), \quad (9)$$

where ω_i is the weight. According to the value of the grey comprehensive correlation degree, the influence degree of the risk assessment index of back hometown entrepreneurship and the risk assessment result of back hometown entrepreneurship can be obtained, so as to realize the screening of the risk assessment index of back hometown entrepreneurship.

Let the input x and the output y be an unknown joint distribution probability $F_{X,Y}(x, y)$, for N samples $\{(x_i, y_i)\}_{i=1}^{N}$ that are independent and identically distributed. The problem of machine learning is to construct a set of input-output mapping functions as follows:

$$y = f(x, w). \quad (10)$$

Among them, y is the actual output of the mapping function, w is the weight value, and the difference between the actual output and the expected value input by $f(x, w)$ is expressed by the formula $L(y, f(x, w))$, thereby defining the risk functional as follows:

$$R(w) = \int L(y, f(x, w)) \mathrm{d}F_{X,Y}(x, y). \quad (11)$$

From the definition, it can be seen that the smaller the risk functional $R(w)$ is, the closer the model will be to the actual output, and the purpose of machine learning is to minimize the risk functional. However, in general, the joint distribution probability $F_{X,Y}(x, y)$ of the input and output cannot be known, so the minimum risk functional cannot be obtained. The traditional statistical method is to use empirical risk instead of risk functional. The empirical risk is as follows:

$$R_{\text{emp}}(w) = \frac{1}{N} \sum_{i=1}^{N} L(y_i, f(x_i, w)). \quad (12)$$

Thus, the functional problem of minimizing risk is transformed into the problem of minimizing empirical risk.

Usually, it refers to the process of venture capital, in which high returns are usually accompanied by high risks, while low-risk venture capital projects generally only bring low returns to entrepreneurs. Because high-risk venture capital projects will create high-risk obstacles for other investors who want to enter the industry, they will not dare to enter them easily to carry out venture capital activities, which will enable venture investors who successfully enter the industry to obtain higher risk returns in a certain period of time. If the risk of a venture capital project is relatively low and the income is high, it will inevitably lead to a large influx of venture capital investors, which will eventually lead to intensified competition and lower income, so that only lower risk income can be obtained.

4. Result Analysis and Discussion

4.1. Risk Assessment Simulation of Back Home Entrepreneurship. If the number of attributes with null values comprises a significant fraction of the total number of samples, this attribute and the samples with an excessive

number of null attribute values can be eliminated. For discrete variables, count the occurrence times of each discrete factor and draw the overall histogram, and count the percentage of the factors in the overall sample number. For discrete variables, outliers may be some factors with relatively small occurrence times or particularly large occurrence times, which need to be judged according to specific businesses. The possible outliers can be qualitatively analyzed through the direct view diagram and verified by combining with specific businesses. The estimated value of the whole training set is obtained by averaging the accuracy of the classified data, and the obtained results are shown in Table 1.

For the accuracy of the training model, the size of the sample may also have some influence. When the ratio of the quantity of two categories is 1 : 1, training models with different sample numbers are used for testing. The specific results are shown in Table 2.

It can be found that when the quantity of samples reaches a certain level, the classification accuracy will be improved, while when the quantity of samples is too small, the classification accuracy will be greatly reduced. At the same time, with the increase of the quantity of samples, the training time is also improved. According to the above-mentioned test, this paper will use a total of 160 training sets, including 80 entrepreneurs with normal finance and 80 entrepreneurs with abnormal finance. A total of 80 samples were tested, including 40 entrepreneurs with normal finance and 40 entrepreneurs with abnormal finance. Figure 3 shows the comparison of the accuracy of different algorithms when different sparsity is selected.

It can be seen that after many iterations, the accuracy of the algorithm is gradually improved and tends to be stable. The purpose of precision poverty alleviation is to help farmers get rid of poverty, while rural revitalization is intended to realize agricultural and rural modernization, and they are mutual mechanisms. At the same time, rural laborer's mobility between urban and rural areas makes them have dual identities and becomes an important link between urban and rural development, which is conducive to helping poverty alleviation and reshaping the new urban-rural relationship. The average absolute error results of different algorithms are shown in Figure 4. The recall results of different algorithms are shown in Figure 5.

It is a complex and dynamic process for rural laborer's back home to start undertaking. Whether they can succeed in starting a business in the end is not only due to individual conditions but their entrepreneurial behavior is deeply embedded in their social relations and structures and is influenced by multiple factors. In the process of rural laborer's back home to start undertaking, all kinds of resources and policies, such as policy regulation and public environment in this paper, will restrict or promote their entrepreneurial activities to some extent. In the process of interaction between entrepreneurial behavior and external structure, due to the differences of entrepreneurs' individual conditions, resources and policies, some returning rural laborer's can successfully start a business, while some returning rural laborers can only achieve a part of their entrepreneurial goals or fail to start a business, resulting in different entrepreneurial results. The risk assessment results of homecoming entrepreneurship based on big data analysis are shown in Figure 6.

Table 1: Parameter optimization accuracy.

Error penalty function	Gauss parameter	Accuracy (%)
0.1	0.1	68.95
0.1	1	54.85
0.1	10	55.67
0.2	0.1	54.28
0.2	1	56.27
0.2	10	71.28
0.4	0.1	63.95
0.4	1	58.43
0.4	10	57.64
0.8	0.1	61.29
0.8	1	60.18
0.8	10	58.99

Table 2: Effect of sample size on model accuracy.

Total sample number	Number of samples per type	Accuracy (%)	Training time (S)
40	20	65.29	0.0318
60	30	71.88	0.0315
80	40	71.87	0.0345
100	50	76.99	0.0411
120	60	79.01	0.0425
140	70	80.24	0.0456
160	80	78.89	0.0467

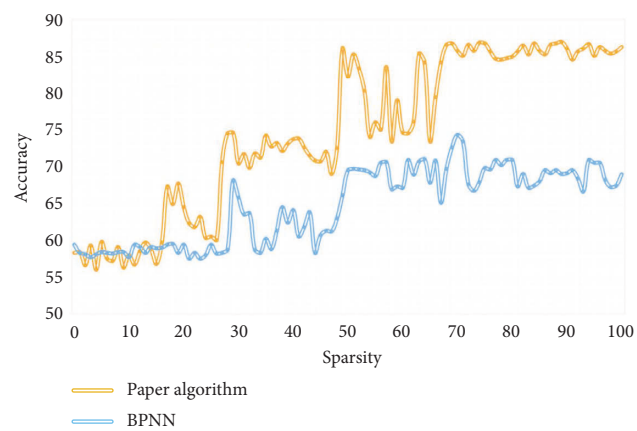

Figure 3: Comparison of algorithm accuracy when different sparsity is selected.

From the analysis of the experimental results in Figure 6, it can be seen that the return venture risk assessment value of the algorithm in this paper is very close to the actual return venture risk value, and there is almost no deviation, thus obtaining a high-precision return venture risk assessment result. The experimental results show that this algorithm is an excellent risk assessment tool for homecoming entrepreneurs.

There are many situations that affect rural laborers starting their own businesses when they return to their

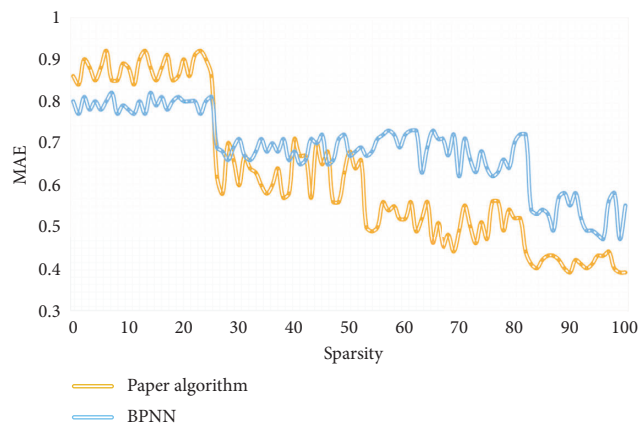

Figure 4: Comparison of the error between the algorithm in this paper and BPNN.

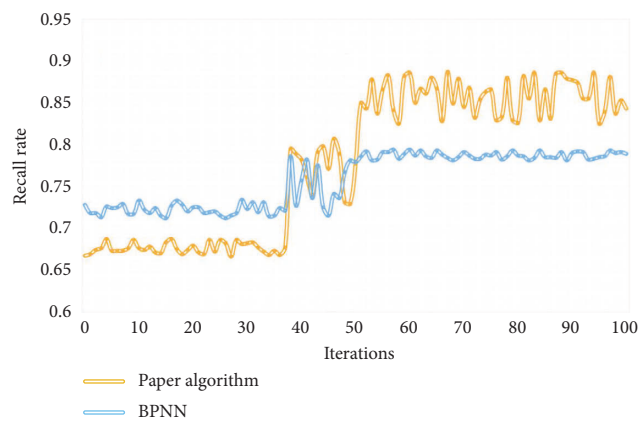

Figure 5: Comparison of the recall rate between the algorithm in this paper and BPNN.

hometowns. They are not alone, so we cannot blindly choose variables in econometric analysis. Volume values can only reflect most variables. For variables that cannot be specifically reflected, some processing should be done to ensure that the variables can be digitized. This algorithm is compared to the present traditional BPNN in order to make the risk assessment result of returning home to begin a project more persuasive. The change curve of BPNN's risk assessment results of back home to start undertaking is shown in Figure 7.

As can be seen from Figure 7, although BPNN has obtained a high-precision risk assessment result of back home to start undertaking, the assessment accuracy is lower than that of this algorithm. In this paper, the accuracy rate of venture risk assessment for back home is 93.95%, and the error is 10.24% lower than that of BPNN. At the same time, in the test process, it is found that the result time of back home venture risk assessment of this algorithm is shorter than that of BPNN, which improves the efficiency of back home venture risk assessment.

4.2. The Development Path of Rural Laborer's Entrepreneurship and Targeted Poverty Alleviation. It is necessary to cooperate with a series of institutional measures to ensure

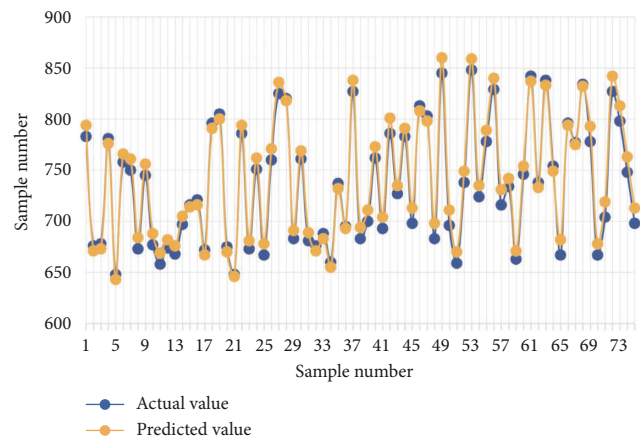

Figure 6: The results of the risk assessment of returning to the hometown of the algorithm in this paper.

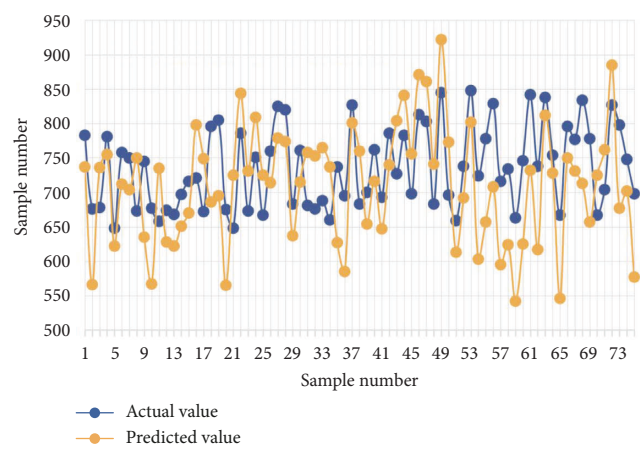

Figure 7: The risk assessment results of returning to hometown entrepreneurship by BPNN.

that rural laborer's can rely on each other to start their own businesses and help the poor accurately and form a linkage development trend of mutual promotion and common progress. Through the role of rural laborer's back home to start undertaking in stimulating the urban-rural infrastructure connectivity and promoting the equalization of urban-rural public services, we can improve the appearance of rural villages and create a corresponding social environment atmosphere for enterprises, so as to realize the integration of urban and rural areas, cooperative development and poverty alleviation. The docking of rural laborer's entrepreneurship and precision poverty alleviation needs the concerted efforts of the government and the market. As the main body of the media, rural laborer's entrepreneurship in their hometowns has a good communication advantage between the government and the market. At the same time, rural laborer's entrepreneurship in their hometowns can help ease the bonding effect between the government and the market in poverty alleviation and improve the efficiency and effectiveness of poverty alleviation. It is particularly important to carry out technical training for rural laborers and poor farmers to enhance their entrepreneurial ability and poor farmers' employability, which is the key to ensure the

effective connection between rural laborer's entrepreneurial ability and their skills requirements for employed poor farmers. It is necessary to establish an interest link system to realize the effective connection between accurate poverty alleviation and back home to start undertaking and promote poverty alleviation. Through the poor farmers' shareholding in agricultural land, subletting, and other forms, the interest link between rural laborer's and farmers who return home to engage in agricultural production and management can be established, so as to realize the co-construction, sharing, and win-win between precision poverty alleviation and back home to start undertaking.

5. Conclusion

The proposal of rural revitalization strategy provides good development conditions for rural laborer's back home to start undertaking. With the continuous expansion of the number and scale of entrepreneurs, it is more important to improve the quality of rural laborer's back home to start undertaking. Due of their lack of managerial skills, experience, and capital, returning rural laborers generally handle their challenges by seeking out partners with similar objectives and launching a business with friends and family. Therefore, the stability of the management of this entrepreneurial enterprise is very important. The results of venture risk assessment can provide guidance for university entrepreneurship. Aiming at the shortcomings of the current venture risk assessment algorithm for back home, this paper proposes a venture risk assessment algorithm for back home based on big data analysis combined with the characteristics of venture risk assessment for back home. The experimental results show that the algorithm in this paper improves the accuracy and speed of risk assessment of homecoming entrepreneurship and solves the problems existing in the current process of homecoming entrepreneurship risk assessment, which has a high practical application value. It is necessary to strengthen the vocational training of local rural surplus labor force, transport qualified, and skilled labor force for enterprises founded by returning rural laborer's guide and cooperate with returning rural laborer's entrepreneurs to carry out pre-job and induction training for employees according to the actual needs of enterprises and solve the brain drain phenomenon of returning rural laborers to start enterprises. [1].

Data Availability

The data used to support the findings of this study are included within the article.

Conflicts of Interest

The authors declare that they have no conflicts of interest.

Acknowledgments

This work was funded by the Guizhou Philosophy and Social Science Project (21GZQN13): Study on the Coupling Mechanism and Boosting Path of Entrepreneurship and Rural Revitalization of Returnee Migrant Workers in Guizhou, and the Key Project of Humanities and Social Sciences Research of Guizhou Department of Education (No. 2022ZD008): Efficiency Measurement and Coupling Machine Research on the Effect of Returning Migrant Workers' Entrepreneurship on Rural Revitalization in Guizhou.

References

[1] C. Viet Nguyen and A. Ngoc Tran, "The role of crop land during economic development: evidence from rural Vietnam," *European Review of Agricultural Economics*, vol. 41, no. 4, pp. 561–582, 2014.

[2] A. Gambardella, M. Ganco, and F. Honoré, "Using what you know: patented knowledge in incumbent firms and employee entrepreneurship," *Organization Science*, vol. 26, no. 2, pp. 456–474, 2015.

[3] Y. C. J. Wu, T. Wu, and Y. Li, "Impact of using classroom response systems on students' entrepreneurship learning experience," *Computers in Human Behavior*, vol. 92, no. 3, pp. 634–645, 2019.

[4] H. Schumacher, K. Gerling, and M. Kowalik, "Entrepreneurial risk choice and credit market equilibria," *The B.E. Journal of Economic Analysis & Policy*, vol. 15, no. 3, pp. 1455–1480, 2015.

[5] J. Yang, J. Černevičiūtė, and R. Strazdas, "The sustainable development of rural troupes under the rural vitalization strategy in China," *Entrepreneurship and Sustainability Issues*, vol. 7, no. 3, pp. 1951–1962, 2020.

[6] G. Wang, "Route choice of rural economic development in offshore areas from the perspective of modern agriculture," *Journal of Coastal Research*, vol. 98, no. sp1, p. 247, 2019.

[7] T. C. Sebora, T. Theerapatvong, and S. M. Lee, "Corporate entrepreneurship in the face of changing competition," *Journal of Organizational Change Management*, vol. 23, no. 4, pp. 453–470, 2010.

[8] G. M. Angeletos and V. Panousi, "Financial integration, entrepreneurial risk and global dynamics]," *Journal of Economic Theory*, vol. 146, no. 3, pp. 863–896, 2011.

[9] C. Clemens and M. Heinemann, "On entrepreneurial risk-taking and the macroeconomic effects of financial constraints," *Journal of Economic Dynamics and Control*, vol. 34, no. 9, pp. 1610–1626, 2010.

[10] C. Cruz Serrano and K. H. Brigham, "Introductory comment to "entrepreneurial risk taking in family firms: the wellspring of the regenerative capability"," *Family Business Review*, vol. 31, no. 2, pp. 214-215, 2018.

[11] C. Wang, Y. Yang, and Y. Zhang, "Economic development, rural livelihoods, and ecological restoration: evidence from China," *AMBIO: A Journal of the Human Environment*, vol. 40, no. 1, pp. 78–87, 2011.

[12] K. R. G. Martínez, Á Herrero Crespo, and A. Fernandez-Laviada, "Influence of perceived risk on entrepreneurial desirability and feasibility: multidimensional approach for nascent entrepreneurs," *Journal of Risk Research*, vol. 20, no. 2, pp. 218–236, 2017.

[13] D. Zhou and B. Li, "How the new media impacts rural development in China: an empirical study," *China Agricultural Economic Review*, vol. 9, no. 2, pp. 238–254, 2017.

[14] E. Feinerman and M. H. Komen, "Agri-environmental instruments for an integrated rural policy: an economic

analysis," *Journal of Agricultural Economics*, vol. 54, no. 1, pp. 1–20, 2003.

[15] K. Cieslik and O. D'Aoust, "Risky business? Rural entrepreneurship in subsistence markets: evidence from Burundi," *European Journal of Development Research*, vol. 30, no. 4, pp. 693–717, 2018.

[16] G. P. K. Ngorora and S. Mago, "Rural entrepreneurship and welfare in South Africa: a case of nkonkobe municipal area in the eastern cape province," *Journal of Economics*, vol. 7, no. 2-3, pp. 169–178, 2016.

[17] K. A. Deng, "Chinese economic revolution, rural entrepreneurship in the twentieth century. by L. Grove. lanham, MD: Rowman & littlefield publishing, inc. 2006. pp. xi, 303. $74.00, hardcover," *The Journal of Economic History*, vol. 71, no. 3, pp. 819-820, 2011.

[18] E. Y. Naminse, J. Zhuang, and F. Zhu, "The relation between entrepreneurship and rural poverty alleviation in China," *Management Decision*, vol. 57, no. 9, pp. 2593–2611, 2019.

[19] Ö Güzel, R. Ehtiyar, and C. Ryan, "The Success Factors of wine tourism entrepreneurship for rural area: a thematic biographical narrative analysis in Turkey," *Journal of Rural Studies*, vol. 84, no. 2, pp. 230–239, 2021.

[20] W. Zhao, J. B. Ritchie, and C. M. Echtner, "Social capital and tourism entrepreneurship," *Annals of Tourism Research*, vol. 38, no. 4, pp. 1570–1593, 2011.

[21] M. Jaafar, A. R. Abdul-Aziz, S. A. Maideen, and S. Z. Mohd, "Entrepreneurship in the tourism industry: i," *International Journal of Hospitality Management*, vol. 30, no. 4, pp. 827–835, 2011.

Hindawi
Mobile Information Systems
Volume 2022, Article ID 6447578, 6 pages
https://doi.org/10.1155/2022/6447578

Research Article

Fuzzy Application in the Design of QR Code Data Binding Based on the GD Packaging Machine

Wei Taicheng, Chen Hao, and Zhu Haoran

China Tobacco Guangxi Industrial Co. Ltd., 530001 Nanning, China

Correspondence should be addressed to Zhu Haoran; 2019020428@stu.cdut.edu.cn

Received 6 July 2022; Revised 7 August 2022; Accepted 9 August 2022; Published 3 October 2022

Academic Editor: Chi Lin

The tracking of raw materials, production, and circulation links is carried out using QR codes in cigarette products. Each link's current data collection and correlation analysis are still in the research and development stage. When used in conjunction with the GD packing machine's production process feature, the QR code reader serves as an acquisition element for the process of data acquisition and the associated design for the tobacco packets and boxes, and the software is used to associate the received data and correct process exceptions. The system satisfies the design requirements, according to the results of the field verification.

1. Introduction

The tobacco industry is propelled by consumer demand. With the advancement of science and technology, distinguishing the authenticity of tobacco products from the outer packaging has become difficult. On the other hand, because of my country's strict control over tobacco propaganda in traditional media and limited media, consumers find it difficult to broaden their awareness of tobacco brands. With the research and statistics of the tobacco industry in recent years, the traditional tobacco industry has been continuously integrated with high and new technologies such as "Internet +" and the Internet of things [1]. As a carrier, the QR code is widely used in the tobacco industry and can effectively control production, processing, quality inspection, logistics, sales, and other links. Make analysis and judgments based on the data collected in each link, and make timely responses to abnormal situations. The construction of the Internet of things in the tobacco industry has effectively improved production efficiency, ensured product quality, and made consumers feel at ease. At the same time, it becomes a link for consumers [2].

With the rapid development of the tobacco industry, the most common GD X2 (hard pack) model in the market has a small box packing capacity of 400 packs per minute. Through manual identification and manual entry of the QR code analysis data, it cannot respond to actual production requirements. In addition, the market is in the research and development stage for the data correlation between the small box and the bar box QR code. Most of the methods are to use multistation and multihardware collection, background data screening, and hardware redundancy, and the system is too complicated. The visual analysis of QR code data technology is currently fairly developed and can reach a recognition rate of more than 99 percent without impacting the efficiency of package production. The electrical and software design of the GD packaging machine realizes data association when combined with the product packaging process [3].

This article primarily describes how the Nanning Cigarette Factory's packaging workshop implemented data correlation technology between the tiny box and the box QR code based on the GD X2 (hard pack) concept.

2. Two-Dimensional Code Analysis Design

2.1. QR Code Format. Both the small box and the bar box use the fast-reading two-dimensional matrix code known as a QR code for their two-dimensional data collection. The black-and-white modules, placement patterns, data regions, and error-correcting codes that make up a QR code. The

positioning pattern is distributed along the three corners of the QR code, which supports fast reading. From any position of the pattern, the ratio of black and white modules is 1 : 1 : 3 : 1 : 1, which is not disturbed by the image position, and the QR code format is shown in Figure 1.

There are 40 versions of the QR code. According to the standard, the QR code starts with a matrix of version 1 (21 ∗ 21) and increases by 4 symbol units in both the horizontal and vertical directions until it reaches version 40 (177 ∗ 177). Different versions of the QR codes are printed after decoding the same data, which affects the speed of parsing to a certain extent [4].

2.2. Code Reader. Combined with the production speed requirements of the GD machine, in order to quickly collect the two-dimensional code information, the two-dimensional code reader is used as the acquisition element [5]. A QR code reader's hardware integrates a CCD camera, multicore processor, memory, and digital I/O. With one-key tuning, it can automatically adjust the best-captured image setting parameters (exposure gain and focal length automatic correction), parallel processing of captured images, parsing QR codes (pipeline operation reduces parsing time), multiple parsing algorithms, multiple codes, and symbols in one image application, with a high recognition rate [6].

2.3. Light Source. Comparing the contrast between the printed code and the background is typically how two-dimensional code analysis is accomplished [7]. While the skins of cigarette packs at the location are primarily white and yellow, the standard cigarette pack's QR code is printed with black patterns. The background color of the QR code will reflect the emitting light source to appear brilliant, whereas the black code will absorb the light source and appear dark when using a strong red LED light source. Therefore, a higher contrast image, as shown in Figure 2, can be obtained, which is easy to convert into a high-quality binary image [8].

There are some textures on the surface during the QR code collection process [9, 10]. When the light source illuminates the box, the surface forms diffuse reflection, as shown in Figure 3. By increasing the light intensity, the concave and convex parts of the printing surface appear white, so as to avoid some black spots around the two-dimensional code when converting the binary image, which makes the two-dimensional code unable to be parsed. Code images with enhanced light intensity, as shown in Figure 4, are in a state of high-quality recognition [11, 12].

3. The Composition of the Electrical System

3.1. The Overall Structure of the Two-Dimensional Code System. The incremental encoder is used as the input signal for acquisition, and the main control board composed of an ARM chip outputs the trigger signal of the code reader [13]. The code reader sends the parsed data to the industrial computer through the serial port, and the software receives the data for analysis, processing, and correlation [14–16]. Interaction between humans and computers, between computers and software, and between humans and code readers all takes place on the display. When the program detects a deviation from the norm, it sends a signal to the main control board by way of the GPIO ports. After the main control board has been given the abnormal enable signal, it will send the alarm and error-related data, as well as the cigarette bar rejection signal, to the machine that it came from. The system structure diagram is shown in Figure 5 [17].

3.2. Two-Dimensional Code Acquisition Synchronization Signal. In the packaging process of the GD machine, the box packaging machine and the small box transparent paper packaging machine use a unified power [18]. The carton packaging machine runs for one cycle, and the small box transparent paper packaging machine runs for five cycles. Incremental encoders are installed on the motion spindle of the carton packer. According to the input of the A-phase, B-phase, and Z-phase pulse signals, as shown in Figure 6, the main control board outputs the code reading box trigger signal, the bar box trigger signal, and the push bar signal, respectively [19].

4. Software Design

4.1. Software Design Framework. The little box and the bar box both have two-dimensional codes on them, and the two-dimensional code reader is able to conduct image recognition on those codes. The bar code scanner sends the data that it has processed to the industrial computer, and the program receives the information that has been identified by the little box in turn. A new data list is formed by associating and binding the two-dimensional code data of the cigarette pack with the two-dimensional code data of the box corresponding to the packaging relationship. The overall design flow chart of data acquisition is shown in Figure 7.

The background data and display data of the two-dimensional code detection and correlation system mainly include two parts: one part is the real-time data collected by the system from the field equipment, and the other part is the storage of the relationship data of the small box-bar box two-dimensional code information [20]. These data primarily cover three different types of data: the first type is the two-dimensional code information that is recognized by the code reader; the second type is the record of some operating system log machine abnormal information data; and the third type is logically associated data that is processed by software through real-time data [21].

4.2. Software Related Measures. The collected data follows the "first-in, first-out" data queue method, and defines the cigarette pack data from the location where the small box collects the QR code to the location where the small box and the carton are packaged as the cached data. In the software, the number of cigarette packs will be set as the pair length, and the data will form a circular queue buffer of small boxes and double stacks as shown in Figure 8. When the length of the received data is equal to the set pair length, the small box

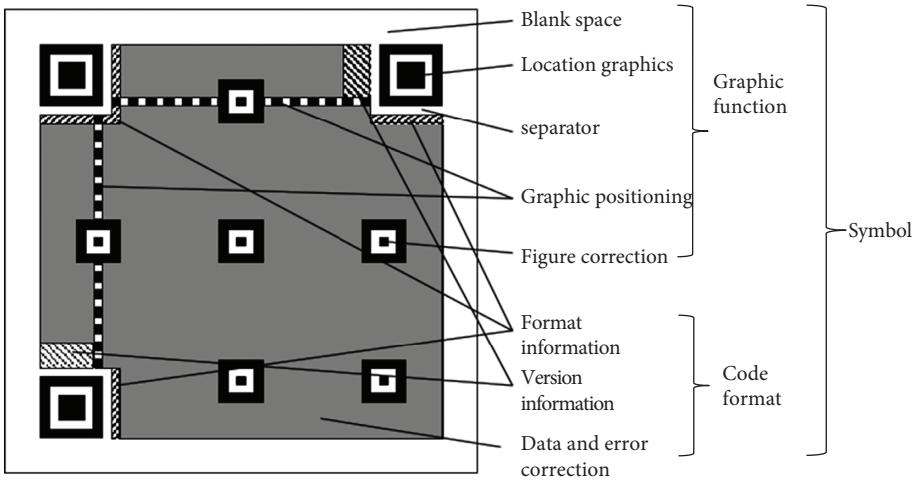

Figure 1: QR code structure.

Figure 2: Capture QR code pictures.

Figure 3: Ordinary red light.

Figure 4: Highlight red light.

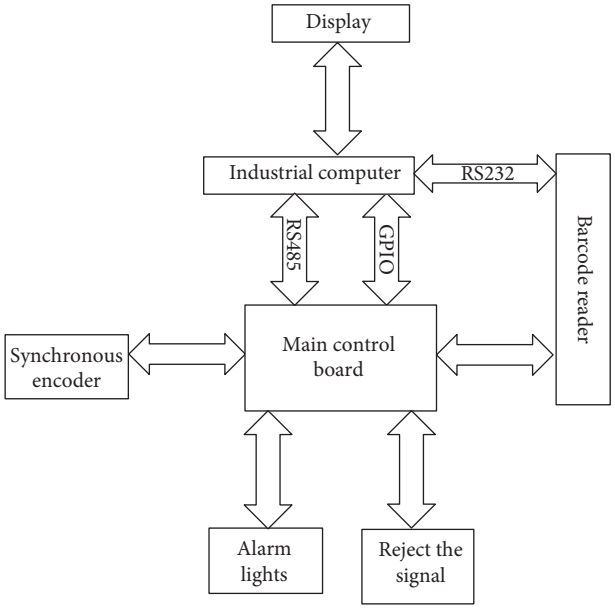

Figure 5: Overall system structure.

first enters the pair of data out of the queue, and the number of dequeues is based on the received push bar signal as a node, and the small box QR code data is associated with the large QR code data [22].

#define Max size 50//Set according to the capacity of cigarette packs in the on-site channel

type def int Queue;

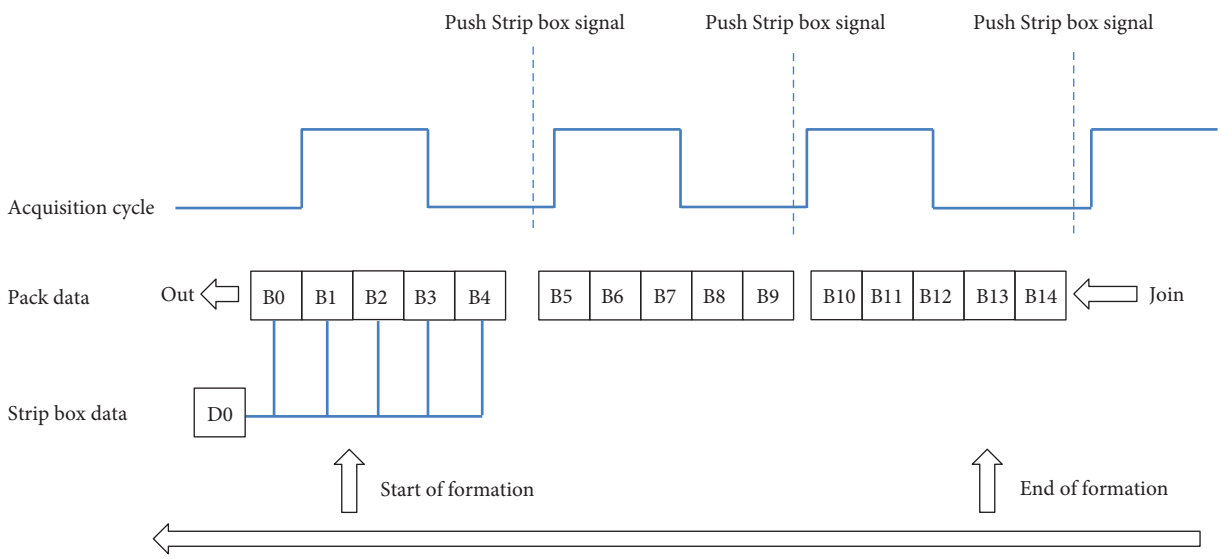

Figure 6: Input and output pulse signals.

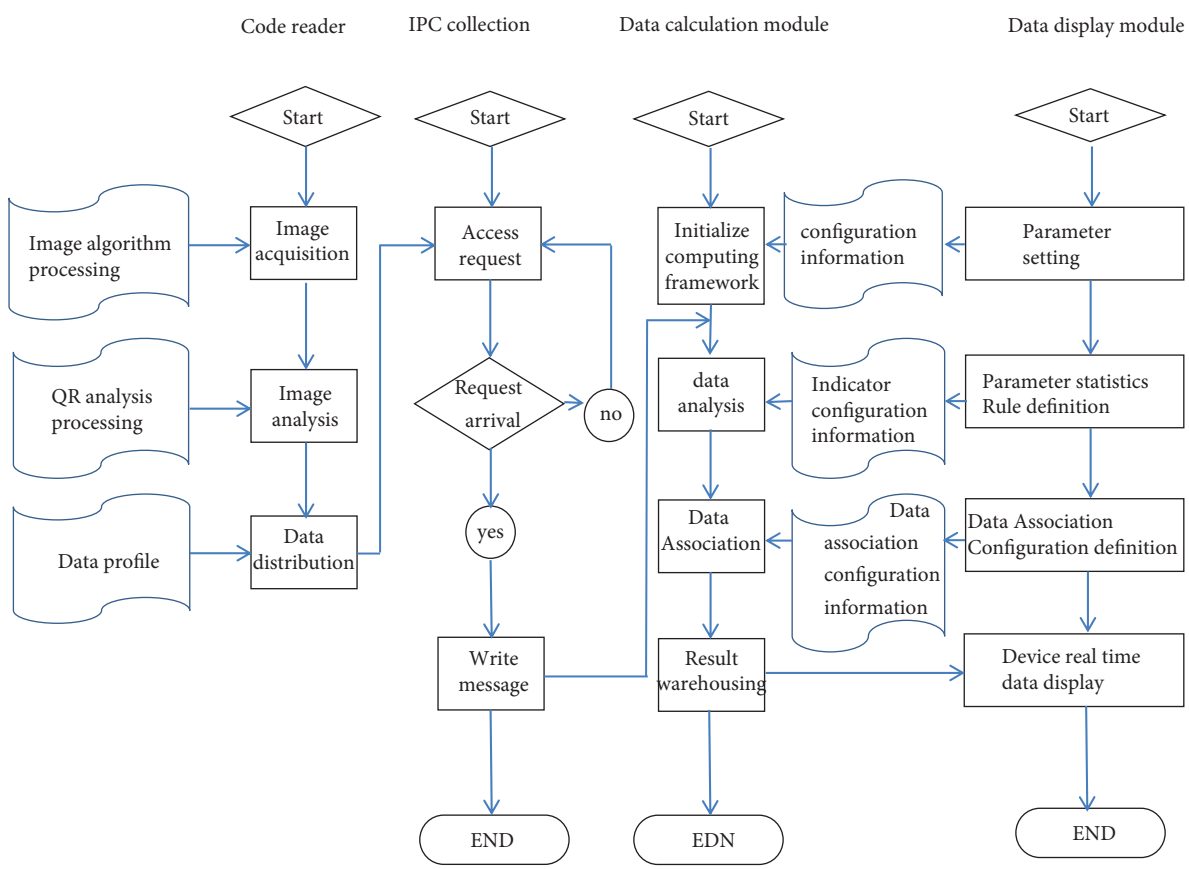

Figure 7: A flow chart of overall software design.

```
type def Struct {
Queue[Max size];
int front; \
int rear;
}SqQueue;
bool Push (SqQueue* &q, ElemType num){
if (q -> rear < Max size – 1);//Determine whether the capacity of the cigarette pack has been met
q -> rear++; //join the team
q -> data[q -> rear] = num;
}
bool deQueue (SqQueue* &q, ElemType num) {
```

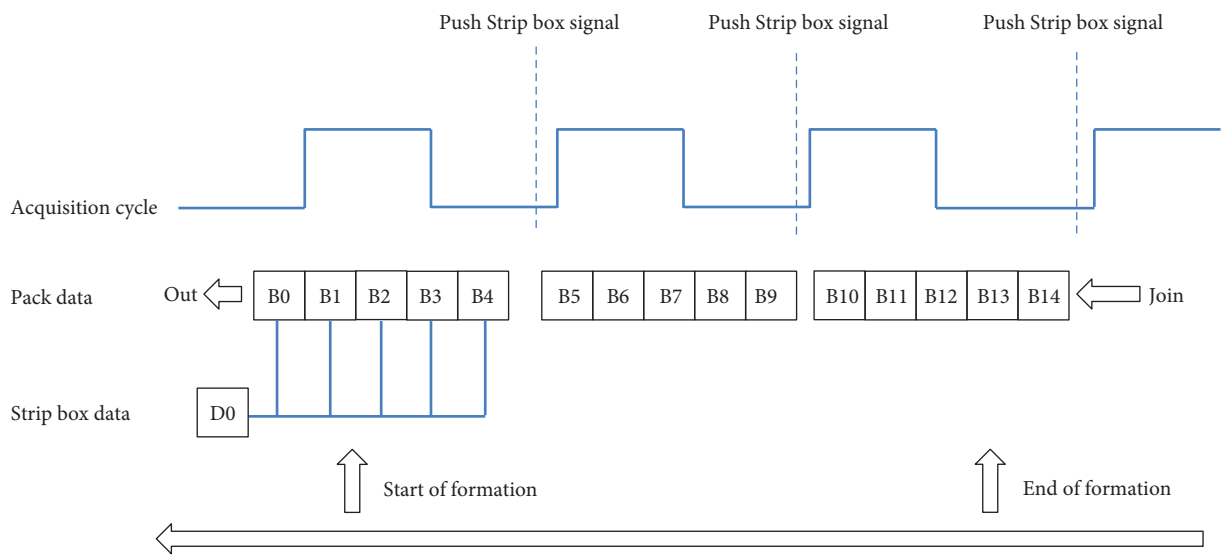

Figure 8: Locket queue data.

```
if(q -> rear = Max size – 1)//Judgment is full
Pull_I/O -> read_DI0; //Read the push bar signal;
q -> front++; //out of the team
num = q -> data[q -> front];
}
```

There will be delays in data transmission, frame loss of serial data, and irregular initialization of the system when the production is carried out. The validity of the data association cannot be guaranteed by anything other than the queue relationship. The small box in the machine's peripheral rhythm takes data, and the program encodes it into a queue. The machine's peripheral rhythm is moving. The reading of the push bar signal is interpreted as a signal, and the gathered data of the current packaging box is dequeued. Additionally, the cached data from the small box queue is dequeued, and the two processes combine to form a data binding relationship.

Small box dequeue data basis: icount = N-(buffer-BarCode num).

icount: the number of small boxes associated; N: the number of packages; the number of buffer queue caches; BarCode num: the number of reading small packages.

When the QR code data is not parsed by the reader or the data is not received during the software cycle, the software polls the GPIO signal of the lower computer. When the software reads the I/O signal, it avoids the accumulation of errors, and the software automatically fills in the occupancy data. At the same time, the abnormal signal is output to the main control board, and the main control board controls the output of the alarm device or rejection. If the received collected data exceeds the number of queue buffers and cannot match the I/O signal pulse count, the software will reinitialize the data and redetermine the pairing and data association [23].

4.3. Data Association Check. After the data is associated, the software outputs the JSON file in a certain format. It includes date, shift, machine, small box QR code data, and bar box QR code data. According to the running time or the number of data associations, the output JSON file is made.

Tobacco bar samples are collected manually to test the correctness of the association between the QR code data of the small box and the QR code data of the box [24, 25].

5. Conclusion

The GD machine packaging machine is equipped with a two-dimensional code detection and association system, which enables the data association of a two-dimensional code between a small box and a bar box. This is made possible by the GD machine packaging machine. According to the findings, the recognition rate of a code reading can get up to 99 percent, the accuracy of data association can get up to 99.5 percent, and the feedback effect is satisfactory. At a later stage, further optimization designs might be applied in order to achieve a higher recognition rate.

Data Availability

The data used to support the findings of this study are included within the article.

Conflicts of Interest

The authors declare that they have no conflicts of interest.

Acknowledgments

This work was supported by the Science and Technology project of the China Tobacco Guangxi Industrial Co., Ltd., "Research on Key Technology of Cigarette Packet Condition Associated Acquisition Equipment Adapted to Multiple Production Lines" (GXZYCX2019E006).

References

[1] G. P. Neupane, T. Yildirim, L. Zhang, and Y. Lu, "Retracted: emerging 2D MXene/organic heterostructures for future nanodevices," *Advanced Functional Materials*, vol. 30, no. 52, Article ID 2005238, 2020.

[2] W. Nong, H. Liang, S. Qin, Y. Li, and C. Wang, "Computational design of two-dimensional boron-containing compounds as efficient metal-free electrocatalysts toward nitrogen reduction independent of heteroatom doping," *ACS Applied Materials & Interfaces*, vol. 12, no. 45, pp. 50505–50515, 2020.

[3] C. J. Zhang, Y. Ma, X. Zhang et al., "Two-dimensional transition metal carbides and nitrides (MXenes): synthesis, properties, and electrochemical energy storage applications," *Energy & Environmental Materials*, vol. 3, no. 1, pp. 29–55, 2020.

[4] U. T. Lieu and N. Yoshinaga, "Inverse design of two-dimensional structure by self-assembly of patchy particles," *The Journal of Chemical Physics*, vol. 156, no. 5, Article ID 054901, 2022.

[5] Q. Zhou, S. Lu, Y. Wu, and J. Wang, "Property-oriented material design based on a data-driven machine learning technique," *The Journal of Physical Chemistry Letters*, vol. 11, no. 10, pp. 3920–3927, 2020.

[6] T. Takayanagi, T. Ueno, K. Horino, A. Ono, K. Yamamoto, and M. Kinsho, "Comparative studies of three-dimensional analysis and measurement for establishing pulse electromagnet design," *IEEE Transactions on Applied Superconductivity*, vol. 30, no. 4, pp. 1–5, 2020.

[7] R. Rajabi, H. Minoonejad, M. E. Varkiani, and M. H. Alizadeh, "360 the design and implementation of sport injury surveillance system," *British Journal of Sports Medicine*, vol. 54, no. Suppl 1, p. A147, 2020.

[8] S. K. Lee, M. Beltempo, D. D. Mcmillan et al., "Outcomes and care practices for preterm infants born at less than 33 weeks' gestation: a quality-improvement study," *Canadian Medical Association Journal*, vol. 192, no. 4, pp. E81–E91, 2020.

[9] K. C. Vranas, A. L. Lin, D. Zive et al., "The association of physician orders for life-sustaining treatment with intensity of treatment among patients presenting to the emergency department," *Annals of Emergency Medicine*, vol. 75, no. 2, pp. 171–180, 2020.

[10] H. Zhang, H. Zhang, L. Zhang, and Y. Wu, "Fastudp: a highly scalable user-level udp framework in multi-core systems for fast packet i/o," *The Journal of Supercomputing*, vol. 77, no. 5, pp. 5148–5175, 2020.

[11] Z. Lu, Y. Lu, C. Q. Li, and P. Zhou, "Construction of a two-dimensional-vwooc based on time domain/frequency domain optical cdma system," *Optoelectronics Letters*, vol. 16, no. 5, pp. 384–389, 2020.

[12] I. Ahmad, I. Shahid, A. Ali, L. Gao, and J. Cai, "Electronic, mechanical, optical and photocatalytic properties of two-dimensional Janus XGaInY (X, Y;= S, Se and Te) monolayers," *RSC Advances*, vol. 11, no. 28, pp. 17230–17239, 2021.

[13] A. E. Hassan, J. Wise, E. M. Burke, and W. G. Tekle, "Visualization of flow diverter stent wall apposition during intracranial aneurysm treatment using a virtually diluted cone beam ct technique (vessel assist)," *Neuroradiology*, vol. 63, no. 1, pp. 125–131, 2021.

[14] T. Chantakit, C. Buajong, and C. Warisarn, "Long-short term memory-based application on adaptive cross-platform decoder for bit patterned magnetic recording," *IEEE Access*, vol. 8, no. 99, pp. 155248–155259, 2020.

[15] D. Parashar and D. K. Agrawal, "Automatic classification of glaucoma stages using two-dimensional tensor empirical wavelet transform," *IEEE Signal Processing Letters*, vol. 28, pp. 66–70, 2021.

[16] C. Liu, "Visualizing logical correlation in trace data for system debugging," *Computer*, vol. 54, no. 3, pp. 28–36, 2021.

[17] J. Chen, I. Tavakkolnia, C. Chen, Z. Wang, and H. Haas, "The movement-rotation (mr) correlation function and coherence distance of vlc channels," *Journal of Lightwave Technology*, vol. 38, no. 24, pp. 6759–6770, 2020.

[18] F. Song, Y. Chen, and P. Lai, "Conditional distance correlation screening for sparse ultrahigh-dimensional models," *Applied Mathematical Modelling*, vol. 81, pp. 232–252, 2020.

[19] S. Fauser, E. Trushin, C. Neiss, and A. Görling, "Chemical accuracy with σ-functionals for the Kohn–Sham correlation energy optimized for different input orbitals and eigenvalues," *The Journal of Chemical Physics*, vol. 155, no. 13, Article ID 134111, 2021.

[20] R. H. Dong, X. Y. Li, Q. Y. Zhang, and H. Yuan, "Network intrusion detection model based on multivariate correlation analysis – long short-time memory network," *IET Information Security*, vol. 14, no. 2, pp. 166–174, 2020.

[21] L. Peng, G. Jing, Z. Luo, X. Yuan, Y. Wang, and B. Zhang, "Temperature and strain correlation of bridge parallel structure based on vibrating wire strain sensor," *Sensors*, vol. 20, no. 3, p. 658, 2020.

[22] J. Xu, W. Wu, K. Wang, and G. Li, "C-vine pair copula based wind power correlation modelling in probabilistic small signal stability analysis," *IEEE/CAA Journal of Automatica Sinica*, vol. 7, no. 4, pp. 1154–1160, 2020.

[23] A. Maan, E. Ostrowski, R. Kaita et al., "Plasma facing component characterization and correlation with plasma conditions in lithium tokamak experiment-β," *IEEE Transactions on Plasma Science*, vol. 48, no. 6, pp. 1463–1467, 2020.

[24] I. Tada, R. Chaleckis, H. Tsugawa et al., "Correlation-based deconvolution (CorrDec) to generate high-quality MS2 spectra from data-independent acquisition in multisample studies," *Analytical Chemistry*, vol. 92, no. 16, pp. 11310–11317, 2020.

[25] P. J. Smith, A. S. Lawless, and N. K. Nichols, "The role of cross-domain error correlations in strongly coupled 4d-var atmosphere-ocean data assimilation," *Quarterly Journal of the Royal Meteorological Society*, vol. 146, no. 730, pp. 2450–2465, 2020.

Hindawi
Mobile Information Systems
Volume 2022, Article ID 9270271, 12 pages
https://doi.org/10.1155/2022/9270271

Review Article

Wireless Multifunctional Display Platform for Visual Communication Design Based on IoT Big Data

Baoqing Wang

ZWU Faculty of Design and Architecture, Zhejiang Wanli University, Ningbo 315100, Zhejiang, China

Correspondence should be addressed to Baoqing Wang; wangbaoqing@zwu.edu.cn

Received 12 August 2022; Revised 12 September 2022; Accepted 16 September 2022; Published 30 September 2022

Academic Editor: Chi Lin

An important role of display visual design is advertising and advertising communication, which is an integrated medium, that is, a medium for communicating information. Visual communication design is the most direct way of information transmission in modern society. In today's increasingly complex and diversified information, visual communication design has been more and more widely used in terms of form and function. On the display platform, the use of visual elements and the expression of visual communication design allows us to examine the different spatial experiences that visual communication design brings to people from a new perspective and adjust the way it is communicated, so as to find a scientific expression. This paper focused on the role of visual communication in display design and discussed its specific application in display design. The use of visual elements in the display space provides a new visual platform for spatial information, making the space design more connotative and cultural. For the smooth experience of media fusion design, it is necessary to ensure that information can be transmitted quickly and smoothly in every link of its processing. In the data write throughput experiment of the microperceptual data layer, the maximum write speed increased by 85.2% compared with the direct write method using the TSBPS method. The findings demonstrated that the IOT-HSQM model's strategy of first queuing and then segmentation writes may more effectively fulfill the demands of high bandwidth than straight data transmission to HDFS (Hadoop Distributed File System).

1. Introduction

The Internet of things (IoT) refers to the use of various proprietary networks such as communication networks, sensor networks, and industry-specific networks to connect people with people, people with things, and things with things, so as to achieve the purpose of information exchange. To improve the portability, connectivity, and accessibility of the Internet of things, the World Wide Web Consortium (W3C) created a group of specifications described as the Web of Things (WoT). In order to facilitate compatibility between IoT systems and software categories, the W3C Web of Things (WoT) was created. The WoT's overarching objective is to maintain and enhance current IoT protocols and technologies. The Web of Everything is the next wave of computer intelligence, and it is another revolution in the information industry after computers and modern communications. Transfer of data has become quicker, cheaper, simpler, and greater effective thanks to modern technology. One should not forget about cybercrime and the dangers they pose to our well-being. Visual design has become an important element for people to recognize, appreciate, and realize their own needs. Utilizing the fundamentals of effective graphic arts in images may boost accessibility and enhance learning. The concepts of production appearance explain how components such as contour, structure, color, grid, and area combine to produce well-rounded and meaningful graphics. Particularly, in today's era of rapid development of interaction design, designers need to achieve a harmonious "realm" between people to meet people's growing visual needs. People are no longer satisfied with the visual effects displayed by plane images, and the visual design of realistic, three-dimensional, interactive, experiential, and human-computer interaction is more in line with the needs of the times. The existence, development, and basic principles of visual space are of great significance to the current and future visual communication design.

The show system's pictorial structure should be contemporary. The upgradation has significantly improved the quality of life for humans. The quality of life for most people has been significantly improved by the integration of science, technologies, and market mechanisms. Using simulators as a foundation, online advertising seeks a fusion of "virtual" and "real." Network virtual display advertising is a new type of visual communication, and its development has brought it to a new level. Wu conducted an in-depth discussion on the characteristics of online advertising and virtual display, analysed its design elements, and summarized its characteristics and laws. The research has certain practical significance, which can provide new ideas for the development of virtual advertising in the future, and add new vitality to the harmonious e-commerce era [1]. The role of British graphic designers and authors in the international dissemination of "Swiss style," "Swiss graphic design," or "Swiss typography" is obvious, but little is known about the process and effects of cross-border communication of design. Lzicar followed the trajectory of objects and texts, revealing how they created and disseminated labels in the UK and abroad, thereby contributing to the current understanding of "Swiss graphic design." Its conclusion was an example of an alternative historiography of modern visual communication as an ongoing process of communication that revealed the complex international interactions of design discourse [2]. As modern scientific techniques develop incessantly, the industry of media of advertising has experienced enormous changes, and the forms of traditional printing have been transformed into digital printing gradually. Different from conventional ones, digital advertising has greater flexibility and can be created in different forms according to the feature of the product itself. In addition, visual communicative design also plays a crucial role, and it is an essential way to strengthen digital commercials. Consequently, it is imperative to optimize the visual communication design to improve the quality of digital advertising. To further advance the growth of the commercial digital economy, Li undertook an extensive investigation and examination of both the graphical development of embedded news in Google AdWords [3]. Manufacturers can produce more inspiration and increase the author's capacity for invention in order to enhance the present computer image technology of image processing. Fan and Li used data in the area of aesthetic and partner services as the focus of their study. He looked into the significance of visual effects becoming a cost-effective and efficient way to transmit real info to the design of mobile media interface through the clarification of graphic data to develop, the technical implementation, and the investigation of clinical science, linguistics, and other concepts that are relevant to digital editing data visualization. In 2022, the field for feature extraction and illustrations will grow to 755.5 million yuan in size. It is certain that, as a future evolvement, the broadcast technique of material and picture fusion will also be used in more domains and play a bigger role [4].

In the near future, self-driving cars are an emerging technology to provide a safe and efficient transportation experience. Driverless cars must have in-vehicle channels to wirelessly share road markings. Current new networks are initially demonstrating their limitations due to the explosive growth of traffic patterns. Kong et al. talked about narrowband technology's potential for use with driverless vehicles. With its number of cosignal strength and channel estimation technologies, mmWave is the next level of wireless technology. Based on these traits, a unique architecture for a vehicle mmWave system is devised that incorporates the benefits of the cloud and IoT. Radar systems that operate at millimetre waves (mmWave) send and collect incident radiation impulses. A radar system can identify the proximity to objects, their solution that can be applied, and their arrival angle by analysing the duration of passage of such radiation impulses through a number of frequencies. Through cloud computing, this underwater acoustic technology enables vehicles to distribute a number of codata about their environment and recognize things in real time. As a result, robot cars can decide on the best driving approach right away [5, 6]. Saxena studied and showed that banks in Oman can use big data analytics and IoT technologies to help them "predict" and "predict now" what it means and can better manage their customers by improving and making their services more efficient. Stergiou combined mobile cloud computing and IoT with big data technologies to study their common features and discover which of the advantages can improve the application of big data. Finally, the respective contributions of mobile cloud computing and IoT to big data technologies are presented [7].

These approaches provided some references for study, but this research has not been recognized by the general population due to the short duration of the related research and the small sample size.

This paper conducted an experiment of microperception data layer data write throughput, and found that the maximum write speed of the TSBPS method increased by 85.2% and the average write speed increased by 41.2%. HDFS write operations can better meet the requirements of high throughput. The data generated by a SensorId in a certain period of time were queried in the HDFS sensor data directory, and it was found that in a 10-minute period, the index-based query time was 7.2 times that of an index-free query. The data locations of different states in a certain period of time on HBase were queried, and it was found that the query based on the cached index is better than the query without the cached index. In the 80 min time period, the query time was 1.88 times that of the uncached. It was verified that the index server caches the index data in the model to improve the query, the hit rate of different strategies with different cache capacity ratios was explored, and it was found that when the cache capacity accounted for 20% of the total data, the HRPB cache hit rate increased by about 30% compared with the LRU cache hit rate.

The rest of the structure is organized as follows: Section 2 presents the method of wireless multifunctional display platform for visual communication design; Section 3 illustrates the experimental design of wireless multifunctional display platform based on IoT big data; Section 4 depicts the data of wireless multifunctional display; and finally, Section 5 concludes the study.

2. Method of Wireless Multifunctional Display Platform for Visual Communication Design Based on IoT Big Data

Vision is the most developed and most important of human functions, and it is superior to other senses. In daily life, the environment is observed through our eyes, and our eyes are used to identify things to obtain information [8]. Words, graphics, and images are settled on the retina through the eyeball so that they can be perceived, which is related to the constancy and attraction of vision. The advantages of big data are as follows: it provides instantaneous reaction and improves a deeper comprehension of information; trends are discovered at a large scale; it detects faults and measures risk; better items and services are created; it provides direct power and surveillance, etc.

The constancy of vision means that our eyes have formed a fixed concept in the long-term cognition. Regardless of whether the distance has changed or the viewing angle has changed, it will be regarded as an eternal thing. In visual constancy, the eyeball is also subject to a series of constancy, such as size, color, and shape constancy [9].

When it comes to visual communication, some flat graphics, symbols, etc., will come to mind. If the literal meaning of the word "visual communication" is understood, it is difficult to give a clear definition, because the scope of visual communication is too wide. Everything that can be seen contains more or less elements of visual communication [10].

With the development of the times and people's in-depth research on visual communication, the most basic elements of visual communication are given academically, namely, "vision" and "communication" [11]. "Vision," as the name suggests, refers to the images that the eyes can see, such as text, pictures, videos, buildings, abstract light, shadow, electro-optic symbols, and music symbols. "Communication" refers to the process of transmitting information from one party to another. This process can be either within the individual or between the individual and the outside world, such as the information transmission within the human body, between people, and between people and the natural environment [12]. In short, when people see something and react to it and get some information from it, this is the most basic visual communication.

Eye imaging is a very complex process. The physician can now discover indications of eye diseases that were previously undetectable thanks to imaging technology. Retinal imaging can be used to identify eye disorders including diabetic retinopathy, hypertension, age-related vision problems, and damaged optic. Each of these eye conditions requires prompt professional attention to avoid loss of vision. After the light refracted by the object itself enters the eyeball, the pupil starts to adjust its size according to the information of the incoming light, and the lens judges the distance and adjusts the focal length according to the information transmitted by the object, forming an object image on the retina. The retina's important transmission units are ganglion cells. At the eye region, wherein their neurons congregate, the olfactory nerves are formed through myelination. Streams of peaks, sometimes referred to as nerve impulses or input features, are used to encrypt their information because it must travel a great distance. A chemical process considered a photochemical reaction is one that is started by the sunlight's energy being absorbed. As a result of atoms collecting sunlight, transitory stimulated phases are produced, which have very different biochemical and physiological characteristics from the initial atoms. After rods and cones receive information, they undergo photochemical reactions to generate bioelectricity, which makes nerve cells generate impulses, which are then transmitted to the cerebral cortex through the bilevel cell layer and ganglion cell layer to form a visual image (Figure 1) [13].

By understanding the complex mechanisms of eye imaging, causes of dilated pupils and how the eye works will be understood. The causes of dilated pupils are using drugs recreationally, head trauma, tumescence of sexuality, vision test, epinephrine, etc. Some people are insensitive to certain colors because of the lack of several color-sensing cone cells in the retina [14]. When two eyes of a person look at an object at the same time, the spatial position of the object can be obtained from the visual information. It is very helpful to understand the visual elements and display the modeling language of spatial art by understanding the formation mechanism of human vision.

Visual communication design is the use of visual symbols by designers for various forms of design. The designer is the person who transmits the information, and the transmitter is the person who receives the information [15]. "Looking" is a form of communication between people in visual communication design. People who come from different countries, different fields, and languages can communicate culturally and emotionally through visual communication. "Visual symbol" and "communication" are two basic concepts, and "visual symbol" is the visual organ, that is, what people see through vision. Books, posters, architecture, and movies can be used as a visual symbol here. The fact that symbolism is mostly ubiquitous, recognized, and acknowledged on a global scale makes it crucial in visual language. Because of this, many symbol and icon concepts are meaningful. Symbols are used in various types of vector illustrations as well, including advertising, posters, and webpages, to guide people and convey information. "Conveying" refers to the use of symbols by the sender of information to convey the information to the receiver [16]. Individual-to-individual communication is expressed in visual form. As a branch of design, visual communication design, the basic principles of design must be mastered by every well-educated visual designer, namely, plane composition, color composition, and three-dimensional composition [17]. As an important component in the field of visual communication, visual communication design elements have been developed from two-dimensional space form to three-dimensional or even four-dimensional wireless space environmental design, and its principles and methods are constantly changing and expanding in practical applications [18]. The design flow chart is shown in Figure 2.

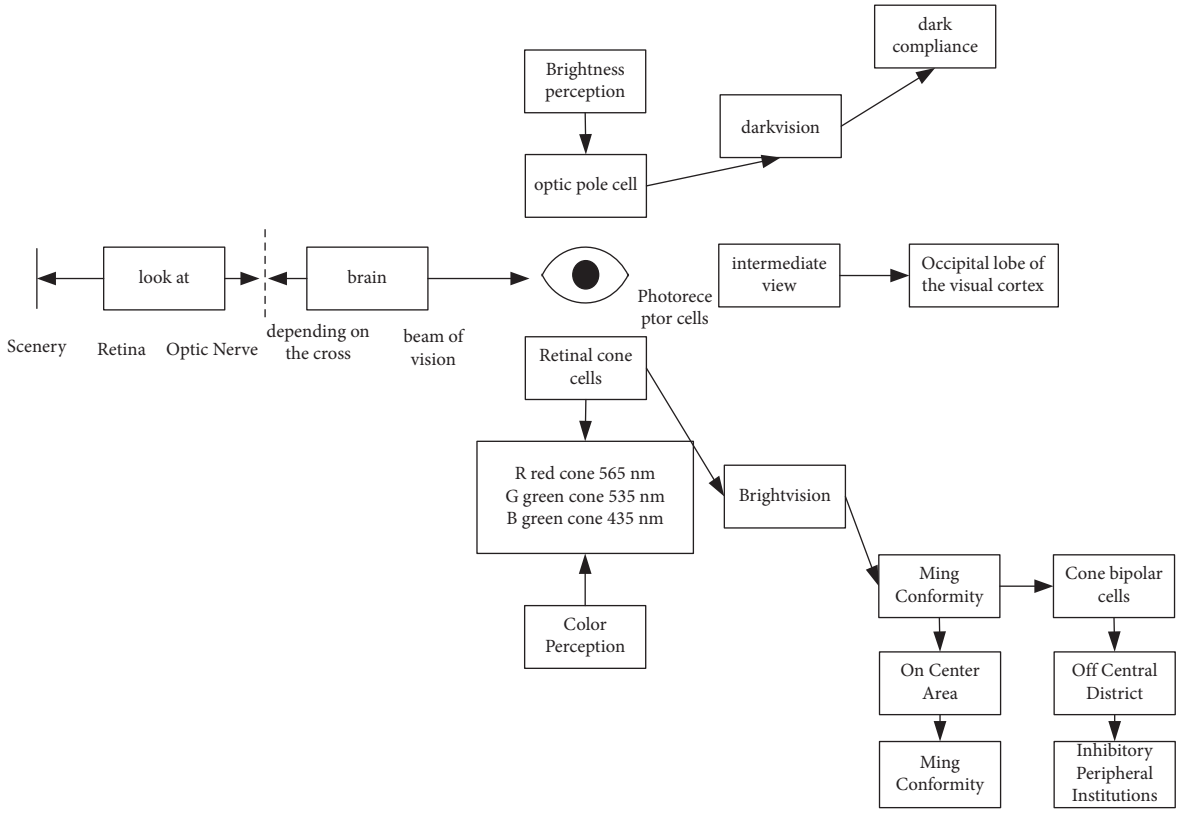

Figure 1: Schematic diagram of the function of the optic nervous system.

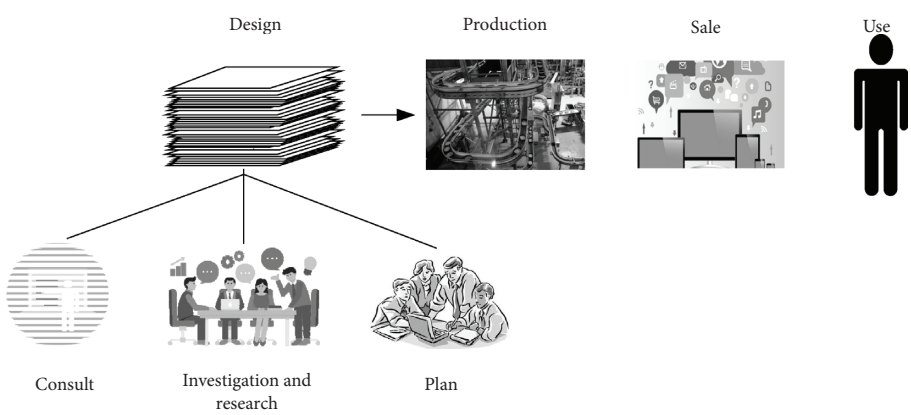

Figure 2: Design flow chart.

Wireless multifunctional display refers to the unlimited transmission of information to people in a limited space. Its communication language has the characteristics of representativeness of the times, communication efficiency, persuasion, etc. It has strong memory and far-reaching influence [19]. With the advancement of science and technology, many industries have been successfully applied to their respective fields and achieved good results. On the display platform, due to the constraints of various objective factors, such as various functions, the development of IoT technology in this field is slow, as shown in Figure 3 [20].

Individuals can preserve aids in identifying, information, and programmes in nonpersistent VDI systems using user layers, which are levels that are viscoelastic provided. The common communicating techniques and interface techniques utilized by guests in a network infrastructure are specified at the protocol stack, which is an intermediate level. Application logic and regulations are upheld by the client side. The user experience and associated presenting software are stored in the presentation layer. The transport layer offers dependable data transmission services to the surface layer by facilitating explicit transmission of data among end customers. By control valves, categorization and lack of discipline, and error management, the transportation layer manages the dependability of a direct source. A sensing layer denotes a certain data kind that originates from a specific

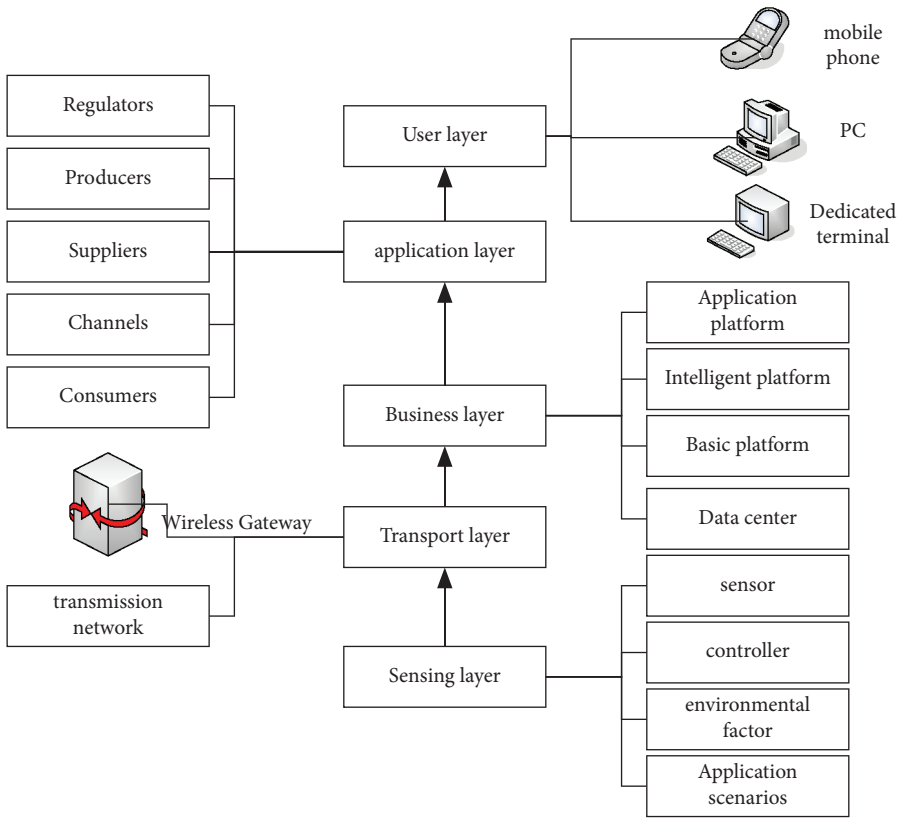

Figure 3: IoT multifunctional display application system.

information resource, including cloud services, conventional wireless sensor systems, or PSNs. The display design architecture includes the core content of the display, the communication of the display content, the interactive experience, and the environmental space. This process requires a systematic arrangement of the structure of the display content, space division, streamlined layout, prop selection, and interface settings for the platform. In this process, it is not only necessary to complete the display theme established before, but also necessary to carry out display design on this basis, and to create the atmosphere of the display space [21].

Model establishment is divided into four steps: training set calibration, shape alignment, shape and texture modeling, and appearance model establishment. In order to reduce the disparity among an occurrence of a modeling that is generated and the subject of concern in an image, active appearance models (AAMs) outline an optimizing issue. The process of locating texture boundary via background subtraction is referred as pattern segment. Whenever typical adaptive threshold approaches are ineffective because an organism's roughness rather than brightness best describes it, texture analysis might be useful.

(1) The shape model refers to the geometric information that is retained after the training samples and reflects the changing laws of the target shape. The establishment process of the shape model is divided into feature point calibration, shape alignment, and model establishment. The n marked points in the image are linearly combined, and several vertices are triangulated to obtain a $2n$-dimensional face shape model R, as shown in formula (1). Among them, (x_i, y_i) represents the coordinates of the marker point on the image.

$$R = (x_1, x_2, \cdots, x_n, y_1, y_2, \cdots, y_n)^T. \quad (1)$$

The face shape model S is calculated using the covariance formula of shape samples, as shown in the following formula:

$$r = \bar{r} + b_r p_r. \quad (2)$$

In the formula, $\bar{r}$ is the average shape obtained from the training set; p_r is the shape transformation matrix; and b_r is variable shape model parameters.

(2) Establishment of a texture model is divided into texture feature extraction and model establishment.

Extraction of texture features: the texture part uses RGB images. First, the corresponding shape model is triangulated by Delaunay, the entire texture is divided into several triangular patches to obtain the benchmark network, and then, the texture feature information is mapped to the piecewise linear affine method. In the average shape, the extraction of texture features is realized. By generating or originating additional factors, PCA uses this strategy to eliminate the extraneous characteristics that are found in the data. The underlying factors are combined linearly to form these elements. Using a minimal group of "basic indexes" that are

simpler to display and understand, PCA is an analytical package that lets you condense the data contained in huge information sets. A well-liked unsupervised learning method for lowering the dimensions of data is principal component analysis. While minimizing data redundancy, it simultaneously improves comprehensibility. It helps to make easier to display in 2D and 3D and aids in identifying the dataset's key important properties. PCA is used to reduce the texture information, and the unified standardized model g is obtained, as shown in the following formula:

$$g = \overline{g} + b_g p_g. \tag{3}$$

In the formula, g is the average texture model; p_g is the texture transformation matrix composed of PCA; and b_g is variable texture model parameters.

The appearance model is obtained by integrating the shape model and the texture model in a unified dimension. To enable quadratic transformations intelligible, eigenvectors are utilized. Eigenvectors can be compared with X-Y line charts that have been compressed or stretched without affecting their orientation. In order to better adjust the newly formed apparent model, a new apparent eigenvector b is obtained by passing b_r and b_g through a certain weight, as shown in the following formula:

$$b = \begin{pmatrix} w_r b_r \\ b_g \end{pmatrix} + \begin{pmatrix} w_r \varphi_r^T (r - \overline{r}) \\ \varphi_g^T (g - \overline{g}) \end{pmatrix}. \tag{4}$$

In the formula, w_r is the diagonal matrix to adjust the weights.

By adjusting the variable parameter p, the difference between the input image $I(x)$ and the average texture $A_0(x)$ is minimized. That is, the energy-optimized nonlinear iterative solution is obtained as shown in formula (5), and the appearance coefficient Y that minimizes the matching error is obtained to complete the model matching.

$$\operatorname{argmin}\left(\sum_{x \in R_0} \left[A_0(x) + \sum_{i=1}^{m} q_i A_i(x) - I(N(W(x;p);u)) \right]^2 \right). \tag{5}$$

Among them, $A_0(x) + \sum_{i=1}^{m} q_i A_i(x)$ (6) represents the estimated texture, $I(N(W(x;p);u))$ represents the texture obtained by mapping the input image into the average shape, and u is translation and rotation scaling parameters.

The concept of the Internet of things was originally proposed by radiofrequency identification technology (RFID), which allows everything in daily life to be connected through the Internet, thus becoming a major trend in the field of logistics. Tags and readers are the two halves of the wireless technology recognized as radiofrequency identification (RFID). The scanner is an electronic gadget including one or more transmitters that transmit electromagnetic radiation and take in information from RFID tags. The scanning distance specifications, sensing demands, pricing, shape, mass, and the nature of the application all have an impact on the choice of qualities. Reading range, length, and price are the main differences among resistive and capacitive labels. The current consumption of RFID in repositories and leveraging the information to release workers for tasks that entail greater engagement with users are two of the mankind's several benefits. With the growth of sensing technologies such as infrared, 4G, and IoT, IoT is defined as a number of networks that connect various objects to the Internet. The present "IoT architecture" normally involves three levels: sensing layer, cyber layer, and applying layer, illustrated in Figure 4.

The main sense tier is made up of sensitive instruments, such as RFID labels and cameras. Their main features are to gather and transport controlled signals. The specific implementation procedure of the perceptual layer is classified into two stages: the communication modem must be authenticated to connect to the LAN; and once the connectivity is succeeded, the perceptual layer can transmit data by the portal or accept information such as control instruction from the terminal to accomplish relative operations.

The least recently used (LRU) caching is a popular technique. Whenever the database is filled, it specifies the strategy to remove pieces in order to create a place for new ones, with the lowest frequently utilized things being removed initially. As the cache server of the meso-aware data layer, Redis itself supports the LRU cache strategy, and the expiration time can be set for the cached data. Redis will follow the volatile-lru strategy. When triggering the cache replacement strategy, Redis selected the least recent data from the expired data. The accessed data were deleted. However, the core idea of this LRU strategy is that recently accessed data have a high possibility of being accessed in the future. If the data belong to hot data for a long time, the LRU strategy is used very effectively. However, in the case of frequent queries with periodic characteristics, the hit rate will decrease, resulting in serious cache pollution.

The HRPB method proposed a way to score the cached data by weights. The weights represent the possibility of future access. Data with a larger weight are the data most likely to be reused recently, and data with a smaller weight will be preferentially replaced when the cache exceeds the threshold and new data need to be cached. When the access to the data in the cache increases, the weight of the hit data is increased. On the contrary, when the access to a certain block of data decreases, the weight of the data is decreased.

$$w = tv * k + (1 - k) * \frac{a * f}{\text{size}}. \tag{6}$$

The formula for calculating the weight in the HRPB method is shown in the above formula, which is calculated based on the predicted value of the access frequency trend, the data size, and the data validity period. In the formula, w represents the weight of the data, and tv represents the validity period of the data, as shown in formula (8); the parameter k is used to adjust the influence of the data validity period on the weight w; f is used to represent the frequency trend prediction value, as shown in formula (7); size is the size of the data occupied space; and a is an adjustable parameter to ensure the range of the weight w value.

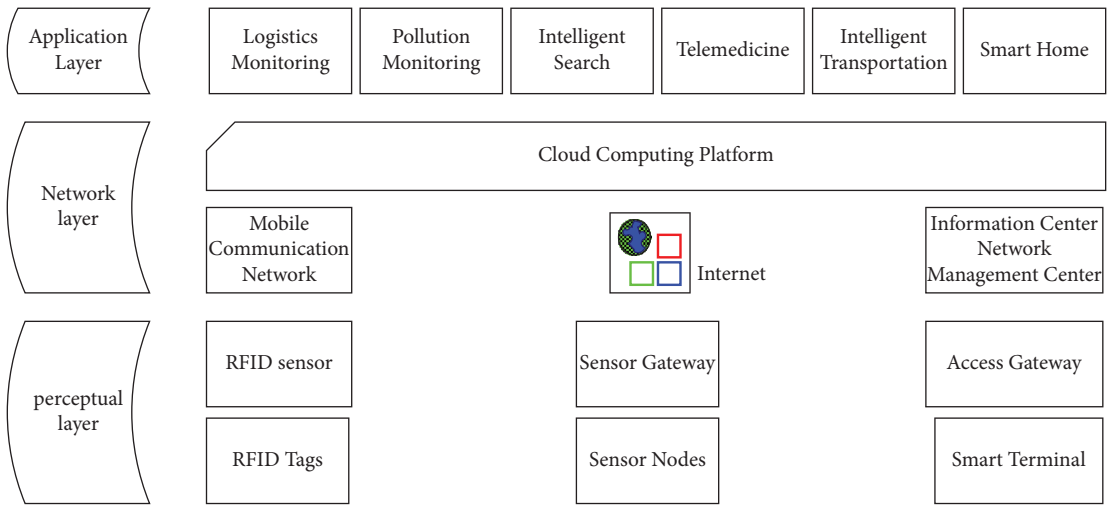

Figure 4: Schematic diagram of the IoT architecture.

$$f = \frac{\text{cout}}{tl} * (1 - h) + h * f_o. \tag{7}$$

In the above formula, tl represents the last fixed time length. The time length is configurable. cont represents the number of accesses to resources in this stage. f_o is the last access frequency value saved last time. h is an adjustable parameter, indicating the proportion of historical frequency and current frequency in the result.

$$\text{tv} = \frac{(\text{exTime} - \text{curTime})}{(\text{exTime} - \text{addTime})}. \tag{8}$$

In the above formula, exTime represents the validity period of the data, that is, the expiration time; curTime represents the current time, and addTime represents the entry time into the cache.

Spatial propagation can transform coarse depth maps into new, finer, and more accurate images. The image space propagation guided by the affinity matrix is equivalent to the standard anisotropic diffusion process. The graph's beneficial characteristics are related to the Laplacian matrix in numerous ways. It may be utilized in conjunction with Kirchhoff's theory to determine how many bridging branches there are in a directed sequence. Therefore, LG has orthogonally eigenvalues with eigenvalue nonexistent: [0 1] and [1 0], in which the directions have been divided up much like the LG grid. The transformation of the image is controlled by the Laplacian matrix, which consists of the parameters of the spatial propagation module.

X and H are denoted as two two-dimensional matrices of size $n \times n$. Among them, x_u and y_u represent their u columns, each with n elements. Using an $n \times n$ linear transformation matrix w_u, the information is linearly propagated between adjacent columns from left to right, as shown in the following formula:

$$\begin{aligned} f &= w_u h_{u-1}, \\ h_u &= (I - d_u)x_u + f, t \in [2, n]. \end{aligned} \tag{9}$$

Among them, I is an $n \times n$ identity matrix and the initial conditions are as follows:

$$h_1 = x_1, \tag{10}$$

d_u is a diagonal matrix; among them, element $d_u(i, i)$ is the sum of all elements of row i.

$$d_u(i, i) = \sum_{j=1, j \neq i}^{n} w_u(i, j). \tag{11}$$

The matrix H is updated recursively in a columnwise fashion. For each column, h_u is a linearly weighted combination of the previous column h_{u-1} and the corresponding column x_u in X.

When the whole recursive process is completed, the updated H can be expressed as follows:

$$\begin{aligned} H_d &= \begin{bmatrix} I & 0 & \cdots & \cdots & 0 \\ w_2 & \alpha_2 & 0 & \cdots & \cdots \\ w_3 w_2 & w_3 \alpha_2 & \alpha_3 & 0 & \cdots \\ \cdots & \cdots & \cdots & \cdots & \cdots \\ \cdots & \cdots & \cdots & \cdots & \alpha_n \end{bmatrix}. \\ X_d &= G X_d \end{aligned} \tag{12}$$

Among them, G is a $n^2 \times n^2$-dimensional lower triangular matrix, and H_d and X_d are the vectorized X and H. α_u, w_u, d_u, and I are all $n \times n$-dimensional submatrices; among them,

$$\alpha_u = I - d_u. \tag{13}$$

The transformation process represented by formula (12) can be expressed as a spatially anisotropic diffusion process, and the propagation matrix is the affinity matrix composed of all w_u.

IoT sensing data are the data generated by IoT sensors. The sensor data generation cycle is short, and a large amount of data are transmitted to the data center in real time. The IoT perception data include spatiotemporal data and attribute data. The spatiotemporal data are used to describe the time information and location information of the sensor. Attribute data are used to describe the current state of the

sensor. A large amount of dense IoT sensor data are continuously transmitted to the data center. Since each piece of sensor data is small data, if these data are written in pieces, the number of HDFS files opened at the same time is limited, and the file connection is continuously opened and closed, which slows down the writing speed. Because the order in which the perceived data arrive is not strictly chronological, the written data will be stored out of order in the file. Therefore, the data should be preprocessed and the directory structure of the HDFS file should be designed.

Since the queries related to the Internet of things are often related to space and time, the HDFS directory structure based on space and time characteristics is designed in the IOT-HSQM system model, and the TSBPS writing method is used to preprocess the data. The specific process is described as follows:

(1) The received sensory data by space-time blocks, and the data according to the space-time block classification numbers are classified

(2) The classified original sensory data in combination with the space-time block where it is located and the characteristics of the dataset itself are compressed and cached

(3) When the data cached in the space-time block meet the write data volume threshold and duration threshold, the content of the space-time block is written out to the corresponding HDFS file

Data are obtained from the upper layers and subsequently communicated to other systems at the protocol stack, where this function is most important. It also immediately sends to the user devices at the same time. One way is that the node changes the format of the data gathered first from network layers so that it may be transmitted easily over the World Wide Web, and 2G, 3G, and 4G networks, among others. Additionally, it is organized after being collected from other connections and given back towards the network layers. The transceiver, broad connection, GPRS, MH network, ZigBee, Gigabit, and other technologies make up the majority of the network layer. In order to combine with the existing system and big data environment, this paper proposed a cloud computing model deployment scheme based on cloud computing, as shown in Figure 5.

Remote Dictionary Server is abbreviated as Redis. It is a storage solution that operates by collecting information in a critical data format for short-term storage. Since it is supported by practically all common computing platforms, Redis cache is well-liked. The web browser delivers queries towards the WebSEAL centralized server, where it then communicates with the Redis host to handle sessions in a Redis transaction caching scenario. After receiving the original sensory data in the Redis cache, the sensory data are cleaned asynchronously, and the data items that may be used by the upper-layer application are retained, and converted into a format that is convenient for processing. The cleaned microscopic sensory data are called valid data. After accumulating a certain amount of data in the Redis cluster, these data are written out to HBase in batches. Column-oriented, nonrelational databases such as HBase are common. This indicates that information is organized into categorical variables and referenced using a special column keyword. Using this design, it is possible to efficiently scan through specific fields in a database and quickly get certain rows or columns. Since HBase searches on the row key most efficiently, the row key for storing awareness data should be reasonably designed, and relevant auxiliary indexes should be established.

The broadband connection acts as a transmitter and the receiver function to the application layer. These data are transferred into CVS services and XInsight-PDS, which are further divided into three different protocols, namely, industrial control communication protocol 1, industrial control communication protocol 2, and industrial control communication protocol 3. The application tier is a collection terminal for data. The application layer gathers sensor data first, then carries out memory, analysis, and computation to deliver particular kinds of services to users. Or in a specific case, in order to meet the corresponding control requirements, the actual control command is transmitted to the object of the perception layer.

3. Experimental Design of Wireless Multifunctional Display Platform Based on IoT Big Data

This data cloud platform provides data management services for massive sensor devices, realizes the collection, identification, storage, and display of sensor device resources, and ultimately achieves the goal of providing stable and efficient sensor data management services. The benefits of the cloud platform are durability, reduction in the IT system management and upkeep costs, cooperation effectiveness, lower IT expenses, and accessibility to automated upgrades, which are all desirable qualities. The relevant basic functions of the IoT data cloud platform design are shown in Figure 6.

The sensor device collects data and uploads it to the data management server through the data interface. The user can view the data information of the corresponding sensor device through the client. The functions of the entire cloud platform include four parts: user management function, sensor management function, sensor data query function (chart display), and setting management:

(1) User management function: the data cloud platform provides sensor data management services for multiple different roles independently, and needs to save the basic information of the user, including the user's permission information, registration information, and description information. In the process of data processing, storage, and viewing, it is necessary to distinguish according to the corresponding permissions of users.

(2) Sensor management function: sensor management is the basic function of the data cloud platform. Different types of sensors, including their geographic

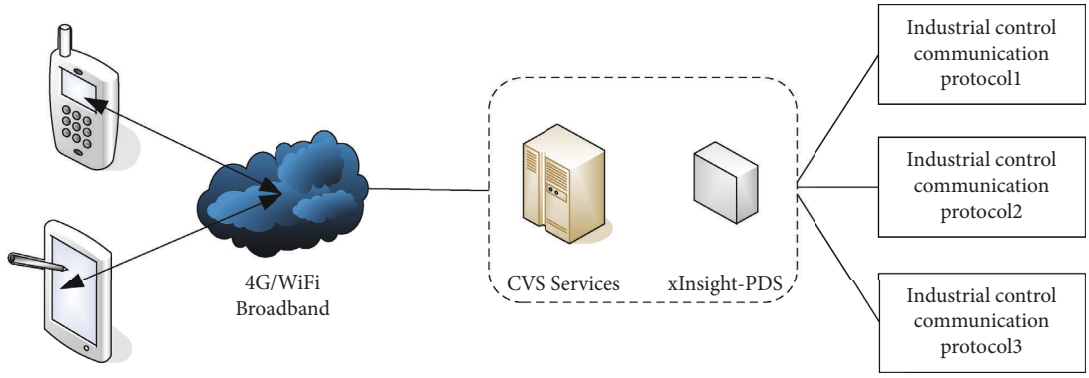

Figure 5: Cloud mode deployment.

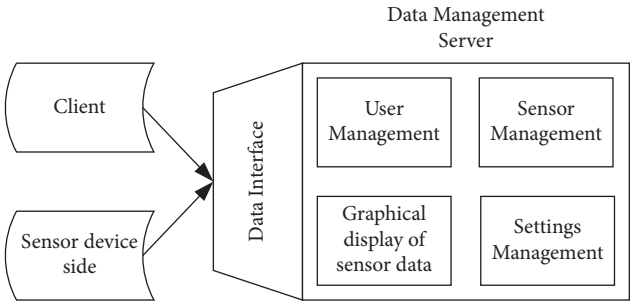

Figure 6: Cloud platform system functional design module diagram.

location information, sensor description information, and sensor status information, are stored in the database. Some of these data are classified according to user permissions, some are shared information, and different sensor gateways and users need to be stored separately. The system can collect data through sensors, and then, users can add, delete, modify, and query the data through the database.

(3) Sensor data query function: the data of the data cloud platform are open to accounts with different permissions. These accounts can view the basic information and data collection information of various types of sensors in the form of chart display through the client according to their respective permissions, and it is necessary to provide them with a unified data interface API.

(4) Setting management function: this module can set the user's personal information under this account, such as changing the password and user name.

The experimental environment is a cluster composed of 6 servers. The CPU, memory, and hard disk size of the 4 machines are shown in Tables 1 and 2, and the experimental data are shown in Table 3.

4. Data of Wireless Multifunctional Display Platform Based on IoT Big Data

For the experiment of microperceived data layer data writing throughput, different amounts of data are taken out for writing experiments. For writing, HDFS makes use of the catalog hierarchy and filename approach of the IOT-HSQM model. The average data writing speed and the maximum data writing speed between directly storing data in HDFS and the method of first caching and then clustering write based on space-time blocks are compared. In order to ensure the accuracy of the test results, most of the original sensory data are cached in the memory in advance, and when writing out, the occurrence time of the data is modified in advance to the current time. Figure 7 is a comparison chart of writing speed.

Table 1: Hardware and software information.

Name	Value
CPU	Intel (R) Core (TM) i5-3470
Memory	8 GB
Operating system	Windows 7
Available hard drive capacity	120 GB
Network	50 M
—	—

It is clear from Figure 7 that the written speed increases by 85.2% for the maximum write speed and 41.2% for the average write speed compared with the direct write method. The write speed of the TSBPS methodology is significantly better than the direct write speed. Consequently, the method of caching first and then writing in clusters in the sample model can fulfill the demand of high capacity better than direct writing to HDFS.

Query 1: The data generated by a SensorId in a certain period of time in the HDFS sensor data directory are queried. The results are shown in Figure 8.

As can be seen from Figure 8, the index-based HDFS query is significantly better than the nonindexed HDFS query. In the 10 min time period, the index-based query time is 7.2 times that of the nonindexed query.

Query 2: The data location of different states in a certain period of time on HBase is queried. The results are shown in Figure 9.

According to the comparison chart of the experimental results, it can be seen that the query based on the index is obviously better than the query without the index, and the query based on the cached index is better than the query without the cached index. In the 80 min time period, the query time is 1.88

Table 2: Server configuration information.

Serial number	1	2	3	4
Server address	172.21.20.147	172.21.20.10	172.21.20.107	172.21.20.111
Name	Node1	Node2	Node3	Node4
CPU (s)	8	8	8	8
Total hard disk memory	1.8 T	1.8 T	1.8 T	1.8 T

Table 3: Experimental data.

Serial number	1	2
Data volume	10000 MB	5000 MB
Serial number	3	4
Data volume	10000 MB	5000 MB

times that of no cache. It is verified that the index server caches the index data in the model to improve the query.

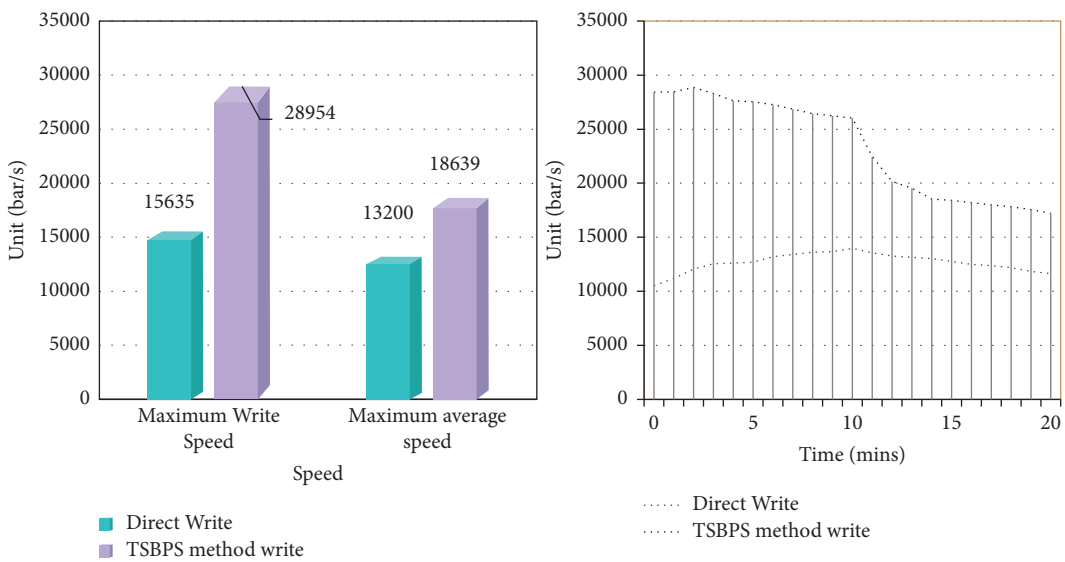

Figure 7: Comparison chart of write speed.

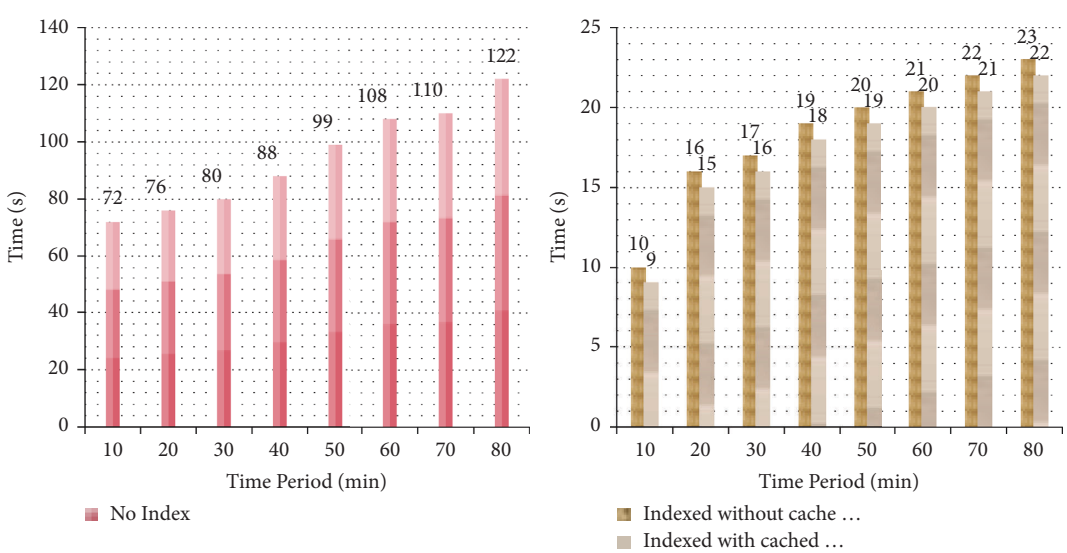

Figure 8: Comparison chart of HDFS query experimental results.

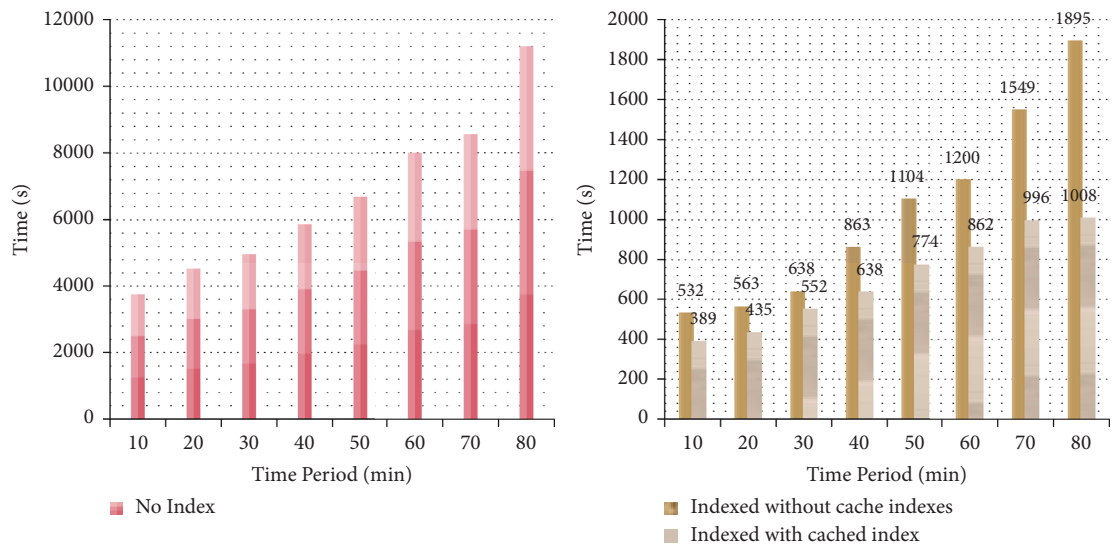

Figure 9: Comparison chart of HBase query experimental results.

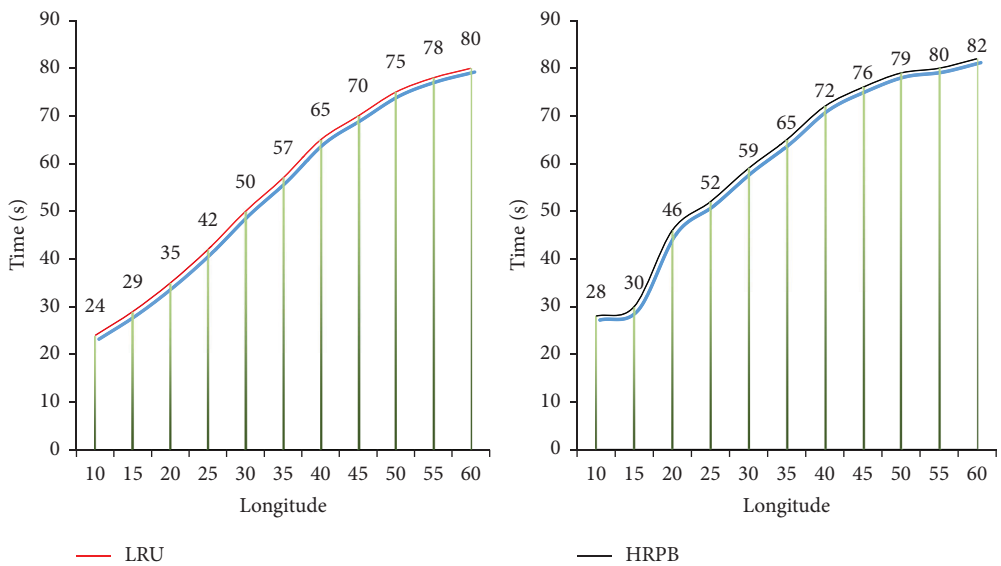

Figure 10: Cache hit ratio comparison chart.

According to the size of the experimental data, the Redis cache size to 30%–70% of the total data volume is set, and the hit rates of different strategies with different cache capacity ratios are recorded. The experimental results are shown in Figure 10.

As can be seen from Figure 10, the HRPB cache replacement strategy has a significantly higher cache hit rate than the LRU replacement strategy. The smaller the cache capacity, the greater the difference in the hit rate between the two strategies. When the cache capacity accounts for 20% of the total data, the HRPB cache hit rate is about 30% higher than the LRU cache hit rate.

5. Conclusion

There are many types of IoT sensing data, and the data with mobile sensors and the sensor data with fixed positions are distinguished by whether the sensor position moves. Aiming at the high-throughput capacity and efficient query and statistical analysis requirements of massive data in the Internet of things, a large-scale data storage and query model IOT-HSQM based on the perception of the Internet of things was proposed to achieve efficient retrieval purposes. With the development of the economy and the frequent foreign trade exchanges, more and more traditional enterprises have become aware of the crisis and realize that the future development trend is bound to be the rapid development of network coverage and globalization, which needs to be combined with the big data technology of the Internet of things. This is not only to promote their own products, but more importantly to display and disseminate culture. Users can understand the functions of the multifunctional display platform through interaction, breaking the traditional display effect of a single picture and text. In the era of the

Internet of things, visual communication design has been carried out from a single medium, and more and more attention is paid to the use of various media in design. The redesign of multimedia fusion is a new design content of it. It focuses on diversified design experience, communication across time and space, nonlinear narration, and personalization of information, making the interaction and experience of information more fluid.

Abbreviations

HDFS: Hadoop Distributed File System
IoT: Internet of things
WoT: Web of Things
LRU: least recently used
PCA: principal component analysis
AAM: active appearance model
RGB: red, blue, green images
RFID: radiofrequency identification technology
LAN: local area network
GPRS: General Packet Radio Services.

Data Availability

All data generated or analysed during this study are included in the manuscript.

Conflicts of Interest

The author declares no conflicts of interest.

Authors' Contributions

Baoqing Wang contributed to the design and methodology of this study, the assessment of the outcomes, and the writing of the manuscript.

References

[1] Y. Wu, "Design and implementation of virtual advertising based on visual communication design," *Boletin Tecnico/Technical Bulletin*, vol. 55, no. 18, pp. 604–610, 2017.
[2] R. Lzicar, "Swiss graphic design: a British invention," *Design Issues*, vol. 37, no. 1, pp. 51–63, 2021.
[3] H. Li, "Visual communication design of digital media in digital advertising," *Journal of Contemporary Educational Research*, vol. 5, no. 7, pp. 36–39, 2021.
[4] M. Fan and Y. Li, "The application of computer graphics processing in visual communication design," *Journal of Intelligent and Fuzzy Systems*, vol. 39, no. 4, pp. 5183–5191, 2020.
[5] L. Kong, M. K. Khan, F. Wu, G. Chen, and P. Zeng, "Millimeter-wave wireless communications for IoT-cloud supported autonomous vehicles: overview, design, and challenges," *IEEE Communications Magazine*, vol. 55, no. 1, pp. 62–68, 2017.
[6] S. Saxena and T. Ali Said Mansour Al-Tamimi, "Big data and internet of things (IoT) technologies in Omani banks: a case study," *Foresight*, vol. 19, no. 4, pp. 409–420, 2017.
[7] C. Stergiou and K. E. Psannis, "Recent advances delivered by mobile cloud computing and internet of things for big data applications: a survey," *International Journal of Network Management*, vol. 27, no. 3, Article ID 19300, pp. 1–12, 2017.
[8] M. Al-Rawi, "Design of 2.4 GHz transceiver for wireless communication," *Land Forces Academy Review*, vol. 24, no. 3, pp. 232–241, 2019.
[9] F. Xiaodan, "Design and implementation of remote health monitoring system for 3D visual bridge," *Procedia Engineering*, vol. 174, pp. 1330–1335, 2017.
[10] N. I. U. Qingsong, "A design of modern greenhouse environmental monitoring system," *Asian Agricultural Research*, vol. 7, no. 149, pp. 61–64, 2017.
[11] E. Pober and M. Cook, "Thinking in virtual spaces: impacts of virtual reality on the undergraduate interior design process," *International Journal of Virtual and Augmented Reality*, vol. 3, no. 2, pp. 23–40, 2019.
[12] W. Zhao, "The redesign of brand visual identity in the information age," *Acta Technica CSAV (Ceskoslovensk Akademie Ved)*, vol. 62, no. 1, pp. 279–288, 2017.
[13] M. A. Razzaque, M. Milojevic-Jevric, A. Palade, and S. Clarke, "Middleware for internet of things: a survey," *IEEE Internet of Things Journal*, vol. 3, no. 1, pp. 70–95, 2016.
[14] A. Yanar, F. Söylemezoğlu, Z. Erdoğan, and O. Ozgen, "Preservation of tangible and intangible cultural heritage: sample of Turkish bath," *The Turkish Online Journal of Design Art and Communication*, vol. 11, no. 1, pp. 1–19, 2021.
[15] G. C. Nobre and E. Tavares, "Scientific literature analysis on big data and internet of things applications on circular economy: a bibliometric study," *Scientometrics*, vol. 111, no. 1, pp. 463–492, 2017.
[16] L. Chettri and R. Bera, "A comprehensive survey on internet of things (IoT) toward 5G wireless systems," *IEEE Internet of Things Journal*, vol. 7, no. 1, pp. 16–32, 2020.
[17] R. Wang, "Computer-aided interaction of visual communication technology and art in new media scenes," *Computer-Aided Design and Applications*, vol. 19, no. S3, pp. 75–84, 2021.
[18] W. Jianhua, G. Zhang, and S. Zhengxiang, "Internet of things, big data, intelligent electrical apparatus—the future development of power equipment," *Gaoya Dianqi/High Voltage Apparatus*, vol. 54, no. 7, pp. 1–9, 2018.
[19] G. Kokkonis, K. E. Psannis, M. Roumeliotis, and D. Schonfeld, "Real-time wireless multisensory smart surveillance with 3D-HEVC streams for internet-of-things (IoT)," *The Journal of Supercomputing*, vol. 73, no. 3, pp. 1044–1062, 2017.
[20] D. Furuncu Kutluhan and A. Zinderen, "Data journalism in the COVID-19 period: a descriptional review of coronavirus news," *The Turkish Online Journal of Design Art and Communication*, vol. 11, no. 1, pp. 85–102, 2021.
[21] H. Y. Lin and M. Y. Hsieh, "A dynamic key management and secure data transfer based on m-tree structure with multi-level security framework for Internet of vehicles," *Connection Science*, vol. 34, no. 1, pp. 1089–1118, 2022.

Hindawi
Mobile Information Systems
Volume 2022, Article ID 4817463, 11 pages
https://doi.org/10.1155/2022/4817463

Research Article

Comparative Analysis of Volleyball Serve Action Based on Human Posture Estimation

Bo Zhou[1] and Omer Saeed[2]

[1]*School of Physical Education, Southwest Minzu University, Chengdu 610000, Sichuan, China*
[2]*Institute of Management, Kyrgyz International Universal College, Bishkek, Kyrgyzstan*

Correspondence should be addressed to Omer Saeed; omersaeed@mail.cu.edu.kg

Received 20 June 2022; Revised 7 August 2022; Accepted 9 August 2022; Published 30 September 2022

Academic Editor: Chi Lin

Serving is one of the most crucial techniques in volleyball. Serving is a method that does not require team interaction and is difficult for the opponent to immediately interfere with. The feature migration module with a fixed offset is suggested in this work. This module can be thought of as a cross-channel dilated convolution approximation of dilated convolution. The reason cross-channel dilated convolution is not worse than standard dilated convolution with few parameters is discussed in this article. An improved random forest model is put forth to address the issue of the human pose estimation system's high memory consumption when utilizing random forest as the classifier. This model presents the Poisson process and incorporates it with the depth data to create a filter before using Bootstrap sampling. In order to optimize and reconstruct the training dataset, a portion of the feature sample points that do not contribute positively to subsequent classification is removed from the original training dataset. This allows the training dataset to better account for the repeated sampling of the random forest during the sampling process. Resampling has some drawbacks, but they are not very representative. The effectiveness of the optimization model, which significantly lowers the system's time and space complexity and increases the system's applicability, is demonstrated by experiments.

1. Introduction

Taking an overview of today's volleyball world, the techniques and tactics in volleyball games are developing in the direction of "comprehensive, high, fast, flexible, and changeable." Volleyball is one of the better-developed sports in my country. With the Chinese women's volleyball team standing on the championship podium again after many years at the Rio Olympics in 2017, the Chinese people's attention to volleyball has increased significantly [1]. Mass sports are carried out in various forms. While participating teams continue to use new technologies, new tactics, and new styles of play, they also put forward higher requirements on the overall abilities of volleyball players [2]. Excellent volleyball players can maximize the accuracy and offensive characteristics of serving, which is undoubtedly an effective supplement to the overall offensive strength of the team [3]. The precision of the athlete's serve technique must therefore be continually improved during the volleyball training process if they are to win the match. Technical and psychological training are the sources of the elements impacting volleyball serve accuracy. The effectiveness of an athlete's serve and his degree of expertise are closely related, and it also depends on subjective elements like athletes' psyche and is influenced by objective factors like the venue's equipment, environment, and setting [4].

Human body pose estimation is the process of detecting a given image or video and calibrating the key parts or main joint points of the human body in the video or picture [5]. Since the concept of pose estimation was put forward, scholars at home and abroad have conducted a lot of research for this [6, 7]. When estimating the human body pose, two main solutions are used, namely, the traditional image processing method and the method based on deep learning

[8]. Although the traditional method has high time efficiency, it mainly extracts SHIFT features and HOG features, and these features are manually set, which will lead to different viewing angles, appearances, occlusions, and their inherent geometry in the image [9]. Fuzziness will have a certain impact on the performance of the algorithm, so that the full use of image information cannot be realized. Aiming at the influencing factors of the serving technique, while training the athletes' serving technique, the combination of sports psychological indicators and the accuracy of volleyball serve for investigation and analysis is not only conducive to the improvement of the athletes' serving skills but also can be used for coaches and teachers in volleyball players [10]. It applies the depth perception ability and muscle exertion of volleyball students to the volleyball technique, reveals the law of the influence of the depth perception ability and muscle exertion of volleyball students on the accuracy of volleyball serve, and improves the technical level of volleyball students and the application of psychological principles [11]. It can play an active role in the training of volleyball technical skills, and at the same time, it can provide a theoretical basis for solving problems in the service of volleyball students in training, provide a theoretical basis for future volleyball players' psychological selection indicators, and improve the psychological principles [12]. The theoretical system applied to the learning of sports technical skills provides research inspiration.

Translating other spatial location features to the location is an easy and direct way to increase the model's receptive field. We suggest a method for translating each channel feature map by a predetermined offset, enabling the integration of each point with other location features at predetermined periodic intervals. We categorize this technique as a module, a module for long-distance relationships. This module may be thought of as a particular variety of dilated convolution. In order to improve the random forest model in the experiment and analysis sections, this research highlights the drawbacks and inadequacies of the random forest classifier in the human pose estimation system. The system's time and space usage before and after the forest model optimization are compared. According to the experimental data, this optimization is quite successful in decreasing the system's time and space complexity without significantly affecting the accuracy of system identification. Analyzing the test results reveals that there was no statistically significant variation in the movement skill difficulty between the three groups and that the subject's serving motion essentially took the shape of an automatic frontal overhand serve. For the jumping technique where the skill difficulty is medium and the subjects are still in the stage of differentiation to automation, the three training groups also showed no significant differences. Among them, sequence exercises have the most obvious improvement in accuracy and total score, while random exercises are still only the best for improving motor skills. Jumping ball is a technique between basic and difficult serving techniques in volleyball. It is not easy to send high-quality jumping ball, even for volleyball students. The sequence practice mode with moderate background interference can enable the subjects to correct some wrong actions in time during the whole training process and establish the correct action mode, so that the subjects can be allowed to perform under the premise of moderate background interference.

The rest of this article is organized as follows. Section 2 discusses related work. Section 3 analyzes the global feature extraction method based on feature map migration. Section 4 designs the human pose estimation strategy. In Section 5, a comparative analysis of the experimental results of the volleyball serve action was carried out. Section 6 summarizes the full text.

2. Related Work

Generally, two solutions are mainly used when estimating the human body pose, that is, the traditional image processing method and the method based on deep learning [13]. Among them, the method based on deep learning is the mainstream method used now. In the traditional method, some tree diagram models can be used to express the joint structure of the human body, and these models have dynamic a priori. They divide the joints of the human body, which can be divided into the head, trunk, upper and lower left arm, upper and lower right arm, upper and lower left leg, and upper and lower right leg. Related scholars have proposed a very classic graph structure algorithm [14]. The author uses a collection of multiple parts to express the human body, and there are certain spatial constraints between these parts. The graph structure mainly includes two parts: a space model and a component model. The component model is used to describe the various components that make up the human body.

Related scholars have proposed a greedy parts allocation algorithm, which can utilize the inherent structure of the human body, thereby reducing the complexity of the graphic model [15]. In addition, in order to fuse feature information at different scales, the existing network structure often performs repeated upsampling of pictures, resulting in low spatial sensitivity of the final high-resolution features [16]. In response to this phenomenon, related scholars have proposed a high-resolution representation network, which uses a distinctive parallel structure to ensure that the resolution is not reduced in different stages of the network [17]. Researchers have proposed a method of posture refinement, which is model-independent and does not require prior knowledge and code support from other algorithms, which makes it easy to complete related operations during post-processing [18, 19]. Experiments show that, compared with our commonly used multistage network structure, this method has a better detection effect [20]. In addition, related scholars have proposed a new method using bottom-up thinking to complete the estimation of multiperson 2D human body pose [21]. This method uses the "parts intensity field" to locate the various joint points of the human body. In addition, in order to obtain a complete body posture, the

aforementioned "part affinity field" is used to associate the various joint points belonging to the same person [22]. This method has very good applicability for application scenarios such as delivery robots and unmanned driving.

Relevant scholars have summarized the inadequate completion of the volleyball player's serve technique and smash technique in sports and believe that the higher the athlete's bounce when smashing the ball, the better, because the higher the jump, the smashing will have more lethality [23, 24]. However, the fact is that athletes often do not jump high when doing the above two technical actions. This is mainly related to the lack of muscle ability when jumping. The buckle and serve skills need to have the early approach speed. There are certain requirements for athletes' waist and leg muscle abilities, and they need to have strong coordination and contractility. In response to this shortcoming, scholars also proposed that short-distance running and weight load can be used to exercise this part of the muscle strength [25–27]. The second aspect is that the error of the spiking action is due to the premature squatting when hitting the ball, which cannot be normal. Under normal circumstances, when volleyball takes off, the coordination of each link has a great influence on the completion of the take-off. Relevant scholars have mentioned in the research that the extension of the knee cannot be fully exerted when the human body is stepping and jumping [28, 29]. At this time, the cooperation of the ankle joint is urgently needed. In short, the cooperation of the lower limbs of the human body is crucial to the effect of jumping.

3. Global Feature Extraction Method Based on Feature Map Migration

3.1. Baseline Model. Instead of using regression models in our approach, we employ categorization models to forecast where the important body parts will be located. The location of important sites in the human body is predicted by this model using categorization rather than regression. For each pixel classification, it tries to ascertain the existence and type of key points. The deep CNN needs to maintain an output scale that is similar to the input scale in order to accomplish pixel-level prediction. In comparison to conventional CNNs, this characteristic can be obtained with fewer pooling layers, although less pooling necessitates higher computing and storage costs in the deep layers of the network. U-shaped networks are increasingly being used in computer vision techniques to attain this goal [30]. The U-shaped network can be divided into two stages. Its shallow layer is the first stage, the downsampling stage. The network is convolved and downsampled like the traditional CNN network. The feature map is downsampled to a relatively small size to extract features and reduce the optimization space [31, 32]. This stage is followed by an upsampling stage; some upsampling layers and convolutional layers expand and shrink the feature maps together. Subsequently, the upper-level sampled feature map is added to the downsampling stage feature map of the same size. This jump addition method is usually called a shortcut connection [33–35].

3.2. Dilated Convolution. Let S denote the discrete 2D spatial location on a feature map, and let F denote the feature map defined on $s \in S$. Let $\Omega r = [-r, r]\ 2 \cap Z2$ represent the offset space of a convolution kernel element, that is, the horizontal or vertical spatial offset of each convolution kernel should be between $-r$ and r (including boundary). We define k: $\Omega r \longrightarrow R$ as a convolution kernel with size $(2r+1) \times (2r+1)$. Then, the dilated convolution can be expressed as follows:

$$Fk_{*l}(p) = \prod_{p=lt-s} F(s)Zk(t), \tag{1}$$

where $*l$ is called the l-dilated convolution (l-DConv), and $l \in Z+$ is the dilation step.

We extend this definition to the concept of convolutional neural networks. For a convolutional layer with M input feature maps and N output maps, the expanded convolutional layer can be written as follows:

$$G_n(p) = \prod_{m=0}^{M-1} k_{m,n} F_{m*l}(p) n = 0, 1, 2, \ldots, N-1. \tag{2}$$

3.3. Cross-Channel Dilated Convolution. Assuming that $(2r+1)\ 2$ is a factor of M, we divide a total of M feature maps into W groups so that $M = W \cdot (2r+1)\ 2$ is satisfied. Assume that adjacent feature maps are grouped into the same group. Note that the concept of "group" here is orthogonal to the "offset group" mentioned in the feature migration process, that is, the wth group is equivalent to the wth element in all H offset groups. Our wth feature group can be expressed as follows:

$$F_i^w(p) = F_{(w-2)(H-i)}(p) \quad i = 0, 1, 2, \ldots, H-1. \tag{3}$$

We define the cross-channel expansion convolutional layer as follows:

$$G_n(p) = \prod_{w=0}^{W-1} \left[k_{n,w} F_{\oplus l}^{(w)} \right](p), \tag{4}$$

where $\otimes 1$ is the l-cross-channel dilated convolution (l-XDConv) operation, assuming that the finite set Ωr is ordered, and $t(i)$ is the ith element of Ωr. Note that lt (i) is equivalent to u used in the feature migration process. Unlike traditional convolution or dilated convolution, the cross-pass dilated convolution operation applies the $(2r+1) \times (2r+1)$ convolution kernel to $H = (2r+1)2$ channels.

$$\left[k_{n,w} F_{\oplus l}^{(w)} \right](p) = \prod_{p=s-lt(i)} k\left[t^{(i)}\right] \bullet F_i^{(w)}(s). \tag{5}$$

The traditional convolution kernel and the traditional expansion convolution kernel focus on extracting the local features in each feature map and weighting the sum of the extracted features. They can be regarded as a broader version of cross-channel dilated convolution because they can achieve the same operation as cross-channel dilated convolution by setting the weight of each convolution kernel to

only one nonzero, that is, the in-channel operation of the traditional convolution is turned off.

4. Human Pose Estimation Strategy

4.1. Deep Feature Selection and Poisson Process. Poisson distribution is a common discrete probability distribution in statistics and probability. Poisson distribution is suitable for describing the number of random events occurring in unit time, and its probability distribution function is as follows:

$$P(X = k) = (k!)^{-1}\lambda^k e^{-\lambda} \quad \lambda k > 0. \tag{6}$$

The parameter λ represents the average occurrence rate of random events in unit time (area). If the random variable $N(t)$ represents the total number of "events" that have occurred until time t, then the random process $\{N(t), t \geq 0\}$ is called the counting process.

The number of events in any interval of length t obeys Poisson distribution with λt as the mean, that is, for all $s, t \geq 0$ satisfies

$$P[N(s) - N(s-t) = n] = (n!)^{-1}e^{-\lambda t}(\lambda t)^{n-1}. \tag{7}$$

Then, the above counting process is called the Poisson process with rate $\lambda\,(\lambda > 0)$. It can be seen that the Poisson process is the partial unitization of Poisson, that is, the Poisson process describes the count of the number of occurrences of events (number of occurrences of particles) in a unit time interval.

4.2. Poisson Optimized Random Forest. In this study, the Poisson process is introduced and used as a filter to filter the original sample dataset. First, we scan the image and calculate the filter factor L of all feature points in the image. Suppose the depth value of the feature point X to be operated is De, and the depth values of the feature point X1, the feature point X2 on the left, and the feature point X3 on the right, which are adjacent to and directly above the feature point X, are De1, De2, and De3, where the Euclidean distance is integrated. We calculate the Euclidean distance L' between the feature point De and De1, De2, and De3 as in (8) and then use (9) to obtain the characteristic point X filtering factor L. Then, we sort the filtering factors of all feature points in the image. Finally, the sorted filtering factor is regarded as a counting process, and the Poisson value of each feature point is calculated by formula (10), and the filtering threshold is set at the same time. According to the filtering threshold and the calculated value of each feature point, the size of the Poisson value is selected and left, so as to reconstruct the training dataset.

$$L' = \prod_{i=0}^{2}\left(De_i - 2De\right)^{-2}, \tag{8}$$

$$L = De \bullet L', \tag{9}$$

$$\text{Poisson}\left[L_u = N(u) - N(u-1)\right] = \left(L_u\right)!\lambda^{L_u}e^{-\lambda}. \tag{10}$$

In formula (10), $N(u)$ is the value of the uth filtering factor after sorting, and λ is the average of all filtering factors in the image.

4.3. Experiment and Result Analysis. In Figure 1, the first row represents the experimental sample pictures. There are 600 pictures in the sample library, which are divided into 3 categories according to the characters, and each category of pictures is a continuous action made by the same person. The second line is the experimental effect diagram before random forest optimization, and the third line is the experimental effect after optimization. The optimized random forest model did not cause the classification accuracy to drop too much. The specific accuracy comparison is shown in Figure 2.

Following optimization, the random forest's recognition accuracy increases consistently as the number of decision trees increases. The more decision trees there are, the less the accuracy rate will fluctuate, making the system more stable. Prior to optimization, the system will run out of memory when there are 700 decision trees, causing it to crash. Therefore, once there are 700 decision trees, the matching graph from before optimization will stop. In order to verify the influence of the optimization of the random forest model on the accuracy of human pose estimation, this study designs a comparison of the accuracy of the model before and after optimization, as shown in Figure 2. Figure 2 shows that the optimization of the model has increased the recognition accuracy of the system to a certain extent, and at the same time, it has further improved the robustness of the system.

While ensuring that the accuracy of system identification will not be too reduced, this study designs a comparison of the system time costs before and after model optimization, as shown in Figure 3. Before model optimization, the time cost of the system increases with the increase of decision trees. When the number of decision trees reaches a certain number, the system cannot run on ordinary PCs. However, after the model is optimized, the time cost of the system has been greatly reduced compared with that before the optimization, and it also shows a more stable trend. The optimized random forest model has made great progress in the time cost of the original human pose estimation system.

This work designs a comparison of the memory used by the system operation, as shown in Figure 4, in order to demonstrate the contribution of the improved random forest model to the space overhead of the original system. Prior to model optimization, as the number of decision trees grew, the system's memory overhead grew along with it. When the number of decision trees reached a certain point, the memory footprint reached roughly 1900MB, rendering standard PCs impossible to function. The optimized model has been kept between 750 MB and 1050 MB, with minimal adjustments, indicating a consistent trend. This prevents the system's memory cost from rising as the number of decision trees increases. This demonstrates how the optimized random forest model has significantly reduced the original system's space overhead.

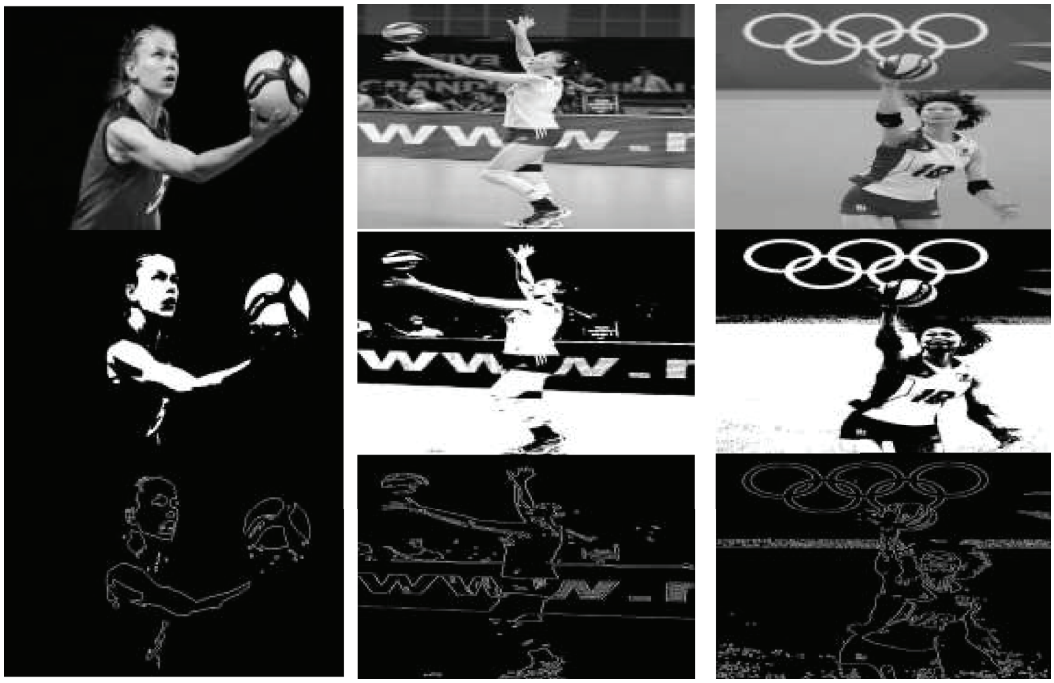

Figure 1: Experimental results before and after optimization.

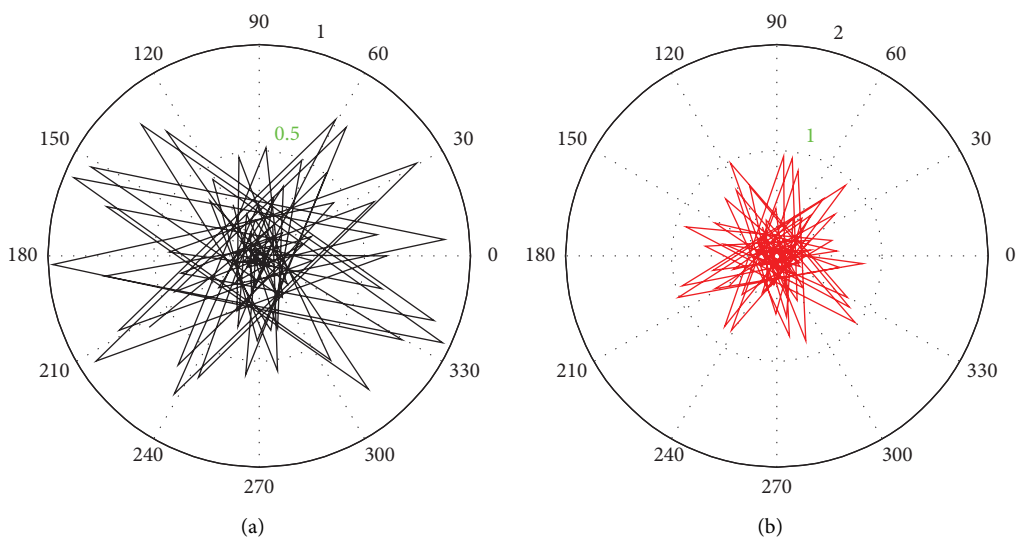

Figure 2: Comparison of accuracy before and after optimization. (a) Poisson optimized random forest. (b) Random forest.

5. Comparative Analysis of Experimental Results of Volleyball Serve

5.1. Subjects Maintain Test Scores. 72 hours after the end of the last training arrangement, the straight ball skill retention test was performed on the frontal overhand serve and jump ball practiced in this experiment. In order to discuss in detail the training effects of each training method for each serving technique and the overall training effects of each practice group's serving skills after three weeks of practice, under the conditions of fixed technical difficulty factors, the front-hand serve and jump ball analysis of variance was performed.

5.1.1. Test Results of Frontal Overhand Serve in Different Practice Groups. First, the homogeneity test of the frontal overhand serve of the movement skills with lower operational difficulty is carried out, and the result is shown in Figure 5. Subsequently, a one-way analysis of variance was performed on the scores of the retention test of frontal overhand serve skills, as given in Table 1. The results showed that serving accuracy $F = 1.33$, $P = 0.176$, action technique $F = 0.178$, $P = 0.645$, and total score $F = 0.415$, $P = 0.507$; P values were all greater than 0.05, and there was no significant difference between the three groups. Among them, the fixed practice group has the best serving accuracy and total score. The average serving accuracy reached 9.14, and the average

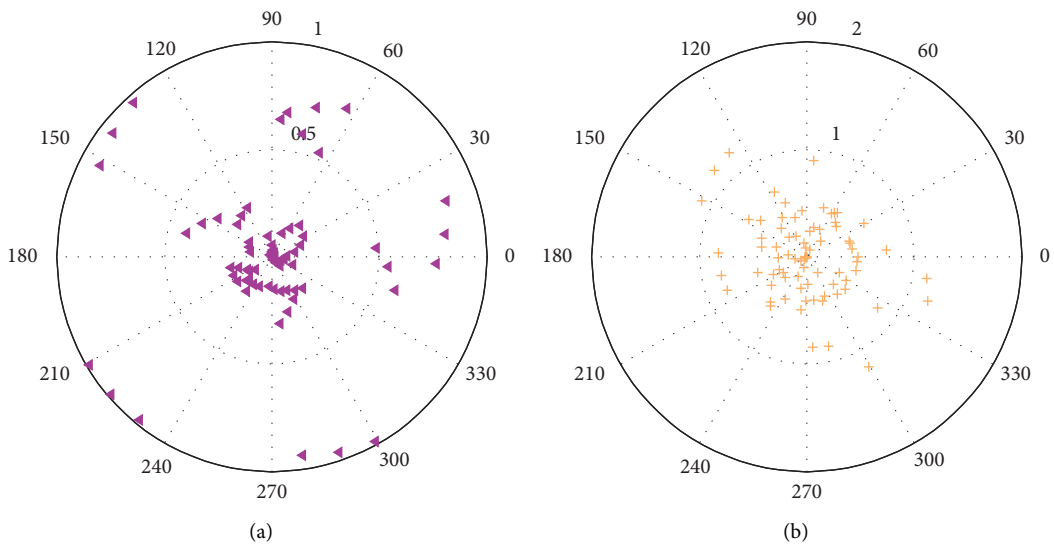

Figure 3: Comparison of system time. (a) Poisson optimized random forest. (b) Random forest.

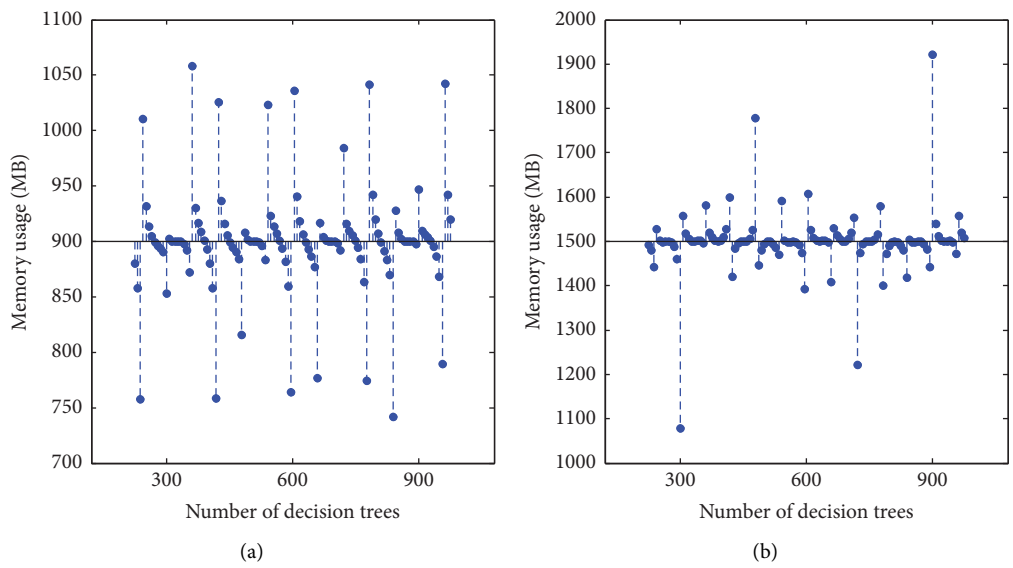

Figure 4: Comparison of system memory usage. (a) Poisson optimized random forest. (b) Random forest.

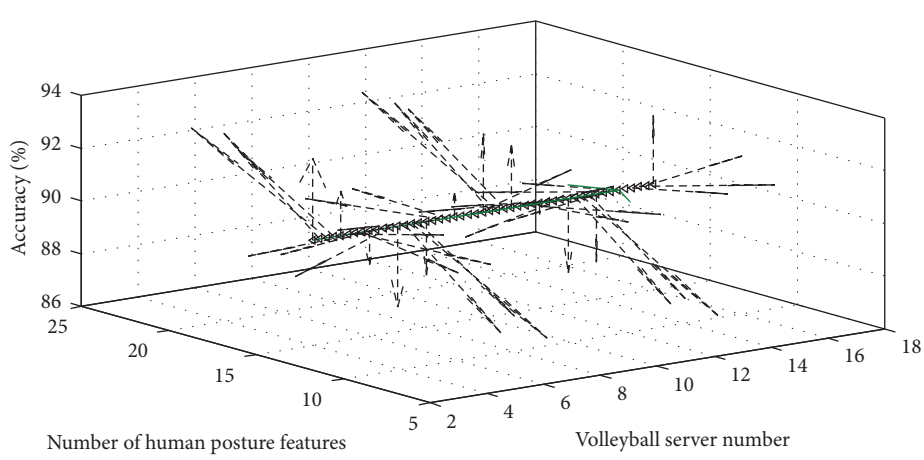

Figure 5: The homogeneity test of frontal overhand serve in different practice groups.

Table 1: Frontal overhand serve results of different practice groups.

	F value	P value	Random practice group	Sequence practice group	Fixed practice group
Volleyball serve accuracy	1.33	0.176	8.14	8.64	9.14
Volleyball technique	0.178	0.645	7.07	6.7	6.74
Total score	0.415	0.507	15.21	15.34	15.88

total score reached 16.0, followed by the sequential practice group, with an average serving accuracy of 8.64. In comparison, the random practice group has the worst performance, with an average accuracy of 8.14 and an average total score of 15.22. However, in the performance of the action technique, the random practice group achieved the best performance with an average of 7.07, followed by the fixed practice group with an average of 6.74, and the sequential practice group has a poorer performance with an average of 6.70. In addition, the standard deviations of the three performances in the fixed practice group are all the lowest. The serving accuracy is 0.40, the action technique is 0.06, and the total score is 0.31. In the random practice group, the standard deviation of the serving accuracy is the same as that of the sequence practice group. The standard deviations of the technique and total score were both in the middle, 0.176 and 1.05, respectively, and the standard deviations of the sequence practice group were the highest, 0.77 and 1.34, respectively. It shows that the performance fluctuations in the fixed practice group are relatively small and stable, followed by the random practice group, and the sequential practice group has the largest fluctuations. Overall, the fixed practice group, followed by the sequential practice group and the random practice group, has relatively poor effects on low-difficulty front-hand serve practice. The frontal overhand serve performance during interference practice with varied backgrounds varies, but there is no statistically significant difference between them, according to the difference test of the three groups of measured data.

5.1.2. Jumping Ball Test Results of Different Practice Groups. Similarly, the homogeneity test of jumping ball with medium-difficulty action skills is carried out, and the result is shown in Figure 6. Subsequently, a one-way analysis of variance was performed on the retention test scores of jumping ball skills, as given in Table 2. The results showed that the P value is greater than 0.05, and the three groups are not significantly different. Among them, the sequence practice group performed the best in serving accuracy and total score. The average serving accuracy was 9.64, and the total score was 16.57. The movement technique was second to the random practice group and higher than the fixed practice group, reaching 6.82; the mean value of serving accuracy is the same as that of the random practice group, which is 8.64, while the random practice group has the highest mean value of movement skills, reaching 7.04, and the total score is higher than that of the sequence practice group and higher than the fixed practice group, with an average value of 15.8, so the score is in the middle. Compared with the fixed practice group, the performance is the worst, with the average value of the movement technique and total score being 6.72 and 15.47, respectively. In addition, the standard deviation of serve accuracy in the sequence practice group is 0.4, the standard deviation of movement technique is 0.04, the standard deviation of the total score is 0.36, and the standard deviation of the three items is the lowest, indicating that the performance fluctuations in the group are relatively stable; the random practice group excludes the service. The standard deviation of accuracy is the same as that of the fixed practice group, both are 0.85. The standard deviations of the movement technique and total score are both higher than the sequence practice group and lower than the fixed practice group, which is in the median. The standard deviations are 0.06 and 1.01, respectively. The standard deviation of the action technique was 0.32, and the standard deviation of the total score was 1.25. The standard deviations of the two performances were the highest, indicating that the jumping skills in this group fluctuate greatly and are the most unstable. On the whole, the sequence practice group has the best results for the medium-difficulty movement technique jumping ball practice, followed by the random practice group. In comparison, the fixed practice effect is the least satisfactory. After the difference test of the three groups of measured scores, it can be seen that under different levels of background interference practice, the jumping ball with medium skill difficulty maintains scores, but there is no significant difference between them.

5.2. Subject Transfer Test Results

5.2.1. Test Results of Frontal Overhand Serve of Subjects in Different Practice Groups. We test the homogeneity of the frontal overhand serve of the movement skills with lower operational difficulty, and the results are shown in Figure 7. Table 3 shows the single-factor variance of the test scores for the transfer of frontal overhand serve skills. The P values are all greater than 0.05, and there is no significant difference. Among them, the fixed practice group has the highest serving accuracy and average total score of 9.40 and 16.04, respectively. The action technique is the same as the sequence practice group, both are 6.54, next to the random practice group, which has an average of 7.07, and the random practice group has a relatively middle score. The average total score is 15.47, second only to the fixed practice group; the total score of the sequential practice group is poor, with an average of only 15.04. In addition, the three results of the fixed practice group have relatively small fluctuations within the group, and the standard deviations are the lowest, respectively, 1.00, 0.30, and 1.17. In the sequential practice group, except for the movement technique standard deviation of 0.63, which is higher than the random practice group of 0.34, the accuracy and the standard

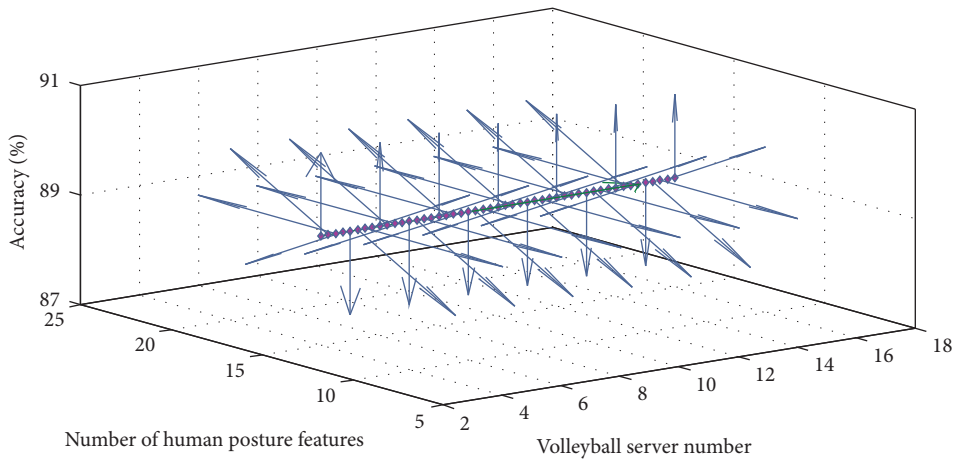

Figure 6: Homogeneity test of jumping balls in different practice groups.

Table 2: Floating ball performance of different practice groups.

	F value	P value	Random practice group	Sequence practice group	Fixed practice group
Volleyball serve accuracy	1.81	0.101	8.64	9.64	8.64
Volleyball technique	1.304	0.181	7.04	6.82	6.72
Total score	1.044	0.247	15.68	16.46	15.36

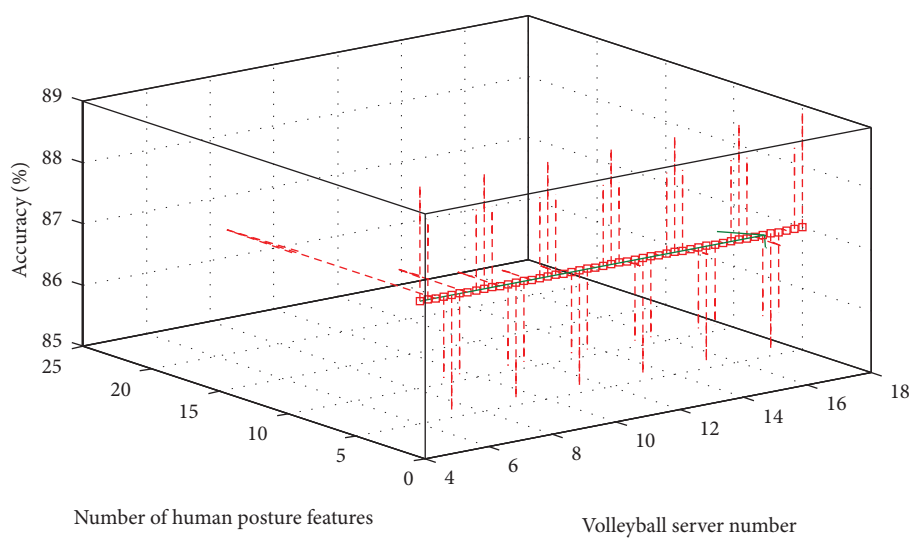

Figure 7: The homogeneity test of frontal overhand serve of subjects in different practice groups.

deviation of the total score are both in the middle, 1.81 and 1.31, respectively; the random practice group has relatively unstable fluctuations in the group, the standard deviation of serve accuracy is as high as 3.00, and the standard deviation of the total score is as high as 3.16. On the whole, the fixed practice group has the best results for the low-difficulty technique of frontal overhand serve, followed by the random practice group. In comparison, the sequential practice effect is the least satisfactory. After the difference test of the three groups of measured scores, it can be seen that under different levels of background interference practice, there are high and low scores for the transfer of frontal overhand serve with lower skill difficulty, but there is no significant difference between them.

5.2.2. Floating Ball Test Results of the Subjects in Different Practice Groups. Figure 8 shows the outcome of the homogeneity test of the leaping ball using a medium-difficulty action skill. The results of the leaping ball skill transfer test's single-factor variance are displayed in Table 4. According to the data, there was a fairly noticeable difference between the three groups that practiced jumping and floating. Among them, the fixed practice group has the best results in three performances, with a serve accuracy of up to 10 points, a movement technique

Table 3: Frontal overhand serve results of different practice groups.

	F value	P value	Random practice group	Sequence practice group	Fixed practice group
Volleyball serve accuracy	1.82	0.642	8.4	8.4	9.4
Volleyball technique	0.678	0.372	7.07	6.54	6.54
Total score	0.100	0.703	15.47	14.94	15.94

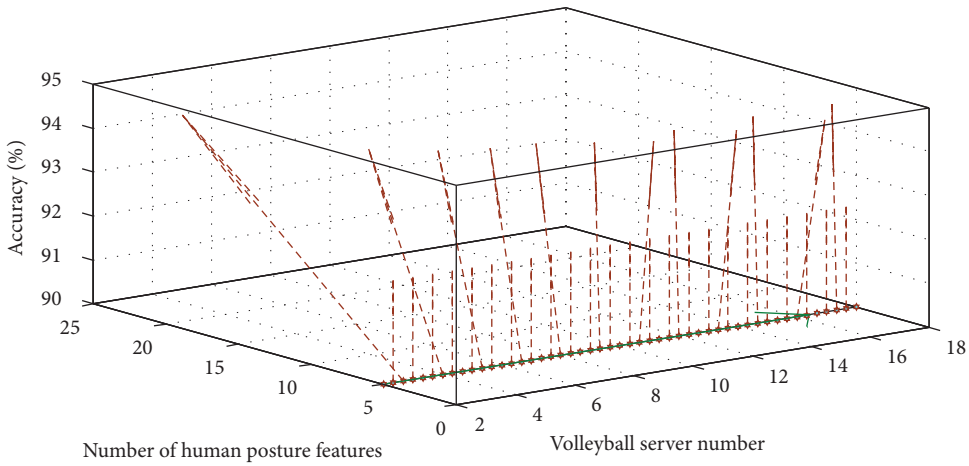

Figure 8: The homogeneity test of jumping balls in different practice groups of subjects.

Table 4: Jumping ball performance of different practice groups.

	F value	P value	Random practice group	Sequence practice group	Fixed practice group
Volleyball serve accuracy	9.521	0.005	10	9	7.64
Volleyball technique	3.607	0.056	7.04	6.64	6.66
Total score	9.317	0.005	17.04	15.64	14.3

of 7.04, and a total score of 17.04, followed by the sequence practice group, except that the average movement technique is slightly inferior to the fixed practice, which is 6.64. The other two average scores are in the middle, the serving accuracy is 9.00, and the total score is 15.64; the fixed practice group scores are the most unsatisfactory, except for the average movement technique only 0.02 points higher than the sequence practice, the average scores of the other two scores ranked last. The average serve accuracy is 7.64 and the average total score is 14.41. In addition, the results in the random practice group are relatively stable. Except for the standard deviation of the movement technique, which is only higher than the fixed exercise by 0.02, the other two grades have the lowest standard deviation; the sequence exercise also has the highest standard deviation of the movement technique. It is higher than the random practice group, and the score distribution within the group is in the middle; the fixed practice group has a lower standard deviation of movement techniques than the other two groups, and the service accuracy and the standard deviation of the total score are both the highest, indicating that the results within the group are fluctuating largely.

6. Conclusion

The relationship between this module and the expansion convolution is demonstrated in this article using a fixed offset translation feature map. This module's operation method is referred to as cross-channel expansion convolution. The purpose of the cross-channel dilated convolution is discussed in this article, and it is demonstrated that it performs similar to the dilated convolution while having significantly smaller parameters. Prior to the sampling operation in the training of the random forest classifier, the depth information and the Poisson process theory are combined to create a filter net. The filter's purpose is to exclude other training data that will not be helpful for the follow-up work while keeping the sample data that will be kept from the training dataset that will be sampled. To compensate for the random forest classifier's repetitive sampling and resampling samples' inadequate representativeness, the training sample dataset can be rebuilt.

The purpose of the experiments was to assess the accuracy of recognition and the time and space consumption before and after model optimization. The results demonstrate that this optimization is highly efficient, drastically lowering the time and spatial complexity of the entire system while maintaining a relatively high level of identification accuracy and increasing the system's applicability. The frontal overhand serve and jumping ball indications did not significantly differ between the fixed practice group, sequence practice group, and random practice group in the skill maintenance test ($P > 0.05$). The three groups differ significantly in serve accuracy and overall score during the ferocious leap serve (P 0.05). The sequence practice group is

in the middle, the random practice group is less effective, and the fixed practice group has the best results. The action technical indicators do not significantly differ from each other ($P > 0.05$). The three groups' serving accuracy was significantly different in the overall score (P 0.05). The fixed practice group performed the best, followed by the sequence practice group, which performed averagely, and the random practice group, which performed poorly.

Data Availability

The data used to support the findings of this study are included within the article.

Conflicts of Interest

The authors declare that they have no conflicts of interest.

Acknowledgments

This study was supported by the Southwest Minzu University (1231119059).

References

[1] F. A. Salim, F. Haider, D. Postma et al., "Towards automatic modeling of volleyball players' behavior for analysis, feedback, and hybrid training," *Journal for the Measurement of Physical Behaviour*, vol. 3, no. 4, pp. 323–330, 2020.

[2] P. X. Fuchs, H. J. K. Menzel, F. Guidotti, W. Herbert, and B. Jeffrey, "Spike jump biomechanics in male versus female elite volleyball players," *Journal of Sports Sciences*, vol. 37, no. 21, pp. 2411–2419, 2019.

[3] G. Zhang and L. Zhong, "Research on volleyball action standardization based on 3D dynamic model," *Alexandria Engineering Journal*, vol. 60, no. 4, pp. 4131–4138, 2021.

[4] K. Idrizovic, B. Gjinovci, D. Sekulic et al., "The effects of 3-month skill-based and plyometric conditioning on fitness parameters in junior female volleyball players," *Pediatric Exercise Science*, vol. 30, no. 3, pp. 353–363, 2018.

[5] K. Sato, K. Watanabe, S. Mizuno, M. Manabe, H. Yano, and H. Iwata, "Development and assessment of a block machine for volleyball attack training," *Advanced Robotics*, vol. 31, no. 21, pp. 1144–1156, 2017.

[6] A. Umek and A. Kos, "Sensor system for augmented feedback applications in volleyball," *Procedia Computer Science*, vol. 174, pp. 369–374, 2020.

[7] B. Molik, N. Morgulec-Adamowicz, J. Marszałek et al., "Evaluation of game performance in elite male sitting volleyball players," *Adapted Physical Activity Quarterly*, vol. 34, no. 2, pp. 104–124, 2017.

[8] L. d S. Oliveira, T. B. M. A. Moura, A. L. F. Rodacki, M. Tilp, and V. H. A. Okazaki, "A systematic review of volleyball spike kinematics: i," *International Journal of Sports Science & Coaching*, vol. 15, no. 2, pp. 239–255, 2020.

[9] J. Sarvestan, Z. Svoboda, and P. Linduška, "Kinematic differences between successful and faulty spikes in young volleyball players," *Journal of Sports Sciences*, vol. 38, no. 20, pp. 2314–2320, 2020.

[10] Y. Wang, Y. Zhao, R. H. M. Chan, and W. J. Li, "Volleyball skill assessment using a single wearable micro inertial measurement unit at wrist," *IEEE Access*, vol. 6, pp. 13758–13765, 2018.

[11] J. Prieur, G. Le Du, M. Stomp, S. Barbu, and C. Blois-Heulin, "Human laterality for manipulation and gestural communication: a study of beach-volleyball players during the Olympic Games," *Laterality*, vol. 25, no. 2, pp. 229–254, 2020.

[12] Y. Yu, A. García-De-Alcaraz, L. Wang, and T. Liu, "Analysis of winning determinant performance indicators according to teams level in Chinese women's volleyball," *International Journal of Performance Analysis in Sport*, vol. 18, no. 5, pp. 750–763, 2018.

[13] A. Paulo, F. T. J. M. Zaal, L. Seifert, S. Fonseca, and D. Araujo, "Predicting volleyball serve-reception at group level," *Journal of Sports Sciences*, vol. 36, no. 22, pp. 2621–2630, 2018.

[14] O. Solovey, V. Hunchenko, D. Solovey, and K. Wnorowski, "Influence of static balances level on competitive performance indicators of athletes 17-21 years old in beach volleyball," *Physical education of students*, vol. 24, no. 6, pp. 332–339, 2020.

[15] A. Oliveira, L. Vaz, and J. Pastore, "Discriminate scoring skills and non-scoring skills according to results in the Brazilian men's volleyball SuperLeague," *Montenegrin Journal of Sports Science and Medicine*, vol. 7, no. 1, pp. 73–79, 2018.

[16] I. S. Sopa, "Developing attack point in volleyball game using plyometric exercises at 13-14 years old volleyball players," *Series IX Sciences of Human Kinetics*, vol. 12(61), no. 2, pp. 67–76, 2019.

[17] J. Ying, F. Ren, and G. Fekete, "Dynamic testing of volleyball players' body posture using a formetric 3D device," *Biosurface and Biotribology*, vol. 6, no. 4, pp. 114–117, 2020.

[18] A. T. Erdoğan, G. Umutlu, and N. E. Acar, "Evaluation of shoulder strength characteristics in overhead sports and range of motion related changes during isokinetic testing," *Isokinetics and Exercise Science*, vol. 27, no. 2, pp. 153–161, 2019.

[19] A. Kitsiou, K. Sotiropoulos, and S. Drikos, "Tendencies of the volleyball serving skill with respect to the serve type across genders," *Journal of Physical Education and Sport*, vol. 20, no. 2, pp. 564–570, 2020.

[20] G. Giatsis, V. Panoutsakopoulos, and I. A. Kollias, "Biomechanical differences of arm swing countermovement jumps on sand and rigid surface performed by elite beach volleyball players," *Journal of Sports Sciences*, vol. 36, no. 9, pp. 997–1008, 2018.

[21] T. D'Isanto, G. Altavilla, and G. Raiola, "Teaching method in volleyball service: intensive and exenstive tools in cognitive and ecological approach," *Journal of Physical Education and Sport*, vol. 17, pp. 2222–2227, 2017.

[22] G. Conti, A. Freire, B. Evangelista, G. Pedrosa, H. Ugrinowitsch, and H. Castro, "Brazilian high level men's volleyball: characterization of the attack performed by the opposite player," *Kinesiology*, vol. 50, no. 2, pp. 211–217, 2018.

[23] C. S. Ho, K. C. Lin, M. H. Hung, C. Y. Chang, and K. C. Chen, "System design and application for evaluation of digging agility in college male volleyball players," *Proceedings of the Institution of Mechanical Engineers - Part P: Journal of Sports Engineering and Technology*, vol. 233, no. 3, pp. 424–431, 2019.

[24] P. D. ZahraaJawadAhmed, "Pivotal thinking and its relationship to the performance of the skills of preparing and receiving serve volleyball for female students," *Annals of the Romanian Society for Cell Biology*, vol. 25, no. 6, pp. 7950–7958, 2021.

[25] I. S. Sopa and M. Pomohaci, "Evaluation of motor development and skills in mini-volleyball game (10-12 years old)," *Bulletin of the Transilvania University of Brasov. Series IX, Sciences of Human Kinetics*, vol. 11, no. 1, pp. 95–104, 2018.

[26] M. M. Çelebi, C. Akarçeşme, and B. E. Dalbayrak, "Evaluation of postural balance and hamstring/quadriceps peak torque ratios according to leg dominancy in Turkish female volleyball players," *Turkish Journal of Sports Medicine*, vol. 53, no. 3, pp. 123–130, 2018.

[27] L. Laporta, B. Valongo, J. Afonso, and I. Mesquita, "Game-centred study using eigenvector centrality in high-level women's volleyball: play efficacy is independent of game patterns or is it?" *Montenegrin Journal of Sports Science and Medicine*, vol. 10, no. 1, pp. 19–24, 2021.

[28] A. Tsoukos, S. Drikos, L. E. Brown, K. Sotiropoulos, P. Veligekas, and G. C. Bogdanis, "Upper and lower body power are strong predictors for selection of male junior national volleyball team players," *The Journal of Strength & Conditioning Research*, vol. 33, no. 10, pp. 2760–2767, 2019.

[29] N. Ukita, "Pose estimation with action classification using global-and-pose features and fine-grained action-specific pose models," *IEICE - Transactions on Info and Systems*, vol. E101.D, no. 3, pp. 758–766, 2018.

[30] S. D. Papadopoulou, G. Giatsis, and E. Billis, "Comparative analysis of the technical-tactical skills of elite male beach volleyball teams," *Sport Science*, vol. 13, no. 1, pp. 59–66, 2020.

[31] N. Coito, K. Davids, H. Folgado, T. Bento, and B. Travassos, "Capturing and quantifying tactical behaviors in small-sided and conditioned games in soccer: a systematic review," *Research Quarterly for Exercise & Sport*, vol. 93, no. 1, pp. 189–203, 2022.

[32] J. M. Marzano-Felisatti, J. I. Priego-Quesada, and J. F. G. Luján, "Women' s volleyball performance indicators according to age category and teams' final position in international competitions," *European Journal of Human Movement*, vol. 48, pp. 21–34, 2022.

[33] S. Drikos, "Pass level and the outcome of attack for age categories in male volleyball," *J Phys Act Nutr Rehabil*, vol. 13, pp. 428–438, 2018.

[34] B. Masanovic, "Comparative study of anthropometric measurement and body composition between junior basketball and volleyball players from Serbian national league," *Sport Mont*, vol. 16, no. 3, pp. 19–24, 2018.

[35] A. N. Ungureanu, P. R. Brustio, G. Boccia, A. Rainoldi, and C. Lupo, "Effects of presession well-being perception on internal training load in female volleyball players," *International Journal of Sports Physiology and Performance*, vol. 16, no. 5, pp. 622–627, 2021.

Hindawi
Mobile Information Systems
Volume 2022, Article ID 4419952, 11 pages
https://doi.org/10.1155/2022/4419952

Research Article

Teaching Improvement Strategies of University English Audiovisual or Speaking Course under the Background of Hadoop

Jing Han

School of Foreign Language, Jilin University of Architecture and Technology, Changchun, Jilin 130114, China

Correspondence should be addressed to Jing Han; hanjing@jluat.edu.cn

Received 4 July 2022; Revised 12 July 2022; Accepted 16 July 2022; Published 27 September 2022

Academic Editor: Chi Lin

Under the background of "Internet plus," the social application and penetration of cloud computing and big data have produced far-reaching impacts in many aspects in the field of education. Taking college English audio-visual teaching at present. However, there are still many problems in classroom teaching practice. Focusing on college English listening and speaking teaching, this study explores the teaching strategies of college English listening and speaking to improve college pupils' comprehensive listening and speaking ability. With the rapid development of information technology, relying on information technology and using modern technologies such as multimedia to conduct three-dimensional audio-visual teaching can effectively improve the efficiency of audio-visual classrooms by 16%. Based on the background of Internet plus, this study tries to reconstruct the evaluation model of college English audio-visual courses by using multivariate and multidimensional evaluation models and combining quantitative and qualitative evaluation to improve the teaching quality and effect of college English audio-visual course.

1. Introduction

Over the years, in the teaching management system, the emergence of information-based teaching management systems has provided great convenience for university teaching management, improved the operating efficiency of university management, and reduced the cost of running a school. At present, information teaching management systems are basically equipped to varying degrees. These basically include functional modules, such as curriculum management for pupils and teachers, and performance management [1]. With the help of big data technology, we can establish a dynamic learning management system for each pupil, pay attention to each pupil's dynamics in real time, and implement precise teaching, which lays a solid foundation and guarantees college English teaching reform [2]. As higher education is related to the future of pupils, there is a long way to go to improve the comprehensive application ability of college English in the situation of global economic integration and the real-time updating of social employment demand [3].

The traditional English audio-visual teaching mode is a learning mode in which teachers use players, tape recorders, or other equipment and play them in class, or pupils record them through the teacher's explanation [4]. In this mode, the learning content is only reading or writing, or the teaching mode is boring, which inhibits pupils' interest in learning or makes the whole learning process of audio-visual-oral lack of individuality, resulting in low-classroom efficiency [5]. Single teaching materials or fixed teaching methods make it difficult to teach pupils in accordance with their aptitude, resulting in pupils with a poor foundation, declining English scores, or reluctance to communicate orally, which leads to the general weakness of college pupils' English listening or speaking ability [6]. At present, the teaching methods or forms of University English audio-visual-oral courses are relatively simple, or the traditional multimedia (such as computers, stereos, and projectors) is mainly used for teaching. The teaching form is mainly that teachers explain or read new words, or play audio or video. Pupils practice the test questions according to the played audio or video. After checking the listening answers, the teachers repeat the video

or audio several times or briefly explain the important knowledge points or difficulties in the materials. Finally, pupils practice related oral dialogue.

Improving English learning achievements for other language learners in Internet plus's time is docking with "Internet plus." Faced with massive learning resources, their learning methods have undergone tremendous changes, from the traditional mode to electronic learning, mobile learning, ubiquitous learning, intelligent learning, or deep learning [7]. These new learning methods provide a solid platform or foundation for human information exchange or innovation or development. In this context, clarify the teaching objectives, collect, or organize network resources. Teachers start with the content of teaching materials, analyze all kinds of resources needed for teaching with the guidance of teaching objectives, or then collect or collate them through the Internet in a targeted manner so that the network resources can actually meet the teaching needs or do not deviate from the teaching materials [8]. The Internet is rich in resources, including a large number of high-quality teaching resources, which can be effectively used in college English teaching as long as they are reasonably developed or utilized. Under the background of "Internet plus," teachers adopt the teaching goal as the guidance, collect or sort out online teaching, use online resources to establish a special teaching database, or build a networked teaching environment for college English teaching so that pupils can enjoy the learning benefits brought by the Internet. "Internet plus" education promoted the birth of new teaching methods, such as microclass, flipped classroom, multimedia teaching, and online teaching, all of which have advantages that traditional teaching methods do not have [9]. In college English teaching, teachers can integrate the above teaching methods, enrich English teaching forms, or construct a new form of English teaching with these teaching methods. By changing the innovation of weak links in the past and relying on the advantages of the era of information technology or big data, we can enrich the content or mode of English teaching evaluation, so as to build a scientific, diversified, and efficient evaluation index system.

(1) This study adopts the path of University English audio-visual or speaking precision teaching under the background of Hadoop, or the effectiveness evaluation model of University English audio-visual or speaking precision teaching under the background of Hadoop

(2) This study aims to optimize the course content, clarify the teaching objectives, create a good language learning environment, enrich teaching methods, or adopt diversified modern teaching modes

Section 3 describes the significance of the integration of information technology into University English teaching. This section mainly looks at the current external developing environment or the influence of various technological developments on University English. Section 4 is the method of teaching evaluation, which states that English teaching should pay more attention to the evaluation of innovation or practice, break through the previous mastery of the original knowledge, or strengthen the proportion of self-dialectic or self-evaluation. Section 5 is about the future direction of University English teaching.

2. Related Work

The development of information technology has pushed us into the era of Hadoop. Under the background of Hadoop, a large amount of English teaching data or resources can be collected or utilized, which provides resources or technical support for the development of individualized University English teaching or can well solve the problem that current University English teaching lacks pertinence or effectiveness. Pupils' learning methods or states are also different under different forms of teaching organization [10].

Tan thinks that pupils' application or exploration of mobile application assistant software or platform is insufficient; it is inefficient for pupils to rely on information equipment to learn in class or to interact with teachers; and teachers' ability to control mobile-assisted language teaching or the evaluation strategy of pupils' comprehensive ability of seeing, hearing, or speaking in the intelligent classroom is immature enough [11]. Wang believed that, under the influence of traditional exam-oriented education, there has been long-term cultivation of listening or speaking, rereading, writing, or translating abilities in University English teaching [12]. Zhang L believed that the class hours of University English audio-visual or speaking courses are small or the class capacity is large, so if teachers want to complete the relevant teaching tasks within the limited class hours, pupils will naturally have fewer opportunities to participate in listening or speaking practice [13]. Li believes that it can stimulate pupils' motivation or interest in language learning, change their learning concepts, or encourage pupils to truly realize the importance of audio-visual courses from the bottom of their hearts, so as to actively learn or actively cooperate with related teaching activities [14]. Long believed that the establishment of a diversified evaluation system of University English audio-visual-oral courses is mainly to further test the learning effects of pupils or the teaching achievements of teachers. A perfect evaluation system of University English audio-visual or oral courses can help English teachers find or solve the problems in the teaching process of audio-visual or oral courses in time to realize the mutual learning between teaching and learning [15]. Othman et al. believed that the quietly coming of the era of Hadoop has had a strong impact on University English education for cultivating applied or innovative foreign language talents [16]. At present, in University English teaching, the teaching content depends heavily on textbooks. Teachers rely on English textbooks to carry out various teaching activities, or the teaching emphasis is also placed on the explanation of various vocabulary, grammar, sentence patterns, or articles in textbooks. As a result, pupils' knowledge of content is limited to some extent, or the cultivation of comprehensive English quality is not balanced

enough. In particular, different college pupils have different majors or future developed goals, or expect richer or more targeted teaching contents to meet their individualized needs. Therefore, it is essential to use data technology or resources to select individualized teaching content [17].

In the past, most of the teachers in English teaching only taught step-by-step mechanically, or the teaching organization form was often unchanged, so pupils' interest in learning was not high, or individualized teaching was difficult to realize. Therefore, according to the scientific application of Hadoop or other analytical tools, teachers should make an overall analysis of pupils' situations or adopt a personalized teaching organization form to effectively incorporate pupils of different levels into the teaching organization system, so as to improve the teaching quality or pertinence. It is necessary to combine the advantages of Hadoop technology in English teaching or explore effective countermeasures to implement personalized teaching.

3. Integration of Hadoop or University English Teaching

3.1. Analysis of the Significance of the Integration of Information Technology or University English Teaching. In the current external development environment, with the development or popularization of various technologies, English plays an increasingly important role in various fields, such as economic activities, cultural exchanges, education or teaching, and people's daily work or life. As an educator, it is necessary to combine the developed trends of the times, establish talent training objectives, take applied talents as the training core, or adjust teaching content or teaching methods. Let pupils' attitude towards English learning change from the inefficient way of memorizing words or grammar in the past or gradually take English application as the learning goal so that pupils can not only master the theoretical content of English words or grammar but also strengthen their language application ability, improve their confidence in the language expression, or speak fluent or standard English [18].

The functional advantages of using technology assist teaching or improve the efficiency or quality of classroom teaching. In the era of Hadoop, the development of information technology is accelerating, but the combination of information technology or English teaching activities is still relatively short, which also causes many teachers to apply information technology to English teaching, but the actual teaching effect or quality has not reached the ideal state. Because of this phenomenon, educators realize that the method for integrating information technology with English teaching still lacks systematicness. Therefore, if we want to make better use of information technology to improve the English teaching effect, we must find the key to the integration of the two, that is, how to introduce information technology in a timely or appropriate way in actual teaching, or what is the method of introduction or the interaction between teachers and pupils. All these problems require teachers' comprehensive planning or detailed thinking to formulate an efficient teaching plan suitable for pupils' development. If teachers lack awareness of the integration of information technology or English teaching or still carry out English subject teaching according to traditional teaching methods, they will not be able to assist teachers in effectively completing their teaching tasks or objectives. However, the integration of modern information technology or English teaching can provide services for building efficient classrooms. Learn English through the Internet. Compared with the past book learning methods, not only the learning content is enriched but also the learning channels are exposed. Pupils can use software to learn words, take online open classes or overcome difficult or important knowledge with the help of microclasses; thus, the learning efficiency is significantly improved. Moreover, the diversification of online learning also brings more novelty to pupils, which is conducive to mobilizing pupils' learning initiative, enabling them to learn English more actively, thus achieving higher learning efficiency, as shown in Figure 1.

3.2. University English Audio-Visual-Speaking Teaching Combined with Hadoop Technology. Affected by long-term quality education, both teachers and pupils regard learning English as a task or learning English as just to pass the exam. Moreover, most of the exams are written, lacking the test of oral learning, or the proportion of listening is mostly less than 20% [19]. With the advent of the Internet era, the demo for English listening or speaking professionals has increased dramatically. Traditional English teaching has trained many experts in reading or composition, which cannot meet modern needs. Besides, universities can introduce new teaching modes such as the Internet in time, resulting in poor teaching effects of University English listening, speaking, or listening. With the emergence of rapid development of corpus technology or the establishment of large-scale corpora, it is possible to acquire knowledge from corpora, followed by some statistical methods based on corpora. The main methods are the boundary statistical method, the example-based method, and the mutual information method. The example-based method is also called the memory-based method or similarity-based learning method, which is a guided machine learning method based on classification. It stores a large number of example sets according to specific tasks, or each example is associated with a feature vector, or it also corresponds to a certain class, that is, the solution formula as shown in the following:

$$\triangleright (X, Y) = \sum_{I=1}^{N} O(xi, yi). \tag{1}$$

Choose a feature that appears many times to correspond to multiple classes, that is, when its solution is ambiguous, as the result. X or y are characteristic vectors to be compared, or I of these two vectors are publicized as follows:

$$Y(xi, ti) = 0 \succ if\,(xi = ti). \tag{2}$$

If there is more chance that they appear together than they do at room, then the higher the mutual information value is, the greater the possibility of or forming a phrase, or the lower the mutual information value, the greater the

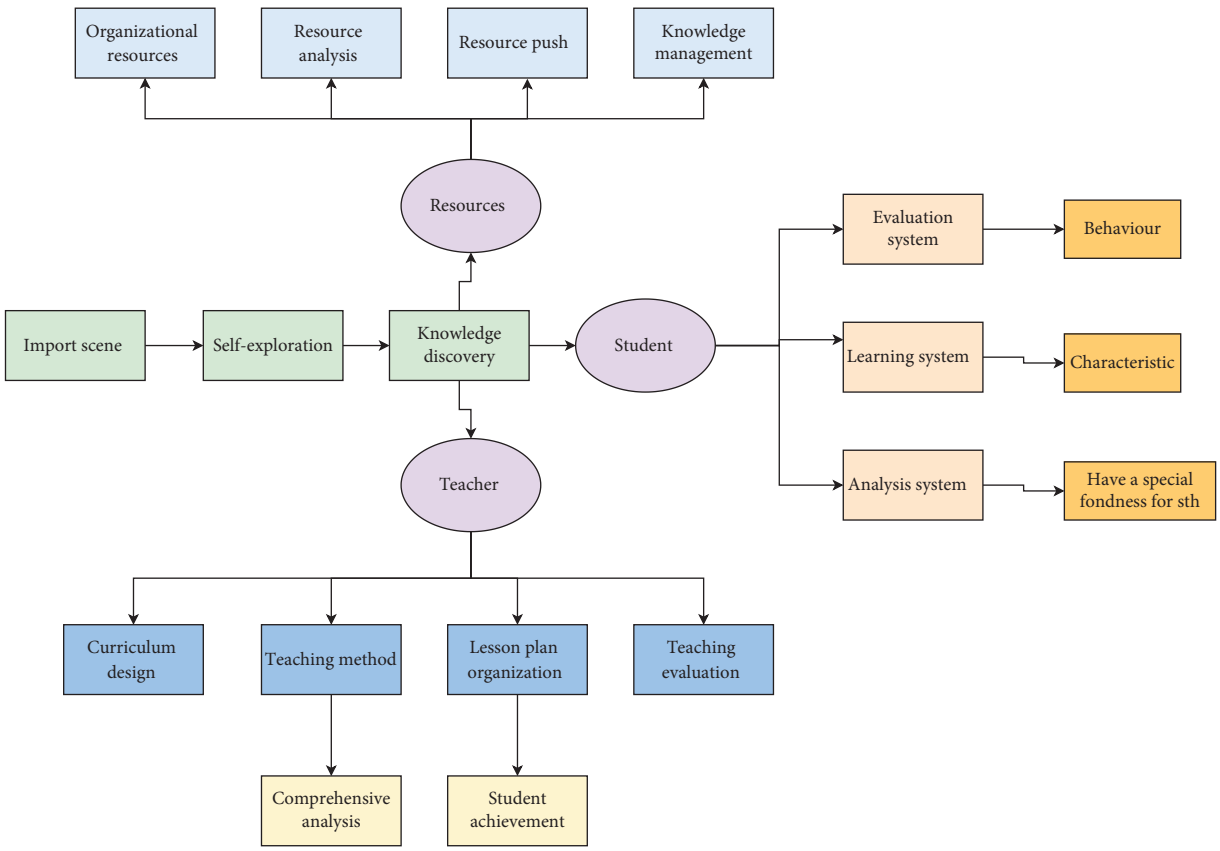

Figure 1: Learning efficiency analysis diagram.

possibility of a phrase boundary. Because a phrase is not necessarily composed of only two words, it is necessary to calculate the mutual information within a symbol combination. The theoretical basis of phrase boundary division based on mutual information is that, in one, the position of the phrase boundary is between a pair of markers with the smallest local generalized mutual information value. The calculation formula of generalized mutual information is as shown in the following:

$$\text{GMI } N_{I(I+J)}(X1 \ldots XI, Y1 \ldots YI). \tag{3}$$

The mutual information method is a method based on boundary statistics. Mutual information is a concept in information theory, which is used to measure the interdependence between two signals in a message. Binary information is the formula of the probability of two events, such as

$$MI(X,Y) = IB\frac{P(X,Y)}{P(X) \times P(Y)}. \tag{4}$$

In this algorithm, each feature is given an information gain, or when the eigenvalue is known, the uncertainty of the class solution corresponding to the eigenvalue is reduced by the information gain:

$$H(D[f]) = \sum pibq. \tag{5}$$

The most important thing for language learning is a good communication environment. The teaching or learning of University English audio-visual or speaking is mostly in the voice classroom. Due to poor teaching equipment, tight seats in the voice classroom, too many pupils, and less than 30% of the audio-visual or speaking classes with less than 50 pupils, it is difficult for teachers or pupils to communicate effectively, pupils' oral problems to be corrected in time, or their listening or speaking abilities to be improved. Moreover, over the years, universities have been exploring their enrollment. As a public basic course, audio-visual-speaking is hard to be effectively improved in a short time due to the huge pressure of teaching equipment or venues [20], as shown in Figure 2.

It can be seen from the figure that, with the continuous enrollment expansion of universities, audio-visual or speaking as a public basic course, the huge pressure of teaching equipment or venues has led to a sharp decline in the number of pupils, constructing the data resource base of University English audio-visual-oral learning. It is necessary to establish a learning platform for English audio-visual-speaking majors in universities, which is divided into four major sections: listening, speaking, reading, and writing, or each section uploads specific learning resources, which should be updated dynamically [21]. Each pupil can download the learning materials that meet their own learning situation on the platform at any time by registering an account on the mobile device side, to meet the individual learning needs of each pupil. Thirdly, assist teachers in teaching activities. Through the Hadoop technology to build

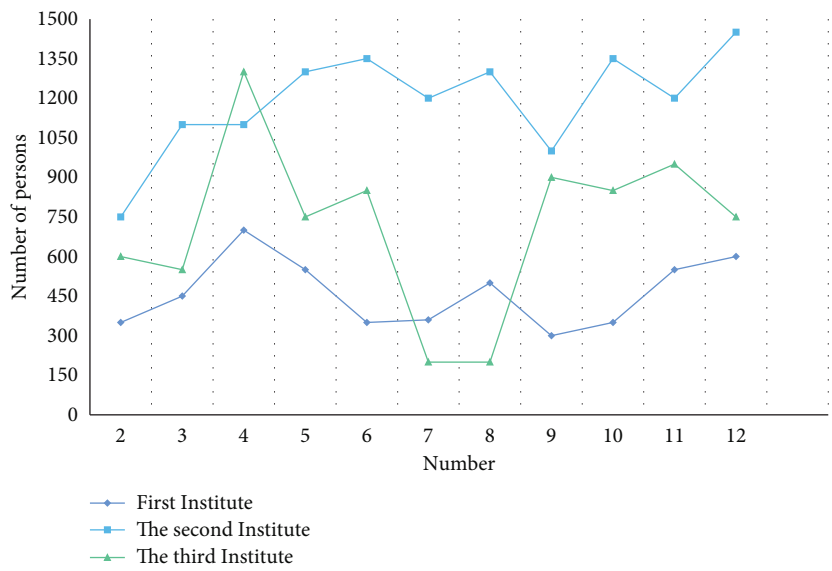

Figure 2: Audiovisual number of university English pupils.

a database or establish each pupil's learning ledger, teachers can learn about each pupil's learning status according to the data. For example, if a pupil's reading or writing scores are high, but his listening or speaking scores are not satisfactory, the teacher will either strengthen the pupil's listening or speaking learning for sex or urge the pupil to pay close attention to listening or speaking practice. See Table 1 for the number of pupils in college audio-visual classes.

Table 1: Table of number of pupils in college audition class.

Class number	Investigate colleges or universities	Proportion of (%)
Less than 30 people	16	8.56
Between 30 or 50	35	9.63
More than 50	50	11.33

4. Effectiveness Evaluation Model of University English Listening, Speaking, or Listening Precision Teaching in Hadoop Context

College English audio-visual speaking is a subject with strong application or practice. Secondly, in the era of "Internet plus," pupils become the main body of teaching, or teachers can answer questions based on individual pupils' requirements to make the teaching evaluation more scientific, objective, or comprehensive. The teaching objectives of college English audio-visual speaking courses are only generally included in the overall teaching objectives of college English. The short-, medium- or long-term teaching objectives of listening practice or oral training are not set separately, which stimulates pupils' motivation or interest in language learning. Change the learning concept or urge pupils to truly realize the importance of audio-visual or oral courses from the bottom of their hearts, to actively study or actively cooperate with related teaching activities. In actual teaching, the lack of a sound or reasonable listening or oral testing mechanism or the diversification of evaluation subjects in the evaluation system can help teachers or pupils carry out teaching practice to the maximum extent [22]. The evaluation mode is shown in Figure 3.

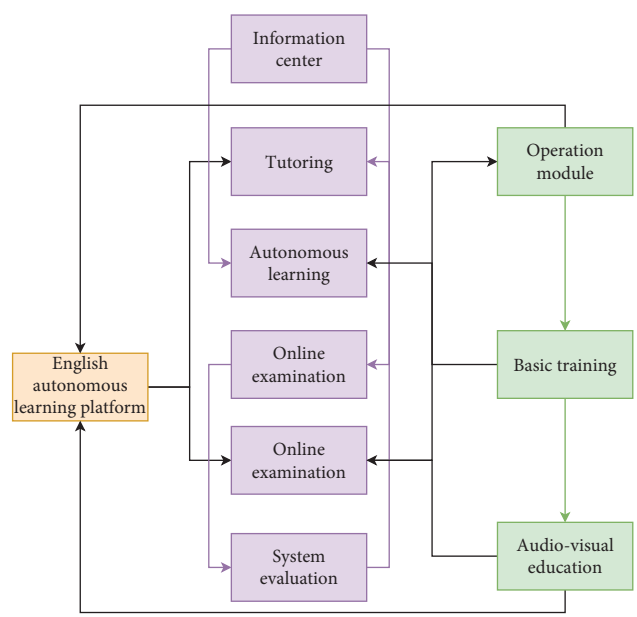

Figure 3: Evaluation mode.

The algorithm consists of two parts: one is to put the instance in the decision tree, and the other is to extract the classification information from the tree. In the process of establishing a decision tree, the plum path between nodes represents an instance, or all nodes contain a test item. Based on the default classification value of a certain feature or a classification identifier representing that point, the order of the feature of the instance to be tested in the tree is determined, which is fixed in advance. According to the vertebra, the most important feature to determine its

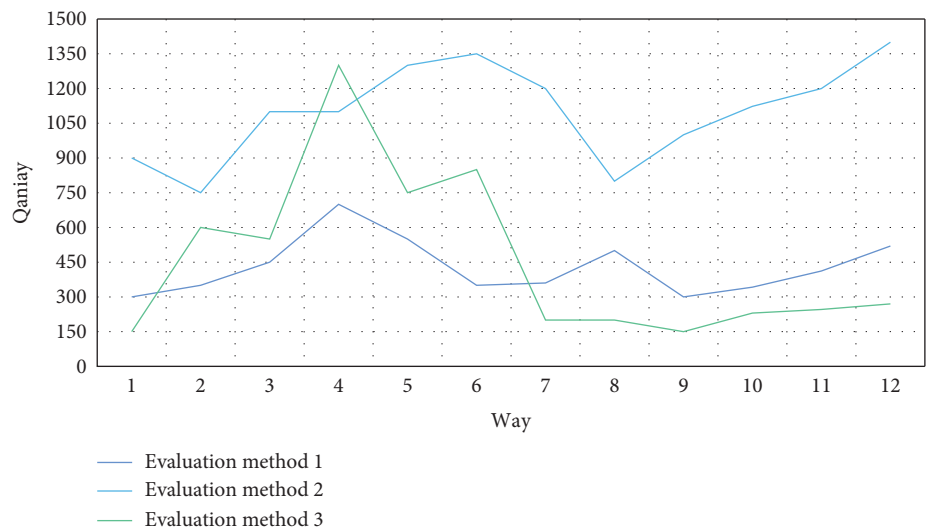

Figure 4: Number of diversification evaluation methods.

classification is placed on the first level. The default classification information corresponding to each characteristic value was calculated in advance. In the search process, compare the feature value of the sentence to be marked with the features of the layers in the tree. For example, when you go to the leaf node, take the classification value corresponding to the leaf node; otherwise, take the default value. The algorithm prunes the tree by information gain, so the time complexity is obviously reduced:

$$C(X) = \mathrm{EXP}\left[\sum UX - Y\right]. \tag{6}$$

English teaching should pay attention to the evaluation of pupils or practice, break through the previous mastery of the original knowledge, or strengthen the proportion of self-dialectic or self-evaluation. Through the implementation of diversified evaluation methods, pupils can better reflect on their autonomy, or their interest or subjective initiative will be greatly enhanced. Teachers should further increase the proportion of guiding evaluation or make effective use of constructivism theory so that different levels or types of cultures can rub against each other to produce due effects, or lay a solid foundation for the quality of training applied English talents. The teaching evaluation should also highlight objectivity, accuracy, or scientificity, promote pupils' cognitive level in coordination, or focus on changing pupils into the main position of evaluation so that pupils can really improve the effect of precision teaching through a sound evaluation mechanism, as shown in Figure 4.

The seven attributes of the English teaching comprehensive ability evaluation system are intelligence cultivation, personality-oriented teaching, motivation or attitude, social environment, learning environment, natural environment, or capital investment. The evaluation of teachers' teaching quality is an important aspect to evaluate the teaching effect in colleges or universities, an important basis for the evaluation of teachers' professional titles or a major component of teaching management in colleges or universities. At present, the evaluation methods of teaching quality are mainly based on statistics or simple calculations; that is, statistics, a collection of pupils' evaluations or achievements, or weighted calculation of teachers' scores as the evaluation index of their teaching quality [23]. However, this method is not scientific or authoritative, and a large amount of data collected in the teaching process has not been fully mined. A more scientific method is to fully mine all kinds of data through the method of association rules or get valuable information as the evaluation basis of teachers' teaching quality. At present, all or most of them contain functional modules such as pupil management, teacher management, course management, or achievement management [24, 25] (Figure 5).

You can also use the decision tree method for data mining. Because the research goal is the passing situation of CET-6, you can take "CET-6 passing situation" as the category attribute of the sample set, with two values, "passing" and "failing." Run the decision tree algorithm program, and finally, you can get a decision tree formula such as

$$h(t) = h(h.t), h(2)\bullet 3. \tag{7}$$

The constraint parameter index analysis of English teaching ability evaluation analysis was constructed or the quantitative recursive analysis method was adopted to analyze the Hadoop information model of English teaching ability evaluation. In order to improve the quantitative evaluation ability of the English teaching level, an English teaching ability evaluation method based on Hadoop fuzzy K-means clustering or information fusion was proposed, which transformed the problem of English teaching ability evaluation into the problem of solving the objective function of K-means clustering as the least square estimation. The least-square problem is to find the consistent estimate of the resource constraint vector β of the English teaching ability assessment so that $Y - X\beta$ can be minimized, where F norm is the norm of European generation. The entropy characteristic formula of English teaching ability constraint characteristic information is

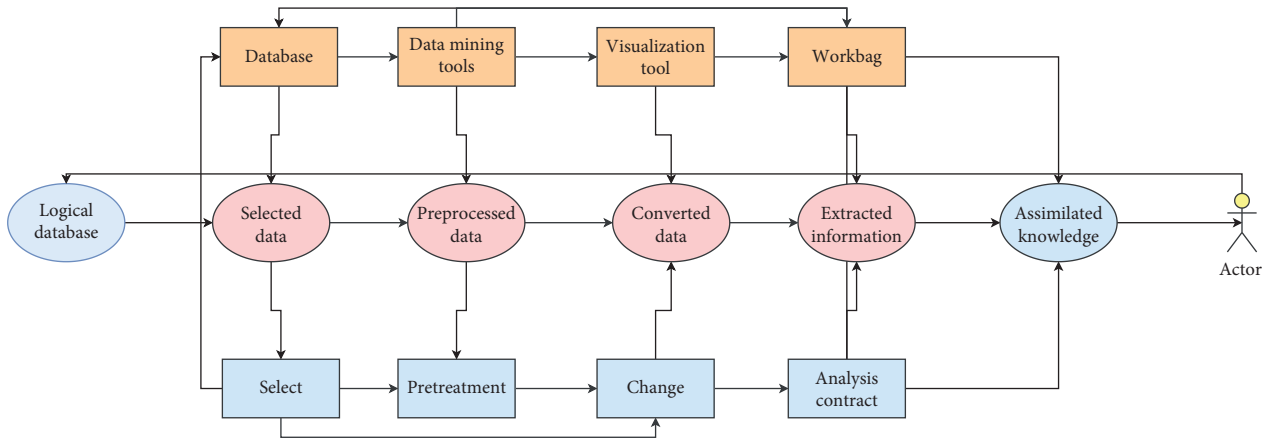

Figure 5: Basic management information.

$$P = 1 - \frac{1-P}{P} = \frac{P+P-1}{P} = \sum n = 1. \quad (8)$$

Under the background of "Internet plus," University English teachers should combine the Internet with traditional teaching, enrich or export English teaching resources by using network resources, construct new forms of English teaching by means of microclasses, flipped classrooms, multimedia, etc., or promote communication between teachers or pupils by means of online social platforms, to create a new form of English teaching, improve the informatization or networking level of English teaching as a whole, or make English teaching better adapt to modern education. At the same time, University English teachers should keep pace with the times, constantly learn about "Internet plus" education, constantly learn new teaching ideas or methods, or improve their teaching ability to meet the needs of English teaching under "Internet plus." With the support of an online social platform, teachers can share high-quality courseware with pupils, assign holiday homework, or guide pupils to learn after class. Pupils can receive teaching resources from teachers, you can reflect on your own learning situation with teachers at any time, or communicate with teachers online when you encounter problems you do not understand, as shown in Table 2.

We need to adopt the Hadoop information fusion method to construct the interdomain classification objective function of the distributed Hadoop information flow for English teaching ability evaluation; that is, the Hadoop clustering objective function is

$$J(U,V) = \sum 4 \sum N(d)^2. \quad (9)$$

The constraint parameter index analysis model of English teaching ability evaluation or analysis is a developed open source project, which is an enhanced language implementation based on the algorithm. The algorithm is encapsulated into a core module; then, a series of peripheral modules are added to export its functions. The rule file for the project is in a custom format. Basic semantics are defined by a language. Add feet or semantic modules. Developers can also customize their own dedicated semantic modules

Table 2: Learning situation.

Attribute	Confidence level			
Gender	25.2%	53.7%	60%	20
	23%	65%	50%	54
Education	23%	35%	42.5%	56
	25.6%	56%	53.2%	45
Title	26.3%	25%	20%	67
	21.4%	45%	50%	35
Teaching age	82.5%	50%	70%	90
	31.5	40%	90%	45

according to their needs. Each rule file includes a unique rule set, or the rule set includes one or more rules. Each rule includes one or more parameters. These parameters are used to judge or perform corresponding operations in the conditions of the rules. The parameters correspond to a class, which will be automatically instantiated when the working memory is created. Each rule includes one or more conditions or the last action. The formula is

$$X = x(i + n\triangleright = h) = h[z(l+n)] + \phi. \quad (10)$$

5. Direction of University English Audio-Visual Speaking Teaching

At present, the role of Hadoop in economic and social development or education is increasingly prominent. People can get valuable information through Hadoop analysis, which can provide guidance for the smooth development of various activities. Hadoop analysis usually involves deep data mining or analysis, not just simple statistics or calculations. Therefore, the analysis of English education data will have more advantages in terms of accuracy and intelligence. Over the years, the rapid development of artificial intelligence has also provided new technical capabilities for Hadoop analysis. The development of artificial intelligence has greatly promoted the development of computer hardware performance or software technology or provided technical support for fast or accurate processing of massive data. Therefore, future Hadoop processing cannot be

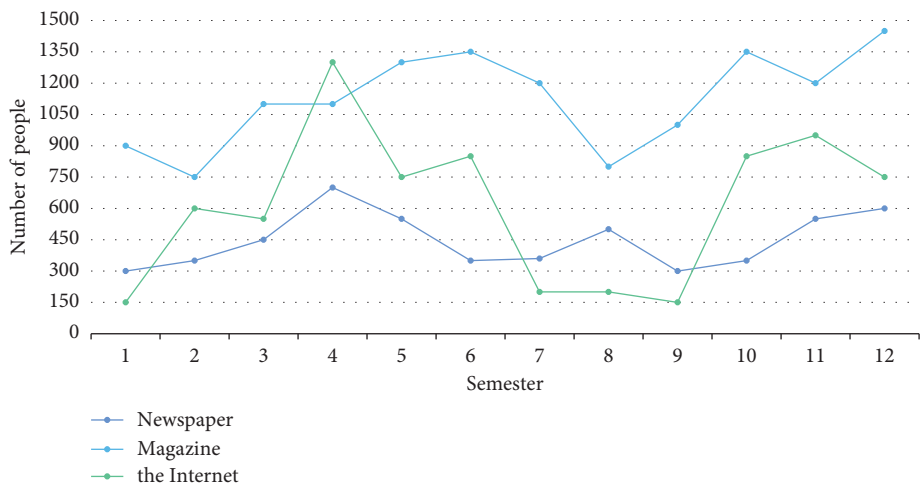

Figure 6: Different ways of pupils' knowledge acquisition.

separated from artificial intelligence, or the application of Hadoop in English personalized education will inevitably improve the intelligence level of personalized teaching.

The primary task of implementing individualized English teaching under the background of Hadoop is to formulate individualized teaching objectives so that teachers can perform teaching design around accurate teaching objectives. First, teachers should make use of Hadoop technology to investigate or count pupils' personal status or English learning status, such as majors, English basics, English specialties, learning ability, hobbies, and future development direction, and then, summarize or analyze the collected data or use it as the basis for setting teaching objectives to ensure that the teaching objectives are more personalized. Secondly, teachers should analyze the teaching content, formulate teaching objectives at different levels according to pupils' different situations, and express different subobjectives according to pupils' individual learning or development needs, to guide pupils to diversify their development. For example, when relying on textbooks to cultivate pupils' reading ability, the public goal is to emphasize pupils' reading or mastering the content of the text or to develop their basic reading ability. The stratified goal requires pupils to choose appropriate reading materials according to their hobbies or professional development direction, which can be selected from newspapers, magazines, the Internet, or other resources. The amount of knowledge acquired by different pupils from newspapers, magazines, or the Internet is different, as shown in Figure 6.

Whether the choice of teaching method is scientific or effective, it will greatly affect the implementation effect of various teaching activities or the smooth realization of teaching objectives. To ensure the smooth implementation of English personalized teaching, we must change the previous unified or general teaching methods or make full use of Hadoop technology to innovate the teaching method system to meet the implementation requirements of English personalized teaching. The evaluation methods of blended teaching should also refer to the teaching steps, design scientifically or rationally, or make comprehensive use of various evaluation methods. Before class, pupils conduct autonomous learning or online learning on the online platform. Pupils' self-evaluation or peer-to-peer evaluation can be used to test their achievements in autonomous learning or online learning. Teachers can also evaluate pupils according to their learning reports on the network platform, online discussions, etc., or can combine the evaluation of pupils or pupils. In class, teachers can evaluate pupils according to their classroom performance, such as through classroom tests or questions. After class, teachers can also conduct mutual evaluations between teachers and pupils, or between pupils and pupils according to the learning situation of the pupils' online platform. In the mixed teaching mode of University English, the combination of summative evaluations or formative evaluation, teacher evaluation or pupil evaluation, and paper evaluation or time-space evaluation forms a pluralistic or three-dimensional teaching evaluation system. The number of systems is shown in Figure 7.

Mobile language learning mode refers to the introduction of the "Internet plus" concept on the basis of the traditional University English teaching mode to promote "intelligent classroom teaching." Mobile-assisted language teaching mode does not only provide classroom teaching to machines but also combine all kinds of systematic education, or teaching theories, or teaching psychological knowledge summarized by predecessors, with the idea of computer-based teaching, so that mobile-assisted devices can help teachers design more colorful classrooms to meet pupils' learning needs. This is one of the backgrounds for the development or practical exploration of a mobile-assisted language learning mode. Besides, structuralism or cognitivism also regards pupils' self-inquiry or self-learn construction as the core of subject teaching. As an important part of English classroom teaching, a successful teaching introduction can create a good start for the follow-up teaching. Therefore, teachers must pay attention to the design of teaching introduction, introduce new lessons in a lively or interesting way, or strive to stimulate pupils' interest quickly to lead out the classroom teaching content smoothly.

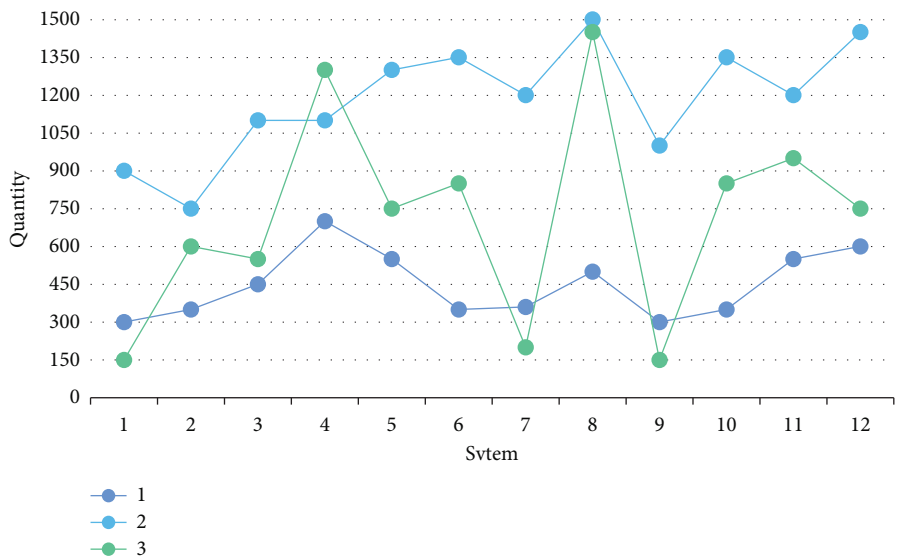

Figure 7: Number of systems.

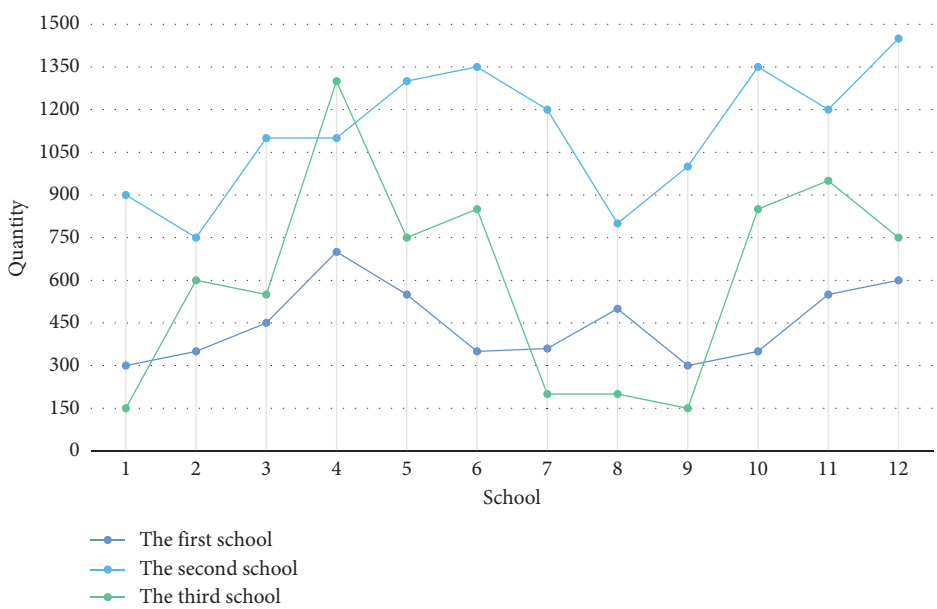

Figure 8: Number of pupil accounts.

The combination of multimedia or audio-visual teaching has a powerful audio-visual effect, which can stimulate pupils' senses or arouse their curiosity or interest. Therefore, in the classroom, teachers can create teaching situations through multimedia videos, ask questions in line with the curriculum through the situations, subtly lead out the new lesson content, or successfully complete the teaching introduction.

Assist teachers in teaching activities. By building a database with Hadoop technology or establishing each pupil's learning account, teachers can learn about each pupil's learning status according to the data. For example, if a pupil's reading or writing scores are high, but his listening or speaking scores are not satisfactory, the teacher will either strengthen the pupil's listening or speaking skills or urge the pupil to pay close attention to listening or speaking skills. Through the monthly, quarterly, or annual learning track, we can clearly understand each pupil's learning situation, establish relevant modes, or find the best teaching mode, which can effectively improve the level of University English audio-visual or oral teaching. It is necessary to listen to or train students individually. The audio-visual course is highly practical, and pupils must train many times to achieve the ideal learning effect. Therefore, teachers must strengthen the training of listening or speaking ability. However, after the expansion of university enrollment, teachers have become weak and the number of professional audio-visual or speaking teachers has been insufficient, so it is difficult to consider every pupil. In the era of Hadoop, the emergence of

artificial intelligence technology can effectively improve this scenario (Figure 8).

6. Conclusions

University English audio-visual teaching also highlights innovation or practice. It is necessary to break through the mastery of previous knowledge or strengthen the proportion of self-dialectic or self-evaluation. University English teaching workers should actively apply convenient conditions, turn challenges into opportunities, or extract valuable things from a large amount of information for our use. Audio-visual teaching is very complicated and involves a relatively wide range. In the selection of data resources, we must select the best pupils, change the traditional teaching idea, teach accurately, or use multidimensional or multivariable evaluation mode to realize the unified evaluation of summative or formative evaluation so that the evaluation mechanism becomes an important part of the teaching process. Only by ensuring concrete, objective, or effective evaluation can we really give full play to the advantages of audio-visual teaching in the era of Hadoop, changing thinking concepts or roles, paying close attention to pupils' real time dynamics before, during, or after class, optimizing teaching contents or methods in the intelligent classroom environment, forming a scientific system of intelligent teaching with distinctive characteristics, effectively improving the quality of University English teaching, or thus promoting the rapid development of intelligent teaching of University English in the era of Hadoop. To realize accurate teaching, we should use multivariate or multidimensional evaluation modes, combine quantitative or qualitative evaluation, reconstruct the evaluation mode of the University English audio-visual course, or rely on information technology or multimedia to improve the efficiency by 16% to improve the teaching quality or effect of University English audio-visual or oral courses or promote the improvement of pupils' comprehensive English ability.

Data Availability

The data used to support the findings of this study are included within the article.

Conflicts of Interest

The author declares that there are no conflicts of interest regarding this work.

References

[1] S. Shanshan, L. Wenfei, and L. Lijuan, "Applying lean six sigma incorporated with big data analysis to curriculum system improvement in higher education institutions," *International Journal of System Assurance Engineering and Management*, vol. 13, no. 2, pp. 641–656, 2022.

[2] H. Y. Huang, "The opportunities, myth or suggestions to the develop of curriculum teaching in university under the Hadoop background," *Journal of Yichun University*, vol. 4, no. 23, pp. 5–9, 2017.

[3] L. Liu, B. Xin, and H. N. University, "A new perspective of the curriculum or teaching for higher education——based on the knowledge view of the Hadoop era," *China Educational Technology*, vol. 7, no. 46, pp. 1–6, 2017.

[4] J. Shen, P. Xu, and Q. Zhang, "Research on the construction of university data literacy curriculum group in the era of Hadoop," *Library or Information Service*, vol. 6, no. 15, pp. 4–6, 2019.

[5] R. R. RahmiE, "Journal of English language teaching pupilS`pupilS`PERCEPTION on program specification of elt curriculum based on AUN-QA criteria," *English Language or Linguistics*, vol. 15, no. 24, pp. 6–9, 2018.

[6] J. J. Zhang, "On hadoop's influence on English teaching," *Journal of Jiamusi Vocational Institute*, vol. 11, no. 75, pp. 12–16, 2018.

[7] Y. U. Fang, "The analysis of the way of realizing high quality English teaching in college in the era of Hadoop," *Journal of Guiyang University(Social Sciences)*, vol. 14, no. 19, pp. 20-21, 2018.

[8] W. Sun, "Strategic research on the integration of primary school English story teaching or primary school English curriculum resources," *The Guide of Science & Education*, vol. 16, no. 80, pp. 2-3, 2018.

[9] D. Li and G. A. Mashour, *NeuroImage*, vol. 196, no. 51, pp. 32–40, 2019.

[10] L. I. You and H. I. University, "Research on the reform of basic English teaching model or the optimization of curriculum system in application-oriented universities," *Journal of Qiqihar Junior Teachers' College*, vol. 22, no. 30, pp. 20–23, 2019.

[11] H. Tan, "The problems or improvement measures of university English teaching objectives or curriculum in private undergraduate colleges——taking guangdong peizheng college as an example[J]," *Journal of Zhongzhou University*, vol. 24, no. 23, pp. 8-9, 2018.

[12] Y. Q. Wang and L. University, "Analysis of the curriculum or teaching characteristics of "primary school English teaching skills training"," *Teacher Education Forum*, vol. 23, no. 24, pp. 30–35, 2019.

[13] L. Zhang, "Combining the "healthy China strategy" or the pupil's storard needs to talk about the reform of English teaching in preventive medicine," *The Guide of Science & Education*, vol. 24, no. 30, p. 29, 2019.

[14] B. Li, "Teacher learning based on school-oriented learn practice research of middle school English teachers," *Curriculum, Teaching Material or Method*, vol. 3, no. 21, p. 30, 2017.

[15] F. Long, "Reform in university English teaching in the education Hadoop era," *Journal of Qilu Normal University*, vol. 5, no. 20, p. 19, 2017.

[16] O. Othman, Z. H. Iksan, and R. M. Yasin, "Teachers' views towards changes in curriculum and the use of real-time big data in statistics education," *Creative Education*, vol. 12, no. 10, pp. 2424–2440, 2021.

[17] L. V. Zhi-Feng and H. H. University, "Research on the improvement of teaching system of large-scale database application course in the Hadoop era," *Heilongjiang Science*, vol. 57, no. 2, pp. 75–86, 2019.

[18] W. Wang and X. JayachandranLiXuLuo, *Microchimica Acta*, vol. 185, no. 3, pp. 156–159, 2018.

[19] H. M. Truong and V. T. Vuong Pham, "Teachers' and students' appraisal of the ITEC English curriculum: a comparative study," *Global Journal of Foreign Language Teaching*, vol. 10, no. 3, pp. 167–181, 2020.

[20] K. Wang, "Research on experimental teaching for economics or management majors in Hadoop era," *Journal of Harbin Engineering University*, vol. 19, no. 16, pp. 12–16, 2017.

[21] C. X. Chen and M. Polytechnic, "Learn on leap-forward develop of university English teachers in Hadoop era," *Education Teaching Forum*, vol. 18, no. 12, pp. 80–83, 2017.

[22] Q. Liu, "Analysis on intelligent transportation system course teaching reform under Hadoop[J]," *The Science Education Article Collects*, vol. 17, no. 1, pp. 6-7, 2017.

[23] Y. X. . Liang, "Research on the reform mode of university teaching method in the era of Hadoop[J]," *Heilongjiang Science*, vol. 15, no. 9, pp. 2–6, 2018.

[24] S. Mu, "Research on online learning curriculum in the context of Hadoop," *IOP Conference Series: Materials Science and Engineering*, vol. 750, no. 5, Article ID 012034, pp. 63-80, 2020.

[25] A. Yap and S. Drye, "The challenges of teaching business analytics: finding real Hadoop for business pupils," *Information Systems Electronic Journal*, vol. 16, no. 1, pp. 41–50, 2018.

Hindawi
Mobile Information Systems
Volume 2023, Article ID 9860170, 1 page
https://doi.org/10.1155/2023/9860170

Retraction

Retracted: Analysis of Ancient Literary Works Based on Intelligent Image Text Recognition

Mobile Information Systems

Received 1 August 2023; Accepted 1 August 2023; Published 2 August 2023

This article has been retracted by Hindawi following an investigation undertaken by the publisher [1]. This investigation has uncovered evidence of one or more of the following indicators of systematic manipulation of the publication process:

(1) Discrepancies in scope
(2) Discrepancies in the description of the research reported
(3) Discrepancies between the availability of data and the research described
(4) Inappropriate citations
(5) Incoherent, meaningless and/or irrelevant content included in the article
(6) Peer-review manipulation

The presence of these indicators undermines our confidence in the integrity of the article's content and we cannot, therefore, vouch for its reliability. Please note that this notice is intended solely to alert readers that the content of this article is unreliable. We have not investigated whether authors were aware of or involved in the systematic manipulation of the publication process.

Wiley and Hindawi regrets that the usual quality checks did not identify these issues before publication and have since put additional measures in place to safeguard research integrity.

We wish to credit our own Research Integrity and Research Publishing teams and anonymous and named external researchers and research integrity experts for contributing to this investigation.

The corresponding author, as the representative of all authors, has been given the opportunity to register their agreement or disagreement to this retraction. We have kept a record of any response received.

References

[1] J. Fan, "Analysis of Ancient Literary Works Based on Intelligent Image Text Recognition," *Mobile Information Systems*, vol. 2022, Article ID 1113856, 9 pages, 2022.

Hindawi
Mobile Information Systems
Volume 2022, Article ID 1113856, 9 pages
https://doi.org/10.1155/2022/1113856

Research Article

Analysis of Ancient Literary Works Based on Intelligent Image Text Recognition

Jia Fan

School of Literature and Journalism, Xihua University, Chengdu, Sichuan 610039, China

Correspondence should be addressed to Jia Fan; 1701100116@xy.dlpu.edu.cn

Received 20 July 2022; Revised 26 August 2022; Accepted 29 August 2022; Published 27 September 2022

Academic Editor: Chi Lin

The analysis of ancient literary works in the era of digital intelligence needs to keep pace with the times. In order to improve the analysis effect of ancient literary works, this paper combines the intelligent image text recognition algorithm to extract the features of ancient literary works and proposes an intelligent algorithm that can be used for the analysis of ancient literary works. Moreover, this paper combines the analysis needs of literary works to improve the algorithm. In order to verify the role of the intelligent image text recognition algorithm proposed in this paper in the analysis of ancient literary works, this paper scans a large number of pictures of ancient literary works in the library by scanning to construct the experimental database of this paper. Finally, this paper combines experimental research to verify the algorithm proposed in this paper. From the experimental results, it can be seen that the method proposed in this paper has a certain effect, and it can be used as a reference for the digital processing and digital preservation of subsequent literary works, and it can also be used as a reference for the management of digital libraries.

1. Introduction

Human beings have always evolved and developed along with image culture and have deep historical origins with it. In ancient times, the ancestors generally used the method of physical records to record daily events. Recording in kind means that the primitive ancestors recorded figures in kind or expressed their opinions and feelings. This kind of method of remembering things in the image of real objects existed in large numbers in the ancient times of many nations or countries. They have a certain impact on other methods of note-taking and the invention of later writing. This primitive calculation method in kind is still used by many ethnic groups (including some ethnic minorities in our country) that are still in a primitive state in today's world. For example, when the Li ethnic minority group in Hainan Island settled accounts, every few tens of straws were put in one section to remember that human beings have always evolved and developed along with image culture. In ancient times, the ancestors generally used the method of physical records to record daily events. Recording in kind means that the primitive ancestors recorded figures in kind or expressed their opinions and feelings. This method of remembering things in the image of objects existed in large numbers in the ancient times of many nations or countries [1]. They have a certain impact on other methods of note-taking and the invention of later writing. This primitive calculation method in kind is still used by many ethnic groups (including some ethnic minorities in our country) that are still in a primitive state in today's world.

In ancient times, the level of social productivity was extremely low, and the living conditions of primitive people were very difficult. Moreover, the living environment is extremely dangerous, social life and spiritual life are also in a barbaric and ignorant state, there is little production experience, and the level of labor skills and knowledge is very low. In order to survive, people have to use primitive and crude production tools to fight against nature. In order to exchange ideas and convey information, language came into being [2]. However, language is fleeting, neither can it be preserved nor can it be transmitted to distant places. Moreover, it is impossible to rely solely on human brain memory. As a result, the original method of note-taking, namely, pictures, naturally appeared. Before social

production and social relations have developed to the point that people feel that they must use language to record things or transmit information, they can only use pictures directly to represent things, and they do not think of using them to record the names of things—words in the language. Over time, these have become customary. With the passage of time, more and more such pictures have played a role in mutual communication [3].

This paper combines intelligent image text recognition technology, proposes an intelligent algorithm that can be used for the analysis of ancient literary works, combines the needs of literary works analysis to improve the algorithm, and combines experimental research to verify the algorithm of this paper.

2. Related Work

In order to solve the problem of binarization of degraded document images, scholars have devoted themselves to research and proposed many methods. Among the traditional threshold calculation methods, the representative algorithms of the global threshold method include the simple iterative method, Otsu algorithm, and histogram peaks algorithm. [4]. The global threshold method determines a threshold according to the gray value of the image and then divides the image into two parts, the foreground and the background, according to this value. The method is simple to implement and fast in execution. However, when the background noise of the image to be processed is complicated, the use of a fixed threshold may lose the foreground information or retain a large amount of noise information, which is obviously not the most ideal method for binarization. Therefore, a local threshold method based on histogram was born, among which the more representative algorithms mainly include the Niblack algorithm [5], Sauvola algorithm [6], Wolf algorithm [7], and other methods. Some scholars have proposed binarization algorithms based on local contrast, such as the Bernsen algorithm [8], a contrast calculation method based on local maximum and minimum gray levels, also known as the LMM algorithm [9], Gatos algorithm [10], and BESE algorithm [11]. Compared with the global threshold method that selects a single threshold, the local threshold effect is more accurate. However, because the threshold adjustment of this method varies according to the size of the sliding window, there may also be phenomena such as misjudgment of the foreground and background. In addition to some methods based on histograms, traditional threshold processing algorithms also appear to select thresholds based on image features, such as threshold segmentation algorithms based on image texture features [12]. This method first uses the Otsu algorithm to iteratively extract candidate thresholds and then extracts the texture features associated with each candidate threshold from the run-length histogram. Finally, the optimal threshold was selected to maintain the ideal document texture characteristics. Some scholars also consider the image as a three-dimensional terrain and put forward a very interesting thresholding idea. On this basis, a water flow model is proposed, which extracts characters from the background through a thresholding method. Compared with histogram-based methods, feature-based methods can usually get more robust binarization results because high-resolution image features can be used to classify foreground and background pixels [13]. This type of algorithm is more suitable for images with relatively single noise information. Since the noise of the degraded document image is more complicated and the noise information of most images has a low contrast with the foreground text, it is difficult to effectively remove the noise without losing the strokes of the foreground text.

Using a single traditional threshold segmentation method for binarization processing, it is difficult to show ideal results on complex degraded document images. Therefore, some scholars combine a variety of image processing techniques and make full use of certain characteristics of the image to perform binarization processing. The main methods include global and local combination methods [14] and the edge detection method used in literature [15], [16] The proposed methods include background estimation method, gradient normalization and saliency map method [17], and Laplace energy method [18], and so on. This type of algorithm is more adaptable and can achieve ideal results for general image binarization problems. However, due to the complexity and diversity of the types of degraded document images, in the current existing multithreshold fusion algorithm, even if a nonfixed threshold is used for processing, it is difficult to remove the background without losing the foreground text. Noise information is removed cleanly.

The method based on statistical learning refers to the application of the method in mathematical statistics to the binarization of the image; that is, the problem is transformed into a clustering or classification problem. Among them, the representative methods based on statistical learning mainly include the support vector machine algorithm [19], k-means algorithm [20], and fuzzy c-means algorithm [21]. Under the premise of a large number of data sets, using this type of method to process general types of images with a single noise information has an ideal effect. However, various types of degraded document images with complex noise causes the processed binarized image to be disconnected from the foreground text, hollow strokes, and even information loss. This is a problem that is not allowed for some precious archive files. If you want to get better binarization results, you need to perform secondary processing on this basis. In addition, the model built by this type of method depends on the data set. If the processed image is similar to the data set, the effect is better; otherwise, the effect is poor. Therefore, the generalization ability of this type of algorithm is poor.

3. Intelligent Ancient Literature Image Text Recognition Algorithm

The global threshold refers to the process of selecting a threshold for an image and applying it to the entire image. The algorithm mainly traverses each pixel of the image and compares it with the selected threshold and uses a formula to determine the category of the point. The global threshold

method is simple to implement and fast in execution. However, if the background noise of the document image is complex, the effect of the global threshold will be unsatisfactory. The following mainly introduces Otsu as a representative algorithm.

The Otsu algorithm is also called the Otsu method, which is a clustering algorithm. According to the characteristics of the gray value of the image, the algorithm obtains the best threshold when the variance between classes is the largest, and then divides the image into two categories: background and foreground. If there is a wrong classification of the categories, this will cause the variance between the two categories to become smaller. Therefore, we have to choose an appropriate threshold to maximize the variance between classes and minimize the probability of class misclassification.

We use L to represent the number of gray levels of the image, and use $\sum_{i=1}^{L} p_i$ to represent the total number of image pixels. Among them, n_i represents the number of pixels when the gray level is i. Relative to the histogram, the probability of gray level i is given as

$$p_i = \frac{n_i}{\sum_{i=1}^{L} n_i}, \sum_{i=1}^{L} p_i = 1. \tag{1}$$

If it is assumed that the best threshold value is$T = K, T \in (I, L)$, then we can use this value to divide the image into target and nontarget categories, which are represented by C_1andC_2 respectively. Among them, the gray value range of class C_1 is $[1, K]$, and the gray value range of class $C_2$is $[k+1, L]$. Then, the probability that a pixel may be divided into the foreground $p_1(k)$ and the background probability $p_2(k)$ can be given as

$$\begin{aligned} p_1(k) &= \sum_{i=1}^{K} p_i, \\ p_2(k) &= \sum_{i=k+1}^{L} p_i = 1 - p_1(k). \end{aligned} \tag{2}$$

Then, the average gray values of pixels classified into foreground $C_1$and background C_2 are, respectively, given as follows:

$$\begin{aligned} g_1(k) &= \frac{1}{p_1(k)} \sum_{i=1}^{K} i p_i, \\ g_2(k) &= \frac{1}{p_1(k)} \sum_{i=k+1}^{L} i p_i. \end{aligned} \tag{3}$$

The overall gray value of the image can be expressed as

$$g_{avg}(k) = \sum_{i=1}^{L} i p_i. \tag{4}$$

The between-class variance of foreground and background is

$$\sigma_{12}^2(k) = p_1(k) p_2(k) [g_1(k) - g_2(k)]^2. \tag{5}$$

It can be obtained from formula (7) that when the difference between g_1 and g_2 is larger, the variance $\sigma_{12}^2(k)$ between foreground and background is also larger, and vice versa. Therefore, the between-class variance can be used as a measure of the separability between the foreground and the background, which represents the difference between the two categories. The Otsu algorithm mainly uses the normalized histogram to select the segmentation threshold, so the operation is simple, relatively easy to implement, and it is widely used in the image processing neighborhood. The following will show the results of degraded document images processed by the Otsu algorithm. Among them, Figure 1 is the original picture, and Figure 2 is the effect picture after the Otsu algorithm is used.

From Figure 2, we can see that when there are smudges around the text, that is, when the contrast between the text and the background area is low, the foreground text area will be misclassified as the background area. In addition, the Otsu algorithm uses a uniform threshold to process the entire image, so some noise information is still retained, and the background area is not cleanly processed. It can be seen that the Otsu algorithm can get better results when the foreground and background present high contrast, but when the target area and the background area have low contrast or when dark blocks are formed due to ink pollution, the results of the algorithm are not ideal. Therefore, the Otsu algorithm is not suitable for degraded document images with complex backgrounds.

When the contrast between the foreground and the background in an image is not constant due to ink, lighting, etc., the effect of the global threshold method will become unsatisfactory. Therefore, the threshold segmentation method based on the local characteristics of the image should be adopted. The local threshold algorithm is an algorithm that takes into account the different characteristics of the local area of the image and selects different optimal thresholds for segmentation in different areas. The local threshold algorithm determines the local area of the image to be processed according to the size of the sliding window. Therefore, the size of the sliding window has a great influence on the effect of the local threshold method. Because the foreground text size, font, and stroke of the degraded document image vary, it is necessary to adjust the size of the sliding window according to the characteristics of different images in order to obtain the best binarization effect. The following mainly introduces four representative local threshold binarization algorithms: Niblack algorithm, Sauvola algorithm, Bernsen algorithm, and LMM algorithm.

The Niblack algorithm is a simple and effective local binarization algorithm. Its main idea is to take a pixel as the center and calculate the best threshold in the area according to the point in its neighborhood. If it is assumed that there is a pixel point p on an image, and its coordinates are (x, y), then the threshold T_p of this point is given as

$$T_p(x, y) = \mu_p(x, y) + k * \sigma_p(x, y). \tag{6}$$

Among them,$\mu_p(x, y)$ represents the average gray value of all pixels within the size of the sliding window around the

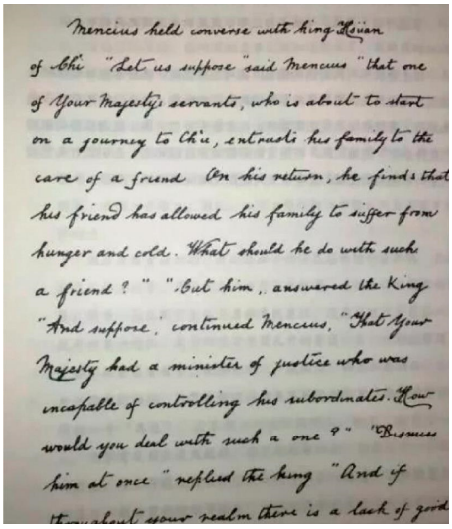

Figure 1: Original image.

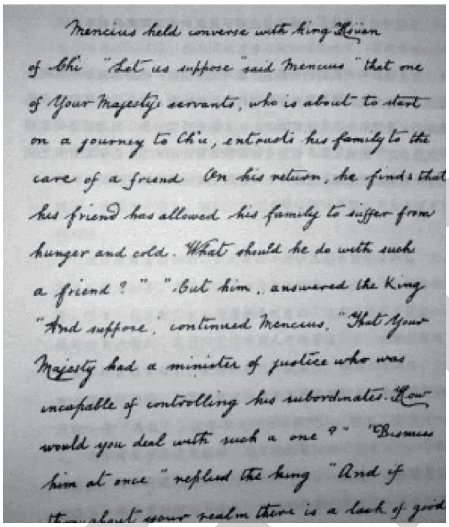

Figure 2: The result after Otsu processing.

pixel p, k is the coefficient for dynamically adjusting the threshold, and $\sigma_p(x, y)$ represents the standard deviation in the neighborhood. The following will show the result of the degraded document image processed by the Niblack algorithm. Among them, Figure 3 is the original picture, Figure 4 is the effect picture after using Niblack algorithm processing.

The Sauvola algorithm is a local threshold algorithm that uses the local mean as a benchmark and then fine-tunes the binarization effect according to the standard deviation. This algorithm can well solve the problem that the global threshold method cannot solve, that is, the binarization of the image with uneven illumination. The Sauvola algorithm is a local binarization algorithm for degraded document images, which is improved on the Niblack algorithm. If it is assumed that there is a pixel point P on the image, and its coordinates are (x, y), then the threshold T_p of this point is

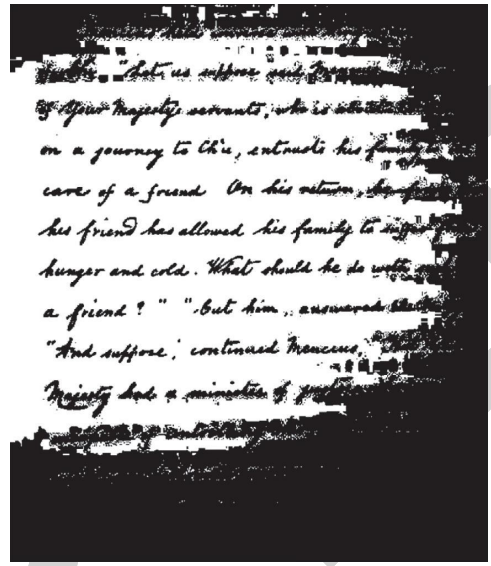

Figure 3: Original image.

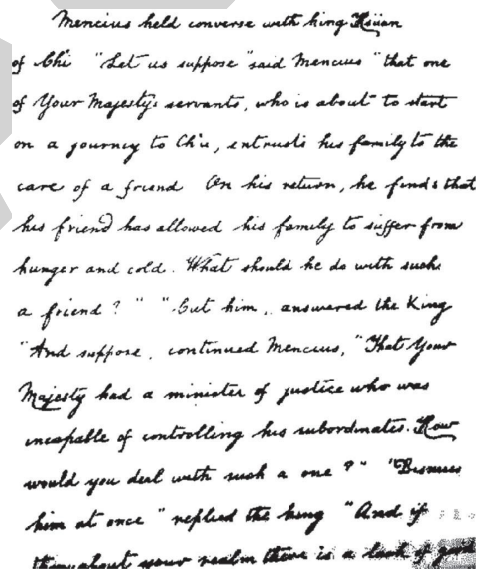

Figure 4: Effect picture after processing with the Niblack algorithm.

$$T_p(x, y) = \mu_p(x, y) * \left[1 - \frac{K * \left(1 - \sigma_p(x, y)\right)}{R}\right]. \quad (7)$$

Among them, $C_p(x, y) = f_{\max}(x, y) - f_{\min}(x, y)$ represents the average gray value of all pixels within the size of the sliding window around the pixel p, k is a coefficient for dynamically adjusting the threshold, $\sigma_p(x, y)$ represents the standard deviation in the neighborhood, and R represents a constant. Generally, $R = 128$ and $k = 0.5$. When we choose the size of the sliding window to be $40 * 40$, the experimental results of the Sauvola algorithm are shown in the figure below. Among them, Figure 5 is the original picture, and

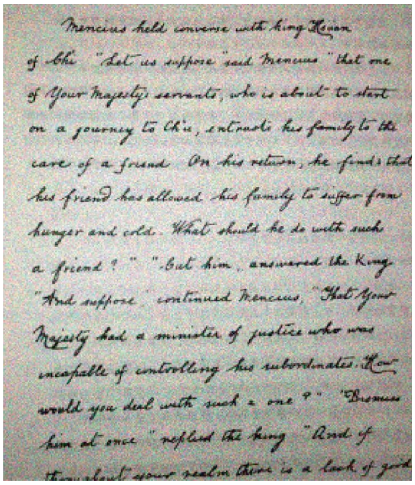

Figure 5: Original image.

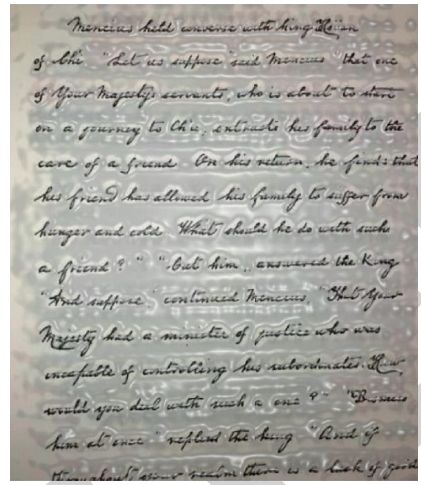

Figure 6: Sauvola processed results.

Figure 6 is the effect picture after the Sauvola algorithm is used.

From the experimental results, it can be clearly seen that the Sauvola algorithm has a better improvement than the Niblack algorithm with the presence of large ink spots in the image. However, when the image contrast is low, a large number of noise points are generated around the font, as shown in Figure 6, or the foreground is misjudged as background pixels, resulting in the loss of foreground fonts.

The Bernsen algorithm is a binarization algorithm based on local contrast. The so-called local contrast refers to the assumption that there is a pixel P on the image. Its coordinates are (x, y) and the local contrast$C_p(x, y)$ of the pixel is given as

$$C_p(x, y) = f_{\max}(x, y) - f_{\min}(x, y). \tag{8}$$

Among them, $f_{\max}(x, y)$ represents the maximum gray value in the sliding window centered on the point P, and $f_{\min}(x, y)$is the minimum gray value. The average gray value $T_p(x, y)$ in the neighborhood of this pixel is

$$T_p(x, y) = \frac{f_{\max}(x, y) - f_{\min}(x, y)}{2}. \tag{9}$$

First, we artificially set the value s, and $S = 15$ in the algorithm. For any pixel, the algorithm calculates the value of its local contrast. If the contrast value is greater than S, set the threshold of the current point as the average gray value in the neighborhood and perform threshold segmentation according to the threshold. If the value of contrast is less than the preset value S, indicating that the area is a background area, set the current gray value to 255. The experimental results of Bernsen algorithm are shown in the figure below. Among them, Figure 7 is the original picture, and Figure 8 is the effect picture after processing with Bernsen algorithm.

From the experimental results shown in Figure 8, we can see that the Bernsen algorithm can effectively solve problems such as traces. However, there are still a large number of misjudgment points, and too much noise is retained, and even part of the foreground area is misjudged as noise. In

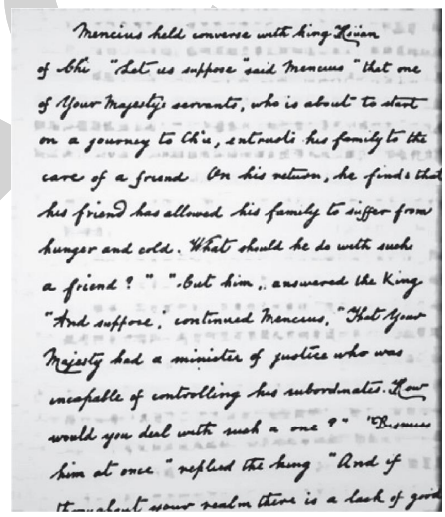

Figure 7: Original image.

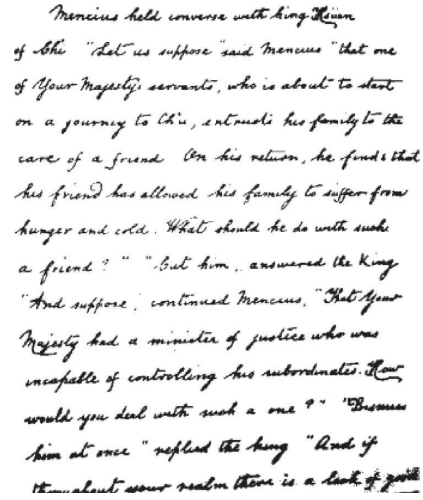

Figure 8: Bernsen processing results.

addition, the algorithm takes too long to run, which is very time-consuming and not very practical when it needs to process large quantities of data.

The LMM method normalizes the contrast, which can avoid the influence of the appeal situation on the binarization effect. The definition of image contrast is as follows:

$$C_p(x, y) = \frac{f_{\max}(x, y) - f_{\min}(x, y)}{f_{\max}(x, y) + f_{\min}(x, y)}. \tag{10}$$

Among them, $f_{\max}(x, y)$ is the maximum gray value in the neighborhood of the sliding window centered on the pixel (x, y), and $f_{\min}(x, y)$ represents the minimum gray value. The denominator is the sum of the maximum gray value and the minimum gray value. This method is used to normalize the contrast of the image, which is also the difference in the definition of image contrast between the LMM algorithm and the Bernsen algorithm. The advantage of normalizing the contrast of the image is that no matter whether the image is dim or bright, it can get a similar contrast value. After that, the algorithm uses the Otsu method to extract high-contrast pixel values and then uses the following formula to perform threshold segmentation:

$$H(x, y) = \begin{cases} 0, & N_c > N_{\min} \& f_p \le \mu_p(x, y) + \dfrac{\sigma_p(x, y)}{2}. \\ 1, & \text{others}. \end{cases} \tag{11}$$

The following parameters are for sliding windows. Among them, $N_{\min}$ is the minimum number of pixels in the sliding window, $C_p(x, y) = f_{\max}(x, y) - f_{\min}(x, y)$ is the average gray value of the pixels in the sliding window, $\sigma_p(x, y)$ is the standard deviation of the pixels in the sliding window, and N_c is the number of foreground pixels in the sliding window.

The support vector machine algorithm has good generalization ability for unknown samples, so the model can be applied to the fields of pattern recognition, regression estimation, probability density function estimation, time series forecasting, and so on. At the same time, it is also widely used in many fields such as handwritten digit recognition, text classification, image classification, and recognition in pattern recognition. The support vector algorithm is to find a hyperplane, through training samples, so that the sample points fall on both sides of the hyperplane, that is, divided into two categories. At the same time, the separation distance between the two sides to the hyperplane is maximized to distinguish the difference between the perceptron and the support vector machine algorithm. The problem of image binarization can actually be regarded as a pixel-level classification problem. Given a large amount of training data, the main method is to train a model for classification tasks. Among them, each pixel is assigned to a foreground or background label. Let us assume that we have N sample data as follows:

$$S = \{(x_1, y_1), (x_2, y_2), \ldots, (x_i, y_i)\}, i \in [1, N]. \tag{12}$$

Among them, x_i is the i-th instance, and y_i is the category of x_i, $y_i \in \{-1, +1\}$; that is, when binarization is performed, y_i may be the foreground or the background category. We assume that the hyperplane is $g(x)$: wx + b = o, and the distance $d_i$from the sample points on both sides to the hyperplane is

$$d_i = \frac{|g(x_i)|}{\|w\|}. \tag{13}$$

From this, a binary classification problem is transformed into

$$\begin{aligned} &\min_{w,b} \frac{1}{2}\|w\|^2, \\ &\text{s.t. } y_i(wgx_i + b) - 1 \ge 0, i = 1, 2, \ldots, N. \end{aligned} \tag{14}$$

The optimal solutions w^*, b^* are obtained by solving, and the hyperplane can be obtained from this as

$$w^* x + b^* = 0. \tag{15}$$

The classification decision function is

$$f(x) = \operatorname{sign}(w^* x + b^*). \tag{16}$$

We directly use the support vector machine algorithm to process the degraded document image. Because the problems of degraded document images are more complex and diverse, the effect of directly performing linear classification binarization is not ideal. Therefore, Xiong et al. made improvements based on this algorithm and proposed a low-quality document image binarization based on support vector machines. In this algorithm, the support vector machine algorithm has been successfully applied to the processing of old degraded documents. The main method is to use the algorithm to preprocess the image, classify the image block, and achieve rough segmentation. After getting different types of image blocks, different methods are used to process, correct, and adjust details for different classification results. For an image, the algorithm divides it into three categories, but for some complex document images, the three categories may not be enough, and different follow-up threshold processing is required for different categories. Therefore, the generalization ability of the algorithm is not strong.

We assume that for the given n data sets $X = \{x_1, x_2, ..., x_n\}$, the data set X is divided into C clusters. Among them, the center of each cluster is m_j, $1 \le j \le C$, and the cluster loss function based on the membership function is defined as (17)

$$J_L = \sum_{j=1}^{C} \sum_{i=1}^{n} \left[\mu_j(x_i)\right]^b \left\|x_i - m_j\right\|^2. \tag{17}$$

Among them, i and j are the membership functions of the i-th sample corresponding to the j-th category, $\sum_{j=1}^{C} \mu_j(x_i) = 1$, and b represents the smoothing factor. Generally, $b = 2$.

We used J_L to obtain partial derivatives of m_j, μ_j, respectively and to make the result equal to 0. At this point, we get the following formula:

$$m_j = \frac{\sum_{i=1}^{n}\left[\mu_j(x_i)\right]^b g x_i}{\sum_{i=1}^{n}\left[\mu_j(x_i)\right]^b}, \mu_j(x_i) = \frac{\left\|x_i - m_j\right\|^{(2/b-1)}}{\sum_{s=1}^{C}\left\|x_i - m_j\right\|^{(2/b-1)}}. \tag{18}$$

Through the iterative solution, we get the optimal solution.

We use F-measure to directly evaluate the binarization process. This metric is suitable for two types of problems with unbalanced sample distribution. The F value is calculated as follows:

$$F = \frac{2 \times RC \times \mathrm{PR}}{RC + \mathrm{PR}}. \tag{19}$$

Among them, RC means recall rate, and PR means precision rate. The calculation methods are as follows:

$$\begin{aligned} RC &= \frac{TP}{TP + FN}, \\ \mathrm{pr} &= \frac{TP}{TP + Fp}. \end{aligned} \tag{20}$$

Among them, TP is a case where it is judged to be a positive sample, but it is actually a positive sample. The meaning of FP is actually a negative sample, but it is classified as the number of positive samples. FN is actually a positive sample and is classified as a negative sample. The F value is a measure of the number of correct foreground pixel values in the generated result. The higher the F value, the higher the accuracy of the algorithm.

3.1. Peak Signal-to-Noise Ratio (PSNR). The calculation method of peak signal-to-noise ratio is as follows:

$$\begin{aligned} PSNR &= 10\log\left(\frac{C^2}{MSE}\right), \\ MSE &= \frac{\sum_{x=1}^{M}\sum_{y=1}^{N}\left(I(x,y) - K(x,y)\right)^2}{MN}. \end{aligned} \tag{21}$$

Among them, M represents the length of the image, N represents the width of the image, $I(x, y)$ and$K(x, y)$, respectively, represent the original image and the true value image, and C represents the absolute error value between the foreground and the background. The peak signal-to-noise ratio was originally used in the communication field to represent the ratio between the maximum possible power of a signal and the noise power that affects the signal. We now apply it to the algorithm to measure the processing of degraded document images to calculate the similarity between the document image processed by the algorithm and the true value image. The larger the ratio, the better the performance of the algorithm, and the closer the binarization result is to the true value image.

The degree of distortion is inversely proportional to the distance between adjacent pixels. The distance on the diagonal is larger than the distance between the horizontal and vertical directions, so the distortion caused by changing the pixels on the diagonal is smaller than the horizontal or vertical direction. Therefore, the reciprocal distance distortion metric can be used as a criterion for judging the binarization result of degraded documents. The calculation method is as follows:

$$DRD = \frac{\sum_{k=1}^{S} DRD_k}{NUBN}. \tag{22}$$

Among them, NUBN represents the number of image blocks that are not completely black or not completely white in the Ground Truth image. DRD_k represents the weighted sum of distortion of the K-th flipped pixel, and the calculation method is as follows:

$$DRD_k = \sum_{i=-2}^{2}\sum_{j=2}^{2}\left|GT_k(i,j) - B_k(x,y)\right| gW_{NM}(i,j). \tag{23}$$

Among them, W_{NM}represents the weight matrix, $GT_k(i, j)$ represents the pixel value of the K-th pixel at the flip center pixel point (x, y) in the Ground Truth image, and $B_k(x, y)$ is the k-th pixel in the image to be measured at the pixel (x, y). The smaller the reciprocal distance distortion metric, the smaller the distortion and the better the algorithm performance.

The error rate metric is calculated as follows:

$$NRM = \frac{NR_{FN} + NR_{FP}}{2}. \tag{24}$$

Among them, NR_{FN}represents the false negative rate, and NR_{FP} represents the false positive rate. The calculation methods are as follows:

$$\begin{aligned} NR_{FN} &= \frac{FN}{FN + TP}, \\ NR_{FP} &= \frac{FP}{FP + TN}. \end{aligned} \tag{25}$$

Among them, TN refers to the situation where the actual result and the judgment result are both negative samples. The error rate measurement also compares the difference between the image processed by the algorithm and the Ground Truth image. However, the error rate measurement mainly focuses on the ratio of false matches. Therefore, the smaller the calculation result, the better the algorithm performance.

4. Analysis of Ancient Literary Works Based on Intelligent Image Text Recognition

In order to verify the role of the intelligent image text recognition algorithm proposed in this paper in the analysis of ancient literary works, a large number of pictures of ancient literary works are scanned in the library by scanning, and an experimental database is constructed. After that, this

Table 1: Statistical table of the analysis effect of ancient literary works based on intelligent image text recognition.

No	Text feature recognition	Literary analysis
1	93.56	76.82
2	92.23	76.28
3	95.73	76.40
4	96.73	79.06
5	93.32	86.39
6	96.94	77.57
7	94.06	74.32
8	96.58	76.42
9	94.88	84.43
10	94.06	80.55
11	97.78	78.35
12	92.85	80.04
13	97.14	78.04
14	93.67	79.98
15	97.66	87.95
16	95.76	74.34
17	97.81	85.82
18	96.27	86.41
19	93.14	80.78
20	93.90	78.80
21	94.70	86.67
22	97.36	88.34
23	95.88	84.65
24	97.18	86.21
25	97.29	75.04
26	93.35	81.64
27	95.07	79.78
28	94.65	85.94
29	92.42	85.69
30	97.38	74.48
31	92.90	86.89
32	93.15	82.49
33	96.48	80.40
34	92.11	80.31
35	95.45	86.53
36	93.70	77.92
37	95.83	77.72
38	93.68	83.26
39	94.16	84.45
40	95.45	83.66
41	92.38	85.04
42	97.43	86.89
43	93.53	86.54
44	95.27	81.42
45	96.30	76.33
46	97.60	78.75
47	93.32	85.46
48	94.69	81.35
49	92.33	84.80
50	95.67	86.98
51	94.64	84.85
52	92.82	78.34
53	93.93	86.57
54	92.53	85.14
55	95.07	88.14
56	97.81	81.00
57	94.27	81.57
58	96.15	85.73
59	97.96	81.52
60	92.52	80.27

paper randomly combines these database files to obtain multiple sets of image collections of ancient literary works. At the same time, this paper recognizes these images, counts the recognition accuracy and work analysis effect of the intelligent image text recognition algorithm proposed in this paper, and obtains the results shown in Table 1.

From the above research, it can be seen that the intelligent image-based text recognition method proposed in this paper can play an important role in the analysis of ancient literary works, and it can be used as a reference for the digital processing and digital preservation of subsequent literary works. At the same time, it can also be used as a reference for the management of digital libraries.

5. Conclusion

The form of literary works began to generalize, and the literary form showed a trend of diversification. As we all know, literature in the traditional sense is now fading from the sacred aura of the superstructure in the "image age," and its era as the darling of the art temple is gone forever. Moreover, it will gradually become a new industry in the commodity society, seeking survival and development like other industries. Facing the increasingly fierce competition and challenges, the pure and serious traditional literature began to decline. The real life of the novel and the creation and fiction are obviously out of balance, the spiritual sublimation and the ideological connotation are mostly poor, and the concern for human nature is gradually disappearing, and the quality is beginning to be rapidly vulgar. This paper combines intelligent image and text recognition technology to propose intelligent algorithms that can be used for the analysis of ancient literary works and improves the algorithm based on the needs of literary works analysis. Finally, this paper combines experimental research to verify the algorithm of this paper. From the experimental results, we can see that the method proposed in this paper has a certain effect.

Data Availability

The data used to support the findings of this study are included within the article.

Conflicts of Interest

The authors declare that they have no conflicts of interest.

References

[1] J. Zhao, X. Xu, H. Jiang, and Y. Ding, "The effectiveness of virtual reality-based technology on anatomy teaching: a meta-analysis of randomized controlled studies," *BMC Medical Education*, vol. 20, no. 1, pp. 127–136, 2020.

[2] S. J. Bennie, K. E. Ranaghan, H. Deeks et al., "Teaching enzyme catalysis using interactive molecular dynamics in virtual reality," *Journal of Chemical Education*, vol. 96, no. 11, pp. 2488–2496, 2019.

[3] S. F. M. Alfalah, J. F. M. Falah, T. Alfalah, M. Elfalah, N. Muhaidat, and O. Falah, "A comparative study between a virtual reality heart anatomy system and traditional medical

Hindawi
Mobile Information Systems
Volume 2022, Article ID 5776642, 9 pages
https://doi.org/10.1155/2022/5776642

Research Article

Intelligent Action Recognition and Dance Motion Optimization Based on Multi-Threshold Image Segmentation

Yang Han[1] and Kaza Mojtahe[2]

[1]*Zhengzhou Preschool Education College, Henan 450000, China*
[2]*Department of Computer Engineering, Kyrgyz-Turkish Manas University, Bishkek, Kyrgyzstan*

Correspondence should be addressed to Kaza Mojtahe; kaza.mojtahe@mail.cu.edu.kg

Received 25 August 2022; Revised 8 September 2022; Accepted 14 September 2022; Published 24 September 2022

Academic Editor: Chi Lin

In order to improve the recognition and optimization effect of dance movements, this paper combines multi-threshold image segmentation technology to perform intelligent recognition of dance movements. Moreover, this paper analyzes the window focus calibration process in the cascade multi-threshold expansion method and focuses the window on the object body to expand from small to large. Then, due to the local optimum problem of single-layer expansion, this paper proposes a cascade expansion method, and comparative experiments analyze the effect of this method on window optimization. In addition, this paper combines the actual situation of dance movement training to construct an intelligent action recognition and dance movement optimization system based on multi-threshold image segmentation. The research shows that the intelligent action recognition and dance motion optimization method based on multi-threshold image segmentation proposed in this paper has a good effect.

1. Introduction

The training level of dance skills can intuitively reflect the professional level of dancers. It contains both kinematics and medical skills and can show the graceful and steady movements of the human body in the form of performance. At the same time, human action has always been a topic of discussion in the field of science, and dance includes not only human kinematics but also exercise physiology and psychology. At present, the scope of scientific application of dance teaching in our country includes human body warm-up methods, body therapy, related research on various functions of the body, and exercise methods. These dance teaching methods should be used more in practical training. Of course, it is not just for dance learners to learn more complex physical movement skills but through the explanation and study of the above dance teaching methods to understand the various movements that the body can reflect in dance teaching. At the same time, they need to feel the charm from dance skills, and then they can be enthusiastic about learning dance skills and show stable, graceful, unrestrained, and euphemistic dance charm.

The training of dance skills is a method, and only by mastering its essence, we can perform better dance. There is a certain way of learning. First, you must have a comprehensive understanding of the content of the subject of dance and your own experience. The so-called "one minute on-stage, ten years of work off stage," the mastery of skills does not happen overnight. Only by mastering the dance training method can you train in dance. Therefore, the discussion of dance skills in class should be paid special attention and then the specific demonstration of dance will be followed. In dance teaching, we must pay attention to the explanation of dance movements, so that students are familiar with the connection and transformation skills between the front and rear movements. The strength and flexibility of the body are inseparable during training, which has high physical requirements for some movements. Therefore, the understanding of basic knowledge is what students must master. Second, dance teaching is to cultivate the artistic quality of

dancers. Art has the ability to express, and dance can better exercise the expressive ability of dancers. In dance training, although the fluidity and coherence of body movements make the viewer feel comfortable, this is not the ultimate goal of dance teaching. Third, the time available for dance teaching classes is limited. Before the dance training starts, students should warm-up enough to keep their bodies active so as to avoid physical injuries during the training. In this case, the warm-up has taken up most of the classroom teaching time, leaving little time for students to actually learn dance skills.

This paper combines multi-threshold image segmentation technology for intelligent recognition of dance movements and builds an intelligent system to improve the optimization effect of subsequent dance movements.

2. Related Work

Using gesture recognition to analyze human motion behavior has become an important research direction of relevant experts and scholars in recent years [1]. Dancing tossing skills are an important indicator for evaluating dancers' basic skills and comprehensive abilities. Identifying dancing tossing gestures are of great significance to art teaching and research. At present, human gesture recognition has achieved great results. The method of literature [2] first establishes a high-level description model of human body structure information through the spatio-temporal features of human posture and then uses image feature recognition to identify human posture. This method needs to recognize the pose through the human contour with high integrity, and most of the images in the video cannot extract the human contour with high integrity, so the recognition accuracy is low. The method of literature [3] first extracts human behavior features, uses human behavior features to establish a spatio-temporal and/or the graph model and then uses video sequence moving target detection and recognition methods to identify human poses in the spatio-temporal and/or graph model. This method can only recognize the human posture in the two-dimensional image and does not consider the change of the video image, resulting in poor recognition stability. The method in [4] uses emotion-oriented speech recognition to identify human pose features. This method selects a single feature to identify human poses, resulting in the inability to accurately distinguish the target area and the background area, and the accuracy of the recognition results is poor. Literature [5] proposes a dance tossing gesture recognition model based on the spatial frequency domain features of contour images. First, the frequency domain features and airspace contour features of the contour images are extracted, and then the hidden Markov model is used to identify the dancing tossing gesture features, which have a strong recognition ability performance, which is convenient for people to recognize the dancing and tossing gestures in the video.

Dance training refers to a teaching activity that comprehensively develops the professional ability of the dance body through systematic reconstruction of the body structure and function of dancers and processing of movement techniques based on scientific principles. Different training courses in dance teaching have different content settings and course objectives, but the core is to train dancers' physical quality, function, psychology, technical skills, and artistic performance by applying training load stimulation, so that it meets the needs of dance majors [6]. The physical function of a dancer is largely determined by genetic factors, and some physiological indicators with high heritability should be used as an important basis for selecting dance materials. In addition, acquired growth and development, especially long-term professional training, will also affect it [7]. Therefore, dancers' physical functions are different from ordinary people, and they are also very different from athletes, with professional characteristics. After a long period of professional dance training, the dancer's motor system, circulatory system, respiratory system, and nervous system will all undergo adaptive changes, which is a manifestation of the improvement of the level of physical function [8]. For example, the impact of dance training on the motor system is manifested in changes in bone mineral density (BMD) and increases in muscle strength. Studies have shown that ballet training increases hip bone mineral density in adolescent females [9]. Long-term professional dance training can significantly improve the muscle strength of dancers' lower limbs, especially the relative strength is significantly higher than that of ordinary people. Long-term dance training can also enhance the elasticity of the lungs and the strength of the respiratory muscles and improve respiratory function [10].

The physical function monitoring and evaluation of dancers is to apply the theories and methods of medicine, psychology, biochemistry, dance physiology, dance biomechanics, and other disciplines to the dance training process and use comprehensive methods and means to study the training process and the training effect. The purpose is to help the instructors adjust the training plan scientifically, so that the dancers can achieve the best physical, psychological, and technical state, so as to maximize the training effect and professional ability [11]. Physical function, as an internal factor that affects dancers' physical fitness, technical skills, and expressiveness, should be an important part of the monitoring and evaluation of dancers in dance training and competitions. The functional monitoring and evaluation of dance training is an important manifestation of the scientization of dance training [12]. A series of physiological changes of the body when dancers participate in dance training is the objective reflection of the body's training load, that is, the body's ability to stress to dance training. If the training load is too small, the improvement of professional ability will not be obvious; if the training load is too large, it will not only fail to improve the professional level, but also may damage the health and cause the occurrence of dance injury [13]. Through scientific monitoring of dancers' physical function indicators and athletic ability indicators during dance training, we can study the regular characteristics of dancers' physical function changes during training, select dance materials, implement dance training, improve dancers' professional level and prevent excessive fatigue and fatigue. The occurrence of dance injury provides a scientific guarantee [14].

The selection of physical function monitoring indicators in dance training should be based on comprehensive consideration of training purposes, training methods, monitoring purposes, and dancer training levels [15]. At the same time, it should be noted that the selected indicators should be as simple as possible, strong pertinence, high accuracy, easy to operate, and fast feedback. Each index should have its own independence and can more sensitively reflect the changes of the training load or function from different aspects and can complement each other in order to obtain a more comprehensive evaluation [16]. In the process of operation, special attention should be paid to individual differences, professional characteristics, and systematic observation of dancers. Some indicators can reflect the situation of a training session, while other indicators need to be tracked for a long time and combined with other indicators for comprehensive comparative evaluation. It reflects the training effect and dancer's physical function level within a week or a period of time. The functional monitoring and evaluation indicators of professional dancers should include the physical functions that can reflect the dancers' skeletal muscle system, cardiovascular system, respiratory system, nervous system, and other systems [17].

3. Multi-Threshold Image Segmentation Algorithm

The superpixel segmentation method based on graph theory has problems such as parameter setting, low computational efficiency, and poor segmentation effect. Aiming at the above problems, this paper applies the adaptive threshold SLICO method to general object generators for the first time. The experimental results verify that this method can generate adaptive thresholds for superpixel segmentation and has better segmentation results at faster processing speed, which solves the above problems well. The post-processing method proposed in this paper contributes in exploiting superpixel cues.

Graph theory-based superpixel segmentation is a top-down global segmentation method. It regards the whole image as a weighted undirected graph, in which each pixel represents a node, the adjacent relationship between pixels represents a node, and the difference or similarity between pixel features corresponds to the weight on the edge. Then, the previous nodes are divided by various segmentation criteria on the established graph, so as to complete the superpixel segmentation process.

The superpixel segmentation method based on graph theory maps an image to an undirected graph and defines the weight of each edge e as w(e). W(e) represents the degree of difference between the vertices v_i and v_j connected by edge e. The vertex set in the graph is V, and dividing V into different regions is a division s. A connected subgraph of the graph $G'=(V, E')$ corresponds to each small region C ∈ S, where the non-empty subset of E is denoted by E'.

This method defines the internal difference of CeV as the maximum weight of the component's minimum spanning tree MST(C, E), as shown in the following formula:

$$\operatorname{int}(C) = \max_{e \in MST(C,E)} w(e). \tag{1}$$

Then, it defines the difference between two parts $C_1, C_2 \subseteq V$ as the minimum weight edge connecting the two parts. The specific definition is shown in the following formula:

$$dif\ (C_1, C_2) = \min_{v_i \in C_1, v_j \in C_2, (v_i, v_j) \in E} w((v_i, v_j)). \tag{2}$$

The threshold function is used to control that the degree of difference between the components must be greater than the minimum degree of internal difference, and the pairwise comparison judgment formula $D(C_1, C_2)$ is specifically defined as follows:

$$D(C_1, C_2) = \begin{cases} true\ if\ dif\ (C_1, C_2) > MInt(C_1, C_2) \\ false \quad otherwise. \end{cases} \tag{3}$$

Its minimum internal difference degree MInt is defined as follows:

$$MInt(C_1, C_2) = \min\ (Int(C_1) + \tau(C_1)), (\operatorname{int}(C_2) + \tau(C_2)). \tag{4}$$

Among them, for some regions, the function Int(C) does not perform well for data local feature evaluation. For example, in extreme cases, the region size $|C| = 1$ and Int(C) = 0. Therefore, a threshold function $\tau(C) = k/|C|$ based on the region size needs to be used, where k is a constant. That is, for small regions, stronger boundary evidence needs to be relied on.

The graph-based method uses clustering to divide the nodes on the graph, and the minimum spanning tree of its pixel set is the superpixel. The segmentation effect diagram of the graph-based method is shown in Figure 1.

It can be observed from Figure 1 that although the graph-based method can segment images more accurately, the segmented superpixels are not very regular, there are many glitches, and multiple parameters need to be set. Usually, the parameter setting will have a greater impact on the final segmentation effect.

The algorithm initializes the seed point. The seed point spacing is $S = \sqrt{N/K}$, where N is the number of pixels in the image, and K is the number of superpixels to be segmented. The algorithm then centers the seed on the edge of the image and moves it to the lowest gradient position within the 3×3 neighborhood. The purpose of this is to avoid centering superpixels on edges and reduce the possibility of seeding superpixels with noisy pixels. In the assignment step, each pixel is associated with the nearest cluster center whose search area and its location overlap, as shown in Figure 2. Since the expected spatial extent of a superpixel is a region roughly S × S in size, SLIC performs a similar pixel search in a 2S × 2S region around the center of the superpixel.

Finally, the distance is measured, that is, the distance between the pixel point and the cluster center is calculated, and the most similar seed point label is attached to the pixel, and the process is iterated until convergence. The color of a pixel is represented in the CIELAB color space [l,a,b]T, the range of which is known. The position of the pixel is

(a) (b)

Figure 1: Graph-based segmentation rendering. (a) Original image. (b) Segmentation rendering.

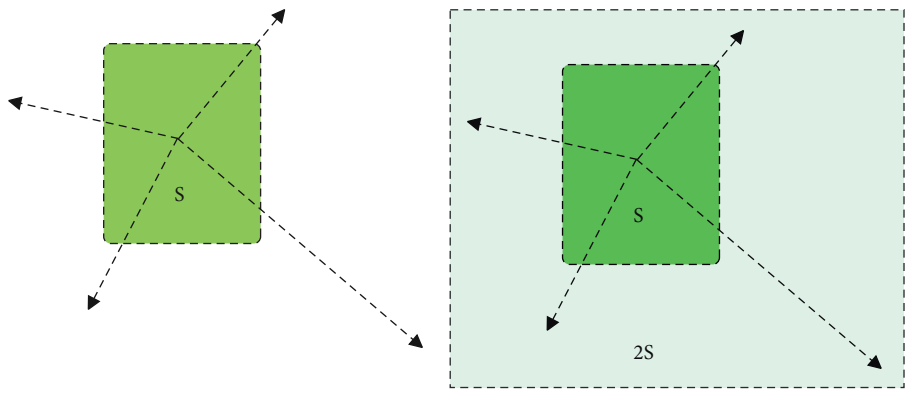

(a) (b)

Figure 2: SLIC reduces the search range of pixels. (a) Search in the entire image. (b) SLIC searches within the restricted area.

represented by $[x,y]$T. In order to combine the two distances into a single metric, it is necessary to normalize their respective color proximity max distance d and spatial proximity max distance d within the cluster. Then, the similarity D between pixels j and k is defined, and the specific formula is as follows:

$$\begin{aligned} d_c &= \sqrt{\left(l_j - l_k\right)^2 + \left(a_j - a_k\right)^2 + \left(b_j - b_k\right)^2}, \\ d_p &= \sqrt{\left(x_j - x_k\right)^2 + \left(y_j - y_k\right)^2}, \\ D_s &= d_c + \frac{m}{S} d_p. \end{aligned} \tag{5}$$

Making full use of the superpixel set generated after image segmentation plays a very important role in the post-processing process of this paper. Therefore, this part will focus on introducing the superpixel strategy, detailing the relationship between superpixel, objects and windows, and the application strategy. First, we will focus on the concept of superpixel straddling.

Superpixel segmentation divides objects into small regions of uniform color or texture. Therefore, an important property of superpixels is to preserve the boundaries of objects, which can be considered as dividing objects into many superpixels. However, these superpixels do not cross the original boundary of the object.

We assume that the initial generator generates a window set BB, and the initial window bb is some window in BB. A superpixel sp is considered to span the window bb if at least one pixel of the superpixel sp is outside bb and one pixel is inside bb. The superpixel spanning fraction SS is defined as follows:

$$SS\left(bb, \theta_{ss}\right) = 1 - \sum \frac{\min\left(|sp \backslash bb|, |sp \cap bb|\right)}{|bb|}. \tag{6}$$

Among them, $SP(\theta_{ss})$ is the set of superpixels with segmentation scale θ_{ss}. The above formula also calculates the area $|sp \cap bb|$ of the superpixel inside the window bb and the area $|sp \backslash bb|$ of the outer area, and the minimum value of the above two items is divided by the window area value.

If most of the spanning superpixel is inside or outside, its numerator value is small and contributes little to the overall summation formula. Therefore, the SS score will be highest when a window bb closely surrounds an object with a numerator value of 0, which is exactly the desired window.

Figure 3 is a superpixel spanning clue map. Figure 3(b) is the image obtained by superpixel segmentation of Figure 3(a). Observing the image, it is found that the object is composed of a subset of superpixels, and the boundary outside the superpixel is basically the boundary of the object itself. The superpixel spanning degree $SS(bb, \theta_{ss})$ is

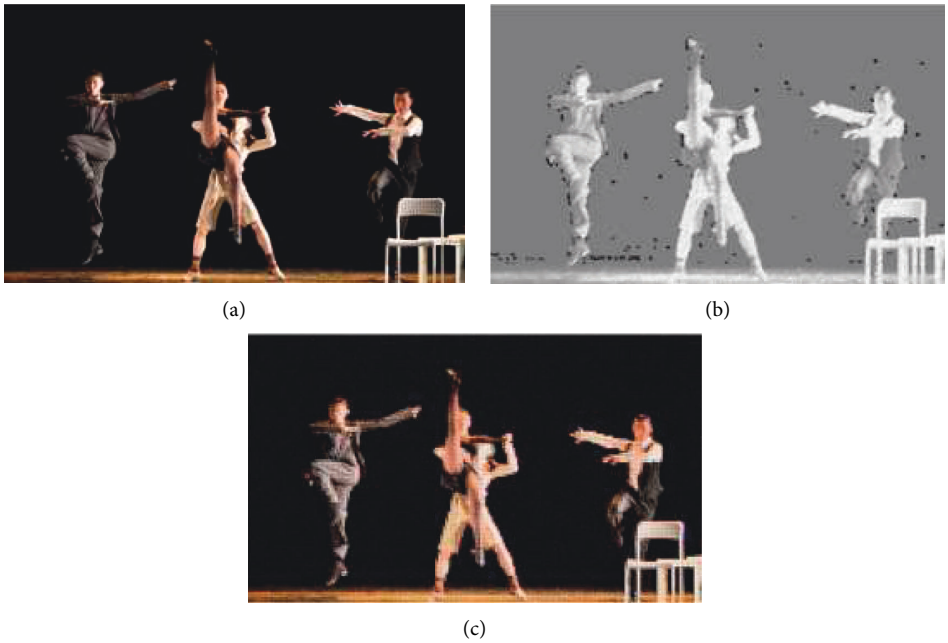

Figure 3: Superpixels spanning clues. (a) Original image. (b) Graph-based segmentation graph. (c) Superpixels spanning clues.

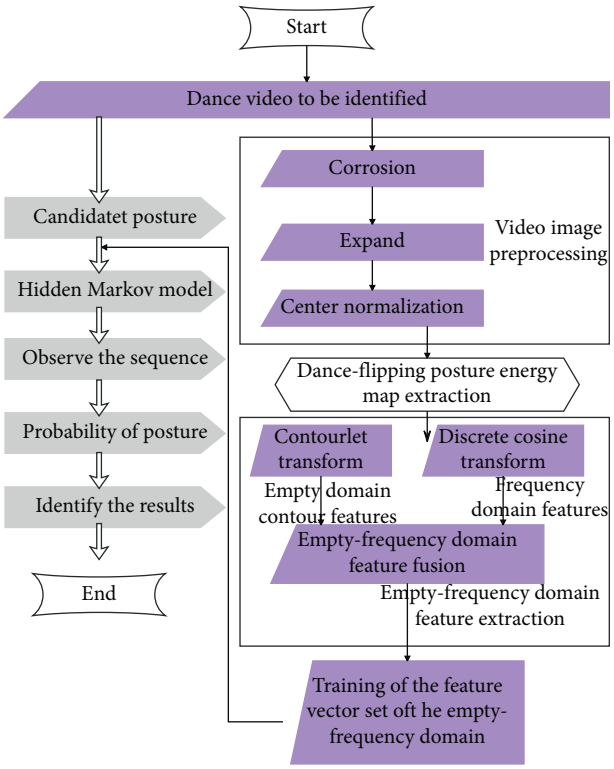

Figure 4: Intelligent action recognition and dance motion optimization based on multi-threshold image segmentation.

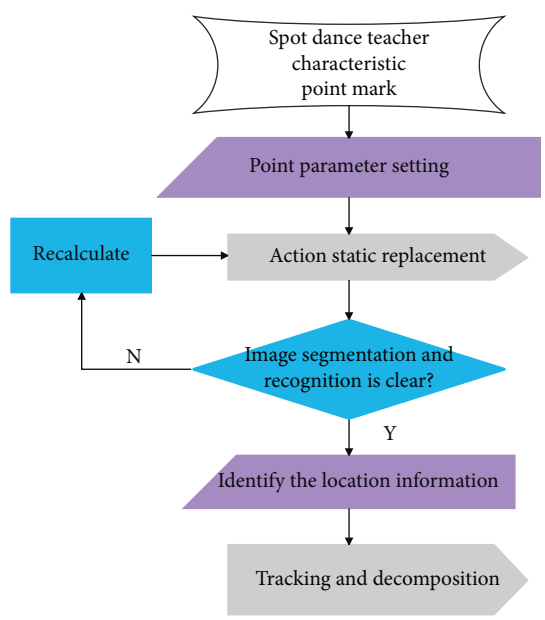

Figure 5: Flow chart of the dance visual action tracking decomposition method.

calculated according to the relationship between the window bb and the superpixel. In Figure 3(c), most of the superpixels are inside the boundary of the window bbs, whereas most of the superpixels are outside the window $w2$. Therefore, bb_1 has a higher SS score than bb_2, and bbs has a higher score because of its ability to closely fit the object.

In order to facilitate the application of the above concepts, a concept of superpixel straddling degree (SSD) is proposed. The specific definitions are shown in the following formulas:

$$SSD(sp, bb) = \frac{|sp \cap bb|}{|sp|}, \tag{7}$$

$$SP_{st} = \{sp_{st} \mid SSD(sp_{st}, bb) \in (0, 1)\}. \tag{8}$$

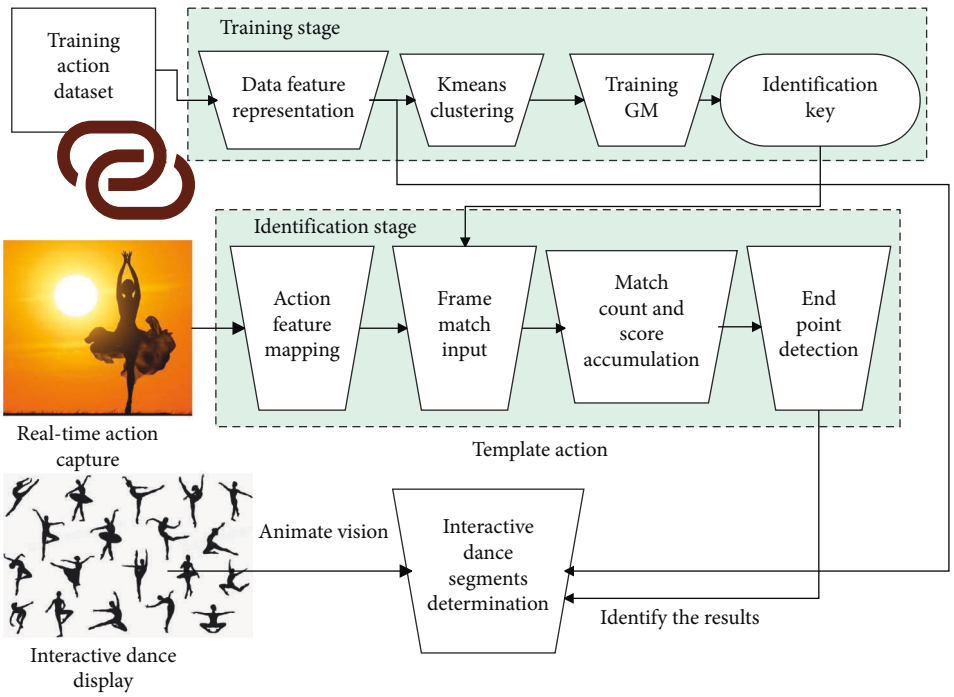

Figure 6: Overview of the structure of the dance interaction system.

The definition of superpixel density ST is shown in the following formula:

$$ST(bb) = \sum_{sp \in SP} \frac{|sp| \cdot \delta(|sp| - |sp \cap bb|)}{|bb|}. \quad (9)$$

Among them, δ denotes an impulse function that is non-zero if and only if $|sp| - |sp \cap bb| = 0$, where SP refers to the set of superpixels.

The window focus correction procedure is used to adjust the initial window to focus on the main body of the object, which facilitates subsequent superpixel-based expansion across the threshold.

Generally speaking, the initial window set generated by the initial generator can be directly input into the cascaded multi-threshold expansion model for correction. However, the window tightness of the initial window is actually very low, which may lead to the failure of the correction process. Taking BNG as an example, the windows have only 36 uniform scales, and such windows generally do not closely surround objects, so their window tightness is usually very low. However, cascading multi-threshold expansion directly on such a window usually cannot achieve very good results. The reason is that for such an already large window, expanding and optimizing it will usually only increase the positioning error of the window and frame more backgrounds.

Therefore, using the window focus calibration method to generate a calibrated window is more beneficial for subsequent expansion. Since the true boundary of the object is not known in practical situations, the method adopts an approximation idea to calibrate the initial window. The window is aligned with the edge alignment of a superpixel set if it can just closely surround a subset of superpixels. If an initial window bb is given, and the entire superpixel set is SP_{all}, the calculation formula of the superpixel set SP_{in} inside the window and the superpixel set SP_{st} spanned by the window is defined as follows:

$$SP_{in} = \{sp \in SP \mid SSD(sp, bb) = 1\}, \quad (10)$$

$$SP_{st} = \{sp \in SP \mid 0 < SSD(a, b) < 1\}. \quad (11)$$

We assume that window bb(SP) is the smallest window that can just tightly enclose the superpixel set SP, and $IOU(bb_m, bb_n)$ denotes the intersection ratio between windows bb_m and bb_n. Then, according to the intersection ratio between each superpixel and the window of the spanned superpixel set SP_{st}, the superpixels $\{sp_i, \ldots, sp_j\}$ inside SP_{st} are sorted in descending order, and they satisfy the following formula:

$$IOU(bb(SP_{in} \cup \{s_m\}), bb) \geq IOU(bb(SP_{in} \cup \{s_m\}), bb), \forall m < n. \quad (12)$$

Single-layer multi-threshold extension (MTSE) extends the focus-corrected window in multiple superpixel cross-threshold directions. Formula (13) represents the process of modifying the window ab according to the superpixel span threshold tr.

$$SP_{t_1}(ab) = \{sp \in SP \mid SSD = 1\}. \quad (13)$$

If $SP_{in}(ab) = \{sp \in SP \mid SSD = 1\}$ is satisfied, it means that the window ab tightly encloses the superpixel set that satisfies this condition. If there are other superpixels that satisfy the constraint $SSD \geq t_1$, they are combined into the previously tightly enclosed superpixel set $SP_{in}(ab)$, and the scale of the window ab will be adjusted accordingly to just tightly surround the new superpixel set $SP_{t_1}(ab)$. The

Table 1: Segmentation effect of dance movements.

Num	Identify
1	90.19
2	91.69
3	90.03
4	86.65
5	90.52
6	84.81
7	91.70
8	85.87
9	86.92
10	87.20
11	88.47
12	91.59
13	90.84
14	91.26
15	88.49
16	85.97
17	89.87
18	86.01
19	88.38
20	87.81
21	86.55
22	86.80
23	85.54
24	90.50
25	84.88
26	84.71
27	91.81
28	84.17
42	88.73
43	90.70
44	88.25
45	89.89
46	88.35
47	90.78
48	88.13
49	91.39
50	88.21
51	84.63
52	91.87
53	90.37
54	87.13
55	88.71
56	90.47

Table 2: Optimization effect of the dance movement.

Num	Optimization
1	83.38
2	86.19
3	81.94
4	82.32
5	82.47
6	82.11
7	79.56
8	87.95
9	83.83
10	80.67
11	78.21
12	82.57
13	83.05
14	81.57
15	77.59
16	82.94
17	84.51
18	78.03
19	85.24
20	86.99
21	86.01
22	85.82
23	85.06
24	77.11
25	82.83
26	84.86
27	79.98
28	84.31
42	87.94
43	81.55
44	77.25
45	80.48
46	87.35
47	85.83
48	81.68
49	77.33
50	78.29
51	80.92
52	86.29
53	84.07
54	77.46
55	80.34
56	79.97

threshold t_l is the spanning criterion for single-layer superpixel expansion. The value of t_l is smaller, the deformation of the corresponding window ab is larger, so that it is easier to approach the standard window of the manually calibrated object.

4. Intelligent Action Recognition and Dance Motion Optimization Based on Multi-Threshold Image Segmentation

After preprocessing the dance video image to be recognized through erosion, expansion, center normalization, etc., the energy map of dance tossing posture is extracted. In this paper, discrete cosine transform and transformation methods are used to extract the frequency domain features and multi-directional and multi-resolution spatial contour features in the energy map of dancing tossing poses. Moreover, this paper uses the extracted features to distinguish the high and low frequency components of the human body in the dance tossing posture and capture the detailed information of the dance tossing features. In addition, this paper adopts the feature-level fusion method to fuse the above features to obtain the spatial frequency domain feature vector set of the contour image for processing. Intelligent action recognition and dance motion optimization based on multi-threshold image segmentation are shown in Figure 4.

In the process of visual motion tracking in basic dance training, the spatial limit range of the 3D motion tracking system should be selected first, and then the extreme points of the 3D motion tracking system should be located. In the

extreme lattice, the lattice data of each key action and the parameters of each key action lattice vector are obtained, and then the key lattice feature vector is calculated. The three-dimensional tracking and decomposition of dance visual movements is completed by applying a multi-directional dual-camera space plane imaging system, as shown in Figure 5.

As shown in Figure 6, the system mainly includes three components, namely the optical motion capture system, the real-time motion recognition engine, and the animation drive engine. The motion capture system is responsible for capturing the user's dance movements in real time and expressing them into effective feature forms such as joint angle feature forms. The action recognition engine is responsible for segmenting and identifying the captured dance movements in real time and determining whether they are legal movements so that the system can make corresponding decisions. If the current input action is a legal action, the animation driving engine needs to determine the frame block exactly corresponding to the current input segment from the interactive dance action of the legal action. At the same time, it displays the actions with animated characters, so that the user's dance and the displayed interactive dance are kept in sync with each other as much as possible.

In this paper, the improved inverse kinematics method is used to decompose the video action tracking, and the multi-key points and key action parts in the dance movement are marked with the feature points and the marking parameters are set. The static displacement data of dance movements is calculated through the principle of visual action tracking and decomposition, and the dynamic capture is performed after the image segmentation and identification are clear. If the image is not segmented and marked clearly, the coefficient correction and recalculation will be performed until the dance action image is clearly segmented and marked. When a certain action is analyzed in detail, the system automatically tracks and decomposes without the need for teachers to make corresponding actions. The three-dimensional action tracking and decomposition imaging can be performed through the projection system or the teaching display. On this basis, the effect of the intelligent action recognition and dance motion optimization method based on multi-threshold image segmentation proposed in this paper is verified, and its dance motion segmentation effect and dance motion optimization effect are calculated, as shown in Tables 1 and 2.

It can be seen from the above research that the intelligent action recognition and dance motion optimization method based on multi-threshold image segmentation proposed in this paper has good results.

5. Conclusion

If we want to dance gracefully and naturally, and make our body movements full of power and beauty, then we need to match our body movements and breathing to the right musical frequency. When discussing a certain movement or a technical point in dance teaching, dance teachers have to make corresponding movements and explain them accordingly, which causes a lot of inconvenience. The traditional dance basic training adopts the uncalibrated global visual feedback method for training, that is, the traditional video decomposition training. When the visual motion is decomposed, the visual changes of adjacent key nodes and cannot be calculated, and there are problems of large 3D visual motion tracking error and unclear decomposition contours. This paper combines multi-threshold image segmentation technology to perform intelligent dance movement recognition, builds an intelligent system and improves the effect of subsequent dance movement optimization. The research shows that the intelligent action recognition and the dance movement optimization method based on multi-threshold image segmentation proposed in this paper has good results.

Data Availability

The data used to support the findings of this study are available from the corresponding author upon request.

Conflicts of Interest

The authors declare that there are no conflicts of interest regarding this work.

References

[1] K. Aso, D. H. Hwang, and H. Koike, "Portable 3D human pose estimation for human-human interaction using a chest-mounted fisheye camera," *Augmented Humans Conference 2021*, pp. 116–120, 2021, February.

[2] A. Azhand, S. Rabe, S. Müller, I. Sattler, and A. Heimann-Steinert, "Algorithm based on one monocular video delivers highly valid and reliable gait parameters," *Scientific Reports*, vol. 11, no. 1, p. 14065, 2021.

[3] A. Bakshi, D. Sheikh, Y. Ansari, C. Sharma, and H. Naik, "Pose estimate based yoga instructor," *International Journal of Recent Advances in Multidisciplinary Topics*, vol. 2, no. 2, pp. 70–73, 2021.

[4] J. Bhombe, A. Jethwa, A. Singh, and T. Nagarhalli, "Review of pose recognition systems," *VIVA-Tech International Journal for Research and Innovation*, vol. 1, no. 4, pp. 1–8, 2021.

[5] S. L. Colyer, M. Evans, D. P. Cosker, and A. I. T. Salo, "A review of the evolution of vision-based motion analysis and the integration of advanced computer vision methods towards developing a markerless system," *Sports medicine-open*, vol. 4, no. 1, pp. 24–15, 2018.

[6] R. G. Díaz, F. Laamarti, and A. El Saddik, "DTCoach: your digital twin coach on the edge during COVID-19 and beyond," *IEEE Instrumentation and Measurement Magazine*, vol. 24, no. 6, pp. 22–28, 2021.

[7] S. Ershadi-Nasab, E. Noury, S. Kasaei, and E. Sanaei, "Multiple human 3d pose estimation from multiview images," *Multimedia Tools and Applications*, vol. 77, no. 12, pp. 15573–15601, 2018.

[8] Z. Li, J. Bao, T. Liu, and W. Jiacheng, "Judging the normativity of PAF based on TFN and NAN," *Journal of Shanghai Jiaotong University*, vol. 25, no. 5, pp. 569–577, 2020.

[9] S. Liu, Y. Li, and G. Hua, "Human pose estimation in video via structured space learning and halfway temporal evaluation,"

IEEE Transactions on Circuits and Systems for Video Technology, vol. 29, no. 7, pp. 2029–2038, 2019.

[10] W. McNally, A. Wong, and J. McPhee, "Action recognition using deep convolutional neural networks and compressed spatio-temporal pose encodings," *Journal of Computational Vision and Imaging Systems*, vol. 4, no. 1, p. 3, 2018.

[11] D. Mehta, S. Sridhar, O. Sotnychenko et al., "VNect: real-time 3d human pose estimation with a single RGB camera," *ACM Transactions on Graphics*, vol. 36, no. 4, pp. 1–14, 2017.

[12] N. V. Dr P Prabhavathy, "The analysis of the impact of yoga on healthcare and conventional strategies for human pose recognition," *Turkish Journal of Computer and Mathematics Education (TURCOMAT)*, vol. 12, no. 6, pp. 1772–1783, 2021.

[13] X. Nie, J. Feng, J. Xing, S. Xiao, and S. Yan, "Hierarchical contextual refinement networks for human pose estimation," *IEEE Transactions on Image Processing*, vol. 28, no. 2, pp. 924–936, 2019.

[14] Y. Nie, J. Lee, S. Yoon, and D. S. Park, "A multi-stage convolution machine with scaling and dilation for human pose estimation," *KSII Transactions on Internet and Information Systems (TIIS)*, vol. 13, no. 6, pp. 3182–3198, 2019.

[15] I. Sárándi, T. Linder, K. O. Arras, and B. Leibe, "MeTRAbs: metric-scale truncation-robust heatmaps for absolute 3d human pose estimation," *IEEE Transactions on Biometrics, Behavior, and Identity Science*, vol. 3, no. 1, pp. 16–30, 2021.

[16] J. Xu and K. Tasaka, "[Papers] keep your eye on the ball: detection of kicking motions in multi-view 4K soccer videos," *ITE Transactions on Media Technology and Applications*, vol. 8, no. 2, pp. 81–88, 2020.

[17] A. Zarkeshev and C. Csiszár, "Rescue method based on V2X communication and human pose estimation," *Periodica Polytechnica: Civil Engineering*, vol. 63, no. 4, pp. 1139–1146, 2019.

Hindawi
Mobile Information Systems
Volume 2022, Article ID 3291030, 9 pages
https://doi.org/10.1155/2022/3291030

Research Article

Simulation Model of Enterprise Financial Management Activities Based on the Random Forest Algorithm

Fang Zhao

School of Accounting, Henan Logistics Vocational College, Zhengzhou, Henan 450000, China

Correspondence should be addressed to Fang Zhao; 2111602035@e.gzhu.edu.cn

Received 5 July 2022; Revised 26 August 2022; Accepted 8 September 2022; Published 20 September 2022

Academic Editor: Chi Lin

In the era of information and data, big data and cloud computing have been widely used in all walks of life, especially for promoting the transformation of business model and the financial administration model of corporations. Building various management systems based on the financial sharing center can realize centralized management of business finance and improve enterprise management efficiency. Enterprises must establish a set of perfect financial administration systems to prevent and resolve financial crisis, reduce financial losses and ensure the normal operation of corporations. Based on situational learning theory and simulation experiment technology, this paper constructs a comprehensive simulation experiment system of financial administration and focuses on three key technologies: case decomposition and task-driven, business simulation expansion, and scientific evaluation. Based on the random forest algorithm, a preparation setup model of accounts receivable and payable audit is constructed, and its application in case corporations is analyzed, which provides new ideas for the modern audit work mode and creates a dynamic and open business simulation environment for the financial administration experiment. The results show that the classification accuracy of the improved K-fold random forest algorithm is 1.54% higher than that of the traditional random forest algorithm, and the accuracy of the crisis preparation setup model in predicting the actual enterprise financial crisis reaches 90.327%, which is feasible and effective in the preparation setup of enterprise financial administration and provides a new research idea for the construction of the preparation setup model of enterprise financial administration. Financial management is the core part of enterprise management activities, and it is also an important factor affecting the comprehensive competitiveness of corporations. Therefore, on the basis of fully studying the objective regularity of financial activities, improving the financial administration algorithm, applying the random forest algorithm to enterprise management, and building a perfect management system can comprehensively control the financial administration activities of corporations and realize the innovation of financial administration activities from the aspects of data collection, fund management, and internal control, which is conducive to promoting the continuous improvement of the efficiency of enterprise financial administration.

1. Introduction

With the rapid development of the market economy, the market competition environment faced by corporations is becoming increasingly fierce. In order to enhance their comprehensive competitiveness, corporations must continuously improve their internal management models and improve management efficiency. Financial management is the core part of enterprise management activities and also an important factor affecting the comprehensive competitiveness of corporations. In the traditional internal audit, the audit of accounts receivable and accounts payable needs to use the confirmation method most of the time, but due to the extremely low response rate of the confirmation, it is impossible to obtain the necessary external audit evidence. In recent years, through the policy guidance and guidance of government departments such as the Ministry of Finance, the financial shared service model has caused a new upsurge. Financial Shared Service Center is from the perspective of the market, using modern information technology, to provide professional financial services for the internal and external customers of the group enterprise, it is a new type of financial administration model and is the Internet economy and enterprise management sharing concept a new

application in the field of financial administration of group companies [1].

The random forest algorithm cited in this paper is to randomly construct a number of unrelated decision trees to form a forest. Each decision tree makes a decision on the attribute category of each data put into the random forest and finally predicts the financial risk level of each data according to the decision results of all decision trees. Real-time data collection and timely uploading of output audit warning results in the process of enterprise production, operation and financial administration can be realized by the management through the financial sharing center. The results show that the classification accuracy of the improved K-fold random forest algorithm is 1.54% higher than that of the traditional random forest algorithm, and the prediction accuracy of the crisis preparation setup model to the actual enterprise financial crisis reaches 90.327%, which is feasible and effective in the enterprise financial administration preparation setup and provides a new research idea for the construction of the enterprise financial administration preparation setup model [2].

While fully considering the openness and dynamics of the financial sharing environment, this paper studies and solves the key scientific problem of the audit preparation setup of accounts receivable and payable in the enterprise financial sharing center and constructs the audit preparation setup framework of accounts receivable and payable from the perspective of classification by using the random forest theory and develops the implementation framework in combination with the evidence theory, which verifies the correctness and effectiveness of the evaluation method in the case analysis. The model is verified by using *R* software, and the conclusion is drawn, which provides an effective method and a reasonable way for the enterprise financial sharing center to study the audit preparation setup of a/P [3]. The innovation lies in the following:

(1) The financial preparation setup model of accounts receivable and payable under the financial sharing mode based on the random forest is constructed. On the basis of in-depth analysis, first build a financial preparation setup framework and then analyze the current situation and existing problems of the company's receivables and payable management, select financial preparation setup indicators and then use the random forest algorithm to select features and then build a random forest model. Finally, the financial warning threshold is obtained. According to the financial preparation setup model established by a random Senli algorithm, the application of the model is explained in combination with the actual situation of the enterprise, and the validity of the model is proved.

(2) Taking an enterprise under the financial sharing model as an example, a new idea and scheme of financial preparation setup is introduced, which is conducive to the development of internal finance and provides new ideas for the construction of an intelligent financial system [4]. On the basis of in-depth analysis of the features of the enterprise financial sharing mode, the financial preparation setup model of accounts receivable and payable is analyzed in detail. The data source before the implementation of the on-site financial procedures is collected and cleaned through big data technology, and the big data technology is further used. Analysis of massive financial data, compared with traditional financial sampling, expands financial scope, improves financial efficiency, and provides new ideas for financial preparation setup methods of accounts receivable and payable, so as to realize the random forest method in internal financial research innovation.

This paper is divided into six chapters from the organizational structure.

The first chapter is the introduction. This part analyzes the application status of the business model and financial administration model, summarizes the causes of problems and compares new technologies and algorithms to improve the efficiency of enterprise management. The second chapter mainly summarizes the relevant literature, summarizes its advantages and disadvantages and puts forward the research ideas of this paper. The third chapter introduces in detail the objectives of enterprise financial administration activities and the establishment of the financial administration simulation system. The fourth chapter introduces the enterprise financial administration activity simulation model based on the random forest algorithm and the financial crisis preparation setup based on the improved *K*-fold random forest algorithm. The fifth chapter describes the data processing and the construction of financial indicators. The sixth chapter is the conclusion, which summarizes the research results of the full text.

2. Related Work

From the perspective of financial practice, Wu Jing compared the financial risk preparation setup and the financial preparation setup, constructed the framework of the financial preparation setup and explained the important points in the construction process and put forward some suggestions. Constructive comments [5]. Wu pointed out that a new type of financial model is online finance, an important part of which is financial preparation setup. According to the features of China's online finance, a financial preparation setup model is constructed, and the most important part is the collection and detection of databases and incomplete data [6]. Starting from the principles of financial administration, Wu and Chen finds out errors and frauds and makes preparation setups according to financial goals, studied the necessary elements for building a financial preparation setup system, designs a financial preparation setup framework flow standard and constructs a tax preparation setup system framework through five aspects and pointed out the functional role and limitations of this indicator [7]. Forsaith uses the Granger causality test for the financial administration index system to determine the

weight of management indicators and designs a financial preparation setup index. The direct invisible risk has the greatest impact on finance [8]. Anna selects tax risk management from the macro level and the micro level [9].

Since the concept of the random forest algorithm was proposed, scholars have conducted a lot of research on it and put forward many improved algorithms on this basis. Jie summarized the main theoretical decision trees and integrated learning of random forests and then proposed an improved algorithm for the classification of ultra-high dimensional attribute data. The weight of random forest features is determined according to the size of statistics, which can improve the classification accuracy [10]. Tu compared the similarities and differences between the cart algorithm and the C4.5 algorithm and created a new splitting algorithm by combining the two algorithms, focusing on the construction of weighted nodes of binary numbers. He applied this algorithm to the random forest algorithm and proposed the concept of the hybrid random forest algorithm [11]. Scholars have also proposed many improved methods for the classification of random forests. Wang and Liu proposed that after building the decision tree, the decision tree should be sorted according to its classification ability, and the decision tree with strong classification ability should be selected to build a new random forest [12]. Li and Wang pointed out that different weights are allocated according to the classification ability of the decision tree, and then the classification is carried out. In the classification process, the weighted voting method should be used, that is, the weight of the decision tree is given to each ballot [13]. Liu and Song used a vector space model and potential topic representation to construct a decision tree and classified the random forest composed of these two features with experimental data. The final classification result was calculated by the weighted average formula [14].

3. Objectives of Corporate Financial Administration Activities

3.1. Goal Theory. The objectives pursued by enterprise financial administration activities can be roughly divided into the following three aspects:

(1) Maximize profits. It is generally believed that profits represent the wealth created by corporations. The more profits, the more wealth the enterprise has. As an independent entity, corporations must pursue profits driven by the principle of self-interest. Therefore, the greater the profit, the closer to the goal of the enterprise. In recent years‘ the view of profit maximization has been questioned and denied. The reason is that the profit maximization financial administration goal does not consider the time value and risk of money. The relationship between input and output is not considered.

(2) Development of the view that earnings per share maximization is profit maximization. To a certain extent, it makes up for the lack of profit maximization. It is generally believed that this view not only reflects the pursuit of profits by corporations but also links the profits of corporations with the capital invested by shareholders. However, the risk and time of earnings acquisition are still not considered [15].

(3) Enterprise value maximization measures the overall value of the enterprise. It represents the judgment and evaluation of entrepreneurs made by capital market participants. It is generally believed that this view comprehensively and fully considers the company's current and future possible profitability, time factors, risks, and other factors.

3.2. Financial Management Simulation System. First, collect and preprocess the dynamic financial data of the time series of corporations and then conduct the stationarity test and the pure randomness test. If it fails the test, it will be stabilized by differential operation and transformed into a stationary time series and then select a mature model to complete the time series modeling. The modeling process of time series is shown in Figure 1.

The research object of the financial administration comprehensive simulation system is the enterprise, that is, how to flexibly formulate financial administration strategies in the process of operation and development and use internal and external resources to carry out various financial accounting and decision-making activities, so as to maximize the economic benefits of the enterprise. It integrates financial strategy formulation, accounting operation, financial decision simulation, business operation simulation, and other modules, with huge data stock and flow [16]. Based on the basic idea of comprehensive experiments, a virtual financial business environment is constructed through computer simulation technology in the network environment, and a variety of positions and roles of the financial administration department are set for overall operation or decision-making. An experimental platform system, such as shown in Figure 2.

4. Simulation Model of Enterprise Financial Administration Activities

4.1. Introduction to the Random Forest Algorithm. Random forest is to plant many decision trees that are not related to each other by using random methods. These decision trees form a forest, which is called a random forest. After the random forest is established, assuming that there is a new sample, it is put into the random forest, and then each decision tree in the random forest is allowed to make a decision on the attribute category of the sample to be entered. Each tree has one vote. The minority obeys the majority method. The category with the largest number of votes in the decision tree is the final classification result of the sample [17]. The working principle of random forest algorithm can be divided into the following four steps, as shown in Figure 3.

Step 1: Randomly sample the training set p times with replacement and form a subset of the training set with the obtained p samples and use it as a new training set P.

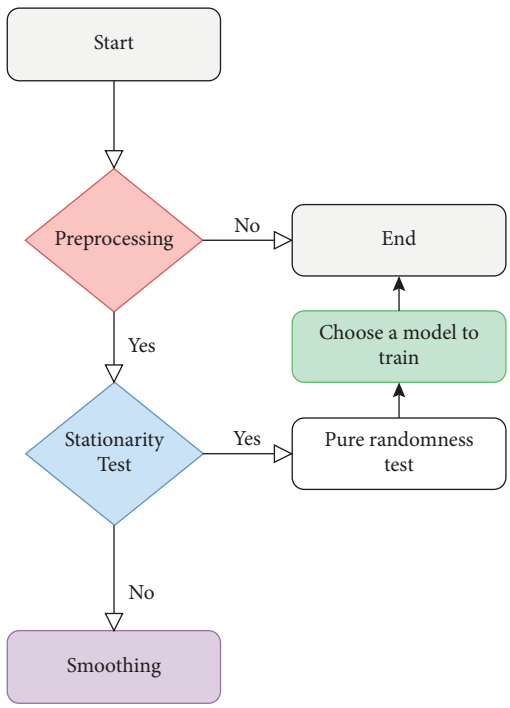

Figure 1: Time series modeling flow chart.

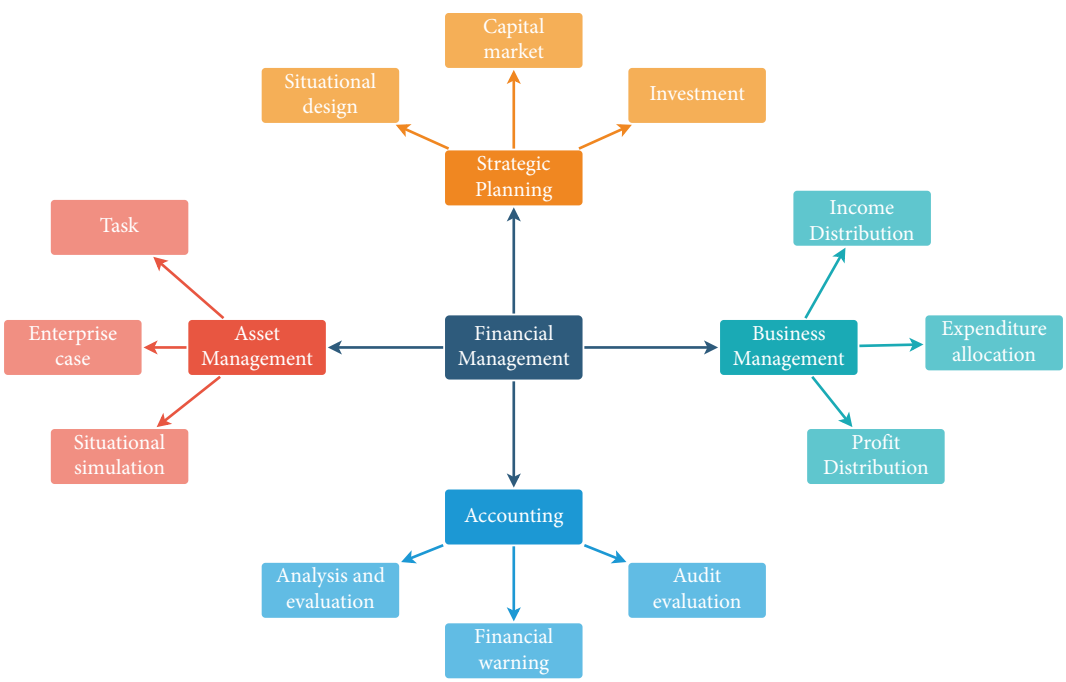

Figure 2: The structure of the financial administration simulation system.

Step 2: Randomly extract k features of the training set from P to form a subset and use this subset to perform a decision tree. During the decision-making process, let the decision tree grow sufficiently without pruning it [18].

Step 3: Repeat steps 1 and 2 until m decision trees are generated to establish a random forest.

Step 4: The test sample to be classified is given to the decision tree in the forest for classification decision, and the classification voting results of each decision tree are counted, and the category with the most votes in the decision tree is used as the final classification result of the test sample.

4.2. Financial Crisis Warning based on the Improved K-Fold Random Forest Algorithm. Use the time series model to make a short-term forecast on the historical financial index data of

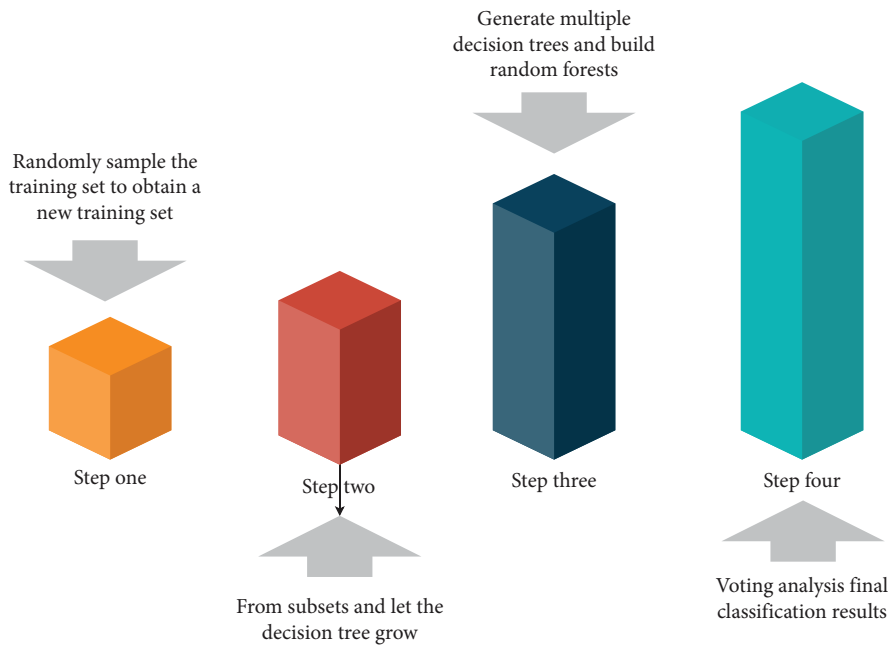

Figure 3: Random forest working steps.

the enterprise and then use the K-fold random forest algorithm to make a financial analysis on the forecast data and finally realize the preparation setup of the enterprise's financial crisis [19]. Test the pure randomness of the time series data to ensure that the time series data have correlation and can be effectively predicted through the historical data. The test original hypothesis function is shown as follows:

$$\rho_1 = \rho_2 = \cdots = \rho_{\mathrm{m}} = 0, \forall m \geq 1. \tag{1}$$

In the formula, ρ represents the autocorrelation coefficient of the sequence samples. For large sample data, the QBP statistic is used to judge the randomness, and the function is expressed as follows:

$$Q_{BP} = n \sum_{k=1}^{m} \rho_k^2 \sim \chi(m). \tag{2}$$

In the formula, n represents the sequence observation period, m represents the specified delay period, and $\chi(m)$ represents the quantile. When faced with small sample data, the function of the QLB statistic is expressed as follows:

$$Q_{LB} = n(n+2) \sum_{k=1}^{m} \left(\frac{\rho_k^2}{(n-k)} \right) \sim \chi(m). \tag{3}$$

The time series model selection is carried out according to the features of the autocorrelation diagram and the partial autocorrelation diagram of the time series. When the autocorrelation diagram has tailing phenomenon, and the partial autocorrelation diagram has the tailing phenomenon, the AR autoregression model is used, and the function is expressed as follows:

$$X_i = \sum_{i=1}^{p} \phi\alpha + \alpha_i + c. \tag{4}$$

In the formula, φ represents the autoregressive coefficient, p represents the autoregressive order, α represents the random error term, and c represents the constant term. When the autocorrelation graph is truncated, when the partial autocorrelation graph is smeared, the MA moving average model is used. When $\varphi = 0$, the function is expressed as follows:

$$X_i = \alpha_i - \sum_{i=1}^{q} \theta_i + c. \tag{5}$$

In the formula, θ_i represents the moving average coefficient, and q represents the moving average order. When the autocorrelation graph and the partial autocorrelation graph both show tailing phenomenon, the ARMA autoregressive moving model or the ARIMA autoregressive difference moving average model is used, and the ARIMA model is used for the sub-differentiated time series. The ARMA function is expressed as follows:

$$X_i = \sum_{i=1}^{p} \phi_i x_{i-1} - \sum_{j=1}^{q} \theta_j \alpha_{j-1} + \alpha_i + c. \tag{6}$$

The improved K-fold random forest algorithm is used to analyze the financial situation of corporations and realize the preparation setup of financial crisis. Random forest algorithm is based on classification regression tree, combined with a bagging algorithm and a random subspace method. It has the features of high accuracy, good scalability and parallelism, low demand for prior knowledge, less vulnerable to the negative impact of interfering data, wide applicability, and simple and clear structure [20]. The random sampling method is used to select y training sample sets from N original data samples, and the optimal splitting feature is selected to split the classification regression tree for training.

Y classification regression trees are generated through the learning of the sample sets. Finally, the simple majority voting method is used to obtain the final classification results.

In the process of random forest sample extraction, taking bagging idea as the core, the self-help sampling method with the random selection method of putting back is adopted. After repeated operations for many times, the number of training sample sets is consistent with the number of original sample sets, and the out of pocket data is a part of the sample data that has not been selected. Add noise to a single feature and measure the importance of the feature by reducing the change of prediction accuracy. First, use the corresponding out of pocket data to calculate the out of pocket data error of each classification regression tree, carry out random noise interference on each sample feature x_i in the out of pocket data and calculate the out of pocket data error again. Repeat the operation for many times until the two out of pocket data error calculations of all classification regression trees are completed. Finally, calculate the importance of the feature, and the calculation function is shown as follows:

$$T_{x_i} = \sum_{i=1}^{Q} \frac{OOB2(x_i) - OOB1(x_i)}{Q}. \tag{7}$$

In the formula, Q represents the number of decision trees, $OOB1(x_i)$ represents the out-of-bag data error obtained for the first time, $OOB2(x_i)$ represents the out-of-bag data error after interference, $T(x_i)$ represents the importance of the feature x_i, and the value of $T(x_i)$ is positively correlated with the importance, when $T(x_i)\langle 0$, the noise of feature x_i has a negative disturbing effect on the model.

4.3. Data Dimensionality Reduction Processing. The data dimensionality reduction process first compares the algorithms before and after dimensionality reduction and uses decision tree, random forest, and support vector machine algorithms for comparative analysis. The first 770 data are used as training samples, and the last 30 data are used as test samples. First normalize the data, and then perform matrix analysis and calculate the MSE values before and after dimensionality reduction. The calculation formula is as follows:

$$MSE = \frac{\sum_{i=1}^{n}\left(y_i - y_q\right)}{n}. \tag{8}$$

The results obtained from the calculation are shown in Table 1.

It can be seen that the error rate has decreased significantly and the accuracy has been improved after dimensionality reduction by factor analysis.

In order to obtain the audit warning threshold suitable for the enterprise, the enterprise should use its own data to verify and optimize the set financial threshold: generally, the enterprise should make a financial evaluation once a month or every quarter, and the financial department should make a comprehensive evaluation at the end of the year. First, the actual financial data are used to determine the actual financial early-warning interval of the enterprise, then the actual early-warning interval is compared with the set threshold interval, the financial differences between them and the reasons for the differences are analyzed, and the early-warning interval of each financial supervisor is adjusted. Finally, the financial audit early-warning threshold of the enterprise is comprehensively verified, adjusted, and optimized in combination with the enterprise's financial status and the market environment. Finally, we get the most suitable audit warning threshold for ABC corporations.

Let function $f(x) = f(x_1, x_2, x_3, \cdots, x_s)$, where $(x_1, x_2, x_3, \cdots x_s)$ is the independent variable in random forest. The partial correlation of function $f(x)$ on x_j is

$$f_j\left(x_j\right) = E_x[f(x)]. \tag{9}$$

For the k classification problem, let $\rho_k(x)$ be the vote probability of category k, then the partial correlation function corresponding to category k is

$$f_k(x) = \log\rho_k(x) - \frac{1}{k}\sum_{j=1}^{k}\log\rho_j(x). \tag{10}$$

In this paper, a similar integration idea is applied to the data level, and the data mining software is R language. R language is not only compatible with various operating systems but also has many mature and stable data mining models, which is conducive to the accuracy of audit warning indicators. The training set used in each round of the fitting process of the model is a new data set obtained by random reorganization on the original data set, and the process of data reorganization is completely randomized and independent of the generation process of the previous training set. The final prediction result of the algorithm in this paper is also estimated using the average value, which is similar to the random forest.

5. Data Processing and Financial Indicator Construction

In order to carry out the enterprise financial crisis preparation setup more comprehensively and accurately, based on the classification features and the feature importance measurement method of the K-fold random forest algorithm, a new financial preparation setup index system is established, and the financial crisis analysis that has a high impact on the enterprise is screened out. Indicators are established to improve the prediction accuracy of crisis preparedness setting. Based on the financial statements of listed manufacturing corporations, starting from the features of the financial situation of the financial crisis of the enterprise, the preliminary screening of financial indicators is carried out from the five aspects of the enterprise's profitability, solvency, operating ability, development space, and cash flow. It includes 26 financial indicators such as current ratio, asset-liability ratio, and total asset turnover ratio, which are numbered from A to Z. Using OOB out-of-bag data to carry out importance measurement analysis, the top six financial indicators in the order of importance are shown in Table 2, and a new financial

Table 1: Comparison of MSE before and after dimensionality reduction.

	Before dimensionality reduction	After dimensionality reduction
Decision tree	0.092	0.087
Random forest	0.054	0.012
SVM	0.128	0.031

Table 2: Top 6 financial indicators in order of importance.

Order of importance	Indicator number	Index	Importance
1	A	Current ratio	0.8392
2	G	Quick ratio	0.8123
3	J	Cash flow ratio	0.8023
4	C	Fixed asset turnover	0.7987
5	R	Total asset turnover	0.7638
6	Y	Sales cash ratio	0.7348

crisis preparation setup indicator system based on the K-fold random forest algorithm is obtained.

In this part, we use the decision tree model and random forest model introduced earlier to analyze and process the financial data, and test the classification effect of each model.

(1) Decision tree classification. First, we set the parameters of the decision tree, including the maximum number of features, the maximum depth, and other attributes. After SMOTE sampling, the optimal hyperparameters are found, and the model is trained and evaluated by 10-fold cross-validation. Then we verify the model on the test set. After modeling, we found that the maximum depth of the decision tree was 8: 00, and the accuracy rate was 87.63%. Too deep a decision tree will cause the data to be overfitted, which will lead to the decline of judgment results. The specific maximum depth traversal results are shown in Figure 4.

(2) Random forest classification. The random forest model also needs to do each of the parameters first. Considering that each decision tree in the random forest requires cross-validation, its fold does not have much impact. Considering the calculation performance, we will randomly select the number of cross-validation folds in the forest as 3. At the same time, we traverse the total number of decision trees and the maximum depth in different situations. The specific values are shown in Table 3.

The results of data analysis showed that the best judgment rate was 800 decision trees at the maximum depth of 5 layers of random forest, and the value was 88.27% (See Figure 5 for details).

According to the above experimental results, we have constructed 14 financial indicators based on financial data, which are related to the five aspects of the enterprise's solvency, operating ability, profitability, development ability, and risk level. Based on these data, a decision tree model and a random forest model are constructed. From the empirical results, the random forest model has a higher analysis accuracy than the decision tree model. The results based on the model need to be checked manually in the

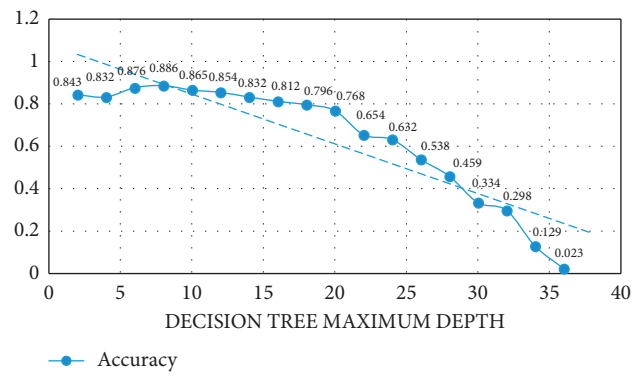

Figure 4: Judgment accuracy at different maximum depths of the model.

follow-up, and the judgment accuracy rate close to 90% can effectively reduce the time cost of manual checking.

Algorithm Accuracy Analysis. In order to verify the effectiveness and optimization of the improved K-fold random forest algorithm, three data sets in the UCI database were used for simulation experiments, 80% of which were used as training data sets and 20% as test sets. Experiments are carried out in the Anaconda3+ VScode environment, and the classification accuracy of the traditional random forest algorithm and the K-fold random forest algorithm under different numbers of classification and regression trees is compared. The comparison results are shown in Figure 6.

The input data in this model is the financial information of listed corporations. In this chapter, the data processing process and the construction of financial indicators will be introduced. There are many methods to judge the financial irregularities of listed corporations, among which we adopt a more credible method, that is, to judge whether there are any irregularities in the financial reports of the year through the statistical caliber of the problems and results of the handling of irregularities disclosed by CSRC. We downloaded all the processing file announcements of A stock exchange and B stock exchange since 2017, marked them according to the name of the offending enterprise and the offending time

Table 3: Random forest related parameter values.

	Whole school (%)	Whole class (%)	Student A (%)
Math	82.30	79.30	90.60
Accounting	84.20	91.80	94.20
Programming	83.60	79.30	84.20
Management	84.30	81.20	77.20
Computer application	87.20	86.10	87.30

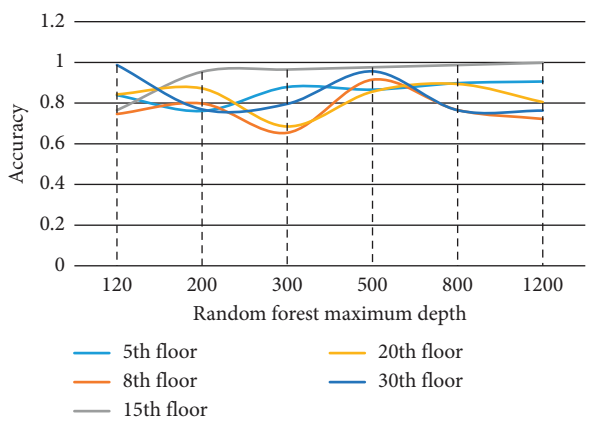

Figure 5: Accuracy of the random forest model in different situations.

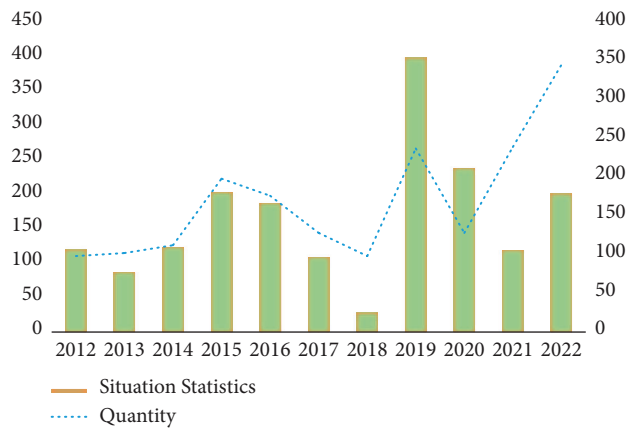

Figure 7: Statistics on violations.

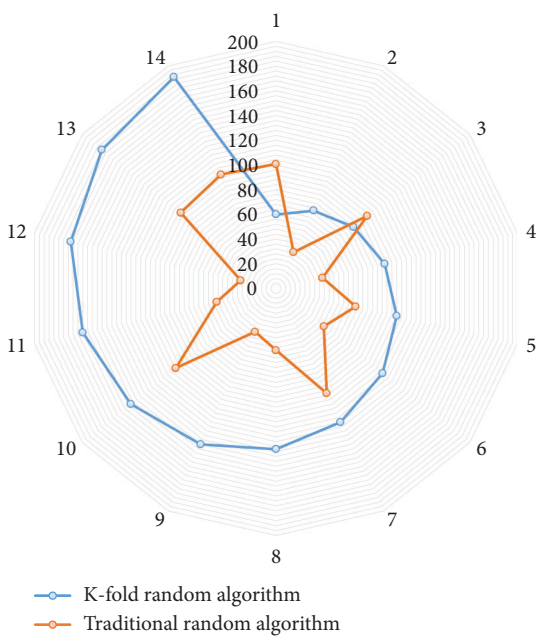

Figure 6: Comparison of the classification accuracy of the two algorithms.

disclosed therein and completed the processing of the forecast variables, as shown in Figure 7.

Therefore, it is particularly important to establish a number of decision tree individuals with independence and distinctiveness in building a random forest model. If we simply use the original data to judge the data, it is difficult to realize a diversified decision tree model, and it is also difficult to reflect the advantages of integrated learning. Therefore, when building a random forest model, we need to sample the data according to certain rules, and each decision tree uses part of the total sample for training, which can not only reduce the repetition of the training data but also make the database of each decision tree different and increase the difference of individual decision trees.

In the era of big data, the financial sharing center provides great convenience for the data collection of the financial preparation setup model. The corporate account information data can be directly extracted from the business module of the financial sharing center. In addition to the internal financial data of the enterprise, the average data of various indicators of various industries and the related information data of the bank-enterprise interconnection system should also be collected. The data required by the financial preparation setup model must be authentic, accurate, and complete in order to ensure the accuracy of the financial risk preparation setup output by the financial model. However, the information and data initially collected are numerous and complicated and need to be sorted and processed uniformly. The information data collected initially needs to firstly screen out the data required by the financial preparation setup model and digitally process and store it in the database; secondly, use the data mining technology to convert the data in the database and the financial preparation setup indicators correspondingly and eliminate the correlation and noise. Big data is as shown in Figure 8; finally, the transformed and eliminated data is copied to the DBMS management system, and the Hadoop platform is used to normalize the data.

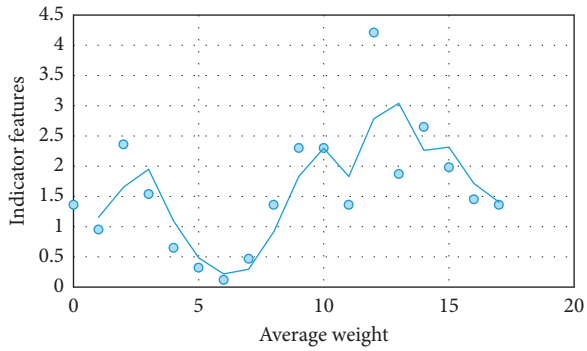

Figure 8: Scatter plot of average weight of preparation setup indicator features.

6. Conclusion

The new economic development trend requires companies to monitor their financial status in real time and strengthen their risk management and control capabilities. In order to realize the timely and accurate preparation setup of enterprise financial crisis, an preparation setup model of enterprise financial crisis is constructed based on time series and improved K-fold random forest algorithm. The results show that, compared with the traditional random forest algorithm, the classification accuracy of the improved K-fold random forest algorithm is improved by 1.54%, and the classification accuracy rate reaches 82.6%, K-fold cross-validation idea is optimized for the random forest algorithm. In the application of enterprise financial crisis preparation setup, the prediction accuracy of the preparation setup model is 90.327%. The positive and negative classes are 91.869% and 88.785%, respectively. The prediction accuracy is high. There are differences in the actual data of financial indicators of corporations in different industries, and it is difficult to use a unified indicator standard for financial crisis preparation setup. The research limits the type of sample data and can further design the financial preparation setup indicator system in different industries to improve the adaptability of the preparation setup model.

Data Availability

The data used to support the findings of this study are available within the article.

Conflicts of Interest

The author declares that there are no conflicts of interest.

References

[1] W. Long, L. Song, and L. Cui, "Relationship between capital operation and market value management of listed companies based on random forest algorithm," *Procedia Computer Science*, vol. 108, pp. 1271–1280, 2017.

[2] Q. Wu, Y. Ye, H. Zhang, M. K. Ng, and S. S Ho, "ForesTexter: an efficient random forest algorithm for imbalanced text categorization," *Knowledge-Based Systems*, vol. 67, no. sep, pp. 105–116, 2014.

[3] Y. Song, X. Liang, and R. Zhang, "Feature selection based on statistical random forest algorithm[J]," *Journal of Computer Applications*, vol. 5, no. 15, pp. 145–254, 2018.

[4] Y. Cai, Q. Yin, Q. Su, X. Huang, Y. Zhang, and T. Liu, "Prediction method of enterprise return on net assets based on improved random forest algorithm," *Journal of Physics: Conference Series*, vol. 1682, no. 1, Article ID 012083, 2020.

[5] J. Wu, "An enterprise credit scoring model based on improved random forest algorithm," *[J]. Conference on Management Science*, vol. 26, no. 2, pp. 14–25, 2020.

[6] Z. Wu, "Using machine learning approach to evaluate the excessive financialization risks of trading enterprises," *Computational Economics*, vol. 59, no. 4, pp. 1607–1625, 2022.

[7] H. Wu and J. Chen, "Prediction of cash holdings using random forest algorithm [J]," *Journal of Physics*, vol. 23, no. 25, p. 2, 2019.

[8] D. Forsaith, R. Mcmahon, and S. Holmes, "Small enterprise financial management: theory and practice[J]," *Small Enterprise Research the Journal of Seaanz*, vol. 12, no. 1/2, pp. 19–21, 2017.

[9] N. Z. Anna, "Enterprise financial administration quality control[J]," *International Conference on Management Science & Engineering*, vol. 59, no. 14, pp. 23–65, 2018.

[10] L. Jie, "On Assets quality control of enterprise financial management," *Journal of Beijing Economic Management Institute*, vol. 12, no. 4, pp. 362–541, 2019.

[11] J. Tu, "The evaluation method of enterprise financial management skill[J]," *Applied Mechanics and Materials*, vol. 59, no. 13, pp. 56–91, 2021.

[12] L. Wang and H. Liu, "Research on the mode of enterprise financial management in the Internet age," *IOP Conference Series: Materials Science and Engineering*, vol. 394, Article ID 042024, 2018.

[13] Z. Li and J. Wang, "An optimization application of artificial intelligence technology in enterprise financial administration [J]," *Boletin Tecnico/technical Bulletin*, vol. 55, no. 11, pp. 83–89, 2017.

[14] Q. Liu and Y. K. Song, "Creating blockchain driven ecosystem model for enterprise financial management[J]," *Proceedings of the International Academic Conference on Frontiers in Social Sciences and Management Innovation (IAFSM 2019)*, vol. 154, no. 03, pp. 12–36, 2020.

[15] D. Cheng, "On the aim of business financial management[J]," *JOURNAL OF JIANGHAN PETROLEUM INSTITUTE*, vol. 55, no. 23, pp. 98–120, 2018.

[16] F. Livingston, "Implementation of Breiman's random forest machine learning algorithm[J]," *ece591q machine learning journal paper*, vol. 4, no. 1, pp. 22–36, 2020.

[17] F. Wang, "Forest algorithm based staff incentive mechanism design of non-public enterprise from the perspective of positive organizational behavior," *Cognitive Systems Research*, vol. 52, no. 33, pp. 132–137, 2018.

[18] Z. Ding, "Force identification from vibration data by response surface and random forest regression algorithms[J]," *Financial Management*, vol. 89, no. 11, pp. 02–13, 2022.

[19] S. Chakraborty, "Hierarchic information structure design for corporate financial administration simulation software," *Winter Simulation Conference*, vol. 3, no. 10, p. 37, 2018.

[20] S. Shiotani, "Low-cost carriers in Japan: challenges and paths to success - using a corporate simulation model for empirical analysis[J]," *Cellular Physiology & Biochemistry International Journal of Experimental Cellular Physiology Biochemistry & Pharmacology*, vol. 31, no. 1, pp. 37–43, 2019.

Hindawi
Mobile Information Systems
Volume 2022, Article ID 7056149, 10 pages
https://doi.org/10.1155/2022/7056149

Research Article

Siamese Attention Networks with Adaptive Templates for Visual Tracking

Bo Zhang, Zhixue Liang, and Wenyong Dong

School of Computer Science, Wuhan University, Wuhan 430072, China

Correspondence should be addressed to Wenyong Dong; dwy@whu.edu.cn

Received 23 May 2022; Revised 20 August 2022; Accepted 27 August 2022; Published 19 September 2022

Academic Editor: Chang Wu Yu

Visual object tracking takes an important role in realistic applications, such as video understanding, unmanned auto vehicles, and autonomous robots. Although the Siamese-based tracker has achieved good performance in tracking tasks, the existing methods using initial template or updating template with simple strategy result in the performance degradation of the model when the target varies in realistic scenarios such as target occlusion, scale variation, and deformation. In this paper, we propose a visual tracking framework with adaptive template update and spatiotemporal attention, named SiamAttnAT. Specially, we propose a historical template selecting strategy and a template adaptively generating method for robust tracking. In addition, we apply the proposed mechanisms to the employed baseline SiamRPN++. Extensive experiments and comparisons with state-of-the-art trackers on short-term and long-term visual tracking benchmarks including VOT2018, OTB-100, UAV123, NFS, and LaSOT show that the proposed framework achieves the outstanding performance with a considerable real-time speed, verifying its efficiency and effectiveness.

1. Introduction

Visual object tracking (VOT) is one of fundamental tasks in computer vision, which applied widely in automatic driving, human–computer interaction, robot sensing, visual surveillance, and augmented reality. VOT aims to automatically locate a specific target object at each frame given its initial location in a changing video sequence [1]. Recently, VOT has received considerable attention and gained significant progress [2]. However, it is still a highly challenging task, which is to learn an appearance model of an arbitrary target object online, due to complicated scenarios including target occlusion, appearance changes, scale variation, deformation, and environmental aspects such as motion blur or illumination changes [3].

In [4], the tracking approaches are roughly categorized into traditional methods and deep learning (DL)-based methods. The former employs various visual frameworks to model the appearance and motion of a target, including discriminative correlation filters (DCF), silhouette tracking, Kernel tracking, and point tracking. The latter employs either deep off-the-shelf features or end-to-end networks. There are two most prominent paradigms: discriminative correlation filters (DCFs) and deep Siamese tracking methods. The DCF-based trackers [5–7] attempt to train filters to learn the correlation between the target and background appearance. The target is then detected in consecutive frames by convolving the trained filter via the fast Fourier transform (FFT) [5]. The DCF-based trackers have the advantages to update the appearance model over time through the loss function [5]. However, these trackers based on the discriminative correlation filters (DCF) have inherent limitations [6]. In general, DCF-based trackers have inflexible assumptions about training samples for learning an online classifier, which leads to undesirable boundary effects that severely degrade the quality of the target model [4].

With strong capacity of learning and powerful deep features, deep learning technologies have significantly advanced the performance of visual object tracking [8], especially the emergency of the Siamese trackers. Trackers based on Siamese networks [9–14] have received significant

attention in visual tracking community. The Siamese-based trackers employ two subnetworks and convert tracking problems into similarity learning between the target template and the current image. The features of the target template and the search region can be extracted through training a deep neural network offline on large datasets. Then the trackers match the template and the search region and output the similarity with the target for each location in the search region. Due to the competitive performance, especially well-balanced accuracy and speed, Siamese trackers have drawn the increasing attention of many researchers. Some excellent Siamese-based tracking frameworks, such as SiamRPN [15], SiamRPN++ [10], SiamBAN [16], SiamCAR [17], and SiamCorners [18], have demonstrated their superior capabilities in different aspects of visual object tracking by introducing semantic network, cross correlation, region proposal network, feature pyramid network, corner prediction, and so on [3, 4]. This work is mainly based on Siamese trackers.

Although the Siamese trackers have achieved remarkable progress, the tracking is still a highly challenging task due to the vast amount of challenging scenes [15]. The appearance of target may change due to the complicated real scene. And it will result in the low similarity between initial template and the search region. Therefore, the model is ambiguous to locate target when facing the scene changes. Some Siamese trackers employ the object template, which is initialized in the first video frame and keep it fixed during the remainder of the video. Therefore, this method is prone to lead to early failure of the tracker [3]. While some Siamese trackers adopt update strategies to update the object template for robust tracking, the update strategies are inadequate to adapt to the changes of different tracking situations. Additionally, it is important to consider both spatial and temporal information in video sequence for object tracking. However, previous trackers do not simultaneously model the spatiotemporal relationships.

Inspired by the prior works, we propose a novel template updating strategy and adapt it to Siamese attention network name SiamAttnAT. Specially, our method fully utilizes the reliable prediction of the model to select the historical templates actively for generating the current template subsequently. So the feature representation of the template is enhanced to cope with the complicated tracking scenarios. Besides, spatiotemporal attention mechanism is adopted to the tracker to improve the tracking accuracy and robustness. Figure 1 shows the qualitative comparison of our SiamAttnAT tracker with three state-of-the-art trackers on OTB100 benchmark. Summarily, the main contributions of this work are three-fold.

(i) We present a novel template selecting strategy in feature level. It can determine which historical frame feature should be selected for adaptive template generating.

(ii) We propose a learnable and adaptive template generating method, which is used to update the current template online to adapt to the tracking object variances.

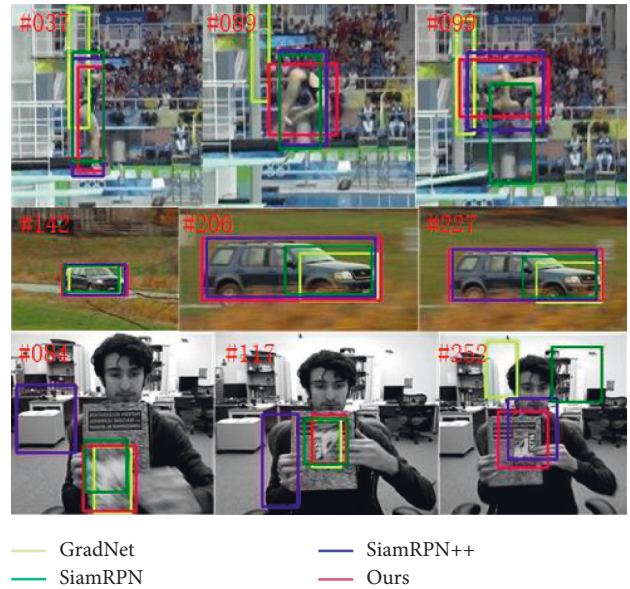

Figure 1: Qualitative comparisons of our tracker with three state-of-the-art trackers on OTB100 benchmark. Observed from the visualization results, our tracker is better than the other three trackers. Best viewed in colour.

(iii) We adapt above methods to a well-known tracking network, SiamRPN++. We verify the proposed method on five short-term and long-term tracking benchmarks and has achieved obvious improvement over existing methods

2. Related Works

In this section, we briefly introduce recent development of object trackers, template update, and attention mechanism. We focus on the Siamese trackers in this work.

2.1. DCF-Based Trackers. With the efficiency and expansibility of correlation filter theory, correlation filter-based object trackers have recently shown excellent performance on several tracking benchmarks. Among the approaches, discriminative correlation filter (DCF)-based trackers are the most prominent. These trackers learn a correlation filter from example patches of the target appearance to discriminate between the target and background appearance [3]. With the adoption of deep learning technologies [12], multichannel formulations and spatial constraints, attention mechanisms in correlation filter framework, the performance of correlation filter-based trackers have been notably improved [8]. In ASTCA [5], a learnable and adaptive spatial-temporal context-aware network is proposed to reduce the influence of boundary effect and improve the tracking accuracy. In CFML [19], a metric learning model is presented to solve the target scale problems in correlation filter framework. SRDCF [20] tracker proposed a penalty function to reduce the filter coefficients of the boundary regions of the image patch. More specially, in [1], a probabilistic regression formulation is proposed to predict the

conditional probability density of the target state instead of confidence-based regression strategy, which is shared by the previously dominant DCF paradigm. Integrating the strategy to the DiMP [21] tracker achieves a new state-of-the-art performance on six datasets.

2.2. Siamese-Based Trackers. The other dominant tracking framework is Siamese-based trackers. By learning massive data on pairs of video frames offline and employing an effective similarity function, Siamese network-based trackers have made much progress and achieved the best balance between accuracy and efficiency [17]. As pioneering work, [9] first introduced SiamFC framework for visual object tracking, by using Siamese networks to measure the similarity between target and search image [8]. Reference [12] further proposed the CFNet architecture and received higher performance by integrating correlation filter to the Siamese networks for tracking.

The trackers, such as SiamFC, CFNet, and DSiam, use multiscale bounding boxes to locate the target object in the search area, resulting in a large amount of calculation and limited performance. Reference [15] proposed SiamRPN by applying region proposal network (RPN) into Siamese architectures to reduce calculation. Reference [14] further designed a novel distractor-aware module for incremental learning and applied the module to the SiamRPN, referred to as DaSiamRPN. Due to some limitations as translation invariance, the above trackers built their networks upon an architecture similar to AlexNet. Reference [10] overcame the restrictions of strict translation invariance and proposed SiamRPN++ with a deep network ResNet. By introducing layerwise and depthwise cross correlations to learn sufficient semantic information and produce multiple similarity maps at multiple levels, tracking performance and robustness had been highly improved. The above Siamese trackers all employ anchor-based object detectors. In addition, some anchor-free trackers are proposed for higher performance, such as SiamBAN [16], SiamCAR [17], and SiamFC++ [13]. Furthermore, [22] proposed an accurate bounding-box regression with distance-IoU loss to optimize the objective function to make the target estimation more accurate.

2.3. Template Update. It is important to possess the online model adaptability for the Siamese trackers. However, most Siamese trackers adopt the fixed-model trained offline, which cannot cope with appearance changes in tracking scenarios. While some Siamese-based trackers introduce update strategies to update the model online for robust tracking, the update strategies are insufficient to adapt to the changes of different tracking scenarios. DSiam [23] adopt a fast transformation learning module to online update the tracking model. In [3], a learned update strategy is proposed, which use the initial template, the accumulated template from all previous frames, and the feature template in the current frame. In [24], the current template will be replaced when the thresholds of the dynamic template update interval and the confidence threshold are satisfied. Although template update methods are introduced into some Siamese trackers, the update strategies are either simple template replacement or use all historical templates without selection. The template representation will be weakened without selecting strategy of historical templates since some templates have lower similarity with the search region. In this work, we propose selecting strategy of historical templates and adaptive template update methods. Using the selected historical templates as the input, a trained subnetwork can generate the different weight matrixes to obtain the current tracking template by matrix multiplication.

2.4. Attention Mechanism. It is a core problem to employ the attention mechanisms to explore the inherent spatial and temporal relations in the video sequence in object tracking. The spatial relations contains object appearance information, which help localize the target. The temporal dependencies include the state changes of objects across video frames, which help cope with the challenging scenes such as occlusion, scale variation, and object deformation. Some trackers have introduced attention mechanisms to enhance the template representation and improved the tracking robustness. However, some previously Siamese trackers [6, 10, 13, 17, 25] only exploit the spatial relations for tracking, and some methods [3, 21, 26] only explore the temporal relationships by updating the model with historical predictions. In this work, we consider spatial and temporal information simultaneously to leverage them for robust tracking.

3. Siamese Attention Networks with Adaptive Templates

In this section, we describe our proposed tracking architecture SiamAttnAT, with an overview in Figure 2. And then we elaborate the main components of the proposed network, including backbone, template selection module, memory pool, and template generation module.

3.1. Backbone. We employ the modified ResNet50 like [10] as the backbone of SiamAttnAT architecture to extract the multilevel features of search regions and target templates, respectively. Features from different blocks of the backbone focus on different hierarchical information of target object. Features from earlier layers contain shallow semantic information such as shape and colour, which help locate the target object. Features from latter layers have richer and more abstract semantic information, which is beneficial to cope with the challenging scenarios such as occlusions, deformation, and target disappearance in visual object tracking.

The backbone consists of two subbranches: a template branch and a search branch. The template branch is used to extract features from the target patch z, and the search branch is for extracting features from the current search patch x. The two branches share parameters in CNN [15]. In this work, we use the block 3, block 4, and block 5 of the ResNet50 to extract multilevel features of the target template

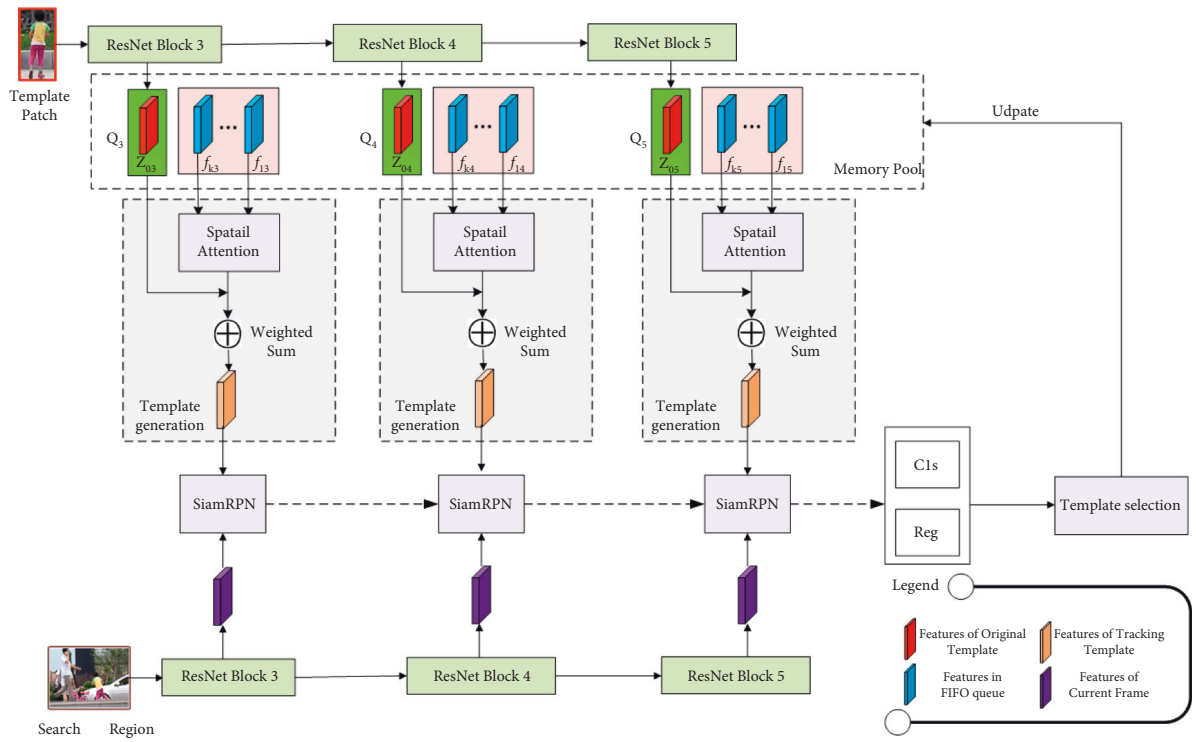

FIGURE 2: Illustration of main framework of SiamAttnAT. The network consists of backbone (ResNet50), memory pool, template generation module, template selection module, and Siamese Region Proposal (SiamRPN) modules. The network generates the classification and regression boxes by fusing the outputs from multiple SiamRPN blocks with weighted sum. Best viewed in colour.

and the search region. The sizes of template patch and search region are $127 \times 127 \times 3$ pixels and $255 \times 255 \times 3$ pixels.

3.2. Memory Pool. We construct memory pool to store historical feature templates. By fusing the different feature templates, we capture the temporal dependencies across video frames to enhance the feature representation of the current template, improving the tracking robustness. The memory pool is composed of three First-in First-out (FIF0) queues (i.e. Q_3, Q_4, Q_5). The size of queue is a hyper-parameter. In this work, we set the queue size to 4. If the template selecting strategy is satisfied, we first crop the template image at a size of $127 \times 127 \times 3$ pixels from the current frame, then feed the new template image into ResNet50 network. We store the new feature templates generated from block 3, 4, and 5 of the backbone to the template queues. In general, the latest feature template has the most advantages to reflect the state of the current object. So we adopt FIFO strategy to update the template queues. Considering that the initial template is given in the first frame containing only ground-truth information, while other templates are based on predictions. For this reason, we retain the initial template throughout the tracking process.

In SiamAttnAT framework, for convenience, we denote $\varphi_i(z_j)$ and $\varphi_i(x)$ as the output feature maps of z_j and x from L_i (i is 3, 4, 5, denotes the block 3, 4, and 5 of the ResNet50) in the backbone, where j represents the j-th target template in the template queue. In particular, $\varphi_i(z_0)$ denotes the initial feature templates of different layers given in the first frame and could not be deleted throughout the tracking process.

3.3. Template Generation Module. Template generation module can adaptively generate the target template online to achieve more accurate and robust tracking performance. The module take as input the initial object template and the historical templates stored in the template queues. Since linearly combined these templates leads to information decay over time, we adopt learnable weighted sum to aggregate the templates. We first fuse the historical templates by constructing a spatial attention model to generate weighted matrixes, and then we adopt fixed weighted sum to fuse the initial template and the output of spatial attention module. Due to the most reliable signal provided the initial template, we use a parameter σ_0 to denote the initial template weight.

The spatial attention module is composed of four nonshared full convolution networks, each of which contains two consecutive 3×3 convolutions, one 1×1 convolution, and a sigmoid activation function. The spatial attention model generates four weight matrixes, denotes asσ_j (j is from 1 to 4). The output of the template generation module ($\varphi_i(\check{z})$) is calculated as

$$\varphi_i(\check{z}) = \sum_{j=1}^{4} \left(\sigma_j \times \varphi_i(z_j)\right) + \sigma_0 \times \varphi_i(z_0). \quad (1)$$

When tracking on a new frame of video sequence, the candidate image (named as x) of the current frame is fed into

the search branch of the backbone to generate the features$\varphi_{\mathrm{i}}(x)$. When we feed the feature maps $\varphi_{\mathrm{i}}(\check{z})$ and $\varphi_{\mathrm{i}}(x)$ into corresponding RPN network individually, the RPN network outputs classification feature (referred to as A_i^{cls}) and the regression feature (referred to as A_i^{reg}), respectively. We denote trainable parameters ω_i^{cls} and ω_i^{reg} as classification weights and regression weights of the i-th convolutional layer. The fusion outputs of each RPN modules are combined by weighted-fusion layer and calculated by weighted sum as follows:

$$\mathrm{A}^{cls} = \sum_{i=3}^{5}\left(\omega_i^{cls} \times \mathrm{A}_i^{cls}\right), \mathrm{A}^{reg} = \sum_{i=3}^{5}\left(\omega_i^{reg} \times \mathrm{A}_i^{reg}\right) \tag{2}$$

3.4. Template Selection Module. Which historical templates should be memorized is the core of dynamically generating the current template. In our work, we adopt the confidence score between the current template and the search region to decide whether to update the memory pool.

The selecting strategy is described as follows: we denote θ_i (i is 3, 4 and 5) as the i-th layer confidence threshold and θ as the final similarity threshold. When the conditions of $\mathrm{A}_i^{cls} > \theta_i$ and $\mathrm{A}^{cls} > \theta$ are satisfied, we crop the template image at a size of 127×127 pixels from the current frame, then feed the new template image into ResNet50 network. The ResNet50 network output new feature maps from the 3, 4, and 5 block. We update the i-th template queue using the i-th layer feature maps with the FIFO strategy.

The selected historical feature map is the target feature map with high accuracy. But if we overly focus on the correctness and set the threshold of access to the memory to a high level, it will cause the memory pool to update slowly, and all the feature maps in the memory are highly similar. Therefore, the balance between accuracy and speed is essential for selecting strategies. Our strategies are as follows.

We determine the relationship among the thresholds for accessing the memory through a large number of experiments, as shown in equation (3).

$$\theta_3 < 0_4 < 0_5 \tag{3}$$

We find that the deep features representing high semantic information must be highly consistent with the first frame to make the template accurate. In order to ensure the high diversity of the memory, the shallow features that characterize appearance information such as shape and colour require a lower threshold to maintain target with various appearance changes.

In addition, the confidence is still high after tracking the wrong target, but the score between two consecutive frames will suddenly change when there is semantic interference in the case of a clean background. The sudden change of two frames is also judged as a situation with low confidence and the feature is not allowed to enter the memory pool in this case. We denote hyperparameter ρ as the change threshold of two consecutive frames, as shown in (4).

$$\left|\max\left(\mathrm{A}_i^{cls}\right)_k - \max\left(\mathrm{A}_i^{cls}\right)_{k-1}\right| > \rho. \tag{4}$$

We denote $(\mathrm{A}_i^{cls})_k$ as the classification result of the i-th layer and the k-th frame through the RPN module.

4. Experiments and Results

We conduct experiments on five short-term and long-term benchmark databases: VOT2018 [27], OTB-100 [28], UAV123 [29], NFS [30], and LaSOT [31] datasets. Furthermore, we conduct ablation study to verify the effects of each proposed module.

4.1. Datasets.

VOT2018. The VOT [27] dataset has been updated every year since 2013, which is composed of high-resolution colour sequences [14]. VOT2018 is a widely used dataset for online free single object tracking. It consists of 60 challenging videos collected from real-life datasets.

OTB-100. OTB-100 [28] is the most authoritative and widely used benchmark dataset. The dataset contains 100 video sequences which is extended from the OTB-2013 (50 videos) including a quarter of the grayscale images.

NFS. NFS [30] is higher frame rate video dataset (called Need for Speed - NfS) and benchmark for visual object tracking. The dataset consists of 100 videos (380K frames) captured with now commonly available higher frame rate (240 FPS) cameras from real-world scenarios.

UAV123. The UAV123 [29] dataset is proposed in 2016 which contains a set of video sequence for drone tracking. It contains 123 high-resolution aerial video sequences annotated, totaling more than 110K frames [14].

LaSOT. LaSOT [31] is a large-scale dataset which contains 1400 video sequence in total, with more than 3.5 M image frames, and 280 videos in the testing set in total. Since such challenging scenarios as occlusion, deformation, target disappearance are common in LaSOT, it is widely used into performance evaluation for long-term object tracking.

4.2. Implementation Details

4.2.1. Experimental Environment. The operating system used for the experiment is Ubuntu 18. The experiment is implemented using PyTorch, and 2 11 GB NVIDIA GeForce RTX 2080Ti GPUs to conduct the experiments.

4.2.2. Training. We use SiamRPN++ [10] as baseline. In proposed SiamAttnAT network, we use ResNet50, which is pretrained on ImageNet, as the backbone of tracking architecture. The whole network are trained and fine-tuned on the training sets of COCO, ImageNet DET, ImageNet VID, YouTube-BoundingBoxes Dataset, and LaSOT. In addition, we use an image of 127×127 pixels as target template and an image of 255×255 pixels as candidate image in training and testing.

Our model is trained in an end-to-end fashion. We employ stochastic gradient descent (SGD) as the optimizer with weight decay of 0.0005 and momentum of 0.9. The learning rate is exponentially decayed from 0.005 to 0.0005. By following SiamRPN [15], the training loss is the sum of classification loss and regression loss. We adopt the cross-entropy loss for the former and smooth L1 loss for the latter.

4.2.3. Inference. The first template provides the most reliable information, while the latest template provides the most similar appearance to the target in the current frame. In our work, we set the weight of the first template to 0.5. Furthermore, we set hyperparameters θ_3, θ_4, θ_5, θ, ρ to 0.98, 0.985, 0.99, 0.985, and 0.1, respectively. Comparison with State-of-the-Art Methods.

4.2.4. On OTB-100. We draw some experimental comparisons of the proposed SiamAttnAT and other 9 state-of-the-art trackers including SiamFC [9], ECO [32], SiamRPN [15], DaSiamRPN [14], SiamRPN++ [10], ATOM [26], DiMP [21], SiamBAN [16], and GradNET [11] on this dataset. We adopt success plots and precision plots as the evaluation indicators of tracking performance on OTB-100. Figure 3 illustrates comparisons of the success and precision plots over all 100 testing videos. As shown in Figure 3, SiamAttnAT outperforms all other trackers for both indicators. Especially, our tracker achieves a success score of 0.715 and a precision score of 0.928. Compared with the baseline SiamRPN++, our tracker has improved success score and precision score by 1.9% and 1.4%, respectively, verifying the effectiveness and efficiency of the proposed tracker.

4.2.5. On UAV123. To evaluate the tracking performance of the proposed tracking framework, we report some experimental comparisons of our tracker and several other state-of-the-art trackers including Staple [33], SRDCF [20], SiamFC [9], ECO-HC [32], ECO [32], SiamRPN [15], DaSiamRPN [14], SiamRPN++ [10], and SiamCAR [17]. Figure 4 illustrates the precision and success scores of the compared trackers on UAV123 dataset. Specifically, our tracker achieves an AUC score of 0.636, which surpasses that of DaSiamRPN (0.586) and SiamCAR (0.614) by 5.0% and 2.2%, respectively. Compared to the baseline SiamRPN++, our tracker has improved success score and precision score by 2.3% and 4.6%.

4.2.6. On VOT2018. We conduct our experiment on VOT2018 dataset [27] in comparison with 10 different methods including UPDT [34], ECO [32], DaSiamRPN [14], DRT [35], RCO [27], SiamRPN [15], ATOM [26], SiamRPN++ [10], and DiMP [21].

Following the evaluation protocol of VOT2018, we use the expected average overlap (EAO), accuracy, and robustness as evaluation indicators of different trackers. Table 1 presents the comparison results in EAO score, accuracy score, and robustness score with almost all the top-performing trackers in the VOT2018 benchmark. As shown in Table 1, our tracker has achieved good results in EAO and accuracy. In comparison with the baseline tracker SiamRPN++, our approach gains of 3.2%, 1.8%, and 3.3% on EAO, accuracy, and robustness, respectively.

4.2.7. On NFS. We evaluate the proposed tracker on the 30 fps version of the NFS [30] dataset. As shown from Table 2, our tracker achieves better performance. Compared with the baseline SiamRPN++, AUC score is improved by 2.3%.

4.2.8. On LaSOT. We conduct experiments on LaSOT [31] to further validate the long-term performance of proposed tracker on a large-scale database. As shown in Table 3, our method attains the best normalized precision and AUC score. Compared with SiamRPN++, our tracker has improved AUC and normalized precision by 6.7% and 5.4%, respectively.

4.3. Ablation Study. We provide detailed ablation studies about the different strategies including historical templates selection, template queue size, and the fusion methods of the historical templates to analyze their effects to the tracking performance. To achieve better balance of the different factors, we conduct extensive studies. All the ablation experiments are conducted on the VOT2018 benchmark.

4.3.1. Effect of Historical Templates Selecting Methods. Historical template selection method is the main components of our proposed tracker. We perform extensive experiments to analyze the effects of it to the tracking performance.

We construct a template selection module to determine which template can be stored in the memory pool. Besides our selecting strategy, there are two other methods including random selection and continuous selection. The former is to randomly select the multiple templates from the last 10 historic video frames, and the latter is to continuously select them. We set template queue size to 4 and perform numerous experiments to explore their effects to the tracking performance.

Table 4 displays the results comparisons of our tracker with different selecting strategies. From the table, we can observe that the tracker with our selecting strategy performs better than the tracker with continuous selection and random selection. Compared with the random selection, the tracker with continuous selection has slightly better performance.

4.3.2. Effects of Spatial Attention Module. There are two strategies to aggregate the historical templates in the template queues: fixed weighted sum and learnable weighted sum. To study the effects of the two strategies to the tracking performance, we conduct experiments on VOT 2018 benchmark. We set the fixed weights of four templates in the template queue (f_{1i}, f_{2i},f_{3i}, and f_{4i}, i is 3, 4, and 5) as 0.05, 0.1,

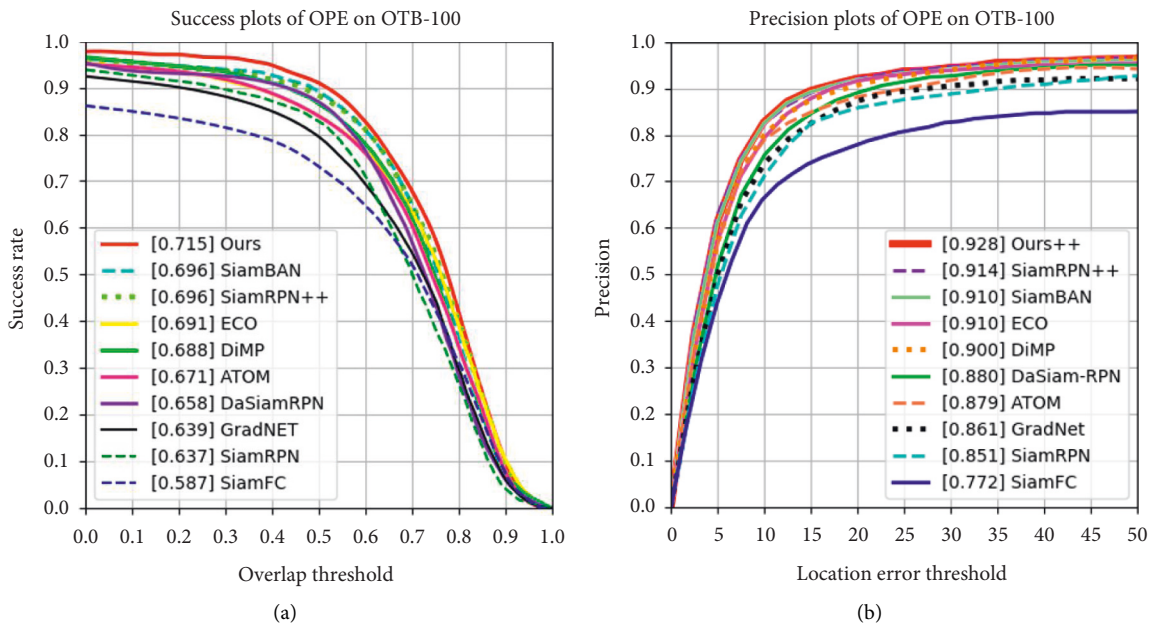

Figure 3: Success and precision plots on OTB-100. (a) Success plot. (b) Precision plot.

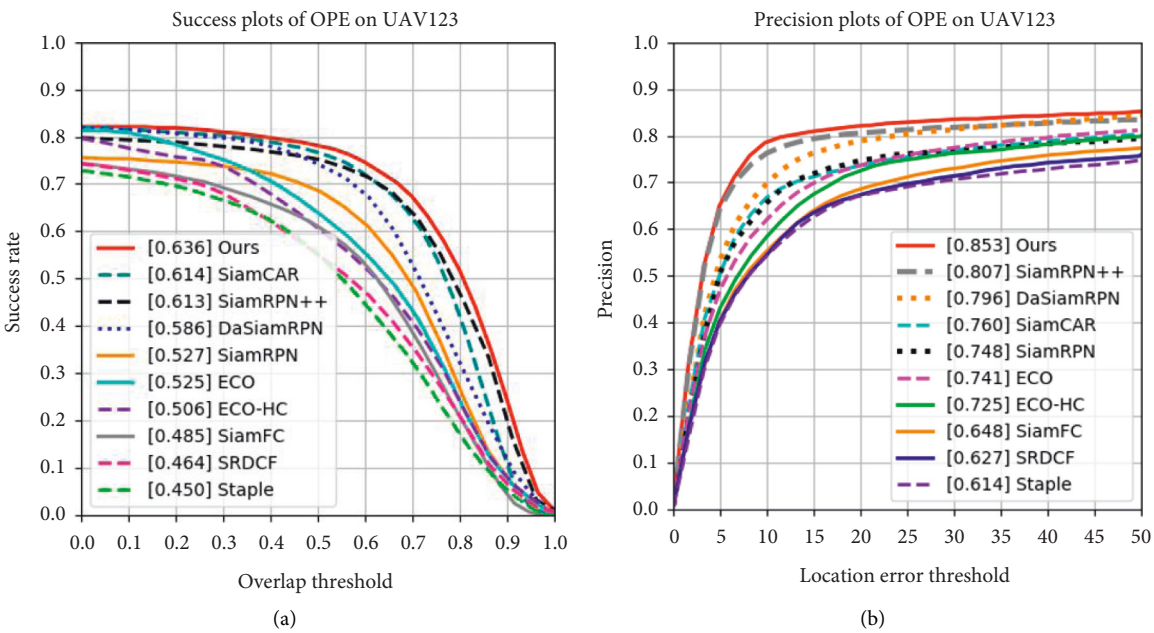

Figure 4: Success and precision plots on UAV123. (a) Success plot. (b) Precision plot.

Table 1: Comparison with state-of-the-art trackers on VOT2018. The best results are highlighted in red, blue, and green, respectively. SiamRPN++ is baseline.

	ECO	DRT	RCO	UPDT	SiamRPN	ATOM	SiamRPN++	DiMP	Ours
EAO↑	0.280	0.355	0.376	0.379	0.384	0.401	0.414	0.441	0.445
Accuracy↑	0.484	0.518	0.507	0.536	0.586	0.590	0.600	0.597	0.618
Robustness↓	0.276	0.201	0.155	0.184	0.276	0.204	0.234	0.152	0.202

0.15, and 0.2, respectively. The latest template to the current tracking frame is assigned the greater weight. The attention module composed of convolution neural network generate the learnable weight to fuse the template. Table 5 shows the comparison results of different fusion strategies in terms of accuracy, robustness, and EAO.

Table 2: Comparison with State-of-the-art trackers on the NFS dataset in terms of AUC. The best results are highlighted in red, blue, and green, respectively. SiamRPN++ is baseline.

	ECO	UPDT	ATOM	SiamRPN++	DiMP	Ours
AUC↑	0.466	0.537	0.584	0.602	0.620	0.625

Table 3: Results on LaSOT. The best results are highlighted in red, blue, and green, respectively. SiamRPN++ is baseline.

	ECO	MDNet	DaSiam	SiamRPN++	ATOM	Ours
Success (%)	32.4	39.7	41.5	49.5	51.5	56.2
Norm.Pr (%)	30.1	46.0	49.6	56.9	57.6	62.3

Table 4: Comparison results of different selecting methods on VOT2018. SiamRPN++ is baseline. "-" denotes without template selecting strategy.

Template selecting strategy	Accuracy↑	Robustness↓	EAO↑
- (Baseline)	0.600	0.234	0.414
Random	0.610	0.216	0.431
Continuous	0.612	0.214	0.436
Our selecting strategy	0.618	0.202	0.445

Table 5: Comparison results of different templates fusion strategies on VOT2018. SiamRPN++ is baseline. "-" denotes without templates fusion.

Templates fusion strategies	Accuracy↑	Robustness↓	EAO↑
- (Baseline)	0.600	0.234	0.414
Fixed weighted sum	0.610	0.223	0.436
Learnable weighted sum (spatial attention module)	0.618	0.202	0.445

As shown in Table 5, the tracker with fixed weighted sum or with learnable weighted sum achieves better results than the baseline SiamRPN++. Compared with the fixed weighted sum, the tracker with attention module has improved accuracy, EAO, and robustness by 0.8%, 0.9%, and 2.1%, respectively. It can be interpreted that spatial attention can enhance the representation capability of the template to help improve the tracking performance.

5. Conclusions

In this work, we present a new tracking framework named Siamese Attention Network (SiamAttnAT). We propose a new method to update template during tracking, which is composed of a historical template selecting strategy and a template dynamically generating approach. More specially, our method fully utilizes the reliable prediction of the model to select the historical templates actively for generating the current template subsequently. Compared with existing template update methods, our strategy gets rid of treating all historical templates equally or simply updating template with the fixed interval and thus enhances the representation capability of the template to improve the tracking performance of the model. Extensive experiments on five short-term and long-term benchmarks demonstrate that our method achieves competitive performance, while running at a real-time speed. In future, we will conduct further studies to reduce the limitations of the tracker on certain aspects of tracking video, such as slow motion, fewer target disappearance, and fewer similar distractors.

Data Availability

All data included in this study can be obtained from the corresponding author upon request.

Conflicts of Interest

The authors declare that they have no conflicts of interest.

References

[1] M. Danelljan, L. V. Gool, and R. Timofte, "Probabilistic regression for visual tracking," in *Proceedings of the conference on computer vision and pattern recognition*, pp. 7183–7192, Seattle, WA, USA, June 2020.

[2] S. Javed, M. Danelljan, and F. S. Khan, "Visual object tracking with discriminative filters and siamese networks: a survey and outlook," arXiv preprint arXiv:2112.02838, 2021.

[3] Z. Lichao, A. Gonzalez-Garcia, J. D. V. Weijer, M. Danelljan, and F. S. Khan, "Learning the model update for siamese trackers," in *Proceedings of the international conference on computer vision*, pp. 4010–4019, Seoul, Korea (South), October 2019.

[4] S. M. Marvasti-Zadeh, L. Cheng, H. Ghanei-Yakhdan, and S. Kasaei, "Deep learning for visual tracking: a comprehensive survey," *IEEE Transactions on Intelligent Transportation Systems*, vol. 23, no. 5, pp. 3943–3968, 2022.

[5] D. Yuan, X. Chang, Z. Li, and Z. He, "Learning adaptive spatial-temporal context-aware correlation filters for UAV tracking," *ACM Transactions on Multimedia Computing, Communications, and Applications*, vol. 18, no. 3, pp. 1–18, 2022.

[6] S. M. Marvasti-Zadeh, J. Khaghani, H. Ghanei-Yakhdan, S. Kasaei, and L. Cheng, "COMET: context-aware IoU-guided network for small object tracking," in *Proceedings of the Asian Conference on Computer Vision*, Kyoto, Japan, December 2020.

[7] D. Yuan, X. Chang, P. Y. Huang, Q. Liu, and Z. He, "Self-supervised deep correlation tracking," *IEEE Transactions on Image Processing*, vol. 30, pp. 976–985, 2021.

[8] Y. Yuechen, X. Yilei, H. Weilin, and R. S. Matthew, "Deformable siamese attention networks for visual object tracking," in *Proceedings of the Conference on Computer Vision and Pattern Recognition*, pp. 6728–6737, April 2020.

[9] L. Bertinetto, J. Valmadre, J. F. Henriques, A. Vedaldi, and P. H. Torr, "Fully-convolutional siamese networks for object tracking," in *Proceedings of the European Conference on Computer Vision*, pp. 850–865, Amsterdam, The Netherlands, October 2016.

[10] L. Bo, W. Wei, and W. Qiang, "Siamrpn++: evolution of siamese visual tracking with very deep networks," in *Proceedings of the Conference on Computer Vision and Pattern Recognition*, pp. 16–20, Long Beach, CA, USA, United State Of America, August 2019.

[11] L. Peixia, C. Boyu, and Y. Wanli, "Gradnet: gradient-guided network for visual object tracking," in *Proceedings of the International Conference on Computer Vision*, pp. 6162–6171, Seoul, Korea (South), September 2019.

[12] V. Jack, B. Luca, H. Joao, V. Andrea, and H. T. Philip, "Endto-end representation learning for correlation filter based tracking," in *Proceedings of the Conference on Computer Vision and Pattern Recognition*, pp. 2805–2813, Honolulu, HI, USA, united state of america, July 2017.

[13] Y. Xu, Z. Wang, Z. Li, Y. Yuan, and G. Yu, "Siamfc++: towards robust and accurate visual tracking with target estimation guidelines," *Proceedings of the AAAI Conference on Artificial Intelligence*, vol. 34, no. 07, pp. 12549–12556, 2020.

[14] Z. Zheng, W. Qiang, and L. Bo Li, "Distractor-aware Siamese networks for visual object tracking," in *Proceedings of the European Conference on Computer Vision*, pp. 101–117, ECCV), Munich, Germany, September 2018.

[15] L. Bo, Y. Junjie, W. Wei, Z. Zheng, and H. Xiaolin, "High performance visual tracking with Siamese region proposal network," in *Proceedings of the Conference on Computer Vision and Pattern Recognition*, pp. 8971–8980, Salt Lake City, UT, USA, United state of america, June 2018.

[16] C. Zedu, Z. Bineng, L. Guorong, Z. Shengping, and J. Rongrong, "Siamese box adaptive network for visual tracking," in *Proceedings of the Conference on Computer Vision and Pattern Recognition*, pp. 6668–6677, Seattle, WA, USA, March 2020.

[17] G. Dongyan, W. Jun, C. Ying, W. Zhenhua, and C. Shengyong, "Siamcar: siamese fully convolutional classification and regression for visual tracking," in *Proceedings of the Conference on Computer Vision and Pattern Recognition*, pp. 6269–6277, Seattle, WA, USA, June 2020.

[18] K. Yang, Z. He, W. Pei et al., "SiamCorners: siamese corner networks for visual tracking," *IEEE Transactions on Multimedia*, vol. 24, pp. 1956–1967, 2022.

[19] D. Yuan, W. Kang, and Z. He, "Robust visual tracking with correlation filters and metric learning," *Knowledge-Based Systems*, vol. 195, Article ID 105697, 2020.

[20] M. Danelljan, G. Hager, F. S. Khan, and M. Felsberg, "Learning spatially regularized correlation filters for visual tracking," in *Proceedings of the IEEE international conference on computer vision*, pp. 4310–4318, Santiago, Chile, December 2015.

[21] G. Bhat, M. Danelljan, L. V. Gool, and R. Timofte, "Learning discriminative model prediction for tracking," in *Proceedings of the International Conference on Computer Vision*, pp. 6182–6191, Seoul, Korea (South), October 2019.

[22] D. Yuan, X. Shu, N. Fan, X. Chang, Q. Liu, and Z. He, "Accurate bounding-box regression with distance-IoU loss for visual tracking," *Journal of Visual Communication and Image Representation*, vol. 83, Article ID 103428.

[23] G. Qing, F. Wei, and H. Rui, "Learning dynamic siamese network for visual object tracking," in *Proceedings of the International Conference on Computer Vision*, pp. 1763–1771, Venice, Italy, October 2017.

[24] Y. Bin, P. Houwen, F. Jianlong, W. Dong, and L. Huchuan, "Learning spatio-temporal transformer for visual tracking," in *Proceedings of the International Conference on Computer Vision*, pp. 10448–10457, March 2021.

[25] W. Sanghyun, P. Jongchan, L. Joon-Young, and I. S. Kweon, "Cbam: convolutional block attention module," in *Proceedings of the European Conference on Computer Vision*, pp. 3–19, Munich, Germany, October 2018.

[26] M. Danelljan, G. Bhat, F. S. Khan, and M. Felsberg, "Atom: accurate tracking by overlap maximization," in *Proceedings of the Conference on Computer Vision and Pattern Recognition*, pp. 4660–4669, Long Beach, CA, USA, June 2019.

[27] M. Kristan, A. Leonardis, and J. Matas, "The sixth visual object tracking vot2018 challenge results," in *Proceedings of the European Conference on Computer Vision*, no. 0–0, September 2018.

[28] W. Yi, L. Jongwoo, and Y. Ming-Hsuan, "Online object tracking: a benchmark," in *Proceedings of the Conference on Computer Vision and Pattern Recognition*, pp. 2411–2418, Portland, OR, USA, June 2013.

[29] M. Matthias, N. Smith, and B. Ghanem, "A benchmark and simulator for uav tracking," in *Proceedings of the European Conference on Computer Vision*, pp. 445–461, Amsterdam, Netherlands, September 2016.

[30] H. K. Galoogahi, A. Fagg, C. Huang, D. Ramanan, and S. Lucey, "Need for speed: a benchmark for higher frame rate object tracking," in *Proceedings of the International Conference on Computer Vision*, pp. 1125–1134, Venice, Itly, October 2017.

[31] F. Heng, L. Liting, Y. Fan, C. Peng, D. Ge, and B. Hexin, "Lasot: a high-quality benchmark for large-scale single object tracking," in *Proceedings of the Conference on Computer Vision and Pattern Recognition*, pp. 5374–5383, March 2019.

[32] M. Danelljan, G. Bhat, F. S. Khan, and M. Felsberg, "Eco: efficient convolution operators for tracking," in *Proceedings of the Conference on Computer Vision and Pattern Recognition*, pp. 6638–6646, Honolulu, HI, USA, July 2017.

[33] L. Bertinetto, J. Valmadre, S. Golodetz, O. Miksik, and P. H. S. Torr, "Staple: complementary learners for real-time tracking," in *Proceedings of the IEEE Conference on Computer Vision and Pattern Recognition*, pp. 1401–1409, Las Vegas, NV, USA, June 2016.

[34] G. Bhat, J. Johnander, M. Danelljan, F. S. Khan, and M. Felsberg, "Unveiling the power of deep tracking," in *Proceedings of the European Conference on Computer Vision*, pp. 483–498, Munich, Germany, September 2018.

[35] S. Chong, W. Dong, L. Huchuan, and Y. Ming-Hsuan, "Correlation Tracking via Joint Discrimination and Reliability Learning," Conference on Computer Vision and Pattern Recognition," in *Proceeding of the 2018 IEEE/CVF Conference on Computer Vision and Pattern Recognition*, pp. 489–497, Salt Lake City, UT, USA, United state of america, June 2018.

Hindawi
Mobile Information Systems
Volume 2022, Article ID 4650250, 10 pages
https://doi.org/10.1155/2022/4650250

Research Article

The College English Teacher Behavior and Teaching Effect Based on Big Data Technology

Jiang Ling,[1] Liu Jianhua,[2] Wang Haijie,[3] and Zhang Li[3]

[1]*College of Foreign Studies, Hubei Normal University, Huangshi, Hubei 435000, China*
[2]*School of Humanities and Law, Hebei University of Engineering, Handan, Hebei 056038, China*
[3]*Western Languages Department, Hebei Institute of International Business and Economics, Hebei, Qinhuangdao 066311, China*

Correspondence should be addressed to Wang Haijie; yaigek@163.com

Received 17 May 2022; Revised 11 July 2022; Accepted 23 August 2022; Published 17 September 2022

Academic Editor: Chi Lin

In order to explore the correlation between college English teacher behavior and teaching effects, this paper applies data mining technology to related research. Moreover, this paper uses Bloom Filter to represent the efficiency of insert queries and space usage of dynamic data sets and designs a multichannel balanced matrix Bloom Filter. In addition, this paper uses the longest prefix matching filling algorithm when selecting the element insertion position in multiple candidate Bloom Filters, and uses this algorithm to process the college teacher behavior and teaching effect data. Finally, this paper combines investigation and experiment to conduct research. Through the investigation, it can be seen that the teaching behavior of college English teachers will have a certain impact on students, and the positive behavior of teachers can effectively improve the teaching effect, which can be used as a reference for the formulation of subsequent teaching plans.

1. Introduction

With the continuous deepening of the reform of the new curriculum standard, the reform of China's college English curriculum education and teaching has become more and more important. The new educational philosophy requires "health as the core." As one of the school's basic education courses, the English and health curriculum focuses on the multidirectional development of students' English ability. Through the comprehensive teaching of sports knowledge and skills, the realization of the various goals of English and health courses can help students better master English skills and improve English learning, which can further promote the deepening reform of college English education and teaching. Under a new type of talent training model aimed at improving students' ideological and moral character, scientific and cultural knowledge, and comprehensive development of physical and mental health, the new curriculum standard puts forward higher and higher requirements and goals for the personal comprehensive ability of English teachers [1]. English teachers are the implementers of English curriculum standards, as well as the guides of classroom teaching, and their comprehensive ability level is mainly manifested through the teachers' own leadership behavior [2]. Teacher leadership behavior is a research branch of behavioral science and has a certain behavior pattern. Moreover, it is an external behavior manifested in the psychological process of teachers' physical and mental quality, and a meaningful leadership activity that governs the internal spiritual motivation of teachers [3].

In the implementation of the new curriculum, teaching behavior research has become one of the effective methods of classroom teaching research, and it has received widespread attention and application in the education field. The development of teacher professionalization has become the trend of international teacher education reform, and it has been valued by many countries. It is also a subject of great theoretical significance put forward by the current education reform practice. Compared with other industries, the turnover rate of teachers in this industry is relatively low. Many teachers have been engaged in education for life, serving as teachers for 30–40 years, which is relatively rare in

other industries. In the case of a long-term education environment, teachers need to constantly adjust their educational concepts and values, enrich professional knowledge and professional skills, and meet their own needs at different levels, so as to show teacher role behaviors that are table for a specific stage of professional development.

Previous studies have suggested that teachers' teaching concepts will affect teaching behavior, but there has been no thorough and detailed research on how to influence them. This research explores the relationship between the concepts of teaching, teacher, student, and learning concepts and behaviors in teaching design, teaching environment, classroom teaching, and teaching reflection by refining teaching concepts and behaviors, and derives different concepts The degree of influence on different aspects of teaching behavior is different, so as to provide theoretical support for the update of teaching concepts and the transformation to teaching behaviors, enrich and improve the research on the relationship between teaching concepts and teaching behaviors, and enrich the relevant theoretical basis for teachers' professional growth. The renewal of teachers' teaching concepts and the transformation of teaching behaviors are part of the research content in the field of teacher professional growth. The ultimate goal of the renewal of teachers' teaching concepts and efficient transformation of teaching behaviors is to help teachers' professional growth. Therefore, this research on the status quo and the relationship between teaching concepts and teaching behaviors can enrich the connotation of teachers' professional growth and supplement the theoretical foundation of teachers' professional growth.

This article combines big data technology to study the behavior and teaching effect of college English teachers, conducts research based on actual cases, and builds an intelligent model through big data technology to provide theoretical references for subsequent teaching reform research.

2. Related Work

Regarding the relationship between teaching philosophy and behavior, early foreign scholars also agreed that teaching philosophy and teaching behavior are consistent. The literature [4] proposed that teachers' ideas determine their teaching behavior to students. The literature [5] pointed out that the ideas held by teachers profoundly affect their behaviors, and based on their ideas, we can more accurately predict the behaviors they will take. Literature [6] believes through research that "concepts are the tendency of action and the decision of behavior," and concepts guide behavior. Concepts are the internal basis of behaviors, behaviors are the external manifestations of concepts, and teachers' teaching concepts strongly influence their teaching behaviors. However, with the deepening of research, many scholars have proposed that the relationship between teacher's teaching philosophy and teaching behavior is not a simple one-to-the-other relationship. The two are related to each other and influence each other. There are both consistency and difference. The literature [7] used a self-compiled questionnaire to investigate the low-level teachers in elementary school, and tried to explore the relationship between their ideas and behaviors. Its research shows that teachers with developmental awareness and new teaching concepts tend to be student-centered, and tend to have a free and open teaching concept. However, teachers, who do not have developmental awareness and stick to the old teaching concepts, are mostly self-centered, and their teaching concepts also remain conservative and closed.

The literature [8] found that the influence of teacher's concept and teaching behavior is interactive: teacher's concept affects their teaching behavior, and the teacher's day-to-day teaching behavior affects the change of teacher's teaching concept to a certain extent. Literature [9] used questionnaires, interviews, and video analysis to study the teaching concepts and teaching behaviors of inquiry teaching on 8 new science teachers who had received inquiry teaching training. It was found that even if new teachers believed in student-centered teaching concepts, they could not be implemented in practice, there was a gap between the concepts and behaviors of new teachers. These studies have revealed the complexity of the relationship between teachers' individual teaching concepts and teaching behaviors.

Literature [10] developed a "checklist for important factors of teacher's character" after a lot of research, which provides specific tools for frontline teachers to improve their teaching behavior. Literature [11] believed that teachers should have the same professional knowledge as doctors and lawyers, and first proposed the concept of pedagogical content knowledge (PCK), which is an important condition for teachers to practice teaching.

The interaction between teachers and students is a necessary condition for teaching and learning. Scholars have studied the interaction between teachers and students from different angles, and the research focuses on the impact of the interaction between teachers and students on student behavior. Literature [12] studied the influence of different leadership styles on personal behavior and obtained the relationship between authoritative, leadership, and laissez-faire teacher leadership styles and student behavior. Literature [13] started from the perspective of the status of teachers, students, and knowledge, and studied the behavior of teachers in the classroom. They divide teacher-student interaction into three ways: teacher-centered, student-centered, and knowledge-centered. The central teacher-student relationship is a relationship of control and obedience, the student-centered teacher-student relationship is a dual subject, and the knowledge-centered teacher-student relationship is a partnership with a common goal.

3. Teaching Data Mining Algorithm

The basic principle of Bloom Filter is to represent the element set $S = \{x_1, x_2, \cdots, x_n\}$ through a bit vector of length m. Among them, the set S contains n elements, and the initial state of each bit in the vector is 0. For each element in the set, k hash functions are used to map it to the vector, and the corresponding position of the hash value is set to 1, and the other bits remain O unchanged. When we are asked to query

whether an element belongs to a certain set, we use k hash functions to calculate the element and check whether the corresponding position of each hash value in the vector is 1. As long as the position of a certain hash value in the vector is 0, then it can be determined that the element does not belong to the set, otherwise the element is considered to belong to the set with a certain misjudgment rate. The algorithm structure of Bloom Filter is shown in Figure 1, [14].

Then, the probability that the positions of the k hash function mappings of the element are all 0 is given as follows:

$$\left(1-\frac{1}{m}\right)^{k}. \tag{1}$$

The probability that the positions of k hash function mappings of n elements in the set are all 0 is given as follows:

$$\left(1-\frac{1}{m}\right)^{kn}. \tag{2}$$

Then the probability that a certain hash function of an element is mapped to 1 is given as follows:

$$1-\left(1-\frac{1}{m}\right)^{kn}. \tag{3}$$

Due to its simplicity and efficiency, Bloom Filter has recently received widespread attention in the network and storage fields. When using Bloom Filter, performance parameters such as misjudgment rate, memory size, and the number of sets to be managed are mainly considered [15].

Therefore, the false positive rate of Bloom Filter is given as follows:

$$p=\left(1-\left(1-\frac{1}{m}\right)^{kn}\right)^{k}\approx\left(1-e^{(kn/m)}\right)^{k}. \tag{4}$$

Although Bloom Filter is an efficient retrieval data structure, it still cannot solve problems such as the dynamic growth and change of collection elements. With the increase of elements in the set, the false positive rate of a single Bloom Filter will increase, which will eventually lead to the failure of the Bloom Filter. In recent years, some substantial improvements have been made to the Bloom Filter for the problem of dynamic collections, resulting in the split Bloom Filter algorithm and the dynamic Bloom Filter algorithm as well as improved algorithms based on these two algorithms.

The basic idea of split the Bloom Filter is to use r bit vectors to represent the data set. When the number of elements in the set increases to a certain extent and affects the initial design of the misjudgment rate index, a $r\times m$ two-dimensional bit vector is regenerated. If the added element does not reach the preset maximum number of sets, a bit vector is randomly selected to represent the element. If the mapped hash function is evenly distributed, the number of elements that can be inserted by each Bloom Filter in the split Bloom Filter is the same. That is, the number of elements that each Bloom Filter can hold is n/r. The structure of the split Bloom Filter is shown in Figure 2.

For split Bloom Filter, the probability that one of the Bloom Filters will be misjudged is given as follows [16]:

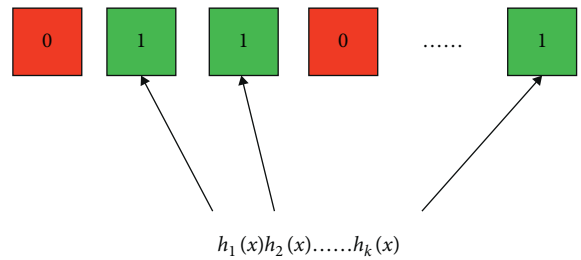

Figure 1: Bloom filter algorithm structure.

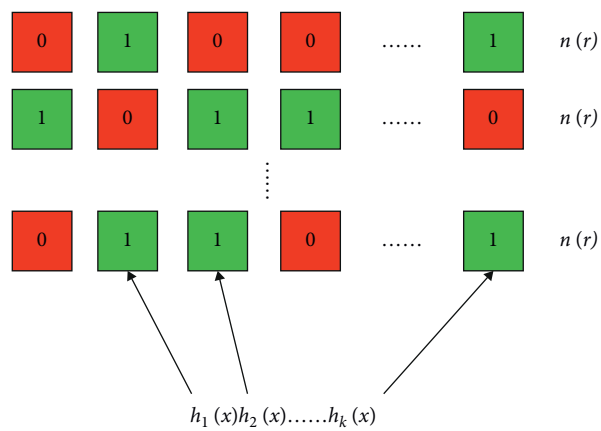

Figure 2: Split bloom filter algorithm structure.

$$p'_{BF}=\left(1-\left(1-\frac{1}{m}\right)^{kn}\right)^{k}\approx\left(1-e^{(kn/m)}\right)^{k}. \tag{5}$$

Then, the probability that Bloom Filter does not make a misjudgment is given as follows:

$$p_{BF}=1-\left(1-\left(1-\frac{1}{m}\right)^{kn}\right)^{k}\approx 1-\left(1-e^{(kn/m)}\right)^{k}. \tag{6}$$

The probability that r Bloom Filters does not make a misjudgment is given as follows:

$$p'_{SBF}=1-\left(1-\left(1-\frac{1}{m}\right)^{kn}\right)^{k}\approx 1-\left(1-e^{(kn/m)}\right)^{k}. \tag{7}$$

Then, the probability that split Bloom Filter makes a misjudgment is given as follows:

$$p'_{SBF}=1-\left(1-\left(1-\left(1-\frac{1}{m}\right)^{kn}\right)^{k}\right)^{r}\approx 1-\left(1-\left(1-e^{(kn/m)}\right)^{k}\right)^{r}. \tag{8}$$

Dynamic Bloom Filter dynamically increases Bloom Filter according to the growth of elements. The number of elements that the predesigned Bloom Filter can store is n, the number of initialized Bloom Filters is 1, and the current Bloom Filter that can be inserted is the active Bloom Filter. When we need to insert an element, we first query whether the element exists in the collection. If it does not exist, we

determine whether the currently active Bloom Filter is full. If it is not full, it will be inserted into the currently active Bloom Filter. If it is full, it will dynamically grow a Bloom Filter and insert the element. It should be noted that only the last Bloom Filter of the dynamic Bloom Filter is the currently active Bloom Filter, and the $r-1$ Bloom Filters on it are the inactive Bloom Filters, which only allow query operations and cannot insert elements. The structure of the dynamic Bloom Filter is shown in Figure 3. It can be seen from the structure diagram of the dynamic Bloom Filter that when the mapping hash function distribution is sufficiently uniform, the number of elements that can be accommodated by the previous $r-1$ inactive Bloom Filters is the same, which are all n, as long as the elements stored in the currently active Bloom Filter are less than n_0.

When the dynamic Bloom Filter looks for an inactive Bloom Filter, the probability of no misjudgment is given as follows:

$$p_{r-1} = \left(1-\left(1-\left(1-\frac{1}{m}\right)^{kn_0}\right)^k\right)^{r-1} \approx \left(1-\left(1-e^{(kn_0/m)}\right)^k\right)^{r-1}. \quad (9)$$

When searching for the currently active Bloom Filter, the probability of no misjudgment is given as follows:

$$p_{r-1} = 1-\left(1-\left(1-\frac{1}{m}\right)^{kn_0}\right)^k \approx 1-\left(1-e^{(kn_0/m)}\right)^k. \quad (10)$$

The probability of no misjudgment of the entire dynamic Bloom Filter is given as follows:

$$p'_{DBF} = \left(1-\left(1-e^{(kn_0/m)}\right)^k\right)^{r-1}\left(1-\left(1-e^{(k(n-n_0)(r-1)/m)}\right)^k\right). \quad (11)$$

Then, the probability of misjudgment of dynamic Bloom Filter is given as follows:

$$p_{DBF} = 1-\left(1-\left(1-e^{(kn_0/m)}\right)^k\right)^{r-1}\left(1-\left(1-e^{(k(n-n_0)(r-1)/m)}\right)^k\right). \quad (12)$$

Although splitting Bloom Filter and dynamic Bloom Filter solves the problem of dynamic growth of elements, they do not effectively solve the problem of space utilization of a single Bloom Filter. At the same time, these algorithms have brought new problems. In terms of element query performance, they run counter to the constant time complexity of Bloom Filter. The time complexity of the standard Bloom Filter is $O(k)$. However, split Bloom Filter and dynamic Bloom Filter need to search for each Bloom Filter sequentially when inserting and querying data, so its time complexity is related to the number of Bloom Filters, namely, $O(kr)$, where r is the number of Bloom Filters. When the number of Bloom Filters is large, the query performance is poor. Matrix Bloom Filter is improved based on the query performance of split Bloom Filter. It quickly locates a Bloom Filter through a special hash function, and searches or inserts elements in this Bloom Filter. This algorithm no longer uses the inserted element count as the full condition of the Bloom Filter, but introduces the concept of saturation, and uses the saturation as the full condition of the Bloom Filter. In addition, it dynamically grows the Bloom Filter by means of a vector group, and selects the Bloom Filter that uses the least space in the vector group as the element insertion position to achieve the effect of inserting more elements. Although 2BDBF can represent more elements, its query performance has not been improved [17].

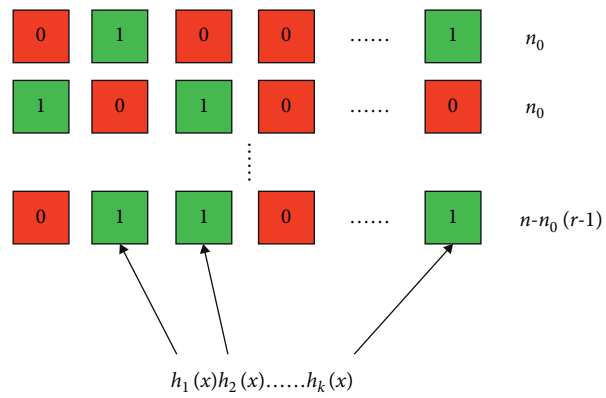

Figure 3: Dynamic bloom filter algorithm structure.

The false positive rate of the Bloom Filter is $p = (1-(1-1/m)^{kn})^k \approx (1-e^{kn/m})^k$, where m is the bit length of Bloom Filter, n is the number of inserted elements, and k is the number of hash functions.

Theorem 1. *The false positive rate function of the Bloom Filter is a monotonically increasing function.*

Proof. Under the premise that the number of hash functions k and the vector length m of Bloom Filter are determined, in order to find the minimum misjudgment rate of Bloom Filter, p is derived from n:

$$\frac{dp}{dn} = k\left(1-e^{(kn/m)}\right)^k \cdot \left(-e^{(kn/m)}\right) \cdot \left(-\frac{m}{n}\right). \quad (13)$$

Since the exponential function e^x increases monotonically at $x \geq 0$, and $kn/m > 0$, so $e^{kn/m} > e^0 = 1$and $0 < e^{kn/m} < 1$. At this point, we can get $1-e^{kn/m} > 0$. Since $k > 0$, $\mathrm{d}p/\mathrm{d}n > 0$. From the abovementioned derivation, it can be concluded that the false positive rate of Bloom Filter is a monotonically increasing function. Therefore, when $\mathrm{d}p/\mathrm{d}n = 0$, the misjudgment rate is the smallest.

The false positive rate is kept to a minimum, and the Bloom Filter bit space usage rate when the number of inserted elements reaches the maximum is 50% [18]. □

Proof. According to Theorem 1, when the misjudgment rate is the smallest, the maximum number n of set elements that can be represented in the vector satisfies $n = \mathrm{In}2$. If it is assumed that the hash function obeys a uniform distribution, when inserting an element, the probability that a certain hash function of Bloom Filter maps to a certain bit is 1. Then, when n elements are inserted, the probability of any bit being 0 is given as follows:

$$p' = \left(-\frac{1}{m}\right)^{kn}. \tag{14}$$

When formula $n = k/\mathrm{m} \ln 2$ is inserted into formula (14), we can get

$$p' = \left(1 - \frac{1}{m}\right)^{k+(m/k)+\ln 2} \approx e^{-(1/m)+m\ln 2} = \frac{1}{2}. \tag{15}$$

It can be seen that the probability that any bit in the Bloom Filter is O is, at this time, it can be considered that the number of bits 1 accounts for 50% of the total length of the vector. That is, when the maximum number of inserted elements is reached, the bit space usage rate of the Bloom Filter is 50%.

As mentioned above, the work of this paper mainly uses Bloom Filter to express the efficiency of insert queries and space usage of dynamic data sets. This text has designed a kind of multichannel balanced matrix Bloom Filter (M-BMBF), its algorithm design structure is shown in Figure 4.

In order to solve the problem of the efficiency of inserting and querying dynamic data sets, M-BMBF introduces multiple positioning hash function concepts. The basic design idea of M-BMBF is to express the dynamic set as a bit matrix of $r \times m$. The behavior r of the matrix indicates that there are r Bloom Filters, and the column of the matrix is m, which indicates that the vector length of each Bloom Filter is m bits. Here, the line r is a constant, which must be predetermined according to the maximum estimate of the size of the collection. In order to improve the search performance of elements, this paper designs s location hash functions h0,. . ., hs − 1. These s hash functions are specially defined and different from other k-independent hash functions. In order to reduce the probability of collision of s hash functions, r Bloom Filters are divided into s groups, where each group has r/s Bloom Filters, and each positioning hash function maps a set of Bloom Filters. Before adding an element, you need to determine which Bloom Filter the element should be added to. At this time, we can use these s hash functions to perform positioning calculations, and select the Bloom Filter corresponding to the element in each group as the candidate insertion position [19].

We can convert the maximum number of inserted elements of the Bloom Filter under the lowest misjudgment rate into its bit space usage. Based on this, we use the longest prefix matching filling algorithm to improve the space utilization efficiency of Bloom Filter. The main design idea of the longest prefix matching filling algorithm is to map the hash function value of the element to the position of 1 in the Bloom Filter vector as much as possible when inserting the element. Then, it is possible to insert more elements than n, while keeping p unchanged.

Specifically, when inserting, we use é hash functions to calculate the k hash function values of the element x, and compare them with the corresponding address positions of the candidate Bloom Filter. If it is found that the addresses of the k hash functions corresponding to one of the Bloom Filters are all 1, it is considered that the element already exists and does not need to be inserted. Otherwise, the

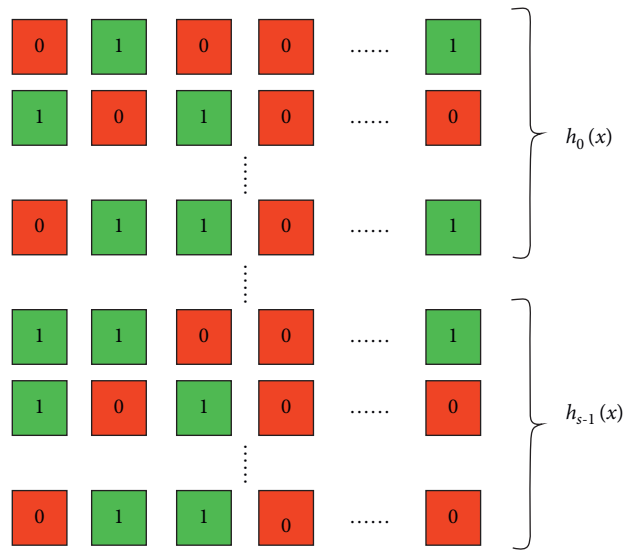

Figure 4: M-BMBF algorithm structure.

position with the corresponding address value of 1 in the s candidate Bloom Filters that overlaps the k hash addresses of x the most is selected as the insertion position. In M-BMBF, the hash range of each location hash function is $\{0, 1, 2, ...r/s\}$, and the range of other k hash functions is $\{0, 1, ..., m-1\}$. Therefore, before the construction of M-BMBF, the number of hash functions is not the number of days actually used in the algorithm. In fact, $k+s$ hash functions will be used. When we assume that the location hash function is perfectly random, the number of elements that can be contained in each group should be the same, which is n/r. □

3.1. Time Complexity. When we want to query whether an element belongs to a certain set, split Bloom Filter and 2BDBF are to query each Bloom Filter in order until it is found. The query time for each Bloom Filter is $O(k)$, where k is the number of hash functions, then the worst-case average query time for splitting Bloom Filter and 2BDBF is $O(kr)$. Its time complexity is $O(s)$. Then, this paper performs the mapping of k hash functions in these s Bloom Filters, and the time complexity is $O(k)$. Therefore, the total query time complexity of the algorithm in this paper is $O(ks)$. Since s is generally much smaller than r, the algorithm constructed in this paper can effectively solve the problem of query efficiency [20].

3.2. Analysis of Misjudgment Rate. As far as Bloom Filter is concerned, when querying an element, if the element does not belong to a dynamic collection but returns true during the query process, a misjudgment will occur. From the analysis of the misjudgment rate of split Bloom Filter, it can be seen that the misjudgment rate of split Bloom Filter is given as follows:

$$F = 1 - \left(1 - \left(1 - e^{(kn/m)}\right)^k\right)^r. \quad (16)$$

For the algorithm proposed in this paper, when $0 \le d \le s - 1$, if we assume that the probability of misjudgment of the Bloom Filter corresponding to the d-th location hash function is f_d, then the probability of no misjudgment in all location rows of the algorithm is $(1 - f_d)$. Therefore, the probability of misjudgment of at least one Bloom Filter is $1 - (1 - f_d)$. The misjudgment rate of M-BMBF can be obtained as follows:

$$F_{M-\mathrm{BMBF}} = 1 - \left(1 - \left(1 - e^{(kn/mr)}\right)^k\right)^s. \quad (17)$$

Compared with the split Bloom Filter, the misjudgment rate of M-BMBF is related to the number of positioning hash functions s. In the case of the same inserted elements, because of $s \le r$, $F_{M-\mathrm{BMBF}} \le F$.

3.3. Space Performance. Bloom Filter itself is a data structure with efficient spatial performance. It uses bit arrays to express a collection very concisely. Compared with other data structures related to data sizes, such as B-trees and hash tables, the storage space is very small, so it can be resident in memory. This paper uses the longest prefix matching filling algorithm when selecting the element insertion position in multiple candidate Bloom Filters. Before the bit space usage rate of Bloom Filter reaches 50%, more elements can be inserted to save the storage space of Bloom Filter. At the same time, from the analysis of formulas (16) and (17), it can be seen that when the variable parameters m, k and r are the same, if the misjudgment rate is also controlled to be equal, because of $s \le r$, M-BMBF inserts more elements than split Bloom Filter, which can save space.

4. Research on College English Teacher Behavior and Teaching Effect Based on Big Data Technology

Teacher's teaching behavior refers to all the activities and performance of teachers in order to complete teaching tasks, achieve teaching goals, and promote students' learning in classroom teaching. This behavior includes both implicit reactions (such as feelings and emotions) and explicit reactions, but both can be observed and recorded, and both can be perceived and understood by students. Students learn mainly under the guidance of teachers' teaching behavior, which is a direct influence factor on teaching quality.

The research objects are mainly English teachers in ordinary colleges and universities. The data of this research are representative.

This study made two predictions before the formal investigation. The first prediction was carried out in March 2020. This article mainly uses random sampling methods to consciously collect and summarize the relevant questions reflected by the participants in the process of answering the questionnaire. After the investigation, the data obtained will be entered and analyzed using SPSS 21.0 for Windows. After that, the

Table 1: Evaluation results of college English teacher's observation behavior.

Number	Scores
1	69.28
2	74.33
3	72.74
4	78.44
5	77.48
6	86.58
7	73.80
8	83.01
9	80.80
10	76.13
11	69.37
12	69.61
13	80.09
14	83.31
15	77.12
16	72.63
17	79.88
18	74.45
19	83.76
20	84.01
21	73.90
22	85.90
23	71.72
24	70.16
25	81.51
26	86.95
27	86.09
28	74.19
29	69.32
30	81.16
31	73.94
32	84.55
33	77.79
34	83.25
35	72.54
36	69.51
37	70.70
38	70.67
39	78.50
40	76.47
41	77.08
42	82.39
43	75.62
44	80.34
45	74.10
46	69.37
47	70.06
48	69.53
49	77.82
50	83.37
51	78.81
52	79.40
53	85.15
54	87.72
55	84.33
56	70.47
57	76.57
58	69.84
59	71.02
60	83.50

Table 2: Evaluation results of time control behavior of college English teacher.

Number	Scores
1	50.93
2	60.78
3	51.34
4	53.25
5	55.17
6	56.05
7	51.87
8	56.40
9	57.72
10	54.75
11	52.40
12	56.91
13	50.78
14	55.83
15	50.13
16	54.64
17	52.41
18	51.74
19	56.55
20	60.75
21	55.62
22	50.55
23	56.87
24	51.44
25	50.50
26	57.29
27	60.44
28	60.15
29	56.20
30	56.21
31	50.39
32	53.89
33	51.77
34	54.92
35	60.16
36	49.16
37	54.71
38	53.35
39	57.49
40	56.22
41	49.59
42	52.41
43	50.15
44	54.26
45	53.86
46	54.20
47	51.74
48	52.95
49	57.93
50	54.82
51	57.72
52	54.71
53	57.58
54	59.49
55	50.16
56	58.52
57	50.76
58	54.07
59	51.75
60	55.41

Table 3: Evaluation results of college entertainment behavior of English teacher.

Number	Scores
1	69.61
2	73.08
3	72.19
4	64.31
5	69.59
6	83.59
7	77.07
8	74.50
9	78.19
10	71.22
11	67.24
12	69.68
13	65.66
14	68.42
15	64.85
16	72.89
17	79.48
18	66.56
19	73.06
20	64.81
21	72.71
22	71.39
23	65.46
24	67.63
25	71.55
26	82.32
27	65.16
28	72.89
29	64.19
30	77.28
31	69.54
32	73.72
33	78.62
34	83.99
35	78.66
36	68.89
37	72.47
38	77.35
39	73.98
40	82.91
41	76.13
42	76.30
43	70.18
44	67.97
45	69.72
46	71.63
47	77.23
48	72.94
49	68.52
50	80.80
51	66.85
52	64.70
53	64.52
54	64.55
55	82.26
56	70.32
57	67.95
58	77.15
59	80.56
60	76.33

Table 4: Evaluation results of teaching summary behavior of college English teacher.

Number	Scores
1	72.98
2	70.58
3	78.06
4	76.24
5	67.78
6	70.25
7	77.39
8	69.41
9	67.66
10	78.51
11	79.99
12	69.35
13	73.54
14	77.59
15	76.49
16	72.83
17	68.43
18	67.82
19	71.00
20	73.35
21	79.01
22	77.73
23	67.63
24	79.82
25	79.13
26	76.72
27	71.66
28	73.63
29	72.30
30	76.34
31	71.56
32	74.23
33	67.46
34	76.31
35	67.43
36	73.18
37	67.12
38	77.03
39	79.72
40	71.52
41	72.91
42	71.84
43	79.37
44	75.80
45	76.37
46	68.72
47	73.87
48	73.92
49	72.26
50	72.87
51	75.55
52	70.54
53	77.34
54	74.45
55	67.65
56	72.93
57	71.96
58	79.82
59	71.04
60	68.80

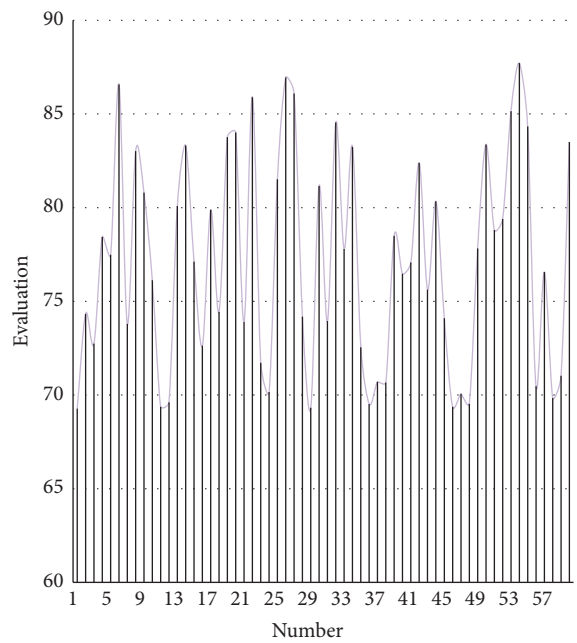

Figure 5: Statistical diagram of the correlation between college observation behavior of English teacher and teaching effect.

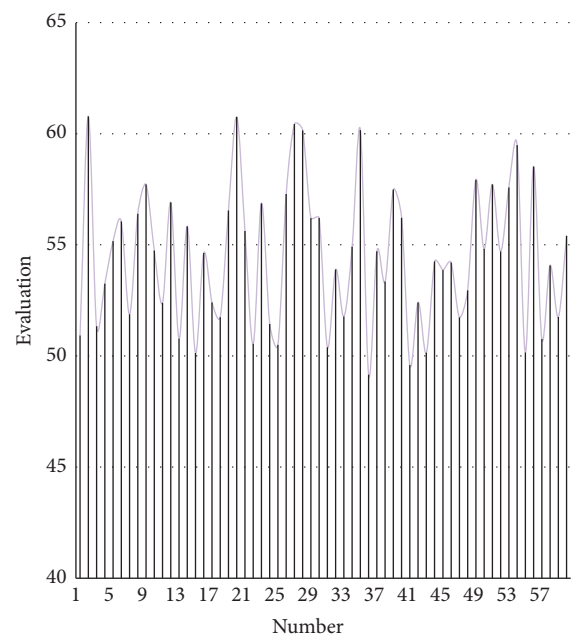

Figure 6: Statistical diagram of the correlation between time control behavior of college English teacher and teaching effect.

research team summarizes the problems that the subjects reported during the survey process, such as an excessive number of questions, duplication of some items, or lack of utility. Moreover, this paper invites expert teachers with many years of rich educational research experience to provide guidance to discuss the necessity of the questions in the survey and the rest of the questionnaire, and the rationality of the textual expression. After many meetings and discussions, this paper combines the results of data analysis to finally, delete some items and streamline the questionnaire.

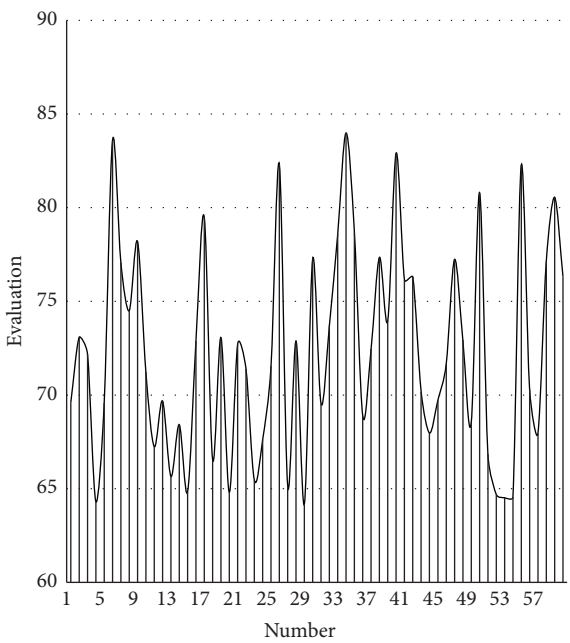

Figure 7: Statistical diagram of the correlation between entertainment behavior of college English teacher and teaching effect.

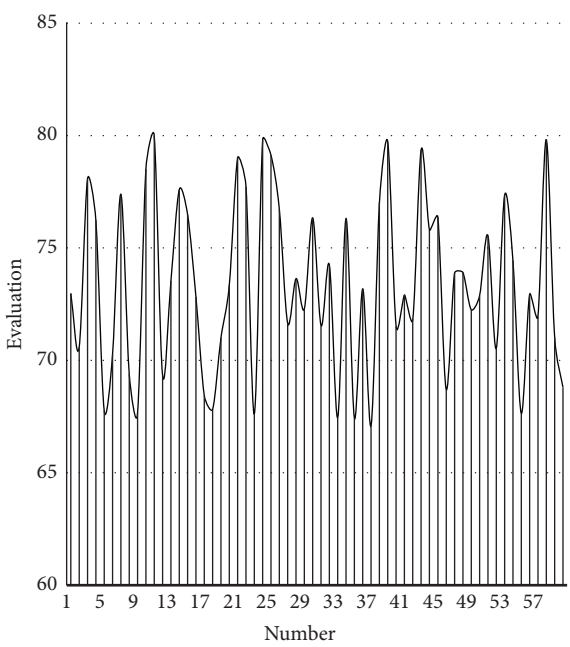

Figure 8: Statistical diagram of the correlation between teaching summary behavior of college English teacher and teaching effect.

The second prediction was conducted in June 2021. A total of 60 English teachers in colleges and universities are surveyed, 0 questionnaires are distributed, 60 questionnaires are returned, and the recovery rate is 100%.

This experiment mainly counts teachers' classroom behavior and teaching effect. Because there are many teacher behaviors, this paper analyzes the correlation between teacher observation behavior, time control behavior, entertainment teaching behavior, summary behavior, and teaching effect. Moreover, this paper combines big data technology to carry out data processing, and counts the test results, as shown in Table 1–Table 4 and Figure 5–Figure 8.

From the abovementioned research, it can be seen that the teaching behavior of college English teachers will have a certain impact on students, and the positive behavior of teachers can effectively improve the teaching effect, which can be used as a reference for the formulation of subsequent teaching plans.

5. Conclusion

Teachers are the implementers and organizers of courses, and teaching activities are the main manifestations of courses. Since the launch of the new round of basic education curriculum reform, the concept, structure, content, implementation, evaluation, and management of the curriculum have made major breakthroughs and innovations compared to the past. Teachers' educational philosophy and whether they can understand the new curriculum, student, teaching, and evaluation perspectives will directly affect the implementation of the new curriculum and the effectiveness of this round of curriculum reform, and these will be reflected in the teaching behavior of teachers The leadership behavior of English teachers involved in this paper refers to the various behaviors and activities shown in the process of influencing students through their physical or mental activities in the English curriculum teaching of the school, so as to achieve a certain teaching goal.

The main purpose of this research is to explore the relationship between college English teachers' teaching behavior and teaching effect. This article mainly uses the method of questionnaire survey and combines big data technology to carry on the data processing.

Data Availability

The data used to support the findings of this study are included within the article.

Conflicts of Interest

The authors declare that they have no conflicts of interest.

References

[1] X. Li, "The construction of intelligent English teaching model based on artificial intelligence," *International Journal of Emerging Technologies in Learning (iJET)*, vol. 12, no. 12, pp. 35–44, 2017.

[2] S. Zou, "Designing and practice of a college English teaching platform based on artificial intelligence," *Journal of Computational and Theoretical Nanoscience*, vol. 14, no. 1, pp. 104–108, 2017.

[3] F. Kong, "Application of artificial intelligence in modern art teaching," *International Journal of Emerging Technologies in Learning (iJET)*, vol. 15, no. 13, pp. 238–251, 2020.

[4] M. Pantic, R. Zwitserloot, and R. J. Grootjans, "Teaching introductory artificial intelligence using a simple agent framework," *IEEE Transactions on Education*, vol. 48, no. 3, pp. 382–390, 2005.

[5] C. Yang, S. Huan, and Y. Yang, "A practical teaching mode for colleges supported by artificial intelligence," *International Journal of Emerging Technologies in Learning (IJET)*, vol. 15, no. 17, pp. 195–206, 2020.

[6] K. Kim and Y. Park, "A development and application of the teaching and learning model of artificial intelligence education for elementary students," *Journal of The Korean Association of Information Education*, vol. 21, no. 1, pp. 137–147, 2017.

[7] O. Zawacki-Richter, V. I. Marín, M. Bond, and F. Gouverneur, "Systematic review of research on artificial intelligence applications in higher education–where are the educators?" *International Journal of Educational Technology in Higher Education*, vol. 16, no. 1, pp. 39–27, 2019.

[8] S. C. H. Yang, W. K. Vong, R. B. Sojitra, T. Folke, and P. Shafto, "Mitigating belief projection in explainable artificial intelligence via Bayesian teaching," *Scientific Reports*, vol. 11, no. 1, pp. 9863–9917, 2021.

[9] Y. Lee, "An analysis of the influence of block-type programming language-based artificial intelligence education on the learner's attitude in artificial intelligence," *Journal of The Korean Association of Information Education*, vol. 23, no. 2, pp. 189–196, 2019.

[10] J. M. Alonso, "Teaching explainable artificial intelligence to high school students," *International Journal of Computational Intelligence Systems*, vol. 13, no. 1, pp. 974–987, 2020.

[11] R. Yang, "Artificial intelligence-based strategies for improving the teaching effect of art major courses in colleges," *International Journal of Emerging Technologies in Learning (iJET)*, vol. 15, no. 22, pp. 146–160, 2020.

[12] P. Ribeiro, H. Simões, and M. Ferreira, "Teaching artificial intelligence and logic programming in a competitive environment," *Informatics in Education*, vol. 8, no. 1, pp. 85–100, 2009.

[13] V. Rampton, M. Mittelman, and J. Goldhahn, "Implications of artificial intelligence for medical education," *The Lancet Digital Health*, vol. 2, no. 3, pp. e111–e112, 2020.

[14] Q. Zhou, "Reforms in teaching the course of introduction to artificial intelligence," *Solid State Technology*, vol. 64, no. 2, pp. 6331–6335, 2021.

[15] K. I. M. Haejoong and L. E. E. Sangmin, "Do less teaching, do more coaching: toward critical thinking for ethical applications of artificial intelligence," *Journal of Learning and Teaching in Digital Age*, vol. 6, no. 2, pp. 97–100, 2021.

[16] P. H. Lin, A. Wooders, J. T. Y. Wang, and W. M. Yuan, "Artificial intelligence, the missing piece of online education?" *IEEE Engineering Management Review*, vol. 46, no. 3, pp. 25–28, 2018.

[17] C. Guan, J. Mou, and Z. Jiang, "Artificial intelligence innovation in education: a twenty-year data-driven historical analysis," *International Journal of Innovation Studies*, vol. 4, no. 4, pp. 134–147, 2020.

[18] D. Ni, "The application of artificial intelligence technology in international Chinese language teaching," *Chinese Journal of Social Science and Management*, vol. 5, no. 1, pp. 101–112, 2021.

[19] R. Dilmurod and A. Fazliddin, "Prospects for the introduction of artificial intelligence technologies in higher education," *Academicia: An International Multidisciplinary Research Journal*, vol. 11, no. 2, pp. 929–934, 2021.

[20] S. Huang, "Analysis of psychological teaching assisted by artificial intelligence in sports training courses," *Journal of Applied Science and Engineering*, vol. 24, no. 5, pp. 743–748, 2021.

Hindawi
Mobile Information Systems
Volume 2022, Article ID 2970335, 13 pages
https://doi.org/10.1155/2022/2970335

Research Article

Excessive Defense of Antitakeover Provisions and Enterprise Value Based on PSM-DID Quasi-Natural Experimental Method

Zhang Yao,[1] **Guo Xuemeng**,[2] **and Jia Jia**[3]

[1]*Capital University of Economics and Business, Beijing, China*
[2]*Beijing Jiaotong University, Beijing, China*
[3]*Beijing Union University, Beijing, China*

Correspondence should be addressed to Zhang Yao; 20150810063@m.scnu.edu.cn

Received 20 June 2022; Revised 20 July 2022; Accepted 26 August 2022; Published 14 September 2022

Academic Editor: Chi Lin

Under the background of frequent hostile takeover events in China and the autonomy of the articles of association, the articles of association of listed companies even set up antitakeover provisions with an excessive defense that unreasonably restricts the rights of shareholders. Based on the role orientation of innovative supervision, the Small and Medium-sized Investors Service Center (hereinafter referred to as "Investment and Service Center") proposes to modify the relevant noncompliance provisions in the form of a shareholder recommendation letter. As the basic requirements of the articles of association and the relevant laws in corporate governance are increasingly inconsistent, the legal review of the articles of association is particularly important. This article determines the identification standard of excessive defense of antitakeover provisions by manually collecting the shareholder suggestion letter of the investment service center, the announcement on amendment of association articles of listed companies, and relevant laws and regulations. On this basis, the PSM-DID quasi-natural experimental method is used to empirically test the impact of excessive defense of antitakeover provisions on enterprise value. The study finds that the excessive defense of antitakeover provisions significantly inhibited the enterprise value. In this article, taking a-share listed companies in Shanghai and Shenzhen stock markets in 2007–2018 as an example, with the construction of antiacquisition clause excessive defense index (ATP end), relying on the "quasi-natural experiment" method of PSM-DID, we discuss the impact of excessive defense antiacquisition clause on the value of the enterprise and its impact path analysis. Further study found that its restriction mechanism was reflected in the significant increase of the first type of agency cost and the second type of agency cost. At the same time, the correlation between management compensation and performance and the correlation between management and professional performance are further reduced. Excessive defense against antiacquisition terms can reduce the corporate value, and the impact path of this effect is achieved by increasing type 1 agent costs and type 2 agent costs. It shows that the controlling shareholders are more likely to collude with the management, which aggravates the agency problem. The research conclusion of this article provides legal and economic empirical evidence for listed companies to reasonably set up antitakeover provisions and is also of great significance to innovative regulatory methods such as investment service centers. Excessive defense against antitakeover terms will enhance the dual-ditch effect and ultimately damage corporate value.

1. Introduction

With the rise of the split share structure reform and the wave of acquisition in the capital market in 2007, antitakeover has increasingly become the focus of research. The management and major shareholders of listed companies have attached importance to the setting of antitakeover provisions of "shark repellent." As the current relevant laws and regulations represented by the Administrative Measures for the Anti-takeover of Listed Companies do not clearly specify the scope of autonomy of the association articles, the antitakeover provisions in the association articles of listed companies have the new feature of excessive defense [1]. The shareholding ratio of the nomination right of director candidates is up to 30%, and the nomination of director candidates holds shares continuously for up to 5 years. Even

some articles of association directly restrict the qualification of director candidates, and the compensation multiple of the golden parachute provision is even up to 1000 times the total annual salary of the dismissed directors [2]. The above statistics fully show that some counterprovisions set up in the articles of association of listed companies have seriously infringed on the basic rights and interests of shareholders. With more and more inconsistencies between the articles of association and the basic requirements of relevant laws in corporate governance, the legal review of the articles of association is particularly important [3]. A hostile takeover is a relative goodwill takeover without the consent of the actual controller (or management) of the listed company. Once the hostile acquisition is successful, the acquirer will gain the actual control of the listed company.

Facing the practical problem of "excessive defense" of the antitakeover provisions in the articles of association of listed companies, the investment service center responded to the call for "innovative supervision mode" put forward by the party, combined "the essence of public implementation mechanism" with "the form of private implementation mechanism," and innovated "shareholding and exercise." Under the essence of official supervision background, exercising the basic rights and interests of ordinary shareholders and combining "prior supervision" and "in-process supervision" not only extends the supervision path but also overcomes the lag of postsupervision. Since its establishment, on the basis of its existing positioning and functions, the investment service center has carried out a series of work in the retrieval and analysis of corporate governance and articles of association and actively urged listed companies to modify their nonconforming and illegal articles of association by sending shareholder suggestions [4, 5]. Therefore, based on the special research background of China's reality, directly using the antitakeover provisions set in the articles of association of listed companies as the research object cannot truly reflect the external governance role of the antitakeover provisions. It is more necessary to effectively identify the excessive defense of antitakeover provisions and study their real governance effects based on the legal perspective of antitakeover provisions and the practice of scientific exercise of power in the investment and service center [6]. It is worth noting that most of the existing studies on antiacquisition terms are based on mature capital markets, with very little research on emerging capital markets. Compared with mature capital markets such as the United States, the laws and regulations of emerging capital markets are not sound enough, and the company's equity is highly concentrated. The first type of agency problem between management and shareholders and the second type of agency problem between major shareholders and minority shareholders exist at the same time, and the second type of agency problem is particularly prominent. This institutional difference makes the influence path and result of the antiacquisition terms on the company value may be different from that of the mature capital markets.

At the same time, there is no unified conclusion on how antitakeover provisions affect enterprise value in academic research. Some scholars believe that there is a positive correlation between antitakeover provisions and enterprise value, which supports the long-term value hypothesis. Other scholars believe that antitakeover provisions have a negative correlation with enterprise value, which verifies the trench hypothesis. It is worth noting that most of the existing studies on antitakeover provisions are based on mature capital markets, and most of the relevant studies are based on the simple perspective of "whether to set antitakeover provisions," and there is no in-depth analysis of the legal effect of antitakeover provisions. Under the background of China's special system, the autonomy of the articles of association leads to the excessive defense of antitakeover provisions, which provides a rare opportunity to study the economic consequences of antitakeover provisions in emerging market countries [7, 8]. Therefore, based on the characteristics of different institutional environments, this article studies how to scientifically measure the excessive defense of antitakeover provisions under the realistic background of China? How is the impact of excessive defense of antitakeover provisions on enterprise value reflected? How is its influence mechanism realized? The differences in the institutional environment and the provisions of the articles of association provide a rare opportunity to study the influence of the antiacquisition provisions in the articles of association of listed companies in emerging markets on the corporate governance mechanism and corporate value.

Based on the above problems, this article manually collects the antitakeover provisions, the recommendation letter of the investment service center, the characteristic rights protection services of the investment service center, and other data in the articles of association, corresponding to the requirements of specific provisions such as the company law and the measures for the administration of the acquisition of listed companies with the contents of the recommendation letter of the investment service center one by one, so as to determine the identification standard of excessive defense of antitakeover provisions. On this basis, the quasi-natural experimental method of PSM-DID is used to test the impact of excessive defense of antitakeover provisions on enterprise value. The empirical results show that there is a significant negative correlation between the excessive defense of antitakeover provisions and enterprise value [9]. With the construction of antiacquisition clause overdefense index (ATP end), based on the "quasi-natural experiment" method of PSM-DID, the influence of overdefense antiacquisition clause on enterprise value and its influence path are analyzed. After testing the changes in type I and type II agency costs, R&D input, and output before and after setting excessive defense antitakeover provisions, the study finds that excessive defense of antitakeover provisions will increase the type I and type II agency costs of enterprises. It leads to collusion between controlling shareholders and management, which verifies the trench hypothesis and reduces the long-term value of the enterprise. The research conclusion of this article provides legal and economic empirical evidence for listed companies to reasonably set up antiacquisition clauses, which is of great significance to innovative regulatory means such as investment service centers.

The research contributions of this article are as follows: firstly, based on the special background of the autonomy of the association articles of listed companies in China, it provides new empirical evidence for the study of the economic consequences of antitakeover provisions in emerging markets. The existing antitakeover literature is mainly based on the mature capital market environment [10, 11]. As a representative of emerging markets, due to the need to improve the formulation and implementation of laws and regulations, there is a special economic phenomenon of "excessive defense of antitakeover provisions." Its setting motivation and governance effect are different from those in developed markets. Therefore, combined with China's special institutional background, this article analyzes the governance effect of excessive defense of antitakeover provisions and supplements the relevant research on antitakeover provisions in China. Secondly, this article deeply analyzes the impact path of excessive defense of antitakeover provisions on enterprise value and enriches the research results of the impact mechanism. In addition to verifying the first type of agency cost and the second type of agency cost, it also further tests its impact on the salary performance relevance of the management and the level of professional performance relevance of the management, verifies the collusion tendency between the controlling shareholder and the company's management, and supplements the relevant literature on its mechanism. Thirdly, based on the legal and economic perspectives, this article deeply discusses the legal effect of antitakeover provisions from the legal perspective and discusses its impact on enterprise value from the economic perspective. Previous studies are only based on a single legal perspective or economic perspective and rarely combine the two for in-depth analysis. The research conclusions of this article have positive reference significance for the formulation of policies of relevant regulatory institutions and the implementation effect of innovative regulatory methods for investment service centers [12].

2. Theoretical Analysis and Research Hypothesis

2.1. Excessive Defense of Antitakeover Provisions and Enterprise Value. With the rise of the M&A wave, many companies have set up antitakeover provisions, and many scholars have also conducted in-depth research on them. Foreign scholars prefer to study M&A results, financial performance, market response, enterprise innovation, etc. However, Chinese scholars prefer the impact on the rotation of executive directors, the protection of minority shareholders' rights and interests, agency costs, and risk perception. Because of China's highly centralized ownership structure, domestic scholars prefer to study the impact of antitakeover provisions on agency costs and the protection of minority shareholders' rights and interests. The research results are more in line with China's actual national conditions [13].

Previous studies have found that the setting of antitakeover provisions was more likely to be one of the ways to maintain the position of management. Many scholars have verified the trench hypothesis. In order to avoid the acquisition of enterprises at low prices, the management of the company usually tends to invest in short-term projects that bring faster and more definite benefits to the company, resulting in insufficient long-term innovation investment and damaging the long-term value of the enterprise. It was found that the long-term market wealth effect was negative after the implementation of the "poison pill plan," indicating that the capital market generally believes that the trench effect is greater than the housekeeper effect. Cohen and Wang used the natural experimental method to find that the terms of a hierarchical board of directors will reduce the enterprise value. It was found that the stronger the company's defense ability was, the more inclined it was to establish a business empire without considering the optimization of investment decisions, which impairs the improvement of enterprise value. Based on the practical data on China's emerging markets, Zhang Weihua found that the setting of antitakeover provisions had a significant negative effect on the company's value and significantly increased the second type of agency cost [14].

On the contrary, many scholars support the long-term value hypothesis and believe that antitakeover provisions can reduce the acquired risk to a certain extent and have a positive impact on enterprise value. Sanjeev et al. believed that antitakeover provisions could become a shield against short-term market pressure, and there was no need for real earnings management to meet the needs of investors so as to promote the improvement of enterprise value. It was found that the layered board provision could encourage the company's management to invest in long-term projects, thus improving the enterprise value. It was found that the antitakeover provisions did not necessarily reduce the enterprise value, and its main role was to improve the company's negotiation ability so as to avoid the risk of M&A. Taking state laws as exogenous events, we mainly studied the value effect of innovative companies, and it was found that antitakeover provisions could promote the improvement of enterprise value. It was found that for companies with high management quality, antitakeover provisions were conducive to improving enterprise financial indicators. Johnson et al. took IPO companies as the research object and the research found that antitakeover provisions helped to stabilize the relationship between enterprise management and upstream and downstream and improved the value and performance of IPO companies [15, 16].

To sum up, based on the foreign real capital market, the impact of antitakeover provisions on the company's value has not reached a unified conclusion. In the context of China's special autonomy of the articles of association, many listed companies modify the articles of association and introduce antitakeover provisions with excessive defense. In addition, compared with foreign capital markets, the equity of China's listed companies is more concentrated. Compared with the management trench hypothesis, the controlling shareholder trench hypothesis is more suitable for China's actual national conditions. It can read the articles of association, the announcement on amendment of articles of association, the announcement of the relevant board of

directors, and the recommendation letter of the investment service center according to the accounting year. Through the one-to-one comparison of data, it is found that the problem of excessive defense of antitakeover provisions is mainly reflected in three types of provisions, such as the nomination right of director candidates, hierarchical board of directors, and golden parachute. Starting from different stakeholders, the study found that the nomination right of director candidates and the layered board of director's provision more safeguard the control right of the board of directors, while the golden parachute provision more safeguards the control right of the management [17, 18].

The golden parachute provision of excessive defense supports the management trench hypothesis and believes that its excessive defense is reflected in the self-interest behavior of the company's management, and it is more to maintain the control of the management. The excessive defensive nomination right of director candidates and the layered board of directors provision more support the trench hypothesis of controlling shareholders and believe that the antitakeover provisions not only protects the management but also consolidates the position of controlling shareholders, thus providing shelter for the tunneling behavior of major shareholders. However, as the representative of shareholders, there is a certain contradiction between the board of directors and the management. In order to reduce the risk of being acquired, the management chooses to reduce the shareholder value to a certain extent, and the board of directors supports the long-term value hypothesis. The long-term value hypothesis holds that the establishment of antitakeover provisions can send a positive signal to investors that the management and major shareholders have confidence in the long-term operation and development of the enterprise, protect the management and major shareholders from market pressure and avoid short-term decision-making behavior. Under the special institutional background of China, how the excessive defense antitakeover provisions affect the enterprise value depends on the combined influence of the trench hypothesis (management trench, shareholder trench) and the long-term value hypothesis. Therefore, this article puts forward the competitive hypothesis:

(i) Hypothesis 1a: setting antitakeover provisions with excessive defense in the articles of association will lead to the loss of enterprise value [19–21].

(ii) Hypothesis 1b: setting antitakeover provisions with excessive defense in the articles of association will promote the promotion of enterprise value.

2.2. Excessive Defense of Antitakeover Provisions, Agency Cost, and Enterprise Innovation. There are two completely opposite paths for the impact of excessive defense of antitakeover provisions on enterprise value, one is the agency cost path based on the management trench hypothesis and the controlling shareholder trench hypothesis, and the other is the enterprise innovation path based on the long-term value hypothesis. Through the above analysis, the impact mechanism of excessive defense of antitakeover provisions on enterprise value is the result of the comprehensive action of agency cost path and innovation path [22].

Under the agency cost hypothesis, the antiacquisition clause protects the manager status at the expense of reducing the shareholder wealth, thus intensifying the agency conflict between managers and shareholders. There are several important assumptions in the agency cost hypothesis. First, managers attach great importance to control rights, and their desire for control right makes the interests of management go against the interests of shareholders. This conflict of interest is very costly for shareholders. Second, the control market is a kind of corporate governance mechanism, which can alleviate the agency cost of external equity.

The agency cost path shows that when listed companies set antitakeover provisions with excessive defense, the management will not receive serious punishment and its company reputation will not be damaged under the pretext of autonomy of the articles of association. At most, it will receive the shareholder recommendation letter from the public welfare shareholder investment service center. In addition, setting antitakeover provisions with excessive defense in advance to prevent malicious mergers and acquisitions is easier to obtain the sympathy of public opinion and shape a good image of tragic heroes. Under the condition that the restrictive effect of the reputation mechanism is gradually weakened, the possibility of improper investment and financing decisions by the management will increase, and the enterprise value will further decrease. The controlling shareholders support the listed company to set up antitakeover provisions with excessive defense, which prevents the transfer of the company's control. If the controlling shareholders firmly grasp the company's control, it is likely to damage the interests of minority shareholders and ignore the growth of the long-term value of the enterprise. Therefore, based on the above analysis, this article puts forward Hypothesis 2.

(i) Hypothesis 2a.: setting antitakeover provisions with excessive defense in the articles of association will lead to the increase of the first kind of agency cost [22–25].

(ii) Hypothesis 2b: setting antitakeover provisions with excessive defense in the articles of association will lead to the increase of the second kind of agency cost.

As an external governance mechanism, antitakeover provision is very important to solve the contradiction between short-term market pressure and long-term interests represented by innovation. The path of the housekeeper theory hypothesis and long-term value creation theory hypothesis is to overdefend the antitakeover provisions, protect the management from the performance pressure and acquisition risk of the capital market, and reserve development space for long-term innovation of the management, so as to enhance the enterprise value. Therefore, based on the above analysis, this article puts forward Hypothesis 3.

(i) Hypothesis 3a: setting antitakeover provisions with excessive defense in the articles of association will promote the increase of enterprise innovation investment [26].

(ii) Hypothesis 3b: setting antitakeover provisions with excessive defense in the articles of association will promote the improvement of enterprise innovation output.

3. Research Design

3.1. Sample Selection and Data Source. Foreign antitakeover research is relatively mature, and the measurement of antitakeover terms mostly adopts the form of an index. The more mature indexes include the FK index created by Field and Karpoff et al. [26], *G* index created by Gompers et al. [16], and *E* index created by Bebchuk et al. [27]. Because there are significant differences in the formulation of articles of association between domestic and foreign listed companies, Chinese scholars mostly use the form of a single index to measure antitakeover provisions. Early scholars mostly used the cumulative voting system as the measurement index [28, 29]. With the widespread emergence of the cumulative voting system in the setting of the articles of association, some scholars focused on the staggered board of directors [30]. However, some scholars prefer multi-index measurement but have not formed a relatively mature index form.

The preliminary design of the identification method for the excessive defense of antitakeover terms is as follows: (1) it clarifies the basic concepts. This article introduces the concept of "Excessive defense" in psychology and finds that such antitakeover provisions focus on protecting the acquiree's own control while ignoring the principles of conforming to mandatory corporate legal norms and not damaging the interests of minority shareholders. (2) It determines the basic principles of identification methods. The first is to comply with the mandatory legal norms of the company, and the second is not to damage the overall interests of the company and minority shareholders. (3) It determines the basic content of the identification method. According to the revised contents of the articles of association of the listed company, the basic contents of identification shall be determined in combination with the shareholder recommendation letter of the investment service center and the characteristic rights protection service cases of the investment service center. It is found that there are no new types of antitakeover provisions in the articles of association of listed companies in China, but the contents of three types of antitakeover provisions such as the nomination right of director candidates, hierarchical board of directors, and golden parachute have changed greatly while increasing information disclosure obligations and cumulative voting are not of typical significance. (4) It determines the basic criteria for identification methods. The requirements of the specific provisions of the company law and the measures for the administration of the acquisition of listed companies are combined with the contents of the shareholders' recommendation letter of the investment service center to determine the basic standards. The specific identification criteria for the excessive defense of antitakeover provisions are shown in Table 1.

To sum up, the basic identification criteria for excessive defense of antitakeover provisions are as follows: (1) the shareholding ratio of recommended director candidates increased to more than 5%; (2) imposing continuous holding time as a condition for shareholders to recommend candidates for the board of directors; (3) conditions for directly depriving the hostile acquirer of the right to nominate director candidates; (4) restrictions on the replacement of directors; (5) determining that the compensation amount of the dismissed directors and their senior managers whose term of office has not expired shall exceed 80% of the total remuneration of the remaining term of office. As long as the antitakeover provisions in the articles of association of listed companies meet any of the above standards, they are excessive defense of antitakeover provisions.

Taking the listed companies in Shanghai and Shenzhen stock markets from 2007 to 2018 as the research object, the samples of companies in special industries such as finance and insurance, special operating companies such as ST and ST* , and listed companies with missing data are excluded, and the continuous variables are reduced by 1%. The final sample includes the data of 2621 listed companies and 20144 research samples. The antitakeover provisions in the articles of association are collected manually, and the data are obtained through keyword identification and manual judgment according to the identification standard for excessive defense of antitakeover provisions. In this article, Stata 14.0 software is used for data sorting and analysis.

3.2. Variable Definition

3.2.1. Explained Variable. Enterprise value: based on the research of Cremers [31] and Bhojraj [32], this article selects Tobin's *Q* as the index to measure enterprise value.

Agency cost: based on the research of Jiang and Jiranyakul [33], this article uses *Cost* to represent agency cost. The first kind of agency cost *Cost1* is measured by the sales management expense rate. The second kind of agency cost *Cost2* is measured by the capital occupation rate of major shareholders to minority shareholders.

Enterprise innovation: based on the research of Chemanur [34], this article uses Innovation to represent enterprise innovation. *R* and *D* investment *RNDR* is measured by the *R*&*D* investment ratio. The *R*&*D* output *IPantent* is measured by the number of enterprise invention patent applications that best reflect the innovation ability. Considering the lag of *R*&*D* output, this study uses the *R*&*D* output variable of the next period as the explained variable.

3.2.2. Explanatory Variables. The explanatory variable is the excessive defense of antitakeover provisions (*ATP over*), which mainly includes the following five types of excessive defense of antitakeover provisions. The number of excessive defense of antitakeover provisions (*ATP over*) is a dummy variable. When any of the following antitakeover provisions with excessive defense is set in the articles of association of a listed company, the value of *ATP over* is 1; otherwise, it is 0. (1) If the articles of association of the listed company in year *t* set the excessive defense provision (*SL over*) on the shareholding ratio restriction of the nomination right of directors,

Table 1: Identification criteria for excessive defense of antitakeover provisions.

	Nomination right of director candidates	
Identification criteria	Legal basis	Case support of investment service center exercise
Increase the shareholding ratio of recommended director candidates to more than 5%	Paragraph 2 of Article 102 of the company law	Dexin transportation (603032) Shareholder's proposal letter of Investment Service Center [2017] no. 1242
Impose continuous holding time as a condition for shareholders to recommend candidates for the board of directors	Paragraph 2 of Article 102 of the company law	Emeishan a (000888) Shareholder recommendation letter of Investment Service Center [2017] no. 1146
Directly deprive the malicious acquirer of the right to nominate director candidates	Paragraph 2 of Article 102 of the company law Article 53 of the guidelines for the articles of association of listed companies	Tianye Co., Ltd. (600807) Shareholder recommendation letter of Investment Service Center [2017] no. 134
	Hierarchical board of directors	
Identification criteria	***Legal basis***	***Case support of investment service center exercise***
Replacement of specific directors	Article 45, Paragraph 1, Articles 16, 121, and 142 of the company law. Articles 8 and 33 of the measures for the administration of the acquisition of listed companies	Maoye communication (000889). Shareholder recommendation letter [2017] no. 374 of Investment Service Center
	Golden parachute	
Identification criteria	***Legal basis***	***Case support of investment service center exercise***
Determine the compensation amount of the dismissed directors and their senior managers whose term of office has not expired, which shall exceed 80% of the total remuneration of the remaining term of office	Paragraph 1 of article 21, paragraph 2 of article 37, paragraph 9 of article 46 and paragraph 2 of article 103 of the company law. Article 32 of the governance standards for listed companies. Article 33 of the measures for the administration of the acquisition of listed companies	Polyfluorodox (002407). Shenzhen stock exchange inquiry

the value from *SL* $over_t$ to *SL* $over_{t+n}$ is 1, and the value of *SL* $over_{t+n}$ is 0. (2) If the articles of association of the listed company in year t set the excessive defense provision (*TL over*) on the shareholding time limit of the nomination right of directors, the value from *TL* $over_t$ to *TL* $over_{t+n}$ is 1 and *TL* $over_{t+n}$ is 0. (3) If the articles of association of a listed company set the excessive defense provision (*QE over*) on the qualification examination of directors, the value from *QE* $over_t$ to *QE* $over_{t+n}$ is 1, and *QE* $over_{t+n}$ is 0. (4) If the articles of association of a listed company sets the excessive defense provision (*SB over*) on staggered board of directors, the value from *SB over* to *SB* $over_{t+n}$ is 1, and the value of *SB* $over_{t+n}$ is 0. (5) If the articles of association of the listed company set the excessive defense provision (*GP over*) on the golden parachute, the value from *GP* $over_t$ to *GP* $over_{t+n}$ is 1, and the value of *GP* $over_{t+n}$ is 0.

3.2.3. Control Variables. Referring to the relevant literature of Chen [35], the control variables selected in this article are shown in Table 2.

3.3. Model Design. This article adopts the PSM-DID analysis method, which is divided into two steps: the first step is divided into an experimental group and matched control group according to the determinant model. The decisive factor model for testing the impact of excessive defense of antitakeover provisions is adopted, and model (1) is as follows:

$$\begin{aligned} ATP\_\mathrm{over}_i = {} & \alpha_0 + \alpha_1 \mathrm{Board}_{it} + \alpha_2 \mathrm{IndDir}R_{it} \\ & + \alpha_3 \mathrm{Mana\_hold}_{it} + \alpha_4 \mathrm{Top1}_{it} \\ & + \alpha_5 \mathrm{Size}_{it} + \alpha_6 \mathrm{Lev}_{it} + \alpha_7 \mathrm{ROA}_{it} \\ & + \sum \mathrm{Year}_t + \sum \mathrm{Industry}_i + \varepsilon_{it}. \end{aligned} \tag{1}$$

For companies with an excessive defense of antitakeover provisions, if the excessive defense of antitakeover provisions (*ATP over*) is set in the articles of association of listed companies in year t, the value from *ATP* $over_t$ to *ATP* $over_{t+n}$ is 1 and *ATP* $over_{t-n}$ is 0. For companies without the excessive defense of antitakeover provisions, *ATP over* is 0. Through model (1), it can test the impact of various factors in the model on the company when deciding whether to set excessive defense of antitakeover provisions.

Through the determinant model, it can match to form the tendency score. For the whole sample period, a company j in the control group without the excessive defense of antitakeover provision is found, which is as similar as possible to the determinant of the experimental group i with an excessive defense of antitakeover provisions, so that an effective control group with similar probability to the experimental group can be found, and applied to the follow-up test [32].

Table 2: Variable names and definitions.

Variable	Variable symbol	Variable description
Explained variable	Tobin's Q	Company market value/asset replacement cost
	Cost1	(Sales expenses + administrative expenses)/main business income
	Cost2	(Other receivables - other payables)/total assets
	$RNDR$	R&D investment/operating income
	IPantent	Number of invention patent applications of the enterprise in the next phase
Explain variable	ATP_over	Overdefense antitakeover provisions mainly include five types of overdefense antitakeover provisions. As long as one of the overdefense antitakeover provisions is set in the articles of association, the value is 1; otherwise, it is 0ATP *over*
Control variable	Board	Natural logarithm of the number of directors
	IndDir$R$	Number of independent directors/total number of directors
	Mana_hold	Number of shares held by management/total number of shares of the company
	Top1	Number of shares held by the largest shareholder/total number of shares of the company
	Size	Natural logarithm of total assets at the end of the year
	Lev	Total liabilities/total assets
	ROA	Net profit/average balance of total assets
	Ind_dum	Industry dummy variable
	Year_dum	Annual dummy variable

The second step is to use the double difference method. This article uses the following model (2):

$$\begin{aligned}\text{Consequences}_i = {} & \beta_0 + \beta_1 ATP\_\text{over}_i + \beta_2 \text{After}_{\text{it}} \\ & + \beta_3 ATP\_\text{over}_i \times \text{After}_{\text{it}} \\ & + \sum \text{Controls}_{\text{it}} + \sum \text{Year}_t \\ & + \sum \text{Industry}_i + \varepsilon_{\text{it}}.\end{aligned} \tag{2}$$

In model (2), the excessive defense of antitakeover provisions (ATP *over*) is a dummy variable. When the excessive defense of antitakeover provisions is set in the articles of association, the value is 1. When the excessive defense of antitakeover provisions is not set in the articles of association, the value is 0. *After* is a virtual variable. When the articles of association are set with an excessive defense of antitakeover provisions, the value is 1; otherwise, it is 0. For the control group, *After* is 1 in the same year after the experimental group companies with an excessive defense of antitakeover provisions are matched accordingly. $ATP\ over_i{}' After_{it}$ indicates the difference between the experimental group and the control group before and after setting the excessive defense of antitakeover provisions. The explained variable (Consequence) represents enterprise value (Tobin's Q), the first kind of agency cost (Cost1), the second kind of agency cost (Cost2), enterprise innovation input ($RNDR$), and enterprise innovation output (IPantent), respectively. In addition, the model controls the fixed effects of industries and years to eliminate the influencing factors of macroeconomy and specific industries.

4. Empirical Test

4.1. Descriptive Statistics and Correlation Analysis. Table 3 shows the results of descriptive statistical analysis of the main variables. According to the identification criteria of excessive defense of antitakeover provisions, this article focuses on five types of excessive defense antitakeover provisions: shareholding ratio limit of director nomination right (*SL over*), time limit (*TL over*), director qualification examination (*QE over*), staggered board of directors (*SB over*), and golden parachute (*GP over*). Therefore, the excessive defense of antitakeover provision means that as long as any one or more of the above five provisions are set, the ATP *over* value is 1; otherwise, it is 0. It can be seen from Table 3 that the average number of ATP *over* is 5%, indicating that 5% of the listed companies in the sample of listed companies have set excessive defense of antitakeover provisions. The results of other variables are shown in Table 3.

Table 4 shows the Pearson correlation coefficients of the main variables. It can be seen from the results in Table 4 that although the correlation of the main variables is significant, the relative coefficient is small, which further verifies that there is no multicollinearity problem between the variables. However, the correlation coefficients between different types of antitakeover provisions may be different, which further verifies the uniqueness of antitakeover provisions.

Among them, *SL over* and *SB over* are negatively correlated with enterprise value and *R&D* input-output and positively correlated with the type 2 agency cost. *TL over* and *QE over* are positively correlated with enterprise value, *R&D* input-output, and the type 2 agency cost. The *GP over* is negatively correlated with enterprise value and *R&D* input-output and positively correlated with the first type of agency cost. This shows that the terms with the maintenance of the control of the board of directors as the core are mainly positively correlated with the type 2 agency cost, while the terms with the maintenance of management control as the core are mainly positively correlated with the type 1 agency cost. For the impact of enterprise value, the positive and negative effects of different antitakeover provisions are different, and the governance effects of antitakeover provisions will also be affected by each other. Therefore, this article makes an empirical test by setting the dummy variable ATP *over*. From the correlation analysis table of main

Table 3: Descriptive statistics.

Variables	Number of observations	Mean value	Standard deviation	Minimum value	Median	Maximum value
Tobin's Q	20144	2.42	2.18	0.22	1.77	12.25
COST1	20144	0.18	0.13	0.01	0.15	0.78
COST2	20144	0.67	1.11	-2.58	0.41	6.01
RNDR	20144	0.05	0.04	0.00	0.04	0.25
IPantent	20144	14.09	32.63	0.00	4.00	237.00
SL over	20144	0.12	0.10	0.00	0.00	1.00
TL over	20144	0.01	0.05	0.00	0.00	1.00
QE over	20144	0.05	0.09	0.00	0.00	1.00
SB over	20144	0.01	0.10	0.00	0.00	1.00
GP over	20144	0.02	0.04	0.00	0.00	1.00
ATP over	20144	0.05	0.03	0.00	0.00	1.00
Board	20144	2.10	0.17	1.11	2.22	2.90
IndDirR	20144	0.38	0.05	0.19	0.34	0.81
Mana hold	20144	0.11	0.17	0.00	0.03	0.65
Top1	20144	0.34	0.15	0.08	0.32	0.76
Size	20144	21.85	1.18	19.93	21.71	25.70
Lev	20144	0.37	0.18	0.05	0.35	0.79
ROA	20144	0.06	0.05	−0.07	0.05	0.19

Table 4: Correlation Analysis of main variables.

Variables	*Tobin's Q*	*COST1*	*COST2*	*RNDR*	*IPantent*	*SL over*	*TL over*	*QE over*	*SB over*	*GP over*	*ATP over*
Tobin's Q	1										
COST1	0.365***	1									
COST2	−0.034***	-0.221***	1								
RNDR	0.238***	0.242***	−0.034**	1							
IPatent	0.004***	0.005***	−0.001*	0.007***	1						
SL over	−0.012**	0.020	0.017*	−0.003**	−0.012**	1					
TL over	0.013**	0.012	0.023*	0.002**	0.021**	0.094**	1				
QE over	0.019**	0.016	0.014*	0.003**	0.018**	0.212**	0.067***	1			
SB over	−0.024**	0.017	0.012*	−0.005**	−0.015**	0.121***	0.089***	0.065***	1		
GP over	−0.017**	0.019**	0.017	−0.007**	−0.011**	0.087***	0.102***	0.098***	0.086***	1	
ATP over	−0.015**	0.022**	0.007	−0.008**	−0.023**	0.312***	0.087***	0.096***	0.103***	0.092***	1

variables in Table 4, it can be seen that the correlation coefficient between *ATP over* and *Tobin's Q* is negative. Consistent with Hypothesis 1A proposed above, that is, setting excessive defense of antitakeover provisions in the articles of association will reduce the enterprise value.

4.2. Propensity Score Matching. According to the research design, this article conducts PSM analysis. The experimental group is the listed companies with an excessive defense of antitakeover provisions from 2007 to 2018, and the control group is the listed companies without the excessive defense of antitakeover provisions from 2007 to 2018. The propensity score is estimated through the regression model of model (1) and paired in a ratio of 1 : 3. The reliability requirements of PSM in pairing require that there is no significant difference in determinant variables between the matched experimental group and the control group. Therefore, this article first tests the balance of matched samples. Table 5 lists the balance test of matched samples. Compared with the relevant data of the experimental group and the control group before matching, the differences between the experimental group and the control group after matching are significantly reduced in the following table. Therefore, the decisive variables and matching methods selected in this article are correct, and the estimation results of the PSM matching method are reliable.

Table 6 shows the regression results of the decisive factors of model (1). The results show that there is a significant positive correlation between the management shareholding ratio and the excessive defense of antitakeover provisions, and its actual coefficient is 2.121, which shows that the management shareholding ratio of listed companies with an excessive defense of antitakeover provisions is obviously high. The shareholding ratio of the first largest shareholder is significantly negatively correlated with the excessive defense of antitakeover provisions, and its actual coefficient is −5.532, which shows that the shareholding ratio of major shareholders of listed companies with excessive defense provisions is obviously low and the equity is relatively scattered. The leverage level is significantly negatively correlated with the excessive defense of antitakeover provisions, and its actual coefficient is −0.824, indicating that the asset-liability ratio of listed companies with excessive defense provisions is not high.

The outstanding characteristics of listed companies with an excessive defense of antitakeover provisions are low

Table 5: Balance test of matched samples.

Variables	Before matching			After matching		
	Experience group	Control group	Difference	Experience group	Control group	Difference
Board	2.118	2.128	−0.01	2.118	2.119	−0.001
IndDirR	0.373	0.372	0.001	0.373	0.373	0.0001
Mana hold	0.124	0.103	0.021*	0.124	0.122	0.002
Top1	0.271	0.364	−0.093*	0.271	0.270	0.001
Size	21.834	21.780	0.054	21.834	21.815	0.007
Lev	0.426	0.441	−0.015*	0.426	0.432	−0.006
ROA	0.047	0.040	0.007	0.047	0.050	−0.003

Table 6: Decisive factor analysis model.

Variable design	Prediction coefficient	Actual coefficient	*P* Value
Board	?	−0.023	0.311
IndDirR	?	0.281	0.614
Mana hold	+	2.121**	0.013
Top1	—	−5.532*	0.001
Size	?	0.031	0.705
Lev	—	−0.824*	0.092
ROA	?	1.832	0.235

leverage and low shareholding ratio of major shareholders, indicating that listed companies with good operating performance and dispersed equity are more likely to be valued by the acquirer, and the risk of being acquired is greatly increased. In order to effectively reduce the risk of the hostile takeover, listed companies prefer to set antitakeover provisions with excessive defense in their articles of association. At the same time, listed companies with high management shareholding ratio are also more inclined to set antitakeover provisions with excessive defense in the articles of association to ensure the safety of the company's control.

4.3. Double Difference Test. After being processed by the PSM method, this article uses the PSM-DID method to test model (2). The double difference model controls the fixed effects of industry and year. Table 7 lists the panel DID results of model (2), in which the difference between columns (1), (3), (5), (7), (9) and columns (2), (4), (6), (8) and (10) is mainly reflected in the regression results of whether to add control variables.

Columns (1) and (2) mainly test the impact of excessive defense of antitakeover provisions on enterprise value. In column (2), the regression coefficient of the multiplication term *ATP over´*After is −0.507, which is significant at the statistical level of 5%, which indicates that compared with the company without the excessive defense of antitakeover provisions, the enterprise value with an excessive defense of antitakeover provisions is significantly reduced, thus verifying Hypothesis 1a; that is, setting antitakeover provisions with excessive defense in the articles of association will reduce the enterprise value. Columns (3) and (4) mainly test the impact of excessive defense of antitakeover provisions on the type 1 agency cost. In column (4), the regression coefficient of the multiplication term *ATP over´After* is 0.007, which is significant at the statistical level of 10%, which verifies Hypothesis 2a; that is, the excessive defense of antitakeover provisions effectively protects the position of the management, invalidates the role of supervision and governance for the management, and increases the type 1 agency cost. Columns (5) and (6) mainly test the impact of excessive defense of antitakeover provisions on the type 2 agency cost. In column (6), the regression coefficient of the multiplication term *ATP over´*After is 0.132, which is significant at the statistical level of 10%, thus verifying Hypothesis 2b, that is, setting antitakeover provisions with excessive defense in the articles of association will increase the type 2 agency cost and greatly increase the tunneling probability of major shareholders. Columns (7) and (8) mainly test the impact of excessive defense of antitakeover provisions on enterprise innovation investment. In columns (7) and (8), the regression coefficients of ATP over´After are −0.019 and −0.012, respectively, but they are not significant. Columns (9) and (10) mainly test the impact of excessive defense of antitakeover provisions on enterprise innovation output. In columns (9) and (10), the regression coefficients of the cross multiplication term ATP over´After are −0.002 and −0.001, respectively. This further verifies that the antitakeover provisions with excessive defense have no significant value effect on the long-term innovation of enterprises [34].

From the perspective of control variables, the regression coefficient of *Board* is significantly negative in column (6), indicating that with the increase in the number of directors, an effective supervision mechanism to restrict the tunneling behavior of controlling shareholders can be better established. The regression coefficient of *Top1* is significantly negative in column (4) and significantly positive in column (6), indicating that the shareholding ratio of controlling shareholders has a negative correlation with the type 1 agency cost, while it has a positive correlation with the type 2 agency cost, indicating that the controlling shareholders have played a positive supervisory role for the management but failed to effectively inhibit the tunneling behavior of major shareholders. The regression coefficient of *ROA* is significantly positive in columns (8) and (10), indicating that enterprises with higher income levels are willing to invest more funds in *R&D* investment, and the long-term value of enterprises can increase.

To sum up, setting antitakeover provisions with excessive defense in the articles of association has significantly reduced the enterprise value. Hypothesis 1a, Hypothesis 2a, and Hypothesis 2b have been effectively verified, and the

Table 7: Analysis of DID regression results of setting antitakeover provisions with excessive defense.

Variables	*Tobin's Q*		*COST1*		*COST2*		*RNDR*		*IPantent*	
	(1)	(2)	(3)	(4)	(5)	(6)	(7)	(8)	(9)	(10)
ATP over	0.232	0.354	−0.019	−0.018	−0.243**	−0.144***	0.025	0.018	0.002	0.001
	(1.21)	(1.33)	(−1.11)	(−0.99)	(−2.43)	(−2.77)	(1.47)	(1.08)	(1.44)	(1.01)
After	0.165	0.087	−0.004	−0.011	−0.065	−0.078	−0.004	−0.014	−0.001	−0.001
	(0.89)	(0.55)	(−0.30)	(−1.01)	(−0.68)	(−1.51)	(−0.56)	(−0.68)	(−0.34)	(−0.56)
ATP over′ After	−0.543**	−0.507**	0.025*	0.007*	0.251**	0.132*	−0.019	−0.012	−0.002	−0.001
	(−2.20)	(−2.01)	(1.75)	(1.87)	(2.21)	(1.76)	(−0.89)	(−0.77)	(−0.88)	(−0.69)
Board		0.006		0.003		−0.021***		−0.011**		−0.001**
		(0.37)		(0.91)		(−4.14)		(−2.04)		(−2.11)
IndDirR		−0.541		0.036		−0.211		0.012		0.001
		(−0.99)		(0.80)		(−1.16)		(0.22)		(0.22)
Mana hold		0.132		0.023		0.341		0.015		0.003
		(0.45)		(0.87)		(0.45)		(0.43)		(0.56)
Top1		−0.281		−0.084*		0.745*		0.013		0.004
		(−0.75)		(−1.62)		(1.88)		(0.83)		(0.85)
Size		0.084		0.011		0.271***		0.011		0.001
		(0.75)		(1.22)		(5.12)		(1.02)		(1.13)
Lev		−2.101**		−0.177***		−0.133		−0.011***		−0.010***
		(−2.57)		(−5.87)		(−1.12)		(−4.55)		(−4.12)
ROA		2.253		−0.265		3.126***		0.035**		0.031**
		(1.34)		(−0.87)		(5.67)		(2.58)		(3.11)
Constant	3.315***	4.711***	−0.157***	−0.081	−0.431	−4.122***	0.015*	0.014	0.542	0.327
	(10.54)	(3.75)	(−10.11)	(−0.66)	(−1.03)	(−5.11)	(1.43)	(0.57)	(0.91)	(0.43)
Industry	YES	YES	YES	YES	YES	YES	YES	YES	YES	YES
Year	YES	YES	YES	YES	YES	YES	YES	YES	YES	YES
N	2587	2514	2587	2514	2587	2514	2587	2514	2587	2514
Adj.R^2	0.17	0.28	0.12	0.18	0.09	0.20	0.22	0.28	0.21	0.19

Note. ***, **, and * indicate significance at the confidence level of 1%, 5%, and 10%, respectively.

trench hypothesis and agency path have been confirmed. This shows that the setting of antitakeover provisions with excessive defense by listed companies not only exceeds its judicial recognition standards in terms of law but also brings the loss of long-term value of enterprises in terms of economic consequences, which verifies the value loss caused by the increase of two types of agency costs.

4.4. Robustness Test. In order to prove the robustness of the above results, this article uses the nomination right provisions of director candidates, including three types of antitakeover provisions with excessive defense: shareholding ratio limit (*SL over*), shareholding time limit (*TL over*), and director qualification review (*QE over*) as alternative variables. This article tests the differences and changes in the relevant economic consequence variables represented by enterprise value before and after setting the director candidate nomination right provisions with excessive defense. The specific robustness results are shown in Table 8.

It can be seen from Table 8 that setting the provisions on the nomination right of over defensive director candidates will still reduce the enterprise value, and the type 2 agency cost will increase significantly, but the coefficient of the type 1 agency cost is not significant, which may only increase the type 2 agency cost because such provisions are more to safeguard the interests of controlling shareholders. It has no significant impact on the type 1 agency cost. The coefficients of *R&D* input and *R&D* output are still not significant, indicating that the original conclusion is still valid after replacing the original measurement method of antitakeover provisions with excessive defense. The sign direction and significance of the regression coefficient are not significantly different from the previous results. In conclusion, the research results are relatively robust.

5. Further Analysis

In the previous study, we verified the impact of excessive defense of antitakeover provisions on agency costs. The study found that listed companies with excessive defense antitakeover provisions not only significantly increase the type 1 agency costs but also increase the type 2 agency costs. In view of the simultaneous occurrence of the management trench problem and the controlling shareholder trench problem, it should further analyze whether the controlling shareholder will collude with the management to realize its "Tunnel" effect.

In the market economy environment, the salary level of the management is closely related to the real performance level of the enterprise. The management will strictly resist the private interest behavior of the controlling shareholders out of consideration of its own salary level. At the same time, the tunneling behavior of the controlling shareholder will also have a negative impact on the reputation of the listed

Table 8: Analysis of DID regression results of setting the terms of nomination right of director candidates.

Variables	*Tobin's Q*		*COST1*		*COST2*		*RNDR*		*IPantent*	
	(1)	(2)	(3)	(4)	(5)	(6)	(7)	(8)	(9)	(10)
ATP over	0.342	0.241	−0.021	−0.016	−0.213*	−0.167*	0.021	0.010	0.003	0.002
	(1.27)	(1.01)	(−1.05)	(−0.87)	(−1.85)	(−1.89)	(1.23)	(1.06)	(1.33)	(1.12)
After	0.211	0.120	−0.005	−0.016	−0.078	−0.122	−0.011	−0.025	−0.001	−0.001
	(1.10)	(0.67)	(−0.30)	(−0.11)	(−0.87)	(−1.41)	(−0.76)	(−0.86)	(−0.35)	(−0.65)
ATP over′ After	−0.573**	−0.461**	0.021	0.008	0.257**	0.168*	−0.021	−0.017	−0.003	−0.002
	(−2.27)	(−2.27)	(1.15)	(1.04)	(2.05)	(1.65)	(−0.98)	(−0.87)	(−0.78)	(−0.66)
Board		0.014		0.002		−0.012		−0.013**		−0.001
		(0.77)		(0.88)		(−1.14)		(−2.14)		(−1.17)
IndDirR		−1.11*		0.057		−0.801		0.013		0.002
		(−1.78)		(0.85)		(−1.31)		(0.24)		(0.21)
Mana hold		0.121		0.032		0.344		0.021		0.002
		(0.32)		(0.84)		(0.47)		(0.34)		(0.51)
Top1		−0.281		−0.124*		0.998*		0.015		0.004
		(−0.55)		(−1.72)		(1.98)		(0.98)		(0.81)
Size		0.087		0.007		−0.011*		0.015		0.001
		(0.85)		(1.22)		(−1.72)		(1.12)		(1.02)
Lev		−3.011**		−0.207***		0.253		−0.012***		−0.010***
		(−2.57)		(−5.48)		(1.57)		(−3.45)		(−3.23)
ROA		2.753		−0.425		6.132***		0.041**		0.030**
		(1.44)		(−0.87)		(8.72)		(2.87)		(2.76)
Constant	3.655***	3.511*	−0.166***	−0.081*	−0.427	−2.722***	0.011*	0.015	0.542	0.370
	(12.54)	(1.75)	(−7.11)	(−1.66)	(−1.12)	(−4.96)	(1.45)	(0.75)	(0.91)	(0.41)
Industry	YES	YES	YES	YES	YES	YES	YES	YES	YES	YES
Year	YES	YES	YES	YES	YES	YES	YES	YES	YES	YES
N	1978	1906	1978	1906	1978	1906	1978	1906	1978	1906
Adj.R^2	0.20	0.27	0.11	0.17	0.06	0.16	0.20	0.21	0.19	0.17

Note. ***, **, and * indicate significance at the confidence level of 1%, 5%, and 10%, respectively.

company and further consume the personal career reputation of the company's management. Therefore, the management generally does not cooperate with the interest mining behavior of the controlling shareholder for the dual consideration of salary and reputation. However, the controlling shareholders may choose the way of joint management to realize their tunneling behavior, mainly through the following two forms. The first is to reduce the risk that the management is involved and reduce the correlation between the management's salary and performance. The management does not have to worry about the impact of the company's performance on its salary. The second is to improve the stability of management positions, reduce the risk of management replacement, and reduce the relevance of management to professional performance.

Based on the above analysis, we test the relationship between setting antitakeover provisions with excessive defense in the articles of association and the correlation between management compensation and performance. In this article, the natural logarithm of the average salary of the top three executives with the highest salary level and directors, supervisors, and senior managers is used as the measurement index of management salary performance, which is expressed as *Execomp* and *Dsecomp,* respectively. It can be seen from columns (1) and (2) of Table 9 that the multiplier coefficient of the variable *ATP over′* R*OA* is significantly negative in the model, indicating that compared with the listed companies without the excessive defense of antitakeover provisions, the listed companies with an excessive defense of antitakeover provisions have a lower level of salary performance relevance of their management. The relationship between the setting of antitakeover provisions with excessive defense in the articles of association and the correlation between management's professional performances are further investigated. The CEO change is used as the measurement index of management turnover, and the control variables include executive education, age, tenure, and other company characteristics. It can be seen from column (3) of Table 9 that the multiplier coefficient of the variable *ATP over′ ROA* is significantly positive, which shows that in listed companies with an excessive defense of antitakeover provisions, the possibility of CEO replacement due to poor corporate performance is relatively small, and the correlation level of CEO's resignation performance is relatively low. Through the analysis of the above regression results, the listed companies that set excessive defense of antitakeover provisions in the articles of association not only have the tunneling behavior of the controlling shareholders but also show the increase of the second kind of agency cost and the further reduction of the level of correlation between management compensation and performance and the level of correlation between turnover performance. It also proves that the controlling shareholders are more likely to collude with the management, which aggravates the agency problem.

Table 9: Regression result analysis of salary performance relevance and resignation performance relevance.

Variables	*Execomp* (1)	*Dsecomp* (2)	*CEO change* (3)
ATP over	−0.021	−0.001	0.140***
	(−0.56)	(−0.04)	(3.81)
ATP over′ ROA	−0.732***	−0.720***	1.617***
	(−2.88)	(−2.98)	(3.89)
ROA	1.302***	1.317***	−1.879***
	(5.12)	(5.13)	(−4.99)
Size	0.351***	0.361***	0.053***
	(13.11)	(12.89)	(3.51)
Fage	0.011	0.021	0.043
	(0.36)	(0.77)	(1.12)
TOP1	0.002	0.002	−0.003**
	(1.26)	(1.21)	(−2.71)
Institution	0.007***	0.005**	−0.002
	(2.66)	(2.44)	(−1.20)
LEV	−0.081*	−0.052*	0.033
	(−1.78)	(−1.78)	(0.66)
Board	0.033***	0.027***	−0.005
	(4.12)	(4.17)	(−0.33)
IndDirR	0.351	0.306	0.277
	(1.55)	(1.12)	(0.76)
Education			−0.029**
			(−1.99)
Age			0.012***
			(3.98)
Tenure			−0.212***
			(−7.81)
Duality			−0.081***
			(−3.12)
Constant	3.112***	4.023***	−1.691**
	(5.51)	(4.12)	(−2.22)
Industry	YES	YES	YES
Year	YES	YES	YES
N	2502	2178	2076
Adj.R^2	0.37	0.31	0.18

6. Research Conclusion

Taking the A-share listed companies in Shanghai and Shenzhen stock markets from 2007 to 2018 as a sample, based on the construction of excessive defense index of antitakeover provisions (*ATP over*), and relying on the "quasi-natural experiment" method of PSM-DID, this article focuses on the impact of excessive defense of antitakeover provisions on enterprise value and its impact path analysis. The results show that excessive defense of antitakeover provisions will reduce enterprise value, and its impact path is realized by increasing the type 1 agency cost and the type 2 agency cost. By manually collecting the shareholders' suggestion letter of the Investment Service Center, the amendment announcement of the articles of association of the listed companies and the relevant laws and regulations, this paper determines the identification standard of the excessive defense of the antiacquisition provisions. Further analysis found that listed companies with the excessive defense of antitakeover provisions in the articles of association also further reduced the correlation between management compensation and performance and the correlation between management and professional performance, indicating that not only the controlling shareholders have tunneling behavior but also the controlling shareholders are more likely to collude with the management to aggravate the agency problem. The comprehensive practical results show that the excessive defense of antitakeover provisions will enhance the double trench effect and eventually damage the enterprise value.

At present, China has not set up special laws and regulations to strictly regulate the legal effect of antitakeover provisions. Based on the dual perspectives of law and economy, and on the basis of defining the legal effect of antitakeover provisions, this article studies the impact of excessive defense of antitakeover provisions on enterprise value, which provides strong practical support for legislators and regulators to deeply think about the legal effect of antitakeover provisions. It is conducive for regulators to carry out reasonable legal framework supervision on antitakeover provisions, give full play to the positive effects of antitakeover provisions, and abandon the management inertia caused by excessive defense, so as to realize the final growth of enterprise value. In the current capital market environment, the regulatory authorities should, within the legal framework, strictly supervise the behavior of listed companies in revising the articles of association and joining the antiacquisition clause, and strengthen the protection of the interests of small and medium investors, in order to maximize the positive role of the antiacquisition clause.

Data Availability

The data used to support the findings of this study are included within the article.

Conflicts of Interest

The authors declare that they have no conflicts of interest.

Acknowledgments

This work was supported by the Beijing Municipal Education Commission Social Science General Projects (SM201910038013).

References

[1] T. Sokolyk, "The effects of antitakeover provisions on acquisition targets," *Journal of Corporate Finance*, vol. 17, no. 3, pp. 612–627, 2011.

[2] M. S. Goktan and R. Kieschnick, "A target's perspective on the effects of ATPs in takeovers after recognizing its choice in the process," *Journal of Corporate Finance*, vol. 18, no. 5, pp. 1088–1103, 2012.

[3] R. Daines and M. Klausner, "Do IPO charters maximize firm value? antitakeover protection in IPOs," *Journal Of Law, Economics, and Organization*, no. 1, pp. 83–120, 2001.

[4] A. Agrawal and C. R. Knoeber, "Managerial compensation and the threat of takeover," *Journal of Financial Economics*, vol. 47, no. 2, pp. 219–239, 1998.

[5] L. A. Bebchuk, A. Cohen, and A. Ferrell, "What matters in corporate governance?" *Review of Financial Studies*, vol. 22, no. 2, pp. 783–827, 2009.

[6] P. Chintrakarn, N. Jiraporn, and P. Jiraporn, "The effect of entrenched boards on corporate risk-taking: testing the quiet life hypothesis," *Applied Economics Letters*, vol. 20, no. 11, pp. 1067–1070, 2013.

[7] J. E. Core, W. R. Guay, and T. O. Rusticus, "Does weak governance cause weak stock returns ?" *The Journal of Finance*, no. 2, pp. 655–687, 2006.

[8] J. Atanassov, "Do hostile takeovers stifle innovation? Evidence from antitakeover legislation and corporate patenting," *The Journal of Finance*, vol. 68, no. 3, pp. 1097–1131, 2013.

[9] J. M. Karpoff and M. D. Wittry, "Institutional and legal context in natural experiments: the case of state antitakeover laws," *The Journal of Finance*, vol. 73, no. 2, pp. 657–714, 2018.

[10] T. J. Chemmanur and X. Tian, "Do anti-takeover provisions spur corporate innovation? a regression discontinuity analysis," *Journal of Financial and Quantitative Analysis*, vol. 53, no. 3, pp. 1163–1194, 2018.

[11] Yu Cheng, *Research on the Impact of Investor protection Provisions in the Articles of Association on the Probability of Control Transfer*, Sun Yat sen University, Guangzhou, China, 2014.

[12] J. Xu, Y. Zeng, S. Li, and J. Kang, "Mechanism of anti-takeover provisions: a perspective of controlling shareholder's tunneling," *Journal of Management Sciences in China*, vol. 21, no. 2, pp. 37–47, 2018.

[13] S. Li, J. Xu, and D. Zhang, "Do anti-takeover provisions protect the rights of minority investors? Evidence from China's a type-share listed companies," *Nankai Business Review*, vol. 19, no. 4, pp. 49–62, 2016.

[14] Y. Chen, Y. Yang, and Y. Liu, "Does the director rotation system increase the agency cost of the company?" *Securities market guide*, vol. 2018, no. 4, pp. 35–41, 2018.

[15] K. Wang, H. fan, K. K. Xue, and J. Xu, "Research on board capital, layered board terms and corporate risk taking," *Journal of Management*, vol. 16, no. 3, pp. 351–432, 2019.

[16] P. A. Gompers, J. Ishii, and A. Metrick, "Corporate governance and equity prices," *Quarterly Journal of Economics*, vol. 118, no. 1, pp. 107–156, 2003.

[17] Y. Chen and S. Fang, "Anti takeover clauses, merger probability and corporate value," *Accounting research*, vol. 2014, no. 2, pp. 34–40, 2014.

[18] J. C. Stein, "Takeover tmm," *Journal of Political Economy*, vol. 96, no. 1, pp. 61–80, 1988.

[19] A. Cohen and C. C. Y. Wang, "Reexamining staggered boards and shareholder value," *Journal of Financial Economics*, vol. 125, no. 3, pp. 123–157, 2017.

[20] T. A. Gormley and D. A. Matsa, "Playing it safe? Managerial preferences, risk, and agency conflicts," *Journal of Financial Economics*, vol. 122, no. 3, pp. 433–455, 2016.

[21] W. Zhang, Yi Yao, and C. Wang, "Setting of anti takeover clauses in the articles of association and company value," *China soft science*, vol. 10, pp. 129–144, 2019.

[22] B. J. Sanjeev, S. Partha, and Z. Suning, "Takeexcessive defenses: entrenchment and efficiency," *Journal of Accounting and Economics*, vol. 63, no. 1, pp. 142–160, 2017.

[23] K. M. Cremers, L. P. Litov, and S. M. Sepe, "Staggered boards and long-term firm value, revisited," *Journal of Financial Economics*, vol. 126, no. 2, pp. 422–444, 2017.

[24] M. Stráska and H. G. Waller, "Antitakeover provisions and shareholder wealth: a survey of the literature," *Journal of Financial and Quantitative Analysis*, vol. 49, no. 4, pp. 933–956, 2014.

[25] T. J. Chemmanur, I. Paeglis, and K. Simonyan, "Management quality and antitakeover provisions," *The Journal of Law and Economics*, vol. 54, no. 3, pp. 651–692, 2011.

[26] J. M. Karpoff, W. C. Johnson, and S. Yi, "The bonding hypothesis of takeover defenses: evidence from IPO firms," *Journal of Financial Economics*, vol. 117, no. 2, pp. 307–332, 2015.

[27] L. Bebchuk, A. Cohen, and A. Ferrell, "What matters in corporate governance?" *Review of Financial Studies*, vol. 22, no. 2, pp. 783–827, 2009.

[28] H. Chen and M. Chen, "Flipping photons backward: reversed Cherenkov radiation," *Materials Today*, vol. 14, no. 1-2, pp. 34–41, 2011.

[29] B. Zhang, W. Huang, J. Li et al., "Principles, developments and applications of computer vision for external quality inspection of fruits and vegetables: a review," *Food Research International*, vol. 62, pp. 326–343, 2014.

[30] K. Wang, H. M. Zhang, S. B. Tsai et al., "Does a board chairman's political connection affect green investment?—from a sustainable perspective," *Sustainability*, vol. 10, no. 3, p. 582, 2018.

[31] K. Cremers, M. Ernicke, F. Gaessler et al., "Patent litigation in europe," *European Journal of Law and Economics*, vol. 44, no. 1, pp. 1–44, 2017.

[32] S. Bhojraj, C. M. C. Lee, and D. K. Oler, "What's my line? a comparison of industry classification schemes for capital market research," *Journal of Accounting Research*, vol. 41, no. 5, pp. 745–774, 2003.

[33] J. Jiang and K. Jiranyakul, "Capital structure, cost of debt and dividend payout of firms in New York and Shanghai stock exchanges," *International Journal of Economics and Financial Issues*, vol. 3, no. 1, pp. 113–121, 2013.

[34] T. J. Chemmanur, E. Loutskina, and X. Tian, "Corporate venture capital, value creation, and innovation," *Review of Financial Studies*, vol. 27, no. 8, pp. 2434–2473, 2014.

[35] Y. Chen, W. Li, and K. J. Lin, "Cumulative voting: investor protection or antitakeover? Evidence from family firms in C hina," *Corporate Governance: An International Review*, vol. 23, no. 3, pp. 234–248, 2015.

Hindawi
Mobile Information Systems
Volume 2022, Article ID 5066994, 10 pages
https://doi.org/10.1155/2022/5066994

Research Article

Stroke Extraction Algorithm of Clerical Script in Han Dynasty Based on Contour: Take "Stele of Cao Quan" as an Example

Liu Guoqing,[1] Hao Changning,[2] Yan Jingbo,[3] Dong Jing,[4] Zhao Zuolong,[5] and Hao Lujia[6]

[1]*Education Management Leadership, School of Education, Bangkok Thonburi University, Bangkok 10170, Thailand*
[2]*Faculty of Modern Languages and Communication, Universiti Putra Malaysia, Selangor 43400, Malaysia*
[3]*School of Arts, Shandong Cultural Industry Vocational College, Qing Dao 266600, China*
[4]*School of Distance Education, Universiti Sains Malaysia, Penang 11800, Malaysia*
[5]*School of Calligraphy, Jilin Jianzhu University, Chang Chun 130119, China*
[6]*School of Calligraphy, Hebei Academy of Fine Arts, Shijiazhuang 050700, China*

Correspondence should be addressed to Hao Changning; gs60380@student.upm.edu.my

Received 15 July 2022; Revised 10 August 2022; Accepted 16 August 2022; Published 5 September 2022

Academic Editor: Chi Lin

Under natural conditions, the inscription will be damaged by corrosion and oxidation, which is very unfavorable for the inheritance of this cultural heritage. Therefore, how to protect and study ancient calligraphy inscriptions by modern scientific and technological methods is a scientific and technological problem before us. In this paper, taking "Stele of Cao Quan" as an example, a stroke extraction algorithm of clerical script in Han Dynasty based on contour is proposed. Starting from the Chinese character skeleton, the basic skeleton is extracted by parallel thinning algorithm, and the redundant points in the skeleton are eliminated by matching with the construction template. In addition, the contour tracking thinning algorithm is analyzed. Aiming at the problems that the starting point is difficult to determine and the tracking process is complicated, the method of determining the tracking starting point is given, and some problems existing in the tracking process are solved. The experimental results show that the accuracy of regular script, running script, and clerical script is 88.35%, 86.71%, and 84.09%, respectively. Experiments show that the contour-based clean script stroke extraction algorithm can correctly extract clean script strokes.

1. Introduction

Inscription refers to the words engraved on the vertical stone. Stone inscriptions left over from history are the precious wealth of the Chinese nation, and they are an ancient and rich artistic form. "Stele of Cao Quan" is an important tablet in the Eastern Han Dynasty of China. This tablet is a vertical square with a height of 272 cm and a width of 95 cm. With the appearance of this monument, clerical script has developed to a certain extent, and there has also been a new turning point in aesthetics. Because of its early excavation, large quantity, exquisite calligraphy, and modeling, it has become the most important object for later generations to learn about calligraphy of Han Dynasty and study clerical script for a long period of history. Chinese character recognition is a branch of pattern recognition. Through the unremitting efforts of scientific researchers, online handwritten recognition and offline printed recognition in Chinese character recognition have become increasingly mature, and many products with practical value have appeared. Therefore, the study of image acquisition and digital visualization and three-dimensional modeling of ancient inscriptions and stone carvings is conducive to our deeper understanding of traditional culture and inheritance of ancient culture, which is also the significance of this topic.

In Chinese character recognition, there are two main categories: statistical features and structural features, according to the different features on which the recognition is based. Among them, thinning method is easy to cause false pen segment and shape distortion, and even if various

correction methods are adopted, it is not satisfactory [1, 2]. Because the handwriting process of Chinese characters will be recorded and saved, the coordinate data of each pixel in time sequence will be obtained. This unified data are very convenient for comparison and further research. However, for discrete Chinese characters, it is necessary to get all the strokes of Chinese characters, which requires a lot of work. As a part of our Chinese traditional culture, calligraphy is not only a font and symbol but also represents the historical heritage of China for five thousand years [3]. It is necessary to use technical methods to extract strokes of Chinese characters in traditional calligraphy works in terms of time uniqueness and two-dimensional space uniqueness and then to reproduce the three dimensions, which is a concrete process that learners can intuitively observe writing. Therefore, stroke extraction plays a very important role in guiding traditional calligraphy teaching.

Chinese calligraphy art has a long history and is profound, which is a precious historical treasure of our country. It embodies the culture of the Chinese nation for 5,000 years and is one of the most worthy of inheritance. It has a profound cultural connotation and is a treasure of the world art forest. It takes Chinese characters as the carrier, involves language, literature, history, aesthetics, and other aspects, and is connected with music and art. The "Stele of Cao Quan" rules are generally sparse and clear, and the characters are arranged neatly, horizontally and vertically, and orderly. Its word spacing is larger than line spacing, which is closely related to its stretching posture. The loose line spacing makes the works more ethereal, free and easy, elegant, and beautiful. This paper focuses on stroke extraction of Chinese characters and proposes a new algorithm integrating all levels of contour information. The extracted stroke outline has complete parameters and feature points and is easy to identify. Experiments show that the stroke extraction algorithm designed in this paper has a high accuracy and good stability, and it can correctly process oblique fonts without correction.

2. Related Work

2.1. Research on Chinese Character Stroke Extraction Method. In a large number of related studies of computer calligraphy, the recognition of clerical script is generally not based on the stroke features of clerical script, but on the contour pixel level of the word, which makes the feature extraction and recognition of clerical script have great limitations. Compared with hard pen characters, brush clerical script has greater changes in the thickness of strokes, the degree of adhesion, and the strength of pen movement. Many clerical scripts used in the past are no longer used in modern Chinese character writing.

Tan et al. extracted calligraphy strokes on the basis of pixel points of strokes in clerical script skeleton, but did not describe the acquisition of strokes skeleton in detail [4]. Yang et al. put forward stroke extraction algorithm and contour restoration algorithm based on stroke contour features by analyzing the contour features of Chinese characters [5]. Bag and Harit constructed a brush model. They abstract the brush tip as an inverted cone, and regard the cross section between the virtual brush and the paper as the actual contact surface. The geometric model of this method is simple, and it has a certain effect on the simulation of strokes, but it does not take into account the deformation when the real brush touches the paper [6]. Ye et al. established a stroke relation graph according to the direction of the strokes connected by each bifurcation point and applied bidirectional connection rules to extract strokes [7].

In order to solve the problem that skeleton distortion and spur phenomenon will have unnecessary influence on the extraction results in the skeleton-based stroke extraction method, some researchers change directions and abandon the idea of extracting strokes from skeleton. Chang et al. proposed a method of extracting boundary points from the outline of Chinese characters, screening out control points and inflection points from the set of boundary points according to certain rules, dividing the Chinese character shape image 3 into linear areas and nonlinear areas by using the corresponding feature points on the selected outline, and modeling the stroke features of the corresponding areas [8]. Liu et al. put forward a method of dividing strokes into overlapping areas and independent areas according to the turning point information of Chinese characters' shapes and contours and then recombining the obtained areas to evaluate the combination results and finally obtaining complete basic composition strokes [9]. Yang et al. proposed a parallel thinning algorithm with high efficiency. Different from iterative thinning algorithm, noniterative thinning algorithm, such as contour tracking thinning algorithm, does not need to process all pixels, but only the pixels on the contour calculate the center point and obtain the skeleton by interpolation [10].

2.2. Research on Chinese Character Recognition. The imitation of human functions of machines has been proved to be a very challenging research field, involving the knowledge of artificial intelligence, pattern recognition, human-computer interaction, natural language processing, signal processing, and other fields. Word recognition technology can be divided into printed Chinese character recognition and handwritten Chinese character recognition, while handwritten Chinese character recognition can be divided into online Chinese character recognition and off-line Chinese character recognition [11, 12]. According to different processing methods, it is usually divided into off-line Chinese character recognition methods based on structural patterns, off-line Chinese character recognition methods based on neural networks, and off-line Chinese character recognition methods based on statistical patterns.

Liu et al. incorporated the invariant features based on the tangent and curvature of strokes, then combined preprocessing and invariant feature extraction, and used point-oriented and stroke-oriented methods to recognize characters on small, medium, and large character sets, respectively [13]. Wong et al. have shown through experiments that the hidden Markov method is effective in recognizing conjoined characters. Because the character samples are too

large, there are still great problems in efficiency and accuracy of the hidden Markov model recognition method with large character sets [14]. Siddiqi et al. put forward Bayesian network. Compared with the traditional classifier, Bayesian network has higher recognition efficiency. However, because each node has to maintain a conditional probability table, it needs many samples, and its analysis and calculation are complicated [15]. Sadeghi et al. described the stroke width, stroke curvature, stroke continuity, and other information of Chinese characters by using the contour features and gray features of Chinese characters images and segmented and extracted Chinese characters strokes according to these information [16].

In online handwriting recognition, users input the images of characters one by one through touch screen, tablet, and other input devices. The system can judge and recognize the input characters according to the type and sequence of each stroke and the speed change of the pen. Ou et al. proposed an off-line handwritten Chinese character recognition method based on variable precision rough sugar set. Taking Chinese character samples and their corresponding feature vectors as an information system, a decision information system for off-line handwritten Chinese character recognition was constructed [17]. Zhang et al. proposed a clear script retrieval method based on clear script contour similarity. Using this method, 20 clear scripts were tested, and the precision rate was close to 90% at 90% recall [18]. Yao and Cheng proposed an interactive high-dimensional vector indexing method based on local distance graph, which mainly establishes the relationship between the concept of Chinese character semantic hierarchy and the underlying shape features through user feedback and improves the retrieval speed of massive clerical script databases [19].

3. Research Method

3.1. Inscription Image Preprocessing. When the original clerical script works are converted into digital images, the noises that will have unnecessary influence on the subsequent processing will be generated due to the influence of scanning equipment and the works themselves. Therefore, these noises need to be preprocessed at the beginning of the stroke extraction operation of the given clerical script images. According to the characteristics of clerical script, the preprocessing process needs to carry out image binarization, edge smoothing, hole filling, and other separate noise removal steps.

The research sample of this paper is "Stele of Cao Quan" image obtained by high-definition shooting. According to the clarity of the inscription image, the inscription image can be briefly divided into two situations. In the first case, the imaging degree of the stone inscription image is relatively clear. For this type of inscription image, common methods such as image filtering and image segmentation can meet the requirements of inscription image processing [20]. In the second case, the image quality of stone inscriptions is poor, so it will be complicated and difficult to extract the character outline of the image.

The "Stele of Cao Quan" images scanned from books or historical calligraphy works often contain many noises, including spots, scratches, and small holes in fonts caused by natural weathering or worn candle decay. The binarized single "Stele of Cao Quan" image is a binary color matrix with black characters on a white background. In this paper, first, "Stele of Cao Quan" image is converted into gray image, and then the obtained gray image of clerical script is binarized by iterative method. In this method, the best threshold is obtained by setting the new threshold to the midpoint of the average above and below the old threshold.

The principle of iterative optimal threshold method is to assume a threshold before all the work starts and set the initial value of the threshold as the average of the maximum gray value and the minimum gray value in the image.

$$T_0 = \frac{g_{\max} + g_{\min}}{2}, \tag{1}$$

where T_0 represents the initial threshold, $g_{\max}$ represents the maximum gray value of the image, and $g_{\min}$ represents the minimum gray value of the image.

Then, according to the threshold value, the image is divided into two parts: foreground and background. The pixels whose gray value is greater than the threshold value are designated as foreground, and the pixels whose gray value is less than the threshold value are designated as background. The average values of foreground and background are calculated, respectively.

$$A_b = \sum_{g=g_{\max}}^{T_0} g \times \frac{h(g)}{\sum_{g=g_{\min}}^{T_0} h(g)}, \tag{2}$$

where A_b represents the average gray value of the background and $h(g)$ represents the number of each gray value g.

Then, divide the number of pixels in each interval by the total number of pixels in the image, and the result is the proportion of pixels in each interval to the total number of pixels in the whole image. Calculated gray average of background and foreground. Iterate the threshold T from 0 to 255 and calculate the interclass variance of the image background and foreground under each threshold. Figure 1 shows the "Stele of Cao Quan" image before and after binarization.

If the noise in the image is not removed in time, it may be recognized by our algorithm as glyph area in the later calculation, which will affect the later matching work, so it is necessary to remove it in the preprocessing stage. The concrete principle is that after corrosion, the corresponding structure operator will remove the earlier part of the image, and the image at this time will be reduced by one circle compared with the previous image, so it is necessary to restore the image at this time by an expansion operation here.

Mean filtering method and Gaussian filtering method. Block filtering refers to the convolution of pixels in a filter kernel with a value of 1 and a size of $w \times h$. If the convolved value is divided by $w \times h$, it is consistent with the mean filtering. Gaussian filtering is the weighted average

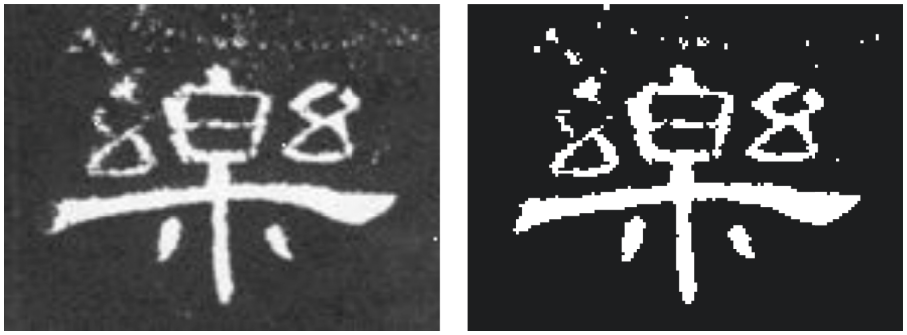

Before binarization (a) After binarization (b)

Figure 1: "Stele of Cao Quan" image before and after binarization. (a) Before binarization. (b) After binarization.

processing of the whole image by using the filtering kernel. Its core is that the weight of the filtering kernel conforms to the two-dimensional Gaussian filtering, namely:

$$G_0(x, y) = \frac{1}{2\pi \cdot \sigma^2} \cdot \exp\left(\frac{-(x - x_0)^2 - (y - y_0)^2}{2\sigma^2}\right). \quad (3)$$

From the image observation and analysis, it can be concluded that the stroke width will affect the threshold-the wider the stroke, the larger the threshold; Therefore, a dynamic threshold method is used here, namely:

$$S = S_0 * \frac{(a + \delta * S_1/S_0)}{100}, \quad (4)$$

S_0 is the area of Chinese character circumscribed rectangular frame; a, δ is a constant related to the threshold, $a = 0.4, \delta = 0.1$; and $S_1$is the area of Chinese characters.

The actual effect pairs are shown in Figure 2 below:

Threshold segmentation of image is a common and mature image segmentation method. Its algorithm is simple in implementation, small in computation, and stable in performance, so threshold segmentation is a basic and widely used image segmentation technology. The obtained subset of each pixel's gray value is a region corresponding to the image object, and the gray values of the pixels in this region are consistent, as are the neighboring regions. The division of the pixel gray value set can be carried out by using one or more image thresholds from the image gray level [15].

When recognizing clerical script, it is necessary to compare the similarity between "Stele of Cao Quan" images. Different sizes of "Stele of Cao Quan" images cannot be directly compared, so it is necessary to normalize the "Stele of Cao Quan" images and scale them to the same size images. Nonlinear normalization is complicated in calculation and requires a lot of computation, but it can keep the density information of clerical script and will not change the stroke structure. Therefore, this paper adopts a nonlinear normalization method based on the number of strokes crossing, and all clerical script are normalized to 70 pixels.

Let $H(x), V(y)$ represent the density projection of the density function in both horizontal and vertical directions, and then there are

$$H(x) = \sum_{x=1}^{M_0} d(x, y), V(y) = \sum_{xy=1}^{N_0} d(x, y), \quad (5)$$

M candidate recognition results are sorted according to the probability calculated by the above formula, and finally the label with the highest probability is output as the final recognition result.

3.2. Clerical Script Stroke Extraction. Clerical script has a long evolution process, and there are always obstacles in every process. When it captures the most remarkable features of life, it can vividly and profoundly reflect the phenomenon. Every time the evolution of clerical script permeates the integrity of life structure, the form of clerical script is richer than that of society, and its content is constantly derived. It is not easy to determine the logical relationship between the social conditions of the Eastern Han Dynasty and the form of clerical script, because the art of clerical script will inevitably change with the changes of society, and the inscriptions will also develop with the development of society.

The characters in "Stele of Cao Quan" are not only an important carrier for people's communication at that time but also an important form for recording historical documents. Clerical script is closely related to our life, which is not only the demand of daily life but also an artistic work. Each factor has a special meaning under specific conditions. Viewed from the overall background of the artistic experience of clerical script, these are just some abstract factors. No matter how important they are to the formation of Han Li's aesthetic concept, they cannot produce artistic works alone. It can be said that the two peaks of clerical script appeared in the Han Dynasty (development) and the Qing Dynasty (revival). The excavation of "Stele of Cao Quan" played a transformational role in the evolution of clerical script and played a mainstay role in the transformation of calligraphy aesthetics in the Tang, Song, Yuan, and Ming Dynasties and the late Ming and early Qing Dynasties.

"Stele of Cao Quan" became the main object of calligraphers in the late Ming Dynasty and early Qing Dynasty

Before denoising (a) After denoising (b)

Figure 2: Contrast image before and after removing isolated noise. (a) Before denoising (b) After denoising.

because of its beautiful style, fine print, and perfect readability. Its enlightenment and nourishment to the past calligraphy is obvious, which is the ancient value. For the enlightenment teaching of children's calligraphy, it is also an important model of temporary learning. From it, it is helpful for calligraphy aesthetic education and enlightens students' aesthetic thinking; taking it as the source, it is convenient for students to be familiar with the law of character development and enlighten the cognition of calligraphy history; taking it as a mirror, we know that the knowledge of writing and calligraphy skills should be combined, which is the value of today.

This section is to extract the character outline of the preprocessed inscription image. The specific method is to propose a character backbone extraction method based on the stroke characteristics of Chinese characters according to the analysis of the character structure in the inscription image in the previous chapter, combined with the theory and method of mathematical morphology and wavelet transform, so as to obtain the character outline in the inscription image. Many contents in digital image processing, such as image segmentation, feature extraction, image filtering and other work, can be completed by these basic operators and their combinations [14].

The feature point set in this study is obtained from the skeleton of Chinese character picture, and the skeleton extracted from Chinese character picture has connectivity. According to this feature, the feature point set in this study can be treated differently from the common point set mapping problem. On the basis of the above calculation method, according to the obtained point set mapping relationship, the corresponding relationship between the pixel set of clerical script single-character skeleton image and the template point set can be established. The process of stroke extraction method is shown in Figure 3:

The feature points in the extracted Chinese character skeleton are mapped and matched with the feature points in the template, and the corresponding mapping relationship is established. Traverse the point set in each stroke segment with established mapping relationship, calculate the stroke corresponding to the template point corresponding to each point in the stroke segment, and set it as the stroke corresponding to the extracted feature point in the skeleton. Wherein the stroke with the most feature points is set as the stroke to which the stroke segment belongs.

The method proposed in this paper can determine the shape and size of the intersection area according to the shape and thickness of strokes, and the extraction effect is good. In order to adapt to different fonts of Chinese characters and different strokes of the same font, an adaptive algorithm for extracting the intersection area of Chinese characters strokes is proposed. This method does not need to manually set the segmentation radius and can find out the concave point and obtain the intersection area according to the distance from the intersection point to the outline, which can be suitable for Chinese characters of different fonts. At the same time, it shows that this method has a good performance in segmentation accuracy and efficiency.

In order to conveniently determine the position of each region and its corresponding node in the undirected graph in the stroke combination process, a coordinate system is established for the whole character, and the point in the lower left corner of the image is taken as the coordinate origin. Take the center of gravity of each region to represent the region and its corresponding node in the undirected graph [20]. The formula of center of gravity $A_i(x_i, y_i)$ is as follows:

$$x_i = \frac{\sum_{j=1}^{n} x_j}{n}, y_i = \frac{\sum_{j=1}^{n} y_j}{n}, \tag{6}$$

where n is the number of pixels in the area and x_j, y_j is the x, y-axis coordinate of each point in the area.

For similar "Stele of Cao Quan" images retrieved, the first N images are selected as candidate "Stele of Cao Quan" images in descending order. These "Stele of Cao Quan" images may have different semantic annotations. This paper gives weight according to its ranking and similarity.

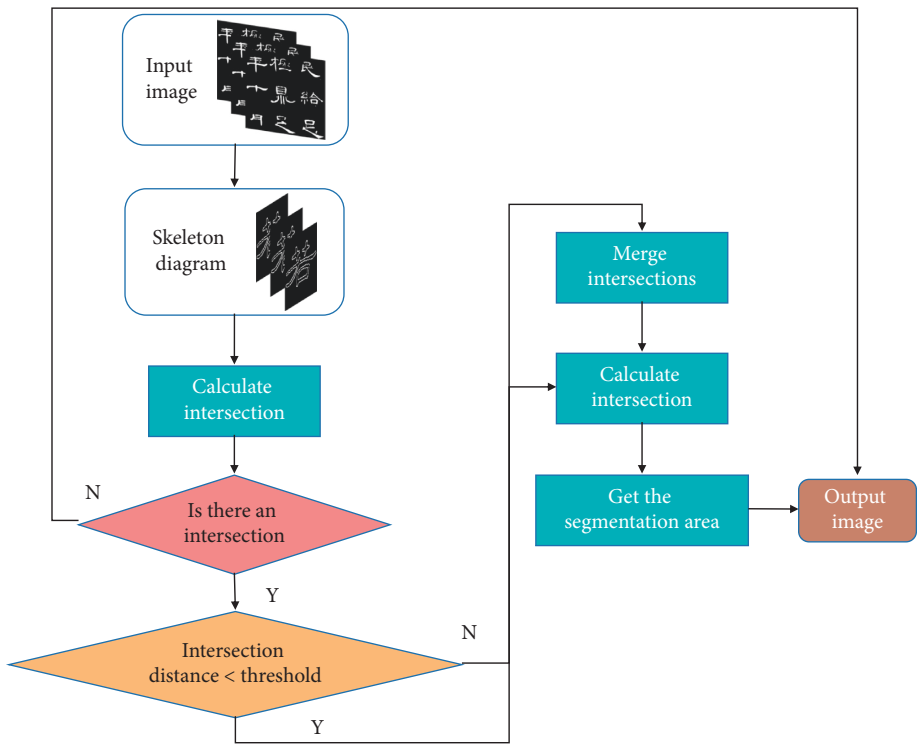

Figure 3: Flow chart of adaptive cross-region extraction algorithm.

The input image of Stele of Cao Quan to be recognized is A, N candidate clerical script: $B_1, B_2, \ldots, B_N$, and the weight $w_i\,(i = 1, 2, \ldots, N)$ is defined as follows:

$$w_i = \frac{\lambda}{i^2} + \text{Similarity}\left(A, B_i\right), \tag{7}$$

λ is an empirical parameter, which indicates the importance of the serial number in the search results in the weight.

Image processing based on wavelet transform is to adjust the approximate component and detail component coefficients generated in the process of image decomposition, so that the reconstructed image can meet specific conditions, thus realizing image processing. Wavelet transform has two remarkable characteristics: the first one is "small," which means that it has compact support set or approximate set in time domain; the second feature is characterized by "volatility" in the alternation of positive and negative.

a, b is discretized so that $a = 2^{-j}, b = 2^{-j}k$; $j, k \in Z$. The form of discrete wavelet transform can be obtained:

$$\left(DW_{\psi} f\right)(j, k) = \langle f(t), \psi_{j,k}(t)\rangle. \tag{8}$$

According to the research sample in this paper, on the basis of the existing trunk extraction algorithm, combined with the analysis of the text structure in the inscription image in the previous article, the original algorithm is improved, and a contour extraction method based on the stroke features of Chinese characters is proposed. According to the wavelet transform of the inscription image and its edge detection method, the edge features of the characters in the inscription image correspond to the local extremum points of the transformed wavelet coefficients, which can accurately describe the edge contour and structural features of Chinese characters in the inscription image.

For Chinese character writing, one structure is usually written before the next one is written. Therefore, the structures are preliminarily divided here, and the writing order between structures is determined according to the distance l_i between $O_i\,(x_{O_i}, y_{O_i})$ and the origin of coordinate axis, namely:

$$l_i = \sqrt{x_{O_i}^2 + y_{O_i}^2}. \tag{9}$$

If $l_a < l_b$ is used, the writing priority of structural component $S_a$is higher than that of S_b.

The writing sequence of structural components is determined by the distance between the center of the connected domain and the origin of coordinates, but there are different strokes in each structural component, that is, there may be multiple strokes in a structural component, so it is necessary to arrange the writing sequence of the strokes in each structural component in running script.

Because of the complex structure of Chinese characters' strokes, there is no certain rule to follow whether the horizontal and vertical strokes intersect, and the skeleton obtained by thinning algorithm has a certain degree of deformation, so there may be multiple intersections in the same intersection area, which will inevitably increase the workload, and the matching will fail because of the different number of intersections in the matching stage, which will inevitably affect the accuracy of stroke extraction.

In this paper, the intersection number $N_c\,(P)$ of each pixel is calculated for the skeleton map corresponding to each stroke structure:

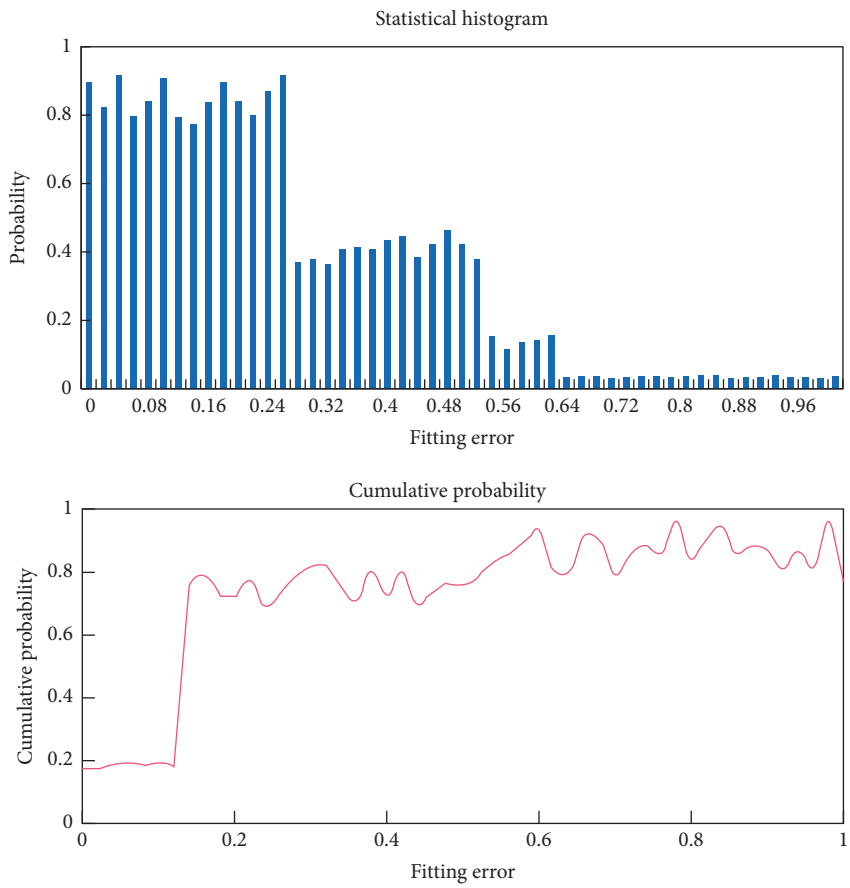

Figure 4: Parabolic fitting error of single word image.

$$N_c(P) = \frac{1}{6}\sum(x_{i+1} - x_i). \tag{10}$$

In which $x_i\,(i = 1, 2, \ldots, 9)$ is the adjacent point of pixel p.

For the stroke structure without intersection, we directly output strokes without stroke extraction. If p is not empty, it means that the stroke structure contains at least two strokes. Therefore, we need to perform stroke extraction operations such as intersection extraction, intersection area extraction, and stroke segment combination for the stroke structure with p not empty.

4. Result Analysis

Fifty single-character images were randomly selected from Stele of Cao Quan, and then continuous single-character contours were manually marked in these single-character images. Finally, a total of 150 partial word contours were obtained. Each local word contour line is fitted by parabola, and the mean square distance between the parabola and the corresponding point on the marked word contour line is calculated to obtain the parabola fitting error of the local word contour line. The final fitting error is normalized by using the distance between words in the corresponding picture. Figure 4 shows the parabola fitting error of a single word image.

It can be observed that the parabola fitting error of more than 72% of the local word contours is below 0.024 word-to-word distance. About 91% of the parabola fitting errors of local word contours are within the range of 0.06 word-to-word distance. This shows that these local word contours can be well fitted by parabola and also shows that the local word contours have parabolic characteristics.

In this paper, continuous high-quality clerical script contour lines are extracted from sparse key points. Therefore, in this section, the method in this paper will be compared with the existing stroke alignment methods. In addition, the outline of the stroke is found by other methods in this paper, and this section will also compare it with the existing edge contour extraction methods. This section runs the executable program on the test picture.

In this section, DME (dense mean error) and SME (sparse mean error) are used to express errors. The results are shown in Figures 5 and 6:

The cumulative error distribution diagram in the above figure shows the advantages of this method. This figure shows the proportion of the contour lines or key points of clerical script extracted within a certain allowable DME or SME error range. It can be seen that this method outperforms the other three methods, which shows the good performance of this clerical script extraction method. This clerical script contour extraction method is more accurate than the other three methods.

Table 1 compares the accuracy of stroke extraction on three different font data sets with the method in this paper. In this paper, the stroke combination stage adopts two arbitrary stroke segments in two combination, and then the correct combination mode is selected and the strokes are extracted by the statistical data of distance from point to edge and distance from edge to edge.

Comparatively speaking, the stroke extraction scheme of clerical script proposed in this paper achieves the accuracy rates of 88.35%, 86.71%, and 84.09%, respectively, on three different fonts: regular script, running script, and clerical script. In most cases, the angle-based combination of stroke segments can find the optimal combination, which proves that the correct intersection set in the standard reference data set and the correct combination of stroke structure can improve the accuracy of stroke extraction. The system proposed in this paper achieves the goal of stroke extraction, basically all strokes are completely extracted, most strokes are smooth, and only a few strokes have redundant strokes near the intersection area.

The model of writing depth and pen width information is established by the method of experimental test and data analysis. To verify the explanatory degree of the model to each data, the variance of each group of data based on the model is calculated, as shown in Figure 7.

It is found that after the depth $d = 6$, the variance increases significantly, which is related to the brush structure. The main writing part of the brush is at the tip, which is called an inverted triangle shape, while the middle part tends to be full gradually, which is the main ink storage area. This shows that the correct writing depth of this brush should be within 6 mm. In the later writing experiment, this threshold should not be exceeded.

Because the stroke details and some stroke information of clerical script are abandoned, the final effect cannot keep the original state of clerical script, which leads to the abandonment of stroke information and the relatively low stroke extraction rate. This paper mainly compares the experimental results with the stroke extraction method. The results are shown in Table 2.

The results show that the recognition sum of ref [10] method is lower than 90.37% in this paper. It can be seen that the stroke extraction algorithm based on BP neural network is slightly superior in recognition rate.

The refinement of Chinese characters is very important. Because in binary dot matrix images, the feature information of Chinese characters that is valuable for recognition is mainly concentrated on the skeleton of Chinese characters, and the refined skeleton of Chinese characters can retain most of the features of the original Chinese characters, which is conducive to feature extraction. These thinning algorithms have achieved good results when dealing with western characters. Because there is a big difference between the glyphs of Chinese characters and those of western characters, when these traditional thinning algorithms are applied to Chinese characters thinning, they often cause new distortion, increase the interference and difficulty of recognition, and the algorithm itself is time-consuming. This is because any local association cannot fully express the global association, so the thinning algorithm based on template cannot completely avoid burrs and whiskers in the thinning results.

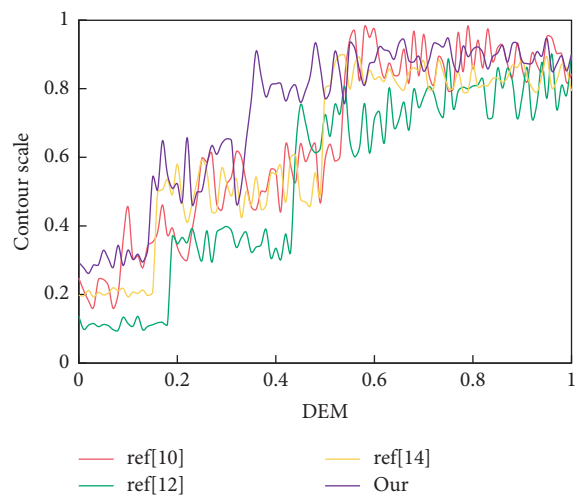

Figure 5: DME error distribution.

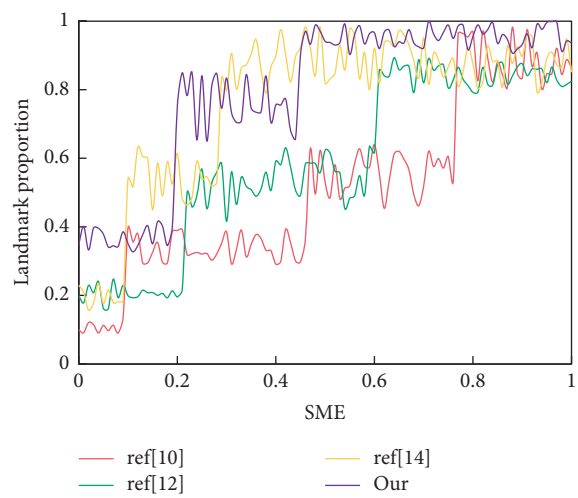

Figure 6: SME error distribution.

Table 1: Comparison of accuracy.

Method	Regular script (%)	Running script (%)	Clerical script (%)
Ref [10]	81.25	75.14	82.25
Ref [12]	86.01	70.12	77.14
Ref [14]	84.11	66.38	81.27
Our	88.35	86.71	84.09

From the statistical data of the above experimental results, it can be found that the skeleton stroke extraction method of clerical script proposed in this paper has certain stability when extracting skeleton strokes of clerical script, and shows strong robustness when the program runs without crash or downtime. When the noise is large, it will

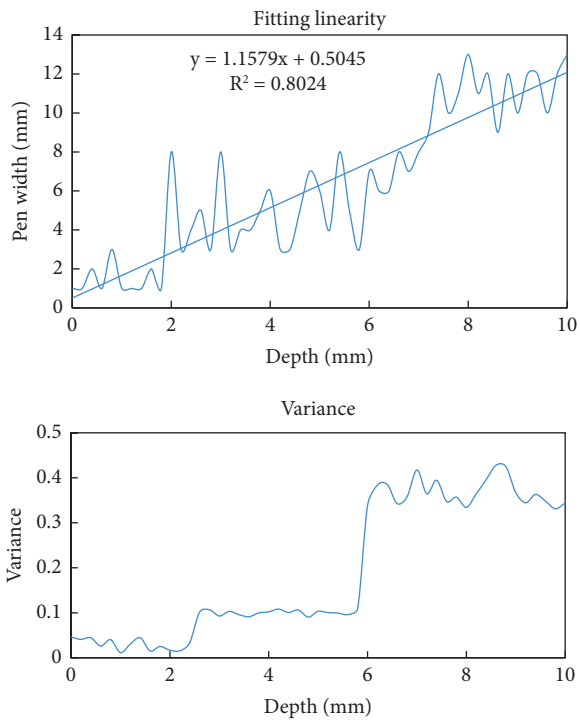

Figure 7: Fitting linear variance diagram.

Table 2: Experimental result.

Method	Number of strokes	Extract the correct number	Accuracy (%)
Ref [10]	1080	739	68.43
Ref [12]	1080	814	75.37
Ref [14]	1080	886	82.04
Our	1080	976	90.37

have a serious impact on the denoising process in the initial stage of processing, so that all the noise cannot be perfectly removed, thus causing interference to the later processing, thus making the extraction work fail.

Fuzzy region detection is used to determine the intersection of strokes. Through comparative analysis, the detection method based on dynamic window scaling is not as effective as that based on thinned intersection. After the corresponding area of the root node is found, each starting point and end point of the known stroke clerical script can find the unique corresponding area in the self-writing character. Traversing the tree topology diagram of the known stroke clerical script, using the end point number of each stroke path of the known stroke clerical script to represent the stroke, and corresponding the path to the self-writing character, the stroke in the self-writing character is extracted.

5. Conclusion

The computer simulation research of tablet inscription clerical script is one of the most challenging topics of computer application technology, and it is of immeasurable value to the protection, development, and application of Chinese calligraphy. "Stele of Cao Quan" became the main object of calligraphers in the late Ming Dynasty and early Qing Dynasty because of its beautiful style, fine print, and perfect readability. Its enlightenment and nourishment to the past calligraphy is obvious, which is the ancient value. Starting from the basic composition of clerical script, we classify and extract the stroke information of clerical script, which is a key step in the research field of computer calligraphy. In this paper, a contour extraction method based on stroke features of Chinese characters is proposed, which can determine the shape and size of the intersection area according to the shape and thickness of strokes, and the extraction effect is good and can be applied to Chinese characters with different fonts. At the same time, it shows that this method has a good performance in segmentation accuracy and efficiency. In this paper, the stroke extraction scheme of clerical script proposed in this paper achieves the accuracy rates of 88.35%, 86.71%, and 84.09%, respectively, on three different fonts: regular script, running script, and clerical script. It is proved that the correct intersection set in the standard reference data set and the correct combination of stroke structures can improve the accuracy of stroke extraction.

Data Availability

The data used to support the findings of this study are included within the article.

Conflicts of Interest

The authors declare that there are no conflicts of interest regarding this work.

References

[1] J. Zeng, W. Feng, L. Xie, and Z. Q. Liu, "Cascade Markov random fields for stroke extraction of Chinese characters," *Information Sciences*, vol. 180, no. 2, pp. 301–311, 2010.

[2] T. Lei, "Stable tracking point extraction for infrared extended target based on contour smoothing and minimal inscribed circle," *Optical Engineering*, vol. 52, no. 11, Article ID 113101, 2013.

[3] W. Y. Liu and J. L. Jiang, "A new Chinese character recognition approach based on the fuzzy clustering analysis," *Neural Computing & Applications*, vol. 25, no. 2, pp. 421–428, 2014.

[4] L. Tan, X. Sun, and G. Sun, "Print-scan resilient text image watermarking based on stroke direction modulation for Chinese document authentication," *Radioengineering*, vol. 21, no. 1, pp. 170–181, 2012.

[5] G. Yang, H. Liang, and Y. Su, "Generating Chinese characters based on stroke splitting and feature extraction," *Displays*, vol. 34, no. 4, pp. 258–269, 2013.

[6] S. Bag and G. Harit, "An improved contour-based thinning method for character images," *Pattern Recognition Letters*, vol. 32, no. 14, pp. 1836–1842, 2011.

[7] N. Ye, X. Qin, L. Dong, X. Zhang, and K. Sun, "Chinese named entity recognition based on character-word vector fusion," *Wireless Communications and Mobile Computing*, vol. 2020, no. 3, Article ID 8866540, pp. 1–7, 2020.

[8] L. Y. Chang, J. Z. Stafura, B. Rickles, H. C. Chen, and C. A. Perfetti, "Incremental learning of Chinese orthography: ERP indicators of animated and static stroke displays on character form and meaning acquisition," *Journal of Neurolinguistics*, vol. 33, no. 1, pp. 78–95, 2015.

[9] L. Liu and C. Cao, "A seed-based method for generating Chinese confusion sets," *ACM Transactions on Asian and Low-Resource Language Information Processing*, vol. 16, no. 1, pp. 5.1–5, 2016.

[10] K. Yang, S. Liu, H. Wang, W. Liu, and Y. Wu, "Effect of pixel's spatial characteristics on recognition of isolated pixelized Chinese character," *The Open Biomedical Engineering Journal*, vol. 9, no. 1, pp. 234–239, 2015.

[11] H. Y. Hsiung, Y. L. Chang, H. C. Chen, and Y. T. Sung, "Effect of stroke-order learning and handwriting exercises on recognizing and writing Chinese characters by Chinese as a foreign language learners," *Computers in Human Behavior*, vol. 74, no. sep, pp. 303–310, 2017.

[12] C. H. Tung and E. Y. Jean, "Stroke-order-free on-line Chinese character recognition by stroke adjustment of two-layer bipartite weighted matching," *Future Generation Computer Systems*, vol. 81, no. 6, pp. 219–234, 2018.

[13] C. L. Liu, F. Yin, D. H. Wang, and Q. F. Wang, "Online and offline handwritten Chinese character recognition: benchmarking on new databases," *Pattern Recognition*, vol. 46, no. 1, pp. 155–162, 2013.

[14] L. H. Wong, I. Boticki, J. Sun, and C. K. Looi, "Improving the scaffolds of a mobile-assisted Chinese character forming game via a design-based research cycle," *Computers in Human Behavior*, vol. 27, no. 5, pp. 1783–1793, 2011.

[15] M. H. Siddiqi, R. Ali, A. M. Khan, E. S. Kim, G. J. Kim, and S. Lee, "Facial expression recognition using active contour-based face detection, facial movement-based feature extraction, and non-linear feature selection," *Multimedia Systems*, vol. 21, no. 6, pp. 541–555, 2015.

[16] F. Sadeghi, H. Izadinia, and R. Safabakhsh, "A new active contour model based on the conscience, archiving and mean-movement mechanisms and the som," *Pattern Recognition Letters*, vol. 32, no. 12, pp. 1622–1634, 2011.

[17] J. Ou, J. Zhou, X. Zhu, Y. Yuan, Y. Shang, and X. Zhang, "Large stack-yard three-dimensional measurement based on videogrammetry and projected-contour scanning," *Optical Engineering*, vol. 51, no. 6, pp. 1–10, 2012.

[18] X. Y. Zhang, Y. Bengio, C. L. Liu, and X. Y. Zhang, "Online and offline handwritten Chinese character recognition: a comprehensive study and new benchmark," *Pattern Recognition*, vol. 61, no. 61, pp. 348–360, 2017.

[19] C. Yao and G. Cheng, "Approximative Bayes optimality linear discriminant analysis for Chinese handwriting character recognition," *Neurocomputing*, vol. 207, no. Sep.26, pp. 346–353, 2016.

[20] X. Feng, H. Yao, and S. Zhang, "Focal CTC loss for Chinese optical character recognition on unbalanced datasets," *Complexity*, vol. 2019, no. 1, Article ID 9345861, 11 pages, 2019.

Hindawi
Mobile Information Systems
Volume 2022, Article ID 1642988, 13 pages
https://doi.org/10.1155/2022/1642988

Research Article

An Improved Online Folk Sports Culture Exchange Model Based on Multimedia Data Analysis and Edge Computing

Sheng-li Cui[1] and Kalra Anurag[2]

[1]*Sports and Health College, Sanming University, Fujian, Sanming 365004, China*
[2]*Ecological and Environmental Research Center, Kyrgyz-Turkish Manas University, Bishkek, Kyrgyzstan*

Correspondence should be addressed to Kalra Anurag; anurag@email.cu.edu.kg

Received 14 July 2022; Revised 10 August 2022; Accepted 12 August 2022; Published 5 September 2022

Academic Editor: Chi Lin

In order to improve the effect of folk sports cultural exchange, this study proposes an improved online folk sports cultural exchange model based on multimedia data analysis and edge computing. Moreover, this study explores the factors that affect the local popularity of media content and establishes a relationship model between user request volume and edge node location characteristics. In addition, this study designs customized edge storage strategies under different conditions, which effectively increases the amount of user requests processed by edge nodes and enhances the agility of edge nodes to respond to user content requests. Finally, in order to improve the effectiveness of content crowdsourcing collection, the edge platform needs to select the optimal set of participants to complete the content collection task under a given task budget. The experimental research shows that the improved online folk sports culture exchange model based on multimedia data analysis and edge computing can realize the effective exchange of folk culture.

1. Introduction

Culture belongs to the field of ideology and obeys the law that material determines consciousness, and changes at the level of material form will also lead to corresponding changes at the level of culture. The main source of folk culture is a cultural belief, and many folk sports activities are derived from belief worship. For example, the "Maogus" of the Tujia people in western Hunan originated from the worship of reproductive organs. The peacock dance of the Dai people in Yunnan originates from the fact that the local residents regard the peacock as the spiritual symbol of their own nation, thus imitating the dance of the peacock to express their ideals and wishes. Moreover, traditional folk sports activities transcend the closure and restrictions of primitive beliefs, transcend their own national and regional restrictions, and spread to a wider area and receive a higher degree of acceptance. For example, wrestling, which is prevalent in the life of the Yi nationality people, was originally a religious sacrifice for the Yi nationality people to entertain the gods in order to pray for good weather and prosperity of the six animals. With the development of society, people have a better understanding of nature, and the religious sacrificial color of wrestling activities of the Yi nationality gradually fades, but it still reflects strong cultural and folk customs.

In addition to the influence from modern cultural civilization, Western sports culture, which is the dominant sports culture in the world today, has also had a great impact on the ecology of traditional folk sports culture. Comparing the natural ecosystem with the cultural ecosystem, the traditional folk sports culture is like the rice we often eat, while the western sports culture is like the corn that we are very common now. Corn originates from Central America and was introduced to China during the Ming Dynasty in the sixteenth century. Now China is the second largest corn producer in the world, and one of the main grains for the people in the wadi regions of northern and southwestern China. It is almost equal to rice, its economic value and use value are no less than that of rice, and it has more advantages

than rice as feed for livestock. Compared with the local folk sports culture ecosystem, Western sports culture is a kind of foreign cultural species. It already has a mature and close cultural system, its adaptability and influence are greater than that of traditional folk sports culture, and its expansion is relatively stronger. It is undeniable that Western sports culture spreads rapidly in China like corn, and even its development level far exceeds that of traditional folk sports, and its acceptance is quite high. Moreover, under the trend of global economic integration, the invasion of foreign cultures is almost inevitable. In the face of this irreversible trend, we should not blindly reject it, but should "take what is long and make up for our shortcomings" and adjust together. And adapt to the new cultural ecosystem, strive to seek common ground while reserving differences, and achieve a win-win situation. Moreover, Western sports culture is not without merit. On the one hand, it brings a more advanced sports culture and a more active sports spirit, and also brings a sense of crisis and competition to folk sports culture, as well as opportunities and challenges., forcing folk sports out of the closed circle to cross geographical restrictions and spread to a wider area.

This study proposes an improved online folk sports culture exchange model based on multimedia data analysis and edge computing to improve the effect of online folk sports culture exchange.

2. Related Work

Regarding the definition of the concept of folk sports, scholars use different disciplinary theories to define it from different angles. Literature [1] believes that "folk sports is a collection of diverse sports and games". The common element of this collection is the formation of customs among the people and is related to folk culture. Folk sports include traditional sports, National sports, indigenous sports, and games also include new sports activities based on traditional behaviors, such as bar games, and noncompetitive walks. Folk sports correspond to modern sports and are closer to all sports for the public [2]. Literature [3] pointed out according to the connotation of "custom" of folklore: "The ontology attribute of folklore sports lies in the ontology attribute of folklore. Folklore sports are created by certain people, inherited and enjoyed by certain people, and integrated into and attached to it. A collective, patterned, traditional, and daily sports activity in the customs and habits of people's daily life (such as festivals, etiquette, etc.) is not only a sports culture but also a life culture. Literature [4] defines folk sports from the perspective of cultural forms as: "The sports form spread in folk customs or folk culture and folk way of life is a special kind of sports that is produced and developed to meet and meet the various needs of the people cultural form". Literature [5] believes that from the perspective of life mode: "Folk sports refers to the sports life mode that the people (the common people) have inherited from generation to generation in social life, and it is a social group in sports language, behavior, and psychology." Literature [6] believes that: "Folk sports is a form of activity related to fitness, entertainment, competition, and performance that is produced in folk activities, depends on the development of folk festivals, and spreads in a certain time and space." "Folk custom sports is a kind of physical exercise cultural habit that a nation slowly co-creates and forms a tradition in the place where it lives." It has a common national outlook on life, long-standing living habits, and typical behavior patterns. The physical exercise of this nation's culture must use gross muscle activity as a way to increase health and use the educational opportunities of physical activity to cultivate the ability of social life and achieve the purpose of education for the balanced development of body and mind [7]. In addition to the folk sports in the school sports, the more important thing is the activities in the social and folk welcome games and festivals.

Regarding the research on the characteristics of folk sports, the literature pointed out that folk sports have internal characteristics such as competition, entertainment, dependence, ethnic differences, and commonality of all human beings, while external characteristics include historical, regional, inheritance, Variability and ornamental. Literature [9] pointed out that the characteristics of folk sports are: people's ideas and intentions to participate in folk sports activities are relatively clear, mainly from beliefs and tendencies of passion; there is a considerable time and space span of tradition; relatively strict normative, participants can consciously respect and maintain; have a certain universality; focus on mass activities, with very competitive characteristics; obvious social benefits; most projects have more or less religious colors. It is believed that the characteristics of sports folklore are the embodiment of the internal form of folklore events, which are mainly nationality, regionality, inheritance, variability, collectivity, and program. In the research on the characteristics of folk sports, most scholars are based on the essential attribute of folk sports, and by grasping the characteristics of folk sports, they summarize the universal characteristics of folk sports [10]. Most of the studies on the characteristics of these folk sports are macroscopic and general studies, and there are few studies on the characteristics of regional folk sports from a microscopic perspective. "Commonality resides in individuality", the research on the characteristics of regional folk sports is an important guarantee for the general research on the characteristics of folk sports, and the research on the characteristics of regional folk sports needs to be further improved [11]. Regarding the classification of folk sports, folk sports are divided into: running, jumping, throwing, gymnastics, ball, water, shooting, riding, wrestling, martial arts, dance, and games according to the form and content of sports and others [12]. Literature [13] divides folk sports into Han folk sports and ethnic minority folk sports according to nationality and physical education. Literature [14] divides folk sports into: playful entertainment, competition, and festival customs according to the application of folk sports in physical education courses. Literature [15] is divided into traditional labor production, folk sports in daily life, Chinese marriage custom culture, folk sports in festivals, flower fairs, temple fairs, and folk sports in sacrificial rituals. Literature [16] classifies the folk sports culture in traditional festivals and divides them into the sports of gambling and

competition in festivals and the sports of entertainment and viewing in festivals according to the nature of the activities. Due to the different research perspectives and classification standards chosen by different scholars, the classification of folk sports is also different. The above classification of folk sports will provide a certain literature for the classification of traditional festival folk sports in this study.

3. Multimedia Content Storage Strategy Based on Location Characteristics of Edge Nodes

The d-dimensional vector $x_{f,n} \in \mathbb{R}^d$ represents the parameter vector of file f at edge node n. Taking video content as an example, this parameter can describe the video's definition, style, theme, length, and historical data requested at an edge node (Figure 1). We assume that $d_{f,n}$ represents the request volume of file f at the edge node n, and we assume that the following linear model exists:

$$d_{f,n} = \mathbf{x}_{f,n}^{\mathrm{T}} \boldsymbol{\theta}_n^* + w_n. \tag{1}$$

Among them, $\theta_n^* \in \mathbb{R}^d$ is the position feature vector of the edge node n to be predicted. In the actual scene, the position feature vector will change with time. w_n is the random noise associated with edge node n. It is affected by many factors, including the social function of the node's location, the number of users served, and the frequency of stored content updates.

We assume that the set $\mathscr{F} = \{1, 2, \ldots, F\}$ is the set of all storable files, and denote the storage capacity at each edge node by $c < F$. The model divides time into a series of time slots $\mathscr{T} = \{1, 2, \ldots, T\}$, and sets $\mathscr{F}_{n,t}$ to be the set of files stored at edge node n in time slot t, while setting $d_{f,n,t}$ to be the amount of requests for file f at edge node n in time slot t. The goal of formulating the storage strategy in this study is to maximize the average number of requests processed locally within each time slot. Its mathematical description is as follows:

$$\max \frac{1}{T} \sum_{t \in \mathscr{T}} \sum_{n \in \mathscr{N}} \sum_{f \in \mathscr{F}_{n,t}} d_{f,n,t}, \tag{2}$$

$$\text{Subject to} \left| \mathscr{F}_{n,t} \right| \le c, \quad \forall n \in \mathscr{N}, t \in \mathscr{T}. \tag{3}$$

Since the user's request volume is unknown, the set $\mathscr{F}_{n,t}$ of stored files is also unknown, and the above optimization problem cannot be solved directly. To this end, we solve the above optimization problem by approaching the optimal storage strategy. We assume that $\mathscr{F}_{n,t}^*$ represents the optimal set of timeslot t stored at node n, then for $\forall n \in \mathscr{N}, t \in \mathscr{T}$, we have

$$\mathscr{F}_{n,t}^* = \underset{\left|\mathscr{F}_{n,t}\right| \le c}{\operatorname{argmax}} \sum_{f \in \mathscr{F}_{n,t}} d_{f,n,t}. \tag{4}$$

For any given storage strategy, the time-averaged storage utility loss function $R(t)$ is defined as follows:

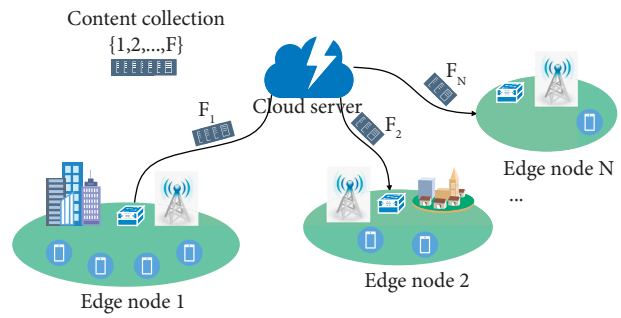

Figure 1: Edge storage system model.

$$R(T) = \frac{1}{T} \mathbb{E}\left[\sum_{t \in T} \sum_{n \in \mathscr{N}} \left(\sum_{f \in \mathscr{F}_{n,t}^t} d_{f,n,t} - \sum_{f \in \mathscr{F}_{n,t}} d_{f,n,t} \right) \right]. \tag{5}$$

Then, the problem of maximizing content requests described in formula (2) can be transformed into the following problem:

$$\min_{\mathscr{F}_{n,t}, \forall n \in \mathscr{N}, t \in \mathscr{T}} R(T). \tag{6}$$

Considering that the noise process described by the linear model 1 is an ideal zero-mean scene, at this time, the influence of various uncertain factors at the edge node n on the user's request volume has a mean value of zero. That is, $\mathbb{E}[w_n] = 0$. From formula (1), we can obtain:

$$\mathbb{E}\left[d_{f,n} \mid \mathbf{x}_{f,n} \right] = \mathbf{x}_{f,n}^{\mathrm{T}} \boldsymbol{\theta}_n^*. \tag{7}$$

Specifically, least squares estimation is the solution to the following problems:

$$\boldsymbol{\theta}_n^* = \underset{\boldsymbol{\theta}_n}{\operatorname{argmin}} \left\| \mathbf{y}_{f,n} - \boldsymbol{\Phi}_{f,n} \boldsymbol{\theta}_n \right\|^2. \tag{8}$$

Among them, $\mathbf{y}_{f,n} \in \mathbb{R}^m$ is the historical request vector of the file f at the edge node n, and $\Phi_{f,n} \in \mathbb{R}^{m \times d}$ is the parameter matrix composed of the corresponding historical parameter vector. Accordingly, the unbiased estimate of θ_n^* can be obtained as $\theta_n^* = (\Phi_{f,n}^{\mathrm{T}} \Phi_{f,n})^{-1} \Phi_{f,n}^{\mathrm{T}} \mathbf{y}_{f,n}$.

Compared with the unbiased estimation of least squares, ridge regression can solve the problem of \$3.8\$ and get a biased but more stable estimation. Specifically, ridge regression adds a penalty term when solving the minimization problem of (8), as follows:

$$\boldsymbol{\theta}_n^* = \underset{\boldsymbol{\theta}_n}{\operatorname{argmin}} \left(\left\| \mathbf{y}_{f,n} - \boldsymbol{\Phi}_{f,n} \boldsymbol{\theta}_n \right\|^2 + \mu \left\| \boldsymbol{\theta}_n \right\|^2 \right). \tag{9}$$

Among them, $\mu > 0$ is a constant, which controls the size of the estimator. The larger the μ, the smaller the magnitude of θ_n. Thus, a more stable estimation of θ_n^* can be obtained, and the explicit expression of the estimation result is

$$\boldsymbol{\theta}_n^* = \left(\boldsymbol{\Phi}_{f,n}^{\mathrm{T}} \boldsymbol{\Phi}_{f,n} + \mu \mathbf{I}_d \right)^{-1} \boldsymbol{\Phi}_{f,n}^{\mathrm{T}} \mathbf{y}_{f,n}. \tag{10}$$

Among them, $\mathbf{I}_d$ is a D-dimensional unit matrix. To simplify the formula symbol, $\mathbf{V}_{f,n} = \Phi_{f,n}^{\mathrm{T}} \Phi_{f,n} + \mu \mathbf{I}_d$ is defined, and the error of the ridge regression estimate is analyzed.

We assume $\mathbf{h}_{f,n} = \Phi_{f,n}^{\mathrm{T}}\mathbf{y}_{f,n}$, and the ridge regression estimation error can be rewritten as:

$$\left|\mathbf{x}_{f,n}^{\mathrm{T}}\widetilde{\boldsymbol{\theta}}_n - \mathbf{x}_{f,n}^{\mathrm{T}}\boldsymbol{\theta}_n^*\right| = \left|\mathbf{x}_{f,n}^{\mathrm{T}}\mathbf{V}_{f,n}^{-1}\mathbf{h}_{f,n} - \mathbf{x}_{f,n}^{\mathrm{T}}\mathbf{V}_{f,n}^{-1}\left(\boldsymbol{\Phi}_{f,n}^{\mathrm{T}}\boldsymbol{\Phi}_{f,n} + \mu\mathbf{I}_d\right)\boldsymbol{\theta}_n^*\right|. \tag{11}$$

$$= \left|\mathbf{x}_{f,n}^{\mathrm{T}}\mathbf{V}_{f,n}^{-1}\boldsymbol{\Phi}_{f,n}^{\mathrm{T}}\left(\mathbf{y}_{f,n} - \boldsymbol{\Phi}_{f,n}\boldsymbol{\theta}_n^*\right) - \mu\mathbf{x}_{f,n}^{\mathrm{T}}\mathbf{V}_{f,n}^{-1}\boldsymbol{\theta}_n^*\right|. \tag{12}$$

Due to $\|\theta_n^*\| \le \zeta$, according to Hölder inequality $|\mu\mathbf{x}_{f,n}^{\mathrm{T}}\mathbf{V}_{f,n}^{-1}\theta_n^*| \le \zeta\mu\|\mathbf{x}_{f,n}^{\mathrm{T}}\mathbf{V}_{f,n}^{-1}\|$ is established. Then, the estimated error in the formula (12) can be further written as

$$\begin{aligned}\left|\mathbf{x}_{f,n}^{\mathrm{T}}\widetilde{\boldsymbol{\theta}}_n - \mathbf{x}_{f,n}^{\mathrm{T}}\boldsymbol{\theta}_n^*\right| &\le \left|\mathbf{x}_{f,n}^{\mathrm{T}}\mathbf{V}_{f,n}^{-1}\boldsymbol{\Phi}_{f,n}^{\mathrm{T}}\left(\mathbf{y}_{f,n} - \boldsymbol{\Phi}_{f,n}\boldsymbol{\theta}_n^*\right)\right| \\ &+ \zeta\mu\left\|\mathbf{x}_{f,n}^{\mathrm{T}}\mathbf{V}_{f,n}^{-1}\right\|.\end{aligned} \tag{13}$$

Two nonequivalent right sides are variance (Variance) and deviation (Bias) in the ridge regression estimation error, respectively.

It can be seen from the formula (7) $\mathbb{E}[\mathbf{y}_{f,n} - \Phi_{f,n}\theta_n^*] = 0$. If the requests of each content are independent of each other, the McDiarmid inequality of the Azuma inequality can be obtained by the following variance probability:

$$\begin{aligned}&\mathbb{P}\left\{\left|\mathbf{x}_{f,n}^{\mathrm{T}}\mathbf{V}_{f,n}^{-1}\boldsymbol{\Phi}_{f,n}^{\mathrm{T}}\left(\mathbf{y}_{f,n} - \boldsymbol{\Phi}_{f,n}\boldsymbol{\theta}_n^*\right)\right| > \delta\left\|\mathbf{x}_{f,n}\right\|_{\mathbf{V}_{f,n}^{-1}}\right\} \le \\ &\qquad 2\exp\left(-\frac{2\delta^2\left\|\mathbf{x}_{f,n}\right\|_{\mathbf{V}_{f,n}^{-1}}^2}{\left\|\mathbf{x}_{f,n}^{\mathrm{T}}\mathbf{V}_{f,n}^{-1}\boldsymbol{\Phi}_{f,n}^{\mathrm{T}}\right\|^2}\right) \le 2e^{-2\delta^2}.\end{aligned} \tag{14}$$

Among them, the last inequality is:

$$\begin{aligned}\left\|\mathbf{x}_{f,n}\right\|_{\mathbf{V}_{f,n}^{-1}}^2 &= \mathbf{x}_{f,n}^{\mathrm{T}}\mathbf{V}_{f,n}^{-1}\left(\boldsymbol{\Phi}_{f,n}^{\mathrm{T}}\boldsymbol{\Phi}_{f,n} + \mu\mathbf{I}_d\right)\mathbf{V}_{f,n}^{-1}\mathbf{x}_{f,n} \\ &\ge \mathbf{x}_{f,n}^{\mathrm{T}}\mathbf{V}_{f,n}^{-1}\boldsymbol{\Phi}_{f,n}^{\mathrm{T}}\boldsymbol{\Phi}_{f,n}\mathbf{V}_{f,n}^{-1}\mathbf{x}_{f,n} \\ &= \left\|\mathbf{x}_{f,n}^{\mathrm{T}}\mathbf{V}_{f,n}^{-1}\boldsymbol{\Phi}_{f,n}^{\mathrm{T}}\right\|^2.\end{aligned} \tag{15}$$

It can be seen from formula (14) that the probability that the upper boundary of the variance term of the estimation error is $\delta\|x_{f,n}\|_{V_{f,n}^{-1}}$ is not lower than $1 - 2e^{-2\delta^2}$. For the bias term, its upper bound can be directly given by the following formula:

$$\begin{aligned}\left\|\mathbf{x}_{f,n}^{\mathrm{T}}\mathbf{V}_{f,n}^{-1}\right\| &= \sqrt{\mathbf{x}_{f,n}^{\mathrm{T}}\mathbf{V}_{f,n}^{-1}\mathbf{I}_d\mathbf{V}_{f,n}^{-1}\mathbf{x}_{f,n}} \\ &\le \sqrt{\mathbf{x}_{f,n}^{\mathrm{T}}\mathbf{V}_{f,n}^{-1}\left(\boldsymbol{\Phi}_{f,n}^{\mathrm{T}}\boldsymbol{\Phi}_{f,n} + \mu\mathbf{I}_d\right)\mathbf{V}_{f,n}^{-1}\mathbf{x}_{f,n}} \\ &= \left\|\mathbf{x}_{f,n}\right\|_{\mathbf{V}_{f,n}^{-1}}.\end{aligned} \tag{16}$$

Substituting formulas (14) and (16) into (13), the following lemma holds.

Lemma 1. *If $\forall n \in \mathcal{N}$, and $\|\theta_n^*\| \le \zeta$ is established, then $\forall\delta > 0$, and the upper bound of the ridge regression estimation error is:*

$$\left|\mathbf{x}_{f,n}^{\mathrm{T}}\widetilde{\boldsymbol{\theta}}_n - \mathbf{x}_{f,n}^{\mathrm{T}}\boldsymbol{\theta}_n^*\right| \le (\delta + \zeta\mu)\left\|\mathbf{x}_{f,n}\right\|_{\mathbf{V}_{f,n}^{-1}}. \tag{17}$$

The probability of the above formula is not lower than $1 - 2e^{-2\delta^2}$.

The above lemma shows that the actual value $\mathbf{x}_{f,n}^T\theta_n^*$ of the user request quantity falls within the high probability confidence interval $[\mathbf{x}_{f,n}^{\mathrm{T}}\widetilde{\theta}_n - (\delta + \zeta\mu)\|\mathbf{x}_{f,n}\|_{\mathbf{V}_{f,n}^{-1}}, \mathbf{x}_{f,n}^{\mathrm{T}}\widetilde{\theta}_n + (\delta + \zeta\mu)\|\mathbf{x}_{f,n}\|_{\mathbf{V}_{f,n}^{-1}}]$ of the estimated value $\mathbf{x}_{f,n}^{\mathrm{T}}\widetilde{\theta}_n$, and the size of the interval is determined by the parameters δ, ζ, μ and the video content parameter matrix.

Specifically, the operation of each part is as follows.

In each time slot t, the edge node \$n\$ firstly updates the estimated $\widetilde{\theta}_{n,t}$ of its location feature vector based on the user's observation of the amount of storage content requested at the previous moment. Then, according to the linear prediction model 7, the edge node makes a prediction $\widetilde{d}_{f,n,t}$ for the content f requested by users in this time slot. Considering the influence of zero-mean noise, we add the perturbation term $p_{f,n,t}$ to the estimate of the request volume of each file and obtain the upper boundary of its request volume $\widehat{d}_{f,n,t} = \widetilde{d}_{f,n,t} + p_{f,n,t}$. Among them, there are

$$p_{f,n,t} = \alpha_t\left\|\mathbf{x}_{f,n,t}\right\|_{\mathbf{V}_{f,n}^{-1}}. \tag{18}$$

Furthermore, there is $\alpha_t = [\ln(tF^{1/2})]^{1/2} + \zeta^{\mu^\circ}$.

It is worth noting that the value of α_t is formally consistent with the upper bound of the error given by formula (11). The value form of α_t is consistent with the upper bound of the probability of Lemma 1, and there is $\alpha_t = [\ln(tF^{1/2})]^{1/2}$. Further, the probability that the upper bound of the estimated error holds is $1 - 2F^{-1}t^{-2}$. With the increase of time t, the value of the above tail probability rapidly approaches 1.

The theoretical analysis of the storage strategy is now carried out, and the specific form of the time-averaged storage utility loss function is solved. By Lemma 1, the high-probability confidence interval for the estimation error of the RPUC algorithm for the user request volume is defined as:

$$J_{f,n,t} = \left[\mathbf{x}_{f,n}^{\mathrm{T}}\widetilde{\boldsymbol{\theta}}_n - p_{f,n,t}, \mathbf{x}_{f,n}^{\mathrm{T}}\widetilde{\boldsymbol{\theta}}_n + p_{f,n,t}\right]. \tag{19}$$

We assume that event $x_{n,t} = \{\exists f \in \mathcal{F}: |d_{f,n,t} - \widetilde{d}_{f,n,t}| \ge p_{f,n,t}\}$ means that there is at least one content whose estimated value of the request volume falls outside the corresponding confidence interval, and $\overline{X}_{n,t}$ is the complementary event of event $x_{n,t}$, that is, the estimated value of the request volume of all content falls within the corresponding confidence interval. Further, $r_{n,t}$ is set to be the instantaneous storage utility loss of edge node n in time slot t. It can be seen from formula (5) that the immediate storage utility loss of edge nodes is positively related to the difference between the storage content set $\mathcal{F}_{n,t}$ and the optimal storage set $\mathcal{F}_{n,t}^*$ selected by the RPUC algorithm, that is,

$$r_{n,t} = \sum_{f\in\mathcal{F}_{n,t}^*} d_{f,n,t} - \sum_{f\in\mathcal{F}_{n,t}} d_{f,n,t}. \tag{20}$$

Moreover, the statistical mean of storage loss utility is:

$$R(T) = \frac{1}{T}\sum_{t\in T}\sum_{n\in\mathcal{N}} r_{n,t} = \frac{1}{T}\sum_{t\in\mathcal{T}}\sum_{n\in\mathcal{N}} 1_{\{x_{n,t}\}}r_{n,t} + \frac{1}{T}\sum_{t\in\mathcal{T}}\sum_{n\in\mathcal{N}} 1_{\{\overline{x}_{n,t}\}}r_{n,t}. \tag{21}$$

Among them, $1_{\{x_{n,t}\}}$ indicates the truth value function of the event. When the event $\mathcal{X}_{n,t}$ occurs, its value is 1, otherwise, it is 0. The discussion of the estimation error of the user's request amount in formula (21) is divided into two cases according to whether the event $x_{n,t}$ occurs or not, and its influence on the average storage utility is discussed accordingly.

When the event $\mathcal{X}_{n,t}$ occurs, the value of α_t indicates that $\forall n \in \mathcal{N}, t \in \mathcal{T}, f \in \mathcal{F}$, and $\mathbb{P}\left\{\left|d_{f,n,t} - \widetilde{d}_{f,n,t}\right| \geq p_{f,n,t}\right\} \leq 2F^{-1}t^{-2}$ is established. Therefore, the upper bound on the occurrence frequency of event $\mathcal{X}_{n,t}$ on the full-time scale is:

$$\begin{aligned}\sum_{t\in\mathcal{T}}\sum_{n\in\mathcal{N}} 1_{\{x_{n,t}\}} &\leq \sum_{t\in\mathcal{T}}\sum_{n\in\mathcal{N}}\sum_{f\in\mathcal{F}} \mathbb{P}\left\{\left|d_{f,n,t} - \widetilde{d}_{f,n,t}\right| \geq p_{f,n,t}\right\} \\ &\leq \sum_{t\in\mathcal{T}}\sum_{n\in\mathcal{N}}\sum_{f\in\mathcal{F}} 2F^{-1}t^{-2} = 2N\sum_{t\in\mathcal{T}} t^{-2} \\ &\leq 2N\sum_{t=1}^{\infty} t^{-2} \leq \frac{\pi^2}{3}N.\end{aligned} \tag{22}$$

Since the user request quantity $d_{f,n,t} \leq \gamma$. According to formula (20), the upper bound of the immediate storage loss can be roughly written as $r_{n,t} \leq c\gamma$, where $c = |\mathcal{F}^*_{n,t}|$ represents the storage capacity of the edge node. Accordingly, the first term on the right side of formula (21), that is, the loss of storage utility when the event $\mathcal{X}_{n,t}$ occurs, satisfies the following formula:

$$\frac{1}{T}\sum_{t\in\mathcal{T}}\sum_{n\in\mathcal{N}} 1_{\{x_{n,t}\}} r_{n,t} \leq \frac{\pi^2 c\gamma}{3T}N. \tag{23}$$

When the event $\overline{X}_{n,t}$ occurs, the predictions of the RPUC algorithm for all content requests fall within the confidence interval of high probability, so $|d_{f,n,t} - \widetilde{d}_{f,n,t}| \leq p_{f,n,t}$ is always established. From $\widehat{d}_{f,n,t} = \widetilde{d}_{f,n,t} + p_{f,n,t}$, we can obtain:

$$d_{f,n,t} - \widetilde{d}_{f,n,t} \leq 2p_{f,n,t}. \tag{24}$$

Combining formulas (20) and (24), it can be obtained that when the event $\overline{X}_{n,t}$ occurs, that is, the loss of storage utility can be defined as:

$$\begin{aligned}1_{\{\overline{x}_{n,t}\}} r_{n,t} &= \sum_{f\in\mathcal{F}^*_{n,t}\setminus\mathcal{F}_{n,t}} d_{f,n,t} - \sum_{f\in\mathcal{F}_{n,t}\mathcal{F}^*_{n,t}} d_{f,n,t} \\ &\leq \sum_{f\in\mathcal{F}^*_{n,t}\setminus\mathcal{F}_{n,t}} \widehat{d}_{f,n,t} - \sum_{f\in\mathcal{F}_{n,t}\mathcal{F}^*_{n,t}} d_{f,n,t} \qquad (25) \\ &\leq \sum_{f\in\mathcal{F}_{n,t}\setminus\mathcal{F}^*_{n,t}} \left(\widehat{d}_{f,n,t} - d_{f,n,t}\right),\end{aligned}$$

$$\leq 2\sum_{f\in\mathcal{F}_{n,t}/\mathcal{F}^*_{n,t}} p_{f,n,t}. \tag{26}$$

Among them, formula (25) is established because the content in the set $\mathcal{F}_{n,t}/\mathcal{F}^*_{n,t}$ is selected by the RPUC algorithm, so compared with the set $\mathcal{F}^*_{n,t}/\mathcal{F}_{n,t}$, the estimated value of its request volume is higher, that is:

$$\sum_{f\in\mathcal{F}_{n,t}\mathcal{F}^*_{n,t}} \widehat{d}_{f,n,t} \geq \sum_{f\in\mathcal{F}^*_{n,t}/\mathcal{F}_{n,t}} \widehat{d}_{f,n,t}. \tag{27}$$

In order to further define the immediate storage utility loss, recalling Lemmas 1 and 2, the following formulas hold:

$$\begin{aligned}\sum_{t\in\mathcal{T}}\sum_{n\in\mathcal{N}} 1_{\{\overline{x}_{n,t}\}} r_{n,t} &\leq 2\sum_{t\in\mathcal{T}}\sum_{n\in\mathcal{N}}\sum_{f\in\mathcal{F}_{n,t}/\mathcal{F}^*_{n,t}} p_{f,n,t}, \qquad (28) \\ &\leq 2c\alpha_T \sum_{t\in\mathcal{T}}\sum_{n\in\mathcal{N}} \left\|\mathbf{x}_{f,n,t}\right\|_{V^{-1}_{f,n}}, \qquad (29) \\ &\leq 2c\alpha_T \sum_{n\in\mathcal{N}} \sqrt{T\sum_{t\in\mathcal{T}} \left\|\mathbf{x}_{f,n,t}\right\|^2_{V^{-1}_{f,n}}}, \qquad (30) \\ &\leq 2c\alpha_T N\sqrt{2T\ln\frac{\left(\mu + T\eta^2/d\right)^d}{\mu}}. \qquad (31)\end{aligned}$$

Among them, inequality (28) is established because α_t increases with time, and formula (30) is established because the arithmetic average of the sequence is less than its root mean square value. Meanwhile, formula (31) can be obtained directly by applying Lemmas 1 and 2. Finally, the model substitutes formulas (31) and (23) into (21), and combines $\alpha_T = [\ln(TF^{1/2})]^{1/2} + \zeta\mu$ to get:

$$\begin{aligned}R(T) &\leq 2c\alpha_T N\sqrt{\frac{2}{T}\ln\frac{\left(\mu + T\eta^2/d\right)^d}{\mu}} + \frac{\pi^2 c\gamma}{3T}N \\ &= O\left(cN\sqrt{\frac{d\ln T}{T}\ln\left(\mu + T\eta^2/d\right)}\right).\end{aligned} \tag{32}$$

Accordingly, the following theorem holds.

Theorem 1. *If the noise of the state model is zero mean, the storage algorithm RPUC asymptotically approaches the optimal storage strategy. Its average storage utility loss function $R(T)$ is of the order of $O(cN\sqrt{d(\ln T)/T\ln(\mu + T\eta^2/d)})$. That is, when $T \longrightarrow \infty$, $R(T) \longrightarrow 0$.*

Considering the situation of a specific file at an edge node, in order to simplify the notation, we omit the subscripts f and n, and rewrite formula (1) as the following state and observation formulas:

$$\begin{cases}\boldsymbol{\theta}_{t+1} = \boldsymbol{\theta}_t, \\ d_t = \mathbf{x}_t^{\mathrm{T}}\boldsymbol{\theta}_t + w_t.\end{cases} \tag{33}$$

To predict θ^* in a dynamic environment, the following prediction loss function is defined:

$$\mathcal{J}_0 = \frac{\sum_{t=0}^{T}\left\|\boldsymbol{\theta}^* - \widetilde{\boldsymbol{\theta}}_t\right\|^2}{\left\|\boldsymbol{\theta}_0 - \widetilde{\boldsymbol{\theta}}_0\right\|^2_{P_0} + \sum_{t=0}^{T}\left|w_t\right|^2}. \tag{34}$$

Among them, $\mathbf{P}_0$ is a symmetric positive definite matrix, which is used to represent the confidence value of the initial prediction $\widetilde{\theta}_0$. When the initial prediction has high uncertainty, a small (eigenvalue) $\mathbf{P}_0$ can be used, and vice versa. The goal of the H_∞-filtering algorithm is to make a series of predictions for θ^* that minimize the numerator of the loss

function $\mathcal{J}_0$. The denominator of $\mathcal{J}_0$ can be seen as a combination of all possible initial state predictions as well as arbitrary noisy processes.

The initial state θ_0 and noise sequence combination $\{w_t\}_{t=1}^{T}$ must be carefully designed. Specifically, the game problem can be described by the following min–max optimization problem:

$$\mathcal{J}_0^* = \min_{\vec{\theta}_t} \max_{\theta_0, W_t} \mathcal{J}_0. \tag{35}$$

For the form of the prediction loss function of formula (34), it is very difficult to directly solve the above min–max optimization problem. In practical scenarios, H_∞ filtering starts from the preset parameter $\psi > 0$, and obtains the suboptimal solution of the above problem. Specifically, there are:

$$\sup \mathcal{J}_0 < \psi^2. \tag{36}$$

That is, the H_∞ filtering method attempts to control the supremum of the prediction loss function by preset parameters under the conditions of the game.

To solve the above minimum–maximization problem, we rewrite the prediction loss function as follows:

$$\min_{\boldsymbol{\theta}_t} \max_{\boldsymbol{\theta}_0, w_t} \mathcal{J} \triangleq -\frac{1}{2}\psi^2 \left\|\boldsymbol{\theta}_0 - \widetilde{\boldsymbol{\theta}}_0\right\|_{P_0}^2 + \frac{1}{2}\sum_{t=0}^{T}\left[\left\|\boldsymbol{\theta}^* - \widetilde{\boldsymbol{\theta}}_t\right\|^2 - \psi^2 |w_t|^2\right]. \tag{37}$$

The transformed min–max problem above can be viewed as a zero-sum game problem. For a given value of ψ, our optimization goal is to find a series of estimates $\{\widetilde{\theta}_t\}_{t=1}^{T}$ such that the prediction loss function $\mathcal{J} < 0$. With the help of the Lagrange multiplier method H_∞ filtering method, the solution of the above dynamic restricted optimization problem is obtained in an iterative manner. Specifically, there are:

$$\widetilde{\boldsymbol{\theta}}_{t+1} = \widetilde{\boldsymbol{\theta}}_t + \mathbf{R}_t\left(d_t - \mathbf{x}_t^{\mathrm{T}}\widetilde{\boldsymbol{\theta}}_t\right). \tag{38}$$

Among them, the initial value of $\widetilde{\theta}_t$ is $\widetilde{\theta}_0 = 0_d$, and R_t is the filter gain, which is given by the following formula:

$$\mathbf{R}_t = \mathbf{M}_t \mathbf{x}_t \left(1 + \left\|\mathbf{x}_t\right\|_{\mathbf{M}_t}^2\right)^{-1}. \tag{39}$$

Furthermore, there are:

$$\mathbf{M}_{t+1}^{-1} = \mathbf{M}_t^{-1} + \mathbf{x}_t\mathbf{x}_t^{\mathrm{T}} - \psi^{-2}\mathbf{I}_d. \tag{40}$$

Among them, the initial value of $\mathbf{M}_t^{-1}$ is $\mathbf{M}_0^{-1} = \mathbf{P}_0 - \psi^{-2}\mathbf{I}_d$.

We assume that ψ_{t+1} represents the preset error value in the $t+1$th time slot, in order to ensure that $\mathbf{M}_{t+1}^{-1}$ in formula (40) is not singular, the following formula holds:

$$\mathbf{M}_t^{-1} + \mathbf{x}_t\mathbf{x}_t^{\mathrm{T}} - \psi_{t+1}^{-2}\mathbf{I}_d > 0. \tag{41}$$

We assume that $\lambda_{\max}(\mathbf{A}) = \lambda_1(\mathbf{A}) \geq \cdots \lambda_k(\mathbf{A}) \cdots \geq \lambda_d(\mathbf{A}) = \lambda_{\min}(\mathbf{A})$ represents the eigenvalue of the d-order invertible square matrix A, and $\lambda_k(\mathbf{A})$ is the kth largest eigenvalue. According to the minimum–maximum theorem of matrix eigenvalues, ψ_{t+1} needs to satisfy the following formula:

$$\lambda_k\left(\mathbf{M}_t^{-1} + \mathbf{x}_t\mathbf{x}_t^{\mathrm{T}}\right) > \lambda_k\left(\psi_{t+1}^{-2}\mathbf{I}_d\right), \quad \forall k \in \{1, 2, \ldots d\}. \tag{42}$$

Since $\forall k \in \{1, 2, \ldots d\}$ has $\lambda_k(\psi_{t+1}^{-2}\mathbf{I}_d) = \psi_{t+1}^{-2}$ established, then $\lambda_{\min}(\mathbf{M}_t^{-1} + \mathbf{x}_t\mathbf{x}_t^{\mathrm{T}}) > \psi_{t+1}^{-2}$. For this reason, the following formula is established.

$$\psi_{t+1}^{-2} = \xi^{-2}\lambda_{\min}\left(\mathbf{M}_t^{-1} + \mathbf{x}_t\mathbf{x}_t^{\mathrm{T}}\right). \tag{43}$$

Among them, ξ is a constant close to 1 but greater than 1, which minimizes the amplitude of ψ_t and is always positive, thus ensuring that the matrix $\mathbf{M}_{t+1}^{-1}$ is always nonsingular.

Considering the crowdsourcing system model based on the edge network shown in Figure 2.

Definition 1 (first-order probability dominance). we define the cumulative distribution function $F(\pi|(\varepsilon, \zeta)) = \int_\pi^1 p(\pi'|(\varepsilon, \zeta))\mathrm{d}\pi'$ as the probability that the participant's degree of completion is higher than π when the level of willingness and ability of the participant is (ε, ζ). If $\pi \in [0, 1]$ holds for any $F(\pi|(\varepsilon, \varsigma))) \geq F(\pi|(\varepsilon', \varsigma))$, then ε is said to dominate the first-order probability of ε'.

For any function $p(\cdot)$ that satisfies the first-order probability dominance, the following lemma holds.

Lemma 2. *When users have the same ability level, the participants with a higher willingness to participate have higher task completion.*

The proof is as follows: we assume that $\varepsilon \geq \varepsilon'$, and $F'(\pi|(\varepsilon, \varsigma))$ is the cumulative distribution function of the completion probability function $p(\pi|(\varepsilon, \varsigma))$. The definition of first-order probability possession shows that the following formula holds: $F'(\pi|(\varepsilon, \varsigma)) = 1 - F(\pi|(\varepsilon, \varsigma)) \leq 1 - F(\pi|(\varepsilon', \varsigma)) \leq F'(\pi|(\varepsilon', \varsigma))$. For a participant whose willingness to participate is ε, the expected completion value is $\Pi_\varepsilon = \int_0^1 \pi p(\pi|(\varepsilon, \zeta))\mathrm{d}\pi = [\pi F'(\pi|(\varepsilon, \zeta))]_0^1 - \int_0^1 F'(\pi|(\varepsilon, \zeta))\mathrm{d}\pi = \pi - \int_0^1 F'(\pi|(\varepsilon, \zeta))\mathrm{d}\pi$. According to this, $\Pi_\varepsilon - \Pi_{\varepsilon'} = \int_0^1 [F'(\pi|(\varepsilon', \varsigma)) - F'(\pi|(\varepsilon, \varsigma))]\mathrm{d}\pi \geq 0$.. The lemma is proven.

We assume that $v(\cdot)$: $2^w \longrightarrow \mathbb{R}^+$ represents the utility metric function of the edge platform. For a selected set of participants $\mathcal{S} \subset \mathcal{W}$ and $\mathcal{A} \subseteq \mathcal{W}/\mathcal{S}$, the set function is defined as follows:

$$\Psi_v(\mathcal{A}|\mathcal{S}) = v(\mathcal{A} \cup \mathcal{S}) - v(\mathcal{S}). \tag{44}$$

The above formula is the marginal value of the participant set δ for a given participant set $\mathcal{A}$. At the same time, we assume that the participants' feedbacks are different from each other, so there is $v(\{w_1, w_2\}) > \max\{v(\{w_1\}), v(\{w_2\})\}$. The descending characteristics and monotonicity of the marginal platform utility function are defined as follows:

Definition 2 (below model characteristic). The aggregate function $v(\cdot)$: $2^W \longrightarrow \mathbb{R}^+$ is defined. If for $\mathcal{A} \subseteq \mathcal{B} \subseteq \mathcal{W}$ and $w_k \in \mathcal{W}/\mathcal{B}$, $\Psi_v(w_k|\mathcal{A}) \geq \Psi_v(w_k|\mathcal{B})$ is always established, then the set function $v(\cdot)$ has the lower model property. Correspondingly, for $\mathcal{A} \subseteq \mathcal{W}$ and $w_1, w_2 \in \mathcal{W}/\mathcal{A}$, $\Psi_v(w_1|\mathcal{A}) + \Psi_v(w_2|\mathcal{A}) \geq \Psi_v(\{w_1, w_2\}|\mathcal{A})$ holds.

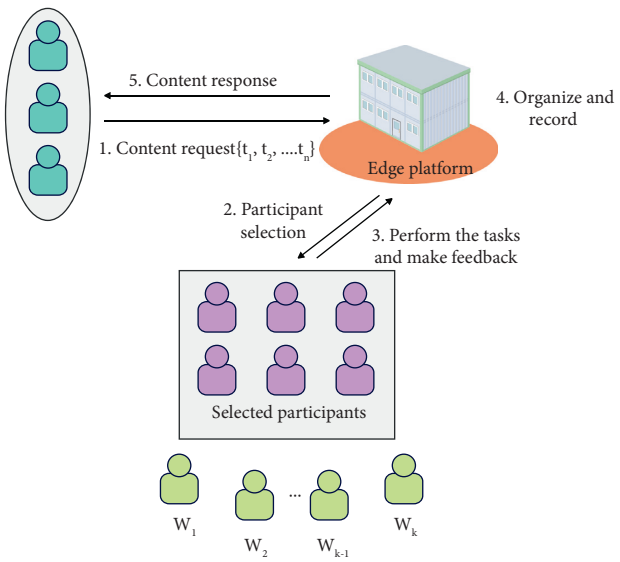

Figure 2: Crowdsourcing system model based on edge platform.

Definition 3 (monotonicity). If for any $\mathscr{A} \subseteq \mathscr{B} \subseteq \mathscr{W}$, $v(\mathscr{A}) \leq v(\mathscr{B})$ holds, then the set function $v(\cdot)$ is said to be monotonic.

The goal of an edge crowdsourcing platform is to select a set of participants δ_i to maximize its utility function, that is,

$$\delta_i = \underset{S \subseteq W, |S| \leq b}{\operatorname{argmax}}\, v_i(\delta). \tag{45}$$

The utility loss function $R(n)$ is used to characterize the cumulative utility gap between the speculative learning algorithm design algorithm and the posterior optimal strategy, that is,

$$\widetilde{R}(n) = \max_{|S| \leq b}\left[\sum_{i=1}^{n} v_i(\delta)\right] - \mathbb{E}\left[\sum_{i=1}^{n} v_i(\delta_i)\right]. \tag{46}$$

To reach the $(1 - 1/e)$-optimal, the utility loss function is changed to the following form:

$$R(n) = \left(1 - \frac{1}{e}\right) \cdot \max_{|S| \leq b} \mathbb{E}\left[\sum_{i=1}^{n} v_i(\delta)\right] - \mathbb{E}\left[\sum_{i=1}^{n} v_i(\delta_i)\right]. \tag{47}$$

It mainly solves the problem of minimizing the cumulative utility loss as follows:

$$\min_{\{\delta_i\}_{i=1}^{n}} R(n). \tag{48}$$

We define $\delta_t = \{w_j\}_{j=1}^{t}$ as the set of the first t content crowdsourcing participants selected in turn by the greedy algorithm, and $\Psi_t = \mathbb{E}[\Psi_v(w_t|(\delta_{t-1})]$ as the marginal utility gain function of the tth participant. According to the monotonicity and lower model characteristics of the utility function of the crowdsourcing platform, the following formula is established:

$$\begin{aligned} &\mathbb{E}[v(\mathscr{P})] \leq \mathbb{E}[v(\mathscr{P} \cup \delta_t)] \\ &\mathbb{E}\left[v(\delta_t) + \sum_{w_k \in \mathscr{P} \setminus \delta_t} \Psi_v w_k|(\delta_t)\right] \end{aligned} \tag{49}$$

We assume that $\widehat{v}(\cdot)$ is the perturbation utility function based on the perturbation completion degree sequence $\{\widehat{\pi}_k\}_{k=1}^{K}$, and $\widehat{\Psi}_t = \mathbb{E}[\Psi_{\widehat{v}}(w_t|(\delta_{t-1})]$ is the marginal utility gain function of the perturbation, then $\widehat{v}(w_k) \leq v(w_k) + \epsilon_k$ is established. Since in the t+1th cycle of the algorithm, w_{t+1} is selected among the remaining participants; therefore, $\forall w_k \in \mathscr{P}/\delta_t$ has $\Psi_{\widehat{v}}(w_t|(\delta_t) \geq \Psi_{\widehat{v}}(w_k|(\delta_t))$. established. Since $|\mathscr{P}/\delta_t| \leq b$, inequality 49 can be written as:

$$\mathbb{E}[v(\mathscr{P})] \leq \mathbb{E}[v(\delta_t)] + b\overset{\cap}{\Psi}t + 1. \tag{50}$$

Using the lower model properties of the utility function $v(\cdot)$, $\widehat{\Phi}_{t+1} \leq \Psi_{t+1} + \epsilon_{t+1}$ is established, and the inequality 50 can be iteratively transformed into

$$\mathbb{E}[v(\mathscr{P})] \leq \Psi_1 + \cdots \Psi_t + b\Psi_{t+1} + b\epsilon_{t+1}. \tag{51}$$

We assume $\Psi_0 = 0$, and $t = 0, 1, \ldots, b - 1$ respectively. The formula (52) can be transformed into b different inequalities. We multiply the t th inequality above by the coefficient $(1 - 1/b)^{b-1-t}$, in turn, and accumulate all the b inequalities. The coefficient of the $\mathbb{E}[v(\mathscr{P})]$ term on the left side of the obtained inequality is $\sum_{t=0}^{b-1}(1 - 1/b)^{b-1-t} = \sum_{t=0}^{b-1}(1 - 1/b)^t = b(1 - (1 - 1/b))^b$, and the coefficient of the right side term of the inequality Ψ_t is $b(1 - 1/b)^{b-t} + \sum_{i=t}^{k-1}(1 - 1/b)^{b-1-i} = b$. Hence, there are:

$$b\left(1 - (1 - 1/b)^b\right)\mathbb{E}[v(\mathscr{P})] \leq \sum_{t=1}^{b} \Psi_t + \sum_{w_k \in \mathscr{S}} \epsilon_k. \tag{52}$$

Since the inequality $b(1 - (1 - 1/b)^b) \leq e^{-1/b}$ is always established, the following theorem is established.

Theorem 2. *The upper bound of the utility gap between the expected utility of the linear greedy algorithm and the posterior optimal strategy is $\sum_{w_k \in \mathscr{E}} \epsilon_k$, that is,*

$$\mathbb{E}[v(\mathscr{S})] \geq \left(1 - \frac{1}{e}\right) \cdot \mathbb{E}[v(\mathscr{P})] - \sum_{w_k \in \mathscr{S}} \epsilon_k. \tag{53}$$

By setting the perturbation term $\epsilon_k = 0$ in Theorem 1, the single-task crowdsourcing utility of greedy algorithm 1 can reach $(1 - 1/e)$-optimal.

We assume that $\widetilde{\pi}_{i,k}$ represents the experience completion value of the participant w_k when the crowdsourcing task t_i arrives, and $\overline{\pi}_{i,k}$ represents the upper bound of the experience value. Since $\pi_k \in [0, 1]$, we have:

$$\overline{\pi}_{i,k} = \min\left\{\widetilde{\pi}_{i,k} + c_{i-1, f_{i-1}(k)}, 1\right\}. \tag{54}$$

Among them, the perturbation is as follows:

$$c_{i, f_i(k)} = \mu\sqrt{\frac{\log i}{f_i(k)}}. \tag{55}$$

Lemma 3 (Chernoff–Hoeffding inequality). *If $X_1, X_2, \ldots, X_n \in [0, 1]$ is a sequence of random variables and $\mathbb{E}[X_t|X_1, X_2, \ldots, X_{t-1}] = \xi$ is established. We assume $S_n = X_1 + X_2 + \cdots + X_n$, then for $\forall a \geq 0$, the following inequality holds:*

$$\mathbb{P}\{S_n \geq n\xi + a\} \leq e^{-2a^2/n}, \mathbb{P}\{S_n \leq n\xi - a\} \leq e^{-2a^2/n}. \tag{56}$$

By applying the Chernoff–Hoeffding inequality, the actual completion degree $\pi_{i,k}$ of the crowdsourcing task of the participants can be obtained as follows:

$$\mathbb{P}\left\{\left|\widetilde{\pi}_{i,k} - \pi_k\right| \geq c_{i,f_i(k)}\right\} \leq 2e^{-2\mu^2 \log i} = 2i^{-2\mu^2}. \tag{57}$$

That is, the disturbance term form of the formula (54) effectively guarantees: when $\mu \geq 1$, the actual completion degree π_k of the crowdsourcing task of the participants falls within the interval $[\widetilde{\pi}_{i,k} - c_{i-1,f_{i-1}(k)}, \widetilde{\pi}_{i,k} + c_{i-1,f_{i-1}(k)}]$ with a high probability.

We assume that $\mathcal{S}^* = \underset{|\mathcal{S}| \leq b}{\operatorname{argmax}} \mathbb{E}[\sum_{i=1}^n v_i(\mathcal{S})]$ represents the posterior optimal participant selection scheme for all n crowdsourcing tasks, and the set $\mathcal{P}$ is the suboptimal solution obtained in polynomial time based on the greedy algorithm. From Theorem 4.1, we can obtain:

$$\mathbb{E}\left[\sum_{i=1}^n v_i(\mathcal{P})\right] \geq \left(1 - \frac{1}{e}\right) \cdot \mathbb{E}\left[\sum_{i=1}^n v_i(\mathcal{S}^*)\right]. \tag{58}$$

We assume that δ_i represents the set of participants selected by the UCBG algorithm for the crowdsourcing task t_i and define the loss of the crowdsourcing utility of the platform after the set of participants completes the task as $R_i = \mathbb{E}[v_i(\mathcal{P})] - \mathbb{E}[v_i(\mathcal{S}_i)]$. According to the formula (47), the cumulative utility loss of the crowdsourcing platform satisfies the following formula:

$$R(n) \leq \mathbb{E}\left[\sum_{i=1}^n v_i(\mathcal{P})\right] - \mathbb{E}\left[\sum_{i=1}^n v_i(\delta_i)\right] = \sum_{i=1}^n R_i. \tag{59}$$

Since $\pi_k \in [0, 1]$ and $|\mathcal{P}| = |\mathcal{S}_i| = b$, then $R_i \leq b$ holds for $\forall t_i \in \mathcal{T}$.

We assume that event $x_i = \{\exists w_k \in \mathcal{W}: |\widetilde{\pi}_{i-1,k} - \pi_k| \geq c_{i,f_i(k)}\}$ means that when assigning participants to a crowdsourcing task t_i, there is at least one participant whose actual completion degree π_k falls outside the high confidence interval of the estimated value $\widetilde{\pi}_{i-1,k}$. We assume that $\overline{X}_i$ represents a complementary event to x_i, that is, the actual completion of π_k for all participants falls within the high confidence interval of the estimated value $\widetilde{\pi}_{i-1,k}$. Accordingly, we decompose the cumulative utility loss shown in formula (49) into the following three categories and analyze them separately:

$$R(n) \leq \sum_{i=1}^{i_0} R_i + \sum_{i=i_0+1}^n 1_{\{x_i\}} R_i + \sum_{i=i_0+1}^n 1_{\{\overline{x}_i\}} R_i. \tag{60}$$

Here, $1_{\{x_i\}}$ is an indicator function; when the event x_i occurs, its value is 1, otherwise, its value is 0.

Since all participants are selected at most once in the initialization phase of the algorithm, the utility loss in this phase satisfies the following formula:

$$\sum_{i=1}^{i_0} R_i \leq i_0 b \leq K. \tag{61}$$

In the online selection stage, the cumulative frequency of event x_i can be obtained from the Chernoff–Hoeffding inequality to satisfy the following formula:

$$\begin{aligned}\sum_{i=i_0+1}^n 1_{\{x_i\}} &\leq \sum_{w_k \in \mathcal{W}} \sum_{i=1}^n \sum_{f=1}^i \mathbb{P}\left\{\left|\widetilde{\pi}_{i,k} - \pi_k\right| \geq c_{i,f_i(k)}\right\} \\ &\leq 2 \sum_{w_k \in \mathcal{W}} \sum_{i=1}^n \sum_{f=1}^i i^{-2\mu^2} \\ &\leq 2K \sum_{i=1}^\infty i^{-2\mu^2+1}.\end{aligned} \tag{62}$$

When $\mu^2 \geq 3/2$, $\sum_{i=1}^\infty i^{-2\mu^2+1} \leq \sum_{i=1}^\infty i^{-2} = \pi^2/6$ holds. Since $R_i \leq b$ holds for $\forall t_i \in \mathcal{T}$, the second term on the right-hand side of Inequality (59) satisfies the following formula:

$$\sum_{i=i_0+1}^n 1_{\{x_i\}} R_i \leq \pi^2 \frac{Kb}{3}. \tag{63}$$

When the event $\overline{X}_i$ occurs in the online selection stage, the actual completion degree π_k of all participants falls within the high confidence interval of the estimated value $\widetilde{\pi}_{i-1,k}$, that is, for $\forall w_k \in \mathcal{W}$, $\pi_k - c_{i-1,f_{i-1}(k)} \leq \widetilde{\pi}_{i-1,k} \leq \pi_k + c_{i-1,f_{i-1}(k)}$ holds. From $\pi_k \in [0, 1]$ and $\overline{\pi}_{i,k} = \min\{\widetilde{\pi}_{i,k} + c_{i-1,f_{i-1}(k)}, 1\}$, the following inequality holds:

$$\pi_k \leq \widetilde{\pi}_{i,k} \leq \pi_k + 2c_{i-1,f_{i-1}(k)}. \tag{64}$$

For the sake of brevity, the intersection $\mathcal{J}_i = \delta_i \cap \mathcal{P}$ is defined, and the complements $\delta_i^d = \delta_i/\mathcal{P}, \mathcal{P}_i^d = \mathcal{P}/\delta_i$ are defined. The utility loss for completing the crowdsourcing task t_i is rewritten as:

$$\begin{aligned}R_i &= \mathbb{E}\left[v_i(\mathcal{J}_i) + \Psi_{v_i}\left(\mathcal{P}_i^d | \mathcal{J}_i\right)\right] - \mathbb{E}\left[v_i(\mathcal{J}_i) + \Psi_{v_i}\left(\mathcal{S}_i^d | \mathcal{J}_i\right)\right] \\ &= \mathbb{E}\left[\Psi_{v_i}\left(\mathcal{P}_i^d | \mathcal{J}_i\right)\right] - \mathbb{E}\left[\Psi_{v_i}\left(\delta_i^d | \mathcal{J}_i\right)\right].\end{aligned} \tag{65}$$

At the same time, $\overline{v}(\cdot)$ represents the upper bound function of crowdsourcing utility calculated based on participant completion degree UCB. Since the participant set δ_i is selected by the algorithm, the upper bound of its crowdsourcing utility is higher than the upper bound of the crowdsourcing utility obtained by the posterior optimal participant set $\mathcal{P}$, that is, $\overline{v}_i(s_i) \geq \overline{v}_i(\mathcal{P})$. Furthermore, the following inequality holds:

$$\Psi_{\overline{v}_i}\left(\delta_i^d \mid \mathcal{J}_i\right) \geq \Psi_{\overline{v}_i}\left(\mathcal{P}_i^d \mid \mathcal{J}_i\right). \tag{66}$$

According to the lower model properties of the utility function and inequality (63), the independent utility upper bound for a single player satisfies the following formula:

$$\mathbb{E}\left[v_i(w_k)\right] \leq \overline{v}_i(w_k) \leq \mathbb{E}\left[v_i(w_k)\right] + 2c_{i-1,f_{i-1}(k)}. \tag{67}$$

Accordingly, for the participant set S_i^d, the upper bound of its marginal utility gain relative to the set J_i satisfies the following inequality:

$$\Psi_{\overline{v}_i}\left(\delta_i^d|\mathcal{J}_i\right) \le \mathbb{E}\left[\Psi_{v_i}\left(\delta_i^d|\mathcal{J}_i\right)\right] + 2\sum_{w_k\in\mathcal{S}_i^d} c_{i-1,f_{i-1}(k)}. \tag{68}$$

Meanwhile, the inequality holds as follows:

$$\Psi_{\overline{v}_i}\left(\mathcal{P}_i^d|\mathcal{J}_i\right) \ge \mathbb{E}\left[\Psi_{v_i}\left(\mathcal{P}_i^d|\mathcal{J}_i\right)\right]. \tag{69}$$

The inequalities (65), (66), (68), and (69) can be combined to obtain that when the event $\overline{X}_i$ occurs, that is, when the utility loss satisfies the following formula:

$$R_i \le 2\sum_{w_k\in\mathcal{S}_i^d} c_{i-1,f_{i-1}(k)}. \tag{70}$$

The set of participants with fewer selections in set δ_i^d is as follows:

$$\mathcal{Q}_i \triangleq \left\{w_k \in \mathcal{S}_i^d:\ f_{i-1}(k) \le \alpha \log n\right\}. \tag{71}$$

Accordingly, the following two events are defined:

$$\begin{aligned} y_i^1 &= \left\{|Q_i| \ge \gamma\right\}, \\ y_i^2 &= \left\{|Q_i| < \gamma, \left[\exists w_k \in \mathcal{S}_i^d:\ f_{i-1}(k) \le \beta \log n\right]\right\}. \end{aligned} \tag{72}$$

Among them, α and β are positive constants. $R_{\min} = \min_i R_i$, the following lemma can directly get the cumulative utility loss when the event $\overline{X}_i$ occurs.

Lemma 4. *When event $\overline{x}_i$ occurs, $0 < \gamma \le b, \alpha = 16\mu^2 b^2/R_{min^2}, \beta = 16\mu^2\gamma^2/R_{min^2}$, then one of event y_i^1 and event y_i^2 must happen. The cumulative frequency of event y_i^1 and event y_i^2 satisfies $\sum_i 1_{\{y_i^1\}} \le (K/\gamma)\alpha \log n$ and $\sum_i 1_{\{y_i^2\}} \le (K\beta \log n/\gamma)$, respectively.*

The above lemma can be briefly proved in two steps as follows. First, the event is defined as follows:

$$\overline{y}_i = \left\{|Q_i| < \gamma, \left[\forall w_k \in \delta_i^d:\ f_{i-1}(k) > \beta \log n\right]\right\}. \tag{73}$$

The above definition shows that events y_i^1, y_i^2, and $\overline{y}_i$ are mutually exclusive events, and the sum of their probability of occurrence is 1. Therefore, if event $\overline{y}_i$ does not occur, then one event y_i^1 and event y_i^2 must occur. It is now proved that event $\overline{y}_i$ cannot happen because of the following paradox:

$$\begin{aligned} R_i &\le 2\sum_{w_k\in\mathcal{S}_i^d} c_{n,f_{i-1}(k)} \\ &= 2\sum_{w_k\in\mathcal{S}_i^d/Q_i} c_{n,f_{i-1}(k)} + 2\sum_{w_k\in\mathcal{Q}_i} c_{n,f_{i-1}(k)}, \end{aligned} \tag{74}$$

$$\begin{aligned} &< 2\mu b\sqrt{\frac{\log n}{\alpha \log n}} + 2\mu\gamma\sqrt{\frac{\log n}{\beta \log n}} \\ &= R_{\min}. \end{aligned} \tag{75}$$

We assume $R_{\max} = \max_i R_i$; according to Lemma 3, the third term of formula (60) satisfies the following formula:

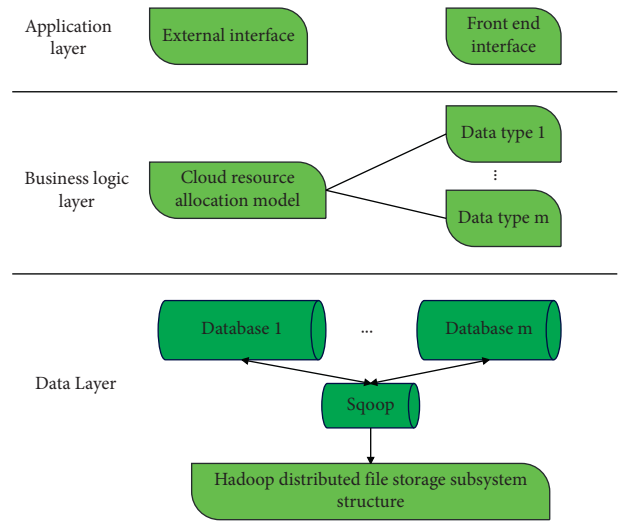

Figure 3: The structure diagram of the optimization system of folk sports cultural resources based on cloud platform. The structure of the Hadoop distributed file storage subsystem is shown in Figure 4.

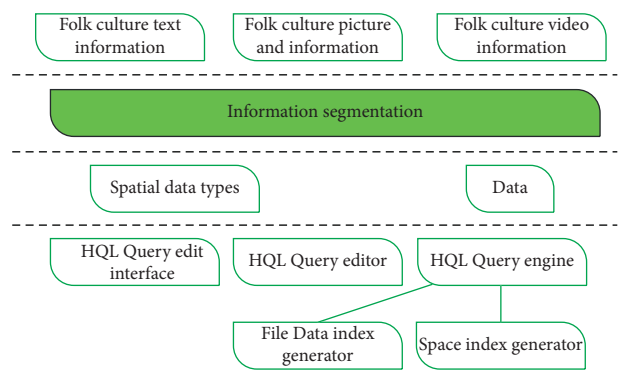

Figure 4: Structure diagram of distributed file storage subsystem.

$$\begin{aligned} \sum_{i=i_0+1}^{n} 1_{\{\overline{x}_i\}} R_i &\le R_{\max} \sum_{i=i_0+1}^{n} \left(1_{\{y_i^1\}} + 1_{\{y_i^2\}}\right) \\ &\le 16\mu^2 K\left(\frac{b^2}{\gamma} + \gamma^2\right)\frac{R_{\max}}{R_{\min^2}}\log n. \end{aligned} \tag{76}$$

We assume $\gamma = b^{2/3}$, and substitute formulas (61), (63), and (75) into formula (60) to obtain the mean cumulative crowdsourcing utility that satisfies the following formula:

$$R(n) = 32\mu^2 K b^{4/3}\frac{R_{\max}}{R_{\min^2}}\log n + \frac{\pi^2}{3}Kb + K. \tag{77}$$

It can be seen from the above formula: when $n \longrightarrow \infty$, $R(n)/n \longrightarrow 0$. Therefore, the above theorem holds.

4. An Improved Online Folk Sports Culture Exchange Model Based on Multimedia Data Analysis and Edge Computing

Through the edge computing mentioned above, the data processing of cultural and communication platforms is

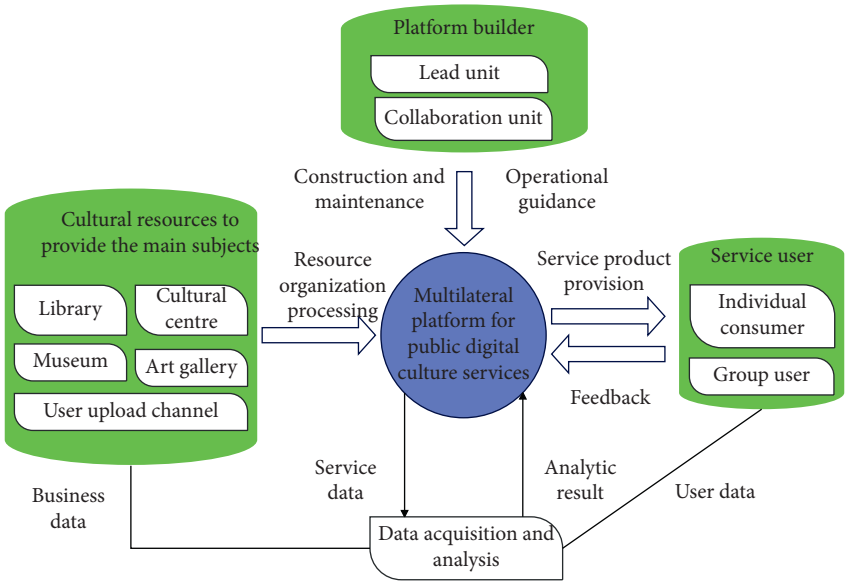

Figure 5: Conceptual framework of the multilateral platform for public digital cultural services.

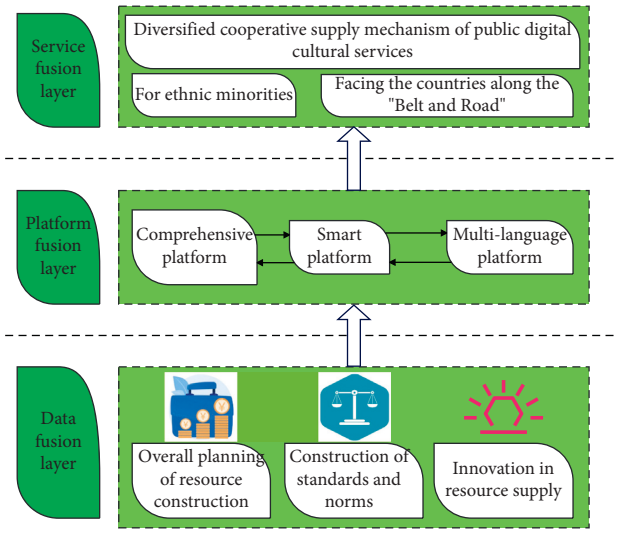

Figure 6: Model of the integration path of public digital cultural resource.

carried out to improve the efficiency of data sharing. Figure 3 shows the structure of the folk culture resource optimization system based on the multimedia data platform. The system is divided into the application layer, business logic layer, and data layer. The application layer mainly serves users, and users can log into the system on the front-end interface of the system, and the external interface is the communication carrier between the application layer and the business logic layer. The business logic layer can schedule diverse folk sports and cultural resources according to user requests. The data layer provides distributed storage services for folk sports and cultural resources. Hadoop is a distributed file storage system composed of a variety of databases, and the database uses the open source tool Sqoop to realize the transmission of folk sports and cultural resources. This distributed file storage system has good stability, and the storage of folk sports and cultural resources has extremely high security. Therefore, users can make full use of the advantages of cloud platform clusters for fast resource scheduling and storage without knowing the underlying details of the distribution.

The multilateral platform for public digital cultural services takes co-construction, co-governance, and sharing as the strategic goal, and its service principles are inclusive, open, and equal. According to the development status of public digital cultural services and the multilateral platform model introduced above, this research constructs a conceptual framework of multilateral platforms for public digital cultural services that conforms to the characteristics of public digital cultural services (Figure 5).

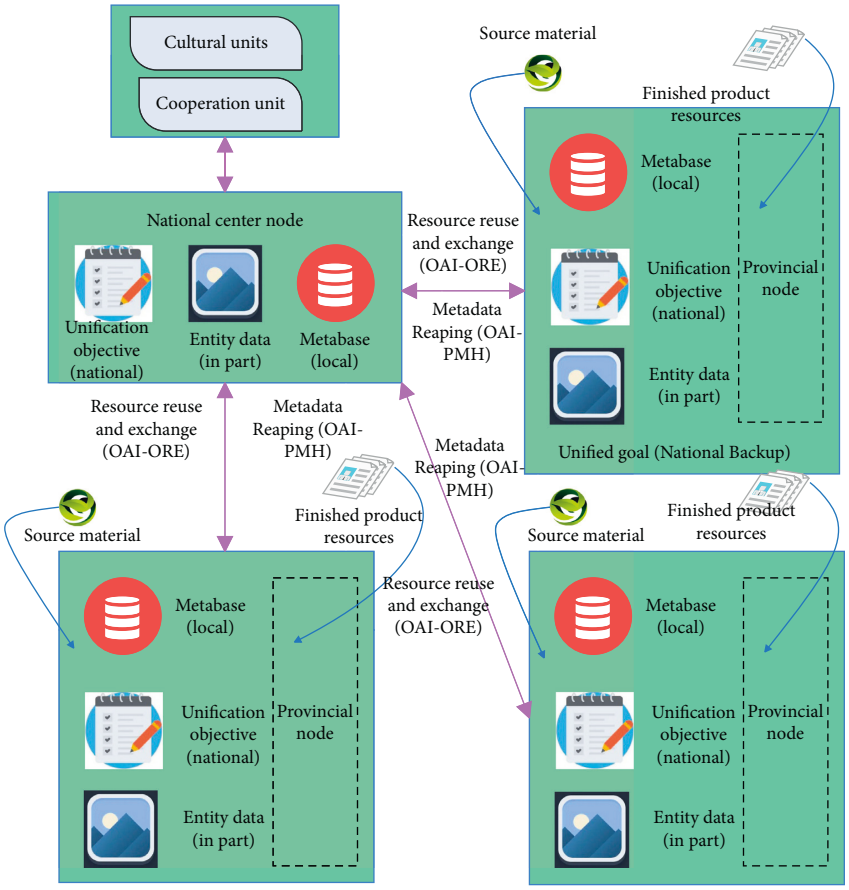

Figure 7: Resource sharing mode.

(a) (b) (c)

Figure 8: Example of folk sports culture. (a) Example 1 of folk sports culture. (b) Example 2 of folk sports culture. (c) Example 3 of folklore sports culture.

From the perspective of resource integration, this study proposes a bottom-up overall construction idea from the three levels of data, platform, and service, and builds a path model for the integration of public digital cultural resources, as shown in Figure 6.

In order to achieve nationwide resource sharing, a unified interoperability model for national resources is defined, as shown in Figure 7. Provincial nodes and national central nodes save their own resource data, including material and finished product resources and metadata of resources, as well as the local resource directory of the node.

Figure 8 shows an example of folk sports culture. In the cultural exchange model constructed in this study, the feature extraction of the above folk culture can be realized, which is convenient to achieve effective folk culture sharing. On this basis, the effect of the folk culture communication model in this study is verified, and the results shown in Table 1 are obtained.

It can be seen from the above research that the improved online folk sports culture exchange model based on multimedia data analysis and edge computing can realize the effective exchange of folk culture.

Table 1: Improved online folk sports culture exchange model based on multimedia data analysis and edge computing.

Number	Cultural exchange
1	91.07
2	93.06
3	89.73
4	89.95
5	92.44
6	91.67
7	89.34
8	93.39
9	93.74
10	93.07
11	92.06
12	88.68
13	91.02
14	87.09
15	92.84
16	88.38
17	92.59
18	91.91
19	90.19
20	88.69
21	91.82
22	88.11
23	87.26
24	90.31
25	90.91
26	87.33
27	89.13
28	88.91
29	93.52
30	89.91
31	91.62
32	93.78
33	91.91
34	88.72
35	90.30
36	92.28
37	88.27
38	92.70
39	93.35
40	87.25

5. Conclusion

Changes in cultural beliefs can most directly reflect changes in folk sports activities. With the improvement of people's material living standards and cultural level, the folk sports activities that were originally intended to entertain gods and pray for good fortune, physical fitness or force to protect one's family, and entertainment have now evolved into cultural and entertainment activities that focus on entertainment and performance, which have completely lost the seriousness and sublime of cultural beliefs. On the other hand, these changes are not without merit. On the contrary, it reflects the adaptation and adjustment of folk culture to modern culture. This study proposes an improved online folk sports culture communication model based on multimedia data analysis and edge computing. The experimental study shows that the improved online folk sports culture communication model based on multimedia data analysis and edge computing can realize the effective communication of folk culture.

Data Availability

The data that support the findings of this study are available from the corresponding author upon reasonable request.

Conflicts of Interest

The authors declare no potential conflicts of interest with respect to the research, authorship, and/or publication of this article.

Acknowledgments

Fujian Provincial Social Science Fund Project (project no. FJ2021B139) and National Social Science Fund Cultivation Project of Sanming University (project no. PYS2005).

References

[1] M. Li, Z. Zhou, and X. Liu, "Multi-person pose estimation using bounding box constraint and LSTM," *IEEE Transactions on Multimedia*, vol. 21, no. 10, pp. 2653–2663, 2019.

[2] J. Xu, K. Tasaka, and M. Yamaguchi, "[Invited paper] fast and accurate whole-body pose estimation in the wild and its applications," *ITE Transactions on Media Technology and Applications*, vol. 9, no. 1, pp. 63–70, 2021.

[3] G. Szűcs and B. Tamás, "Body part extraction and pose estimation method in rowing videos," *Journal of Computing and Information Technology*, vol. 26, no. 1, pp. 29–43, 2018.

[4] R. Gu, G. Wang, Z. Jiang, and J. N. Hwang, "Multi-person hierarchical 3d pose estimation in natural videos," *IEEE Transactions on Circuits and Systems for Video Technology*, vol. 30, no. 11, pp. 4245–4257, 2020.

[5] M. Nasr, R. Osama, H. Ayman, N. Mosaad, N. Ebrahim, and A. Mounir, "Realtime multi-person 2D pose estimation," *International Journal of Advanced Networking and Applications*, vol. 11, no. 6, pp. 4501–4508, 2020.

[6] N. T. Thành, L. V. Hùng, and P. T. Cong, "An evaluation of pose estimation in video of traditional martial arts presentation," *Journal of Research and Development on Information and Communication Technology*, vol. 2019, no. 2, pp. 114–126, 2019.

[7] I. Petrov, V. Shakhuro, and A. Konushin, "Deep probabilistic human pose estimation," *IET Computer Vision*, vol. 12, no. 5, pp. 578–585, 2018.

[8] G. Hua, L. Li, and S. Liu, "Multipath affinage stacked—hourglass networks for human pose estimation," *Frontiers of Computer Science*, vol. 14, no. 4, Article ID 144701, 2020.

[9] D. Mehta, S. Sridhar, O. Sotnychenko et al., "Vnect: real-time 3d human pose estimation with a single rgb camera," *ACM Transactions on Graphics*, vol. 36, no. 4, pp. 1–14, 2017.

[10] S. Liu, Y. Li, and G. Hua, "Human pose estimation in video via structured space learning and halfway temporal evaluation," *IEEE Transactions on Circuits and Systems for Video Technology*, vol. 29, no. 7, pp. 2029–2038, 2019.

[11] S. Ershadi-Nasab, E. Noury, S. Kasaei, and E. Sanaei, "Multiple human 3d pose estimation from multiview images,"

Multimedia Tools and Applications, vol. 77, no. 12, Article ID 15573, 2018.

[12] X. Nie, J. Feng, J. Xing, S. Xiao, and S. Yan, "Hierarchical contextual refinement networks for human pose estimation," *IEEE Transactions on Image Processing*, vol. 28, no. 2, pp. 924–936, 2019.

[13] Y. Nie, J. Lee, S. Yoon, and D. S. Park, "A multi-stage convolution machine with scaling and dilation for human pose estimation," *KSII Transactions on Internet and Information Systems (TIIS)*, vol. 13, no. 6, pp. 3182–3198, 2019.

[14] A. Zarkeshev and C. Csiszár, "Rescue method based on V2X communication and human pose estimation," *Periodica Polytechnica: Civil Engineering*, vol. 63, no. 4, pp. 1139–1146, 2019.

[15] W. McNally, A. Wong, and J. McPhee, "Action recognition using deep convolutional neural networks and compressed spatio-temporal pose encodings," *Journal of Computational Vision and Imaging Systems*, vol. 4, no. 1, p. 3, 2018.

[16] R. G. Díaz, F. Laamarti, and A. El Saddik, "DTCoach: your digital twin coach on the edge during COVID-19 and beyond," *IEEE Instrumentation and Measurement Magazine*, vol. 24, no. 6, pp. 22–28, 2021.

Hindawi
Mobile Information Systems
Volume 2022, Article ID 3158314, 8 pages
https://doi.org/10.1155/2022/3158314

Research Article

Folk Music Audio Enhancement Method Combining Internet of Things and GA

Cheng Ming

Taiyuan University, Taiyuan 030032, China

Correspondence should be addressed to Cheng Ming; qu82783@163.com

Received 31 May 2022; Revised 22 July 2022; Accepted 29 July 2022; Published 1 September 2022

Academic Editor: Chi Lin

The current methods of music sound enhancement mainly use the way of enhancing the intensity of the sound source, which ignores the spatial noise cancellation of the human ear, resulting in poor sound enhancement effect. Therefore, this paper proposes an audio enhancement method for folk music combining Internet of Things and GA. After acquiring folk music audio by Internet of Things technology, the postprocessing algorithm of wavelet packet decomposition combined with Wiener filter is used to suppress the noise in music. On the basis of HRTF, genetic algorithm is used to reduce the output error of left and right sound channels and realize the enhancement of music sound effect. The simulation experiment verifies the method of application research. The reverberation is established at 65 ms and lasts for a long time, which has good effect of sound enhancement.

1. Introduction

Folk music has a unique musical beauty, but limited by the skill proficiency of players, quality of instruments, etc., it is difficult to guarantee a stable and high-quality experience of folk music. Sound enhancement is a forensic audio enhancement service that uses nondestructive methods to enhance audio recordings while preserving voice clarity. This is important so that the fact-finder can assess the events described in the documentary evidence. The music sound enhancement has the function of beautifying the sound color and improving the output sound quality. The principle of the sound enhancement is mainly to carry on the special reprocessing to the left and right sound channel signal, enlarge the sound field, produce the extremely realistic positioning sound effect around the listener, and bring the real auditory experience [1]. Literature [2] uses DNN sound source enhancement technology to improve high music sound effects, but the range of sound source intensity enhancement for folk music instruments is limited, and the realization is difficult. The DNN source enhancement architecture is utilized to estimate the latent parameters in the T-F mask processing output signals' continuous probability density function (PDF). Literature [3] uses the excitation loudspeaker in the OLED panel for sound enhancement. The principle behind OLED panel speaker technology is that an OLED panel works as a speaker diaphragm by adding an oscillator called an exciter to the back of the OLED panel. With the ability to play back both the sound and the video in the same place, the technology allows listeners to experience the panel directly and clearly while also enhancing the interactive experience. This method has a good effect on audio enhancement in video, but it is not good for pure audio processing. In addition, there are certain limitations in the sound enhancement methods that use front and rear dimensional 3D enhancement, base-missing harmonic control bass enhancement, sound source localization, and sparse Bayesian learning, which cannot achieve ideal effects for the sound enhancement of folk music [4–7].

The Internet of Things is a kind of network that connects any terminal to the Internet through radio-frequency identification, wired and wireless data transmission, etc., to realize data exchange. In essence, the Internet of Things is a new omnidirectional and multiangle communication network with communication network as the carrier, and its overall architecture consists of the perception layer, the network layer, and the application layer from bottom to top [8]. It can reduce the signal interference in the signal

transmission process. Genetic algorithm has good iteration and can improve the sound enhancement [9].

The Internet of Things (IoT) allows diverse physical items to share information over a 6G wireless communication network. IoDs get access to the main spectrum by acting as an orthogonal frequency-division multiplexing (OFDM) relay using energy gathered from a radio-frequency (RF) transmission received. IoT network is powered by UAVs that uses orthogonal frequency-division multiplexing (OFDM). Two ground nodes (GNs) are supplied with electricity by two UAVs in the proposed network through a down link WPT. In order to resolve the suggested optimization issue, we use sequential convex programming (SCP) approach. Simulation findings demonstrate that our suggested design provides a higher total average transmission rate than the benchmark methods [10, 11].

The main motivation of the work is discussed as follows.

This paper will study the folk music audio enhancement method combining the Internet of Things and GA. Further, the postprocessing algorithm of the wavelet packet decomposition method is combined with Wiener filter to reduce noise after obtaining folk music audio by IoT. And, the output error of the left and right sound channels is reduced by using HRTF.

2. Folk Music Audio Enhancement Method Combining Internet of Things and GA

2.1. Internet of Things Technology to Access Music Audio. In order to improve the efficiency of enhancing the sound effects of folk music, this paper uses sound sensors to collect the occurrence of each folk music playing instrument and uses wireless Internet of Things for data transmission. The sensor measures noise levels effectively at frequencies ranging from 3 kHz to 6 kHz. The human ear can detect noises in this frequency range. Acoustic pressure sensors, pressure microphones, high amplitude pressure microphones, prepolarized condenser microphones, probe microphones, condenser microphones, and prepolarized free-field condenser microphones are some of the sensors used in the sound enhancement process. Multiple audio sensor nodes with association are divided into clusters, and one sensor node within each cluster is selected as the cluster head node based on certain algorithmic mechanisms, which is used to manage and coordinate the work of its cluster member nodes, collect node information, and perform specific processing and forwarding functions such as music signal denoising [12–14]. The cluster head node in the lower level network can become a cluster member node in the higher level network and continue to cluster up to the highest level. The highest level cluster head node communicates directly with the base station [15].

Due to the different parts distribution and sound modes of different folk music instruments, there are differences in the intensity of music signals collected. In order to ensure that the final output music is in a relatively harmonious state, it is necessary to conduct intensity balance processing through the audio analyzer before the sound enhancement [16–20]. After the signal is picked up by the sound sensors on the different instruments being played, it needs to be processed by an audio analyzer, which uses a CMOS chip to divide the audio spectrum into seven bands: 63 Hz, 160 Hz, 400 Hz, 1 kHz, 2.5 kHz, 6.25 kHz, and 16 kHz. The auditory spectrum, which ranges in frequency from 20 Hz to 20,000 Hz, is the range at which humans can hear. The audio spectrum ranges from 20 Hz to 20,000 Hz and may be efficiently divided into seven distinct frequency bands, with each band having a particular effect on the overall sound. The complementary metal-oxide semiconductor (CMOS) chip, which stores configuration and other data for the hard drive, is battery-operated. CMOS chips often offer CMOS memory and real-time clock (RTC) in microcomputers and microcontrollers. The seven frequencies detected provide a DC band amplitude for the multiplexed output. No additional components are used as a response to the selection filter. Only one of the chip's resistors and capacitors needs to be switched off to select the clock oscillator frequency on the chip. The filter center frequency tracks the clock oscillator frequency [21, 22]. It is often described as the geometric mean or the arithmetic mean of the lower and higher cutoff frequencies of a band-passing or band-stopping system. The center frequency of a filter or channel is a measurement of the frequency that is in the middle of the upper and lower cutoff frequencies. The chip power supply provides the best performance for 5 volts. The multiplexer allows multiple inputs by resetting the control gate, but the multiplexer has only 2 pins to read out. The read speed of the multiplexer is also output by the decay time control, which decays by about 10% per read. The music signal after the initial equalization processing by the audio analyzer is transmitted to the processing center through the Internet of Things for the actual ethnic sound enhancement processing [23–25].

The real-time message transmission protocol (RTMP) is used to transmit music signal, so as to improve the timeliness of music sound effect enhancement. RTMP is an application layer protocol based on TCP. It is designed for real-time communication, mainly for audio communication between Flash/AIR platform and server that supports RTMP. Internally, ActionScript 3.0 is the main programming language used by AIR, and it shares a codebase with the rendering engine of Flash Player. A TCP-based technology called RTMP provides for low-latency communication while still maintaining persistent connections. It divides streams into segments, and their sizes are constantly negotiated between the client and server in order to deliver streams smoothly and transfer as much information as feasible. RTMP meets the real-time requirements of this design, and the open source RTMPDump toolkit can be used to reduce the development effort [23]. RTMPDump is a free software project aimed at the development of an RTMP toolkit. RTMPDump, Rtmpsrv, and Rtmpsuck are the three applications included in the package. Similar to regular Flash video player clients, RTMPDump can connect to RTMP servers, capture the network stream, and save it to a file. It allows for the construction of instructions utilizing connection and authentication details previously collected by rtmpsrv from the RTMP server.

To stream music over the RTMP, there are four steps: shake hands, establish a connection, establish a stream, and

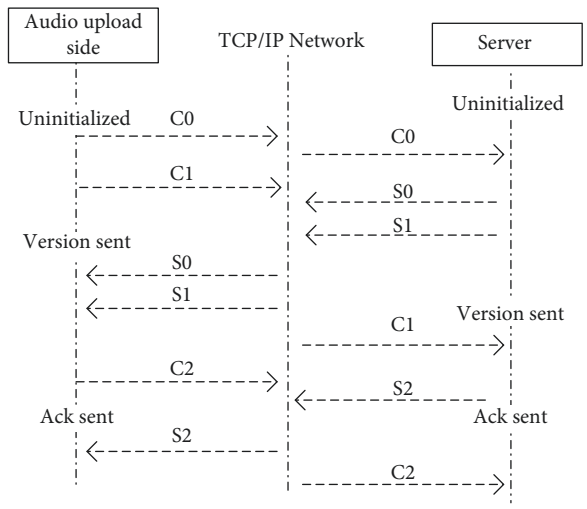

Figure 1: RTMP handshake process.

send. After the handshake is successful, it is necessary to realize the network connection of the Internet of Things in the establishment of connection stage, then complete the construction of network flow between the C/S structures of the Internet of Things in the establishment of stream stage, and complete the transmission of audio data in the transmission stage. In the handshake stage, the server and the music uploader need to send three fixed-size data blocks, respectively [26–30]. The brief process is as follows [31].

(1) At the beginning of the handshake, the upload end sends $C0$ and $C1$ data blocks, and the server end sends $S1$ and $S1$ data blocks to the upper transmission end after receiving $C0$ or $C1$.

(2) After the uploader and server receive $S0$ and $S1$, $C0$ and $C1$, respectively, they send $C2$ and $S2$ to the opposite end.

(3) When $C2$ and $S2$ are received, the handshake process is completed. The RTMP handshake process is shown in Figure 1 [32].

The process of establishing the connection phase is as follows:

(1) The upload side sends the "connect" command to the server side to initiate the connection request.

(2) After the server receives the connection request, it sends the confirmation window size message and the bandwidth setting message to the client and connects to the application mentioned in the connection request.

(3) After receiving the server bandwidth setting message, the uploader sends the confirmation window size message to the server.

(4) The server sends the control message of "stream start" and the command message of "result" to the upper transmission end to inform the upload end of the status of the connection.

Establish the flow process:

(1) The uploader sends the "Create Stream" message to the server.

(2) After receiving the command "Create Stream," the server sends the "result" message to the top end to inform the state of the stream.

Sending process:

(1) The upload side transmits the "Send" command to the server side.

(2) The server sends the message of setting block size after receiving the command.

(3) The server sends the "stream start" control message to the upstream end, including the music stream ID.

(4) After the successful execution of the command, the server sends the "response status" message to the upload end to inform the execution status of the command at the upload end.

After using the Internet of Things to obtain folk music signals, in order to achieve better music sound effects, it is necessary to denoise the music signals to improve the quality of audio signals.

2.2. Music Noise Reduction Processing. Signal collected by sound sensors in the Internet of Things will contain unavoidable noise during performance. In this paper, the postprocessing algorithm of wavelet packet decomposition combined with Wiener filtering is used to suppress noise in music. The Wiener filter may be used to remove the noise from a distorted signal and estimate the relevant underlying signal. The minimal mean square error (MMSE) estimator article provides a more statistical explanation of the idea as the Wiener filter is based on a statistical methodology. The Wiener filtering achieves the best trade-off between noise smoothing and inverse filtering. At the same time, it reverses the blurring and eliminates the additional noise. The Wiener filtering has the best mean square error performance.

The first step of wavelet packet decomposition is to select the appropriate wavelet packet base. The choice of wavelet packet basis is not unique; as long as the function satisfies the wavelet packet condition in the wavelet packet basis, the appropriate wavelet packet basis is very important for the decomposition of the wavelet packet. The principle of selecting the wavelet packet basis is that the higher the coincidence degree between the wavelet packet basis and the useful signal, the better. Since the time-domain medium and small wave packet bases and signals are convolved, if the waveform of wavelet packet bases and useful signals are close, the features of useful signals will also be amplified, while those with different shapes will be suppressed, which is conducive to signal denoising. Noise is generally nonstationary, with time-varying and mutagenicity. It is proved that the wavelet packet basis of Daubechies (DB) series is a compactly supported orthogonal wavelet packet basis, which is suitable for processing abrupt signals. Daubechies wavelets are frequently employed to address a variety of issues, including the self-similarity characteristics of a signal, fractal issues, and signal discontinuities. Therefore, the wavelet

packet base of Daubechies series is selected in this study. Using the DB2-DBLL wavelet packet base of DB wavelet, the music signal with noise is decomposed into four layers of wavelet packet for denoising [33]. Using mean square error and signal-to-noise ratio to judge, it is found that DB4 is the best of 10 wavelet packet basis, so DB4 in Daubechies series is selected as the wavelet packet basis, and the number of decomposes layers in the wavelet packet decomposition of suppressing music noise is set as 3. For a given signal $F(x)$, its orthogonal wavelet decomposition formula is as follows [34]:

$$\begin{aligned} M_{j-1}F(x) &= M_jF(x) + N_jF(x), \\ M_jF(x) &= \sum_n p_n^j \cdot \varphi_{j,n}(x), \\ N_jF(x) &= \sum_n q_n^j \cdot \psi_{j,n}(x). \end{aligned} \tag{1}$$

In the above equation, M and N are the frequency bands of the approximate part and the detail part in the multi-resolution analysis, respectively. p_n^j and q_n^j are coefficients, which can be determined, recursively.

The wavelet packet reconstruction formula for the music signal is as follows [35]:

$$t_l^{j,n} = \sum_k \left[h_{l-2k} q_k^{j+1,2n} + g_{l-2k} q_k^{j+1,2n+1} \right]. \tag{2}$$

In the above equation, $t_l^{j,n}$ is the signal reconstructed by wavelet packet; h_{l-2k} and g_{l-2k} are the filter coefficients. Mallat algorithm can implement wavelet packet decomposition and wavelet packet reconstruction as filter, low-pass filter is equivalent to scale function, and high-pass filter is equivalent to wavelet function. The Mallat algorithm inverts a single-scale orthogonal expansion into a multiscale orthonormal expansion. The generalization of the coefficients is not necessary for the Mallat method for some function's Fourier coefficients. Wavelet packet decomposition filter is to get the first layer coefficient of wavelet packet decomposition by low-pass filtering and high-pass filtering, respectively, and the next layer coefficient is obtained by low-pass filtering, high-pass filtering, and low sampling of the upper layer coefficient until the set number of decomposition layers. The wavelet packet reconstruction filter realizes the inverse process equivalent to the wavelet packet decomposition filter; that is, the coefficients of the lowest layer are sampled up and then summed up through the corresponding low-pass reconstruction filter and high-pass reconstruction filter to get the coefficients of the upper layer until the original signal of the uppermost layer is reconstructed.

The prior signal-to-noise ratio of the current frame audio signal can be obtained from the prior signal-to-noise ratio of the previous frame and the posterior signal-to-noise ratio of the current frame. After obtaining the prior signal-to-noise ratio $\widehat{\xi}_i(k)$ of the voice signal of the current frame, the following equation can be used to obtain Wiener filter's transfer function for the audio signal in the current frame [36]:

$$S(k) = \frac{\xi(k)}{1+\xi(k)} = 1 - \frac{1}{\gamma(k)}. \tag{3}$$

In the above formula, $\xi(k)$ and $\gamma(k)$ represent prior SNR and posterior SNR, respectively. The ratio between the clean signal's and the noisy signal's power is known as the a priori SNR, whereas the posteriori SNR is defined as the ratio of the observed noisy signal's squared magnitude to the noise power. Both SNRs are calculated for each frequency bin. The transfer function of Wiener filter is as follows:

$$S_i(k) = \frac{\widehat{\xi}_i(k)}{\widehat{\xi}_i(k)+1}. \tag{4}$$

The output of Wiener filter can be calculated as follows:

$$B(k) = S_i(k) A_i(k). \tag{5}$$

After denoising the audio signals transmitted and collected by the Internet of Things in accordance with the above process, GA is used to enhance the sound effects of folk music.

2.3. GA to Enhance Music Sound Effects. The enhancement processing of folk music sound effect is mainly realized according to the principle of spatial hearing characteristic of human ear. Therefore, this design will use genetic algorithm to improve the HRTF, so as to achieve sound efficiency. The head related transfer function (HRTF) defines how an ear receives sound from a sound source. A sound wave is created when a sound is generated and travels across space in all directions. The sound wave emitted by the sound source reaches the ears after scattering and reflection through the head, auricle, trunk, etc., which changes the sound and enables the human ear to locate it. This physical process can be regarded as a linear time-invariant (LTI) filtering system, whose characteristics can be fully described by the frequency domain transmission function of the system. HRTF is the frequency domain transfer function of the acoustic filtering system. In the case of free field, HRTF is defined as [37]:

$$\begin{aligned} H_L &= H_L(r,\theta,\varphi,\omega,a) = \frac{P_L(r,\theta,\varphi,\omega,a)}{P_0(r,\omega)}, \\ H_R &= H_R(r,\theta,\varphi,\omega,a) = \frac{P_R(r,\theta,\varphi,\omega,a)}{P_0(r,\omega)}. \end{aligned} \tag{6}$$

In the above formula, P_L and P_R are the complex sound pressures generated by the sound source in the listener's left and right ears, respectively. P_0 is the complex sound pressure at the center of the head when the head does not exist. H_L and H_R are functions of the horizontal azimuth of the sound source θ, elevation φ, the distance from the center of the sound source to the head r, and the angular frequency of the sound wave ω. In addition, the size and shape of the head and auricle and trunk of different people are different; so strictly speaking, the HRTF of each person is different; that is to say, the HRTF is a physical quantity with personalized characteristics. HRTFs are usually measured in an anechoic room to reduce the impact of early reflections and

reverberation on the recorded response. Interpolation is used to generate HRTFs at arbitrary positions of. HRTFs are recorded at modest increments, such as 15° or 30° in the horizontal plane. In the formula, a represents the parameter with personalized characteristics.

The morphology of spectrum peaks or valleys in the HRTF amplitude spectrum can be described by three parameters, namely, the center frequency, the height of the peak or the depth of the valley, and the width of the peak or valley. These three parameters are used to uniquely determine a filter, so a second-order notch filter can be used to control the synthesis of a single spectrum peak or spectrum valley, which can better approximate the spectrum peak and spectrum valley actually measured. The shape positions of spectrum peaks and valleys vary significantly between individuals, which is the main source of errors in the use of nonpersonalized HRTF for sound enhancement synthesis. Using genetic algorithm to improve the HRTF can reduce the error of sound enhancement synthesis.

In this study, multiple continuous variables of HRTF are encoded by genetic encoding in the form of real encoding, and N dimensional real vectors are used to represent N real variables. The most classic method of selecting operations is roulette selection. It uses the proportion of fitness to determine the size and proportion of the central angle of the fan on the roulette. If N individuals are selected as parents, the roulette wheel needs to be rotated N times, which is equivalent to doing N times of uniform probability distribution sampling. Using small selection pressure in the early stages of genetic search makes the search area wider and directs the search location to the promising neighborhood. In the late stage of search, high selection pressure is applied to accelerate the convergence of the algorithm to the optimal solution of the current covered neighborhood [38, 39]. According to the HRTF optimized by genetic algorithm, the sound effect enhancement of folk music can be realized by controlling the intensity difference between the left and right sound channels during the audio output. At this point, the method combining the Internet of Things and GA is realized to enhance the sound effect of folk music and improve the auditory experience of folk music. A genetic algorithm is a type of search-based algorithm used in machine learning to solve optimization issues. This method is significant because it quickly resolves challenging issues that would otherwise require a lot of effort.

3. Sound Enhancement Method Testing

The sound enhancement method of folk music combining IT and GA is proposed above. According to the requirement of the sound display effect when folk music is performed, this section will test the studied sound enhancement method.

3.1. Sound Effect Enhancement Test Content. The actual effect of the method is tested from two aspects: the spatial sense of music and the anticrosstalk effect of the music signal after the processing of the ethnic music sound enhancement method. The term "spatial music" refers to music in which the listener's attention is drawn primarily to the listener's location and movement in relation to the sound sources' positions and movements. It could include a single mobile sound source or several simultaneous fixed or mobile sound events occurring in various places. The easiest technique to avoid crosstalk is to take advantage of the parallelism that causes it by tightly connecting the return path to the ground to your high-speed signals. Because the return path is same in amplitude but opposite in direction, the fields cancel out and decrease crosstalk. In order to make the test results credible, the sound enhancement method based on is chosen as a comparative reference. Through the form of comparative test, the feasibility of the sound enhancement method proposed in this paper is visually verified.

3.2. Test Preparation and Process. Five students from a music school majoring in folk instruments are invited to participate in this test, and all students will play famous music excerpts from the corresponding folk instruments. The folk music played by the students on different instruments will be used as the test data for this experiment to test the actual effect of the sound enhancement method. In order to avoid interference from the outside environment and equipment, the equipment will be tested and noise interference from the outside environment will be eliminated as much as possible before the recording of the students' instrumental pieces. 5 students will play the pieces as required, and pickups will be attached to the vocal positions of the playing instruments to capture the instrumental pieces. After the folk music was performed, the clips were intercepted using music editing software. To facilitate the subsequent analysis of the test data, the 30 s length of the music was intercepted from the more obvious segments of the music waveform and numbered. All the music for the test was only intercepted in length, without any other processing operations.

The experimental group for comparison test is the sound enhancement method designed in this paper, and the sound enhancement method based on sparse Bayesian learning is used as the reference group. The two groups of sound enhancement methods were used to enhance the sound of the input music clips. The music output after the two groups of sound enhancement methods is played back using the audio, and the output signals of the left and right channels of the audio are collected using a sound acquisition device. On the premise of ensuring the clarity of the audio output music, the reverberation waveform of the enhanced music signal is collected, and the reverberation delay and reverberation time of the output music signal and other parameters are counted.

When conducting the anticrosstalk test, the input signal of one channel is used to test the output signal of the other channel separately. By comparing the magnitude of the crosstalk rejection of the two channels, the anticrosstalk ability of the enhancement method is judged. In accordance with the above design of the sound enhancement method of comparison test content, the sound enhancement method to test summarizes all test data analysis content to obtain the final experimental results.

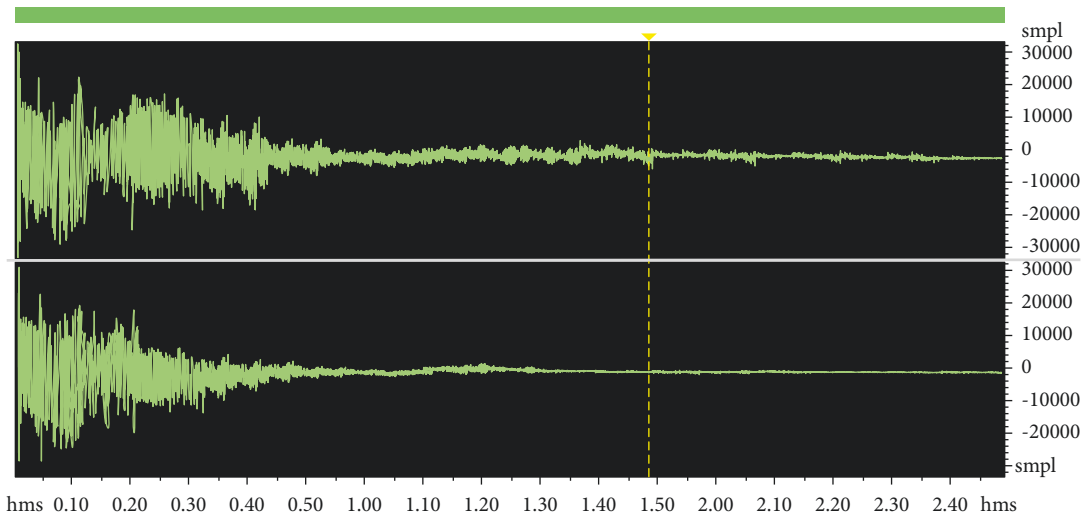

Figure 2: Audio reverberation comparison.

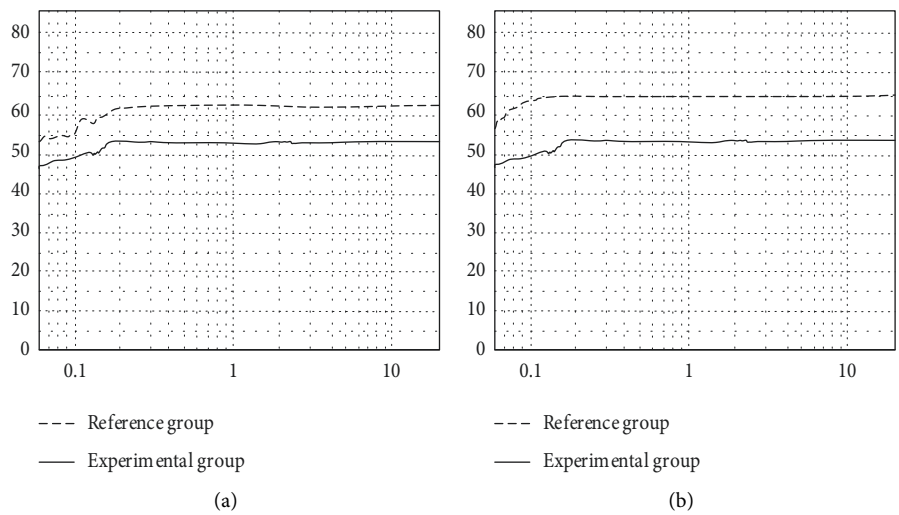

Figure 3: Comparison of crosstalk suppression response curves of sound channels. (a) Left channel to right channel anticrosstalk. (b) Right channel to left channel anticrosstalk.

3.3. Experimental Results. The reverberation test after sound enhancement using actual ethnic music performance clips is shown in Figure 2, the upper part of the signal is the audio reverberation after the experimental group method, and the lower part is the audio reverberation after the reference group method. Each unit of the horizontal coordinate in the figure is 1.25 s. Reverberation is the continuation of sound after the source of the sound has ended. It is the consequence of several reflected waves that the brain can interpret as a continuous sound. On the other hand, an echo happens when a sound pulse is audible twice. Reverberation effects are frequently employed in studios to give sounds depth. The pitch of a sound is unaffected by reverberation, but the apparent spectral structure is changed. The sound bouncing in a large speaker is an illustration of reverberation.

Comparative analysis of the upper and lower parts of the signal in Figure 2 shows that, for the audio signal processed by the experimental group method, when the reverberation is established after 65 ms of the end of the input performance clip, the entire reflection sound still exists until about 5 s or even 6.5 s, thus achieving the most significant extension of the reverberation time, to ensure the purpose of the reflection density. Considering the reference group method of processing the audio signal in the end of the performance clip 74 ms after the establishment of reverberation, the reflection sound only lasted until about 3 s, and the reflection density is also rapidly declining abd cannot achieve a better sound enhancement effect.

Figure 3 shows the application of two sound enhancement methods and the output speaker crosstalk suppression response curve of the left and right channels. The horizontal axis of the figure is the frequency of the speaker output signal, while the vertical axis indicates the response curve signal amplitude. The greater the amplitude of the channel crosstalk suppression response curve, the worse the channel crosstalk suppression effect and the more violent fluctuations in the

channel crosstalk suppression response curve, representing the more serious channel crosstalk problem.

Separate analysis of Figure 3, the application of the experimental group sound enhancement method after processing, the left and right channels, respectively, on the other channel of the maximum amplitude of interference is only 45 dB; and the reference group method after processing, the left channel on the right channel of the sound channel crosstalk suppression effect is slightly better than the right channel on the left channel of the sound channel crosstalk suppression effect, but the application of the method, the left and right channels respectively on the other channel of the crosstalk effect is poor.

Summarizing the above experimental data analysis, the ethnic music sound enhancement method combining IoT and GA proposed in this paper can most significantly extend the reverberation time and has the advantages of improving the output spatial sense and optimizing the anticrosstalk effect. The ratio of each voice part of the processed audio sound is more coordinated and even, and the overall output sound is remarkable and the actual experience is better.

4. Conclusion

The application of sound effect enhancement methods is promising, but constrained by the economic cost and processing capacity, there are currently common problems of poor output and poor user experience. To this end, this paper proposes an ethnic music sound enhancement method combining IoT and GA. In the future, in-depth research will be conducted on further improving the processing efficiency and sound field detail adjustment of sound enhancement.

Abbreviations:

HRTF:	Head related transfer function
GA:	Genetic algorithm
DNN:	Deep neural network
OLED:	Organic light-emitting diodes
CMOS:	Complementary metal-oxide semiconductor
RTC:	Real-time clock
DC:	Direct current
RTMP:	Real-time messaging protocol
TCP:	Transmission control protocol
C/S structures:	Client/server structure
ID:	Identification
DB:	Daubechies
SNR:	Signal-to-noise ratio
LTI:	Linear time-invariant
IoT:	Internet of Things.

Data Availability

The datasets used and/or analyzed during the current study are available from the corresponding author on reasonable request.

Conflicts of Interest

The authors declare that they have no conflicts of interest.

Acknowledgments

Shanxi Tourism and Performing Arts Industry Research Project, a philosophical and social science planning project in Shanxi Province (2020YY285).

References

[1] N. Sasaoka, E. Akamatsu, A. Kawamura, N. Hayasaka, and Y. Itoh, "4th order moment-based linear prediction for estimating ringing sound of impulsive noise in speech enhancement: regular section," *IEICE - Transactions on Fundamentals of Electronics, Communications and Computer Sciences*, vol. E103.A, no. 10, pp. 1248–1251, 2020.

[2] Y. Koizumi, K. Niwa, Y. Hioka, K. Kobayashi, and Y. Haneda, "DNN-Based source enhancement to increase objective sound quality assessment score," *IEEE/ACM Transactions on Audio, Speech and Language Processing (TASLP)*, vol. 26, no. 10, pp. 1780–1792, 2018.

[3] S. Lee, K. Park, S. Park, J. Lee, and H. Park, "Improved sound quality by using the exciter speaker in OLED panel," *Journal of the Society for Information Display*, vol. 28, no. 3, pp. 297–307, 2020.

[4] D. D. Lu and X. Y. Zeng, "3D sound effect enhancement of front and back," *INTER - NOISE and NOISE - CON Congress and Conference Proceedings*, vol. 259, no. 9, pp. 177–183, 2019.

[5] Y. T. Geng, M. Nakayama, and T. Nishiura, "Virtual bass enhancement based on harmonics control using missing fundamental in parametric array loudspeaker," *INTER - NOISE and NOISE - CON Congress and Conference Proceedings*, vol. 259, no. 7, pp. 2660–2671, 2019.

[6] R. W. Li, D. M. Pan, and S. Zhang, "Speech enhancement algorithm based on sound source localization and scene matching for binaural digital hearing aids," *Journal of Medical and Biological Engineering*, vol. 39, no. 3, pp. 403–417, 2019.

[7] A. Xenaki, J. Bünsow Boldt, and M. Græsbøll Christensen, "Sound source localization and speech enhancement with sparse Bayesian learning beamforming," *Journal of the Acoustical Society of America*, vol. 143, no. 6, pp. 3912–3921, 2018.

[8] E. Suganya and C. Rajan, "An adaboost-modified classifier using particle swarm optimization and stochastic diffusion search in wireless IOT networks," *Wireless Networks*, vol. 27, no. 4, pp. 2287–2299, 2020.

[9] V. Anand and S. Pandey, "New approach of GA–PSO based clustering and routing in wireless sensor networks," *International Journal of Communication Systems*, vol. 33, no. 16, Article ID e4571, 2020.

[10] W. Lu, P. Si, G. Huang et al., "SWIPT cooperative spectrum sharing for 6G-enabled cognitive IoT network," *IEEE Internet of Things Journal*, vol. 8, no. 20, pp. 15070–15080, 2021.

[11] W. Lu, P. Si, Y. Gao et al., "Trajectory and resource optimization in OFDM-based UAV-powered IoT network," *IEEE Transactions on Green Communications and Networking*, vol. 5, no. 3, pp. 1259–1270, 2021.

[12] B. Cao, Y. Zhang, J. Zhao, X. Liu, L. Skonieczny, and Z. Lv, "Recommendation based on large-scale many-objective optimization for the intelligent Internet of Things system," *IEEE Internet of Things Journal*, vol. 9, no. 16, pp. 15030–15038, 2022.

[13] Q. Sun, K. Lin, C. Si, Y. Xu, S. Li, and P. Gope, "A secure and anonymous communicate scheme over the Internet of Things," *ACM Transactions on Sensor Networks*, vol. 18, no. 3, pp. 1–21, 2022.

[14] X. Zenggang, Z. Mingyang, Z. Xuemin et al., "Social similarity routing algorithm based on socially aware networks in the big data environment," *Journal of Signal Processing Systems*, vol. 12, 2022.

[15] J. Pak and J. W. Shin, "Sound localization based on phase difference enhancement using deep neural networks," *IEEE/ACM Transactions on Audio, Speech and Language Processing (TASLP)*, vol. 27, no. 8, pp. 1335–1345, 2019.

[16] C. Qin, G. Shi, J. Tao et al., "An adaptive hierarchical decomposition-based method for multi-step cutterhead torque forecast of shield machine," *Mechanical Systems and Signal Processing*, vol. 175, Article ID 109148, 2022.

[17] C. J. Qin, D. Y. Xiao, J. F. Tao et al., "Concentrated velocity synchronous linear chirplet transform with application to robotic drilling chatter monitoring," vol. 1, Measurement, 2022.

[18] Y. Feng, B. Zhang, Y. Liu et al., "A 200-225-GHz manifold-coupled multiplexer utilizing metal wave guides," *IEEE Transactions on Microwave Theory and Techniques*, vol. 69, no. 12, pp. 5327–5333, 2021.

[19] A. Yan, Y. Chen, Y. Hu et al., "Novel speed-and-power-optimized SRAM cell designs with enhanced self-recoverability from single- and double-node upsets," *IEEE transactions on circuits and systems. I, Regular papers*, vol. 67, no. 12, pp. 4684–4695, 2020.

[20] A. Yan, Z. Wu, J. Guo, J. Song, and X. Wen, "Novel double-node-upset-tolerant memory cell designs through radiation-hardening-by-design and layout," *IEEE Transactions on Reliability*, vol. 68, no. 1, pp. 354–363, 2019.

[21] A. Yan, Y. Hu, J. Cui et al., "Information assurance through redundant design: a novel tnu error-resilient latch for harsh radiation environment," *IEEE Transactions on Computers*, vol. 69, no. 6, pp. 789–799, 2020.

[22] A. Yan, Z. Xu, X. Feng et al., "Novel quadruple-node-upset-tolerant latch designs with optimized overhead for reliable computing in harsh radiation environments," *IEEE transactions on emerging topics in computing*, vol. 10, pp. 404–413, 2022.

[23] S. Roy, D. Sarkar, and D. De, "Entropy-aware ambient IOT analytics on humanized music information fusion," *Journal of Ambient Intelligence and Humanized Computing*, vol. 11, no. 1, pp. 151–171, 2020.

[24] B. S. Kim, S. Kwon, S. Y. Jeong, and J. Park, "Semi-active control of smart porous structure for sound absorption enhancement," *Journal of Intelligent Material Systems and Structures*, vol. 30, no. 17, pp. 2575–2580, 2019.

[25] M. R. Bai, S. S. Lan, J. Y. Huang, Y. C. Hsu, and H. C. So, "Audio enhancement and intelligent classification of household sound events using a sparsely deployed array," *Journal of the Acoustical Society of America*, vol. 147, no. 1, pp. 11–24, 2020.

[26] A. Yan, Z. Fan, L. Ding et al., "Cost-effective and highly reliable circuit components design for safety-critical applications," *IEEE Transactions on Aerospace and Electronic Systems*, vol. 58, pp. 517–529, 2022.

[27] X. Liang, L. Luo, S. Hu, and Y. Li, "Mapping the knowledge frontiers and evolution of decision making based on agent-based modeling," *Knowledge-Based Systems*, vol. 250, Article ID 108982, 2022.

[28] W. Zheng, X. Liu, and L. Yin, "Research on image classification method based on improved multi-scale relational network," *PeerJ Computer Science*, vol. 7, p. e613, 2021.

[29] Z. Ma, W. Zheng, X. Chen, and L. Yin, "Joint embedding VQA model based on dynamic word vector," *PeerJ Computer Science*, vol. 7, p. e353, 2021.

[30] W. Zheng, L. Yin, X. Chen, Z. Ma, S. Liu, and B. Yang, "Knowledge base graph embedding module design for Visual question answering model," *Pattern Recognition*, vol. 120, Article ID 108153, 2021.

[31] R. Hao, Y. Qiang, X. Liao et al., "An automatic detection method for lung nodules based on multi-scale enhancement filters and 3D shape features," *KSII Transactions on Internet and Information Systems*, vol. 13, no. 1, pp. 347–370, 2019.

[32] I. Afshankaleem and P. Santi, "Enhancement of urban sound classification using various feature extraction techniques," *International Journal of Recent Technology and Engineering*, vol. 7, no. 5s3, pp. 507–514, 2019.

[33] L. Liao, L. Du, and Y. Guo, "Semi-supervised SAR target detection based on an improved faster R-CNN," *Remote Sensing*, vol. 14, no. 1, p. 143, 2021.

[34] D. Holland and D. Chapman, "Introducing new audiences to sound-based music through creative engagement," *Organised Sound*, vol. 24, no. 3, pp. 240–251, 2019.

[35] D. Glista, M. Hawkins, J. M. Vaisberg, N. Pourmand, V. Parsa, and S. Scollie, "Sound quality effects of an adaptive nonlinear frequency compression processor with normal-hearing and hearing-impaired listeners," *Journal of the American Academy of Audiology*, vol. 30, no. 07, pp. 552–563, 2019.

[36] M. A. Steadman, C. Kim, J. H. Lestang, D. F. M. Goodman, and L. Picinali, "Short-term effects of sound localization training in virtual reality," *Scientific Reports*, vol. 9, no. 1, p. 18284, 2019.

[37] C. Porschmann, J. M. Arend, and F. Brinkmann, "Directional equalization of sparse head-related transfer function sets for spatial upsampling," *IEEE/ACM Transactions on Audio, Speech and Language Processing (TASLP)*, vol. 27, no. 6, pp. 1060–1071, 2019.

[38] G. Fuertes, M. Vargas, M. Alfaro, R. Soto-Garrido, J. Sabattin, and M. A. Peralta, "Chaotic genetic algorithm and the effects of entropy in performance optimization," *Chaos*, vol. 29, no. 1, Article ID 013132, 2019.

[39] M. Noura, M. Atiquzzaman, and M. Gaedke, "Interoperability in Internet of Things: taxonomies and open challenges," *Mobile Networks and Applications*, vol. 24, no. 3, pp. 796–809, 2019.

Hindawi
Mobile Information Systems
Volume 2022, Article ID 1351908, 12 pages
https://doi.org/10.1155/2022/1351908

Research Article

The Diversified Communication Methods of Chinese and Korean Cultural Education Based on New Media Technology

Guanen Wang[1] and Duan Li[2]

[1]*Academy of Global Governance and Area Studies Sichuan Normal University, Chengdu 610066, China*
[2]*Sichuan Academy of Social Sciences, Chengdu 610071, China*

Correspondence should be addressed to Duan Li; yi65434@163.com

Received 31 May 2022; Revised 28 July 2022; Accepted 8 August 2022; Published 28 August 2022

Academic Editor: Chi Lin

In the current era of multicultural exchange and integration, the Chinese and Korean cultures have shown the ideal effect of cultural deep integration through interaction and exchange to promote cultural exchanges better, to view the diversified communication between Chinese and Korean cultures with correct cultural views, so as to better find the common points of effective integration of the two cultures, understand and respect the differences between Chinese and Korean cultures, and effectively improve the effect of the application of Chinese and Korean cultural integration by selecting appropriate integration perspective. Based on the understanding of cultural connotation and the analysis of the current situation of cultural education in China and South Korea, this study explores the mechanism of cultural and educational diversification exchange in China and South Korea under the cultural background and puts forward relevant optimization suggestions.

1. Introduction

China and South Korea are geographically adjacent and belong to the East Asian cultural circle. There are many similarities between Chinese and South Korean cultures. Therefore, it is of great significance to deepen the exchanges between them. Culture is a kind of fusion culture based on the value consensus [1]. Through the systematic analysis of the cultural communication process, all countries have a stable cultural state in different stages of development, and the effect and value of culture are systematic. Both China and South Korea belong to the greater Chinese cultural circle. At the same time, in the history of South Korea's development, they are deeply influenced by the cultural habits of our country and deeply influenced by the culture of South Korea. However, in modern times, influenced by historical factors, South Korea has been occupied by Japan and the United States, and Western culture has also been integrated into South Korea [2]. Therefore, to a certain extent, the current Korean culture is a cultural system with diverse contents and forms [3]. With the improvement of China's economic strength and the expansion of openness and inclusiveness, the cultural exchange between China and South Korea has ushered in a new historical stage. Both the level of cultural exchange and the content of cultural exchange have changed substantially. When the cultural and educational exchanges between China and South Korea are diversified, the forms they present are also extremely diversified, such as joint education, international students in Colleges and universities, and even Confucius Institutes [4]. Through various forms of cultural exchanges, the level of cultural and educational exchanges between China and South Korea is comprehensively upgraded.

2. Diversified Communication Methods of Culture and Education between China and South Korea

2.1. Construction of the Characteristic System of Cultural Exchange between China and South Korea Based on New Media Technology. At present, there are many problems in

the educational activities between China and South Korea, such as the imperfection of ideas, the incomprehensibility of methods, and the insufficient integration of contents. For a long time, due to the influence of one-sided cultural exchange thinking, the value of foreign cultural exchange and cultural education has not been paid enough attention. In addition, the openness of the whole education market is not enough [5]. The public is more inclined to public education, and the cultural exchange between China and South Korea is more reflected in interest, understanding and nongovernmental exchange. Both the perfection of cultural exchange and the power of public participation are relatively insufficient. Therefore, the enthusiasm of cultural exchange between China and South Korea is relatively poor. In the era of increasingly diverse and three-dimensional cultural exchanges, the exchanges between cultures are increasingly showing an era environment of deep exchange and continuous integration [6]. With the development of new technologies, our ability to engage with people from all over the world has expanded our understanding of cultures. We have formed ties and common interests and ideals that are distinct from those of past generations as a result of the expansion of our contact circles made possible by digital technologies. Social media and other digital technologies have made it possible for us to exchange and interact in real time beyond conventional cultural barriers and across the globe. Nevertheless, the information technology can actually widen the gap between interconnected and non-interconnected societies. In the end, efficient communication is all about interactions between people. Therefore, the comprehensive innovation of the cultural exchange mechanism between China and South Korea has become a key demand to improve the use of various resources, optimize the cultural exchange system, and improve the talent training mode and specialty setting. In order to meet the diversified demands of public education today, in addition to the overall innovation of the whole cultural exchange system, we should also start from the value perspective of cultural exchange and mining, establish the era concept of cultural inclusion, strengthen the practice and application of culture, and promote the education and cultural exchange between China and South Korea, so as to achieve the most ideal effect [7]. On the basis of logical thinking of the analytical framework and according to the design principles of the index system, the four levels of the evaluation index system are taken as the first level indicators, which are the enhancement of national cohesion, the formation of a correct multicultural view, the reasonable integration of multicultural, and the safety of cultural exchange, and then refined into operable second and third level indicators one by one, which formed the following evaluation index system of cultural exchange security (Table 1).

The value of cultural exchange between China and South Korea is diversified. In addition to meeting the public's understanding of South Korea's culture, it also effectively exports China's cultural content and values to South Korea, which helps to enhance the value influence of China's culture and meet the demands of current multicultural exchange [8–10]. The diversified communication mechanism of cultural education between China and South Korea can form a positive and effective guidance for students' cultural ideas. The transmission of ethnic cultures will be significantly impacted by increased educational diversity. The importance of the heritage of diverse communities within the globalization process is enhanced in light of the modern age and current societal changes. The richness of this cultural diversity benefits people's lives and their growth. Therefore, any nation's understanding of its native civilization and foreign cultures is extremely important. People are now concerned that the global communications stream may degrade each ethnic firm's rich and distinct culture. Regional, economic, cultural, and behavioral diversity are the main ways in which this diversed communication is expressed. In particular, there are many advanced contents in the current Korean culture, and the output power of Korean culture is extremely amazing [5]. If we cannot treat the differences and fusion values between Chinese and Korean cultures with a correct attitude, it is difficult to effectively play the advantages and influence of advanced culture. For the current education and training of students, in addition to actively guiding students to master knowledge content and practical skills, we should also pay full attention to effectively enlighten and reasonably influence students from the deep perspective of cultural concept. Recognizing and learning advanced culture is actually a manifestation of self-confidence [11–14]. Therefore, at present, the real purpose of the diversified cultural exchange activities between China and South Korea is to guide students to form a correct cultural mentality through cultural exchange and comparison, and "absorb" advanced cultural knowledge and thinking content from each other's culture, which is the effect that the normalized cultural exchange activities cannot achieve (Figure 1).

Multicultural communication is one of the important ways of multicultural integration and acculturation. It is called adaptive cultural communication, which is based on students' different cultural experience. It is connected with the multicultural curriculum. As one of the practice subjects of the multicultural curriculum and cultural exchange, teachers must carefully consider the relationship and main problems of their own cultural background and cultural exchange style, students' learning characteristics and style, curriculum, and teaching materials, and cultural exchange strategies and methods, so as to cultivate students' ability to choose between different cultures and form critical thinking [15–17] in order to deepen the understanding of multiculturalism to eliminate cultural bias. The concept of "cross-cultural education policy" refers to the policy related to cross-cultural education, which is based on the general meaning of "policy," highlights the special significance and value of cross-cultural education, and is the special expression of the general nature of policy in the field of cross-cultural education [18–20]. The benefits of the re-emergence of regional and national individuality on the axes of value diversification and multidimensionality of education are increased as a result of helping to promote an education policy for cultural diversity. This decreases the challenges that the higher education system continues to face, impliedly

Table 1: Safety evaluation index system of cultural exchange between China and South Korea.

First level dimension	Secondary dimension	Three level dimension
Correct multiculturalism	The cultural view of pluralistic and integrated culture	What is the cultural attitude of teachers and students towards "pluralistic integration"
	Cultural view of ethnic minorities	Is the attitude of teachers and students towards minority culture respect and tolerance
	Cultural view of overseas culture	Do border people selectively absorb foreign culture
National cohesion has been enhanced	The identity of Chinese culture	Language identity National identity
	Identification of national culture	Religious identity Customs identification
Reasonable integration of multiculture	The booster of multicultural integration: community education and family education	Active cooperation between the community and school education
	School education: the main front of multicultural integration	The subject of multicultural integration: teachers The carrier of multicultural integration: curriculum Multicultural integration channel: multicultural teaching

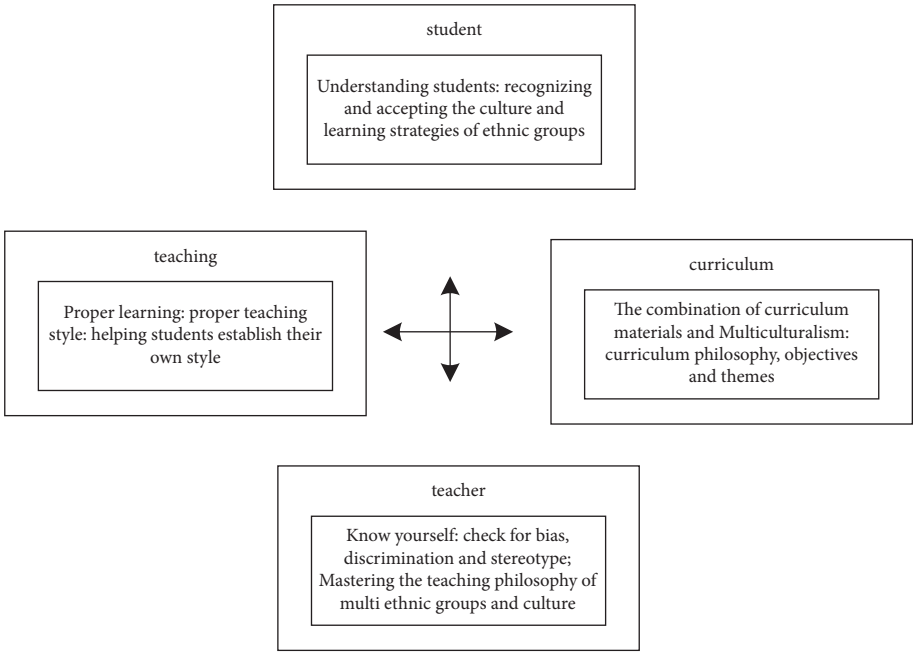

Figure 1: The relationship between China and South Korea in the field of multicultural exchange.

social challenges that insist on the value of cultural engagement and access for fostering democratic citizenship and community stability as well as being a key component of cultural diversity, interchange, and conversation. Intercultural education policy is one of the components of education policy, which should be treated as a subordinate concept of "education policy." At the same time, the cultural policy also has an impact on cross-cultural education policy, which can be understood as the embodiment of cultural policy in the field of education. Therefore, the logical relationship among the four concepts of policy, education policy, cultural policy, and cross-cultural education policy is shown in Figure 2. Learning visits can help students gain the knowledge they need to better comprehend other cultures and people, the knowledge that is essential for developers working in today's globally integrated society. Learners know more deeply about the particular topic when collaborating and listening in a classroom with people from different origins and cultures. In addition, it helps learners how to participate in a diverse workplace using their unique skills and perspectives.

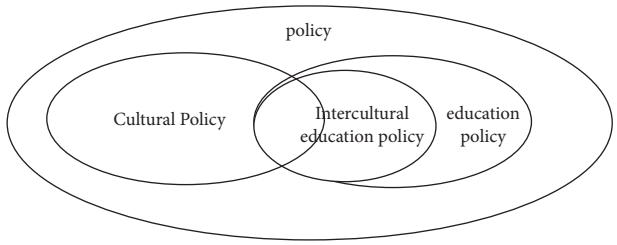

Figure 2: The logical hierarchy of cultural and educational exchanges between South Korea and China.

At present, with the deepening of cultural exchange Display and practice test, when conducting diversified cultural exchanges between China and South Korea, we should base ourselves on continuous innovation, in-depth exchanges, and help multicultural education and exchanges. For students, participating in diversified education of Chinese and South Korean cultures can enable students to understand and understand the specific differences between Chinese and South Korean nationalities and societies with a correct attitude, so as to form a correct cultural concept [21–23]. Through reasonable education and guidance, we can cultivate students' ability to judge multiculture. When students deal with and understand the relationship and substantial influence between their own culture and Korean culture with correct cultural attitude, they should develop correct cultural thinking to help students achieve all-round self-development. A good cultural exchange mechanism can help students realize the spiritual enlightenment and humanistic significance of culture to students' growth while learning knowledge and growing skills. The communication between Chinese and Korean cultures is of great significance to students [24]. A good cultural exchange mechanism not only enables students to better understand the development of other cultural systems but also broadens their horizons in this process [25]. Therefore, it is very important to respect the growth of students, care about students' cultural awareness, and guide students to form a good concept of cultural exchange and application ability by highlighting teachers' specific love and interest in the connotation of Chinese and Korean culture.

2.2. Evaluation Algorithm of Multiculture Communication between China and South Korea Based on New Media Technology. In the evaluation of multicultural exchange, the evaluators can be experts, teachers, students, etc., the evaluation method can adopt the combination of quantitative evaluation and qualitative evaluation, the evaluation period can be very long or very short, and the evaluation results can be displayed immediately or after a period of time [26]. The essence of the evaluation of multicultural exchange is the evaluation model. The evaluation model determines the evaluation content, evaluation relationship, and evaluation method. The evaluation content of the diversified evaluation model should be diversified, covering all aspects of cultural exchange, and the evaluation relationship should be diversified, including not only the normal evaluation relationship between teachers and students, but also the evaluation relationship between experts and parents [27]. The evaluation methods should also be diversified, using both quantitative and qualitative methods. The evaluation model of diversified cultural exchange is flexible. Different evaluation models should be established for different cultural exchange objectives [28]. The process of multicultural exchange evaluation is basically consistent with that of general cultural exchange evaluation, including three stages of evaluation preparation, evaluation implementation, and evaluation result analysis and processing, as shown in Figure 3.

The preparation of evaluation is the first step. The quality of preparation will directly affect the quality and effect of cultural exchange evaluation. The main tasks of this link are to determine the object and purpose of the evaluation, to determine the evaluation system, to establish an evaluation group, to formulate an evaluation implementation plan, and to train personnel. Among them, determining the evaluation system is a very difficult task and often requires senior education experts, using fuzzy mathematics or the AHP method, on the basis of the existing evaluation system to establish an evaluation model that meets the evaluation objectives and is suitable for the evaluation object [29]. An organized term to describe the current decision is using an AHP hierarchy. A group of variations or possibilities for achieving the goal are included, as well as a number of elements or characteristics that connect the possibilities to the overall goal. The key benefit of the AHP method is that it creates hierarchies of criteria by breaking down a decision-making problem into its component elements. Assessors can record both positivist and interpretivist evaluation measures for culture quality using AHP. In addition, the AHP approach offers a more organized assessment of a particular culture education quantitative performance measure. It might serve as a practical and quantifiable benchmark for evaluating progress [30]. The implementation of evaluation is the second link, which is directly related to the success of evaluation and the real effect. In this link, the main work includes ideological mobilization of evaluation, evaluation data collection, statistical processing of evaluation data, analysis, and evaluation, writing evaluation conclusions, etc. Among them, the workload of evaluation data statistical processing, analysis, and evaluation is very large, and many statistical charts need to be generated [31]. The evaluation relationship model is the abstraction and description of the evaluation relationship in the evaluation of multicultural communication. Evaluation relationship refers to who evaluates who, including the evaluator and the evaluated. The quantitative evaluation model, qualitative evaluation model, assessment evaluation model, and process evaluation model each have an evaluation relationship model corresponding to them. The data mining model specifies and describes the collection of mining data, the use of mining algorithms, and the display of mining results in the evaluation of diversified cultural exchanges. The quantitative evaluation model, qualitative evaluation model, assessment evaluation model, and process evaluation model each have a corresponding data mining model. The formal definition of the evaluation model is as follows:

$$\mathrm{MTAM} = \{\mathrm{ACM}, \mathrm{ARM}, \mathrm{DMM}, R_1, R_2, A_1, A_2, A_3, M\}. \quad (1)$$

Further, the evaluation characteristics of the evaluation examples of diversified cultural exchanges are standardized as follows:

$$\mathrm{ACM} = \{C_0, C_1, \cdots, C_n\}, \quad (2)$$

where $n = 0, 1, 2, 3, C_n \in \{\mathrm{QutAM}, \mathrm{QuaAM}, \mathrm{CAM}, \mathrm{PAM}\}, C_0, C_1, \ldots, C_n$.

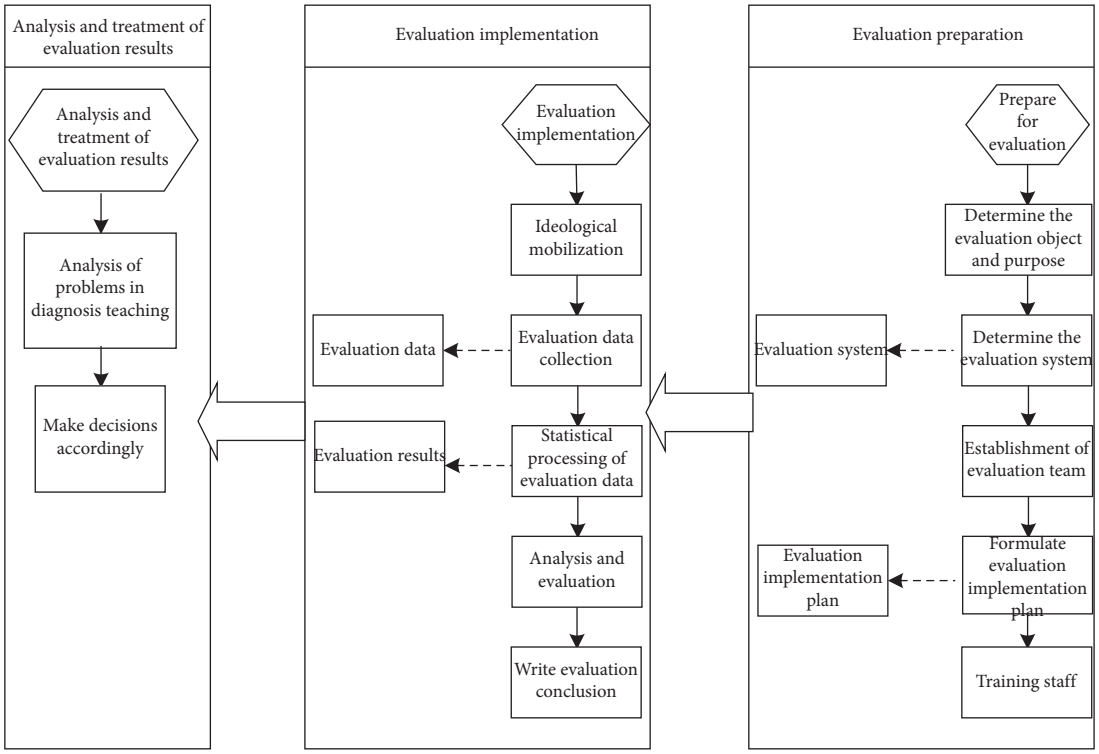

Figure 3: Information processing flow of diversified education exchange.

Indicators usually refer to the provisions reflecting the characteristics of a certain aspect of the target. It is a concrete, measurable, behavioral, and operational goal. In essence, the evaluation index of cultural exchange is the symbol of one aspect of the goal of cultural exchange and the decomposition of the connotation of cultural exchange. The evaluation index system is a systematic and closely related index group formed by the integration of individual indexes. In general, the tree structure is used to explain the link between each index, and the weight is used to define the importance of each index in the system. The following is the quantitative evaluation raw data MOC gathering methodology: Prior to determining the score, the specific evaluation relationship is determined in accordance with the evaluation relationship model that corresponds to the quantitative evaluation model. Each attribute selects the nomenclature of its own scheme and the terminology for Maintenance of Certification (MOC) is always changing. The motivation of cultural evaluation metrics should accurately reflect the theories and precepts that serve as the foundation for cultural programs, the fundamental rules for the development of educational culture, the fundamental traits of the interpreting trends as a guidance, and the cultural process. The essential components of the appraisal must therefore be highlighted, but other components could be disregarded. The key component of evaluation work is the evaluation index system. This component influences assessment results, which in turn influences how accurately schools are evaluated. Then, the evaluators in the evaluation relationship score the evaluation objects one by one according to the quantitative evaluation index system, and the software system calculates the score of nonleaf node index items according to the formula, Finally, the original data of quantitative evaluation are stored in the database.

$$ps = \mathrm{MTAM} \sum_{i=1}^{n} \frac{cs_i \times w_i}{\mathrm{ACM}}, \tag{3}$$

where ps is the score of the parent node and cs_i is the score of the child node. The real number between the specified maximum score, w_i is the weight value of the child node, and the value range is a real number between 0 and 1. The original data of quantitative evaluation of the same evaluation object are summarized. For each evaluation index item, the highest score and the lowest score are removed, and the average score is calculated as the final score of the evaluation index item. The final fractal of all evaluation index items is the quantitative evaluation result. Sometimes, experts will adjust the quantitative evaluation index system, change the weight value of some or all indicators, and reprocess the original data of quantitative evaluation to form a new quantitative evaluation result. According to the evaluation model, the specific evaluation relationship is determined, that is, who should fill in the original data of the evaluation. Then, according to the evaluation system, the evaluation objects fill in the evaluation content with their actual work or learning results. Finally, the software system stores the original data of the evaluation in the database. The processing method of original data MOA is as follows: summarize the original data of the same evaluation object, calculate the workload of the evaluation object in each evaluation according to the formula, and then add the

workload of each evaluation to get the total workload, thus forming the evaluation result.

$$w = \sum_{i=1}^{n} w_i \times q_i - ps. \tag{4}$$

Among them, w is the workload of an evaluation object in an evaluation system, w_i is the workload of an evaluation object in an evaluation raw data, q_i is the workload coefficient of this evaluation raw data, which is defined in the evaluation standard, and w_i and q_i are positive real numbers. Furthermore, the scale of the judgment matrix and its meaning are explained in Table 2.

After normalization, the eigenvalue problem of the judgment matrix A is the ranking weight of the relative importance of the corresponding factors at the same level to a factor at the upper level. This process is called hierarchical single ranking. By breaking down the same ranking categories of elements into sub-levels till every sub-level just contains a single object, the aggregated rating is created hierarchically. Hierarchically, the ranking aggregate is performed with the uncertain elements at the bottom. It combines various level ranks based on the criterion. In order to test the consistency of hierarchical single sorting, it is necessary to calculate the value of consistency index CI and average random consistency index RI, which meet the requirements of Table 3. An indicator of how well a specific character matches on a phylogenetic analysis is the consistency index. It is computed by taking the relatively small number of steps that can be taken and reducing it by the actual series of phases. Furthermore, the mean consistency indexes of a set of random number pairwise comparisons are calculated using the average random consistency index.

If the consistency index of some factors of level B for a single ranking is CIA, and the corresponding average random consistency index is CRS, then the random consistency ratio of level B total ranking is RI, and its calculation method is shown in the formula. When RI < 0.10, it is considered that the ranking result of the hierarchy is consistent, otherwise, the element value of the judgment matrix needs to be readjusted.

$$\mathrm{RI} = \frac{\sum_{j=1}^{m} a_j \mathrm{CI}_j}{\sum_{j=1}^{m} a_j \mathrm{CR}_j}. \tag{5}$$

When the random consistency ratio CR = CI/RI < 0.10, it is considered that the result of the hierarchical single sort has satisfactory consistency, otherwise, it is necessary to adjust the element value of the judgment matrix (Table 4).

The ranking weight of the relative importance of all factors at the same level to the highest level (overall goal) is calculated to be the overall ranking of the level. This process is carried out layer by layer from the highest level to the lowest level, so as to ensure the accuracy and effectiveness of the evaluation results.

2.3. Diversified Communication Strategies of Culture and Education between China and South Korea. Because the meaning of culture itself has diversity, the definition of multiculturalism is different. Although people from different countries and backgrounds have different understandings of multiculturalism, the existence of culture has both existential and externality. This is a consensus among scholars. Based on this, this study holds that multiculturalism mainly refers to the society in which a country or a nation exists. In many cultures, except for the mainstream culture, other cultures have common and equal development. Among them, "many" is embodied in the dialectical unity of "one" and "many," that is to say, "cultural diversity" takes "unity" as the premise and "unity" and "diversity" as the basis, thus forming the dialectical unity of cultural unity and diversity. It contains a kind of pluralistic values and also a kind of cultural openness, tolerance, and equality, through education to improve cultural identity, respect different nationalities, cultures and promote the understanding and harmonious unity between cultures. The core of global security lies in "people," including people's needs, religious customs, national beliefs, ideas, etc., which are closely related to all kinds of education at all levels. Education is not only about people's basic rights, but also a kind of security. Based on this, this study analyzes the association rules of education security, as shown in Figure 4. A broad concept that has received considerable attention in recent cultural heritage arguments is cultural security. It provides suggestions on how to develop and include economic and cultural safety modules in a range of higher education programs.

With the advent of economic integration and information globalization, the process of China's modernization is constantly advancing. The degree of education opening is deepening, the international exchange and cooperation of cultural exchange are becoming more frequent, and the degree of mutual influence and interdependence with neighboring countries is constantly improved. The internationalization of education has become the trend of cultural exchange and development. In this process, China and South Korea in the border areas face double challenges: first, how to adapt to the challenge of globalization under the macro background, and preserve the diversity and nationality of culture; second, how to adapt to the challenges of the overall modernization of the country under the background of the Chinese view, and realize the protection and inheritance of Chinese and Korean culture. In such challenges and adaptations, China and South Korea have been experiencing a series of problems such as cultural reconstruction, psychological gap, personality conflict, survival pursuit, and value mutation. In order to survive in the border areas full of the multicultural atmosphere, they should choose multicultural, which means they should learn the mainstream culture and inherit multi-ethnic culture. Therefore, it is an inevitable choice to grasp and develop cultural exchange from the perspective of multiculturalism. So far, individual experience gradually accepts all aspects of the host country culture and loses its original cultural characteristics more and more. In this mode, assimilation is considered to be an inevitable and one-way result, but the stage of maintaining national culture and accepting mainstream culture is only a temporary feature, and its final result must be consistent with the mainstream culture. This theoretical model

Table 2: Scale of judgment matrix.

Scale	Meaning
1	The two factors are equally important
3	The former is slightly more important than the latter
5	The former is more important than the latter
7	The former is more important than the latter
9	Compared with the two factors, the former is more important than the latter
2, 4, 6, 8	The median value of two adjacent judgments
1, 1/2,. . .,1/9	If b_{ij} is obtained by comparing factor i with j, then $b_{ji} = I/b_{ij}$

Table 3: The value of RI.

Matrix order	1	2	3	4	5	6	7	8	9
RI value	0.00	0.00	0.59	0.91	1.13	1.25	1.34	1.42	1.45

Table 4: Total ranking of levels.

Level A / Level B	A_1 / a_1	A_2 / a_2	... / ...	A_m / a_m	Total sorting weight of level B
B_1	b_{11}	B_{12}	...	b_{1m}	$\sum_{j=1}^{m} a_j\ b_{1j}$
B_2	b_{21}	b_{22}	...	b_{2m}	$\sum_{j=1}^{m} a_j\ b_{2j}$
...	...	...	...	...	...
B_n	b_{n1}	b_{n2}	...	b_{nm}	$\sum_{j=1}^{m} a_j\ b_{nj}$

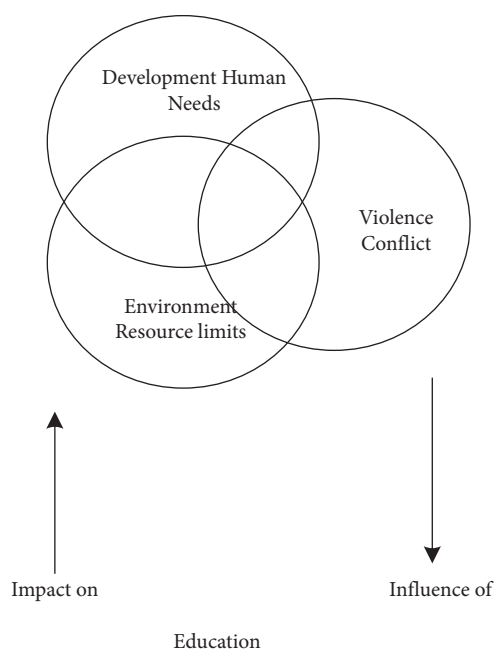

Figure 4: Safety association rules of transnational cultural and educational exchanges.

emphasizes the objectivity and necessity of assimilation, but neglects the subjective and active role of cultural adaptation, which is not enough to summarize the whole connotation of the process of cultural adaptation, which is one-sided (Figure 5).

When the mainstream ethnic groups tend to adopt a strategy of allowing them to integrate into the mainstream ethnic groups based on the cultural recognition of the nonmainstream ethnic groups, and at the same time, it is consistent with the cultural orientation of the nonmainstream ethnic groups, it may produce a harmonious ethnic relationship. On the contrary, if the strategies adopted by the mainstream ethnic groups are inconsistent with the orientation of the nonmainstream ethnic groups, and at the same time, the mainstream ethnic groups do not recognize the nonmainstream ethnic culture or allow them to integrate into it, it may lead to problems or conflicts between ethnic groups. On this basis, the researchers further pointed out that education is one of the important factors affecting cultural adaptation. The deliberate adjustment of an evidence-based treatment or interventions procedure to take languages, culture, and context into account in order to make it consistent with the client's cultural norms, meanings, and values is known as cultural adaptation. It may encourage more interest and involvement in an organization. Among them, the focus of cultural integration is the primary principles of culture, and the fundamental values and actions embodied in these principles. Its starting point strength comes from each individual's choice, exclusion, and modification of culture with his own subjective judgment. The various forms of cultural integration directly or indirectly affect how education makes use of its own conditions to carry out cultural integration. In education, there are three ways of integration: horizontal, vertical, and historical, but it reflects more on the integration of history. That is to say, through the transmission of the cultural tradition of the previous generation, the educated can consciously or unconsciously achieve a relative balance between tradition and reality. So that culture can achieve harmony between "unity" and "diversity." The deliberate adjustment of an evidence-based treatment or interventions procedure to take languages, culture, and context into account in order to make it consistent with the client's cultural norms, meanings, and values is known as cultural adaptation. It may encourage more interest and involvement in an organization.

To sum up, in order to realize the harmony, stability, and long-term development of the border, the education representing the mainstream culture should adopt the multicultural cultural strategy, adhere to the multicultural value orientation, recognize the value of multiculturalism and make it fully integrated into the mainstream culture, while meeting the educational needs of the local people so that the ethnic cultural groups can adopt the corresponding integration strategy. It can produce the best result of cultural adaptation, avoid inducing ethnic conflicts and insecurity, form harmonious and United ethnic relations, and ultimately promote the border education security. Cultural

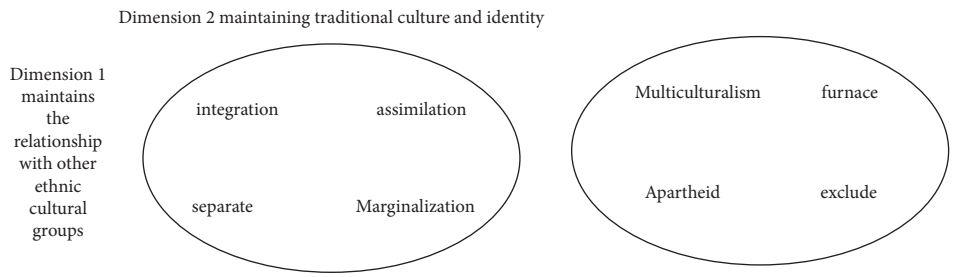

Figure 5: Information management strategy of educational and cultural exchanges between China and South Korea.

harmony is bound to pursue the identification, adaptation, and integration of multicultures. Therefore, cultural identity is the cultural foundation of the harmonious coexistence of different cultures and the energy cornerstone of coordinating social well-being. The accurate multicultural view advocates seeking to coordinate the same and seek common ground while reserving differences on the premise of respecting differences. This kind of energy of seeking new "harmony" of coordinated growth provides a favorable thinking basis for the fair integration of multicultures and the coordinated coexistence of multicultures. Improving cultural identity and enhancing national cohesion are the cornerstone of ensuring the security of cultural exchanges and promoting social stability and harmony in border areas. The correct multicultural view advocates that we should respect differences and cherish the bribe guidance, so as to better guide cultural action. Through school teaching and enhancing the integration of school teaching with community and family, it is difficult for multicultural integration to be fair. The inevitable cultural integration mode forms a kind of coordinated cultural energy and achieves unity, education, and peace, After all, the national unity and society in the United areas will remain unchanged, and there is a progressive relationship between them. Based on the above analysis, the author takes national cohesion, correct multicultural view, and reasonable integration of multiculture as the first level indicators of the analysis framework, and determines the logical schematic diagram of the analysis framework of cultural exchange security around these core factors, as shown in Figure 6.

In the aspect of the integration of justice of multicultural, the integration of culture in education includes two aspects: the integration of the internal education system and the integration outside the education system, community culture, and regional culture are closely related to the culture of China and South Korea. Therefore, we can conclude that cultural integration in education includes the integration of school education itself and community culture in order to actively participate in the training of multicultural education and carry out multicultural education. The curriculum is the carrier of multicultural integration. The course of multicultural integration is essentially a reflection and re-study of a specific culture. The special geographical environment in border areas requires the border people to face multicultural and excellent achievements of ethnic culture with an open mind and compatible position. And we should take a broad view of our national traditional culture, and the contemporary cost of fair interpretation of traditional culture is to establish a curriculum concept of cultural diversity, integrate the cultural essence or characteristics of China and South Korea into the existing curriculum of China and South Korea, and actively adopt multicultural integration channels to teach multicultural, in order to reflect the concept of cultural diversity. To integrate the multiculture dialectically and impartially. In addition to the active role of school education, the integration of multiculturalism is also a booster of community cooperation. School education should actively form a benign cooperative relationship with the community and family, advocate the cooperation of schools, families, and communities, comprehensively utilize the family resources of the community and promote the integration of multicultural. In terms of cultural exchange security, through the above analysis of the concept and characteristics of cultural exchange security, it can be concluded that the connotation of cultural exchange security includes the healthy development of education in border areas, which requires improving cultural exchange identity, ensuring the quality of cultural exchange and further developing cultural exchange undertakings. At the same time, it emphasizes the realization of cultural exchange function, including social function, economic function, and cultural function of cultural exchange, especially the function of inheritance and integration of national culture.

3. Analysis of Experimental Results

In order to verify the feasibility of the diversified communication method of culture and education between China and South Korea based on new media technology, the border areas of China and South Korea were selected as the investigation area, and some students, teachers, and parents were selected for investigation and analysis. In order to ensure the validity of the experimental results, first of all, the data samples of the participants are counted, and the specific illustrations are shown in Table 5 and Figure 7.

Teachers are the key factor in the development of education in border areas, and the construction of a good teaching staff is the premise and guarantee for the development and improvement of education in border areas. To this end, the state, autonomous county, and local governments have adopted a variety of policies and measures to improve the level of cultural exchanges, and encourage and attract teachers from other regions to teach in border areas. The implementation of these policies and measures has

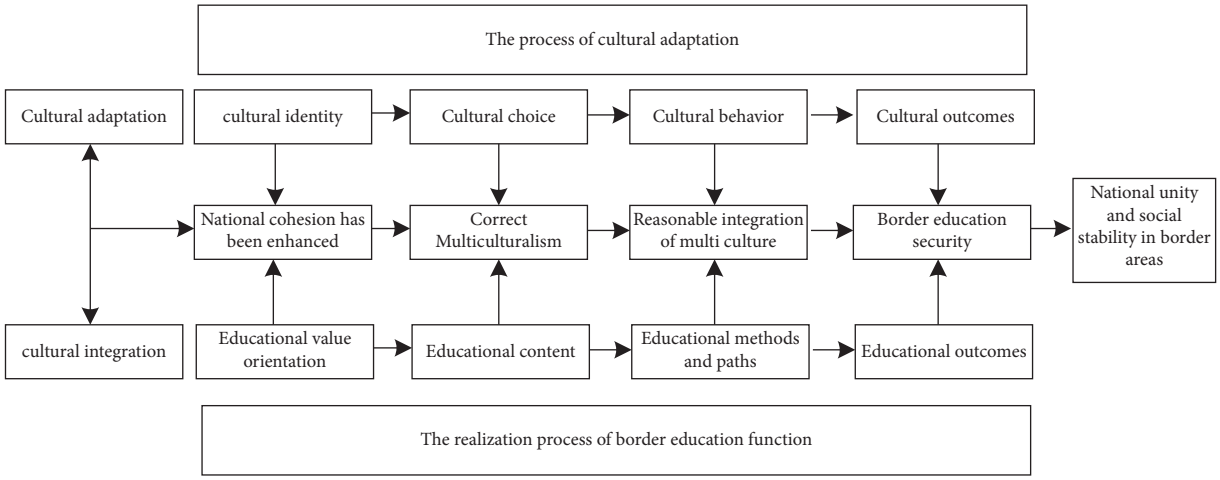

Figure 6: Management system of cultural and educational exchanges between China and South Korea.

Table 5: Collection of basic information of inspection samples.

High school			Junior middle school			Primary school		
Enrollment rate	Consolidation rate	Graduation rate	Enrollment rate	Consolidation rate	Graduation rate	Enrollment rate	Consolidation rate	Graduation rate
40.8	60.57	38.1	97.62	82.45	45.05	99.52	92.29	72.93
38.5	59.37	32.5	98	91.25	44.2	99.43	93.32	74.79
43.6	51.15	36	95.02	80.12	40.5	99.45	93.33	80.13

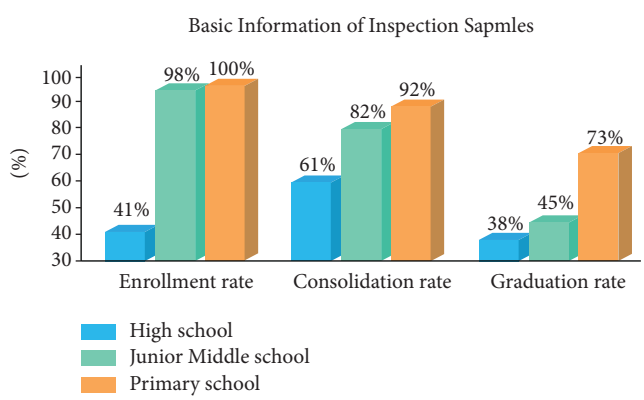

Figure 7: Survey results of collected inspection samples.

promoted the development and growth of teachers in border areas and improved the quality of teachers. However, there are many unreasonable phenomena in the structure of teachers. For example, the subject structure, age structure, and ethnic structure of teachers need to be constantly optimized (Table 6).

According to the Ministry of education's "primary and secondary school staff establishment standard," the teacher–student ratio of primary schools in counties and towns is 1 : 21 And 1 : 23 respectively, while that of secondary schools in counties and towns is 1 : 16 And 1 : 18, respectively. Among them, the average ratio of teachers to students in middle schools is 1 : 7.9, and the number of teachers in border areas is sufficient, reaching the basic national standard. However, there is a shortage of teachers in some subjects, such as music, natural science, physical education, English, and so on. Identifying with the mainstream culture of a country is an indispensable part of educational security, including identifying with the country's religious beliefs, political ideals, and core values. A country's education security must begin with the desire to learn and understand its national culture and tradition, and be able to firmly believe that national culture and tradition should be protected. Therefore, the identification of national culture is the primary condition to ensure the safety of cultural exchange, and the low identification of national culture is the primary threat to the safety of cultural exchange. According to Fei Xiaotong's cultural theory of "pluralistic integration" and the special geographical location of the border area between China and South Korea, the ethnic cultural identity we emphasize here includes two aspects: one is the identity of Chinese national culture. On the other hand, it is the identification of the national culture. The theory gives a broad conceptual overview of how cultural education is formed and how it is structured. It shows how a united, multiethnic country is formed and developed in reference to the relationship between nation and state. It engaged in extensive, systematic current discussions on the emergence and growth of multiculturalism unity in a variety of fields, including ethnic hypothesis, ethnic background, ethnography and ethnography, and global nationalities, thereby advancing the main objective of fostering a real sense of community. Therefore, we investigate and analyze the students, teachers, and parents' cultural identity of the Chinese nation, Chinese traditional cultural identity, and national cultural identity. This part of the survey uses the Likert 5-

Table 6: Statistical table of the teacher-student ratio of various schools.

High school			Junior middle school			Primary school		
On campus students	Full time teacher	Teacher-student ratio	On campus students	Full time teacher	Teacher-student ratio	On campus students	Full time teacher	Teacher-student ratio
712	41	1 : 17.4	3077	386	1 : 7.9	26730	1696	1 : 15.7
3165	174	1 : 18.2	10034	671	1 : 14.9	26028	1482	1 : 17.6
1822	111	1 : 16.3	10187	621	1 : 16.4	7534	652	1 : 11.6

Table 7: Attitudes towards Chinese cultural identity.

Evaluation project	Attitude (%)					Mean value	Standard deviation
	Totally disagree	Basically disagree	Indifferent	Basically agreed	In full agreement		
I am proud of Chinese traditional culture	4.4	36.6	11.9	10.4	36.7	2.41	0.76
I understand Chinese traditional culture	13.5	41.2	2.7	7.5	35.1	2.66	1.03
I have a strong interest in learning Chinese	15.2	25.6	7.4	15.3	36.5	2.33	1.05
I like to speak Chinese	3.2	6.4	11.5	14.6	64.3	1.75	0.86

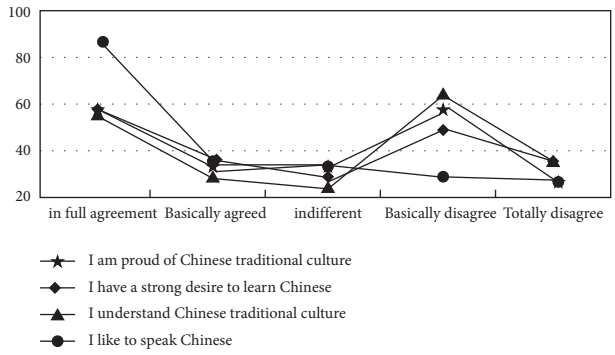

Figure 8: Survey results of the identity of Chinese cultural diversity.

Table 8: Views on the effect of the diversified exchange of overseas culture and education.

Evaluation project	Attitude (%)					Mean value	Standard deviation
	Totally disagree	Basically disagree	Indifferent	Basically agreed	In full agreement		
I think overseas education and culture can enter China	11.8	11.0	14.2	43.6	19.5	1.89	1.25
I will resist the bad culture abroad	20.9	27.8	15.4	21.2	14.6	3.19	1.37
I think foreign culture will have a bad influence on us	25.7	30.1	9.8	20.7	13.4	3.15	1.34

point scoring method to set the attitude options as "completely agree," "basically agree," "indifferent," "basically disagree" and "completely disagree." Both surveyed managers and participants will have no trouble using the 5-point Likert scale. Compared to higher-point measures, it requires less time in completing and monitors superior. There are options for responders without overwhelming the evaluating activities. The results are shown in Table 7.

The research results are further plotted in Figure 8.

From the chart, we can see that the students have a low sense of cultural identity of the Chinese nation and basically express their disapproval. On the issue of "like to speak Chinese," the students agree, but 25.6% of them have no strong desire to learn Chinese. On the issue of "understanding Chinese traditional culture," the average value is 2.66, which indicates that most of the students do not know much about Chinese traditional culture, and even 41% of the students are not proud of Chinese traditional culture.

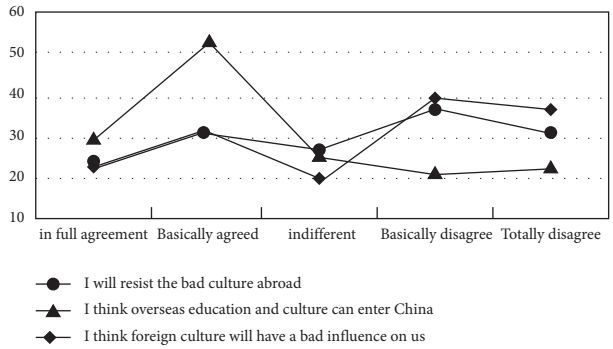

Figure 9: Survey results of Korean cultural diversity communication identity.

According to the survey results of students, parents, and teachers' views on overseas culture, the average value is taken and consolidated into the following statistical chart. The results are in Table 8.

We further draw the statistical results in Figure 9.

It can be seen from the table that the border people are too tolerant of foreign culture and lack the concept and consciousness of absorbing foreign culture. 55.7% of the border people think that foreign culture will not have adverse effects on themselves, 63.1% of the border people think that foreign education and culture can enter China, especially 48.7% of the border people say that they will not resist foreign bad culture, and the average value of this item reaches 3.19. From the picture, we can see that there are many problems in the outliers' view of overseas culture. Most of the outliers say that they basically disagree with or completely disagree with "I think overseas culture will have a bad impact on us" and "I will boycott bad overseas culture," and "I think overseas education and culture can enter China," they all agreed.

4. Conclusions

Today, with the increasingly comprehensive and perfect cultural exchange system, integration and application has become the theme of cultural exchange activities. Therefore, mining the value connotation of different cultures between China and South Korea, enriching cultural concepts, and changing cultural exchange thinking have become the key demands of diversified cultural and educational exchanges between China and South Korea. In addition, the richness and application value of cultural content also provide positive significance for the construction of the current diversified communication mechanism. In fact, it has gradually become a new requirement for the society to realize its best responsibility in cultural exchange activities. From the objective performance of culture, the content is diverse and hierarchical. In the future, personal exclusion and even space-time constraints decided to bring on by pandemic, reconfigure the information sharing the ecological balance of cultural heritage, and genetic makeup and use the treasured riches left to humanity in the future, digital communication subject matter of cultural heritage displaying the qualities from real and virtual interconnection of cultural heritage in a fully integrated media landscape.

Data Availability

The datasets used and/or analyzed during the current study are available from the corresponding author on reasonable request.

Conflicts of Interest

The authors declare no conflicts of interest.

Acknowledgments

This study was supported by the Special Fund of "Academy of Global Governance and Area Studies" of Sichuan Normal University in 2021 (NO. GJZD2021001).

References

[1] Z. Wang and N. Yu, "Education data-driven online course optimization mechanism for college student," *Mobile Information Systems*, vol. 2021, Article ID 5545621, 8 pages, 2021.

[2] F. Cappellano and T. Makkonen, "Cross-border regional innovation ecosystems: the role of non-profit organizations in cross-border cooperation at the US-Mexico border," *Geojournal*, vol. 85, no. 6, pp. 1515–1528, 2020.

[3] H. Zhang, X. Li, H. Yu et al., "The impacts of new media on marketing effectiveness: a comparative study of China and South Korea tourism souvenirs website," *iScience*, vol. 22, no. 2, pp. 16–27, 2019.

[4] Y. Gao, Y. Fan, J. Wang, X. Li, and J. Pei, "The mediating role of safety management practices in process safety culture in the Chinese oil industry," *Journal of Loss Prevention in the Process Industries*, vol. 57, no. 2, pp. 223–230, 2019.

[5] Y. Latif, N. Harrison, and H. E. Chu, "Interpreting the cultural and academic experiences of PhD students from the Indian sub-continent and the Chinese regions in Australian universities," *International Journal of Emerging Technologies in Learning (iJET)*, vol. 15, no. 19, p. 171, 2020.

[6] B. Balakrishnan, F. Tochinai, H. Kanemitsu, and A. Ali, "Engineering ethics education from the cultural and religious perspectives: a study among Malaysian undergraduates," *European Journal of Engineering Education*, vol. 46, no. 2, pp. 1–12, 2021.

[7] M. Jaeger, S. Gang, and D. Adair, "Impact of cultural differences among engineering managers on assessing competencies of engineering graduates – a case study," *International Journal of Engineering Education*, vol. 36, no. 1(A), pp. 117–129, 2020.

[8] T. Jiang and J. Yang, "Teaching of practice innovation of new media interactive for art design training in college," *International Journal of Electrical Engineering Education*, Article ID 002072092094444, 2020.

[9] X. Zenggang, Z. Mingyang, Z. Xuemin et al., "Social similarity routing algorithm based on socially aware networks in the big data environment," *Journal of Signal Processing Systems*, 2022.

[10] A. Li, D. Spano, J. Krivochiza et al., "A tutorial on interference exploitation via symbol-level precoding: overview, state-of-the-art and future directions," *IEEE Communications Surveys & Tutorials*, vol. 22, no. 2, pp. 796–839, 2020.

[11] K. Liew and P. Lindborg, "A sonification of cross-cultural differences in happiness-related tweets," *Journal of the Audio Engineering Society*, vol. 68, no. 1/2, pp. 25–33, 2020.

[12] A. Li, C. Masouros, A. L. Swindlehurst, and W. Yu, "1-Bit massive MIMO transmission: embracing interference with symbol-level precoding," *IEEE Communications Magazine*, vol. 59, no. 5, pp. 121–127, 2021.

[13] W. Zheng, Y. Zhou, S. Liu, J. Tian, B. Yang, and L. Yin, "A deep fusion matching network semantic reasoning model," *Applied Sciences*, vol. 12, no. 7, p. 3416, 2022.

[14] W. Zheng and L. Yin, "Characterization inference based on joint-optimization of multi-layer semantics and deep fusion matching network," *PeerJ Computer Science*, vol. 8, p. e908, 2022.

[15] D. P. Sang, J. Y. Lee, and W. Bo, "The main factors affecting cultural exchange between Korea and China: a semantic network analysis based on the cultural governance perspective - ScienceDirect," *International Journal of Intercultural Relations: International Journal of Information Retrieval*, vol. 71, no. 12, pp. 72–83, 2019.

[16] W. Zheng, X. Tian, B. Yang et al., "A few shot classification methods based on multiscale relational networks," *Applied Sciences*, vol. 12, no. 8, p. 4059, 2022.

[17] J. Li, K. Xu, S. Chaudhuri, E. Yumer, H. Zhang, and L. Guibas, "GRASS: generative recursive autoencoders for shape structures," *ACM Transactions on Graphics*, vol. 36, no. 4, pp. 1–14, 2017.

[18] C. Chung, "Contemporary art exchange between Korea, China and taiwan: when Korea and China established diplomatic relations (1992)," *Art History*, vol. 39, no. 6, pp. 303–331, 2020.

[19] H. Zhao, C. Zhu, X. Xu, H. Huang, and K. Xu, "Learning practically feasible policies for online 3D bin packing," *Science China Information Sciences*, vol. 65, no. 1, Article ID 112105, 2021.

[20] Z. Xiong, Q. Liu, and X. Huang, "Thinkingfluence of digital educational games on preschool Children's creative thinking," *Computers & Education*, vol. 189, Article ID 104578, 2022.

[21] S. Hong, "The cultural exchange between China and Korea under the network media environment," *Journal of Physics: Conference Series*, vol. 1325, no. 1, Article ID 012110, 2019.

[22] D. M. Yu, Z. M. Ma, and R. J. Wang, "Efficient Smart Grid Load Balancing via Fog and Cloud Computing," *Mathematical Problems in Engineering*, vol. 2022, Article ID 3151249, 11 pages, 2022.

[23] D. M. Yu, J. T. Wu, W. D. Wang, and B. Gu, "Optimal performance of hybrid energy system in the presence of electrical and heat storage systems under uncertainties using stochastic p-robust optimization technique," *Sustainable Cities and Society*, vol. 83, Article ID 103935, 2022.

[24] Z. Zhou, K. Sohn, H. Yoon, and O. Kwon, "The empirical study on the effect of technology exchanges in the fourth industrial revolution between Korea and China: focused on the firm social network analysis," *The Journal of Society for e-Business Studies*, vol. 25, no. 3, pp. 41–61, 2020.

[25] L. C. Bresser-Pereira, E. Jabbour, and L. F. D. Paula, "South Korea's and China's catching-up: a new-developmentalist analysis," *Brazilian Journal of Political Economy*, vol. 40, no. 2, pp. 264–284, 2020.

[26] I. Belousova, S. Bairamova, and S. Ova, "Linguistic and cognitive analysis of inter-cultural business discourse from the perspective of "dialogue of cultures" in the formation of inter-cultural communicative competence," *International Journal of Emerging Technologies in Learning (iJET)*, vol. 15, no. 09, p. 173, 2020.

[27] J. Liu and T. Zhu, "Application of blockchain technology in cultural and creative design and education," *International Journal of Emerging Technologies in Learning (iJET)*, vol. 16, no. 04, p. 228, 2021.

[28] B. Balakrishnan, F. Tochinai, H. Kanemitsu, and A. Altalbe, "Engineering ethics education from the cultural and religious perspectives: a study among Malaysian undergraduates," *European Journal of Engineering Education*, vol. 46, no. 5, pp. 707–717, 2021.

[29] E. Nectara and N. E. Mircioag, "Identification of cultural dimensions specific to pre-university education," *Risk Analysis*, p. 398, 2021.

[30] L. Xiujuan, M. K. Kagita, and L. Kumar, "Machine learning techniques for multi-media communications in business marketing," *Journal of Multiple-Valued Logic and Soft Computing*, vol. 36, no. 1-3, pp. 135–150, 2021.

[31] X. Wang and Z. Liu, "Online engagement in social media: a cross-cultural comparison," *Computers in Human Behavior*, vol. 97, pp. 137–150, 2019.

Hindawi
Mobile Information Systems
Volume 2022, Article ID 1454855, 15 pages
https://doi.org/10.1155/2022/1454855

Research Article

The Safe Financial Processing Method for Realizing Supply Chain Integrated Business Intelligence Using Blockchain Application Scenarios

Xianqiu Tan[1] and Kaza Mojtahe[2]

[1]*Nanjing Institute of Railway Technology, Nanjing 210031, China*
[2]*Department of Computer Engineering, Kyrgyz-Turkish Manas University, Bishkek, Kyrgyzstan*

Correspondence should be addressed to Kaza Mojtahe; kaza.mojtahe@mail.cu.edu.kg

Received 16 June 2022; Revised 12 July 2022; Accepted 16 July 2022; Published 24 August 2022

Academic Editor: Chi Lin

In order to improve the financial processing effect of supply chain integrated business intelligence, this study applies blockchain technology to the financial processing of supply chain integrated business intelligence and conducts an evolutionary game analysis on the factors that affect the selection of information-sharing strategies for logistic service supply chain nodes. By establishing the evolutionary game model of logistic service integrators and logistic service providers under the strategy of information sharing and information nonsharing, the value of information sharing in the logistic service supply chain is discussed from a qualitative and quantitative perspective. In addition, this study constructs the expected profit mathematical model of a two-level logistic service supply chain composed of logistic service integrators and logistic service providers. The experimental research results show that the safe financial processing method for realizing supply chain integrated business intelligence using blockchain application scenarios has good results.

1. Introduction

Nowadays, with the development of science and technology and the continuous improvement of people's demand for a high-quality life, the entire social needs, production methods, and social division of labor are constantly changing. The production of commodities has changed from a model of complete production by a single company to a model of cooperative production by multiple companies. Moreover, market competition has evolved from simple customer competition to competition between the entire supply chain involving multiple links in commodity production [1]. Banks and other funding parties radiate financial products and services to the upstream and downstream and even the entire industry chain around relevant core companies to solve the financial problems of corporate procurement, sales, and inventory in the supply chain. This financial operation mode is called supply chain finance. Supply chain finance mainly includes financing services such as goods mortgage, advance payment, and accounts receivable. The supply chain finance business is mainly participated by banks and other funders, large-scale core enterprises, small and medium-sized suppliers, and other enterprises. Due to the special requirements of the supply chain finance industry for information privacy and security, the current supply chain finance system has many problems [2].

The blockchain technology is an organic collection of many existing technologies, which mainly include cryptography, consensus algorithms, and distributed systems. The blockchain is simply a distributed ledger, which allows every distributed node in the blockchain network to participate in the blockchain, and each participant shares the same permanent and transparent transaction record ledger. Blockchain technology uses cryptography-related technologies to realize that every transaction in the blockchain can

be traced back, and it ensures that no one can change the transactions recorded in the blockchain shared ledger. At the same time, the distributed consensus algorithm protocol is used to allow each participant of the blockchain to reach a consensus on the transaction result and record it in the shared ledger. Blockchain smart contract technology can replace manual operations, set the trigger conditions of the smart contract in advance, and automatically execute the smart contract to complete the transfer of assets after the transaction is executed to a certain stage [3].

The blockchain system can be regarded as a distributed multinode shared database ledger. Each distributed node in the blockchain system communicates through a peer-to-peer protocol, that is, P2P technology; and each transaction in the system can use a one-way hash function, asymmetric encryption, and other related cryptography technologies to achieve high security. Since the blockchain is equivalent to a distributed system in which all participants share the ledger, any company participating in the same blockchain has a copy of the entire ledger as the upstream supplier of the financial participants of the blockchain supply chain. Downstream buyers, core companies, and financial institutions can share benefits from related financing businesses, while minimizing policy and operating risks without the need to build a financial system.

This study combines the blockchain technology to analyze the security financial management of the supply chain integrated business intelligence, builds an intelligent system, and verifies the performance of the system to improve the security financial management effect of the supply chain integrated business intelligence.

2. Related Work

The "ghost protocol" proposed in document [4] ensures the integrity of the blockchain, records the entire process of value transfer (transaction) immutably, and uses decentralization and trustless methods to collectively maintain the reliability of a databook sexual solution; this databook is completely public and not under the control of any organization. Literature [5] proposes that blockchain is a technology with breakthrough significance across the ages, and the core ideas behind this technology, such as decentralization, trustlessness, and national accounting, are its greatness. Therefore, blockchain technology will be the core technology that has the most potential to trigger the fourth industrial revolution after steam engine, electricity, information, and internet technology.

The core feature of blockchain technology is that the transaction information on the chain cannot be tampered with, and it is difficult to interfere, modify, or delete it under the existing technical conditions. Literature [6] proposes that immutability is also the most important difficulty in realizing landing applications. The immutability of blockchain may turn its advantages into disadvantages in the activities of reversing financial services. Literature [7] pointed out that for some time, blockchain technology wanted to replace legal currency in the form of blockchain tokens, and even wanted to replace government agencies with decentralized functions, but it was difficult to achieve in actual operation. Yes, blockchain technology is just a technology, and it needs to find an application scenario suitable for this technology in order to play its own role. Literature [8] believes that the blockchain has an "impossible triangle" in the three aspects of "decentralization," "high efficiency and low energy," and "security." It is difficult to achieve three goals at the same time. To achieve two of them, it is necessary to abandon another goal, which means that if two of the attributes are strengthened, the third attribute will be automatically weakened. The premise of the use of blockchain technology is that users should keep the private key they generated. Once the private key is lost, they cannot perform any operations on the assets in their account. Individual ordinary users or users without much technical experience may feel private. If the key is lost, it is enough to apply for a replacement like an ID card, but in fact, it is impossible. Literature [9] believes that with the development of society, a large number of mathematical algorithms have been developed, resulting in the blockchain algorithm that may be cracked by new algorithms, so it may be a blockchain formed by mathematical principles someday in the future. The algorithmic security of the technology will be threatened. Such risks may not exist in the short term but may exist in the long term. Therefore, the application of blockchain technology to the business process of the securitization of accounts receivable assets may bring risks.

The blockchain technology is an emerging field of research. Domestic and foreign scholars in various industries use the theory of blockchain technology to solve problems that arise. Most scholars analyze the application of this technology theoretically. Literature [10] believes that the development of blockchain technology can not only make the asset securitization of accounts receivable become a reality but can also become a boost to social development; taking the application of blockchain technology in various industries as the research direction, the new intermediary will be based on blockchain technology, which provides the possibility to build a trust mechanism that does not rely on third-party platforms. One argument for the popularity of blockchain in society is that blockchain technology can rebuild business models, so it will change the production relations of traditional society. In essence, it is a human cognitive revolution, and capital is profit-seeking. Yes, the financial industry takes the lead after the emergence of a new technology. The literature [11] surveyed more than 1,300 financial institutions around the world. It can be seen that the number of financial institutions that use the combination of blockchain technology and traditional business processes will account for 55%; in 2020, it will reach 77%. Literature [12] starts with the business process of asset securitization of accounts receivable. The problems encountered in the business process of the asset securitization of accounts receivable are reflected in the following aspects [13]: the authenticity of the relevant assets in the pool cannot be effectively determined; the lack of repayment rules after the financial institution itself has problems;

in accounts receivable, the characteristics of asset securitization products are that there are many trading entities, the transaction structure of securitization products is relatively complicated, and the data transmission chain is long. These difficulties also indirectly lead to deeper problems, that is, it is difficult to obtain low capital costs for issuing securitized products, and the cost limits its further development [14]. Literature [15] believes that the traditional problem of the securitization of accounts receivable assets is that the transaction structure is complicated, the transaction chain of the participants is very long, and there may be external uncertain factors, which further trigger the problem of information asymmetry. Literature [16] proposes to establish a negative list system. Starting from the top level, the regulatory authorities play an intermediate role to solve the relationship between blockchain service organizations and specific landing application scenarios, and better regulate the development of blockchain technology.

3. Blockchain-Based Supply Chain Business Intelligence Security Financial Processing Model

The final profit of the game subject is determined by the strategy chosen by itself and the strategy chosen by the other party in the game. It represents the expected return when the two parties in the game choose to share or not share information.

Game party 1 adopts the information-sharing strategy, and the expected benefits are [17] as follows:

$$U_{11} = y\left(R_1 + gK_1Q_2 + \alpha Q_1 - C_1 - \theta Q_1\right) + (1-y)\left(R_1 - C_1 - \theta Q_1\right). \tag{1}$$

Game party 1 adopts the information nonsharing strategy, and the expected benefits are as follows:

$$U_{12} = y\left(R_1 + K_1Q_2\right) + (1-y)R_1. \tag{2}$$

The average expected return of the game party 1 is as follows:

$$\overline{U_1} = xU_{11} + (1-x)U_{12}. \tag{3}$$

Game party 1 chooses the copy dynamic equation of the information-sharing strategy as [18] follows:

$$F(x) = \frac{dx}{dt} = x\left(U_{11} - \overline{U_1}\right). \tag{4}$$

Substituting formulas (1)–(3) into (4), we get the following:

$$\begin{aligned}\frac{dx}{dt} &= x(1-x)\left(U_{11} - U_{12}\right)\\ &= x(1-x)\left\{y\left[K_1Q_2(g-1) + \alpha Q_1\right] - C_1 - \theta Q_1\right\}.\end{aligned} \tag{5}$$

According to formula (5), when $dx/dt = 0$, three possible equilibrium solutions can be obtained as follows: $x_1^* = 0, x_2^* = 1$, and $y^* = C_1 + \theta Q_1/K_1Q_2(g-1) + \alpha Q_1$. However, these three solutions are not necessarily all evolutionary stable strategies. According to the stability theorem of differential equations, when $dx/dt = 0$ and $F'(x) < 0$ are satisfied, it is an evolutionary stable strategy in a stable state. Therefore, when we find the first derivative of formula (5), we get the following:

$$F'(x) = (1-2x)\left\{y\left[K_1Q_2(g-1) + \alpha Q_1\right] - C_1 - \theta Q_1\right\}. \tag{6}$$

Through formulas (5) and (6), it can be analyzed that the evolutionary stable strategies of game party 1 are [19] as follows:

(1) If $y = y^* = C_1 + \theta Q_1/K_1Q_2(g-1) + \alpha Q_1$, then $dx/dt \equiv 0$, which shows that the three solutions are all evolutionary stable strategies.

(2) If $y \neq y^* = C_1 + \theta Q_1/K_1Q_2(g-1) + \alpha Q_1, x_1^* = 0, x_2^* = 1$ are all evolutionary stable equilibrium points of x. Therefore, the different situations of $C_1 + \theta Q_1/K_1Q_2(g-1) + \alpha Q_1$ are discussed and analyzed.

(i) When $C_1 + \theta Q_1 > K_1Q_2(g_1 - 1) + \alpha Q_1$, for any $y(0 \le y \le 1), F'(x^* = 0) < 0$, and $x_1^* = 0$ is the evolutionary stable strategy of game party 1.

(ii) When $C_1 + \theta Q_1 < K_1Q(g-1) + \alpha Q_1$, we discuss in two situations.

When $y < y^* = C_1 + \theta Q_1/K_1Q_2(g-1) + \alpha Q_1, F'(x_1^* = 0) < 0, F'(x_2^* = 1) > 0$, so $x_1^* = 0$ is a stable equilibrium point. When $y > y^* = C_1 + \theta Q_1/K_1Q_2(g-1) + \alpha Q_1$, $F'(x_1^* - 0) > 0, F'(x_2^* - 1) < 0$, so $x_2^* = 1$ is a stable equilibrium point. It can be seen that in the case of $C_1 + \theta Q_1 < K_1Q_2(g-1) + \alpha Q_1$, the steady state is affected by the value of y^*. The larger the y^* is, the smaller the probability that y will fall within the interval $[y^*, 1]$, and the probability that game party 1 chooses the information-sharing strategy will decrease accordingly.

Game party 2 chooses the expected benefits of the information-sharing strategy as [20]follows:

$$U_{21} = x\left(R_2 + gK_2Q_1 + \alpha Q_2 - C_2 - \theta Q_2\right) + (1-x)\left(R_2 - C_2 - \theta Q_2\right). \tag{7}$$

The expected return of the game party 2 who chooses the information nonsharing strategy is as follows:

$$U_{22} = x\left(R_2 + K_2Q_1\right) + (1-x)R_2. \tag{8}$$

The average expected return of the game party 2 is as follows:

$$\overline{U_2} = yU_{21} + (1-y)U_{22}. \tag{9}$$

The copy dynamic equation for the game party 2 to choose the information-sharing strategy is as follows:

$$F(y) = \frac{dy}{dt} = y\left(U_{21} - \overline{U_2}\right). \tag{10}$$

Substituting formulas (7)–(9) into (10), we get the following:

$$\frac{dy}{dt} = y(1-y)(U_{21} - U_{22}) = y(1-y)\{x[K_2Q_1(g-1) + \alpha Q_2] - C_2 - \theta Q_2\}. \quad (11)$$

According to formula (11), when $dy/dt = 0$, three possible stable solutions can be obtained as follows: $y_1^* = 0, y_2^* = 1, x^* = C_2 + \theta Q_2/K_2Q_1(g-1) + \alpha Q_2$. However, these three solutions do not necessarily belong to evolutionary stable strategies. From the stability theorem of differential equations, we know that when $dy/dt = 0$ and $F'(y) < 0$, it is an evolutionary stable strategy in a stable state. Therefore, by taking the first-order derivative of equation (11), we obtain the following:

$$F'(y) = (1-2y)\{x[K_2Q_1(g-1) + \alpha Q_2] - C_2 - \theta Q_2\}. \quad (12)$$

Through formulas (11) and (12), it can be analyzed that the evolutionary stable strategies of game party 2 are as follows:

(1) If $x = x^* = C_2 + \theta Q_2/K_2Q_1(g-1) + \alpha Q_2$, then $dy/dt \equiv 0$, which means that the three solutions are all evolutionary stable strategies, and the results of the two strategies of information sharing and non-sharing for game party 2 are the same.

(2) If $x \neq x^* = C_2 + \theta Q_2/K_2Q_1(g-1) + \alpha Q_2$, $y_1^* = 0$, $y_2^* = 1$ are all evolutionary stable equilibrium points of y. Therefore, the different situations of $C_2 + (\theta - \alpha)Q_2/K_2Q_1(g-1)$ are discussed and analyzed.

(i) When $C_2 + \theta Q_2 > K_2Q_1(g-1) + \alpha Q_2$, for any $x(0 \le x \le 1), F'(y^* = 0) < 0$, $y_1^* = 0$ is the evolutionary stable strategy of game party 2.

(ii) When $C_2 + \theta Q_2 < K_2Q_1(g-1) + \alpha Q_2$, we discuss in two situations [21].

If $x < x^* = C_2 + \theta Q_2/K_2Q_1(g-1) + \alpha Q_2, F'(y_1^* = 0) < 0, F'(y_2^* = 1) > 0$, so $y_1^* = 0$ is a stable equilibrium point. If $x > x^* = C_2 + \theta Q_2/K_2Q_1(g-1) + \alpha Q_2$, $F'(y_1^* = 0) > 0$, $F'(y_2^* = 1) < 0$, so $y_2^* = 1$ is a stable equilibrium point. It can be seen from the above that in the case of $C_2 + \theta Q_2 < K_2Q_1(g-1) + \alpha Q_2$, the steady state is affected by the value of x^*. The larger the x^*, the smaller the probability that x falls within the $[x^*, 1]$ interval, and the possibility of the player 2 choosing the information-sharing strategy will decrease.

The two parties of the game are independent of each other. However, it requires the cooperation of both parties to form a stable evolution strategy. This is not only to analyze the evolution process of information-sharing behavior among supply chain members but also to consider the situation of both parties. From formulas 5 and 11, it can be seen that the possible stable strategies are $(0,0)$, $(0,1)$, $(1,0)$, $(1,1)$, (x^*, y^*), and the existing evolutionary situations are as follows:

(1) When $C_1 + \theta Q_1 > K_1Q_2(g-1) + \alpha Q_1, C_2 + \theta Q_2 > K_2Q_1(g-1) + \alpha Q_2$, the additional benefits obtained by both parties of the game by taking information-sharing behaviors are small, and they are not enough to make up for the cost and existing risks of information-sharing inputs. As shown in Figure 1(a), the evolution process converges to $x^* = 0, y^* = 0$, and the stable point is (0,0). The evolutionary stable strategy of integrators and providers is (not sharing and not sharing).

(2) When $C_1 + \theta Q_1 > K_1Q_2(g-1) + \alpha Q_1, C_2 + \theta Q_2 < K_2Q_1(g-1) + \alpha Q_2$, the cost and risk borne by the integrator for information sharing are higher than the benefits that can be obtained by information sharing. However, the additional benefits obtained by the provider's choice of information-sharing strategy are greater than the costs and risks involved in information sharing. As shown in Figure 1(b), the evolution process converges to $x^* = 0, y^* = 1$, and the stable point is (0,1). The evolutionary and stable strategy of integrators and providers is (not sharing and sharing).

(a) Dynamic evolution phase diagram of case 1.

(b) Dynamic evolution phase diagram of case 2.

(3) When $C_1 + \theta Q_1 < K_1Q_2(g-1) + \alpha Q_1, C_2 + \theta Q_2 > K_2Q_1(g-1) + \alpha Q_2$, when the integrator's information cost and risk are less than the shared benefits, information sharing is the best strategy for the integrator. However, the cost and risk of provider information sharing exceed the benefits obtained, and the best strategy is to not share information. Therefore, as shown in Figure 2(a), the evolution process ends at $x^* = 1, y^* = 0$, the stable point is (1,0), and the evolutionary stability strategy is (shared and not shared).

In the two situations shown in formulas (2) and (3), the game player unilaterally adopts an information-sharing strategy, with one party choosing information sharing and the other party choosing not to share. Entities that adopt information-sharing strategies can obtain greater additional benefits when they begin to share. However, as the game process is repeated, the information input cost and information-sharing risk of the information-sharing party will gradually rise. In the end, it will also evolve into unwillingness to share information. Therefore, in both cases, the final result of the information-sharing game between integrators and providers is that information is not shared, and the evolutionary stability point is (0, 0), as shown in Figure 2(b).

(4) When $C_1 + (\theta - \alpha)Q_1 < K_1Q_2(g-1), C_2 + \theta Q_2 < K_2Q_1(g-1) + \alpha Q_2$, the benefits obtained by the integrator and the provider by adopting the information-sharing strategy are greater than the cost and risk of the input. However, there are two evolutionary stable points (0,0) and (1,1) for both parties, which are (shared and shared) and (not shared and not shared), as shown in Figure 3.

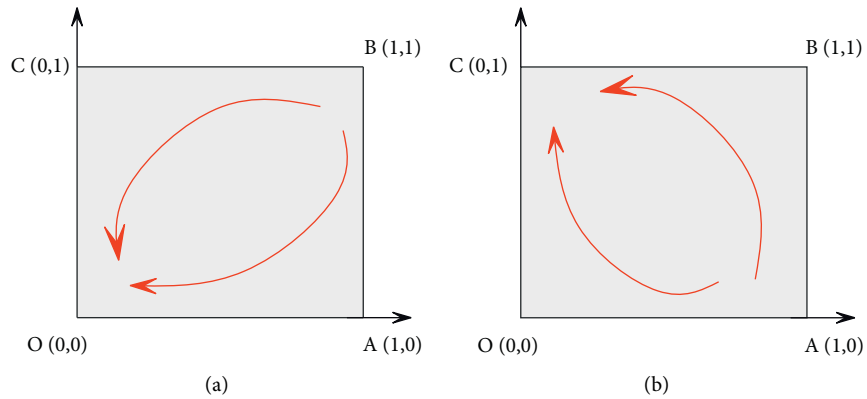

Figure 1: Dynamic evolution phase diagram 1. (a) Dynamic evolution phase diagram of case 1. (b) Dynamic evolution phase diagram of case 2.

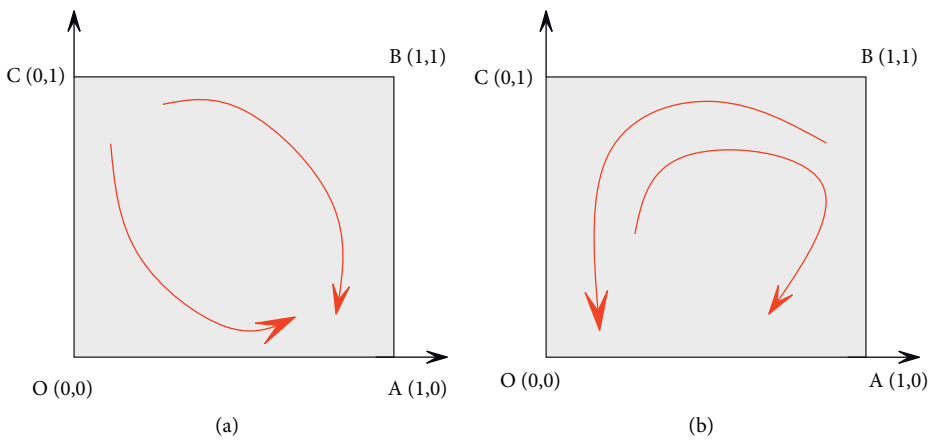

Figure 2: Dynamic evolution phase diagram 2. (a) Dynamic evolution phase diagram of case 3. (b) The dynamic evolution phase diagram of case 2 and case 3.

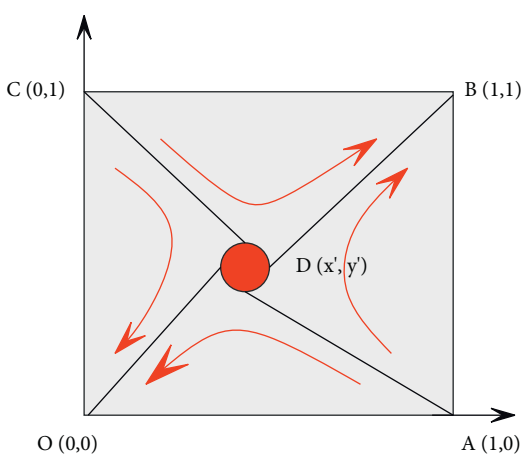

Figure 3: Dynamic evolution phase diagram of case 4.

The broken line ADC is the dividing line of the two evolutionary results (0,0) and (1,1). In the OADC region, the evolution process converges to $x^* = 0, y^* = 0$, and the stable point is (0,0). In the end, both parties of the game will choose the information nonsharing strategy. In the ABCD region, the evolution process gradually converges to $x^* = 1, y^* = 1$, the final stable state is (1,1), and both players in the game choose to share information. The critical point $D(x^*, y^*)$ determines the final result of the evolutionary game, and the strategic choice of the game player will change with the change in the critical point. When the critical point $D(x^*, y^*)$ is close to the origin, the area OADC decreases and the area ABCD increases, and the game player is more likely to choose an information-sharing strategy. Conversely, if the value of the critical point $D(x^*, y^*)$ becomes larger, the area of OABC becomes larger, the area of ABCD decreases, and the two sides of the game are more likely to tend to nonsharing of information. The change in the critical point $D(x^*, y^*)$ is closely related to the parameters of both parties. Among them, the area of ABCD is as follows:

$$S_{ABCD} = 1 - \frac{1}{2}\left[\frac{C_1 + \theta Q_1}{K_1 Q_2 (g-1) + \alpha Q_1} + \frac{C_2 + \theta Q_2}{K_2 Q_1 (g-1) + \alpha Q_2}\right]. \tag{13}$$

From the above evolutionary game analysis process, it can be seen that whether a logistic service supply chain node enterprise will choose to share information depends on the enterprise's own capabilities, the payment matrix of the evolutionary game, and the initial values of various

parameters. With the passage of time and the repeated progress of the game process, the changes in the values of various parameters may cause the players of the game to choose different strategies. This study uses critical points $D(x^*, y^*)$ to analyze various parameters that may affect the outcome of the evolutionary game.

From $x^* = (C_2 + \theta Q_2)/[K_2 Q_1 (g-1) + \alpha Q_2]$, $y^* = (C_1 + \theta Q_1)/[K_1 Q_2 (g-1) + \alpha Q_1]$, it can be seen that the information-sharing cost, risk coefficient, incentive coefficient, synergy coefficient, information absorption and utilization capacity, and information-sharing degree of each node of the supply chain are important factors that affect the size of the critical point.

Under uncertain market conditions, customer demand is generally price-sensitive. Therefore, the market logistic service demand Q faced by integrators is uncertain. Here, the random variable Q has the characteristics of the probability distribution F (Q), and the customer enterprise logistic service demand can be expressed by the following formula:

$$\begin{aligned} Volume &= initial\ demand\ volume \\ &+ volume\ decrease\ rate \times (price) \\ &+ volume\ variation\ range \\ &\times sin\left(\frac{price}{variation\ cycle}\right). \end{aligned} \tag{14}$$

Among them, initial demand volume is the initial demand for logistic services, volume decrease rate is the slope of change in service demand, volume variation range is the range of change in service demand, and variation cycle is the price cycle of service demand changes.

The change in customer demand described by a sine curve is shown in Figure 4.

From Figure 4 above, we can see the impact of price changes on the anticipated demand for logistic services by client companies. Demirkan (2008) uses a normal distribution function to describe the effect of random demand on price. In order to facilitate model analysis and calculation, this study uses a uniform distribution function to express the demand price sensitivity in the logistic service supply chain model, that is, we assume that the demand for logistic services of price-sensitive client companies in a period is uniformly distributed in the interval $[Q(p) - \theta, Q(p) + \theta]$ (θ is the demand fluctuation coefficient, $\theta > 0$), as shown in Figure 5 below as follows:

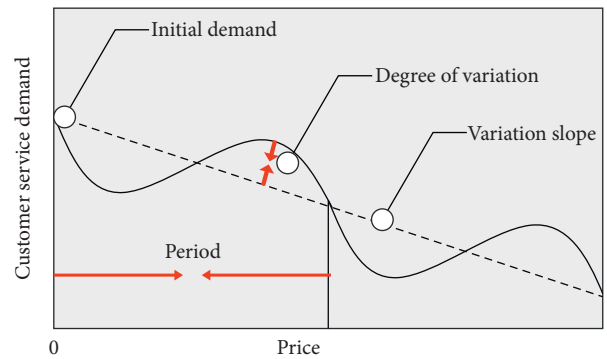

Figure 4: Price-sensitive customer service demand curve.

$$Q(p) = a - bp. \tag{15}$$

Among them, a is a known constant, such as the actual demand in the previous cycle. b is a constant, which is the price sensitivity coefficient of market demand, $a>$, and $b > 0$.

In order to simplify the model, this study does not consider the marginal cost of both the supply chain and the demand side, and directly uses revenue instead of profit for calculation. According to the uniform distribution probability density function F (Q) in the above figure, the expected profit function of the integrator is as follows:

$$\begin{aligned} \prod \text{collection} &= \int_{Q(p)-\theta}^{s} [(P-V)Q(p)]F(Q)dQ + \int_{S}^{Q(p)+\theta} [(P-V)S]F(Q)dQ \\ &= \frac{-(P-V)S^2 + 2(P-V)[Q(p)+\theta]S - (P-V)[Q(P)-\theta]^2}{4\theta} \\ &= -\frac{P-V}{4\theta}\{S - [Q(P)+\theta]\}^2 + (P-V)Q(p) \\ &= -\frac{P-V}{4\theta}[S - (a - bP + \theta)]^2 + (P-V)(a-bP). \end{aligned} \tag{16}$$

The first term in formula (15) represents the income when the actual logistic service demand is less than the logistic service capacity S purchased by the integrator. The second term represents the income when the actual logistic service demand is greater than the logistic service capacity S purchased by the integrator.

The income of the logistic service provider is equal to the product of the logistic service capability S purchased by the

integrator and the unit logistic service price V. The cost of the provider is mainly composed of two parts. One is the unit logistic service capacity cost m, such as fixed costs such as logistic elements, which reflect the normal economic scope of capacity. The other is the operation and management cost n, which is related to the management of the enterprise and mainly includes the cost of improving the management ability and the increase in the complexity of the business model. That is, the profit function of the logistic service provider is as follows:

$$\prod_{\text{Supply}} = VS - mS - nS^2. \tag{17}$$

Due to the randomness of customer demand, uncertain market demand will affect the logistic service costs of integrators and providers. When the logistic service capabilities cannot meet customer needs, integrators and provider groups will incur lost opportunity costs. When the logistic service capacity is higher than the customer's demand, this will produce waste.

The expected cost when the logistic service capacity purchased by the integrator is lower than the actual logistic demand is as follows:

$$\begin{aligned} L(Q) &= \int_{S}^{Q(p)+o} \alpha[Q(p) - S]F(Q)dQ \\ &= \frac{\alpha}{2\theta}\left\{\frac{S^2}{2} - S[Q(p) + \theta] + \frac{[Q(p) + \theta]^2}{2}\right\} \\ &= \frac{\alpha}{4\theta}\{S - [Q(p) + \theta]\}^2 = \frac{\alpha}{4\theta}[S - (a - bP + \theta)]^2. \end{aligned} \tag{18}$$

The parameter α represents the opportunity cost of unit loss caused when the customer's needs cannot be met. Therefore, the expected cost when the logistic service capability purchased by the integrator is higher than the logistic demand is as follows:

$$\begin{aligned} M(Q) &= \int_{Q(p)-\theta}^{S} V[S - Q(p)]F(Q)dQ \\ &= \frac{V}{2\theta}\left\{S^2 - S[Q(p) - \theta] - \frac{S^2}{2} + \frac{[Q(p) - \theta]^2}{2}\right\} \\ &= \frac{V}{4\theta}\{S - [Q(p) - \theta]\}^2 = \frac{V}{4\theta}[S - (a - bP - \theta)]^2. \end{aligned} \tag{19}$$

Unlike the product supply chain, logistic services are intangible and perishable. Therefore, excess service capacity neither generates inventory nor residual value.

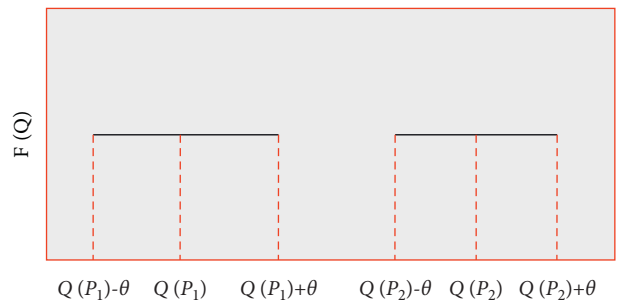

Figure 5: Price-sensitive customer service demand.

The single-loop information flow mode refers to the unidirectional flow of information on the chain. In this model, logistic service supply chain integrators and providers independently predict the logistic demand of the market, and there is no demand information sharing between the two. The integrator makes the logistic service integration planning decision based on the customer's demand information, and the provider makes the logistic service supply planning decision based on the integrator's order information, as shown in Figure 6.

Under the single-loop information-sharing model, integrators and providers reach a consensus on services through negotiation. In this mode, because the integrator directly contacts with the customer and grasps important customer information and market demand status, it belongs to the dominant party, and the provider belongs to the follower. Therefore, the logistic service integrator first maximizes its expected profit and determines the optimal purchase amount S. However, integrators will generate uncertain capacity risks and need to bear the uncertain cost of logistic service volume. Therefore, the expected profit function of the integrator is as follows:

$$\begin{aligned} \Psi_{\text{collection}} &= \Pi_{\text{collection}} - M(Q) - L(Q) \\ &= -\frac{P + \alpha}{4\theta}[S - (a - bP + \theta)]^2 + P(a - bP) - VS. \end{aligned} \tag{20}$$

However, the provider's profit function is $\Psi_{\text{Supply}} = \Pi_{\text{Supply}}$, and the provider determines the optimal price V through the integrator's service purchase volume S. We assume that $d\Psi_{\text{Supply}}/dS = V - m - 2nS = 0$, and the relationship between the provider's optimal pricing and purchase volume can be obtained as follows:

$$V = m + 2nS. \tag{21}$$

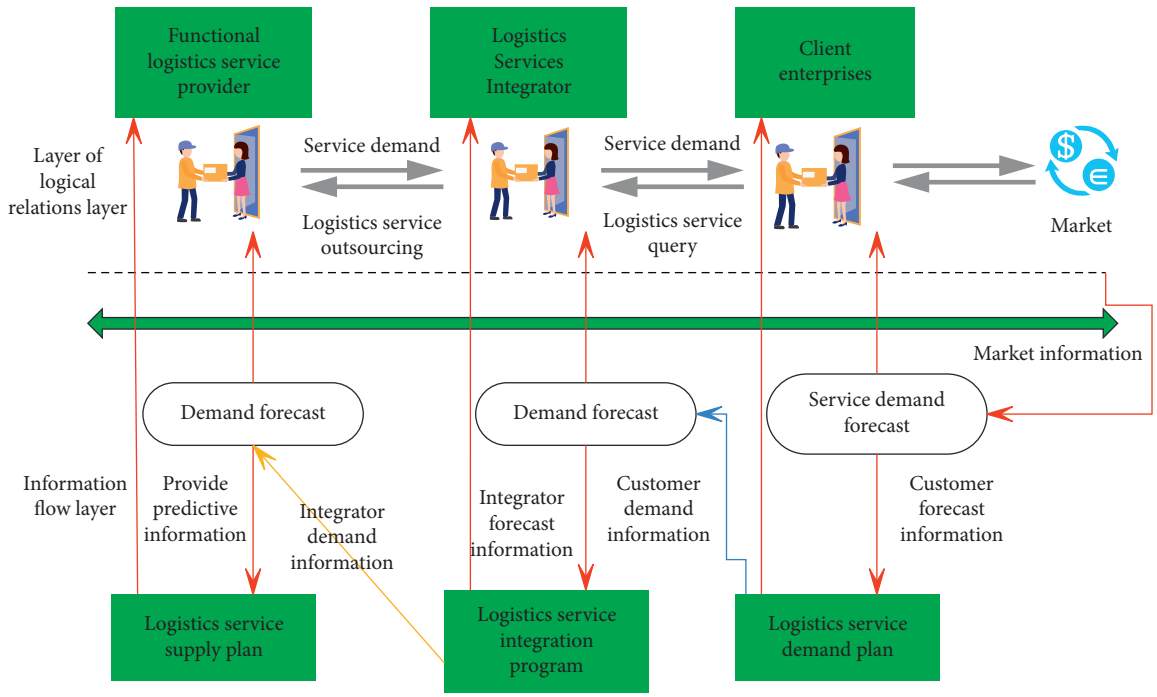

Figure 6: Single-loop information flow mode.

Incorporating formula (20) into the integrator's profit function equation (19), when the following two conditions are met, the integrator's own expected profit is the largest as follows:

$$\begin{cases} \dfrac{\partial \Psi_{\text{collection}}}{\partial S} = -\left(\dfrac{P+\alpha}{2\theta} + 4n\right)S + \dfrac{(P+\alpha)(a-bP+\theta)}{2\theta} - m = 0 \\ \dfrac{\partial \Psi_{\text{collection}}}{\partial P} = -\dfrac{S^2}{4\theta} + \dfrac{(a-bP+\theta)}{2\theta}S - \dfrac{(a-bP+\theta)^2}{4\theta} + \dfrac{b(P+\alpha)(a-bP+\theta)}{2\theta} - \dfrac{b(P+\alpha)}{2\theta} + a - 2bP = 0 \end{cases}. \tag{22}$$

According to equation (22), the optimal purchase quantity of the integrator can be obtained as follows:

$$S_1 = \frac{(P+\alpha)(a-bP+\theta) - 2m\theta}{P+\alpha+8n\theta}. \tag{23}$$

It is the optimal logistic service volume of the logistic service supply chain, and the provider determines the optimal unit logistic service capacity price V through the optimal purchase volume S to maximize its own revenue.

Then, the total expected profit of the logistic service supply chain is as follows:

$$\begin{aligned} \Psi_1 &= \Psi_{\text{collection}} + \Psi_{\text{Supply}} = \Pi_{\text{collection}} - M(Q) - L(Q) + \Pi_{\text{Supply}} \\ &= -\left(\frac{P+\alpha}{4\theta} + n\right)S^2 + \left[\frac{(P+\alpha)(a-bP+\theta)}{2\theta} - m\right]S - \frac{(P+\alpha)}{4\theta}(a-bP+\theta)^2 + P(a-bP). \end{aligned} \tag{24}$$

We bring the optimal solution S_1 into formulas (16), (19), and (23) to obtain the expected profits of logistic service providers, integrators, and the entire supply chain, respectively.

The collaborative control information flow model is an information-sharing model led by logistic service integrators. The integrator takes the initiative to share the customer's logistic service demand information with the provider for collaboration. In this mode, the provider makes

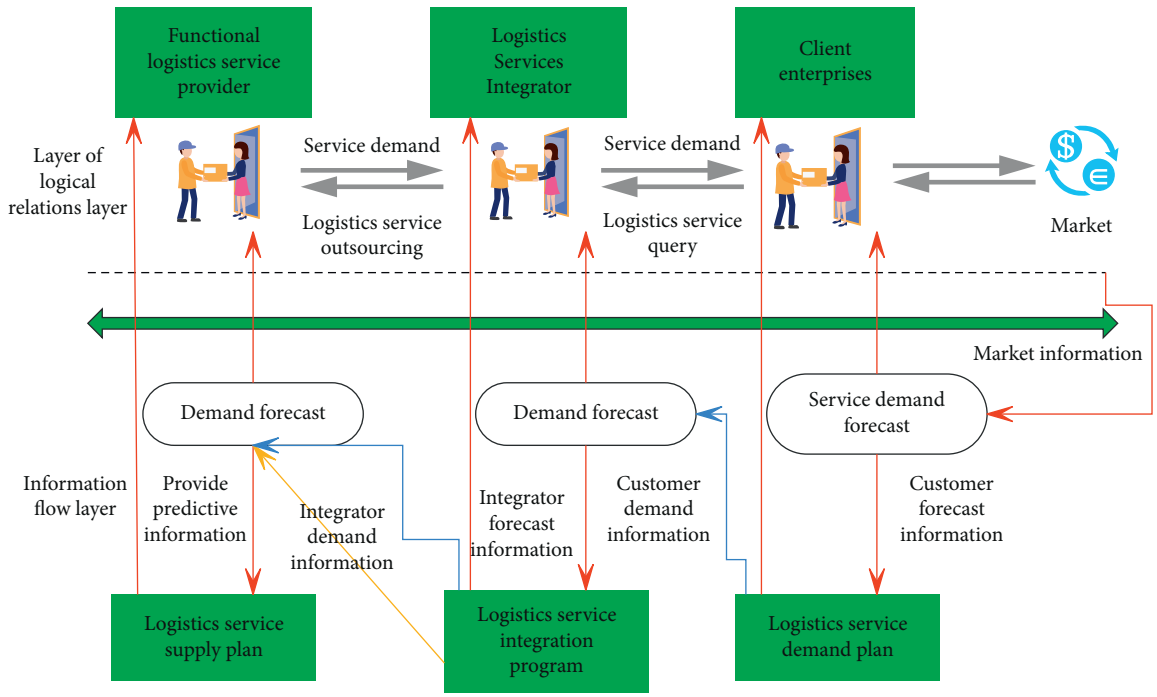

Figure 7: Cooperative control information flow mode.

logistic service supply planning decisions based on the integrator's order information and the customer's service demand information, as shown in Figure 7.

Under this information flow model, information asymmetry may occur between the integrator and the provider. That is, the order volume predicted by the integrator differs from the customer demand predicted by the provider. At this time, the provider coordinates the supply chain by adjusting the number S of logistic service capabilities. Therefore, the cost of uncertain capacity is borne by the provider. However, the integrator only needs to bear the purchase cost of the logistic service capability, that is, the expected profit function of the integrator is as follows:

$$\Psi_{\text{collection}} = \Pi_{\text{collection}} = -\frac{P-V}{4\theta}[S-(a-bP+\theta)]^2 + (P-V)(a-bP). \tag{25}$$

When formula (15) satisfies the following two conditions, the integrator expects the profit to be maximized as follows:

$$\begin{cases} \dfrac{\partial \Psi_{\text{collection}}}{\partial S} = \dfrac{(P-V)(a-bP+\theta-S)}{2\theta} = 0 \\ \dfrac{\partial \Psi_{\text{collection}}}{\partial P} = -\dfrac{S^2}{4\theta} + \dfrac{(a-bP+\theta)-b(P-V)}{2\theta}S - \dfrac{(a-bP+\theta)^2}{4\theta} + \dfrac{b(P-V)(a-bP+\theta)}{2\theta} + a - 2bP + bV = 0 \end{cases}. \tag{26}$$

From equation (26), the optimal purchase amount of the integrator can be obtained as follows:

$$S_{\text{collection}} = a - bP + \theta. \tag{27}$$

This shows that when integrators do not have to bear the cost of uncertain capabilities; in order to meet customer needs, integrators always tend to purchase the maximum amount of logistic services.

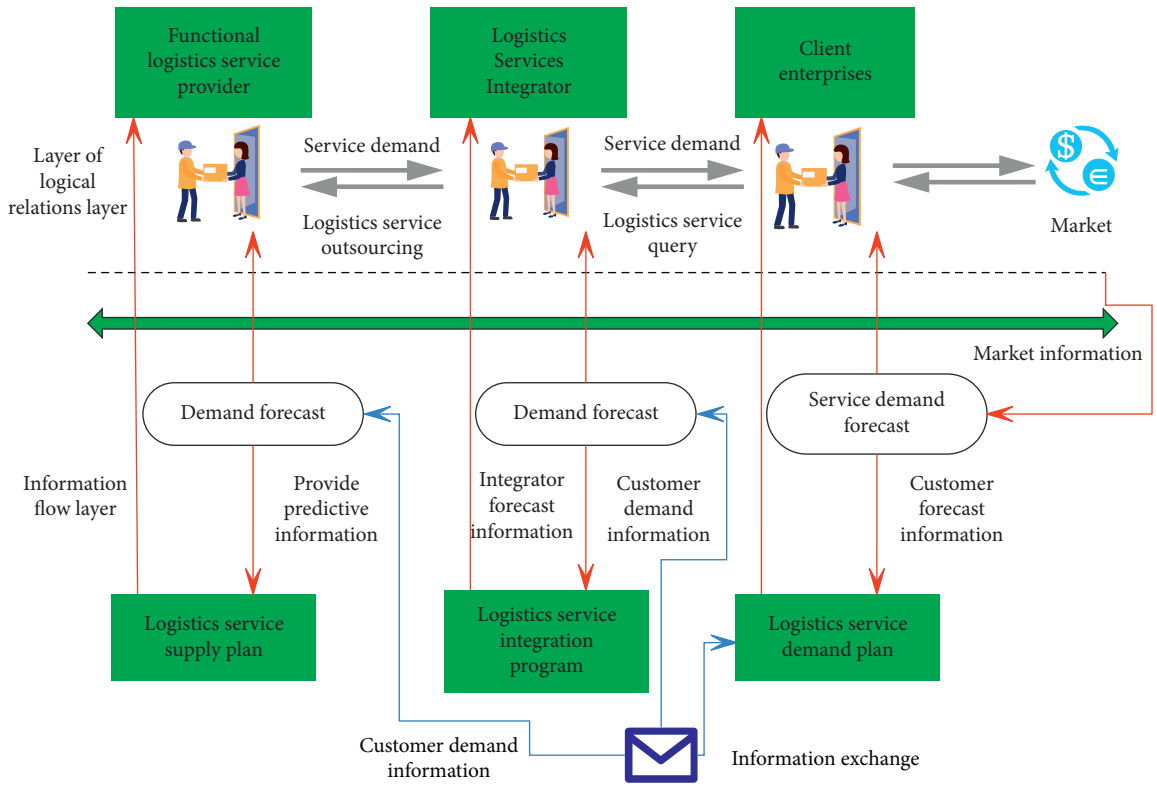

FIGURE 8: Centralized control information flow mode.

Substituting formula (26) into the expected profit function of the provider, we get the following:

$$\Psi_{\text{Supply}} = \Pi_{\text{Supply}} - M(Q) - L(Q) = -\left(\frac{V+\alpha}{4\theta} + n\right)S^2 + \left[\frac{\alpha}{2\theta}(a - bP + \theta) + \frac{V}{2\theta}(a - bP - \theta) + V - m\right]S - \frac{\alpha}{4\theta}(a - bP + \theta)^2 - \frac{V}{4\theta}(a - bP - \theta)^2 = -nS^2 + (V - m)S - m\theta. \tag{28}$$

We assume that $d\Psi_{\text{Supply}}/dS = -2nS + V - m = 0$, and the optimal service volume of the available provider is $S_{\text{Supply}} = V - m/2n$, that is, $V = m + 2nS$. It shows that no matter how the cost of the provider changes, the optimal pricing strategy is always only related to the volume of logistic services. In order to balance the capabilities of the entire supply chain, the integrator's purchase volume should be equal to the provider's supply volume. We assume $dS_{\text{collection}}/dP = -b < 0$, and $S_{\text{collection}}$ is a monotonically decreasing function of P. We assume $dS_{\text{Supply}}/dV = 1/2n > 0$, and S_{Supply} is a monotonically increasing function of V. It shows that there must be a unique equilibrium solution for $S_{\text{collection}} = S_{\text{Supply}}$ to maximize the profits of both, that is, $P = 2n(a + \theta) - V + m/2nb$. The provider decides the price V that maximizes its own interests based on the integrator's maximum purchase volume, and the integrator decides the price P for the customer on the basis of the provider's price V. The total expected profit of the logistic service supply chain is as follows:

$$\Psi_2 = \Psi_{1/4^-} + \Psi_{1©} = \Pi_{1/4^-} + \Pi_{1©} - M(Q) - L(Q). \tag{29}$$

We bring the optimal solution of $S_2 = S_{\text{collection}} = S_{\text{Supply}}$ into formulas (15), (23), and (26) to obtain the expected profits of logistic service integrators, providers, and the entire supply chain.

The centralized control information flow model is a way to use information technology to share information in the supply chain network. In this model, a decentralized supply chain can achieve optimal organizational performance. Information sharing among supply chain members can produce

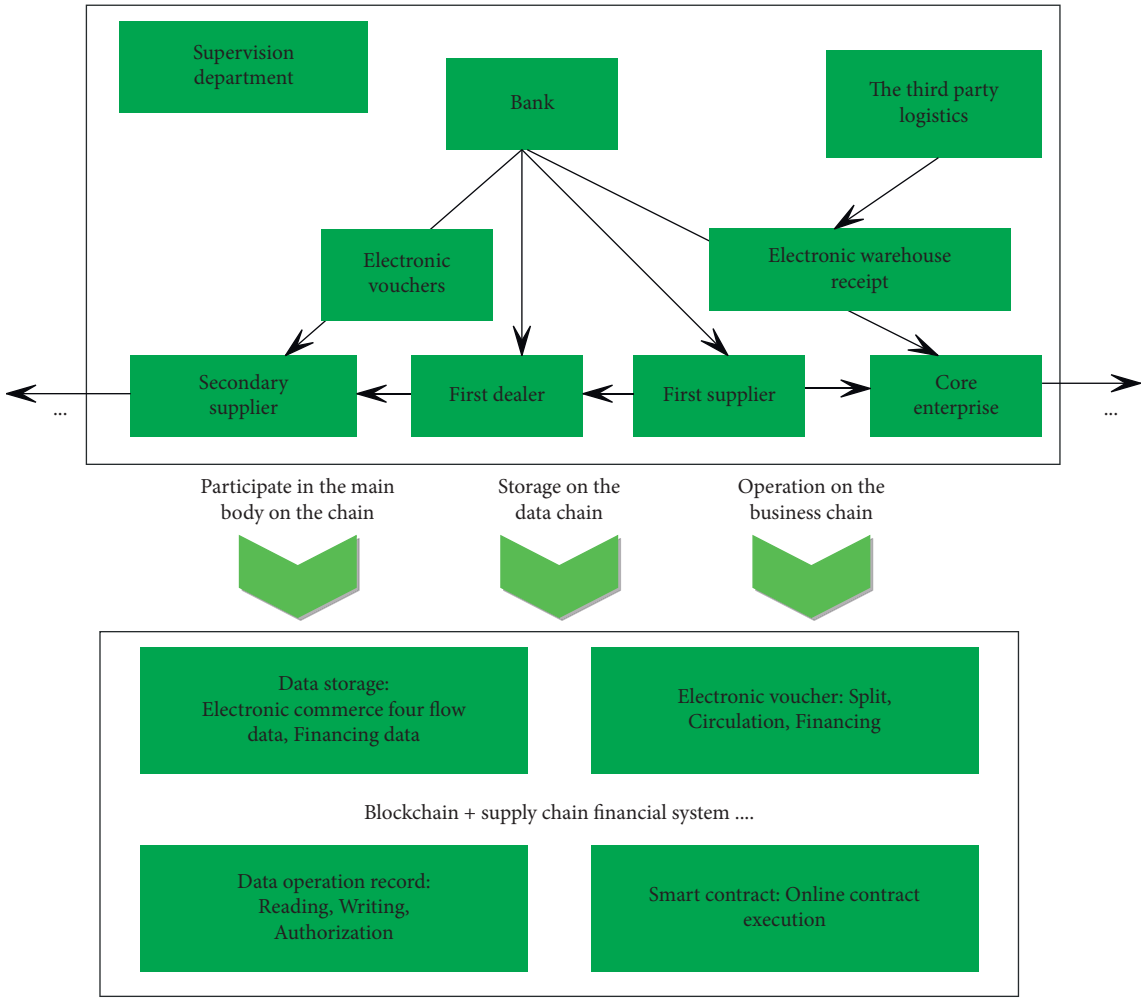

Figure 9: The operating mechanism of blockchain + supply chain finance.

deterministic changes, such as reducing or eliminating the "bullwhip effect." The use of information transmission and interaction technology to increase vertical information sharing can improve the service performance of providers in the logistic service supply chain and the entire supply chain. Providers use information-sharing technology to shorten the distance with customers and can synchronize with integrators to obtain customer logistic demand information in the market, and providers can directly make service supply chain decisions based on customer demand information. In this way, the provider can take the initiative to adopt corresponding strategies to support the integrator's decision-making, in order to achieve the balance of capabilities of the entire logistic service supply chain, as shown in Figure 8.

Under this information-sharing model, in the logistic service supply chain of integrators, providers, and customer enterprises, each member shares market demand information and makes unified decisions, with the goal of maximizing the overall benefits of the logistic service supply chain. Therefore, the expected profit of the entire supply chain is the sum of the expected profit of the integrator and the provider. Subsequently, the uncertain capacity cost is eliminated, and the cost is ultimately borne by the integrator and the provider. To simplify the model and

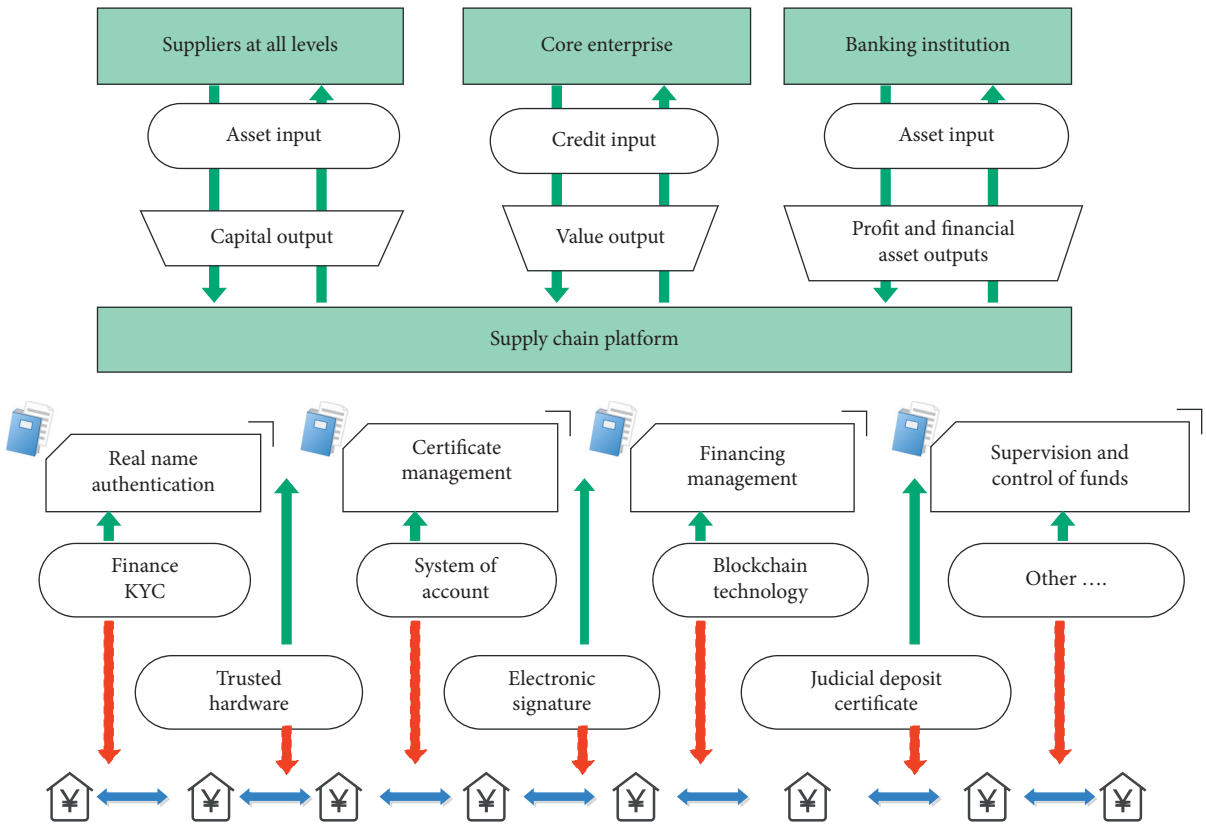

Figure 10: Schematic diagram of using blockchain application scenarios to realize the core functions of supply chain integrated business intelligence financial processing.

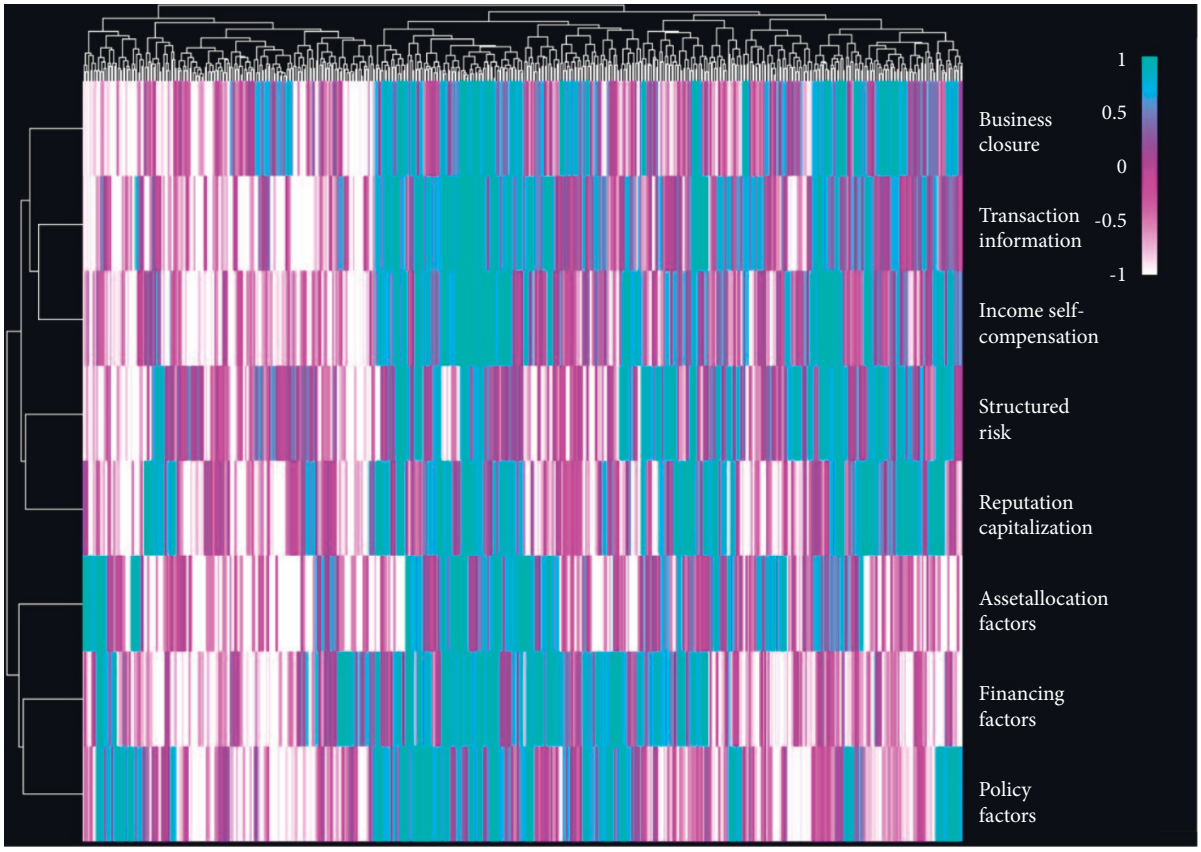

Figure 11: The processing effect of the safe financial processing method for realizing supply chain integrated business intelligence using blockchain application scenarios.

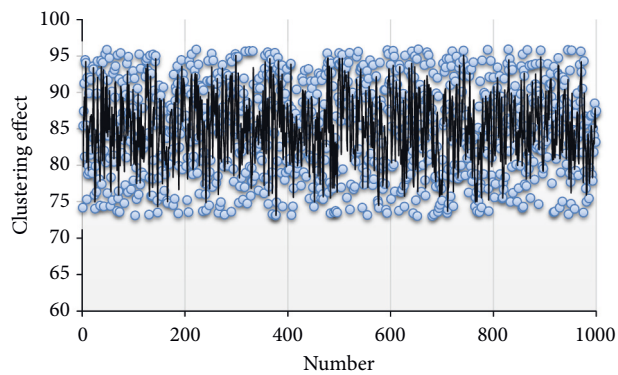

Figure 12: The clustering effect of the system.

calculations, we assume that the commitment ratio is 1 : 1, that is, $\Psi_{\text{collection}} = \Pi_{\text{collection}} - 1/2[M(Q) + L(Q)]$, $\Psi_{\text{Supply}} = \Pi_{\text{Supply}} - 1/2[M(Q) + L(Q)]$. Therefore, the total revenue of the supply chain is simply calculated as follows:

$$\begin{aligned}\Psi_3 &= \Psi_{\text{collection}} + \Psi_{\text{Supply}} \\ &= -\left(\frac{P+\alpha}{4\theta} + n\right)S^2 + \left[\frac{(P+\alpha)(a-bP+\theta)}{2\theta} - m\right]S - \frac{(P+\alpha)}{4\theta}(a-bP+\theta)^2 + P(a-bP)\end{aligned} \tag{30}$$

In order to maximize the total revenue of the supply chain, the following two conditions must be met as follows:

$$\begin{cases}\dfrac{\partial\Psi}{\partial S} = -\left(\dfrac{P+\alpha}{2\theta} + 2n\right)S + \dfrac{(P+\alpha)(a-bP+\theta)}{2\theta} - m = 0 \\[2ex] \dfrac{\partial\Psi}{\partial P} = -\dfrac{S^2}{4\theta} + \dfrac{(a-bP+\theta)}{2\theta}S - \dfrac{(a-bP+\theta)^2}{4\theta} + \dfrac{b(P+\alpha)(a-bP+\theta)}{2\theta} - \dfrac{b(P+\alpha)}{2\theta} + a - 2bP = 0\end{cases} \tag{31}$$

According to formula (29), the optimal logistic service volume of the supply chain is as follows:

$$S_3 = \frac{(P+\alpha)(a-bP+\theta) - 2m\theta}{P+\alpha+4n\theta}. \tag{32}$$

We assume that $d\Psi_{\text{collection}}/dS = -2P - V + \alpha/4\theta S + 2P - V + \alpha/4\theta(a - bP + \theta) - V/2 = 0$, and the available service volume of the integrator is $S_{\text{collection}} = a - bP + \theta - 2V\theta/2P - V + \alpha$. We assume that $d\Psi_{\text{Supply}}/dS = -(V + \alpha/4\theta + 2n)S + V + \alpha/4\theta(a - bP + \theta) + V/2m = 0$, and the optimal service volume of the available provider is $S_{\text{Supply}} = (V + \alpha)(a - bP + \theta) + 2V\theta - 4m\theta/V + \alpha + 8n\theta$.

4. The Safe Financial Processing Method for Realizing Supply Chain Integrated Business Intelligence Using Blockchain Application Scenarios

On the basis of the above algorithm analysis, the blockchain application scenario is used to realize the secure financial processing of supply chain integrated business intelligence, and the model in this study is constructed and the performance is analyzed. The behaviors and activities of multiple participating entities involved in the development of supply chain finance business, banks, core enterprises, upstream and downstream enterprises, and related service entities must comply with commercial rules and contract requirements. However, the complex structure and sophistication of business operations increase the difficulty of risk control for banks. The characteristics of blockchain technology can effectively meet the control of the causes of supply chain financial risks. The application of blockchain to the supply chain financial business can effectively reduce the difficulty of business risk management, thereby reducing the probability of risk occurrence. Figure 9 shows the operating mechanism of blockchain technology embedded in supply chain financial services.

As shown in Figure 10, the core functions of the supply chain platform mainly include four parts: real-name authentication, credential management, financing management, and capital management and control.

Based on the above model, the safe financial processing method for realizing supply chain integrated business intelligence using blockchain application scenarios was validated, and the results shown in Figure 11 below were obtained.

From the results shown in Figure 11 above, the safe financial processing method for realizing supply chain integrated business intelligence using blockchain application scenarios has good results. On this basis, this study clusters the effects of the model and obtains the results shown in Figure 12.

From the above analysis, it can be seen that the safe financial processing method for realizing supply chain integrated business intelligence using blockchain application scenarios has good results and can play an important role in the safe financial processing of supply chain integrated business intelligence.

5. Conclusions

The blockchain-based supply chain financial system mainly uses core companies and suppliers to record the information involved in transactions. When the core enterprise participates in the transaction in the supply chain financial system, it only needs to confirm the transaction order with the corresponding private key, which reduces the risk of banks and other financial institutions in the supply chain to a certain extent. Furthermore, the reduction in financing risks has further reduced the financing costs of participating companies in the supply chain and promoted the efficient operation of the supply chain financial system. In addition, the blockchain-based supply chain financial system uses smart contracts to replace manual operations. This study combines the blockchain technology to analyze the security financial management of the supply chain integrated business intelligence, builds an intelligent system, and verifies the performance of the system to improve the security financial management effect of the supply chain integrated business intelligence. The experimental research results show that the safe financial processing method for realizing supply chain integrated business intelligence using blockchain application scenarios has good results.

Data Availability

The data used to support the findings of this study are included within the article.

Conflicts of Interest

The authors declare that there are no conflicts of interest regarding this work.

Acknowledgments

This research was supported by the Research Fund of China's Jiangsu Province Higher Education Teaching Reform Project (2021JSJG439).

References

[1] N. Nizamuddin, H. Hasan, K. Salah, and R. Iqbal, "Blockchain-based framework for protecting author royalty of digital assets," *Arabian Journal for Science and Engineering*, vol. 44, no. 4, pp. 3849–3866, 2019.

[2] M. E. Peck, D. Wagman, N. Scarpato, L. Di Nunzio, F. Fallucchi, and M. Raso, "Smarter city: smart energy grid based on blockchain technology or sell your own-it'll all be on a blockchain," *IEEE Spectrum*, vol. 54, no. 10, pp. 56–61, 2018.

[3] A. Pieroni, N. Scarpato, L. Di Nunzio, F. Fallucchi, and M. Raso, "Smarter city: smart energy grid based on blockchain technology," *International Journal of Advanced Science, Engineering and Information Technology*, vol. 8, no. 1, pp. 298–306, 2018.

[4] K. Gai, Y. Wu, L. Zhu, M. Qiu, and M. Shen, "Privacy-preserving energy trading using consortium blockchain in smart grid," *IEEE Transactions on Industrial Informatics*, vol. 15, no. 6, pp. 3548–3558, 2019.

[5] L. N. Chavali, N. L. Prashanti, K. Sujatha, G. Rajasheker, and P. B. Kishor, "The emergence of blockchain technology and its impact in biotechnology, pharmacy and life sciences," *Current Trends in Biotechnology and Pharmacy*, vol. 12, no. 3, pp. 304–310, 2018.

[6] K. Luchoomun, S. Pudaruth, and S. Kishnah, "Implementation of a proof of concept for a blockchain-based smart contract for the automotive industry in Mauritius," *International Journal of Advanced Computer Science and Applications*, vol. 11, no. 3, pp. 71–81, 2020.

[7] A. Whitaker and R. Kräussl, "Fractional equity, blockchain, and the future of creative work," *Management Science*, vol. 66, no. 10, pp. 4594–4611, 2020.

[8] A. Verma, "Security of Internet of things using blockchain: an overview," *International Journal of Managment, IT and Engineering*, vol. 9, no. 6, pp. 406–412, 2019.

[9] F. Antonucci, S. Figorilli, C. Costa, F. Pallottino, L. Raso, and P. Menesatti, "A review on blockchain applications in the agri-food sector," *Journal of the Science of Food and Agriculture*, vol. 99, no. 14, pp. 6129–6138, 2019.

[10] A. S. Yadav and D. S. Kushwaha, "Query optimization in a blockchain-based land registry management system," *Ingénierie des Systèmes d'Information*, vol. 26, no. 1, pp. 13–21, 2021.

[11] A. Kumar, A. Prasad, and R. Murthy, "Application of blockchain in usage based insurance," *International Journal of Advance Research, Ideas and Innovations in Technology, IJARIIT*, vol. 5, no. 2, pp. 1574–1577, 2019.

[12] E. Huerta and S. Jensen, "An accounting information systems perspective on data analytics and Big Data," *Journal of Information Systems*, vol. 31, no. 3, pp. 101–114, 2017.

[13] S. Balne, "Analysis on research methods in bigdata applications," *International Journal of Innovative Research in Computer and Communication Engineering*, vol. 8, no. 10, pp. 4059–4063, 2020.

[14] P. B. de Laat, "Algorithmic decision-making based on machine learning from Big Data: can transparency restore accountability?" *Philosophy & technology*, vol. 31, no. 4, pp. 525–541, 2018.

[15] G. Tucker, "Sustainable product lifecycle management, industrial big data, and Internet of things sensing networks in cyber-physical system-based smart factories," *Journal of Self-Governance and Management Economics*, vol. 9, no. 1, pp. 9–19, 2021.

[16] P. B. de Laat, "Big data and algorithmic decision-making," *ACM SIGCAS - Computers and Society*, vol. 47, no. 3, pp. 39–53, 2017.

[17] T. E. Marshall and S. L. Lambert, "Cloud-based intelligent accounting applications: accounting task automation using IBM watson cognitive computing," *Journal of Emerging Technologies in Accounting*, vol. 15, no. 1, pp. 199–215, 2018.

[18] D. Chessell and O. Neguriţă, "Smart industrial value creation, cyber-physical production networks, and real-time big data analytics in sustainable Internet of Things-based manufacturing systems," *Journal of Self-Governance and Management Economics*, vol. 8, no. 4, pp. 49–58, 2020.

[19] B. Abdualgalil and S. Abraham, "Efficient machine learning algorithms for knowledge discovery in big data: a literature review," *Database*, vol. 29, no. 5, pp. 3880–3889, 2020.

[20] J. R. A. Q. Al Natour, "The impact of information technology on the quality of accounting information (SFAC NO 8, 2010)," *Turkish Journal of Computer and Mathematics Education (TURCOMAT)*, vol. 12, no. 13, pp. 885–903, 2021.

[21] A. P. Aaron, M. L. Kohlstrand, L. V. Welborn, and S. T. Curvey, "Maintaining medical record confidentiality and client privacy in the era of big data: ethical and legal responsibilities," *Journal of the American Veterinary Medical Association*, vol. 255, no. 3, pp. 282–288, 2019.

Hindawi
Mobile Information Systems
Volume 2023, Article ID 9829310, 1 page
https://doi.org/10.1155/2023/9829310

Retraction

Retracted: Regular Flow Field Sparse Processing and Blue Finance of Ocean City Research Based on GIS System

Mobile Information Systems

Received 31 October 2023; Accepted 31 October 2023; Published 1 November 2023

This article has been retracted by Hindawi following an investigation undertaken by the publisher [1]. This investigation has uncovered evidence of one or more of the following indicators of systematic manipulation of the publication process:

(1) Discrepancies in scope
(2) Discrepancies in the description of the research reported
(3) Discrepancies between the availability of data and the research described
(4) Inappropriate citations
(5) Incoherent, meaningless and/or irrelevant content included in the article
(6) Peer-review manipulation

The presence of these indicators undermines our confidence in the integrity of the article's content and we cannot, therefore, vouch for its reliability. Please note that this notice is intended solely to alert readers that the content of this article is unreliable. We have not investigated whether authors were aware of or involved in the systematic manipulation of the publication process.

Wiley and Hindawi regrets that the usual quality checks did not identify these issues before publication and have since put additional measures in place to safeguard research integrity.

We wish to credit our own Research Integrity and Research Publishing teams and anonymous and named external researchers and research integrity experts for contributing to this investigation.

The corresponding author, as the representative of all authors, has been given the opportunity to register their agreement or disagreement to this retraction. We have kept a record of any response received.

References

[1] Y. Sun and K. Anurag, "Regular Flow Field Sparse Processing and Blue Finance of Ocean City Research Based on GIS System," *Mobile Information Systems*, vol. 2022, Article ID 7650704, 10 pages, 2022.

Hindawi
Mobile Information Systems
Volume 2022, Article ID 7650704, 10 pages
https://doi.org/10.1155/2022/7650704

Research Article

Regular Flow Field Sparse Processing and Blue Finance of Ocean City Research Based on GIS System

Ying Sun[1] and Kalra Anurag[2]

[1]*Yantai University of Science and Technology, Shandong 430074, China*
[2]*Ecological and Environmental Research Center, Kyrgyz-Turkish Manas University, Bishkek, Kyrgyzstan*

Correspondence should be addressed to Kalra Anurag; anurag@email.cu.edu.kg

Received 3 June 2022; Revised 20 July 2022; Accepted 28 July 2022; Published 24 August 2022

Academic Editor: Chi Lin

In order to explore the development path of blue finance in ocean cities, this paper combines GIS to conduct blue finance research in ocean cities, draws on the traditional direct visualization method of point icons, and uses arrow symbols to render vector flow field data. Moreover, this paper uses GIS means to perform statistical analysis on flow field data, studies the adaptive sparse algorithm of flow field data spatial structure based on GIS, and proposes a program implementation method for regular flow field sparse processing suitable for the general flow of the sparse algorithm. The experimental research shows that the GIS technology proposed in this paper can play an important role in the research of blue finance in ocean cities and has a certain role in promoting the development of ocean blue finance.

1. Introduction

The development of the world economy shows that the coastal areas have become the regions with the most concentrated population, the highest degree of urbanization, and the most developed economy. The coastal areas of the world are about more than 2/3 of the world's population, and 60% of the large and medium cities are distributed. China is one of the major maritime countries in the world, and most of the developed cities are concentrated in the coastal areas. Among them, the coastal area, which accounts for 15% of the country's land area, carries more than 40% of the country's population, 50% of large and medium-sized cities, and 60% of its GDP.

The ocean industry is the production and service activities carried out by human beings to develop, utilize, and protect the ocean and refers to the sum of various material production and nonmaterial production sectors formed by human development, utilization, and protection of ocean resources. That is, it is the various production and service activities carried out by human beings using ocean resources and ocean space, or the social production, exchange, distribution, and consumption activities of human beings in the ocean and targeting ocean resources [1].

Finance is the engine of economic development, and the level of financial development will directly affect the degree of economic development [2]. At present, the continuous development of financial globalization, the continuous enhancement of international capital mobility, and the continuous increase of mergers and reorganizations of financial institutions have undoubtedly exacerbated the phenomenon that financial activities, financial factors, and financial institutions are highly concentrated in some large financial centers [3]. At present, the three most eye-catching international financial agglomeration areas are New York, Tokyo, and London. Beijing Financial Street and Shanghai Lujiazui agglomeration area are currently formed and basically perfected financial agglomeration areas in China. Qingdao, as the vanguard of the blue economic zone in Shandong Peninsula, has formulated a development plan for building a regional financial center in order to realize the blue leap. This era is not only an era led by science and technology, but also an era of soaring oceans. With the emergence of resource crisis, people's attention is once again focused on the ocean.

Therefore, exploring the treasures of the ocean and finding development forces from the ocean have become the new direction for the economic development of various countries.

The ocean economic theory is an important part of the blue economic theory. Before the twentieth century, restricted by the level of technology, the development and utilization of marine resources could only stay at the surface—fishing, salt production, sea transportation, etc. Later, with the progress and innovation of technology, people gradually began to explore the development and utilization of marine resources. The term "ocean economy" was first proposed in the United States in the early 1970s. As population growth put a heavy pressure on land resources, some developed countries began to formulate some marine development plans and invested a lot of capital into them.

Marine economy is a general term for marine activities carried out by all marine-related industrial sectors in a country or a region to develop or utilize marine resources. Its essence is activities related to marine resources, and it has two characteristics of comprehensiveness and sea-related. After the continuous development of traditional marine activities, a marine economy in the modern sense has been formed. The marine economy in the modern sense is a collective economic concept, including not only productive activities for scientific and technological development of marine resources and expansion of marine space, but also service activities that provide support for marine development and space expansion.

This paper combines the GIS to carry out the research on the blue finance of the ocean city, to improve the exploration effect of the blue finance of the ocean city, and to provide a theoretical reference for the further development of the blue finance of the ocean city.

2. Related Work

Marine Geographic Information System (MGIS) is a combination of geographic information system technology and marine science and applications. The application of GIS in the marine field can be traced back to the marine automation carried out by the National Ocean Survey (NOS) in the 1960s. However, some initial researchers simply applied GIS directly to the management of the marine environment. Literature [4] designed a sharing service system for marine stereoscopic monitoring data based on distributed database, WebGIS, and other technologies and elaborated in detail. The data organization structure, overall framework, business function modules, and implementation methods of spatial data publishing and services are adopted by the shared service system.

Literature [5] studies the preliminary application of GIS in coastal zone management. Try to explore the application of GIS in coastal environment. Literature [6] affirmed the importance of GIS in managing and displaying marine data and also discussed the three-dimensional modeling, visualization, and quantitative analysis of marine data. Literature [7] proposed the spatial structure of marine GIS and spatial simulation integration. Literature [8] conducted in-depth research on the expression, analysis, and visualization of marine data. Literature [9] combines JavaJJava3d, visualization toolkit, and ESRI's ArcGIS Engine to build a GIS prototype system including ocean models. Through ArcGIS Engine's spatial analysis capabilities and Java3D's complex visualization capabilities, users can input data and perform spatial and scientific analysis and virtual visualization of the output results. Literature [10] advocated the research and development of coastal and marine GIS and put forward the concept of "global database with coastal chain as the baseline." Literature [11] combined GIS and tidal current model to study tidal wave system. Literature [12] studied and analyzed the visualization of tidal current numerical simulation from the perspective of geographic information system and designed and implemented a virtual reality prototype of coastal ocean current simulation. On the basis of analyzing the advantages and disadvantages of various data models, literature [13] proposed a three-dimensional GIS data model and a marine spatiotemporal data model suitable for marine information management. Literature [14] takes the multisource, multidimensional, and dynamic massive data of coastal zones and oceans as the research object and designs a GIS spatial data model for marine data to realize the unified management and expression of multisource, multidimensional, and massive data, especially the three-dimensional dynamic expression. Literature [15] uses GIS technology to study the management and visualization methods of marine hydrological data. Based on the spatial location management of hydrological data, the visual expression of hydrological data is realized in the form of vector graphics and statistical histograms, and GIS visualization tools are used to detect the seabed. The data is managed, and the spatial visualization relationship between the profile data and the planar distribution data is established, which provides a shortcut for the visualization of seabed scientific research. Literature [16] established a seabed sediment visualization simulation environment by establishing a marine sediment database. Based on bathymetry data, multibeam data, borehole data, and stratigraphic trawl samples, a three-dimensional visualization simulation system for the seabed was built. On the basis of analyzing the demand for information expression of digital ocean water elements, literature [17] proposed a water cube liter data model and its establishment method and realized the simulation of sea surface, the three-dimensional expression of water elements, and the construction of virtual ocean scenes. Literature [18],considering the combination of geographic information system and virtual reality technology, uses multisource and heterogeneous basic data to establish a realistic and dynamic three-dimensional virtual ocean environment and visualize the observation data in the virtual ocean. With the development of network technology, WebGIS is used in marine science. The application research of marine information is also more and more extensive. Literature [19] analyzed the development of marine basic geographic basemap for marine information sharing and the implementation of marine information WebGIS and realized the sharing of marine information and hazards based on WebGIS. In literature [20], aiming at the shortcomings of the existing WebGIS in

the field of marine information sharing, a method based on Spatial Database Engine (SDE) to manage marine remote sensing data is proposed, thus realizing the marine remote sensing WebGIS oriented to the distributed heterogeneous database environment.

3. GIS Visualization Technology Analysis of Flow Field

GIS stores spatial data in the form of layers, the flow field is multitime data, and each time data is a vector layer. These layers are integrated into a layer group (Group Layer), which is convenient for data management and observation and analysis of flow field motion in time series. Therefore, when rendering the flow field, a uniform flow velocity threshold and the length and color of the corresponding rendering symbols should be specified. However, observing the data, it can be found that the numerical distribution range of the data velocity at different times is very different. Figure 1 shows the numerical distribution characteristics of the flow velocity at the first and 72nd time during the storm surge. The value distribution at the first time is between 0 and 0.1, while the range at the 72nd time is between 0 and 1.5.

If the data is rendered linearly, the spatial characteristics of the flow velocity cannot be highlighted. Therefore, in order to enhance the contrast effect of the flow field, in this paper, when the flow field is uniformly rendered, the symbol length and symbol color are processed, and the flow field is rendered nonlinearly.

3.1. Length Map Rendering. The flow field data is rendered with arrow symbols, and the length of the arrow indicates the magnitude of the flow velocity. Since the change of the flow field is a dynamic process in a long-term sequence, when rendering the data at each moment, the maximum value of the flow velocity at all moments should be uniformly selected as the upper limit of the rendering. In this paper, the maximum velocity range of the Jiaozhou Gulf flow field at multiple times is about 1.5. When the symbol length is linearly corresponding to the velocity value, the formula is as follows:

$$size = \left(V \div V_{\max}\right) \times 1000. \tag{1}$$

In the formula, $V_{\max}$ represents the flow rate, g is the maximum flow rate, and the maximum value of the symbol length corresponding to the maximum flow rate is 1000. However, since the numerical ranges of the flow velocity in the flow field at different times are different, the spatial distribution of the flow velocity in the flow field at the same time is not uniform.

In order to avoid this problem and highlight the numerical variation characteristics of most elements, it is necessary to set the symbol length within an appropriate range according to certain rules. This paper nonlinearly maps the symbol size to between 70 and 600, as shown in Figure 2.

The formula for nonlinear mapping is as follows:

$$aftersize = \begin{cases} size \in (0, 70), \\ size, size \in (70, 500), \\ 500 + (size - 500) \times 0.2. \end{cases} \tag{2}$$

In the formula, aftersize is the symbol size after nonlinear mapping, and size is the size of linear mapping.

Figure 3 shows the comparison of the effect of general linear mapping and nonlinear mapping of symbol length in the same region of the flow field. Although the vortex characteristics of the water flow can be seen in both Figures 3(a) and 3(b), the symbols of the general linear mapping have little difference in the length of the vortex, which cannot reflect the changing law of the water flow velocity at the vortex. However, Figure 3(b) clearly shows that the flow velocity in the center of the vortex is small, and the flow velocity increases toward the outside.

3.2. Color Stretching Rendering. In flow field rendering, the color stretching of symbols is also a way to express the magnitude of the flow velocity. The color stretching of the flow field, that is, the rendering of the color by subshort, is to divide the elements of the flow field into several segments according to the flow rate and then select a starting color and an ending color to form a color band. Finally, the corresponding relationship between the flow velocity of each segment and the color on the ribbon is established according to certain rules, and the arrow symbols of the flow field elements at each level are rendered into corresponding colors.

The formula for nonlinear mapping is as follows:

$$colorin\ de\ x = \begin{cases} breakvalue \times 140, breakvalue \in [0, 1], \\ breakvalue \times 20 + 140, breakvalue \in [1, 1.5]. \end{cases} \tag{3}$$

In the formula, breakvalue is the flow velocity value of the flow field element, and colorindex is the index number of the color block corresponding to the color ribbon.

Figure 4 shows the comparison of the effect before and after the nonlinear mapping of the flow field symbol color. Figure 4(a) is a single-color map, and the color of the flow field symbol does not change. Figure 4(b) is a nonlinear color mapping. With the change of the flow rate, the color of the flow field symbol also changes, and the expression of the seawater flow law is more vivid.

Figure 5 depicts the relationship between map scale and flow field feature display. As the scale is reduced, the size of the spatially fixed features on the map is smaller. However, the size of the computer screen is fixed, which results in a large number of features on a small-scale map and a small distance between features.

The degree of sparseness of the data is related to the cell size of the grid used to control the display of features. To achieve adaptive sparsification, the size of grid cells should change with the scale. It can be seen from Figure 6 that when browsing the map in a large scale at a small scale, the grids with larger unit size (smaller number) are used for thinning. At this time, the level of detail of the data is lower; that is, the

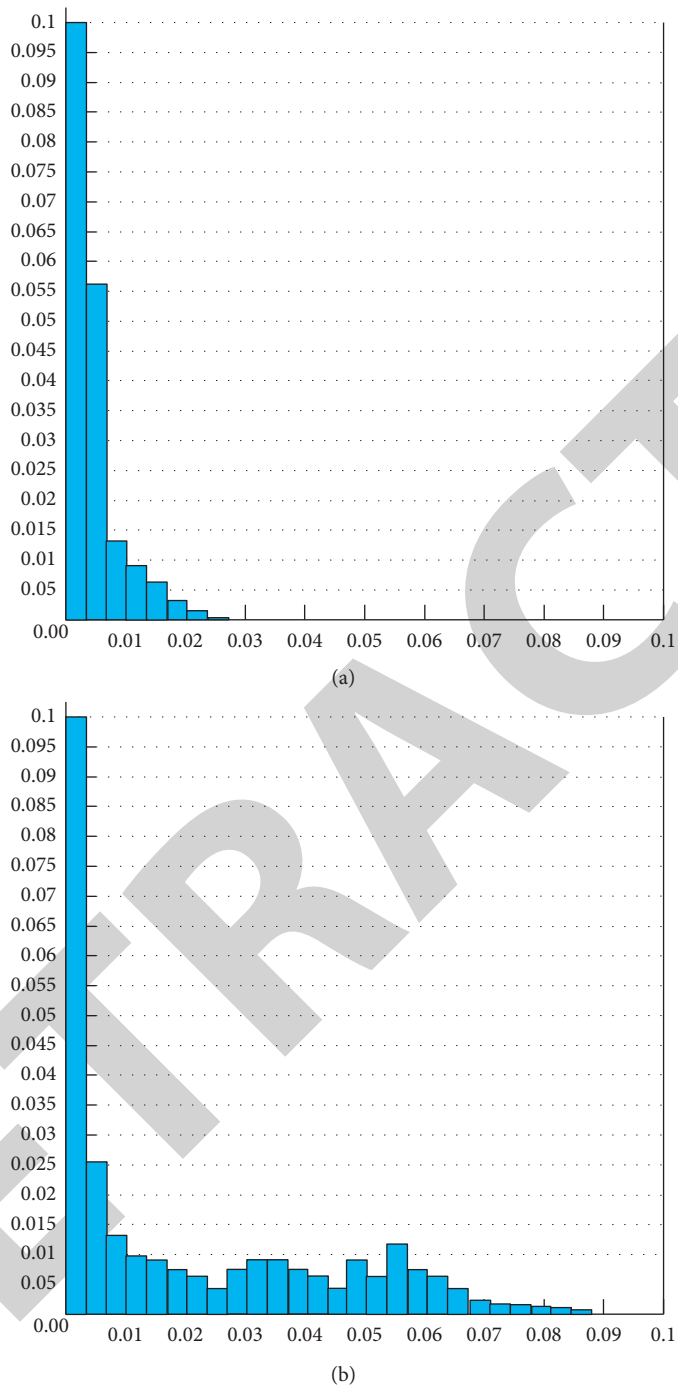

Figure 1: Numerical distribution characteristics of flow velocity. (a) The first moment. (b) The 72nd moment.

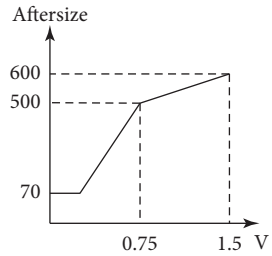

Figure 2: Nonlinear mapping of symbol length.

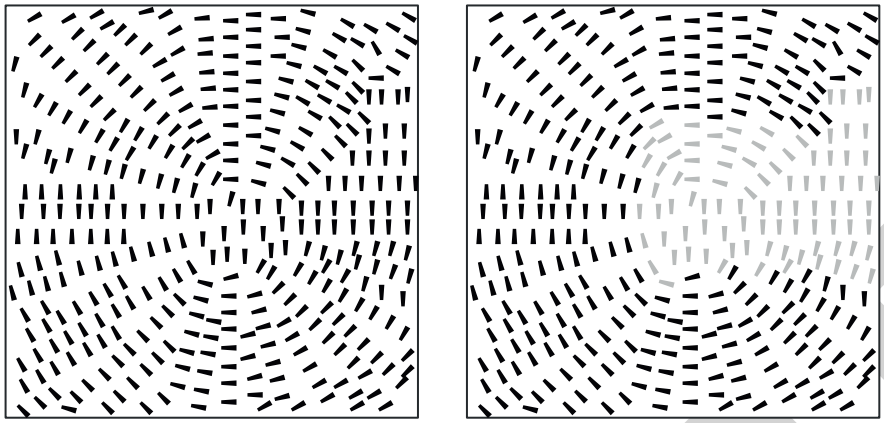

(a) (b)

Figure 3: Comparison of flow field symbol length mapping effects. (a) General linear mapping. (b) Nonlinear mapping.

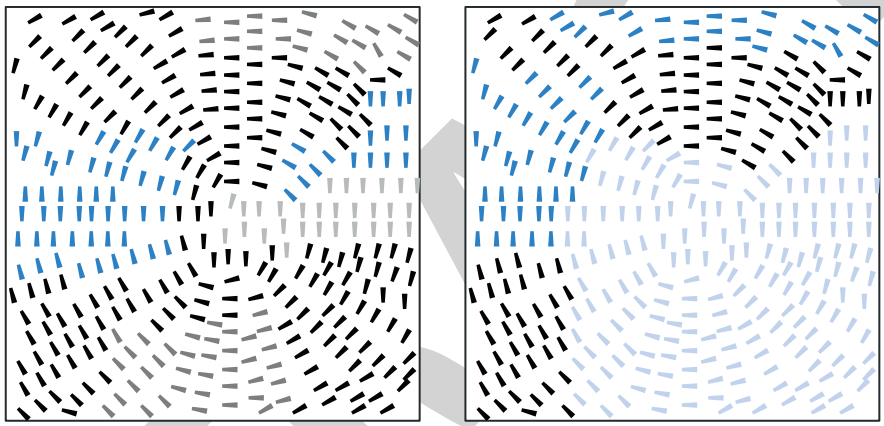

(a) (b)

Figure 4: The rendering before and after nonlinear color mapping. (a) Single-color mapping. (b) Nonlinear mapping.

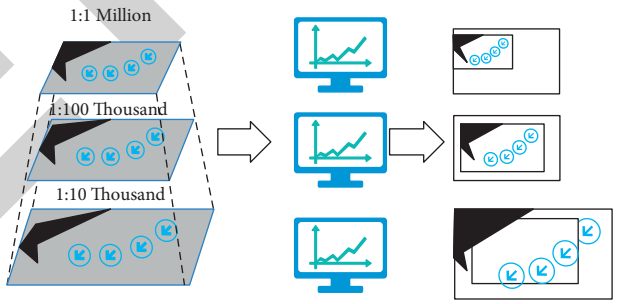

Figure 5: The relationship between map scale and element display.

degree of sparseness is higher. When viewing in a large scale and a small area, that is, when the map is enlarged, in order to highlight the details of the flow field and display more elements, a grid with a smaller unit size (more number) is used for thinning. At this time, the data display has a higher level of detail, that is, a lower degree of sparseness, as shown in Figure 6.

Therefore, the adaptive thinning processing is divided into the following steps: determining the scale range of the adaptive processing, the scale classification, and the calculation of the grid size at each level. Finally, an adaptively processed grading table is obtained, and the scale and grid size of each level are recorded.

To realize the adaptive sparse processing of the flow field, the key step is to determine the relationship between the map scale and the grid size. This paper calculates that, for the flow field data with specific spatial distribution (element range, element location), the distance between the displayed elements at any scale should be kept the same. Then, there is a constant relationship between the scale and the size of the

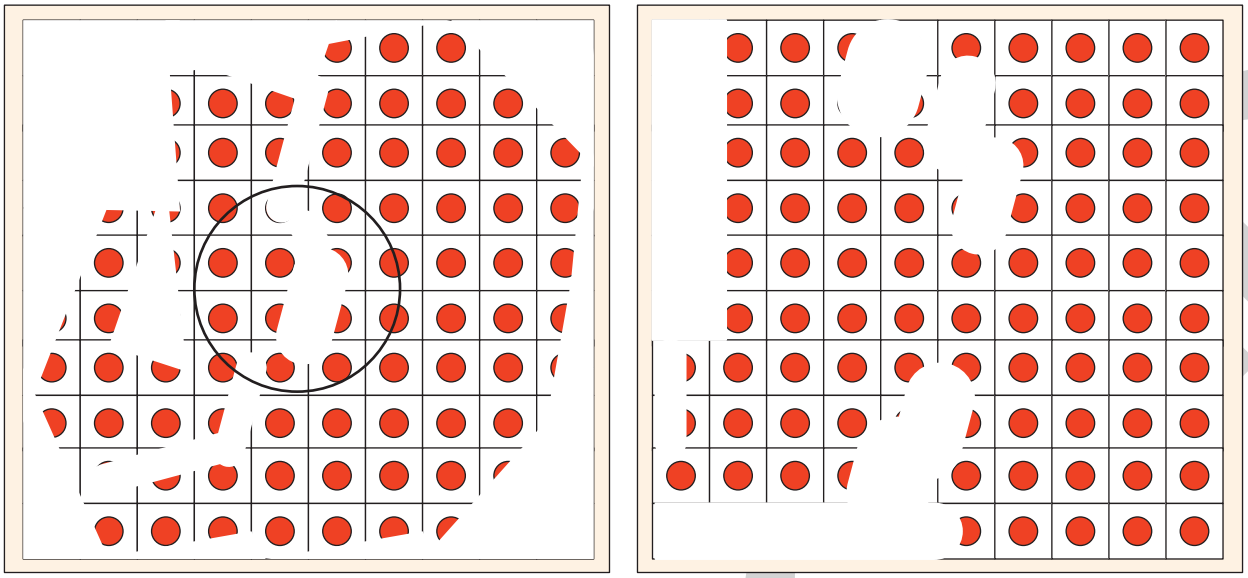

(a) (b)

Figure 6: Grid size at different scales. (a) Grid size at 1 : 60,000. (b) Grid size at 1 : 22,000.

corresponding grid, which is defined as the spatial density eigenvalue in this paper. It can be seen that the spatial density eigenvalue is an important parameter to describe the relationship between flow field sparse processing and scale.

First, we define several variables: width represents the real spatial width of the ocean field, and L represents the width of the computer screen that displays the ocean field. num represents the number of points in a single direction (here, the horizontal direction is used as an example) within the screen range after thinning, and space is the point interval. As mentioned above, the empirical value is space e [1.8, 2.3 cm].

This paper selects any two display levels to analyze the relationship between scale and grid number. We set these two grid levels as i, j. Under the level i, the corresponding scale is S_i, the actual space width of the screen coverage is L_i, and the number of horizontal grids of the matching grid is N_i. Under the j level, the corresponding scale is S_j, the actual space width of the screen coverage is L_j, and the grid number of the matching grid is N_j, as shown in Figure 7.

Since the scale bar = distance on the map/distance on the ground, such as 1/5,000, means that 1 meter on the map represents the distance on the ground of 5 kilometers, we obtain

$$S_i = L/L_i, \tag{4}$$

$$S_j = L/L_j. \tag{5}$$

Since the number of points displayed on the current screen is fixed and the real width of the current screen = the real width of the point interval $*$ the number of points, we obtain

$$L_i = wi\ dt\ h/N_i \times num, \tag{6}$$

$$L_j = wi\ dt\ h/N_j \times num. \tag{7}$$

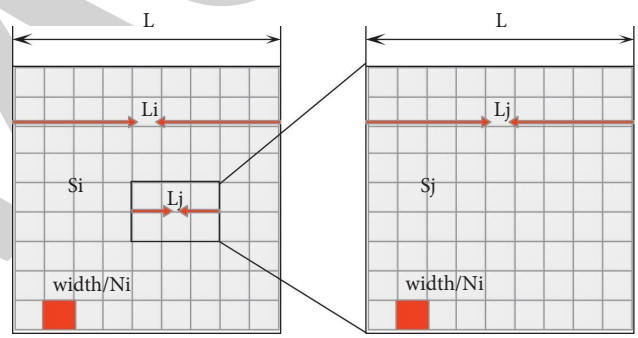

Figure 7: Quantitative relationship under any two display levels.

From formulas (1)–(4), the following is calculated:

$$N_i/S_i = N_j/S_j = num \times wi\ dt\ h/L = \lambda. \tag{8}$$

It can be seen from formula (8) that the ratio of the number of grids at any level to the corresponding scale is a constant. In this paper, this number is defined as the eigenvalue of the spatial density of the massive field, and formula (8) is called the eigenvalue formula. Based on the characteristics of this formula, the number of cells and corresponding scales of grids at each level can be calculated.

According to the relationship between the number of grids and the scale obtained above, it can be seen that the number of grids corresponding to each level of scale can be calculated only by the spatial density characteristic value of the massive field, and vice versa, and the display scale corresponding to each level of grid can also be calculated.

There are two methods for the estimation of spatial density eigenvalues. The first method is to combine formulas (8) and (9):

$$num = L/space. \tag{9}$$

The following formula can be obtained:

$$N_i/S_i = N_j/S_j = width/space = \lambda. \quad (10)$$

Therefore, the spatial density eigenvalue is the ratio of the real spatial width of the ocean field to the spatial density coefficient. In this way, when the scale grading is completed, the size of the grid and the number of grid cells at each level can be calculated.

Another method is to adjust the display scale to the adaptive maximum scale. In this state, the solid distance of the grid spacing can be determined. The number of cells in the corresponding grid can be obtained from the field width of the flow field, and the spatial density characteristic value can be obtained according to formula (10).

If the value of the level increment coefficient is too small, it lacks practical significance, and if the value is too large, the data cannot be effectively thinned. Through continuous experiments, the empirical value k of the level increment coefficient is obtained, which is roughly 1.1–1.6. In actual operation, this value can be manually adjusted according to the display accuracy.

$$\begin{aligned} S_i * k &= S_{i+1} \\ N_i * k &= N_{i+1}, k \in [1.1, 1.6]. \end{aligned} \quad (11)$$

In this formula, S_i , S_{i+1} represent the scale at level i, i+1, $V_{\max}$, N_j represent the number of grids at grid level i, j, and k is the level increment coefficient.

The ocean flow field data is divided into regular uniform flow field and irregular flow field according to its spatial distribution characteristics. Since the data elements of the regular flow field and the sparse grid are uniform and regular, the adaptive sparseness processing of the regular flow field data can achieve the uniform adaptive sparse effect by using the idea of the above general algorithm.

Moreover, since each point in the uniform lattice is identified by a unique set of row and column index (i, j), which is convenient for retrieving elements and extracting point sets, the specific operations of sparse processing do not need to generate grids and other data step by step. Moreover, it can easily and quickly retrieve elements in the application and display them. In this paper, ArcEngine is used as the platform for the program implementation of stream field data sparse processing.

The basic idea of the realization of the regular flow field sparse program can be reduced to two transformations. First, the size of the sparse grid is transformed into the problem of "taking a point for every few points" and then transformed into the mathematical law satisfied by the row and column index numbers (i, j), and the qualified point set is searched and retrieved.

The distances between the elements of the flow field data with uniform lattice distribution are equal everywhere, and the cell size of the sparse grid is also the same. Therefore, if it is assumed to be n times of the point spacing, then when superimposed, the number of feature points that fall in the horizontal or vertical direction in the grid cell where the feature points fall is also N. The result of sparse processing is that at most one element point is extracted from each grid unit, so as long as every n points in both horizontal and vertical directions are taken—one element. Its conversion to (i, j) satisfies the condition that i and j are divisible by N at the same time.

Figure 8 shows the situation when the grid cell contains exactly two feature points in the horizontal and vertical directions. At this time, as long as the feature points whose row and column numbers are divisible by 2 are extracted, it is the result of sparseness at the current level.

Based on the basic idea of transforming grid size into index condition, the key to program realization of regular flow field data sparse processing lies in solving the corresponding relationship between grid size and n value. The solution formula is as follows:

$$n = \begin{cases} R/N, R > C \\ C/N, C > R \end{cases}. \quad (12)$$

N is the number of cells in one direction of each grid level. R and C are the number of rows and columns of the regular flow field data lattice, respectively. The adaptive flow field sparse algorithm classifies the scale, and the size of the sparse grid corresponding to each level is usually expressed by the number of grid cells. Since the range of uniform grid division is the smallest circumscribed square of the flow field, the number of cells in each level of grid is equal in the horizontal and vertical directions. Therefore, the size of a pair of grids is expressed as $N \times N$.

The extraction of point sets theoretically requires retrieval control in both horizontal and vertical directions. The number of rows and columns of the regular flow field data lattice is R and C, respectively, but the flow field data with unequal R and C only reach the edge of the minimum circumscribed square in one direction of the horizontal or vertical direction. Therefore, according to formula (13), the grid size of each level is converted into the corresponding n value.

When the user browses the map, the program locates the corresponding level and the n value of the level according to the scale of the current map, queries the elements of the flow field, and obtains the elements whose row and column numbers are divisible by n, which can be seen on the map. The query statement is as follows:

$$[i] \bmod n = 0 and [j] \bmod n = 0. \quad (13)$$

4. Research on Blue Finance of Ocean City Based on GIS

The overall structure of the system is shown in Figure 9. The whole system is divided into data service layer, application service layer, and client application layer from bottom to top. The application service layer consists of two parts: the open-source framework layer and the GIS function service layer. The open-source framework layer is the core framework for data sharing and also provides standard format communication data for the GIS function service layer. The GIS function service layer is the main part of realizing the sharing of ocean data processing service functions, mainly realizing ocean scene modeling, ocean data analysis, and other

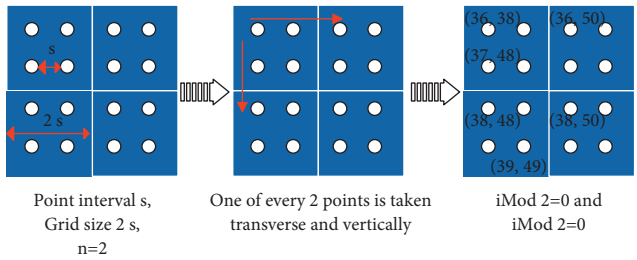

Figure 8: Conversion of grid and retrieval conditions.

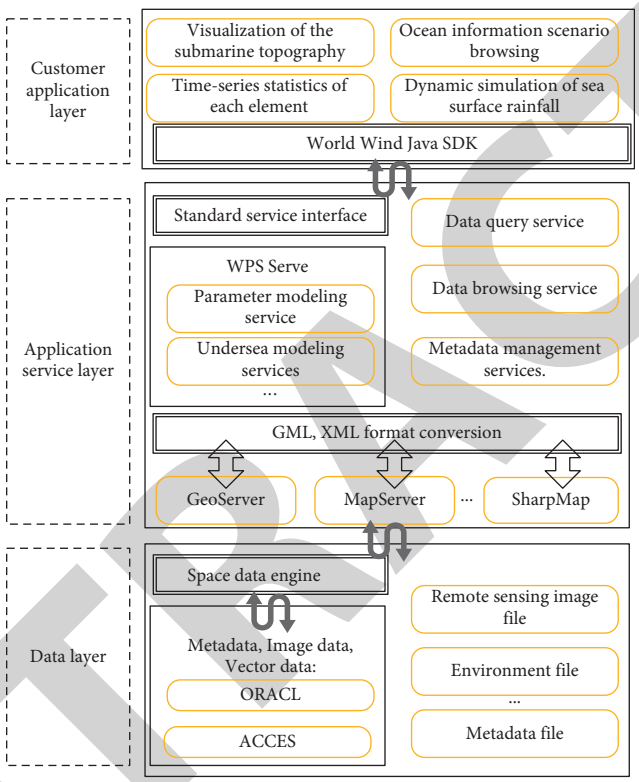

Figure 9: Service-based Web 3D GIS architecture.

services. The client application layer is the interface for the client to realize data browsing and interaction.

The data service layer is the basis for the entire demonstration system to build network application services and is responsible for saving all the data and control information required by the system. According to the characteristics of basic spatial data, data includes not only structured data records, but also unstructured files and image data. For image data, this paper adopts metadata management technology. The multisource, heterogeneous, dynamic, multidimensional, and massive characteristics of ocean environmental comprehensive data determine the complexity of its data management. Moreover, this complexity is reflected in the diversity of data and the complexity of the image vector data itself. According to the sharing requirements of ocean data, the unified interoperability of different data types must be realized. This demonstration system supports a variety of data storage methods. Ocean data can be stored in the form of files or in spatial databases such as Oracle.

The application service layer is the core function layer of the service-based ocean 3D visualization system, including the open-source framework layer and the GIS function service layer. The system is developed on the basis of open-source GIS software to realize operations such as reading multisource ocean data and convert multisource data into standard format communication data to realize network data interoperability. After the open-source GIS framework layer completes data conversion and realizes data interoperability, the GIS function service layer can realize GIS function analysis with standard communication data. The functional interface of the service layer can not only be published in the form of ordinary web service interface, but also follow the WPS specification of OGC to realize the collaborative sharing of multiple GIS functional services. The client application layer mainly realizes the 3D visualization of ocean information, including the visualization of seabed terrain, dynamic simulation of rainfall on the sea surface, simulation of clouds in the sea and sky, and

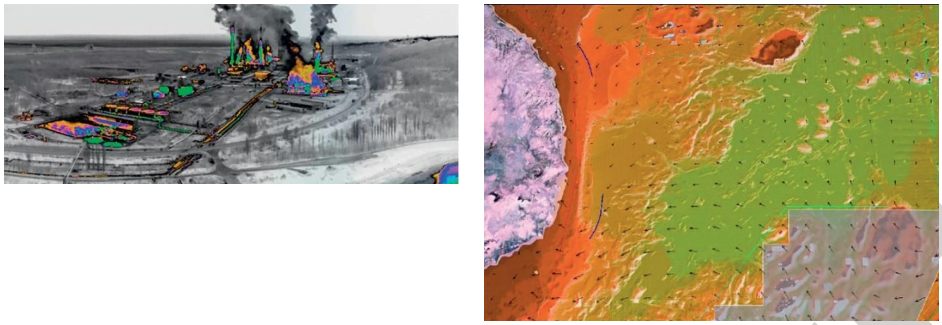

(a) (b)

Figure 10: Simulation of ocean city blue finance based on GIS. (a) Image simulation of coastal economic development (corporate carbon emissions). (b) Ocean climate modeling and its impact on coastal economies.

Table 1: Evaluation of the role of GIS in the development of blue finance in ocean cities.

Number	Test evaluation	Number	Test evaluation	Number	Test evaluation
1	87.25	21	89.19	41	82.25
2	83.43	22	87.20	42	83.57
3	76.59	23	84.13	43	77.19
4	77.75	24	78.46	44	84.40
5	86.72	25	89.35	45	80.67
6	84.83	26	77.16	46	79.79
7	81.15	27	88.76	47	80.73
8	84.37	28	82.14	48	82.68
9	84.47	29	78.38	49	86.57
10	83.21	30	84.05	50	79.52
11	79.44	31	85.06	51	76.18
12	80.65	32	88.96	52	79.20
13	90.01	33	84.53	53	79.05
14	85.61	34	90.73	54	77.20
15	80.21	35	84.40	55	86.40
16	81.63	36	82.27	56	80.05
17	89.48	37	90.91	57	81.61
18	78.90	38	82.47	58	78.13
19	81.00	39	83.68	59	77.69
20	79.44	40	89.53	60	77.92

browsing of ocean scenes. The client calls the application service layer interface to obtain the data information after the analysis and processing of the service layer for rendering and expression of the client. The application layer completes the realization of the application system through the service interface. The client integrates the service interface defined by the application layer and accesses the underlying resources through the protocol of the application layer and no longer needs to care about the complicated and cumbersome implementation mechanism of access. Figure 10 shows an example image of the simulation model in this paper.

On the basis of the above research, the role of GIS in the development of blue finance in ocean cities is explored, and the statistical results are shown in Table 1.

From the above research, it can be seen that the GIS technology proposed in this paper can play an important role in the research of blue finance in ocean cities and has a certain role in promoting the development of ocean blue finance.

5. Conclusion

The ocean provides various resources and environmental support for the development and evolution of human society. The development of the ocean economy must be guaranteed to be sustainable, ensuring the coordinated advancement of the ocean economy, human survival and ecological stability. Moreover, the ocean is an important guarantee for the continuous development and progress of human beings, and without a healthy ocean, the survival of human beings will be difficult to maintain. The ocean economy is an important part of the blue economy, and the development status of the main body of the blue economy will directly affect the development level of the blue economy. Therefore, in order to realize the rapid and healthy blue economy, the ocean economy and ocean related industries will be the focus of development and attention. This paper combines the GIS to carry out the research on the blue

Hindawi
Mobile Information Systems
Volume 2022, Article ID 9113683, 10 pages
https://doi.org/10.1155/2022/9113683

Research Article

The Path of Agricultural Policy Finance in Smart Service for Rural Revitalization under Big Data Technology

Yingzhi Wu

Shanxi Vocational University of Engineering Science and Technology, Taiyuan, Shanxi 030619, China

Correspondence should be addressed to Yingzhi Wu; 2020240288@mail.chzu.edu.cn

Received 18 June 2022; Revised 20 July 2022; Accepted 21 July 2022; Published 21 August 2022

Academic Editor: Chi Lin

In order to explore the path of agricultural policy finance in the intelligent service of rural revitalization under the background of big data, this paper combines data mining technology for financial data processing and big data technology for rural revitalization data analysis. Moreover, this paper combines rural revitalization with agricultural policy-based financial smart services. In addition, with the support of data mining technology, this paper constructs a research system on the path of agricultural policy finance in smart services for rural revitalization based on big data technology. Finally, this paper analyzes the data from the National Statistical Yearbook. Through experimental research, it can be known that the system constructed in this paper has certain effects. Moreover, with the support of the data mining system, this paper conducts research on the path of agricultural policy finance in smart services for rural revitalization and puts forward some suggestions.

1. Introduction

China's agricultural policy financial institutions implement low interest rates on agricultural industries in order to better stimulate agricultural production. According to the "financial constraints" theory [1], our country should implement artificially priced low interest rates lower than the equilibrium interest rate in the rural financial market under the premise of stable food prices to overcome the incomplete information of the rural financial market and solve the problem of the incentive mechanism of agricultural policy financial institutions in the process of investing and financing agricultural production activities. The essence of the theory of financial constraints is that the government intervenes in financial market interest rates and creates rental income to encourage banks and enterprises [2]. The theory of financial restraint is different from the theory of financial restraint. (1) It advocates that the government control interest rates, implement low-interest deposits to reduce financing costs, issue mid- and long-term loans, and control loan interest rates to achieve economic stability. (2) Under the premise of an imperfectly competitive market, market mechanisms will aggravate information asymmetry. Therefore, the government should restrict bank competition, control franchise rights, formulate market access mechanisms, and restrict disorderly market competition to ensure rental income. (3) The government needs to pull deposits and restrict the transfer of deposits to nonfinancial institutions in order to improve the efficiency of resource allocation of financial institutions. For China, the government set up a special agricultural policy financial institution (Agricultural Development Bank) to ensure that agricultural policy financial institutions can obtain sufficient rental income to maintain their operations through concessions. At the same time, the financing channels of agricultural policy financial institutions include government appropriations, capital funds, bond markets and deposits, etc., and there are stable sources of funds to extend loans to obtain profits and achieve stable and sustainable operations [3].

The strategy of rural revitalization refers to the starting point for socialism with Chinese characteristics to enter a new era. Under the guidance of a series of theoretical systems of the Sinicization of Marxism, it is necessary to follow the basic laws of the market around the "three rural" issues in the new era, activate the main body, elements, and the market, and break the urban-rural dual structure by

cultivating the endogenous force of rural development. At the same time, it is necessary to promote the overall prosperity and recovery of rural areas, accelerate the modernization of agriculture and rural areas, build and improve the integration of urban and rural economic and social development as the core, and accelerate major strategic measures to promote my country's agricultural power to become an agricultural power country.

In this paper, the path of agricultural policy finance in smart services for rural revitalization research is carried out in combination with big data technology. On this basis, this paper combines experimental research to verify the effect of the method.

2. Related Work

Due to different development stages and foundations, the research on modern agriculture and agricultural modernization started from developed countries and derived from modernization theories. Moreover, these studies are a combination of agricultural development and progress, and they define, summarize, and promote modern agriculture from the perspective of the development conditions, development momentum, and development effectiveness of agricultural production. In [4], the authors put forward the concepts of "traditional society" and "modern society" and at the same time put forward the "analysis" and "motivation" of modernization that constitute the source of Western modernization theory. Under the tide of the industrial revolution, in [5], the authors compared the differences between "traditional (agricultural)" and "modern" societies from different disciplines. However, these theories are full of the ideology of "Western supremacy," which believes that modernization is Westernization and Americanization. In [6], the authors questioned and impacted the westernized modernization theory. Some scholars began to develop modernization theories from different standpoints and perspectives. The authors from [7] believed that agriculture is by no means useless; on the contrary, it can become the driving force of economic growth, and agricultural modernization can be like a booster for launching satellites to promote economic take-off. In [8], the authors emphasized the need to transform from "consumption type" to "ecological type," from "open" to "closed" economic growth mode, and pursued the improvement of human welfare instead of output. This is considered to be the source of ideas for agricultural circular economy. The authors from [9] believed that modernization mainly includes industrialization, urbanization, social mobility, democratization, and intellectualization. Because modernization theory brings about a major change in the concept of modernization, the authors from [10] believed that any society has the possibility of developing modernity from tradition and adapting to the development of new functions from the original system of the country is more effective than copying the Western system. The authors from [11] believed that no matter what kind of country there is a path for modernization development, and meticulous research from different levels and different channels can establish a suitable modernization theory. In [12], the authors put forward the theory of induced technological innovation and showed that the relative scarcity of resource endowments induces farmers to choose different technologies. Since the new century, relevant research on modern agriculture has analyzed and explained modern agriculture from the perspective of the application of new technologies and new systems. Moreover, it has gradually transformed from emphasizing the increase of input elements to emphasizing the role of technological innovation and institutional innovation in agricultural development, improving production relations, and applying modern machinery and information technology to equip agriculture. With the acceleration of the world modernization process, the current foreign scholars' research on agriculture is increasingly in the field of ecology, green and sustainable development of agriculture [13]. The research on modern agriculture carried out by foreign scholars from different perspectives and different priorities provides a useful reference for my country to conduct modern agricultural theoretical research and promote agricultural progress.

The authors from [14] believed that modern agriculture is a highly technologically intensive industry based on biotechnology and information technology, and a new type of industry in the direction of diversification. In [15], the authors pointed out that the foundation of modern agriculture is modern industry and science and technology, and the core is scientificization. Moreover, it is a comprehensive agricultural system based on market demand and operating rules, using modern agricultural science and technology, modern industrial equipment, and modern management concepts. In [16], the authors suggested that efforts should be made in four aspects: technological innovation capability, technological promotion capability, infrastructure construction, and agricultural product subsidy system to accelerate the promotion of modern agriculture. The authors from [17] believed that the core issue of agricultural modernization is to break the constraints of agricultural production factors and market demand through technological innovation and institutional innovation. The authors from [18] believed that the essence of modern agriculture is a process of upgrading, and the only goal is to develop agricultural productivity. The authors from [19] believed that modern Internet technology is deconstructing the modern agricultural industry chain and business model and will become a key means for the transformation of modern agricultural development methods and the improvement of agricultural production efficiency. Through the panel data analysis of the level of agricultural mechanization and the scale of wheat planting, in [20], the authors proposed that prioritizing investment in mechanization and cultivating the outsourcing service market can effectively induce wheat growers to be involved in the division of labor and introduce smallholder production into the development track of modern agriculture.

3. High-Order Autoencoder Based on Subspace Mapping

This paper uses big data technology to analyze rural revitalization data and combines rural revitalization with agricultural policy-based financial smart services. The high-order automatic coding model based on subspace mapping maps the input data to an independent subspace by replacing the hidden layer of the basic depth calculation model with a subspace mapping layer, as shown in Figure 1.

In the subspace high-order autoencoder, the input data are mapped to two independent subspaces: $h_1 \in R^{P_1 \times P_2 \times \cdots \times P_S}$ and $h_2 \in R^{Q_1 \times Q_2 \times \cdots \times Q_T}$, as shown in the following formula:

$$H = \begin{pmatrix} h_1 \\ h_2 \end{pmatrix} = f\left(\begin{bmatrix} W_1^{(1)} \\ W_2^{(1)} \end{bmatrix} X + \begin{bmatrix} b_1^{(1)} \\ b_2^{(1)} \end{bmatrix} \right). \quad (1)$$

Among them, $W_1^{(1)} \in R^{I_1 \times I_2 \times \cdots \times I_N \times P_1 \times P_2 \times \cdots \times P_S}$ and $W_2^{(1)} \in R^{I_1 \times I_2 \times \cdots \times I_N \times Q_1 \times Q_2 \times \cdots \times Q_T}$ represent the weight tensors, and $b_1^{(1)} \in R^{P_1 \times P_2 \times \cdots \times P_S}$ and $b_2^{(1)} \in R^{Q_1 \times Q_2 \times \cdots \times Q_S}$ represent the bias tensors.

The subspace mapping hidden layer H is mapped to the output layer Y through the $(S+T+N)$-order tensor $W_2^{(1)} \in R^{I_1 \times I_2 \times \cdots \times I_N \times Q_1 \times Q_2 \times \cdots \times Q_T \times I_1 \times I_2 \times \cdots \times I_N}$, as shown in the following formula [21]:

$$y_{i_1 i_2 \cdots i_N} = f\left(\sum_{p_1=1 \cdots p_S=1}^{P_1 \cdots P_S} \sum_{q_1=1 \cdots q_T=1}^{Q_1 \cdots Q_T} w^{(2)}_{p_1 \cdots p_S, q_1 \cdots q_T, i_1 \cdots i_N} h_{1 p_1 \cdots p_S} \cdot h_{2 q_1 \cdots q_T} + b^{(2)}_{i_1 i_2 \cdots i_N} \right). \quad (2)$$

For an image with a title, h_1 represents the text feature learning subspace and h_2 represents the image feature learning subspace. Then, formula (2) associates with the features of the two subspaces by assigning a weight $w^{(2)}_{p_1 \cdots p_S, q_1 \cdots q_T, i_1 \cdots i_N}$ to each feature value $h_{1 p_1 \cdots p_S}$ and $h_{2 q_1 \cdots q_T}$ of the two subspaces to obtain the output $Y_{i_1 i_2 \cdots i_N}$.

Figure 2 shows an equivalent model of the subspace mapping high-order auto-encoding model. In the equivalent model of the subspace mapping high-order automatic coding model, the associated representation of the two subspaces h_1 and h_2 is defined as μ, as shown in the following formula:

$$\mu = h_1 \otimes h_2. \quad (3)$$

Among them, $\otimes$ represents the Kronecker product of two tensors. For two tensors $A \in R^{I_1 \times I_2 \times \cdots \times I_N}$ and $B \in R^{J_1 \times J_2 \times \cdots \times J_N}$, the Kroc product definition is as follows:

$$\begin{aligned} C &\in R^{I_1 J_1 \times I_2 J_{12} \times \cdots \times I_N J_N}, \\ c_{(i_i, j_1) \cdots (i_N, j_N)} &= a_{i_1, \cdots, i_N} b_{j_1, \cdots, j_N}. \end{aligned} \quad (4)$$

Among them, $(i_n, j_n) = j_n + (i_n - 1) J_n$. Formula (2) can be equivalent to

$$y_{i_1 i_2 \cdots i_N} = f\left(\sum_{p_1 \cdots p_S q_1 \cdots q_T}^{P_1 \cdots P_S Q_1 \cdots Q_T} w^{(2)}_{p_1 \cdots p_S, q_1 \cdots q_T, i_1 \cdots i_N} \cdot v_{p_1 \cdots p_S, q_1 \cdots q_T} + b^{(2)}_{i_1 i_2 \cdots i_N} \right). \quad (5)$$

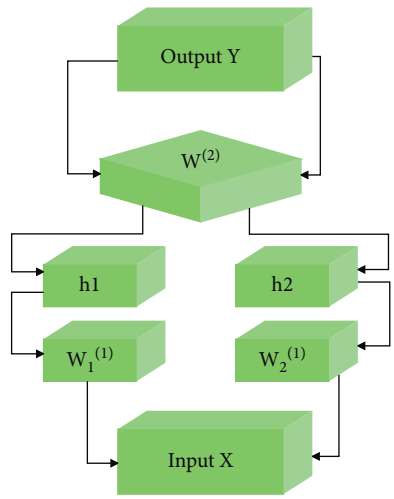

Figure 1: Subspace mapping high-order automatic coding model.

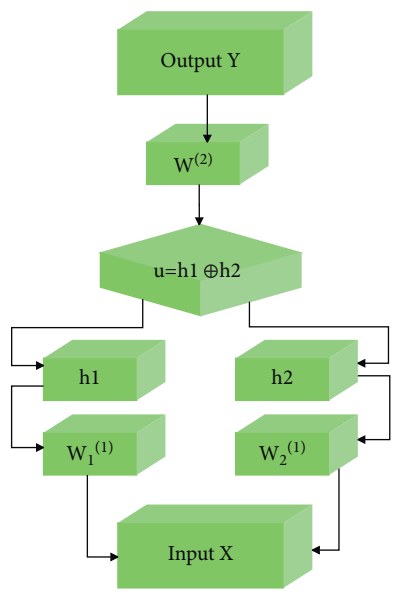

Figure 2: Equivalent model of subspace mapping high-order automatic coding model.

With the form of formula (5), the parameters of the subspace mapping high-order automatic coding model can be trained through the backpropagation strategy.

For any training sample X, the subspace mapping high-order automatic coding model defines its error function $J_{\mathrm{DPTAE}}(\theta, X)$ as shown in the following formula:

$$J_{\mathrm{DPTAE}}(\theta; X) = \frac{1}{2}(X - \hat{X}) = \frac{1}{2} \sum_{i_1}^{I_1} \cdots \sum_{i_N}^{I_N} \left(x_{i_1 i_2 \cdots i_N} - \hat{x}_{i_1 i_2 \cdots i_N} \right)^2. \quad (6)$$

Among them, $\theta = \{W_1^{(1)}, b_1^{(1)}, W_2^{(1)}, b_2^{(1)}; W^{(2)}, b^{(2)}\}$ represents the parameter to be trained and $\hat{X}$ represents the output of the subspace mapping high-order automatic coding model. For a dataset with m training samples, the subspace mapping high-order automatic coding model defines the overall error cost function as

$$J_{\mathrm{DPTAE}}(\theta)=\left[\frac{1}{m}\sum_{i=1}^{m}\left(\frac{1}{2}(X-\hat{X})^{T}(X-\hat{X})\right)\right]+\frac{\lambda}{2}\left(\sum_{i_1\cdots i_N}^{I_1\cdots I_N}\sum_{p_1\cdots p_S}^{P_1\cdots P_S}\left(w_{1(i_1\cdots i_N p_1\cdots p_S)i}^{(1)}\right)^2+\sum_{i_1\cdots i_N}^{I_1\cdots I_N}\sum_{q_1\cdots q_T}^{Q_1\cdots Q_T}\left(w_{2(i_1\cdots i_N q_1\cdots q_T)}^{(1)}\right)^2+\sum_{p_1\cdots p_S}^{P_1\cdots P_S}\sum_{q_1\cdots q_T}^{Q_1\cdots Q_T}\sum_{i_1\cdots i_N}^{I_1\cdots I_N}\left(w_{2(p_1\cdots p_S,q_1\cdots q_T,i_1\cdots i_N)}^{(2)}\right)^2\right). \tag{7}$$

In order to train the parameters of the subspace mapping high-order automatic coding model, first calculate the partial derivative of the error function $J_{\mathrm{DPTAE}}(\theta,X)$ with respect to each parameter through the following steps:

(1) The algorithm performs forward conduction and calculates the input and output of each neuron in the hidden layer and output layer. The calculation process is shown in formulas (8) to (13):

$$z_{(p_1p_2\cdots p_S)}^{(2)}=\sum_{i_1}^{I_1}\cdots\sum_{i_N}^{I_N}w_{1(i_1\cdots i_N,p_1\cdots p_S)}^{(2)}\cdot x_{i_1i_2\cdots i_N}+b_{1(p_1p_2\cdots p_S)}^{(1)}, \tag{8}$$

$$h_{1(p_1p_2\cdots p_S)}=f\left(z_{1(p_1p_2\cdots p_S)}^{(2)}\right), \tag{9}$$

$$z_{2(p_1p_2\cdots p_S)}^{(2)}=\sum_{i_1}^{I_1}\cdots\sum_{i_N}^{I_N}w_{1(i_1\cdots i_N,p_1\cdots p_S)}^{(2)}\cdot x_{i_1i_2\cdots i_N}+b_{1(q_1q_2\cdots q_S)}^{(1)}, \tag{10}$$

$$h_{2(p_1p_2\cdots p_S)}=f\left(z_{2(q_1q_2\cdots q_S)}^{(2)}\right), \tag{11}$$

$$z_{i_1i_2\cdots i_N}^{(3)}=\sum_{p_1\cdots p_S}^{P_1\cdots P_S}\sum_{q_1\cdots q_T}^{Q_1\cdots Q_T}w_{p_1\cdots p_S,q_1\cdots q_T,i_1\cdots i_N}^{(2)}\cdot h_{1(p_1p_2\cdots p_S)}\cdot h_{2(q_1q_2\cdots q_T)}+b_{i_1i_2\cdots i_N}^{(2)}, \tag{12}$$

$$y_{i_1i_2\cdots i_N}=f\left(z_{i_1i_2\cdots i_N}^{(3)}\right). \tag{13}$$

(2) For each neuron in the output layer, the algorithm uses formula (14) to calculate its "residual term" $\delta_{i_1i_2\cdots i_N}^{(3)}$.

$$\begin{aligned}\delta_{i_1i_2\cdots i_N}^{(3)}&=\frac{\partial I_{\mathrm{DPTAE}}(\theta,X)}{\partial z_{i_1i_2\cdots i_N}^{(3)}}\\&=\frac{\partial}{z_{i_1i_2\cdots i_N}^{(3)}}\left[\frac{1}{2}\sum_{i_1}^{I_1}\cdots\sum_{i_N}^{I_N}\left(y_{i_1\cdots i_N}-x_{i_1\cdots i_N}\right)^2\right]\\f'\left(z_{i_1i_2\cdots i_N}^{(3)}\right)\left(y_{i_1\cdots i_N}-x_{i_1\cdots i_N}\right)&=y_{i_1\cdots i_N}\left(1-y_{i_1\cdots i_N}\right)\left(y_{i_1\cdots i_N}-x_{i_1\cdots i_N}\right).\end{aligned} \tag{14}$$

(3) The algorithm uses formulae (15) and (16) to calculate the residual term of each neuron in the hidden layer:

$$\begin{aligned}\delta_{1(p_1p_2\cdots p_S)}^{(2)}&=\frac{\partial J_{\mathrm{DPTAE}}(\theta,X)}{\partial z_{1(p_1p_2\cdots p_S)}^{(2)}}\\&=\sum_{i_1}^{I_1}\cdots\sum_{i_N}^{I_N}\frac{\partial I_{\mathrm{DPTAE}}(\theta,X)}{\partial z_{i_1i_2\cdots i_N}^{(3)}}\cdot\frac{\partial z_{i_1i_2\cdots i_N}^{(3)}}{\partial z_{1(p_1p_2\cdots p_S)}^{(2)}},\\&=\sum_{i_1}^{I_1}\cdots\sum_{i_N}^{I_N}\delta_{i_1i_2\cdots i_N}^{(3)}\cdot\frac{\partial}{\partial z_{1(p_1p_2\cdots p_S)}^{(2)}}\\&\quad\left(\sum_{p_1\cdots p_S}^{P_1\cdots P_S}\sum_{q_1\cdots q_T}^{Q_1\cdots Q_T}w_{p_1\cdots p_S,q_1\cdots q_T,i_1\cdots i_N}^{(2)}\cdot h_{1(p_1p_2\cdots p_S)}\cdot h_{2(q_1q_2\cdots q_T)}+b_{i_1i_2\cdots i_N}^{(2)}\right),\\&=\sum_{i_1}^{I_1}\cdots\sum_{i_N}^{I_N}\delta_{i_1i_2\cdots i_N}^{(3)}\sum_{q_1\cdots q_T}^{Q_1\cdots Q_T}w_{p_1\cdots p_S,q_1\cdots q_T,i_1\cdots i_N}^{(2)}h_{1(p_1p_2\cdots p_S)}\cdot h_{2(q_1q_2\cdots q_T)}\left(1-h_{1(p_1p_2\cdots p_S)}\right),\end{aligned} \tag{15}$$

$$\begin{aligned}\delta_{2(q_1q_2\cdots q_T)}^{(2)}&=\frac{\partial J_{\mathrm{DPTAE}}(\theta,X)}{\partial z_{2(q_1q_2\cdots q_T)}^{(2)}}=,\\&\sum_{i_1}^{I_1}\cdots\sum_{i_N}^{I_N}\left(\delta_{i_1i_2\cdots i_N}^{(3)}\sum_{p_1\cdots p_S}^{P_1\cdots P_S}w_{p_1\cdots p_S,q_1\cdots q_T,i_1\cdots i_N}^{(2)}h_{1(p_1p_2\cdots p_S)}\cdot h_{2(q_1q_2\cdots q_T)}\left(1-h_{2(q_1q_2\cdots q_T)}\right)\right).\end{aligned} \tag{16}$$

(4) The algorithm uses formulae (17) to (19) to calculate the error term of each neuron in the hidden layer and the output layer:

$$\frac{\partial z^{(3)}_{i_1 i_2 \cdots i_N}}{\partial w^{(2)}_{p_1 \cdots p_S, q_1 \cdots q_T, i_1 \cdots i_N}} = \frac{\partial \left(\sum_{p_1 \cdots p_S}^{P_1 \cdots P_S} \sum_{q_1 \cdots q_T}^{Q_1 \cdots Q_T} w^{(2)}_{p_1 \cdots p_S, q_1 \cdots q_T, i_1 \cdots i_N} \cdot h_{1\left(p_1 p_2 \cdots p_S\right)} \cdot h_{2\left(q_1 q_2 \cdots q_T\right)} + b^{(2)}_{i_1 i_2 \cdots i_N} \right)}{\partial w^{(2)}_{p_1 \cdots p_S, q_1 \cdots q_T, i_1 \cdots i_N}} = h_{1\left(p_1 p_2 \cdots p_S\right)} \cdot h_{2\left(q_1 q_2 \cdots q_T\right)}, \tag{17}$$

$$\frac{\partial z^{(2)}_{1\left(p_1 p_2 \cdots p_S\right)}}{\partial w^{(1)}_{1\left(i_1 \cdots i_N, p_1 \cdots p_S\right)}} = x_{i_1 i_2 \cdots i_N}, \tag{18}$$

$$\frac{\partial z^{(2)}_{2\left(q_1 q_2 \cdots q_T\right)}}{\partial w^{(1)}_{2\left(i_1 \cdots i_N, q_1 \cdots q_T\right)}} = x_{i_1 i_2 \cdots i_N}. \tag{19}$$

(5) The algorithm uses formulae (20) to (22) to calculate the partial derivative of the error function for each parameter:

$$\frac{\partial J_{\mathrm{DPTAE}}(\theta, X)}{\partial z^{(2)}_{2\left(q_1 q_2 \cdots q_T\right)}} = \delta^{(2)}_{1\left(p_1 p_2 \cdots p_S\right)} \cdot x_{i_1 i_2 \cdots i_N}, \tag{20}$$

$$\begin{aligned} \frac{\partial J_{\mathrm{DPTAE}}(\theta, X)}{\partial b^{(l)}_{i_1 i_2 \cdots i_N}} &= \frac{\partial J_{\mathrm{DPTAE}}(\theta, X)}{\partial z^{(l)}_{i_1 i_2 \cdots i_N}} \cdot \frac{\partial z^{(l)}_{i_1 i_2 \cdots i_N}}{\partial b^{(l)}_{i_1 i_2 \cdots i_N}} \\ &= \delta^{(l)}_{1\left(p_1 p_2 \cdots p_S\right)} \left(l = 1, 2\right), \end{aligned} \tag{21}$$

$$\begin{aligned} \frac{\partial J_{\mathrm{DPTAE}}(\theta, X)}{\partial w^{(1)}_{2\left(i_1 \cdots i_N, q_1 \cdots q_T\right)}} &= \frac{\partial J_{\mathrm{DPTAE}}(\theta, X)}{\partial z^{(2)}_{2\left(q_1 q_2 \cdots q_T\right)}} \cdot \frac{\partial z^{(2)}_{2\left(q_1 q_2 \cdots q_T\right)}}{\partial w^{(1)}_{2\left(i_1 \cdots i_N, q_1 \cdots q_T\right)}} \\ &= \delta^{(2)}_{2\left(q_1 q_2 \cdots q_T\right)} \cdot x_{i_1 i_2 \cdots i_N}. \end{aligned} \tag{22}$$

After obtaining the partial derivative of the error function with respect to the parameter, the algorithm can use formulae (23) and (24) to calculate the partial derivative of the overall error cost function $J_{\mathrm{DPTAE}}(\theta, X)$ with respect to the parameter:

$$\frac{\partial J_{\mathrm{TAE}}(\theta)}{\partial W^{(l)}} = \left[\frac{1}{m} \sum_{i=1}^{m} \frac{\partial J_{\mathrm{TAE}}\left(\theta; X^{(i)}\right)}{\partial W^{(l)}} \right] + \lambda W^{(l)}, \tag{23}$$

$$\frac{\partial J_{\mathrm{TAE}}(\theta)}{\partial b^{(l)}} = \frac{1}{m} \sum_{i=1}^{m} \frac{\partial J_{\mathrm{TAE}}\left(\theta; X^{(i)}\right)}{\partial b^{(l)}}. \tag{24}$$

Finally, the parameters are updated through the gradient descent method. If the learning rate is assumed to be α, the formula for updating the parameters using the gradient descent method is shown in (25) and (26):

$$W^{(l)} = W^{(l)} - \alpha \frac{\partial J_{\mathrm{DPTAE}}(\theta)}{\partial W^{(l)}}, \tag{25}$$

$$b^{(l)} = b^{(l)} - \alpha \frac{\partial J_{\mathrm{DPTAE}}(\theta)}{\partial b^{(l)}}. \tag{26}$$

Connecting multiple subspace mapping high-order autoencoders from bottom to top can form a depth calculation model based on subspace mapping, as shown in Figure 3.

h^0 and h^l, respectively, represent the input layer and output layer of the depth calculation model based on subspace mapping. The depth calculation model based on subspace mapping first maps the input layer h^0 through two weight tensors $W_1^{(1)}$ and $W_2^{(1)}$ and two bias tensors $b_1^{(1)}$ and $b_2^{(1)}$ to a hidden layer h^1 with two independent subspaces h_1^1 and h_2^1. Then, each subspace in the hidden layer h^1 is divided and mapped to a second hidden layer h^2 with two independent subspaces h_1^2 and h_2^2. This mapping relationship is iterated upwards until the output layer h^l.

Figure 4 shows the equivalent model of the depth calculation model based on subspace mapping. In the equivalent model shown in Figure 4, the interaction of the two subspaces of each hidden layer is mapped to a feature tensor through the Kronecker product of the tensor, which is used as the input tensor of the next hidden layer.

4. Research on Path of Agricultural Policy Finance in Smart Service for Rural Revitalization Based on Big Data Technology

Agricultural policy finance has not given it a definite concept in academia. Generally speaking, "agriculture" is the object of the concept and the object of policy efforts and financial regulation. Various financial instruments will be limited to its scope; "policy" reflects the publicity of the concept and shows the social and economic effects the government wants to achieve, and the achievement of such effects cannot be achieved without the strictness of the government's credit and legal system; "finance" is the category of means in this concept, including all funds storage except administrative power and loan issuance. Industry policy-based finance is not profitable, and it takes agency behavior as a prerequisite and uses government integrity as an endorsement to cooperate with the implementation of relevant policies to support the development of agriculture and the construction of rural areas and promote the solution of the three rural issues. In addition, special financial law assistance should be provided for agricultural activities in terms of borrowing funds.

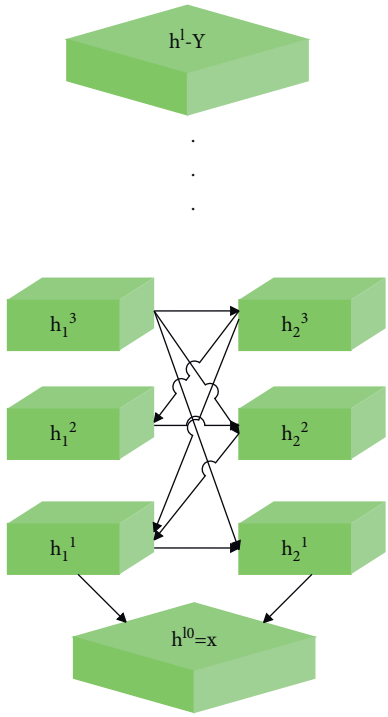

Figure 3: Depth calculation model based on subspace mapping.

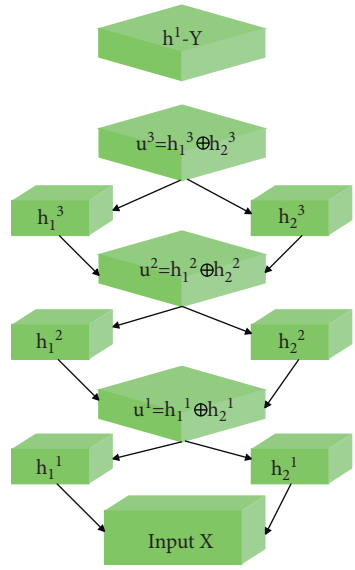

Figure 4: Equivalent model of the depth calculation model based on subspace mapping.

If local governments want to achieve steady economic development, it is closely related to the support of financial funds. However, in the common practice of commercial financial institutions, instead of pulling out local funds, the purpose of asset injection is not achieved. A major feature of China is its large population, accounting for 20% of the global population. In order to solve the problem of the survival of the large population, the steady development of agriculture must be realized. Only the health of agriculture can guarantee the basic conditions for the survival of all citizens. At this stage, various parts of China are facing a shortage of funds. One of the reasons is that local funds have fled the place through commercial financial institutions. Due to the shortage of funds, various localities are generally inadequate in agricultural investment. The agricultural policy financial institution, as a functional department that guides the market, is the implementer of the national macro-control objectives and therefore should also be the solver of local funding problems. The basis for the existence of agricultural policy finance is that there are deficiencies in market means, and the free competition system cannot achieve good regulation. Therefore, the country has to adjust the supply and demand of funds with the help of policy means to achieve the full play of social resources at all levels. In the context of the free market, funds will exhibit the "Matthew effect" and excessive concentration in wealthy areas will result in the flow of funds from rural areas to cities, which will make agriculture, which lacked investment in the past, face a greater crisis. In addition, through policy arrangements, the return of funds to the countryside can achieve a balanced allocation of social capital to a certain extent, adjust the social layout, improve agricultural efficiency, and realize the rational use of social resources.

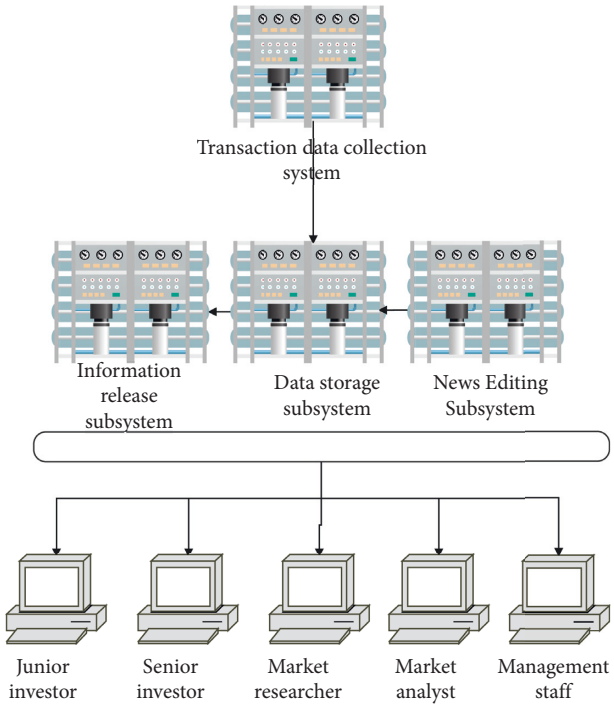

Figure 5: System overall architecture diagram.

The overall structure of the agricultural policy-based financial intelligent service knowledge system is shown in Figure 5. It is divided into four parts: transaction data collection, news data collection, data storage, information release, and knowledge service. The knowledge service part runs on the user's computer terminal in the form of client software, providing knowledge services for junior investors, senior investors, market researchers, market analysts, and information management personnel.

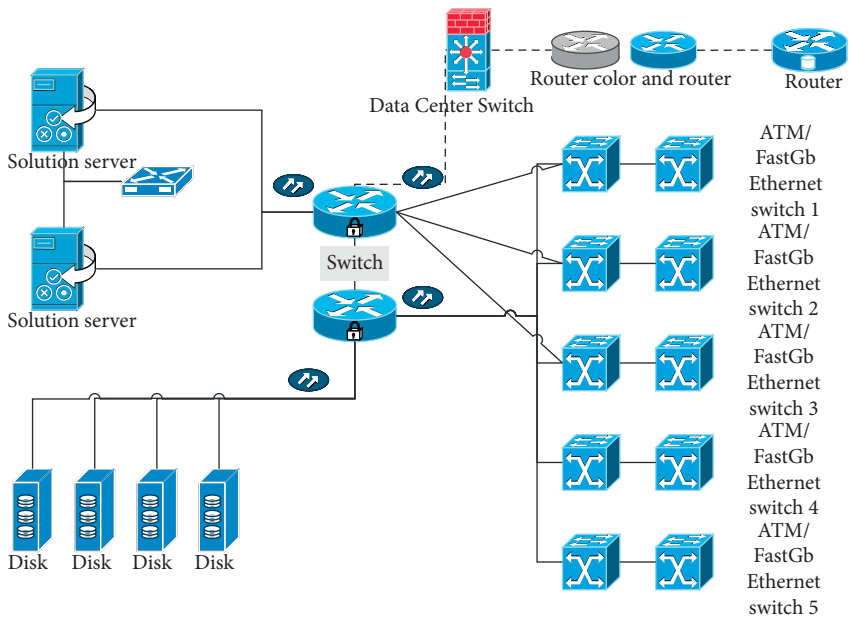

Figure 6: Product hardware architecture and topology scheme.

The hardware architecture and topology of the product are shown in Figure 6, which contains the following components.

The system includes a client, load balancing, an application server, a web server, a database server, a full-text index server, an ETL server, an information analysis and mining server, a manual editing and maintenance platform, an ETL manual verification platform, and various data sources, as shown in Figure 7. Among them, the client, ETL manual verification client, and information manual editing and maintenance client are placed on the external network and separated from the internal network by a firewall. For other tentative intranets, the application server and the web server are placed on the same network segment. Moreover, the database server and the full-text index server are placed on a separate network segment, and the external network is not visible. The ETL and the information analysis part are placed on the same network segment. The data source is processed according to the actual deployment situation, and the same network segment is tentatively determined.

In the process of three-dimensional search, there are three main processes: The first part is the establishment of the search domain. This step is the most critical. The information needs to be cleaned, word segmented, and coded and other preprocessing, and then multi-dimensional analysis is performed, such as the information to which the information belongs The multiple categories of, establish the corresponding relationship with the structured data according to the association relationship of the category. Discover hot topics based on clustering, discover market-related sentiments through sentiment analysis, and extract and analyze information-focused objects through keyword extraction. On this basis, the management of the retrieval domain is realized. The second part is the storage of search objects. Because the search is based on the full-text index and the related information needs to be queried at the same time,

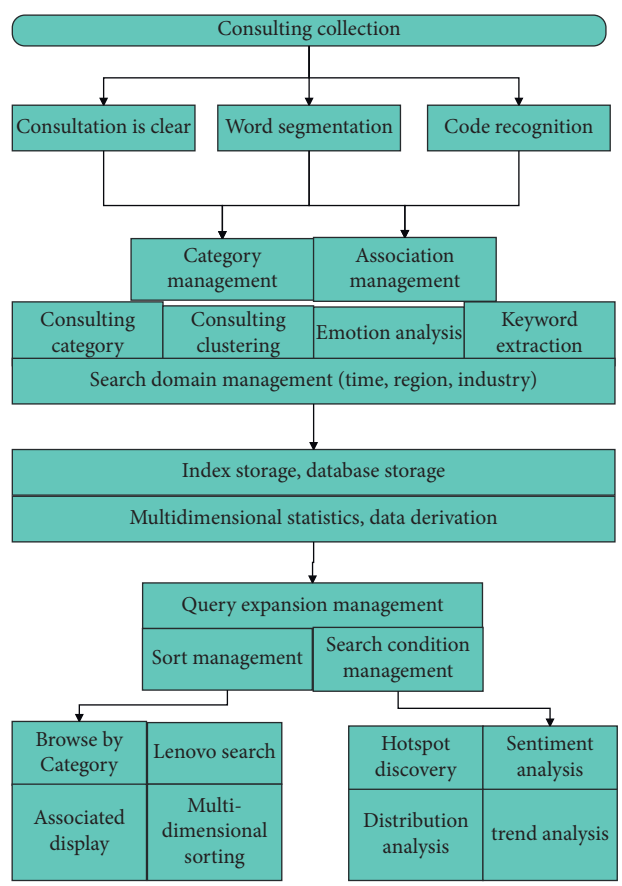

Figure 7: System workflow.

the information data need to be stored in the full-text index and structured database at the same time. In addition, in order to increase the richness of the search level, it is necessary to establish a statistical derivative table based on

the business. The third part is the display part of the search results, including query expansion management, which is used to automatically map the most suitable query object according to the query conditions input by the user. Sorting management is to return the returned results according to the needs of users. Search condition management is to provide users with search conditions. The retrieval part shows the returned results seen by the user in different ways. Derivative results are a series of statistical analysis results based on user input query conditions, including keyword distribution analysis, trend analysis, sentiment analysis, hot spot discovery, and other results derived according to business needs.

The status of financing institutions engaged in policy guarantees is twofold. It is between the borrower and the lender. While reducing the loan issuance risk of financial institutions, it also bears the risk of unrecoverable loans. Due to the policy endorsement, it will stimulate the speculative psychology and negative behavior of some financial institutions and lenders. Under the influence of speculative psychology, in order to realize their own interests, both borrowers and lenders will ignore or falsely report important information, which will increase the risk and cause the consequences of harm to others. Since there are policy guarantees, lenders will focus their attention on high-risk projects because once the project succeeds, the return will be very fast, and once the project fails, it will be backed by a policy guarantee. In this way, it will have a reverse elimination effect, which will exclude many projects with high security but low returns. However, there is a positive relationship between the higher risk and lower loan repayment rate, and the process of reverse elimination will eventually damage the effectiveness of agricultural policy finance, thereby undermining the implementation of agricultural support policies. On the other hand, the party receiving the loan will not use the funds in areas with a higher margin of safety, but will invest in areas with higher risks. The idea is nothing more than if the risk is successful, you can get huge profits, and if the risk fails, there is a guarantee provided by the state as a shared responsibility. The meaning of negative actions is that the parties who should have taken positive measures chose a negative attitude when they had the conditions to act positively. For the parties who provide loans, having national credit as an endorsement will lead to problems of relaxation of review and negligence of supervision, thereby increasing the possibility of not being able to recover the loan. In addition, the parties who obtain loans will also relax management and neglect risk factors, which will lead to the accumulation of risks and increased hidden dangers. This will also weaken the enthusiasm of relevant state agencies for guaranteeing agricultural projects, resulting in a shortage of funds for agricultural support and long-term development restricted.

Relevant institutions that undertake agricultural policy-based financial functions can directly provide funds to agricultural practitioners so as to provide efficient financing for the development of agriculture. Because commercialized financial entities are subject to the purpose of maximizing profits, they are relatively indifferent to agricultural projects with low returns. Therefore, it is not easy for agricultural borrowers to obtain loans from commercial banks and other institutions. In addition, private financing also exists in agricultural areas. Private financing has the advantages of wide coverage, simple procedures, and more ways to obtain it. However, it also has shortcomings such as strict interest requirements and illegal subject qualifications. In addition, due to the restrictions of national laws and regulations, it is unable to make great achievements in supporting agriculture and benefiting agriculture. Therefore, in the process of developing the rural economy, policy financing has become the best choice. It has a nonprofit business method and does not pursue an excessively high profit rate so that it can provide more low-interest loans than commercial banks. This will greatly promote the development of weak industries, especially the agricultural product purchase industry. However, agricultural policy-based finance can play a limited role in directly supporting agriculture and cannot provide all the funds needed for agricultural revitalization. Therefore, the driving effect of its financing must be used to indirectly promote rural prosperity. The statistical agricultural production index is shown in Table 1 and Figure 8. Table 1 and Figure 8 show the agricultural production indexes in the past few years (source: China Statistical Yearbook).

This article combines the statistical yearbook data to study the system of this paper, explores the effect of formulating related strategies, conducts research on data analysis and decision-making effects through multiple sets of data, and obtains the results shown in Table 2 and Figure 9.

From the above research, this paper introduces the following strategies.

At the current stage, the Agricultural Development Bank can consider focusing its work on the following three main industries. The first is the agricultural productive service industry, such as companies that supply all kinds of materials needed for production, companies that master newer industrial technologies, companies that carry out mechanical operations and lease and sell institutional power to the outside world, companies that provide third-party agricultural labor and employment, companies that are committed to expanding agricultural product marketing networks, and agricultural companies that operate Internet platforms to expand their influence. This achieves the intensive use of labor and increases the stock of large-scale modern industrial economies. The second is rural leisure and tourism. The Agricultural Development Bank needs to maintain a sensitive vision of social and market changes and select those agricultural projects that have advantageous geographical locations and distinctive products and are suitable for free market competition. Moreover, the Agricultural Development Bank needs to provide large-scale funding to help develop more tourism industries in rural areas and attract urban populations and other resources to migrate to the countryside, thereby invigorating the rural economy and increasing farmers' incomes. The third is the rural elderly care service industry. Rural elderly care has its unique advantages. With the rapid increase of the elderly population, urban elderly care faces a variety of difficulties, which has also generated huge social needs. The Agricultural

Table 1: Agricultural production index.

Years	Total index	Crops	Forest industry	Animal husbandry	Fishery
2008	105.10	101.60	232.70	97.80	126.60
2009	103.30	102.60	236.60	97.40	115.20
2010	105.50	105.40	217.30	98.70	117.40
2011	109.40	111.90	214.50	102.00	115.70
2012	107.50	107.30	222.20	100.60	118.80
2013	106.30	106.70	241.50	98.60	117.30
2014	107.40	110.20	207.20	98.70	116.20
2015	103.80	105.10	125.60	98.10	110.50
2016	100.00	100.00	100.00	100.00	100.00
2017	105.70	109.70	84.90	99.70	105.20
2018	108.50	113.10	61.20	102.70	105.30

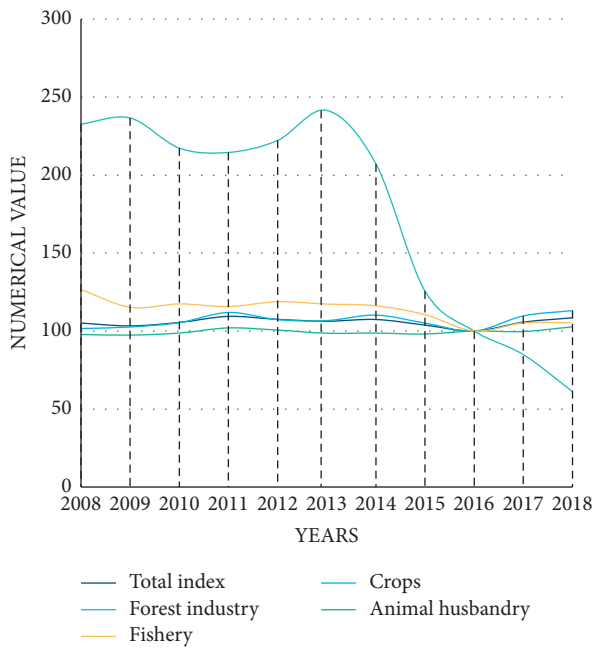

Figure 8: Line chart of agricultural production index.

Table 2: System test research.

Number	Data analysis	Decision effect
1	96.99	85.46
2	95.21	72.43
3	95.22	79.75
4	97.21	79.88
5	94.39	75.16
6	97.27	87.24
7	94.68	71.75
8	94.19	80.84
9	97.75	72.63
10	97.52	90.11
11	94.25	75.28
12	95.25	81.36
13	97.87	87.68

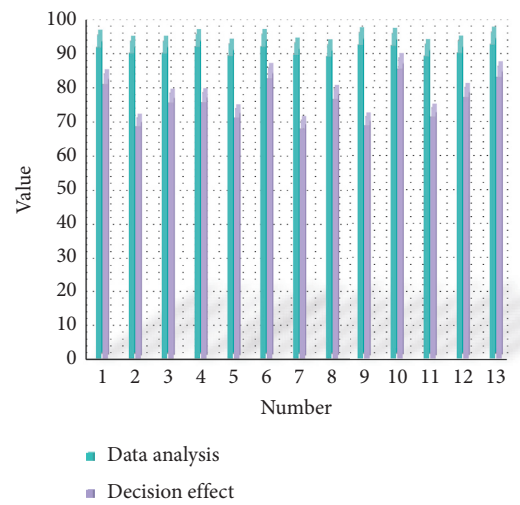

Figure 9: Performance verification of the platform system.

Development Bank should have sufficient foresight and increase investment in the industry. It is possible to select those villages with sufficient medical resources, convenient transportation, and pleasant environment to develop the industry, and provide financing services to them to cultivate the market.

As a financial institution that implements national policies, the service policy is the first responsibility of the Agricultural Development Bank, and the implementation of the policy requires the Agricultural Development Bank to maintain close contact with relevant state institutions. Therefore, the Agricultural Development Bank should maintain a close relationship with the local management at all levels and promote the financing of agriculture with the help of the good cooperation system between the government and the bank.

5. Conclusion

This paper uses big data technology to analyze rural revitalization data and combines rural revitalization with agricultural policy-based financial smart services. Based on the rural revitalization policy, this paper conducts research on the impact of agricultural policy-based financial institutions in supporting the transformation and upgrading of rural industries from two aspects: theoretical analysis and empirical research. Our country's rural economic foundation is poor, industrial development is lagging behind, and rural financial services such as commercial bank loans and commercial insurance have reduced capital investment, and there are frequent chaos in private financial lending. Under this current situation, agricultural policy-oriented financial institutions actively respond to national policies and can effectively promote the upgrading of rural industrial structure. This paper uses big data technology to analyze rural revitalization data and combines rural revitalization with agricultural policy-based financial smart services.

Moreover, this paper constructs a path of agricultural policy finance in smart services for the rural revitalization research system based on big data technology and analyzes it with data from the National Statistical Yearbook. Through experimental research, it can be known that the system constructed in this paper has certain effects.

Data Availability

The data used to support the findings of this study are available from the author upon request.

Conflicts of Interest

The author declares that he has no conflicts of interest.

References

[1] D. K. Dimitrov and M. Ivanova, "Trends in organic farming development in Bulgaria: applying circular economy principles to sustainable rural development," *Visegrad Journal on Bioeconomy and Sustainable Development*, vol. 6, no. 1, pp. 10–16, 2017.

[2] F. Andreola, I. Lancellotti, T. Manfredini, and L. Barbieri, "The circular economy of agro and post-consumer residues as raw materials for sustainable ceramics," *International Journal of Applied Ceramic Technology*, vol. 17, no. 1, pp. 22–31, 2020.

[3] N. M. Trendov, "Index of circular agriculture development in the republic of Macedonia," *Visegrad Journal on Bioeconomy and Sustainable Development*, vol. 6, no. 1, pp. 35–38, 2017.

[4] M. Carus and L. Dammer, "The circular bioeconomy-concepts, opportunities and limitations," *Industrial Biotechnology*, vol. 14, no. 2, pp. 83–91, 2018.

[5] N. Gontard, U. Sonesson, M. Birkved et al., "A research challenge vision regarding management of agricultural waste in a circular bio-based economy," *Critical Reviews in Environmental Science and Technology*, vol. 48, no. 6, pp. 614–654, 2018.

[6] W. Peng and A. Pivato, "Sustainable management of digestate from the organic fraction of municipal solid waste and food waste under the concepts of back to earth alternatives and circular economy," *Waste and biomass valorization*, vol. 10, no. 2, pp. 465–481, 2019.

[7] B. Garske, J. Stubenrauch, and F. Ekardt, "Sustainable phosphorus management in European agricultural and environmental law," *Review of European, Comparative & International Environmental Law*, vol. 29, no. 1, pp. 107–117, 2020.

[8] D. Fytili and A. Zabaniotou, "Circular economy synergistic opportunities of decentralized thermochemical systems for bioenergy and biochar production fueled with agro-industrial wastes with environmental sustainability and social acceptance: a review," *Current Sustainable/Renewable Energy Reports*, vol. 5, no. 2, pp. 150–155, 2018.

[9] M. Kouhizadeh, Q. Zhu, and J. Sarkis, "Blockchain and the circular economy: potential tensions and critical reflections from practice," *Production Planning & Control*, vol. 31, no. 11-12, pp. 950–966, 2020.

[10] K. R. Skene, "Circles, spirals, pyramids and cubes: why the circular economy cannot work," *Sustainability Science*, vol. 13, no. 2, pp. 479–492, 2018.

[11] S. R. Paramati, N. Apergis, and M. Ummalla, "Dynamics of renewable energy consumption and economic activities across the agriculture, industry, and service sectors: evidence in the perspective of sustainable development," *Environmental Science and Pollution Research*, vol. 25, no. 2, pp. 1375–1387, 2018.

[12] B. Aydoğan and G. Vardar, "Evaluating the role of renewable energy, economic growth and agriculture on CO_2 emission in E7 countries," *International Journal of Sustainable Energy*, vol. 39, no. 4, pp. 335–348, 2020.

[13] I. Mocanu, I. Grigorescu, B. Mitrică, and P. E. Ana, "Regional disparities related to socio-economic determinants of agriculture in the Romanian Plain," *Journal of Urban and Regional Analysis*, vol. 10, no. 1, pp. 79–99, 2018.

[14] A. C. Ruane, J. Antle, J. Elliott et al., "Biophysical and economic implications for agriculture of +1.5° and +2.0°C global warming using AgMIP Coordinated Global and Regional Assessments," *Climate Research*, vol. 76, no. 1, pp. 17–39, 2018.

[15] W. Khan and S. A. Ansari, "Does agriculture matter for economic growth of Uttar Pradesh (India)?" *Economy of Region*, vol. 14, no. 3, pp. 1029–1037, 2018.

[16] M. Paul, "Community-supported agriculture in the United States: social, ecological, and economic benefits to farming," *Journal of Agrarian Change*, vol. 19, no. 1, pp. 162–180, 2019.

[17] I. Pattnaik, K. Lahiri-Dutt, S. Lockie, and B. Pritchard, "The feminization of agriculture or the feminization of agrarian distress? Tracking the trajectory of women in agriculture in India," *Journal of the Asia Pacific Economy*, vol. 23, no. 1, pp. 138–155, 2018.

[18] G. Salmoral, D. Rey, A. Rudd, P. Margon, and I. Holman, "A probabilistic risk assessment of the national economic impacts of regulatory drought management on irrigated agriculture," *Earth's Future*, vol. 7, no. 2, pp. 178–196, 2019.

[19] B. Lanz, S. Dietz, and T. Swanson, "Global economic growth and agricultural land conversion under uncertain productivity improvements in agriculture," *American Journal of Agricultural Economics*, vol. 100, no. 2, pp. 545–569, 2018.

[20] J. Cai, J. Luo, S. Wang, and S. Yang, "Feature selection in machine learning: a new perspective," *Neurocomputing*, vol. 300, pp. 70–79, 2018.

[21] J. N. Goetz, A. Brenning, H. Petschko, and P. Leopold, "Evaluating machine learning and statistical prediction techniques for landslide susceptibility modeling," *Computers & Geosciences*, vol. 81, pp. 1–11, 2015.

Hindawi
Mobile Information Systems
Volume 2022, Article ID 9672693, 9 pages
https://doi.org/10.1155/2022/9672693

Research Article

International Law Protection of Cross-Border Transmission of Personal Information Based on Cloud Computing and Big Data

Xu Ziyi

Hebei University of Economics and Business, 050000 Shijiazhuang, China

Correspondence should be addressed to Xu Ziyi; 20150810238@m.scnu.edu.cn

Received 25 May 2022; Revised 16 June 2022; Accepted 21 June 2022; Published 18 August 2022

Academic Editor: Chi Lin

Cross-border data flow brings new growth and opportunities for the development of digital economy, but disordered cross-border data flow may damage national security, public interests, enterprise interests, and data sovereignty. At present, the unified rules for global regulation of cross-border data flow have not yet been formed. The existing rules are mainly led by developed countries like Europe and the United States. There is huge room for improvement in the international legal protection of cross-border transmission of personal information. This paper introduces the privacy protection mechanism of personal information data under the digital trade environment in China, that is, the privacy protection framework under the background of big data, cloud computing, and the cloud service selection method of data life cycle privacy protection. At the same time, we combined with many problems existing in the cross-border transmission of personal privacy information in China and compared with foreign advanced experience, and this paper puts forward China's response path to clarify the obligations of data controllers and exporters, improve the responsibilities of regulators, improve the legislation of cross-border data flow, and improve the operability of the law; we vigorously carry out international cooperation and actively participate in the formulation of international rules, so as to further protect the rights and interests of personal privacy information protection.

1. Introduction

In today's society, with the rapid development of informatization, especially with the support of cloud computing, big data, Internet of Things and other technologies, the era of informatization and big data not only brings convenience to people's life but also increases the concentration of social data. At present, the collection, storage, processing, and application of personal information have reached an unprecedented level. With the in-depth development and continuous development of cross-border e-commerce and other businesses, and with the more and more extensive collection and processing of personal information, the risks are also higher and higher. For relevant enterprises, how to make natural persons clearly understand the scope of information collection, the location of information storage, and the purpose of information analysis is a very important notification. On the other hand, if the relevant enterprises that control and stand as personal information cannot fully and clearly understand the personal information protection laws, and do not know which information collection or information processing should be clearly authorized by the data subject, it will even produce greater compliance risks. We should pay more attention to the process of data protection in different jurisdictions, especially in the process of cross-border data transmission. Some developed countries have started the legal practice of cross-border data flow, typical examples are the chapter on digital trade in the United States–Mexico-Canada agreement (USMCA) led by the United States, and the EU-U.S. privacy shield agreement reached between the United States and the European Union, and the EU general data protection regulation (GDPR). The rules on cross-border data flow in these three specifications provide an institutional model for cross-border data sharing. China should learn from these mature international mechanisms on the control of cross-border data flow and combine with its own data protection practice, from the establishment of data classification and review system,

strengthening the construction of technical security, improving the rights and responsibilities of data subjects, strengthening international cooperation and other dimensions, build a legal supervision mechanism for the collection, and release of coordinated cross-border data flow, so as to achieve the incentive compatibility between data exit governance and economic growth needs [1].

2. Literature Review

No matter how personal information is stored, and its most important function is to identify the identity of natural persons and reflect the activities, behaviors, and preferences [2]. Moreover, due to the development of big data and cloud computing technology, the fragmented information can also identify the identity of a specific natural person and reflect the activities of the natural person after integration, analysis, and processing. Therefore, some scholars believe that in the context of international law, the so-called "personal information" refers to the information that can identify or have identified the identity of a natural person alone or in combination with other information, or the information that reflects the customary preferences, identity, and status of a specific natural person [3]. In the process of research, the author found that "personal information" and "personal data" are mixed or defined together in bilateral and multilateral international treaties and other normative documents. However, whether personal information or personal data, its connotation emphasizes the identification of identity and the mapping of personal characteristics, habits, and preferences [4].

Domestic research on the international law of personal information protection mostly focuses on specific legal rules, while foreign research mostly starts from regional documents and only studies the role of relevant documents in the protection of personal information in this region, but there are relatively few papers on the international legal rules as a whole. Moreover, the basic principles of international legal protection of personal information are rarely mentioned in the existing research, and the research on the rights of data subjects mostly focuses on the historical evolution, and the research on the cooperation and connection of the rights of data subjects is not clear enough [5]. This paper intends to study the international legal rules of personal information protection as a whole. Combining the privacy protection framework in the context of big data and cloud computing and the cloud service selection method model of privacy protection in the data life cycle, more intuitively finding the problems of international legal protection of personal information, we sort out the principles of international legal protection of personal information in different documents and summarize the basic principles of personal information protection; analyze the rights of data subjects and the obligations of data controllers and data processors, and put forward relevant improvement suggestions for the insufficient provisions; and study the international cooperation on personal information protection, clarify its cooperation mode, analyze the cooperation effect, and clarify that the cross-border flow of personal information should be promoted and guaranteed by signing bilateral or multilateral treaties [6].

3. Privacy Protection of Personal Information in My Country under the Digital Trade Landscape

With the advent of the era of big data, learning and analysis technology has become a new wave to solve international law problems. Through the data model framework, the process of information storage and cross-border transmission can be more intuitively understood, so as to find the existing legal problems. This part introduces the construction of data privacy protection framework and the cloud service selection method of privacy protection through the data life cycle, and understands data privacy security mechanism, which will affect the country's specific design and selection of international cooperation mechanism and international rules. China needs to think prospectively about the global rules of cross-border information flow, and become the creator of international rules.

3.1. Privacy Protection Framework. From the perspective of cloud service scenarios, this section constructs the research framework of data privacy protection in the cloud environment; attributes the data privacy security in the cloud environment to the three links of cloud service selection, access control, and trusted implementation of privacy policies; and tries to ensure the privacy security of users in these three links. This section mainly describes the application scenarios and assumptions of the proposed data privacy protection framework in the cloud environment. For the detailed application scenarios of the research contents of each part in this framework, please refer to the scene description of each chapter [7]. The cloud application scenario is shown in Figure 1.

As shown in Figure 1, in the above cloud application scenario, users can interact with cloud service providers indirectly or directly based on trusted third parties. Aiming at the above cloud application scenarios, this paper solves three problems: the choice of cloud services for data privacy protection, the protection of user data and identity attribute information, and the implementation of privacy policies. Due to their different emphases, they have different dependences on trusted third parties in this scenario. Therefore, this data privacy protection framework needs to be built at both ends of the trusted third party and the cloud service party. Its framework is shown in Figure 2.

As shown in Figure 2, in this framework, the left side is the deployment scheme of the cloud service selection method for data life cycle privacy protection proposed for the service selection problem for data privacy protection in this framework, and its components are deployed in a trusted third party. In the middle, it is the problem of protecting the privacy of user data, identity, and attributes [8].

3.2. Cloud Service Selection Method for Data Life cycle Privacy Protection

3.2.1. Scene Description. The cloud service selection scenario in this article is shown in Figure 3.

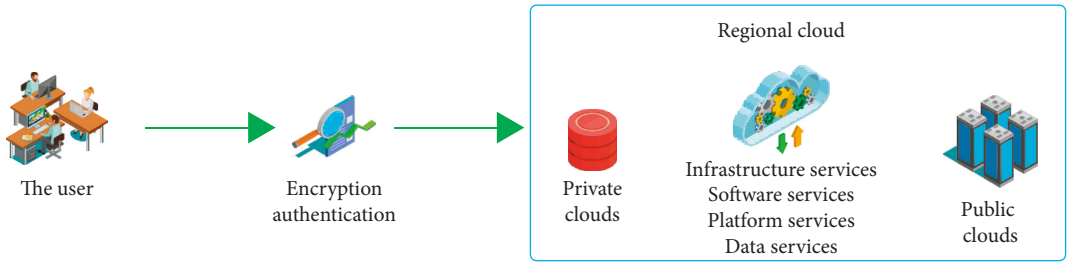

Figure 1: Schematic diagram of cloud application scenario.

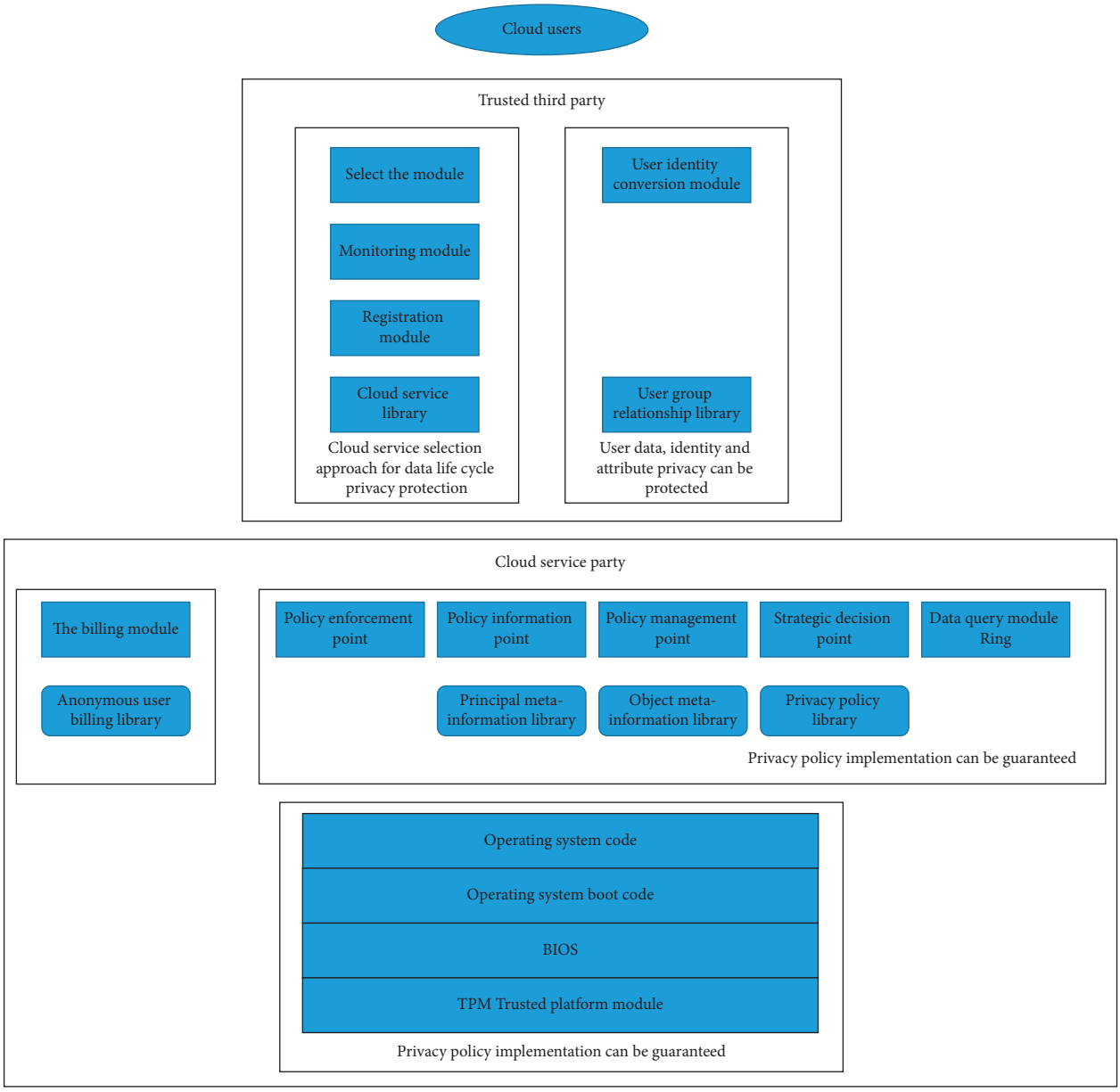

Figure 2: Data privacy protection framework in cloud computing environment.

As shown in Figure 3, in the cloud service selection application scenario based on a trusted third party, the user's selection of cloud service providers is completed by the trusted third party. This third party is responsible for supervising the status of cloud services. For example, TapInSystems, TechOut, and Hyperic can test the availability, response time, throughput, and other information of cloud services provided by Amazon. This paper studies such

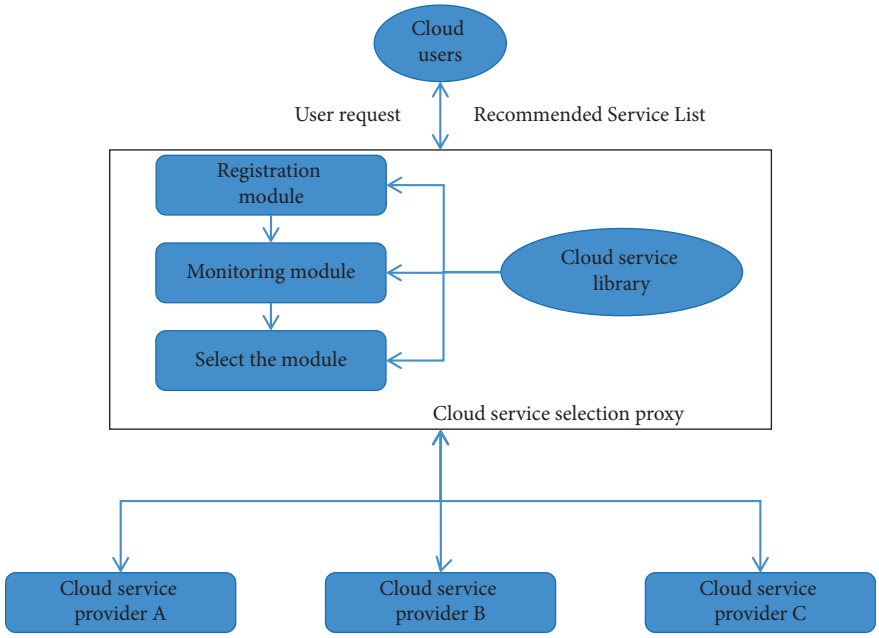

Figure 3: Cloud application scenario based on trusted third party.

third-party scenarios [9]. Specifically, in the above scenario, the trusted third party needs to regularly send performance query requests to each service and accept the performance parameters returned by each service to sort out and maintain a service library. After that, when the user submits the cloud service selection request, the trusted third party queries the service library according to the user's request and gives the cloud service recommendation list for the user to choose. For the above cloud application scenarios, this paper presents a cloud service selection method for data life cycle privacy protection [10]. This method extracts and quantifies the data privacy protection capability (CoPP) index of each target cloud service from the perspective of data life cycle in the cloud. On this basis, it calculates the data privacy protection capability (CoPP) and gives the cloud service recommendation list for data privacy protection.

3.2.2. Evaluation Index System. The cloud service selection evaluation index system, as the standard to measure and detect cloud services, mainly takes each stage of the data life cycle in the cloud environment as the index of data privacy protection capability (CoPP), including seven stages of data generation, transmission, storage, access, derivation, archiving, and destruction, as well as the data privacy security mechanism under each stage, as shown in Table 1.

Next, this paper analyzes the influencing factors of the privacy protection ability of the privacy security mechanism in each stage. Due to space reasons, we take each privacy security mechanism in the data generation stage as an example, including identity authentication, access control, and authorization mechanisms, which need to be analyzed and evaluated from the following aspects, as shown in Figure 4.

Identity authentication is an effective means to verify the identity of users, mainly in several ways in Figure 4. In cloud services, one or more ways are often used at the same time [10]. Generally speaking, it is generally believed that the security of the above authentication methods increases from top to bottom, and the security of multiple authentications is higher than that of single authentication [11]. Authorization mechanism is a method to grant permissions to reliable users. As shown in Figure 4, its security judgment mainly includes authorized environmental monitoring and judging whether it is authorized in real time. Among them, environmental monitoring includes supplier and client detection. At present, cloud computing providers generally use environmental monitoring to ensure the security of authorization in the authorization process. Access control is an important guarantee for users to safely operate cloud data and prevent privacy disclosure. Its principles and types are mainly shown in Figure 4. The integrated access control strategy integrates the technical advantages of a variety of mainstream access control and more effectively ensures the integrity and privacy of data. Therefore, the evaluation of access control should be comprehensively considered from two aspects: the satisfaction of principles and the security of policy types [12].

4. Current Situation and Deficiencies of Cross-Border Transmission and Protection of Personal Information in China under the Background of Digital Trade

4.1. Lack of Integration with the International Protection Model. The concepts of digital trade have been clearly defined, and cross-border transfer of personal information has also been clarified [13–15]. The protection and free flow of personal information must not be neglected. Secondly, it is necessary to protect the cross-border transmission of

Table 1: Evaluation index system of cloud service selection.

Evaluation index system	Life cycle data	Privacy security mechanism at all stages
Privacy protection capability (CoPP)	Data generation G	Access control protocol selection (P_1)
		Autonomous access control (P_2)
		Anonymous access control (P_3)
	Data transmission T	Digital certificate (P_4)
		Transmission encryption (P_5)
		Virtual machine isolation (P_6)
	Data storage S	Legal storage (P_7)
		Storage encryption (P_8)
	Data access Ac	Identity authentication (P_9)
		Trusted execution of access control policy (P_{10})
	Data derivation reuse R	Data derivation (P_{11})
		Safety measures (P_{12})
	Data archiving Ar	Track encryption (P_{13})
		Offsite storage (P_{14})
		Recovery mechanism (P_{15})
	Data destruction D	Disk replication (P_{16})
		Data destruction method (P_{17})

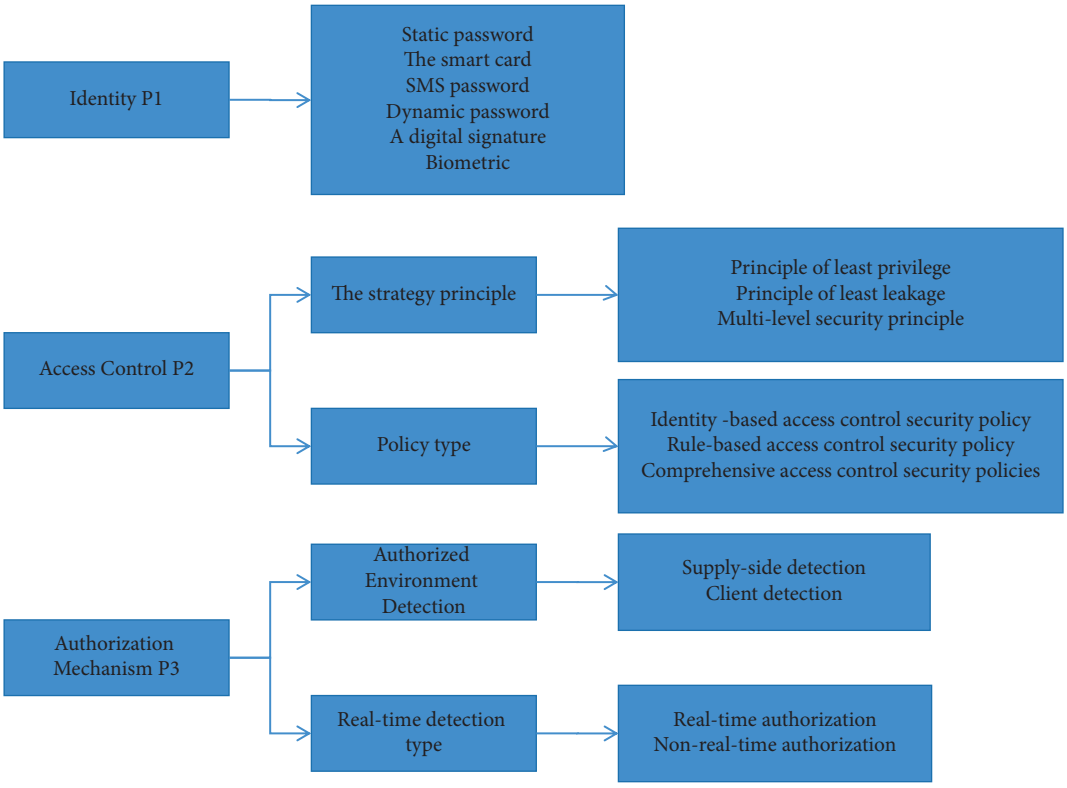

Figure 4: Evaluation of privacy security mechanisms in data generation stage.

personal information at the level of international law. On the one hand, digital trade, as an emerging economic momentum, is in the process of enhancing the vitality of the global economy. On the other hand, the frequent cross-border flow of personal information puts forward requirements for international law; secondly [16], it poses a threat to the security of personal information, and the necessity of international legal protection of personal information is evident [17, 18]. From the analysis of the international legal protection of cross-border transmission of personal information in digital trade from the three levels of bilateral norms, regional norms, and global norms, we can see that among the bilateral norms, the bilateral privacy agreement between Europe and the United States reflects a higher level of personal information protection [19]. In the regional norms, the relevant norms formulated by the EU and APEC give full play to their geographical advantages and form a joint force in the region to effectively regulate the cross-border transmission of information [20]; in the global norms, the personal information protection formulated by

the WTO and the UN Norms is the most representative, providing a framework and model for national legislation [19, 21]. There are many deficiencies in the existing international protection methods for personal information. The scope of application of bilateral agreements is too narrow, the process of negotiating and negotiating with different countries one by one is relatively complicated, and the existing bilateral protection methods are relatively simple as shown in Figure 5.

The cross-border transmission of personal information has been paid more and more attention; firstly, China's efforts in cross-border information protection cannot be ignored. In recent years, China has used the Boao Forum, the Asian infrastructure open bank, the BRICs countries, and the Belt and Road initiative to carry out regional cooperation or rule negotiation on cross-border information flow, so as to enhance China's voice in this field [21]. But compared with other digital trading countries in the world, China lacks cooperation in cross-border information protection, unable to integrate with the international protection model.

There are two reasons for the lack of international cooperation in personal information protection: firstly, in China, the regulation of cross-border data flow is distributed in various laws, regulations, and departmental rules, which are relatively scattered. In general, the existing regulations severely restrict the transfer of domestic data to overseas. China tries to avoid the possible national security risks and personal privacy risks of cross-border data through data localization and retention. But in an environment where cross-border data flows act as an economic engine, the protection measures may aggravate the information asymmetry phenomenon, thus affecting the competitiveness of our country, and there is a lack of confidence in international negotiations on personal information protection. Harsh cross-border data flow restrictions may make a market isolated or limited, it is difficult for the domestic-related enterprises to participate in the international competition, and consumers cannot enjoy the benefits of global scale, which bring negative impact to economic development [22]. Secondly, although China's digital trade has developed rapidly in recent years, it is still in the exploration and initial stage, and many digital enterprises are still in the stage of "going out." There is still a large gap compared with the level of personal information protection in developed countries; once China joins regional or international information protection organizations or platforms, digital enterprises are bound to be constrained in the protection of cross-border transmission of personal information, which will increase the operating costs of enterprises and is not conducive to China's digital enterprises to open the international market in a short time [20, 22].

4.2. Imperfect Legal Provisions on Personal Information Protection in China. The role of the development of big data in promoting global economic growth should not be underestimated. As one of the countries with the best development momentum of digital trade, China is still not in place in protecting the personal information transferred across borders, which is mainly manifested in the imperfect legal provisions. China has not formulated a special personal information protection law, the relevant legal norms and systems are not perfect, and the data commissioner system and information authentication system have not been established. The lack of personal information protection law makes it difficult to get relief when the interests of information subjects are infringed, and it is also unable to connect with the protection mode of other countries. China's special laws are under preparation, which also gives the public a shot in the arm. The special laws will be able to protect the legitimate information rights of individuals to a greater extent, and the contents on the protection of cross-border transmission of personal information will also be stipulated [23, 24]. The national security law also deals with the cross-border flow of personal information data; that is, important data should be stored locally and other data should be evaluated before cross-border transfer [25]. Firstly, important data are not clearly defined, and the scope of important data cannot be known; secondly, only before the cross-border transfer of data is determined, the supervision during and after the event is difficult to reflect, and the existing supervision system is difficult to implement in place. The essence of security assessment is to serve the exit of data. We should promote the cross-border flow of data on the premise of ensuring security. Only using security assessment as a supervision means in a single way may not meet the needs of real massive data transfer [26] as shown in Figure 6.

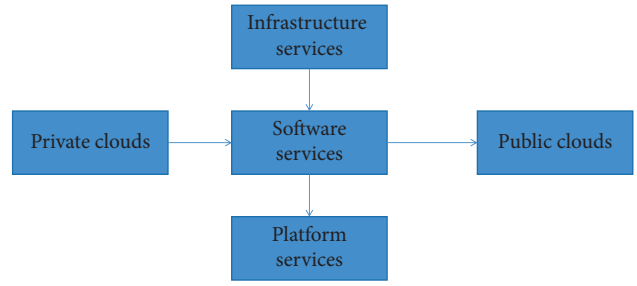

Figure 5: Cross-border transmission of human information.

5. Legal Protection Countermeasures for Cross-Border Transmission of Personal Information in China

5.1. Actively Participate in International Cooperation on the Protection of Cross-Border Transmission of Personal Information. In an era of connectivity, collaboration, openness, and sharing as themes, cooperation at the international level on cross-border data flow regulation is inevitable. Despite the active regulation of cross-border data flows by regions or countries such as the EU, on a global scale, unified international rules and treaty norms have not yet been formed. In this window period, China needs to make forward-thinking about the global rules of cross-border data flow, deploy research in advance, and strive to be

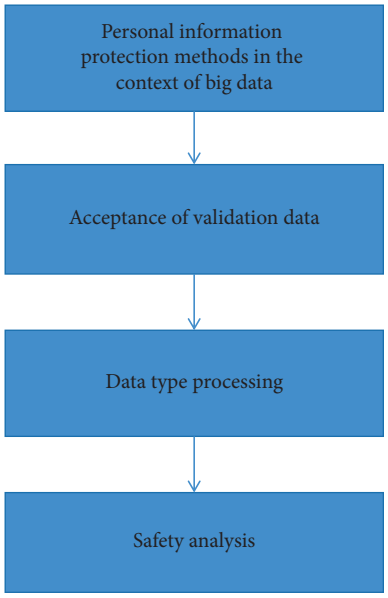

Figure 6: Big data protection law.

the builder of international rule making, rather than becoming a passive recipient of the rules.

Due to the need for the development of digital trade and expanding market influence, it is difficult to shake the leading position of Europe and the United States in rule making. In concrete practice, on the one hand, China should actively participate in the discussion on cross-border data flow rules on international platforms and issue China's voice on behalf of the interests of Chinese enterprises; on the other hand, regional negotiation platforms such as the Regional Comprehensive Economic Partnership (RCEP) and Free Trade Area of the Asia-Pacific (FTAAP) provide favorable conditions for China to actively participate in rule making, and promote the construction of regional rules for cross-border transmission of personal information with the help of regional comprehensive economic partnership [25]. As China's status in international affairs improves, China can make better use of changes such as the Boao Forum, the Asian Infrastructure, the Open Bank, and the BRICS Belt and Road strategy to carry out regional cooperation agreements or rule negotiations on cross-border data flow, so as to enhance China's voice in this field. In short, China's data power image through the negotiation of multilevel international rules or the construction rate that matches China's international status is not only the need to safeguard domestic interests but also a requirement for ensuring cross-border data flow, the healthy development, and sustainable development of international cooperation.

In addition, compared with China, developed countries have higher requirements on domestic personal information protection standards and information transfer conditions. Therefore, China should also strengthen cooperation with trading partners in mutual legal assistance and information law enforcement, keep up with the high standards of personal information protection, and share personal information governance experience. We need to keep close contact with international professional privacy protection organizations, learn advanced experience, reflect China's determination and confidence in personal information governance, enhance China's influence and voice in the field of personal information protection, and win opportunities for China's digital enterprises to enter overseas markets.

5.2. Effectively Learn from International Experience in Cross-Border Protection and Governance of Personal Information. As the two digital trade giants, the EU and the United States have different legal paths for personal information protection, and there are obvious differences in the protection modes between the two countries, which are closely related to the long-standing values and tradition of the rule of law. Many scholars believe that the United States does not pay attention to the protection of personal information, and personal privacy is vulnerable to infringement. The EU's general data protection regulations are too strict and complicated, which is not conducive to the development of digital trade. It is considered that privacy protection and trade need not be combined. In short, it is difficult to strike a balance between the development of big data and personal information protection. Economies are also exploring the path of both. The EU and the United States are also facing challenges and urgently need to find better solutions. Latecomers should also seek the development of personal information protection from the experience and training of Europe and the United States. As the saying goes, China should learn from others' strong points, draw on their essence, and learn from the beneficial experience of European and American information protection models to serve the improvement of China's rules. Both European and American models have advantages and common laws to follow. In order to achieve the expected protection results, we must follow the way of incentive compatibility. If they are incompatible, it is difficult to implement, and we cannot ignore one and lose the other. Otherwise, it will hinder economic development and personal information protection [26].

Therefore, it is necessary to analyze the advantages and disadvantages of each personal information protection mode and whether the system design of personal information governance is scientific. To improve the degree of personal information protection in China, on the basis of summarizing the experience and lessons of personal information governance in developed countries, we should draw useful experience from the two models, not only see the differences between the two but also summarize the common laws. The EU's cross-border protection model of personal information is characterized by a strict legal system, including the setting of personal information supervision institutions and data protection commissioners. It is worth learning from China's specific practice of personal information protection to review the cross-border transmission of personal information before, during, and after the event, and clarify the main responsibilities of all parties. China is a civil law country. It is a good choice to learn from the advanced experience of the EU in the formulation of legal norms. Secondly, the personal information protection system of the United States

combines departmental decentralized legislation with industry self-discipline system, although the effect of departmental decentralized legislation is far less than that of formulating a unified personal information protection law. However, the relatively perfect industry self-discipline system in the United States is still worthy of reference in the practice of personal information protection in China. The industry norms are more flexible. The formulation of self-discipline norms in line with the industry development characteristics and economic development trend in various industries and assisting the government in relevant law enforcement work will be an important direction of personal information protection in the future.

5.3. Vigorously Improve the Laws and Regulations on the Protection of Cross-Border Transmission of Personal Information. In terms of cross-border flow of personal information, China should apply the hierarchical and classified management systems of different cross-border flow management mechanisms to the personal information and important data, general personal information, and business data of network operators, and establish an international data flow circle in line with its own security standards and the needs of industrial interests on this basis. Specifically, first is dual supervision of local data storage and cross-border data flow. China can encourage localized data storage and processing for the reasons of promoting data aggregation and protecting national security. For the flow of cross-border data, China can set a regulatory threshold. For the normal cross-border flow of data, there are no obstacles, but only the cross-border flow of data reaches the corresponding threshold [27].

Second is dual track supervision of personal information and important data. Personal information is essentially different from important data. Personal information mainly protects the private rights of data subjects, while important data focus on the protection of national interests and national security. Due to the significant differences between personal information and important data in regulatory objectives, scope of application, and evaluation procedure indicators, China can formulate regulatory norms applicable to personal information and important data, respectively. The cross-border flow of personal information can be solved based on civil means such as evaluation, agreement, express consent, and certification, while the cross-border flow of important data should mainly rely on administrative supervision [28].

Third, the legal reasons for the cross-border flow of personal information are diversified. Looking at the legitimacy of the cross-border flow of personal information all over the world, it roughly includes the adequacy identification of the information receiving country, the adoption of adequate safeguard measures, authentication mechanism, and interstate peer-to-peer agreement. China can learn from the content above and add legal reasons such as authentication mechanism and adequacy safeguard measures to make the flow of personal information more convenient [29].

6. Conclusion

Digital trade with the Internet as the carrier has greatly promoted the growth of the global economy. At present, Internet users have exceeded 3/4 of the global population. At the same time, it is also accompanied by the transnational transfer of massive information. How to coordinate the contradiction between cross-border transmission of personal information and personal information protection has become an urgent practical problem to be solved. Firstly, there are huge differences in the level of digital technology between countries, and digital trade protectionism still exists; secondly, digital trade lacks a universal global rule system and exists fragmentation of digital trade rules; finally, China lacks perfect legislation on cross-border data flow and cannot integrate with the protection mode of other countries.

To solve these problems, firstly, each country's norms in the field of personal information protection are not similar, which leads to huge differences in national legal norms. If a country imposes domestic norms on its international dealings with other countries, it is bound to cause conflicts. It is the general consensus of the international community to oppose the implementation of hegemonism and protectionism, so it is necessary in the process of cross-border information transfer countries should carry out cooperation and consultation on this issue, which can effectively reduce the occurrence of conflicts. Whether within the European Union or between the European Union and the United States, data cross-border flow has been realized under a certain legal framework or relevant norms, which provides a reference for China to realize the protection of data cross-border flow. At the same time, China should actively participate in the discussion of cross-border data flow rules on international platforms and make a Chinese voice on behalf of the interests of Chinese enterprises. We learn from RCEP, FTAAP, and other regional negotiations to seek to establish cross-border data flow rules in line with China's interests. This can enhance the trust of the international market in Chinese enterprises, strive for opportunities for enterprises to participate in global competition, cultivate industry self-discipline in this process, and promote the improvement of China's data protection level and the sustainable development of related industries [30].

Secondly, China's personal information protection legal system is gradually improving, but it is still a certain distance from the high level of personal information protection, and little attention is paid to the protection of cross-border transmission of personal information. As an important member of APEC and a new force in the development of global digital trade, China should actively participate in the formulation of international rules for cross-border information transmission, draw on the strengths of others, absorb useful foreign experience, actively connect with international rules, accelerate the process of digital trade globalization, improve China's information protection level, and play a more important role in the process of digital trade globalization.

Data Availability

The data used to support the findings of this study are included within the article.

Conflicts of Interest

The author declares that there are no conflicts of interest.

References

[1] Q. Ma, "Li Xiaonan on the construction of supervision rules for cross-border data flow in China," *Research on the rule of law*, vol. 1, pp. 91–101, 2021.

[2] D. Guo, *Open the Rudder Research on Legal Regulation of Cross-Border Data Flow*, University of international business and economics, Beijing, China, 2018.

[3] M. Xiaying, "Legal attribute of data and its civil law positioning," *Chinese Social Sciences*, vol. 40, no. 9, pp. 164–183+209, 2016.

[4] M. Ferracane, "Restrictions on Cross-Border data flows: a taxonomy," *ECIPE Working Paper No. 1/2017*, 2017.

[5] S. A. Aaronson, "Data is different, and that's why the world needs a new approach to governing cross-border data flows," *Digital Policy, Regulation and Governance*, vol. 3, 2019.

[6] R. Pepper, J. Garrity, and C. LaSalle, "Cross-border data flows, digital innovation, and economic growth," *Global Inf. Technol. Rep*, vol. 2016, pp. 39–47, 2016.

[7] D. W. Trabay, I. El-Henawy, and W. Gharibi, "A trust framework utilization in cloud computing environment based on multi-criteria decision-making methods," *The Computer Journal*, vol. 65, no. 4, pp. 997–1005, 2021.

[8] "Zhang Jing Systematic literature review of data sovereignty research in China," *Journal of Intelligence*, vol. 41, no. 04, pp. 128–134, 2022.

[9] Q. Abbas and A. Alsheddy, "Driver fatigue detection systems using multi-sensors, smartphone, and cloud-based computing platforms: a comparative analysis," *Sensors*, vol. 21, no. 1, p. 56, 2020.

[10] J. Gong and N. J. Navimipour, "An in-depth and systematic literature review on the blockchain-based approaches for cloud computing," *Cluster Computing*, vol. 25, no. 1, pp. 383–400, 2021.

[11] R. Gopi, S. T. Suganthi, R. Rajadevi, P. Johnpaul, N. Bacanin, and S. Kannimuthu, "An enhanced green cloud based queue management (gcqm) system to optimize energy consumption in mobile edge computing," *Wireless Personal Communications*, vol. 117, no. 4, pp. 3397–3419, 2021.

[12] Z. Jin, "Retracted article: green city economic efficiency based on cloud computing and machine learning," *Arabian Journal of Geosciences*, vol. 14, no. 11, p. 1007, 2021.

[13] W. Wu and A. Plakhtii, "E-learning based on cloud computing," *International Journal of Emerging Technologies in Learning (iJET)*, vol. 16, no. 10, p. 4, 2021.

[14] C. H. Tran, T. K. Bui, and T. V. Pham, "Virtual machine migration policy for multi-tier application in cloud computing based on q-learning algorithm," *Computing*, vol. 104, no. 6, pp. 1285–1306, 2022.

[15] T. Liu, "Retracted article: urban ecological environment investigation based on a cloud computing platform and optimization of computer neural network algorithm," *Arabian Journal of Geosciences*, vol. 14, no. 15, p. 1536, 2021.

[16] T. Lin, Y. Zhao, H. Zhang, G. Li, and J. Zhang, "Research on information security system of ship platform based on cloud computing," *Journal of Physics: Conference Series*, vol. 1802, no. 4, Article ID 042032, 2021.

[17] F. Liu, "Era of big data is based on the study of physical education teaching mode in mooc," *Journal of Physics: Conference Series*, vol. 1744, no. 3, Article ID 032008, 2021.

[18] D. Yu and Z. Li, "Study on users' travel behavior of urban car sharing system based on spatio-temporal big data in chengdu," *Journal of Physics: Conference Series*, vol. 1910, no. 1, Article ID 012046, 2021.

[19] "Dai long on the protection of personal privacy under the background of digital trade," *Contemporary law*, vol. 34, no. 1, pp. 148–160, 2020.

[20] "Li MoSi Game and cooperation of cross-border data flow rules between Europe," *America and Japan International trade*, vol. 2, pp. 82–88, 2021.

[21] Z. Huizhong, M. Fanrong, W. Gui, B. Mago, and T. Puyalnithi, "Research on the automation integration terminal of the education management platform based on big data analysis," *Advances in Data Science and Adaptive Analysis*, vol. 14, Article ID 01n02, 2022.

[22] F. Fang and L. Zhang, "Progress Dilemma and Enlightenment of EU personal data governance," *German Research*, vol. 36, no. 4, pp. 49–66+157, 2021.

[23] "Xu DuoQi International pattern of regulation of cross-border flow of personal data and China's response," *Law forum*, vol. 33, no. 3, pp. 130–137, 2018.

[24] Q. Zhao, "Information system construction and prediction model of leaving using big data mining and random forest," *Journal of Physics: Conference Series*, vol. 1982, no. 1, Article ID 012152, 2021.

[25] J. P. Meltzer, "The Internet, cross-border data flows and international trade," *Asia & the Pacific Policy Studies*, vol. 2, no. 1, pp. 90–102, 2015.

[26] Y. Chen, "Gao Yuning the strategic choice of digital trade opening -- Based on the comparative analysis of the United States, Europe, China and India," *International trade*, vol. 5, pp. 49–55, 2022.

[27] P. Sun and L. Gu, "Optimization of cross-border e-commerce logistics supervision system based on Internet of things technology," *Complexity*, vol. 2021, Article ID 4582838, 11 pages, 2021.

[28] C. Kuner, "Regulation of transborder data flows under data protection and privacy law: past, present, and future," *TILT Law & Technology Working Paper*, vol. 16, 2010.

[29] Ye Jingtian, "Administrative supervision of cross-border flow of personal data -- Analysis Based on the principle of proportion," *International business accounting*, vol. 9, pp. 79–83, 2022.

[30] P. Yue, "Digital trade governance and its regulation path," *Comparative study*, vol. 4, pp. 158–173, 2021.

Hindawi
Mobile Information Systems
Volume 2022, Article ID 1693365, 10 pages
https://doi.org/10.1155/2022/1693365

Research Article

The Application of Big Data Technology in the Construction of Financial Shared Service Center of Agricultural Enterprise Group

Chen Wang

School of Accounting, Shanxi Vocational University of Engineering Science and Technology, Taiyuan, Shanxi 030619, China

Correspondence should be addressed to Chen Wang; 2111602027@e.gzhu.edu.cn

Received 27 June 2022; Revised 15 July 2022; Accepted 30 July 2022; Published 17 August 2022

Academic Editor: Chi Lin

The prerequisite for the reasonable construction and successful implementation of the financial sharing center of the agricultural enterprise group is that the agricultural enterprise group must fully understand the financial sharing center, understand the steps and key points of its construction, and comprehensively design and re-engineer the business process. This paper combines the big data technology to construct the financial sharing center system of agricultural enterprise groups, combines the machine learning algorithm to improve the big data processing algorithm, and builds the intelligent financial sharing platform with the support of the improved algorithm, and builds the overall system architecture and operation process. After constructing the system, the performance verification and practical verification of this system are carried out through experimental research. From the research results, it can be seen that the system constructed in this paper has good data processing effects and data sharing effects, and has good security, which meets the financial sharing needs of agricultural enterprise groups.

1. Introduction

In recent years, the level of industrialization of the agricultural industry has been continuously improved, and there have been more and more large-scale agricultural material enterprises, which has provided a strong boost to the improvement of farmers' living standards and the modernization of the primary industry, and the social and economic level of rural areas has been continuously improved. The first is that my country's large-scale agricultural enterprises have greatly improved both in quantity and quality [1].

Since the reform and opening up, China's economy has developed rapidly, and many large enterprise groups have also been established. This organizational form of enterprise group is generally centered on a relatively powerful enterprise, and small enterprises whose main business is the operation and development of capital, production links, and key technologies related to the core enterprise are the peripheral layers. Then, each enterprise follows certain related systems and obeys the unified leadership of the core enterprise. This kind of tedious and huge organizational form prevents enterprise groups from being able to grasp the operation of the entire enterprise as quickly as small enterprises. Therefore, at this time, the internal audit department is particularly important as a supervision and control department. The work efficiency of the audit department directly affects the work efficiency of decision-makers [2]. In particular, in the past few years, many influential large-scale enterprise groups have been exposed to financial fraud scandals, which have caused huge losses to the society and economy, and are also not conducive to the development of their own enterprises. This makes major enterprise groups pay more attention to the financial operation risks of their enterprises, which further shows the importance of the internal audit department [3].

Since the beginning of the last century, science and technology have developed by leaps and bounds, and the business environment of enterprises is constantly changing. Only companies that efficiently handle the collection and application of financial data can remain invincible in the ever-changing development environment. However, for the large-scale enterprise organization form of enterprise group, the traditional financial processing method is no longer suitable for their development, and even will have an adverse

effect on the business development of the enterprise. Because, in the entire enterprise group, if each branch company processes its own financial data separately, it will easily lead to "information islands," and will lead to the duplication of financial work, increase the cost of financial work, and reduce the efficiency of financial work. What is more serious is that due to performance reasons, some branch companies sometimes exaggerate their operating performance, misrepresent their operating results, or even directly falsify financial data. This makes it difficult for the parent company to obtain accurate information in time and make wrong decisions. The enterprise caused huge losses. For this reason, many enterprise groups are trying to improve this situation. In this economic environment, the financial shared service center emerged as a new financial processing model. This financial processing mode applies unified procedures and specifications to centralize financial data to a semi-self-service data processing platform so that the standardization unifies financial data, while also reducing financial processing costs and improving work efficiency.

Financial crisis is the final transformation process of financial risk accumulation from small to large. Therefore, in the process of business development, the state of financial risks must be monitored in real time in order to avoid bankruptcy. Once problems with the state of financial risks are discovered, correct advance decisions can be made to prevent them in time. For financial risks, most companies take after-the-fact management measures after the financial risk has caused a financial crisis. The after-event measures are often not timely enough. Therefore, the financial risk early-warning system as a pre-predicted financial risk early-warning system is becoming more and more important. We can start from the combination of the company's past operating conditions and current status, and strive to make correct predictions before the occurrence of financial crises to prevent fatal risks.

This paper studies the application of big data technology in the construction of financial shared service centers of agricultural enterprise groups, improves the development efficiency of agricultural groups, builds intelligent data sharing centers, and promotes sustainable agricultural development.

2. Related Work

The study of financial risk early warning in foreign countries began in the 1930s, and the initial early warning model was the simplest univariate model. Through the efforts of many scholars and researchers, the research on financial risk early warning models has evolved from the simplest univariate model to a complex multivariate model, which has become more perfect and more realistic year after year. In terms of financial early warning models, the literature [4] established an unprecedented logistic regression early warning model to deal with the financial risks of high-risk industries. This model can accurately measure the risk area that high-risk enterprises are in, and make corresponding financial risk predictions based on specific risk areas. The literature [5] abandoned the traditional logistic regression early warning model when studying the financial industry, and established a brand new semiparametric single index model. The literature [6] believed that quantitative and qualitative methods should be used when facing financial risks of real estate enterprises and establishing financial early warning models. The two are indispensable, and new elements such as external financing capacity, EVA, cash flow, board size, and board of supervisors have been added to the traditional financial early warning model to form a brand new model. The literature [7] proposed a new type of multivariable early warning model. This kind of multivariable early warning model can make in-process analysis during the Lehman crisis or help postcrisis financial decision-making, and is of great benefit to the financial crisis of the entire country. The literature [8] established a logistic regression early warning model with higher accuracy than traditional models and verified the accuracy of the logistic regression early warning model by using nonfinancial efficiency indicators of data envelopment analysis. This analysis method is also completely new. In the face of the recently extremely active Internet financial industry, the literature [9] proposed that the financial early warning model should be combined with the big data system, and based on this, established a new financial early warning model for the Internet financial industry. The literature [10] proposed that a targeted financial early warning model should be established for the entire industry environment, and at the same time believed that the entire industry environment has a particularly profound impact on corporate financial risks in the market. The literature [11] studied the banking financial risk early warning system, established a number of logistic regression early warning models and binomial logistic regression early warning models, and compared the accuracy of the model predictions. Finally, it is compared that the multinomial logistic regression early warning model is better than the binomial logistic regression early warning model.

The literature [12] used genetic algorithm to analyze the financial risk early warning of the banking industry when establishing the financial early warning model, and after obtaining the final test prediction result, it is considered that this algorithm is feasible and reliable. The literature [13] combined artificial neural network (ANN) and multivariate linear analysis (MDA) technology to conduct financial early warning analysis of large enterprises. After research, it is found that more than 15% of the enterprises have various financial risks. The literature [14] established a financial early-warning model based on SOM and BP neural network to study the financial early-warning of listed enterprises. The literature [15] studied and proposed to establish an effective financial risk early warning model that can use various indicators other than financial indicators. The literature [16] successfully built a financial risk early warning system, which can achieve the expected early warning effect through 16 kinds of financial information. The literature [17] built a universal EWS financial risk early warning model for various enterprises in the economic market, and verified its reliability. The literature [18] proposed that in addition to ordinary financial information, other nonfinancial information should be paid attention to in the financial risk early

warning system. For example, nonfinancial information such as economic weakness can provide good help to the early warning results. The literature [19] found that the importance of cash flow is irreplaceable during the establishment of a financial risk early warning model. When studying the financial risk of underdeveloped countries to establish a model, the literature [20] found that adding time indicators greatly improves the accuracy of the early warning model. The literature [21] proposed that enterprises and institutions facing the financial industry do not necessarily have to use a multivariate early warning model, and believed that a univariate model can have a good early warning effect.

3. Improved Application of Big Data Technology in Financial Shared Service Center of Agricultural Enterprise Group

The current Dropout model sets a constant dropout rate for each hidden layer of the deep learning model, which is 0.5. In other words, each neuron of the deep learning model is randomly activated with a probability of 0.5. This method ignores the relationship between the dropout rate and the position of the hidden layer. A large number of studies have shown that the features of the underlying hidden layer have a higher effect on data feature learning and classification than the features of the upper hidden layer. Therefore, the number of activated neurons that need to be retained in the bottom layer should be more than the number of activated neurons retained in the upper hidden layer. To this end, this paper designs an adaptive distribution function that takes the position of the hidden layer as the independent variable, and takes the activation probability of the hidden layer neurons as the dependent variable. The activation probability of each hidden layer is set according to the position of the hidden layer. Through the above analysis, the adaptive distribution function decreases monotonically with the increase of the hidden layer position. In addition, Hinton's Dropout model shows that the activation probability of each layer of neurons should be about 0.5. At this time, it can ensure that enough activated neurons are retained, and at the same time, enough neurons can be discarded, which is conducive to the generalization of the deep calculation model. Finally, the value range of the Dropout rate of each layer needs to be in the (0, 1) interval.

Therefore, the adaptive distribution function designed in this paper is shown as follows:

$$\rho = f(l) = \begin{cases} 1 - \dfrac{1}{\sigma\sqrt{2\pi}} \displaystyle\int_{-\infty}^{l} \exp\left(-\dfrac{(l-n/2)^2}{2\sigma^2}\right) \mathrm{d}l & n = 2k\,(k \in N_+) \\ 1 - \dfrac{1}{\sigma\sqrt{2\pi}} \displaystyle\int_{-\infty}^{l} \exp\left(-\dfrac{(l-n+1/2)^2}{2\sigma^2}\right) \mathrm{d}l & n = 2k+1 \end{cases}. \tag{1}$$

Among them, ρ represents the dropout rate, l represents the position of the hidden layer, and n represents the number of layers of the depth calculation model. At the same time, σ indicates that the parameter is used to control the change range of the Dropout rate.

The adaptive function $\rho = f(l)$ satisfies the following three properties:

(1) Monotonically decreasing. That is, as the hidden layer rises, the probability of neurons being activated decreases.

(2) The activation probability of neurons in the middle hidden layer is 0.5.

(3) $\rho \in (0, 1)$. That is, the probability of each neuron being activated is between (0, 1). The proof is as follows:

(1) The derivative of function f() to l is shown as follows:

$$f(l) = \frac{\mathrm{d}\rho}{\mathrm{d}l} = \begin{cases} -\dfrac{1}{\sigma\sqrt{2\pi}} e^{-(l-n/2)^2/2\sigma^2} < 0 n = 2k\,(k \in N_+) \\ -\dfrac{1}{\sigma\sqrt{2\pi}} e^{-(l-n+1/2)^2/2\sigma^2} < 0 n = 2k+1 \end{cases}. \tag{2}$$

Because of $f'(l) < 0$, $\rho = f(l)$ is a monotonically decreasing function.

(2) When the number of hidden layers is even, that is, when $n = 2k\,(k \in N_+)$:

$$\rho = f\left(\frac{n}{2}\right) = 1 - \int_{-\infty}^{n/2} \frac{1}{\sigma\sqrt{2\pi}} \exp\left(-\frac{(l-n/2)^2}{2\sigma^2}\right) \mathrm{d}l = 0.5. \tag{3}$$

When the number of hidden layers is odd, that is, when $n = 2k + 1\,(k \in N_+)$:

$$\rho = f\left(\frac{n+1}{2}\right) = 1 - \int_{-\infty}^{n/2} \frac{1}{\sigma\sqrt{2\pi}} \exp\left(-\frac{(l-n+1/2)^2}{2\sigma^2}\right) \mathrm{d}l = 0.5. \tag{4}$$

Therefore, the activation probability of each neuron in the middle hidden layer is 0.5.

(3) Since $f()$ is a strictly decreasing function, formula (5) satisfies

$$f(n) < f(l) < f(1). \tag{5}$$

When the number of hidden layers is even, that is, when $n = 2k\,(k \in N_+)$:

$$\rho_{\max} = f(1) = 1 - \int_{-\infty}^{1} \frac{1}{\sigma\sqrt{2\pi}} \exp\left(-\frac{(l-n/2)^2}{2\sigma^2}\right) dl = 1 - \left(\lim_{x\longrightarrow-\infty}\left(\frac{1}{2} erf\left(\frac{\sqrt{2}\,(-2l+n)}{4\sigma}\right) - \frac{1}{2} erf\left(\frac{\sqrt{2}\,(-2+n)}{4\sigma}\right)\right)\right) < 1, \quad (6)$$

$$\rho_{\min} = f(n) = 1 - \int_{-\infty}^{n} \frac{1}{\sigma\sqrt{2\pi}} \exp\left(-\frac{(l-n/2)^2}{2\sigma^2}\right) dl = 1 - \left(\lim_{x\longrightarrow-\infty}\left(\frac{1}{2} erf\left(\frac{\sqrt{2}\,(-2l+n)}{4\sigma}\right) + \frac{1}{2} erf\left(\frac{\sqrt{2}\,(-2+n)}{4\sigma}\right)\right)\right) > 0. \quad (7)$$

When the number of hidden layers is odd, that is, when $n = 2k + 1\,(k \in N_+)$:

$$\rho_{\max} = f(1) = 1 - \int_{-\infty}^{1} \frac{1}{\sigma\sqrt{2\pi}} \exp\left(-\frac{(l-n+1/2)^2}{2\sigma^2}\right) dl = 1 - \left(\lim_{x\longrightarrow-\infty}\left(\frac{1}{2} erf\left(\frac{\sqrt{2}\,(-2l+n+1)}{4\sigma}\right) - \frac{1}{2} erf\left(\frac{\sqrt{2}\,(n-1)}{4\sigma}\right)\right)\right) < 1, \quad (8)$$

$$\rho_{\max} = f(n) = 1 - \int_{-\infty}^{n} \frac{1}{\sigma\sqrt{2\pi}} \exp\left(-\frac{(l-n+1/2)^2}{2\sigma^2}\right) dl = 1 - \left(\lim_{x\longrightarrow-\infty}\left(\frac{1}{2} erf\left(\frac{\sqrt{2}\,(-2l+n+1)}{4\sigma}\right) + \frac{1}{2} erf\left(\frac{\sqrt{2}\,(n-1)}{4\sigma}\right)\right)\right) > 0. \quad (9)$$

From formulas (6)–(9), we can see $df(l) \in (0,1), \forall l$. Therefore, the probability of each neuron being activated is between (0, 1).

Figures 1 and 2 show the image of the adaptive distribution function when $\sigma = 1$ and $\sigma = 10$.

When the adaptive distribution function is applied to the depth calculation model, a depth calculation model based on adaptive Dropout can be obtained. Figures 3 and 4 show the difference and connection between the basic depth calculation model and the depth calculation model based on adaptive Dropout.

Figure 3 shows a depth calculation model based on adaptive Dropout with three hidden layers and a total of 5 layers (input layer, hidden layer, and output layer). Among them, the activation probability of the neurons in the first hidden layer is 80% and the activation probability of neurons in the second and third layers is 50% and 40%, respectively.

We assume that L represents the total number of layers based on the adaptive Dropout depth calculation model, that is, the number of hidden layers is $L-2$. $l \in \{0, 1, \ldots, L-1\}$ is the index number of each layer. That is, $1 = \mathrm{O}$ indicates the input layer, and $l = 1$ indicates the first hidden layer. $l = L - 1$ represents the output layer. For the depth calculation model in which each layer is represented by an N-th order tensor, $z^{(l+1)}_{j_1 j_2 \cdots j_N}$ represents the input of the $j_1 j_2 \cdots j_N$-th neuron of the lth layer, and $y^{(l+1)}_{i_1 i_2 \cdots i_N}$ represents the output of the $i_1 i_2 \cdots i_N$-th neuron of the lth layer. At the same time, $y^{(0)} = x$ represents the input data and $y^{(L-1)}$ represents the output of the model. $W^{(l)}$ and $b^{(l)}$ represent the weight tensor and bias tensor of the lth layer. Then, the forward propagation process of the basic depth calculation model is shown in formulas (10) and (11):

$$z^{(l+1)}_{j_1 j_2 \cdots j_n} = W^{(l)}_{\alpha} \odot Y^{(l)} + b^{(l)}_{j_1 j_2 \cdots j_n} \left(\alpha = j_n + \sum_{i=1}^{N-1} (j_i - 1) \prod_{t=i+1}^{N} J_t\right), \quad (10)$$

$$y^{(l+1)}_{j_1 j_2 \cdots j_n} = f\left(z^{(l)}_{j_1 j_2 \cdots j_n}\right), \quad (11)$$

where $\odot$ represents the multipoint product of two tensors, $H \in R^{J_1 \times J_2 \times \cdots \times J_N}\,(J_1 \times J_2 \times \cdots \times J_N = \alpha)$ represents the result of the multipoint product of tensor $H \in R^{\alpha \times I_1 \times I_2 \times \cdots \times I_N}$ to g and tensor $A \in R^{I_1 \times I_2 \times \cdots \times I_N}$, that is, $H = W \odot A$. Each element in H is defined as follows:

$$h_{j_1 j_2 \cdots j_n} = W_{\beta} \cdot A\left(\beta = j_n + \sum_{i=1}^{N-1} (j_i - 1) \prod_{i=j+1}^{N} J_t\right). \quad (12)$$

Among them, f is the activation function. The depth calculation model based on adaptive Dropout proposed in this paper uses the Sigmoid function as the activation function of the neuron, that is $f(x) = 1/(1 + \exp(-x))$.

For the depth calculation model based on adaptive Dropout, the forward propagation process is as shown in formulas (13)–(16):

$$r^{(l)}_{i_i i_2 \cdots i_N} \sim \text{Bernoulli}\left(\rho^{(l)}\right), \quad (13)$$

$$\widetilde{y}^{(l)}_{i_i i_2 \cdots i_N} = r^{(l)}_{i_i i_2 \cdots i_N} \cdot y^{(l)}_{i_i i_2 \cdots i_N}, \quad (14)$$

$$z^{(l+1)}_{j_1 j_2 \cdots j_n} = W^{l}_{\alpha} \odot \widetilde{Y}^{(l)} + b^{(l+1)}_{j_1 j_2 \cdots j_n} \left(\alpha = j_n + \sum_{i=1}^{N} (j_i - 1) \prod_{i=j+1}^{N} J_t\right), \quad (15)$$

$$y^{(l+1)}_{j_1 j_2 \cdots j_n} = f\left(z^{(l+1)}_{j_1 j_2 \cdots j_n}\right). \quad (16)$$

Among them, $\rho^{(l)}$ represents the activation probability of each hidden layer neuron in the first layer, and $r^{(l)}_{i_i i_2 \cdots i_N}$ obeys the Bernoulli distribution and takes the value 1 according to the probability $\rho^{(l)}$. From the perspective of the depth calculation model based on adaptive Dropout, the activation probability of each hidden layer neuron is set through an adaptive function, and each training obtains a submodel of the basic depth calculation model. The adaptive Dropout

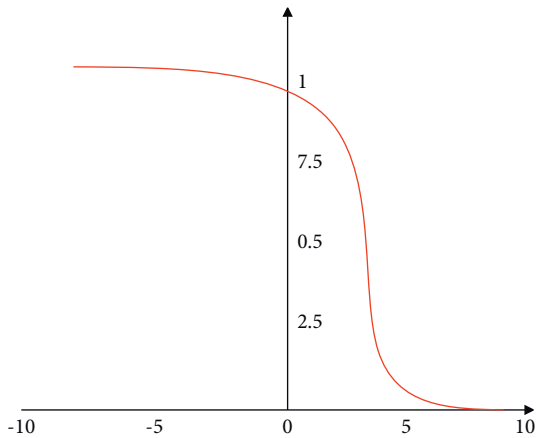

Figure 1: Adaptive distribution function with $\sigma = 1$.

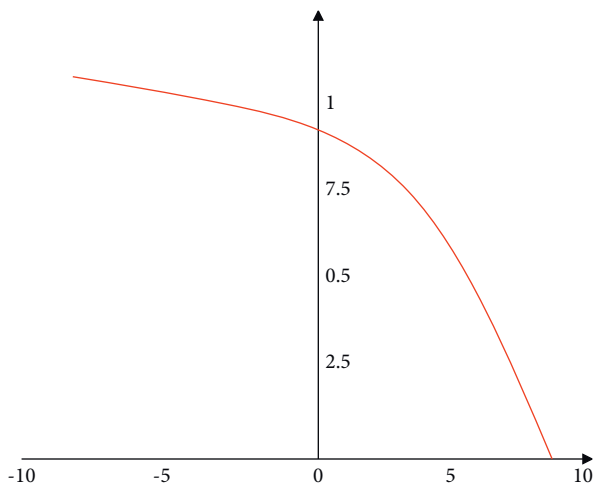

Figure 2: Adaptive distribution function with $\sigma = 10$.

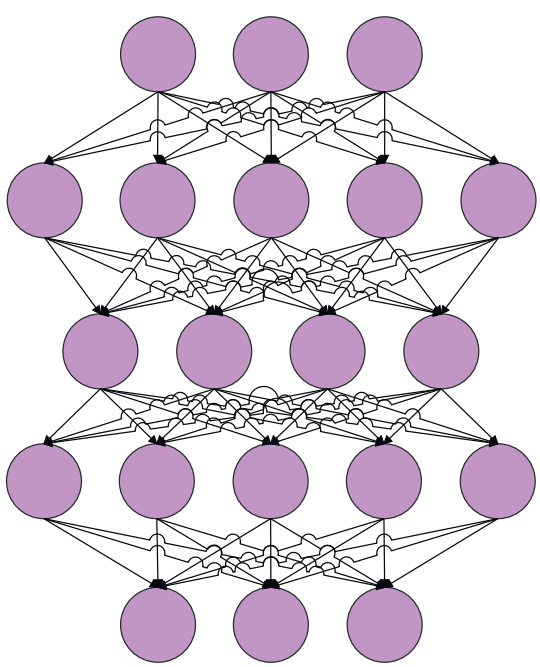

Figure 3: Basic deep computation model.

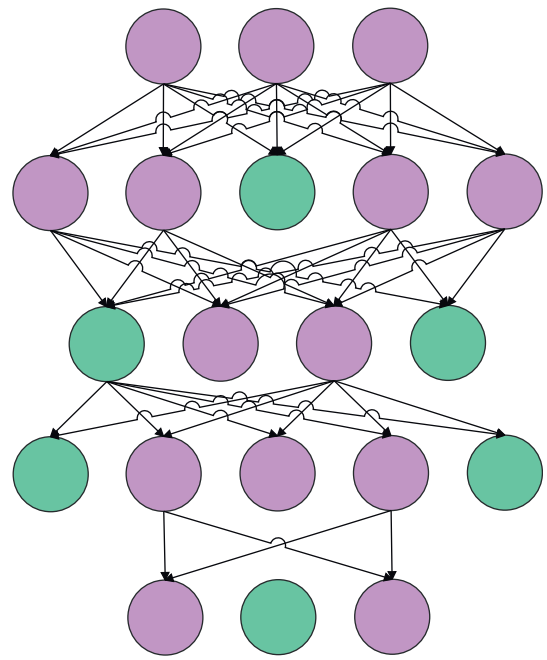

Figure 4: Adaptive dropout deep computation model.

model improves the generalization ability of the deep computing model by training multiple submodels that share weights.

The training process based on the adaptive Dropout depth calculation model is the same as the training process of the basic depth calculation model. In the pretraining process, it uses the principle of automatic coding to train the parameters of each hidden layer from the bottom up to obtain the initial parameters. In the fine-tuning process, it uses labeled supervision examples to fine tune the parameters from top to bottom.

It is assumed that there are m instances in the training dataset. Among them, x represents one of the instances. For the lth hidden layer (the second hidden layer in Figures 2 and 3 is taken as an example), the corresponding high-order automatic coding model of the basic depth model and the high-order automatic coding model based on the adaptive Dropout model are shown in Figures 5 and 6.

The reconstruction error function is shown as follows:

$$J_{TAE}(\theta;l)=\frac{1}{2}\left(h_{W,b}\left(\tilde{y}^{(l-1)}\right)-\tilde{y}^{(l-1)}\right)^{T}G\left(h_{W,b}\left(\tilde{y}^{(l-1)}\right)-\tilde{y}^{(l-1)}\right). \tag{17}$$

Among them, $\theta = \left\{W^{(l-1)}, b^{(l-1)}; W^{(l-1)\prime}, b^{(l-1)\prime}\right\}$ is a parameter, and $\tilde{y}^{(l-1)}$ is the expansion vector corresponding to the output tensor of the activated neuron in the 1-1th layer.

Similar to the basic depth calculation model, the depth calculation model based on adaptive Dropout uses gradient descent to update the parameters of the model. However, for each step of the training process of the depth calculation model based on adaptive Dropout, the forward propagation

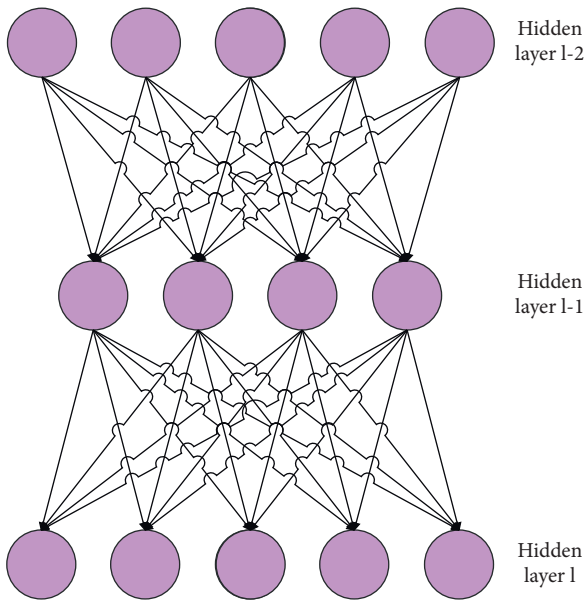

Figure 5: The lth hidden layer in basic deep computation model.

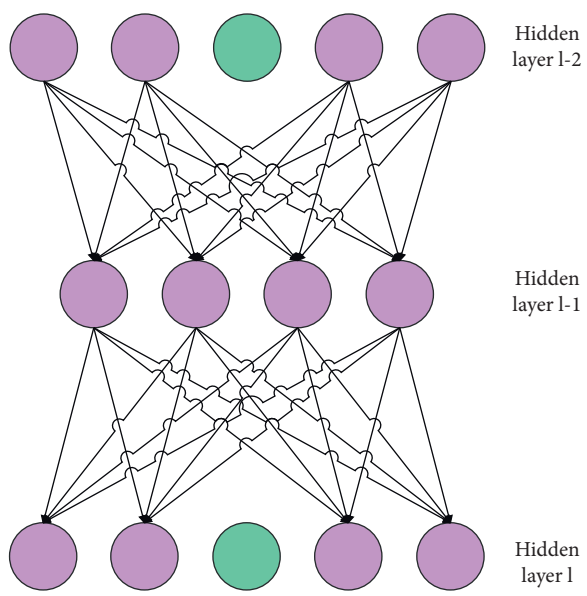

Figure 6: The lth hidden layer in adaptive dropout deep computation model.

and back propagation are trained on a submodel set by the adaptive distribution function. Therefore, when calculating the parameter gradient, only activated neurons are calculated.

It can be seen from the algorithm process that the main step of the algorithm is to calculate the partial derivative of the objective function with respect to the parameters. Therefore, the overall complexity of the algorithm is $O(M \times \prod_{t=1}^{N} I_t \times \prod_{s=1}^{N} J_s \times k)$. Among them, M represents the number of training samples, $\prod_{t=1}^{N} I_t$ and $\prod_{s=1}^{N} J_s$ represent the number of neurons in the input layer and hidden layer, respectively, and k represents the number of iterations.

4. Financial Shared Service Center of Agricultural Enterprise Group Based on Big Data Technology

The financial sharing center has a relatively obvious effect on improving the traditional financial control mode, can meet more needs of enterprise management, and is in line with the development trend of today's technological progress. The establishment of a financial sharing model has become a mainstream means for large enterprises to optimize financial control. However, people have some misunderstandings about building a financial sharing center. The most common misunderstandings are as follows. First, any enterprise can achieve data and process standardization by establishing a financial sharing center. Second, the establishment of a financial sharing center will effectively reduce the financial cost of the enterprise. Therefore, before constructing a financial sharing center, enterprises must clarify the types of enterprises and the scope of business they are applicable to. Moreover, enterprises need to rationally analyze whether they are applicable to the financial sharing model based on their own organizational structure, operating conditions, and business types.

The financial sharing center is a relatively centralized financial control model, which can correct the problems caused by the excessive decentralization of power of the group company. The headquarters of the group company have strong control and supervision powers over the core financial business, and arrange and allocat the economic resources within the group. For noncore financial businesses, member companies also have certain financial powers, but they need to strictly abide by unified standards and process guidelines in decision-making and implementation, and do not violate the overall strategic goals of the group. One of the types of enterprises that the financial sharing center is suitable for is a large cross-regional or multinational company. This type of enterprise has complex organizational structures, a wide geographical range of institutions, and large differences in policy, economic, and cultural backgrounds. There are certain difficulties in the process of implementing management and control. In large-scale trans-regional or multinational companies, each business unit independently conducts noncore and repetitive financial operations, which will cause a lot of redundancy in business departments and business personnel. Due to the geographical distribution of institutions, the parent company needs to implement remote management, which is less timely, difficult to play an effective role, and more difficult to manage. The differences in policies, economics, and humanities make it difficult for the overall policies and goals of the enterprise group to be effectively implemented. The business volume of manual adjustment is huge, and it is difficult to truly achieve unified management. The establishment of a financial sharing center can help this type of enterprise solve the above-mentioned problems and difficulties. Through the integration of noncore and repetitive financial services, cross-regional remote network management, financial data search, calculation, and switching

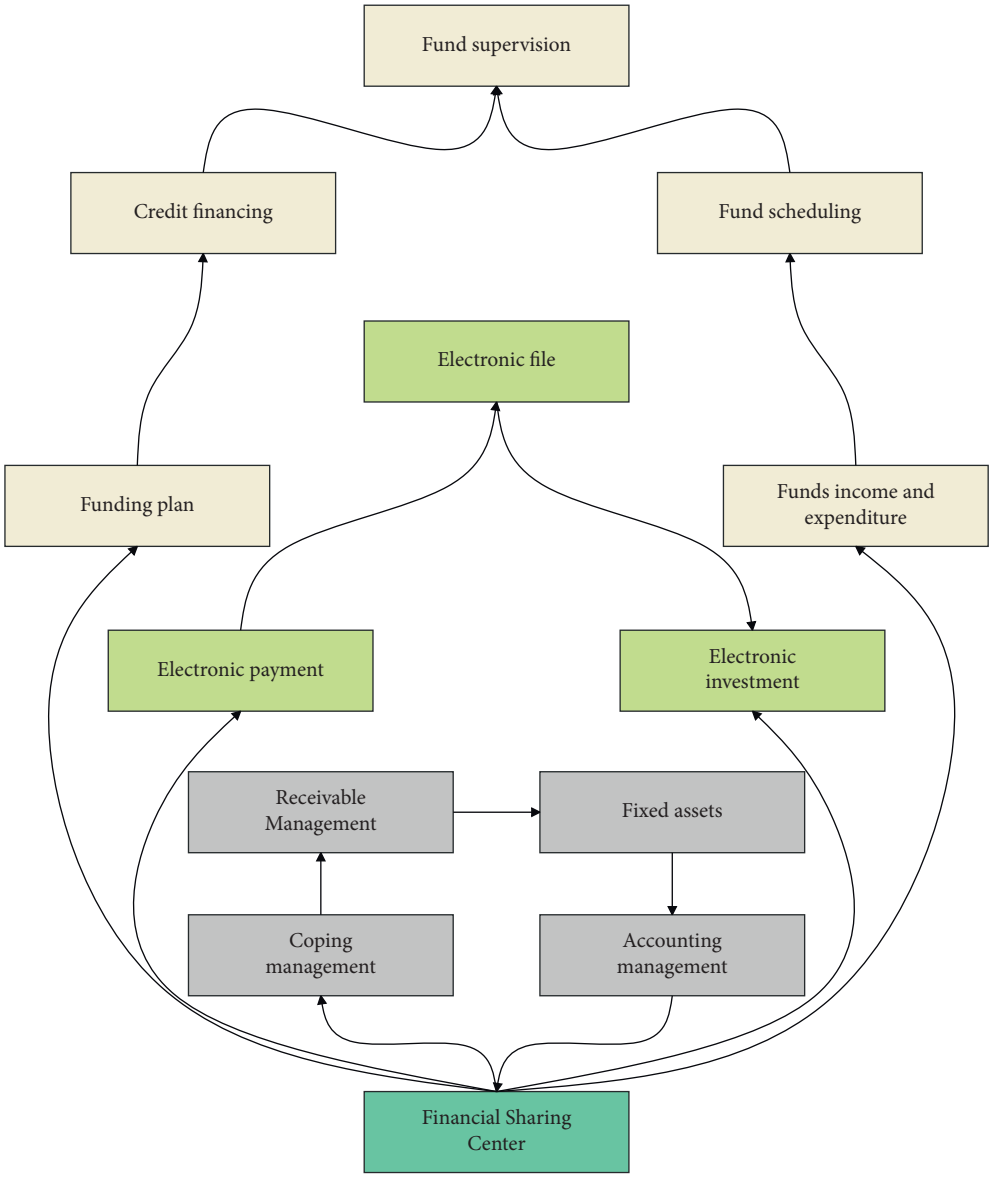

Figure 7: The functional scope of the financial sharing center of agricultural enterprise groups.

functions, it will help such enterprises to improve work efficiency, control management costs, and strengthen parent company supervision functions, ensure the implementation and implementation of group policies, and aslo ensure the quality of financial information and timely feedback. Another type of enterprise that the financial sharing center applies to is enterprise groups that frequently undergo mergers and acquisitions, reorganizations, and organizational changes. In the process of mergers, reorganizations, and organizational structure changes, such enterprises need to establish, merge, or cancel related business departments many times. Frequent changes make the management more difficult for enterprises, and they are prone to negligence and loopholes. The establishment of multiple complete functional department systems will lead to various cost increases. The staff expends a lot of energy on the handling of the basic financial business of various changes, which restricts the formulation and execution of business plans and goals. The establishment of the financial sharing center, through its integration function, eliminates the need to separately establish a complete financial system for them when new businesses or new institutions are established, which can reduce the management difficulty. The rapid transmission of information within the central system can also help companies promote the rapid integration of new businesses.

The specific functions of the financial sharing center can be divided into accounting center, reimbursement center, and settlement center. The business of the accounting function includes payable management, receivable management, fixed asset management, and accounting management. The business of the reporting function includes electronic payment, electronic reporting, and electronic files. The business of the settlement function includes fund planning, credit financing, fund monitoring, fund

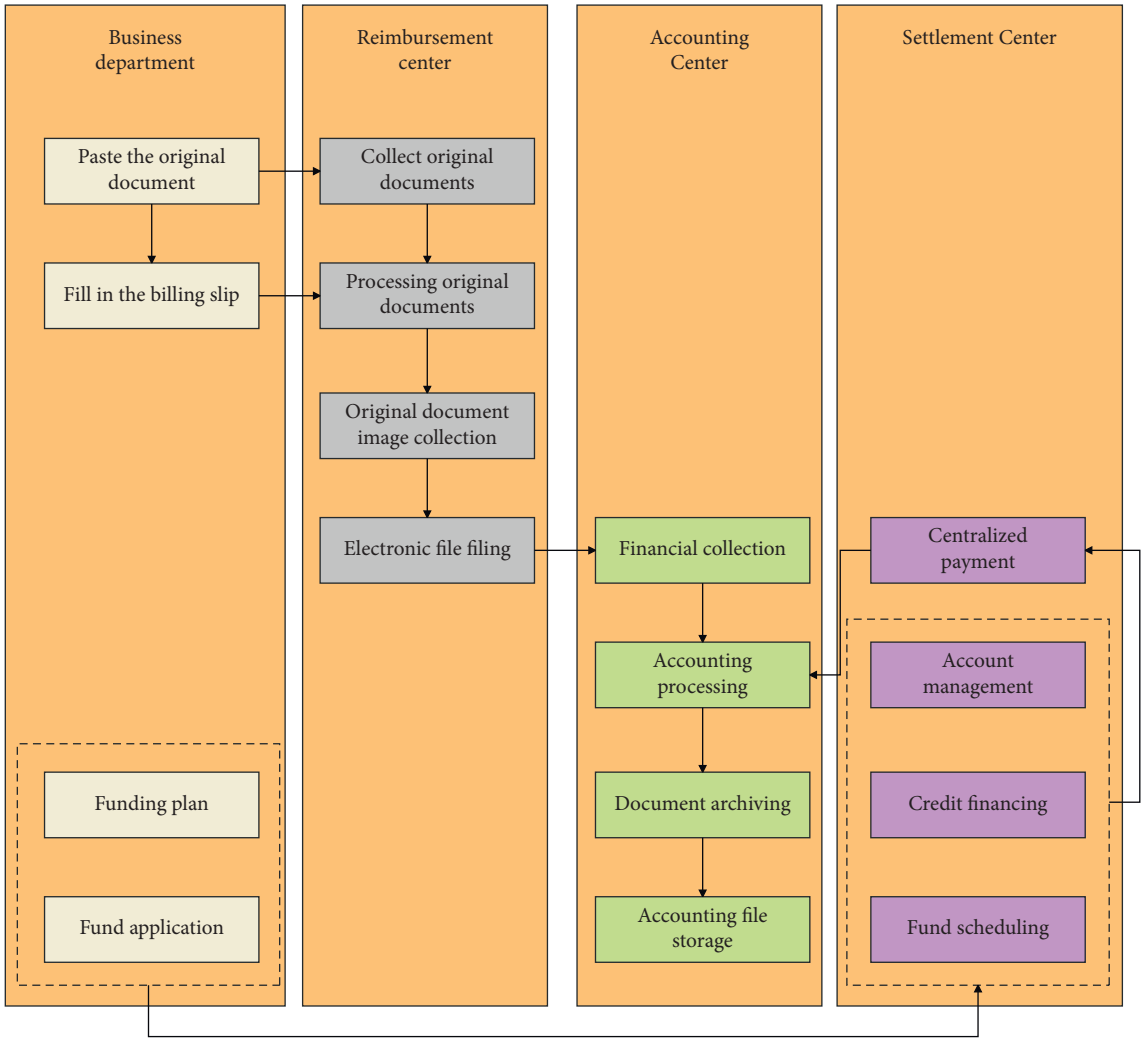

Figure 8: The overall business process of the financial sharing center of the agricultural enterprise group.

scheduling, and fund revenue and expenditure. Enterprises can gradually expand the scope of shared business based on the business they are concerned about, and finally form an integrated application of centralized accounting, centralized accounting, and centralized settlement, as shown in Figure 7.

The establishment of the process and system of the financial sharing center involves the internal financial process and related business processes, and they need to be unified planning and reasonable adjustments. In this link, companies need to rely on the ERP system to achieve. The process and system are composed of four parts: process specifications, job responsibilities, management methods, and assessment methods. Among them, the process specification mainly describes the main business process, operation process, and approval specification. Job responsibilities are to regulate the specific responsibilities and operational requirements of each position on the assembly line. The management method is to provide for the supporting systems for employee accounts, accounting file management, etc.; the assessment method is a method for evaluating and assessing the operation and effectiveness of the financial sharing center. The construction of the financial sharing center is essentially the optimization and re-engineering of business processes. The business processing flow of the financial sharing center covering a complete range of functions is shown in Figure 8. The three major functional centers complete the corresponding business processing according to their professional division of labor.

This paper constructs the above-mentioned agricultural enterprise group financial shared service center based on big data technology, and then verifies the performance of the system. First of all, this article evaluates the agricultural financial data processing and agricultural financial data storage of the system, and the results are shown in Table 1 and Figure 9.

From the above chart analysis, it is not difficult to conclude that the big data agricultural enterprise constructed in this article has good data processing and data storage effects according to the financial shared service system. After that, this article evaluates the financial sharing effect of the system and evaluates the data security, and the results shown in Table 2 and Figure 10 are obtained.

Table 1: Evaluation of agricultural financial data processing and storage of agricultural financial data.

Number	Data processing	Data storage
1	94.89	96.96
2	96.20	96.75
3	97.06	98.21
4	96.40	97.88
5	97.91	98.94
6	97.70	97.69
7	93.95	96.08
8	93.44	98.32
9	97.24	96.03
10	95.54	96.27

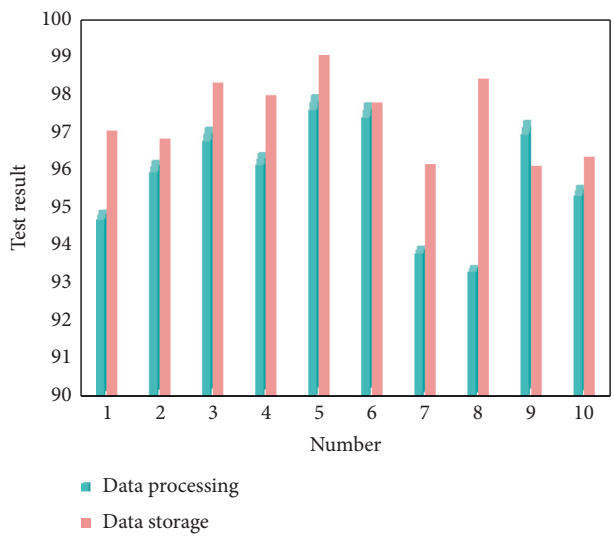

Figure 9: Histogram of evaluation of data processing and storage.

Table 2: Evaluation of the practical effect of the financial sharing system.

Number	Shared evaluation	System security
1	85.90	97.80
2	88.59	97.37
3	87.67	97.21
4	90.25	97.93
5	85.72	98.58
6	89.34	97.09
7	87.62	97.76
8	82.79	98.92
9	88.41	97.55
10	86.21	97.63

From the above test results, the financial shared service system of agricultural enterprise groups based on big data technology constructed in this paper has good performance and good practical effects.

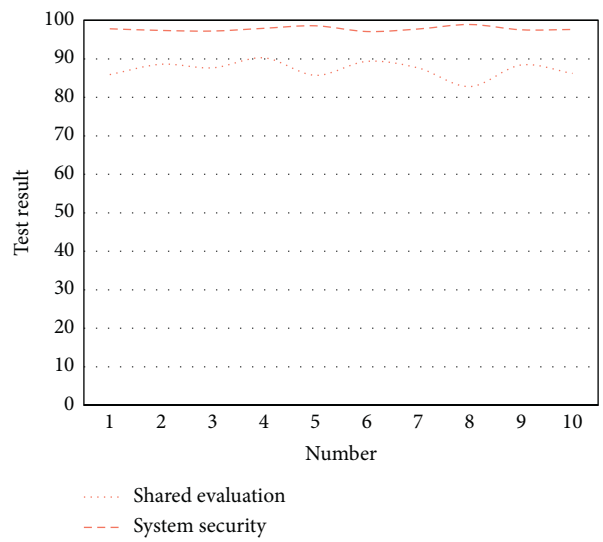

Figure 10: Histogram of the practical effect of the financial sharing system.

5. Conclusion

The advantage of the financial sharing model of agricultural enterprise groups is that it achieves the reduction of operating and management costs under the effect of scale, the improvement of financial management level and efficiency, and the improvement of the core competitiveness of enterprise groups. First of all, the establishment of the financial sharing center of the agricultural enterprise group enables the agricultural enterprise group to reduce the number of financial personnel and middle management of the agricultural enterprise group while the overall business volume remains unchanged, which improves the work efficiency of employees and reduces operation and management costs. Secondly, the agricultural enterprise group financial sharing center adopts a unified standard, which simplifies the steps and processes of business processing. The grasp of the financial data and indicators of the agricultural enterprise group ensures the control of each member company. Moreover, with the support of the ERP system, it not only ensures the transmission and accuracy of information but also avoids the omission of information, thereby improving the level and efficiency of the financial management of agricultural enterprise groups. Third, after the establishment of the financial sharing center, corporate managers can focus on higher-value core businesses, provide external customers with paid financial services, and create new economic growth points for the company.

Data Availability

The data used to support the findings of this study are included within the article.

Conflicts of Interest

The author declares that there are no conflicts of interest regarding this work.

References

[1] J. Hedlund, S. B. Longo, and R. York, "Agriculture, pesticide use, and economic development: a global examination (1990–2014)," *Rural Sociology*, vol. 85, no. 2, pp. 519–544, 2020.

[2] J. M. Antle and C. O. Stöckle, "Climate impacts on agriculture: insights from agronomic-economic analysis," *Review of Environmental Economics and Policy*, vol. 11, no. 2, pp. 299–318, 2017.

[3] S. R. Paramati, N. Apergis, and M. Ummalla, "Dynamics of renewable energy consumption and economic activities across the agriculture, industry, and service sectors: evidence in the perspective of sustainable development," *Environmental Science and Pollution Research*, vol. 25, no. 2, pp. 1375–1387, 2018.

[4] B. Aydoğan and G. Vardar, "Evaluating the role of renewable energy, economic growth and agriculture on CO_2 emission in E7 countries," *International Journal of Sustainable Energy*, vol. 39, no. 4, pp. 335–348, 2020.

[5] I. Mocanu, I. Grigorescu, and B. Mitrică, "Regional disparities related to socio-economic determinants of agriculture in the Romanian Plain," *Journal of Urban and Regional Analysis*, vol. 10, no. 1, pp. 79–99, 2018.

[6] A. C. Ruane, J. Antle, J. Elliott et al., "Biophysical and economic implications for agriculture of +1.5° and +2.0°C global warming using AgMIP Coordinated Global and Regional Assessments," *Climate Research*, vol. 76, no. 1, pp. 17–39, 2018.

[7] W. Khan and S. A. Ansari, "Does agriculture matter for economic growth of Uttar Pradesh (India)?" *Economy of Region*, vol. 14, no. 3, pp. 1029–1037, 2018.

[8] M. Paul, "Community-supported agriculture in the United States: social, ecological, and economic benefits to farming," *Journal of Agrarian Change*, vol. 19, no. 1, pp. 162–180, 2019.

[9] I. Pattnaik, K. Lahiri-Dutt, S. Lockie, and B. Pritchard, "The feminization of agriculture or the feminization of agrarian distress? Tracking the trajectory of women in agriculture in India," *Journal of the Asia Pacific Economy*, vol. 23, no. 1, pp. 138–155, 2018.

[10] G. Salmoral, D. Rey, A. Rudd, P. Margon, and I Holman, "A probabilistic risk assessment of the national economic impacts of regulatory drought management on irrigated agriculture," *Earth's Future*, vol. 7, no. 2, pp. 178–196, 2019.

[11] B. Lanz, S. Dietz, and T. Swanson, "Global economic growth and agricultural land conversion under uncertain productivity improvements in agriculture," *American Journal of Agricultural Economics*, vol. 100, no. 2, pp. 545–569, 2018.

[12] J. Cai, J. Luo, S. Wang, and S Yang, "Feature selection in machine learning: a new perspective," *Neurocomputing*, vol. 300, pp. 70–79, 2018.

[13] J. N. Goetz, A. Brenning, H. Petschko, and P Leopold, "Evaluating machine learning and statistical prediction techniques for landslide susceptibility modeling," *Computers & Geosciences*, vol. 81, pp. 1–11, 2015.

[14] H. Darabi, B. Choubin, O. Rahmati, A. Torabi Haghighi, B. Pradhan, and B Klove, "Urban flood risk mapping using the GARP and QUEST models: a comparative study of machine learning techniques," *Journal of Hydrology*, vol. 569, pp. 142–154, 2019.

[15] A. Rajkomar, J. Dean, and I. Kohane, "Machine learning in medicine," *New England Journal of Medicine*, vol. 380, no. 14, pp. 1347–1358, 2019.

[16] Y. Xin, L. Kong, Z. Liu et al., "Machine learning and deep learning methods for cybersecurity," *IEEE Access*, vol. 6, Article ID 35365, 2018.

[17] B. Meredig, A. Agrawal, S. Kirklin et al., "Combinatorial screening for new materials in unconstrained composition space with machine learning," *Physical Review B*, vol. 89, no. 9, Article ID 94104, 2014.

[18] L. Ward, A. Agrawal, A. Choudhary, and C. Wolverton, "A general-purpose machine learning framework for predicting properties of inorganic materials," *Npj Computational Materials*, vol. 2, no. 1, pp. 1–7, Article ID 16028, 2016.

[19] P. Feng, B. Wang, D. L. Liu, C. Waters, and Q Yu, "Incorporating machine learning with biophysical model can improve the evaluation of climate extremes impacts on wheat yield in south-eastern Australia," *Agricultural and Forest Meteorology*, vol. 275, pp. 100–113, 2019.

[20] K. Kourou, T. P. Exarchos, K. P. Exarchos, M. V. Karamouzis, and D. I. Fotiadis, "Machine learning applications in cancer prognosis and prediction," *Computational and Structural Biotechnology Journal*, vol. 13, pp. 8–17, 2015.

[21] S. Amershi, M. Cakmak, W. B. Knox, and T. Kulesza, "Power to the people: the role of humans in interactive machine learning," *AI Magazine*, vol. 35, no. 4, pp. 105–120, 2014.

Hindawi
Mobile Information Systems
Volume 2022, Article ID 7557015, 10 pages
https://doi.org/10.1155/2022/7557015

Research Article

Artificial Intelligence Application in the Design of Children's Service Robot Based on Context Perception

Jing Gao

Institute of Design, Hefei University, Hefei, Anhui 230601, China

Correspondence should be addressed to Jing Gao; 2201304@s.hlju.edu.cn

Received 23 June 2022; Revised 12 July 2022; Accepted 16 July 2022; Published 11 August 2022

Academic Editor: Chi Lin

In the era of artificial intelligence, children's service robots will surely become one of the conventional hardware. This paper combines artificial intelligence technology and the space algorithm to design the child service robot system, improves the situational space perception algorithm, and applies the algorithm to the robot system. Moreover, this paper constructs the system structure of the children's service robot according to the actual needs and obtains the system function modules. In addition, this paper constructs a child service robot based on context perception and verifies the performance of the robot system. Finally, this paper combines the simulation experiment to carry out the interactive effect of the robot system and the service effect to children and investigates the satisfaction of parents. Through experimental research, it can be seen that the child service robot system based on situational awareness constructed in this paper has good service effects, can effectively take care of children, and has high parent satisfaction.

1. Introduction

In recent years, with the development of artificial intelligence technologies such as big data, deep learning, cloud computing, sensors, and machine vision, more and more intelligent products endowed with AI technology have penetrated into various fields of life, and the intelligence of traditional products has become an inevitable trend [1]. The field of children's products is no exception. Traditional static children's products can no longer meet the complex, dynamic, and emotional scenes in life. Therefore, various technology companies and traditional manufacturers actively introduce new technologies and develop intelligent and emotional products that truly meet the needs of children [2]. As one of the important branches of the robotics field, the companion robot for children is favored by the parents of the post-80s and post-90s due to its own emotional, interactive, and intelligent advantages. The high pressure of life, the fast pace, and the less time to spend with children are the main pain points of parents nowadays. However, the emergence of child companion robots has alleviated this problem to some extent. Children's companion robots can provide children with enlightenment education and scene-based entertainment companions through technologies such as big data computing, deep learning, and sensor capture. Moreover, it can effectively strengthen the interaction between children and the outside world, which is conducive to early childhood physical and mental development [3].

In recent years, with economic development and changes in lifestyles, people have put forward higher requirements for the quality of life. On the one hand, as the pace of life accelerates and work pressure increases, people hope to be relieved from the complicated housework; on the other hand, the problem of aging population has become prominent, and the pressure on social pensions is increasing. In addition, the number of people with disabilities is gradually increasing, and the elderly and the disabled need more care. The development of service robots has brought new technical ideas to solve the above problems, and can play a huge role in improving people's quality of life. Therefore, there has been an upsurge in the development of service robots at home and abroad. As an inevitable extension of the modern information technology revolution, service robots will follow the path of smartphones and PCs,

with diversified application scenarios, fast updating, and very broad market prospects. After the realization of personal robots (PR) in the future, the global market capacity will exceed 3 billion units, and a service robot market of 100 billion US dollars can be born, that may reach to an unimaginable scale.

As a typical representative of service robots, escort robots are in a rapid development stage. People have higher and higher functional requirements for escort robots. However, traditional escort robots are designed to operate in a stand-alone mode, which has complex software and hardware systems, expensive construction, and difficult development and maintenance. Skill sharing has seriously hindered its promotion and application. In recent years, technologies such as cloud computing, big data, and virtualization have continuously made breakthroughs, which have promoted the informatization and modularization of the science and technology field, thus forming a new concept "cloud service", which has high resource utilization and data processing capabilities It has the advantages of strong, high fault tolerance, and low cost. It can coordinate management and scheduling of cloud resources, provide powerful computing capabilities, and provide users with on-demand services. It is widely used in aerospace, medical, financial, and education fields. Based on the intensive computing power of cloud computing, big data, and the analysis and processing capabilities of massive data, the escort robot body function is virtualized to the cloud, and the corresponding cloud service is constructed. While simplifying the software and hardware structure of the robot body, it also reduces the cost of the robot itself., and expand its function beyond the limitations of its physical body, thus realizing the real "good quality and low price." Therefore, the combination of escort robots and cloud technology is an inevitable trend in the development of service robots in the future.

This article combines intelligent technology to construct a children's service robot based on situational perception, combines intelligent space technology to improve the immersion that children's service robot brings to children, and combines experimental research to verify the performance of the system.

2. Related Work

The literature [4] has conducted sufficient research on home service robots in the intelligent era. Firstly, it conducted in-depth research from five aspects: the concept of service robot, the control mode of the product, the movement mode of the product, the functional attribute of the product, and the structural design. Then, it divided user research into three parts: children's physical characteristics, behavioral characteristics, and psychological characteristics. Finally, from the user's point of view, it took the principle of humanity and modularity as the guiding principles for the design of the child care robot. The literature [5] took children's robots as the research object, used perceptual engineering methods to study its modeling design elements, and established a quantitative model between perceptual images and children's robot modeling design elements. The literature [6] analyzed and studied children's behavioral characteristics and emotional characteristics, and proposed that the study of children's groups should pay special attention to the catharsis of negative emotions in children's emotions. Moreover, it illustrated the importance of emotional catharsis to the growth of children and focused the research on the problems of loneliness and negative emotions encountered in the process of children's growth. In addition, it took emotional design as a guiding principle and combined the existing theoretical basis of children's robot design to innovate its shape and function, which reduces the distance between the robot and the user. The literature [7] put forward the concept and the design method of remote parent-child interaction from the perspective of parent-child games based on user research, so that parents can remotely accompany and communicate with children and communicate emotionally. Child robots are an auxiliary tool for parents to accompany their children in education.

Literature [8] took the emotional design as the theoretical basis, analyzes, and compares the existing products on the market in terms of the design elements, and uses the three levels in the Norman emotional design to target the children's emotional needs. The innovative design of the product is divided into four levels: form, color, function, and action, and carries out innovative design of the product shape.

Literature [9] proposed the characteristics of children's products in the 020 mode and introduced the commercialized 020 mode into the design of children's interactive products. Literature [10] proposed to explain the app interaction strategy of early childhood education in the three parts of information architecture, information presentation, and information efficiency. Literature [11] proposed that children's interaction problems should be based on children's spiritual and behavioral needs to meet children's aesthetic requirements for interfaces. Literature [12] pointed out the importance of other sensory experiences in product interactions in addition to visual experience in the research on the interactive interface of children's products and proposed related research results on graphical and sound interactive interfaces.

Literature [13] proposed a brand-new interactive method that uses multiple thermal sensations in parent-child interaction design to achieve wearable remote interaction. Literature [14] established a user-centered interactive evaluation method for children's robots. Literature [15] proposed that using music interaction to communicate with children for emotional communication and parent-child interaction is superior to other methods.

Literature [16] proposed that when children are playing games with application software, they should actively help children understand the principles of freedom and flexibility of the extensibility of the objects and interaction methods in the interface. The development of service robots is inseparable from the development of interactive technology. Takeo Igarashi provided children with a simple pen and gesture interaction that can generate a rough 3D model. It is a 3D drawing model based on outline Teddy [17]. MIT multimedia laboratory has developed an interface system Doll

Talk [18] that exercises children's conversational ability. This system can simulate speech recognition by capturing children's gestures and language information, and then inform children of the conversation content by changing the pitch, thereby guiding children to improve their own narrative. IaTAR is an immersive simulation creation system developed by Pohang University in South Korea. The system emphasizes "what you see is what you get" and can cultivate children's imagination and creativity in space [19]. These interactive technologies play a vital role in the interaction between robots and users.

3. Spatial Algorithm Based on Context Perception

As the most typical adaptive beamforming algorithm, the MV algorithm has a certain degree of contribution to improve the imaging resolution, but the algorithm's robustness are not as good as the traditional nonadaptive DAS algorithm: and if the expected direction vector of the MV algorithm is not accurate, or the estimation of the sample covariance matrix is not accurate, which will greatly affect the imaging effect. In engineering practice, due to various noises and interferences in the detection environment, there are errors between the echo signal of the ultrasonic array and the expected direction vector, which makes it difficult to meet the normal working conditions of the MV adaptive algorithm, which leads to a decrease in the output signal-to-noise ratio. This section mainly analyzes the robust form of the MV algorithm under error conditions, that is, an improved algorithm that overcomes the influence of error factors such as noise and interference to improve the output performance and robustness of the MV algorithm. At present, the common beamforming robust algorithms for the MV algorithm includes diagonal loading method to obtain a more accurate sample covariance matrix, a spatial smoothing method to reduce the strong correlation of ultrasonic signals, and a feature space method to filter out the influence of noise interference. This section will conduct detailed analysis and research on the principles and performance of the above robust algorithms [20].

According to the basic principle of the MV algorithm, the acquisition of the optimal dynamic weight vector involves the determination of the desired direction vector and the inverse operation of the sample covariance matrix $R = E[x_d, x_d^H]$. In the actual detection process, the number of ultrasonic echo data samples are limited by the influence of noise interference, so that the estimation error of the sample covariance matrix increases, and it is even irreversible. When there is an error in the expected direction vector, the expected signal will be cancelled, which will cause the image quality to deteriorate. In order to effectively improve the estimation accuracy of the sample covariance matrix, some scholars have proposed the diagonal loading method to correct the error of the estimated sample covariance matrix. A constant is added to the diagonal element of the sample covariance matrix. On the one hand, the loaded covariance matrix can be full-rank invertible, so the problem of too few samples is compensated. On the other hand, it can compensate the weakened desired signal to a certain extent, and produce a robust effect on the error of the desired direction vector. The specific principle of the algorithm is described as follows [21]:

$$\widehat{R} = R + \varepsilon B. \tag{1}$$

Among them, B represents a unit variance random matrix with a mean value of 0, and ε represents an error factor, which generally takes an integer value. Then, the estimated sample covariance matrix after diagonal loading compensation can be expressed as

$$\widehat{R}_{DL} = R + \varepsilon B + \lambda I. \tag{2}$$

Among them, λ represents the diagonal loading factor, and I represents the identity matrix. According to the principle of the MV algorithm, the minimum variance criterion after diagonal loading compensation will be transformed into

$$\begin{gathered} \min_{w} w^H \widehat{R}_{DL} w + \lambda w^H w, \\ \text{subject to } w^H a = 1. \end{gathered} \tag{3}$$

It can be obtained that the mathematical expression of the optimal weight vector of the MV algorithm after diagonal loading can be modified as

$$w_{\text{opt}} = \frac{\widehat{R}_{DL}^{-1} a}{a^H \widehat{R}_{DL}^{-1} a}. \tag{4}$$

Secondly, although the diagonal loading method can enhance the robustness of the MV algorithm against the number of echo signal samples and the desired direction vector, the selection of the diagonal loading factor A is very critical. If the value of A is too small, the estimated sample covariance matrix is irreversible, and the loading effect will be lost; if the value is too large, the algorithm's anti-interference ability will decrease. To solve this problem, a method to determine the value based on the ultrasonic echo signal is proposed. The specific selection criteria are as follows:

We assume that there is $\varepsilon\|B\| \le \|R + \lambda I\|$, and the approximate inverse operation of the estimated sample covariance matrix can be performed by the following formula to obtain the optimal weighting vector of the MV algorithm:

$$\widehat{R}_{DL}^{-1} \simeq (R + \lambda I)^{-1} \left\{ I - \frac{\varepsilon}{\lambda + \delta^2} B \left[I - A\left(A^H A + \left(\lambda + \delta^2\right) \wedge^{-1} \right) A^H \right] \right\}. \tag{5}$$

Among them, A represents the array flow matrix, and $\wedge = \text{diag}\{\sigma_1^2, \sigma_2^2, \ldots, \sigma_N^2\}$ is the diagonal matrix composed of the noise power σ_i^2 $(i = 1, 2, \ldots, N)$ of the diagonal elements. At the same time, δ represents the loading factor selection parameter, and N represents the number of array elements. According to formula (5), in order to obtain a more accurate estimated covariance inverse matrix, while making the left half term $R + \lambda I$ closer to the true sample covariance matrix, the value of the right half term that mainly causes estimation errors should be reduced to zero. That is, the formulas (6) and (7) are satisfied, respectively [22]:

$$\lambda \leq R(i,i),\ i = 1, 2, \ldots, N, \tag{6}$$

$$\begin{aligned} y(k) &= w^H(k) x_d(k) \\ &= \sum_{i=1}^{N} w_i(k) x_i(k - \Delta_i). \end{aligned} \tag{7}$$

Among them, there is $k_d(x) = [x_1(k-\Delta_1), \ldots, x_N(k-\Delta_N)]^T$. According to formula (6) and formula (7), the value range of diagonal loading factor Δ_i is

$$w(k) = \left[w_i(k), \ldots, w_N(k)\right]^T. \tag{8}$$

Among them, the error factor $[\cdot]^T$ in formula (8) and the diagonal element $P = E[|(k)|^2] = E[|w^H x_d(k)|^2] = E[w^H x_d(k)(x_d(k))^H w]$ of the real sample covariance matrix are unknown items in engineering practice, and the value range of $R = E[x_d(k)(x_d(k))^H]$ can only be obtained based on the estimated value of the sample covariance matrix.

According to the mean variance characteristics of matrix B, the diagonal elements and error factors of the real sample covariance matrix can be estimated by estimating the mean and standard deviation of the diagonal elements of the sample covariance matrix $\min_w w^H R w$, *subject* to $w^H a = 1$, as shown in formulas (9) and (10):

$$J = \frac{1}{2} w^H R w + \lambda\left[1 - w^H a\right], \tag{9}$$

$$\begin{aligned} \frac{\partial J}{\partial w} &= Rw - \lambda a \\ &= 0. \end{aligned} \tag{10}$$

Among them, trace(·) represents the trace calculation operation, std(·) represents the standard deviation operation, and diag(·) represents the diagonal element solving operation. According to formulas (9) and (10), the value range of $w = \lambda R^{-1} a$ can be obtained as

$$\lambda = \frac{1}{a^H R^{-1} a}. \tag{11}$$

In summary, by adopting the diagonal loading method with appropriate parameters, the full-rank reversible estimated sample covariance matrix $w_{\text{opt}} = (R^{-1}a / a^H R^{-1} a)$ can be obtained, thereby increasing the robustness of the MV algorithm.

In the ultrasonic detection process, the echo signal received by each element of the ultrasonic transducer comes from the reflection or scattering of the object to be detected. Therefore, the received ultrasonic echo signal exhibits a strong correlation, resulting in the cancellation of the expected signal, which seriously affects the quality of ultrasonic imaging. In this regard, the spatial smoothing method is proposed to weaken the strong correlation between the echo signals received by the ultrasonic array element. The basic principle of the method is as follows: first, the echo signals received by the ultrasonic transducer arrays with the same array flow pattern are divided, and several overlapping sub-arrays are obtained. Secondly, the sub-array covariance matrix corresponding to each sub-array is solved in turn and

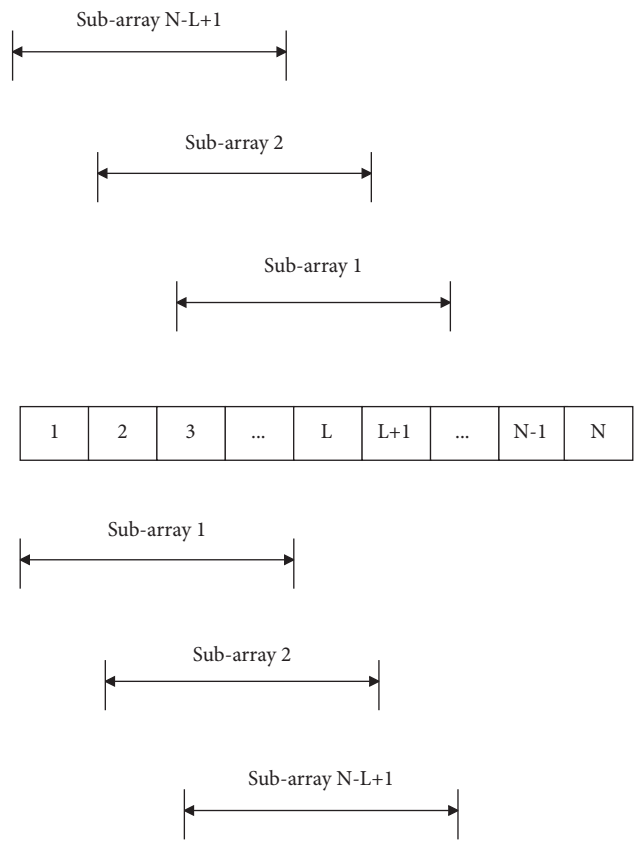

Figure 1: The principle of forward and backward spatial smoothing.

its average value is obtained. Finally, this value is used to replace the original sample covariance matrix for adaptive weighting. The ultrasonic linear transducer array of N elements is taken as an example, and the detailed schematic diagram of the forward and backward spatial smoothing is shown in Figure 1 [23].

It can be seen from Figure 1 that the forward and backward spatial smoothing method uses the translation invariance of the linear array to achieve the uniform division of the sub-arrays. Among them, the forward smoothing method divides all array elements uniformly into $N-L+1$ overlapping sub-arrays including L array elements in the order from left to right. The first sub-array is taken as an example, the received echo signal (k) after forward smoothing can be expressed as

$$y_{mv}(k). \tag{12}$$

It can be seen that the subsample covariance matrix corresponding to the lth submatrix after forward smoothing can be expressed as

$$y_{mv}(k) = w_{\text{opt}}^H x(k). \tag{13}$$

Among them, $CF = (|\sum_{n=1}^{N} x_n(k)|^2 / N | \sum_{n=1}^{N} x_n(k)|^2) = (|(1/N) \sum_{n=1}^{N} x_n(k)|^2 / |(1/N) \sum_{n=1}^{N} x_n(k)|^2 + (1/N) \sum_{n=1}^{N} |x_n(k) - \overline{x}(k)|^2)$ represents the expected operation and $(\cdot)^H$ represents the conjugate transpose operation. The $N-L+1$

subsample covariance matrix obtained by equation (13) is averaged, and the sample covariance matrix smoothed by the forward space can be expressed as

$$x_n(k). \tag{14}$$

Therefore, the spatial smoothing method weakens the strong correlation of the ultrasonic echo signal by averaging the covariance matrix of all sub-arrays, and the dimension of the covariance matrix is reduced from the number of elements N to the number of elements L of the sub-array. As a result, the complexity of the inversion of the covariance matrix is reduced, and the efficiency of the algorithm is improved. However, the application of the forward spatial smoothing method will cause the loss of the array aperture, which will adversely affect the imaging resolution. Therefore, a forward and backward spatial smoothing method is proposed, and N$-L+1$ backward sub-arrays are added to perform backward smoothing on the basis of the former. The Ith sub-array is taken as an example, and the received echo signal $|\cdot|$ after backward smoothing can be represented as

$$m_{mv-cf}(k) = CF(k) \cdot \sum_{i=1}^{N} w_{\text{opt}}^{H} x(k). \tag{15}$$

In the same way, the corresponding subsample covariance matrix of the lth submatrix after the backward smoothing process can be represented as

$$\begin{aligned} SNR(j) &= \frac{S(j)}{N(j)} \\ &= \frac{\left((1/M)\sum_{i=1}^{M} x(i,j)\right)^2}{(1/M)\sum_{i=1}^{M}\left(x(i,j) - (1/M)\sum_{i=1}^{M} x(i,j)\right)^2}. \end{aligned} \tag{16}$$

Similar to the principle of formula (14), the sample covariance matrix smoothed by the backward space can be represented as

$$SNR_{dB}(j) = 10 * \lg(SNR(j)). \tag{17}$$

By taking the arithmetic average of the matrices R^f and R^b, the forward and backward spatial smoothing matrix R^{fb} can be obtained as

$$\begin{aligned} r_a &= c\frac{\tau_p}{2} \\ &= \frac{c}{2B_w}. \end{aligned} \tag{18}$$

However, although the above method can effectively reduce the loss of the array aperture, it doubles the calculation amount compared to the one-way spatial smoothing method. In order to reduce the computational complexity of the algorithm, an appropriate matrix J can be constructed to directly solve R^{fb} through R^{f}. The specific conversion steps are as follows:

$$R^{fb} = J\left(R^f\right) * J. \tag{19}$$

Among them, J represents a conversion matrix whose anti-angle element is 1 and the remaining elements are 0,

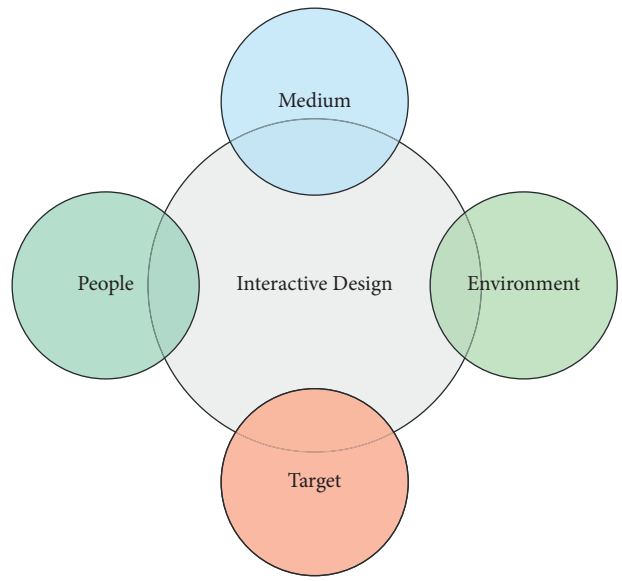

Figure 2: Elements of the interactive design system.

and $r_i = 2R\sin(\theta_{ml}/2)$ represents a matrix conjoint operation.

The echo signal received by the ultrasonic transducer contains both the desired signal and the noise signal. If the noise signal cannot be effectively filtered out, it will result in a reduction in the signal-to-noise ratio of the adaptive beamforming output, and seriously affect the imaging quality. In this regard, the feature space method is proposed to suppress the noise content in the echo signal, thereby improving the robustness of the MV adaptive beamforming algorithm. The basic principle of the algorithm is: first, the sample covariance matrix of the echo signal received by the array element is decomposed by the eigenvalue, and it is sorted in descending order according to the size of the obtained eigenvalue. Secondly, the aforementioned covariance matrix is decomposed in the signal subspace and the noise subspace that are orthogonal to each other. Since the noise subspace contains noise and interference signals in the ultrasonic echo signal, a specific threshold can be set according to the feature value, and the signal subspace can be set to the feature space corresponding to the feature value greater than the set threshold. Finally, the weighted vector obtained in the adaptive algorithm is projected to the signal subspace to obtain the desired echo signal, and the signal subspace and the noise subspace are orthogonal to each other to filter out the noise component in the signal. Finally, the optimal adaptive weight vector is obtained. The specific principle of the algorithm is described as follows:

First, the eigenvalue decomposition of the estimated sample covariance matrix θ_{ml} is represented by its corresponding signal subspace and noise subspace:

$$\begin{aligned} \widehat{R} &= \sum_{i=1}^{\text{num}} \lambda_i e_i e_i^H + \sum_{i=\text{num}+2}^{N} \lambda_i e_i e_i^H \\ &= E_s \Lambda_n E_n^H. \end{aligned} \tag{20}$$

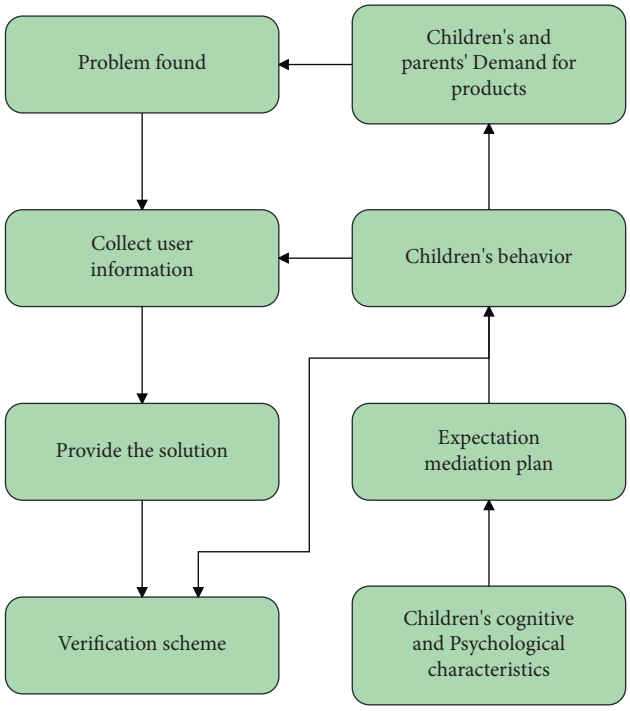

Figure 3: Flow chart of children's interaction design based on CAPS theory.

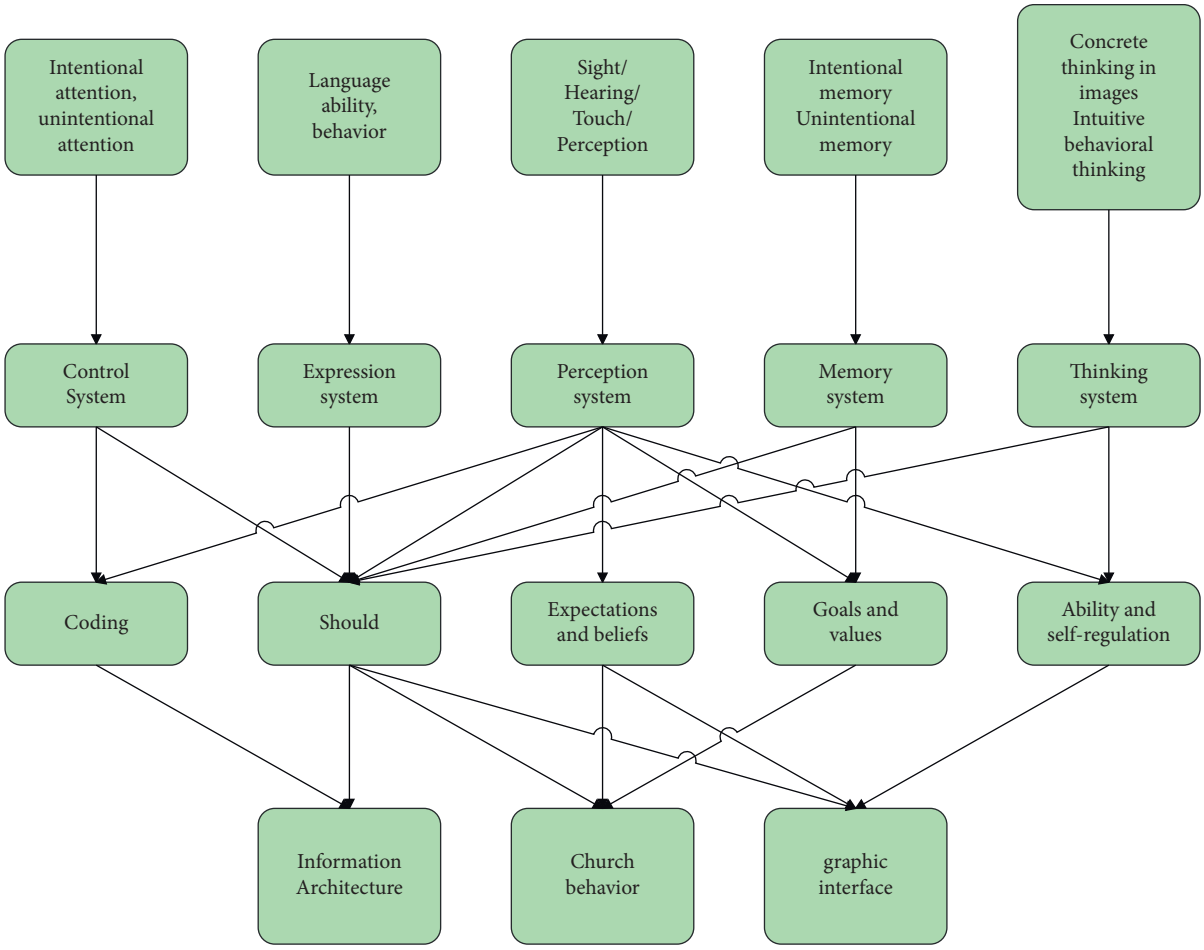

Figure 4: Children's cognitive emotion system and interaction design.

Among them, $CR = 20 * \lg(\mu_B/\mu_C)$ is the signal subspace, num represents its spatial dimension, and θ_{ml} is the noise subspace. At the same time, μ_C is the N eigenvectors corresponding to the N eigenvalues $SD = \sqrt{\sigma_B^2 + \sigma_C^2}$ of the covariance matrix, and its eigenvalue σ_B satisfies σ_C. $\Lambda_s = \mathrm{diag}\{\lambda_1, \lambda_2, \ldots, \lambda_{num}\}$ and $\Lambda_s = \mathrm{diag}\{\lambda_{\mathrm{num}+1}, \lambda_{\mathrm{num}+2}, \ldots, \lambda_N\}$ are diagonal matrices formed by the corresponding eigenvalue elements of the signal subspace and the noise subspace.

Secondly, after the signal subspace E_s corresponding to the covariance matrix is obtained, the optimal weight vector ω_{opt} obtained in the adaptive algorithm is projected to the signal subspace, which can filter out the component of the weight vector in the noise subspace. Furthermore, the optimal weighting vector based on the feature space is obtained as

$$\begin{aligned} \omega_{esbmv} &= E_s E_s^H, \omega_{\mathrm{opt}} \\ &= E_s E_s^H \frac{\widehat{R}_{DL}^{-1} a}{a^H \widehat{R}_{DL}^{-1} a}. \end{aligned} \tag{21}$$

In summary, the application of the feature space method can effectively improve the resolution and contrast of ultrasound imaging, and improve the performance of the adaptive algorithm and the imaging effect. However, the operation of this algorithm involves matrix eigenvalue decomposition, eigenvalue sorting, and matrix inversion operations. The amount of calculation and complexity are high, which seriously affects the operating efficiency of the algorithm.

4. Children's Service Robot System Based on Context Perception

The essence of interaction design is to improve the user's experience through the communication between individuals and make users feel emotional, so that users can experience the product more conveniently and comfortably, and complete the target tasks. Therefore, interaction design is essentially a subject that focuses on interactive experience. In the process of using products and various services, it is actually interacting with them. The feeling during the use is a kind of interactive experience. The interaction design system contains five elements: human, actions, media, goals, and scenarios, as shown in Figure 2.

Applying the psychological CAPS theory to interaction design is to better interpret the user, and from the user's point of view, it is to respect the user's behavior and habits. In particular, for children, a special user group, their cognitive, psychological, and emotional characteristics are different from those of adults. Therefore, it is more necessary to study the cognitive and emotional characteristics of children from the perspective of this special group of children, and then apply them to the design, so that users can feel the "care" that the product brings to people. Therefore, in the interaction design process, we should pay attention to the discovery of user needs, use the theoretical methods of psychology to collect user information, and apply the CAPS theory to the specific design process of children's interaction design, as shown in Figure 3.

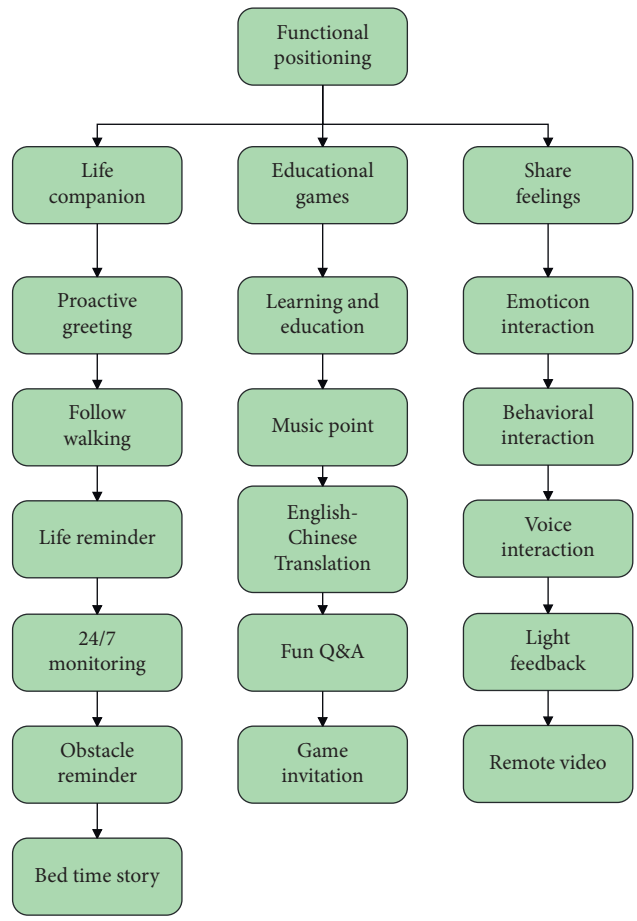

Figure 5: Summary of existing product functions of children's service robots in the market.

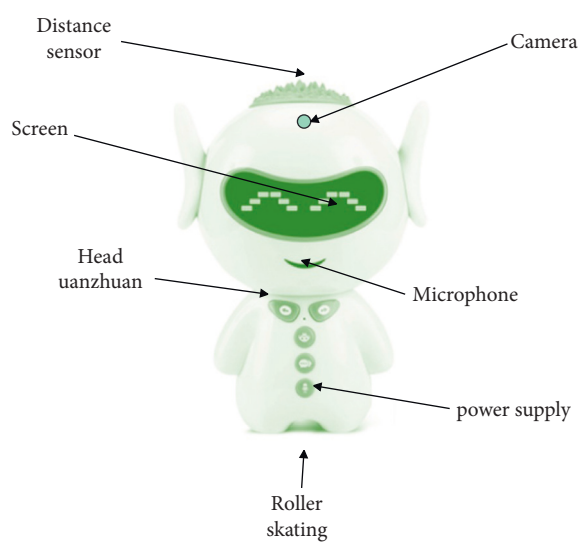

Figure 6: Hardware infrastructure of children's service robots.

The child's cognitive and emotional system is further generalized and divided into five subsystems: control system,

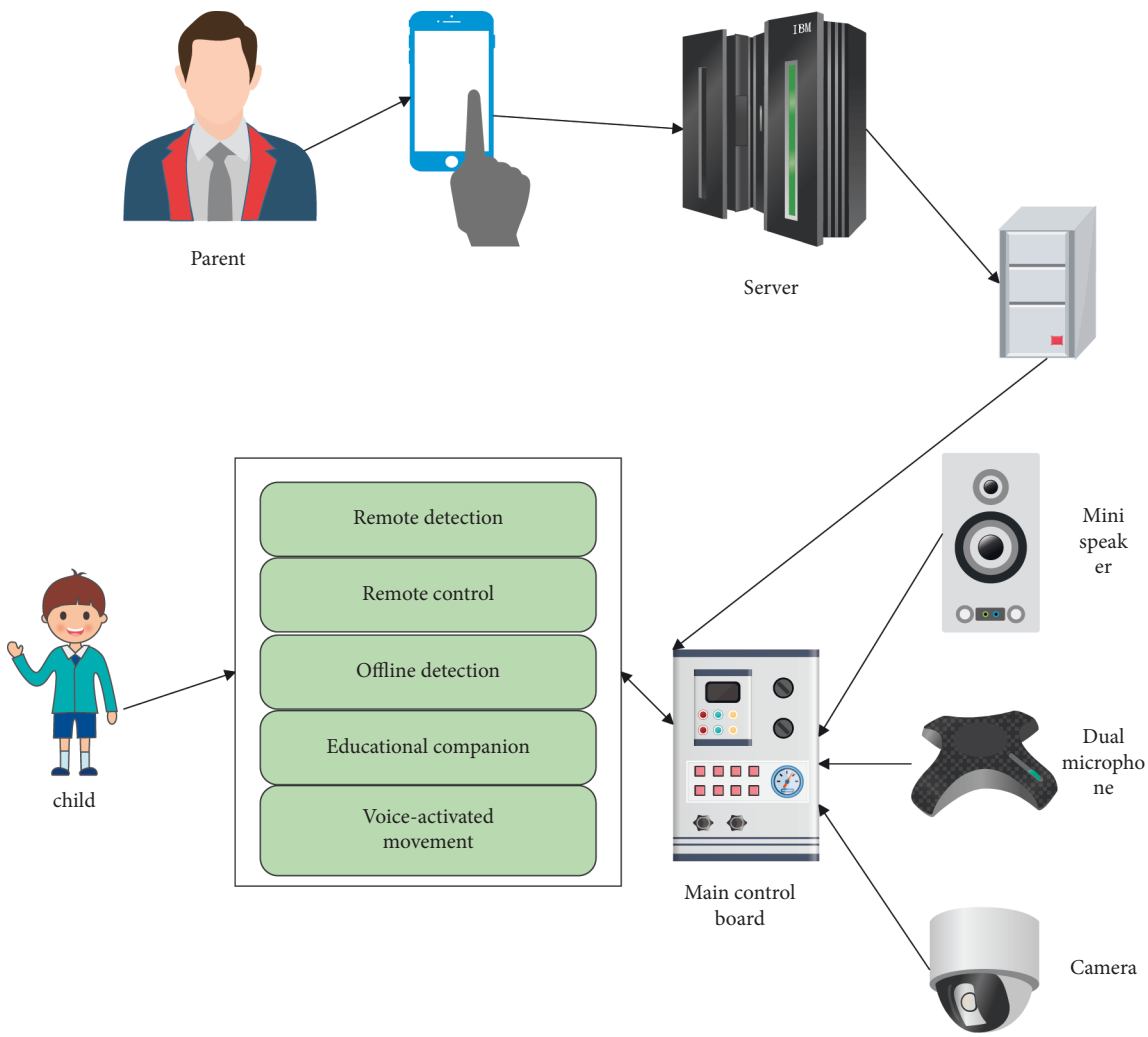

Figure 7: The overall control structure of the child service robot.

Table 1: Experimental research results of the child service robot system.

	Interactive effect	Service effect	Satisfaction
1	93.97	92.79	91.88
2	93.08	83.58	94.51
3	93.98	88.68	93.53
4	91.46	93.64	94.69
5	90.12	87.23	91.12
6	92.73	94.53	96.16
7	92.34	88.75	91.50
8	86.29	91.52	95.46
9	92.50	86.19	96.73
10	87.92	87.53	87.63

perception system, expression system, memory system, and thinking system, which correspond to and influence children's cognitive and emotional units, respectively. Thus, the corresponding relationship between the children's cognitive emotion system and the three parts of the product's interactive design solution is summarized, as shown in Figure 4.

According to the analysis of user needs and the current situation of the product, this paper will study the interactive

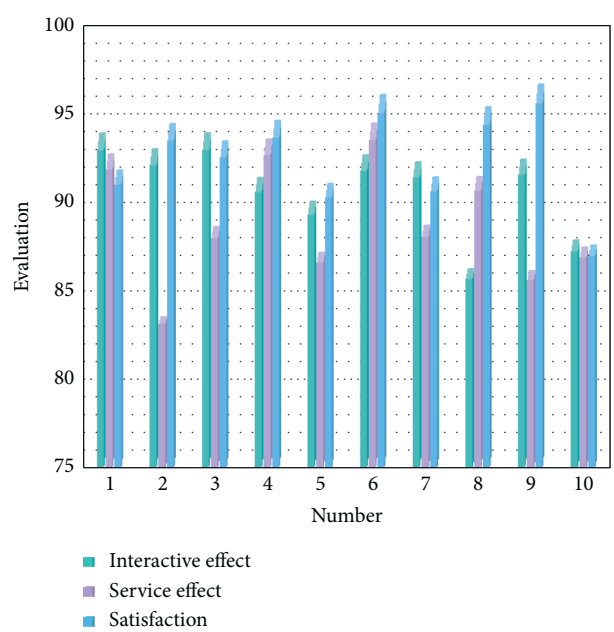

Figure 8: The practical effect of the intelligent child service robot.

design of the child escort robot at the content level from three aspects, that is, interaction design based on "accompanying" requirements, interaction design based on "educational" functions, and interaction design based on "interest" requirements. This article summarizes the commonality and individuality of existing products, and the results are shown in Figure 5.

As shown in Figure 6, the hardware facilities of the child service robot should include distance sensors, cameras, screens, LED lights, microphones, speakers, power buttons, and roller skating.

The functions of remote real-time monitoring, remote control, and offline monitoring are to meet the needs of parents. Remote monitoring and remote control mean that parents can operate the robot through media devices to observe the child's dynamics when they are working or on a business trip. The purpose of offline monitoring is to understand what has happened. The method adopted is to upload the dynamic scene in front of the camera to the Baidu cloud disk in the form of pictures. In their leisure time, parents learn about the child's dynamics by browsing pictures, on the other hand, they record the child's growth process and monitor the safety of the home at the same time. Therefore, to meet the needs of parents and children at the same time, the child service robot should have the above six functions: education companion, voice-controlled movement, graphical programming, remote monitoring, remote control, and offline monitoring. In summary, the overall structure design of the child service robot is obtained, as shown in Figure 7.

After constructing a child service robot based on context perception, the performance of the robot system is verified. This paper combines the simulation experiment to carry out the interactive effect of the robot system and the service effect to children, and investigates the satisfaction of parents. The results are shown in Table 1 and Figure 8.

From the above research, it can be seen that the child service robot system based on context perception constructed in this paper has good service effects, can effectively take care of children, and has high parent satisfaction.

5. Conclusion

Solving the problem of left-behind children through service robots is a new solution to social problems. Based on the research results of domestic and foreign scholars, this paper summarizes basic theories such as children's physiological and psychological characteristics and interaction design theory. Then, this paper further studies the needs of the left-behind children on the companion robot through interactive behavior experiments, and further explores the design concepts and methods of the companion robot for children. In addition, based on the above research results, a targeted design plan is made as a practice and test of the design theory. Finally, starting from the existing emotional design theory, through actual case analysis, literature search, and practical research, the children's emotional needs in life and learning are clarified, and a child companion robot design plan is formed, and the product design and practice of children's companion robots are carried out based on the research conclusions.

Data Availability

Data used to support the findings of this study are available from the corresponding author upon request.

Conflicts of Interest

The author declares that there are no conflicts of interest regarding this work.

References

[1] K. W. C. Shin and J. H. Han, "Qualitative exploration on children's interactions in telepresence robot assisted language learning," *Journal of the Korea Convergence Society*, vol. 8, no. 3, pp. 177–184, 2017.

[2] D. Belanche, L. V. Casaló, C. Flavián, and J Schepers, "Service robot implementation: a theoretical framework and research agenda," *Service Industries Journal*, vol. 40, no. 3-4, pp. 203–225, 2020.

[3] H. Lee, W. Shin, and H. Cho, "A study on preschool children's perceptions of a robot's theory of mind," *Journal of Korea Robotics Society*, vol. 15, no. 4, pp. 365–374, 2020.

[4] C. E. Farrier, J. D. R. Pearson, and T. N. Beran, "Children's fear and pain during medical procedures: a quality improvement study with a humanoid robot," *Canadian Journal of Nursing Research*, vol. 52, no. 4, pp. 328–334, 2020.

[5] N. F. Valchkova and R. Z. Zahariev, "Optimization of model operator for service robot, intended to service persons with disability," *IFAC-PapersOnLine*, vol. 52, no. 25, pp. 174–179, 2019.

[6] S. Kim and K. You, "Analysis of effects on children's operation ability and fine motor skills depending on various remote controls and game controller [J]," *International Information Institute (Tokyo). Information*, vol. 21, no. 2, pp. 555–562, 2018.

[7] M. R. Daud, "Design of service taekwondo robot for simulation "kwon" movement[J]," *Journal on Technical and Vocational Education*, vol. 4, no. 3, pp. 44–48, 2019.

[8] M. Jin and J. Kim, "A survey of nurses' need for care robots in children's hospitals," *CIN: Computers, Informatics, Nursing*, vol. 38, no. 7, pp. 349–357, 2020.

[9] S. Ali, R. Manaloor, K. Ma et al., "A randomized trial of robot-based distraction to reduce children's distress and pain during intravenous insertion in the emergency department," *Canadian Journal of Emergency Medicine*, vol. 23, no. 1, pp. 85–93, 2021.

[10] M. I. Ahmad, O. Mubin, S. Shahid, and J. Orlando, "Robot's adaptive emotional feedback sustains children's social engagement and promotes their vocabulary learning: a long-term child-robot interaction study," *Adaptive Behavior*, vol. 27, no. 4, pp. 243–266, 2019.

[11] E. S. Secim, M. C. Durmuşoğlu, and M. Çiftçioğlu, "Investigating pre-school children's perspectives of robots through their robot drawings," *International Journal of Computer Sciences and Engineering Systems*, vol. 4, no. 4, pp. 59–83, 2021.

[12] C. Sinoo, S. van der Pal, O. A. Blanson Henkemans et al., "Friendship with a robot: children's perception of similarity between a robot's physical and virtual embodiment that

supports diabetes self-management," *Patient Education and Counseling*, vol. 101, no. 7, pp. 1248–1255, 2018.

[13] H. W. Lee and W. Shin, "Exploring factors affecting acceptance intention and recognition of robot-based education for mother with young children[J]," *Journal of the Korea Academia-Industrial cooperation Society*, vol. 21, no. 7, pp. 462–474, 2020.

[14] A. K. Chung and S. J. Byun, "A study on the factors affecting on pre-service early childhood teachers' adoption intention of robot-based education[J]," *The Journal of The Institute of Internet, Broadcasting and Communication*, vol. 18, no. 4, pp. 227–235, 2018.

[15] H. P. Yueh, W. Lin, S. C. Wang, and L. Fu, "Reading with robot and human companions in library literacy activities: a comparison study," *British Journal of Educational Technology*, vol. 51, no. 5, pp. 1884–1900, 2020.

[16] K. D. Adams, A. M. Rios Rincón, L. M. Becerra Puyo et al., "An exploratory study of children's pretend play when using a switch-controlled assistive robot to manipulate toys," *British Journal of Occupational Therapy*, vol. 80, no. 4, pp. 216–224, 2017.

[17] M. T. Choi, J. Yeom, Y. Shin, and I. Park, "Robot-assisted ADHD screening in diagnostic process," *Journal of Intelligent and Robotic Systems*, vol. 95, no. 2, pp. 351–363, 2019.

[18] C. J. Moerman, L. van der Heide, and M. Heerink, "Social robots to support children's well-being under medical treatment: a systematic state-of-the-art review," *Journal of Child Health Care*, vol. 23, no. 4, pp. 596–612, 2019.

[19] C. L. van Straten, J. Peter, and R. Kühne, "Child-robot relationship formation: a narrative review of empirical research," *International Journal of Social Robotics*, vol. 12, no. 2, pp. 325–344, 2020.

[20] B. Lee, J. Y. Cho, H. W. Lee, Y. Choi, Y. S. Yoon, and HS. Han, "Successful ABO-incompatible living donor liver transplantation using splenectomy and intravenous immunoglobulin in high isoagglutinin titer patients," *Korean journal of transplantation*, vol. 34, no. 2, pp. 109–113, 2020.

[21] K. A. Brink, K. Gray, and H. M. Wellman, "Creepiness creeps in: uncanny valley feelings are acquired in childhood," *Child Development*, vol. 90, no. 4, pp. 1202–1214, 2019.

[22] N. Hasegawa and Y. Takahashi, "Control of soap bubble ejection robot using facial expressions," *International Journal of Manufacturing, Materials, and Mechanical Engineering*, vol. 11, no. 2, pp. 1–16, 2021.

[23] C. de Jong, J. Peter, R. Kühne, and A. Barco, "Children's acceptance of social robots," *Interaction Studies*, vol. 20, no. 3, pp. 393–425, 2019.

Hindawi
Mobile Information Systems
Volume 2022, Article ID 5046869, 9 pages
https://doi.org/10.1155/2022/5046869

Research Article

Performance evaluation of agricultural financial funds based on smart big data analysis

Min Kuang

School of Public Administration, Sichuan University, Chengdu 610000, China

Correspondence should be addressed to Min Kuang; 2020020147@stu.cdut.edu.cn

Received 18 June 2022; Revised 15 July 2022; Accepted 18 July 2022; Published 9 August 2022

Academic Editor: Chi Lin

This paper attempts to build a performance evaluation system for agricultural financial project expenditures to make the performance evaluation of financial support for agriculture more maneuverable and provide a reference for the management of agricultural funds. Moreover, this paper combines the intelligent big data technology to construct the agricultural financial fund performance evaluation system, and describes the characteristics of the relevance of geographic elements in the entire spatial region through global spatial autocorrelation. Simultaneously, this paper uses different spatial weight matrices to examine the rationality and robustness of the results. In addition, this paper introduces covariates and removes trends through regression methods. Further, taking into account the characteristics, scientificity and operability of agricultural financial funds, the dimensions and structure of the performance evaluation of agricultural financial expenditures are drawn up. Finally, this paper verifies the effectiveness of this method through case studies, and gives several targeted suggestions.

1. Introduction

Agriculture is the foundation of the national economy, and financial support for agriculture is an important direction of public finance expenditure. In recent years, all levels of finance have increased their investment in agriculture-related funds year by year, and the scale of agricultural fiscal expenditure has risen sharply, and a stable growth mechanism for fiscal support of agriculture has been gradually established and improved [1]. In terms of the use of funds, the financial support for agriculture has a direct bearing on the vital interests of the broad masses of farmers. Therefore, it is a people's livelihood fund with a wide audience and a high degree of social attention, and it is of inestimable economic and political significance to manage and use fiscal funds to support agriculture [2]. However, judging from the current management and use of domestic financial support funds for agriculture, it can be seen that there are many types, scattered use, random distribution, and frequent occurrences. These problems are difficult to meet the needs of the development of the situation. Therefore, it is imperative to carry out the performance evaluation of agricultural financial expenditure, to reflect the input and output, cost and benefit of agricultural production to an operable and quantifiable level, and to impel power into the cage of the system [3].

With the continuous growth of the population, the pressure on the demand for food has gradually emerged, and the living standards and quality of life of farmers have also been paid special attention. To this end, China has been committed to the development and progress of rural areas and agriculture. However, in the process of development, there are still many influencing factors that restrict development, such as poor rural infrastructure, imperfect road traffic, imperfect water, electricity, and network communications, and a reduction in rural labor. As these influencing factors have not been improved for a long time, it has led to the accumulation of more contradictions, the development of urban and rural areas has begun to become seriously unbalanced, the basic resources of rural society are scarce, and the income gap between urban and rural residents has become increasingly prominent. Facing the severe situation of rural and agricultural development, the Party Central Committee and the State Council have formulated a

series of policies to strengthen the development of rural, agricultural, and peasants, and they have made rural, agricultural development and increasing peasants' income the top priority of government work. Among the influencing factors restricting the development of rural agriculture, weak rural basic production conditions, facilities, and limitations of rural farmers' development concepts have a great impact on rural development. In response to this situation, the state finance has invested a large amount of funds to support the development of agriculture and rural economy.

Fiscal expenditure is an important part of the national income distribution and redistribution. It is a resource allocation activity carried out by the state to meet the common needs of society, and it is an important aspect of public finance. With the continuous deepening of the reform of my country's fiscal budget management system and the establishment of the public finance framework system, strengthening the management and supervision of fiscal expenditures and improving the efficiency of the use of fiscal funds have become a very important task in fiscal management. At the same time, the establishment of a sound scientific fiscal expenditure performance evaluation system and the implementation of evaluation and control of fiscal expenditure performance are effective ways to improve the efficiency of fiscal expenditure.

The method of national finance to support agriculture is generally direct investment, tax incentives and subsidies. The subsidies also include income subsidies, price subsidies, and financial discounts. Among them, the agricultural financial interest subsidy is an important part of the fiscal expenditure for supporting agriculture, and it is the national finance according to the agricultural development policy and industrial policy of the party and the government. It refers to the government granting a certain percentage of interest subsidies to certain specific loans within a certain period of time. It has an obvious financial leverage function, which can stimulate the investment enthusiasm of social funds and guide the investment direction of social funds. Under the background that all sectors of society pay more and more attention to the issue of fiscal expenditure efficiency, as a component of fiscal expenditure, the "tracking and testing" of agricultural fiscal discount interest and the evaluation of its use performance are of great significance to strengthening the management of public fiscal expenditure.

2. Related work

With the continuous progress of comprehensive agricultural development projects, in order to study the effects and efficiency of comprehensive agricultural development projects, many scholars try to evaluate the performance of agricultural projects by constructing a reasonable evaluation method and a scientific and reasonable indicator system. The unified indicator system framework cannot meet different evaluation needs, and many indicators do not truly reflect the performance of funds but are more directed toward work evaluation. Therefore, the purpose of evaluation should become the starting point of the internal logic of evaluation [4]. Based on the theory of balanced scorecard and system theory, 12 specific and relatively independent indicators are selected from the four dimensions of beneficiaries, finance, management and operation and sustainability to form the project performance evaluation system [5]. The analytic hierarchy process is used to determine the weight of the performance evaluation index of land governance project funds [6]. Based on the process of agricultural comprehensive development project activities, the evaluation indicators are involved in two aspects: capital input and capital output [7].

From the perspective of project content classification, China's performance evaluation of agricultural development projects is done in accordance with the project. Due to the continuous refinement of land governance projects, the current research on land governance projects has gradually shifted from theoretical research on land governance project planning and feasibility analysis to empirical research. The method of combining theoretical analysis and expert consultation is used to establish an evaluation system to form a quantitative index evaluation and quantitative evaluation of the economic benefits after land consolidation [8]. The literature [9] established a provincial-based implementation index of domestic agricultural land quality, discussed domestic agricultural land changes, and re-division and evaluation of the domestic high-yield, middle-yield, and low-yield fields and their regional distribution. The literature [10] analyzed and evaluated the status quo of low-yield farmland transformation in my country from the perspective of food security.

In the qualitative research on the management of comprehensive agricultural development funds, many domestic scholars analyze the management status and existing problems of comprehensive agricultural development funds from the aspect of fund management, and then put forward suggestions for optimizing management. Through the research on the current situation of fund management for comprehensive agricultural development on the ground, it is found that there are problems in fund management such as low quality of financial personnel, irregular reimbursements, delayed fund audits, and lax project acceptance. The literature [11] proposed that the leadership should pay attention to the management of comprehensive agricultural development funds, strictly implement the county-level accounting system for fiscal funds, strengthen the audit of comprehensive agricultural development funds, strengthen the management of paid funds, and increase recovery efforts. Through a comprehensive analysis of the process of raising, allocating, appropriating, monitoring, and performance evaluation of agricultural comprehensive development funds, it was found that the contradiction between project funding needs and fund raising was prominent, and there were still system loopholes in the appropriation, use, and supervision of funds. Literature [12] proposes to improve the investment mechanism of comprehensive agricultural development, gradually expand the scale of investment, strengthen capital supervision, play a positive role in performance evaluation, and improve the quality of the comprehensive agricultural development fund management team. Taking the investment cycle data of a comprehensive agricultural development fund as an example, it analyzes from two aspects: the land governance capital chain and the industrialized management

capital chain. Moreover, it reveals the problem of address changes and inaccurate budgets during the implementation of the agricultural development project due to inadequate preliminary work, which in turn led to poor circulation of agricultural development funds during the project implementation. The literature [13] proposed to speed up the construction of the financial system, implement supporting funds in place, strengthen rolling development, improve the quality of accounting personnel, and strengthen supervision, inspection and supervision. From the perspective of auditing, literature [14] used a combination of normative and empirical analysis to find many problems in the management of agricultural comprehensive development funds. These problems are all caused by the serious principal-agent relationship in public management, and performance auditing is an effective measure to solve this problem. The management of comprehensive agricultural development funds is out of touch with project management. Since project management and fund management are not the same department, each department performs its own duties, and there is no complete right to know each other, resulting in poor fund allocation. The literature [15] suggested that the relevant departments of comprehensive agricultural development should correspondingly strengthen project plan management, make more detailed budgets for projects, improve project and fund declaration procedures, and strengthen communication and coordination and information sharing among relevant departments.

3. Smart big data inspection algorithm

Global spatial autocorrelation describes the description of the characteristics of the relevance of geographic elements in the entire spatial region. Global Moran's I is a widely used global spatial autocorrelation statistic. The calculation formula is as follows [16]:

$$I = \frac{n}{S_o} \times \frac{\sum_{i=1}^{n} \sum_{j=1}^{n} w_{ij} (z_i - \overline{x})(z_J - \overline{x})}{\sum_{i=1}^{n} (z_i - \overline{x})^2}. \tag{1}$$

Among them, $S_0 = \sum_{i=1}^{n} \sum_{j=1}^{n} w_{ij}$, $\overline{x} = \sum_{i=1}^{n} (z_i/n)$, and n is the total number of observation variables, $(z_i - \overline{x})$ is the deviation of the observation value on the i-th spatial unit from the average value, and w_{ij} is the weight of the spatial observation variables i and j. i and j represent two different regions. The spatial weight matrix w is defined as:

$$W = \begin{pmatrix} w_{11} & \cdots & w_{1n} \\ \vdots & \ddots & \vdots \\ w_{n1} & \cdots & w_{nn} \end{pmatrix}. \tag{2}$$

Among them, the spatial weight matrix w is a real symmetric matrix. The elements on the main diagonal indicate the distance of the same area, and $W_{11} = \ldots = W_{nn} = o$ indicates that the distance between the same area is 0. The most commonly used distance function is "adjacent", that is, if the area i and the area j have a common boundary, when it is expressed by the indicator function (also called the Heavyside function), $w_{ij} = l$, otherwise, $w_{ij} = 0$. For the convenience of description, the vector Z can be used to represent the attribute variable of the space object, $Z = (x_1, x_2, x_3, \ldots . x_n)$.

When applying the model, the weight matrix should be subjected to "row standardization" processing. That is, each element in the matrix (denoted as $\overline{\overline{w_{ij}}}$) is divided by the sum of the elements in its row to ensure that the sum of the elements in each row is 1. The advantage of implementing row standardization is that if the row standardization matrix W is multiplied by z, the average value of the attribute values around each area can be obtained. The calculation formula for row standardization is as follows [17]:

$$w_{ij} = \frac{\overline{\overline{w_{ij}}}}{\sum_j \overline{\overline{w_{ij}}}}. \tag{3}$$

Similarly, for the space-time weight matrix, $W^{st}X$ is called the "spatial lag" of X, that is, the average value of X's surrounding attribute values. Since the sum of the elements in each row is 1, this means that the sum of the influences of its neighbors on the area i must be equal to the sum of the influences of its neighbors on the area j (any $i \neq j$).

There are two issues worthy of attention when carrying out the Moran's I spatial autocorrelation test in the traditional space. First, the value of Moran's I has a strong correlation with the spatial weight matrix W. If the weight matrix is not properly selected or set, unreasonable or false spatial autocorrelation results will be obtained. Second, the core component of Moran's I model is $(z_i - \overline{x})(z_j - \overline{x})$, which implicitly assumes that the expected value of $\{z_i\}_{i=1}^{n}$ is constant. Therefore, the premise of using this model is that there is no trend in the attribute value of the geospatial object, that is, it is stable in the spatial dimension.

In order to make the calculation results of the model more in line with reality, the appropriate spatial weight matrix should be selected first, or different spatial weight matrices should be used to examine the rationality and robustness of the results. Secondly, covariates can be introduced, the trend can be removed by the regression method, and Moran's I statistical test can be performed on the residual items. When performing statistical inference, it is necessary to make assumptions about the distribution of the spatial variable Z in advance. There are generally two assumptions: the first is to assume that the spatial variable Z obeys a normal distribution, and the second is to use randomization to get the approximate distribution of Z when the distribution is unknown. Under the two assumptions of normal distribution or random uniform distribution, the expected value and variance of the spatial autocorrelation coefficient are obtained and tested [18].

Under the assumption of normal distribution, the expected value and variance of Moran'sI are:

$$\begin{aligned} E_n(I) &= -\frac{1}{n-1}, \\ \mathrm{Var}_n(I) &= \frac{n^2 S_1 - n S_2 + 3S_0^2}{S_0^2 (n^2 - 1)} - E_n(I)^2. \end{aligned} \tag{4}$$

Under the assumption of random uniform distribution, the expected value and variance of Moran's I are:

$$E_R(I) = \frac{1}{n-1},$$
$$\mathrm{Var}_n(I) = \frac{n\left[\left(n^2-3n+3\right)S_1 - nS_2 + 3S_0^2\right] - k\left[\left(n^2-n\right)S_1 - 2nS_2 + 6S_0^2\right]}{(n-1)(n-2)(n-3)S_0^2} - E_R(I)^2. \tag{5}$$

Here $S_0 = \sum_{i=1}^{n}\sum_{j=1}^{n} w_{ij}$, $S_1 = (\sum_{i=1}^{n}\sum_{j=1}^{n}(w_{ij}+w_{ji})^2/2)$, $S_2 = \sum_{i=1}^{n}(\sum_{j=1}^{n} w_{ij} + \sum_{j=1}^{n} w_{ji})^2$. When n is large enough, Moran's I expectation is close to zero.

The value range of Moran's I is [−1, 1]. The closer the value is to ±1, the higher the spatial autocorrelation; when the value of Mroan's I is greater than its expected value, the adjacent area or position. The attribute values of both tend to be similar, showing a positive autocorrelation: when the value of Moran's I is less than its expected value, the variable attribute values in adjacent areas or locations tend to be different, showing a negative autocorrelation. When Moran's I>0, it indicates a positive correlation, that is, areas with high attribute values are clustered with areas with high attribute values (high-high aggregation, or IHIH aggregation for short), and areas with low attribute values are clustered with areas with low attribute values. (Low low poly, LL aggregation for short), as shown in Figure 1(a). The closer Moran's I is to 1, the higher the degree of spatial aggregation and the smaller the overall spatial difference; on the contrary, when Moran's I <0, it indicates a negative correlation, and the attribute values of the observation unit present a discrete spatial pattern, as shown in Figure 1(b) Shown. The closer Moran's I is to −1, the greater the overall spatial difference. When Moran's-0, the observed variables are independent of each other, and there is no spatial autocorrelation in the attribute values of the observation units, and they are randomly distributed in space. At this time, Moran's I is close to $-1/(n-1)$, as shown in Figure 1(c) as shown [19].

If it is assumed that the observed variable does not have spatial autocorrelation in space, but presents a random distribution, in the statistical test, the standardized Moran's I value is generally used, namely [20]:

$$Z(I) = \frac{[I - E(I)]}{\sqrt{\mathrm{Var}(I)}}. \tag{6}$$

Among them, *E(I)* is Moran's I expected value of spatial autocorrelation, var(I) and *S(I)* represent the variance and standard deviation of spatial autocorrelation Moran's I, respectively. *Z(I)* is a multiple of the standard deviation. It is used to test the size of the spatial autocorrelation.

At the 0.05 confidence level, $|Z(I)| = 1.96$. $Z(I) > 1.96$ means: there is a significant positive correlation between the observed variables. That is, high observations and high observations have spatial aggregation (HH), and low observations and low observations have spatial aggregation (LL), which presents a spatial aggregation distribution. $|Z(I)| < -196$ means: there is a significant negative correlation between observations, that is, high observations and low observations are clustered together (HL), and low observations and high observations are clustered together (LH), which presents an abnormal spatial distribution. $|Z(I)| < 1.96$ means: the correlation of the spatial observation variable is not significant, and it presents an independent random distribution in the region.

The global spatial autocorrelation statistics are based on the implicit assumption of spatial stationarity, that is, the expected value and variance of the attribute values of the observed variables at all positions are constant. However, most of the geospatial processes are non-stationary, especially when the amount of data is very large, the requirement of spatial stability becomes very unrealistic. From the perspective of the research area, there are often different degrees of spatial autocorrelation among spatial elements. This phenomenon is also called Spatial heteroge-neity. Local spatial autocorrelation statistics can identify different spatial association patterns (or spatial aggregation patterns) that may exist at different spatial locations. Therefore, observing the local instability at different spatial locations can find spatial heterogeneity between data. It is this spatial heterogeneity that provides the basis for the classification or division of spatial patterns.

In essence, the local space Moran's I model decomposes the global space Moran's I model into various regional units. For a certain space i, local Moran's I is expressed as follows [21]:

$$I_t = \frac{(x_i - \overline{x})\sum_{j=1}^{n}\left(x_j - \overline{x}\right)}{(1/n)\sum_{i=1}^{n}(x_i - \overline{x})}. \tag{7}$$

When $I_t > 0$, it means that the spatial objects with similar observation values are in a clustered state in space, which can be high-value clustering or low-value clustering, and this phenomenon is called "cluster". Conversely, when I0, it means that the spatial objects with dissimilar observations gather in space, and this phenomenon is called "outlier". The so-called "cluster" or "outlier" only represents the deviation state of the attribute value of the spatial unit, and does not represent the geographical distribution of the spatial objects.

The exact distribution form of local Moran's I statistic is generally unknown, and its test usually adopts conditional randomization or random arrangement method. Conditional randomization refers to the empirical distribution

1	1	1	0	0	0
1	1	1	0	0	0
1	1	1	0	0	0
1	1	1	0	0	0
1	1	1	0	0	0
1	1	1	0	0	0

(a)

1	0	1	0	1	0
0	1	0	1	0	1
1	0	1	0	1	0
0	1	0	1	0	1
1	0	1	0	1	0
0	1	0	1	0	1

(b)

1	0	1	1	0	1
0	1	0	0	1	0
1	0	1	1	0	0
0	0	1	0	0	1
0	0	0	0	0	0
1	1	1	1	0	0

(c)

Figure 1: Schematic diagram of spatial autocorrelation positive and negative Moran's (I) (a) $t > 0$, (b) $t < 0$, (c) $t = 0$.

function that fixes the observation value of the position and arranges other observation values randomly in the entire space position.Under the assumption of complete randomness, the mean and variance of I_t are respectively;

$$E(I_t) = -\frac{W_i}{n-1}, \tag{8}$$

$$\mathrm{Var}_n(I_t) = -\frac{(n-a)W_i^{(2)}}{n-1} + \frac{(2a-n)\left(W_i^2 - W_i^{(2)}\right)}{(n-1)(n-2)} - E(I_t)^2. \tag{9}$$

In the above formulas (8) and (9), $W_i = \sum_{j=1}^{n} W_{ij}$, $W_i^{(2)} = \sum_{j=1}^{n} W_{ij}^2$, and $a = (n\sum_{t=1}^{n}(z_t - \overline{z})^4 / [\sum_{t=1}^{n}(z_t - \overline{z})^2]^2)$.

The constructed test statistics are:

$$Z_t = \frac{[I_t - E(I_t)]}{\sqrt{\mathrm{Var}(I_t)}}. \tag{10}$$

In addition, Moran scatter plots can also identify spatial anomalies and local instabilities. The Moran scatter diagram describes the correlation between the observation vector Z of a certain unit and its spatial lag vector *WZ* (that is, the weighted average of the observation values of the surrounding units of the space unit). For example, the Moran scatter corresponding to (*Z*, *WZ*) In the dot plot, the slope corresponding to the straight line fitted by the scatter points is the size of the global Moran'sI value. Because the data set (*Z*, *WZ*) is processed by row standardization, the results at different times are comparable Sex.

The Moran scatter diagram has 4 quadrants, which correspond to the 4 local spatial connection forms between the regional unit and its neighbors: the first quadrant represents the high observation value of the regional unit and the surrounding area is high (HH); the second quadrant represents The area around the area unit with low observation value is high value (LH): the third quadrant represents the area around the area unit with low observation value is the same as the low value (LL); the fourth quadrant

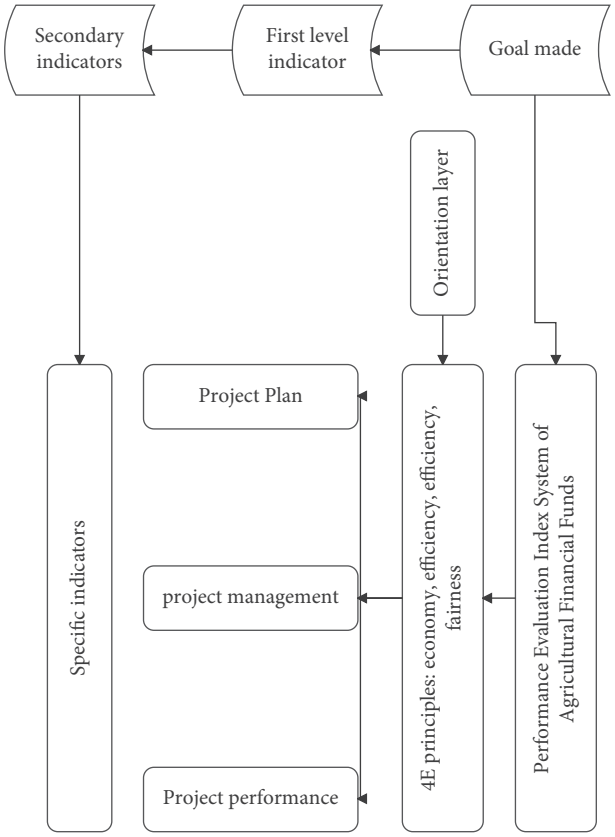

Figure 2: Schematic diagram of the idea of constructing the evaluation index system.

represents the area around the area unit with high observation value It is a low value (HL).

Compared with the local Moran's I, the advantage of the Moran scatter plot is that it can further specifically distinguish which spatial association mode among the HH, LL, HL, and LH the observation values between the regional unit and its adjacent units belong. Therefore, according to the different quadrants of the data points (*Z, WZ*) in the Moran scatter diagram, it is possible to identify what kind of spatial distribution the observed value of the research object of the regional unit belongs to.

4. Case analysis of performance evaluation of agricultural financial funds

This article takes the A region as an example to conduct a case study. Taking into account the characteristics of agricultural financial funds, scientificity and operability, this paper draws up the dimensions and structure of agricultural financial expenditure performance evaluation, as shown in Figure 2, which includes three dimensions: project plan, project management, and project performance.

According to the statistical data of expert judgment, we first construct the judgment matrix A of the first-level index, as shown in Table 1, and carry out the consistency test.

We get that W(A1) =0.1841, W(A2) =0.3062, W(A3) =0.5113, CI=0.011, CR=0.0306. Therefore, CR<0.1, which proves that the judgment matrix has good consistency, can pass the test, and the weight distribution of each first-level indicator is reasonable, as shown in Table 2.

The first step is to construct a paired comparison matrix B by judging the importance of the two factors. Numbers are used as a scale to judge the relative importance of two factors and the two factors are compared one by one to form a paired comparison matrix, as shown in Table 3.

The second step is to calculate the weights through the consistency check method and judge the rationality of the index weight settings. Using YAAHP software, the following results are obtained: W(B1) =0.1634, W(B2) =0.2970, W(B3) =0.5396, CI=0.0046, CR=0.0079. We define the consistency ratio as CR=CI/RI. When analyzing the paired comparison matrix B, we take 0.1 as the boundary value. When its value is below the boundary value, it is considered to have a certain degree of consistency. Otherwise, it is necessary to reconstruct the comparison matrix B to adjust the relative importance of each index. CR < 0.1, so the hierarchical ranking passes the consistency test. The consistency test and index score calculation table are shown in Table 4 below.

We choose Area A from January 2020 to May 2021 for 26 projects, involving agricultural technology promotion, green food, agricultural information, planting, breeding, agricultural talent training, and agricultural land planning. Due to the large number of projects, in order to facilitate the visual display of related data and layout, 26 projects are replaced by projects 1 to 26.

Table 1: Pairwise comparison matrix A.

	Project plan (A1)	Project management (A2)	Project performance (A3)
Project plan (A1)	1	1/2	1/4
Project management (A2)	2	1	1/2
Project performance (A3)	4	2	1

Table 2: Consistency test and index score calculation table.

Index layer	Weight	Score
Project plan	0.1841	20
Project management	0.3062	30
Project performance	0.5113	50

Table 3: Pairwise comparison matrix B.

	Management system	Financial management	Business management
Management system	1	1/2	1/3
Financial management	2	1	1/2
Business management	3	2	1

Table 4: Consistency test and index score calculation table.

Index layer	Weight	Score
Management system	0.1634	5
Financial management	0.297	9
Business management	0.5396	16

Table 5: Self-assessment and empirical average scores.

NO	Self-evaluation	Empirical	NO	Self-evaluation	Empirical
1	95.56	90.71	14	95.09	90.28
2	93.57	92.44	15	94.19	92.13
3	93.90	91.42	16	93.41	92.25
4	93.31	92.61	17	92.12	91.96
5	95.72	90.54	18	92.22	89.58
6	94.95	89.31	19	95.05	90.37
7	94.85	92.87	20	94.53	89.71
8	95.47	91.35	21	95.67	90.85
9	93.56	89.51	22	94.35	89.49
10	94.03	91.22	23	92.31	91.42
11	93.70	89.62	24	95.86	89.11
12	94.01	91.90	25	92.93	89.76
13	93.87	90.42	26	94.45	91.16

From the perspectives of self-evaluation and third-party evaluation of the project unit, performance evaluation empirical studies are carried out, and there are still some differences in the evaluation scores. Unit self-assessment is to better obtain basic information, self-assessment reports, key supporting materials, etc. of various fund authorities and user units for reference. By carrying out third-party evaluation and combining with the self-evaluation results of the project unit to form a comparison, it will help to further discover problems and differences and make up for the lack of self-evaluation, as shown in Tables 5 and 6, and Figures 3 and 4.

From the above experimental research, it can be seen that when each unit conducts project self-evaluation, there is a tendency to score in a good direction as much as possible. However, the performance evaluation carried out from the

Table 6: Comparison of self-assessment and empirical performance levels.

Grade	Self-evaluation	Empirical
1	0	0
2	0	0
3	0	0
4	0	0
5	0	0
6	0	1
7	2	3
8	2	2
9	5	6
10	17	14

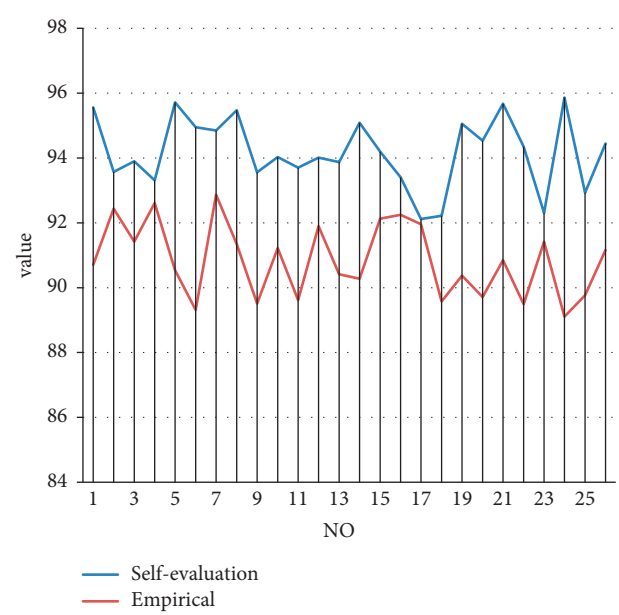

Figure 3: Line chart of self-evaluation and empirical scores.

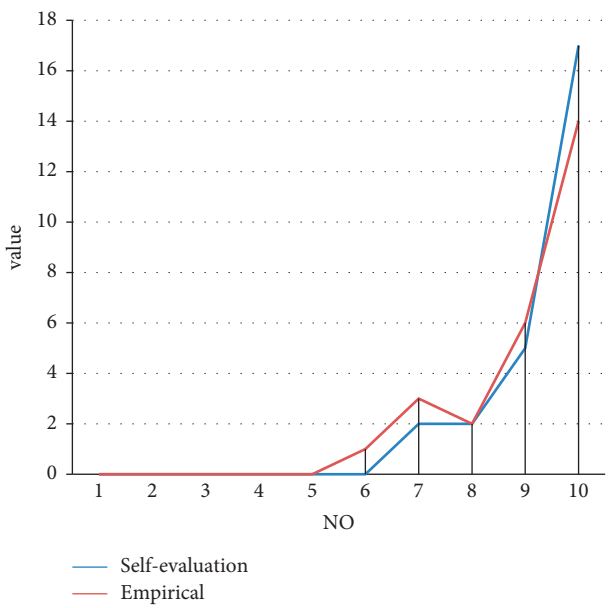

Figure 4: Line chart of comparison of self-assessment and empirical performance ratings.

perspective of a third party can more objectively and reasonably examine the actual overall performance of the agricultural financial fund project.

5. Conclusion

The performance of agricultural financial funds has a bearing on agriculture, rural areas and farmers, as well as the implementation of rural revitalization strategies. By strengthening the performance evaluation of agricultural financial funds, the efficiency of the use of funds can be improved, and performance management can better serve budget management. It is necessary to promote budget units to establish budget performance management concepts, effectively improve the important role of performance evaluation in daily management, ensure the safe and efficient use of financial funds, and continuously expand performance evaluation models. At the same time, it is necessary to improve the quality of performance evaluation, make full use of the results of performance evaluation, and continuously improve the efficiency of the use of financial funds, so as to achieve the goals of promoting the change of the government's governance concept, strictly controlling the budget, establishing a responsible government, and providing effective public services. This paper combines smart big data technology to evaluate the performance of agricultural financial funds. Moreover, this paper proposes several improvement measures including improving the performance evaluation organization system, attaching importance to the preliminary project demonstration and indicator design, strengthening the process supervision of project performance and funds, and expanding the output and benefits of agricultural financial funds.

Data Availability

The experimental data used to support the findings of this study are available from the corresponding author upon request.

Conflicts of Interest

The author declared that there are no conflicts of interest regarding this work.

References

[1] M. Sultan, T. Miyazaki, S. Koyama, and Z. M. Khan, "Performance evaluation of hydrophilic organic polymer sorbents for desiccant air-conditioning applications," *Adsorption Science and Technology*, vol. 36, no. 1-2, pp. 311–326, 2018.

[2] B. Haralayya, "Financial statement analysis of shri ram city union finance," *Iconic Research And Engineering Journals*, vol. 4, no. 12, pp. 183–196, 2021.

[3] Z. Kish and M. Fairbairn, "Investing for profit, investing for impact: moral performances in agricultural investment projects," *Environment and Planning: Economy and Space*, vol. 50, no. 3, pp. 569–588, 2018.

[4] A. Varghese, P. Sibby, and K. Jayakumar, "IPO mobilisation and allocation: an empirical analysis," *Mukt Shabd Journal*, vol. 9, no. 4, pp. 3462–3472, 2020.

[5] Y. Aleskerova, T. Mulyk, and L. Fedoryshyna, "Improving credit protection analysis methods Reports of main agricultural enterprises," *Baltic Journal of Economic Studies*, vol. 4, no. 2, pp. 1–7, 2018.

[6] P. He, H. Niu, Z. Sun, and T. Li, "Accounting index of COVID-19 impact on Chinese industries: a case study using big data portrait analysis," *Emerging Markets Finance and Trade*, vol. 56, no. 10, pp. 2332–2349, 2020.

[7] A. A. A. Matrood and A. Rhouma, "Penicillium and Aspergillus species characterization: adaptation to environmental factors and sensitivity to aqueous medicinal plants extracts," *Review of Plant Studies*, vol. 8, no. 1, pp. 1–11, 2021.

[8] H. Jia, Z. Wang, X. Zhen, M. Clar, and S. L. Yu, "China's sponge city construction: a discussion on technical approaches," *Frontiers of Environmental Science & Engineering*, vol. 11, no. 4, pp. 18–11, 2017.

[9] G. Pe'er, A. Bonn, H. Bruelheide et al., "Action needed for the EU Common Agricultural Policy to address sustainability challenges," *People and Nature*, vol. 2, no. 2, pp. 305–316, 2020.

[10] J. D. Sachs and G. Schmidt-Traub, "Global fund lessons for sustainable development goals," *Science*, vol. 356, no. 6333, pp. 32-33, 2017.

[11] F. C. Tseng, M. H. Huang, and D. Z. Chen, "Factors of university–industry collaboration affecting university innovation performance," *The Journal of Technology Transfer*, vol. 45, no. 2, pp. 560–577, 2020.

[12] V. B. Nakku, F. W. Agbola, M. P. Miles, and A. Mahmood, "The interrelationship between SME government support programs, entrepreneurial orientation, and performance: a developing economy perspective," *Journal of Small Business Management*, vol. 58, no. 1, pp. 2–31, 2020.

[13] B. Batchimeg, "Financial performance determinants of organizations: the case of Mongolian companies," *Journal of competitiveness*, vol. 9, no. 3, pp. 22–33, 2017.

[14] G. N. S. Miller and C. C. Morphew, "Merchants of optimism: agenda-setting organizations and the framing of performance-based funding for higher education," *The Journal of Higher Education*, vol. 88, no. 5, pp. 754–784, 2017.

[15] M. Ibert, R. Kaniel, S. V. Nieuwerburgh, and R. Vestman, "Are mutual fund managers paid for investment skill?" *Review of Financial Studies*, vol. 31, no. 2, pp. 715–772, 2018.

[16] P. E. Hulme, G. Brundu, M. Carboni et al., "Integrating invasive species policies across ornamental horticulture supply chains to prevent plant invasions," *Journal of Applied Ecology*, vol. 55, no. 1, pp. 92–98, 2018.

[17] B. Aydoğan and G. Vardar, "Evaluating the role of renewable energy, economic growth and agriculture on CO_2 emission in E7 countries," *International Journal of Sustainable Energy*, vol. 39, no. 4, pp. 335–348, 2020.

[18] I. Mocanu, I. Grigorescu, B. Mitrică, E. A. Popovici, and M. Dumitraşcu, "Regional disparities related to socio-economic determinants of agriculture in the Romanian Plain," *Journal of Urban and Regional Analysis*, vol. 10, no. 1, pp. 79–99, 2018.

[19] A. C. Ruane, J. Antle, J. Elliott et al., "Biophysical and economic implications for agriculture of +1.5° and +2.0°C global warming using AgMIP Coordinated Global and Regional Assessments," *Climate Research*, vol. 76, no. 1, pp. 17–39, 2018.

[20] W. Khan and S. A. Ansari, "Does agriculture matter for economic growth of Uttar Pradesh (India)?" *Economy of Region*, vol. 14, no. 3, pp. 1029–1037, 2018.

[21] M. Paul, "Community-supported agriculture in the United States: social, ecological, and economic benefits to farming," *Journal of Agrarian Change*, vol. 19, no. 1, pp. 162–180, 2019.

Hindawi
Mobile Information Systems
Volume 2022, Article ID 6974246, 12 pages
https://doi.org/10.1155/2022/6974246

Research Article

Intelligent Financial Processing Based on Artificial Intelligence-Assisted Decision Support System

Xinyu Zhao [1] **and Omer Saeed** [2]

[1] *School of Mathematics, Liaoning Normal University, Dalian, Liaoning 116029, China*
[2] *Institute of Management, Kyrgyz International Universal College, Bishkek, Kyrgyzstan*

Correspondence should be addressed to Xinyu Zhao; zhaoxinyu161@163.com and Omer Saeed; omersaeed@mail.cu.edu.kg

Received 30 May 2022; Revised 9 July 2022; Accepted 19 July 2022; Published 8 August 2022

Academic Editor: Chi Lin

In order to improve the effect of intelligent financial processing and decision-making, this paper combines the artificial intelligence-assisted decision support system to construct an intelligent financial processing system. Based on the RBF neural network, this paper studies a fast decision-making algorithm based on short-term efficiency in an adaptive burst communication system. The trained RBF neural network can make quick decisions according to the parameters such as the electromagnetic environment information obtained by perception, and has good communication anti-interference ability, good fault tolerance ability and certain generalization ability. Moreover, this paper designs a channel-associated signaling transmission mechanism for adaptive burst communication system, and constructs an intelligent financial processing system based on artificial intelligence-assisted decision support system. The simulation results show that the intelligent decision-making model in this paper has a certain practical effect in the simulation.

1. Introduction

In the process of the continuous development of the globalization of the world economy, the market competition is becoming more and more fierce, and the use of modern science and technology can reasonably manage the company's operation and capital investment. However, the company operates with a relatively large amount of data. For finance, how to analyze the meaning of the data and solve the information association is the main consideration. Moreover, due to the development of computer technology, information processing technology has developed faster, and accounting models are used to deal with traditional complex financial problems. As the development of computer technology has promoted the development of information processing technology, traditional and complex financial problems can be solved by creating accounting models. At the same time, financial management in the new modern society has changed. The original accounting information base has certain limitations, and neither accounting nor financial analysis can meet the actual needs of managers. Artificial intelligence technology can solve this problem very well. Moreover, the traditional accounting-based accounting is developing towards the network, and the financial intelligent decision support system is analyzed, so as to realize the corresponding decision-making and management of the enterprise.

To solve these problems, the intelligence of the financial decision support system is an inevitable way. The deep learning and autonomous learning, natural language processing, data mining, and reasoning perception and other functions that artificial intelligence has developed up to now are the mechanisms and implementation paths of the financial decision support system. Perfection provides ideas. Smart finance can be traced back to the 1980s. Scholars at home and abroad have conducted a lot of research on the definition, characteristics and standards of intelligent finance, which enriches and promotes the theoretical development of intelligent finance management. In the era of big data, intelligent finance has developed rapidly, and the

cloud-based financial robot has been released, making finance more focused on the company's strategic finance and business financial decision-making; UFIDA Cloud Finance uses global treasury, intelligent finance and real-time accounting. Combination as the core, supported by technologies such as artificial intelligence and financial sharing, provides targeted solutions for enterprise cost accounting, financial management and investment financing.

With the gradual increase in the application of big data in various fields of society, the advantages of intelligent finance are also reflected in the real-time interaction of information in the cloud with audit institutions, tax agencies, the China Securities Regulatory Commission and other third-party service agencies, making it more convenient and fast for enterprises. Financial work gives services and support. A large amount of data is generated in the business and operation of an enterprise every day, and what the enterprise needs to do is to analyze the data and use it after processing. For the development of the enterprise, financial personnel should actively improve their use of data analysis tools and analysis. The ability of data to form an efficient service team.

This paper combines the artificial intelligence assisted decision support system to construct an intelligent financial processing system to improve the effect of enterprise financial processing, which provides a theoretical reference for subsequent enterprise financial decision-making.

2. Related Work

Although the term "smart finance" has been born for a long time, the academic community has not given a clear and authoritative definition for it. According to the analysis of "smart finance" by academic researchers, it is usually defined as [1]: Intelligent finance is to carry out the company's financial management activities through the organic cooperation of man and machine, and gradually improve and develop until it can gradually replace some full-time financial personnel to carry out financial management behavior. In short, "smart finance" is a brand-new financial management method. It is based on the latest financial management theories and financial tools. It is a new model with significant advantages such as full-function and whole-process intelligent management [2]. Literature [3] pointed out that intelligent finance mainly takes finance as the core. In the traditional financial category, it is generally divided into two branches: finance and accounting. Among them, accounting is the management of bookkeeping, which converts unstructured information into data and provides accounting reports to external users; finance is financial management. The analyzed financial data information is provided to the internal management personnel of the enterprise, and then it is used in decision-making. With the development of Internet technology, the functions of finance and accounting in enterprises are becoming more and more blurred. The rapid development of enterprises has made it impossible to strictly distinguish between finance and accounting, and it is necessary to re-understand and define enterprise finance [4].

Literature [5] found that the reason why financial management adopts intelligent financial decision support system is that the enterprise has a high degree of business structure. And through the design and development of the intelligent decision support system, it plays an important role in promoting the development of financial management in a better direction [6]. Based on the analysis of the nature of decision-making, it is mainly composed of three types: ① semi-structured decision-making; ② structured decision-making; ③ unstructured decision-making. Intelligent financial management mainly solves semi-structured decision-making and unstructured decision-making problems [7]. Literature [8] believes that intelligent finance includes three branches: first, the intelligent management accounting platform based on business intelligence, which occupies a core position in the field of intelligent finance; The basic department of finance; third, the intelligent financial platform based on artificial intelligence, which represents the in-depth development of intelligent finance, but this expression lacks the internal logical relationship between the three levels. Literature [9] pointed out that the construction of enterprise intelligent finance is analyzed from two aspects of enterprise data and business process. One is to decompose the business process, integrate the activity process that can create value, deeply realize the integration of business and finance, and then improve its intelligent process. The second is the construction of a big data management system, to achieve the full integration of financial data and business data, and to enhance the data management and analysis capabilities of enterprise value creation activities.

The rapid development of economic globalization and big data has made intelligent financial applications mature, and in this development process, the development trend of intelligent finance has emerged. In addition to the general influence of laws and regulations related to smart finance, the needs of enterprises themselves, the development of new science and technology, and the speed of research and development of smart financial systems will have a great impact on the future development trend of smart finance [10]. Reference [11] pointed out that under the background of the vigorous development of financial cloud and big data, the financial information system of enterprises does not need to be purchased outright, nor does it need to arrange a large number of personnel for system maintenance, but directly rent the financial information of software manufacturers service can be. The benefits brought by this streamlined approach to enterprises are also obvious: first, it can reduce the hardware investment and operation and maintenance investment required by enterprises to build information systems, and turn to software service providers to provide professional operation and maintenance and services in the cloud; second It enables all the financial cloud services used by enterprises to be the latest version, and there is no need to spend time and extra money to update and upgrade [12]. With the gradual increase in the application of big data in various fields of society, the advantages of intelligent finance are also reflected in the real-time interaction of information in the cloud with audit institutions, tax agencies, the China Securities Regulatory Commission and

other third-party service agencies, making it more convenient and fast for enterprises. Financial work gives services and support. A large amount of data is generated in the business and operation of an enterprise every day, and what the enterprise needs to do is to analyze the data and use it after processing. For the development of the enterprise, financial personnel should actively improve their use of data analysis tools and analysis. The ability of data to form an efficient service team [13]. Reference [14] pointed out that financial outsourcing business will be affected by intelligent finance. The development of intelligent finance has led to an increase in outsourcing business. Many small and medium-sized companies do not have the ability to conduct independent accounting. Therefore, outsourcing financial work to firms such as firms can effectively reduce costs [15]; for large and medium-sized enterprises, financial sharing the development of services can also bring convenience to them. The main operation steps are as follows: First, write a smart contract through the blockchain, and the other party, as Party *B*, accepts the work tasks issued by Party *A*, and at the same time completes the work according to the specific terms of the contract, and Party *A* according to the workload To pay the salary, it should be noted that Party *A* should determine the work quality assesment specifications in the blockchain in advance, and the accounts of both parties need to be clearly registered. When Party B achieves the work goals on time and passes the assessment requirements, the pre-filled smart contract will be signed. Transfer the salary to Party *B*'s account [16]. In the blockchain, the secret code of the smart contract is compiled according to the code of the computer, and the entire transaction is not controlled by human beings, but is completed automatically by the computer, which can protect the interests of both parties [17]. Reference [18] pointed out that the application scope of financial intelligence will continue to expand in the future, and intelligent robots can replace financial personnel to complete simple and repetitive financial tasks, such as bookkeeping, account reconciliation and reimbursement work. At the same time, the blockchain system can directly connect with the uploaded account book. Although financial personnel can record and backup in the system, they cannot modify the account book privately. In addition, blockchain can also ensure the smooth signing of smart contracts. The signing time is set in advance in the system, and then the system will strictly abide by the agreed time to realize the orderly development of the signing work [19].

3. Intelligence-Assisted Decision-Making Algorithm

The decision-making mechanism of the burst communication system is shown in Figure 1, and the main functions are as follows:

(1) It obtains the working electromagnetic environment information (channel quality, interference characteristics, etc.) of the burst communication system through spectrum resource sensing. According to the information in the knowledge base (spectrum allocation, platform capabilities, regulatory policies, interference characteristics, etc.), this information is mapped to system state parameters;

(2) Based on the results of policy decision-making and spectrum resource perception and identification, it adopts a policy-based decision-making algorithm to make decisions on the system parameter configuration under the support of the policy library, and adjusts the parameter configuration according to the transmission performance information fed back;

(3) It makes quick decisions based on short-term performance, adopts neural network algorithm, and trains the neural network under the database constructed by historical transmission performance. Moreover, it uses the results of spectrum resource perception and recognition as the input of the neural network to make quick decisions, and can quickly obtain effective system parameter configuration;

(4) It evaluates the generated anti-jamming strategy according to the feedback performance results, and updates the database for the strategy that meets the anti-jamming requirements of the burst communication system.

The input of the decision mechanism is: interference type, interference parameters, link quality and performance evaluation parameters. Link quality and transmission performance evaluation parameters include transmit power, estimated Signal-to-Noise Ratio (SNR) value, synchronization detection correlation value, bit error rate, waveform efficiency, and recognition rate. The output is: transmit power, interference processing method and frequency selection, etc.

The block diagram of the decision engine in this paper is shown in Figure 2. When the perceptron receives external information (interference type, interference parameters, link quality, etc.), with the support of the database, the fast decision-making unit based on short-term efficiency is preferentially used for decision-making, and the parameters are configured after the decision-making result is obtained. After the performance feedback is obtained, if the feedback result does not meet the performance requirement, the policy-based decision-making is used as the correction unit to make a new decision until the feedback result meets the performance requirement. The results of this decision are stored in the database in the form of cases, and the database is continuously enriched to continuously improve the learning ability of the system.

The short-term performance-based fast decision unit employs a neural network algorithm (NN) algorithm, which is used to make fast and optimal decisions. The neural network can be trained in advance, extract the required knowledge, and use it directly when a decision is needed, which greatly reduces the decision-making time.

The decision correction unit adopts the Policy-Based Decision (PBD) algorithm to provide backup support in the case of failure of search decision and fast decision. Although the process is slow, it has a feedback mechanism, which can

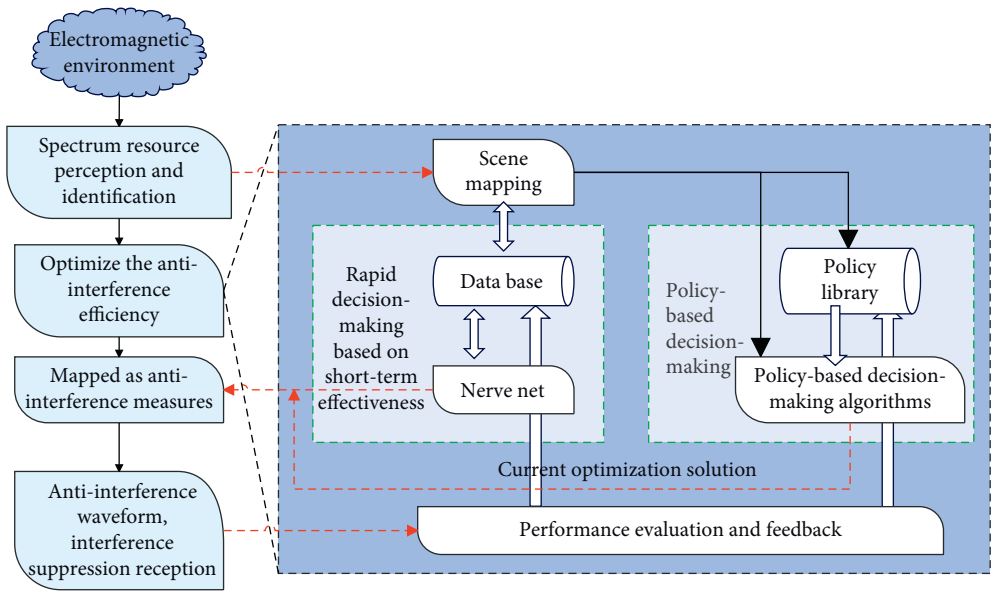

Figure 1: Working principle of the decision-making mechanism of the burst communication system.

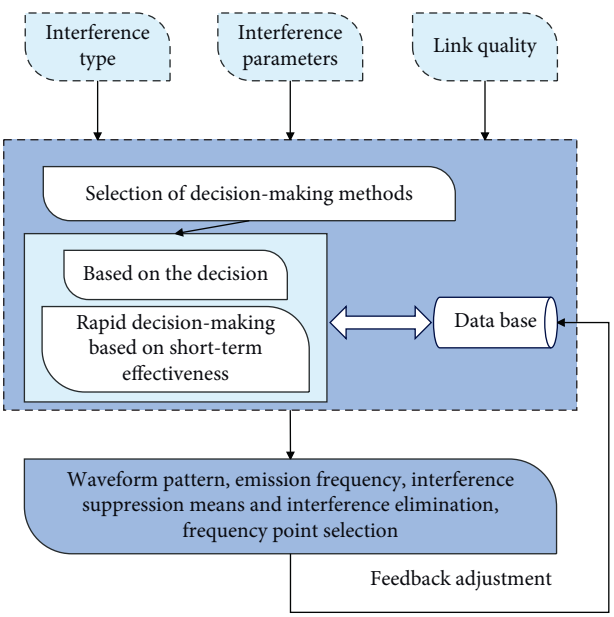

Figure 2: Decision engine block diagram.

monitor the system performance in real time, interact with the environment in an unknown environment, and decide the optimal parameter configuration in the current environment.

According to the goal of realizing the communication with the largest recognition rate with the minimum power consumption and the complexity of the interference suppression and elimination means, the anti-interference performance index and objective function are designed based on parameters such as transmit power, bit error rate, complexity of interference suppression and elimination methods, and recognition rate. Since the dimensions and variation ranges of different indicators are different, all indicators are first de-dimensioned and normalized.

(1) Normalization of minimizing bit error rate.

The bit error rate (BER) is the ratio of the number of bits in a digital signal received in error over a period of time to the total number of bits in the digital signal received at the same time. The de-dimensionalized normalized value of the average bit error rate during the inquiry and response process is shown in the following formula:

$$f_b = \frac{\log_{10} P_{b_{\max}} - \log_{10} P_b}{\log_{10} P_{b_{\max}} - \log_{10} P_{b_{\min}}}. \quad (1)$$

Among them, f_b represents the normalization parameter that minimizes the average bit error rate of the query and response, the average bit error rate of the query and response is $P_b = P_{b1} + P_{b2}$, P_{b1} and P_{b2} represent the bit error rate of the query and response process, respectively. When the synchronization of the inquiry process is unsuccessful, $P_{b1} = 0.5$, and when the synchronization of the response process is unsuccessful, $P_{b2} = 0.5$. We define $P_{b_{\max}} = 0.5, P_{b_{\min}} = 10^{-7}$.

(2) Normalization of minimizing transmit power

The de-dimension normalization of the transmit power P at the transmitter is as follows:

$$f_P = \frac{\log_{10} P_{\max} - \log_{10} P}{\log_{10} P_{\max} - \log_{10} P_{\min}}. \quad (2)$$

Among them, $P_{\max} = 2200\text{W}, P_{\min} = 1800\text{W}$, f_P is the normalized value to minimize the transmit power.

(3) Minimize the complexity of interference processing means

C is the complexity of the interference processing means, which is calculated according to the

complexity of the interference suppression and interference cancellation algorithms. The de-dimensionalized normalization of the complexity of the interference suppression and cancellation means is shown in the following formula:

$$f_C = \frac{C_{\max} - C}{C_{\max} - C_{\min}}. \tag{3}$$

(4) Maximize the average transmission accuracy.

The average transmission accuracy rate is an indicator to measure the recognition rate. The transmission accuracy rate is the average value of the transmission accuracy rate in the query process and the transmission accuracy rate in the response process. The de-dimension normalization process is shown in formula (4).

$$f_R = \frac{R^2 - R_{\min^2}}{R_{\max^2} - R_{\min^2}}. \tag{4}$$

Among them, R is the average transmission accuracy rate $R_{\min} = 0, R_{\max} = 1$.

The goal of this system is to achieve the communication with the largest recognition rate with the smallest power consumption and the smallest complexity of the interference processing means. Therefore, the objective function needs to comprehensively consider the transmission performance, the transmission power and the complexity of the anti-interference means.

(1) Simulation objective function.

In this paper, the simulation objective function is used as the short-term performance. The bit error rate of the communication system can be obtained during the simulation, and the transmission performance is represented by the bit error rate and the average transmission accuracy rate. At the same time, considering the transmit power and the complexity of the anti-jamming method, the design objective function is as follows:

$$E_o = w_b\overline{f_b} + w_R\overline{f_R} + w_P\overline{f_P} + w_C\overline{f_C}. \tag{5}$$

Among them, $\overline{f_b} + \overline{f_R} + \overline{f_P} + \overline{f_C}$ represents the de-dimensioned normalized value of the bit error rate of the query process, the average bit error rate of the response, the average transmission accuracy rate, the transmit power, and the complexity of the interference processing method, respectively. $w_b + w_R + w_P + w_C$ are the weight values of $\overline{f_b} + \overline{f_R} + \overline{f_P} + \overline{f_C}$, respectively.

(2) Decision objective function.

In the case of fast decision-making, since the bit error rate cannot be obtained, only the average transmission accuracy rate $\overline{f_R}$ is used to represent the transmission performance. The objective function is as follows:

$$E_f = w_R\overline{f_R} + w_P\overline{f_P} + w_C\overline{f_C}. \tag{6}$$

The block diagram of the fast decision-making algorithm based on short-term performance using neural network is shown in Figure 3. The decision algorithm mainly includes offline process and online process. In the offline process, the network model is established through the model parameters of the neural network, and the neural network is trained based on the data in the database until the network training reaches the standard. The neural network at this time can be directly used for real-time decision-making in the online process. First, the perceptron receives external information (interference type, interference parameters, link quality). Then, the external information is preprocessed to make it suitable for the neural network model designed in this paper, and then the processed information parameters are input into the neural network. The final decision outputs the optimized parameters in the current environment, including: selection of interference suppression and elimination methods, transmission power, etc. According to the feedback transmission performance, it is judged whether the decision parameters meet the current requirements, and the database is adjusted to enrich the content of the database.

RBF neural network is a fixed neural network with only 3 layers, including an input layer, a hidden layer and an output layer. Because the hidden layer unit of this kind of neural network uses radial basis function for calculation, it is called radial basis function neural network. The structure of the RBF neural network is shown in Figure 4:

The number of neurons in the input layer of the RBF neural network is the same as the dimension of the input vector, and the input layer is directly connected to the hidden layer. The input layer sends the input vector to the hidden layer, and the hidden layer uses the radial basis function to perform nonlinear processing on the input vector. The number of neurons in the hidden layer needs to be reasonably set according to the problem to be solved. In addition, the output layer performs weighted summation of the results of each neuron output in the hidden layer as the result of the network output layer, and the number of neurons in the output layer is determined by the dimension of the output vector. Since the number of neurons in the input layer and output layer of the RBF neural network is determined by the input and output vectors of the problem to be solved, the network size of the RBF neural network under a specific problem depends on the number of neurons in the hidden layer.

The hidden layer usually uses the Gaussian function as the radial basis function. For the input vector of dimension I: $\mathbf{x} = [x_1, x_2, \ldots, x_I]$, the output h_i of the ith neuron in the corresponding hidden layer is shown in formula (7):

$$h_i = \varphi_i(\mathbf{x} - \mathbf{c}_i) = \exp\left(-\frac{\|\mathbf{x} - \mathbf{c}_i\|^2}{2\sigma_i^2}\right). \tag{7}$$

Among them, $\mathbf{c}_i$ is the center of the basis function of the i-th neuron in the hidden layer, and σ_i is the width of the basis function of the i-th neuron. The output of the output

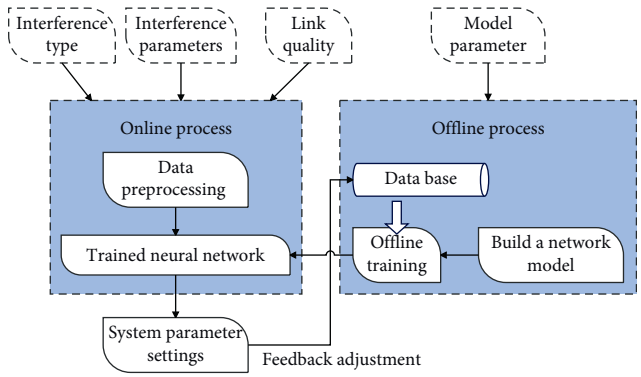

Figure 3: Block diagram of fast decision-making algorithm based on short-term performance using neural network.

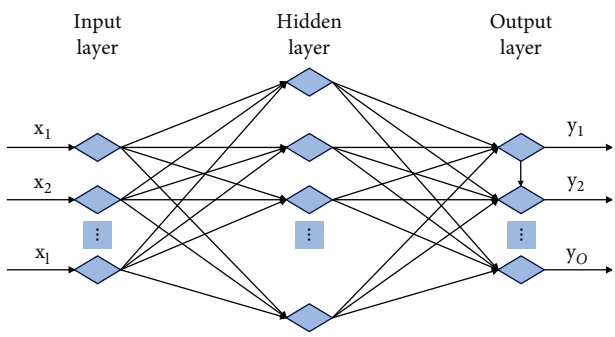

Figure 4: RBF neural network structure.

layer is the weighted sum of the outputs of each neuron in the hidden layer, that is, the expression of the output y_j of the j th neuron in the output layer is shown in formula (8):

$$y_j = \sum_i w_{ij} \exp\left(-\frac{\|\mathbf{x} - \mathbf{c}_i\|^2}{2\sigma_i^2}\right). \tag{8}$$

Among them, w_{ij} is the weight value of the i-th neuron in the hidden layer connecting the j-th neuron in the output layer.

It can be seen that the center of the basis function in the hidden layer and the weight value from the hidden layer to the output layer are two important parameters that need to be solved in the RBF neural network. In the RBF neural network algorithm, the K-means clustering algorithm is usually used to solve the base function center of the hidden layer, and the least squares method is usually used to solve the weight value connecting the hidden layer to the input layer.

The K-means clustering algorithm is a typical algorithm based on distance clustering. The main idea of the algorithm is to classify the sample points in the sample into the category of the nearest mean. The steps of the K-means clustering algorithm are as follows:

(1) The algorithm selects the initial K sample points as the initial cluster center $[\mathbf{c}_1(0), \mathbf{c}_2(0), \ldots, \mathbf{c}_K(0)]$;

(2) The algorithm calculates the Euclidean distance between each sample point in the sample and the cluster center;

(3) For each sample point, the algorithm selects the nearest cluster center point as the cluster center of the sample point to form K domains;

(4) The algorithm calculates the mean of all sample points in each domain as the new cluster center in the domain, replaces the old cluster center with the new cluster center and updates the cluster center $[\mathbf{c}_1(1), \mathbf{c}_2(1), \ldots, \mathbf{c}_K(1)]$. The algorithm repeats (2)–(4) until the cluster centers obtained twice before and after are the same, and then stop training;

(5) The algorithm takes the cluster center obtained by the last iteration as the basis function center $[\mathbf{c}_1, \mathbf{c}_2, \ldots, \mathbf{c}_K]$ of each neuron in the hidden layer.

After the basis function center $[\mathbf{c}_1, \mathbf{c}_2, \ldots, \mathbf{c}_K]$ of each neuron is obtained, the width of the basis function corresponding to each neuron can be calculated. The width of each basis function in the RBF neural network is the same, and the determination method is shown in formula (9):

$$\sigma_i = \frac{c_m}{\sqrt{2N}} \quad (i = 1, 2, \ldots, H). \tag{9}$$

Among them, c_m is the maximum Euclidean distance between the centers of each basis function, N is the number of input training samples, and H is the number of neurons in the hidden layer.

According to formula (8), it can be seen that the calculation of neurons in the output layer is a linear summation, and the weight value matrix $\mathbf{W}$ shown in formula (10) can be solved by the least square method:

$$\mathbf{W} = \begin{pmatrix} w_{11} & \cdots & w_{1O} \\ \vdots & \ddots & \vdots \\ w_{H1} & \cdots & w_{HO} \end{pmatrix}. \tag{10}$$

The core idea of the least squares method for solving weights is to minimize the l_2 norm of the residual between the actual output $\{\mathbf{y}^{(i)}\}_{i=1}^{N}$ and the expected output $\{\mathbf{a}^{(i)}\}_{i=1}^{N}$ of the network through learning. The weight at this time can be used as the weight from the hidden layer to the output layer of the network. The residual between the actual output and the expected output of the network is shown in formula (11):

$$\text{error}_i = \mathbf{y}^{(i)} - \mathbf{a}^{(i)} \quad , i = 1, 2 \ldots, N. \tag{11}$$

One half of the l_2-norm is shown in formula (12):

$$\begin{aligned} J(\mathbf{W}) &= \frac{1}{2}\sum_{i=1}^{N}\left(\mathbf{y}^{(i)} - \mathbf{a}^{(i)}\right)^2 \\ &= \frac{1}{2}\sum_{i=1}^{N}\left(\mathbf{W}^T\mathbf{h}^{(i)} - \mathbf{a}^{(i)}\right)^2 \quad , i = 1, 2 \ldots, N. \end{aligned} \tag{12}$$

Among them, $\mathbf{h}^{(i)}$ is the output $\mathbf{h}^{(i)} = [h_1^{(i)}, h_2^{(i)}, \ldots, h_H^{(i)}]^T$ of the hidden layer corresponding to the i-th training sample $\mathbf{x}^{(i)} = [x_1^{(i)}, x_2^{(i)}, \ldots, x_I^{(i)}]^T$. The input sample matrix is $\mathbf{X} = [\mathbf{x}^{(1)}, \mathbf{x}^{(2)}, \ldots, \mathbf{x}^{(N)}]^T$, the output sample matrix is $\mathbf{Y} = [\mathbf{y}^{(1)}, \mathbf{y}^{(2)}, \ldots, \mathbf{y}^{(N)}]^T$, the hidden layer output matrix is $\mathbf{H} = [\mathbf{h}^{(1)}, \mathbf{h}^{(2)}, \ldots, \mathbf{h}^{(N)}]^T$, and the expected output matrix is $\mathbf{A} = [\mathbf{a}^{(1)}, \mathbf{a}^{(2)}, \ldots, \mathbf{a}^{(N)}]^T$. The formula (12) can be written in the form of formula (13):

$$\begin{aligned} J(\mathbf{W}) &= \frac{1}{2} + \mathbf{Y} - \mathbf{A} +_2^2 \\ &= \frac{1}{2} + \mathbf{HW} - \mathbf{A} +_2^2 \\ &= \sum_{i=1}^{H}\frac{1}{2}\left\|\mathbf{Hw}_i - \mathbf{a}_i\right\|_2^2. \end{aligned} \tag{13}$$

Among them, the column vector $\mathbf{w}_i$ is the i-th column of the matrix $\mathbf{W}$, and the column vector $\mathbf{w}_i = \left\{w_i^{(j)}\right\}_{j=1}^{N}$ is the i-th column of the matrix A. The weight matrix $\widehat{\mathbf{W}}$ obtained based on the least squares method is shown in formula (14):

$$\widehat{\mathbf{W}} = \text{argmin}_{\mathbf{w}}\ J(\mathbf{W}). \tag{14}$$

The least squares solution $\mathbf{w}_i = \mathbf{H}^+\mathbf{a}_i$ of the equation system $\mathbf{Hww}_i = \mathbf{a}_i$ can make the value of $\|\mathbf{Hw}_i - \mathbf{a}_i\|_2^2$ the smallest, so the weight matrix $\widehat{\mathbf{W}}$ obtained from the solution is shown in formula (15):

$$\widehat{\mathbf{W}} = \mathbf{H}^+\mathbf{A}. \tag{15}$$

When the inverse of $\mathbf{H}^T\mathbf{H}$ exists, $\mathbf{H}^+$ can be written in the form of formula (16):

$$\mathbf{H}^+ = \left(\mathbf{H}^T\mathbf{H}\right)^{-1}\mathbf{H}^T. \tag{16}$$

For the RBF neural network algorithm, the parameter that has a greater impact on the decision-making performance is the network size. The number of neurons in the input layer and output layer of the RBF neural network depends on the dimensions of the input and output sample vectors. The mapping method between neurons and output parameters in the output layer can be mapping method 1: one neuron represents one parameter. It can also refer to the idea of one-hot coding and adopt mapping method 2: a neuron represents a possible value of a parameter. The M input parameters are $p_i\,(i = 1, \ldots, M)$, and the parameter $p_i\,(i = 1, \ldots, M)$ has m_i possible values $[p_i(1), p_i(2), \ldots, p_i(m_i)]$, and the specific mapping methods are shown in Figures 5 and 6 respectively.

In the mapping method 1, the output result of the neural network is continuous, while the value of each parameter in this model is discrete. Therefore, the value within the parameter value range $[p_i(1), p_i(2), \ldots, p_i(m_i)]$ that is closest to the actual output value of the neuron corresponding to the parameter $p_i\,(i = 1, \ldots, M)$ is taken as the value of the output parameter p_1. For example, the value range of parameter p_1 is [0, 1, 2, 3]. If the neuron output is 0.8, the value of the output parameter p_1 is 1.

In the mapping method 2 shown in Figure 6 , the neurons in the output layer are divided into M groups according to the output parameters, and the number of neurons in the i-th group and the number of possible values of the parameter p_i are m_i. According to the output value of each neuron in the group, the value of the neuron with the largest output value is set to 1, and the output value of the rest of the neurons in the group is set to zero. The parameter value corresponding to the neuron set to 1 is taken as the value of parameter p_i. For example, the value range of parameter p_1 is [0, 1, 2, 3], which means that the number of neurons in parameter p_1 is 4. If the output is [0.01, 0.07, 0.9, 0.2], the value of parameter p_1 is 2.

The input parameters of the RBF neural network in this paper are: interference type, interference feature and interference power, so the number of neurons in the input layer is 3. The output parameters are signal transmission power and interference processing mode, and there are 15 cases for the value of power. There are three types of interference processing methods: processing or not, interference suppression and interference cancellation. Therefore, if the output layer mapping method 1 is used, the number of neurons in the output layer is 2. If the output

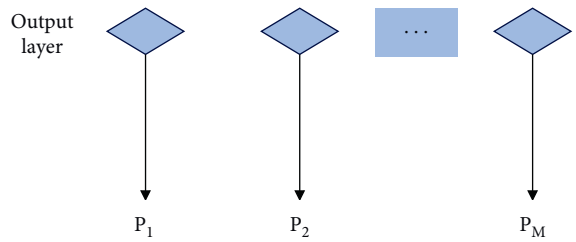

Figure 5: Output layer mapping method 1.

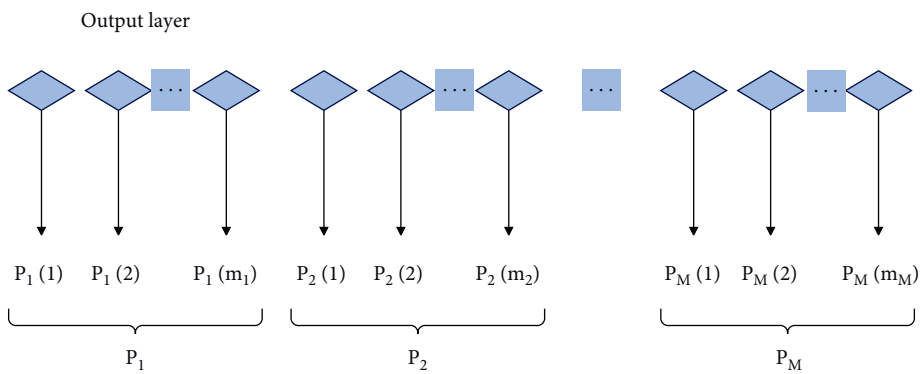

Figure 6: Output layer mapping method 2.

layer mapping method 2 is used, the number of neurons in the output layer is 18. The number of neurons in the hidden layer determines the complexity of the RBF neural network. The larger the number of neurons, the better the fitting of the input sample, and the easier it is to over-fit. The smaller the number of neurons, the lower the fit to the input sample, and the less likely to over-fit. Different numbers of neurons in the hidden layer are set to simulate the output error and correct rate of the network using output layer mapping method 1 and output layer mapping method 2 respectively. The results are shown in Figure 7.

As can be seen from Figure 7, when the number of neurons in the hidden layer is the same, the mean square error and correct rate performance of the training set and the test set under the output layer mapping method 2 can usually be significantly better than the mean square error and correct rate performance of the training set and the test set under the output layer mapping method 1, respectively. When the output layer mapping method 2 is adopted and the number of hidden layer neurons is set to be greater than or equal to 41, the correct rate of the training set and the test set converges to 1. When the output layer mapping method 1 is used and the number of hidden layer neurons is set to 45, the correct rate of the training set and the test set is close to 1. When the number of neurons in the hidden layer is greater than 54, the correct rate of training set and test set converges to 1. To sum up, the network under the output mapping mode 2 is better, and when the number of hidden layer neurons in this mapping mode is 50, the correct rate of the training set and the test set is 1 and the mean square error is small. Therefore, the network output mapping method 2 is selected, and the number of hidden layer neurons is 50.

4. Intelligent Financial Processing Based on Artificial Intelligence-Assisted Decision Support System

In a broad sense, the intelligent financial system has an impact on the development of intelligent finance at the level of the environment, including various information and data resources, information industry, information talents, high-tech technology and informatization-related policies. It can be roughly divided into government departments, industry organizations, application entities and the supply chain of intelligent finance development. Although the process of intellectualization is mainly driven by the internal development power of the application subject, the external environment undoubtedly plays a crucial role in promoting it. The structure of the generalized intelligent financial system is shown in Figure 8.

The intelligent financial decision support system adopts a system structure consisting of four levels, which

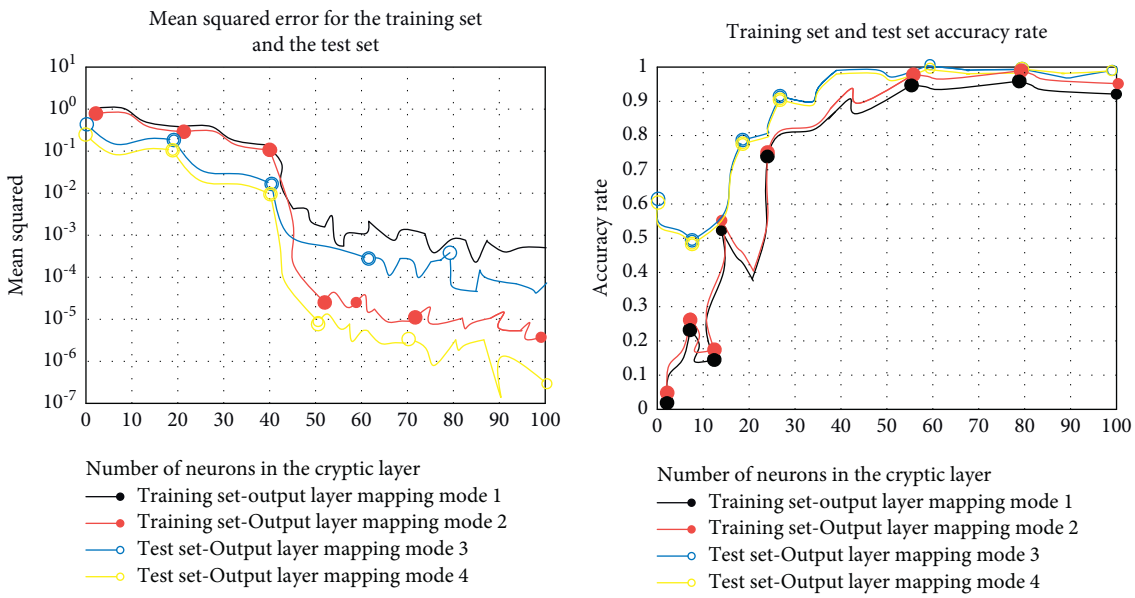

Figure 7: Performance of different output layer mapping methods and different numbers of neurons in the hidden layer.

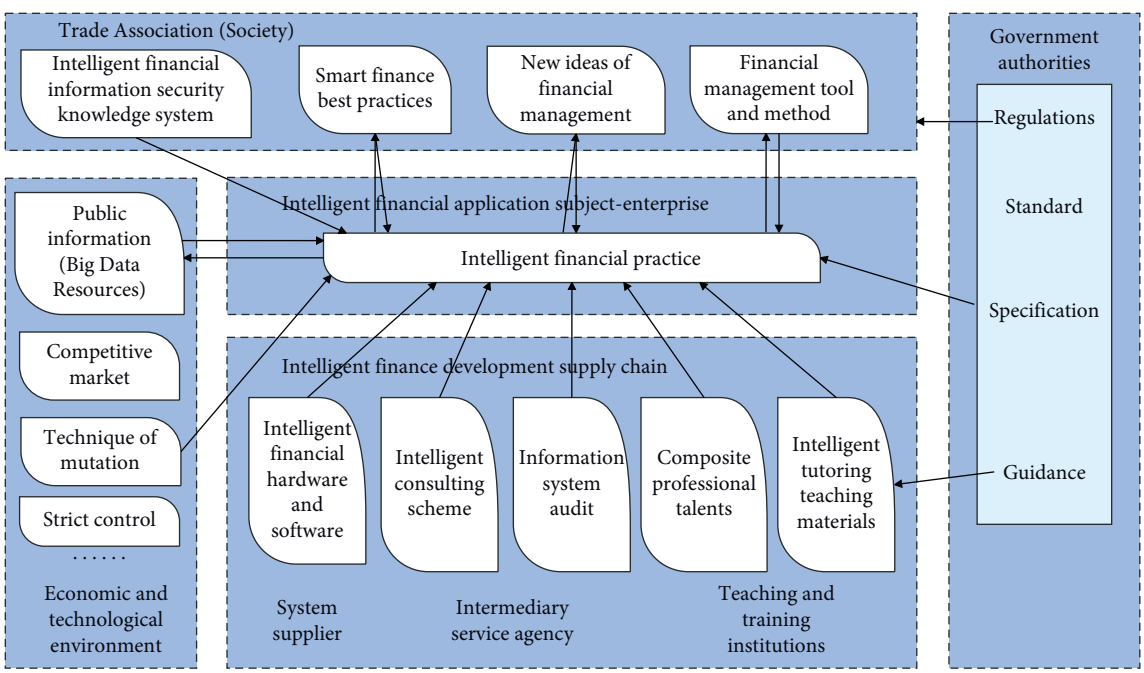

Figure 8: Architecture diagram of intelligent financial system.

can ensure the scalability and scalability of the system, and any level can be independently extended and developed according to actual needs. The system structure diagram is shown in Figure 9.

Figure 10 shows the regression simulation image of intelligent financial processing based on artificial intelligence-assisted decision support. Through the expert evaluation of the group data (Table 1), the simulation

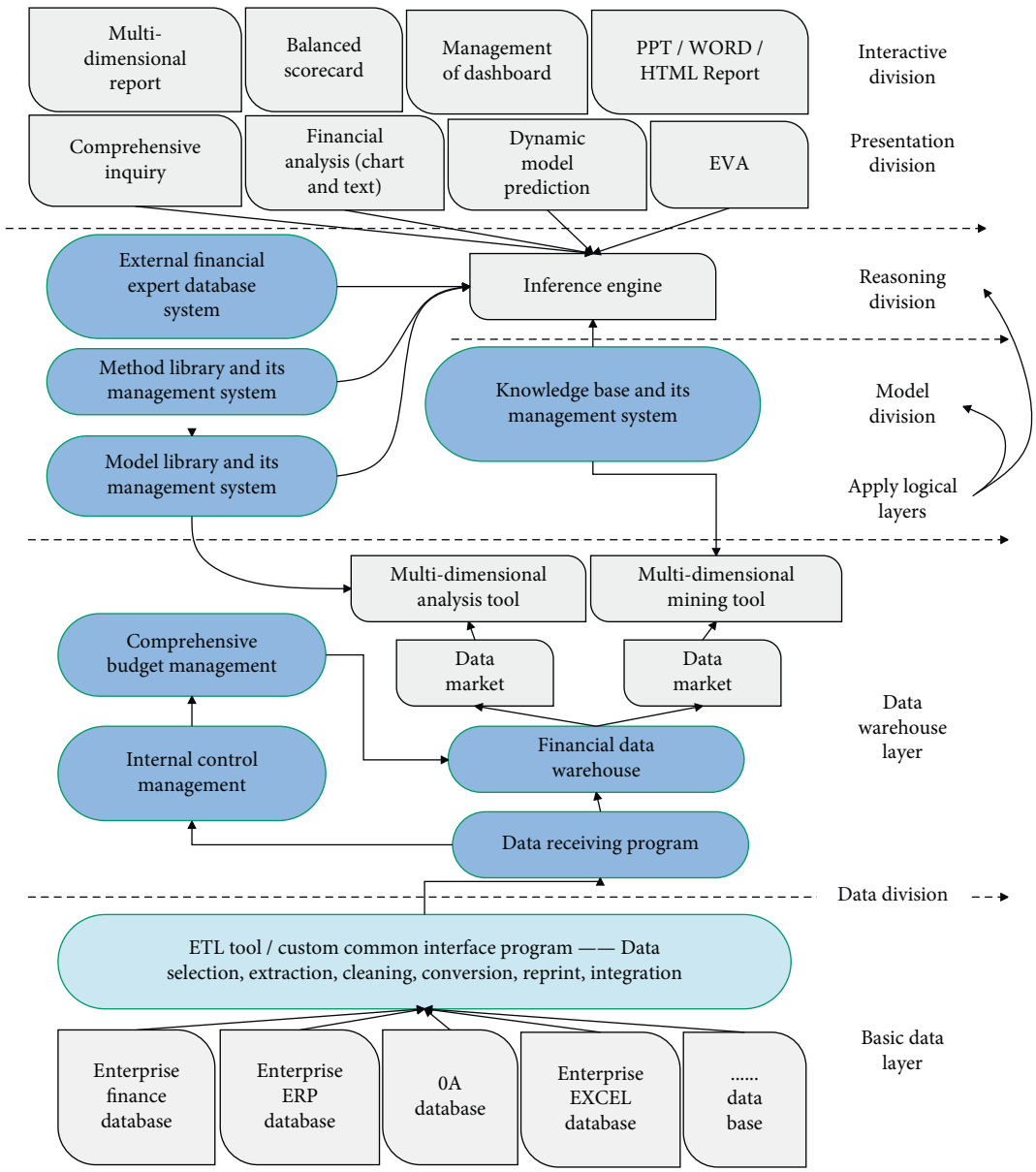

Figure 9: System structure diagram.

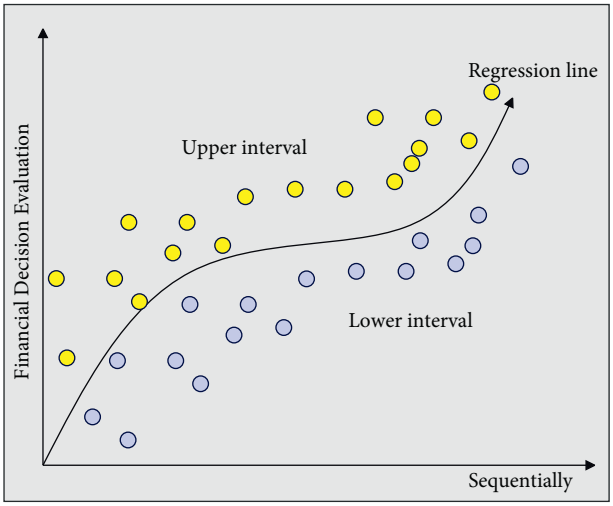

Figure 10: Regression simulation image of intelligent financial processing based on intelligence-assisted decision support.

Table 1: Evaluation of system effect.

Number	System assessment	Number	System assessment	Number	System assessment
1	86.89	16	84.59	31	81.51
2	84.45	17	80.47	32	85.22
3	87.58	18	87.75	33	78.64
4	85.97	19	83.16	34	80.36
5	84.52	20	84.30	35	90.70
6	78.53	21	79.68	36	85.74
7	83.28	22	86.07	37	85.48
8	79.94	23	87.58	38	82.98
9	87.05	24	81.99	39	82.34
10	87.31	25	87.08	40	78.37
11	85.61	26	85.41	41	84.79
12	86.58	27	85.89	42	81.84
13	89.41	28	79.57	43	87.49
14	80.78	29	89.53	44	90.36
15	87.35	30	83.21	45	86.17

results show that the intelligent decision-making model in this paper has a certain practical effect in the simulation.

5. Conclusion

Financial decision-making is an important field of management accounting, and the correctness, timeliness and effectiveness of financial decision-making are related to the future development of an enterprise. With the development of computer and Internet technology, in order to improve the efficiency and accuracy of decision-making and provide necessary assistance for decision-makers, financial decision-making support systems have emerged and continuously developed and improved. However, the current financial decision support system still has many defects in data acquisition and unstructured problem solving, mainly exerting the functions of database and calculator. Moreover, it cannot automatically screen information that may be relevant to financial decision-making or provide differentiated and targeted decision-making recommendations, so it cannot fully meet the needs of managers. This paper combines the artificial intelligence-assisted decision support system to construct the intelligent financial processing system. The simulation results show that the intelligent decision-making model in this paper has a certain practical effect in the simulation.

Data Availability

The experimental data used to support the findings of this study are available from the corresponding author upon request.

Conflicts of Interest

The author declared that there are no conflicts of interest regarding this work.

Acknowledgments

This study did not receive any funding in any form.

References

[1] Z. Lanlan, A. Ahmi, and O. M. J. Popoola, "Perceived ease of use, perceived usefulness and the usage of computerized accounting systems: a performance of micro and small enterprises (mses) in China," *International Journal of Recent Technology and Engineering*, vol. 8, no. 2, pp. 324–331, 2019.

[2] A. Omitogun and K. Al-Adeem, "Auditors' perceptions of and competencies in big data and data analytics: an empirical investigation," *International Journal of Computer Auditing*, vol. 1, no. 1, pp. 92–113, 2019.

[3] K. S. Kumar, "Factors affecting the adoption of computerized accounting system (CAS) among smes in Jaffna District," *SAARJ Journal on Banking & Insurance Research*, vol. 8, no. 6, pp. 11–15, 2019.

[4] B. L. Handoko, A. N. Mulyawan, J. Tanuwijaya, and F. Tanciady, "Big data in auditing for the future of data driven fraud detection," *International Journal of Innovative Technology and Exploring Engineering*, vol. 9, no. 3, pp. 2902–2907, 2020.

[5] Z. Rezaee, A. Dorestani, and S. Aliabadi, "Application of time series analyses in big data: practical, research, and education implications," *Journal of Emerging Technologies in Accounting*, vol. 15, no. 1, pp. 183–197, 2018.

[6] E. Huerta and S. Jensen, "An accounting information systems perspective on data analytics and Big Data," *Journal of Information Systems*, vol. 31, no. 3, pp. 101–114, 2017.

[7] S. Balne, "Analysis on research methods in bigdata applications," *International Journal of Innovative Research in Computer and Communication Engineering*, vol. 8, no. 10, pp. 4059–4063, 2020.

[8] D. Chessell and O. Neguriță, "Smart industrial value creation, cyber-physical production networks, and real-time big data analytics in sustainable Internet of Things-based manufacturing systems," *Journal of Self-Governance and Management Economics*, vol. 8, no. 4, pp. 49–58, 2020.

[9] B. Abdualgalil and S. Abraham, "Efficient machine learning algorithms for knowledge discovery in big data: a literature review," *Database*, vol. 29, no. 5, pp. 3880–3889, 2020.

[10] O. Throne and G. Lăzăroiu, "Internet of Things-enabled sustainability, industrial big data analytics, and deep learning-assisted smart process planning in cyber-physical manufacturing systems," *Economics, Management, and Financial Markets*, vol. 15, no. 4, pp. 49–58, 2020.

[11] E. Nica, C. I. Stan, A. G. Luţan, and R. □. Oa, "Internet of things-based real-time production logistics, sustainable industrial value creation, and artificial intelligence-driven big data analytics in cyber-physical smart manufacturing systems," *Economics, Management, and Financial Markets*, vol. 16, no. 1, pp. 52–63, 2021.

[12] D. B. L. Shallal Almutairi, "Impact of COVID19 on accounting profession from the perspective of a sample of head of accounting departments within KUWAITI manufacturing sector," *Psychology and Education Journal*, vol. 58, no. 2, pp. 4758–4768, 2021.

[13] V. Q. Thong, "Factors defining the effectiveness of integrated accounting information system in ERP environment–Evidence from Vietnam's enterprises," *ECONOMICS AND BUSINESS ADMINISTRATION*, vol. 7, no. 2, pp. 96–110, 2020.

[14] J. R. A. Q. Al Natour, "The impact of information technology on the quality of accounting information (SFAC NO 8, 2010)," *Turkish Journal of Computer and Mathematics Education (TURCOMAT)*, vol. 12, no. 13, pp. 885–903, 2021.

[15] A. P. Aaron, M. L. Kohlstrand, L. V. Welborn, and S. T. Curvey, "Maintaining medical record confidentiality and client privacy in the era of big data: ethical and legal responsibilities," *Journal of the American Veterinary Medical Association*, vol. 255, no. 3, pp. 282–288, 2019.

[16] B. J. Ali and M. S. Oudat, "Accounting information system And financial sustainability of commercial and islamic banks: a review of the literature," *Journal of Management Information and Decision Sciences*, vol. 24, no. 5, pp. 1–17, 2021.

[17] V. Brock and H. U. Khan, "Big data analytics: does organizational factor matters impact technology acceptance?" *Journal of Big Data*, vol. 4, no. 1, pp. 21–28, 2017.

[18] S. Antony Sibi and S. Antony Lucia Merin, "An investigation on accounting information system, Zambia," *Shanlax International Journal of Management*, vol. 8, no. 2, pp. 13–20, 2020.

[19] L. Loku, B. Fetaji, and A. Krsteski, "Automated medical data analyses of diseases using big data," *Knowledge International Journal*, vol. 28, no. 5, pp. 1719–1724, 2018.

Hindawi
Mobile Information Systems
Volume 2022, Article ID 1478626, 10 pages
https://doi.org/10.1155/2022/1478626

Research Article

Sports Personnel Health Monitoring Application Based on Biometric Data Collection Model

Xueqing Hu

Sports Department, Jiangsu University, Zhenjiang, Jiangsu 212013, China

Correspondence should be addressed to Xueqing Hu; 2020020194@stu.cdut.edu.cn

Received 25 May 2022; Revised 11 July 2022; Accepted 16 July 2022; Published 8 August 2022

Academic Editor: Chi Lin

In order to improve the health monitoring effect of sports personnel, this study combines the biometric data acquisition model to construct the sports personnel health monitoring application program. Moreover, this study uses the iterative conjugate gradient method ICGM to prove the correctness of the biometric data acquisition algorithm from the changes of the residual and the objective function in the iterative process. Finally, the optimized cosine similarity is substituted into the SBGI model, and better results are obtained than using the weighted cosine similarity as input. The research shows that the sports personnel health monitoring application based on the biometric data collection model proposed in this study has a good health monitoring effect, and has an important supporting role in improving the fitness effect of group sports.

1. Introduction

The acquisition and transmission of fitness exercise data mainly include two aspects: exercise effect and exercise equipment data. Heart rate data are an important indicator to reflect the exercise effect of practitioners, especially aerobic exercise [1]. Moreover, the size of the heart rate and the speed at which the heart rate returns to normal reflect the physical condition of the practitioner and the effect of the exercise. At the same time, the heart rate data should be matched with specific exercise equipment for analysis. The heart rate changes in aerobic training and the heart rate changes in resistance training are different, and need to be fully excavated [2]. In this study, the heart rate sensor was used to obtain the heart rate data of the exerciser, and the information of the exercise equipment was obtained through the radio frequency identification technology [3].

Fitness exercise can effectively improve physical health, but exercise with a too low heart rate will not have a good training effect, and exercise with a high heart rate increases the risk of training. The basic information of the practitioner, such as name, gender, age, height, and weight, can be read through the smart device, and the maximum heart rate can be calculated based on age and resting heart rate. According to the impact of different heart rate zones on exercise, heart rate zones can be divided into four stages. Among them, the heart rate zone in the warm-up phase is 50%–60% of the maximum heart rate. At this stage, the exercise intensity is relatively low, and it is generally a preparatory activity to improve the function of the body and prevent injury. The heart rate zone during the fat-burning phase is 60%–70% of the maximum heart rate. The intensity of exercise at this stage is greater than that of the warm-up stage. As long as the amount of exercise is reasonable, it will have a good effect of burning fat. Therefore, this stage is of great help to those who need to lose fat. In the endurance phase, the heart rate zone is 70%–80% of the maximum heart rate. At this stage, the exercise intensity is higher than that of the fat-burning stage, and the durability of exercise is lower, but it is of great help to improve the cardiovascular system and respiratory system. Therefore, this stage is more suitable for people who need to improve their cardiopulmonary function. The heart rate in the strength training phase should be above 80% of the maximum heart rate. In this phase, the exercise intensity is very high, the muscle burden is relatively large, and it is easy to cause fatigue. Therefore, this stage is very helpful for muscle growth and is suitable for people who need to improve muscle strength and endurance. Through Internet

technology, the heart rate data of the user during exercise are obtained. Then, according to the needs of users, the system analysis is carried out. For users who need to lose fat, the recommended heart rate range is 60%–80% of the maximum heart rate (fat-burning exercise and aerobic endurance stage), and for users who need to build muscle, it is recommended that the heart rate be more than 80% of the maximum heart rate (strength exercise stage). In addition, monitoring the heart rate of fitness exercise can improve exercise effect, reduce exercise risk, and make fitness exercise more scientific and professional.

In this study, a biometric data collection model is combined to construct a sports personnel health monitoring application program to improve the health monitoring effect of sports personnel.

2. Related Work

Literature [4] designed a telemedicine monitoring system based on ZigBee sensor and wireless local area network, which can realize remote medical monitoring of sick patients at home; Literature [5] proposed to popularize healthy life, build a healthy environment, improve health protection, optimize health services, and develop health industries to comprehensively promote the construction of a healthy China and achieve the grand goal of a healthy China. Literature [6] designed a new type of human health monitoring system based on ZigBee and IGPS positioning technology. The system combines ZigBee technology and smartphones. It not only has the characteristics of low cost, low power consumption, reliable data transmission, and strong anti-interference ability, which reduces the hardware cost, but also improves the system stability and portability, and meets the needs of human health monitoring requirements. As far as the current policies and markets are concerned, its development prospects are very broad.

Literature [7] studies and designs a human vital index detection terminal with a shape similar to a ring. This terminal can realize the collection of human blood oxygen saturation, heart rate information, and pulse information; a French company designed a human health data collection The gloves can realize the collection of human health data such as human skin blood flow velocity, skin conductivity, instantaneous heart rate, and respiration. The system can realize the analysis and processing of health data to obtain the state of human health; Literature [8] developed a portable terminal for the collection and monitoring of human physiological data can collect ECG, blood pressure, body temperature data, and at the same time can realize fall detection and alarm; Literature [9] developed a system for children's health monitoring based on mobile phones; Literature [10] proposed A system equipped with a heart rate sensor to collect the patient's heart rate data, and send the data to the Web terminal remotely via wireless means for doctors and nurses to view. Smart medical care and mobile medical care have attracted the attention of some other mobile medical and medical equipment providers, and they have carried out research in the field of smart medical care. A product designed by MobileOCT, which uses mobile phones, cameras, and algorithms to detect sports health [11]; the system designed in Literature [12] can collect body temperature, ECG, and blood oxygen data, and send the collected data through Bluetooth. Give users a mobile phone for users to view; an APP designed in the literature [13] can realize the functions of collecting sensor data and data analysis, through which it can improve the user's mental health status, and can be applied to depression, chronic pain, and other ailments. In nursing and treatment, improve the effect of treatment and nursing; Literature [14] develops and designs desktop and mobile platforms, which can help users obtain the diagnosis and treatment of minor health problems, and at the same time realize online consultation and obtain treatment prescriptions issued by doctors by paying a certain fee; An embedded biomedical sensor studied in Literature [15] realizes the acquisition of human physiological response and behavior data by carrying a patch and a smartphone, which can be applied in the fields of patient monitoring and clinical trials; [16] The combination of this sensor and APP can realize the management of chronic obstructive pulmonary disease and asthma and the tracking of patients' drug use, and can provide personalized health advice and optimize the treatment plan and treatment time according to the patient's condition.

Not only a physiological parameter of heart rate can be extracted from the pulse wave but also some other physiological parameters can be extracted. Literature [17] uses the camera to obtain the finger image information, and realizes the detection of human pulse, blood oxygen, and respiratory rate through pixel extraction of the image information and simulation of the photoplethysmographic wave signal. Literature [18] used the RGB three-primary color signal sequence on the skin surface to estimate the relative blood oxygen saturation with blue light as the Literature light. Literature [19] proposed a method to obtain blood pressure data by measuring PPG signal with a mobile phone. Because smartphones integrate a variety of sensors, in addition to using the camera and flashing lights of the mobile phone, we can also use the microphone of the mobile phone to measure the lung capacity of the human body. Literature [20] developed the software SpiroSmart, which collects the sound signal of deep breathing and uses machine learning regression to estimate the human vital capacity. With the rapid development of science and technology, researchers have applied some artificial intelligence methods originally used in condition monitoring and machine fault diagnosis to human disease diagnosis and monitoring. At present, these methods have achieved certain results in human health diagnosis and monitoring. Literature [21] proposed an adaptive hidden Markov model based on wearable multisensor devices and used it to prevent and manage chronic diseases. Literature [22] introduced the framework of Bayesian Hierarchical Poisson Models with Hidden Markov Structure to detect the onset of influenza flow.

3. Biometric Data Collection Model

In this study, the biometric data acquisition model is used to construct a health monitoring application, and the biometric data acquisition model is first analyzed.

Before constructing the associated motion association network, it is necessary to calculate the associated motion similarity network, that is, to calculate all the similarity matrices involving associated motions. For the calculation method of similarity between expression profiles, the linear transformation L learned from the association motion knockout and association motion overexpression data based on the LFDA algorithm is used to recalculate the similarity matrix between the association motion knockout expression profiles, and the correlation motion is obtained. In the experiments, we selected 3689 expression profiles of association motor knockout experiments in the MCF7 cell line and calculated the similarity magnitude of all association motor pairs.

Collected from the MSigDB database (version 5.1), all 5936 associated movements with GOBP annotation information constitute a set of GO BP, and 5039 associated movements with GO MF annotation information constitute a set of GPMF. We recorded the knockout on MCF7 in the LINCS data set. The 3689 associated motion sets of the experiment are LINCS, and the Venn diagram (1) represents the intersection of the three. We can analyze two of these subsets, one is the subset A of the associative motor knockout experiment in the LINCS data MCF7 cell line, and has GOBP or GOMF annotation information, and the other is the existing associative motor knockout experiment. There is also associated motion set subset B with GOBP annotation information. The number of elements in the two sets is 2304 and 1905, respectively, and the latter is a subset of the former.

According to the similarity network of the knockout expression profile of the association movement, we can cluster all the association movements according to the cluster analysis, and then construct the association movement association network according to the clustering results. Figure 1 shows the Venn diagrams involving associated motion sets in the three datasets.

According to the hypothesis, there should be similar annotation information of GOBP and GO MF. Therefore, we can perform cluster analysis on the associated motion set A and the associated motion set B, respectively. In the associated motion set A, there are 399 associated motions with unknown GOBP associated motion annotation information. It is the associated motion set whose GOBP annotation information can be predicted later. Moreover, we perform cluster analysis on the two sets, respectively, and we can use the two clustering results to verify the correctness of the clustering results in the subsequent analysis to verify the basic hypothesis.

We selected k-means clustering, spectral clustering, Non-Negative Matrix Factorization (NMF), and AP clustering for analysis. The k-means clustering algorithm and the spectral clustering algorithm cannot obtain stable clustering results during the experiment, so these two clustering methods are not suitable for the clustering analysis of the data. The NMF method is to first use the matrix non-negative decomposition to find the low-dimensional reconstruction of all associated motions, that is, to find the non-negative matrices w and H such that

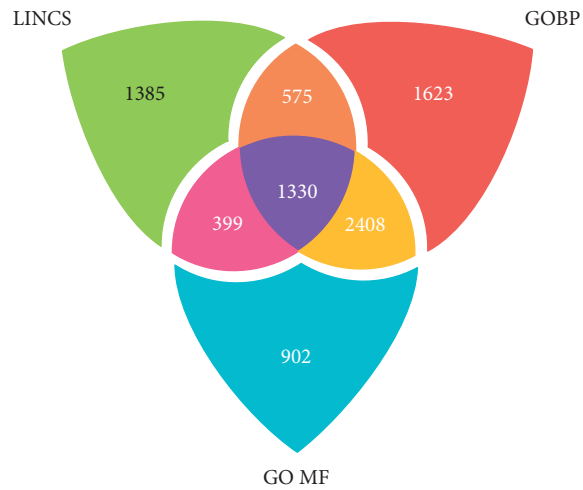

Figure 1: Venn diagrams involving associated motion sets in the three datasets.

$$V \approx WH, W \in R_{+}^{n\times k}, H \in R_{+}^{n\times k}. \quad (1)$$

Then, k-means clustering is performed with one of W/H as a low-dimensional representation of the associated motion. AP clustering is to find the best clustering result of each vertex through the data information propagation and product algorithm (sum-product algorithm) in the probabilistic graph model. The input to both algorithms is the similarity matrix of the samples. However, NMF and spectral clustering need to specify the number of clusters, while AP clustering will automatically choose the optimal number of clusters.

In the clustering process of the NMF method, we set the number of clusters to 9 k values with an interval of 10 from 20 to 100, performed 9 different NMFs, and obtained the performance investigation results of the method, as shown in Figure 2. In the performance survey graph, the larger the cophenetic coefficient, the better the decomposition effect. The RSS value needs to be as small as possible. Residuals represents the residual, which represents the deviation between the decomposed matrix and the original matrix, and also needs to be as small as possible. The consistency curve (Consensus) reflects its cluster consistency, which is a number between [0, 1]. The closer to 1, the better the consistency. Therefore, according to Figure 2, in terms of the number of clusters, the optimal number of clusters is around 80 to 90.

According to the above analysis, we can get the histogram of the coverage. From the Figure 3, we can see that there are 66 sub-communities whose coverage is higher than 0.8, and the remaining 18 sub-communities are lower than 0.8. That is, in the separate clustering analysis of the two sets, most of the clustering communities in the B set are covered by the corresponding large communities in the A set, and the two clustering results are consistent. The clustering results are valid, and the next step can be analyzed.

At the same time, we can compare the clustering performance of the similarity network based on the LFDA algorithm and the similarity network based on the ScoreGSEA algorithm. Figure 4 shows the consistency

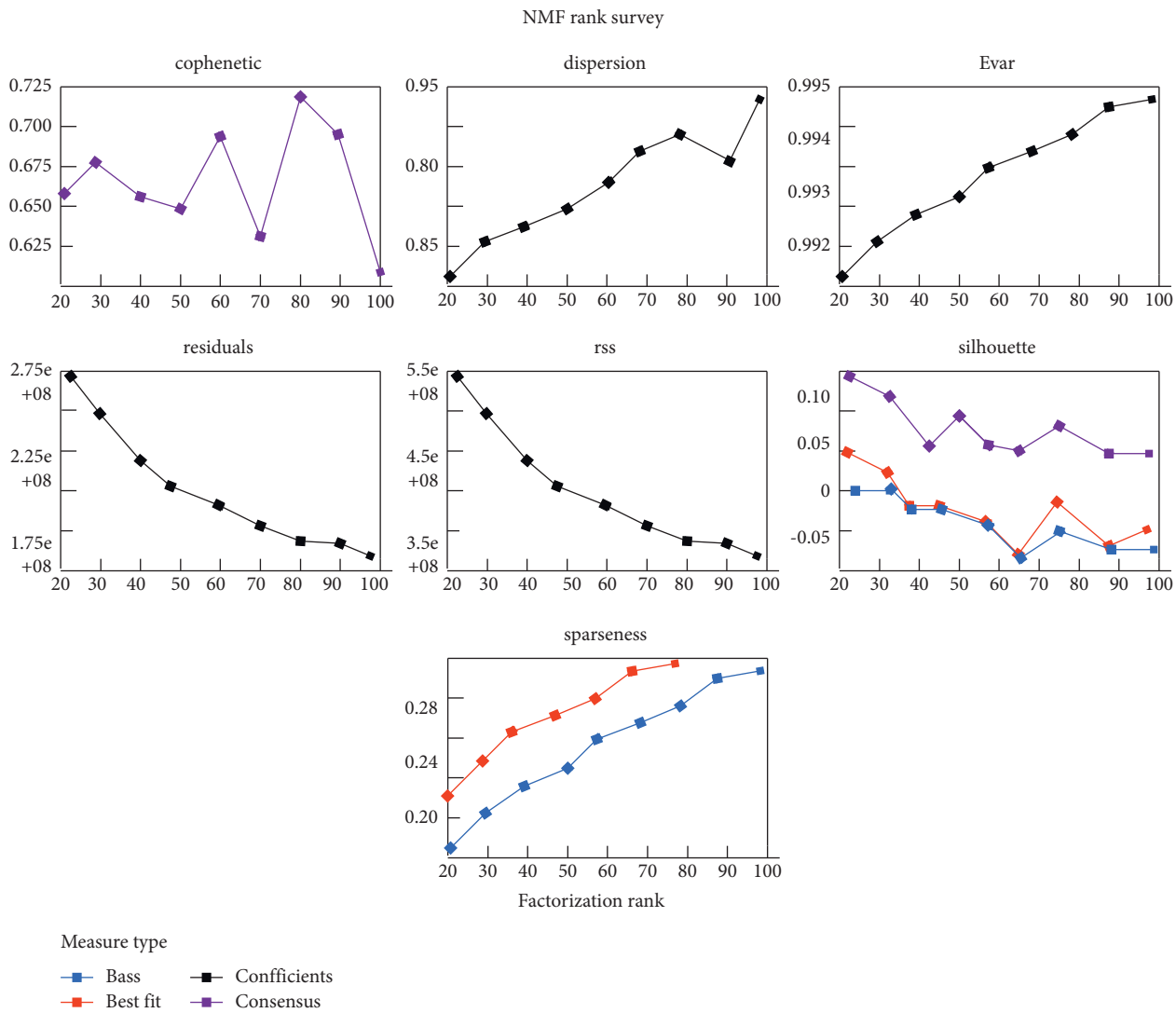

Figure 2: The NMF rank survey results show that the cophenetic coefficient peaks between 80 and 90, but the clustering consistency is consistently low. At the same time, when NMF decomposes the similarity matrix, no matter how many clusters are used, the consistency mainly fluctuates below 0.1, and the consistency of the clustering results is extremely poor, so the NMF method is not suitable for the study of this data.

results of the clustering results in the two sets based on the similarity network of the ScoreGSEA algorithm. Comparing the two figures, we can see that the consistency of the clustering results of the similarity network based on the LFDA method is significantly better than the corresponding results based on the ScoreGSEA algorithm.

After verifying the validity of the clustering, we also need to verify our basic assumptions. Figure 5 below shows the verification results.

Each community is the clustering result of cluster analysis, and two associated movements of the same community are represented by similarity, and they belong to the same class due to their high similarity. Therefore, according to the premise, the associated movement sets of the same community should have the same performance in Go terms, and the associated movements of different communities should have no intersection in GO Terms.

The above proves the validity of the clustering results and verifies the correctness of the basic assumptions. According to the clustering results of the cluster analysis, we can construct the association motion association network according to the communities obtained by clustering, as shown in Figure 6. Each vertex in the graph represents all the associated motions in the A set, each edge represents the similarity between vertices, and the vertices in each area constitute a community, and 10 major communities are drawn in the figure.

In the associative motion graph, the associated motions of each community's sub-communities (i.e., points in the B set) are represented by blue vertices, and these associated motions have known GOBP annotations. The rest of the vertices are represented by red vertices, and these associated motions are unknown for their GOBP annotation information. Through Enrichr's enrichment analysis, the

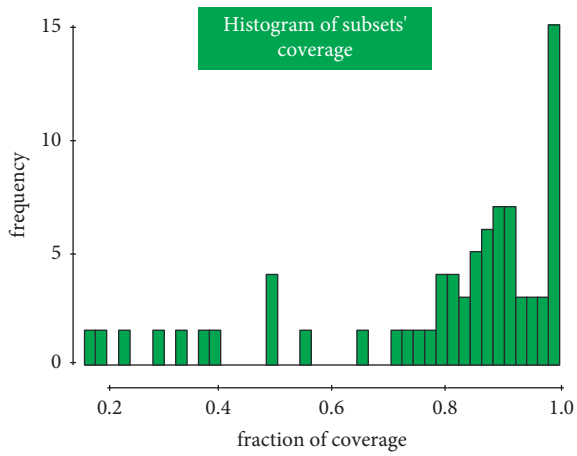

Figure 3: Histogram of coverage statistics of cluster communities in set B corresponding to cluster communities in set A.

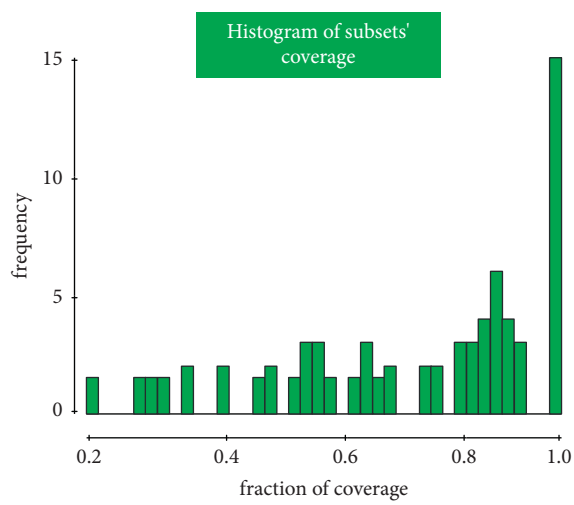

Figure 4: Histogram of coverage statistics of the clustering community in set B in the similarity network based on the ScoreGSEA algorithm in the corresponding clustering community in set A.

enrichment results of sub-communities with known GOBP information in the associated motion association network can be obtained. At the same time, it is speculated that the missing GOBP annotation information represented by the red vertices in the community is related to the GOBP annotation information of the movement. This is the GOBP annotation information prediction process of this model. Through the analysis of the clustering results, we verified the validity of the clustering results and the correctness of the basic assumptions, so the validity of this model has also been proved.

At the same time, we can also analyze the specificity of the clustering results. As shown in Figure 7, the abscissa represents the number of communities, and the ordinate represents the statistics of the number of GO Terms shared by several communities. It can be seen that nearly 500 GO Terms are exclusively within a single community, and the

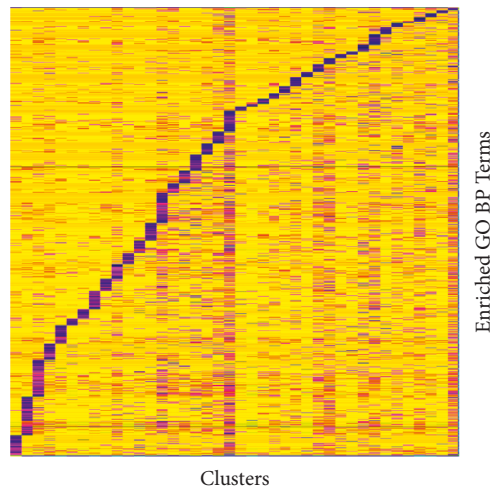

Figure 5: Heat map of the correlation between clustering results and GO BP enrichment results: the horizontal direction in the figure represents the clustering community, the vertical direction represents the term of GOBP, and the value in the heat map is the p value size of each community after enrichment analysis.

clustering results have high specificity and practical analysis significance.

Similar to generalized Mahalanobis distance, first we need to find a new feature space. In this space, the cosine value between samples satisfies that the cosine value between similar samples is high, and the cosine value between dissimilar samples is low. Therefore, we need to define a linear transformation $A \in R^{d\times n}$, that is, to map the original n-dimensional feature vector into a d-dimensional space:

$$A\colon R^n \longrightarrow R^d\,(d \le n). \tag{2}$$

Because $d \le n$, the transformation A also reduces the dimension of the feature data. At this point, the cosine values of samples x and y in the transform subspace are

$$CS(x, y, A) = \frac{(Ax)^T(Ay)}{\|Ax\| \cdot \|Ay\|} = \frac{x^T A^T A y}{\sqrt{x^T A^T A x}\sqrt{y^T A^T A y}}. \tag{3}$$

The set of constraints is S, D. Our goal is to have high cosine values for similar samples and low cosine values for dissimilar samples. Then, there is an objective function:

$$f(A) = \sum_{(x,y)\in S} CS(x,y,A) - \alpha \sum_{(x,y)\notin D} CS(x,y,A) - \beta\|A - A_0\|. \tag{4}$$

Among them, $\alpha, \beta \ge 0$ is a hyperparameter, and $\|A - A_0\|$ is a regular term, which is used to control the distance between the target transformation A and the predefined matrix Ao, control the optimization step size, and prevent overfitting. The parameter α balances the contribution of the positive sample pair and the negative sample pair to the loss function. The optimal value can be determined by the cross-validation method, or it can be directly set to |SVD).

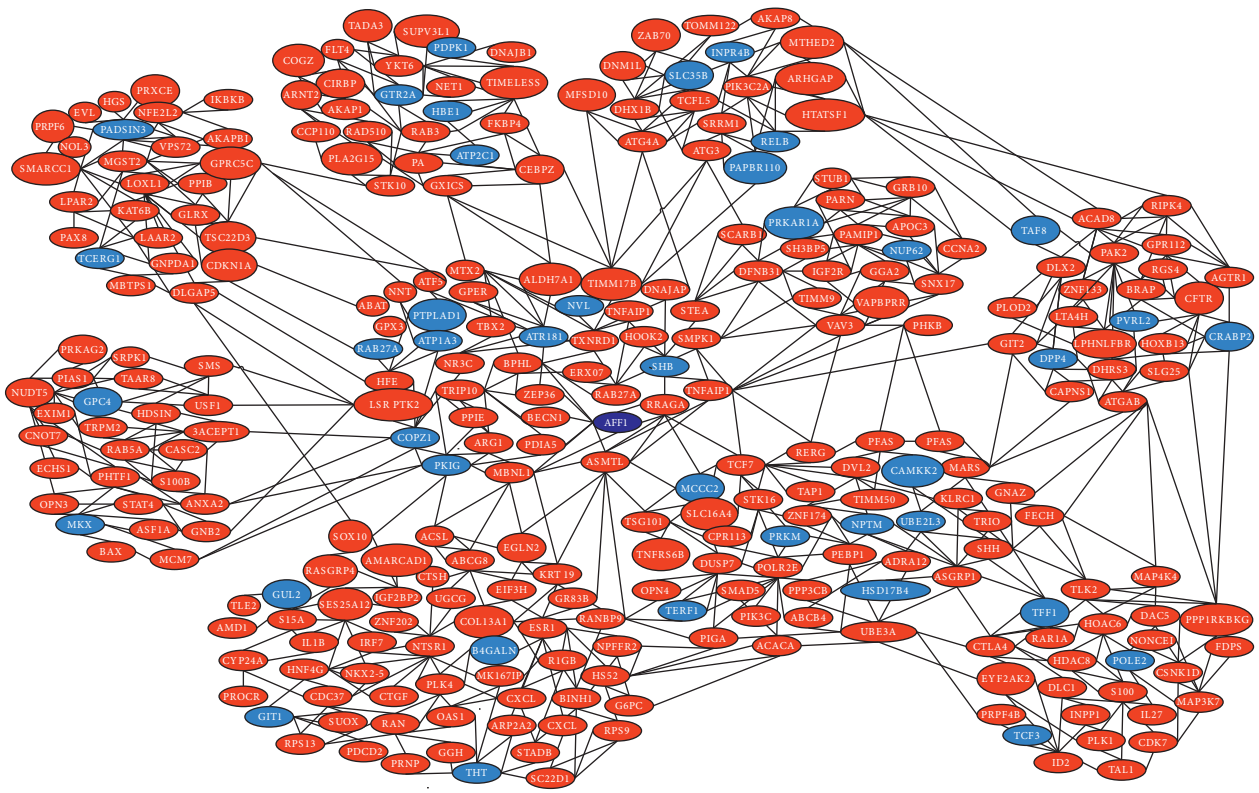

FIGURE 6: Display of the associated motion association network: because there are too many network vertices with 2304 associated motions, only 10 associations of the association network are shown in the figure, and the blue vertices are the associated motions of the known GO BPs.

Therefore, our final optimization goal is to find the transformation A^* that maximizes the objective function, namely:

$$A^* = \underset{A}{arg\,max}\ f(A). \tag{5}$$

Jaccard distance is used to define the similarity of ATC labels between motions:

$$J(d_i, d_j) = \frac{|l_i \cap l_j|}{|l_i \cup l_j|}. \tag{6}$$

Then, we can decide which set of constraints the two motions belong to according to the threshold 8, that is,

$$\begin{aligned} S &= \{(d_i, d_j) | J(d_i, d_j) > \delta\}, \\ D &= \{(d_i, d_j) | J(d_i, d_j) < \delta\}. \end{aligned} \tag{7}$$

We use ATC labels as side information to construct a restricted set, so the model is a weakly supervised algorithm.

The objective function (4) is divided into two parts: the loss function formed by the summation of cosine functions and the regular term. For a fixed predefined matrix Ao, the optimized optimal solution A^* performs better than A_0. Therefore, we use an iterative strategy to continuously optimize. That is, in the next iteration, the A^* value of the previous round is substituted into the new A_0 for calculation, and at the same time, cross-validation is used to ensure that the solution of each round is improving the performance. In addition, the coarse-to-fine strategy is used to update the β value during the iteration, and the β value finally approaches $+\infty$, so the iteration of A^* will eventually stabilize and obtain the final optimal solution.

The next step is to solve the optimal solution in step 4 in the Algorithm Table (1). First, we derive it with respect to the transformation matrix A, and obtain

$$\frac{\partial f(A)}{\partial A} = \sum_S \frac{\partial C\,S(x, y, A)}{\partial A} - \alpha \sum_D \frac{\partial C\,S(x, y, A)}{\partial A} - 2\beta(A - A_0). \tag{8}$$

Among them, the partial derivative with respect to A of a single cosine function is

$$\begin{aligned} \frac{\partial C\ S(x, y, A)}{\partial A} &= \frac{1}{v(A)} \frac{\partial u(A)}{\partial A} - \frac{u(A)}{v(A)^2} \frac{\partial v(A)}{\partial A} \\ &= A\left[\frac{1}{\|Ax\| \cdot \|Ay\|}\left(xy^T + yx^T\right)\right. \\ &\quad \left. - \frac{(Ax)^T Ay}{\|Ax\|^2 \|Ay\|^2}\left(\frac{\|Ay\|}{\|Ax\|} xx^T + \frac{\|Ax\|}{\|Ay\|} yy^T\right)\right]. \end{aligned} \tag{9}$$

The common factor in formula (9) is as follows:

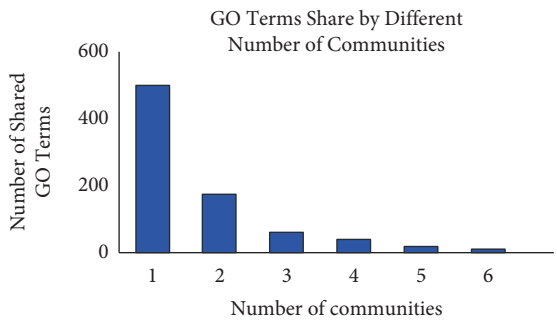

Figure 7: Statistical diagram on the frequency of community sharing of GO Terms.

$$M = \frac{1}{\|Ax\| \cdot \|Ay\|}\left(xy^T + yx^T\right) - \frac{(Ax)^T Ay}{\|Ax\|^2 \|Ay\|^2} \left(\frac{\|Ay\|}{\|Ax\|} xx^T + \frac{\|Ax\|}{\|Ay\|} yy^T\right). \tag{10}$$

From the analysis of formula (10), we can find that the norm and the inner product in the formula are both scalars, and the result of the vector product is a symmetric matrix. To sum up, we can do the following transformation on the derivative of the objective function:

$$\begin{cases} D = \sum_S M_i - \sum_D M_i - 2\beta E = d(A), \\ \beta = -2\beta A_0. \end{cases} \tag{11}$$

Among them, E is the identity matrix, then we can get the simplified formula of formula (8):

$$\frac{\partial f(A)}{\partial A} = AD - B. \tag{12}$$

Among them, $D = d(A)$ is a symmetric matrix, and it is a negative definite matrix when β is large enough. We want to find the extreme value of the objective function, that is, to find the point whose derivative is equal to zero, that is, to find the zero solution of the linear equation system (12). Because the negative definite matrix D is a function of the parameter matrix A, we use the iterative form of the Conjugate Gradient Method (ICGM) to solve the model, that is, to solve d linear equations:

$$DA^T(k) - B^T(k) = O, k = 1, 2, \ldots, d. \tag{13}$$

Among them, $A^T(k)$, $B^T(k)$ is the k-th column vector of matrix A^T, B^T, The solution process of ICGM is shown in Algorithm Table (2).

Algorithm (2) ensures that we can solve the stationary point of the objective function. However, by calculating the second derivative of its derivative, we can find that the objective function does not guarantee convexity, so the solution process of the problem can only obtain a local optimal solution. That is, the solution of the problem depends on the selection of the predefined matrix A_0.

The iterative conjugate gradient method is used to solve the linear equation system, and the direction of the optimized gradient in the original conjugate gradient method is orthogonal to the previous one each time. However, in the ICGM model, since the negative definite matrix D is related to the parameter matrix A, all of them are solved by an iterative method, but the orthogonality of each iteration direction is also lost. However, in fact, in the optimization process, the selection of the initial direction is based on the negative definite matrix D_j of the previous time, and in the calculation of the orthogonal direction in the next step, D_{j+1} is used as the coefficient matrix. Therefore, according to the characteristics of the conjugate gradient method, each optimization ensures that the residual error of the linear equation system is reduced, and finally a zero solution is reached. Figure 8(a) shows the change curve of the residual $R = D'A^T - B^T$ in the iterative process of the linear equation system in the optimization process, and the ordinate in Figure 8 is the logarithmic index. From Figure 8, we can see that despite the use of nonstrictly orthogonal search directions, the optimization speed is still very fast. In the matrix solution of rank 50, the allowable accuracy is achieved in only 32 iterations. At the same time, during the whole optimization process, the residual error is strictly reduced, which proves the correctness of this optimization method.

In the whole iterative process of the algorithm, each small iteration is the ICGM algorithm, and its first layer iterative method is the algorithm (1). The correctness of the algorithm is shown in Figure 8(b). After the optimal solution of the previous round of ICGM is substituted as a predefined matrix in a new round of iteration, its objective function rises steadily and meets the optimization objective, so it can be proved that the iterative strategy is effective.

4. Sports Personnel Health Monitoring Application Based on Biometric Data Collection Model

In this study, the construction of a sports personnel health monitoring application program is combined with the biometric data acquisition model. When designing the monitoring system, several principles were followed for the design, which mainly included the data acquisition part, the associated motion data transmission and the monitoring center part. The data acquisition part is mainly composed of the terminal node structure based on STM32 microprocessor, which includes LoRa wireless communication module and various sensor modules. The data transmission part is composed of an STM32-based associated motion microprocessor, which includes a LoRa wireless communication module and a WIFI module. The monitoring center is mainly constructed based on server-related motion, and corresponding monitoring functions can be realized by deploying a web server. The overall design structure of the system of this subject is shown in Figure 9(a).

The system software part includes the design of the terminal node data acquisition terminal, the aggregation node and the cloud server. The overall design block diagram of system software is shown in Figure 9(b).

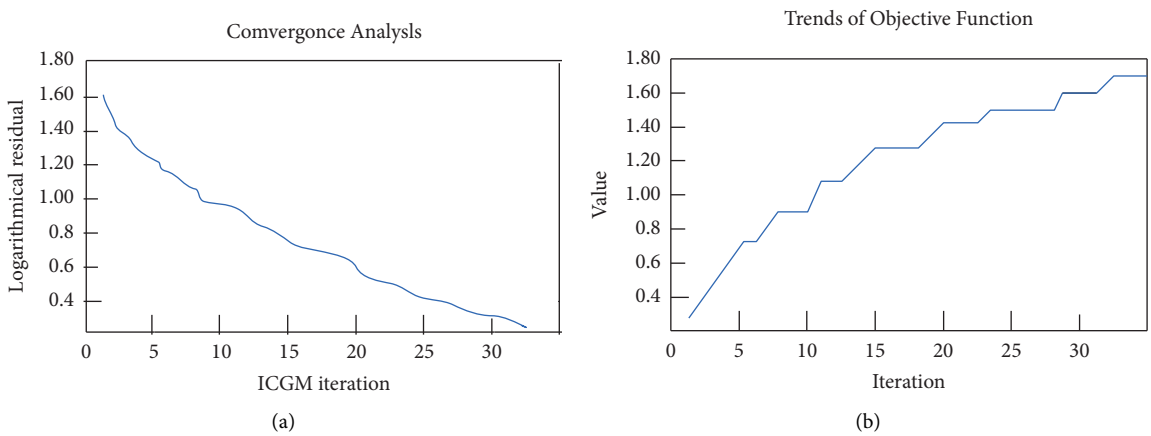

Figure 8: (a) In the optimization process of the iterative conjugate gradient method, the change trend of the residual R of the linear equation system, and the ordinate in the figure is the logarithmic index; (b) as the outer iteration proceeds, the overall objective function rises steadily.

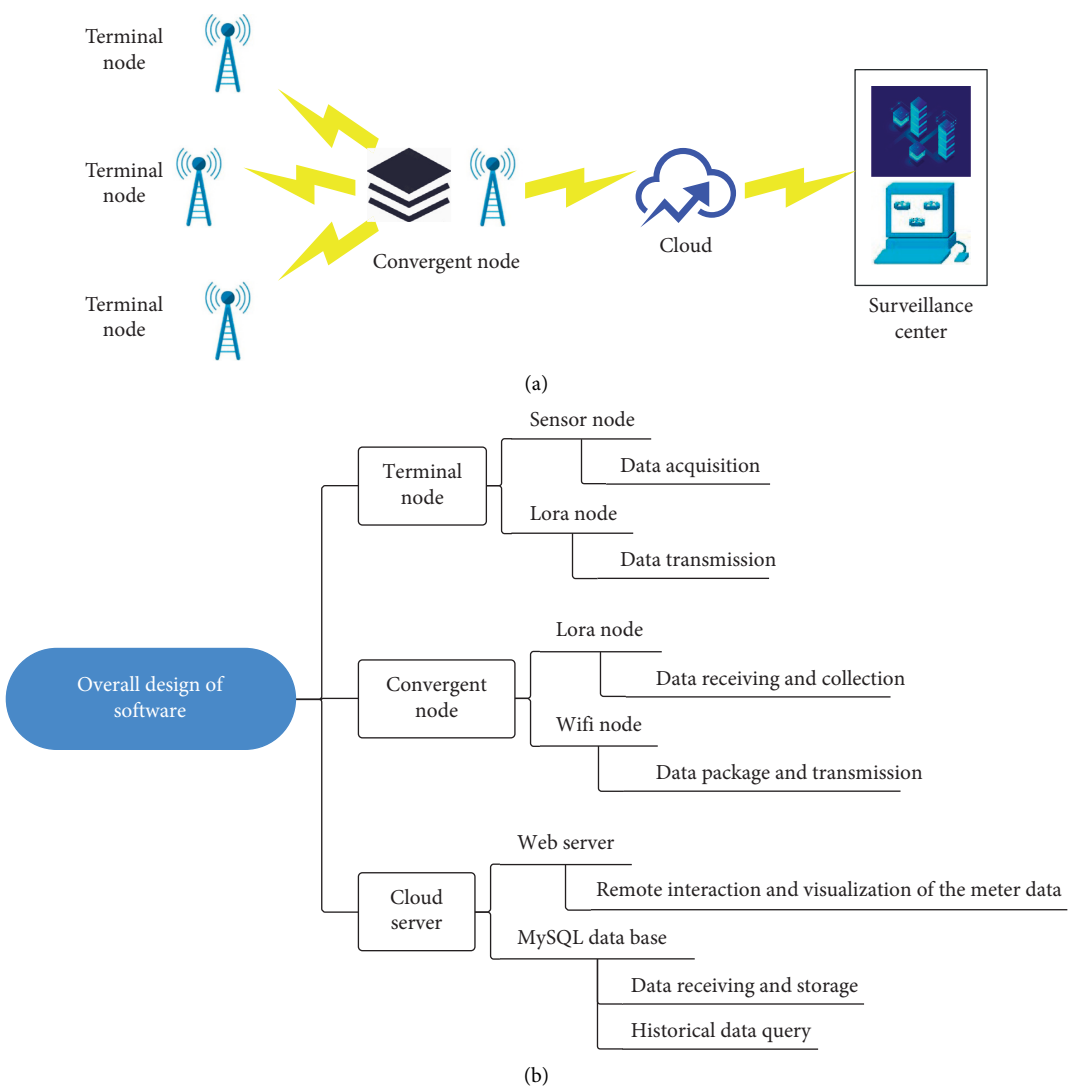

Figure 9: Structure of sports personnel health monitoring application program based on biometric data collection model. (a) System overall design architecture diagram and (b) system software design block diagram.

Table 1: The group sports data collection effect of the model.

Num	Data collection	Num	Data collection	Num	Data collection
1	87.95	20	90.00	39	87.74
2	84.37	21	84.36	40	88.92
3	91.46	22	88.34	41	86.79
4	86.85	23	84.11	42	88.36
5	84.49	24	86.24	43	89.44
6	87.50	25	85.17	44	84.27
7	90.42	26	89.43	45	90.47
8	88.86	27	86.88	46	91.84
9	87.56	28	89.49	47	90.28
10	91.91	29	86.59	48	91.74
11	87.20	30	85.96	49	85.35
12	90.00	31	84.62	50	88.91
13	91.23	32	85.50	51	84.77
14	89.16	33	86.06	52	86.01
15	85.47	34	90.73	53	85.34
16	90.73	35	91.23	54	84.88
17	84.21	36	85.84	55	90.34
18	84.46	37	86.77	56	85.72
19	87.96	38	88.66	57	84.07

Table 2: Health monitoring effect of sports personnel health monitoring application based on biometric data collection model.

Num	Motion monitoring	Num	Motion monitoring	Num	Motion monitoring
1	78.95	20	78.74	39	85.50
2	79.85	21	87.05	40	79.53
3	86.26	22	82.08	41	81.98
4	78.63	23	87.93	42	82.59
5	83.61	24	79.73	43	78.02
6	86.55	25	81.62	44	78.39
7	84.49	26	78.04	45	83.41
8	77.03	27	83.39	46	79.31
9	87.55	28	84.38	47	83.69
10	79.82	29	84.93	48	82.01
11	87.29	30	79.50	49	86.18
12	80.55	31	82.46	50	82.22
13	87.00	32	77.68	51	86.57
14	81.50	33	81.76	52	84.59
15	86.53	34	87.51	53	87.80
16	85.94	35	78.38	54	79.70
17	85.06	36	84.09	55	78.42
18	81.32	37	79.61	56	83.85
19	86.39	38	84.40	57	80.26

After constructing the above model, this study verifies the collection effect of group sports data of the biometric data collection model proposed in this study, and calculates the data collection evaluation results as shown in Table 1.

The above verifies that the sports personnel health monitoring application based on the biometric data collection model has a good effect of group sports data collection. On this basis, this study verifies the health monitoring effect of the sports personnel health monitoring application based on the biometric data collection model, and obtains the results shown in Table 2.

From the above research, it can be seen that the sports personnel health monitoring application based on the biometric data collection model proposed in this study has a good health monitoring effect, and has an important supporting role in improving the fitness effect of group sports.

5. Conclusion

The application of the Internet of Things technology in the sports and fitness industry focuses on the main body with the attribute of "thing" in the fitness system. It is based on the gradually mature information system, and it is supplemented by the application of the core technology of the Internet of Things, and follows the principle of demand orientation, and finally realizes "smart sports." The body area network is "a wireless network based on a wireless sensor network, a wireless network formed by sensors for collecting physiological parameters on the human body or

biosensors transplanted into the human body," which can be used as an information communication solution for a ubiquitous physical health monitoring system. This study combines the biometric data acquisition model to construct the sports personnel health monitoring application program to improve the sports personnel health monitoring effect. The research shows that the sports personnel health monitoring application based on the biometric data collection model proposed in this study has a good health monitoring effect, and has an important supporting role in improving the fitness effect of group sports.

Data Availability

The experimental data used to support the findings of this study are available from the corresponding author upon request.

Conflicts of Interest

The author declared that there are no conflicts of interest regarding this work.

References

[1] D. Henriques-Neto, J. P. Magalhães, M. Hetherington-Rauth, D. A. Santos, F. Baptista, and L. B. Sardinha, "Physical fitness and bone health in young athletes and nonathletes," *Sport Health*, vol. 12, no. 5, pp. 441–448, 2020.

[2] T. M. Kravchuk, N. M. Sanzharova, J. V. Golenkova, and I. B. Katrechko, "Influence of means of parterre gymnastics on physical fitness of young athletes in acrobatic rock and roll," *Health, sport, rehabilitation*, vol. 6, no. 3, pp. 19–25, 2020.

[3] D. Okun and K. Mulyk, "Investigation of the relationship between the indicators of physical preparedness and the basic technique elements of young water-slalom athletes," *Slobozhanskyi Herald of Science and Sport*, vol. 5, no. 61, pp. 69–71, 2017.

[4] O. Politko, "Model characteristics of physical development and special physical preparedness of swimmers 12–15 years old," *Slobozhanskyi Herald of Science and Sport*, vol. 2, no. 64, pp. 37–40, 2018.

[5] G. Chang, "Retracted article: urban air pollution diffusion status and sports training physical fitness measurement based on the Internet of things system," *Arabian Journal of Geosciences*, vol. 14, no. 16, pp. 1555–1611, 2021.

[6] B. Silva and F. M. Clemente, "Physical performance characteristics between male and female youth surfing athletes," *The Journal of Sports Medicine and Physical Fitness*, vol. 59, no. 2, pp. 171–178, 2019.

[7] L. P. Tuti Ariani, "The effect of repetition sprint training method combined with the level of physical fitness toward the speed of 100 meter run," *International Journal of Engineering, Science and Information Technology*, vol. 1, no. 3, pp. 59–63, 2021.

[8] Z. L. Kozina, M. Cieslicka, K. Prusik et al., "Algorithm of athletes' fitness structure individual features' determination with the help of multidimensional analysis (on example of basketball)," *Physical education of students*, vol. 21, no. 5, pp. 225–238, 2017.

[9] A. V. Titova, O. G. Chorniy, A. A. Dolgov et al., "Parameters of biochemical control as a criteria of adaptive changes in the organism of athletes with various fitness levels engaged in the conditions of power fitness," *Ukraïns'kij žurnal medicini, bìologìï ta sportu*, vol. 3, no. 2, pp. 278–283, 2018.

[10] T. Chernykh, V. Mulik, and D. Okun, "Study of the level of physical fitness of young acrobat athletes at the initial stage of training," *Slobozhanskyi Herald of Science and Sport*, vol. 7, no. 73, pp. 27–30, 2019.

[11] P. Kostiantyn, G. Grygoriy, P. Vasyl et al., "Correlation analysis of readiness indicators of athletes and their competitive results in kettlebell sport," *Journal of Physical Education and Sport*, vol. 17, no. 3, pp. 2123–2128, 2017.

[12] L. A. Sarafyniuk, A. V. Syvak, Y. I. Yakusheva, and T. I. Borejko, "Correlations of cardiointervalographic indicators with constitutional characteristics in athletes of mesomorphic somatotype," *Biomedical and biosocial anthropology*, no. 35, pp. 17–22, 2019.

[13] V. V. Artiuh, Z. L. Kozina, V. O. Koval, D. V. Safronov, S. V. Fomin, and Y. O. Novikov, "Influence of application of special means of development of equilibrium and precision-target movements on the level and structure of psychophysiological indicators, physical and technical readiness of archers," *Health, sport, rehabilitation*, vol. 4, no. 4, pp. 7–16, 2019.

[14] Y. Strykalenko, O. Shalar, V. Huzar, R. Andrieieva, I. Zhosan, and S. Bazylyev, "Influence of the maximum force indicators on the efficiency of passing the distance in academic rowing," *Journal of Physical Education and Sport*, vol. 19, no. 3, pp. 1507–1512, 2019.

[15] F. Fachrezzy, I. Hermawan, U. Maslikah, H. Nugroho, and E. Sudarmanto, "Profile physical fitness athlete of slalom number water ski," *International Journal of Educational Research & Social Sciences*, vol. 2, no. 1, pp. 34–40, 2021.

[16] R. L. Kons, E. Franchini, and D. Detanico, "Relationship between physical fitness, attacks and effectiveness in short- and long-duration judo matches," *International Journal of Performance Analysis in Sport*, vol. 18, no. 6, pp. 1024–1036, 2018.

[17] Z. Kozina, I. Sobko, L. Ulaeva et al., "The impact of fitness aerobics on the special performance and recovery processes of boys and girls 16-17 years old engaged in volleyball," *International Journal of Applied Exercise Physiology*, vol. 8, no. 1, pp. 98–113, 2019.

[18] V. I. I. Zalyapin, A. P. Isaev, A. S. Bakhareva, and A. S. Aminova, "Modelling the spectral characteristics of the circulatory system of athletes-skiers," *Journal of Computational and Engineering Mathematics*, vol. 6, no. 4, pp. 57–68, 2019.

[19] P. Kyzim and S. Humeniuk, "Characteristics of the leading factors of special physical preparedness of athletes from acrobatic rock and roll at the stage of preliminary basic training," *Slobozhanskyi Herald of Science and Sport*, vol. 7, no. 71, pp. 20–24, 2019.

[20] D. Detanico, R. L. Kons, D. H. Fukuda, and A. S. Teixeira, "Physical performance in young judo athletes: influence of somatic maturation, growth, and training experience," *Research Quarterly for Exercise & Sport*, vol. 91, no. 3, pp. 425–432, 2020.

[21] E. A. Bondareva, O. I. Parfenteva, A. V. Kozlov et al., "The Ala/Val polymorphism of the UCP2 gene is reciprocally associated with aerobic and anaerobic performance in athletes," *Human Physiology*, vol. 44, no. 6, pp. 673–678, 2018.

[22] R. L. Kons, D. Detanico, J. Ache-Dias, and J. Dal Pupo, "Relationship between physical fitness and match-derived performance in judo athletes according to weight category," *Sport Sciences for Health*, vol. 15, no. 2, pp. 361–368, 2019.

Hindawi
Mobile Information Systems
Volume 2022, Article ID 1375331, 11 pages
https://doi.org/10.1155/2022/1375331

Research Article

Management of Power Marketing Audit Work Based on Tobit Model and Big Data Technology

Wenjie Fu,[1] Hongtao Shen,[1] Bo Feng,[1] Rui Zhang,[1] Jing Liang,[1] Chong Sun,[1] and Kalra Anurag[2]

[1]*State Grid Hebei Electric Power Co., Ltd, Marketing Service Center, Tianjin, Hebei Province, China*
[2]*Ecological and Environmental Research Center, Kyrgyz-Turkish Manas University, Bishkek, Kyrgyzstan*

Correspondence should be addressed to Kalra Anurag; anurag@email.cu.edu.kg

Received 17 June 2022; Revised 12 July 2022; Accepted 16 July 2022; Published 8 August 2022

Academic Editor: Chi Lin

In order to improve the management effect of power marketing audit work, this paper combines big data technology to carry out related data processing, changes the management mode of traditional power marketing audit work, analyzes the overall process and characteristics of the current power marketing audit case selection, and designs an audit system. Moreover, this paper builds a data warehouse based on data mining technology and realizes the process of automatic generation of the index system. In addition, this paper chooses the Tobit model proposed by Tobin, which is a restricted dependent variable model and can be better applied to the relevant analysis of power marketing audit indicators. Finally, this paper evaluates the effects of the method and system designed in this paper through simulation experiments. The experimental research results show that the power marketing audit management system based on big data technology can play an important role in power audits.

1. Introduction

The so-called power marketing audit mainly refers to the use of effective means and methods to carry out feasible and controllable quality audit and supervision of the marketing process of power enterprises. At present, the marketing audit of the electric power industry has become the most critical part of the marketing process of China's power supply enterprises, and it is also an effective measure to control risks in the professional operation of electric power marketing. In fact, the power marketing audit management work can be regarded as a key point in the entire power marketing process, and it is extremely important in the power marketing management work. The specific work it carries out will often directly affect the basic image and fundamental interests of power companies and, at the same time, will have a more important impact on the interests of electricity customers in the electricity market. There are many links in the processing of various electric power business operations, and problems in any one link may cause huge losses to the electric power company [1]. Therefore, the essence of power marketing audit management is a supervision process of management, cooperation, and operation of various links. This is a means implemented in order to maximize the protection of the power companies' own interests and the fundamental interests of electricity customers. This method can avoid the errors that may occur or exist in the various business of power marketing and prevent the occurrence of losses [2].

Many foreign countries have established energy regulatory agencies specifically responsible for economic regulation of energy (electricity). These regulatory agencies are responsible for the investigation and handling of violations of laws and regulations, dispute resolution, and handling of complaints and reports [3]. After long-term practical exploration, foreign regulatory agencies have gradually formed some mature practices and characteristics in the legal system, organizational system, and working procedures of the marketing audit business. It not only ensures the smooth development of the audit work, but also puts forward opinions on the rules and systems of the electricity market and promotes the reform of the national electricity market,

which is worthy of our reference. In the development of marketing audit informatization, the power informatization level of the United States, Japan, and Germany is the best. As early as 2003, the US Department of Energy held a high-level seminar on the future of the US power system and formed the long-term goal of the Grid2030 plan. At present, almost 100% of US electric power companies have basically realized system integration work and realized the use of information technology to conduct auxiliary analysis and audit monitoring of electric power marketing work [4]. The main purpose of power audits in the UK power market, which has achieved the separation of transmission and distribution, is to monitor and evaluate the operational efficiency of the power grid and improve the quality of power supply. For example, the detection of market power demand includes the prediction of the power demand of the whole society on the user side and the expected load growth of the power grid. Among them, the demand forecast on the user side includes power load and power, customer satisfaction, and power supply reliability. In further detail, it also includes power demand forecasts within the jurisdiction of different power companies.

The so-called power marketing audit mainly refers to the use of effective means and methods to carry out feasible and controllable quality audit and supervision of the marketing process of power enterprises. At present, the marketing audit of the electric power industry has become the most critical part of the marketing process of China's power supply enterprises, and it is also an effective measure to control risks in the professional operation of electric power marketing.

This article combines big data technology to construct a power audit work management system, which improves the efficiency of power audit while further improving work efficiency, and provides a theoretical reference for the further development of subsequent power audit work.

2. Related Work

The United Kingdom is the first country in the world to carry out electricity market reforms. The Office of Gas and Electricity Markets in the United Kingdom is an organization independent of the government, and the electricity regulatory agency supervises both electricity and natural gas markets in the United Kingdom [5]. The Competition Policy and Law Enforcement Department is set up under this regulatory agency. Its main task is to be responsible for the audit business of the electricity market and maintain the stable operation of the electricity market. Australia's electricity marketization is also relatively high. The main responsibility of the Australian Energy Regulatory Agency (AER) is to manage the national electricity market, formulate relevant laws and regulations, and promote the reform of the national electricity market. Moreover, AER also includes audit departments, which mainly carry out audit work within the scope of the power market in various regions of the country [6]. The United States has a high degree of electricity marketization. As a federal country, state-level government departments enjoy a high and independent status [7]. Therefore, the United States has formed a federal and state regulatory system in the electricity market. The Federal Energy Regulatory Commission (FERC) is responsible for state-level power economic regulation, and the State Public Utilities Regulatory Commission (PUC) is responsible for state power regulation. FERC and PUC include the departments that deal with complaints and reports, the departments that mediate disputes, and the departments responsible for administrative penalties [8].

Among the institutions set up within FERC, the three offices, the Law Enforcement Office, the Administrative Litigation Office, and the Administrative Judge's Office, are directly in charge of the inspection work. Based on years of auditing practices, the Law Enforcement Office, Administrative Litigation Office, and Administrative Judge's Office coordinated and cooperated with each other to form a complete audit system and process system. The three offices perform their duties, complement each other, and supervise each other [9]. For example, the Audit Department of the Law Enforcement Office regulates and manages the operation and management of relevant electric power companies according to a certain time frame. The inspection department performs investigation duties and is responsible for handling violations reported by the audit department or other institutions that have been ruled by the committee; if the punished person disagrees with the law enforcement, the office's investigation conclusion can exercise the right to appeal. The Administrative Litigation Office accepts its appeal or adopts other effective methods to resolve incidents and disputes to ensure the speed and fairness of the litigation process and ensure that the case resolution complies with FERC regulations [10]. In order to protect the legitimate rights and interests of clients, the Office of the Administrative Judge needs to conduct detailed investigations and fair punishments of violators or adopt mediation to solve problems. Through the accumulation of long-term practical experience, the US Energy Regulatory Agency has gradually formed a sound system in terms of handling appeals and reporting, coordinating disputes and punishing non-compliance with laws and regulations, and investigating the inspection work [11].

It can be seen from the investigation of relevant literature that there is relatively little research in this field at home and abroad regarding the risk of the marketing business of the power supply company. The more mature research is the power market risk in the process of or after the reform of the western power market. And most of them are related to the financial aspect. Among them, the representative research results are presented in the following. Literature [12] studied the risk management in the competitive power market environment and established the VAR model and its improved CVAR model; literature [13] showed that the utility function and the VAR model are mainly used for the risks that users generate when purchasing electric energy. Literature [14] studies the impact of relevant laws, regulations, and policies on the benefits and risks of power companies in the government's deregulated electricity market;

literature [15] studied the risk assessment of load forecasting errors, combined the differential autoregressive moving average model with the artificial neural network model, predicted the load curve, and then calculated the variance of the load change value.

3. Power Marketing Audit Management Algorithm Based on Big Data Technology

The so-called data mining is to extract effective and available resources and knowledge from the ocean of large amounts of information. There is a large amount of basic data in government and enterprises, and this information is often messy and unrelated, and valuable information may be hidden in it. The conventional analysis tools of this information cannot be expressed. Only through data mining can the hidden information and knowledge be extracted, and the knowledge can be used to guide the work planning and research direction of the government and enterprises. The core step of data mining is the process of knowledge discovery in database (KDD), that is, the step of obtaining the required knowledge module by a specific algorithm in KDD; and the result of its operation directly affects the reliability of the discovered knowledge.

At present, knowledge mining is mainly divided into three stages, and the process is shown in Figure 1 [16].

What data mining needs is to use different methods to take relevant tests for different data to complete different tasks. At present, the more common data mining methods include genetic algorithms, artificial neural networks, and other methods. Although each method has its pros and cons, there is still no general data mining method. More often, different methods are combined and connected in a certain way to make a data mining model, so as to solve some specific problems in a targeted manner [17].

Through the existing different known data, the prediction model can predict the future. Although it cannot provide a very detailed prediction for the entire model, it at least provides a raw data, such as the annual turnover of a restaurant and so on. In this way, these relatively primitive data can provide a more valuable and meaningful reference value for future power marketing and other related fields.

The descriptive model is to classify and summarize the relationships and related rules of some related categories in the data. Moreover, compared to the predictive model, the descriptive model is a more advanced model with more variables. The main classification of the two models is well reflected in the figure below, and the difference between the two is also very well represented in Figure 2 [18].

At present, data mining mainly has the following common analysis and prediction methods:

(1) Linear regression analysis method: for tax-related problems with linear characteristics, linear regression forecasting is the main analysis method. Based on the influence factors of the variable in time, it is divided into two methods: unary linear regression analysis and multiple linear regression.

(2) Nonlinear regression prediction method: exponential curve predictive analysis method and quadratic curve predictive analysis method are commonly used methods to deal with nonlinear power marketing problems. For the electricity marketing problem that continues to grow at a steady rate, the corresponding exponential curve model forecasting model can be established through the exponential curve forecasting method to estimate. If there is a quadratic function relationship between power marketing and a certain macroeconomic variable of the country, the quadratic curve model can better explain it.

(3) Association analysis: association mining algorithms can effectively identify the inherent association relationships between different fields in the data. The more classic algorithm is the Apriori algorithm. At present, the association mining algorithm is mainly used to mine the interrelationships of commodities involved in the massive business operations of enterprises and, on this basis, to measure the consumption behavior of potential customers.

(4) Neural network prediction method: for explained variables with many influencing factors, neural network prediction method is the most suitable predictive analysis method. In addition, compared with other analysis methods, the neural network prediction method effectively avoids the process of defining whether the model is linear in the modeling stage and greatly simplifies the construction and operation of the model.

(5) Classification analysis: the classification method is a kind of guided learning, the category must be clear, and there must be a certain amount of data that has been obtained the classification results to create a classification model (the most commonly used are decision trees, neural networks, etc.), and then it can be used. This classification model classifies new data and is often used to classify customer groups and adopt different marketing methods for customers belonging to different categories.

(6) Cluster analysis: the core idea of cluster analysis is data classification; that is, target data is classified according to different similarities, similar data have similar designated characteristics, and different types of data are different from each other. Cluster analysis is similar to association analysis and has the characteristic of exploring the correlation of data attributes. Among them, the dissimilarity of clusters is calculated based on the attribute value of the description object, and the distance is a frequently used measurement method.

(7) Sequence mode analysis: as the name implies, the sequence mode is used to predict a sequence of actions in a chronological order. For example, in a shopping transaction database, it may be found that the user will purchase a printer for a period of time after purchasing a computer. This is a rule. For another example,

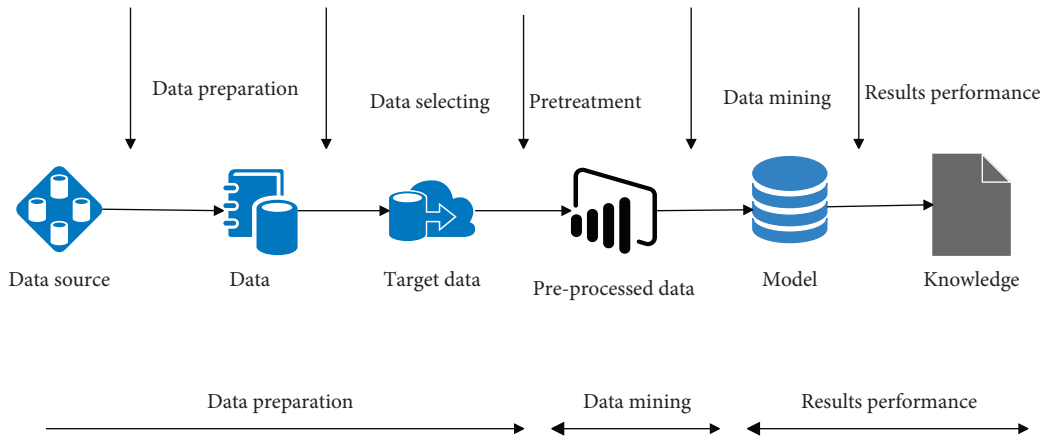

Figure 1: The steps of knowledge mining.

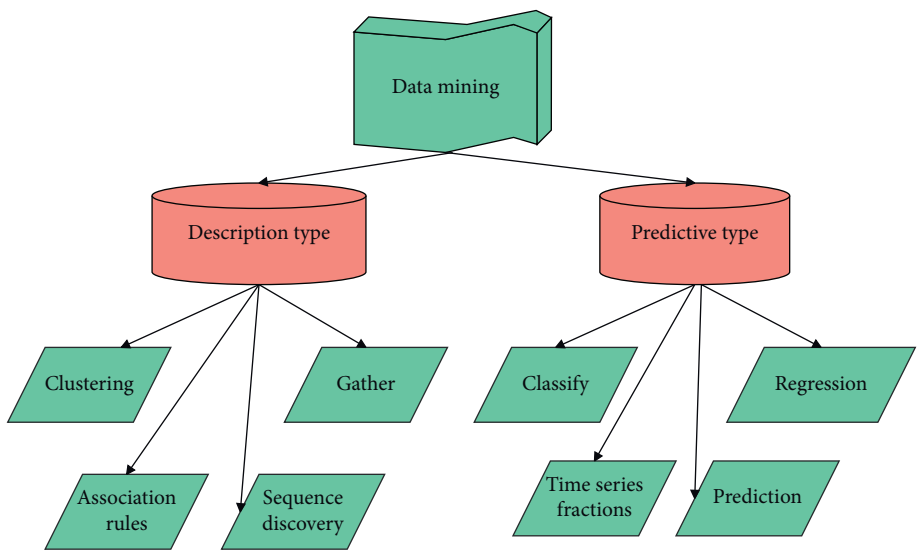

Figure 2: Analysis method of data mining.

through web log analysis, we can find that website viewers usually have a special page flow when browsing pages. Finding such a rule will help the website further provide more user-friendly services.

The various forecasting methods and methods listed above can be classified into two main categories: one is explanatory forecasting methods, which means that some special values are found from different variables or influencing factors. Some specific things establish a very complete linear regression model; the other is a time series analysis method; this method is mainly a systematic and purposeful and targeted research, analysis, and induction of various past data so as to find out the rules and provide relevant suggestions for future decision-making [18].

Data mining technology has broad prospects in the field of electric power marketing audit due to its intuitive, concise, and efficient characteristics. Some experts and scholars at home and abroad have put forward many viewpoints in this regard. The main direction of their research is to mine unknown information through different data mining algorithms from the built data warehouse and apply it to the intelligent selection of audits. After that, by mining the basic information of electric power marketers and analyzing electric power marketing behaviors, the source of the cases that may have problems is screened.

Tobit model: its main form is as follows: it sets a certain electricity expenditure as the explained variable y_i and the corresponding explanatory variable as X_i. Then, we can know that there are only two results for the electricity expenditure level y_i: one is greater than y_0, which represents the minimum expenditure level of the electricity, and the other is directly zero. Therefore, under the research assumption that the model is linear, the relationship between power expenditure y_i and explanatory variable X_i is [19]

$$y_i = \begin{cases} \beta^T X_i + e_i, & \text{if } \beta^T X_i + e_i > y_0 \\ 0, & \text{other} \end{cases}, \quad e_i \sim N\left(0, \sigma^2\right), i = 1, 2, \ldots, n. \tag{1}$$

Among them, Xi is the (k+1)-dimensional explanatory variable vector, and β is the (k+1)-dimensional unknown parameter vector. This model is called a censored regression model. We deform the above model and subtract y_0 from both sides of the equation under the premise that y_0 is known. In the resulting model, the constant term is equal to the original constant minus y_0. The form of this model is called the Tobit model [20].

$$y_i = \begin{cases} \beta^T X_i + e_i, & \text{if } \beta^T X_i + e_i > y_0 \\ 0, & \text{other} \end{cases}, \quad e_i \sim N\left(0, \sigma^2\right), i = 1, 2, \ldots, n. \tag{2}$$

The Tobit model can also be expressed as

$$y_i = \max\left\{\beta^T X_i + e_i, 0\right\}, \quad fdghjk. \tag{3}$$

or

$$y_i = \beta^T X_i + e_i, \quad y_i = \begin{cases} y_i, & \text{if } y_i > 0, \\ 0, & \text{if } y_i \le 0. \end{cases} \tag{4}$$

For the Tobit model, the explanatory variable Xi is observable (that is, Xi takes the actual observation value), and the explained variable y_i cannot be directly obtained, but is observed in a restricted way. When $y_i^* > 0$, $y_i = y_i^* > 0$, y_i at this time is the "unrestricted" observation value. When $y_i^* \le 0$, $y_i = 0$, at this time y_i is the "restricted" observation value. Obviously, "restricted" observations are all truncated to 0, and "unrestricted" observations are taken as actual observations.

For the analysis of the Tobit model, the core idea is to measure the estimated values of β and σ^2 based on n (n> k) observations of y_i and X_i. When using the model, we assume that when $y_i = 0$, the observed value is n_0, and when $y_i > 0$, the observed value is n_1; then the total amount is $n = n_0 + n_1$.

If the observation value n_0 at $y_i = 0$ is ignored, then the remaining n_1 observation values are complete observation values (yi > 0), and β can be estimated by the least square method in the calculation. However, the least squares estimate in this range is biased and inconsistent. Then, the conditional expectation of the observation value y_i at $y_i > 0$ is [21]

$$E\left(e_i | y_i > 0\right) = E\left(e_1 | e_i > -\beta^T X_i\right) = \sigma \cdot \frac{f_i}{F_i}. \tag{5}$$

Therefore,

$$Y_i = \beta^T X_i + e_i = \beta^T X_i + \sigma \cdot \frac{f_i}{F_i} + u_i. \tag{6}$$

Among them, f_i and F_i are, respectively, the probability density function and the distribution function of the standard normal distribution under the condition ($\beta^T X_i/\sigma$). Since the least squares estimator does not calculate the item $\sigma f_i/F_i$ that is not independent of Xi, the least squares estimator is biased and inconsistent. Since $e_i \sim N(0, \sigma^2)$,

$$E\left(e_i | y_i > 0\right) = \sigma \cdot \frac{f_i}{F_i} > 0. \tag{7}$$

That is, the least squares estimator of β is biased.

If $n = n0+n1$ observations are taken into consideration, the unconditional expectation of yi is $E(y_i) = F_i \cdot (\beta^T X_i) + \sigma \cdot f_i$.

Therefore, even if the least squares method is applied to all n observations, the unbiased and consistent estimators of the Tobit model are difficult to obtain. In summary, the maximum likelihood estimators of β and σ^2 are consistent estimators, and the maximum likelihood estimation method is the preferred method for calculating the estimator of the Tobit model.

The core of this research design is to extract appropriate data from the huge power marketing audit management system to establish indicators. This involves the storage and extraction of power marketing data and the process of data mining. At this stage, the establishment of a special audit data warehouse is the development trend of electric power marketing. This chapter will discuss the related concepts of the data warehouse, design the construction process of the data warehouse, and give the Tobit regression analysis steps based on the discriminant method.

Because of the continuous extension and broadening of its concept, the data warehouse itself has continued to develop and expand. As far as we can conclude, the entire data warehouse has the following characteristics:

(1) Subject-orientation: an abstract theme is mainly used to show how different customers are concerned about the analysis of different data. Each topic is a field of data analysis, and the topics are independent of each other.

(2) Integration: the data in the data warehouse is formed by extracting, processing, and analyzing data from different data sources. In this process, the data in each data source should be consistent in order to achieve effective extraction, processing, and analysis from each other.

(3) Relative stability: it refers to the phenomenon that once the data in the data warehouse is loaded or used, it will be stored for a long time and the data will rarely be modified such as changes and deletions.

(4) Reflecting history: the data in the warehouse obviously represents a certain period of time in the past. It stores a certain period of historical data. The choice of time point is mainly to meet the needs of decision support analysis.

(5) Dynamic data: the data in the warehouse is not completely static. In order to meet the needs of decision-making, the latest data must be frequently loaded into the data warehouse, and from the perspective of operational efficiency, the data beyond the scope of statistical analysis must be archived to tape, or it is also nonstatic to make some appropriate corrections to the data in the warehouse, such as on the CD-ROM.

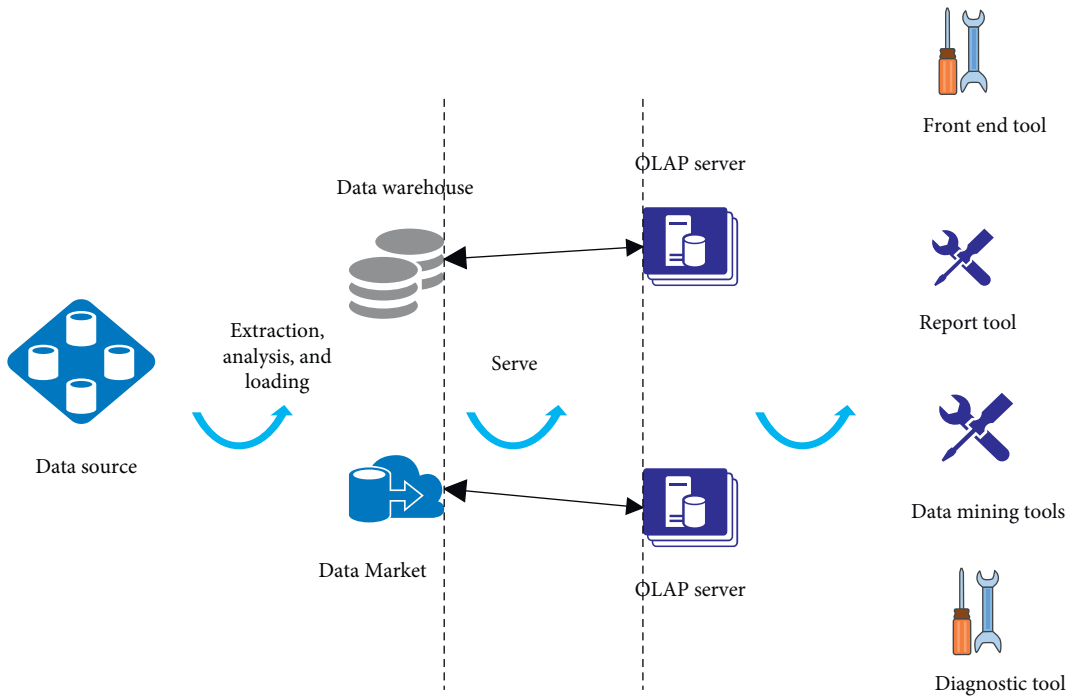

Figure 3: System structure of data warehouse.

According to the above, we can find that the data warehouse is actually a kind of dynamic, can reflect a certain reality very quickly, and can provide relevant decision makers or leaders with very effective data and information in a short time., So as to help them realize an important tool for decision-making. In addition, the data warehouse is therefore regarded by many people as a system and structure and can provide systematic research and analysis.

Data mining technology is based on massive amounts of raw data. In the same way, the use of data mining technology in the power marketing system must rely on a powerful power marketing information platform. The emergence of data warehouses effectively solves this difficulty and provides a strong guarantee for power marketing agencies to implement data mining.

The construction of the data warehouse is based on a large amount of existing business data, as shown in Figure 3. Moreover, the construction of a good data warehouse often requires a lot of manpower and money, and the relevant personnel need to have very good qualities and related technologies, and they must be very careful in the data entry process. Therefore, it is very difficult to build a data warehouse.

The data source is the basic element of the data warehouse. The key to a data warehouse is to store and manage data, conduct targeted information extraction, cleaning, and integration for different business systems, and organize them according to themes. According to the coverage of data, data warehouses can be divided into enterprise-level data warehouses and department-level data warehouses.

Data storage and management are the core of the entire data warehouse system. The main components are ROLAP, MOLAP, and HOLAP. The basic data and aggregated data of ROLAP are stored in RDBMS. The basic data and aggregated data of MOLAP are stored in a multidimensional database. The basic data of HOLAP is stored in RDBMS, and the aggregated data is stored in a multidimensional database.

The OLAP server can effectively integrate the required data and combine them in a certain structure for extraction, processing, and analysis and to find out effective information.

The front-end tools mainly include three stages: various reporting tools, query tools, data warehouse planning, and analysis phase; data warehouse design and implementation phase; and data warehouse use and maintenance. These three stages are a continuous cycle and an improvement process. Under normal circumstances, the data warehouse system cannot be completed in one cycle, but after many cycles of development, each cycle will add new functions to the system, so that the application of the data warehouse will be improved.

The development of everything has its own unique and complete life cycle, and so does the data warehouse. Generally speaking, the development and application cycle of a data warehouse can be divided into the stages shown in Figure 4.

In view of the cyclical principle of its operation and development, when we apply it to the development of the power marketing system platform, we compare its analysis, implementation, and maintenance in the three stages shown in Figure 5.

After establishing the power marketing audit selection data warehouse and the corresponding data mining algorithm, the key step of the research is to filter the appropriate indicator system from the excavated audit information, thereby establishing a Tobit regression model to evaluate the

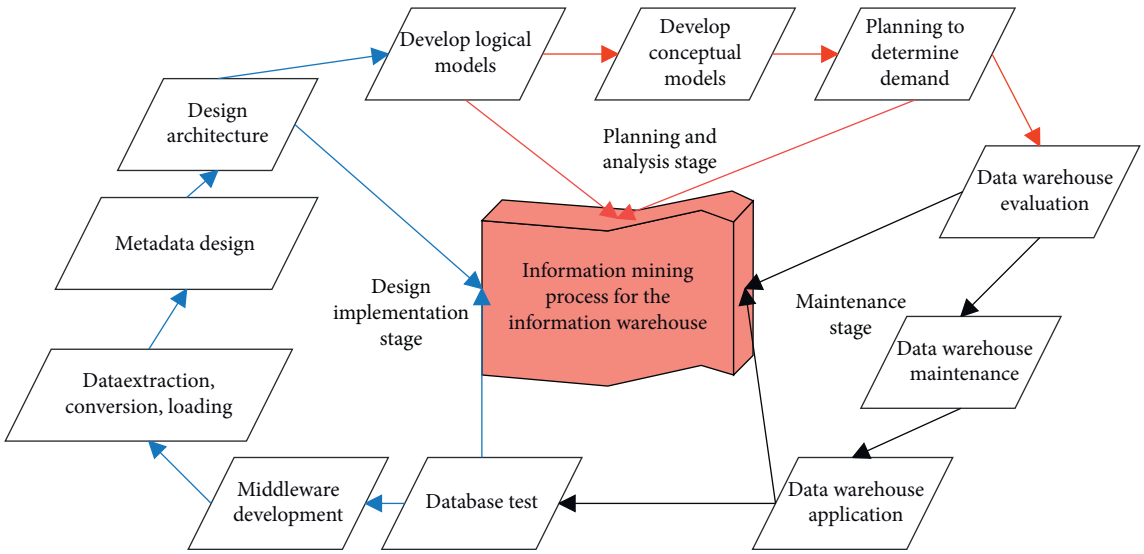

Figure 4: The information development process of the data warehouse.

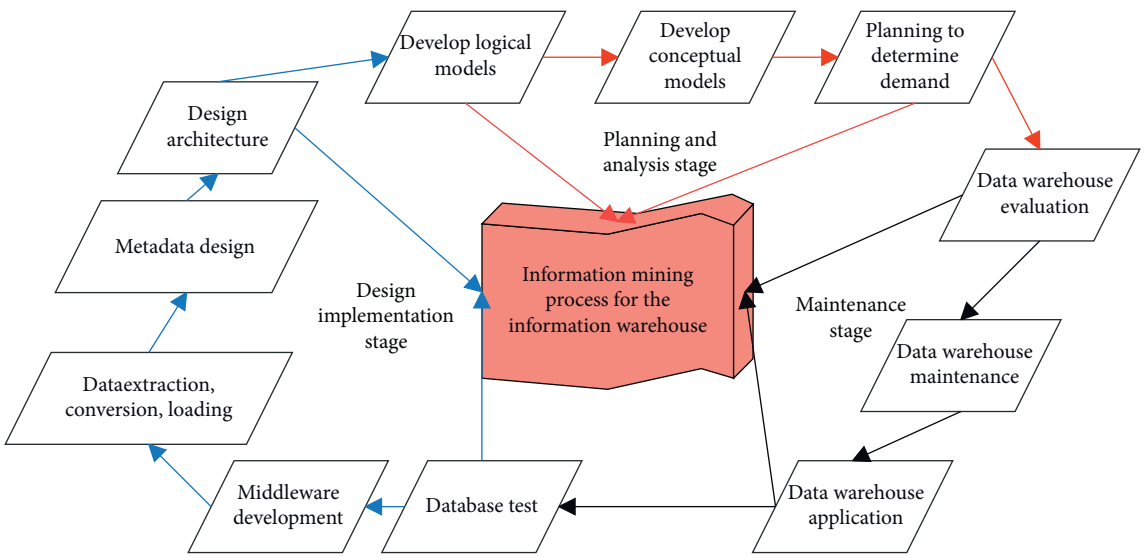

Figure 5: Application model of data warehouse for audit case selection.

power marketing situation and determine the scope of the case selection, as shown in Figure 6. Since the selection methods and principles of the index system have been systematically explained above, the corresponding power marketing analysis model can be simulated in combination with the research data under this research idea.

4. System Construction

The power marketing audit and monitoring system is designed to be centrally deployed at the provincial level, but is independent of the marketing business system; that is, the application release of the two systems does not affect each other. The systems realize application access through the integrated integration platform according to standard interfaces and business services encapsulated by models, call functions to obtain information from each other, and return results in real time. The designed application integration deployment logic diagram is shown in Figure 7.

In order to realize the seamless connection of process authority between the marketing business application system and the marketing audit monitoring system, this paper integrates the organizational authority, work flow of the audit monitoring system, and the marketing business application system to achieve the integration of the organizational authority of the two. At the same time, the data interaction between the production management system and other peripheral systems and the marketing audit monitoring system can also be implemented through the integrated platform. The process integration diagram is shown in Figure 8.

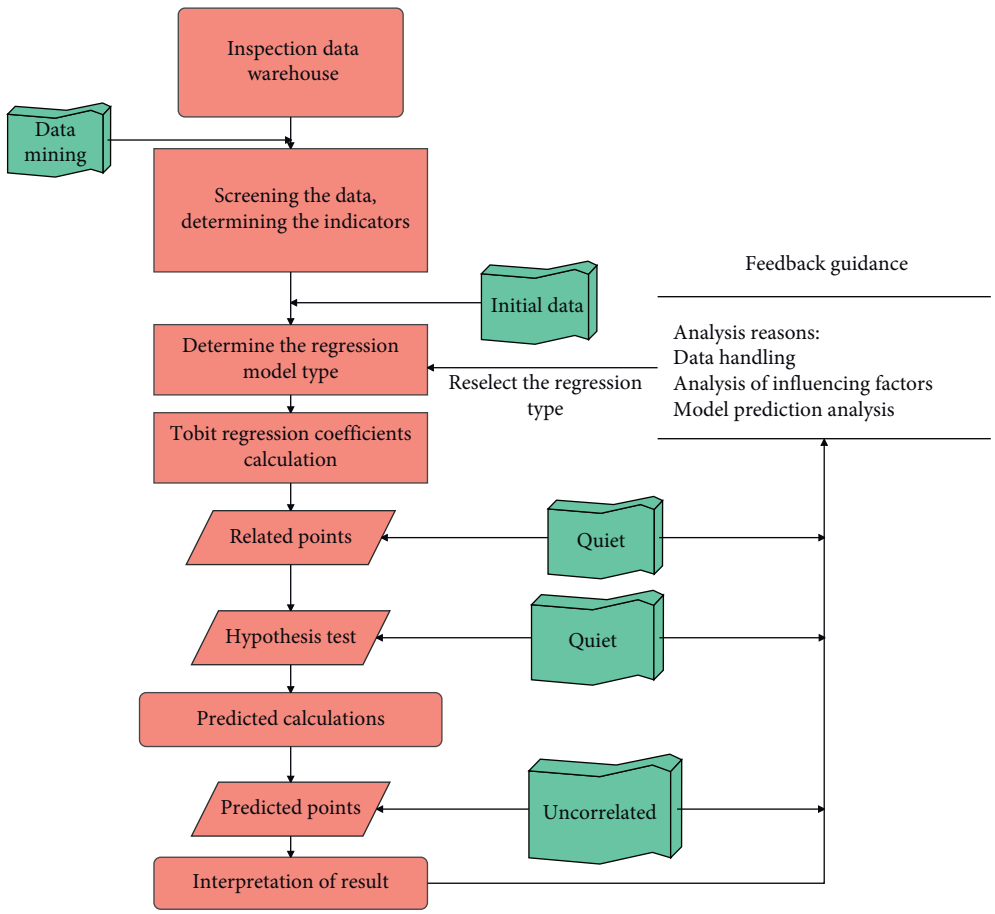

FIGURE 6: Tobit regression model establishment steps.

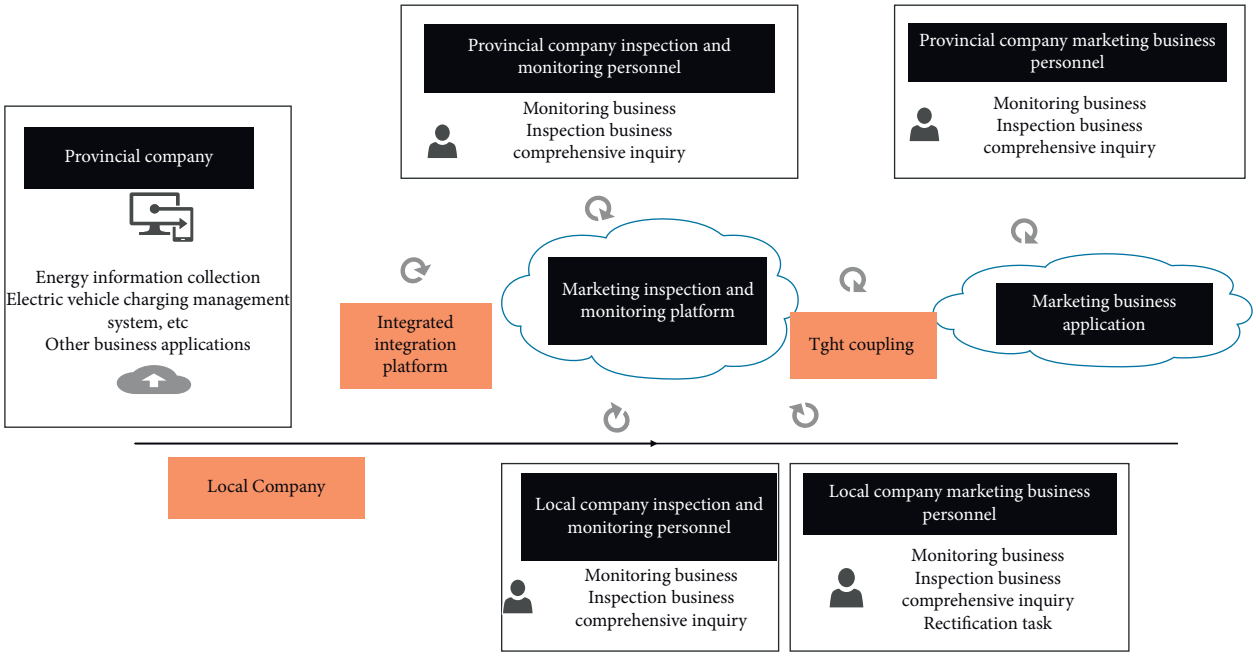

FIGURE 7: Logic diagram of application integration deployment.

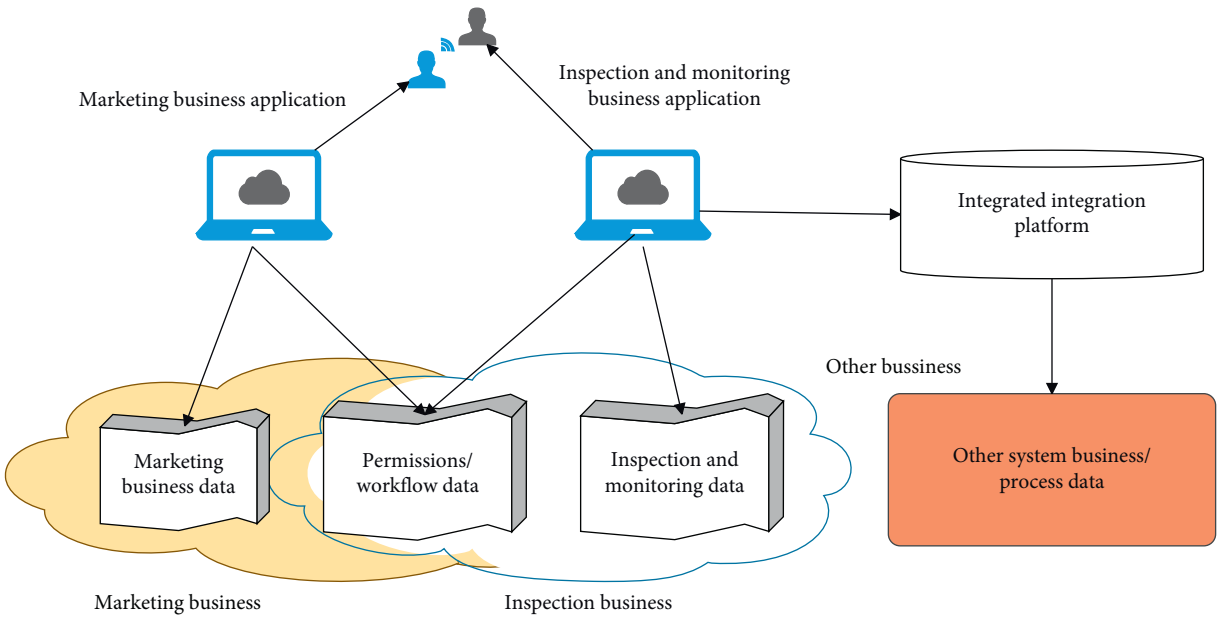

Figure 8: Schematic diagram of process integration.

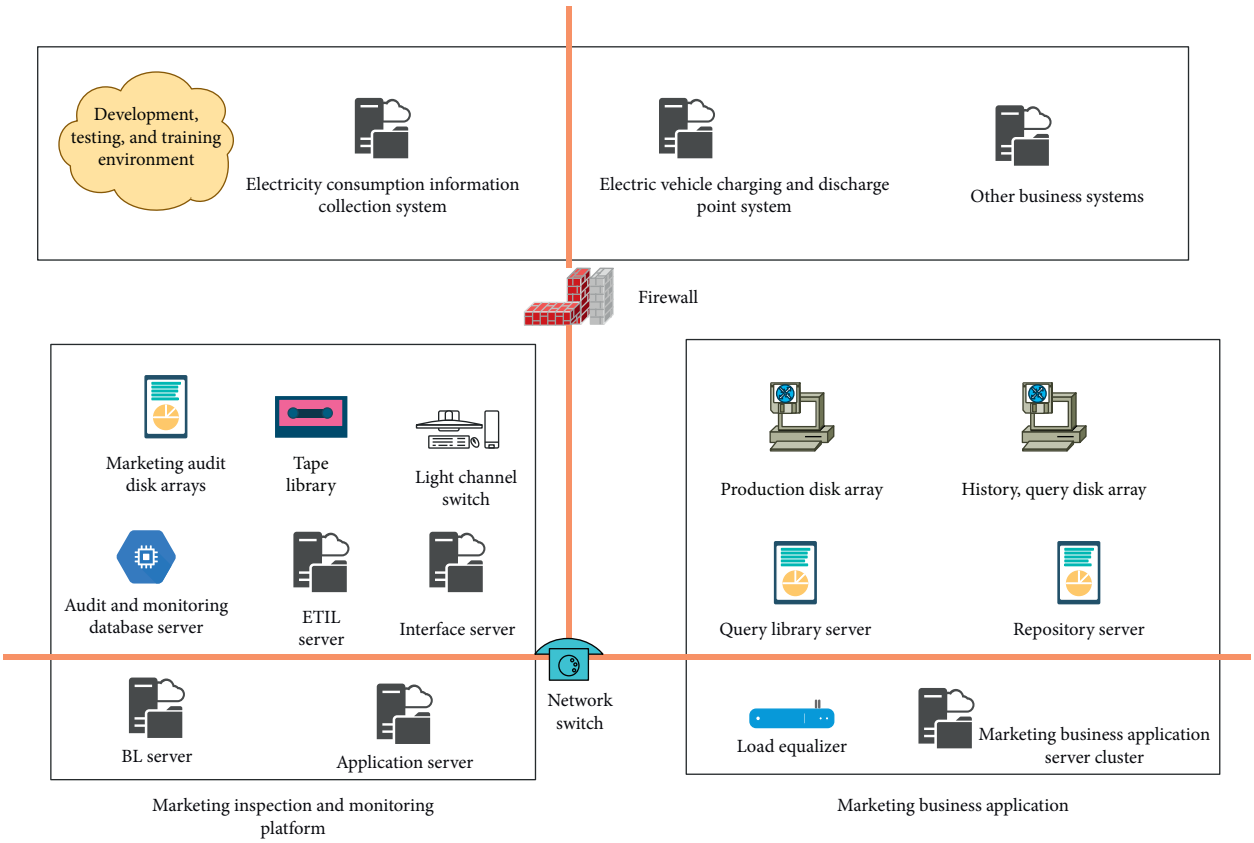

Figure 9: The physical architecture deployment diagram of the electric power marketing audit and monitoring system.

There are roughly two ideas for the design of the marketing audit monitoring platform. The first is to design the monitoring platform as an independent system that can maintain normal communication with related business systems. The second is to deploy the monitoring platform in the existing power marketing system. The two systems share the infrastructure such as the computer room, information security, and backup equipment. The second idea is used in the design of this paper. The physical architecture of the specific monitoring platform is shown in Figure 9.

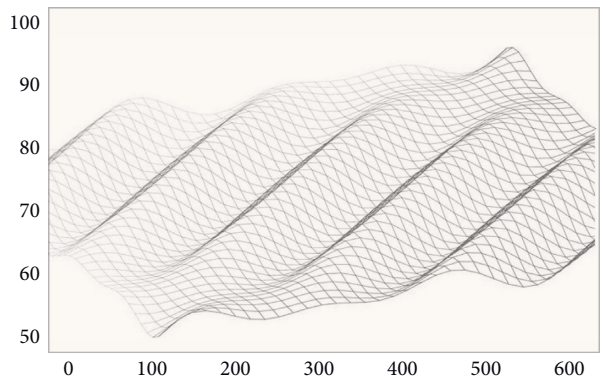

Figure 10: Data mining effect of power marketing audit management system based on big data technology.

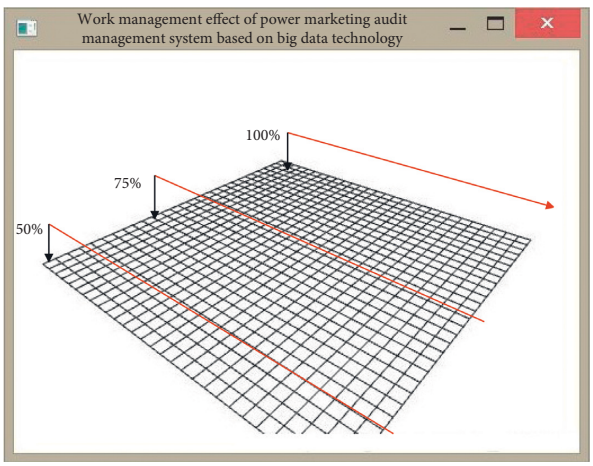

Figure 11: Work management effect of power marketing audit management system based on big data technology.

On the basis of the above research, this paper verifies the power audit data mining effect of the algorithm model proposed in this paper and builds a database based on historical data. Moreover, this paper uses the system proposed in this paper to perform data mining simulation, and the results are shown in Figure 10.

From the perspective of data mining simulation, the power marketing audit management system proposed in this paper can play an important role in power marketing audit data analysis. On this basis, this paper explores the effect of power marketing audit management system on the management effect of power marketing audit work, and the results obtained through simulation are shown in Figure 11.

From the above research, it can be seen that the power marketing audit management system based on big data technology can play an important role in power audits.

5. Conclusion

Power marketing audit management can be regarded as a key point in the entire power marketing process, and it is extremely important in power marketing management. The specific work it carries out will often directly affect the basic image and fundamental interests of power companies and, at the same time, will have a more important impact on the interests of electricity customers in the electricity market. Since there are many links in the processing of various electric power business operations, problems in any one link may cause huge losses to the electric power company. Therefore, the essence of power marketing audit management is a supervision process of management, cooperation, and operation of various links. This is a means implemented in order to maximize the protection of the power companies' own interests and the fundamental interests of electricity customers. In addition, this method is used to avoid errors that may occur or exist in the progress of various power marketing businesses and to prevent losses. This article combines big data technology to construct a power audit work management system, which improves the efficiency of power audit while further improving work efficiency, and provides a theoretical reference for the further development of subsequent power audit work.

Data Availability

The data used to support the findings of this study are included within the article.

Conflicts of Interest

The authors declare that there are no conflicts of interest regarding this work.

References

[1] A. M. P. Milani, F. V. Paulovich, and I. H. Manssour, "Visualization in the preprocessing phase: Getting insights from enterprise professionals," *Information Visualization*, vol. 19, no. 4, pp. 273–287, 2020.

[2] T. C. Huber, A. Krishnaraj, D. Monaghan, and C. M. Gaskin, "Developing an interactive data visualization tool to assess the impact of decision support on clinical operations," *Journal of Digital Imaging*, vol. 31, no. 5, pp. 640–645, 2018.

[3] H. Gubler, N. Clare, L. Galafassi, U. Geissler, M. Girod, and G. Herr, "Helios: history and anatomy of a successful in-house enterprise high-throughput screening and profiling data analysis system," *SLAS Discovery*, vol. 23, no. 5, pp. 474–488, 2018.

[4] J. W. Windsor, F. E. Underwood, E. Brenner et al., "Data visualization in the Era of COVID-19: an interactive Map of the SECURE-IBD Registry," *American Journal of Gastroenterology*, vol. 115, no. 11, pp. 1923-1924, 2020.

[5] M. Jayakrishnan, A. K. Mohamad, and A. Abdullah, "Journey of an enterprise architecture development Approach in Malaysian Transportation industry," *International Journal of Engineering and Advanced Technology*, vol. 8, no. 4, pp. 765–774, 2019.

[6] T. Xu, G. Song, Y. Yang, P. X. Ge, and L. X. Tang, "Visualization and simulation of steel metallurgy processes," *International Journal of Minerals, Metallurgy and Materials*, vol. 28, no. 8, pp. 1387–1396, 2021.

[7] K. Kasemsap, "Knowledge discovery and data visualization," *International Journal of Organizational and Collective Intelligence*, vol. 7, no. 3, pp. 56–69, 2017.

[8] R. C. Basole, A. Srinivasan, H. Park, and S. Patel, "ecoxight," *ACM Transactions on Management Information Systems*, vol. 9, no. 2, pp. 1–26, 2018.

[9] A. Pieroni, N. Scarpato, L. Di Nunzio, F. Fallucchi, and M. Raso, "Smarter city: smart energy grid based on blockchain technology," *International Journal of Advanced Science, Engineering and Information Technology*, vol. 8, no. 1, pp. 298–306, 2018.

[10] K. Gai, Y. Wu, L. Zhu, M. Qiu, and M. Shen, "Privacy-preserving energy trading using consortium blockchain in smart grid," *IEEE Transactions on Industrial Informatics*, vol. 15, no. 6, pp. 3548–3558, 2019.

[11] L. N. Chavali, N. L. Prashanti, K. Sujatha, G. Rajasheker, and P. B. Kishor, "The emergence of blockchain technology and its impact in biotechnology, pharmacy and life sciences," *Current Trends in Biotechnology and Pharmacy*, vol. 12, no. 3, pp. 304–310, 2018.

[12] K. Luchoomun, S. Pudaruth, and S. Kishnah, "Implementation of a proof of concept for a blockchain-based smart contract for the automotive industry in Mauritius," *International Journal of Advanced Computer Science and Applications*, vol. 11, no. 3, pp. 71–81, 2020.

[13] A. Whitaker and R. Kräussl, "Fractional equity, blockchain, and the future of creative work," *Management Science*, vol. 66, no. 10, pp. 4594–4611, 2020.

[14] A. Verma, "Security of Internet of things using blockchain: an Overview," *International Journal of Management, IT and Engineering*, vol. 9, no. 6, pp. 406–412, 2019.

[15] F. Antonucci, S. Figorilli, C. Costa, F. Pallottino, L. Raso, and P. Menesatti, "A review on blockchain applications in the agri-food sector," *Journal of the Science of Food and Agriculture*, vol. 99, no. 14, pp. 6129–6138, 2019.

[16] A. S. Yadav and D. S. Kushwaha, "Query Optimization in a blockchain-based Land Registry management system," *Ingénierie des Systèmes d'Information*, vol. 26, no. 1, pp. 13–21, 2021.

[17] A. Kumar, A. Prasad, and R. Murthy, "Application of blockchain in usage based Insurance," *International Journal of Advance Research, Ideas and Innovations in Technology, IJARIIT*, vol. 5, no. 2, pp. 1574–1577, 2019.

[18] Z. Rezaee, A. Dorestani, and S. Aliabadi, "Application of time series analyses in big data: practical, research, and education implications," *Journal of Emerging Technologies in Accounting*, vol. 15, no. 1, pp. 183–197, 2018.

[19] E. Huerta and S. Jensen, "An accounting information systems perspective on data analytics and Big Data," *Journal of Information Systems*, vol. 31, no. 3, pp. 101–114, 2017.

[20] S. Balne, "Analysis on research methods in Bigdata applications," *International Journal of Innovative Research in Computer and Communication Engineering*, vol. 8, no. 10, pp. 4059–4063, 2020.

[21] P. B. de Laat, "Algorithmic decision-making based on machine learning from Big Data: can transparency restore accountability?" *Philosophy & technology*, vol. 31, no. 4, pp. 525–541, 2018.

Hindawi
Mobile Information Systems
Volume 2022, Article ID 8493004, 12 pages
https://doi.org/10.1155/2022/8493004

Research Article

Dynamic Budget Management of Rural Public Affairs Based on Internet of Things Technology

Xue Pei

Shanxi Vocational University of Engineering Science and Technology, Jinzhong, Shanxi 030619, China

Correspondence should be addressed to Xue Pei; 201603561408@stu.yznu.edu.cn

Received 18 June 2022; Revised 15 July 2022; Accepted 19 July 2022; Published 8 August 2022

Academic Editor: Chi Lin

In order to improve the budget management of rural public affairs, this paper combines the Internet of things technology to construct an information processing system that can be used for dynamic budget management of rural public affairs and optimizes the internal resource processing process of the system. In order to overcome the constraints and differences of resource QoS attributes and ensure that the QoS attribute values of candidate resources are within the user's expectations, this paper introduces penalty factors and grey incidence matrix to analyze the gap between resource QoS attribute values, and calculates the similarity between matching resources and user-requested resources. In addition, this paper combines the dynamic budget requirements of rural public affairs to construct system function modules. Finally, this paper evaluates the Internet of Things data transmission and rural public affairs dynamic budget management effects of the system constructed in this paper, and conducts simulation research based on the data collected by the network. From the experimental research, we can see that the dynamic budget management system of public affairs based on the Internet of things technology constructed in this paper has good results.

1. Introduction

Under the strict registered residence system and the high-speed urbanization, China's economic structure, social structure, and management structure of grassroots public affairs have undergone major changes. Although in recent years, with the rapid advancement of urbanization to rural areas, the rapid flow of population and the gradual weakening of the traditional small-scale peasant economic model based on the household contract responsibility system, and the boundary of urban-rural dual structure are also gradually blurred; on the whole, rural development and rural governance are still important parts of all affairs in China [1].

China is a large agricultural country with a vast territory and a large rural population, accounting for about 80% of the national population. Since the reform and opening up, China's rural economy has achieved good development. However, due to the weak foundation of rural economy and the constraints of the initial development stage of industrialization, the development pattern of urban-rural dual economic structure also brings many problems to rural economic development, such as the widening gap between urban and rural development, the widening income gap between rural residents and urban residents, and the serious pollution of rural environment [2]. These influences, together with other disharmonious factors, bring severe challenges to the long-term, stable, and healthy development of rural areas. The issue of "agriculture, rural areas, and farmers" is a major issue related to the National People's livelihood, and needs to be urgently solved. The Party Central Committee has been paying close attention to the "three rural" issues. The Fifth Plenary Session of the 16th CPC Central Committee proposed to solidly promote the construction of a new socialist countryside in accordance with the requirements of "production development, affluent life, civilized rural style, clean village appearance, and democratic management". This is not only the strategic goal of the current work of "agriculture, rural areas, and farmers" but also an important connotation of accelerating the construction of a new socialist countryside with a well-off society in an all-round way. The goal of building a new socialist countryside puts forward new and higher

requirements for innovative agriculture and rural public management functions. Moreover, this also puts forward higher requirements for the work of township governments. Township government is the most grassroot level government in China and the basis of China's political power. The township government is under the jurisdiction of the superior county government and directly faces the farmers. It is an important bridge and link between the government and farmers and provides public goods and services for the stable development of rural economy [3].

In essence, finance is an important factor affecting the management of rural public affairs. Therefore, this paper combines the Internet of things technology to carry out the dynamic budget management system of rural public affairs and analyzes the dynamic management of rural public affairs through the system, so as to improve the efficiency of rural public affairs management.

2. Related Work

The literature [4] proposed a systematic theory on budget balance, marking the beginning of the midterm rolling budget. The literature [5] pointed out that the focus of the long-term annual budget is only to balance the corresponding budget in a single year. Although it can promote the effective control of the government's expenditure to a certain extent, it seriously deviates from the national macroeconomic policy. Therefore, while improving the quality and efficiency of financial management of government departments, it is necessary to emphasize midterm planning. The literature [6] emphasizes the perfect integration of evaluation results and project budgets, which has played a huge role in improving the efficiency of government budget management and effectively improving the budget efficiency of government departments. The literature [7] conducted a comprehensive study on government budget planning. The author pointed out the role of federal government management efficiency. Using budget performance management and implementing performance budgeting can make the government shift its focus from input to output. At the same time, it reduces the unfairness of the allocation of resources with political factors. Literature [8] systematically studied the performance budget and pointed out that the so-called performance budget means to establish a budget management model that can adapt to the current state of government management according to cost factors based on performance goals. Literature [9] conducted a systematic study on the use of departmental budgets, and pointed out the challenges it faces in the process of government use. For example, the lack of motivation for departmental budget reforms, the consensus on the expected accomplishment of goals, the measurement of service costs and results, and the use of performance in the budgeting process cannot be solved. Literature [10] uses a budget management system to dynamically monitor the execution of all fiscal revenues and expenditures. Literature [11] pointed out that the transparency of government budgets largely determines the authenticity of government financial data. It can be seen that when budget transparency is very high, it means that the more truthful the data, the fewer opportunities for fraudulent accounts. Therefore, we can grasp government financial information as much as possible on the basis of improved budget transparency, so as to promote citizens' participation in government affairs.

In addition, foreign scholars have also analyzed many problems in departmental budgets: first, the department did not pay attention to the importance of consensus when preparing budgets, and the content of determining common consensus was not included in related documents and systems. As mentioned, this has led to the improvement of performance and the scientific nature of the evaluation stage being greatly weakened [12]; second, since agencies do not have a clear and complete understanding of budget goals in the process of expanding business channels, they will focus on most of them, which tend to increase the number of business completions. In addition, the communication between the departments is not sufficient. This is also an objective fact caused by the departments in charge of different projects, which will cause certain difficulties in setting performance indicators. Moreover, the quality and reliability of the project itself cannot be completely determined, which also adds a burden to the performance appraisal [13]. Therefore, it is very difficult to determine the relationship between budget and performance.

Literature [14] analyzed the reasons for the establishment of the departmental budget system and answered in detail the characteristics of the departmental budget system and how to update the system. Their analysis shows that there are still many contradictions in my country's departmental budget reform at this stage, such as conflicts between zero-based budgets and revenue and expenditure items and inconsistent expenditure standards. Literature [15] proposes that departmental budgets should be prepared on a departmental basis, and the financial department should first review them, and then formulate and approve them by the People's Congress. In summary, it fully reflects the overall revenue and expenditure of each department in the budget year. After the audit by the financial department, the audit results will be submitted to the legislature for re-examination. If the relevant standards are met, a comprehensive fiscal plan can be established. The literature [16] further clarified the relationship among the people, administrative agencies, power organs, and government functional departments in departmental budget management and further explained the composition of the delegation and authorization chain in budget management, pointing out that due to information for reasons such as asymmetry, weak supervision, and low levels of punishment for corruption, the establishment of an effective supervision mechanism is the key to solving the agency problem of departmental budgets. Literature [17] pointed out that administrative units generally have problems such as insufficient budget management awareness, poor compilation quality, lack of continuous supervision in the budget process, and low overall quality of the staff involved in the preparation of the budget. A detailed analysis of the causes of these problems has been made. Starting from the two levels of the management and the leadership at the same time, it

proposed solutions to improve the budget management awareness of relevant managers, strengthen the monitoring of the preparation, and strengthen the supervision.

3. Optimal Management of System Resources Based on the Internet of Things

This paper mainly considers the resources with the same service function. The QoS attributes of the resources are set according to user preferences and have certain scalability. In order to facilitate the analysis of the whole evaluation process, we give the following definitions for some parameters involved.

Definition 1. The QoS attribute set of user-requested resources is uq. $uq = \{uq_1, uq_2, \ldots, uq_m\}$ describes the QoS requirements of user requests for resources and determines the QoS attributes to be evaluated. $uq_j\,(1 \le j \le m)$ in the set is represented by the values of different QoS attributes, such as response time, availability, and price.

Definition 2. Dynamic resource price. The dynamic price of resources in the fog computing environment is shown in formula (1) [18]:

$$p_r = U * b\frac{u}{\varphi} * D_{\text{dev}}. \tag{1}$$

Among them, U is the basic price of the service, u is the number of service requests completed per unit time, and φ is the number of service requests received per unit time. B is the price adjustment factor, which is determined by the service provider. D_{dev} indicates the type of equipment. It can generally be divided into static equipment, small mobile equipment, and large mobile equipment. The relative reserved resources of each device are 1, 1.25, and 1.5 times, respectively.

Definition 3. The set of available resources is Rs. $Rs = \{r_1, r_2, \ldots, r_n\}$ is used to describe resources with the same service functions. In the resource set, $r_i\,(1 \le i \le n)$ represents the i th resource. Each resource is evaluated according to the same QoS attribute to determine the matching between user requirements and resources.

Definition 4. The QoS attribute set of available resources is Rq. $Rq = \{rq_1, rq_2, \ldots, rq_m\}$ is used to describe the QoS attribute value of available resources. Each QoS attribute $rq_j\,(1 \le j \le m)$ of the available resource is consistent with the QoS attribute of the user requested resource.

Definition 5. The resource QoS attribute matrix is R. In this paper, it is used as the decision matrix in evaluation. If it is assumed that there are n available resources and each resource has m QoS attributes, the matrix R is

$$R = \left(r_{ij}\right)_{n\times m} = \begin{bmatrix} r_{11} & r_{12} & \cdots & r_{1m} \\ r_{21} & r_{22} & \cdots & r_{2m} \\ \vdots & \vdots & \ddots & \vdots \\ r_{n1} & r_{n2} & \cdots & r_{nm} \end{bmatrix}. \tag{2}$$

Among them, r_{ij} represents the value of the j th QoS attribute of the i th resource.

Definition 6. The resource QoS standardization matrix is $z = (z_{ij})_{n\times m}$. Due to the different unit dimensions of QoS attributes, it needs to be unified. Therefore, formula (3) is adopted for standardization according to the relationship between attribute and user satisfaction [19].

$$z_{ij} = \begin{cases} \dfrac{r_{ij} - 0r_j^{\min}}{r_j^{\max} - r_j^{\min}}, (a) \\ \\ \dfrac{r_j^{\max} - r_{ij}}{r_j^{\max} - r_j^{\min}}, (b) \end{cases}. \tag{3}$$

Among them, (a) is the case where the j th QoS attribute is a positive attribute and (b) is the case where the j th QoS attribute is a negative attribute. When condition (a) is satisfied, the greater the attribute value, the higher the user satisfaction. On the contrary, the smaller the attribute value, the higher the user satisfaction. $r_j^{\min}$ and $r_j^{\min}$ are the minimum and maximum values in column J of the standardized matrix, respectively.

Definition 7. Weight of QoS attribute. In order to ensure the objectivity of the evaluation results, we use the direct weight method to determine the entropy value e_j and entropy weight w_j of each resource QoS attribute according to formulas (4) and (5):

$$e_j = -\frac{1}{\ln n}\sum_{i=1}^{n} f_{ij} \cdot \ln f_{ij}. \tag{4}$$

$$w_j = \frac{1 - e_j}{m - \sum_{j=1}^{m} e_j}. \tag{5}$$

Among them, $f_{ij} = (z_{ij}/(\sum_{i=1}^{n} z_{ij}))$, $\sum_{j=1}^{m} w_j = 1$.

Definition 8. The matching resource set is $R_p = \{rp_1, rp_2, \ldots, rp_k\}$. The matching resource set R_p is a subset of the available resource set R_s, which is used to represent the available resources that need matching calculation. Among them, rp_k is the k-th resource, $1 \le k \le n$.

Definition 9. The candidate resource set is $R_s' = \{r_1', r_2', \ldots, r_l'\}$. The set is composed of resources that meet the matching conditions in the matching resource set R_p. Among them, r_l' is the l th resource in the set, $1 \le l \le k$.

Definition 10. The resource matching matrix is R_p. It is composed of QoS attribute values of each resource in the n set and user requested resources [20].

$$P = \begin{bmatrix} rp_{11} & rp_{12} & \cdots & rp_{1m} \\ rp_{21} & rp_{22} & \cdots & rp_{2m} \\ \vdots & \vdots & \ddots & \vdots \\ rp_{k1} & rp_{k2} & \cdots & rp_{km} \\ uq_1 & uq_2 & \cdots & uq_m \end{bmatrix}. \quad (6)$$

Among them, rp_{kj} is the value of the j th QoS attribute of the k th resource in the R_p set.

Definition 11. The matching resource standardization matrix is p . It is used to describe the standard value of the resource matching matrix P processed by formula (3).

$$P' = \begin{bmatrix} rp'_{11} & rp'_{12} & \cdots & rp'_{1m} \\ rp'_{21} & rp'_{22} & \cdots & rp'_{2m} \\ \vdots & \vdots & \ddots & \vdots \\ rp'_{k1} & rp'_{k2} & \cdots & rp'_{km} \\ uq'_1 & uq'_2 & \cdots & uq'_m \end{bmatrix}. \quad (7)$$

Among them, rp'_{kj} is the normalized value of the j th QoS attribute of the k th resource in the corresponding R_p set. uq'_j is the normalized value of the j th QoS attribute of the user-requested resource.

Before similarity matching, resources are classified to reduce matching time and improve matching efficiency. Taking the QoS attribute value of user requested resources as the standard, each resource is regarded as a point in multidimensional space, and the Euclidean distance is used to measure the proximity between resources and user needs. Since the user has a preference for an attribute or each QoS attribute of the resource has a different impact on the measurement result, an objective weight is set for each QoS attribute according to

$$d(r_i, uq) = \sqrt{\sum_{j=1}^{m} w_j * \left(r_{ij} - uq_j\right)^2}. \quad (8)$$

$$\mathrm{dsim}(r_i, uq) = \frac{1}{1 + d(r_i, uq)}. \quad (9)$$

In formula (8), w_j is the weight of each QoS attribute of the resource, and $d(r_i, uq)$ is the distance between the i th resource and the user requested resource in space. In formula (9), $\mathrm{dsim}(r_i, uq)$ is the proximity between available resources and user requested resources. The range of $\mathrm{dsim}(r_i, uq)$ is between [0, 1]. The smaller $d(r_i, uq)$ is, the closer it is to the resource requested by the user.

According to the proximity between the available resources and the user requested resources obtained from formula (9), the proximity threshold ε is set, and the range is between [0, 1]. The resources are classified by formula (10), and the resources that meet the conditions are classified into one class to form a matching resource set R_p.

$$R'(\varepsilon) = \{r_i | \mathrm{dsim}(r_i, uq) \geq \varepsilon\}. \quad (10)$$

Based on the above resource classification, a resource matching matrix P of user request QoS and resource QoS is established for the resources in R_p set. We use the standardized method of formula (3) to process the matrix P to obtain the standardized matrix P' of matching resources.

This paper uses the Pearson correlation coefficient to calculate the similarity between the resources in the matching resource set R_p and the resources requested by users.

$$\mathrm{sim}(rp_k, uq) = \frac{\sum\left(q_{rp,rp_{kj}} - \overline{q}_{rp_k}\right)\left(q_{uq,uq_j} - \overline{q}_{uq}\right)}{\sqrt{\sum\left(q_{rp,rp_{kj}} - \overline{q_{rp_k}}\right)^2}\sqrt{\sum\left(q_{uq,uq_j} - \overline{q_{uq}}\right)^2}}. \quad (11)$$

In formula (11), $\mathrm{dsim}(r_i, uq)$ represents the similarity between any resource $\mathrm{dsim}(r_i, uq)$ in the set R_p and the resource uq requested by the user. $q_{rp,rp_{kj}}$ and q_{uq,uq_j}, respectively, represent the value of rp_{kj} in the R_p set and the value of uq_j for the resource requested by the user. $\overline{q}_{rp_k}$ represents the average value of all QoS attribute values of the k th resource in the R_p set, and $\overline{q}_{uq}$ represents the average value of all QoS attribute values of the resource requested by the user.

In order to overcome the constraints and differences of resource QoS attributes and ensure that the QoS attribute values of candidate resources are within the user's expectations, we analyze the gap between resource QoS attribute values by introducing penalty factors and grey incidence matrix and calculate the similarity between matching resources and user-requested resources. Taking resource constraints as conditions, a penalty factor λ is set. When the value of the penalty factor is smaller, the closer to the user's expected range, the higher the correlation. Conversely, when the penalty factor is large, the farther it exceeds the user's expected range, the lower the correlation, and the lower the matching degree.

$$\lambda_j = \begin{cases} 0, & rq_j < \delta_j, \\ \dfrac{rq_j - \delta_j}{\gamma_j - \delta_j}, & \delta_j \leq rq_j \leq \gamma_j, \\ 1, & rq_j > \gamma_j. \end{cases} \quad (12)$$

In formula (12), δ_j and γ_j are the minimum and maximum values of the user's expected range corresponding to the jth QoS attribute of the resource, respectively.

The penalty factor calculated by formula (12) is substituted into formula (13) to calculate the correlation coefficient to modify the matching function. The attribute correlation coefficient is calculated as follows:

$$\xi_{kj} = \frac{\min + \eta \cdot \max}{\lambda_j \left| uq_j' - rp_{kj}' \right| + \eta \cdot \max},$$
$$\min = \min \min \left| uq_j' - rp_{kj}' \right|, \tag{13}$$
$$\max = \max \max \left| uq_j' - rp_{kj}' \right|.$$

The grey incidence matrix is expressed as

$$\xi = \left(\xi_{kj}\right) = \begin{bmatrix} \xi_{11} & \xi_{12} & \cdots & \xi_{1m} \\ \xi_{21} & \xi_{22} & \cdots & \xi_{2m} \\ \vdots & \vdots & \ddots & \vdots \\ \xi_{k1} & \xi_{k2} & \cdots & \xi_{km} \end{bmatrix}. \tag{14}$$

In formula (13), ξ_{kj} is the correlation coefficient of the j th QoS attribute of the k th resource, $1 \le k \le n$, $1 \le j \le m$ is the resolution coefficient, which is generally 0.5. λ_j is the penalty factor of the j th QoS attribute; min and max represent the smallest difference between the two levels and the maximum difference between the two levels. From the difference $|uq_j - rp_{kj}|$ between each QoS attribute of each resource and the corresponding QoS attribute of the resource requested by the user, the respective minimum difference and maximum difference are respectively selected. Furthermore, from the minimum difference and the maximum difference of all resources, respectively, the minimum difference and the maximum difference are selected. uq_j' and rp_{kj}' are the standardized values r.

According to the above analysis, the matching function obtained after modifying formula (11) is

$$c\,\mathrm{sim}\left(rp_k, uq\right) = \alpha * \mathrm{sim}\left(rp_k, uq\right) + (1-\alpha) * \frac{1}{m}\sum_{j=1}^{m} \xi_{kj}. \tag{15}$$

Among them, α represents the weight, and the range is between [0, 1]. When the matching degree reaches the threshold K, that is, $c\mathrm{sim}\left(rp_k, uq\right) \ge K$, it indicates that the matching is successful, and the resource is put into the candidate resource set Rs'.

Due to the dynamics and uncertainty of the resource itself, there are certain fluctuations in the QoS data volume and data value. Moreover, the inherent mobility in the Internet of things environment makes mobile users have a certain degree of volatility when using resources. Therefore, by analyzing the load changes of the resources themselves, further resources are selected.

The resource load is random and dynamic, and the load has the characteristics of frequent changes in a short period of time. Short-term resource forecasting facilitates real-time feedback and management of resources, which ensures the efficiency of the provided resources. Therefore, the regression-Markov chain combination forecasting method is adopted to better reflect the changing trend of resources and the characteristics of random fluctuations.

According to the difference of the interval time t, the original data sequence of the resource load value is recorded as $\{X^{(0)}(t)\} = \{X^{(0)}(1), X^{(0)}(2), \ldots, X^{(0)}(l)\}$. The data series may have certain fluctuations due to uncertain external factors, and fluctuations may have an impact on the predicted results. Therefore, in order to weaken the influence of data fluctuations on the prediction results, we add the sequence weight adjustment function to adjust the weight when performing linear regression prediction.

For any data $X^{(0)}(c)$, $1 \le c \le l$, in the original data sequence, the deviation $\Delta_c = |X^{(0)}(c) - \overline{X^{(0)}(t)}|$ of the mean $\overline{X^{(0)}(t)}$ of the sequence is calculated. By calculating the absolute deviation of all the data in the original data series, the deviation sequence $\Delta_{x^{(0)}(t)} = \{\Delta_1, \Delta_2, \ldots, \Delta_l\}$ is obtained. The sequence weight adjustment function is expressed as follows:

$$\xi(c) = \frac{\min\left(\Delta_{x^{(0)}(t)}\right) + \max\left(\Delta_{x^{(0)}(t)}\right)}{\Delta_c + \max\left(\Delta_{x^{(0)}(t)}\right)}. \tag{16}$$

Among them, $\xi(c)$ is the weight number at time c. $\min(\Delta_{x^{(0)}(t)})$ and $\max(\Delta_{x^{(0)}(t)})$ are the minimum and maximum values in the deviation sequence, respectively. When the deviation Δ_c is larger, the value of $\xi(c)$ is smaller, and its weight is smaller.

According to formula (17), the original data sequence is corrected as follows:

$$X^{(0)}(c) = \xi(c) * X^{(0)}(c). \tag{17}$$

For the revised data sequence, we first use linear regression to predict to obtain the predicted value sequence $\left\{\widehat{X}^{(0)}(t)\right\} = \left\{\widehat{X}^{(0)}(1), \widehat{X}^{(0)}(2), \ldots, \widehat{X}^{(0)}(l)\right\}$ of the resource load, and calculate the relative difference between the two sequences to obtain the residual sequence $\{X^{(1)}(t)\} = \left\{\widehat{X}^{(0)}(t) - X^{(0)}(t)\right\}$.

Then, the relative residual sequence $\{X^{(1)}(t)\}$ is divided into s state intervals according to the numerical range, and the residual one-step transition probability matrix $M_{s\times s} = M(s_j)(s_j) = p_{ij}(X_{s+1} = j | X_s = i)$ is calculated according to the distribution of state $S = (1, 2, ..., s)$.

$$M = \begin{bmatrix} M_{11} & M_{12} & \cdots & M_{1s} \\ M_{21} & M_{22} & \cdots & M_{2s} \\ \vdots & \vdots & \ddots & \vdots \\ M_{s1} & M_{s2} & \cdots & M_{ss} \end{bmatrix}. \tag{18}$$

If the condition $M_{ij} \ge 0, \sum M_{ij} = 1,\ i,\ j \in S$ is met, then M is a random matrix, and $P^{(n)} = (p_{ij}^{(n)}) = P^n$ is an n-step transition matrix.

We assume that after n-step transition, the Markov chain reaches a stable state, and the state vector $x = [x_1, x_2, \ldots, x_s]$ in its stable state satisfies the following:

$$\begin{cases} x = xM, \\ \sum_{t'=1}^{s} x_{t'} = 1. \end{cases} \tag{19}$$

In formula (19), the value $x_{t_{\prime}}$ $(1 \le t' \le s)$ corresponding to each state in the state vector x satisfies the condition that the sum is 1. After that, we set the initial state and obtain the probability $p_1, p_2, \ldots, p_s$ corresponding to the error state interval by solving the probability of the steady state distribution.

According to the principle of maximum probability, the error state interval corresponding to the maximum probability is selected from the probability of each prediction interval to be solved, and then the predicted value is substituted into the solution prediction interval value. On this basis, the availability of resources in the short term can be obtained, and appropriate resources can be selected reasonably.

The proposed dynamic resource evaluation method includes two stages: similarity matching method and regression-Markov chain prediction method. First, we establish a resource QoS matrix R, and preliminarily divide the resource into a resource matching set R, through proximity calculation. Then the resource matching matrix P is established, and the matching degree between user QoS requirements and resources is calculated through the Pearson similarity coefficient and the grey incidence matrix. Set the matching degree threshold to select resources that meet the conditions and put them into the candidate resource set *Rs*'. Finally, the regression-Markov chain prediction method is used to analyze the load changes of resources, sort the candidate resources, and select the appropriate resources. The specific process of the evaluation method is shown in Figure 1.

In the far cloud, the data center isolates users from the underlying physical framework through virtualization technology, forming a virtual resource library for external services, and the fog computing microdata center is similar. Each user can request resources from multiple resource providers, and the resources provided by each resource provider can only satisfy a single user's request at the same time. Therefore, the one-to-many bilateral matching game method is used to evaluate and select resources. When multiple users request at the same time, based on the stable matching method, the comprehensive satisfaction of the user and the resource provider is used as the utility function, all matching results are evaluated, the result with the largest comprehensive utility function is selected, and the best one is selected for the user request resources, meet the needs of both users and resource providers, and improve overall resource utilization efficiency.

We set two disjoint sets of user request set and resource set. Among them, the user request set is $Q = \{q_1, q_2, \ldots, q_N\}$, q_i is the request of the i th user, and $1 \le i \le N$. The resource set is $P = \{p_1, p_2, \ldots, p_T\}$, p_j represents the j th resource, $1 \le j \le T$, $N \le T$.

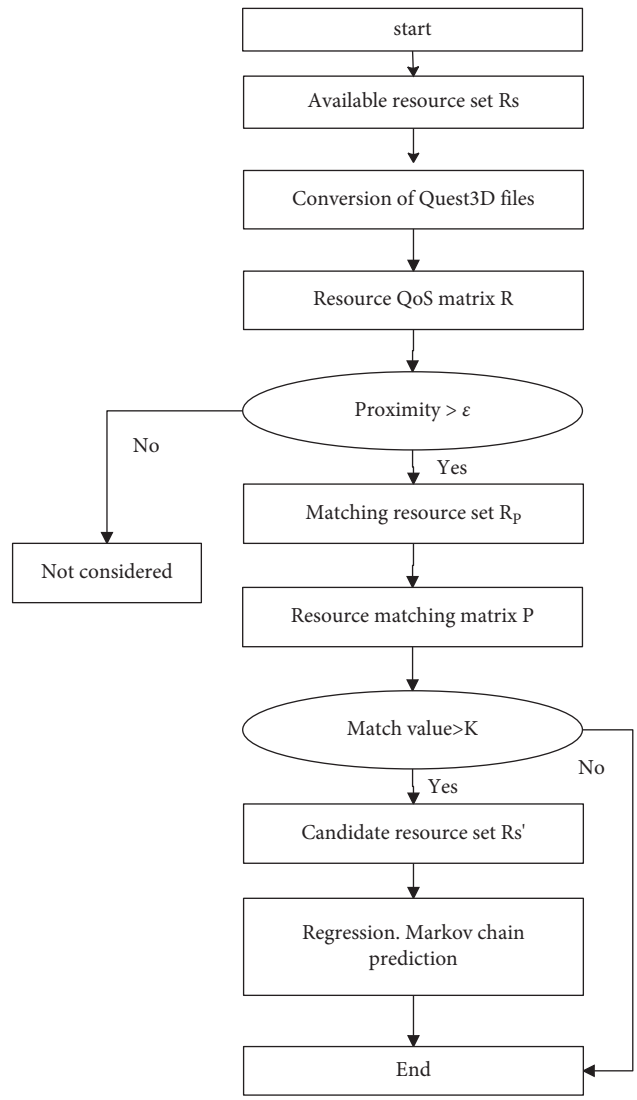

Figure 1: Flow chart of resource assessment method.

For ease of understanding, we give the following related concepts based on the literature.

Definition 1: One-to-many bilateral matching. If any $q_i \in Q$ satisfies the condition $f(q_i) \subseteq q_i \cup P$ and any $p_j \in P$ satisfies the condition $f(p_j) \subseteq Q \cup p_j$, then f represents a one-to-many bilateral match between the user request set Q and the resource set P.

Definition 2: Matching subject pairs. In one-to-many bilateral matching f, if $f(q_i) = p_j$, the subject pair (q_i, p_j) is called the matching subject pair of f. If $f(q_i) = q_i$, it means q_i does not match.

Definition 3: Stable matching. When the following conditions are not met, f is called stable matching.

In the process of stable matching, it is necessary to consider the preference sequence of user requests and resources to each other, which is used to describe the ranking results of user requests and the willingness of the other party to choose resources.

Preference sequence. $Pu_i = (pu_{i1}, pu_{i2}, \ldots, pu_{iT})$ is the sequence of user preferences for resources, and pu_{ij}

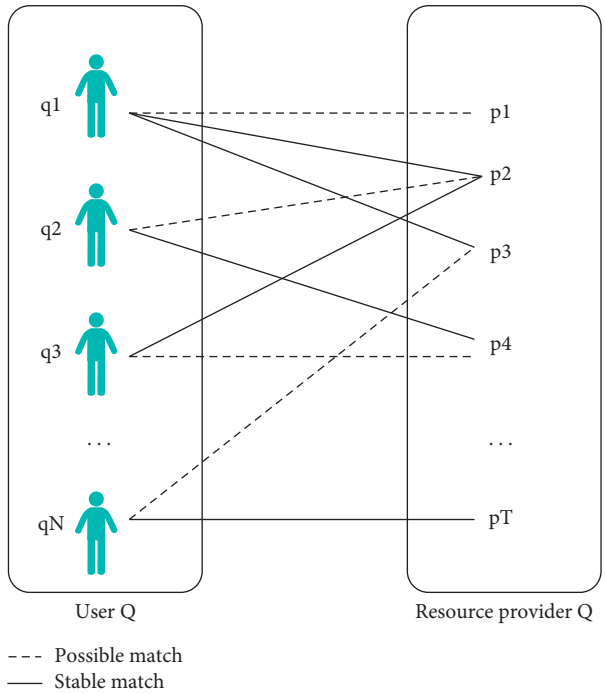

Figure 2: Schematic diagram of next-to-many matching in the fog computing environment.

indicates that that q_i places p_j in the pu_{ij} position. $Pt_j = (pt_{1j}, pt_{2j}, \ldots, pt_{Nj})$ represents the preference sequence of the resource to the user's request, and pt_{ij} represents that q_i ranks p_j in the pt_{ij} position.

Definition 5: Expected number of matches. For a user request, multiple resources may be required to complete the task. The number of resources that the user request q_i expects to match is s_i, $\sum_{i=1}^{N} s_i = k$. The number of user requests that resource p_j expects to match is 1.

We assume that users and resource providers are two disjoint sets, that is, there is no resource provider as a user, and the resource set that completes the user's request is the same, that is, all user requests to calculate the preference of resources in the same set. It can be seen from the above analysis that the evaluation and selection of resources under multiuser requests can be regarded as a one-to-many bilateral matching game process, as shown in Figure 2.

4. Dynamic Budget Management System of Rural Public Affairs Based on Internet of Things Technology

This paper constructs a rural public affairs dynamic budget management system based on Internet of things technology. The system adopts a three-level structure, which is divided into business logic processing layer, centralized data processing layer, and centralized system management layer. At each level, we introduce server integration technology to try to provide the simplest hardware platform. The system deployment view is shown in Figure 3.

The external interface is shown in Figure 4.

Three tier architecture is a new project system development environment as shown Figure 5. The role of database server layer in the use of engineering projects is to fix the logical relationship between data.

The developed audit data comprehensive analysis system adopts B/S architecture. After analyzing the whole work process of the audit department, it is found that auditors require the system to operate simply and quickly, and have high requirements for data security. The network layout of the system is a data server and an application server. The internal auditors of the audit unit can access directly through the internal network, and the external auditors need to pass through the network and firewall. The network topology of the financial budget execution audit data comprehensive analysis system is shown in Figure 6.

As a part of the whole financial online audit system, the budget execution module reuses and realizes its management functions in many aspects based on the application support platform provided by the system, so as to complete the realization of data collection, audit model construction, audit analysis, data early warning management, and audit report. The detailed function framework of the budget execution module is shown in Figure 7.

A general analysis tool is designed in the audit analysis management, which can flexibly query the data, flexibly analyze the data and find audit doubts in combination with the general analysis function, so as to realize the data management function. The specific query includes many aspects of work, and the data parameters need to be set before. By using a variety of tools, the displayed data can be

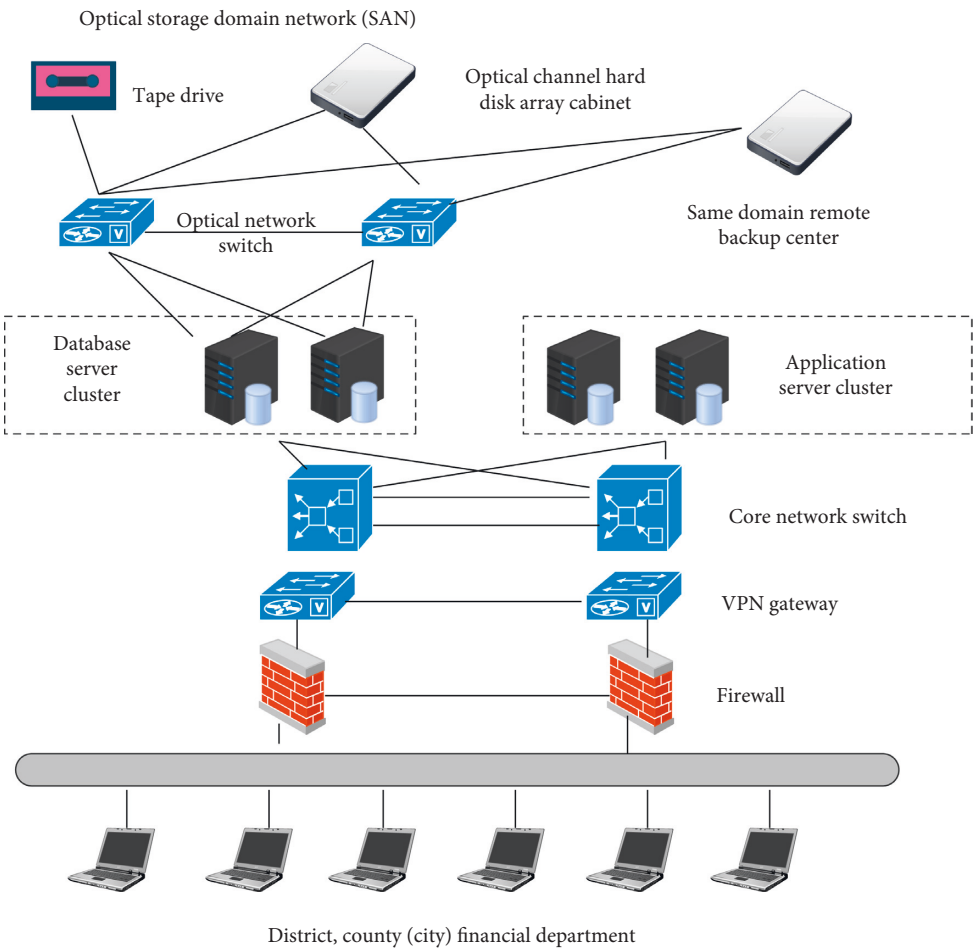

Figure 3: System deployment view.

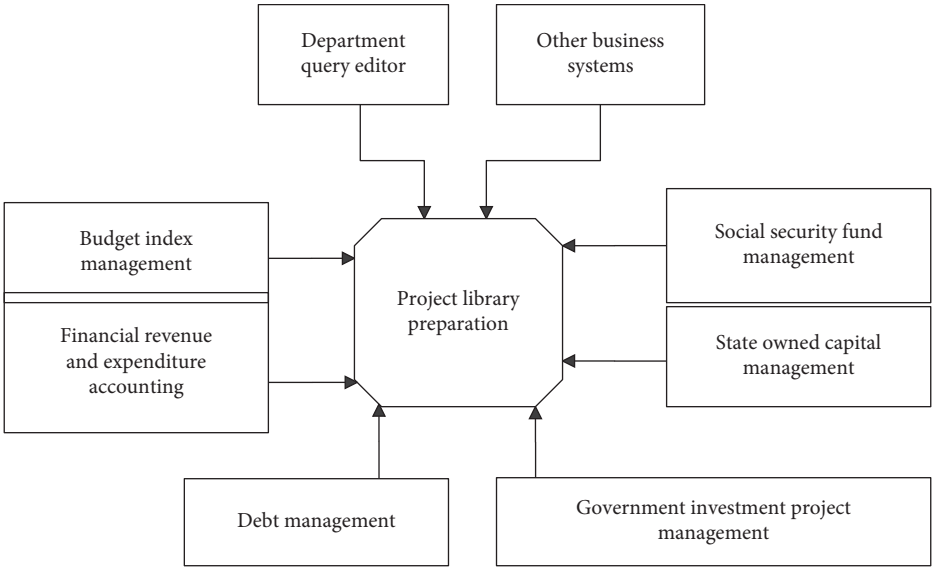

Figure 4: External interface of the project library.

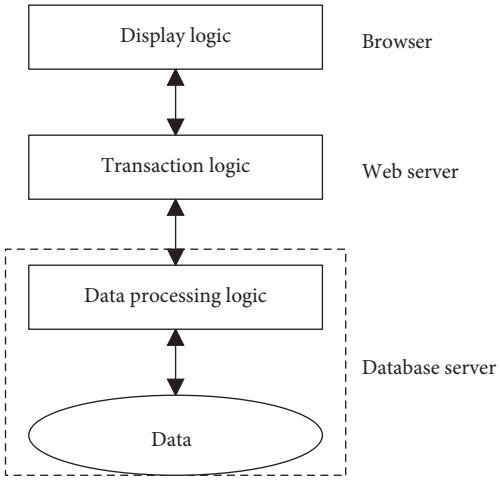

Figure 5: System structure diagram.

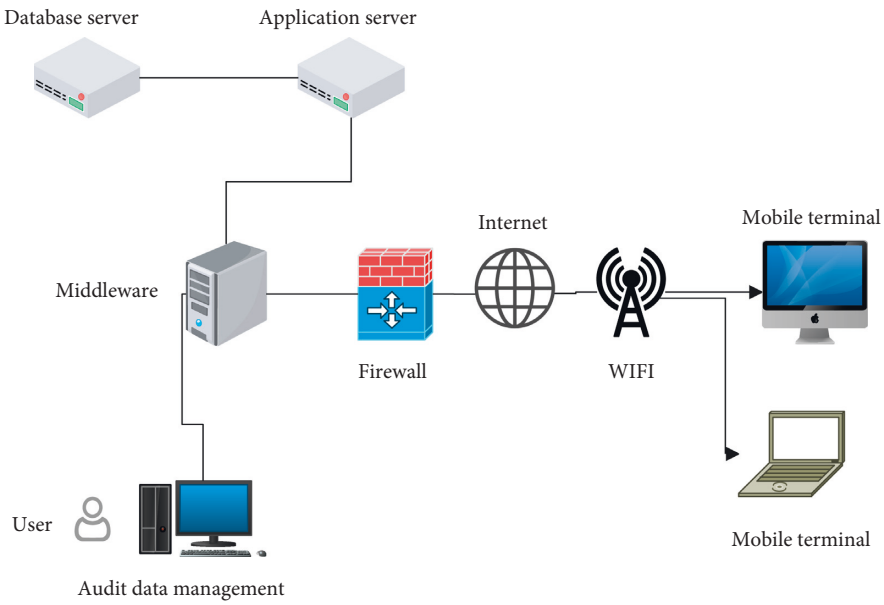

Figure 6: Network topology structure diagram.

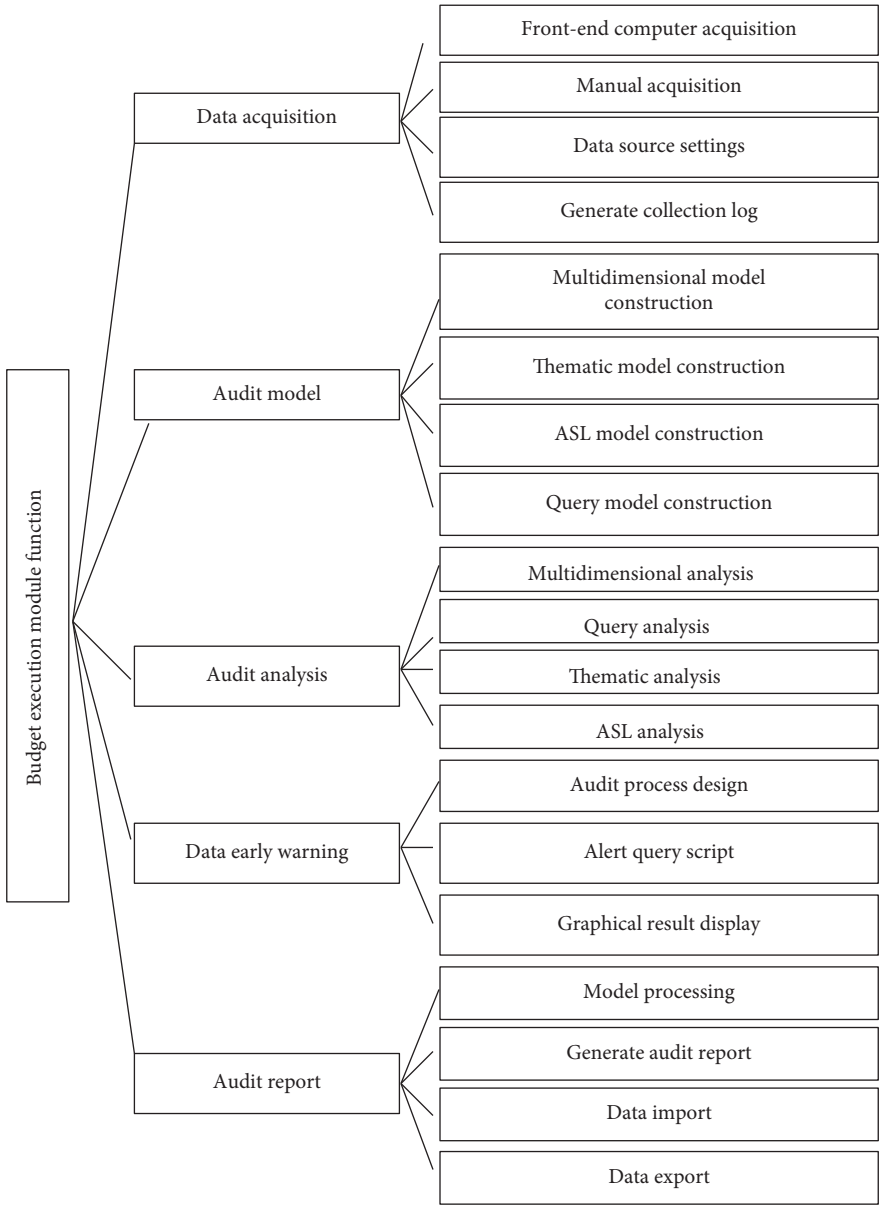

Figure 7: Detailed framework diagram of the functions of the budget execution module.

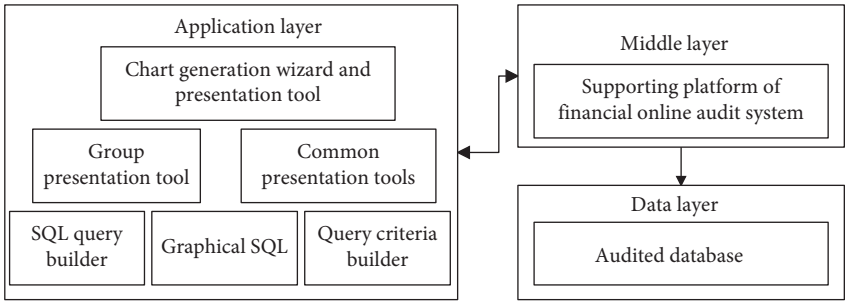

Figure 8: Structure diagram of audit analysis tool.

Table 1: Dynamic budget management effects of rural public affairs.

NO	Data processing	Budget effect
1	83.01	93.01
2	90.65	91.45
3	89.85	82.43
4	84.75	92.46
5	84.04	82.24
6	85.09	92.98
7	90.71	93.36
8	83.51	91.55
9	89.63	83.90
10	87.52	91.39
11	93.74	93.16
12	87.45	86.79
13	93.90	91.75
14	86.73	87.77
15	91.94	86.77
16	85.51	91.35
17	85.45	93.89
18	89.39	84.83
19	83.22	92.04
20	85.17	93.35
21	87.78	91.39
22	86.04	83.74
23	83.77	93.44
24	87.53	89.46
25	89.87	91.73
26	88.62	93.10
27	91.00	87.23
28	89.67	94.37
29	87.77	85.92
30	83.93	90.46
31	90.13	84.28
32	93.98	82.14
33	84.98	82.80
34	91.02	88.98
35	86.45	93.20
36	83.56	87.68
37	88.67	85.39
38	85.03	87.24
39	83.49	92.07
40	93.08	85.91
41	91.58	82.97
42	87.80	90.11
43	92.65	85.48
44	85.87	87.70
45	89.63	88.25
46	85.65	93.25
47	89.45	86.15
48	83.44	89.48
49	84.98	84.03
50	84.22	90.31
51	86.40	94.36
52	90.77	89.47
53	91.09	84.30
54	83.03	83.45
55	85.03	82.26
56	93.72	87.48
57	88.91	85.59
58	91.75	84.55
59	89.66	86.69
60	84.84	84.46

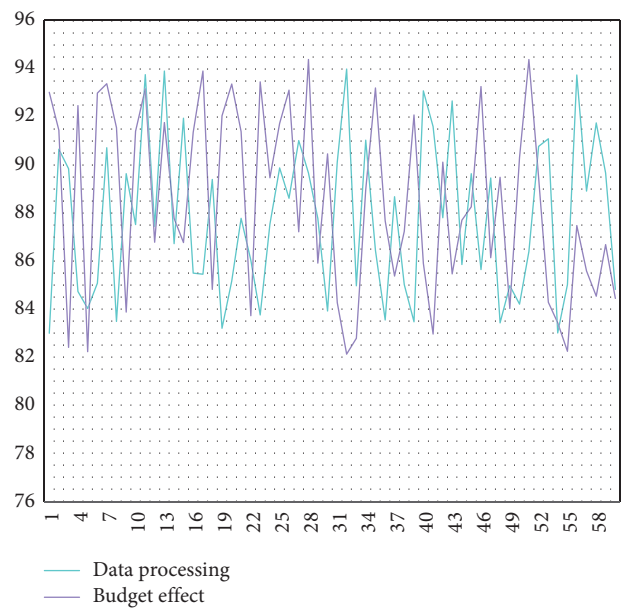

Figure 9: The experimental line chart of the dynamic budget management of rural public affairs.

further analyzed, such as grouping, sorting, filtering, statistics, calculation, and chart display. The structure diagram of audit analysis tool is shown in Figure 8.

After constructing the above system modules, the performance of the model is verified, the effect of the Internet of things data transmission and rural public affairs dynamic budget management of the system in this paper is evaluated, and the simulation research is carried out in combination with the data collected by the network. The results are shown in Table 1 and Figure 9.

From the above research, we can see that the dynamic budget management system of public affairs based on the Internet of things technology constructed in this paper has good results.

5. Conclusion

Since the implementation of the new rural construction, although most rural areas have made some development in infrastructure, environmental health improvement, and hardware conditions, the current situation of rural public services in China is worrying, and rural public services are generally insufficient, the structure is unbalanced and the efficiency is low. Specifically, the rural infrastructure is still relatively backward, the supply of rural education is insufficient, the structure is unbalanced and the efficiency is low. The imperfect and nonstandard township public management system is the biggest software factor restricting the construction of a new socialist countryside. This paper combines the Internet of things technology to construct the dynamic budget management system of rural public affairs, and analyzes the dynamic management of rural public affairs through the system, so as to improve the efficiency of rural public affairs management. In addition, this paper evaluates the effects of the Internet of things data transmission and the

dynamic budget management of rural public affairs in this system, and conducts simulation research based on the data collected by the network. From the experimental research, we can see that the dynamic budget management system of public affairs based on the Internet of things technology constructed in this paper has good results.

Data Availability

The experimental data used to support the findings of this study are available from the corresponding author upon request.

Conflicts of Interest

The author declares that there are no conflicts of interest regarding this work.

References

[1] W. Khan and S. A. Ansari, "Does agriculture matter for economic growth of Uttar Pradesh (India)?" *Economy of Region*, vol. 14, no. 3, pp. 1029–1037, 2018.

[2] M. Paul, "Community-supported agriculture in the United States: social, ecological, and economic benefits to farming," *Journal of Agrarian Change*, vol. 19, no. 1, pp. 162–180, 2019.

[3] I. Pattnaik, K. Lahiri-Dutt, S. Lockie, and B. Pritchard, "The feminization of agriculture or the feminization of agrarian distress? Tracking the trajectory of women in agriculture in India," *Journal of the Asia Pacific Economy*, vol. 23, no. 1, pp. 138–155, 2018.

[4] G. Salmoral, D. Rey, A. Rudd, P. de Margon, and I. Holman, "A probabilistic risk assessment of the national economic impacts of regulatory drought management on irrigated agriculture," *Earth's Future*, vol. 7, no. 2, pp. 178–196, 2019.

[5] B. Lanz, S. Dietz, and T. Swanson, "Global economic growth and agricultural land conversion under uncertain productivity improvements in agriculture," *American Journal of Agricultural Economics*, vol. 100, no. 2, pp. 545–569, 2018.

[6] J. Cai, J. Luo, S. Wang, and S. Yang, "Feature selection in machine learning: a new perspective," *Neurocomputing*, vol. 300, pp. 70–79, 2018.

[7] J. N. Goetz, A. Brenning, H. Petschko, and P. Leopold, "Evaluating machine learning and statistical prediction techniques for landslide susceptibility modeling," *Computers & Geosciences*, vol. 81, pp. 1–11, 2015.

[8] H. Darabi, B. Choubin, O. Rahmati, A. T. Haghighi, B. Pradhan, and B. Kløve, "Urban flood risk mapping using the GARP and QUEST models: a comparative study of machine learning techniques," *Journal of Hydrology*, vol. 569, pp. 142–154, 2019.

[9] A. Rajkomar, J. Dean, and I. Kohane, "Machine learning in medicine," *New England Journal of Medicine*, vol. 380, no. 14, pp. 1347–1358, 2019.

[10] Y. Xin, L. Kong, Z. Liu, Y. Chen, Y. Li, and H. Zhu, "Machine learning and deep learning methods for cybersecurity," *IEEE Access*, vol. 6, pp. 35365–35381, 2018.

[11] B. Meredig, A. Agrawal, S. Kirklin et al., "Combinatorial screening for new materials in unconstrained composition space with machine learning," *Physical Review B*, vol. 89, no. 9, Article ID 094104, 2014.

[12] L. Ward, A. Agrawal, A. Choudhary, and C. Wolverton, "A general-purpose machine learning framework for predicting properties of inorganic materials," *npj Computational Materials*, vol. 2, no. 1, pp. 1–7, 2016.

[13] O. Elijah, T. A. Rahman, I. Orikumhi, C. Y. Leow, and M. N. Hindia, "An overview of Internet of Things (IoT) and data analytics in agriculture: benefits and challenges," *IEEE Internet of Things Journal*, vol. 5, no. 5, pp. 3758–3773, 2018.

[14] A. A. Kimaro, M. Mpanda, J. Rioux et al., "Is conservation agriculture 'climate-smart'for maize farmers in the highlands of Tanzania?" *Nutrient Cycling in Agroecosystems*, vol. 105, no. 3, pp. 217–228, 2016.

[15] F. Terdoo and O. Adekola, "Assessing the role of climate-smart agriculture in combating climate change, desertification and improving rural livelihood in Northern Nigeria," *African Journal of Agricultural Research*, vol. 9, no. 15, pp. 1180–1191, 2014.

[16] A. K. Thakur and N. T. Uphoff, "How the system of rice intensification can contribute to climate-smart agriculture," *Agronomy Journal*, vol. 109, no. 4, pp. 1163–1182, 2017.

[17] C. J. Chae and H. J. Cho, "Smart fusion agriculture based on Internet of Thing," *Journal of the Korea Convergence society*, vol. 7, no. 6, pp. 49–54, 2016.

[18] J. P. Aryal, T. B. Sapkota, D. B. Rahut, and M. L. Jat, "Agricultural sustainability under emerging climatic variability: the role of climate-smart agriculture and relevant policies in India," *International Journal of Innovation and Sustainable Development*, vol. 14, no. 2, pp. 219–245, 2020.

[19] K. Aliev, E. Pasero, M. M. Jawaid, S. Narejo, and A. Pulatov, "Internet of plants application for smart agriculture," *International Journal of Advanced Computer Science and Applications*, vol. 9, no. 4, pp. 421–429, 2018.

[20] A. Chandra, K. E. McNamara, P. Dargusch et al., "Resolving the UNFCCC divide on climate-smart agriculture," *Carbon Management*, vol. 7, no. 5-6, pp. 295–299, 2016.

Hindawi
Mobile Information Systems
Volume 2022, Article ID 2441292, 9 pages
https://doi.org/10.1155/2022/2441292

Research Article

The Practical Application of Agricultural Genetic Breeding Technology in Elm Cultivation Based on Big Data Analysis

Haiguang Huang,[1,2] Rong Yang,[1,2] Lei Hao,[3] and Guosheng Zhang[1]

[1]*College of Forestry, Inner Mongolia Agricultural University, Hohhot 010010, China*
[2]*Inner Mongolia Academy of Forestry, Hohhott 010010, China*
[3]*Inner Mongolia University of Finance and Economics, Hohhott 010010, China*

Correspondence should be addressed to Guosheng Zhang; 2111602032@e.gzhu.edu.cn

Received 16 June 2022; Revised 12 July 2022; Accepted 16 July 2022; Published 8 August 2022

Academic Editor: Chi Lin

In order to explore the role of agricultural genetic breeding technology in elm cultivation, this paper improves the big data technology. According to the test data verification requirements, based on the Monte Carlo idea, a TDSTI statistical test method is proposed, and a set of judgment criteria for the significance of spatio-temporal autocorrelation is given. Moreover, in order to make the observed variables of the time lag series have a clearer geographical significance, the obtained spatio-temporal weight matrix is subjected to row standardization. In addition, this paper combines big data technology and agricultural genetic breeding technology to study the cultivation of elm trees. Finally, this paper conducts a correlation analysis between the distance matrix generated by cluster analysis of leaf shape traits and the distance matrix generated by cluster analysis of SSR molecular markers. The research results show that agricultural genetic breeding technology can play an important role in the cultivation of elm.

1. Introduction

The elm belongs to the genus Ulmus in the Ulmaceae family. It is widely distributed in China and has 24 species including cultivated species. The elm tree grows fast, likes light, has strong cold and drought resistance, strong salt and alkali resistance, strong anti-pollution ability, and straight wood texture, which can be used for construction, furniture, vehicles, sleepers, and farm tools. Bark can be used as raw material for artificial cotton and paper making [1]. The samara can be squeezed into oil for food, medicine, and the light chemical industry. In addition, it is an important tree species for the construction of timber forests, shelter forests, saline-alkali land afforestation, and "four sides" greening in the vast plains and desert areas of Northeast China, North China, and Huaibei. With the development of science and technology, the use of molecular marker technology to study the genetic diversity of elm germplasm resources has become more and more popular [2].

The most widely distributed and important elm species in my country is *Ulmus pumila*. Its material is excellent, and it has good drought resistance, cold resistance, salt and alkali resistance, and wind resistance. Moreover, it is an important tree species for cultivating timber forests, shelter forests, and "four sides" greening on the vast plains, saline-alkali land, and sandy wasteland in the northern country. It grows fast, has a long lifespan, and can grow on dry and barren fixed dunes and chestnut soil. In addition, it has the characteristics of year-by-year fruiting, large fruit size, wide spread of samara, strong germination, rapid rooting, and strong seedlings. Therefore, it has become the most important tree species for soil conservation, sand fixation, and grazing protection in areas with a harsh ecological environment [3].

The elm tree has become a good material for making bonsai because of its "root dew, dry thin and dense leaves." Moreover, it has excellent characteristics such as fast growth, strong germination, pruning resistance, and very good plasticity, and is very popular among bonsai lovers. Because it likes sunlight, elm trees are suitable for growing in a warm and humid environment. Although there are no strict requirements on the soil substrate, the soil must be loose and

breathable because it is afraid of water accumulation. As we all know, the material of bonsai comes from trees, and as the trees grow from seedlings, the degree of difficulty in modeling also increases [4].

There are usually two ways to obtain the material of pile blanks, one is to dig in the mountains and the other is to reproduce asexually. In the past, many flower farmers usually went to the mountains to dig wild elm trees to cultivate and process them as materials for bonsai. The old elm stumps in the mountains have been eroded by natural conditions and bitten by animals over the years, so their shapes are often unique and old and simple. This method of digging old elm stumps from the mountains can greatly shorten the cultivation time of bonsai, but the continuous excavation over the years has made wild old elm stumps very few now, and farmers continue to cut down elm trees for firewood. As time passed, there were almost no wild elms on the mountain. Therefore, in order to obtain a large number of elm tree stumps, while avoiding damage to the ecological environment, current flower farmers can only cultivate elm tree seedlings by breeding, so that a large amount of elm tree bonsai materials can be quickly obtained. The basic methods of elm reproduction are divided into two categories: sexual reproduction and asexual reproduction. Sexual reproduction means sowing and breeding. It takes a long time to grow old stump bonsai after seedlings are formed by sowing and breeding. Therefore, elm trees generally do not use sowing and reproduction; and the method of asexual reproduction can not only maintain the characteristics of the female parent but also can A large amount of stump material is obtained, and the time for bonsai to be formed is also relatively short. The vegetative propagation of elm trees is often carried out by the cutting or ramification method.

This paper combines big data technology and agricultural genetic breeding technology to study the cultivation of elm trees and conducts experimental research in combination with actual conditions.

2. Related Work

Ulmus tree species are relatively drought-tolerant, suitable for growing in limestone mountains, and are mostly excellent timber species, and the bark is rich in fiber [5]. Although there are many Ulmaceae species in my country, they generally have huge crowns, slow growth, unsuitable for afforestation in mountainous areas, poor dry shape, serious damage by dry-boring pests, and low utilization value of wood. At present, it is mainly used for village greening, street trees in some northern urban areas, tree planting in the surrounding areas, etc.

The literature [6] used AFLP molecular technology to analyze the genetic diversity of *Ulmus pumila* clones. The literature [7] used RAPD molecular technology to study the genetic diversity of *Ulmus pumila* in hunshandake. The literature [8] used RAPD molecular technology to study the genetic diversity of natural *Ulmus pumila*. In the past piece of research on the genetic diversity of elm resources, molecular markers are used individually. At present, there are reports on the combination of phenotypic traits and SSR molecular markers to study plant genetic diversity, and there are few studies on the correlation analysis between phenotypic traits of elm and SSR. Therefore, this experiment uses elm leaf shape traits and SSR molecular marker technology to study the genetic diversity of elm trees.

The current research on Ulmus tree species mainly focuses on geographical distribution, population dynamics, biological characteristics, growth and development patterns, community characteristics, etc. There are few reports on special studies on their drought tolerance mechanism and drought tolerance source selection. Moreover, researches mostly focus on a few elm species, such as *Upumila*, U1.amellosa, Uelongata, etc. On seed germination, growth patterns, quantitative classification, drought tolerance, tissue culture, and other research on a few aspects. Literature [9] studied the seedlings of *Ulmus longiflorum*. The elm has a short seedling period, the seed germinates out of the soil faster, the seedling time is relatively concentrated, and the initial growth lasts longer. However, its growth is slow and its growth only accounts for 10.18% of the total annual growth. The peak growth period is one-third of the total annual growth period, and its growth accounts for 34.19% of the total annual growth. The results of multiple regression analysis show that temperature is the main meteorological factor affecting the growth of its height. The literature [10] studied the growth of the seedlings of *Ulmus chenmoui* Cheng and *Ulmus gaussenii* Cheng. The seedling rate of *Ulmus gaussenii* Cheng was 20.30% on average, but the preservation rate was low. The causal wing of *Ulmus gaussenii* Cheng is thicker, and the core is located in the middle of the samara. The emergence rate is only limited to 10%, and the preservation rate is lower. The literature [11] studied the application of auxin in elm seedlings. When the seedling height is about 10 cm, it uses GA3, vitamin B2, choline chloride, high-efficiency auxin, Yemianbao, Aiduoshou, Fengchansu, etc. To spray and observe the 1a elm seedlings. It was found that, except for individual strains that were comparable to the control, the others all increased by 5%–15%, the ground diameter was all better than the control and the increased range was 10%–70%. The literature [12] studied the determination of the wilting coefficient of the too common broad-leaved tree species at the seedling stage and found that the white elm has the same drought resistance as the Chinese locust, black locust, and Ailanthus altissima but is better than walnut, mountain apricot, toon, loblolly pine, and dry willow. The literature [13] adopted P–V technology to measure the moisture parameters of elm and korshinskii, indicating that the elm can tolerate a gradual increase in moisture.

The literature [14] used seeds to propagate small seeds like elm, which should be picked and sown at the same time, and the effect is better. There are only sporadic studies on the salt tolerance of Ulmus species. The literature [15] studied the critical value of salt tolerance of *Ulmus pumila* seeds under compound salt stress of 139/kg, and the critical value of salt tolerance of leaching salt stress of 179/kg. There are some research reports on the salt tolerance of other Ulmus species. There are many research reports on *Ulmus sylvestris* in foreign countries, which are mainly embodied in the

biological characteristics of *Ulmus sylvestris* and *Ulmus crassifolia*, cultivation and management, seedling cultivation, and prevention and control techniques of diseases and insect pests, as well as the wood properties of *Ulmus sylvestris*. However, there has been no report on the salt and drought tolerance characteristics and photosynthesis of *Ulmus pumila* series.

3. TDSTI Statistical Test Method

The null hypothesis H0 of spatial Moran's I statistical test: the spatial variables Z are independent of each other. Therefore, when performing the spatial Moran's I test, it is assumed that the probability distribution of the spatial variable Z is a normal distribution or a random distribution. Under these two assumptions, the expected value and variance of the spatial autocorrelation coefficient are calculated. When the actual expected value is greater than the hypothetical expected value, H0 is rejected and the statistical test is completed [16].

The salient feature of spatial Moran's I test: assumes that the spatial variable Z is independent. If the result of Moran's I test rejects this null hypothesis, it is considered that the spatial autocorrelation is credible under a certain degree of confidence. Similarly, in the TDSTI statistical test, can this idea be used? That is, it is assumed that the spatio-temporal variable X is also independent.

TDSTI is suitable for analyzing the spatio-temporal autocorrelation of data sequences with long-range correlation characteristics. This characteristic is related to two mechanisms: one is the long-range correlation shown by the inherent correlation among data, and the other is the inter-data wide probability density distribution (non-Gaussian normal distribution). The biggest difference between these two mechanisms is that when the attribute values in a time series are randomly sorted to form a new time series, the intrinsic correlation among the new series data will disappear at this time, but the probability among the data remains. The density distribution will not be changed. That is, the new time series is still affected by the wide probability density distribution and still has a certain correlation [17].

Obviously, after implementing statistical tests, even if the null hypothesis is rejected, no reliable results can be obtained. This is because the long-range correlation of spatio-temporal series is related to the probability density distribution of the data series and the correlation between the data. When assuming that the space-time variables X are independent of each other, this assumption only refers to the probability density distribution of the data sequence, that is, assuming that the probability density distribution is independent and identically distributed (i.i.d.), and does not assume the correlation between the data. Therefore, even if the statistical test results reject the null hypothesis, the correlation between the data cannot be determined.

Based on the Monte Carlo idea, a TDSTI statistical test method is proposed, and a set of criteria for judging the significance of spatio-temporal autocorrelation is given. Figure 1 shows the application process of the TDSTI statistical test method [18].

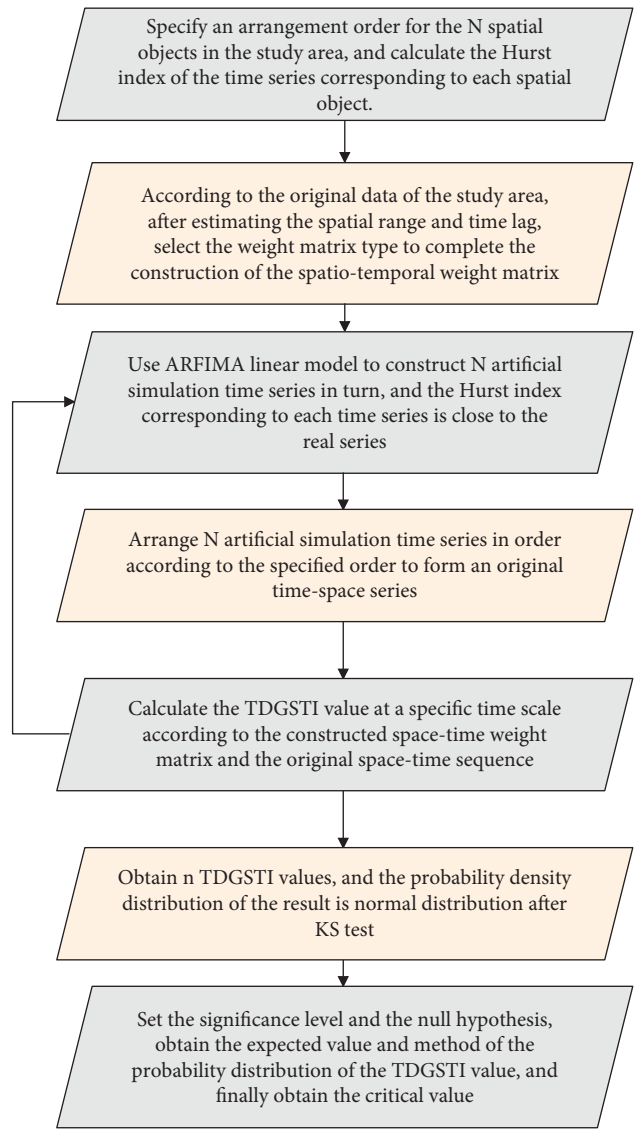

Figure 1: Statistical inspection process.

The application of the TDSTI statistical test method mainly includes the following steps:

(1) The algorithm determines the study area, obtains time series data of sufficient length of space objects in the study area, and analyzes and organizes the original data.

(2) The algorithm determines the time series of N spatial objects. It calculates the Hurst index of these N time series and determines the long-range correlation characteristics of the time series.

(3) The algorithm uses the time autocorrelation analysis method to estimate the time lag parameter h of the time series, uses the semivariogram in geostatistics to estimate the spatial range, selects the appropriate time and space weight function, and determines the time and space weight matrix.

(4) The algorithm uses the ARFIMA linear model to construct N artificial simulation time series whose Hurst index is consistent with the real series and

connects them end to end according to the specified order to obtain an original spatio-temporal series.

(5) According to the determined time-space weight matrix and the original time-space sequence, the algorithm constructs the time-lag sequence and applies the TDSTI model to calculate the TDSTI value under a certain time scale, TDSTI(s).

(6) The algorithm repeats n times steps 4 and step 5. Kolmogorov-Smirnov (K–S) test is performed on the calculated n TDSTI(s) values to verify whether the probability density distribution of TDSTI(s) is a normal distribution.

(7) The algorithm gives the result of the probability density distribution of TDSTI(s). According to the set significance level α and the null hypothesis Io, the expected value and variance of TDSTI are obtained, and the critical value of significant spatio-temporal autocorrelation is obtained.

(8) The algorithm gives a specific TDSTI statistical test criterion.

Many real-world geoscience data have long-range correlation characteristics. Granger and Joyeux proposed the Autoregressive Fractional Integrated Moving Average (ARFIMA) model, which can generate long-range correlation time series.

We use ARFIMA (0, d, 0) linear model to generate artificial (Artificial) simulation data, which is similar to actual data and also has long-range correlation characteristics. The ARFIMA(0, d, O) model is as follows [19]:

$$y(i) = \sum_{j=1}^{x} a_j(d) y(i-j) + \eta(i). \tag{1}$$

Among them, $\eta(i)$ in formula (1) is independent of each other and $\eta(i) \sim N(0,1)$ $a_j(d)$ is the statistical weight, and there is a relationship $a_j(d) = -\Gamma(j-d)/\Gamma(-d)\Gamma(1+j)$, Γ represents the gamma function, d is a free parameter, and the value range is [−0.5, 0.5]. The relationship with the Hurst index is: $H = 0.5 + d$. According to the Fractional Brownian Motion Model (FBM), the Iurst index (H) is an important parameter describing the fractal characteristics of time series, and ARFIMA can be used to generate time series with different Hurst indices.

When $H = 0.5$, the time series is an independent and identically distributed random series, belonging to Brownian motion, the variables are independent of each other, and the corresponding correlation coefficient is zero [20].

When $0 < H < 0.5$, the time series is an antipersistent series, and there is a negative correlation between variables. The antipersistence sequence fluctuates more intensely than the random sequence, and the variation span it produces in a certain period of time is smaller than that of the random sequence, and the intensity of antipersistence is related to the distance between H and O. When H is closer to 0, the mutation or variability of the time series is stronger.

When $0.5 < H \leq 1$, the time series has state persistence and has the characteristics of long-term memory (long-range correlation), which is expressed as a fractal time series. In theory, current changes will have a lasting impact on subsequent changes. Moreover, the long-range correlation of time series does not change with the time scale, and the time series of different time increments (day, week, month, year, etc.) have the same statistical law, which has the key characteristics of fractal time series. The closer the H is to 1, the stronger the degree of continuity of the sequence [21].

Figure 2shows the time series with different Hurst exponents generated by the ARFIMA linear model.

In Figure 3(a)–3(c), the Hurst index is 0.1, 0.5, and 0.9, respectively. The results in Figure 4 show that different Husrt indices have different artificial simulation time series. When $H = 0.1$, the fluctuation of the time series is the most obvious. When $H = 0.5$, the time series appears as a random sequence. When $H = 0.9$, the trend of the time series is the most obvious. This phenomenon is related to the long-range correlation of the fractional Brownian motion.

Figure 3 shows the relationship between the ARFIMA coefficient $a_j(d)$ and j when $d = 0.1, 0.2, 0.3, 0.4$ (i.e., $H = 0.6$, 0.7, 0.8, 0.9).

Figure 4 shows that when j gradually increases, $a_j(d)$ decreases rapidly and quickly approaches zero. This shows that the contribution of the sequence data generated by the ARFIMA linear model mainly comes from the first few items, and the contribution of d to the observed value varies from time to time. As d increases, the contribution increases. Therefore, a significant feature of formula (1) is that y(i) is related to all previous observation points, and this result is consistent with the long-range correlation interpretation of the time series. Moreover, y(i) has a different degree of correlation with all previous observation points.

The choice of the space-time weight matrix W^{st} is very important, where the element W_{uv}^{st} (the space-time weight function) represents the spatio-temporal geographic process between x(p, i) and y(q, j) ($u = \mathrm{PT} + i, v = qT + j, 1 \leq u \leq \mathrm{NT}, 1 \leq V \leq \mathrm{NT}$). Generally speaking, we believe that the process of spatio-temporal geography is the result of the joint effect of spatial and temporal interrelationships. Therefore, the space-time weight matrix will be constructed from two aspects: the space weight matrix and the time weight matrix.

The spatial weight function indicates the degree of interdependence and correlation among spatial objects, which is the prerequisite and basis for spatial metrological analysis. A reasonable and correct selection of the spatial weight function is essential for spatial model testing and spatial metrological analysis. The spatial correlation $\mathrm{WS}_{\mathrm{pq}}$ among spatial objects in different locations is more complicated. Generally, the spatial weight function is divided into three types: inverse function, negative exponential function, and step function. In order to take into account the spatial geographic process effect, an exponential decay matrix is constructed for the attenuation as the distance increases, the purpose of that is to describe this spatial effect more accurately. In this study, the negative exponential function $\exp(-\mathrm{dist}/\lambda)$ is used as the spatial weight function. Because this method is derived from the direct-maximization model proposed by Wilson. The spatial weight function can be expressed as:

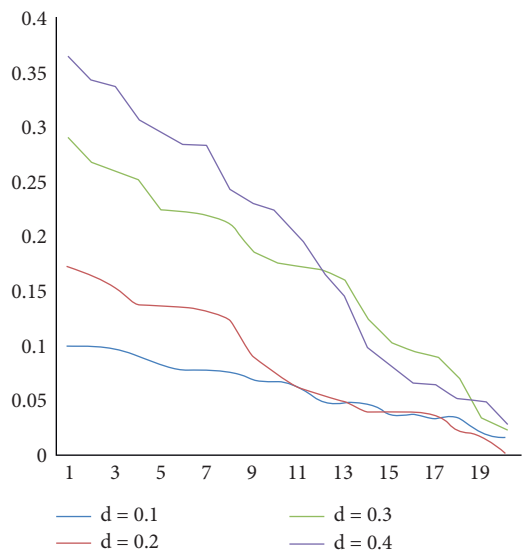

Figure 2: Relationship diagram between $a_j(d)$ and j.

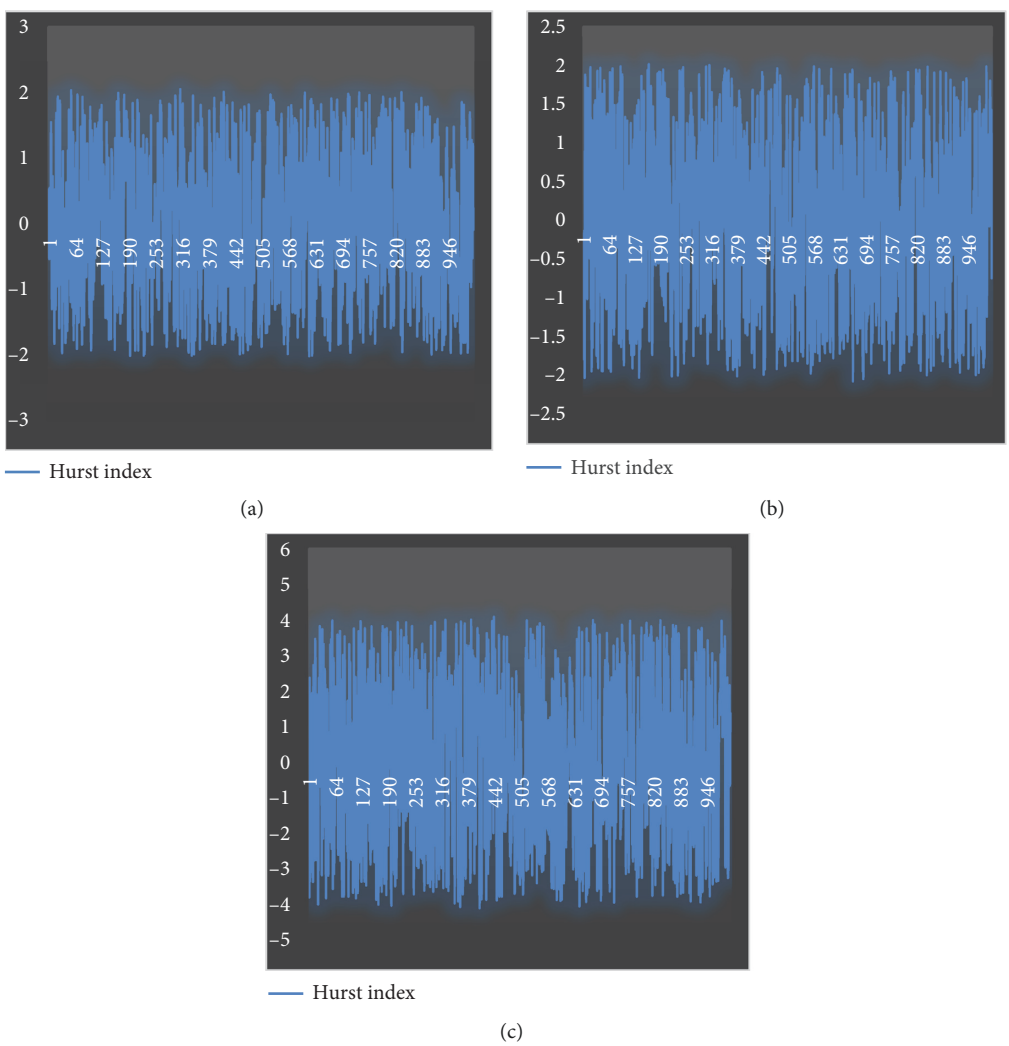

Figure 3: The relationship between artificial simulation time series and Hurst index (a) $H = 0.1$ (b) $H = 0.5$ (c) $H = 0.9$.

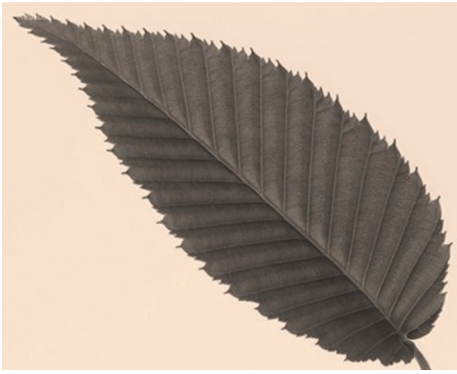

Figure 4: Image of elm leaves.

$$\mathrm{WS}_{pq} = \begin{cases} \exp(-\mathrm{dist}/\lambda), & \mathrm{dist} \neq 0, \\ 0, & \mathrm{dist} = 0. \end{cases} \tag{2}$$

Among them, dist represents the distance between point p and point q in space, and λ is a constant.

The time weight function can be represented by an indicator function, a negative power exponential function, and so on. In order to simplify, this paper chooses the indicator function as the time weight function, which is expressed as:

$$\mathrm{WT}_{ij} = \begin{cases} 1, & |i-j| \leq h, \\ 0, & \text{others}. \end{cases} \tag{3}$$

Among them, h represents the time lag in the time weight function. Formula (3) indicates that when $|i-j| > h$, there is no time correlation between time i and time j, and vice versa.

In order to simplify, the space-time weight function can be considered as the product of the space weight function and the time weight function, namely $W_{\mathrm{UV}}^{st} = \mathrm{WS}_{\mathrm{pq}} \times \mathrm{WT}_{ij}$, so the space-time weight function can be expressed as:

$$W_{\mathrm{UV}}^{\mathrm{st}} = \begin{cases} \mathrm{WT}_{ij}\ \mathrm{dist} = 0, |i-j| \leq h, & i \neq j, \\ \mathrm{WS}_{\mathrm{pq}} \times \mathrm{WT}_{ij}, & \mathrm{dist} \neq 0, |i-j| \leq h, \\ 0, & |i-j| > h, \end{cases} \tag{4}$$

or

$$W_{\mathrm{UV}}^{\mathrm{st}} = \begin{cases} 0, & \mathrm{dist} = 0, |i-j| \leq h, \\ \mathrm{WS}_{\mathrm{pq}} \times \mathrm{WT}_{ij}, & \mathrm{dist} \neq 0, |i-j| \leq h, \\ 0, & |i-j| > h. \end{cases} \tag{5}$$

For all spatio-temporal objects, W usually has two situations. Formula (4) shows that two kinds of autocorrelation have an impact on TDGSTI: one autocorrelation originates from the combined effect of space autocorrelation and time autocorrelation, and the other autocorrelation originates from the effect of time autocorrelation. Therefore, in this case, the spatio-temporal weight matrix type is a hybrid spatio-temporal weight matrix.

Formula (5) shows that spatio-temporal autocorrelation is only derived from the combined action of spatial autocorrelation and temporal autocorrelation. In this case, the spatio-temporal weight matrix type is a complete spatio-temporal weight matrix.

In order to make the observed variables of the time-lag series have a clearer geographical significance, we will perform row-standardization processing on the obtained space-time weight matrix. This is because if we want to analyze how the temperature of a space-time location is affected by the temperature of an adjacent spatio-temporal location, we think that the temperature of each adjacent space-time location will have an impact on the temperature of the spatio-temporal location under study. Therefore, the sum of the weights of the temperature effects on all neighboring space-time locations is 1.

4. Application of Agricultural Genetic Breeding Technology Based on Big Data Analysis in Elm Cultivation

The collected natural wild elm species are grafted on a 1-year-old white elm rootstock, and each clone has 10 plants and normal water and fertilizer management.

After cultivation, we collect 3–5 young leaves from each plant, put them in a ziplock bag, and store them in a refrigerator at -70 °C for SSR marker analysis. The modified CTAB method (Han Qian et al., 2009) is used to extract cloned genomic DNA. After the DNA is purified and dissolved, it is tested with a Nanodrop-2000 nucleic acid analyzer, and the tested DNA is diluted to 30 ng/μL and used for the PCR reaction. A total of 17 pairs of SSR primers are selected, and gel electrophoresis is performed. Finally, 13 pairs of SSR primers with clear bands and high polymorphism are selected and tested. Figure 4 shows an image of elm leaves.

We perform cluster analysis and analysis of variance on the leaf shape traits obtained by using big data technology analysis and calculate the average value, standard deviation, coefficient of variation, and repeatability of each leaf shape trait. In order to eliminate the influence of the dimensions of different phenotypic data, all phenotypic data are standardized, the Euclidean distance between different samples is calculated, and the class average method is used to cluster the phenotypic data. In this paper, the band statistics of the electrophoretic patterns are carried out, and the patterns with bands are recorded as 1, and the patterns without bands are recorded as 0. DPS software is used to calculate the distance coefficient, the class average method (MPGMA) is used for cluster analysis to form a clustering dendrogram, and the PIC software is used to calculate the amount of polymorphic information of each primer. We perform cluster analysis on the phenotypic traits and SSR molecular markers of all varieties and perform correlation analysis based on the genetic distance matrix of the leaf shape trait cluster analysis and the genetic distance matrix of the SSR molecular marker cluster analysis. At the same time, we count the role of agricultural genetic breeding technology in

Table 1: The role of agricultural genetic breeding technology in elm cultivation.

Number	Effect evaluation
1	97.6
2	95.4
3	94.9
4	96.6
5	93.7
6	90.3
7	90.7
8	93.6
9	92.4
10	94.2
11	92.4
12	92.8
13	93.9
14	94.3
15	97.4
16	91.5
17	94.5
18	97.2
19	90.4
20	90.2
21	95.6
22	95.2
23	94.1
24	91.4
25	97.5
26	92.3
27	96.0
28	95.2
29	90.8
30	97.1
31	93.0
32	93.6
33	90.2
34	94.8
35	96.5
36	91.5
37	93.7
38	93.6
39	94.7
40	96.4
41	97.8
42	96.0
43	90.9
44	90.1
45	93.7
46	91.1
47	92.2
48	90.4
49	97.6
50	94.2
51	94.0
52	92.5
53	95.3
54	92.3
55	95.6
56	96.1
57	92.8
58	92.6
59	96.2

Table 1: Continued.

Number	Effect evaluation
60	91.2
61	95.3
62	93.1
63	90.7
64	96.1
65	97.8
66	93.9
67	97.4
68	92.1
69	96.4
70	92.0
71	95.0
72	93.6
73	93.8
74	93.5
75	95.4
76	97.3
77	94.1
78	93.0
79	93.9
80	91.6
81	91.9
82	95.1
83	95.1
84	90.0
85	96.2
86	95.3
87	95.3
88	97.1
89	94.0
90	94.3

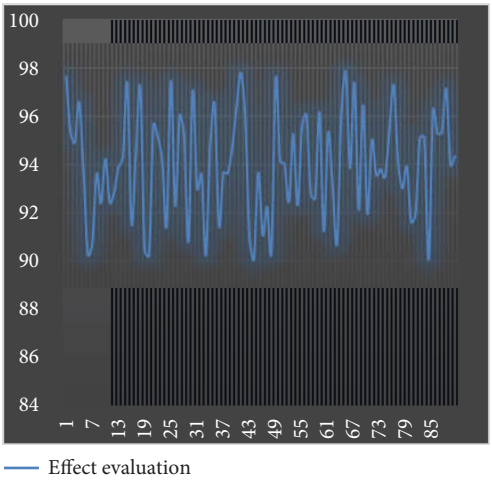

Figure 5: Line chart of data statistics.

the cultivation of elm trees. The statistical results are shown in Table 1 and Figure 5.

In this study, the distance matrix generated by cluster analysis of leaf shape traits and the distance matrix generated by cluster analysis of SSR molecular markers is used for correlation analysis. The experiment showed that the comprehensive leaf shape traits are extremely significantly

correlated with SSR molecular markers, and the correlation coefficient reaches 0.48. In order to further understand the relationship between leaf shape traits and SSR molecular markers, each trait of leaf shape and SSR molecular markers are clustered and analyzed. Moreover, the correlation analysis between the distance matrix produced by the cluster analysis of leaf shape traits and the distance matrix produced by the cluster analysis of SSR molecular markers is carried out. The test results showed that in the pairwise analysis of leaf shape traits and SSR molecular markers, the number of primers for leaf shape traits and SSR primers to reach a level of extremely significant correlation ($p < 0.001$) is between 3 and 11 pairs. There are more than 10 pairs of primers that are extremely significantly related to leaf length traits, the correlation coefficient is up to 0.543, and the repetitive power of leaf length traits is all above 0.9. There are about 10 pairs of primers that are extremely significantly related to leaf width traits, with the highest correlation coefficient being 0.46, and the repetitive power of leaf width traits are all above 0.9. It shows that the variation of leaf shape traits is affected by genetic factors. The results of the study showed that the leaf shape traits of *Ulmus pumila* clones are extremely significantly correlated with SSR molecular markers, and the correlation level between leaf shape traits and SSR loci is relatively high. This study lays the foundation for future research on other phenotypic traits and SSR molecular markers of elm clones and will play a positive role in promoting the collection and genetic improvement of elm germplasm resources.

5. Conclusion

In this paper, the leaf shape traits and SSR molecular markers are performed cluster analysis, and the cluster analysis produced a genetic distance matrix to perform correlation analysis to find the sites closely related to leaf shape traits, to provide a basis for the research on the expression and location of elm-related genes, and to provide technical support for the protection and utilization of elm germplasm resources and molecular marker-assisted breeding.

This paper combines big data technology and agricultural genetic breeding technology to study the cultivation of elm trees and conducts experimental research in combination with actual conditions. Moreover, this paper conducts correlation analysis between the distance matrix generated by cluster analysis of leaf shape traits and the distance matrix generated by cluster analysis of SSR molecular markers and combines big data technology to perform data processing and to count the test results. The research results show that agricultural genetic breeding technology can play an important role in elm cultivation.

Data Availability

The experimental data used to support the findings of this study are available from the corresponding author upon request.

Disclosure

Haiguang Huang and Rong Yang are co-first authors.

Conflicts of Interest

The author declare that there are no conflicts of interest regarding this work.

References

[1] T. A. Volk, B. Berguson, C. Daly et al., "Poplar and shrub willow energy crops in the United States: field trial results from the multiyear regional feedstock partnership and yield potential maps based on the PRISM-ELM model," *GCB Bioenergy*, vol. 10, no. 10, pp. 735–751, 2018.

[2] D. Piou, F. Benest, and É. Collin, "Are there any lessons to be learnt from long-standing introductions of pathogens? The case of Dutch elm disease," *Revue Forestiere Française*, vol. 70, no. 6, pp. 621–637, 2018.

[3] X. Li and Z. H. Huang, "Transcriptome analysis in the process of insect gall formation of elm leaves," *Genomics and Applied Biology*, vol. 38, no. 2, pp. 737–746, 2019.

[4] J. Wang, Q. Zhou, and A. J. Yin, "Self-adaptive segmentation method of cotton in natural scene by combining improved Otsu with ELM algorithm," *Transactions of the Chinese Society of Agricultural Engineering*, vol. 34, no. 14, pp. 173–180, 2018.

[5] M. Chudzińska, M. Litkowiec, M. Pałucka, A. Paalawska, and C. Koziol, "Clonal structure of field elm (Ulmus minor mill.) in Poland," *Sylwan*, vol. 163, no. 10, pp. 839–845, 2019.

[6] M. Chudzińska, M. Pałucka, A. Pasławska, and M. Litkowiec, "Results of preliminary research on genetic variation and genetic differentiation between Wych elm populations (Ulmus glabra Huds.) in Poland," *Sylwan*, vol. 162, no. 9, pp. 727–736, 2018.

[7] X. Li, H. B. Lu, and Z. H. Huang, "Proteomic analysis of leaf gall formation in elm," *Genomics and Applied Biology*, vol. 38, no. 7, pp. 3112–3122, 2019.

[8] J. Webber, "What have we learned from 100 years of Dutch elm disease?" *Quarterly Journal of Forestry*, vol. 113, no. 4, pp. 264–268, 2019.

[9] K. Kiran, K. M. Pawan, and C. Ashu, "Statistical investigations of growth characteristics of cherry-bark elm (Ulmus villosa Brandis) under mid-hill conditions of Himachal Pradesh," *Environment and Ecology*, vol. 36, no. 2A, pp. 551–555, 2018.

[10] D. K. Lee, E. Aberle, E. K. Anderson et al., "Biomass production of herbaceous energy crops in the United States: field trial results and yield potential maps from the multiyear regional feedstock partnership," *Gcb Bioenergy*, vol. 10, no. 10, pp. 698–716, 2018.

[11] W. Zhang, S. Y. Huo, and Y. Jia, "Comparison of machine learning algorithms for reference evapotranspiration estimation in Hebei province, China," *Water Saving Irrigation*, vol. 4, pp. 50–58, 2018.

[12] E. Harris, "The European white elm Ulmus laevis Pall. An elm with potential in Britain," *Quarterly Journal of Forestry*, vol. 111, no. 4, pp. 260–267, 2017.

[13] N. C. Melo, C. Fernandes, E. R. Soares, and E. L. M Coutinho, "Growth and productivity of sugarcane cultivated in soils submitted to chiseling in the planting row and in total area," *Journal of Agricultural Science*, vol. 11, no. 1, pp. 515–526, 2018.

[14] Y. Chen, Q. Cheng, X. Fang, and H. Yu, "Principal component analysis and long short-term memory neural network for

predicting dissolved oxygen in water for aquaculture," *Transactions of the Chinese Society of Agricultural Engineering*, vol. 34, no. 17, pp. 183–191, 2018.

[15] C. M. Brasier and J. F. Webber, "Is there evidence for post-epidemic attenuation in the Dutch elm disease pathogen Ophiostoma novo-ulmi?" *Plant Pathology*, vol. 68, no. 5, pp. 921–929, 2019.

[16] T. M. Fenning, "The use of tissue culture and in-vitro approaches for the study of tree diseases," *Plant Cell, Tissue and Organ Culture*, vol. 136, no. 3, pp. 415–430, 2019.

[17] H. Zhang, G. J. Quan, J. Huang, X. Huang, S. Yan, and R. Liu, "Study on intracellular polymers using near infrared spectroscopy and extreme learning machine in denitrifying phosphorus removal process," *China Environmental Science*, vol. 37, no. 5, pp. 1823–1830, 2017.

[18] C. Gilbert and T. Ellis, "Biological engineered living materials: growing functional materials with genetically programmable properties," *ACS Synthetic Biology*, vol. 8, no. 1, pp. 1–15, 2018.

[19] U. Niggli, C. Andres, H. Willer, and B. P Baker, "Building a global platform for organic farming research, innovation and technology transfer," *Organic Agriculture*, vol. 7, no. 3, pp. 209–224, 2017.

[20] S. Federman and P. Zankowski, "Strategic science planning for responsible stewardship and plant protection at the US Department of Agriculture," *Plants, People, Planet*, vol. 2, no. 1, pp. 53–56, 2020.

[21] L. Zuo, S. Zhang, J. Zhang, X. Liu, X. Yu, and M. Yang, "Primer development and functional classification of EST-SSR markers in Ulmus species," *Tree Genetics & Genomes*, vol. 16, no. 5, pp. 1–11, 2020.

Hindawi
Mobile Information Systems
Volume 2022, Article ID 3389112, 10 pages
https://doi.org/10.1155/2022/3389112

Research Article

Characterization Techniques Application on Pesticide Adsorption Mechanism Research of Corn Straw Biochar Based on KOH Thermal Activation

Minghua Wang, Honglan Cai, Qingan Qiao, and Jiang Zhang

School of Chemistry and Materials Science, Ludong University, Shandong 264025, China

Correspondence should be addressed to Honglan Cai; 2020050028@stu.cdut.edu.cn

Received 22 June 2022; Revised 20 July 2022; Accepted 22 July 2022; Published 3 August 2022

Academic Editor: Chi Lin

In this paper, research on pesticide adsorption mechanism of corn straw biochar based on KOH thermal activation is carried out. In this paper, corn stalks and pine needles are used as raw materials for preparing biomass charcoal, and biochar is prepared at temperatures of 200°C, 400°C, and 600°C. This paper uses thermogravimetric analysis, elemental analysis, electron microscopy scanning, aperture measurement, infrared spectroscopy, and other characterization techniques to analyze the structure and properties of biochar in detail. Moreover, this paper uses batch method to select different organic pesticides diuron and carbaryl to test their adsorption performance. This article discusses the relationship between the adsorption mechanism and structural characteristics of biochar for organic pollutants. In addition, this paper studies the adsorption mechanism of diuron and carbaryl in the loess by adding exogenous biochar to the loess. Finally, this article analyzes the impact of the addition of biochar on the environmental behavior of diesel-contaminated loess adsorption of organic pollutants. This paper studies the role of KOH thermally activated corn stover biochar in agricultural adsorption, and verifies the reliability of the method proposed in this paper through experimental studies.

1. Introduction

With the development of modern agriculture, a large number of pesticides are used for the prevention and treatment of diseases, pests, and weeds. It is of great significance in ensuring a bumper harvest in agriculture, promoting the development of high-yield, high-quality, and efficient modern agriculture, meeting people's demand for agricultural and sideline products, and reducing the intensity of agricultural production. According to incomplete statistics, if pesticides are not used in world food production, the average loss of the three major food crops of wheat, rice, and corn will be more than 30%. If pesticides are not used, the output of agricultural products may be reduced by about 40% in the first year, and the output may be reduced by 60% or even no production in the second year [1]. The use of pesticides in my country can recover 15–30% of the loss of agricultural products every year, and the income from the use of pesticides is about 4 times the cost of pesticides. Therefore, pesticides have become an indispensable means of production in the modern agricultural production [2]. However, while the use of pesticides brings huge benefits to mankind, pesticides and the metabolites and degradation products of some pesticides not only pollute the crops themselves, but also pollute the growth environment of crops such as soil and natural water bodies, posing serious threats to the ecological environment and human health. With the progress of society and the enhancement of human environmental protection awareness and the increasing exposure of the harm caused by the pesticides, people have begun to realize the seriousness of the harm caused by pesticides to human health and environmental pollution. Moreover, all countries in the world have formulated relevant rules and regulations to strictly manage pesticides, and

environmental pollution and governance of pesticides have become a global problem. The United States, Japan, Malaysia, South Korea, Canada, the United Kingdom, Germany, Russia, France, Russia, Taiwan, and other countries and regions have successively established standards for maximum pesticide residue limits, and formulated and promulgated relevant standards. At the same time, the United Nations, European Community, and other world organizations have established a special pesticide residue work system, which is fully responsible for the formulation of pesticide residue standards [3].

The use of pesticides has increased the output of agricultural products. Driven by market demand and economic benefits, people have used more and more pesticides. Although my country has issued relevant industry standards for the safe use of pesticides many times, as well as a list of prohibited pesticides [4], under the temptation of economic interests, the use of pesticides continues to increase; The human body is exposed to organic pesticides remaining in the environment through various channels, and trace amounts of toxic pesticides slowly enter the human body. Accumulation, although it will not cause obvious acute poisoning hazard to the human body in a short time, it will cause chronic potential hazards. For example: organophosphorus and carbamate pesticides can inhibit cholinesterase activity, and prolonged exposure to such pesticides affect the normal function of the human nervous system. Biochar is a carbon-rich substance formed by the pyrolysis of wastes such as wood, straw, manure, or leaves under oxygen-limited or anaerobic conditions. My country produces a large amount of agricultural straw waste every year, but the utilization rate is very low and less than 50%. More than 30% of the straw is directly burned or discarded in the field, which not only causes serious waste of resources, but also causes environmental pollution and other problems. Especially in remote rural areas, the random burning of agricultural straws releases a large amount of CO2 gas, which aggravates the greenhouse effect; on the other hand, the random stacking of agricultural waste makes the toxic and harmful pollutants enter the soil and groundwater with the erosion of rainwater., which can also become the source of agricultural pollution. However, the preparation of biochar can be a new way to deal with agricultural waste straw, because the unique properties of biochar itself determine its utilization value. Applying biochar into the soil can improve the soil environment, and the carbon sequestration effect of biochar can alleviate the greenhouse effect to a certain extent. In addition, because of its special surface structure, biochar has the ability to adsorb pollutants, which is also of great significance for improving the quality and safety of agricultural products.

2. Related Work

Through the research on the environmental behavior of pesticides in soil, literature [5] found that the mobility of pesticides in soil is closely related to the physical and chemical properties of pesticides themselves, which is mainly affected by chemical properties, shape, structure, pH, water solubility, molecular size, and polarity. Ionic pesticides mainly react with soil particles through ion exchange and hydrogen bonding, while organic pesticides that are easily dissociated into cations can be adsorbed in soil or sediments through cation exchange (ionic bonding). The literature [6] found that the content of organic matter in the soil plays a decisive role in the adsorption of nonionic herbicides to a certain extent. However, mineral components have little effect on its adsorption, while ionic herbicides have the opposite effect.

Since the structure of biomass charcoal is relatively loose, it can be mixed with the soil to increase the porosity of the soil, thereby increasing the air and moisture content in the soil. Unlike other organic matter in the soil, biomass charcoal contains more trace elements and the biomass charcoal applied to the soil also has good chemical stability, will not be weathered and decomposed for a long time, and can continuously improve the soil fertility [7]. Literature [8] applied biomass charcoal as fertilizer to corn fields, and found that the yield of corn has been significantly improved. In addition, mixing biomass charcoal and traditional inorganic or organic fertilizers into the soil in a certain proportion can delay the release of nutrients in the fertilizer, which will reduce the loss of nutrients and significantly increase the utilization rate of fertilizers. Biomass charcoal has also played a positive role in improving the absorption of nutrients by crops. The literature [9] found through a series of studies that the nitrogen content in the soil to which biomass charcoal is applied has increased to a certain extent. However, the research on the application of biomass charcoal as a soil amendment to agricultural production is still mainly in a short period of time, and the mechanism of action and long-term effects are still unclear. In addition, since it cannot be ruled out whether it has major side effects, it is currently difficult to promote it on a large scale. Scientists still need to further explore and study the biochar soil amendment.

In modern industry, almost all products that are produced have to go through the process of printing and packaging. In the process of packaging and printing, a large amount of dyes are consumed. This aspect has promoted the continuous development of the printing and dyeing industry. On the other hand, the excessive use of dyes has also caused a considerable degree of environmental problems [10]. If the surplus and unused dyes in the factory cannot be processed in time, they are easily discharged into the environment. Because dye molecules contain more aromatic functional groups, the complex molecular structure often makes them difficult to degrade, which will cause serious pollution to soil and rivers [11]. According to reports, some dyes can irritate human skin and cause allergic symptoms. In severe cases, it can also cause cancer or deformity [12]. For example: Methylene blue is the most common dye for cotton, wood, silk, and other products. It contains certain toxicity. Acute exposure to methylene blue solution can cause increased heart rate, vomiting, shock, cyanosis, jaundice, quadriplegia, and tissue necrosis. Reference [13]. Before being discharged to public water sources, how to

effectively remove dyes from industrial wastewater is the focus of attention nowadays. Adsorption is generally considered to be a reliable technology for the treatment of dye-containing wastewater.

Out of economic considerations, scientists have been studying the process of preparing biomass-activated carbon from agricultural by-products and waste materials as raw materials for a long time. Various agricultural and forestry wastes, such as walnut shells, wood chips, rubber trees, jute fibers, snail shells, castor beans, coconut shells, and oil palm fibers, have been tried to prepare high specific surface area biomass-activated carbon adsorbents, especially for the research on the specific adsorption function of biomass charcoal that has always been valued by the scientific researchers [14].

3. Preparation of Corn Stover Biochar Based on KOH Thermal Activation

Soil is an important place for human activities to survive, and it is also the main destination for environmental behaviors of various external pollutants. The pollutants that enter the environment will eventually accumulate in the soil sediments. It often leads to secondary pollution of the groundwater environment. The organic pesticides remaining in the soil will be enriched and migrated in the food chain, which will cause harm to human health. After pesticides enter the soil environment, processes such as adsorption runoff, biodegradation, and plant absorption will occur. Moreover, it can be degraded into intermediate products or even completely mineralized under the combined action of physics, biology, and chemistry. Or, it migrates through leaching, evaporation, diffusion, absorption and enrichment of animals and plants, and causes pollution to the groundwater environment, atmosphere, and agricultural products (Figure 1). In this process, soil adsorption becomes a key step to lock pesticide pollutants and control their migration. The distribution capacity of pesticides in these media determines its ultimate fate in the environment [15].

The adsorption process of organic pesticide molecules in the soil is the process of their distribution in soil media such as solution, organic matter, and surface minerals (Figure 2). Hydrophobic distribution, covalent bonds, hydrogen bonds, ligand exchange, and chelation are important factors for the adsorption of organic pesticides on soil particles. Studies have pointed out that when atrazine and other herbicides are adsorbed on solids such as activated carbon or clay minerals, compared with soil organic matter, the role of mineral components in sediments to adsorb organic pollutants is not the primary factor. On the one hand, the soluble organic matter in the soil can solubilize pesticides. On the other hand, there are special adsorption sites in the humic acid structure of organic matter, which can still adsorb herbicides on the surface. However, the amount and structural composition of the organic matter in the soil in different regions are different, which makes the environmental behavior of organic pollutants such as pesticides different. Therefore, studying the environmental behavior of pesticide pollutants in soil has far-reaching practical significance for soil pollution control [16].

Broadly speaking, biochar is a type of black carbon. Because of its special structure, it has a wide range of applications in the fields of agriculture, ecological restoration, and environmental protection. It was found that biochar prepared from different sources and different pyrolysis conditions showed differences in the adsorption performance of organic pollutants and heavy metals [17]. Therefore, it is necessary to effectively characterize the prepared biochar to understand the changes in its structure and properties and reveal its influence on the adsorption of organic pollutants by loess. We selected corn stalks and pine needles as the biomass raw materials in this study, and the preparation of biochar was carried out at 200, 400, and 600 temperature conditions by oxygen-limited and temperature-controlled pyrolysis. We use thermogravimetric analysis, elemental analysis, FTIR spectroscopy, specific surface area analysis, and other methods to characterize the structural characteristics of each substance, and analyze the effects of different preparation methods on its elemental composition, surface structure, and surface properties. The problem of soil pollution caused by the abuse of various pesticide pollutants has become more and more serious. This has attracted the attention of my country's environmental protection departments, and relevant laws and regulations have also made further improvements and clear regulations, which have made soil pollution problems in my country. It has become a research hotspot for environmental workers, and the environmental behavior of various toxic and hazardous pollutants in soil has also become an important research topic in the environmental field. Therefore, it is necessary to seek a new way that is cost-effective and can improve soil environmental pollution, while also improving the soil environmental quality. This has also become an objective requirement for ensuring the safety, yield, and quality of agricultural products. There are great differences in soil structure and organic matter content in different regions, and there are also great differences in their ability to adsorb organic pollutants. Up to the present stage, there is a lack of relevant theoretical studies on the adsorption behavior of organic pesticide pollutants in loess in Northwestern cold and early regions by exogenous biochar, especially for some new persistent organic pollutants. At present, the research on the influence mechanism of biochar on the migration and transformation behavior of organic pollutants in the soil environment is not diminishing. The heterogeneity of carbon itself makes the adsorption effect, process, and mechanism of different biochar to have certain differences, so it has great research potential.

Pesticides are widely used in agricultural production to improve the yield and appearance quality of agricultural products. They are a very common environmental pollutant. A large number of residual pollutants entering the soil environment will produce a series of side effects, which will reduce the quality of the soil, affect the activity of microorganisms, and then cause soil compaction, which is not conducive to the long-term growth of crops. Therefore,

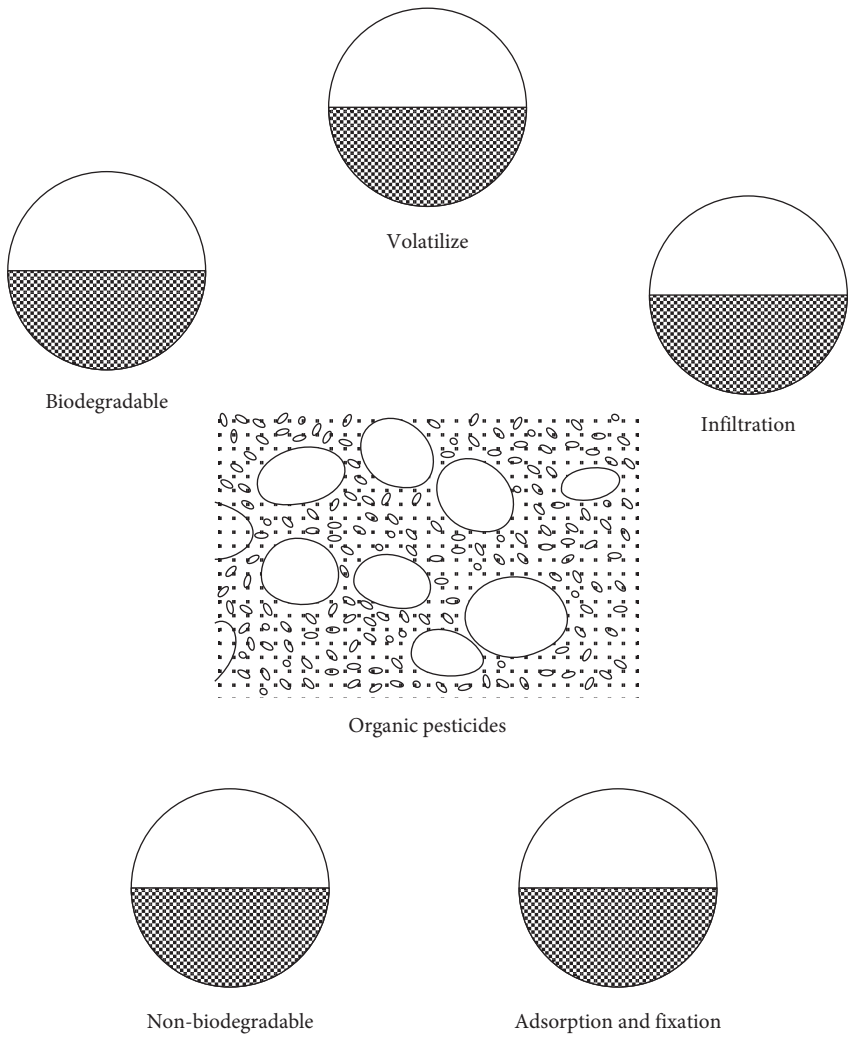

Figure 1: The fate of pesticides in the soil environment.

exploring the adsorption mechanism of pesticide pollutants in soil helps to provide a certain theoretical reference for the treatment and improvement of soil in polluted areas [18].

Based on the above analysis, this paper studies the adsorption mechanism of corn stover biochar pesticides based on KOH thermal activation, and the following research will be carried out in conjunction with the experimental research.

The raw material of biochar is derived from corn stalks in the north. We first wash away the adhering debris on the surface of the straw, then ventilate and dry it under natural conditions, then crush it and sieve it, soak it in a certain amount of deionized water for 24 hours, and then filter it. Finally, it is dried in a drying box and stored for later use. The main instruments include thermogravimetric analyzer, temperature-controlled muffle furnace, Fourier transform infrared spectrometer, element analyzer, scanning electron microscope (SEM), and specific surface area analyzer.

We use limited oxygen temperature control carbonization method, weigh a small amount of straw powder in a crucible, carbonize it at 200, 400, and 600°C, respectively, for 6 h, take it out after cooling to room temperature, sieving, and storing. The sample numbers of corn stover and pine needle biochar are MBC-200, MBC-400, MBC-600, PBC-200, PBC-400, and PBC-600, respectively.

1 mol/l KOH solution and 5 g biochar are mixed. The mixture was magnetically stirred at 80°C in a water bath for 1 h, and then immersed for 11H at room temperature.

We use a cloth funnel to filter and separate the biochar mixture fully impregnated with KOH activator, and place the filtered biochar in a crucible for later use [19].

The biochar precursor obtained in the previous step was placed in a horizontal vacuum tube electric furnace in a nitrogen atmosphere (160 ml/min) (Figure 3). The biochar precursors with different alkali-to-carbon ratios were activated at 600°C, 700°C, and 800°C for 30 minutes, and the heating rate of the reactor was set to 3°C/min.

After taking out the cooled biochar, it was soaked in an excess HCI solution with a concentration of 0.1 mol/L and boiled slightly for 10 minutes. After cooling, it is washed repeatedly with the same concentration of HCl solution, and finally washed with distilled water until the

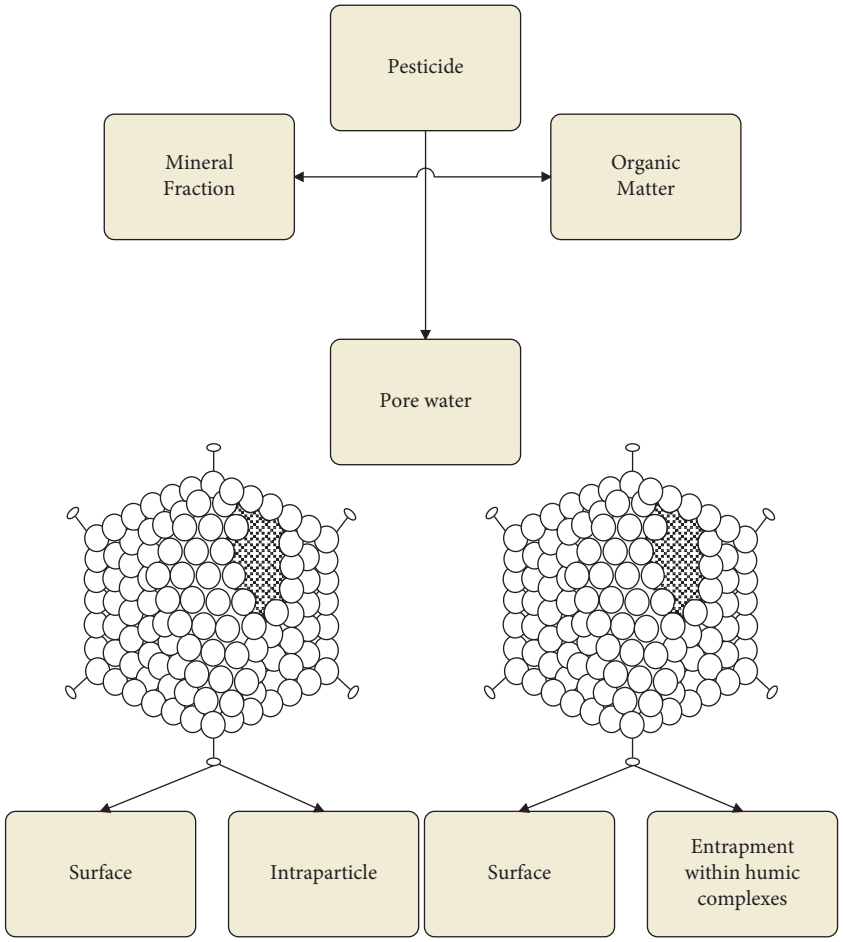

Figure 2: The adsorption of organic pollutants such as pesticides by soil.

pH of the filtrate is 6-7. After filtration and separation, the activated biochar is dried at 105°C for 12 h and cooled to room temperature for later use, which is called activated biochar [20].

When biomass is pyrolyzed, part of the organic matter is destroyed, while relatively stable carbonaceous substances are retained. The ash content and yield of biochar are shown in Tables 1 and 2. From the calculation results in the table, it is concluded that the yield of biochar is related to the pyrolysis temperature in the preparation process. As the pyrolysis temperature increases, the yield shows a certain downward trend. When the pyrolysis temperature is 200°C, the yield of MBC-200 is 67.1%, and the yield of PBC-200 is as high as 75%. At 400°C, the carbonization yield of MBC-400 was reduced to 28.2%, and the carbonization yield of PBC-400 was reduced to 37%. However, when the temperature rises to 600°C, corn stalks and pine needles are carbonized in a large amount, the carbonization yield of MBC-600 drops to 24%, and the carbonization yield of PBC-600 drops to 2.27%. The comparison shows that the carbonization yield of pine needles is higher than that of corn stalks at the three different preparation temperatures. It is mainly due to the differences in the structure and elemental composition of the protoplasm. With the continuous increase of pyrolysis temperature, a large amount of cellulose breaks and loses.

Due to its special physical and chemical properties, biochar has been widely used in sewage treatment and air purification fields. Its application in soil is considered to be a win-win measure to alleviate climate change and increase soil fertility, and it has become a research hotspot in the field of agricultural production and ecological environment. Moreover, there are a wide range of sources of materials for the preparation of biochar. In this paper, corn stalk biochar and pine needle biochar are taken as examples to study the adsorption behavior of organic pollutants (carivin and diuron) of biochar obtained from different pyrolysis conditions. Moreover, this paper determines the adsorption thermodynamics and adsorption kinetics models, and discusses the relevant factors affecting the adsorption behavior.

4. Results

The kinetic adsorption curves of the pollutants diuron and carbaryl on different biochar are shown in Figures 4 and 5. The data is shown in Tables 3–6. It can be seen from the figure that the equilibrium adsorption capacity of biochar for diuron, carbaryl, etc. is positively correlated with its thermal cracking temperature. Whether it is the adsorption of diuron or carbaryl, the adsorption capacity of MBC-00 and PBC-

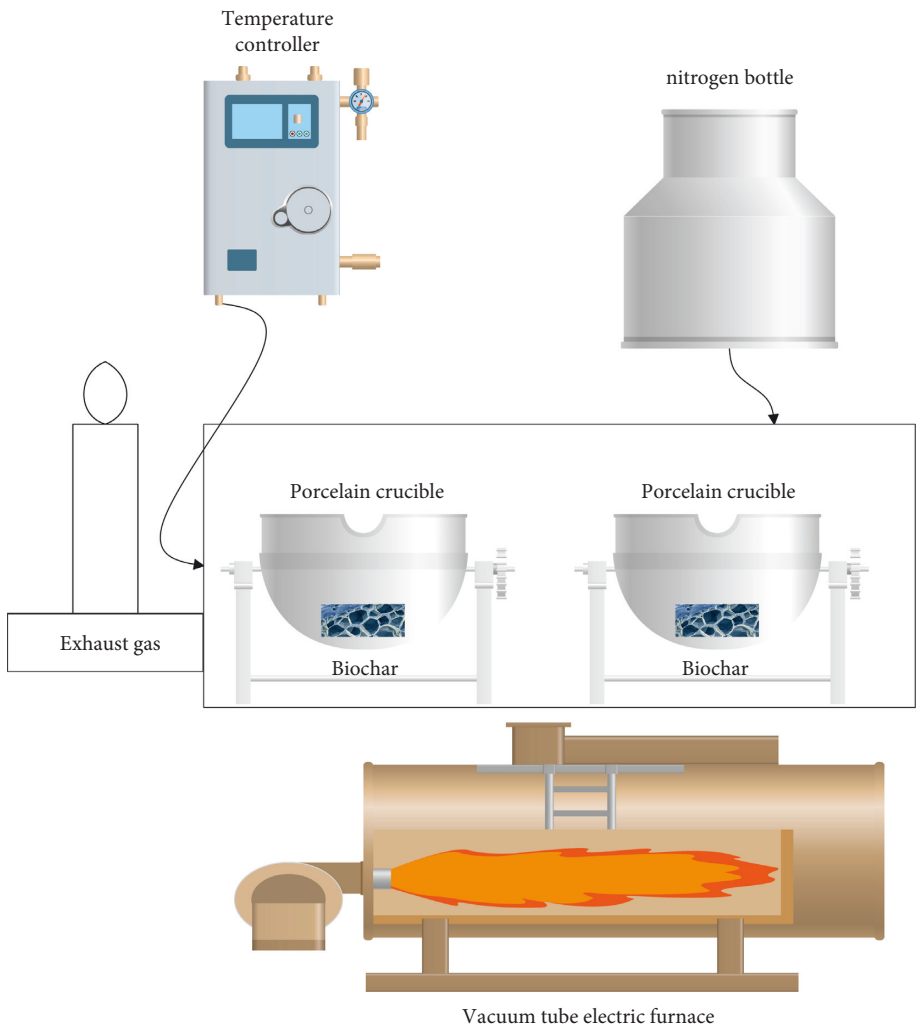

Figure 3: Schematic diagram of activation device.

Table 1: The yield, element composition, and ash content of corn stover biochar.

Sample name	Corn stover	MBC-200	MBC-400	MBC-600
Temperature/°C	—	200	400	600
Yield%	—	67.1	28.1	24.2
Ash content%	—	4.33	11.02	12.35
C%	43.6	51.36	53.22	55.32
H%	5.51	4.78	2.82	1.64
N%	0.44	0.49	0.46	0.47

Table 2: The yield, element composition, and ash content of pine needle biochar.

Sample name	Pine needles	MBC-200	MBC-400	MBC-600
Temperature/°C	—	200	400	600
Yield%	—	75.2	37.1	27.1
Ash content%	—	2.74	7.78	9.22
C%	52.5	65.65	63.94	67.34
H%	6.21	4.71	3.22	1.85
N%	0.31	0.6	54	0.57

600 is much greater than the adsorption capacity of biochar prepared at 200°C and 400°C. Moreover, all the adsorption processes are manifested as a fast reaction stage and a slow reaction stage. The fast reaction stage is mainly controlled by electrostatic gravity, and is mainly exchange adsorption. In this stage, the adsorption of carbaryl and diuron by biochar is first carried out on the surface of biochar. When the surface of biochar reaches adsorption saturation, there are pore structures inside the biochar particles, and these pores can accept more diuron and carbaryl molecules. Therefore, the carbaryl and diuron molecules adsorbed on the surface of the biochar slowly diffuse into the biochar particles, causing the surface of the biochar to become unsaturated again, and more carbaryl and diuron molecules need to be adsorbed. At this time, the concentration of the solution decreases. As the "active sites" that can be adsorbed on the surface of the biochar decrease and the concentration of carbaryl and diuron molecules that can be adsorbed in the solution decreases, the adsorption turns to a slow reaction stage. At this time, the adsorption rate decreases, and the adsorption gradually reaches a saturated state.

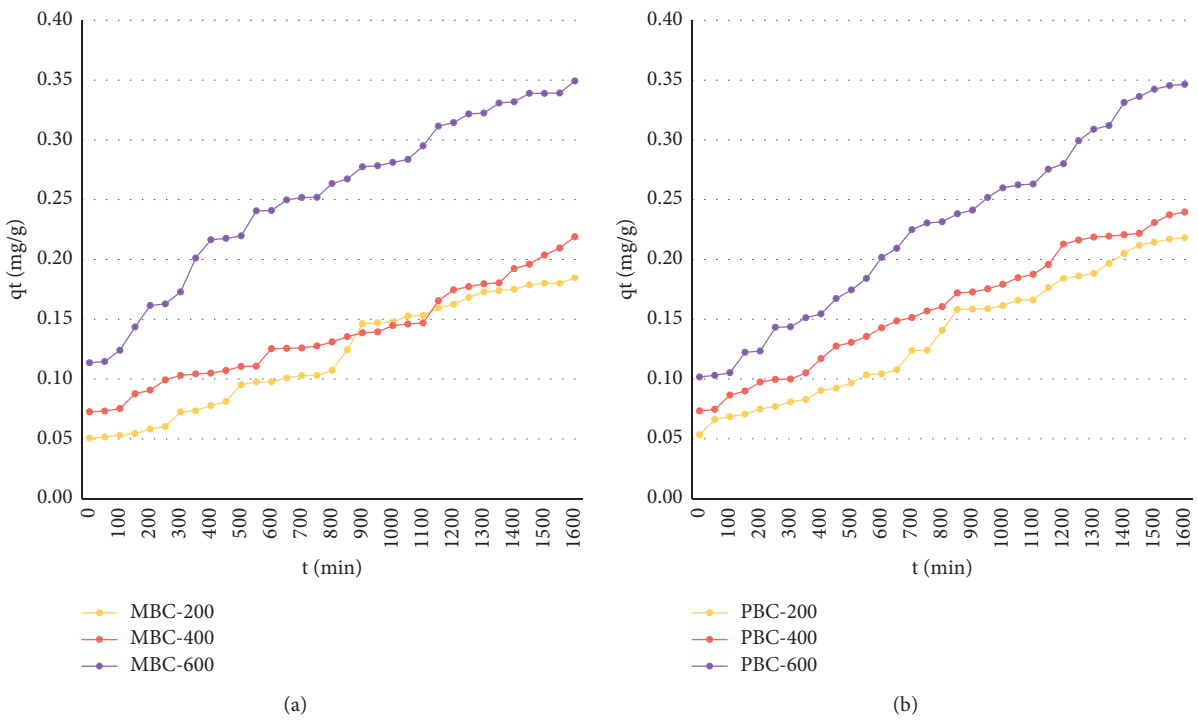

Figure 4: Kinetic adsorption curve of biochar on diuron: (a) diuron adsorption curve 1 and (b) diuron adsorption curve 2.

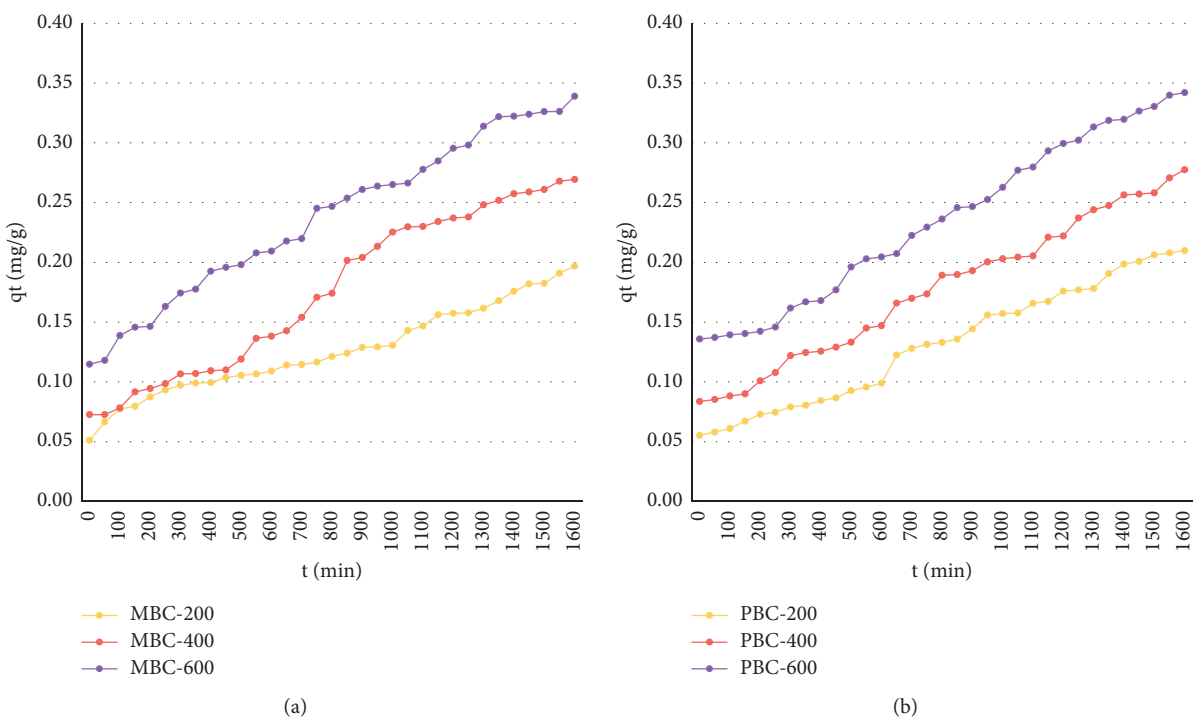

Figure 5: Kinetic adsorption curve of biochar on carbaryl: (a) Carbine adsorption curve 1 and (b) Carbine adsorption curve 2.

Table 3: Diuron adsorption curve 1.

Number	MBC-200	MBC-400	MBC-600
0	0.050	0.073	0.114
50	0.052	0.073	0.115
100	0.053	0.075	0.124
150	0.054	0.088	0.144
200	0.058	0.091	0.161
250	0.060	0.099	0.163
300	0.072	0.103	0.173
350	0.073	0.104	0.201
400	0.078	0.105	0.216
450	0.081	0.107	0.218
500	0.095	0.111	0.220
550	0.098	0.111	0.241
600	0.098	0.125	0.241
650	0.101	0.126	0.250
700	0.103	0.126	0.252
750	0.103	0.128	0.252
800	0.107	0.131	0.263
850	0.125	0.135	0.267
900	0.146	0.139	0.277
950	0.147	0.139	0.278
1000	0.148	0.145	0.281
1050	0.153	0.146	0.284
1100	0.153	0.147	0.295
1150	0.160	0.166	0.311
1200	0.163	0.175	0.315
1250	0.168	0.177	0.322
1300	0.173	0.180	0.322
1350	0.174	0.180	0.331
1400	0.175	0.192	0.332
1450	0.179	0.196	0.339
1500	0.180	0.204	0.339
1550	0.180	0.210	0.339
1600	0.185	0.219	0.349

Table 4: Diuron adsorption curve 2.

Number	PBC-200	PBC-400	PBC-600
0	0.053	0.073	0.102
50	0.066	0.075	0.103
100	0.069	0.086	0.105
150	0.071	0.090	0.122
200	0.075	0.097	0.123
250	0.077	0.100	0.143
300	0.081	0.100	0.144
350	0.083	0.105	0.151
400	0.090	0.117	0.154
450	0.092	0.128	0.167
500	0.097	0.131	0.174
550	0.103	0.135	0.184
600	0.104	0.143	0.202
650	0.108	0.148	0.209
700	0.124	0.151	0.225
750	0.124	0.157	0.230
800	0.141	0.160	0.231
850	0.158	0.172	0.238
900	0.158	0.173	0.241
950	0.159	0.175	0.252
1000	0.161	0.179	0.260
1050	0.166	0.185	0.262
1100	0.166	0.188	0.263
1150	0.176	0.196	0.275
1200	0.184	0.213	0.280
1250	0.186	0.216	0.299
1300	0.188	0.219	0.309
1350	0.197	0.219	0.312
1400	0.205	0.221	0.331
1450	0.212	0.222	0.336
1500	0.214	0.231	0.342
1550	0.217	0.237	0.345
1600	0.218	0.240	0.346

5. Analysis and Discussion

The paper has reached the following conclusions:

(1) The characterization results of biochar show that the surface of biochar contains hydroxyl, carboxyl, and carbonyl groups. With the increase of biochar preparation temperature, O. H, C, a large number of chemical bonds such as H, *C=O,* and phenol-OH are broken and disappeared. It shows that the high pyrolysis temperature during the preparation of biochar will lead to a large loss of polar functional groups on the surface of the biochar, which will increase the hydrophobicity of the biochar surface. The ash content and carbonization degree of biochar increased with the increase of the preparation temperature and the extension of the pyrolysis time, but the yield and organic matter content decreased. At 200°C, biochar exhibits higher polarity and fatness. But with the increase of carbonization temperature, the aromaticity of biochar increases and the polarity decreases. It shows that the heating process is the process of biochar from "soft carbon" to "hard carbon". The preparation temperature of biochar has a great influence on the surface microstructure. As the pyrolysis temperature increases, the number of micropores on the surface of biochar increases, the pore size is irregular, the distribution is uneven, and the pore volume increases. This causes the surface roughness to increase, the specific surface area increases, and the average pore diameter decreases.

(2) The kinetic adsorption of pesticides carbaryl and diuron on loess is divided into fast reaction stage and slow reaction stage, and the time to reach adsorption equilibrium is 14 h and 16 h, respectively. The test results of the biochar adsorption performance show that the adsorption capacity of MBC-600 and PBC-600 is much greater than that of the biochar prepared under the conditions of 200°C and 400°C, regardless of whether it is the adsorption of diuron or carbaryl. Moreover, all the adsorption processes are manifested as a fast reaction stage and a slow reaction stage, and the equilibrium time for the adsorption of diuron and carbaryl by biochar is 12 h and 10 h, respectively. At the same temperature and the same initial concentration, the adsorption capacity of biochar made from pine needles is higher than that of biochar made from

Table 5: Carbine adsorption curve 1.

Number	MBC-200	MBC-400	MBC-600
0	0.051	0.073	0.115
50	0.067	0.073	0.118
100	0.077	0.078	0.139
150	0.080	0.092	0.146
200	0.087	0.094	0.146
250	0.093	0.099	0.163
300	0.097	0.107	0.174
350	0.099	0.107	0.178
400	0.099	0.109	0.193
450	0.104	0.110	0.196
500	0.106	0.119	0.198
550	0.107	0.136	0.208
600	0.109	0.138	0.209
650	0.114	0.143	0.218
700	0.115	0.154	0.220
750	0.117	0.171	0.245
800	0.121	0.174	0.247
850	0.124	0.202	0.254
900	0.129	0.204	0.261
950	0.129	0.213	0.264
1000	0.131	0.225	0.265
1050	0.143	0.230	0.266
1100	0.147	0.230	0.278
1150	0.156	0.234	0.285
1200	0.157	0.237	0.295
1250	0.158	0.238	0.298
1300	0.162	0.248	0.314
1350	0.168	0.252	0.322
1400	0.176	0.257	0.322
1450	0.182	0.259	0.324
1500	0.182	0.261	0.326
1550	0.191	0.268	0.326
1600	0.197	0.269	0.339

Table 6: Carbine adsorption curve 2.

Number	PBC-200	PBC-400	PBC-600
0	0.055	0.084	0.136
50	0.058	0.085	0.137
100	0.061	0.088	0.139
150	0.067	0.090	0.140
200	0.073	0.101	0.142
250	0.075	0.108	0.146
300	0.079	0.122	0.162
350	0.080	0.124	0.167
400	0.084	0.126	0.168
450	0.087	0.129	0.177
500	0.093	0.133	0.196
550	0.096	0.145	0.203
600	0.099	0.147	0.205
650	0.122	0.166	0.207
700	0.128	0.170	0.222
750	0.131	0.174	0.229
800	0.133	0.189	0.236
850	0.136	0.190	0.246
900	0.144	0.193	0.247
950	0.156	0.200	0.253
1000	0.157	0.203	0.263
1050	0.158	0.204	0.277
1100	0.166	0.205	0.280
1150	0.167	0.221	0.293
1200	0.176	0.222	0.299
1250	0.177	0.237	0.302
1300	0.178	0.244	0.313
1350	0.191	0.247	0.319
1400	0.199	0.256	0.320
1450	0.201	0.257	0.327
1500	0.206	0.258	0.330
1550	0.208	0.271	0.340
1600	0.210	0.278	0.342

corn stalks. It is mainly caused by the difference between different biomasses. The analysis and research on the contribution show that the adsorption of biochar prepared at low temperature is dominated by the partitioning effect. With the increase of the preparation pyrolysis temperature, the surface adsorption is enhanced, and the adsorption behavior of biochar prepared by high-temperature pyrolysis is realized by two kinds of adsorption together.

The saturated adsorption capacity of diuron and carbaryl on loess added with exogenous biochar increased significantly. It shows that the physical adsorption is the main reaction type. The adsorption capacity of diuron on loess with exogenous biochar is positively correlated with the temperature of the system and the initial concentration of the solution, indicating that the adsorption is a spontaneous endothermic process. The difference in the amount of biochar added and the pyrolysis temperature has a significant effect on the adsorption of diuron by the loess, and most of the organic pollutants are mainly absorbed by the added biochar in the loess. The pH has a great influence on the adsorption of carbaryl, and the change in the adsorption amount of diuron is negligible.

6. Conclusion

The problem of soil pollution caused by the abuse of various pesticide pollutants has become more and more serious, which has attracted the attention of my country's environmental protection departments. Moreover, relevant laws and regulations have also made further improvements and clear regulations, which makes soil pollution in my country a hotspot for environmental workers to study. At the same time, the environmental behavior of various toxic and harmful pollutants in the soil has also become an important subject in the environmental field. Therefore, it is necessary to seek a new way that is cost-effective and can improve soil environmental pollution, while also improving the soil environmental quality. This has also become an objective requirement for ensuring the safety, yield, and quality of agricultural products. There are great differences in soil structure and organic matter content in different regions, and there are also great differences in their ability to adsorb organic pollutants. Therefore, the research on the influence mechanism of biochar on the migration and transformation behavior of organic pollutants in the soil environment is not diminished. The heterogeneity of carbon itself makes the adsorption effect, process, and mechanism of different biochar have certain differences, so it has great research

potential. This paper studies the role of KOH thermally activated corn stover biochar in agricultural adsorption, and verifies the reliability of the method proposed in this paper through the experimental studies.

Data Availability

The experimental data used to support the findings of this study are available from the corresponding author upon request.

Conflicts of Interest

The author declared that there are no conflicts of interest regarding this work.

References

[1] M. Wang, R. Qu, C. Sun, P. Yin, and H. Chen, "Dynamic adsorption behavior and mechanism of transition metal ions on silica gels functionalized with hydroxyl- or amino-terminated polyamines," *Chemical Engineering Journal*, vol. 221, pp. 264–274, 2013.

[2] S. J Dai, Y. C Zhao, D. J Niu, Q. Li, and Y Chen, "Preparation and reactivation of magnetic biochar by molten salt method: relevant performance for chlorine-containing pesticides abatement," *Journal of the Air & Waste Management Association*, vol. 69, no. 1, pp. 58–70, 2019.

[3] H. Blanco Canqui, "Biochar and water quality," *Journal of Environmental Quality*, vol. 48, no. 1, pp. 2–15, 2019.

[4] M. Wang, R. Qu, C. Sun et al., "Synthesis, characterization, and adsorption properties of m-aramid and chitosan hybrid composite films with the ratio of 100/0, 85/15, 65/35, 50/50 and 35/65 toward Hg(II) ions," *Desalination and Water Treatment*, vol. 146, pp. 197–209, 2019.

[5] M. S. Khorram, A. K. Sarmah, and Y. Yu, "The effects of biochar properties on fomesafen adsorption-desorption capacity of biochar-amended soil," *Water, Air, & Soil Pollution*, vol. 229, no. 3, pp. 1–13, 2018.

[6] J. O. Fernandes, C. A. R. Bernardino, and C. F. Mahler, "Biochar generated from agro-industry sugarcane residue by low temperature pyrolysis utilized as an adsorption agent for the removal of thiamethoxam pesticide in wastewater," *Water, air, & Soil Pollution*, vol. 232, no. 2, pp. 1–13, 2021.

[7] R. Zhao, X. Ma, and J. Xu, "Removal of the pesticide imidacloprid from aqueous solution by biochar derived from peanut shell," *Bioresources*, vol. 13, no. 3, pp. 5656–5669, 2018.

[8] I. Ćwieląg-Piasecka, A. Medyńska-Juraszek, M. Jerzykiewicz et al., "Humic acid and biochar as specific sorbents of pesticides," *Journal of Soils and Sediments*, vol. 18, no. 8, pp. 2692–2702, 2018.

[9] J. Kearns, E. Dickenson, and D. Knappe, "Enabling organic micropollutant removal from water by full-scale biochar and activated carbon adsorbers using predictions from bench-scale column data," *Environmental Engineering Science*, vol. 37, no. 7, pp. 459–471, 2020.

[10] J. P. Kearns, K. K. Shimabuku, D. R. U. Knappe, and R. S Summers, "High temperature Co-pyrolysis thermal air activation enhances biochar adsorption of herbicides from surface water," *Environmental Engineering Science*, vol. 36, no. 6, pp. 710–723, 2019.

[11] A. Mandal and N. Singh, "Optimization of atrazine and imidacloprid removal from water using biochars: designing single or multi-staged batch adsorption systems," *International Journal of Hygiene and Environmental Health*, vol. 220, no. 3, pp. 637–645, 2017.

[12] T. Ding, T. Huang, Z. Wu, W. Li, K. Guo, and J. Li, "Adsorption–desorption behavior of carbendazim by sewage sludge-derived biochar and its possible mechanism," *RSC Advances*, vol. 9, no. 60, pp. 35209–35216, 2019.

[13] S. Manna, N. Singh, T. J. Purakayastha, and A. E Berns, "Effect of deashing on physico-chemical properties of wheat and rice straw biochars and potential sorption of pyrazosulfuron-ethyl," *Arabian Journal of Chemistry*, vol. 13, no. 1, pp. 1247–1258, 2020.

[14] W. Li, R. Shan, Y. Fan, and X. Sun, "Effects of tall fescue biochar on the adsorption and desorption of atrazine in different types of soil," *Environmental Science and Pollution Research*, vol. 28, no. 4, pp. 4503–4514, 2021.

[15] M. Parlavecchia, V. D'Orazio, and E. Loffredo, "Wood biochars and vermicomposts from digestate modulate the extent of adsorption-desorption of the fungicide metalaxyl-m in a silty soil," *Environmental Science and Pollution Research*, vol. 26, no. 35, pp. 35924–35934, 2019.

[16] S. B. Abdel Ghani, S. Al Rehiayani, M. El Agamy, and L Lucini, "Effects of biochar amendment on sorption, dissipation, and uptake of fenamiphos and cadusafos nematicides in sandy soil," *Pest Management Science*, vol. 74, no. 11, pp. 2652–2659, 2018.

[17] K. F. Mendes, R. N. de Sousa, M. O. Goulart, and V. L. Tornisielo, "Role of raw feedstock and biochar amendments on sorption-desorption and leaching potential of three 3H- and 14C-labelled pesticides in soils," *Journal of Radioanalytical and Nuclear Chemistry*, vol. 324, no. 3, pp. 1373–1386, 2020.

[18] L. Zhao, F. Yang, Q. Jiang et al., "Characterization of modified biochars prepared at low pyrolysis temperature as an efficient adsorbent for atrazine removal," *Environmental Science and Pollution Research*, vol. 25, no. 2, pp. 1405–1417, 2018.

[19] M. Li, Z. Zhao, X. Wu, W. Zhou, and L. Zhu, "Impact of mineral components in cow manure biochars on the adsorption and competitive adsorption of oxytetracycline and carbaryl," *RSC Advances*, vol. 7, no. 4, pp. 2127–2136, 2017.

[20] S. Li, J. Lü, T. Zhang, Y. Cao, and J. Li, "Relationship between biochars' porosity and adsorption of three neutral herbicides from water," *Water Science and Technology*, vol. 75, no. 2, pp. 482–489, 2017.